NASA/CR—2020-220487

A Systems Analysis Approach to Understanding the Physiological Adaptation to Spaceflight

Joel I. Leonard
National Space Biomedical Research Institute, Houston, Texas

March 2020

NASA STI Program . . . in Profile

Since its founding, NASA has been dedicated to the advancement of aeronautics and space science. The NASA Scientific and Technical Information (STI) Program plays a key part in helping NASA maintain this important role.

The NASA STI Program operates under the auspices of the Agency Chief Information Officer. It collects, organizes, provides for archiving, and disseminates NASA's STI. The NASA STI Program provides access to the NASA Technical Report Server—Registered (NTRS Reg) and NASA Technical Report Server—Public (NTRS) thus providing one of the largest collections of aeronautical and space science STI in the world. Results are published in both non-NASA channels and by NASA in the NASA STI Report Series, which includes the following report types:

- TECHNICAL PUBLICATION. Reports of completed research or a major significant phase of research that present the results of NASA programs and include extensive data or theoretical analysis. Includes compilations of significant scientific and technical data and information deemed to be of continuing reference value. NASA counter-part of peer-reviewed formal professional papers, but has less stringent limitations on manuscript length and extent of graphic presentations.

- TECHNICAL MEMORANDUM. Scientific and technical findings that are preliminary or of specialized interest, e.g., "quick-release" reports, working papers, and bibliographies that contain minimal annotation. Does not contain extensive analysis.

- CONTRACTOR REPORT. Scientific and technical findings by NASA-sponsored contractors and grantees.

- CONFERENCE PUBLICATION. Collected papers from scientific and technical conferences, symposia, seminars, or other meetings sponsored or co-sponsored by NASA.

- SPECIAL PUBLICATION. Scientific, technical, or historical information from NASA programs, projects, and missions, often concerned with subjects having substantial public interest.

- TECHNICAL TRANSLATION. English-language translations of foreign scientific and technical material pertinent to NASA's mission.

For more information about the NASA STI program, see the following:

- Access the NASA STI program home page at http://www.sti.nasa.gov

- E-mail your question to help@sti.nasa.gov

- Fax your question to the NASA STI Information Desk at 757-864-6500

- Telephone the NASA STI Information Desk at 757-864-9658

- Write to:
  NASA STI Program
  Mail Stop 148
  NASA Langley Research Center
  Hampton, VA 23681-2199

A Systems Analysis Approach to Understanding the Physiological Adaptation to Spaceflight

Joel I. Leonard
National Space Biomedical Research Institute, Houston, Texas

National Aeronautics and
Space Administration

Glenn Research Center
Cleveland, Ohio 44135

March 2020

Level of Review: This material has been technically reviewed by expert reviewer(s).

Available from

A Systems Analysis Approach to Understanding the Physiological Adaptation to Spaceflight

Joel I. Leonard
National Space Biomedical Institute
Houston, Texas 77030

Preface

This book is a summary of interdisciplinary research (physiology, space medicine, engineering, computer science, mathematics) that spans two decades (1972-1992). The research was an attempt to use systems analysis, mathematical modeling, computer simulations, and database systems to integrate the biomedical spaceflight data that was being collected during this period. The goal of the effort was to achieve a better understanding of the human physiological response to short-term and long-term space travel. The activity was primarily devoted to analyzing the biomedical results of Skylab (1973-74), a series of three space missions which is still ranked as the most comprehensive of all long-term biomedical space studies to date.

This work was begun as a coordinated effort between the National Aeronautics and Space Administration (Johnson Space Center) and the General Electric Company's Space Division (Houston, TX). It was the intent that this multi-disciplined, integrative approach could reveal aspects of the then-new science of microgravity adaptation that were not obvious by adhering to the traditional methodology of examining each organ system in isolation. Some joint work with the Russians, including the Apollo-Soyez test project and a joint bedrest study was also supported during this period. In the 1980's the systems analysis group's effort was redirected to support the science management of human and animal experiments on the Space Shuttle. A few examples from this era are also included in the book.

Parts of this work have been published elsewhere, presented at technical meetings, and documented in reports with limited distribution. These publications will be referenced throughout the text and the interested reader is advised to use these as resource material where additional details are desired. The intent of this book is not to reproduce these documents but rather to present a coherent view of the integrative analysis under one cover. This volume contains the first detailed publication (other than in internal reports) of an extensive metabolic balance analysis of Skylab data, the development and validation of the "Whole-Body Algorithm," and simulation studies of diverse hypogravic environments. An analysis of cardiovascular deconditioning and a description of the calcium regulatory model are also new.

A long period has passed between the completion of the main body of work represented in this book and its publication in this form. It was inevitable that new research efforts would lead to developments related to the spaceflight problems addressed and thereby make some of our biomedical conclusions obsolete. Although in some cases reference to more recent work have been included, for the most part this book should be considered an historical summary demonstrating the approach and utility of systems analysis and computer modeling in the NASA Life Sciences program at the time the studies were conducted.

Acknowledgments

Table of Contents

Chapter 1
Executive Summary

1.1 Introduction

One of the most complete set of observations on man's adaptation to weightlessness collected by the United States to date was obtained during the Skylab Program.[*] The primary goal of the Skylab medical experiments was to define the changes which took place in the human body and, thus, to achieve an understanding of the physiological responses which occur during extended exposure to the spaceflight environment. Achieving a unified theory of adaptation to weightlessness, during the Skylab era had been difficult because of the requirement to integrate a voluminous quantity of data obtained by many scientists from various disciplines. This task was further confounded by the need to consider supplementary results from a diverse spectrum of ground-based studies that mimic the hypogravic environment of spaceflight. Interpretation of all these data requires the unraveling of a complex network of feedback regulators involving many individual physiological subsystems. Therefore, a project was developed in the early 1970's, based on an interdisciplinary systems analysis approach, to address this task. The systems analysis approach is particularly applicable in this situation because of the requirements to analyze and assimilate vast quantities of information, to understand the behavior of complex homeostatic systems, and to test scientific hypotheses explicitly and in as unambiguous a manner as possible.

Of the various analytical techniques developed to satisfy these requirements, the primary tool used was a set of mathematical models capable of simulating a number of physiological systems. Physiological function of the human body is often viewed as consisting of an aggregate of subsystems, each one of which is complicated, and these subsystems are integrated so that the organism as a whole maintains homeostasis. Each subsystem may be viewed as a type of control system operating with negative feedback to restore stability following a stress disturbance. These control features are often amenable to mathematical description, and the use of a computer permits such models to be used in a dynamic simulation mode. The benefits of using mathematical models are well known among physiologists who employ them in their research studies. Among other benefits, such models provide a systematic approach for: (a) assembling and organizing existing knowledge about a system; (b) identifying important parameters and determining the overall system sensitivity to the variation in these parameters; (c) predicting the values of quan-

tities that may be difficult or impossible to measure directly; (d) developing and testing hypotheses rapidly, quantitatively, and relatively inexpensively; and (e) identifying specific elements that must be further quantified, thereby suggesting the type of experiments that are needed to obtain missing information.

Although mathematical modeling is now well established in the life sciences, this study represents the first application of a large array of models in a uniform manner to solve problems in spaceflight physiology. Since the time between major space missions is so great and the number of astronaut subjects is relatively small, the decision was made to use mathematical simulation as an alternative means of examining physiological systems and maximizing the yield from previous spaceflight experiments. This use of mathematical models was expected to be complementary to the ongoing NASA program of employing ground-based experimental analogs of zero-g to provide additional insight into man's response to weightlessness.

1.2 Systems Analysis Techniques and Approach

An important objective of the systems analysis program, at the outset, was to develop the mathematical and statistical techniques required to support an extensive integrative effort related to man's response to weightlessness. It was apparent that data from most all of the major flight experiments of Skylab would need to be available in a single database, coupled with the appropriate analysis software. Toward this end, a medical data analysis system was created. The system consisted of an automated database, a computerized biostatistical and data analysis system, and a set of simulation models of physiological systems (see Fig. 1-1).

Data from a wide variety of investigative areas were collected and placed in this database, including cardiopulmonary function, body fluids, biochemistry, nutrition and energy metabolism, musculoskeletal function, body composition, and hematology (see Table 1-1).[†] An indication of the data utilized during the course of these studies is given by the selected parameters shown in Fig. 1-2. The total quantity of data contained in the database is quite large, in spite of the small number of astronaut subjects; information for approximately 900 man-days of spaceflight study is provided by 80,000 measurement values representing over 900 independent parameters. Algorithms were

---

[*] This chapter and accompanying book should be read in the historic context in which it was first drafted – during the period between NASA's first (Skylab, 1973-74) and second generation (Spacelab Life Sciences dedicated missions, 1991-1997) major biomedical flight experiments.

[†] The most significant omission from this list are the experiments related to the neurophysiological aspects of spaceflight. Time and resources did not permit an extensive systems analysis in this area, and therefore, this Skylab data was not included.
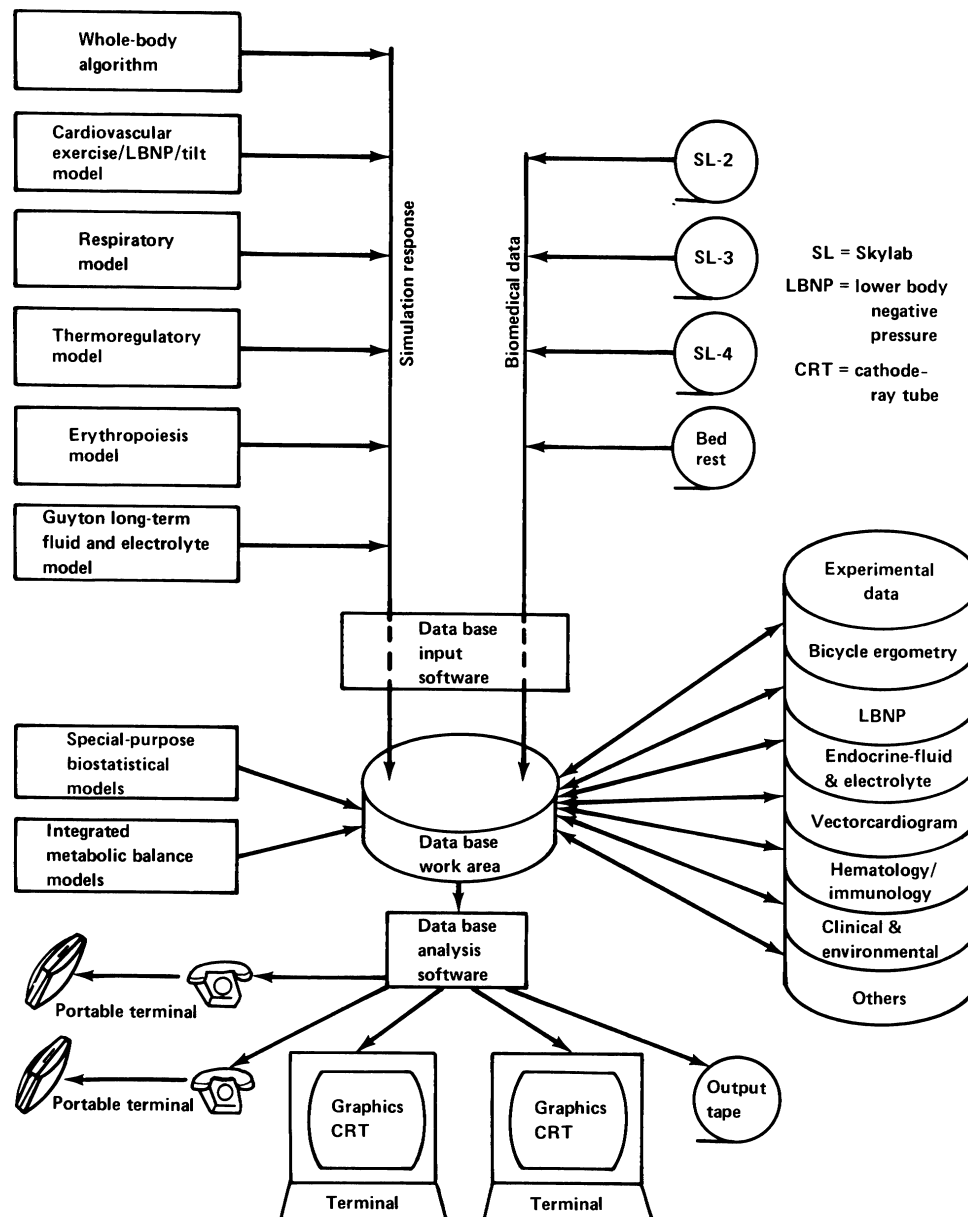
Figure 1-1. Skylab integrated medical data analysis system (SIMDAS)

provided to perform routine statistical tests, multivariate analysis, nonlinear regression analysis, and autocorrelation analysis. Special purpose programs were prepared for rank correlations, factor analysis, and the integration of the metabolic balance data using conservation models for mass, water, and energy.

1.2.1 Simulation Models

Five basic models were employed in this project: a pulsatile cardiovascular model (Fig. 1-3); a respiratory model (Fig. 1-4); a thermoregulatory model (Fig. 1-5); a circulatory, fluid, and electrolyte balance model (Fig. 1-6); and an erythropoiesis regulatory model (Fig. 1-7). A

major objective that was achieved early in the program was the integration of these subsystem models into a common framework termed the "whole-body algorithm" (Fig. 1-8). In addition, the development of a model of calcium regulation was begun but was not completed (Fig. 1-9). The basic similarity of the subsystem models seems evident from the diagrams in Figs. 1-3 to 1-9, since they are all represented by an active controlling system which regulates a relatively passive controlled system, and taken together, these units function as a negative feedback control system. The feedback variables for these models include representations of many of the sensors present in the body including temperature sensors, chemoreceptors, barorecep-

Table 1-1. Biomedical Experiments of Skylab in SIMDAS Database

Cardiovascular System
- Lower body negative pressure (LBNP)
- Submaximal exercise response
- Resting flows, pressures, heart rate

Musculoskeletal Function
- Bone densitometry
- Calcium (Ca$^+$) balance
- Strength measurements
- Anthropometric measurements
- Lean body mass measurements

Pulmonary Function
- Respiratory function during rest and exercise
- Mechanical and metabolic efficiences during exercise

Body Fluids and Composition
- Body fluid volumes
- Composition of plasma, urine, and feces
- Hormones related to fluid electrolyte balance and stress

Nutrition and Biochemical Metabolism
- Metabolic balances of water, nutrients and electrolytes
- Energy balance
- Body mass measurements

Hematology
- Red cell mass (RCM)
- Blood volume
- Hemoglobin (Hb)
- Indices of erythropoiesis
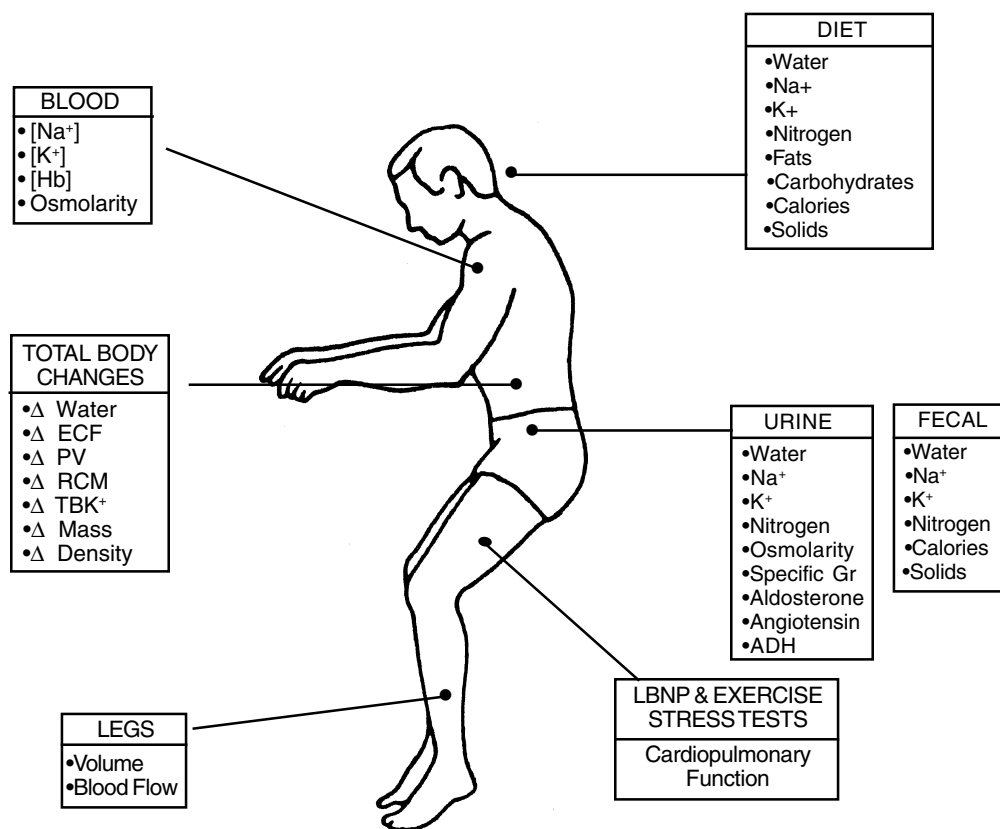
Figure 1-2. Selected data utilized in systems analysis study.

tors, oxygen sensors, and osmoreceptors. A majority of these models resulted from research directly associated with this project.

These models can be characterized as being deterministic, non-linear, and use finite difference formulations. All models operate on a large scale computer in an interactive timesharing mode with the automated capability to display responses graphically on remote terminals, and with the capability to compare experimental data and model responses simultaneously. Most models were modified to include gravity-dependent effects and to enable simulation of a human response to the stresses related to the spaceflight. Some of the experimental and clinical conditions for which the models were validated include

Table 1-2. Stresses Related to Spaceflight That Were Studied Using Simulation Models

- **Hypogravic Stress**
  - Supine Bedrest
  - Head-down Bedrest
  - Water Immersion
  - Spaceflight

- **Orthostatic Stress**
  - LBNP
  - Tilt Table
  - Postural Change

- **Metabolic Stress**
  - Exercise
  - Diet Restriction

- **Environmental Disturbances**
  - Hypoxia
  - Hypercapnia
  - Temperature
  - Ambient Pressure

- **Fluid Shifts** (non-gravity dependant)
  - Hemorrhage
  - Infusion
  - Water and Salt Loading
  - Dehydration

Figure 1-3. Model of Cardiovascular Regulation. A model of the human cardiovascular system and its controls was developed to simulate short-term bicycle ergometry exercise, lower body negative pressure, tilt, and tilt bicycle ergometry. This model includes gravity effects, muscle pumping, venous tone, venous valves, respiratory frequency, and intrathoracic pressure effects. Complex cardiovascular control hypotheses are modeled for the control of the heart period, peripheral flow resistances, venous tone, and other controlled variables. Metabolic control mechanisms are modeled by mathematical representations of oxygen uptake, oxygen deficit, and accumulating metabolites to simulate a transient metabolic state. The cardiovascular circulatory system is divided into 28 compartments to describe pulsatile blood flows, pressures, and volumes. Command inputs to the model are assumed to be from chemoreceptors, neurogenic inputs from muscular activity, and neurogenic anticipation. Other inputs needed are the exercise workload, work rate, blood volume, and angle and magnitude of the gravity vector. Typical outputs that can be selected are oxygen uptake, oxygen deficit, total metabolites, heart rate, various blood flows, systolic pressure, mean pressure, diastolic pressure, stroke volume, venous pressures, and arterial pressures. This model occupies a central position in the short-term segment of the Whole-Body Algorithm and was used to simulate the provocative cardiovascular stress tests used in the spaceflight program.

hypogravic stresses, orthostatic stresses, metabolic stresses, environmental disturbances, and fluid shifts (see Table 1-2). Multiple stresses and sequential degrees of stress can be simulated just as in a real experimental protocol. Many hypotheses can be tested merely by adjusting the value of one or more of the fixed system parameters.

1.2.2 Hypothesis Testing Approach

The combination of the data base analysis system with the group of simulation models formed the basis of the hypothesis testing approach that was used for integrating the Skylab findings (see Fig. 1-10). The basic analysis system enabled the rapid scanning of large arrays of spaceflight data, the graphical visualization of correlations between variables, and the statistical testing of hypotheses. This preliminary evaluation of spaceflight data led naturally to qualitative examination of the mechanism involved in producing the observed responses. This procedure drew heavily upon the theory of physiological feedback regulating systems and often suggested hypotheses capable of
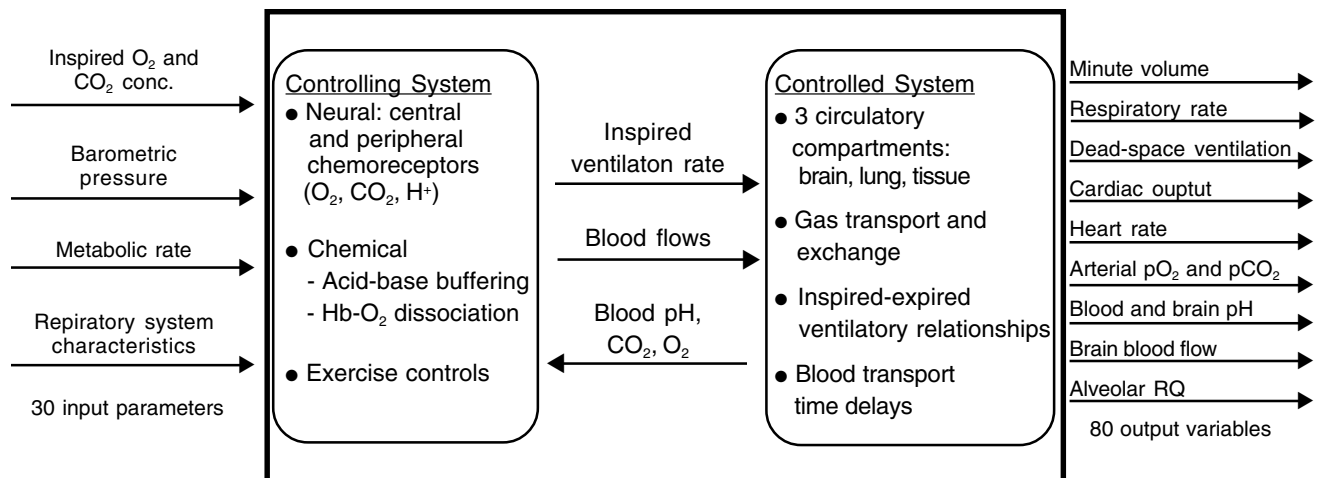
Figure 1-4. Model of Respiratory Regulation. The respiratory system model of Grodins was selected for use in the development of the whole-body algorithm. The controlled system is divided into three compartments (lung, brain, and tissue). The blood passes through the lungs and after a transport delay that is dependent on vascular volume and blood flow rate, the arterial blood arrives at the brain or the tissue compartment. In this model, carbon dioxide (CO_2) and oxygen (O_2) exchange rates are governed by metabolism. Venous blood exiting the brain combines with venous blood from the tissue after a time delay, to form mixed venous blood. After another delay this mixed venous blood enters the lungs to complete the cycle of gas transport and exchange. The real system is composed of receptor elements that monitor chemical concentrations, afferent nerves that transmit this information to the central nervous system, neural centers, and motor nerves to the respiratory muscles that drive the thorax lung pump. In the model of this system, this process is represented by using chemical concentrations at receptor sites as inputs to the system and ventilation as the output. Typical short-term stresses for which this model is suited include hypoxia, hypercapnia and acid-base disturbances. Modification of the original respiratory model for use in the Whole-Body Algorithm provided the capability to simulate exercise.
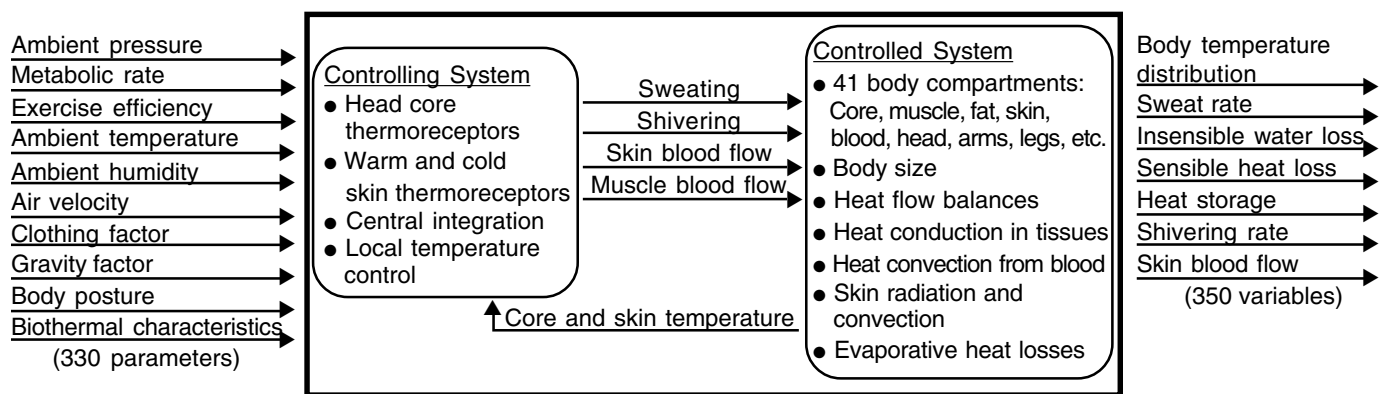
Figure 1-5. Model of Thermal Regulation. A dynamic model of physiological regulation of body temperature in man has been developed by Stolwijk and modified by NASA for various applications to the spaceflight program. The controlled system is the mathematical representation of the thermal characteristics of the various geometric compartments of the body. These compartments (or nodes) represent the head, trunk, arms, hands, legs, and feet and are further divided into concentric layers designated as blood core, muscle, fat and skin. Each of the forty nodes has appropriate metabolic heat production and convective heat exchange with adjacent compartments. The skin exchanges heat with the environment via radiation, convection, and evaporation. The thermoregulatory model receives temperature signals from all tissue compartments and, after integration and processing, the control system sends commands to all appropriate compartments changing metabolic heat production, blood flow, distribution, or the rate of sweat secretion. The thermoregulatory model is well suited to examine short-term stresses such as the effects of external temperature variation (environmental change) and the effects of changing metabolic heat production (exercise level change). This model formed an important link in the Whole-Body Algorithm, especially for the simulation of exercise. It was also employed to predict evaporative water losses in the hypobaric, reduced convective flow environment of Skylab.
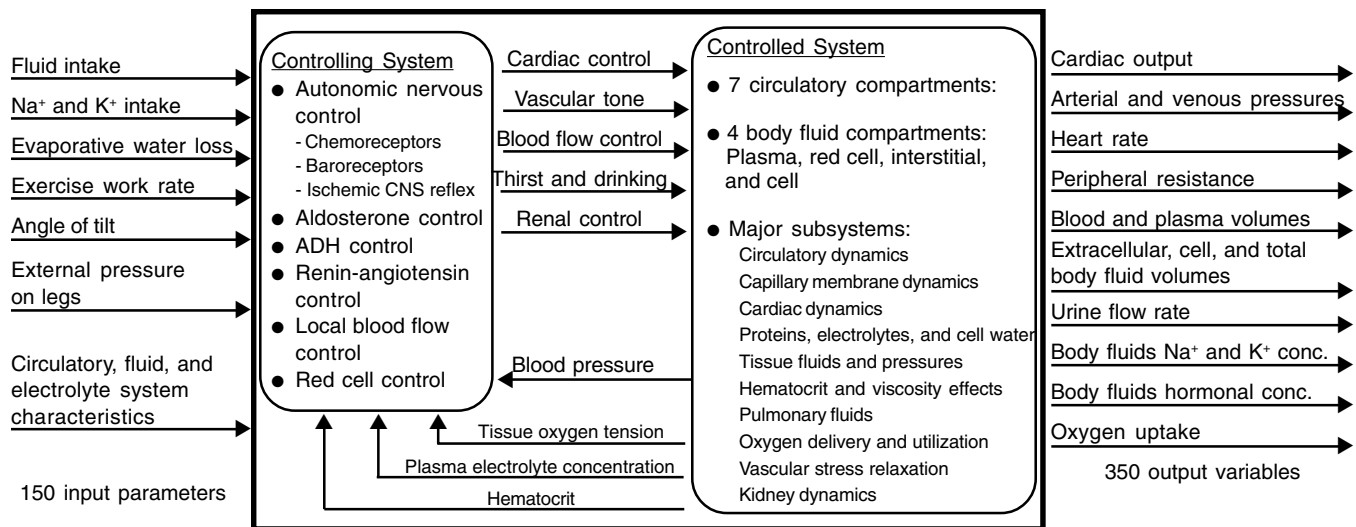
Figure 1-6. Model of Circulatory, Fluid and Electrolyte Regulation. The long-term model of circulatory, fluid, and electrolyte control, which was originally developed by Guyton is the largest and most complex of all the stand-alone models used in this project. It has been modified to include several new representations of certain regulatory functions. This model consists of 354 blocks, each representing one or more mathematical functions that describe an important physiological facet of circulatory regulation including autonomic, metabolic, renal, hormonal and fluid transport function. The circuit of blood flow in the Guyton model is divided into five volume segments: system arteries, system veins, right atrium, pulmonary arteries, and pulmonary veins-left atrium. Exchange of fluids (water and proteins) and electrolytes (sodium and potassium) is permitted to occur between the plasma, interstitial and intracellular fluid compartments by way of diffusion, active transport, transcapillary exchange, and lymph flow. Heart function is represented in a high degree of detail and includes representations for ventricular muscle strength, hypertrophy of the heart, deterioration of the heart, and sympathetic stimulation. Most of the above characteristics of the model can be viewed as the controlled system, while the controlling system consists of three major components: local control, hormonal control, and autonomic control. The inclusion of such elements as hormonal control, autoregulation, baroreceptor adaptation, erythropoiesis control, protein formation and destruction, venous stress relaxation and cardiac conditioning factors clearly indicate that the Guyton model was developed to be useful as a long-term model. Many varied experiments have been simulated with this model including infusions of water, electrolytes, and plasma; congestive heart failure; loss of kidney function; nephrotic proteinuria; and angiotensin infusions. The addition of gravity-dependent stress and the inclusion of leg compartments (developed under the current project) extended the capability of this system to include simulation of orthostasis, bedrest and weightlessness.
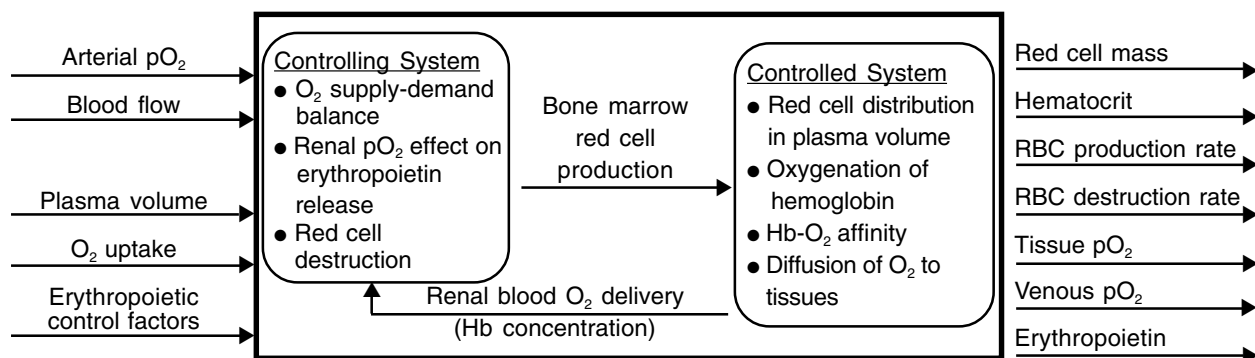
Figure 1-7. Model of Erythropoiesis Regulation. A model representing the control of erythropoiesis was originally developed to replace the red cell control algorithm in the Guyton model, but it has become an important investigative tool in a stand-alone mode as well. Elements in the feedback regulation loop include oxygenation of hemoglobin, oxygen supply by blood transport to a renal site, change in tissue pO_2 based on the balance between oxygen supply and oxygen demand, and secretion of erythropoietin from tissues sensitive to pO_2 levels. Production of red cells is based on the levels of circulating erythropoietin. Hemoglobin concentration in blood is computed from the addition of new cells to existing cells and plasma while accounting for cell destruction. The model is designed to investigate the relative influence of the controlling factors of erythropoiesis on total red cell mass. A wide variety of simulations have been performed with this model including altitude hypoxia, red cell infusions, dehydration, bedrest and spaceflight, as well as certain clinical abnormalities.

Thermoregulatory model

Functions:
- Thermal environment

Blood flow to head
Cardiac output
Oxygen uptake
Muscle blood flow
Trunk blood flow
Skin blood flow

Cardiovascular model

Functions
- Exercise
- Tilt ergometry
- LBNP
- Tilt

Cardiac output
Arterial and venous pressures
Heart rate
Peripheral resistance
Blood and plasma

Respiratory model

Functions:
- CO_2 inhalation
- Hypoxia

Short term

Total blood volume
Unstressed blood volume
Hematocrit
Insensible water losses
Muscle blood flow
O_2-Hb concentration
Renal blood flow
Skin blood flow
Nonmuscle blood flow

Long term

Circulatory, fluid, and electrolyte control model

Functions:
- Fluid balance and distribution
- Electrolyte concentrations
- Circulatory status

Figure 1-8. Whole-Body Algorithm. The design of the whole-body algorithm provides for the simulation of both long- and short-term stresses. The long-term simulation is accomplished by the circulatory, fluid, and electrolyte subsystem model (Fig. 1-6), which then initializes a set of three short-term models representing the cardiovascular, respiratory, and thermoregulatory systems. These three short-term models, which are designed to simulate the responses to acute environmental changes and short-term experimental stresses, operate in parallel fashion interchanging information as often as every half second of simulation time. Modifications were required to interface these subsystem models and to enable simulation of the stresses and experimental conditions of interest. One advantage of combining subsystem models is that each model considers various time lags, fast and slow controllers, and integration step sizes appropriate for their respective simulations. The primary function of this complex model is to enable evaluation of physiological interactions between subsystems. It also provides a capability for realistically simulating spaceflight missions in which long-term adaptation occurs concomitantly with shorter term environmental or experimental stresses. For example, a typical Skylab protocol can be simulated by performing stress tests such as lower body negative pressure or exercise at regular intervals over a prolonged inflight period during which time adaptation to the zero-g environment is achieved. In addition, the whole-body algorithm provides a central repository of hypotheses for explaining changes due to weightlessness in a variety of physiological systems.

being tested by using the predictive capabilities of the simulation models. The elements of the medical data analysis system (Fig. 1-1) were designed to interact in either sequential or parallel fashion, so that, for example, results from a data analysis could be employed as input forcing functions to a simulation model and the model's predicted responses could than be compared to additional data from the data base. Although good agreement between model and data was desirable at times, it was not always essential. The heuristic value of modeling is such that even more important objectives are often realized when this agreement is poor, including suggestions for data analysis, refinements of the mathematical models, changes in the hypothesis being considered, and suggestions for the design of new to be performed either in space or on Earth.

This is an iterative process, as suggested by Fig. 1-10, and is the heart of the systems analysis approach.

Statistical and modeling techniques naturally complemented each other for integrating and correlating results from many different investigative areas. Predicting the consequences of hypotheses on unmeasured variables from many subsystems is within the capability of models, such as the whole-body algorithm, but is impossible if the hypotheses are tested using traditional statistical methods. As the simulation study progressed, it was possible to incorporate increasingly diverse kinds of experimental results and hypotheses into a single model. Although each hypothesis alone would not support a generalized theory, all of them taken together should converge toward a coherent picture of zero-g adaptation.
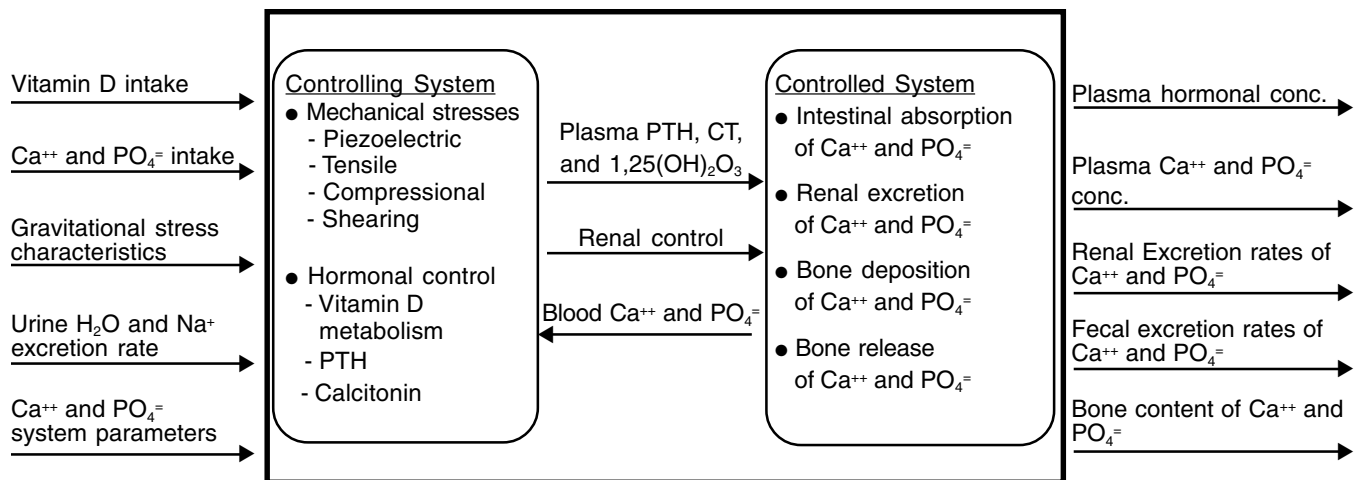
Figure 1-9. Model of Calcium Regulation. Development of this model of calcium metabolism is not complete. The design specifications define the calcium fluxes between the intestinal tract, kidney, bone, and plasma as the controlled system. These elements are controlled by the plasma concentrations of parathyroid hormone (PTH), calcitonin (CT), and the active metabolites of vitamin D, as well as by changes in mechanical stresses due to alterations in the gravitational load. Other controlling elements include the urinary excretion rates of sodium and water. The feedback loops influencing the controlling system are directed via the plasma concentrations of calcium and phosphate (PO_4). Thus, the model is designed to investigate the relative influence of the factors controlling calcium and bone metabolism.

Figure 1-10. Systems analysis approach for evaluation of spaceflight data.

1.3 Subsystem Hypotheses for the Response to Weightlessness

In this study most of the physiological systems that were of major interest to spaceflight researchers prior to and during the Skylab Program, were addressed. These investigative areas will be grouped, for purposes of summation, into five categories: (a) fluid, electrolyte, and renal function; (b) cardiovascular function; (c) hematology; and, (d) musculoskeletal function and (e) body composition. The major systems analysis accomplishments for each area are summarized in Table 1-3. The results from these studies have led to an interpretation of the spaceflight findings that are reviewed briefly in the sections below. Undertaken only recently was an analysis of the musculoskeletal system, with particular emphasis on calcium regulation.

Table 1-3. Accomplishments of Systems Analysis Study

A. Accomplishments: Fluid-Electrolyte Regulation

- Modification of the Guyton model (circulatory, fluid and electrolyte regulation) to include gravity-dependent elements, leg compartments, and improvements in the erythropoietic, renal, autonomic and renin-angiotensin subsystems
- Validation of the modified Guyton model for fluid-loading, hemorrhage, and postural-change studies
- Simulation analysis of the fluid-electrolyte response to hypogravic studies including water immersion, head-down tilt, bedrest, and spaceflight
- Analysis of evaporative water loss in the hypobaric, reduced-convective-flow environment of Skylab using metabolic balance analysis and the modified Stolwijk thermoregulatory model
- Metabolic balance analysis of water, sodium, potassium, calcium, nitrogen, and magnesium including Skylab nine-man composite summaries of dietary intake, renal excretion, and sweat losses
- Composite time profiles of the nine-man Skylab mean responses for plasma and urinary electrolytes, hormones, and total body changes in water, sodium, and potassium
- Analysis of fluid-electrolyte regulatory feedback mechanisms involved in acute and long-term responses to weightlessness
- Interpretation of all Skylab data related to disturbances in body fluid volumes and their composition including an integrated hypothesis to explain the behavior of renal regulating hormones
- Major support of bedrest and Spacelab flight experiment proposals

---

B. Accomplishments: Cardiovascular/Cardiopulmonary Regulation

- Development of a new pulsatile cardiovascular system model
- Validation of cardiovascular model for exercise, tilt, lower body negative pressure (LBNP) in one-g
- Modification of the pulsatile model to include elements responsive to hypoxia and hypercapnia
- Modification of the respiratory model of Grodins to include the capability to respond to exercise
- Simulations of the exercise response using the combined thermoregulatory, respiratory, and cardiovascular subsystem models of the whole-body algorithm
- Simulation analysis of spaceflight LBNP and postflight exercise (supine and sitting) using pulsatile model
- Simulation of disturbances in the circulatory system during short-term water immersion and head-down tilt and long-term bedrest and spaceflight using the modified Guyton model and the whole-body algorithm
- Composite time profiles of the nine-man Skylab mean responses to LBNP
- Sensitivity analyses for effects of blood loss and venous compliance changes on tilt and LBNP responses
- Analysis to examine possible changes in inflight baroreceptor sensitivity
- Analysis of mechanical and metabolic efficiencies and other performance indices during bicycle ergometry flight experiments
- Modification of the pulsatile cardiovascular model to include physical training (conditioning) effects and evaluation of these hypotheses against Skylab exercise data
- Formulation and evaluation of hypotheses to account for decreased orthostatic tolerance and decreased aerobic capacity during inflight and postflight phases
- Analysis of cardiovascular response during the high-g of Shuttle reentry with reduced blood volume including identifying thresholds for visual grayout
- Utilization of models to develop countermeasures for orthostatic intolerance during and after Shuttle reentry including fluid loading and pressure garments
- Support of flight experiment proposal for advanced cardiopulmonary studies

---

C. Accomplishments: Hematology

- Development of new models for control of erythropoiesis in the human and the mouse
- Simulation analysis of hematological responses to altitude hypoxia and descent, red cell infusions, bedrest, water-restricted dehydration, and spaceflight
- Interactive support of a research program that examined suppressed erythropoiesis in dehydrated mice
- Analysis of spaceflight and ground-based studies related to loss of red cell mass during hypogravity
- Formulation and tentative evaluation of candidate hypotheses to explain the "anemia" of spaceflight with particular emphasis on explaining the differences in red cell loss among crewmen
- Simulations of clinical syndromes (anemias, polycythemias, and Hb abnormalities) and partial development of a teaching model of erythropoiesis regulation
- Support of spaceflight experiment by predicting expected results, critical measurements, frequency of measurements, and effect of blood sampling on the hematological response to microgravity.

D. Accomplishments: Musculoskeletal System and Body Composition

- Metabolic mass, water and energy balance analyses including a new method for estimating cumulative total body changes (water, fat, protein, electrolytes) as a function of flight duration
- Analysis of body composition changes (lean body mass and fat) based on body water, body potassium, nitrogen-potassium balance, and body density data
- Analysis of inflight requirements for exercise and diet
- Interpretation of components of body weight loss based on fluid and energy regulation and gravity unloading
- Design and development of a new model for calcium regulation, including validation studies of bedrest and spaceflight
- Support of a flight experiment proposal for advanced calcium regulation studies

---

Therefore, the progress summarized in this area is more limited. In addition, whereas the indirect effects of space motion sickness on diet were considered in some detail, the vestibular system (which is believed to be the origin of this disturbance) and other neurologic aspects were not addressed directly.

The interpretation of the spaceflight data was guided by the need to answer certain questions that can be considered fundamental to a new area of environmental physiology such as weightlessness. These can be briefly stated as follows: (a) can the spaceflight findings be explained in terms of well-known homeostatic systems or are pathological components and non-regulatory characteristics involved?, (b) are there only a few common elements in the spaceflight response (i.e., gravity unloading, fluid shifts, lack of orientation, deconditioning), the identification of which would explain most of the observed findings?, (c) is there a typical "zero-g response" and if so, what are its most characteristic features? Also, is it permissible to treat the nine Skylab crewmen as a composite group in order to delineate this response, or were there significant differences between the three missions (other than duration) that are important to consider?, and (d) in what ways are certain ground-based experimental maneuvers (i.e., water immersion, bedrest, head-down tilt, suitable analogs of weightlessness), and in what significant ways do they differ from the spaceflight environment?

As a starting point in the analysis of each discipline area, an in-depth review was performed to identify findings that appeared paradoxical or otherwise unexplained following Skylab and that would be ripe for systems analysis investigation. A selected group of the most important of these 'critical' areas is listed in Table 1-4. Each was systematically addressed using the hypothesis testing procedures previously outlined and most of these observations and their resolution are mentioned in the following discussion. Taken as a whole, many of the tentative conclusions discussed below might have been considered novel when the original research was completed 20 years ago, although today they could be taken for granted. The book (but not this summary) includes updates that indicate whether the conclusions were subsequently verified or were found to be erroneous or incomplete.

1.3.1 Fluid-Electrolyte Response

There is unequivocal evidence that hypogravic stresses such as bedrest, water immersion, and spaceflight result in significant fluid redistribution within the body. The removal or reduction of the hydrostatic pressure in the blood column, coupled with the normal tissue elastic forces and muscle tone of the lower body, results in shifts of blood and tissue fluid from the lower body to the intrathoracic circulation. The consequences of this event are widespread and long lasting, as suggested by Fig. 1-11. As a result of central volume expansion, a complex set of reactions occurs: (a) stimulation of all cardiopulmonary pressoreceptors and decreased sympathetic activity; (b) increased blood pressures and secondary decreases in peripheral resistance, promoting enhanced renal blood flow;

(c) altered secretion of the fluid-electrolyte regulating hormones including ADH, the renin-angiotensin aldosterone triad, catecholamines, a natriuretic agent, and renal prostaglandins; (d) enhanced renal excretion of fluid and electrolytes as a result of the alterations in sympathetic activity, hormone secretion, and blood pressures and flows; (e) increased transcapillary filtration of plasma into the interstitium; and, (f) a decrease in thirst following reduction in angiotensin levels and augmented by space motion sickness anorexia. The net result of these processes is the loss of extracellular fluid and electrolytes, which has been observed frequently during and following weightless spaceflight.

This description evolved from examining such ground-based studies as water immersion and blood volume infusion. A simulation of immersion demonstrating many of these events is shown in Fig. 1-12. Most, if not all, of the rapidly acting mechanism described previously (which serve to correct the original blood volume disturbance) would most likely be observed only during the first hours of a hypogravic stress. However, based on 24-hour metabolic balances, urine flow in the Skylab crew was not increased and the entire loss of body fluids could be accounted for by deficit fluid intake (possibly as a result of space motion sickness). Computer simulation analysis of the acute stress period indicated that a decrease in fluid intake reduced, but did not abolish, the diuresis response and that the period immediately following this diuresis was accompanied by a reduction of renal excretion below control. Thus, it is postulated that a diuresis was not observed because void-by-void urine samples could not be obtained and because an early diuresis would be masked in a 24-hour pooled sample in the presence of diminished intake. The short-term renal response to spaceflight in well-hydrated subjects is not yet known.

Whatever the mechanism, most of these early fluid losses were believed to be ultimately derived from observed decrements in leg volume involving a contraction of the plasm, interstitial, and possibly intracellular fluid spaces of the lower limbs. By the end of the first 2 days in space the reduction in body water and body sodium was largely complete (see Fig. 1-13). Also during the early stages of flight, significant quantities of potassium escape from intracellular compartments. This shift may be deduced from elevated renal excretion of potassium; increases in plasma potassium; increased levels of cortisol and aldosterone that are involved in releasing and controlling potassium; and potassium balance studies on which the data of Fig. 1-13 are based.

The more prolonged adaptive phase (commencing after the first several days of flight) was characterized by a new steady state with respect to water and sodium and a slightly negative balance of potassium (Figs. 1-13 and 1-14). The modest increase of water and sodium excretion throughout this adaptive phase (not shown) did not necessarily reflect continued body loss inasmuch as excretion could have been offset by a decreased sweat component. Both a steady state metabolic balance analysis and a model simulation analysis support this concept. The continued loss of body potassium is expected from the atrophy of

Table 1-4. Selected Observations from Skylab Experiments Addressed by Systems Analysis

Fluid-Electrolyte System

- Rapid loss of water early in flight
- Much larger increase in leg fluid volume during inflight LBNP compared to preflight and bedrest
- Absence of measurable diuresis following headward fluid shifts contrary to expectations
- Unusual combination of hormonal changes compared to bedrest and water immersion
- Presence of hyponatremic plasma maintained throughout flight
- Increased water and sodium excretion throughout mission without continuous body losses.
- Differences in ADH response between missions.
- Decreased evaporative water loss in presence of hypobaric atmosphere.
- Disproportionate losses of potassium and cell water

Cardiovascular System

- Absence of acute cardiovascular disturbances expected from headward fluid shifts
- Decreased orthostatic tolerance as measured by LBNP tests
- Maintained aerobic capacity *during* flight despite decreased blood volume and decreased orthostatic tolerance
- Decreased aerobic capacity *immediately following* flight.
- Differences in aerobic capacity among the three crews.

Erythropoietic System

- Inflight loss of red cell mass despite normoxic environment
- Delay in postflight recovery of red cell mass on shortest mission.
- Significant differences in rates of red cell loss among the three crews.

Musculoskeletal System

- Progressive loss of calcium from body.
- Urinary calcium stabilizes at elevated level while fecal calcium increases progressively with flight duration
- Changes in PTH during spaceflight dissimilar to changes in bedrest
- Apparent decreases in rates of nitrogen losses as a function of flight duration and increasing levels of exercise

Body Composition

- Apparent disproportion in rates of water, muscle, and fat losses in relation to their normal ratio in body tissues
- Decreases in body mass losses with flight duration
- Water losses in astronauts apparently independent of flight duration
- Large differences in body composition changes between the three Skylab missions
- Apparent similar energy requirements in zero-g and one-g contrary to prior belief

lean body tissue, a consequence of gravity unloading and muscle disuse.

The importance of autonomic, hemodynamic, and hormonal regulators of circulatory and renal function during the chronic phase was ascertained by model simulation. These pathways were influenced by fluid shifts between body compartments, altered metabolic balance, potassium loss from the cells, and plasma electrolyte concentrations. Based on model analysis it appears that plasma volume is depressed about 0.5 liter throughout the flight. This prediction is supported by postflight measurements. The failure of the plasma volume to return to normal in zero g is presumptive evidence of the presence of blood volume controllers responding to the tendency of fluids to pool headward. During the adaptive phase of flight, angiotensin and aldosterone presumably reversed direction from the suppression hypothesized in the acute stress stage. Increased release of these substances can account for the elevated renal potassium rates of excretion. It was necessary to introduce a natriuretic factor in the model (responding to central blood volume expansion) in order to obtain realistic simulations of enhanced sodium excretion in the face of elevated aldosterone, and also to generate the hyponatremic plasma that was observed. The average behavior of ADH for all Skylab subjects (increased during the first 10 days and suppressed thereafter) exhibits the expected inverse correlation with urine output. Not so easy to understand is the elevation of plasma angiotensin I. Since renin-angiotensin is usually released in response to hypovolemia, the reason for elevation of angiotensin in zero-g (and also in some bedrest studies) at a time when there is a tendency for central blood volume expansion (i.e., upper body hypervolemia), is not clear. A mild reduction in plasma osmolarity and sodium concentration occurs early in flight and continues through the longest mission. The mechanisms that maintain this condition are

not clear. However, the combination of mild hypoosmolarity and hyperkalemia, helps account, at least in part, for the increases in angiotensin and aldosterone and decreased ADH.

1.3.2 Hematological Response

The most important hematological finding is a reduction in the circulating red cell mass during the flight interval. Before Skylab, the working hypothesis was that the pure oxygen gaseous atmospheres in the space capsule represented a toxic stimulus and resulted in early destruction of significant numbers (as great as 20% loss) of red cells. For the Skylab crewmen who existed in a supposedly normoxic environment, this hypothesis was no longer tenable to explain their average loss of 10% of total red cell mass. In the absence of a consistent finding of increased red cell destruction, it was assumed that this loss was likely a result of suppressed erythropoietic activity. However, no conclusive proof of this theory is available and no one mechanism has been identified which is consistent with all the data.

The regulation of erythropoiesis during weightless spaceflight was studied using a theoretical model (Fig. 1-7). Several approaches were used, including: (a) parameter sensitivity analyses, which helped identify the factors most likely to have a sensitive influence on erythropoiesis; (b) dynamic simulation of experimental studies such as altitude hypoxia and recovery from altitude hypoxia, red cell infusions, dehydration, and bedrest, all of which helped reveal behavior of the real system; and, (c) collaboration with investigators, performing human and ani-
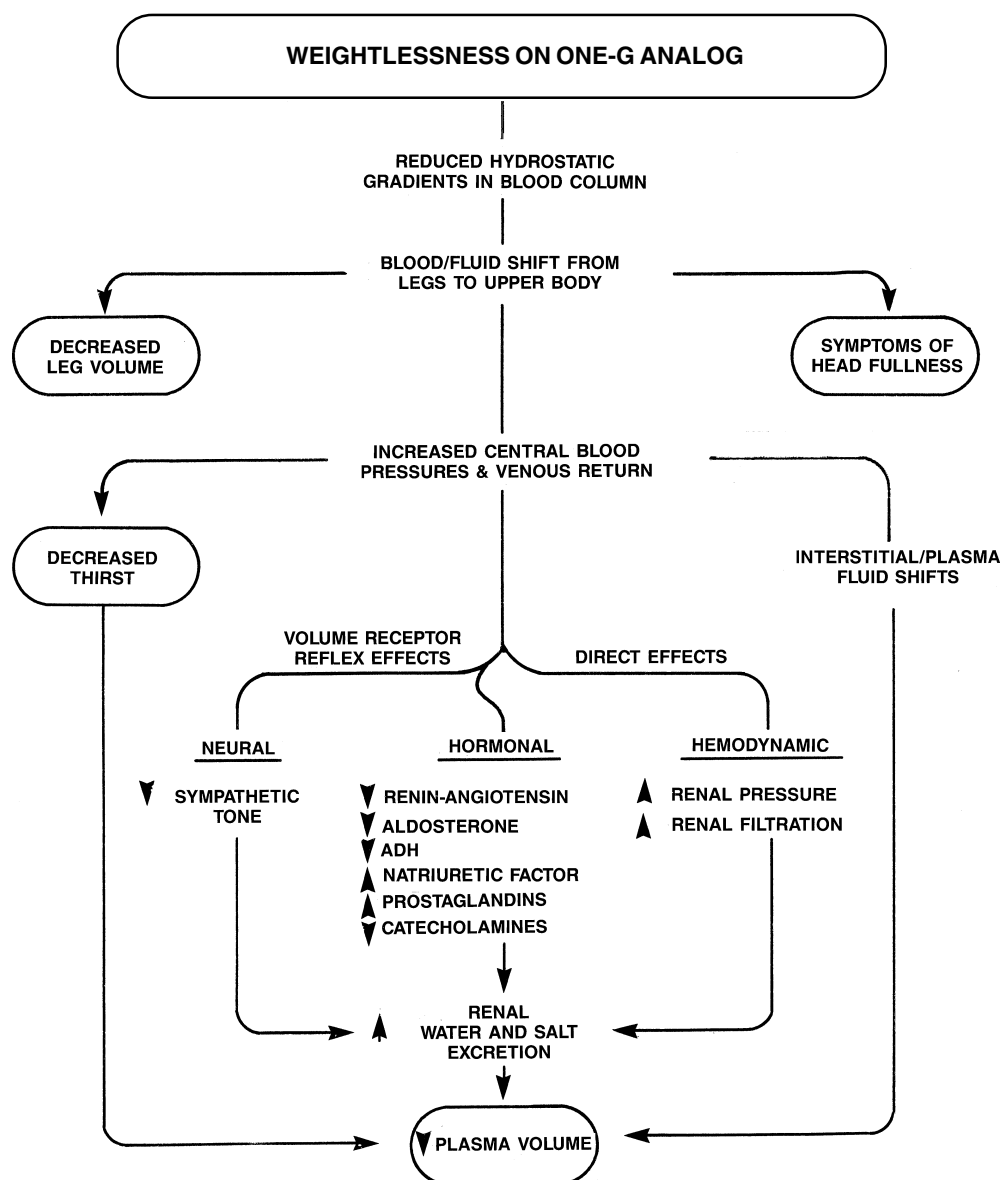
Figure 1-11. Hypothesis of fluid-electrolyte regulation following acute stress of weightlessness leading to a reduction in plasma volume.
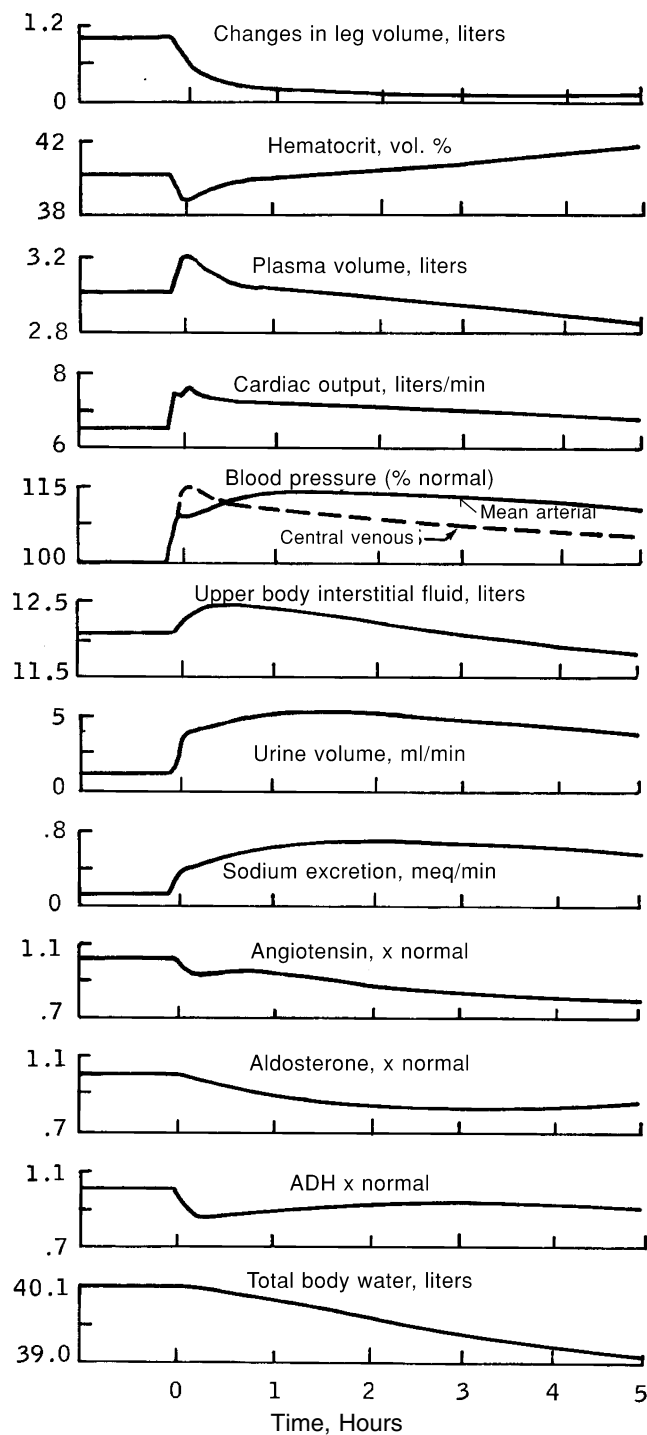
Figure 1-12. Simulation of acute effects of water immersion in normally hydrated subjects using the Guyton model.

Figure 1-13. Changes in body fluids and electrolytes of Skylab crew during first month of flight ($N = 9$).

mal studies, to test in the biological system those hypotheses suggested by the computer model.

The most important finding from these theoretical and experimental studies was that moderate increases in hematocrit, as great as the 12% measured on Skylab, if unopposed by other factors involving oxygen delivery to

tissues, can proportionately increase oxygen tension at a renal sensing site and exert a sensitive suppressant effect on erythropoietin and red cell production (Fig. 1-15). The erythropoietic regulatory system may be viewed, when operating in this fashion, as a hemoglobinometer; (i.e., red cell production) decreases so as to eventually relieve the hyperoxic condition. The final predicted result is a nearly complete restoration of hematocrit accompanied by a diminished red cell mass. Although not yet confirmed experimentally, model simulations suggest that during hypogravic maneuvers red cell mass will eventually stabilize as hematocrit normalizes. Therefore, the Skylab finding of red cell loss in spaceflight can be explained in terms of normal feedback regulation of the erythropoietic system in the face of sustained decreases in plasma volume.

The dissimilarity between red cell mass loss on the different Skylab missions could not be explained by hemoconcentration effects alone. Two theories were examined to explain the findings that the Skylab crews who returned to Earth after longer periods of weightlessness exhibited smaller losses of red cell mass. The time course of red cell loss in spaceflight is not yet known because of difficulties of performing this measurement inflight. But based on a composite of postflight measurement of all crewmembers, it was postulated by the Skylab research team that red cells disappear by some yet unknown mechanism during the first month and then begin to replenish during the second and third months. This notion would predict that after a duration in space longer than 3 months, the red cell mass might return to normal. Acceptance of this hypothesis as a generalized theory of erythropoietic regulation in weightlessness is confounded by the fact that decreasing losses of red cell mass in Skylab were associated not only with longer flight duration but also with increasing levels of diet and exercise. Based on animal studies, it was

Figure 1-14. Fluid-electrolyte response to hypogravity. Acute response is shown in the top portion and in Fig. 1-11, while longer-term adaptive effects are indicated in the bottom portion.

hypothesized that dietary restriction can reduce, and increasing exercise can enhance, erythropoiesis. Diet and exercise also appeared to have demonstrable effects on maintenance of body tissue and cardiovascular condition of the Skylab crewmen, and their further involvement in the oxygen transport-erythropoietic system was postulated in this study.

An alternate and more plausible theory was, therefore, proposed during the current project. This theory suggests there are two components to the suppression of red cell production: one related to energy balance and one related to water balance. Differences among the crewmen's red cell losses were thereby considered a result of different levels of dietary intake and exercise, superimposed on a common loss due to hemoconcentration (see Fig. 1-15). According to this concept, the kinetics of red cell disappearance in space would not include regenerative behavior but would be more similar to the continuous, linear losses observed in bedrest. Statistical correlations between diet levels and red cell losses, as well as model analysis, also tend to support this theory. Thus, it is not necessary to invoke the occurrence of red cell regeneration to explain the Skylab data.

Other factors (also shown in Fig. 1-15) which may have enhanced oxygen delivery and produced the same effects as hemoconcentration cannot be ruled out at this time (i.e., shifts in renal blood flow, oxygen-hemoglobin affinity and arterial pO_2) but direct data are only available to support the hemoconcentration effect. Also, the simulation analysis indicated that a major role of inflight cell destruction was considered unlikely, although it was impossible to rule out some degree of acute red cell destruction early in flight that may have contributed to the reduced red cell loss. Indeed, Skylab measurements indicated that some hemolysis may have occurred on the shortest flight.

Recommendations were proposed for future flights based on this analysis. For example, it is crucial to obtain direct inflight measurements of red cell mass, erythropoietin and bone marrow activity. If reduced erythropoietin levels cannot be demonstrated during spaceflight, then the hemoconcentration theory may have to be abandoned. Also, the importance of diet and exercise on erythropoiesis needs to be studied more carefully in humans with and without accompanying hypogravity. Finally, the differences between postflight and post-bedrest kinetics of red

Figure 1-15. Hypothesis of erythropoiesis regulation during prolonged spaceflight. Erythropoietin is secreted from kidneys in response to tissue pO_2. Erythrocytes are produced in the bone marrow.

cell recovery were not entirely resolved in this study, and it would be desirable to examine bone marrow activity upon recovery from hypogravic maneuvers.

1.3.3 Cardiovascular Response

The most striking changes in the resting cardiovascular system probably occurred early in flight, well before the first measurements could be performed. As simulated by the modified Guyton model and demonstrated by one-g experimental analogs of weightlessness, the primary event of the headward fluid shifts leads to central blood volume expansion, increased venous and arterial pressures, increased stroke volume, and elevated cardiac output. Secondary reactions following stimulation of central mechanoreceptors are immediately activated and include a decrease in heart rate and decreased peripheral resistance. These reflexes, together with enhanced transcapillary filtration and excess renal excretion, tend

to correct both the central blood volume and associated pressures. Although the Guyton model predicts a complete normalization of central blood volume, whether or not this occurs is still a matter of controversy. Engorgement of neck veins and facial tissues and feelings of headfullness, which continue throughout the flight, are symptomatic of the continued tendency of fluids to pool in the upper body in zero g. Also, a residual excess volume in the vicinity of the low-pressure cardiopulmonary receptors may account for the longer-term increase in resting heart rates, e.g., Bainbridge reflex, noted in most of the Skylab crewmen (and in bedrest subjects). Therefore, one of the long-term effects of spaceflight may be that as arterial pressure normalizes, the low-pressure volume receptors increase their influence while the high-pressure receptors decrease their influence with respect to their cardiac influence. Also identified during simulations of weightlessness were other long-term effects that assist the circulation to adapt to a reduced blood volume, an emptying of leg veins, and fluid pooling in the upper body. These poorly defined mechanisms include volume-receptor adaptation, devascularization, stress relaxation, baroreceptor resetting, and autoregulation of blood flow.

Cardiovascular function was evaluated during the Skylab missions by an LBNP orthostatic stress test and by an bicycle ergometry exercise stress test. The most prominent findings from these tests were a decrease in orthostatic tolerance during and following flight and a postflight decrease in aerobic capacity. Hypotheses to explain these findings were formulated and tested in the pulsatile cardiovascular model. (See Figs. 1-3 and 1-16). It was convenient and useful that the same model for the cardiovascular system be used to analyze both LBNP and exercise, each of which represents different challenges to the cardiovascular system with significantly different responses.

1.3.3.1 Analysis of Orthostatic Testing. The observed decrease in orthostatic tolerance is not unexpected in the light of significant loss of blood volume (Skylab avg. = -590 ml). Upon application of LBNP or standing in one-g, the increase in leg pooling coupled with a reduced blood volume significantly lowers central blood volume and venous return to the heart. The model simulations quite accurately predicted the increased heart rates and decreased pulse pressures characteristic of the Skylab crewmens' intolerance to orthostasis (see Chapter 7.4). The inflight heart rate response to maximal LBNP (-50 mmHg) was shown to be nearly equivalent to a 15% hemorrhage. However, blood volume loss alone was not sufficient to explain all of the observed findings. For example, an increase in leg volume pooling

Figure 1-16. Hypotheses to account for inflight cardiopulmonary responses to orthostatic and exercise stress tests. Postflight findings(not shown) reveal degradation in exercise performance as well as continued orthostatic intolerance, both tests being adversely affectedby an anemic blood volume.
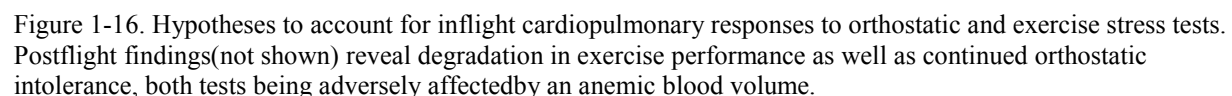
during LBNP (compared to the degree of preflight pooling) was noted during spaceflight. The most promising explanation of this phenomenon, as suggested by simulation analysis, was the partial collapse of leg veins in association with a reduced leg blood volume during the pre-LBNP control period. Small increments of LBNP would be expected to draw significant quantities of blood into the empty leg veins, more so in zero-g than in one-g.

The response to orthostasis was observed to stabilize and even improve in some subjects during the latter part of a mission (i.e., inflight heart rate response) becoming closer to that of the one-g control. One of the more promising hypotheses to explain these findings was a long-term downward adjustment of vascular capacity in the legs (in response to the reduced leg fluid volume) which could be manifested physiologically by retoning, devascularization,or reverse stress relaxation. Changes in plasma electrolyte concentrations (increased potassium and calcium, decreased sodium), may also be involved in altering vascular tone. Little is known concerning autonomic influences on venous tone during long-term adaptation to hypogravity.

1.3.3.2 Analysis of Exercise Response. Tolerance to exercise was essentially maintained during the flight period. It was only after return to Earth that aerobic capacity was found to be diminished. This result is similar to results reported for bedrest. Analyses performed with the whole-body algorithm permitted the circulatory adaptations of long-term bedrest to initialize the short-term LBNP and exercise model so that pre- and post-bedrest stress tests could be simulated with new initial conditions. Results from these studies suggested that decrements in blood volume in association with some reduction in unstressed volume in the legs could quantitatively account for most of the observed changes in post-bedrest exercise (and LBNP) and postflight exercise in the crews of the two shortest Skylab missions. (see Chapter 9.2). However, there was a notable qualitative difference between the degraded postflight exercise responses of the crews of the two shortest flights and the crew of the longest flight that was tentatively ascribed to an inflight exercise training effect. (The level of personal daily exercise increased on each longer flight). A systems analysis task was therefore devoted to developing the most feasible explanation of the interaction of zero-g adaptive changes (deconditioning) and exercise training (conditioning). In this regard, the cardiovascular exercise model was modified and validated to represent the simulation of a highly trained subject's response to bicycle exercise in one -g. This model was used in the"trained" and "untrained" mode to simulate the postflight bicycle ergometry experiments in both sitting and supine positions. The results led to the conclusion that a training effect was quantitatively consistent with the exercise response for the crew that trained the hardest (see Chapter 7.3.2).

The absence of a notable decrease in inflight exercise capacity in any of the Skylab crewmembers indicates that the contracted blood volume is an appropriate adaptation to hypogravity. Nevertheless, the nature of this adaptation is not clear. Results of the current analysis suggested that normal oxygen delivery was maintained in the face of diminished blood volume by the hemoconcentration of weightlessness and by the tendency of fluid to pool in the upper circulation and thereby to augment venous return to the heart. Conversely, the hemodilution observed on recovery (in addition to reduced blood volume) would be expected to contribute to the postflight degradation in exercise performance.

1.3.4 Musculoskeletal Responses to Weightlessness
The Skylab findings support the concept of a generalized atrophic response of the total musculoskeletal system during extended exposure to hypogravity. Losses in bone and muscle mass were among the more significant physiological changes observed in the astronaut subjects (see Fig. 1-17).

1.3.4.1 Muscle Atrophy. The losses in muscular tissue were particularly well documented in the Skylab crew (see Chapter 4). One of the systems analysis projects demonstrated that lean body mass was reduced by approximately1.5 kg (N = 9) over the inflight period. This was revealed by several independent methods that showed losses in body water, potassium, nitrogen, and body volume. More direct evidence of muscle and collogen breakdown was provided by the measured increase in renal excretion of urinary3-methylhistidine, hydroxylycine, and hydroxyproline. Also, excesses of intracellular electrolytes and amino acids appeared in the plasma and urine. Further analysis of spaceflight data indicated a significant degree of local muscle loss in the legs and perhaps in the skeletal muscle groups that normally control anti-gravity or posture. The data supporting these contentions come from spaceflight studies showing a gradual loss of leg volume, decreased leg strength, a reduction in duration of the Achilles reflex, and, in animals, diminished mass and response of red fiber groups. It is well known that atrophy of skeletal muscle occurs in response to disuse, inadequate functional load, and insufficient food intake. Spaceflight may be associated with more than one of these conditions. The absence of gravity results in diminished use of the lower limbs for postural support and locomotion, reduced body weightloading on weight-bearing tissues, and perhaps interference with proprioceptor reflexes which can influence muscle metabolism and function. A reduced caloric intake appears to be capable of increasing the loss of body protein, but increased caloric intake may not prevent this loss. The muscle disuse atrophy hypothesis receives support from the finding that the more intensive exercise performed by the crew of the longest flight (mainly exercise of the leg muscles) was associated with the smallest decreases in leg volume and strength. Little is known, however, about the changes occurring in other muscle groups, particularly those used for postural support in the upper body. If postural muscles are the primary targets of loss induced by zero-g, appropriate locally applied exercise might reverse this trend. Because each Skylab crewmember exercised, it is not possible to quantitatively predict the
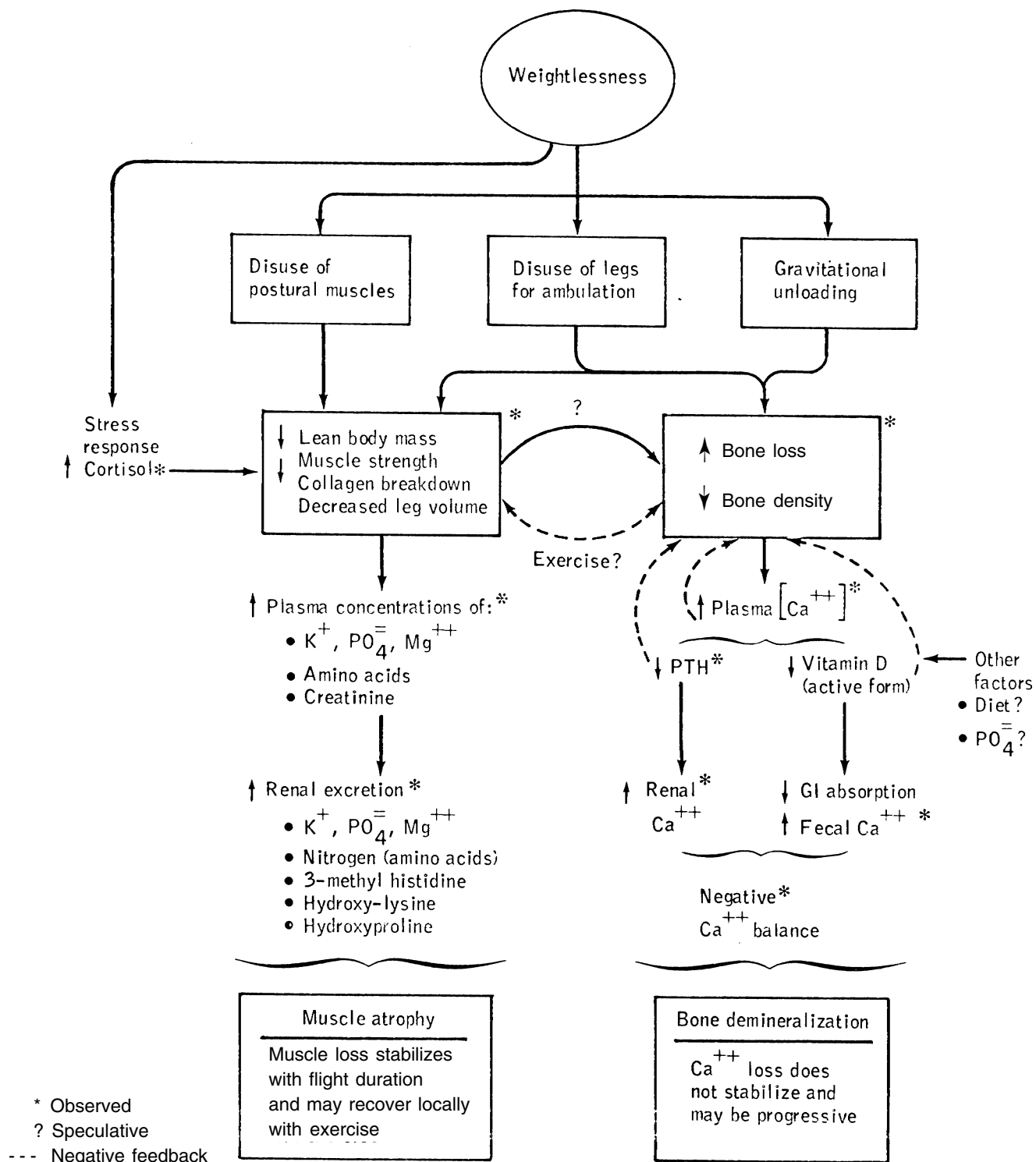
Figure 1-17. Hypotheses of musculoskeletal changes during prolonged spaceflight.

zero-g effect of complete lack of exercise. There is no reason to question, however, that exercise does maintain strength, muscle tone, and probably mass in the legs and improves circulatory condition similar to one-g training.

1.3.4.2 Bone Demineralization. Evidence for inflight loss of bone mass comes primarily from observations of calcium metabolic balance and bone density. Inflight calcium balances were consistently negative on all flights, a result of excess urine excretion throughout the missions and a progressive increase in fecal calcium loss as a function of mission duration. Bone densitometric data indicated losses in the calcaneus (of the heel), but not in the radius and ulna (of the arm), suggesting that losses are concentrated in load-bearing bones. A significant correlation between changes in calcaneus bone density and calcium balance for the nine crewmen was demonstrated. Additional evidence of demineralization is suggested by increases in urinary hydroxyproline and hydroxylycine which indicates breakdowns of the collagen matrix in the bone. As expected, plasma and urine biochemistry showed significant increases in calcium and phosphate, but the calcium regulatory hormones did not reveal a consistent trend. Analysis of all these data suggest that bone losses became progressively more severe on each longer mission, in contrast to the trend toward stabilized losses noted for muscle.

The initiation of bone loss is assumed to come from a reduction of mechanical forces induced by gravitational unloading, and/or reduced musculoskeletal interactions. These forces (piezoelectrical, compressional, tensile, and shearing forces) are known to be important in the normal maintenance and repair of bone. It appears logical that external forces, appropriately applied, might reverse the decalcification process. However, the search for suitable countermeasures has not met with notable success. The effect of exercise on bone demineralization remains unresolved.

Current understanding of the physiology of calcium metabolism, including the systems analysis, provides a partial explanation of the biomedical findings. Upon release from the bone into the extracellular pool, calcium and its concentration in plasma is under the control of a feedback system which is mediated by a hormonal system which influences renal excretion and gastrointestinal absorption as well as new bone formation. The observed elevation of urinary calcium may have been a result of increased plasma calcium concentration, decreased parathyroid hormone, and increased renal tubular sodium (see Figs. 10-8 and 8-9). Progressive losses of fecal calcium have been tentatively attributed to a net decrease in dietary absorption of calcium from the gastrointestinal tract. The active metabolite of vitamin D (1, 25 dihydroxycholecalciferol) is an important regulator of GI tract absorption, and a decrease in circulating levels of this substance could explain the fecal data. As suggested in Fig. 10-8, a depression of parathyroid hormone and Vitamin D could have a negative feedback effect on demineralization and limit the losses of calcium from the bone. These preliminary hypotheses have been incorporated into proposals for future flight experiments that will examine several features

of calcium regulation, including fluxes into and out of the bone and GI tract, hormonal regulation, and the effect of exercise as a countermeasure.

The systems analysis approach for understanding bone demineralization in space centered on understanding the complex feedback systems of calcium regulation including the development of a mathematical model. Various interpretations of spaceflight and bedrest findings were addressed which helped formulate the hypothesis of calcium metabolism adaptation to long-term spaceflight that is summarized above. Although the model is not yet complete, formulation of the model was instrumental in unifying spaceflight and bedrest data and in identifying critical areas in the regulatory system that might become altered in zero-g. When fully developed the model should be able to provide guidance in understanding these mechanisms. Can the acute renal calcium excretion be explained as an initiating event or as a feedback response? Can some primary disturbance in the calcitropic hormones cause renal excretion and bone loss or is there a primary event at the bone level due to alterations in mechanical forces? What biological activity is occurring in the bone tissue during these events?

1.3.5 Body Composition Changes

One of the more consistent findings in astronauts returning from spaceflight of any duration has been a loss in body weight. The dynamic behavior of this weight loss during flight was observed for the first time in the Skylab Program, but ancillary measurements of body composition were performed before and after the flights and, therefore, provided only estimates of gross overall change. Therefore, an analytical method was developed during the current systems analysis program to numerically determine the major components of body weight loss in terms of continuous time profiles for body water, body protein, body fat, body potassium, and body sodium (Fig. 1-18). The basis of the approach was a group of metabolic models for water, mass, and energy balance, which, when combined with whole-body measurements, enabled sequential accumulation of daily balance without incurring unreasonable error. Selected results of this study are illustrated in Fig. 1-19. The general conclusion of this study was that little more than half of the weight loss observed during the Skylab missions can be attributed to loss in lean body mass; the remainder is derived from fat stores. As a working hypothesis, the following conclusions have been assumed: (a) acute water and sodium losses are obligatory as a result of normal physiological responses to headward shifts of fluid in zero-g; (b) protein and intracellular mineral losses are primarily a result of disuse atrophy of postural muscles and may be obligatory in weightlessness (without appropriate exercise), although the losses appear to stabilize after about a month; (c) fat losses are more variable and are probably dependent on the usual one-g influences of diet and exercise; and (d) if present, the anorexia associated with space motion sickness will augment fat and protein losses by virtue of a caloric deficiency and will enhance water loss as a result of reduced fluid
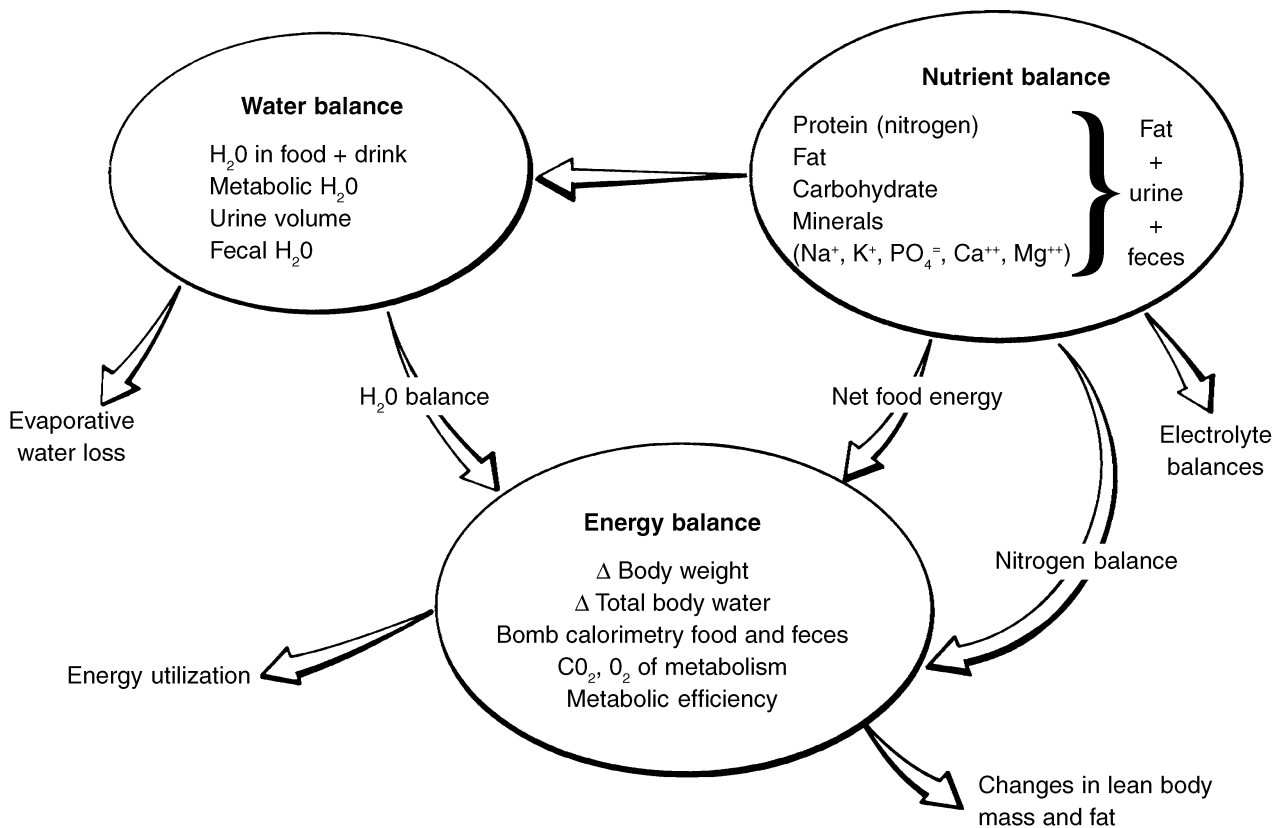
Figure 1-18. Integrated metabolic balance analysis

intake. These conclusions must be considered tentative because of the indirect method of estimation and because adequate experimental controls for assessing the effect of diet and exercise in weightlessness were not available.

1.4 Integration of Subsystem Hypotheses

Figure 1-20 is offered as an integrated hypothesis of the adaptive response to weightlessness. It is obviously limited to the subsystems and specific hypotheses considered in the present analysis. Although a great amount of detail has been omitted for the sake of clarity, of interest here are the interactions between subsystems and the generalizations that can be made about the behavior of the combined systems. The following broad picture has emerged.

Disturbances in the cardiovascular, fluid-electrolyte, erythropoietic, musculoskeletal, and metabolic systems, which are found during and after flights of varying duration, appear to be attributed to two major effects of weightlessness: first, the absence of hydrostatic forces resulting in severe fluid shifts within the body and, second, the absence of deformation forces resulting in degradation of normally load-bearing tissues. The first of these effects leads to a reduction in body fluids, most importantly, blood volume. The consequence of the second effect is a reduction in bone and muscle mass. In addition, a third factor, a long-term alteration of the metabolic state, a reflection of changes in dietary intake and activity levels, was found to have an important effect in the responses of the Skylab crewmen. This latter factor may be within the realm of human intervention and correction on future missions. All of these events have both acute and long-term effects which lead to the notable and consistent findings of a loss in weight, a change in body composition, a decreased tolerance for orthostasis, and additionally, upon return to a one-g environment, a decreased aerobic capacity. Adaptation is said to occur when the body adjusts to these changes and reaches a new steady-state level. Figure 1-21 is an attempt to show the relative time course of adaptation for each major physiological system. The return to new baseline values reflects the establishment of a new homeostatic level appropriate to weightlessness.

These studies have supported the concept that within the time span for which man has so far been studied in space, these responses to weightlessness can be explained in terms of normal feedback regulatory processes. One classical example of these processes concerns the blood volume controllers that reduce plasma volume when challenged by the cephalad shifts of peripheral fluid. Also, the reduction in red cell mass has been postulated to be partly a result of the homeostatic response to hemoconcentration and tissue hyperoxia. Another, of many examples, concerns the biochemical mechanisms which sensitively respond to small changes in electrolyte shifts

Figure 1-19. Body composition changes of the Skylab crew.

rapid decrements in leg volume. At the other extreme is a class of substances that disappear much more slowly. Calcium and, perhaps, red cells are representative of this category. Depending on the degree to which caloric intake matches energy requirements, fat stores can be included in this group as well. Muscle tissue appears to degrade at intermediate rates as exemplified by nitrogen and potassium losses. All these rates of disappearance from the body most likely depend on the nature of the disturbance and on the effective time constant of the correcting homeostatic system.

These studies have confirmed the hypothesis previously suggested that the loss of blood volume is of central importance to the understanding of the zero-g responses of several major systems. Although this loss is essentially an acute circulatory adaptation to volume overload, it was found to have a significant long-term effect on the orthostatic intolerance and reduced exercise performance observed after flight. Also, the reduced plasma volume was found to have a potentially strong influence on the erythropoietic response. Finally, the long-term adaptation of the circulation may depend on the vascular elements responding to accommodate the hypovolemic condition. It should be noted, however, that in none of these cases was the loss of blood volume alone sufficient to explain the entire response . Another event that had a widespread effect was the negative energy balance noted for the crews of the two shortest missions and for all crews during the early flight period. In addition to the obvious effect on fat stores, an inadequate intake of fluid and food was found to be implicated in the lack of expected acute renal response, the loss of muscle tissue, the loss of water, and the differential loss of red cells among the crews.

Although this study has not provided a definitive theory to explain the available data, it has resulted in the examination of available evidence to support or deny various scientific hypotheses, the identification of qualitative and quantitative interactions between various experimentally measured responses to spaceflight, and the formulation of a tentative integrated physiological hypothesis for the adaptive processes. The elements of this hypothesis can be included in the subsystem models or the Whole-Body Algorithm. At that point, the models will serve their main function as a central repository of a detailed integrated hypothesis of zero-g adaptation and can be used for more advanced applications such as development of countermeasures or a quantitative approach for a crew health monitoring and maintenance system.

1.5 Conclusions

The contribution of the simulation models was significant in constructing the hypotheses discussed above, although the limitations of space in this summary may not make this fact apparent. It is appropriate, therefore, to consider several illustrations of these benefits of the modeling process.

The normal functions of simulation models include the capability to evaluate hypotheses retrospectively, and thereby to enable greater use of the acquired information,

resulting from cell demineralization, and, within limits, maintain the plasma composition at the expense of excess renal excretion.

Exposure to weightlessness invariably leads to loss of major body constituents at rates that, according to the present analysis, are disproportionate to their concentrations in the body. The most rapid losses are observed for extracellular fluids and salts, and are reflected by equally

Figure 1-20. Integrated hypothesis of physiological adaptation to prolonged spaceflight.

Neurosensory

Fluids and Electrolytes

Cardiovascular System

Clinical Horizon

Hemoglobal System

Bone and Calcium Metabolism

?

Lean Body Mass

0 g Set Point

1 g Set Point

Time Scale (months)   1   1 1/2   2   4   5   6

Point of Adaption
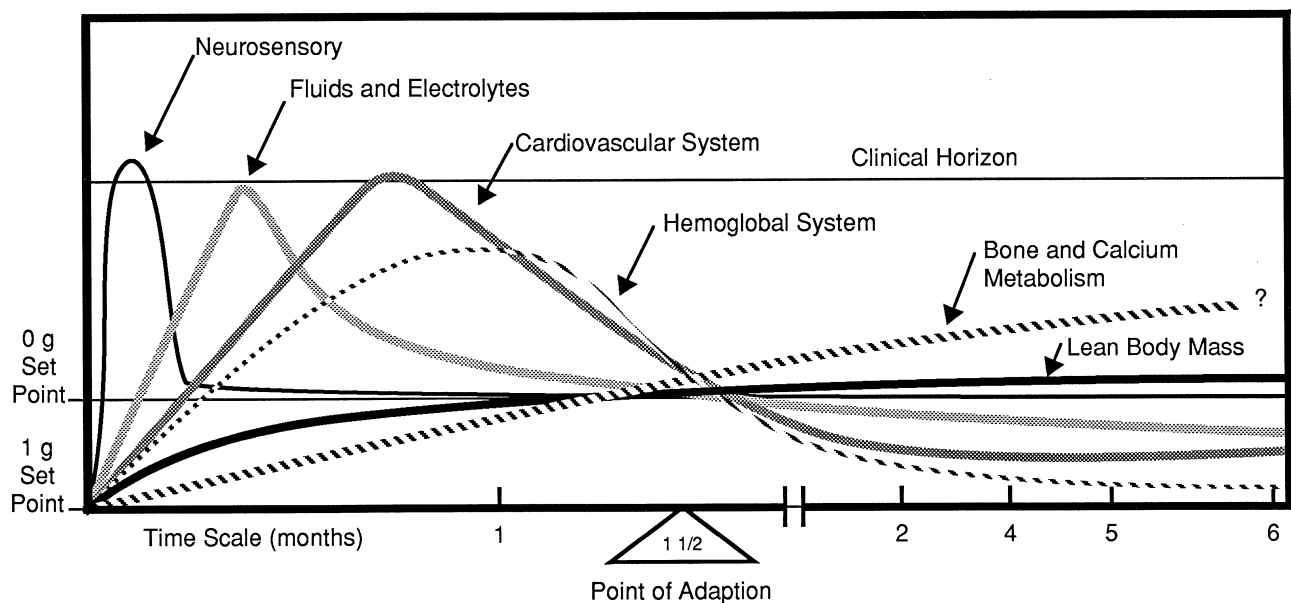
Figure 1-21. A highly idealized view showing the approach toward homeostasis of physiological systems during spaceflight. Each physiological subsystem has a different time course of adaptation and appears to be driving towards a new homeostatic level. Note that the time scale is exponential.

and perhaps lead to the most likely interpretation of the previously collected data. Using the computer simulation, the models predicted the dynamic changes of variables which may have been difficult or impossible to measure during spaceflight. Table 1-5 illustrates two categories of biomedical measures that were found to be very useful or necessary for a characterization of spaceflight adapatation. Quantities in the left column were measured inflight during the Skylab experiments; quantities in the right column were not measured at all during flight. But all quantities shown were capable of being predicted by the computer models.

The utility of models, however, extended beyond these predictive capabilities. A benefit that was attributed to the modeling process related to the ways in which models shaped the data analysis effort. Quantitative modeling often required a new look at data that had already been analyzed by more traditional methods. The simulation approach requires certain patterns of data in very specific forms. Satisfying these model requirements led, in one instance, to the integrated metabolic balance analysis for describing body composition changes during spaceflight. In another situation, the study that led to an analysis of evaporative water loss in the Skylab crew was suggested originally by the need to validate the sweating mechanism in the thermoregulatory model for weightlessness. Another prime benefit of modeling, at this stage of its application to space physiology, was in forcing the analyst to think systematically, comprehensively, and quantitatively about the system of interest. The formation of the model, based on experimental evidence and known concepts, provided insights into the organization of the system elements and the multiple pathways connecting

Table 1-5. Selected Quantities Predicted by Simulation Models

Parameters for Which Inflight Data Exists	Parameters for Which Inflight Data Does Not Exist
Total body water	Extracellular water
Leg volume	Intracellular water
Body potassium	Interstitial water
Extracellular sodium	Plasma volume
Plasma sodium	Red cell mass
Plasma potassium	Red cell production rate
Plasma proteins	Plasma erythropoietin
Plasma hemoglobin	Tissue oxygenation
Plasma angiotensin	Autonomic activity
Plasma aldosterone	Volume receptor stimulation
Plasma ADH	Natriuretic factor
	Capillary filtration
Urine volume	Cardiac output
Urine sodium	Peripheral resistance
Urine potassium	Venous pressure
Evaporative water loss	Local blood flows
Blood pressure	Body temperature
Leg blood flow	Circulatory, renal, fluid, and hormonal changes on first inflight day
LBNP heart rate	LBNP cardiac output
LBNP blood pressure	LBNP venous pressures
LBNP leg volume	LBNP blood volume and flow distribution
Exercise heart rate	Exercise cardiac output
Exercise oxygen uptake	Exercise stroke volume
Exercise minute ventilation	Exercise blood gases

Figure 1-22. Relative duration of various hypogravic stresses showing typical data collection periods. Skylab experiments stretched the time horizon of study to several months but with few measurements during the first day. The ground based experiments helped to fill in this data gap.

Table 1-6. Significant Data Analysis Accomplishments

- A more definitive data analysis of Skylab based on a composite picture of the nine crewmen from all flights

- Estimates of quantities which could not be measured directly but could be derived from metabolic balance models or simulation models

- Integration of data across disciplinary lines

- Quantitative evaluation of hypotheses by computer simulation and interpretation of data in terms of feedback control theory

- Reevaluation and reinterpretation of previously published Skylab data in the light of more recent findings from ground-based studies

these elements. The complexity of models, reflecting the redundancy of the mechanisms in the body helped resolve some paradoxical findings by suggesting the involvement of one or more competing pathways. Also, it was not always possible to explain the long-term adaptation phase of spaceflight in terms of regulatory feedback mechanism more suited to corrective action of acute disturbances. This difficulty suggested a logical division of the spaceflight period into acute and chronic segments for purposes of systems analysis.

A comprehensive approach for relating the experimental findings from various ground-base studies to the spaceflight observations was also facilitated by the integrative qualities of the models. These one-g study employing hypogravic maneuvers often provided more abundant data than spaceflight investigations, especially for the acute stress stage. Postural changes, water immersion, and head-down tilt studies have helped to characterize the short-term phase, whereas bedrest and spaceflight were useful in describing long-term processes (see Fig. 1-22). All of these stresses have the common characteristic of a reduction in hydrostatic gradients and a rapid headward shift of fluid. The modified Guyton model and the whole-body algorithm, both capable of simulating short- and long-term events, provided a framework upon which these diverse experimental results could be systematically examined. Within limits, the approach resulted in a better understanding of the complete temporal spectrum of hypogravic responses and in explaining results which otherwise appeared to conflict.

During the present project, a qualitatively more advanced data evaluation was achieved than was previously available. Some of the key features of these accomplishments are summarized in Table 1-6. The fundamental contribution of the systems analysis effort has been to organize many of the major biomedical findings from spaceflight and correlate these findings with the scientific concepts that describe the requisite organ system. Out of this effort has come an array of methods, tools, and techniques that have proven essential for the handling, processing, and interpretation of experimental data in general and spaceflight data in particular. Another result is an improved understanding of the physiological events that occur during human adaptation to weightlessness. When this understanding is enhanced, it may be possible to predict

individual responses to weightlessness and appropriately define indices of health during prolonged spaceflight and subsequent recovery. Finally, this study led to identification of critical areas ripe for future study. Recommendations for new experimental approaches generated by the current program have already contributed to the design of ground-based and future Spacelab investigations. Full potential of the systems analysis method will be realized only by maintaining an iterative cycle between model development and experiments.

Chapter 2
Introduction

2.1 Introduction

2.1.1 Purpose of the Book

The first set of comprehensive observations on humans in space was collected during the early 1970's aboard the United States' first space station, Skylab. The primary goal of the Skylab medical experiments was directed toward defining the changes in the human body and achieving a better understanding of the physiological responses that occur during extended exposure to the spaceflight environment. The objective of achieving a unified theory of adaptation to weightlessness was confounded by the task of integrating a voluminous quantity of data obtained by many scientists from various disciplines. The experimental findings were interpreted and reported as individual disciplinary studies by the principal investigators [1]. But there was no significant attempt at that time to integrate this collection of disciplinary studies or to develop a theoretical framework to describe these interrelationships. Therefore, separate from the original *experimental* findings of Skylab, a *theoretical* analysis was initiated that was concerned with the very difficult problem of integrating these different studies. This book will summarize the results of this ensuing project whose purpose was to analyze the human physiological response to spaceflight from the unique perspective of *systems analysis*.

At the heart of this interdisciplinary analysis was the recognition that a coherent theory of adaptation to weightlessness should entail integration of data from a large body of research, primarily those from Skylab and other space missions, but also including analogous ground-based studies on both humans and animals. The human body, while conveniently divided into organ systems for research purposes, is of course designed to function as a whole. It is only by crossing the discipline boundaries that we can discover how quite different regulatory elements throughout the body interact, compete with and complement each other as they react to the space environment with an *integrated* response. At the same time it is important to *unravel* the observed total human physiological response to obtain an understanding of the role that each of the major components of the body plays following the transition to and from space. It was believed such an integrative analysis would yield new insights into the overall process of man's adaptation to weightlessness.

2.1.2 Requirements, Objectives and Approach

A systems analysis approach was particularly suited to address three primary *requirements* of the project: a) to analyze and assimilate large quantities of information collected by many investigators from different investigative areas; b) to understand the behavior of complex physiological regulatory processes that may be operating during spaceflight; and c) to pose and analytically test alternative hypotheses in terms of these regulatory systems in order to account for the experimental data.

The following *objectives* were established to meet these project requirements:
1. To identify and develop new and improved mathematical approaches for the solution of problems in the space life sciences,
2. To provide methods of organizing, integrating, and analyzing spaceflight and supportive ground based research data across interdisciplinary lines,
3. To develop and test, using quantitative approaches, individual physiological subsystem hypotheses that attempt to explain the experimental findings,
4. To integrate these hypotheses into a unified and internally consistent understanding of physiological adaptation to weightlessness.
5. To apply the systems analysis techniques to the support of NASA's ongoing research program by contributing to improved experimental design and data analysis.

A *longer-range purpose* was to develop a quantitative approach for a crew health monitoring and maintenance system. This would include the means to establish criteria for zero-g health, detection of clinical deviation from these norms, and development of countermeasures for restoring normal function.

New technology and quantitative methodology would be required to satisfy these ambitious objectives. These new approaches, described fully in Chapter 3, would include several *critical software systems*:
1. An automated database for storage, retrieval and display of experimental results from spaceflight and ground based studies,
2. A biostatistical and data analysis system to support interdisciplinary analysis across the major biomedical flight experiments with the purpose of developing candidate hypotheses for explaining critical spaceflight findings,
3. A group of mathematical models (including an integrated multi-system model of human physiology) capable of simulating a variety of physiological stresses,
4. A wide range of modeling techniques to simulate the experiments performed on Skylab and in ground-based analogs of zero-g, and
5. A software system for quantitatively evaluating candidate hypotheses in the models by comparing simulation responses and spaceflight data.

While today there are special computers and software that make the formulation and solution of mathematical models a relatively simple affair, this was not so true in the

1960's and 1970's when the models used in this project were created. Computer speed and memory storage was an important issue as was the algorithms used to solve the mathematical expressions, usually by iterative procedures. In addition, the user interface was relatively primitive in those early years. In the current project a custom designed interface, using recently developed remote graphical terminals attached to a mainframe computer, was created that permitted the modeler to easily change the independent variables (parameters) of the model and to allow the simulation results to be displayed graphically in a manner that permitted comparisons with experimental data. Likewise, the databases for storing, retrieving and displaying the vast number of Skylab measurements were all custom designed because commercial off-the-shelf software did not exist.

Two facets of the analysis activities will be presented in this volume. One concerns the advantages and limitations of the modeling process itself and how this approach served in integrating and interpreting the spaceflight findings. The other concerns the results of this approach, that is, a description of the spaceflight adaptation process as seen thru the prism of systems analysis. However, it is not the authors intention to provide either a detailed presentation of modeling theory or a comprehensive treatise on spaceflight physiology.

2.2 Background

2.2.1 Systems Analysis in Space Life Sciences

The significant benefit of using systems analysis and mathematical modeling to study the physiological effects of long duration space missions was recognized early in the history of the space program by the National Academy of Sciences [2]. They believed that such an approach would "advance and accelerate knowledge of the functions, control and regulations of the (human) system under space conditions." and would be "particularly useful in those areas where experimentation and actual flights are especially costly in time and resources." Following the Skylab missions the chief biomedical officers of NASA discussed the need for an interdisciplinary analysis approach to assimilate the voluminous quantities of data collected in space [3] and for in-depth studies to resolve some of the paradoxical findings [4]. It was realized that until additional experiments can be performed on future space missions, some years hence at that point, methods such as systems analysis could be very useful for integrating data and testing hypotheses. The projects discussed in this book were meant to address these concerns and recommendations.

The only other broad-based study that was similar to the one reported on in this volume was conducted by the Russian space agency. Throughout the 1970's and 1980's, prior to the normalization of diplomatic and political relationships between the U.S. and the Soviet Union, a group of scientists from NASA and the Institute of Biomedical Problems (Moscow), met on a regular basis to discuss the most pressing biomedical issues confronting human space travel. A regular portion of their deliberations (led by one of the current authors, JAR) was devoted to the systems analysis and mathematical modeling activities of both countries. Some of the material contained in this volume was presented at those meetings. This information on a systems analysis of space biology and medicine was compiled by the Russians, along with their own work [5]. In addition, several overviews of the current project were previously published [6,7,8]. One of these [8] also reviews smaller modeling projects that NASA has sponsored that were not part of the current project.

2.2.2 Project History

This project, representing the work of many NASA investigators and contractor personnel, was initiated in the early 1970's at the Johnson Space Center during the period prior to the Skylab missions. The overriding goal was to use mathematical simulation as an alternative means of examining physiological systems and maximizing the yield from the multi-discipline, large scale Skylab biomedical program. The first effort began in 1970 with *Contract NAS9-11657, Modeling and Integration of Physiological Control Systems*. The objective of this initial effort was to provide information needed to make both technical and managerial decisions regarding the development or use of algorithms of the primary homeostatic regulatory mechanisms of man, and the integration of these algorithms into a total interactive simulation system. Progress was encouraging enough that *Contract NAS9-12932, Automated System for Integration and Display of Physiological Data*, was initiated to develop working models and to simulate the response to various biomedical experiments and environmental stressors. A major objective of this three year study was the development of a Whole-Body Algorithm that was designed for evaluating hypotheses related to the physiological adaptation to spaceflight. The development of customized prototype software systems for organizing spaceflight data conducting hypothesis testing with the models from remote terminals was a secondary benefit. A biostatistical analysis and display system was accomplished as part of a corollary *Contract NAS9-14192, Skylab Endocrine-Metabolic Experiment Data Analysis. Contract NAS9-14523, Skylab Medical Data Evaluation Program (SMEDEP)*, utilized the basic elements previously developed to complete a computerized integrated data base, analysis and simulation system. A major objective was to use this system to process and analyze the major Skylab biomedical experiments, to develop and test individual physiological subsystem hypotheses, and to integrate these hypotheses into a general understanding of physiological adaptation to weightlessness.

2.2.3 Spaceflight and Weightlessness*

Spaceflight presents a unique stress to man; its physiological effects have only been studied since the early 1960's. The spaceflight environment can be considered as

---

* In this text the terms weightlessness, zero-g and microgravity are used interchangeably. Strictly speaking, objects in low earth orbitg are not weightless but are subjected to very small forces, hence the term microgravity.

a multiplicity of factors that affect human physiological systems. These factors include weightlessness, ionizing space radiation, noise and vibrations, accelerations, atmospheric composition, temperature and humidity, hygiene and diet, isolation and emotional stress, and circadian rhythm alteration. Although each of these factors doubtless contributes to the overall response, the factor that appears to have the most important effect on man's physiological systems is weightlessness, or zero-g. Zero-g is known to affect a number of physiological systems including cardiovascular, vestibular, fluid and electrolyte balance, and other hormonal and musculoskeletal systems. Many of the changes that occur cannot be fully appreciated until return to the one-g environment.

Gravitational forces have been present in the evolutionary development of every species of land animal and plant. But because of the ubiquity of Earth's gravity it is difficult to study its physiological influence and therefore one cannot adequately predict the effects of the removal of gravity. For this reason, spaceflight offers the opportunity to not only understand the phenomena of gravity unloading but, by analogy, can teach us much about the mechanisms we possess for living in a gravitational environment. In essence, the "stress" of zero-g is the removal of forces to which our bodies are adapted and genetically designed to counteract. Adaptation to the zero-g environment involves disuse or modified use of these structures and mechanisms. The degree of adaptation that occurs during zero-g affects the severity of problems encountered upon return and adaptation to the one-g environment.

2.2.4 Skylab

Skylab was a large, comfortable habitat containing facilities for conducting biomedical studies. These missions provided the longest stays in space for the U.S. space program until the collaboration with the Russians (and the use of their space station, Mir) in the 1990's. The three manned Skylab flights provided the vast majority of spaceflight data upon which this analysis project was based. Although earlier missions (i.e., Mercury, Gemini, Apollo) included medical evaluations and some physiological testing, the data were severely limited due to operational constraints on the scientific investigations and do not approach the significance of the Skylab data. Prior to Skylab the biomedical evaluations of astronauts were restricted mainly to pre- and postflight measurements. Nothing was known about the time course of physiological events in space beyond three weeks. Skylab was the first (and one of the few ever) NASA program whose primary aim was the gathering of a broad spectrum of inflight biomedical data on space travelers. At the time of this writing much of the data collected on Skylab remains unique in both its scope and duration of inflight exposure to microgravity.

The three Skylab missions were flown consecutively starting in May 1973 and completed the following year. The three missions had durations of 28 days, 59 days and 84 days respectively. On each mission there were three astronauts who served both as investigator and subject for the various biomedical experiments. During the preflight and postflight phases the actual principal investigators were in charge of the research procedures. The capabilities of the Skylab spacecraft to conduct biomedical experimentation is fully described elsewhere [1].

2.3 Scope

2.3.1 Skylab Data

There were many scientific questions still unresolved following the Skylab missions [4,9]. The most pressing of these were addressed in the current study. The data from five major physiological areas were placed in the customized automated data base and were examined using a combination of data analysis and computer simulation. These five areas, shown in Table 2-1 include: a) nutrition, metabolism and body composition; b) fluid-electrolyte regulation; c) hematology and erythropoiesis regulation; d) cardiopulmonary function; and e) musculoskeletal function. Table 2-1 identifies the Skylab researchers that served as the subject matter experts in each area, the types of measurements collected, and the issues and questions that were examined by systems analysis. There was a diverse spectrum of issues from a number of disciplines. Thus, an analysis was undertaken of the primary components of weight loss and changes in body composition, the volume and biochemical changes of the fluid compartments, the loss of red cell mass, the cardiovascular responses to exercise and LBNP, and the atrophy of musculoskeletal tissue. Not all of the "issues" listed in Table 2-1 were objectives of the Skylab experiments, but rather became issues once the data was analyzed. For example, regarding the hematology experiments, it was not expected that red cell loss would even occur in Skylab, much less be quite different on different missions. Yet these questions became critical to the present study following analysis of the Skylab results. The analyses for each of the discipline areas will be presented in separate chapters in the order shown in Table 2-1 (left column) starting with Chapter 4.

The experiments shown in Table 2-1 represent a significant portion, but not all, of the investigations that were conducted during Skylab. There were, in addition, experiments in the areas of vestibular function and motion sickness, biostereometrics, sleep monitoring, muscle function, limb occlusion plethysmography, and other minor investigations and clinical data. While these studies were not the primary focus of our analysis, the data that was generated was often very useful to supplement other findings. For example, motion sickness incidences with its associated restriction of fluid and nutrient intake were used to interpret metabolic balances; body volume segments from biostereometrics was important to confirm body weight loss studies; and muscle strength tests verified the time course of body protein loss. Undertaken rather late in this project was an analysis of the musculoskeletal system, with particular emphasis on calcium regulation (Chapter 8). Therefore, the progress summarized for this area is more limited. In addition to data from the Skylab missions, this analysis project used some data from the Apollo-Soyez Test Project flight in 1975 and from several Shuttle flights from the 1980's.

The findings from this project will be discussed in terms of their physiological, rather than their medical significance. Also, the development and evaluation of countermeasures against the deleterious effects of space travel will not be a major focus except for one study designed to relieve orthostatic impairment during reentry (Chapter 7 and 9).

2.3.2 Zero-g Analogs

In addition to data from spaceflight missions, this analysis takes advantage of data from other related ground-based experiments such as bedrest, water immersion or head-down tilt. These so called "zero-g analog" studies are useful because they approximate the reduced gravity (hypogravic) aspect of spaceflight without introducing the other confounding spaceflight factors discussed in Chapter 2.2.3. Also, ground laboratories can provide more direct measurements than data collected during spaceflight. In the era following Skylab, animal studies became an important adjunct to human studies in both ground laboratories and space. The information from these studies in the mouse, rat and primate, showed sufficient promise that a version of one of the "human" models was adapted especially for animal use (Appendix B). The mathematical models are capable of simulating both the ground-based analogs and spaceflight, in animals and humans, and can, therefore, form a bridge between these experimental environmnets since the same physiological systems are involved in all cases and are also represented in the model.

2.4 Systems Analysis

2.4.1 General Concepts

Novel analytical techniques were required in order to develop mechanistic hypotheses to explain the spaceflight experiments and to integrate these hypotheses into an overall theory of spaceflight adaptation. These techniques were needed to assimilate large quantities of data, account for complex physiological processes, and have the capability to quantitatively test hypotheses both singly and in combination. The analytical techniques chosen for these challenging tasks were those using systems analysis concepts.

Systems analysis is a methodology for logically deducing the behavior of complex processes with the goal of satisfying a set of specific objectives irrespective of the scientific field. A *system* can be defined as one or more elements that bear certain functional relationships to each other and can be identified from their surroundings by a real or conceptual boundary. For example, a cardiac cell, the heart, or the entire circulatory network of vessels and heart pump can each be considered systems worthy of study. The systems analysis approach can be described as follows: 1) careful formulation of the problem to be solved and objectives to be accomplished, 2) development of a logical solution to the overall problem by dividing it into smaller, easily handled problems (i.e., subsystems) according to a prescribed plan, often involving quantitative models, 3) using this "road map" for logically relating the subsystem solutions to the solution of the larger problem, and 4) interpretation and evaluation of the analysis re-

sults so that they directly address the stated objective. A key ingredient of a systems approach is the precise identification and rigorous definition of what, all too often, are vague concepts. The intellectual discipline of even formulating a problem using this methodology often requires systematic and logical thinking and generally provides considerable insight into the complex processes involved. This approach can lead to solutions for many seemingly unsolvable problems.

This is normally the approach used for many years to develop man-made or technological systems. Examples of such applications include the design of chemical processing units, electrical circuits, and software systems. In other cases, of which biological processes are a good example, the system already exists, and the goal is to break the system into smaller units and examine them in a manner that enables one to understand the behavior of the larger system. Physiologists studying the human body must deduce from observation and experimentation, the features and functions of the various anatomical subsystems, including the relationships between these subsystem elements. Systems concepts have only recently (since the 1960's) been applied to studying biological function [10,11,12].

One immediate problem that faces the systems analyst is the level of detail required. For the human body, various levels of organization exist which can form the basis for the modeling of human physiology as shown in Fig. 2-1. Thus, functional areas of physiology are categorized by the "organ systems" such as nervous system, cardiovascular system, etc. Each organ system can, in turn, be built up by a "structural hierarchy" which ranges from subcellular entities to whole organ modules (i.e., *vertical integration*). Also, an organ system may be considered by itself or in combination with one or more other organ systems (i.e., *horizontal integration*). The level of detail is dictated entirely by the models objectives. It is the job of the systems analyst to determine the level of detail necessary to represent the phenomenon of interest in his problem. For example, one circulatory model that was used in this project was designed to simulate blood pressure changes over hours or days, while another was designed for beat-to-beat heart changes and to exhibit pulsatile flow. A guideline of systems analysis is to focus on the grossest level of detail necessary to satisfy the area of interest. Another way of saying this is that models should be designed as simply as possible at each stage of their development. In summary, the physiological systems analyst has to identify the elements of interest and the level of detail necessary to address the particular problem. Conversely, in any systems analysis, it would not be expected that every level of detail would be represented or considered. In the current project, the main emphasis of the systems analysis was on the higher (less detailed) levels describing overall organ systems, with particular interest on addressing the integration of multiple organ systems.

2.4.2 Simulation Models

An essential step in the systems approach is the creation of a facsimile or model to represent both known and
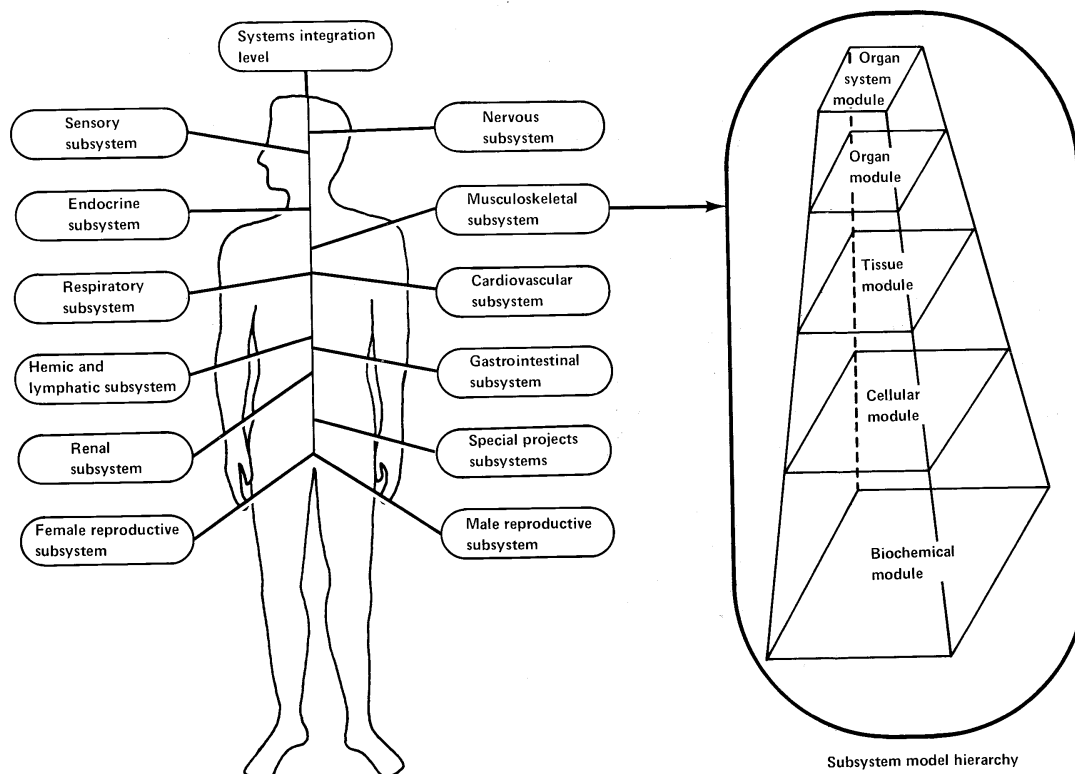
Figure 2-1. Various approaches to modeling human physiology. Left side indicates horizontal integration of organ systems. Right side indicates vertical integration within an organ system.

postulated features of the system. The model is usually in a form that is different and usually less complex than the real-world object being studied. This may include three dimensional physical models or abstract models. The human body is so complex that all who study it must utilize models of some type to relate and interpret the vast amount of experimental data. Modeling of human body functions is a relatively new area of scientific endeavor. Until the middle of the 20th century, models of physiological function have been mostly qualitative with many being entirely verbal and schematic. The quantitative or mathematical model for simulating the behavior of complex physiological systems did not gain importance as an investigative tool until the development of large scale computer systems and the advances in control engineering and integrative physiology [13].

Mathematical modeling is one manifestation of the systems approach to problem solving and has become a very powerful tool for understanding and analyzing complex system operations and interactions. The human body systems are certainly complex, and modeling in the life sciences becomes a way of communicating, a way of testing hypotheses, and a way of designing experiments.

The major body systems that are of concern in this project, including the cardiovascular system, respiratory system, thermoregulatory system, renal regulatory system and the fluid-balance system, all have a similar basic fea-

ture of control. They are characterized by an active controlling system that regulates a relatively passive controlled system, and taken together, these two major components function as a *negative feedback control system*. In physiological systems, control is an inherent feature and is most often exerted to maintain homeostasis of the internal environment of the body. This concept of the stability of the milieu intérieur is perhaps the best known biological generalization attributed to the great physiologist Claude Bernard [14]. Examples of quantities that are thought to be under homeostatic control include, the arterial blood pressure, the partial pressure of oxygen in the blood, the heart rate, core temperature, and electrolyte concentrations in the blood. The body detects these quantities using sensors such as baroreceptors, chemoreceptors, oxygen sensors, temperature sensors and osmoreceptors. Using the control features, the system continuously attempts to restore stress conditions to normal.

Modelers tend to be enthusiastic about their models and researchers who do not use mathematical models tend to be skeptical or outright critics. As in any branch of science objectivity is important. The researchers in this project understood the advantages and disadvantages of modeling, but may have been biased to the extent that they thought the former outweighed the latter. It was gratifying that during the research phase of this project, a prestigious physiology publication was born that attempted

Table 2-1. Biomedical Areas of Investigation on Skylab Studied with Systems Analysis

Physiological Area/(Book Chapter)	Investigators, Measurements and Issues
• **Nutrition, Metabolism and Body Composition** (Chapter 4)	**Investigators**: Drs. P.C. Rambaut, C.S. Leach, M. Whittle, and J. Waligora **Measurements:** The most extensive metabolic and energy balance studies ever made in space of water, nutrients and minerals in diet, urine and feces. Supplementary measurements were made to quantify bone, protein and body mass and volume losses. **Issues:** • Why do astronauts lose body mass in space? • Can differences in body mass loss be attributed to diet and exercise? • What are the components of weight loss and what is their time course? • What are the energetic costs of living in space?
• **Fluid-Electrolyte Regulation** (Chapter 5)	**Investigators:** Drs. C.S. Leach, P.C. Johnson, P.C. Rambaut **Measurements:** Extensive measurements of fluid volumes in plasma, extracellular and body water compartments. Blood and urine biochemistries, including electrolytes and hormones (related to fluid regulation and stress). **Issues:** • What changes in fluid-electrolyte status occur during long-term spaceflight? • What is the role of fluid regulatory mechanisms (renal, endocrine, circulatory, neural) in adaptation to spaceflight? • What changes in the internal distribution of body fluids occur in space? • Is there an early spaceflight dieresis as predicted by many researchers?
• **Hematology and Erytheopoiesis Regulation** (Chapter 6)	**Investigators:** Drs. S. F. Kimzey, C.D.R. Dunn, and P.C. Johnson **Measurements:** Measurements of various indices related to the regulation of the circulating red cell mass, blood volume and hemoglobin. **Issues:** • Why do astronauts lose red cells during spaceflight? • Why is there a two-fold difference in the degree of red cell loss on two separate Skylab missions?
• **Cardiopulmonary Function** (Chapter 7)	**Investigators:** Drs. J.A. Rummel, C. Sawin, and M. Buderer **Measurements:** Measurement of indices of cardiopulmonary status (blood pressure, heart rate, oxygen uptake) at rest and during exercise. Orthostatic intolerance studied inflight and at recovery using lower body negative pressure. **Issues:** • What is the etiology of the loss of blood volume in space and how does the circulatory system adapt? • What other mechanisms regulate circulatory changes in spaceflight? • What changes in exercise performance occur during and following long-term spaceflight? Do increasing periods of personal exercise in space improve the metabolic response to stress tests? • What causes cardiovascular deconditioning and the decrease in orthostatic intolerance seen in astronauts? What is its time course?
• **Musculoskeletal Function** (Chapters 4 and 8)	**Investigators:** Drs. P.C. Rambaut, C.S. Leach, J.A. Rummel **Measurements:** Measurements of blood and urine biochemical markers of muscle and bone loss. Metabolic balance studies of calcium, magnesium, potassium and nitrogen. Supplementary measurements of bone density, muscle strength and total body potassium. **Issues:** • What is the extent and time course of muscle and bone loss during 3 months in space? Do the losses eventually abate? • What regulatory mechanisms are involved? • How are the losses influenced by diet and exercise?

to exemplify the best in life science modeling and set standards in the field [15]. The following sections attempt to introduce the reader to a discussion of advantages and disadvantages of modeling.

2.4.3 Advantages of a Modeling System

In science, mathematical models are built and studied for several reasons. A model is a framework on which all known observations or hypothesized workings of a physiological system along with appropriate real-world data can be integrated. The construction of a model which is composed of separate elements generally provides new insight into the organization of the system elements, the processes within the elements, and the multiple pathways connecting these elements. Any useful model should be able to account for known behavior of the most important variables under consideration. A model built up of component parts allows one to readily isolate each component and its parameters to determine it relative influence on overall system behavior. Simulation enables an investigator to understand how a biological system works through variation of the system's parameters. During simulation, dynamic interaction between various subsystems of the model becomes more apparent. Otherwise regularities and patterns of behavior can be hidden from view simply because one does not know what to look for. By clarifying what to look for, a model may predict both correlations and cause-and-effect relations that are subject to actual verification in the real system.

In contrast to a statistical model or a "black box" model, a deterministic model is based on known physiological processes and feedback pathways. As such, this type of model can predict (not merely extrapolate) beyond the data from which it was generated under a wide range of environmental and metabolic conditions. A biological model will offer some heuristic value and extend the knowledge of the system under study by predicting responses of difficult to measure quantities, by resolving paradoxical behavior, by demonstrating the alterations in the system necessary to produce an observed response, and by design of crucial experiments.

Model building leads almost immediately to the identification of gaps in the experimental knowledge of the system of interest and often suggests the type of experiment needed to obtain missing information. When experimental evidence is conflicting, difficult to interpret or difficult to obtain, it is possible to test the plausibility of a hypothesis by using an appropriate model. By reducing the hypothesis to unambiguous mathematical expression and incorporating it into a model, the consequent changes in the system's behavior often suggests the more significant of alternate hypotheses. By using the model to determine those conditions under which competing hypotheses predict the most divergent results, it is possible to design decisive experiments. These uses of mathematical models provides a new way to look at physiological systems and adds another dimension to experimental physiology.

While it may seem desirable to obtain a successful prediction from a model (i.e., in comparison with real-world data), paradoxically, the most useful results are obtained when the simulation does *not* match observed findings. Analysis of the differences involved can then lead to a modification of the hypotheses that define a portion of the model, or to the need for new and clarifying experiments. Such a practice is generally iterative, being applied over and over again with new stresses designed to force the model to display more and more of its weaknesses. Reconstruction of the model by modification of its hypotheses leads to a stronger model. As the model behavior moves closer to the behavior of the real system through iterative modification of the hypotheses, the probe of science sinks ever deeper into the subject. In fact, this iterative use of models is only a restricted form of the general scientific method. Perhaps the real power of models is not in simply making predictions but in forcing us to think clearly about a problem and its ability to raise the critical questions. Modelers are forced to ask questions in order to understand why a model behaves as it does or why it doesn't behave as we think it should. These critical questions then point the way for further experimentation. Thus, models can lead us not necessarily to the right answers, but to the right questions. There are many examples in this book of this approach in the study of the physiological problems of weightlessness.

Another paradoxical advantage of modeling is that even a relatively simple model or one that is not extremely accurate can provide useful insights. Without a quantitative method of keeping track of different biophysical processes, such as a simulation model, it is impossible to intuitively visualize the dynamic behavior of a system that has short and long time constants, multiple stimuli, interconnecting and redundant pathways, or special effects like time delays, hysteresis and receptor adaptation. Models offer a way of sorting through this complexity. Special modeling techniques are available that allows the researcher to learn much about the behavior of a system that incorporates these features without the need for comparing the theoretical results to real-life data.

In summary, modeling and simulation are useful as a means for providing:
1. A systematic and effective way of assembling existing knowledge about a system,
2. A means for identifying important parameters and to determine the overall system sensitivity to variation in each parameter,
3. Methods for calculating quantitative values of variables that are difficult or impossible to measure,
4. A method to test hypotheses, either individually or in combination, rapidly, efficiently, and inexpensively,
5. Identification of specific elements or information gaps that must be further quantified, thus leading to the suggestions for new experiments.
6. An effective method for predicting the behavior of a real system,
7. A quantitative technique to assist in designing and interpreting biological experiments, and
8. A valuable means of communicating both concepts and detailed function of a system.

2.4.4 Limitations and Considerations in the Design and Use of Models

There are certain limitations of modeling and simulation that should be understood. No model is ever a perfect fit to reality, and the difference between the model and the real system should always be kept in mind. In spite of the fact that models are quantitative and model results may show decimal significance, the response of a model should not be considered more than a prediction subject to verification. Care must be taken in the use of models in order to preclude extrapolating an element of a model beyond the region for which the model element was designed. Therefore, the application of a model should be preceded by an understanding of the simplifying assumptions on which it is based.

The importance of designing a model to meet specific objectives was discussed above but cannot be overemphasized. The fact that most successful models have a fairly narrow set of objectives is sometimes, and erroneously, thought to be a serious deficiency of modeling. However, a biological model is a simplification of the underlying processes; it is not designed to reproduce all or even most aspects of the human body, but rather only a *specific* aspect of the real system. The discussion of Fig. 2-1 illustrated the various levels of model objectives. The best approach is to design a model to meet the desired objective and accept the limitations that naturally follow.

The requirement for good experimental data in the modeling process creates its own problems and limitations. The success of a model will be a function of the degree to which data from the real system can be gathered. Data is used in the construction of the model and the setting of parameter values. Data different from this "construction" data is used to compare with the simulation responses. In many cases it will be found that a model will exhibit a good fit with the results of one experiment only to find that the model's validity is challenged by the results of another. A model must be permitted to evolve as conditions change or as additional data becomes available. Data that is in conflict with the model should never be rejected if it is known to be reliable, rather it should be used to refute, modify, or improve the model. While it is always desirable for the response of a model to correspond closely with a particular set of experimental data, it is even more important to use the model to understand the basic behavior of a system. Using this guideline will assure that the model remains an integral part of the scientific process and does not become a process serving only itself.

There were often major problems in the course of the present study in locating the proper type of data needed for model comparison. Most of the models that were used were capable of simulating dynamic (i.e., non-steady state) responses. However, it was very common in the 1970's, when these studies were conducted, for researchers to collect data only at the beginning and endpoint of their study, rather than make continuous measurements. Models are capable of deriving much more information from a series of measurements when the system is responding or recovering from a highly dynamic stress compared to measure-ments made at steady-state [10]. In a similar vein, because data from spaceflight and bedrest were often collected not more than once a day, and not at the very start of the study, it was not possible to validate the model's capabilities to predict acute changes that occurred during the first few hours after initiation of these hypogravic stresses. In some cases, this led to the use of published ground-based studies to uncover appropriate data; in a few cases it was possible to recommend new data collection protocols to researchers or to develop novel data analysis techniques for deriving the type of data needed from data already collected. But in most cases the model responses were simply offered as predictions awaiting future experimental verification.

Another class of model limitations and design considerations concerns certain mathematical and computer issues. The human system is notoriously nonlinear and the biological modeler is bound to encounter nonlinearities and higher order control systems. The mathematics and numerical solutions of these systems are very difficult, even with the aid of the large high-speed computers available at the time. For this reason, it was necessary when developing models, to simplify as much as possible, to linearize wherever possible, and to limit the scope of the model as much as is acceptable. Special simulation algorithms for computations involving integration step sizes and the use of fast and slow controllers for the same function were developed for this purpose. Simplicity, linearity, and efficiency of operation are worth striving for in model design when they can be accomplished without compromising the basic purpose of the model.

In formulating the individual equations that compose a model, one often creates the simplifying assumptions that make the problem solvable. These typically include lumping compartments and parameters, linearizing otherwise non-linear processes, assuming perfectly mixed compartments, and transforming a system variable into a fixed parameter. Assumptions such as these should be supported by some type of experimental evidence. It may seem that models constructed with these assumptions may bear little relevance to the real system being modeled, but it has been shown that such models can provide useful information that cannot be easily obtained by other methods.

Finally, it should be mentioned that the application of mathematical simulation models to physiology and medicine was not generally accepted as a research tool in the 1970's, even within the ranks of NASA scientists. Not all physiologists have the mathematician's training to critically evaluate the mathematical description given in a model, and they are understandably often skeptical. The simplifying assumptions, described above, do not always receive general acceptance, nor does the building of "black box" transfer functions that often are found in math models. The team approach of systems analysts and modelers on one hand, and the principal investigators and researchers on the other hand was crucial to the success of this project. Modelers contributed their special systems analysis approach including models and data analysis techniques while researchers provided the data, their

understanding of the biology, and hypotheses that could be tested in the models.

2.4.5 Models Considered for Spaceflight Simulation

As the data related to each disciplinary area was examined, the mathematical models were valuable for searching for underlying mechanisms. It was therefore important to utilize models of different organ systems to generally correspond to the different investigative areas of flight research. The following physiological subsystems were identified as being critical for meeting the simulation requirements of the biomedical spaceflight research program and for subsequent inclusion in an integrated whole-body model: cardiovascular, respiratory, thermoregulatory, renal, endocrine, body fluids, autonomic controls and erythropoietic. Candidate biological models were identified and evaluated for their ability to simulate various aspects of the spaceflight physiological testing protocols. This included identifying, developing, or modifying input/output transfer functions, assumptions, verification and validation concepts, limitations, success criteria, and missing model elements. Modifications were necessary in most of the models that currently existed in order to satisfy the research requirements. In several cases, existing models were not available and they were developed under this project. Their utility was greatly increased in all cases by programming them for interactive use on remote terminals with graphical display capabilities – a feature quite uncommon at the time. This initial study provided a basic framework for evaluating models, defining objectives and developing software requirements for models and database management systems.

During the development of a program to study man's physiological adaptation to weightlessness, it became obvious that a large-scale human simulation system would be a valuable asset to such an undertaking. Therefore, a major objective of the study was to develop a Whole-Body Algorithm that would be useful for evaluating hypotheses related to the physiological adaptation to spaceflight. Although the physiologic interaction of major body subsystems had been a subject of interest to researchers for some time, the use of interacting models in concert to study this phenomenon had received little attention. These studies were also limited by the availability of computational equipment and software capable of handling models of the required magnitude and scope (a constraint that no longer exists). By "whole-body", it is meant that the model will include significant aspects of several of the major body regulatory systems including the cardiovascular, respiratory, renal, erythropoietic, endocrine, and thermoregulatory systems. Independently operating subsystem simulations have important applications, but, as such, important interactions between subsystems are lost. The full power of the scientific approach is only utilized when respiratory, cardiovascular, thermoregulatory, renal regulatory system and fluid balance influences are fully accommodated in a dynamic sense. Thus, a disturbance in one subsystem could reveal its influence on other subsystems. Also, the effects of spaceflight are presumably not confined

to any one of these individual subsystems and so the Whole-Body Algorithm would permit evaluation of an integrated total body response.

In addition, the Whole-Body Algorithm would be capable of responding to both long and short-term stresses of various kinds. Perturbations of interest are exercise, chemical imbalances, gravitational changes (i.e., postural change, bedrest, weightlessness), internal fluid disturbances (i.e., LBNP, water immersion), other abnormal environmental conditions (i.e., hypoxia, hypercapnia, ambient temperature excursions), and simple dietary changes of fluids and electrolytes. It was envisioned that such a model would be capable of simulating the integrated physiological response to a "typical" Skylab mission, as shown in Fig. 2-2. This scenario included the entire sequence of major physiological events for long-duration spaceflight consisting of gravitational and environmental disturbances and physiological tests such as exercise and LBNP. With all these models, multiple stresses and sequential stresses of varying degrees can be applied, just as in an actual experimental protocol. For example, a simulation might attempt to show that LBNP tests at regular intervals might exhibit different results as the body adapts to the zero-g environment in a long-term mission, as was observed in Skylab.

Other uses of this technology in medicine and physiology can be realized when subsystem models are joined together to simulate the interaction between major body systems. For example, simulation could be used for real-time monitoring of patients, providing extrapolation of clinical trends in important parameters, identifying the critical parameters in a system and the level of accuracy needed in their measurement, aiding in diagnosis, and indicating patient response to simulated therapy.

In summary, the following mathematical models have been developed and modified for six physiological subsystems and further integrated into a combined model:
1. A pulsatile model of the cardiovascular system
2. A model of the thermoregulatory system
3. A model of respiratory control
4. A model of the circulatory regulation and fluid-electrolyte balance
5. A model of erythropoiesis control
6. A model of calcium and bone regulation.
7. A Whole-Body Algorithm capable of simulating dynamic subsystem interactions for short term experimental stresses and long term adaptation.

The first three models were designed to simulate short-term stress responses (shown in Fig. 2-3) while the next three models were capable of long-term stress responses (shown in Fig. 2-4). The general scheme for incorporating these models (except for the calcium regulatory model) in a Whole-Body Algorithm is illustrated in Fig. 2-5. All these models can be characterized as being deterministic, nonlinear, and continuous, using finite difference formulations. The models themselves are described in detail in Chapter 3 and Appendices. An example of an entire model development, including the physiological overview, the de-
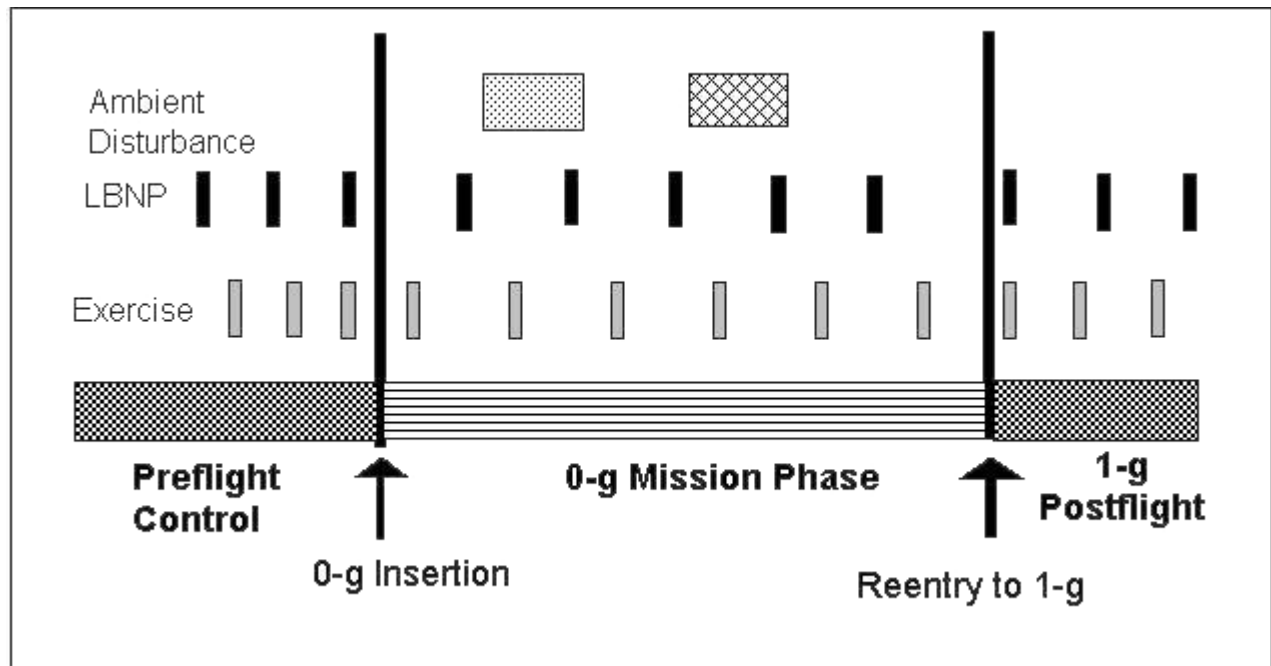
Figure 2-2. A hypothetical spaceflight sequence of events that the Whole-Body Algorithm was designed to simulate. Typical events include changes in gravity including acute and long term adaptation, environmental disturbances such as temperature or carbon dioxide excursions, and periodic physiological tests such as exercise and lower body negative pressure (LBNP).
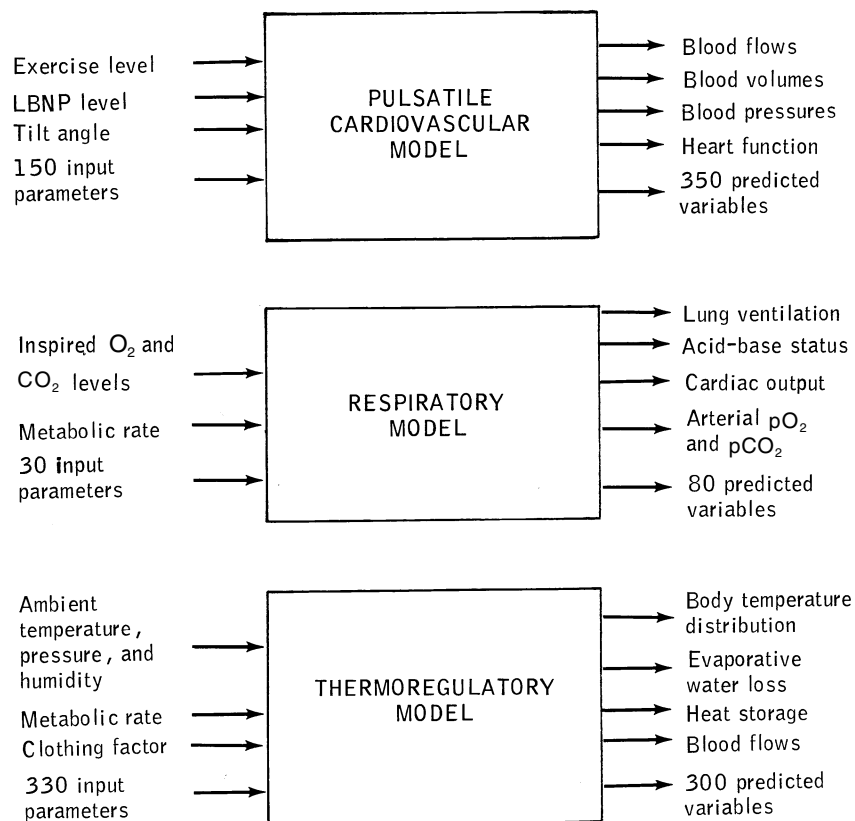
Figure 2-3. Three models use for simulating short-term physiological responses. The numbers of input parameters and output variables indicate the relative complexity of the models. (Key: pO_2 and pCO_2, partial pressures of oxygen and carbon dioxide, respectively).
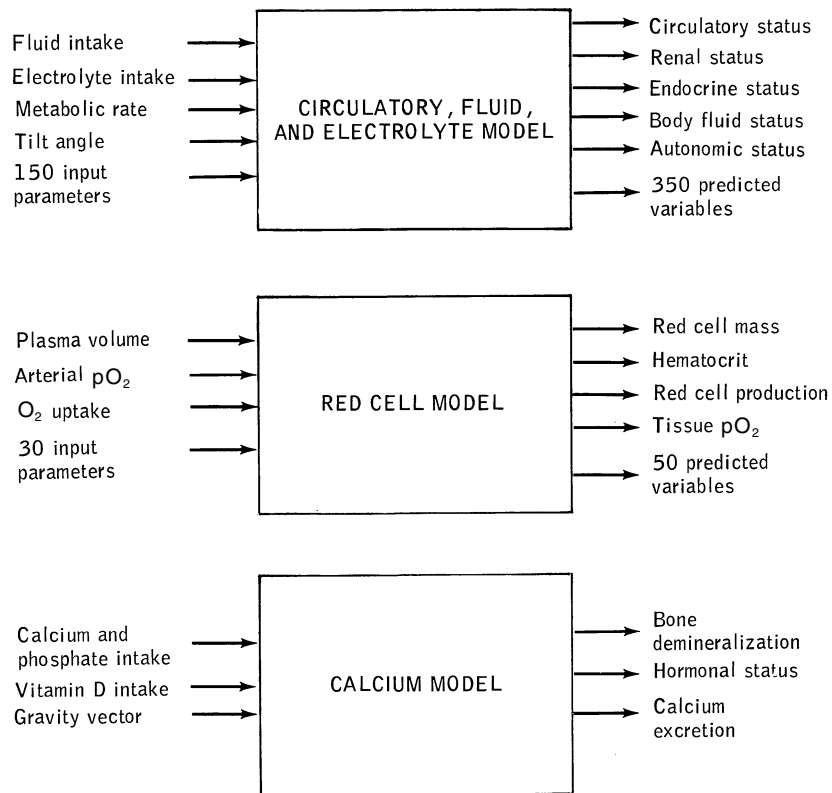
Figure 2-4. Three models used for simulating long-term physiological responses. See caption for Fig. 2-3.
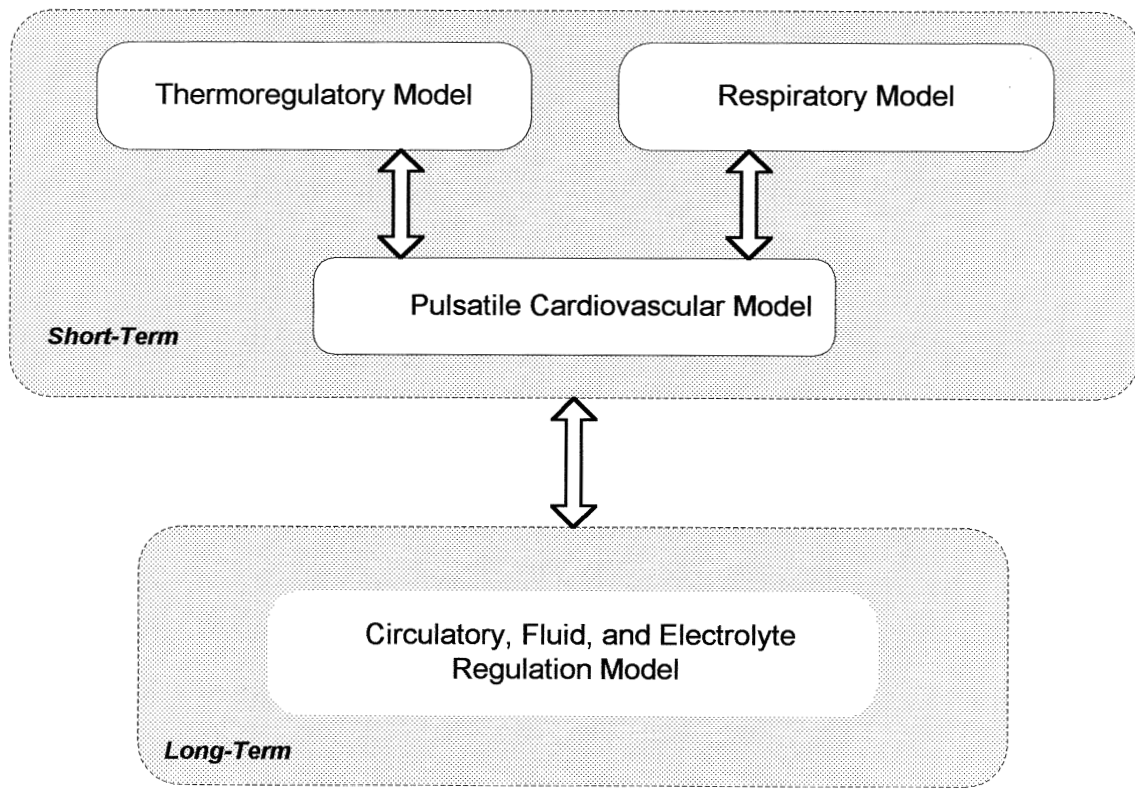
Figure 2-5. Schema of the Whole-Body Algorithm showing the mode of connection between short-term and long-term subsystem models.

tailed equations and the validation simulations are provided for the model of erythropoiesis regulation, a small but very useful model (see Appendix B). Applications for using these models to solve problems in spaceflight physiology are presented in Chapters 5 to 9.

2.5 Approach to Hypothesis Testing

The systems analysis approach used in formulating a deeper understanding of the physiology of weightlessness is illustrated in Fig. 2-6. One of the first steps in the process is to describe the acute and long-term changes that occur during weightless spaceflight. The database and analysis system is an essential tool in this process. This system permits large arrays of data to be scanned rapidly, while variables are correlated visually or automatically, and hypotheses are tested for statistical significance. It is necessary to examine both spaceflight and ground-based data to arrive at a complete a picture as possible of hypogravic responses.

Such an evaluation of experimental data can lead, under appropriate conditions, to a qualitative formulation of alternative mechanisms involved in producing the observed responses. The procedure draws heavily upon the theory of physiological feedback regulating systems and often suggests hypotheses capable of being tested in a model. A qualitative description of these pathways, while useful as a starting point, does little to suggest the relative influence of each mechanism. Only by a quantitative evaluation of that system is it possible to discern if the sum total of positive and negative effects, interacting in a manner previously postulated, will indeed lead to the observed response.

Actual testing of the hypotheses using the mathematical models constitutes the next step in this process. Acceptable candidate hypotheses can be reduced to mathematical expressions and inserted into the models, and by performing the appropriate simulations, they can be used to predict the effect of the hypotheses on other subsystems. It is then possible to study the physiological mechanisms in detail that brought about the appropriate response. As the simulation study proceeds, it is possible to incorporate increasingly more diverse kinds of experimental results and hypotheses into a single model. While each hypothesis alone would not support a generalized theory, all of them taken together may converge toward a coherent picture of zero-g adaptation. Examples that illustrate this important process of hypothesis testing will be found in abundance throughout the book.

The simulation models can be considered a collection of integrated theories and empirical relationships against which a large portion of the spaceflight data can be compared, evaluated, and tested for consistencies or discrepancies. Good agreement between model output and experimental data furnishes a certain level of confirmation for the hypothesis under consideration, but does not "prove" that the hypothesis is true. Poor agreement or contradictions between model output and actual data cause one to question the hypothesis under investigation, the structure of the model itself, or the validity of the experimental data. As emphasized previously, such a state of

poor agreement, at least initially, is the more interesting scenario, and becomes the basis for additional data analysis, the design of new experiments, new model refinements, or new hypotheses. Using this approach, the findings of each of the Skylab experiments could be integrated with each other with a goal of formulating an overall hypothesis of spaceflight adaptation.

The modeling system and hypothesis testing approach developed for the spaceflight biomedical program, was built as a research tool that could evolve along with a long term and broad based physiological research program. This is meant to be an iterative process with the researcher as a crucial element in the loop. It offers the capability for developing, modifying, and refining hypotheses as well as aiding the investigator to visualize the dynamic physiological consequences in the response of the total system due to the hypotheses. By suggesting new experiments and aiding in their design, this process becomes an even more powerful research tool. This combination of theoretical simulation analysis (to test hypotheses and identify gaps in knowledge) and acquisition of experimental data (to reveal actual system behavior) has long been recognized as providing the most effective use of mathematical models [10].

Hypothesis testing is a time-honored approach to solving scientific questions. In hypothesis-driven research, the experimental procedures for collecting data and the subsequent statistical analysis are based, largely, on formulating the hypothesis *prior* to the experimental design. In contrast, it is perfectly acceptable to use model simulations to help interpret data by formulating and testing hypotheses *after* the experiment is completed. This is another reason for viewing modeling as a complement to more traditional research activities.

2.6 Critical Questions

As should be evident from the above discussion, the activities discussed in this volume were not meant to be simply an exercise in technological approaches or mathematical modeling, but rather a meaningful (although non-traditional) contribution to space biology. As is true for most research endeavors, this one was driven by hypotheses, themes, and critical questions. The central overriding hypothesis and theme is dependent upon the systems analysis approach, specifically,

Central hypothesis: A systems analysis approach, including the use of mathematical models of physiological systems, can assist in resolving current issues in space biology and provide a better understanding of the physiological adaptation to spaceflight.

The physiological issues themselves are directly addressed by posing several broad non-trivial critical questions. The answers to these questions, while not dependent on systems analysis, might benefit from the insights of such a quantitative approach. One should read these questions in the context of the time period in which they were
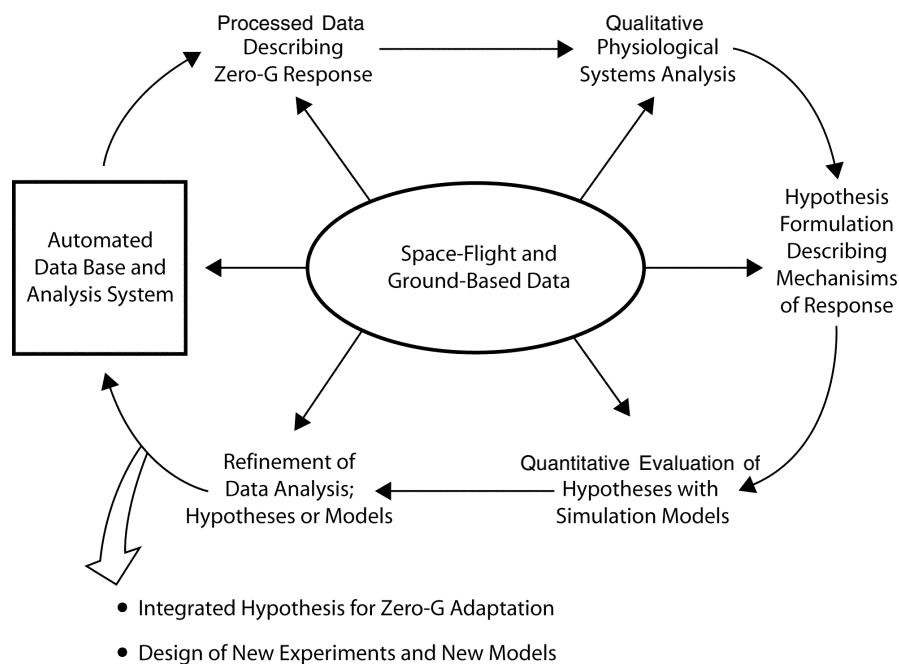
Figure 2-6. Schematic illustrating the systems analysis approach to hypothesis testing in the space life sciences.

posed – approximately 10 years after the first manned flight and with much uncertainty regarding fundamental effects of gravity on the human body.

a) Can the physiological changes observed in humans during space travel be attributed to normal and predictable consequences of known physiological mechanisms and adaptation processes or are they pathological in nature?

b) Are there underlying phenomena common to all the physiological events observed in space, the identification of which would help explain most of the observed findings?

c) What is the common thread between the physiological response to spaceflight and that found during one-g analogs such as water immersion, bedrest and head-down tilt? In what significant ways do they differ?

d) Can the differences between the Skylab missions (i.e., exercise levels) caloric intake, motion sickness incidence, ambient oxygen content, help explain the differences in the responses among the nine crewmembers?

e) Is there a generalized response to spaceflight and other hypogravic maneuvers? Can a unified theory of physiological adaptation to weightlessness be formulated that explains the most significant findings, and if so, what are its most characteristic features?

2.7 Structure of Book

The themes and critical questions discussed above will be addressed in the remainder of the book which may be conveniently divided into four categories:

Systems Analysis Approach

Chapter 3 is a presentation of the systems analysis tools that were developed and used in this project, including the data analysis systems and mathematical models. *Appendix A* is a summary of the fundamentals of modeling and simulation methodology for the unfamiliar reader.

Appendices B, C and D contains supplementary details of the model of erythropoiesis regulation, the Guyton model of circulatory control, and the Whole-Body Algorithm, respectively.

Appendix E is an illustration of sensitivity analysis using the thermoregulatory model.

Subsystem Hypothesis Development

This grouping of chapters focuses on the application of mathematical modeling for the development and testing of hypotheses in four discipline (or subsystem) areas:

Chapter 5, Fluid-Electrolyte Regulation features studies with the Circulatory, Fluid and Electrolyte model of Guyton.

Chapter 6, Erythropoiesis Regulation features studies with the Erythropoiesis Regulatory model.

Chapter 7, Cardiovascular Regulatory features studies with the pulsatile Cardiovascular Regulation model.

Chapter 8, Calcium Regulation features studies with a Calcium Regulatory model.

Integrated Analysis

The two chapters in this "section" emphasize integration of topics in two different types of areas:

Chapter 4, Integrated Metabolic Analysis describes a data analysis, rather than a simulation modeling, activity. It extends the analysis of the valuable metabolic data collected on Skylab (water, electrolytes, protein, and fat) beyond that intended by the Skylab researchers. Several simple but novel approaches for metabolic balances were developed. An integrated approach for computing balances of water, sodium, potassium, evaporative water loss, nitrogen, and calories is contained in this single chapter. The results of this chapter were useful in many of the modeling studies and therefore, they are placed in a chapter which precedes the chapters on Subsystem Hypothesis Development. *Appendix F* contains supplementary information for these analyses.

Chapter 9, Integrated Systems Analysis attempts to integrate the concepts and hypotheses developed in preceding chapters by applying them to major simulation studies of various hypogravic situations. Here you will find simulations of postural changes including orthostasis and head-down tilt, supine bedrest, head-down bedrest and water immersion. The validation study of the Whole-Body Algorithm is also included. Most of the other simulations utilize a modified Guyton model.

Conclusions

Chapter 10, Discussion and Conclusions summarizes the most significant aspects of the project focusing on the two major aspects of this work: a) the advantages and limitations of the systems analysis approach and b) the conclusions reached regarding physiological adaptation to microgravity.

Chapter 11, Future Activities describes possibilities for applications of systems analysis and modeling that are beyond the scope of the current volume, but which were addressed in some fashion during the project. Ideas for new models including an advanced whole-body model are included, as well as applications in countermeasure development, support for flight experiment design, crew health and performance, science management, and teaching models.

Appendix G, Accomplishments and Recommendations succinctly lists the accomplishments of the current project in one place and specific recommendations for model improvements and the research that can provide answers to issues raised in the analysis.

References

1. Johnston, R. S. and L. F. Dietlein, (Eds.), *Biomedical Results from Skylab*, National Aeronautics and Space Administration, NASA SP-377, Washington, D.C., 1977.

2. *Physiology in the Space Environment*, Vol. I, Circulation, Peterson, L.H. (Conf. Chair), National Academy of Sciences, National Research Council, NAS-NRC Publication 1485A, Washington, D.C., 1968.

3. Deitlein, L. F., in *The Proceedings of the Skylab Life Sciences Symposium*, TM X58154, Johnson Space Center, Houston, TX, 1974.

4. Berry, C. A., The medical legacy of Skylab as of May 9, 1974: The Manned Skylab Missions, *Aviation, Space and Environmental Med.*, 47: 418–424, 1976.

5. Verigo, V. V., *Methods of Systems Analysis in Space Biology and Medicine*, Nauka, Moscow, 1987, p. 216 (NASA Technical Translation, NASA TT-20291, NASA, Washington, DC, 1988).

6. White, R. J., Leonard, J. I., Rummel, J. A., and Leach, C. S., A Systems Approach to the Physiology of Weightlessness, *J. Med. Systems*, 6: 343–358, 1982.

7. Leonard, J. I., Understanding Metabolic Alterations in Space Flight Using Quantitative Models: Fluid and Energy Balance, *Acta Astronautica* 13: 441–457, 1986.

8. Srinivasan R. S., Leonard J. I., White R. J., Mathematical Modeling of Physiological States, in *Space Physiology and Medicine*, A. E. Nicogossian, S. R. Mohler, O. G. Gazenco, and A. I. Grigoriev, (Eds.) American Institute of Aeronautics and Astronautics, Reston, VA, and Moscow, Russia, Nauka Press, 1996, vol III, Chapter 26, p. 559–594.

9. Dietlein, L. F., Skylab: A Beginning, Biomedical Results from Skylab, R. S. Johnston and L. F. Dietlein, (Eds.), NASA SP-377, 1977, pp. 408-418.

10. Riggs, D. S.,*Control Theory and Physiological Feedback Mechanisms*, Williams and Wilkins Co., Baltimore, MD, 1970.

11. H. T. Milhorn, Jr., *The Application of Control Theory to Physiological Systems*, W. B. Saunders Co., Philadelphia, PA, 1966.

12. Jones, R. W., *Principles of Biological Regulation: An Introduction to Feedback Systems*, Academic Press, New York, NY, 1973.

13. Defares, J. G., Sneddon, K. N., and Wise, M. E., An Introduction to the Mathematics of Medicine and Biology (2nd ed.), in *Year Book,* Medical Publishers, Inc., Chicago, 1973.

14. Bernard, C., *An Introduction to the Study of Experimental Medicine*, Forward by I. Bernard Cohen, Dover, New York, 1957 (Original publication in French, 1865).

15. Yates, F. E., Good Manners in Good Modeling: Mathematical Models and Computer Simulations of Physiological Systems, (editorial), *Amer. J. Physiol:Regulatory, Integrative, and Comparative Physiol.*, 3: R159–160, 1978.

Chapter 3
A Systems Approach for Understanding Spaceflight Physiology

The Skylab missions provided an opportunity to study the effects of spaceflight on man by enabling the collection of experimental data from several individuals over extended periods. Because such data describing human performance and adaptation was vast in quantity and wide in scope, a systems analysis approach was taken to analyze the data and to develop hypotheses relating to the nature of the physiological events underlying the data.

This approach is illustrated in Fig. 3-1. A unique aspect of this approach is the blending of two separate teams of researchers: an interdisciplinary team of NASA biomedical investigators and a systems analysis team. The NASA team consisted of principal investigators for some of the most important Skylab biomedical experiments in the areas of cardiovascular, musculoskeletal, fluid-endocrine regulation, and hematology. The systems analysis team (from General Electric Co., Space Systems Division) were experts in bioengineering, computer systems, systems analysis and mathematical modeling; they provided analytical tools for interpreting and integrating the spaceflight related data such as simulation models of physiological systems and automated data analysis packages. An hypothesis development and testing approach was used for data interpretation which is described below and at the end of this chapter, the purpose of which was to formulate an integrated hypothesis for human adaptation to the microgravity of spaceflight. It was envisioned that if such an overall hypothesis could be developed and incorporated in simulation models, it would be possible to predict responses that were not previously measurable, design experiments that would test these predictions, and eventually develop a system for real-time physiological monitoring of spaceflight crews.

Figure 3-2 illustrates the typical kinds of interactions that occurred between the principal scientific investigators and the members of the systems analysis team. To begin with, the data are subjected to preliminary analysis and tentative hypotheses are advanced which might explain the observed data. Then, using detailed mathematical models of the systems involved, these hypotheses are tested by comparing the model output for the stress being considered with the experimentally observed responses for the same stress. These comparisons lead to additional and more sophisticated data analysis, to refinements of the mathematical models, to changes in the hypotheses being considered or even suggest the design of new experiments to be performed either in space or on Earth. Given the new data, the modified model, or the changed hypotheses, the entire process is repeated until satisfaction is obtained. This iterative process is the heart of the systems analysis method, because it enables the scientific investigator to visualize the suite of dynamic changes and consequences that accompany certain hypotheses (given the state of the model) and to change either the model or the hypotheses (or both) if the model output does not agree with the experimental data or if an hypothesis proves to have implausible consequences. In this manner, knowledge of the systems in question can be built up in a logical manner.

The following sections contain discussions of the main elements of this approach and the manner in which they were applied to the overall project. These elements include a data base and analysis system, simulation models, and hypothesis testing procedures.

3.1 The Data Base and Analysis System

The Skylab medical experiments yielded data describing many aspects of man's reaction to spaceflight. Inflight experiments were conducted and measurements were made to gather data regarding such investigative areas as circulatory function, biochemistry, body fluids, nutrition, hematology, and body composition. In addition to data collected during flight, additional data were collected through ground-based measurements; some of the nonflight data were used as control data. The data also included extensive clinical and environmental factors (i.e., environmental parameters, medical signs and symptoms, drug usage, and personal exercise) useful for evaluating unusual trends in the experimental observations. The contents of the clinical and environmental data sets have been documented [1], and includes the most significant daily changes in physiological function.

To enable effective use of this information, it was organized into an integrated data system that could be used by scientists and engineers. This database and analysis system, called the Skylab Integrated Medical Data Analysis System (SIMDAS)*, was connected to a high-speed, time-sharing computing system at the Johnson Space Center. Although the number of components integrated into SIMDAS was large, they can be conveniently divided into three main categories: (1) a data base containing all the necessary spaceflight medical data, (2) an automated data analysis system including statistical analysis programs and various special-purpose analysis programs, and (3) computer simulation models of the major physiological systems. The total interactive capability of this system is suggested in Fig. 3-3. The quantity of data contained in SIMDAS is quite large; information for approximately 900 man-days of spaceflight study is provided by 80,000 measurement values representing 860 independent parameters.

*https://ntrs.nasa.gov/archive/nasa/casi.ntrs.nasa.gov/19790017569.pdf
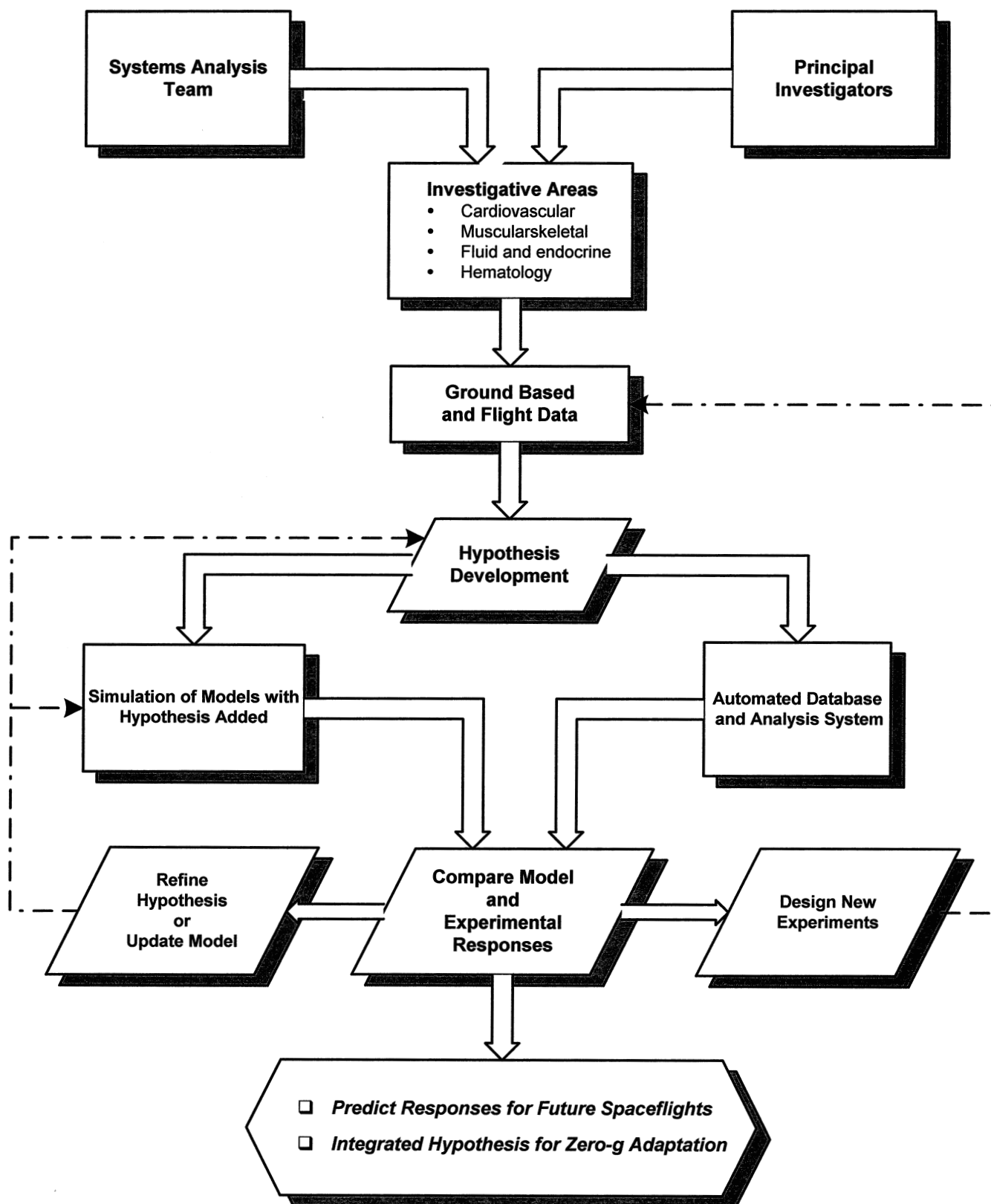
Figure 3-1. Technical approach for Skylab data integration.
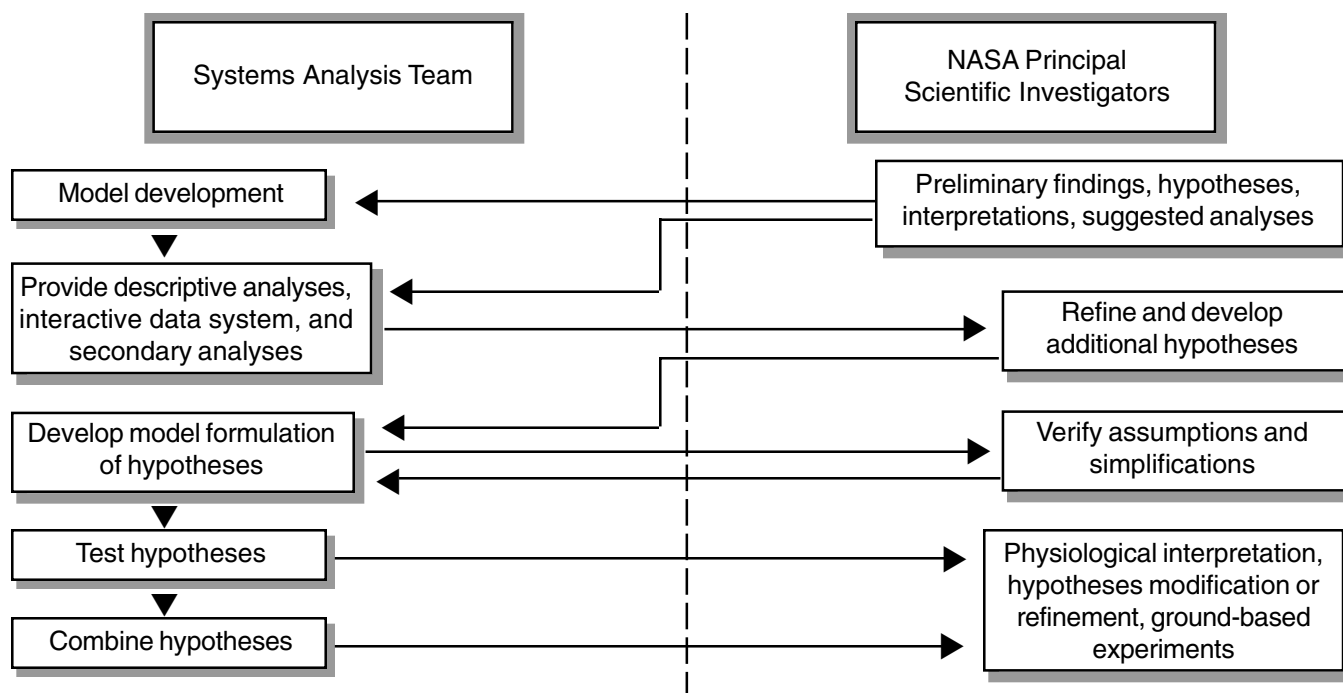
Figure 3-2. Interdisciplinary team concept for testing hypotheses.

3.1.1 Data Analysis System

The data analysis capabilities of SIMDAS helped reveal subtle as well as striking changes in the physiological status of the crewmen at any time during the preflight, inflight, and postflight phases of the missions. The programs included in SIMDAS can retrieve each set of data (all values of a given parameter measured during a specified period) and can generate routine statistical information such as maximum and minimum values, arithmetic means, standard deviation, and 95% confidence intervals (see Fig. 3-4). To assist in hypothesis development and testing, a set of regression functions was also included. Because the data of all experiments were available in a common system, the capability existed to correlate results from different investigative areas and thereby to achieve an interdisciplinary analysis.

To increase the capability of the analysis system, SIMDAS was structured to allow the addition of analysis programs from two large statistical packages, the Univac STAT-PAK and the University of California (Los Angeles) Biomedical Computer Program (BMD). The statistical capabilities offered by these packages include programs for multivariate analysis (including discriminant and factor analysis techniques), time series analysis, analysis of variance, non-linear regression analysis, significance tests, and distribution functions. Cross-correlation and autocorrelation functions can be used to discern periodicities in the data and similarities between different time series.

Several basic programs were written to enable rapid analysis of data from any mission or group of missions. These programs plot the average response of all nine crewmen for specific parameters and provide analysis of variance data from the same crewmen, either separately or collectively. This group of programs also compiles the observations that are outside three standard deviations from the preflight mean for a given parameter.

Another group of programs was designed as a means of scanning the entire database for statistically significant relationships between parameters in different investigative areas. These programs were capable of performing correlation analyses, including data from all nine Skylab crewmen for any group of measurements selected, rank correlation based on the number of significant deviations from the preflight mean, and a factor analysis for any group of measurements selected [2].

A group of more sophisticated programs was designed for converting some of the raw data into meaningful parameters and indices. The programs in this group calculated, among other things, mechanical and metabolic efficiencies during bicycle ergometry tests and also calculated other performance indices during exercise. Conversions such as these contributed extensively to the development of hypotheses concerning the effect of spaceflight on the cardiovascular system.

3.1.2 Integrated Metabolic Balance Analysis

An important set of programs was developed to integrate all of the data relevant to measuring changes in body composition and metabolism. The concept of the integrated metabolic balance analysis is shown in Fig. 3-5. As shown here, the data and the major computed quantities can be categorized into water balance, energy balance and nutri-
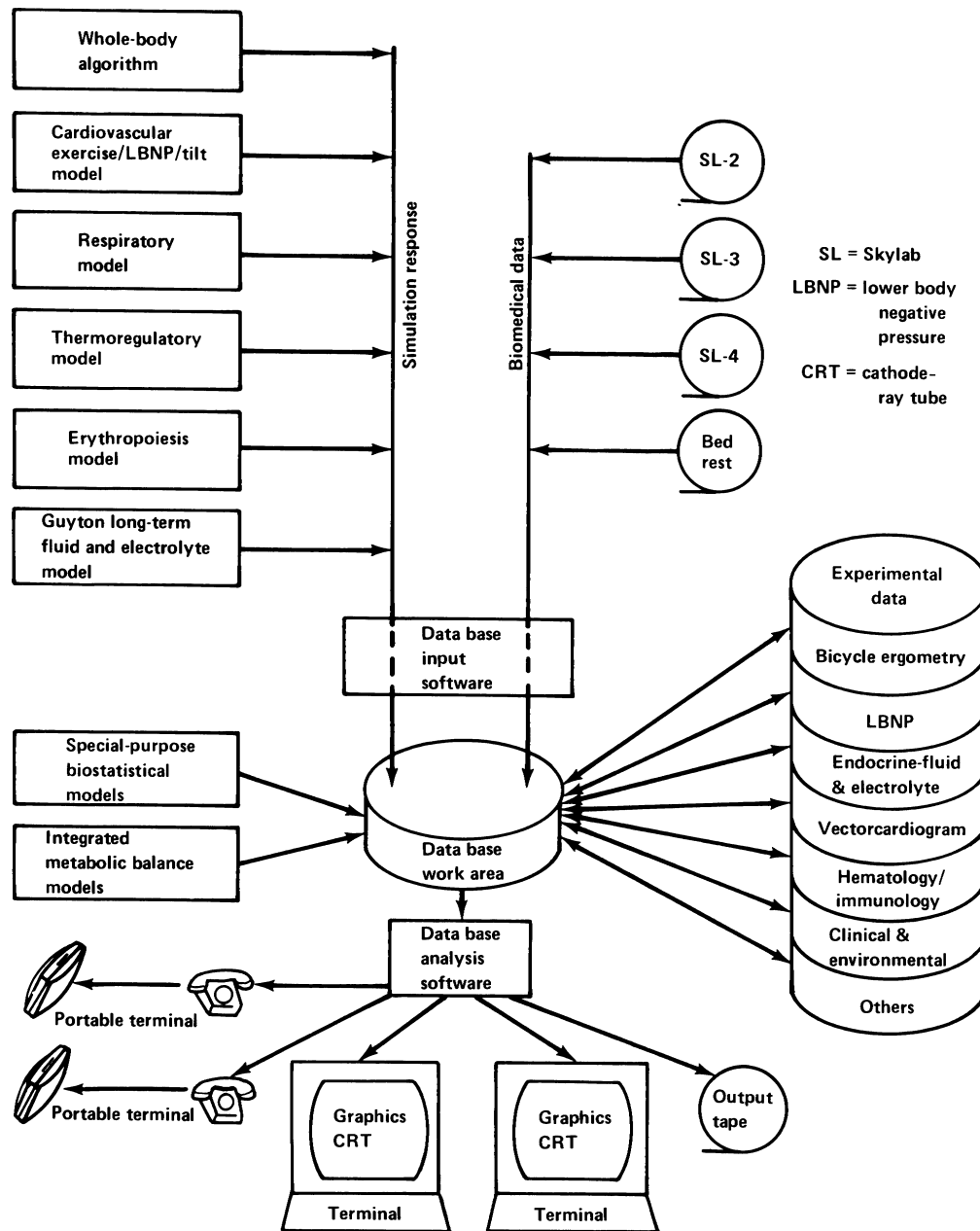
Figure 3-3. Skylab integrated medical data analysis system (SIMDAS).

DATA FUNCTN ....START.... ....STOP.... NO.
IDEN NO. BASE EXPER MAN PHASE DAY HR MN SE DAY HR MN SE DATA
> URVOL1 1 SL2 M073 C PRE 114 144 18
1923.0 = HIGH VALUE 710.0 = LOW VALUE
964.25 = MEAN 247.81 = STD. DEV 1.99 = T AT .95

	NO.	FUNCTN EXPER	MAN	PHASE	DAY		....STOP....
1239.0	115D	H	M	S	APR 25	1973	
911.0	116D	H	M	S	APR 26	1973	
1336.0	117D	H	M	S	APR 27	1973	
901.0	118D	H	M	S	APR 28	1973	
710.0	119D	H	M	S	APR 29	1973	
1503.0	123D	H	M	S	MAY 3	1973	
938.0	124D	H	M	S	MAY 4	1973	
83?.0	125D	H	M	S	MAY 6	1973	
1441.0	126D	H	M	S	MAY 6	1973	
1150.0	127D	H	M	S	MAY 7	1973	
1775.0	128D	H	M	S	MAY 8	1973	
1014.0	129D	H	M	S	MAY 9	1973	
1495.0	130D	H	M	S	MAY 10		1973
1284.0	131D	H	M	S	MAY 11		1973
1923.0	132D	H	M	S	MAY 12		1973
851.0	133D	H	M	S	MAY 13		1973
1883.0	134D	H	M	S	MAY 14		1973
1816.0	137D	H	M	S	MAY 17		1973

Figure 3-4. Typical Skylab data retrieval display. In this example, the preflight (PRE) urine volume (URVOL1) for the commander (C) on the first mission (SL2) is displayed in chronological order in the leftmost column, with the Julian and calendar dates given in the other columns. The notation H,M,S, refers to the time. In certain experiments, several measurements were obtained on the same day and, in that case, the time (hours, minutes, seconds) is also given. Statistical data for the entire set of values are computed and recorded above the tabular listing.
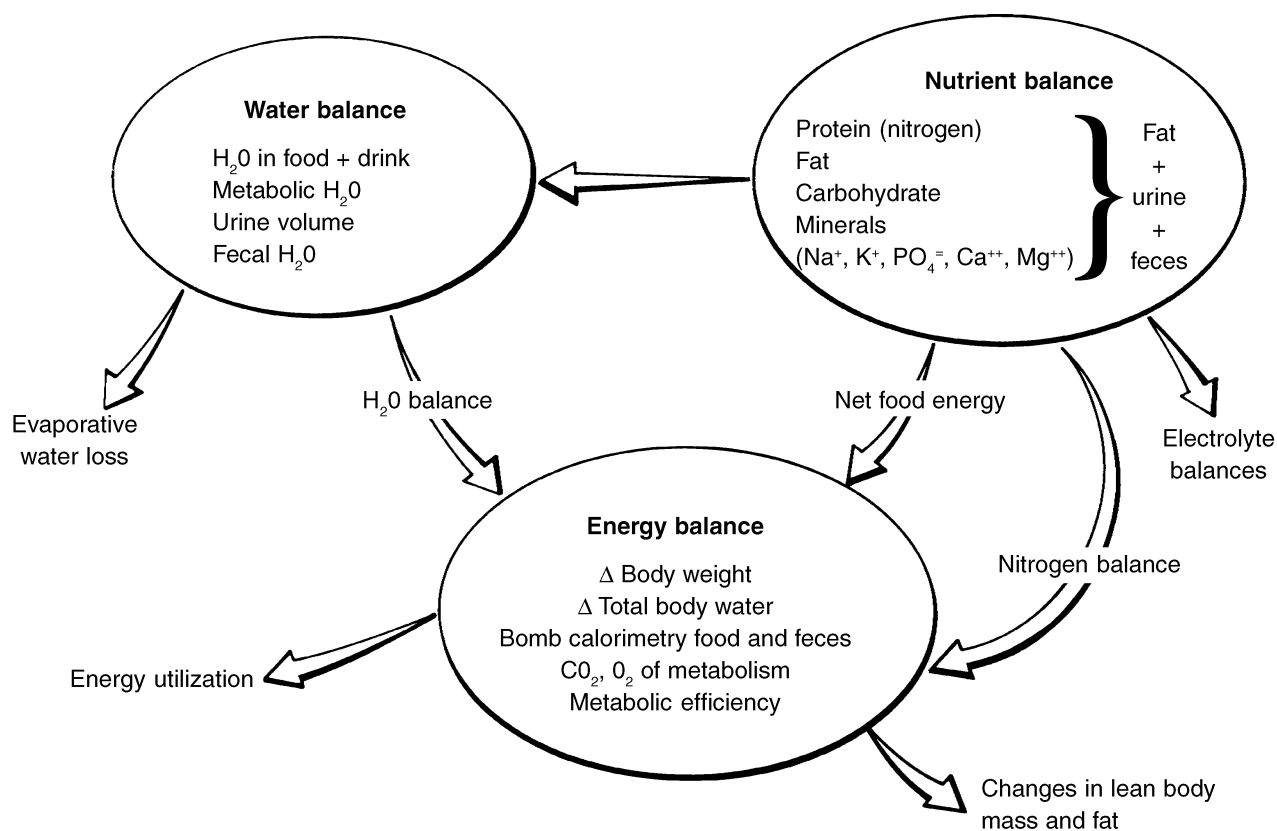
Figure 3-5. Integrated metabolic balance analysis. Complete metabolic data on water, minerals, nutrients, and calories were collected daily for each crewman. The analysis of these data (shown in ovals) enabled calculation of the components shown by the arrows.

URINE CA (MEQ/TV) SL4 PLT
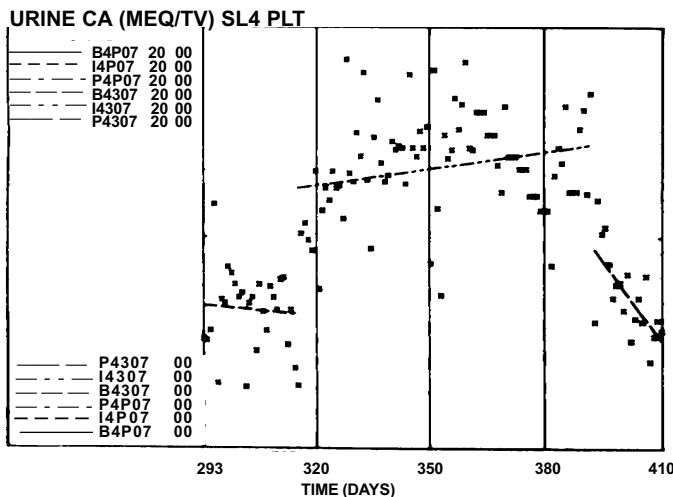
Figure 3-6. Example of cathode-ray-tube (CRT) display of Skylab data (urine calcium for the pilot crewmember on Skylab 4 (SL-4 PLT) with separate regression analysis lines for preflight, inflight, and postflight phases.

URINE VOL VS. OSMOLALITY SL2 CDR

Figure 3-7. Example of a SIMDAS-generated scatter diagram showing relationship between urine volume (abscissa) and urine osmolarity (ordinate) as well as regression line.

ent balance groups. The extensive Skylab data base include such relevant measurements as complete inflight daily metabolic balances for energy, water, nitrogen and electrolytes; body mass; as well as pre- and postflight determinations of changes in body water, body density, and whole-body electrolytes. The analysis yielded the time course for rates of water, electrolyte, protein and fat losses from the body during long-duration spaceflight. The approach for the analysis is based on fundamental equations of conservation for mass, water, and energy. Some quantities shown in Fig. 3-5 were not measured directly, or were measured very infrequently. A new technique for analyzing this metabolic balance data was developed which permits cumulative balances to be computed without incurring the large errors that are normally obtained when this is done. The use of mathematical models resulted in plausible estimates of some changes that were not amenable to direct measurement. The models also provided a means to understand the physiological processes that regulate fluid and electrolyte fluxes and volumes. The results of this extended analysis are presented in Chapter 4.

3.1.3 Graphical Interface

Interpretations of data analyses and of simulation outputs were simplified by using graphical rather than tabular computer monitor display. Discrete jumps, linear trends, periodicity and some other complex functions are more quickly recognized by the user when computer-plotting capabilities are used and the results are displayed in a graphical manner on a monitor screen. Data concerned with a dependent variable can be plotted either against time or against values of another dependent variable to construct time-trend plots or scatter diagrams (Figs. 3-6 to 3-8).

Computer graphics were also used directly with the simulation models, both to display the model output in a
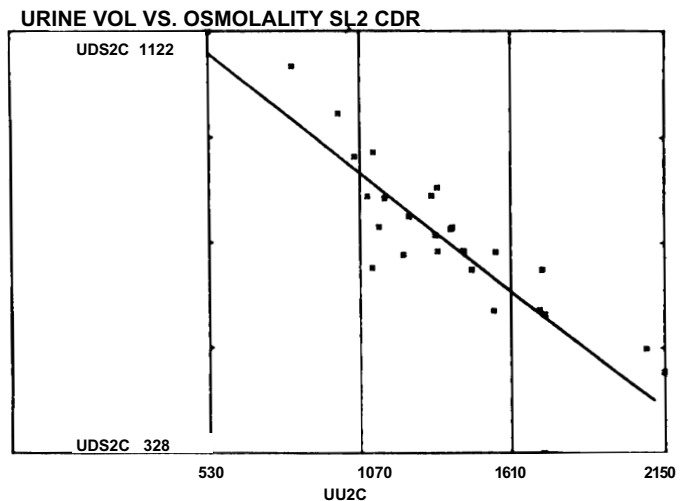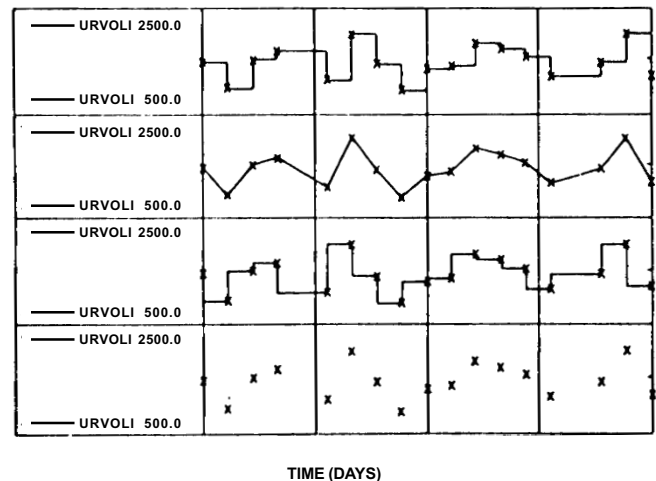
Figure 3-8. Four examples of the variety of formats in which the SIMDAS-generated data can be graphed.

convenient form (Fig. 3-9) and to facilitate comparison of the simulation results with Skylab experimental data (Fig. 3-10). All software for SIMDAS was designed for the Univac 1108/1110 computer under the EXEC 8 remote operating system and programmed using Fortran V language. The approximate core memory required by these programs is 20,000 words.

3.2 The Physiological Models

A distinctive feature of the integrative data analysis was the use of a group of mathematical models describing each physiological system of interest. The object of develop-
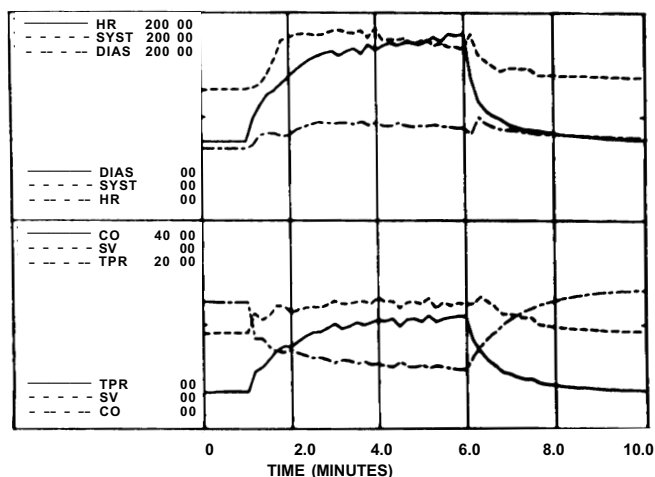
Figure 3-9. Example of SIMDAS-generated CRT display of simulation output from cardiovascular model showing transient responses to exercise (5 minutes at 200 watts). Symbols: HR = heart rate, SYST = systolic blood pressure, DIAS = diastolic blood pressure, CO = cardiac output, SV = stroke volume, and TPR = total peripheral resistance.

Figure 3-10. Example of simultaneous CRT display of Skylab data and simulation results showing preflight LBNP test. Symbols: HR = heart rate, SYS = systolic blood pressure, DIAS = diastolic blood pressure, M = model results, and D = data.

ing models suitable for computer simulation was to predict physiological behavior in weightlessness and to compare the predictions with the experimental data generated in the Skylab Program. This procedure would be expected to provide insight into the process of zero-g adaptation (see Chapter 2). The basic elements of mathematical modeling and simulation are summarized in Appendix A for the reader unfamiliar with these concepts.

Five separate models were employed in this project: a pulsatile cardiovascular model, a respiratory model, a thermoregulatory model, a combined circulatory, fluid and electrolyte balance model, and a red blood cell model. A sixth model, termed a Whole-Body Algorithm, integrates the five basic models into a common framework. In addition, a model of calcium regulation was developed more recently, and its description is also included in this section. The respiratory model and the circulatory, fluid, and electrolyte model were selected from existing models described in the scientific literature and modified to render them appropriate to this project. The remaining models resulted from research directly associated with this project or other NASA programs. These models and their applications have been recently reviewed [3].

Taken as a group, these models are capable of simulating responses to many of the stresses that occurred on the Skylab missions (fluid shifts, lower body negative pressure (LBNP), tilt, exercise tests, and environmental disturbances). The cardiovascular, respiratory, and thermoregulatory models may be considered to be exclusively short-term models, inasmuch as they are useful for simulating events lasting for several hours or less. The circulatory, fluid, and electrolyte model as well as the erythropoiesis (red blood cell) model are noted for their ability to simulate long-term hormonal, reflex, and adaptive influences that last for sev-

eral weeks or months. The combination of both types of models (short-term and long-term) into the Whole-Body Algorithm resulted in a model for studying the interactions between major sub-systems of the body and a means of simulating with one model the short-term and long-term stresses of spaceflight (see Figs. 2-3 to 2-5).
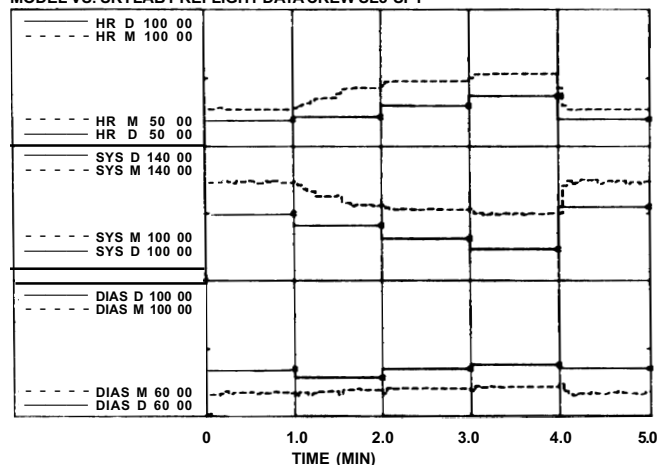
The models of physiological subsystems used in this project provide a flexible method by which hypotheses of spaceflight adaptation can be tested. Multiple stresses and sequential degrees of stress can be simulated just as in a real experimental protocol; by adjusting the value of one or more of the fixed system parameters, many hypotheses can be tested. Other hypotheses requiring a reformulation of program structure may often be evaluated without disturbing the remainder of the model (see Fig. 3-1).

Each physiological model examined in this volume contains the basic elements of a feedback control system, and each model can be represented by an active controlling system that regulates a relatively passive controlled system. The feedback variables for these models include representation of many of the actual sensors present in the body (temperature sensors, chemoreceptors, baroreceptors, oxygen sensors, and osmoreceptors). Each model is constructed of elements that represent real physiological function using algebraic or ordinary differential equations. Such a model is termed deterministic. Less realistic models, often based on a "black box" design, do not have the predictive range of deterministic models.

Many of the model features, including the major input or system parameters and the variables generated or predicted by the models, are summarized in Table 3-1. The total number of parameters and the variables indicated in this table reflect the size and/or complexity of each model. It is apparent that the current models are capable of integrating a

Table 3-1. Capability of Current Models to Utilize and Predict Important Physiological Parameters

Subsystem model	Validated simulations	System parameters (known or assumed)	Output variables (predicted)
Circulatory, fluid-electrolyte regulatory model (7 circulatory compartments; 5 body fluid compartments)	Exercise: salt loading; renal failure; proteinura; intravenous infusions; bedrest; congestive heart failure; hemorrhage; postural change; water immersion; supine bedrest; head-down bedrest	Fluid intake; sodium ion (Na^+) and potassium ion (K^+) intake; evaporative water loss; exercise work rate; arterial oxygen (O_2) saturation; vascular compliances; ventricular strength factor; plasma protein production and destruction rates; red blood cell (RBC) production and destruction rate; external body pressure; angle of tilt (130 parameters)	Cardiac output; heart rate; stroke volume; arterial pressure; venous pressure; peripheral resistance; urine flow rate; Na^+ and K^+ excretion rates; renal and muscle blood flows; blood volume; extracellular fluid; intracellular fluid; total body water; RBC mass; hematocrit; blood viscosity; antidiuretic hormone concentration; aldosterone concentration; renin and angiotensin concentrations; Na^+ and K^+ plasma concentrations; O_2 uptake (370 variables)
Pulsatile cardiovascular model (28 compartments)	Exercise; tilt table; LBNP; hemorrhage; training vs. deconditioning	External workload; exercise efficiency; LBNP intensity; tilt angle; total blood volume; compliances of veins, venules, arteries, and arterioles; fixed flow resistances; stress relaxation sensitivity; length of vascular segments (100 parameters)	Cardiac output; heart rate; stroke volume; total peripheral resistance; systolic blood pressure; diastolic blood pressure; heart period; diastolic filling time; whole-body blood volume distribution; blood pressure (static and dynamic) profiles; whole-body blood flow distribution; resistances to flow; O_2 uptake (350 variables)
Respiratory model (4 compartments)	Hypoxia; hypercapnia; exercise	Inspired O_2; inspired carbon dioxide (CO_2); inspired nitrogen; barometric pressure; metabolic rate; total blood hemoglobin (Hb); blood and tissue gas solubilities; blood-brain gas diffusivities; tissue masses; blood transport delays (30 parameters)	Minute volume; respiratory rate; dead-space ventilation; cardiac output heart rate; arterial partial oxygen pressure (pO_2) and partial carbon dioxide pressure (pCO_2); venous pO_2 and pCO_2; blood and brain pH; brain blood flow; alveolar respiratory quotient; O_2-Hb concentration (80 variables)
Thermoregulatory model (41 compartments)	Environmental heat stress; environmental cold stress; exercise; effects of humidity, clothing, air velocity, and pressure	Total metabolic rate; tissue basal metabolic rates; useful work efficiency; body surface area; body posture; ambient temperature; wall temperature; ambient humidity; ambient free-air velocity; ambient pressure; gravity factor; clothing factor; emissivity of outerwear; specific heat of atmosphere; tissue thermal conductivities; tissue heat capacities; convection and radiation coefficients; basal blood flows; sweat distribution factors; shivering distribution factors (330 parameters)	Body temperature distribution; sweating rate; insensible water losses; sensible heat losses; heat storage; shivering rate; skin blood flow; muscle blood flows (300 variables)

Erythropoietic control model
  Human model
  Mouse model
	Hypoxia; anemia; hyper-volemia; polycythemia; red cell infusion; dehydration; abnormal Hb; bedrest	Arterial pO_2; blood flow; plasma volume; tissue metabolism; O_2-Hb capacity; RBC lifespan, bone marrow gain (20 parameters)	Red cell mass; hematocrit; red cell production rate; red cell destruction rate; tissue pO_2; venous pO_2; erythropoietin (40 variables)

large quantity of information and are capable of predicting behavior of a large number of physiological variables, most of which have been previously identified as important elements in spaceflight biomedical investigations. Simulations performed during this study and by others are also listed in Table 3-1. This table demonstrates the diversity of conditions for which the models can be used in a predictive mode. Details of many of the simulations are provided in this section and throughout this publication.

The mathematical models used in this project were designed or modified through a basic problem-solving approach. First, the system under study was thoroughly analyzed, and its most important elements and parameters were identified. Then, a conceptual model was constructed by specifying the simplifying assumptions to be used and formulating the interactions, which would exist between the elements of the system. All information was translated into mathematical notation and, finally, into computer language (Appendix A).

After the model had been defined in this manner and the computer program had been written, values were selected for the constants (parameters) contained in the model, and the computer program was checked for correctness. The program was then subjected to a series of tests that ensured appropriate model responses when major parameters were changed. This entire process is called *model verification*.

Next, the model was validated to establish its relationship to the real system. Probably the most significant and demanding activity of model development, *validation* usually consists of comparison of model output to real system responses for several specific stresses identified as being related to the model's objectives. It is an important guideline in model develoment that data used for model validation be independent from that used for model verification. Also, validation should be a continual process, using data collected under different conditions; this is vital to ensuring a model's continued credibility. It is critical that the modeler stay abreast of current research regarding the real system that is being modeled; as new knowledge is gained regarding this system, the model, in turn, must be altered to reflect this new knowledge. Each time the model is refined or otherwise modified, it must be validated to ensure that it still accurately represents the real system.

The models were validated for stresses in a one-g environment, and the experimental studies used for validation were derived from the ground-based experiments associated with NASA's training and biomedical program where possible. Such stresses included bicycle ergometry exercise, tilting, LBNP, bedrest, and water immersion. In other cases, such as those involving hypoxia and thermal stress, data from the literature were used. Some simulations could not be properly validated, because data were insufficient. For example, little information regarding sweat losses during exercise at high altitude was available, and this information was necessary to validate the thermoregulatory model for the low ambient pressure of the Skylab environment. Situations such as this identified

Table 3-2. Comparison Between Fluid-Electrolyte Shifts in One-g and Spaceflight

Spaceflight stress	Analogous one-g stress
Acute fluid stress at launch	Water immersion
Blood shift from legs toward head	Blood infusion
Filtrate shift from leg tissues toward head	Isotonic saline infusion
Long-term fluid stress	Bedrest
Loss of 1 to 1.5 liters fluid Loss of sodium	Dehydration Sodium depletion
Recovery fluid stress	Bedrest recovery
Loss of central fluid volume due to loss of total blood volume	Hemorrhage
Loss of central fluid volume due to orthostasis	Hemorrhage and standing

new areas for research. When data was inadequate for quantitative validation, model credibility was demonstrated using simulation techniques, e.g., sensitivity analysis, capable of systematically analyzing the general behavior of a model for subsequent evaluation by subject-matter experts (see Appendix E for example).

A good example of the range of stresses required for demonstrating model capability and credibility is illustrated in Table 3-2. In the left column are the various types of fluid-electrolyte shifts encountered during the acute and chronic inflight and recovery phases of weightlessness. In the right column are well-known one-g stresses that are similar, in many respects, to the zero-g stress. Thus, the response to the fluid shift from the legs in a zero-g environment has many aspects similar to the one-g response to water immersion, blood infusions, or saline infusions. In the same manner, similarities can be seen between one-g stresses such as dehydration, sodium and potassium depletion, and hemorrhage in relation to the spaceflight events of prolonged weightlessness and subsequent recovery. Considerable effort was concentrated on collecting suitable data for validating the circulatory, fluid, and electrolyte model for the one-g counterparts of zero-g stresses (postural changes, water immersion, and bedrest). These studies are described in the remaining sections of this document (especially in Chapter 9). This discussion is not meant to suggest that an appropriate simulation of spaceflight can be performed by combining any or all of the one-g stresses, but this systematic validation approach has suggested improvements in the models and adds credibility to their overall capabilities.

The final step in modeling a system included testing the model over a wider data base than was used for validation, estimating parameters that were not yet measured, predicting responses that are impractical to measure in the real system, evaluating hypotheses, and making inferences

from the model to guide laboratory experimental design. These advanced studies use a number of simulation techniques including dynamic simulation, sensitivity analysis, variation of parameters, error analysis, stability analysis, and parameter estimation procedures (Appendix A). The ultimate objective was to produce valid model simulations for the stresses of interest when accompanied by the long-term absence of gravity.

The models used in this project are described in the following pages and their controlled and controller systems are illustrated in schematic diagrams. These models have been described either in the open literature or in NASA reports referenced under each model description. User guides which include the computer programs (in Fortran) are also available in the Scientific and Technical Aerospace Report (STAR) library retrieval system. When description of some major aspect of the model (such as design concept, mathematical formulation, or modifications for spaceflight simulation) is not readily available in published form, an appendix is provided to describe it. These models were developed in the 1965–1975 timeframe. A brief review of more recent organ system models can be found in Ref. [3].

3.2.1 Pulsatile Cardiovascular Model

A pulsatile model of the cardiovascular system was included in the collection of models to simulate the short-term cardiovascular experiments performed on the Skylab missions and other selected physiological stresses of manned spaceflight. The simulation required a model containing a physiological representation of the circulatory system, including the arterial tree, the veins, the capillary beds, and the heart; pulsatile blood flow; a closed-circuit circulatory system; and the control functions regulating the circulatory system. Such a model should be capable of simulating steady-state and transient responses for short-term events and responding to the selected stresses of exercise, LBNP, and an altered gravity vector to simulate tilt. The cardiovascular model, as defined by these objectives, required a representation of both the heart and the circulatory system and a description of their interactions.

Much of the work on modeling and computer simulation of the cardiovascular system and its controls has been accomplished since the early 1950's, although simple mathematical formulations date back 200 years to Euler. One of the most important models of this early period is that of E. H. Starling [4]. Starling's "law" or model has provided the basis for an initial understanding of some of the dynamic characteristics of the cardiovascular system and has been used directly in other mathematical models. Reviews of this and other cardiovascular models are available [5,6,7,8].

The most recent models of the cardiovascular system can be classified into two basic categories:pulsatile and nonpulsatile. Pulsatile models are designed to account for the inertial components of flow and periodic heartbeats and thereby to enable simulations of the full range of pressure pulses (i.e., systolic and diastolic pressures). In contrast, non-pulsatile models are less complex, have more

linear than nonlinear elements, and provide only continuous blood flow and mean pressures. In these studies, a pulsatile model [9] was used to simulate the short-term cardiovascular events, whereas a non-pulsatile model [10] was used for the longer-term adaptive processes.

Early mathematical analyses of pulsatile blood flow contain assumptions of linearity and steady state. The results from these models agree very well with measured values, unless nonlinear characteristics or transient responses are studied. These limitations in modeling pulsatile blood flow were partly overcome in the present model by a method developed by Rideout and Dick [11]. The method yields difference-differential equations for fluid flow in distensible tubes and forms the basis for solving the fluid flow equations in many pulsatile models. The most significant advantages of this approach are that non-linear terms, important to a particular model, can be included easily and that a complex solution of the model may be avoided. Models using this approach have been found to exhibit a higher fidelity of response and a greater level of system detail.

Non-pulsatile, lumped cardiovascular models developed in recent years are especially effective in simulating the long-term aspects of the circulatory system. In 1972, Guyton and his associates [10] published a non-pulsatile model that is very detailed and includes many mechanisms outside the circulatory system that impact the fluid balance and blood volume within the circulatory system. Elements are also included to account for both short-term and long-term stresses. This design resulted in a powerful model that has been used successfully as a research tool by the present authors. Nevertheless, the portion of the Guyton model representing the circulation consists of a limited number of compartments and does not contain the level of detail required for certain aspects of this project.

The cardiovascular model as used here required pulsatile, nonlinear, and non-steady-state features. In addition, the model needed the capability to respond to exercise and to an altered gravity vector. Because models with the required fidelity and complexity were not available, a puslatile cardiovascular model was developed. The model presented in this section was developed by Croston [9] and was later modified to extend its application to space-flight experiments [12,13].

3.2.1.1 Description of the Croston Model.
The basic mathematical model of the cardiovascular system is represented by two major blocks:the circulatory system, which is the system being controlled, and the regulating or controlling system, which provides feedback control to change various circulatory parameters in response to imposed stress changes (see Fig. 3-11). The circulatory system describes pulsatile blood flows, pressures, and blood volumes for the 28 compartments. Circulatory effects such as venous tone, venous valves, leg muscle pumping, respiratory pressure effects, gravity, and heart pumping are represented. The regulatory system contains neurogenic and metabolic factors that control heart rate, arteriolar resistance, and venous tone. The load disturbances that may be specified
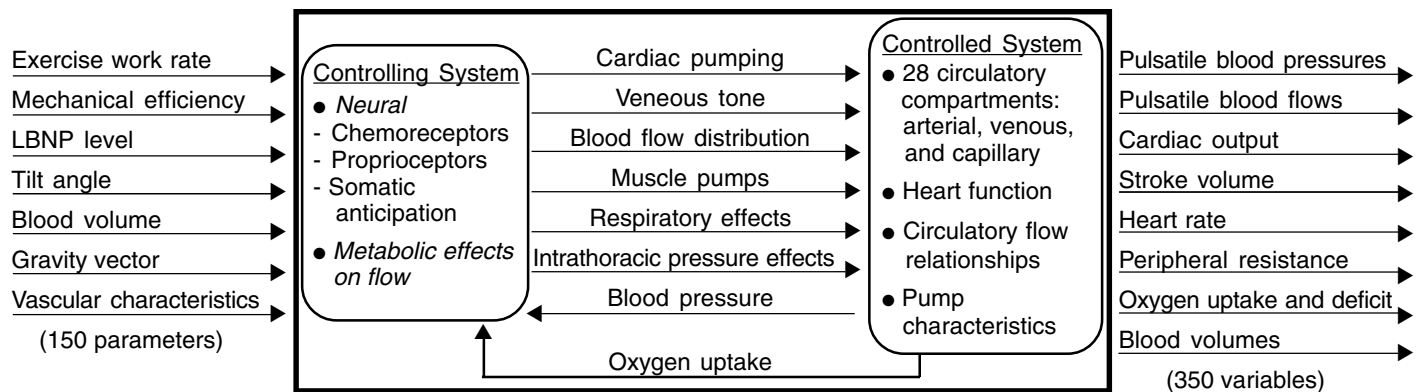
Figure 3-11. Schematic of the pulsatile cardiovascular model showing major input parameters and output responses in addition to elements of the controlled system and mechanisms of the controlling system.

by the simulator include exercise workload, work rate, gravity, LBNP level, and blood volume. Any one of nearly 150 cardiovascular parameters can also be altered to test hypotheses regarding changes in such factors as compliance, controller gain, and heart strength. The more useful output quantities that are generated by the model are oxygen uptake, oxygen deficit, cardiac output, heart rate, various blood flows, systolic pressure, diastolic pressure, mean pressure, stroke volume, and venous and arterial pressures.

3.2.1.1.1 *The Controlled System.* The controlled system consists of the heart and vascular systems. Figure 3-12 illustrates the 28 compartments of the circulatory model, including arterial segments, venous segments, arteriovenous branches, and the heart. Published anatomical and physiological data in addition to selected data from previous models are used to characterize the parameters of the governing differential equations. Nonlinear characteristics are assigned to particular arteriovenous segments, as required, to simulate elastic properties of the vessels over the wide range of pressures observed during exercise. Figures 3-13 and 3-14, derived from Altman and Dittmer [14], illustrate typical nonlinear characteristics of arteries and veins.

The pumping action of the heart is simulated with time-varying inverse compliances. Other pumping actions include the intrathoracic pressure effects, based on a simulated respiratory frequency, and leg muscle pumping. The beat-by-beat mode of operation exhibits a realistic pulsatile response, including the dynamic effects of breathing superimposed on the blood pressure responses for the resting or exercising human subject.

Solution of this mathematical model, which describes unsteady, laminar fluid flow in a distensible tube, requires solution of the Navier–Stokes equations. The previously mentioned method of Rideout and Dick [11] was selected since this technique yields a set of first-order, ordinary differential equations that can be solved routinely on a digital computer. Also, the lumped-parameter coefficients of the equations have anatomical and physiological significance, and gravity forces and nonlinear terms are included easily.

Controlled variables shown in Fig. 3-11 include venous tone, strength of heart contractions, and flow resistances. These variables are controlled in proportion to simulated metabolic and neurogenic factors discussed next.

3.2.1.1.2 *The Controller System.* Figure 3-15 is an overview block diagram of the model's controlling sub-system. Neural commands are assumed to be from baroreceptors, chemoreceptors, muscular activity, and somatic anticipation and arousal inputs. The controller function is assumed to be proportional with a variable set-point based on the sum of the command inputs.

Pressure sensors for the neural control loop consist of stretch receptors located in the aortic arch and the carotid sinuses. The model assumes activity from both the carotid sinuses and the aortic arch, since pressures differ in the vertical position in these two locations because of different hydrostatic pressure. An important effector mechanism of the blood pressure control loop is the sinoatrial (SA) node of the heart, which is the site of neurogenic stimulation. Heart rate is controlled by varying the diastolic depolarization period.

The effects of the sympathetic and vagus nerve efferents are combined into a single signal. This combination is justified by noting that the sum of the two effects is approximately linear over the range of mean arterial pressures encountered during submaximal exercise [15]. Other assumptions are that the controller gain is fixed in this model throughout the range of submaximal exercise and that the set-point for the arterial baroreceptor reflex is elevated during exercise. These assumptions are based on studies by Bevegärd and Shepard [16].

The model uses the accepted hypothesis that metabolic substances that are transported by the blood and are significant factors in the control of heart rate are produced during exercise. The variable "total metabolites" indicated in Fig. 3-15 is meant to include products of metabolism (i.e., lactate) concentrations of several known (i.e., catecholamines, and unknown chemical components), and thermal energy. A key point of this hypothesis is that al-
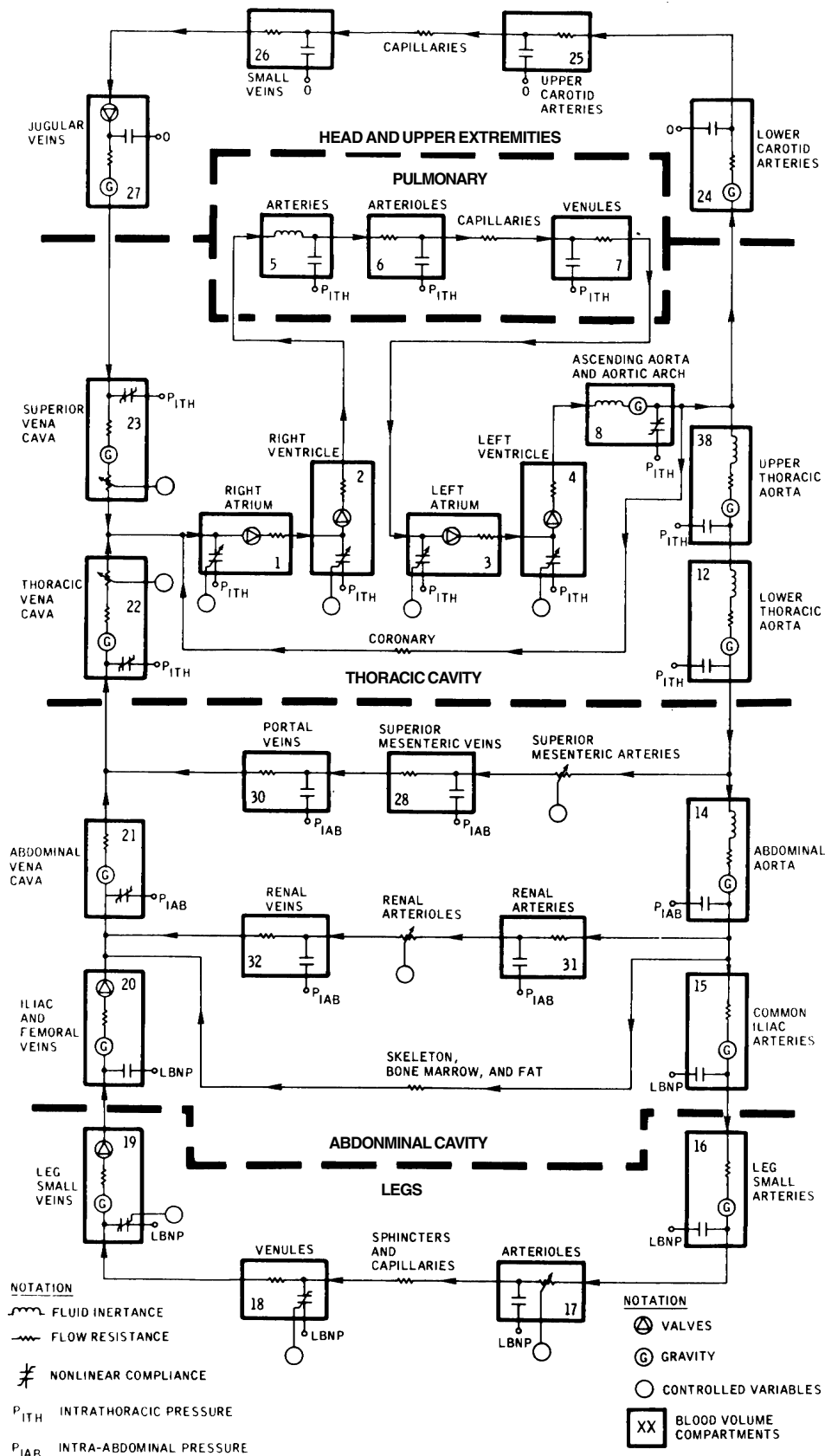
Figure 3-12. Block diagram of the cardiovascular model's controlled system.
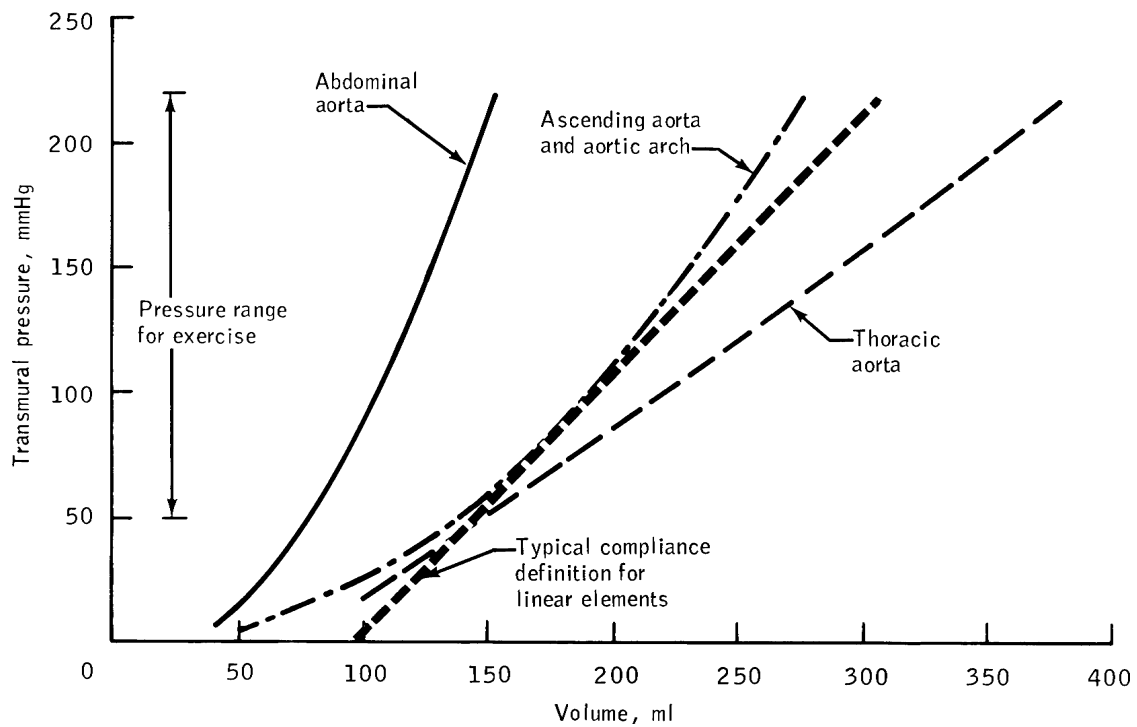
Figure 3-13. Pressure-volume (compliance) relationship for arterial segments.
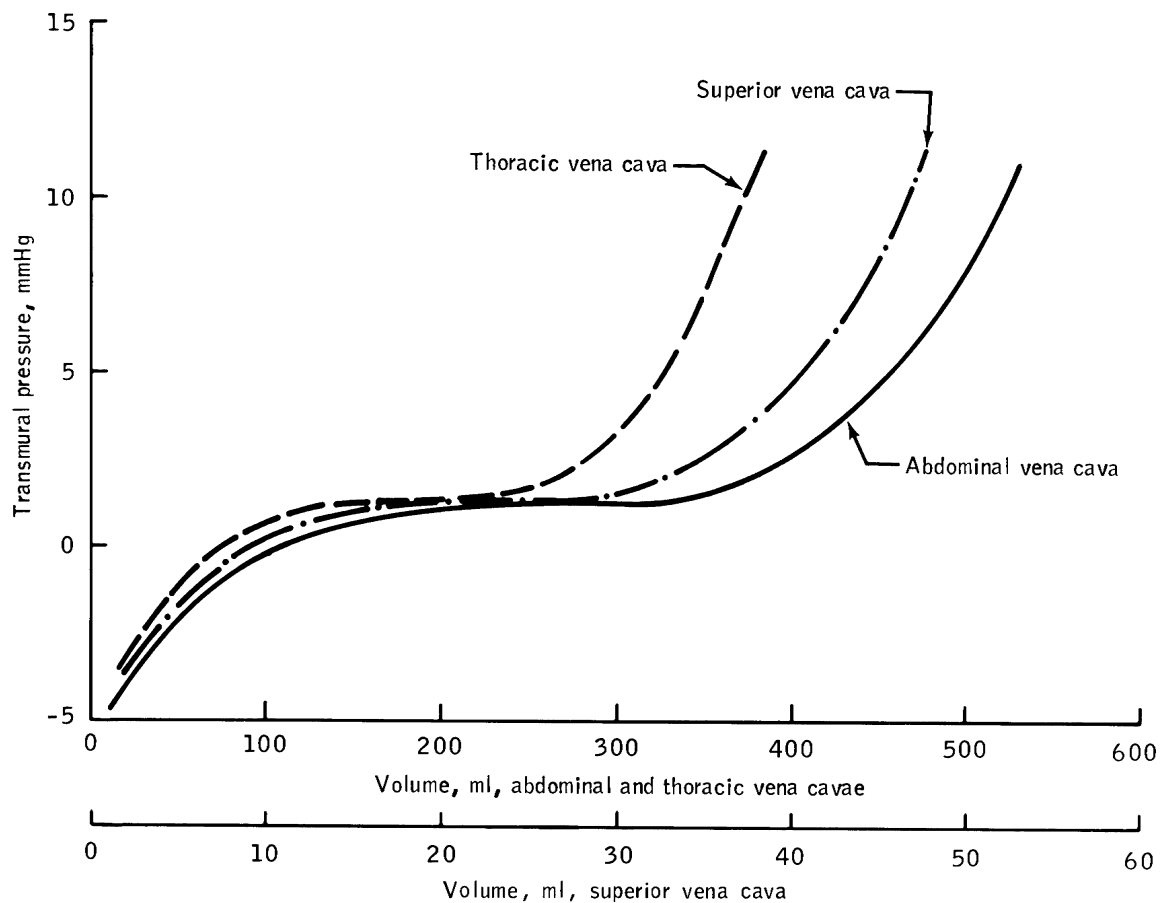
Figure 3-14. Pressure-volume (compliance) relationship for venous segments.

Somatic (arousal and anticipation)

Proprioceptive (muscle activity)

Neuron afferent activity

Arterial stretch receptors

Circulatory system

Proportional control

SA node

Heart rate

Venous tone

Leg blood flow

Arterial pressure

Direct chemical and thermal

Precapillary sphincters

Arterioles

Arterial chemoreceptors

Resting sphincter activity

Total sphincter activity

Total vasodilation

Local tissue control

Exercise workload

Neural references

Oxygen requirement for rest

$\dot{V}O_{2R}$

$K_1\int dt$

M_S

Total metabolites

Transient metabolic indicator factor

M_T

Oxygen deficit

Cardiac output

Work rate

Oxygen requirement for work

$\dot{V}O_{2W}$

$K_2\int dt$

DO_2

Arterial – venous O_2 difference function

Multi- plier

$\dot{V}O_2$

Oxygen uptake

Work efficiency

Figure 3-15. Block diagram of the cardiovascular model's controlling system.

though the total effect of metabolites is not proportional to the exercise workload or to the rate of metabolism, it is proportional to the time-dependent state of a cardiorespiratory metabolic balance. The state is expressed in this model as the sum of metabolic components due to an initial exercise transient (based on oxygen deficit), plus a component due to accumulating metabolites (based on oxygen uptake).

During exercise, these controlling elements elevate cardiac output and leg blood flow by altering flow resistances in the arterioles and the precapillary sphincters. Other flow branches are controlled similarly to produce a realistic cardiac-output distribution. At the same time, venous return is enhanced by vasoconstrictor activity in venules and small veins. This enhancement effectively decreases compliance and decreases the unstressed volume [17].

3.2.1.2 Modifications to the Original Model. Croston's original computer simulation model for exercise was de-

signed to simulate the dynamic response of the cardiovascular system to various levels of exercise. The experiment simulated is bicycle ergometry in which the subject is sitting erect on the bicycle ergometer in a one-g environment. A modification to the cardiovascular model enabled simulation of tilt ergometry, in which the body angle relative to horizontal can be changed while bicycle ergometry is simulated. This modification is related to developing a zero-g simulation of bicycle ergometry for Skylab inflight experiments. A supine or slightly tilted position (such that the heart and the bicycle pedal axis are in the horizontal plane, whereby the gravity heads of the circulatory vessels are nulled) was thought to be a good representation of microgravity effects on the blood column. In addition, a version of the model was developed for simulating LBNP and static tilt experiments. Many of the controlling mechanisms required for exercise simulation are not necessary to simulate LBNP and tilt (such as oxygen debt and total metabolites). The control system model for LBNP and static

tilt simulations is, therefore, a subset of the one shown in Fig. 3-15 [7,8,13].

3.2.1.3 Limitations. During the course of this study, it was apparent that the original exercise model did not contain sufficient detail to simulate all the events of interest to the investigators. Some of these deficiencies were overcome by modifications that provided the capability for simulating static tilt, tilt ergometry, and LBNP as described previously. Other limitations remained; they are described here.

1. The model lacked adequate representation of tissue filtration, hormonal regulation, and baroreceptor adaptation and could not be used to maintain a satisfactory simulation of experimental responses beyond 30 minutes. Consequently, the model is considered a short-term model.
2. The model lacked the capability to simulate maximal oxygen-uptake stress tests. It is likely that cardiac reserve or cardiac filling was inadequately modeled. At intense levels of exercise, the arterial pressure falls and creates an unrealistic reflexive increase in heart rate. This deficiency limits the model to the submaximal range of exercise.
3. The model was validated for subjects who, although not sedentary, were not as physically fit as the astronaut population. In addition, some of the Skylab crewmen were in much better physical condition than others. These differences in physical condition lead to different exercise responses which could not be easily accounted for by the model.
4. The model does not have an explicit representation of chemoreceptors. Although the model has the capability to detect oxygen deficiencies that result from metabolic effects, it could not respond to changes in the content of inspired gases. Modifications were later added to the Whole-Body Algorithm that corrected this limitation during rest but not during exercise (see section entitled "Description of the Whole-Body Algorithm").

In terms of the purpose and objectives of the model, the limitations described are minor. Although they suggested areas for improvement, they did not hinder the initial purposes for which the model was intended.

3.2.1.4 Model Validation. Specific simulations of bicycle ergometry, lower body negative pressure, and tilt experiments were developed and validated for one-g response [12,13]. The validated model was then used to test hypotheses of cardiovascular system changes in weightlessness by comparison of model results with actual crew responses to these experiments while inflight. The one-g validation studies are summarized below, while the zero-g hypothesis testing studies are described in Chapter 7.

a) ***Validation for Exercise.*** The exercise simulation model was initialized with characteristic parameters for a group of young, untrained men in the sitting position. This selection was made because of the applicability and availability of experimental data and the observation that the experimental data are less consistent when age groups are mixed. The steady-state model values are compared (Fig. 3-16) with a set of experimental data published by Ekblom et al. [18]. This particular set of data is for a group of eight male students, age 19 to 27 years, exercising on a bicycle ergometer. The model's oxygen uptake for the particular group simulated is 1.5 liters/min at a work rate of 100 watts with an assumed exercise work efficiency of 25%. Simulation results indicate agreement within plus or minus one standard deviation of the experimental workloads run. Figure 3-9 is an example of the model's graphic output which shows a typical simulation of the transient response to exercise.

b) ***Validation for LBNP and Tilt.*** The computer simulation model for LBNP and tilt experiments [13] is designed to simulate the dynamic response of the cardiovascular system to an induced external negative pressure applied to the lower body or to tilting of the subject (on a tilt table) from supine to a head-up position. Both experiments cause pooling of blood in the lower body and are used by biomedical researchers as a test of orthostatic tolerance. The simulation of LBNP (Fig. 3-17(a)) is accomplished by applying externally to the leg vessels a negative pressure term which increases the transmural pressure and results in an increase in blood volume of the leg compartments. The tilt experiment is simulated in the model (Fig. 3-17(b)) by applying gravity pressure gradient terms to the vascular compartments. The overall effect is a decrease in blood volume above the heart and an increase in all segments below the heart.

The major difference between LBNP and tilt stress is that LBNP causes distention of the leg vascular segments and thereby pulls more blood into the legs from the upper body, whereas the tilt experiment causes a gradient in the direction of the gravity vector in every vascular segment in the body in varying amounts, depending on the length of the segment and its distance from the heart. The response of the cardiovascular system is somewhat different also. The model's response, supported by the experimental data of most investigators, shows a large increase in diastolic blood pressure and little change in systolic blood pressure for the tilt simulation, and a substantial drop in systolic with little change in diastolic blood pressure for the LBNP simulation. For both tilt and LBNP, an increase in leg volume and heart rate and a decrease in stroke volume are obtained.

Table 3-3 contains the steady-state model results obtained for selected variables at rest in the supine position after exposure to three levels of negative pressure on the lower body and after a 70 ° tilt. The variables presented are heart rate (HR) in beats per minute; cardiac output (CO) in liters per minute; stroke volume (SV) in milliliters; mean pressure (PM), systolic
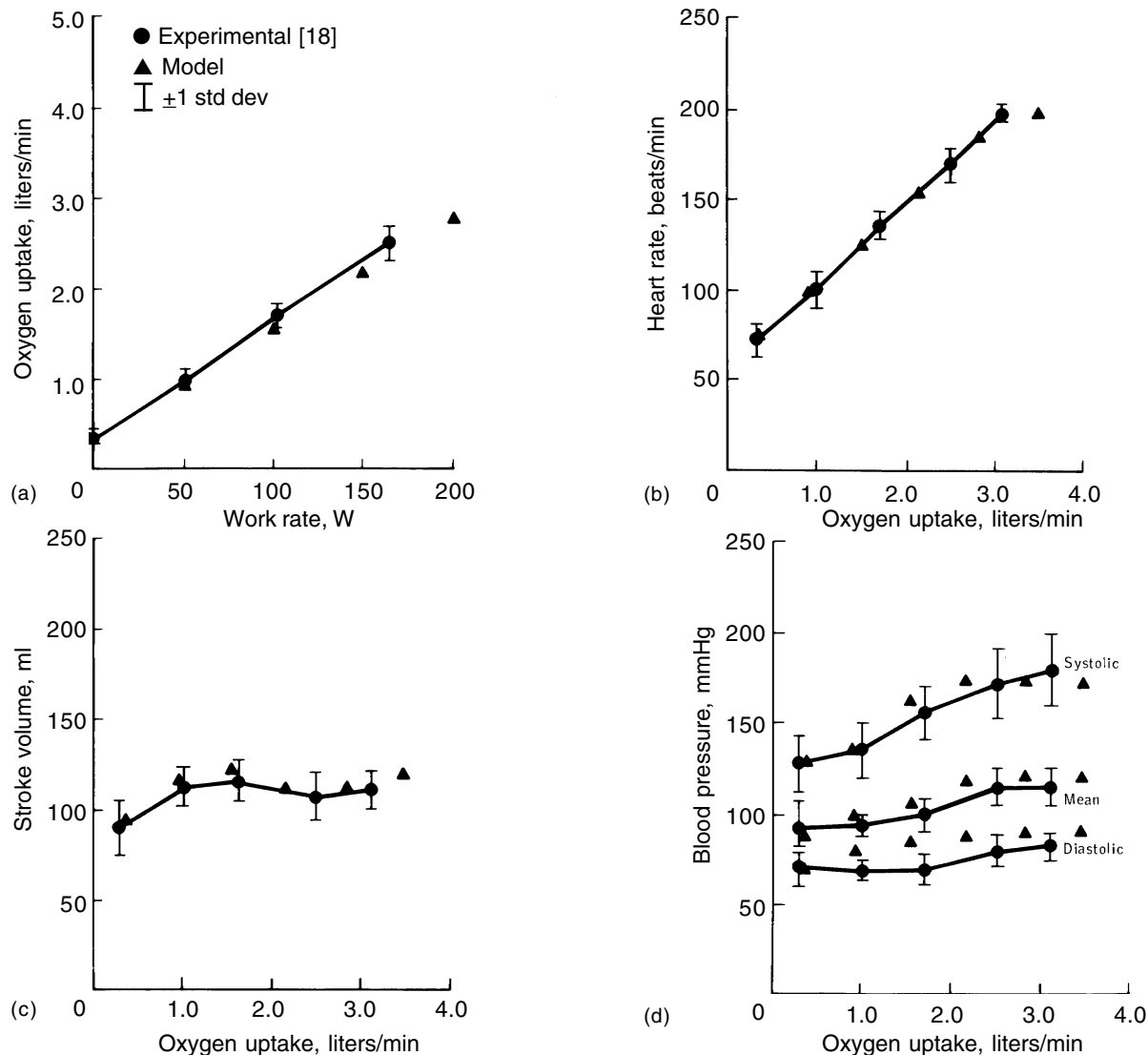
Figure 3-16. Exercise validation study showing steady-state responses of the cardiovascular model compared with experimental data taken from Ref. [18]; (a) Oxygen uptake as a function of work rate, (b) Heart rate as a function of oxygen uptake, (c) Stroke volume as a function of oxygen uptake, and (d) Blood pressure as a function of oxygen uptake.

pressure (SYST), and diastolic pressure (DIAS) in millimeters mercury; and blood volume contained in the legs (LEG BV) in milliliters. The simulations also agree reasonable well with experimental results, including Apollo and Skylab crew preflight data as shown in Table 3-4 for LBNP and Table 3-5 for tilt. There has been some disagreement in the experimental findings with regard to the similarity of response to –40 to –50 mmHg LBNP and 70° head-up tilt. Some investigators consider these to be similar stresses and to produce similar responses (see review by Wolthuis et al. [25]) However, the simulations and the data (Fig. 3-17 and Tables 3-3 to 3-5) demonstrate that in some important respects, they are quite different and produce different responses.

3.2.2 Thermoregulatory Model

The first physiological computer model to be used in the manned spaceflight program was that of the thermoregulatory system. The model selected for the present study resulted from many years of development, modification, and revision by several institutions, including NASA, the John B. Pierce Foundation, Lockheed Electronics Division, and General Electric Company. The NASA sponsored much of this work and participated directly in the model's validation and application to designing life support systems of space cabins and space suits. Five major objectives were formulated for the thermoregulatory model used in this project.

1. Compute modes of heat loss from the body and heat production within the body.

Table 3-3. Steady-State Model Results

Stress	HR	CO	Parameter[a] SV	PM	SYST	DIAS	LEG BV
Supine (rest)	62.4	6.55	105	90.3	126.7	72.4	447
LBNP							
−30 mmHg	69.7	6.46	93	88.7	121.9	72.0	720
−40 mmHg	72.2	6.43	89	88.2	119.2	71.8	812
−50 mmHg	77.2	6.37	82	87.3	115.8	72.6	903
Tilt (70°)	80.9	5.6	69	89.4	124.6	80.4	851

[a] Parameters and units described in text
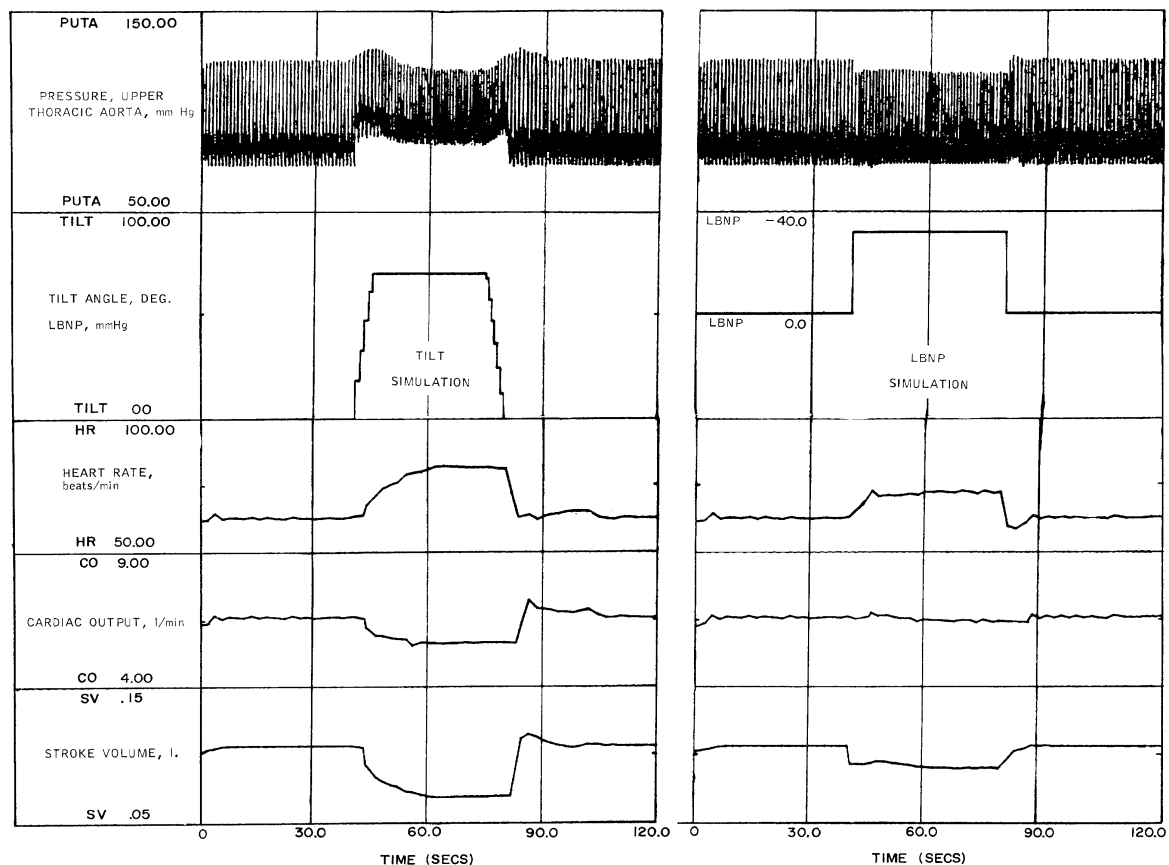
Figure 3-17. Computer simulation of tilt (left) and LBNP (right). Upper pressure trace demonstrates pulsatile capability of model.

2. Compute heat balances, body heat storage, and temperatures for the major segments of the body.
3. Predict body water loss from the three avenues of evaporation: diffusion from skin, sweating, and respiratory losses.
4. Simulate thermoregulatory responses to heat loads caused by variable environmental conditions and exercise rates.
5. Simulate both dynamic responses and steady-state responses of the body in the cases under study.

The thermoregulatory model used in this program was originated by Stolwijk and Hardy [26] as a seven-compartment system. It was later expanded by Stolwijk [27,28] to a 25-node system that was validated not only for environmental effects but also for exercise. To increase the model's fidelity and extend its capabilities, it was subsequently modified for NASA to include options for various layers of clothing and liquid-cooled garments, and the number of passive compartments was expanded to forty-one [29]. Other modifications made under the present program in-

Table 3-4. Comparison of LBNP Model Results with Available Data Sources

Change from rest	Data Source			
	Model	Apollo crew preflight Avg. 12 subjects	Ref. [19]	Ref. [20]
Increase in heart rate, beats/min, for LBNP, mmHg, of				
–30 mmHg	7.3	4.4	—	—
–40 mmHg	9.8	8.9	8.0	11.89
–50 mmHg	15.1	14.6	—	—
Decrease in stroke volume, ml, for LBNP, mmHg, of				
–30 mmHg	12.0	—	—	—
–40 mmHg	16.0	—	—	18.62
–50 mmHg	23.0	—	—	—
Decrease in systolic blood pressure, mmHg, for LBNP, mmHg, of				
–30 mmHg	4.8	—	—	—
–40 mmHg	7.5	—	7.0	6.61
–50 mmHg	10.9	—	—	—
Increase in diastolic blood pressure mmHg, for LBNP, mmHg, of				
–30 mmHg	–0.4	—	—	—
–40 mmHg	–0.6	—	–3.5	0.16
–50 mmHg	0.2	—	—	—
Increase in leg blood volume, ml, for LBNP, mmHg, of				
–30 mmHg	274	—	—	—
–40 mmHg	365	—	–614	[a]419
–50 mmHg	456	—	—	—

[a] Blood volume shifts calculated from percent change in leg volume by conversion factor derived from Ref. [19], where both calf circumference and water plethysmograph measurements are given.

Table 3-5. Comparison of Tilt Model Results with Test Data

Change from rest	Data Source						
	Model	Apollo crew preflight Avg. 12 subjects	Ref. [20]	Ref. [21]	Ref. [22]	Ref. [23]	Ref. [24]
Increase in heart rate, beats/min,	18.5	15.3	15.0	15.5	14.0	15.6	13.0
Decrease in cardiac output, liters/min	0.94	—	—	—	—	—	—
Decrease in cardiac output, percent	15.0	—	—	—	15 to 35	—	19.0
Decrease in stroke volume, ml	36.0	—	—	—	45	—	—
Decrease in stroke volume, percent	34.0	—	—	—	40	—	31.0
Decrease in systolic blood pressure, mmHg	2.1	—	10.0	–1.0	—	1.7	3.0
Increase in diastolic blood pressure mmHg	7.8	—	–2.0	9.0	—	13.0	7.0
Increase in leg blood volume, ml	403.0	—	—	620.0	—	—	—

clude improved equations for convection, radiation, evaporative and respiratory loss, and shivering [30,31,32]. Currently, both a steady-state and a transient version are available for use in the shirt-sleeve model [33,34]. Other approaches to modeling the human thermal system are available and have been reviewed by Fan et al. [35].

3.2.2.1 Description of the Thermoregulatory Model. The thermoregulatory system was modeled as a controlling system and a controlled system (Fig. 3-18). The controlled system consists of the body divided into geometrical segments, each segment having its own thermal characteristics. Changes in environmental thermal
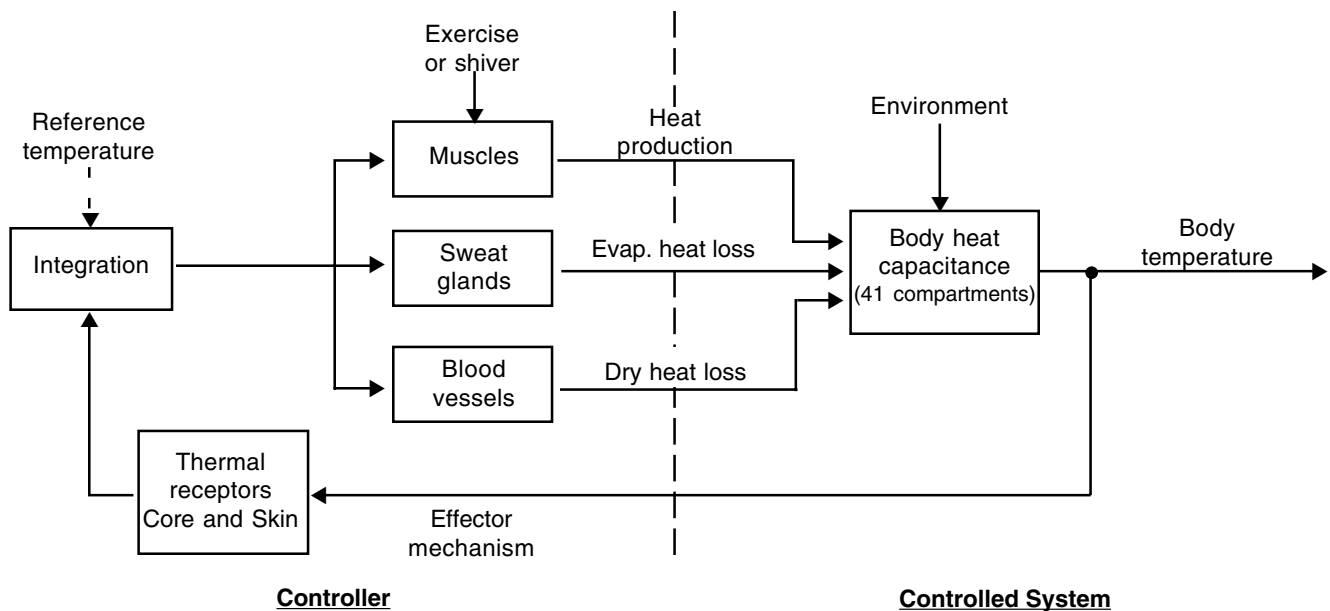
Figure 3-18. Block diagram of the thermoregulatory system showing the determinants of body temperature and the three major regulatory mechanisms.

loads act on the controlled system and change the temperatures of its compartments. Heat production from exercise is also permitted to alter body temperatures by way of increased muscle metabolism. These disturbances are sensed by thermal receptors that transmit temperature signals to an integrating and processing center. The controlling system is designed to maintain a heat balance using all avenues of heat transfer. Control equations consist of functions of the central temperature signal and the integrated skin temperature signal. Appropriate commands are sent to thermoregulatory elements changing skin and muscle blood flow, rates of sweat secretion, and shivering. The blood flow responses act to remove the excess heat load by bringing greater quantities of warm blood to the body surface, where thermal energy can be transferred through the skin to the environment. Evaporation of sweat is also a particularly effective cooling mechanism. In cool environments, metabolic heat production may be increased internally by the shivering mechanism in muscle tissue.

A total of 41 nodes is used to represent the thermal characteristics of the body with 4 nodes each for the head and trunk and each arm, hand, leg, and foot. The forty-first node represents the central blood compartment. The four nodes representing each of the segments are composed of concentric layers treated as core, muscle, fat, and skin. Each node has the appropriate metabolic heat production, convective heat exchange with the central blood compartments, and conductive heat exchange with adjacent compartments. The nodes exchange heat with the environment by way of conduction, radiation, convection, and evaporation. The mathematical basis of the controlled system rests entirely on heat balances taken around each anatomical element. Figure 3-19 is a schematic diagram for one

typical segment; in this case, the head. Each compartment represents a lumped heat capacitance with its own metabolic heat production, conductive heat exchange, evaporative heat loss, and convective heat transfer.

A thermal balance for the body as a whole is illustrated in Fig. 3-20. The rate of heat stored in the body is determined by the rate of metabolic production of energy offset by rates of heat dissipation from convection, radiation, respiratory processes, diffusion of water from skin, and evaporation of sweat. For any particular combination of activity and environment, the rate of heat storage must eventually reach zero (i.e., thermal steady state). This state is ensured by the control elements adjusting such factors as evaporation (by sweat secretion), radiation and convection (by diverting skin blood flow and changing skin temperature), and metabolism (by shivering mechanism). Rates of evaporation, convection, and radiation are also determined by ambient conditions such as temperature, humidity, wind velocity, and pressure.

Figure 3-21 indicates the main features of the model, including the most important input parameters and output variables available. This system is based on a man with a body weight of 74 kilograms and a surface area of 1.9 square meters. Inputs to the system include work rate, basal conditions, environmental conditions, and time or duration of exposure. The thermal properties and the geometric parameters of the body tissues are usually fixed in the model but may be altered to test unusual conditions. For any exposure time, the model generates values for such quantities as temperatures for all 41 nodes, mean skin temperature, mean core temperature, rates of heat storage, sensible and insensible heat and water losses, and blood flow distribution.
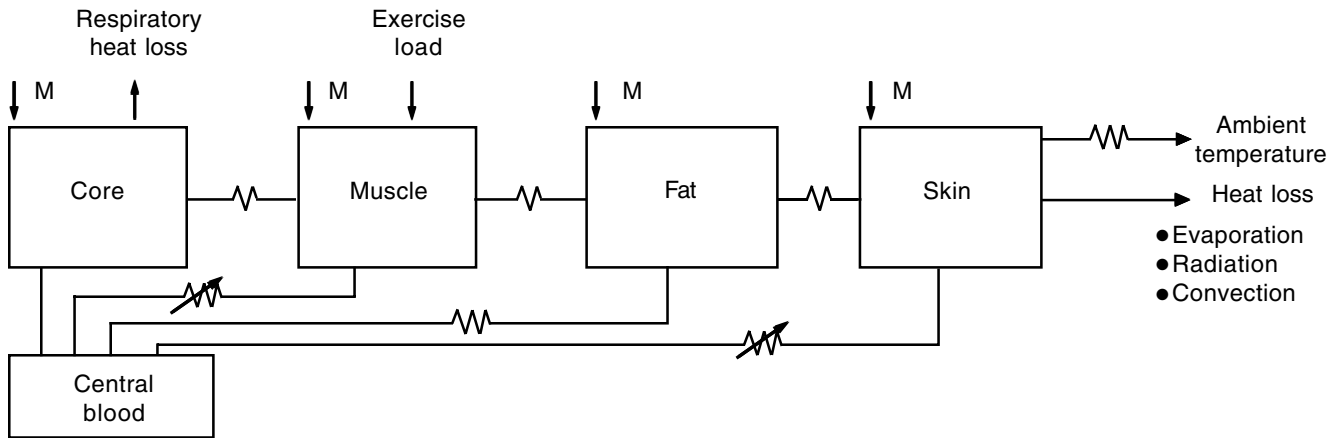
Figure 3-19. Block diagram of the controlled system for one segment: the head. The four major concentric compartments of tissue plus the central blood compartment are indicated as well as their thermal resistances. (*M* = basal metabolic heat production.) Lines connecting each element represent heat flows.

$$\underbrace{\dot{Q}_{metabolic}}_{\text{Heat produced}} - \underbrace{\dot{Q}_{convection} - \dot{Q}_{\substack{mass \\ diffusion}} - \dot{Q}_{sweat} - \dot{Q}_{\substack{lung \\ latent}} - \dot{Q}_{radiation}}_{} $$

$$ \underbrace{= \dot{Q}_{stored}}_{\text{Heat stored}} $$
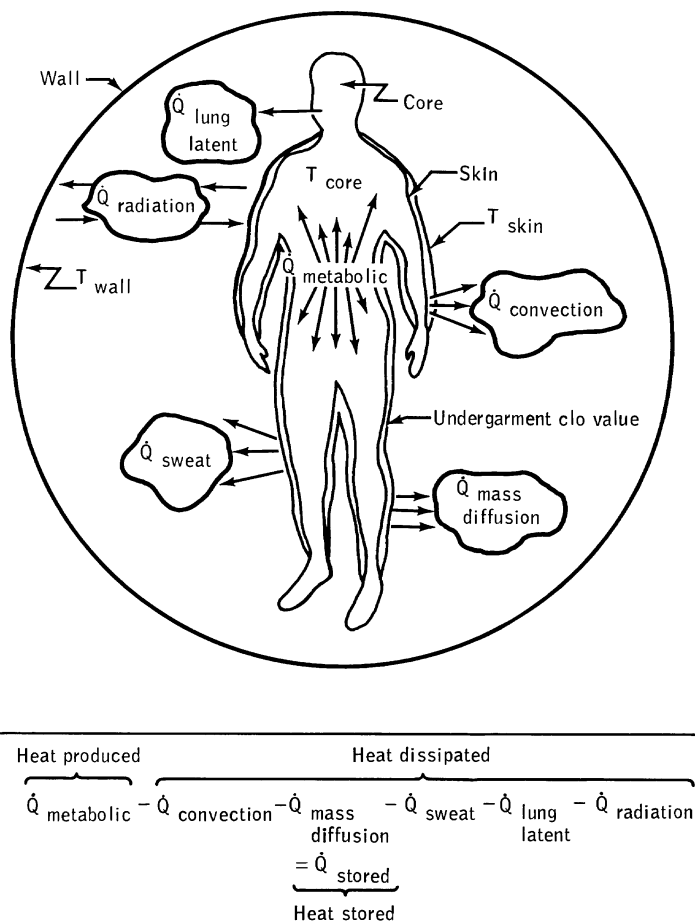
Figure 3-20. The thermal balance for man on which the thermoregulatory model is based. Evaporative heat loss is divided into skin (mass diffusion), respiratory (lung), and sweat components. (*Q* = rate of heat transfer, *T* = temperature.)

3.2.2.2 Validation and Application Studies. Validation of the thermoregulatory model has been reported by the original model developers for a variety of conditions and situations, including experimental fever, disturbances in ambient temperatures, ingestion of cold fluids, and intense bicycle ergometer exercise [26,28]. The model's performance was in reasonable agreement with experimental findings throughout the dynamic range, including the steady-state region, for periods of as long as 5 hours. More recently, the steady-state version of the thermoregulatory model was validated for resting conditions [32], and a sensitivity analysis was performed that demonstrated some unique methods for examining model behavior and uses of the model for guiding research and designing environmental systems [36]; also see Appendix E.

The model has been used by NASA life support system engineers to define the limits of thermal comfort for manned spaceflight [29,37]. This complex model is flexible enough to permit combining it with models of a space life support system so that reasonable predictions can be made about the interactions between the two systems [38].

Coupling the thermoregulatory model with a respiratory control model [39] was another task under NASA sponsorship. This effort demonstrated the feasibility of combining separately developed models and was the forerunner of the Whole-Body Algorithm project. As part of the Whole-Body Algorithm, the thermoregulatory subsystem was validated for both steady-state and dynamic behavior, and the results of these simulations are presented later in this section.

The thermoregulatory model was a useful addition to the Whole-Body Algorithm, primarily because it provided more realistic descriptions of skin blood flow during exercise based on thermal considerations. The capability of the model to predict evaporative water losses was also useful in assessing the importance of this component of water balance in the hypobaric atmosphere of Skylab and during some unusual temperature excursions that were experienced.
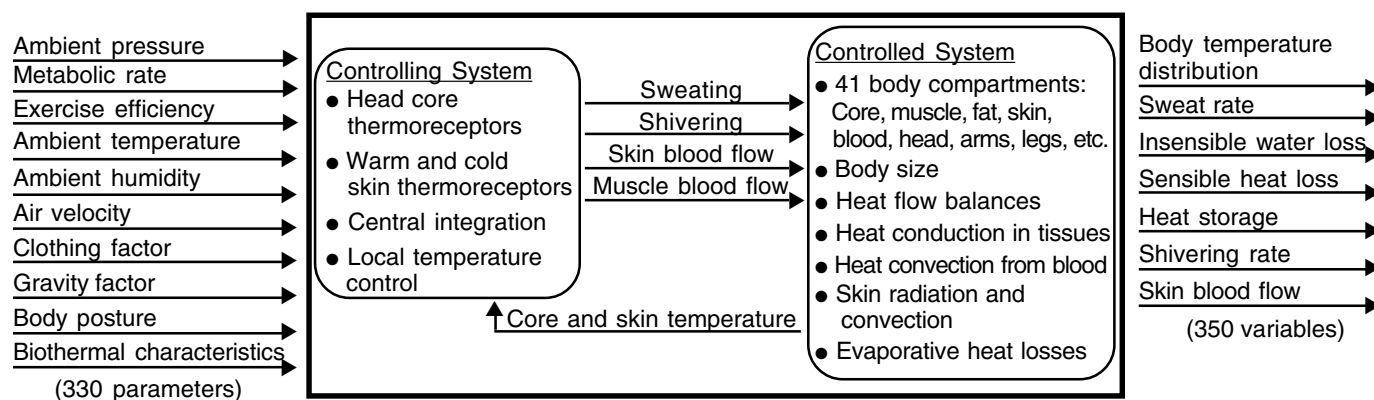
Figure 3-21. Schematic of the thermoregulatory system model.

3.2.2.3 Limitations. Validation studies performed on the thermoregulatory model demonstrated that, as good as the model was, it was not always capable of achieving close correspondence with experimental data when tested over a wide range of stress intensities. In some cases, such as the sweating response to exercise, better agreement was obtained by readjusting several controller sensitivity parameters. Whether such a mechanism is physiologically plausible is not known, although resetting of controller gain is suspected to occur in the thermoregulatory system under certain conditions [40]. In other cases, however, the assumptions used in building the model led to unrealistic responses in certain special situations. For example, blood flow in exercising muscle is assumed to vary in a stepwise fashion with flow proportional to steady-state work rate rather than as a function of local oxygen demand. Another example is the absence of countercurrent heat exchange between large arteries and veins. (A modified countercurrent algorithm was introduced to improve model performance in cool environments (Appendix D)). In addition, the partial inhibition of sweating due to the degree of skin wettedness is not accounted for in the model. This inhibition was suspected to have existed in the Skylab zero-g environment, in which sweat could not drip off the body (see Chapter 4).

3.2.3 Respiratory Control Model

One of the earlier models selected for incorporation into NASA's set of computer models was a description of respiratory control. It was desirable to employ such a model for predicting the respiratory effects of alterations in the artificial gaseous atmosphere of space cabins. The following objectives were formulated for the respiratory model selected for use by NASA. The model should respond to changes in oxygen and carbon dioxide concentrations in inspired gas and respond to exercise ventilatory demand. The model should also be capable of predicting respiratory function in terms of respiratory frequency and minute volume, contain elements to control acid-base status of blood by respiratory compensation, and have the capability to interact with and complement cardiovascular and thermoregulatory models.

Several excellent models were selected for study [41,42,43,44]. Consideration of the previously stated objectives, together with availability, led to selection of the model developed by Grodins and co-workers [45]. The models of Milhorn and co-workers [46,47,48], which are very closely related to Grodins' respiratory model, were in some respects superior to it but were unavailable for immediate use.

Under NASA's sponsorship, the Grodins model was evaluated and modified for spaceflight application [39,49]. The model was originally designed to respond to disturbances in gaseous atmospheres (such as hypoxia and hypercapnia) with the subject in the resting state. The most important structural modifications involved adding an exercise response capability for ventilatory control. Emphasis was placed on the exercise stimulus, since several manned-spaceflight experiments stress man's physiological performance under various exercise levels in an artificial gaseous atmosphere. It was envisioned that this model would appropriately complement the capability of the cardiovascular and thermoregulatory model to simulate exercise and that this synergism would become manifest in the Whole-Body Algorithm. Preliminary studies of these model interactions were performed for the thermoregulatory-respiratory models [39] and for the cardiovascular-respiratory models [50,51].[UPDATE #1]

3.2.3.1 Description of the Respiratory Model.
Grodins' model is a closed-loop control system having a controlled system divided into three compartments corresponding to the lungs, the brain, and the tissue, with a fluid-interconnecting path representing the blood (see Fig. 3-22). A set of differential-difference equations describes a gas transport and exchange system between these compartments. The lungs are treated as a box of constant volume, uniform content, and zero dead space that is ventilated by a continuous unidirectional stream of gas.

The blood passes through the lungs, and after a transport delay, the arterial blood arrives at the brain or tissue compartment. In this model, carbon dioxide (CO_2) and oxygen (O_2) exchange rates are governed by metabolism. If the alveolar respiratory quotient (RQ) differs from unity,

the rates of inspired and expired gas will differ. The time delays associated with transport are not fixed but are realistically based on vascular volume and blood flow rate. The brain compartment communicates with the cerebrospinal fluid (CSF) reservoir by way of a membrane permeable only to respiratory gases. Diffusion rates across the membrane are proportional to their tension gradients. Venous blood exiting from the brain combines with venous blood from the tissue after a time delay to form mixed venous blood. After another delay, this mixed venous blood enters the lungs to complete the cycle of gas transport and exchange. Total cardiac output and local blood flow are considered to vary as functions of arterial CO_2 and O_2 tensions. This assumption is in contrast to that used in Guyton's circulatory model, in which the control of these flows is based only on O_2 tensions (see Chapter 3.2.5).

The actual physiological control system is composed of receptor elements which monitor the chemical concentrations, the afferent nerves that transmit this information to the central nervous system, the respiratory neural centers, the motor nerves of the respiratory muscles, and the respiratory muscles which drive the thorax-lung pump. In this model, the chemical concentrations at receptor sites are used to adjust the respiratory rate. The equations governing the controller system permit inspired ventilation to vary as a function of the hydrogen-ion concentration (pH) in the cerebrospinal fluid and in the arterial blood as well as the arterial blood oxygen partial pressure (pO_2). A mathematical description of acid-base buffering relates blood CO_2 levels and blood pH. The control of respiration is still a subject of controversy, and this model can accept various control functions other than the one originally proposed by Gordins. Thus, the model easily enables evaluation of different basic respiratory control concepts.

3.2.3.2 Modifications.
The original respiratory model developed by Grodins and his associates has been modified to include the effects of performance of physical work on respiratory parameters. A simplified overview of the changes made to Grodins' original model is given in Fig. 3-23. Work performance in the respiratory model primarily affects metabolic rates (oxygen uptake), cardiac output, and alveolar ventilation. The steady-state and dynamic responses for an adult human exercising on a bicycle ergometer at a fixed useful work rate have been determined experimentally by Åstrand and Rodahl [52], Whipp [53], and D'Angelo and Torelli [54]. Simple approximation to their data leads to expressions used in this model. Figure 3-23 suggests that both neural and chemical control are involved in the ventilatory and flow responses. However, there are still some uncertainties as to the degree of neural control in the "on and off" transient responses in ventilation.[UPDATE#2] The functional expressions which simulate this component do not actually describe the physiology involved, and more realistic modeling requires experiments that clarify ventilatory control. The complexities of the interactions between neural and chemical control are manifested during exercise. The individual must increase ventilation to a level sufficient to provide the
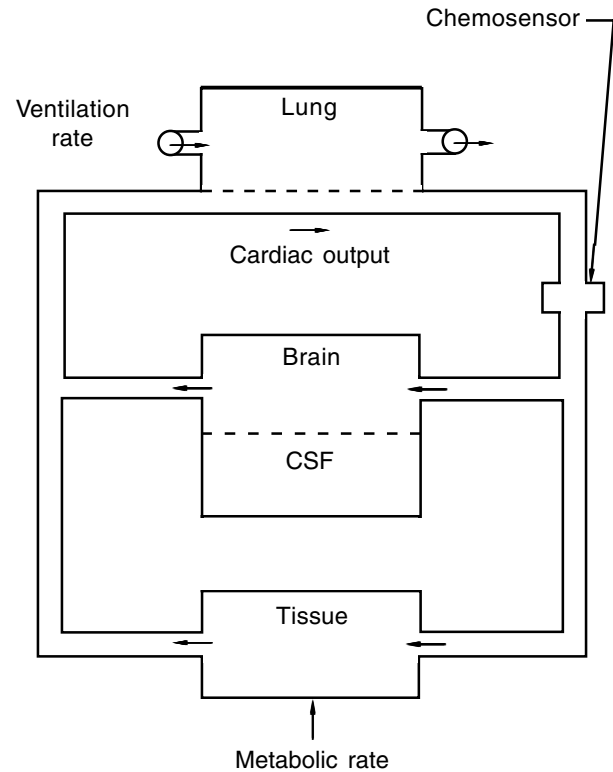
Figure 3-22. Controlled system of the respiratory model. Blood oxygen, carbon dioxide, and hydrogen-ion concentrations are affected by lung ventilation and metabolism. These quantities are continuously monitored by the chemosensor.

additional oxygen intake and carbon dioxide venting demanded by the body's high level of exercise metabolism.

A schematic of the modified respiratory model is given in Fig. 3-24. The output responses of this model include minute volume, frequency of respiration, brain blood flow, and chemical factors (pH, CO_2, and O_2). The fidelity of cardiac-output and heart-rate descriptions in the modified respiratory model differs from that provided by the cardiovascular model. These quantities are provided by the cardiovascular model in the Whole-Body Algorithm.

The strength of the Grodins model lies in its detailed consideration of respiratory chemistry, including the interactions between the O_2 and CO_2 dissociation and bicarbonate buffering. These pathways, which have the ability to "blow off" metabolically produced CO_2, allow the respiratory system to effectively regulate CO_2 and O_2 levels. That is, a change in CO_2 level or a decrease in O_2 level brings about regulatory effects through ventilatory and circulatory parameters.

The model is primarily suited for short-term stress responses lasting not much longer than a half hour. Fortunately, human subjects can approach a new steady-state response within that period for many gaseous and exercise stresses.

3.2.3.3 Simulations.
The basic model as developed by Grodins is capable of responding to disturbances away
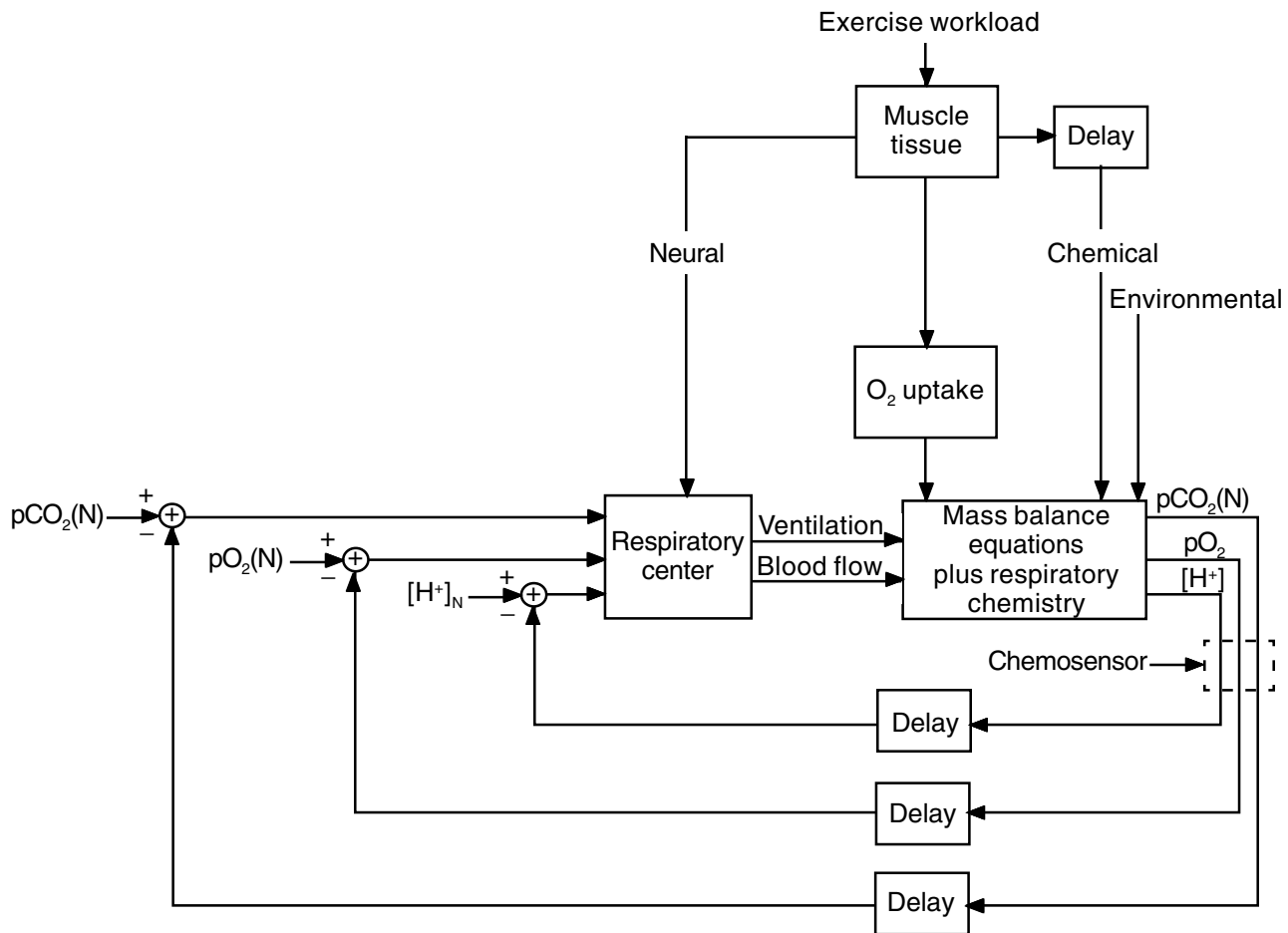
Figure 3-23. Block diagram of respiration control model as modified for exercise. The blood gases and hydrogen-ion concentrations are monitored by the chemosensor and their values compared to the normal set-point value (N).
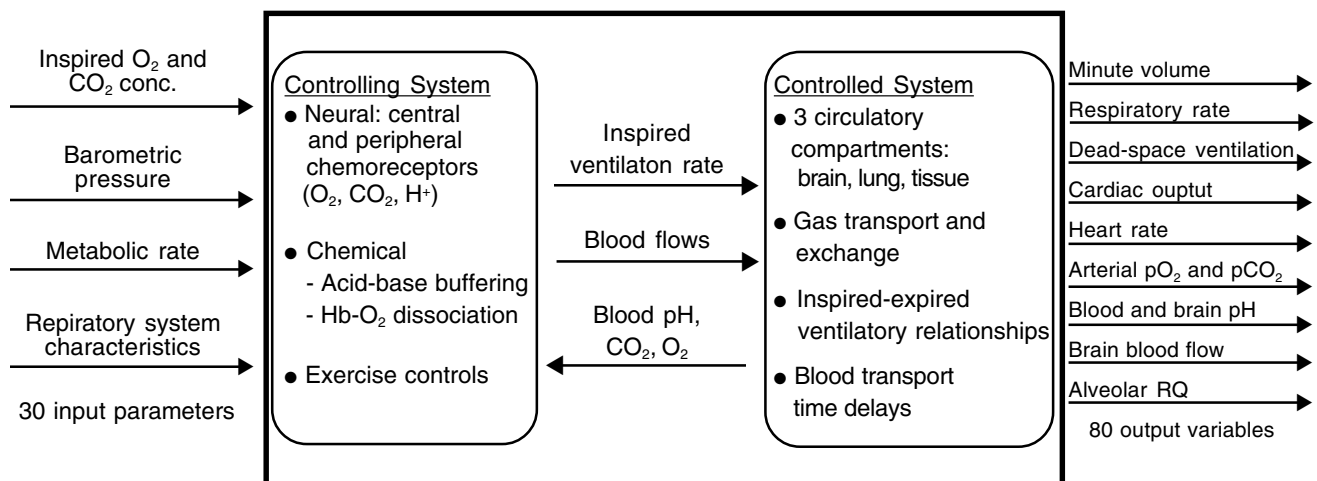
Figure 3-24. Schematic of the respiratory system model.
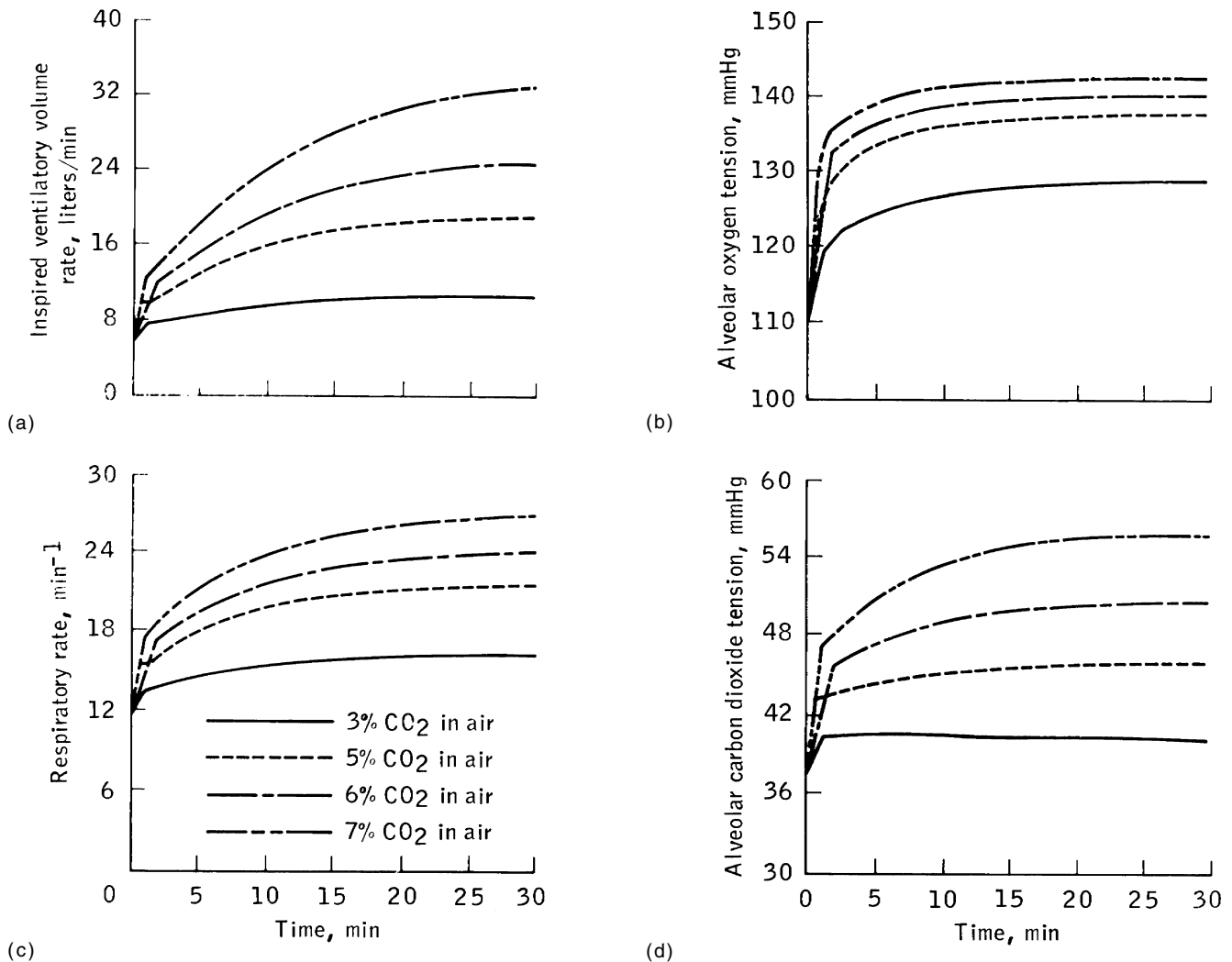
Figure 3-25. Transient responses of the respiratory model to step changes in varying levels of inspired carbon dioxide. (a) Inspired ventilatory volume rate; (b) Alveolar oxygen tension; (c) Respiratory rate; (d) Alveolar carbon dioxide tension.

from the normal resting state, including changes in barometric pressure; in gas composition (i.e., inspired gas fractions, in blood hemoglobin content) and in brain, blood, tissue, and CSF bicarbonate concentration. Simulations of these conditions were reported by Grodins et al. [45] and Gallagher [49]. An example of the model's dynamic responses to varying levels of inspired CO_2 is given in Fig. 3-25. These responses compare favorably with those measured experimentally [47]. Steady-state responses of the respiratory subsystem for hypoxia and hypercapnia are illustrated in a later section as part of the Whole-Body Algorithm validation (see Fig. 3-44).

The added modifications provide the capability to respond to different levels of work, as illustrated in Fig. 3-26. When a transition in exercise level occurs, inspired ventilation is controlled in the simulation by a fast neural component and a slow linear component, related to oxygen consumption. At rest, a control function that consid-

ers changes in blood oxygen, carbon dioxide, and hydrogen-ion levels appears adequate to account for respiratory regulation during such stresses as hypoxia, hypercapnia, or acid-base disturbances. However, blood chemical sensor control does not appear to fully explain the exercise response as can be inferred by the chemical responses shown in Fig. 3-26. Exercising subjects ventilate at rates which exceed increases that could be caused by arterial O_2, pH, and CO_2 alone. Therefore, there appears to be a form of neurogenic control. This control is represented empirically in the model, but it is not well understood.

The first manned space cabins (i.e., Mercury, Gemini, Apollo programs) were equipped to provide a hyperoxic environment (100% O_2 at 1/3 atmosphere) with the CO_2 level maintained by canisters of lithium hydroxide. It was important to ascertain the human responses to breathing in this artificial atmosphere and also to establish toler-
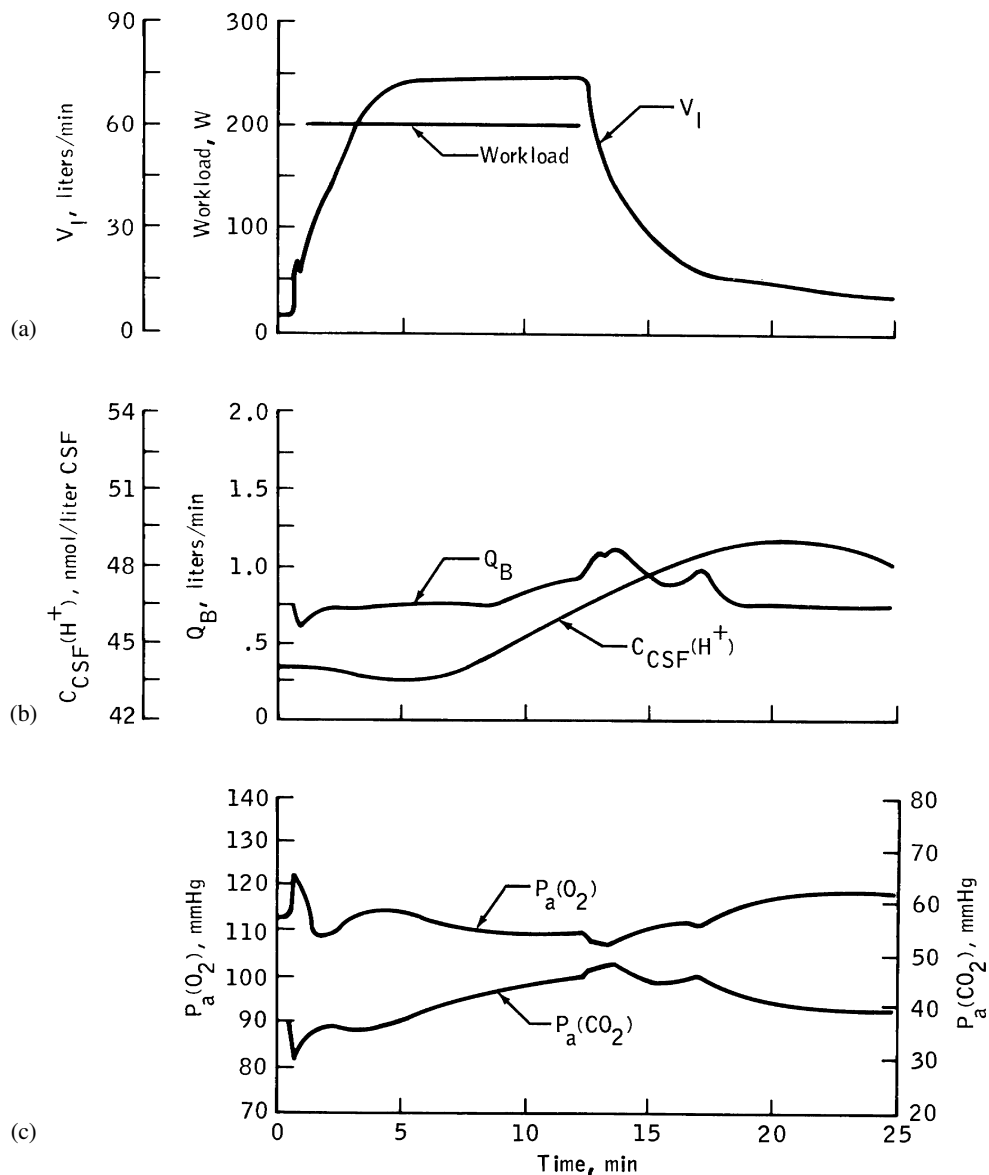
Figure 3-26. Selected variables from the respiratory system simulation of an exercise (workload) excitation using exercise modifications. (a) Inspired ventilatory volume rate V_I and workload; (b) CSF bicarbonate concentration $C_{CSF}(H^+)$ and brain blood flow rate Q_B; (c) Alveolar carbon dioxide tension $P_a(CO_2)$ and alveolar oxygen tension $P_a(O_2)$.

ance levels in the event of failure of the life support system. Computer models of respiration had the potential to assist in predicting human responses and in designing atmospheric control devices as previously described for the thermoregulatory system. However, the Skylab cabin was maintained at nearly normal CO_2 levels, and the CO_2 levels were maintained within design specifications by the efficient regenerable molecular sieve system. In the analysis of Skylab data, there was little need to expect an abnormal respiratory response either at rest or during exercise on the basis of atmospheric factors. As a result, the respiratory computer model by itself received relatively little attention during this modeling activity by comparison to

the other models. Nevertheless, the Whole-Body Algorithm would have been incomplete without the inclusion of the respiratory subsystem model, particularly for simulating exercise responses. The respiratory model provided a more detailed analysis of head blood flow than was available from other subsystems, and it added the capability to study the concentration of respiratory factors to the total exercise response in altered environments.

3.2.4 Erythropoiesis Regulation Model

A mathematical model was developed for use as a tool to investigate the relative influence of the controlling factors of erythropoiesis on total red blood cell (RBC) mass.
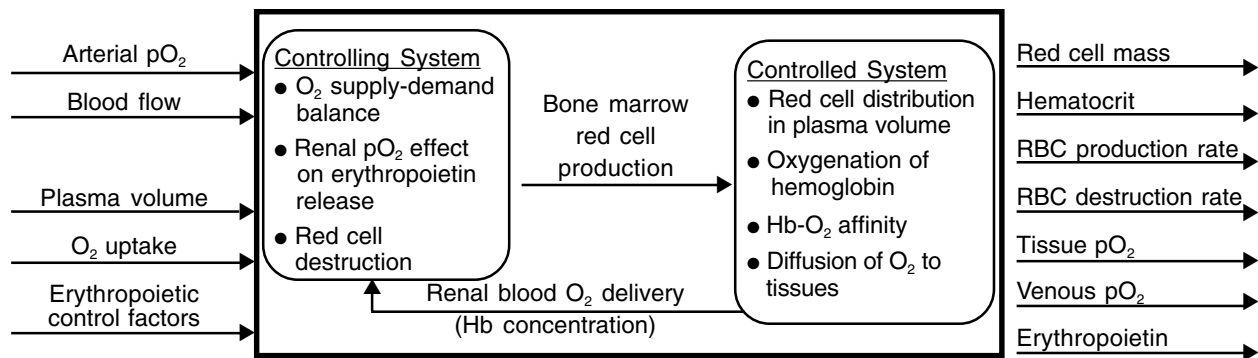
Figure 3-27. Schematic of the erythropoiesis control system model.

The loss of red cell mass has been a consistent finding during spaceflight and certain ground-based analogs of weightlessness such as bedrest. Computer simulation of this phenomenon required a model that could account for oxygen transport, red cell production, and red cell destruction.

The control of erythropoiesis is amenable to a modeling approach, as demonstrated by a variety of investigators. These models have ranged from conceptual, qualitative feedback schemes [56,57] to more detailed mathematical descriptions [58], some of which have led to computer simulation models [10,59]. Quantitative models have been developed for different aspects of erythropoiesis regulation, including ferrokinetic models [60,61] and those describing the control of stem cell production [62,63,64].

A limited number of models are available that integrate the entire feedback circuit in sufficient detail to enable quantitative simulation of diverse hematological stresses directly affecting oxygen transport, tissue oxygenation, erythropoietin release, and red cell production. Hodgson [58] has proposed such a model but apparently has neither implemented it for computer use nor performed the studies necessary for validation. An algorithm capable of predicting red cell mass changes by feedback processes was coupled to a much larger model of circulatory and fluid control [10], but it provided only a gross representation of the renal/bone-marrow axis and failed to recognize renal oxygenation as a major control element. The most complete simulation model previously developed is that of Mylrea and Abbrecht [59]; this model was validated for a single stress (altitude hypoxia in mice).

A review of the factors that control erythropoiesis and of existing models led Leonard to the formulation of a conceptual model and eventually the design and development of a computer model [65]. The initial structure was derived from the best features of the mathematical models of Guyton et al. [10], Hodgson [58], and Mylrea and Abbrecht [59]. The model has a wide range of applicability; the most important application is its simulation of spaceflight events.

3.2.4.1 Description of the Erythropoiesis Model.
Those elements in the feedback regulation loop that have been incorporated into the model are shown schematically in Fig. 3-27. The formulation is based on the accepted concept that erythrocyte production is governed by the balance between oxygen supply and demand in the body and, in particular, at a renal sensing site. The mechanisms and pathways of the control circuit include oxygenation of hemoglobin and oxygenation of tissues by blood transport and diffusional processes. An erythrocyte-stimulating hormone, erythropoietin, is produced and released at a renal site in amounts that vary inversely with the levels of tissue oxygen tension (pO_2). Plasma levels of erythropoietin control the production of erythrocytes in the bone marrow. The amount of circulating red cell mass is based on the addition of new cells to existing cells with allowance for the destruction of older cells. Blood hematocrit, an index of red cell concentration in whole blood, is determined by dividing the circulating red cell mass by the plasma volume. Other features of the model include an oxygen-hemoglobin affinity, which can be varied, and time delays that represent time for erythropoietin distribution in plasma and time for maturation of erythrocytes in the bone marrow.

In terms of control system theory, the controlled system includes the elements of redistribution of new cells, lung oxygenation, blood transport, and tissue oxygen extraction, whereas the controller system consists of erythropoietin release, marrow red cell production, and splenic destruction. The hematocrit (or hemoglobin level) may be considered to be the primary feedback quantity, and the level of tissue oxygenation can be taken as the directly controlled variable. Figure 3-27 indicates the input parameters that have been found most useful in these studies, as well as the predicted output responses that the model is capable of generating. Appendix B and Chapter 6 contain a more complete description of the model system and its applications.

3.2.4.2 Sensitivity Analysis.
The effect of variation of the model parameters on the overall behavior of the system can be studied by sensitivity analysis techniques (see Appendix E). Sensitivity analysis is a systematic method of evaluating the relative importance of different parameters, one at a time, by small increments around the normal control state. Table 3-6 contains the percent change in one dependent variable (red cell production rate) caused by a 1% decrease in the model parameters (shown in the left column) and determined after a new steady-state con-

Table 3-6. Steady-State Sensitivity Coefficients of the Erythropoiesis Regulatory Model*

Parameter	Change in red cell production (percent)
Oxygen uptake, V_m	–4.55
O_2-Hb affinity, P_{50}	3.90
Capillary diffusivity, K_d	3.25
Blood flow, Q	1.45
Mean corpuscular hemoglobin concentration, $MCHC$	1.45
Hemoglobin O_2 carrying capacity, $CHbO$	1.45
Arterial O_2 tension, P_aO	1.10
Plasma volume, PV	–0.90
Red cell half-life, $TRHL$	0.85
Controller gain, G	–0.03

* Values shown are percent change in red cell production at steady state due to a 1% decrease in parameter value.

Figure 3-28. Hypoxic response of erythropoietic model to a 10% constant load disturbance (i.e., step change) of various parameters. Algebraic sign in legend refers to direction of change in each parameter. These simulations are useful for demonstrating dynamic behavior of model and relative sensitivities of important parameters. See Table 3-6 for the definition of each parameter.

dition was reached. Positive values of these coefficients indicate a response to hypoxic conditions, and negative values indicate a response to tissue hyperoxia. In each case, the response is in a direction that agrees with the concepts of erythropoiesis regulation [66]. The unusually high influence of oxygen uptake on red blood cell production indicated may not be representative of the real intact system. Compensatory action by cardiorespiratory factors usually intervene to normalize oxygen transport and thereby limit the correction required by the erythropoietic system (Appendix B). However, this analysis does support the assertion that P_{50} shifts can dramatically augment tissue oxygenation [67,68].

The results from a dynamic sensitivity analysis are illustrated in Fig. 3-28. In this case, the six most important parameters were changed by 10% in a direction that would initiate a hypoxic response. The dynamic behavior of four important dependent system variables during this constant load disturbance is shown over a period of 30 days. It is apparent that the general ranking of parameter importance found in the steady state is maintained for the dynamic state as well. If, however, a new equilibrium state was simulated for a specific hypoxia condition and sensitivity coefficients were obtained by small perturbations from that state, both the magnitude and the ranking of the coefficients might be altered. Such behavior would not be unexpected for a nonlinear control system.

Figure 3-28 also illustrates the wide difference in dynamic properties of the various elements in the model. This model may be viewed as consisting of four sequential processes, each with a characteristic time constant that is correspondingly longer with respect to alterations in tissue oxygenation (seconds to minutes), erythropoietin release (hours), red cell production (days), and red cell mass (days to months). An interesting prediction of these simulations is that the dynamic characteristics of the hypoxia response are similar for a variety of constant load disturbances, whether it is an increase in plasma volume

or a decrease in renal flow rate. Unfortunately, the experiments required to confirm this conclusion are difficult to perform. These simulation results should, therefore, be considered as model-to-model comparisons that demonstrate that the model responds appropriately in a gross sense to both equilibrium and dynamic states.

3.2.4.3 Model Validation. Model-to-data comparison is a more challenging validation process that must be used to establish ultimate credibility of any model system. The erythropoiesis control model has been validated for long-term altitude hypoxia.

Buderer and Pace [69] studied the dynamic changes in red cell mass, hematocrit, and plasma volume in sealevel pigtailed monkeys during 6 months at 3800 meters altitude followed by descent to sea level for 3 months. Comparable data for human subjects were not available. However, the human model would not be expected to be fundamentally different from that for a monkey at sea level, especially if responses are expressed as normalized val-
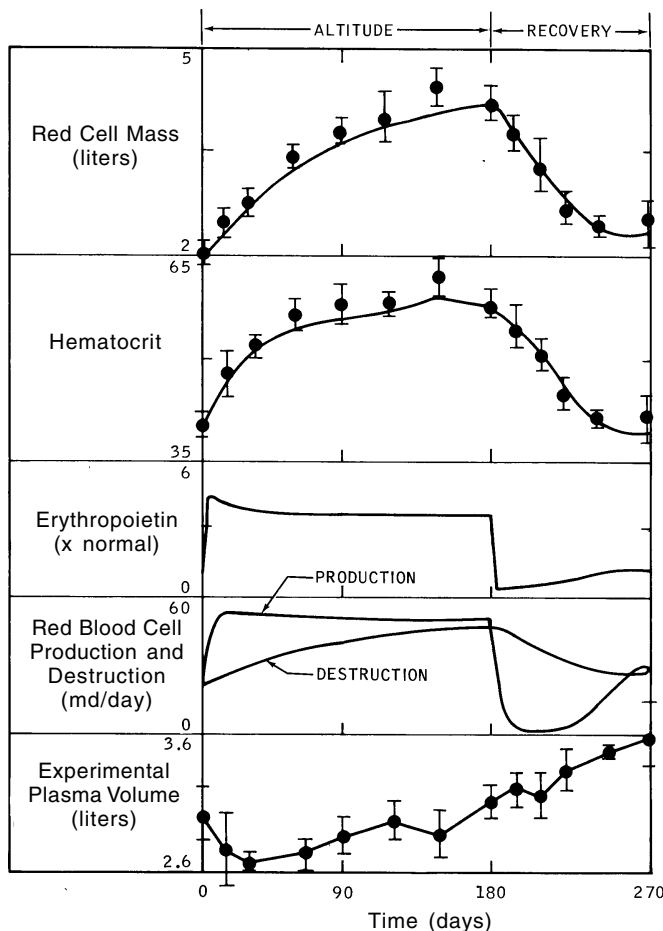
Figure 3-29. Simulation of altitude hypoxia and descent to sea level (solid lines) Experimental data from pigtailed monkeys (filled circles plus or minus standard error) [69]. Hypoxia was simulated by reducing arterial oxygen tension from 95mmHg (sea level value) to 50 mmHg. At 180 days, arterial oxygen tension is returned to 95 mmHg. Experimental plasma volumes (bottom curve) were also used to drive model.

ues. The major driving function for the model was an arterial blood oxygen tension of 50 and 95 mmHg for the altitude and sea-level phases, respectively. The model's response was adjusted using the bone marrow controller gain until a visual "best fit" was obtained. This is an example of parameter estimation (see Appendix A). The comparison of model output and data are illustrated in Fig. 3-29. In combination with the arterial blood oxygen tension, the experimentally determined change in plasma volume (bottom curve) was used as a driver for the simulation, but the effect on the overall response system for this secondary load input was relatively small.

In addition to predicting the measured dynamic changes of red cell mass and hematocrit, the model is capable of predicting other system variables that were not measured, such as plasma erythropoietin and red cell production-destruction rates. The simulation shows the general sequence of events, generally assumed to characterize

the hypoxic response, including tissue hypoxia (not shown), elevated erythropoietin, and augmented red cell production levels, which increase the mass of circulating blood cells [70,72]. Figure 3-29 also shows the opposite scenario for the descent phase. The difference between production and destruction rates provides a visual indication of the dynamic behavior of deviation from steady state. The slow approach to equilibrium at altitude is also evident from the asymptotic nature of the measured quantities. Upon return to sea level, the increased hematocrit serves as a prolonged stimulus for tissue hyperoxia to the extent that red cell production may be totally inhibited for several weeks.

The erythropoietin response in humans and mice during hypoxia is known to return toward control more rapidly than indicated in Fig. 3-29 [70,73]. Adaptive mechanisms of the circulatory, ventilatory, and biochemical systems respond to hypoxia and thereby improve oxygen transport faster than does the more sluggish erythropoietic system [74]. Several simulations were performed to test the hypothesis that some of these pathways contribute to the observed erythropoietin response. Figure 3-30 illustrates the relative influence of three adaptive mechanisms (an increase in pO_2 due to greater ventilation efficiency, a decreased plasma volume, and a diminished oxyhemoglobin affinity) as predicted by the model. These simulations, although not strictly a validation study, not only illustrate a more realistic response for erythopoietin but also indicate the manner in which simulation techniques can be used to test hypotheses regarding physiological mechanisms.

3.2.4.4 Mouse Model. Experiments with animals are routinely conducted in support of spaceflight biomedical investigations. In particular, mice have been examined for their potential use as experimental models for the study of the early erythropoietic disturbances found in astronauts [75]. The desirability of using a species-specific model of erythropoiesis for predicting experimental results with animal subjects prompted the formulation of a "mouse model." This model was based on the human model but incorporated parameter values that describe the unique characteristics of the oxygen transport and erythropoietic system for the mouse. Thus, red cell lifespan, arterial oxygen tension, oxygen-hemoglobin affinity, and many other parameters were found to differ significantly from the human [76].

The mouse model, described in Appendix B, was validated in a preliminary study by examining its responses to hypoxia [75] and to erythropoietin infusions [77]. An example of the dynamic behavior of the mouse model is provided in Fig. 3-31. In this simulation, a pulse decrease in arterial oxygen tension results in a corresponding disturbance in tissue oxygen levels, followed by a short burst of erythropoietin and a resulting wave of erythropoiesis, the effects of which may last 2 weeks or longer. The transient nature of red cell production shown here has been previously observed after injecting erythropoietin into mice [78]. A similar simulation performed with the human model results in more prolonged effects, as indicated in
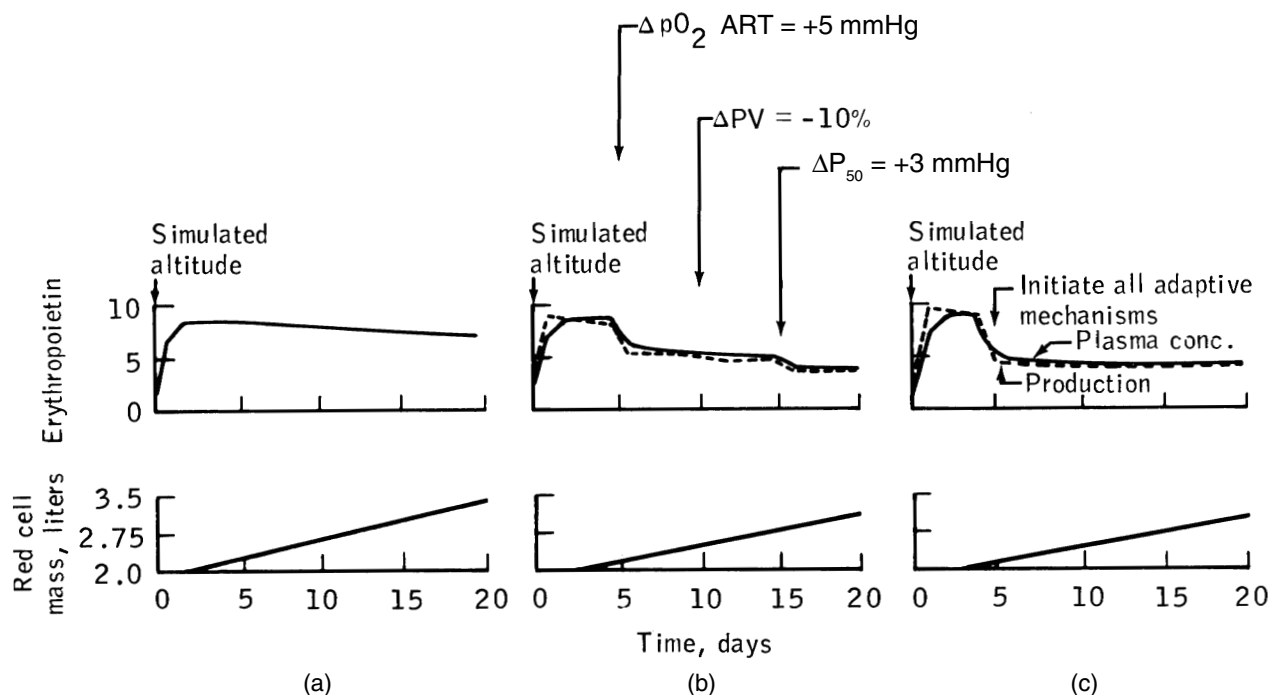
Figure 3-30. Simulations of altitude hypoxia showing effect of three adaptive mechanisms (see text). Models can be useful in studying several simultaneous stresses either in combination or acting alone. Simulated altitude = 4000 meters, pO_2 ART = arterial oxygen tension, PV = plasma volume, P_{50} = parameter describing oxygen-hemoglobin affinity. (a) No adaptive mechanisms; (b) Stepwise addition of three adaptive mechanisms; (c) Combined effect of three mechanisms. The dynamic behavior of erythropoietin illustrated in panel (c) is much closer to the experimentally measured response than is panel (a) [70].

Fig. 3-31. These differences result primarily from the shorter erythropoietin disappearance rates, red cell lifespan, and erythropoietin half-life in the mouse when compared to the human. Simulations such as this suggest that some information regarding erythropoiesis may be obtained in a shorter time interval using the mouse as an experimental model of the human.

3.2.4.5 Other Simulations. Although the major purpose of the erythropoiesis regulation model was to investigate mechanisms related to the loss of red cells during space-flight, other applications have been investigated to validate the model, to test hypotheses, and to introduce refinements. Table 3-7 is a summary of the major simulations accomplished with the human and mouse models. Human bedrest and mouse dehydration studies have been found to be useful experimental analogs of spaceflight effects. A more recent area of model development is in the simulation of hematological disease states that have known physiological etiologies (such as anemias, polycythemias, and abnormalities in hemoglobin functions). Toward this end, a steady-state model based on the dynamic model described previously has been formulated. A program is now in progress to developed a teaching model of patho-physiology based on the human red cell model [65].

3.2.4.6 Limitations. The erythropoiesis control system model is the least complex of all the models used in this project. Various features have been added during its development to increase its simulated realism. These have included elements representing erythropoietin release, cell maturation time delays, and a variable oxygen-hemoglobin affinity. Other limitations have been identified which either are acceptable within the scope of this program or form the basis for suggested improvements. These limitations are summarized here.

1. Red cell production is modulated by factors other than those considered in the model. These include iron levels, hormones other than erythropoietin, and neural stimulation, as well as inhibitors and activators of erythropoietin. Although it may be desirable to include these effects in future model applications, quantitative information regarding them is presently lacking or the need for their inclusion is not yet warranted.
2. The model has a limited representation of bone marrow red cell production. For example, it does not include the full maturation cycle from multipotential cells to denucleated red cells. Furthermore, it has no means of predicting reticulocyte index.
3. The model does not include extrarenal erythropoietin production or extramedullary erythropoiesis. These factors are of much greater importance in the mouse than in the human. However, sufficient quantitative information is lacking for inclusion in a mathematical model.
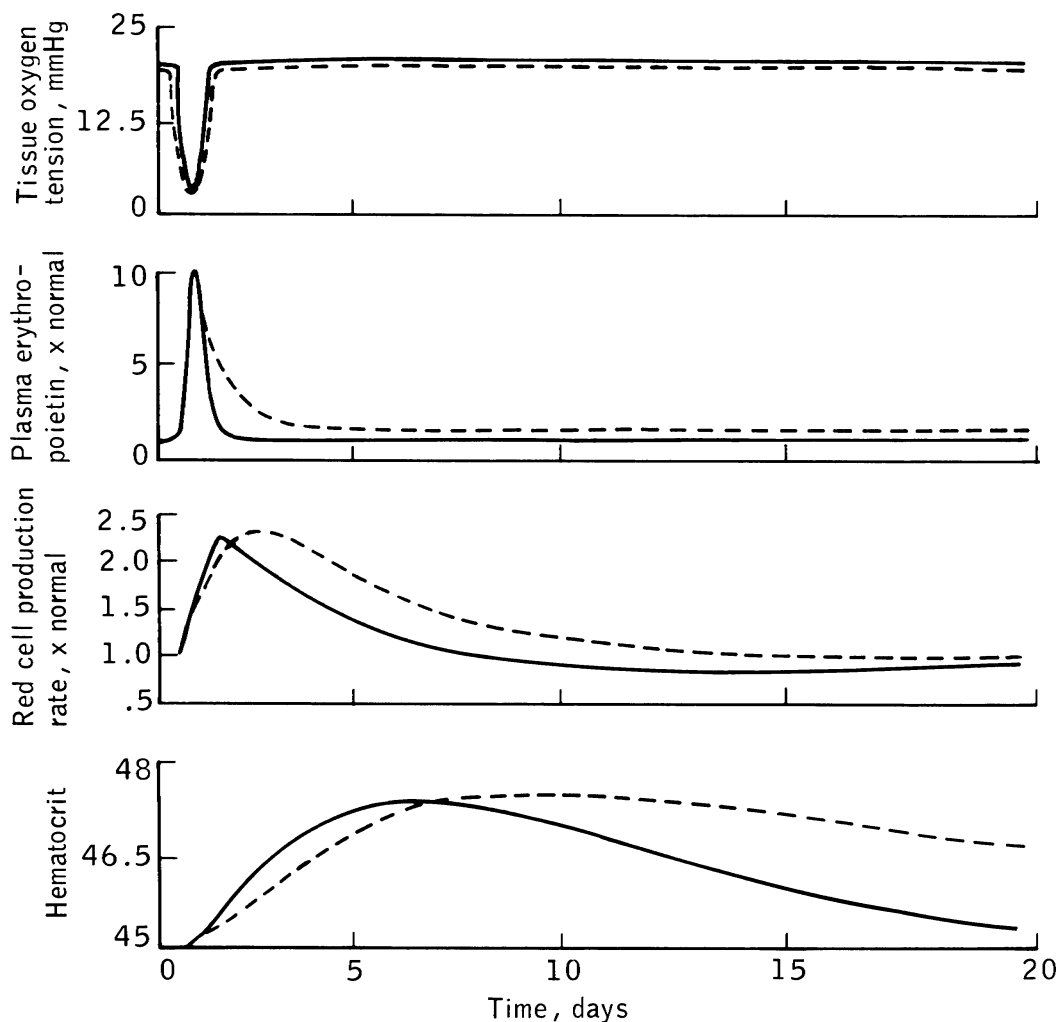
Figure 3-31. Simulation response to a pulse decrease in arterial oxygen tension for the mouse model (solid line) and the human model (dashed line).

4. Blood viscosity and blood volume changes are known to influence blood flow and, thereby, issue oxygenation. These effects are not explicitly represented in the model [87,88].

5. Overall oxygen transport is under the control of homeostatic mechanisms in addition to the erythropoiesis system. Thus, some of the fixed parameters of the model such as blood flow, capillary diffusivity, arterial oxygen tension, plasma volume, and oxygen-hemoglobin affinity can be considered variable elements of circulatory, ventilatory, biochemical, and fluid regulatory feedback mechanisms that are beyond the scope of the present model's design objectives.

Although these mechanisms are not included explicitly in the present erythropoiesis model, their influence can be tested, in most cases, by manual alteration of existing model parameters. Larger models (such as Guyton's model discussed next) that incorporate many of these features are available, and these have been shown to be com-

patible with an erythropoiesis subsystem model. In fact, the erythropoiesis model just presented was inserted into the Guyton model to replace the existing inferior algorithm for red cell production (Appendix C). As a result, performance of the Guyton model was enhanced.

3.2.5 Model of Circulatory, Fluid, and Electrolyte Control

Physiologists have long recognized the intimate relationship between circulatory function and fluid-balance function. Early in the manned spaceflight program, the biomedical investigators of NASA identified the need to monitor these systems for their involvement in the fluid redistribution in microgravity and the orthostatic intolerance usually accompanying recovery. With the extension of flight duration from weeks to months, the need to examine the long-term adaptive responses of both the circulatory and fluid-balance systems with systems analysis and simulation models was proposed by a National Academy of Sciences panel [89].

Table 3-7. Computer Simulation Studies Performed With Erythropoiesis Model

Study	Duration, days	Source
Human model		
Altitude hypoxia and descent	270	Ref. [69]
Altitude hypoxia	6	Ref. [72]
Red cell infusion	120	Ref. [79]
Bedrest	35	Refs. [80,81]
	14, 28	Ref. [82]
Skylab	59, 84	Ref. [83]
Clinical conditions:	Long term	Ref. [84]
Anemia		
(primary, secondary, hemolytic)		
Polycythemia		
(primary, secondary, hypoxic)		
Abnormality (hemoglobin)		
Mouse model		
Multiple sequential		
erythropoietin infusion	7	Ref. [78]
Altitude hypoxia	28	Ref. [73]
Dehydration and recovery	7	Ref. [75, 85]
Red cell infusion	3	Ref. [86]

The following objectives were established for a model of body fluid regulation. The desired model should:

1. Be capable of predicting the volume and electrolyte composition of the major fluid compartments, including plasma, interstitial, and intracellular fluid compartments;
2. Contain the appropriate capillary and membrane interfaces between these compartments and the capability to simulate exchange of fluids and electrolytes under the influence of hydrostatic, oncotic, osmotic, and active transport forces;
3. Contain representation of at least two of the major body cations:sodium (extracellular ion) and potassium (intracellular ion);
4. Contain a representation of the kidney with sufficient detail to predict realistic urine excretion of salts and water under such conditions as fluid/salt loading and restricted fluid intake;
5. Contain neural, hormonal, and hemodynamic feedback control pathways regulating the volume and composition of the extracellular fluid compartment;
6. Contain a circulatory system with sufficient detail to realistically simulate blood pressures, flows, and volumes in arteries and veins during acute and long-term disturbances such as hemorrhage and infusions;
7. Contain an autonomic system with efferents sensitive to blood pressure, plasma osmolarity, and tissue oxygenation and with afferents for controlling blood flow and pressures, hormonal secretion (antidiuretic hormone (ADH), angiotensin, and aldosterone), and body water, the latter by thirst and renal mechanisms;
8. Contain a representation of adaptation effects (both

active and passive) in the heart, vessels, and pressure receptors for controlling long-term blood pressure disturbances.

As this list of objectives suggests, the complete specification of a fluid-electrolyte regulatory system requires the inclusion of several fluid compartments that are controlled by the kidneys acting in conjunction with the endocrine and circulatory systems. An important part of the model selection phase of this project was directed toward identifying models that contained these subsystems or, alternatively, searching for fluid-electrolyte models that could be used to complement existing circulatory models [90,91]. With regard to the latter approach, most of the mathematical models with the required fidelity to simulate responses to circulatory disturbances were relatively short-term models and did not have the elements necessary to account for changes in fluid balance. On the other hand, the models of fluid-electrolyte regulation had representations of cardiovascular function that were highly simplistic or absent altogether.

The renal system is perhaps one of the most complex body systems amenable to a mathematical modeling approach. When the model identification search was initiated, few models were available that contained an adequate representation of the fluid-electrolyte regulating capability of the renal system. Some of the most detailed models of the kidney were presented as complex mathematical formulations unaccompanied by numerical solutions and they, therefore, remained conceptual in nature [92,93,94]. The model of DeHaven and Shapiro [95,96] contained excellent representations of the relationships between more than 100 chemical species in several fluid compartments but was devoid of dynamic regulation as well as direct representations of the circulatory, neural, and endocrine systems. Other models considered a number of important conceptual ideas but had characteristics that limited their applicability [97,98]. Other models of fluid and electrolyte balance include those of Cameron [99], Toates and Oatley [100], and Badke [101]; these were unavailable for consideration in this project and are mentioned here merely for completeness.

The most comprehensive model of fluid and electrolyte control available, and one which satisfied the requirements of the project, was that developed by Guyton and co-workers [10,102,103,104]. This model has been particularly useful in the NASA physiological simulation project, and it formed the cornerstone of the Whole-Body Algorithm. At the time of its formulation, it was perhaps the most complex physiological mathematical model in existence. There have since been few such comprehensive attempts to subject long-term, whole-body biochemical and circulatory function to the rigors of systems analysis and mathematical modeling, which are not directly, related to the fundamental work of Guyton.

3.2.5.1 Description of the Guyton Model. The systems analysis of overall circulatory regulation as developed by Guyton involves a large number of physiological
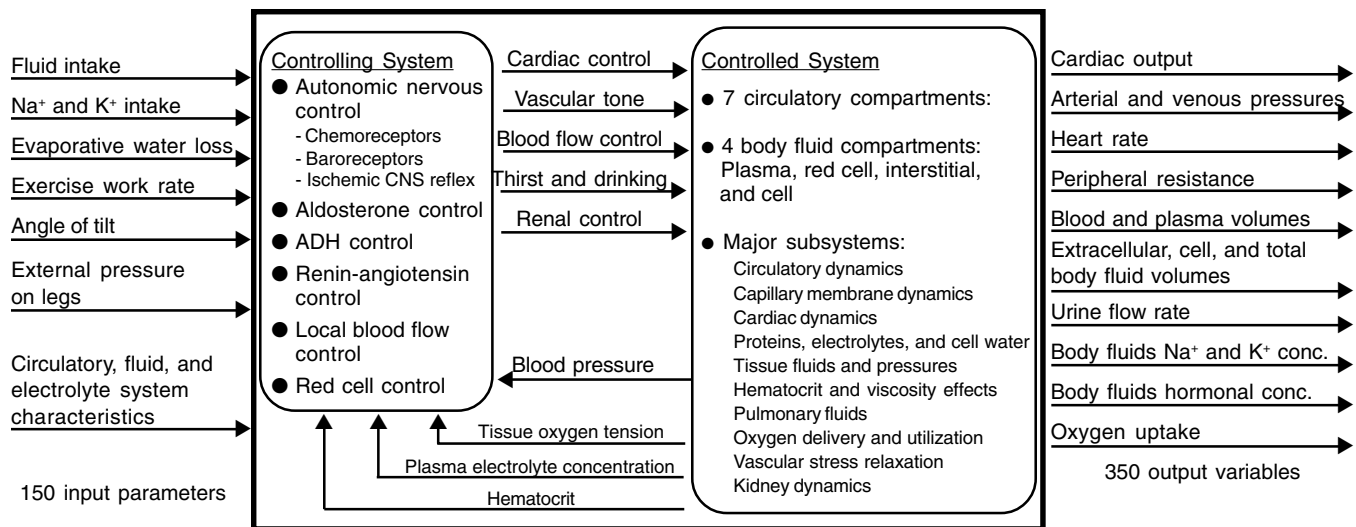
Figure 3-32. Schematic diagram of the circulatory, fluid, and electrolyte regulatory model.

subsystems. The current model, illustrated in Fig. 3-32, is based on cumulative knowledge of the circulation and on experimental data. A model as complex and encompassing as this one is difficult to summarize in one or two diagrams; detailed flow charts and model explanations are available elsewhere [10,90,104,105]. Schematic diagrams are included in the following pages, and a more detailed analog circuit diagram is included in Appendix C.

The relevant physiological systems have been divided into 18 major subsystems, each describing some important physiological aspect of circulatory, fluid, and electrolyte control (Fig. 3-33). The circuit of blood flow in the original model is divided into five volume compartments:arterial volume, venous volume, right atrial volume, pulmonary venous volume, and combined left atrial and pulmonary venous volume (Fig. 3-34). Cardiac output is calculated from function curves, whereas other flow rates are calculated from simple pressure-resistance relationships. Arterial-venous flow is determined by summing flow through three parallel circuits (muscle, renal, and other).

The circulation is not closed but "leaks" through the capillaries, "excretes" through the kidneys, and "drinks" directly into the blood. Fluid intake is controlled by plasma osmolarity and tissue oxygen tension. Fluid excretion is based on glomerular filtration and the action of ADH. The blood, composed of plasma (with dissolved proteins and electrolytes) and red blood cells, serves as a filterable fluid. Other fluid-volume compartments include the interstitial compartment (composed of a gel volume and free fluid volume), the intracellular volume, and pulmonary fluid volume. The relationships between these compartments are illustrated in Fig. 3-35. The capillary filtration rate is determined from a whole-body version of Starling's relationship, which states that net filtration pressure is equal to capillary pressure plus tissue colloid osmotic pressure, minus interstitial fluid pressure, and minus plasma col-

loid osmotic pressure. Lymph flow rate is calculated from free interstitial fluid pressure, total tissue pressure, and lymphatic pumping. Flow into the pulmonary reservoir is obtained by subtracting pulmonary lymph return from pulmonary capillary filtration. Protein (colloid) is produced and lost by the body and is distributed between the interstitial space and the plasma. The representation of the interstitial fluid compartment reflects the years of study by Guyton and co-workers which revealed the importance of the gel-free fluid matrix and sub-atmospheric pressures of this compartment in controlling edema and transcapillary filtration [106]. Fluid flows into the cells are assumed to occur by osmotic imbalance between extracellular and intracellular fluids.

Two electrolytes are considered in the model. Sodium is distributed evenly in the extracellular fluid, and potassium is stored primarily in the intracellular fluid with allowance for active transport from the extracellular to the intracellular compartments. Dietary intake of both these electrolytes is considered as well as renal excretion, the latter being controlled in large part by a renin-angiotensin-aldosterone mechanism. The pathways that regulate fluid and electrolyte balance are described in more detail in Chapter 5.

The model uses basic cardiac function curves modified by the effects of autonomic stimulation, arterial pressure after-load, and cardiac hypertrophy or degeneration of the pumping ability of the heart. The unstressed volumes of each capacitive region are controlled by the level of autonomic stimulation, the level of angiotensin in blood, and the pressure in the veins (through stress relaxation). The flow resistances are controlled by a combination of local effects and hormonal effects. The oxygen transport features of the circulation are present, and hematocrit and red cell control are considered. The autonomic system included is basically regulated by mean blood pressure and tissue oxygen tension and includes the effects of
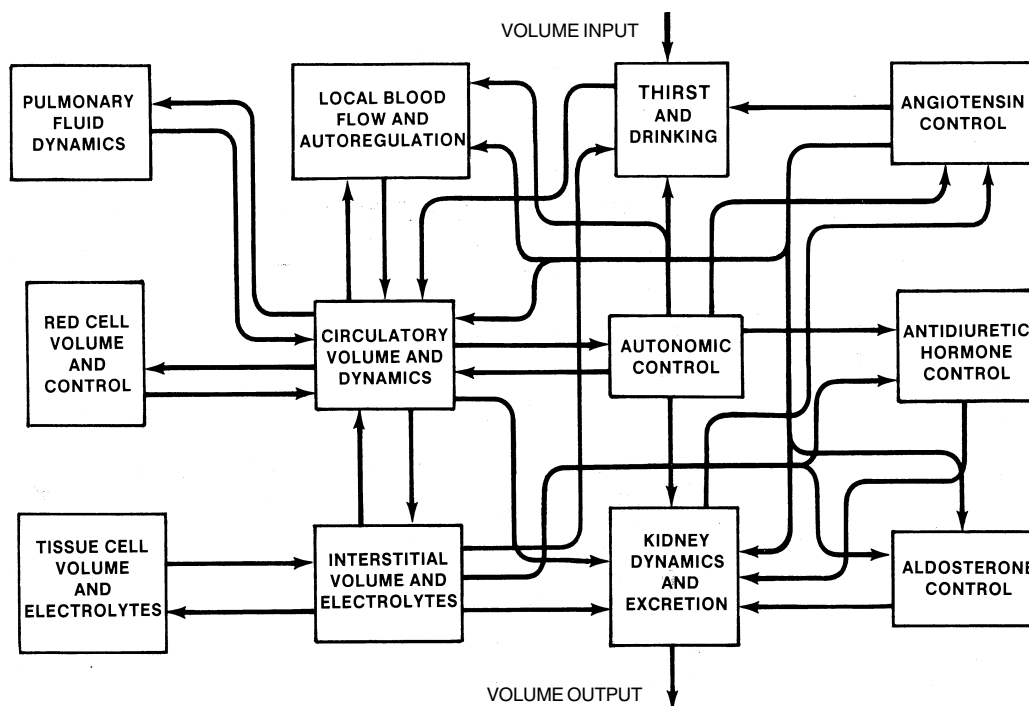
Figure 3-33. Composition of Guyton model of the circulatory, fluid, and electrolyte system. Each block represents a subsystem which consists of a family of function blocks indicated by the numerical figure in parentheses. Modified by Sagawa [4].
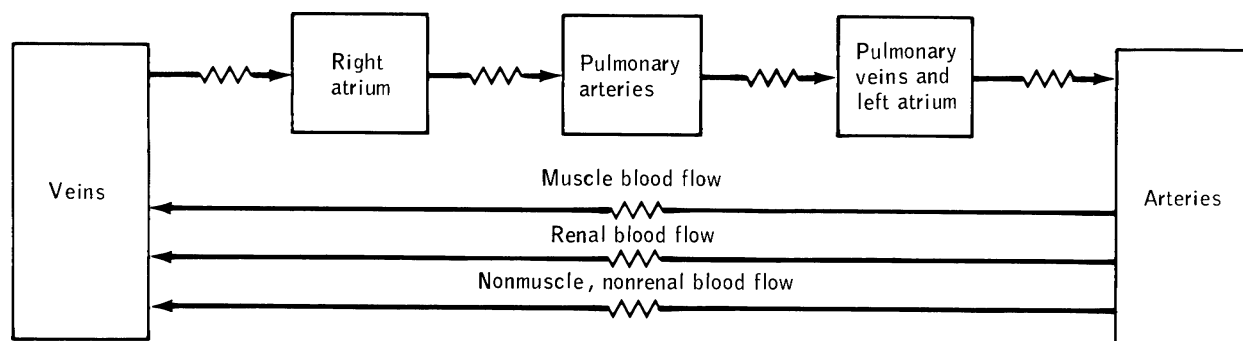
Figure 3-34. Blood volumes and flows in the original Guyton model.

the baroreceptors, chemoreceptors, and ischemia of the central nervous system. Total autonomic output is expressed as a positive effect for sympathetic output and a negative effect for parasympathetic output.

Comparison of the blood flow circuit in the Guyton model (Fig. 3-34) to that of the Croston model shows a great difference in the number of volume segments. These differences reflect a higher fidelity response for short-term stresses in the latter model. However, the Croston model, as well as the other models described earlier, have used a basic closed circulatory flow system with no leaks. This kind of approach can be justified when the simulated challenge is acute. When longer duration simulations are required, a large number of other regulatory mechanisms must be included to describe overall circulatory control,

even in a crude manner. The lack of detail in Guyton's circulatory subsystem can be contrasted with the complexity of the connections between the cardiovascular system and the interstitial-cell complex. The inclusion of such elements as cardiac hypertrophy, cardiac deterioration, baroreceptor adaptation, hormonal pathways, regeneration of red blood cells and plasma proteins, delayed autoregulation of resistance vessels, and stress relaxation of veins clearly indicates that the Guyton model was developed to be useful as a long-term model. This feature has made it very attractive as a companion to a short-term pulsatile model for the Whole-Body Algorithm application.

The evolution of the Guyton model from a basic circulatory system to a much more complex grouping of subsystems revealed that a model of the cardiovascular system
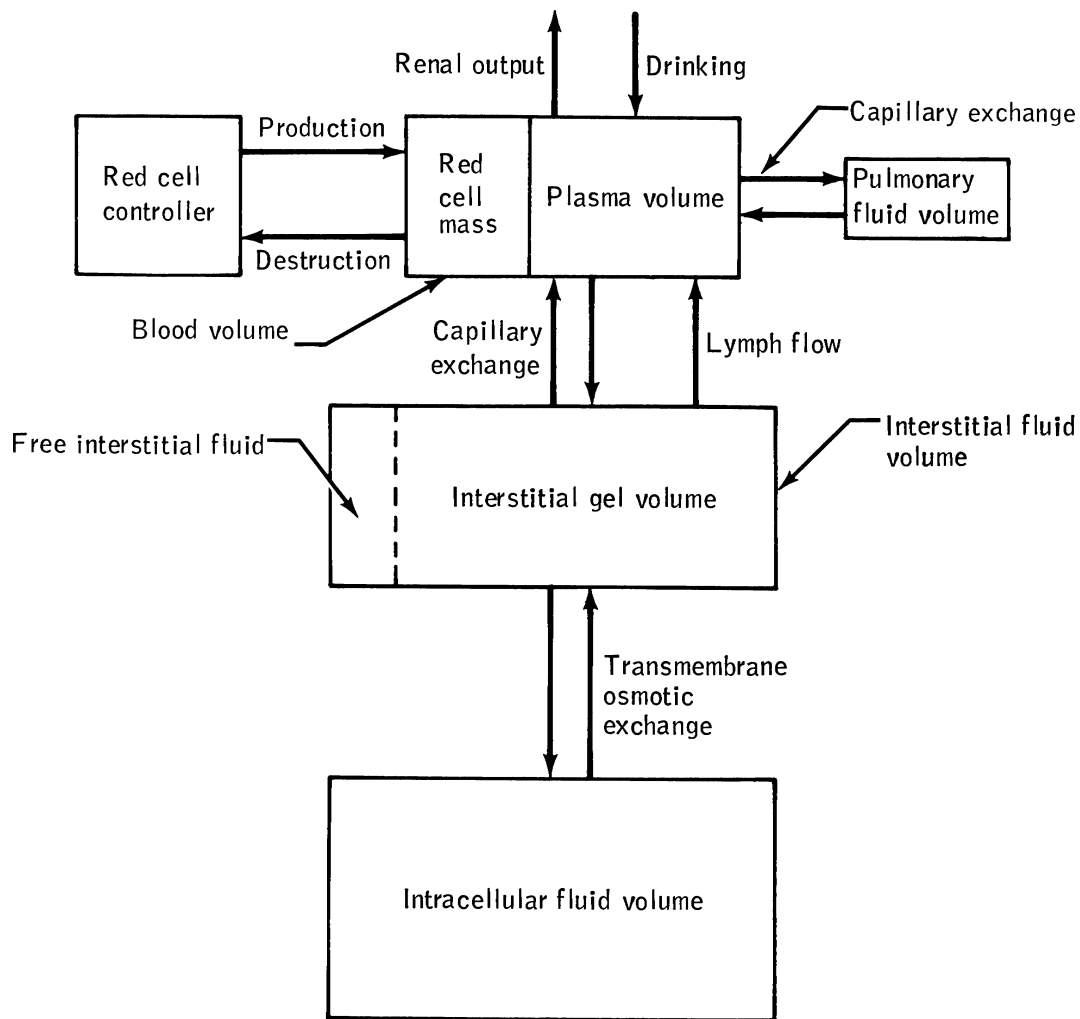
Figure 3-35. Fluid-containing reservoirs of original Guyton model. The volume of each compartment is controlled by active and passive regulators.

must include elements from most of the entire body if it is to be used in the study of intermediate to long-term phenomena. The Guyton model clearly illustrates the importance of considering the interaction between various subsystems in predicting fluid volumes and electrolyte levels. The real system and the model itself are extremely stable, so much so, in fact, that the function of any single control mechanism can be in error by as much as 50% without significantly affecting the overall output of the system. This characteristic is the result of a number of overlapping regulatory circuits that create a large degree of redundancy. One of the most important features of the model is that it is large enough to obtain this stability level, similar to that in the real system, despite the fact that each subsystem is modeled in a gross sense with many minute details omitted. Because of this stability, the model is adequate for predicting the outcome of many long-term experiments.

The system of equations representing this closed-loop model contains more than 370 mathematical relationships and is a large, stiff system with response times ranging from 0.5 second to 40 days. Numerical integration over extended periods would be extremely time consuming unless special techniques were employed. The basic method of integration is a variant of the simple Euler method made possible by the fact that, for many simulations, all short-term subsystems can be separated from the rest of the model and integrated many times using small time steps without disturbing the remainder of the system. When these rapidly acting subsystems have developed near steady-state values, the remainder of the system is numerical integrated, using a relatively large time step, and the whole process is repeated. This procedure is only possible when slow, nonvascular changes are taking place. With rapid overall transitions, as in exercise, a small integration step must often be used for the entire system, greatly slowing the model simulation.

3.2.5.2 Limitations and Modifications. The original Guyton model was built to simulate a large number of diverse situations, but there were some specific stresses for which the model response was inadequate. Since the model did not include separate vascular compartments representing the legs, the model was incapable of realistically responding to either gravitational or postural changes. Analysis of Skylab data has shown that the rapid shifts of fluid from the lower to the upper body as well as a more gradual dehydration of leg tissues play a very important role in the physiological adaptation to zero-g [107,108]. The data from bedrest studies, taken as a ground-based experimental analog to microgravity, have also shown similar important changes involving the legs [109].

There have been a few studies in which the gravitational effects of posture on the body fluid compartments have been modeled. However, no studies have been done to account for long-term simulation of gravity disturbances such as bedrest or weightlessness. Models of the circulatory system that contain short-term gravity effects have met with various degrees of success. The models of short-term circulatory gravity effects include those of Snyder [17], Croston et al. [12], and Green and Miller [110]. Several studies by Luetscher and co-workers [111,112,113] resulted in models that included the effects of intravascular-interstitial fluid shifts on circulatory and renal responses to postural changes and, thereby, allowed for slightly longer term simulations. These latter models, however, were not designed to account for even longer term effects such as lymph return, extravascular protein circulation, and hormonal effects. Nevertheless, the ideas embedded in these models were useful in altering the Guyton model.

The circulatory subsystem of the Guyton model contained only two lumped systemic blood compartments representing the arteries and veins. Modifications made to the model included increasing the number of compartments of the circulatory system so that lower body (i.e., legs) and upper body blood and tissue fluid compartments could be identified separately and adding gravity effects on blood flow and baroreceptor elements to permit the new circulatory system to respond to a variable gravity vector. These structural modifications are illustrated in Fig. 3-36.

Cardiac output was divided into three pathways, as previously described. However, flow through the legs was taken to be the same as the muscle flow of the original model. In addition, a filterable capillary bed was added to this pathway. Details of these modifications are discussed in Appendix C. These changes added the basic capabilities to simulate such stresses as postural change (tilt, including head-up and head-down), LBNP, bedrest, and weightlessness.

Other modifications to the Guyton model, introduced during the course of this project, included alterations in the renin-angiotensin system, the baroreceptor system, the stress relaxation of the vasculature, the autoregulation of muscle blood flow, and the red blood cell control system. Most of these changes were not made because of limitations of the model for spaceflight applications; they were made because other ground-based physiological studies revealed that their inclusion would be more appropriate. Details of these modifications, including the changes for gravity dependency, are available in two study reports and in Refs. [105] and [114] as well as in Appendix C.

One weakness in the Guyton model, for some special circumstances, is the lack of a description of hydrogen-ion regulation (i.e., acid-base balance). Hydrogen-ion levels are controlled by the renal system, the buffering system of the body, and the respiratory system, all acting together. In fact, the hydrogen-ion control system is one of the main links between the circulatory, renal, and respiratory systems. A preliminary analysis that lays the foundation for a model of this valuable subsystem was performed during this project [105], and other researchers have studied this subsystem in some detail [115].

In the latter stages of this project, it became apparent that new techniques were required to simulate the weightlessness of spaceflight and its ground-based experimental analogs such as water immersion and head-down bedrest. These stresses were never contemplated in the design of the original Guyton model. Some of the required features that have been identified include collapsible leg veins, fluid reservoirs above the heart (i.e., jugular vein system) and head tissues, and orthostatic mechanisms. The latter elements would allow the model to assume an upright reference position in addition to its present supine reference. These modifications are presented in Chapter 9.

3.2.5.3 Validation of the Basic Guyton Model. The formulation of the Guyton model was based on a wide variety of experimental data, and the model has been tested extensively. Some of the experiments that have been simulated with this model by Guyton and co-workers are the development of hypertension in a salt-loaded, renal deficient patient; simulation of congestive heart failure; nephrosis; circulatory changes during severe muscle exercise; and unilateral heart failure of the right or left side. Other simulations performed were of the effects of the removal of the sympathetic nervous system on circulatory function, infusions of various types, and the effects of extreme reduction of renal function on circulatory function. The model performed adequately in almost every case. These initial validation studies are discussed in reports issued by Guyton and co-workers [10,102,104,106].

The basic model itself was based on detailed organ level studies and required almost 20 years to develop. But Guyton and his co-workers were primarily interested in developing a model for hypertension research. It remained for the GE/NASA team to demonstrate the capability of the model to predict the appropriate response to fluid-volume shifts in the spaceflight environment. This was accomplished more easily and convincingly by suitable validation studies based on ground-based experiments as suggested in Table 3-2. Since the weightless state is associated with initial expansion of the central blood volume and subsequent partial depletion of plasma and body fluids, the model was validated for such common one-g stresses as infusions, dehydration and hemorrhage for which much data are available. (The reader is referred to the discussion
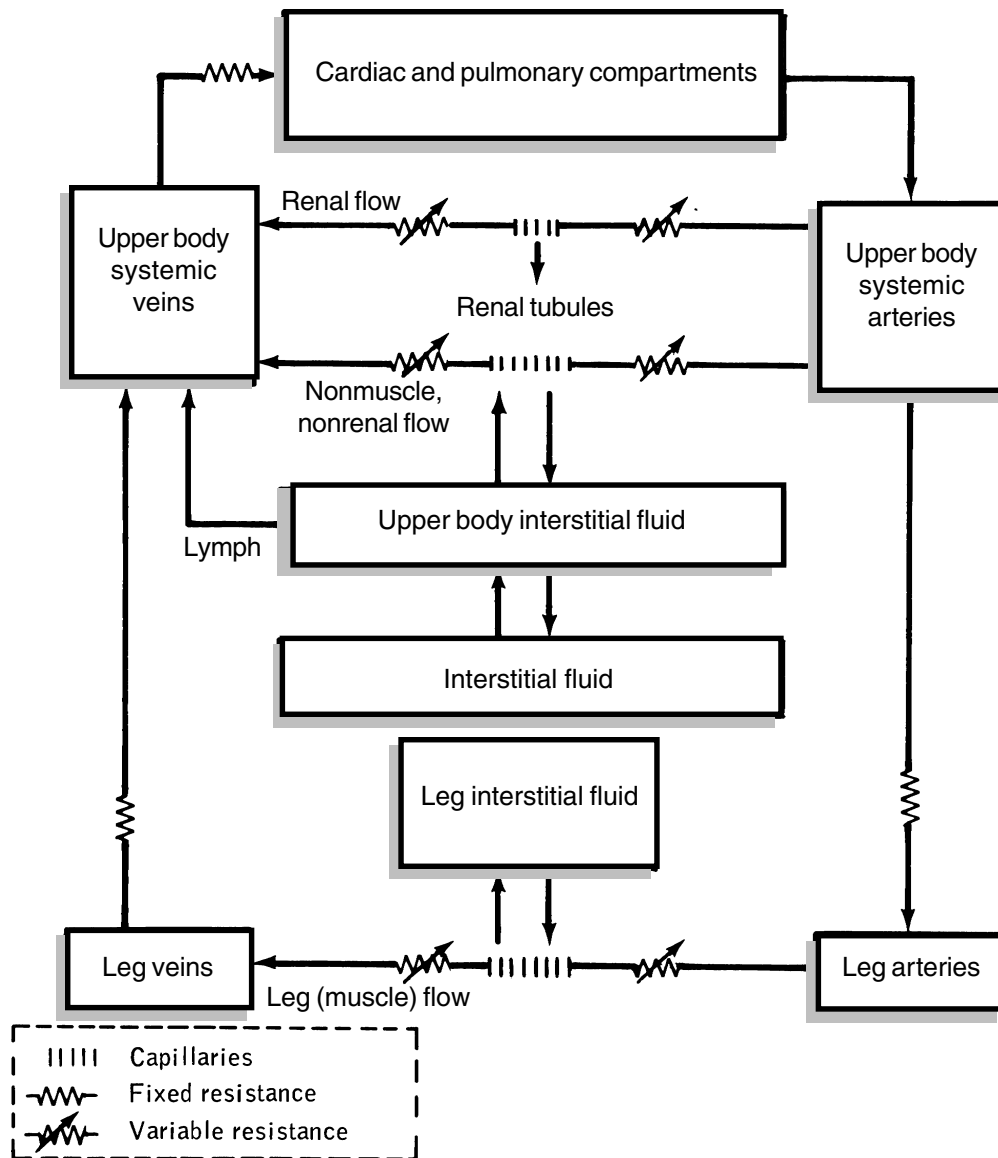
Figure 3-36. Circulatory and fluid compartments in modified Guyton model. Leg blood and interstitial compartments have been added. Gravity influences carotid baroreceptors and blood flow in legs.

associated with this table for the rationale for studying these and other one-g stresses).

Several of these studies are illustrated in Figs. 3-37 to 3-39. The first two figures illustrate the responses to fluid-electrolyte infusions and the third demonstrates the response to dehydration and subsequent rehydration. In all cases, a variety of infusions were performed, including those of hypertonic, isotonic, and hypotonic fluid. The model is obviously capable of distinguishing between variations in the tonicity of the infusion.

In the first series of simulations (Fig. 3-37), 1 liter of water, 150 meq sodium, and 1 liter of isotonic saline (1 liter water plus 150 meq sodium), respectively, were infused. These infusions were made directly into the circu-

lation, so that the response was more rapid and more dramatic than if they had been administered orally. The three infusions all produce appropriate osmotic shifts between extracellular/intracellular spaces and renal excretions of salt and water, as well as proper hormonal responses. Similar responses would be expected for the human subject [118,119]. For water infusion, the diuresis is completed within the first few hours. For isotonic saline, the diuresis is maintained at a lower level but continues beyond several hours. In the case of water or sodium infusion, large variations in cell fluid volume are observed, whereas in the case of isotonic saline, the cell fluid volume is essentially unaffected. Antidiuretic hormone was also appropriately responding to osmotic concentrations of extracellular
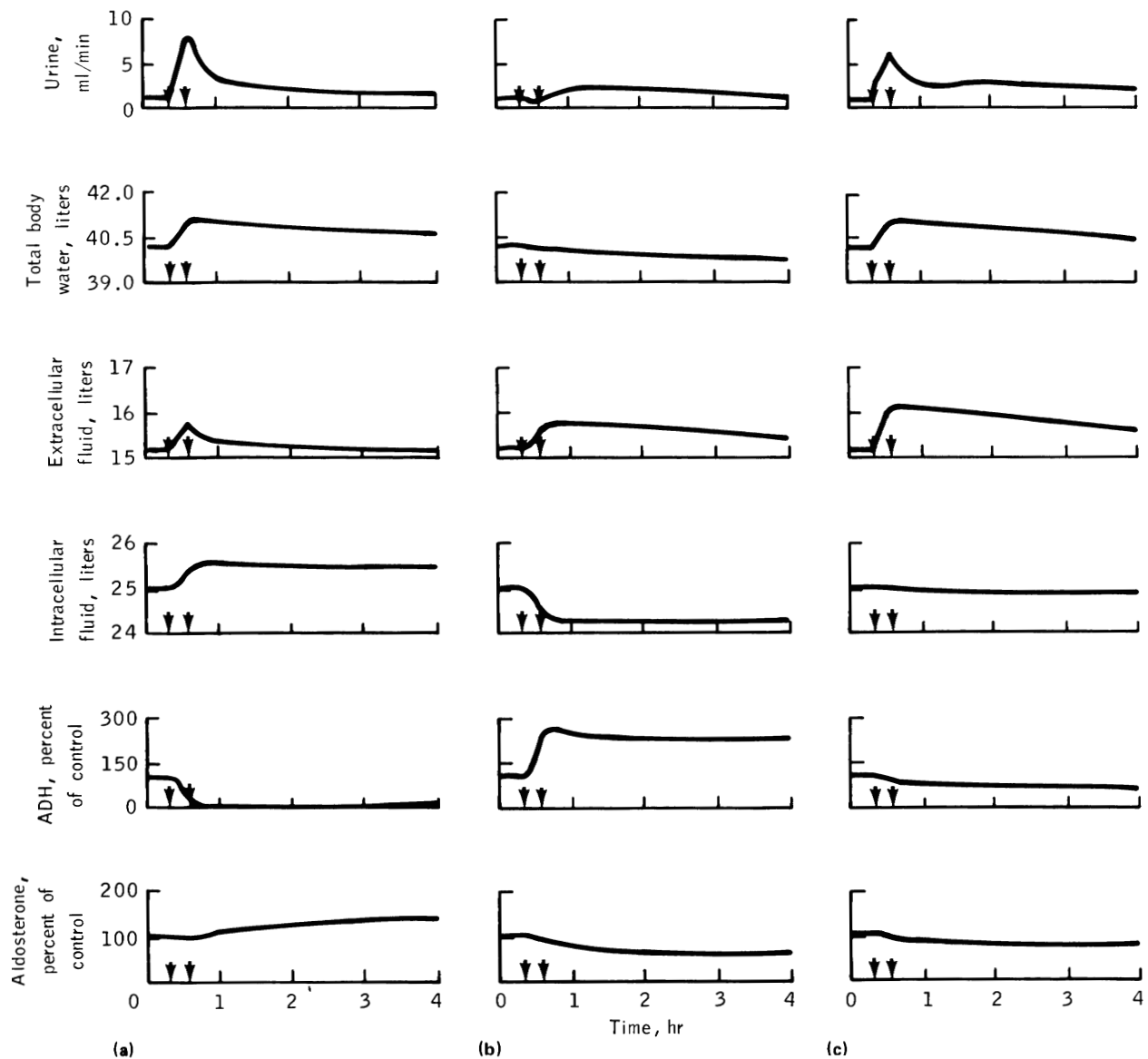
Figure 3-37. Simulated infusion responses using circulatory, fluid, and electrolyte model. These studies demonstrate capability of model to distinguish between the tonicity of fluids in acute water and salt loading. Arrows demarcate infusion period. (a) Infusion: 1000 ml water (hypotonic), (b) Infusion: 150 meq sodium (hypertonic), (c) Infusion: 1000 ml saline (isotonic).

fluid [120], decreasing rapidly in the case of the water infusion, increasing threefold in the case of pure sodium, and barely changing in the case of isotonic saline. Aldosterone in the model is a regulated by angiotensin, extracellular potassium, and extracellular sodium. It reacted appropriately to the primary stress of these experiments by showing a change in extracellular sodium concentration in the first two cases and a fall in angiotensin (not shown) in the last case, due to increased renal arterial pressure. Experiments such as these illustrate the importance of electrolyte considerations in water-balance studies, a concept quite familiar to most clinicians.

A more detailed study of an isotonic saline infusion, particularly as it affects plasma-interstitial fluid exchange,

is shown in Fig. 3-38. The simulation consisted of a 2-liter transfusion over a 30-minute period into a nephrectomized subject. Capillary filtration increases markedly as the transfusion begins and lymph return increases more slowly, resulting in a net outward flow of fluid from the plasma. Since net flow into the interstitial space is less than the transfusion rate, fluid accumulates in the plasma, and plasma volume increases considerable. When the transfusion is stopped, capillary filtration falls to equal lymph flow, and the interstitial fluid continues to expand at the expense of plasma volume until transcapillary flow is reduced and equals lymph flow. At the end of the transfusion, 37% of the added fluid remained in the plasma, but within 30 minutes, only 24% of the transfusion volume
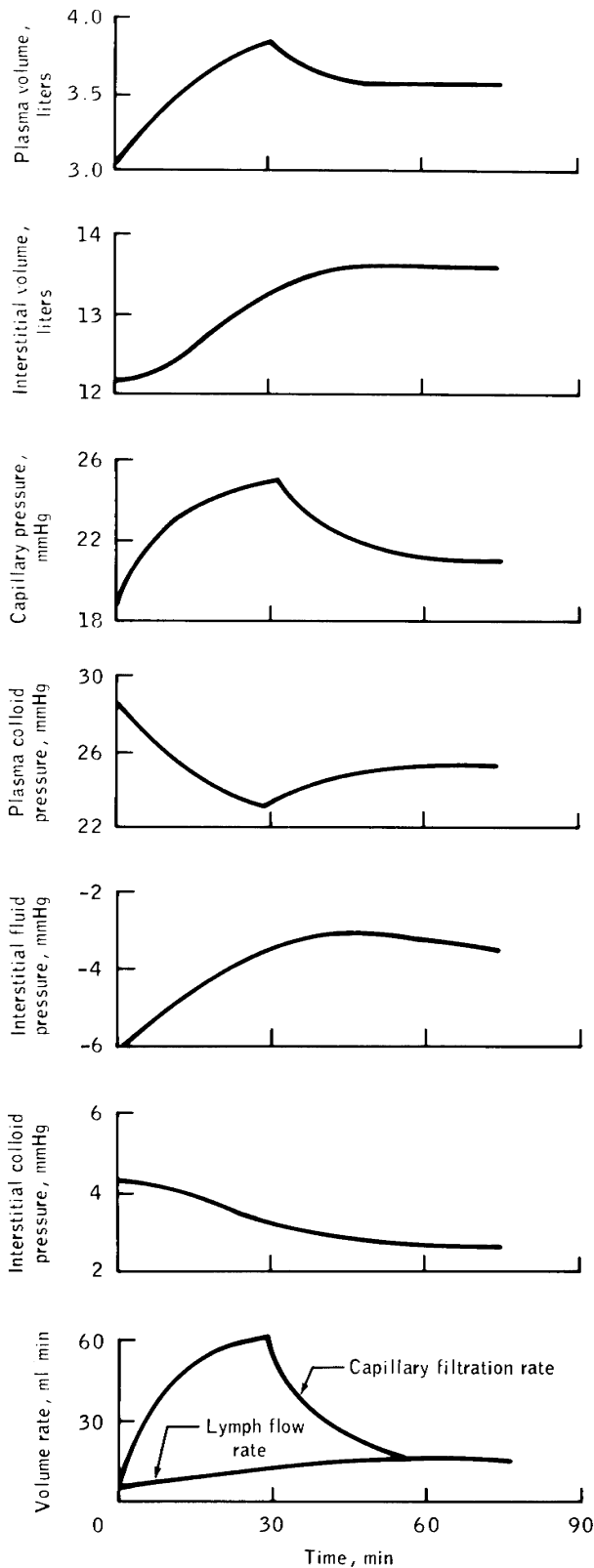
Figure 3-38. Simulation of 2 liters isotonic saline infusion during first 30 minutes showing capillary filtration responses in nephrectomized subject (from [116]).

remained. If the transfusion had been large enough, the interstitial fluid compartment would have entered the region of low compliance and almost all additional fluid beyond a certain point would have entered the interstitial space. The results of this simulation compare quite favorably with recent experiments [121] and demonstrate the suitability of this model for studying situations involving fluid shifts and circulatory function.

Model validation was also extended to include such similar stresses as hemorrhage, salt depletion, and salt loading—for both short-term and long-term changes. Rehydration through use of various fluids has different effects on plasma-volume recovery. In these studies, shown in Fig. 3-39, and others not shown, interstitial fluid does not always act like the fluid reservoir that some investigators have claimed [122]. Following simulated hemorrhage, for example, the interstitial space provides only 20% of the acute plasma refilling response. This has also been noted experimentally by others [123]. After dehydration without rehydration, there is very little tendency for acute refilling of blood either in the model or in the real system. Also, after infusion, the interstitial compartment first expands but, within 24 hours, returns to normal. This has relevancy to the Skylab experience, in which inflight losses from all fluid compartments were observed to change except for the interstitial space.

Simulations that are even more relevant to the zero-g model validation are the water-immersion studies discussed in Chapter 9. Where appropriate, the model was modified slightly in accordance with more recent experimental evidence.

3.2.5.4 Validation of the Modified Guyton Model. Although the validation studies cited are *related* to the fluid shifts associated with weightlessness, they do not *directly* evaluate the new capabilities of the model concerned with the added leg compartments and gravity dependency (see Chapter 3.2.5.2). Therefore, the modified Guyton model was validated for the following four conditions. (Results of these studies are presented in Chapter 9).

a) **Supine Mode at Rest.** The Guyton model is initialized in a so-called "supine position." That is, the values of such quantities as heart rate, blood pressure, and cardiac output agree with measurements from human subjects in the resting horizontal (supine) position. Steady-state values for the gravity-dependent model in the supine, unstressed mode should have agreed with those of the original unmodified model, and they did. This test does not really represent a validation study; however, it was important to ensure that the modifications (of adding leg compartments) did not change the basic output variables of the model such as cardiac output, mean arterial pressure, fluid volumes, concentrations, and renal function. In addition, for the sake of consistency, values of flows, pressures, and volumes of the new lower body compartment should compare favorably with the pulsatile cardiovascular model (Croston model) and with available
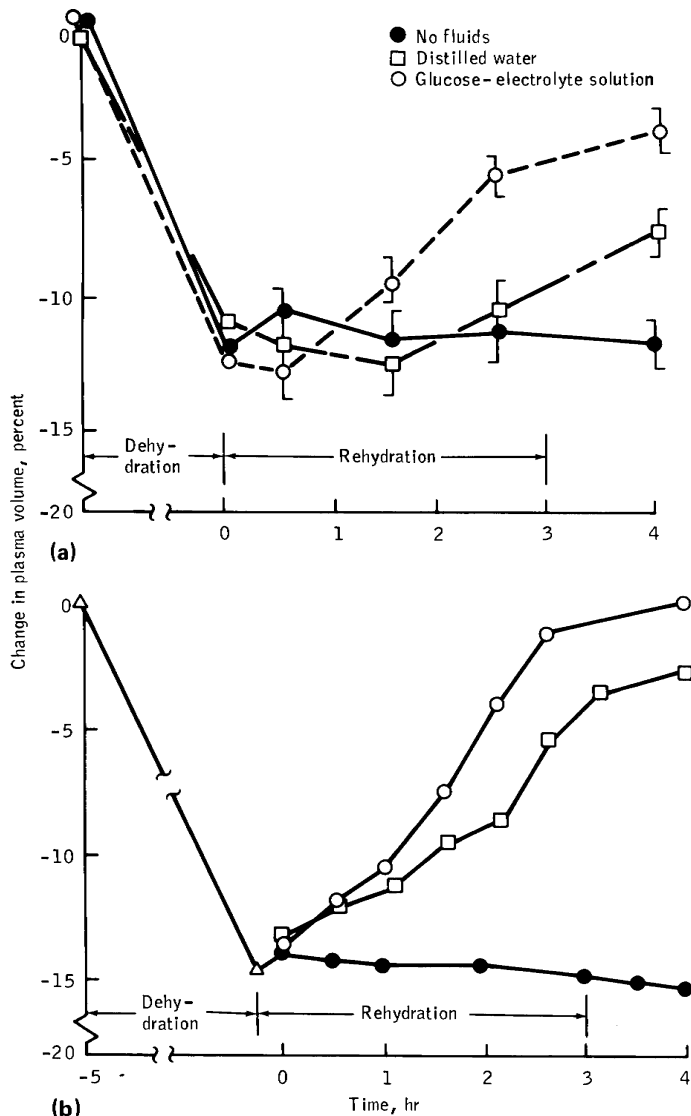
Figure 3-39. Plasma volume response to thermal dehydration and subsequent rehydration with fluids of different tonicity: Guyton model response compared to data. (a) Experimental data [117]. (b) Computer simulation.

data on human subjects who are supine for relatively short periods. Documentation of this study is provided in Ref. [114].

b) ***Supine Mode Under Stress.*** The restructured model responded to various supine stresses in a manner essentially similar to that of the original model. The stresses were those already discussed in the section describing the validation of the basic Guyton model. In addition, the capability to perform LBNP simulations was demonstrated. Simulation results for this stress were compared with results of the pulsatile cardiovascular model that were previously validated for LBNP. The Guyton model did not exhibit the same

degree of accuracy as the Croston model for some cardiovascular indices during LBNP; however, the capability to account for capillary fluid shifts was more realistic (see [114] and Chapter 5.4.2.2).

c) ***Standing Mode at Rest.*** Quiet standing results in different values of circulatory parameters (i.e., cardiac output, blood pressures, hematocrit) than those found in the supine position. Changing posture from supine to upright represents a stress to the individual and a suitable challenge to the model. Values of basic circulatory parameters in the standing mode should agree with data from human subjects performing quiet standing or tilt for relatively short periods of time. The model contains the capability to vary the angle of tilt with respect to gravity but does not include protective orthostatic mechanisms. These simulations of passive tilting and erect standing suggested adding new elements to account for muscle pumps, venous valves, abdominal compression reflex, and venoconstriction, all of which are important in the real system to prevent orthostatic collapse (see [114] and Appendix C). The additional lower body compartment helped to realistically simulate blood pooling, extravascular filtration, and peripheral vasoconstriction (see Chapter 9.6). Comparison of responses was made not only with human data but also with simulation responses from the models of other investigators. The "open" nature of Guyton's circulatory system was expected to provide increased fidelity for simulations of tilt and LBNP. Extremely long-term effects of standing at rest without leg activity will result in continued pooling of blood in the legs, but these effects were not considered. The capability to simulate long-term stress was demonstrated only in the supine position.

d) ***Long-term Bedrest.*** Long-term bedrest can be considered a special case of the supine mode. However, the Guyton model (already initialized in the supine position) required additional modification and hypotheses to simulate the headward shifts of fluids and the dehydration of leg tissues; both are characteristics of bedrest. Incorporation of the lower body segments into the Guyton model and the successful completion of the studies outlined previously has provided a solid foundation and the necessary level of detail with which to test theories of long-term adaptation, including weightlessness. The validation studies discussed here (LBNP, postural change, and long-term bedrest) are fully described in Chapter 9.

The Guyton model represents an attempt to understand the interactions between acute and long-term adaptive control of the body fluids and the circulation. Because there is a notable scarcity of information regarding these complex processes in healthy subjects, long-term bedrest and spaceflight have been of particular importance in validating and modifying the original model of Guyton. This model is clearly relevant to spaceflight because some of the most notable physiological changes that occur can be

traced to disturbances in fluid-electrolyte regulation. By accounting for long-term adaptive effects in the circulatory and autonomic systems, the model has been useful in predicting responses to stresses lasting up to several weeks or months.

3.2.6 The Whole-Body Algorithm

Most previous physiological modeling has emphasized detailed function at the subsystem (organ) level or a more limited whole-body function. In an effort to extend modeling capabilities, an attempt was made to design a combined model of all the sub-system models previously described. The "Whole-Body Algorithm" (a grandiose term used for convenience only) was envisioned to be a large-scale dynamic mathematical model that contained descriptions of the important physiological functions of the major body subsystems and the primary interactions between these subsystems. It was developed to simulate responses to a wide variety of specific stresses related to the spaceflight environment.

To be useful in evaluating hypotheses related to physiological adaptation to spaceflight, such a model must have the capability (1) to contain representations of the cardiovascular, thermoregulatory, respiratory, and fluid-electrolyte systems, (2) to simulate both acute and long-term changes in these systems, (3) to simulate the experiments used to evaluate the spaceflight adaptation process, and (4) to simulate the environmental stresses which may influence the results of these experiments. The experiments of interest include bicycle ergometry (supine and erect), orthostatic tests including LBNP and head-up tilt, and environmental stresses of changes in cabin temperature and atmospheric composition (increased carbon dioxide concentration and hypoxia). The Whole-Body Algorithm was designed such that the entire sequence of major physiological events for long-duration spaceflight could be simulated. This sequence includes preflight (baseline or control) experiments, acute physiological response to zero-g, long-term adaptation to zero-g, changes in cabin environment, inflight responses to the experiments of interest, acute reentry to one-g, long-duration readaptation to one-g, and postflight experiment simulation (see Fig. 2-2). These objectives and design requirements are discussed fully in the Whole-Body Algorithm design specification document [124].

3.2.6.1 Background. Before the development of the Whole-Body Algorithm, there were only a few attempts at modeling interacting physiological subsystems. These attempts were limited in the number of stresses they were capable of simulating [see Refs. 125-132]. Two studies [133,134] represent attempts to integrate the cardiovascular, respiratory, and thermal subsystems. Both models were structured to evaluate exercise response while varying the thermal environmental conditions and inspired gas concentrations.

Guyton et al. [10] successfully integrated the circulatory, fluid, and electrolyte subsystems. However, this model was not capable of simulating thermoregulatory or ventilatory behavior, could not simulate several short-term

experiments of interest, and the capability to simulate exercise was quite redimentary.

In preparation for the development of the Whole-Body Algorithm, two limited studies were performed that involved coupling a thermoregulatory and respiratory model [139] and a circulatory and respiratory model [50].

3.2.6.2 Approach to a Whole-Body Algorithm. Two main approaches were identified for modeling a large system composed of major subsystems. In the first (bottom up) approach, each subsystem could be modeled independently by using hypotheses appropriate for that subsystem. After each subsystem had been verified, the subsystem models could be combined into a unit by restructuring or modifying the subsystems to function together. In the second (top down) approach, the system as a whole could be assembled into a cohesive model using interrelated hypotheses, with all subsystems designed to function as a unit from the outset (for example, Guyton's model).

The concept of coupling existing subsystem models offers the advantage that the validity of each model, operating independently, has been established for simulating each stress of interest. Each model thus incorporates various time lags, fast and slow controllers, and integration step sizes as appropriate for its simulation requirements. Use of the first approach also enables modification of subsystem models without total disruption of the overall system. Then, the Whole-Body Algorithm can evolve as additional experimental data become available, as new information is gained form the literature, as new hypotheses are verified, or as simulation results indicate inappropriate formulations. An additional advantage of this approach is that certain poorly represented elements of one subsystem can often be replaced by a similar, but more accurate algorithm from another subsystem, if one exists. For these reasons, the basic approach of combining previously existing individual subsystem models using physiologically meaningful interactions was selected for developing a first-generation Whole-Body Algorithm. (Of course, this approach also has its disadvantages; these will be discussed following a description of the model validation).

Individual subsystem models were developed or modified from existing models that had been previously validated for the stresses of interest. They were programmed on the same computer system and in the same computer language. Long-term physiological simulation was accomplished by using the Guyton model that incorporated circulatory, fluid and electrolyte subsystems. This long-term model initialized (provided initial values of major system variables) a set of three short-term models representing the cardiovascular, respiratory, and thermoregulatory systems. The three short-term models, designed to simulate physiological responses to acute environmental changes and short-term experimental stresses, operate in parallel fashion, interchanging information as often as every 0.5 second of simulation time. Using this approach, a Whole-Body Algorithm was evolved that is capable of simulating with equal facility those adaptive changes requiring days, weeks, or even months as well as those experimental stresses

evoking significant changes within seconds. Additional information can be found elsewhere [124,125,136].

Joining models designed specifically to simulate different aspects of physiological function into a composite Whole-Body Algorithm required solving several problems that arose because each model may have components that overlap similar components of another model and each model may respond slightly differently to the same stimuli. If the models are compatible with regard to simulation duration, it may be possible to form a composite or bilateral model that offers advantages to each subsystem. Therefore, combining compatible models requires that all overlapping components be eliminated, that the effect of stimuli acting on one model be properly related to the effects of stimuli acting on the other models, and that non-overlapping components function to yield consistent results.

Also essential to the design of a Whole-Body Algorithm was the development of several intramodel interfaces (Fig. 2-5). In addition to the short-term/long-term interface, both circulatory-thermoregulatory and circulatory-respiratory bilateral interfaces were required. The rationale for selecting the appropriate subsystems and the means for dealing with the problems associated with interfacing these subsystems were considered during several preliminary studies [50,51,91,105,124,137] and are summarized in Appendix D.

Other problems arose from the fact that each model was originally developed with no thought of combination with other models, as well as with different goals in mind. Further, each model assumes or calculates common parameters using different techniques, and each model was developed to respond to different specific experimental stresses. To further complicate the model interfacing, baseline data and structure such as blood volumes, basal or resting metabolic rate, control systems, units, variable names, volume compartmentalization, integration schemes, time increments, and programming approaches all differed considerably in the various subsystem models. These and many other details were worked out directly at the program level.

3.2.6.3 Subsystem Models and Modifications.
The individual subsystem models used in the Whole-Body Algorithm were selected and modified to simulate the response of a human subject exposed to the same stresses under investigation in the Skylab medical experiments. These models and the various modifications made during this program have been detailed in earlier sections and in Appendix D. They include the following.
1. The Guyton model [10] with modifications by White [90,105,138] and Leonard and Grounds [114]. This model is capable of simulating intermediate and long-term changes in circulatory, fluid, and electrolyte control;
2. The respiratory model of Grodins [45] with modifications by Gallagher [49,50,51,139];
3. The thermoregulatory subsystem model of Stolwijk [27] with modifications by General Electric Company [31,32,34];

4. The cardiovascular model of Croston [9] for exercise with modifications by Croston and Fitzjerrell [13]. This model simulates LBNP, tilt, and tilt ergometry [9,140,141];
5. The erythropoiesis control model developed by Leonard [65,77,142,143].

(The models of Croston and Leonard, mentioned above, were developed especially for this GE/NASA systems analysis effort).

These models were selected after careful study and with cognizance of the differences in parameters, control systems, and various approximations used as constant parameters or set points, as well as their compatibility with each other and to the requirements of the Whole-Body Algorithm. Each model's structure was modified where necessary to improve the realism of the subsystem performance. These modifications included:
1. Adding a chemoreceptor function to the short-term cardiovascular model to allow blood oxygen and carbon dioxide levels to influence resistance elements in blood vessels, heart rate, and strength of heart contraction;
2. Adding a countercurrent heat exchanger to the blood supply of the thermal model to improve performance in cool environments;
3. Adding a modified oxygen-uptake function for exercise in the respiratory model to improve ventilatory control;
4. Adding a thermoregulatory influence on heart rate.

Appendix D contains further details on these modifications.

3.2.6.4 Description of the Whole-Body Algorithm.
The individual models described earlier are in the form in which they were used in the Whole-Body Algorithm. A diagram illustrating the interfaces developed to represent the interaction between these subsystems is presented in Fig. 3-40. The long-term/short-term interface represents one of the most important relationships in the Whole-Body Algorithm, in that it provides the capability to simulate the spaceflight event sequence.

The basic plan was to use the long-term model to initialize simulations by the short-term models. The short-term experiments or transient environmental conditions would, after steady-state conditions were reached, reinitialize the long-term model for simulation of the subsequent long-term phase. Since the long-term/short-term interchange is sequential rather than simultaneous, the modeling problem was primarily one of providing for the transfer of the interface variables through a common block. A secondary problem involved modeling the mechanism necessary to use these variables on either side of the interface in a physiologically representative manner.

Extensive computer programming was required to initialize and execute the subroutines in a synchronous manner, since integration step sizes of the models were not indentical. An executive program was developed that allowed operation of the models through an "overlay" struc-
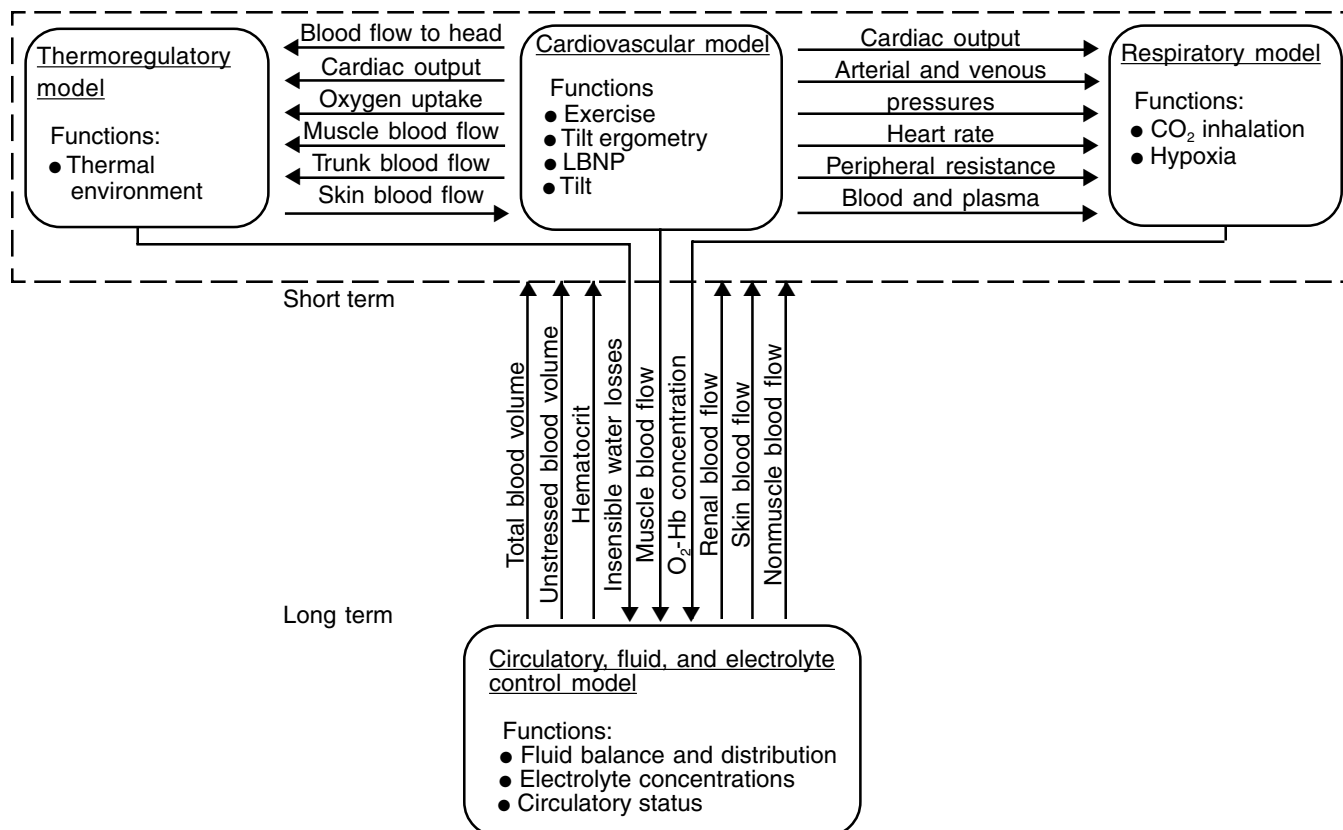
Figure 3-40. Subsystems and interfaces of the Whole-Body Algorithm. Shown are the quantities generated by each subsystem model that are used to influence one or more of the other models.

ture because they were far too large to all fit into core memory at the same time. Limitations of computer technology in the early 1970's required these innovations which would be relatively straightforward today. A description of the executive program is proved in Appendix D.

The variables transferred through the interface are direct functions of the long-term stresses simulated and of the resultant hypotheses that relate to the physiological representation of these stresses. The short-term experiment stresses (other than environmental) do not impose any interface requirement on the long-term model. It is assumed that the short-term experiment simulation will always include recovery to the pre-stress state (i.e., no long-term physiological changes are permitted to result from the simulation of short-term stresses).

The interactions between the short-term models are quite different. These models operate simultaneously, and a stress applied to any one of them evokes a response in all three subsystems. The structure of the Whole-Body Algorithm permits the short-term models to operate essentially independently of the long-term model. The integration of thermal, respiratory, and circulatory mechanisms into a single model structure has been the goal of other investigators; therefore, the short-term portion of the Whole-Body Algorithm constitutes a separate contribution to physi-

ological modeling. The block diagram of Fig. 3-41 describes, in highly schematic form, the integration of major elements of the three models representing the thermoregulatory, respiratory, and cardiovascular control systems. Only those elements essential for proper integration of the feedback signals are shown; other factors important to proper function of only a single subsystem model (such as radiation and convection factors in the thermoregulatory model) are not shown. Many of the blocks represent a considerable degree of complexity in the simulation model. Nevertheless, the diagram is useful for visualizing the integrated system in terms of central controllers which process the input from three kinds of receptors (chemoreceptors, baroreceptors, and thermoreceptors) and in terms of a controlled system which is affected not only by the central controllers but by environmental stimuli as well. (In the case of exercise, environmental stimuli directly affect not only the controlled system but the controller as well, as represented by the block labeled "Somatic and proprioceptor inputs.") Integration of the major regulatory subsystems occurs in both the controller and the controlled systems. Shown on the right of the diagram are the environmental and experimental parameters used to test the responses of the model and also the primary elements they affect.
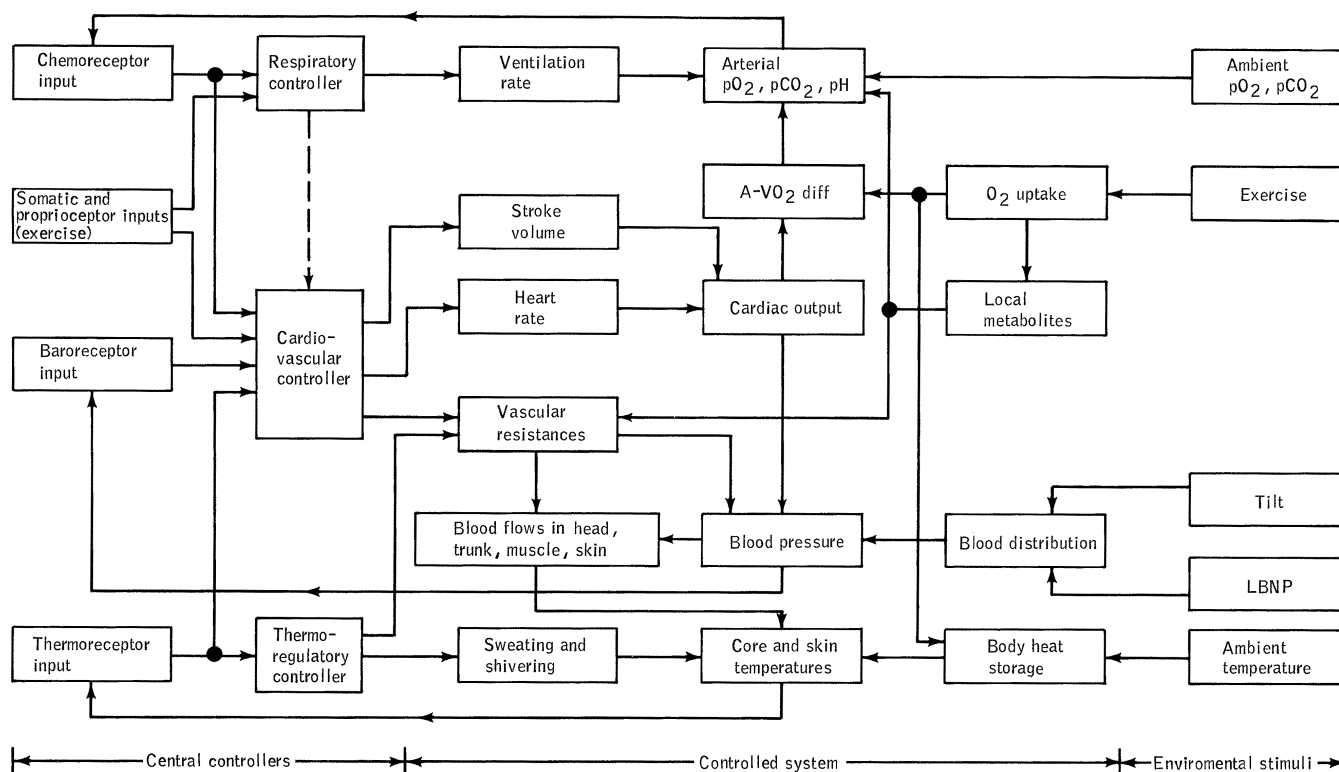
Figure 3-41. Integration of short-term subsystem models of the Whole-Body Algorithm. This diagram indicates the general manner in which environmental and metabolic stimuli can affect the respiratory, cardiovascular, and thermoregulatory systems. Validation of this portion of the WBA is shown in Figs. 3-42 to 3-49.

The individual models differed in structural detail. For example, the number of compartments in the controlled system were vastly different; the thermoregulatory model has 40 compartments for heat transfer, the pulsatile circulatory model has 28 compartments for blood flow, the respiratory model has 3 compartments for gas exchange and the Guyton model has 5 circulatory compartments. Of these, the only overlapping function was blood volume and flow. These differences were reconciled and accommodated by either lumping blood compartments when information flowed in one direction or distributing them when information flowed in another.

The net result of this subsystem integration was a large model that, we believe, was superior to the sum of its parts. This result was achieved by combining the best features of each model and replacing subsystem algorithms known to exhibit poor responses. For example, the segments that compute brain and skin blood flow in the respiratory and thermoregulatory subsystems, respectively, have been used to replace corresponding segments of the cardiovascular model. Conversely, the cardiovascular model contains a better representation of flows in other tissue compartments than is found in either the stand-alone thermoregulatory model or the stand-alone respiratory model.

In another example, the long-term circulatory model can be shown to be a useful counterpart to a short-term, pulsatile cardiovascular model as part of the Whole-Body Algorithm. Disadvantages of the short-term model are the lack of fluid and protein transfer into and out of the central blood compartment and the lack of a drinking mechanism or functioning kidney. Thus, whenever fluid regulation is important (as in dehydration, weightlessness, or water loading), errors are likely. Therefore, the long-term model, which has the capability to account for drinking, renal function, and fluid volume shifts, has been used in the Whole-Body Algorithm to automatically define the fluid status for initializing the short-term model. The short-term model could then be used in a simulation of local exercise, postural change in a gravitational field, or lower body negative pressure. Thus, each subsystem can provide its own unique fine level of detail to the other subsystems where previously only a gross representation existed or was absent entirely.

3.2.6.5 Limitations. As previously discussed, the versatility and performance of each subsystem model was improved to some extent during its incorporation into the Whole-Body Algorithm. However, many of the limitations of each subsystem model were carried over to, and thereby limited the capability of, the Whole-Body Algorithm. In addition to these limitations (which have been discussed in the description of each subsystem model), there are also restrictions that arise because of the combining of several

Table 3-8. Capability of Short-Term Subsystem Models to Simulate Short-Term Stresses Before and After Incorporation into Whole-Body Algorithm

Model	Stress					
	LBNP	Tilt	Hypoxia	Hypercapnia	Thermal stress	Exercise
Cardiovascular subsystem	X*	X	WBA[†]	WBA	WBA	X
Respiratory subsystem	WBA	WBA	X	X	WBA	X
Thermoregulatory subsystem	WBA	WBA	WBA	WBA	X	X

[*]X designates stresses for which subsystem has been previously validated on stand-alone basis.
[†]WBA designates additional capability due to integration of subsystem into Whole-Body Algorithm.

models. One such restriction was the increase in time required for performing simulations. Because of this limitation, it was not always desirable to use the Whole-Body Algorithm when the response to only one of its subsystems was required; the stand-alone model operated much more rapidly. A more fundamental limitation was that the integration of several self-contained models resulted in different control centers and different descriptions of the circulatory system. In addition, short- and long-term controllers were artificially divided by the basic structure of the Whole-Body Algorithm. The difficulties associated with combining these subsystems were largely overcome as previously described, and the final model does achieve most of the simulation objectives established. At the same time, in a number of ways the true capabilities of the Whole-Body Algorithm have yet to be tested and realized. Nevertheless, the lack of a more unified controller and controlled system structure (i.e., a bottoms up design) has resulted in a somewhat unwieldy model that may limit the ease with which major expansion can take place. The knowledge gained from developing the present Whole-Body Algorithm should certainly provide a basis for designing other alternative approaches.

3.2.6.6 Simulation Studies. Validating the Whole-Body Algorithm was more difficult than validation of other physiological models because this large model is more complex than most models. This complexity is reflected in the many subsystems, parameters, and dependent variables that it contains. Also, it is difficult to find data for validating a model as encompassing as this one; very few research laboratories report results from more than one major body systems. The reader should also note that the validation studies reported below were performed in 1975 , which, of course, limited the available data to publications prior to that date.

The short-term stresses chosen for simulation were similar to those used to validate at least one of the short-term subsystem models when operated independently. A summary of the short-term models and the corresponding stresses for which they have been tested on a stand-alone basis is shown in Table 3-8. Not all the models were previously capable of responding to all the stresses; the label "WBA" in Table 3-8 appears whenever a new capability was added to the individual models embedded in the WBA. The formulation of the Whole-Body Algorithm has increased the capability of each model and has provided a basis, through the interfacing links and simultaneous operation of all models, for simulating additional stresses in an integrative manner. Validation of a model as versatile and complex as the Whole-Body Algorithm could involve testing an almost endless variety of conditions and stresses. Table 3-9 is a summary of tests chosen to limit the process to a reasonable number of stresses of interest.

The stresses chosen to validate the Whole-Body Algorithm involve some highly complex physiological interactions and some special formulations to provide an accurate simulation. Appendix D contains a detailed account of these facets as well as the rationale for choosing this subset of validations. The stresses and the results of their simulations follow.

a) ***Lower Body Negative Pressure/Tilt.*** Primary responses to LBNP and tilt occur in the cardiovascular system. Changes in several important variables of the cardiovascular system are shown in Fig. 3-42 and 3-43. Some striking changes occur during these stresses, and different responses occurred in the tilt and LBNP experiments. Most of these changes and differences are reproduced by the simulation response. Both LBNP and tilt cause increases in heart rate and decreases in stroke volume. The change in heart rate for the higher levels of LBNP are similar to those observed for a 70° tilt, but the stroke volume decreases are more severe during tilt. A significant difference between these two stresses is seen in the blood pressure response. Tilt results in a large increase in diastolic pressure with

Table 3-9. Whole-Body Algorithm Validation Tests

Stress	Validation criterion			
	Simulation forcing function	Primary WBA Subsystems validated	Simulation duration, hr	Dynamic mode tested
LBNP (-30 to –50 mmHg)	Decreased extravascular pressure	Short-term (cardiovascular)	0.08	S*
Tilt (70°)	Increased gravity vector	Short-term (cardiovascular)	0.08	S
Hypoxia (8% O_2)	Decreased pO_2 of inspired air	Short-term (respiratory, cardiovascular)	0.12	S
Hypercapnia (7% CO_2)	Decreased pCO_2 of inspired air	Short-term (respiratory, cardiovascular)	0.12	S
Thermal stress (20° to 43°C)	Increased ambient temperature	Short-term (thermoregulatory, cardiovascular, respiratory)	6.0	S
Exercise (0 to 200 W)	Increased external workload	Short-term (thermoregulatory, cardiovascular, respiratory)	0.5	S,T[†]
Bedrest (300 ml change in stressed volume)	Increased vascular stressed volume	Long-term	672.0	S,T
Combination of bedrest with pre-exercise, post-exercise, and tilt (300 ml change in stressed volume, 50 W exercise, 70° tilt)	Combined bedrest, tilt, and exercise plus automatic sequencing between long- and short-term subsystems	Long-term plus all short-term subsystems	672.0	S

[*]S = steady state

[†]T = transient

little change in systolic pressure, whereas LBNP evokes a substantial drop in systolic pressure. The simulation of these two stresses results in different hydrostatic gradients in the blood columns and, hence, in dissimilar effects on the baroreceptors. During the onset of LBNP, blood pressure changes are induced primarily through depletion of central blood volume, whereas during tilt, pressure changes occur because of fluid volume and gravity vector changes. The sympathetic response of the model is different for these two stresses, and the model compares favorably with the data from most investigations shown in Figs. 3-42 and 3-43.

b) *Hypoxia and Hypercapnia.* Validation of the simulation of both hypoxia and hypercapnia was limited by the available data on human subjects. Comparison was attempted for these two cases only with studies in which a large number of physiological variables have been measured. Hypoxia was simulated with 8% oxygen in nitrogen and hypercapnia was simulated with 7% carbon dioxide in air, both at atmospheric pressure. The simulation and experimental results were compared after 7 minutes and are shown in Fig. 3-44. Agreement between model results and experimental

data is good for all cardiorespiratory variables and for both stresses. The major differences between hypoxia and hypercapnia appear to be a much lower blood pressure change for the former and a much higher ventilatory response for the latter. Brain blood flow is considerable increased during the hypercapnia stress. The large increases in cardiac output are not entirely due to direct effects on the heart. Analysis of the simulation experiment shows that decreasing peripheral resistance alone will account for a significant portion of the changes in cardiac output.

It is unfortunate that, because of data limitations, validation was possible for only a single inspired gas composition and for a single point in time for each of these stresses. This is a serious limitation to the modeling process, and it does not represent a complete challenge to a model capable of simulating dynamic responses to a wide range of stress intensities. Nevertheless, the results achieved must be considered significant, inasmuch as the same structural changes that were made in the model to simulate the hypoxic stress also permitted an accurate simulation of the hypercapnic stress. The modeling technique was useful for integrating the dynamic responses to these stresses and the numerous pathways involved (see Appendix D).
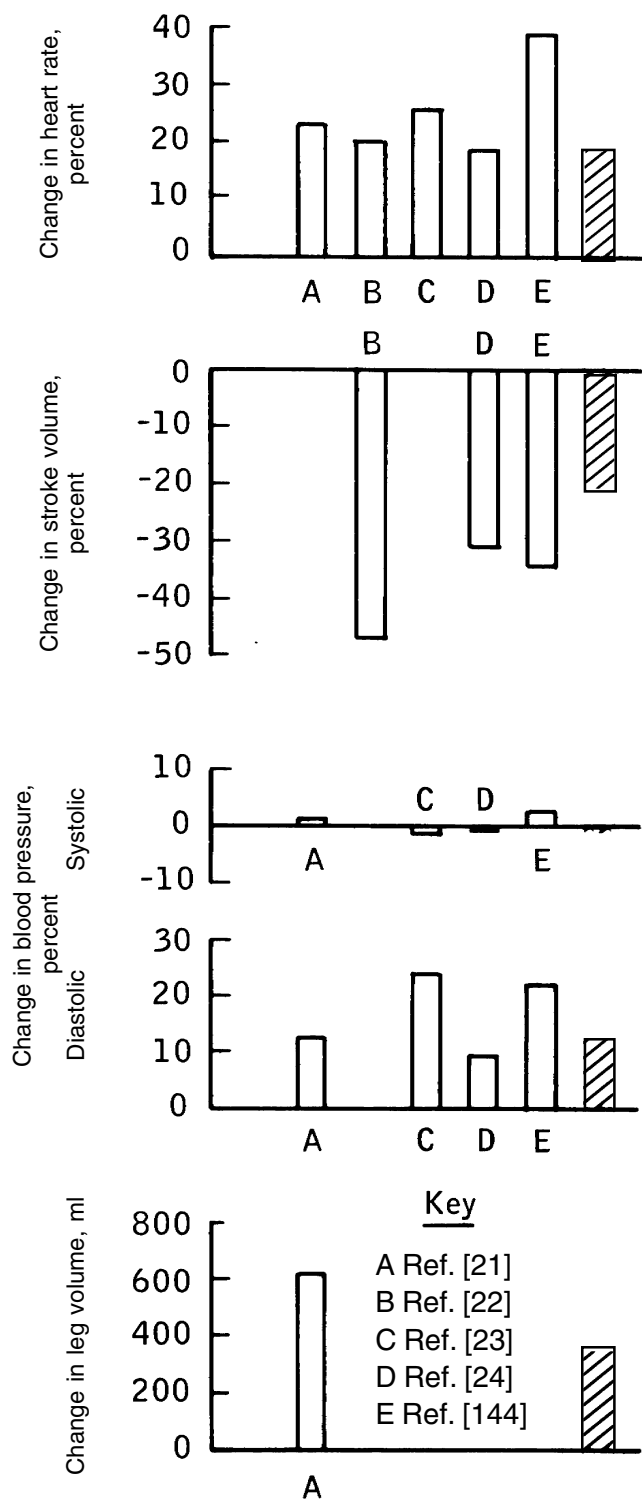
Figure 3-42. Effect of 70° tilt on simulated WBA cardiovascular subsystem response (hatched bars) compared to experimental results (open bars).
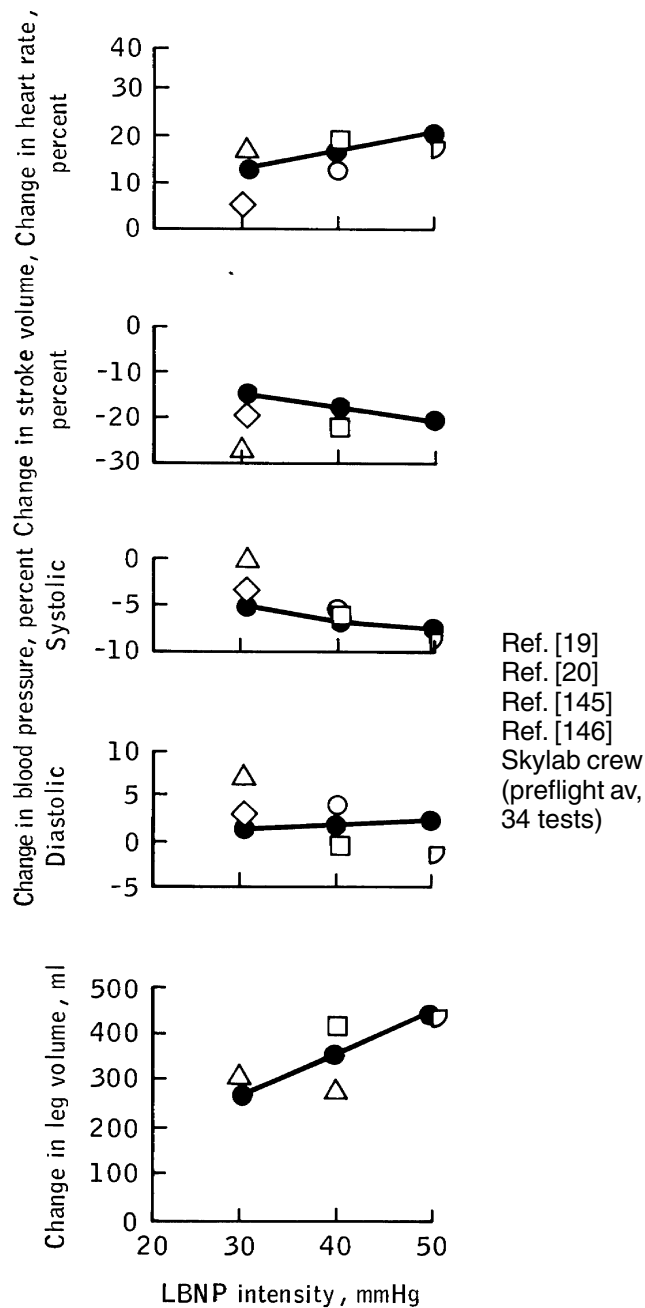
Figure 3-43. Effect of LBNP on simulated WBA cardiovascular subsystem response (solid circles) compared to experimental data (open symbols).

Key

A Ref. [21]
B Ref. [22]
C Ref. [23]
D Ref. [24]
E Ref. [144]

Ref. [19]
Ref. [20]
Ref. [145]
Ref. [146]
Skylab crew
(preflight av,
34 tests)

Figure 3-44. Effect of hypoxia and hypercapnia on simulated WBA cardiorespiratory subsystem response (hatched bars) compared to experimental data (open bars) for following parameters: (A) cardiac output, (B) heart rate, (C) stroke volume, (D) mean arterial pressure, (E) peripheral resistance, (F) arterial pCO_2, (G) arterial pO_2, (H) brain blood flow, and (I) ventilation rate. Scale values for brain blood flow should be multiplied by 2, and values for ventilation rate should be multiplied by 10. (a) Hypoxia; inspired air: 8% oxygen in nitrogen (data from [147] and [148]). (b) Hypercapnia; inspired air: 7% carbon dioxide in air (data from [149] and [150]).

c) *Ambient Temperature.* No previous studies were found which contained reports of simultaneous responses of cardiovascular, thermoregulatory, and respiratory variables in resting man exposed to graded levels of ambient temperature. The greatest experimental effort has been placed on investigating the thermoregulatory system directly, and there are relatively few studies concerning circulatory and respiratory responses. Temperatures from 20°C to 42°C were chosen as a reasonable range over which to test the model. The responses of the model and of human test subjects to this graded heat stress are shown in Figs. 3-45 and 3-46.

It is apparent that the Whole-Body Algorithm correctly predicts responses for a wide variety of variables in all major subsystems throughout the temperature range studied. Inflection points in the data where changes become more marked with increasing temperature (skin temperature, heart rate, cardiac output) are faithfully reproduced by the model. Discrepancies between the model and the data (especially evaporative loss) can be partly explained by the fact that the resting metabolic rate of the model was 10 to 20% higher than that observed experimentally. The stand-alone thermoregulatory model also predicted higher values for evaporative losses than were shown experimentally. Previous work with the thermoregulatory model has shown that evaporative loss rates are particularly sensitive to the choice of metabolic rate [32].

The increasing stroke volume trend of the model as a function of temperature, is at variance with the decreasing experimental values observed, although the divergence is small. This difference may reflect a decreased myocardial contractility but more probably represent a decreased central venous pressure in the human subjects as a result of temperature effects on venous tone. Neither of these effects has been introduced into the model. The decreasing arterial-venous oxygen (A-VO$_2$) difference is a reflection of increased cardiac output being shunted mainly through the skin while oxygen uptake remained constant. Note that between 26°C and 33°C, the cardiac output remained constant during the experiment but increased slightly in the model. The findings suggest that increased skin blood flow at lower temperature is caused by diverting blood flow from the internal organs, whereas at higher temperatures, the further demands on skin blood flow require an increase in cardiac output [152]. This result suggests modifying the cardiovascular subsystem model to include such an effect on the visceral organs. However, any further modifications should be postponed until experiments can be designed to simultaneously measure the cardiovascular, thermoregulatory, and respiratory effects of graded thermal stress.

d) *Exercise.* Understanding the physiology of exercise is a difficult and significant challenge, not only to experimental research but to modeling as well. Because exercise is essentially a short-term stress involving a complex interrelationship of metabolic,

circulatory, respiratory, thermal, and neural activities [52], it represents a stress perfectly suited to rigorously test the validity of the entire short-term section of the Whole-Body Algorithm. Each quantity shown in Fig. 3-41 would be expected to change significantly if the exercise levels were rigorous enough or continued for sufficient time. Each of the three models that comprise this section (respiratory, thermoregulatory, and cardiovascular) had the capability of simulating its respective subsystem response to exercise before incorporation into the Whole-Body Algorithm. However, the representation of certain physiological functions were contained in more than one model and the process of integration provided an opportunity to substitute the algorithm with the best performance. For example, the stand-alone respiratory and thermoregulatory models had a relatively crude representation of the cardiovascular system. During integration, the superior Croston model was used to replace these representations. Also, the thermoregulatory model added appropriate elements to the cardiovascular subsystem, such as changes in skin blood flow that previously did not exist. This substitution process was implemented in most cases via the passing of information through the interface links between subsystem models, as illustrated in Fig. 3-40. These interface modifications and other improvements to the individual subsystems are described in detail in Appendix D.

The Whole-Body Algorithm was validated for exercise by simulating bicycle ergometry in the sitting position for graded levels of exercise. The external workload is entered at the start of simulation as the only required forcing function. Both steady-state and transient responses have been validated for a wide range of activity levels.

The behavior of some of the more important dependent variables of the Whole-Body Algorithm during graded levels of exercise (50, 100, 150, and 200 watts) is illustrated in Fig. 3-47. Comparison with experimental data from a single published source [18] is also shown. Both simulation and experimental values were obtained after 5 minutes of exercise. The model correctly predicted a wide variety of hemodynamic and respiratory responses, including steep linear changes (heart rate and oxygen uptake) and highly nonlinear changes (stroke volume, blood pressures, and ventilation rate) over a wide range of metabolic rates.

Compared to the cardiorespiratory system, the thermoregulatory processes require a much longer time to equilibrate, or reach a quasi-steady state. This delay is partly attributable to the high degree of thermal inertial of the body tissues as well as the relatively slow response of the thermoregulatory feedback processes. Significant changes in such variables as body temperature, sweat rates, and skin blood flows are usually not seen by the end of short-term (5 minutes) exercise [153]. If exercise had been continued for a longer period (both in the human subject and in the model), changes would be expected in the response
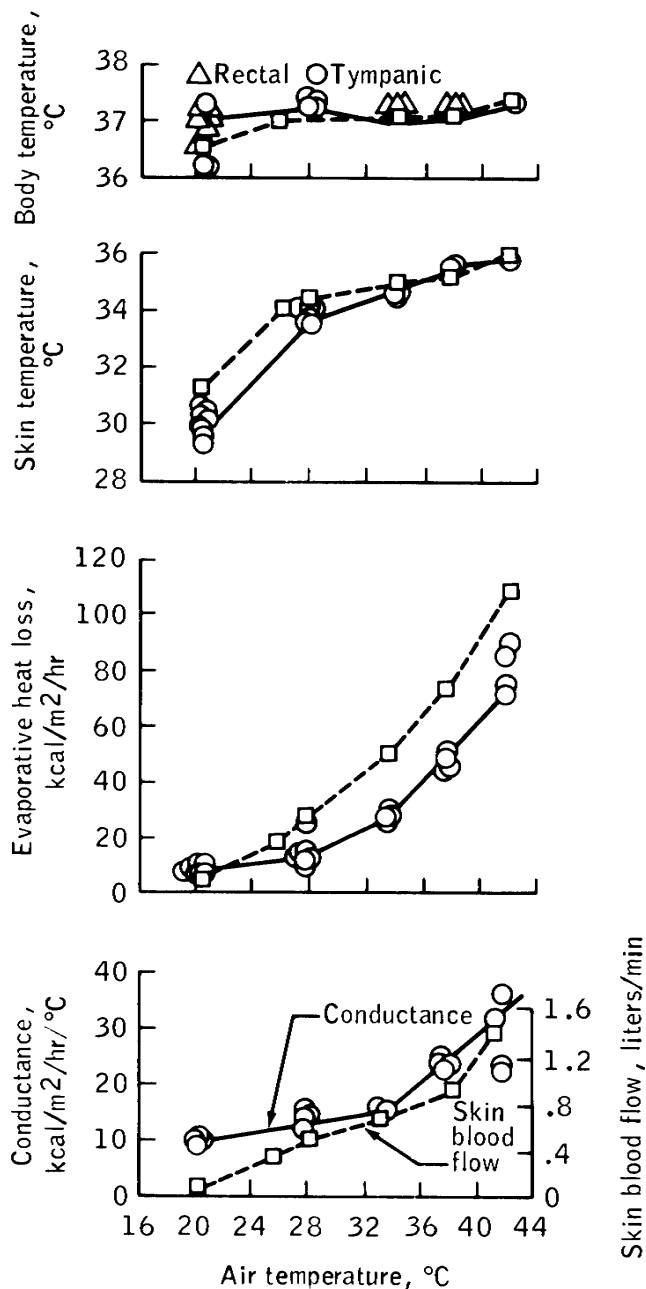
Figure 3-45. Effect of environmental temperature on simulated WBA thermoregulatory subsystem response (dashed lines) compared to experimental data (solid lines) from [151].

Figure 3-46. Effect of environmental temperature on simulated WBA cardiovascular subsystem response (dashed lines) compared to experimental data (solid lines) from [152], shown as percent change from values at 26°C.

that are dependent on heat production as well as in the variables of the cardiorespiratory subsystems that are dependent on skin blood flow (cardiac output, A-VO₂ difference, peripheral resistance, and blood pressure). This effect is shown more clearly in the next two examples, which also demonstrate the capability of the Whole-Body Algorithm to simulate transient as well as steady-state physiological responses.

In the first of these examples (Fig. 3-48), a typical Skylab-type exercise protocol was simulated. The simulation consisted of 5-minute sequences of three graded levels of exercise (50, 100, and 150 watts) followed by a recovery period. Selected responses from all three short-term subsystem models are shown, and all, except heat storage rate and body temperature, tend toward steady-state values at the end of each 5-
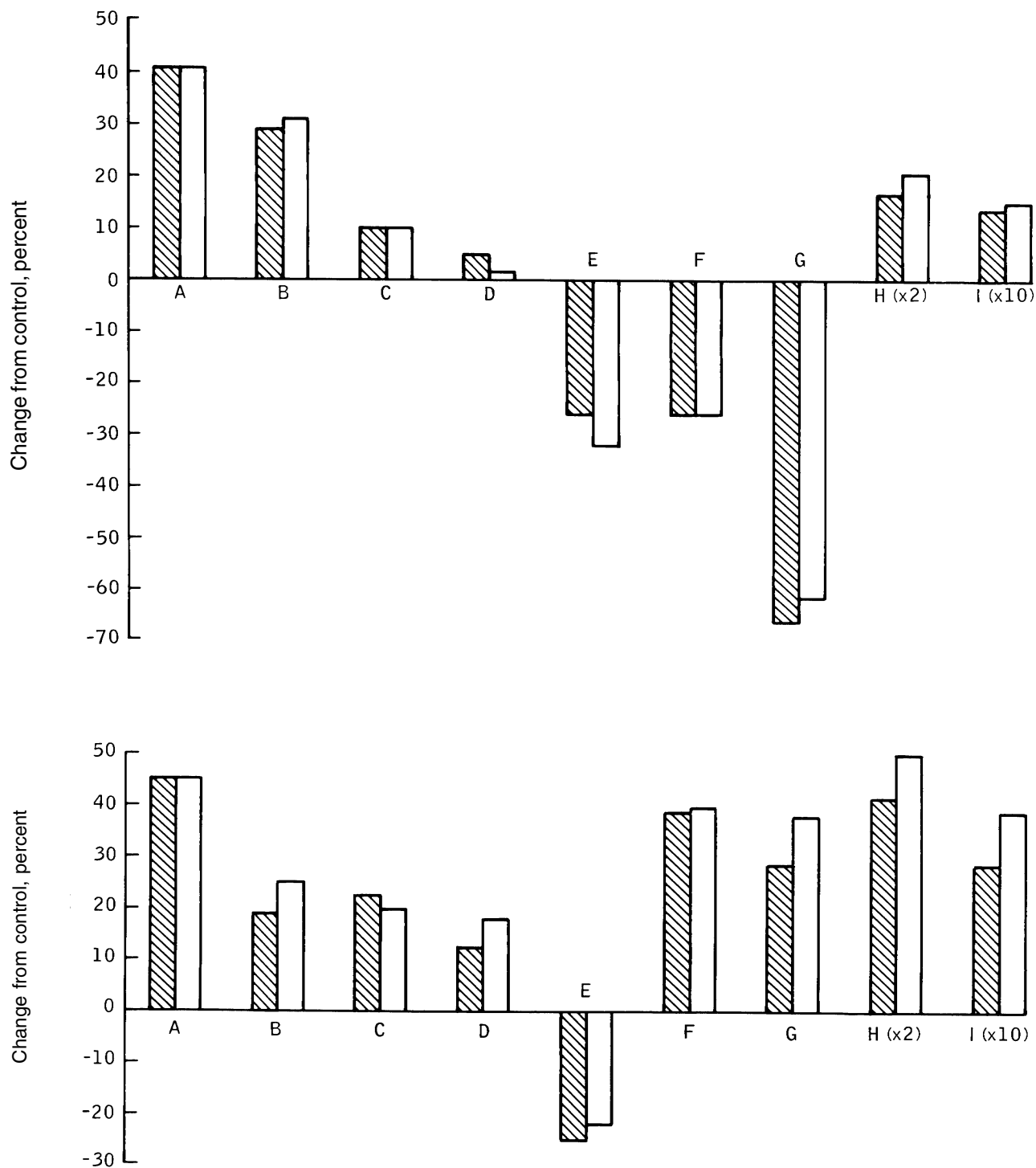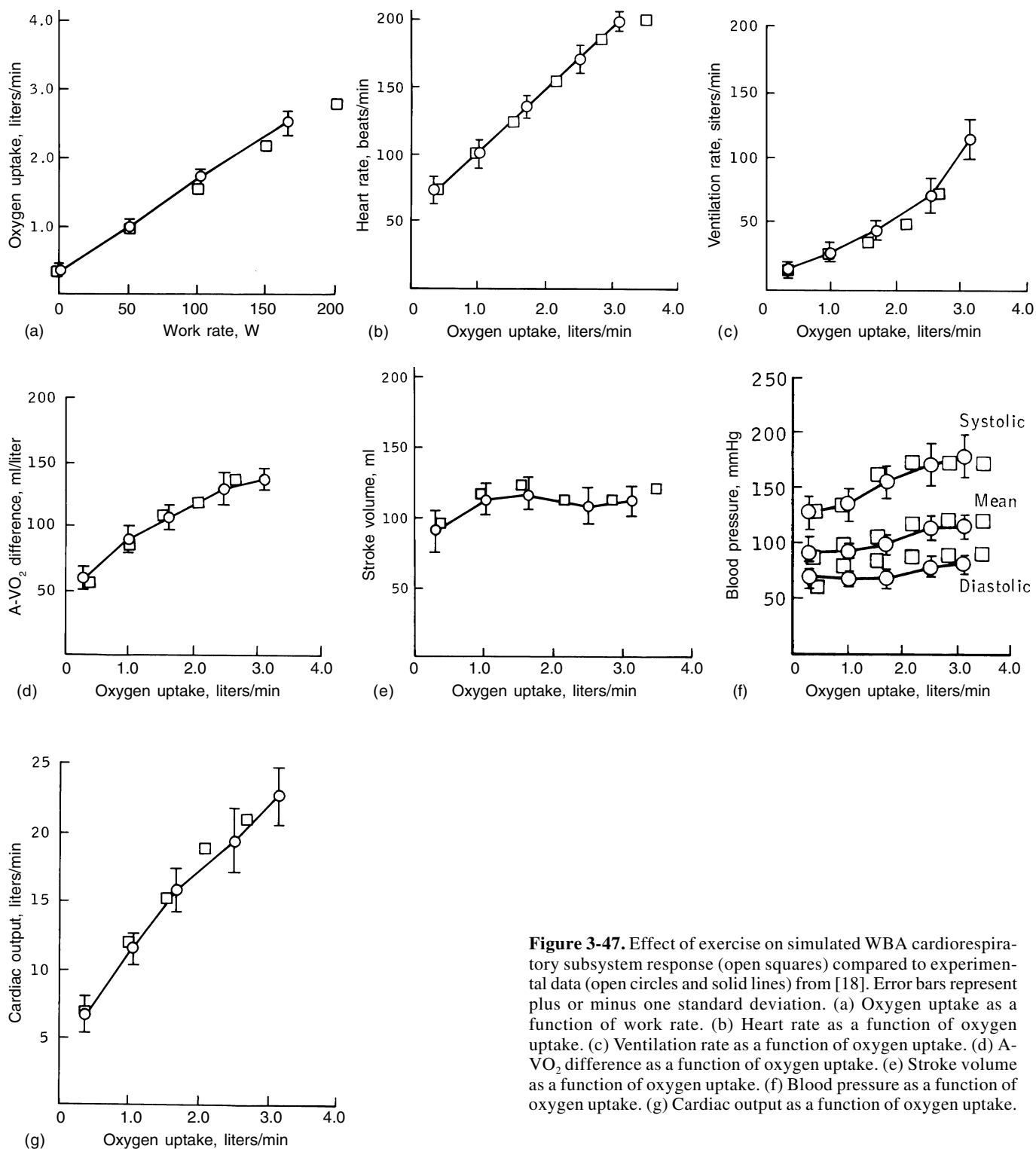
Figure 3-47. Effect of exercise on simulated WBA cardiorespiratory subsystem response (open squares) compared to experimental data (open circles and solid lines) from [18]. Error bars represent plus or minus one standard deviation. (a) Oxygen uptake as a function of work rate. (b) Heart rate as a function of oxygen uptake. (c) Ventilation rate as a function of oxygen uptake. (d) A-VO_2 difference as a function of oxygen uptake. (e) Stroke volume as a function of oxygen uptake. (f) Blood pressure as a function of oxygen uptake. (g) Cardiac output as a function of oxygen uptake.
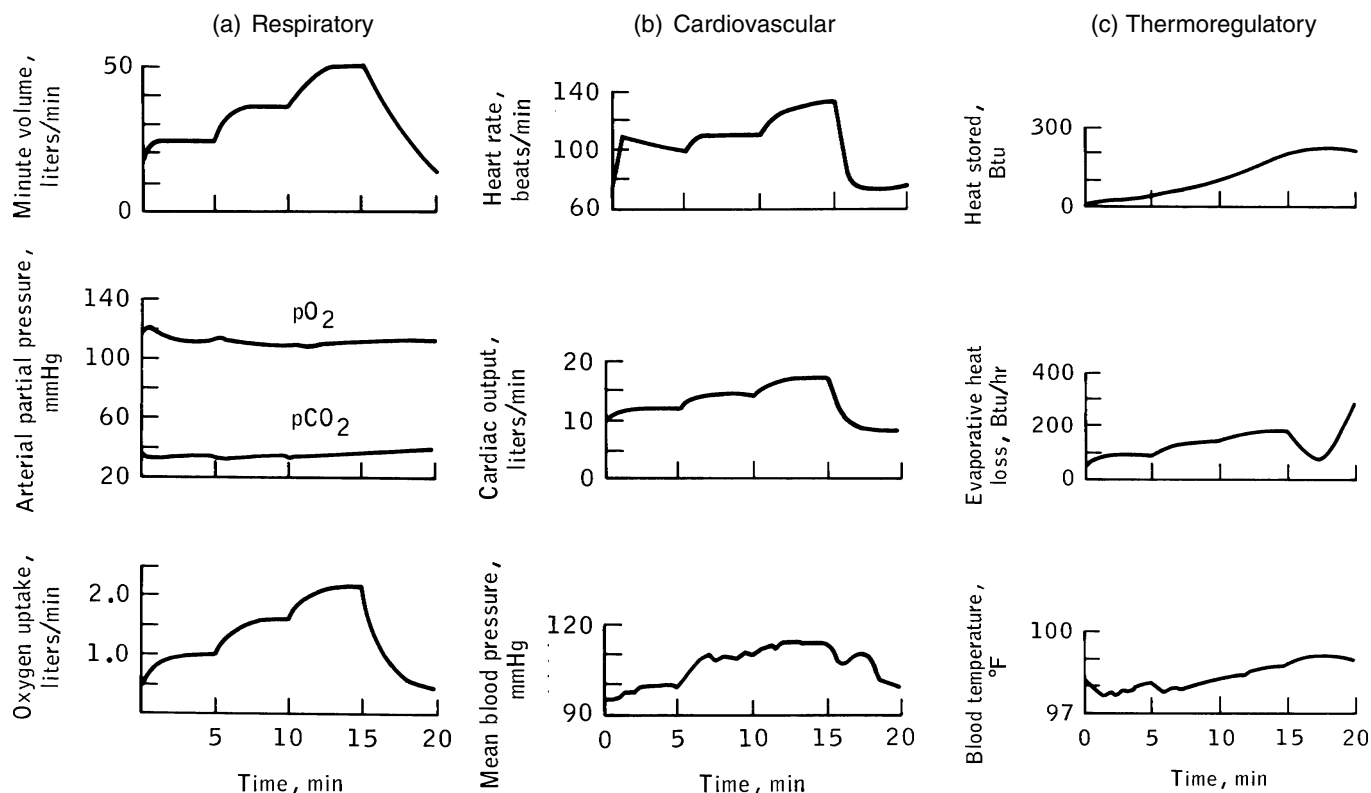
Figure 3-48. Simultaneous subsystem responses of the Whole-Body Algorithm during simulation of a sequential exercise protocol: 5 minutes exercise at 50 watts (0 to 5 minutes on time scale), 5 minutes exercise at 100 watts (5 to 10 minutes on time scale), and 5 minutes exercise at 150 watts (10 to 15 minutes on time scale) followed by a 5-minute recovery period (15 to 20 minutes on time scale). The parameters shown represent only a few of the many variables that can be predicted. (a) Respiratory subsystem. (b) Cardiovascular subsystem. (c) Thermoregulatory subsystem.

minute exercise segment. It also should be observed that no significant changes are predicted to occur for arterial pO_2 and pCO_2 during exercise except for the onset transient. This result supports many physiological observations and illustrates the current dilemma of respiratory physiologists in explaining the striking hyperpnea of exercise despite these small changes in gas tensions.

The capability of the Whole-Body Algorithm to predict significant changes in thermoregulatory responses to longer and more severe exercise (200 watts for 30 minutes) is shown in Fig. 3-49(a). These predictions of transient behavior agree with the observations reported by Saltin et al. [153], which are shown in Fig. 3-49(b). Similar changes in body temperatures are shown by both simulation and experiment. The esophageal temperature of the subject and the blood temperature of the model, both representing deep body temperature, rose half as much as skin temperature. The simulated skin blood flow is characterized by a steep rise similar to the experimentally determined thermal conductance (a crude estimate of skin flow). Maximum sweat rate of the human subject was ap-

proximately 15 g/min, a value also predicted by the model.

Significant delays occurred in the responses of deep body temperature, skin temperature, and sweating rates both in the human experiment and in the simulation. Since conductance measures both skin and muscle blood flow, it would be expected that the delay in skin flow predicted by the model, might not be revealed by this experimental indicator. However, more recent studies have demonstrated a significant delay in skin flow during the onset of exercise [154,155]. The model responses reveals that the extra demands of blood flow to the skin result in a greater cardiac pumping requirement, a decrease in peripheral resistance, and an $(A-V)O_2$ difference. All these predictions are reasonable but not yet fully confirmed in the laboratory.

Also shown in Fig. 3-49 are the predicted responses of the conductive and radiative losses (known to remain relatively constant) and the rate of heat production. In the model, almost 80% of the energy produced during exercise is converted to heat within the body, and the rise in heat production parallels the
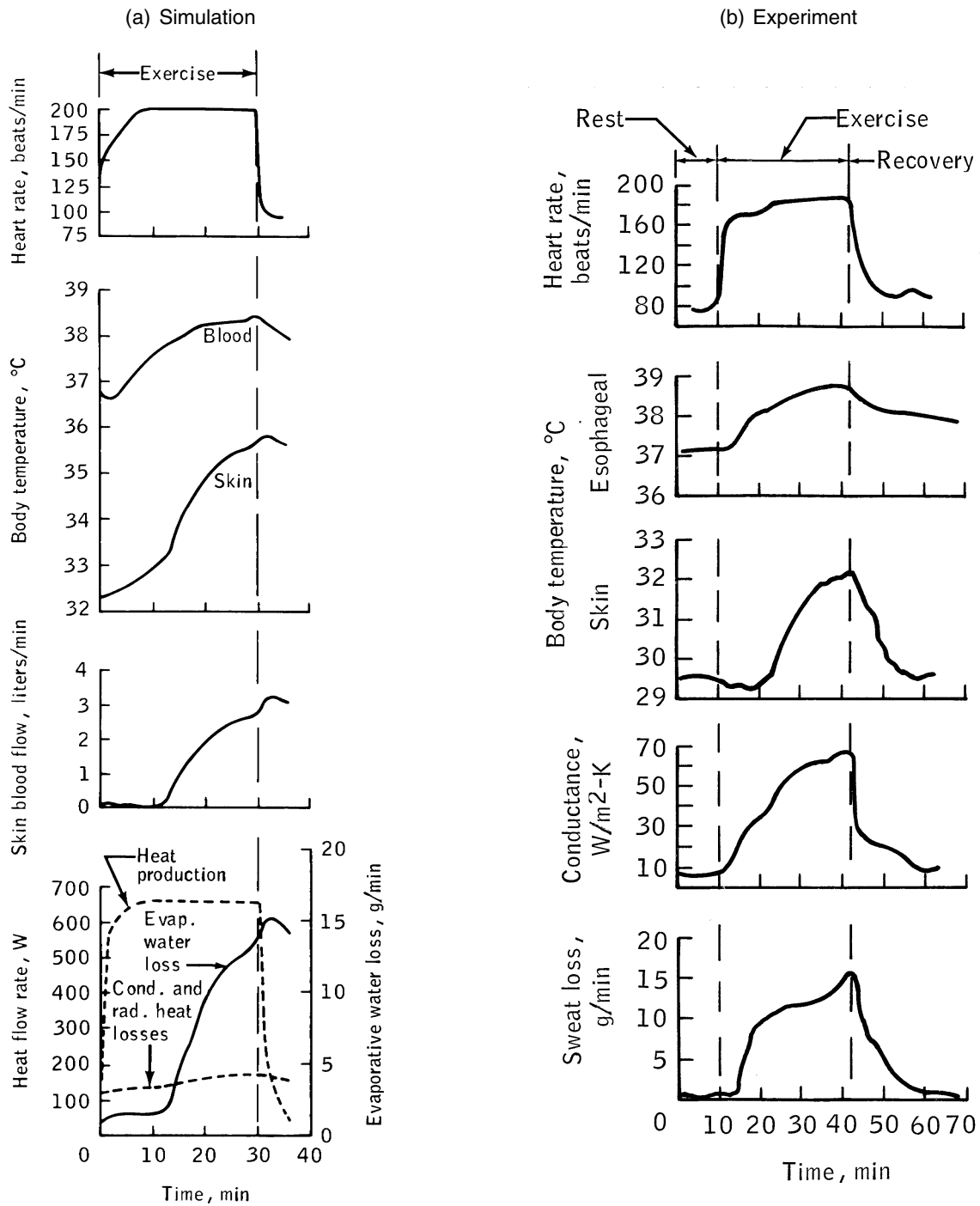
Figure 3-49. Simulated responses of the Whole-Body Algorithm to 200-watt exercise (left side) compared to experimental data from [153] (right side). (a) Simulation. Ventilatory oxygen rate = 2.75 liters/min; air temperature = 24°C. (b) Experimental data. Ventilatory oxygen rate = 3.15 liters/min; air temperature = 20°C.

dynamic behavior of oxygen uptake as well as muscle blood flow.

In comparing the stand-alone cardiovascular model responses to exercise and the response of the Whole-Body Algorithm, it has become apparent that the Whole-Body Algorithm simulation is superior in many respects. This superiority is evident in accuracy of response, stability, and, in particular, the capability to predict detailed simultaneous responses from several important physiological systems involved in the exercise stress. Although still untested, the capability now exists to combine multiple environmental and metabolic stresses for studying some very important physiological conditions. These include supine or sitting exercise in environments of abnormal pressures, temperatures, humidities, and gas concentrations as well as studying the effects of such important parameters as blood volume and hemoglobin concentrations. Because of the importance of exercise as a stress in daily human function and the complexity of the response to exercise, we believe that the ability to simulate short-term exercise is the single most promising aspect of the WBA and one which time (and lack of suitable data) did not permit full exploration.

The initial validation of the Whole-Body Algorithm was limited to a one-g stress simulation as described for short-term subsystems. The stress chosen to validate the long-term (Guyton) subsystem of the Whole-Body Algorithm was bedrest, because it has long been considered an analog to zero-g. This simulation study is presented in Chapter 9.2. The capability of the Whole-Body Algorithm to simulate a typical spaceflight sequence of long-term stress preceded and followed by acute metabolic orthostatic tests will also be demonstrated. The model, validated for sequencing of events in one-g, can then be used to help formulate and test zero-g hypotheses by direct comparison of the model output with the mission data. This aspect also is considered in Chapter 9.

In summary, the development of a Whole-Body Algorithm, has resulted in a model which:
1. Provides a flexible structure for making changes without total disruption of the entire system;
2. Provides a central repository for collecting hypotheses for physiological changes due to the spaceflight environment;
3. Provides the capability to test multiple system interactions and total system hypotheses related to any stress it was designed to simulate;
4. Provides basic capability to simulate multiple and sequential stresses with little or no change in model structure;
5. Provides the basic structure for adding new subsystem models, improved sections in the sub-system models, and the mechanisms and/or interface changes necessary to simulate additional stresses.

3.2.7 Calcium Regulatory Model

Although the Skylab Program provided the first opportunity to study the long-term effects of weightlessness, the much shorter-term Gemini and the Apollo missions suggested the occurrence of a negative calcium balance and bone mineralization [156,157,158]. Data gathered from the Skylab crewmen provided solid experimental evidence supporting the existence of an altered state of calcium metabolism on exposure to zero-g [159]. Because of the complicated nature of calcium regulation, it was decided to develop an appropriate model for use as an analysis tool.

3.2.7.1 Model Rationale. The purpose of the calcium model is to simulate altered states in calcium metabolism and bone demineralization during bedrest and zero-g exposure. To function satisfactorily, the model should have the following characteristics:
1. Be capable of describing plasma concentrations and effects of specific calcium regulatory agents. Initially, the regulatory agents of interest will be vitamin D and its metabolites, parathyroid hormone, and calcitonin;
2. Be capable of simulating both steady-state and transient calcium changes and important interactive biochemical and physiological responses to selected stresses;
3. Embody plausible mechanistic hypotheses for the action of complex stresses such as spaceflight and bedrest on those systems concerned with calcium homeostasis and thereby indicate areas where further study is needed;
4. Provide a validated baseline model of calcium metabolism which can be improved or updated by additional mechanisms or improved formulations of various aspects of the model;
5. Help interpret spaceflight data and related ground-based analog studies with regard to bone demineralization and plasma and urinary levels of associated minerals and their regulatory agents.

Most existing mathematical models capable of simulating calcium metabolism are compartmental models designed to reproduce the distribution kinetics of a tracer. The main objective of such compartmental models is to describe the calcium pools and the fluxes between these pools, primarily in the bone and secondarily throughout the body. The parameters contained in these models are determined from experimental metabolic balance data, and the models can be used to describe the calcium kinetics in either normal or stressed individuals, depending on the experimental procedure used to gather the data. An examination of the results of previous compartmental model analyses helped in the formulation of hypotheses concerning calcium regulation. Some of the compartmental models considered were those of Aubert, Bronner, and Richelle [160]; Cohn et al. [161]; and Neer et al. [162]. Further discussion of existing calcium models is contained in Brand [163].

Unfortunately, most compartmental models have several important disadvantages that greatly limit their application to simulation of low gravity. All compartments and rate constants derived from these models are mathematical constructs which represent a multitude of physiological components and processes that are indistinguishable from each

other; thus, the elements in the calcium regulatory system that are responsible for a particular experimental result cannot be resolved in these type of models. A secondary disadvantage of these models is the assumption of steady-state conditions used to assess the rate of bone activity in calcium regulation. The rate of intestinal calcium absorption is generally assumed to be constant in the models. Then, with steady-state conditions, a constant rate of calcium absorption, and a known rate of calcium excretion (an experimentally supplied value), the changes in calcium balance, theoretically, would be due to changes in bone calcium. Consequently, any changes in calcium balance were assumed to reflect only bone activity (i.e., bone resorption or bone deposition of calcium). In the space-flight environment, these assumptions concerning the calcium balance and bone activity may be realistic, but the steady-state assumption is not. Another disadvantage of compartmental models that represent non-physiological compartments or pools is that such models are difficult to use in a predictive mode, especially in situations that are different from those used to determine the model parameters. Thus, an alternative type of model, a deterministic, physiologically-based model, was sought for the present project.

3.2.7.2 Description of the Calcium Regulatory Model.

Extensive research has been done in deciphering the regulatory features of calcium homeostasis since the discovery of parathyroid hormone, calcitonin, and the metabolites of vitamin D [164-168]. The influence of diet and hormonal activity in the gastrointestinal tract and the kidney and the many feedback pathways between the hormones and plasma calcium concentrations are becoming more clearly defined. The skeleton is perhaps the least understood site of calcium metabolism, but rapid progress is also being made in this area. Consideration of all these facts in relation to the purpose for which the model was being built led to the development of the model shown schematically in Figs. 3-50 and 3-51. Design requirements for this model included the following.

1. The model parameters should have physiological significance in terms of calcium metabolism and should include:
    a. The rate of calcium absorbed from the gastrointestinal tract;
    b. The rate of calcium reabsorbed by the renal tubules or the rate excreted in the urine;
    c. The rate of calcium released or retained by osteocytic regulation of rapidly exchangeable bone calcium;
    d. The rate of calcium derived from bone resorption by osteoclasts or deposited into bone by osteoblasts;
    e. The concentration of plasma parathyroid hormone;
    f. The concentration of plasma 1,25 dihydroxy-cholecalciferol (the active form of vitamin D);
    g. The concentration of plasma calcitonin.
2. The calcium model should be developed as an integrated set of subsystem models, each of which describes one particular aspect of calcium metabolism. With this model structure, modifications and improvements can be easily made in the model without affecting the other subsystems of the model. The subsystem models should describe (1) the plasma concentrations of parathyroid hormone, calcitonin, vitamin D, calcium, and phosphate, (2) the rate of renal clearance of calcium and phosphate, (3) the rate of intestinal absorption of calcium and phosphate, and (4) the skeletal content and the fluxes of calcium and phosphate.
3. The controlling system should include the regulatory features of parathyroid hormone, calcitonin, and 1,25 dihydroxycholecalciferol. The controlled system should include the intestinal tract, kidney, bone, and plasma concentrations of calcium and phosphate. The major regulators in the feedback loops should be the plasma concentrations of calcium and phosphate (see Chapter 8 for a more detailed schemata of the model).
4. Validation of the calcium model should involve two steps. First, as each subsystem model is developed, it should be validated individually. Secondly, the model should be validated as a composite of its subsystems. The calcium model should be validated by simulating the responses to the following stresses:
    a. Calcium loading or deficiency;
    b. Phosphate loading or deficiency;
    c. Vitamin D loading or deficiency;
    d. Parathyroid hormone loading or deficiency;
    e. Calcitonin loading or deficiency;
    f. Changes in dietary calcium or phosphate.
5. Initially, only one-g simulation of stresses should be required. Only after the model is so validated will the simulation of the zero-g stress (bone demineralization) be attempted.

The model should also contain a structure appropriate for the inclusion of additional levels of detail in some subsystems, particularly in the area of bone metabolism. Bone is a dynamic tissue the main function of which is to provide support and structure to the skeletal muscles and body and the secondary function of which is to act as a calcium reservoir in the maintenance of plasma calcium. Bone metabolism may be affected either by the physical stresses induced by its primary function or by the biochemical alterations induced by either function. The biological effects of the physical stresses, such as piezoelectric effects and tensile or shearing forces, affect the bone directly rather than being mediated by any soft-tissue metabolism. The kidneys, the intestinal tract, and the biochemical regulators also influence bone maintenance. Since the soft-tissue kinetics of calcium regulation are better understood at present than the physical effects on hard-tissue metabolism, the initial calcium model should not be a bone model as such but a calcium model encompassing the important biochemical calcium regulatory events in the body. As this model is validated, it should be expanded into the area of physical bone regulation, with the ultimate purpose being to understand the effects of hypogravic environments on bone composition.

In view of the fact that the calcium model is such a recent development in this project, validation studies have not yet been completed. Further details on the design
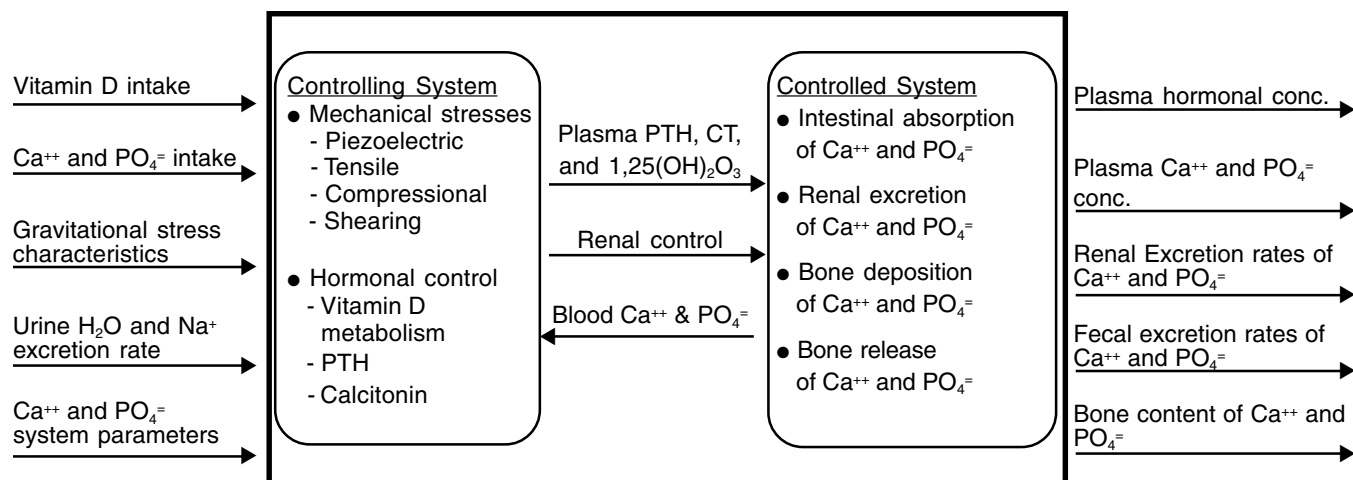
Figure 3-50. Model of Calcium Regulation. Development of this model of calcium metabolism is not complete. The design specifications define the calcium fluxes between the intestinal tract, kidney, bone, and plasma as the controlled system. These elements are controlled by the plasma concentrations of parathyroid hormone (PTH), calcitonin (CT), and the active metabolites of vitamin D, as well as by changes in mechanical stresses due to alterations in the gravitational load. Other controlling elements include the urinary excretion rates of sodium and water. The feedback loops influencing the controlling system are directed via the plasma concentrations of calcium and phosphate (PO_4). Thus, the model is designed to investigate the relative influence of the factors controlling calcium and bone metabolism.

Figure 3-51. General description of calcium model showing the major elements that control plasma calcium and the hormones involved in calcium metabolism. Only the primary pathways are indicated. A more detailed description of the feedback pathways is presented in Chapter 8. PTH = Parathyroid hormone; CT = Calcitonin; Ca = Calcium; P = Phosphate.

specifications for the calcium model can be obtained from Brand [163] and simulation examples are presented in Chapter 8.

3.3 Hypothesis Testing Approach

The overall objective of the study documented herein was to formulate a unified and consistent hypothesis that explained the major physiological responses to weightlessness. To accomplish this objective, it was necessary to process spaceflight crew data into a form appropriate for use with simulation and modeling and then to use these data in the development and testing of hypotheses. The systems analysis approach results in an interactive cycle whereby preliminary data processing suggests hypotheses as well as the type of simulation models required for physiological interpretation. In turn, during the course of the simulation studies, hypotheses are tested and procedures for analyzing and processing data are redefined. Some of the important aspects of this process are discussed in this section (see Fig. 2-6).

3.3.1 Environmental and Metabolic Disturbances

Although weightlessness was the major spaceflight factor of interest in these studies, a number of other environmental and metabolic disturbances are present in spaceflight in general and Skylab in particular. The following factors became important in the data analysis:
- Absence of gravity
- Hypobaric ambient pressure (1/3 atmosphere)
- Artificial gaseous atmosphere (190 mmHg pO_2, 5 mmHg pCO_2)
- Elevated temperatures during early period of 28-day mission
- High g-forces at launch and reentry
- Caloric content of diet that was different on each mission
- Exercise levels which were different on each mission
- Space motion sickness incidence

These factors have the potential to confound conclusions about ascribing the cause of any particular physiological observation to the influence of gravity (or lack of gravity). The data analysis, therefore, included not only a comparison of 1-g and 0-g but also attempted to account for the effect of such factors as oxygen partial pressure, caloric intake, exercise training, and incidence of motion sickness.

3.3.2 Preparation of Crew Data

At the beginning of this effort, it was decided that the analysis of data should be restricted to the support of the program's main objective, which was the use of the theory of feedback regulatory systems to elucidate some of the major physiological mechanisms crucial to weightlessness adaptation. Indeed, one important question that was being pursued was "do the normal feedback pathways that appear to regulate body function in on Earth, operate in a similar manner in weightlessness"? This approach meant that data analysis as such would not be a goal of this project but that such analysis would be used as a tool to develop and test specific hypotheses. Experimental data were to be used in conjunction with simulation models in two ways:first, as a means of providing values for model input or forcing functions and, second, for comparing experimental observations with responses predicted by the model. Each principal investigator had already done extensive data processing, and readily available results, e.g., Johnston and Dietlein [159], defined the point of departure for the project described here. The systems analysis approach was expected to contribute to the *integration* of data from various disciplines; this had not yet been accomplished.

3.3.3 Scope of Data Considered

Table 3-10 illustrates the kinds of information selected for the integrated data analysis project and the Skylab biomedical experiments from which they were derived. This list is merely representative and is not complete, as more data than indicated here were collected for each of the experiments. Despite the fact that all the measured data could not be used in the simulation models, a great deal of interdisciplinary analysis was required, especially since an integrated simulation response which was in basic quantitative agreement with most of the experimental findings was sought. Represented in this list are approximately 80,000 individual measurements spanning the preflight, inflight, and postflight periods of three missions and for nine subjects. In many cases, the analyses were extended by comparing spaceflight and bedrest responses and the total amount of data processed in this integrative effort was increased proportionally as ground-based studies were included.

3.3.4 Grouping of Subjects

One of the primary objectives that guided the data analysis was the characterization of a generalized response to weightlessness. Therefore, the limited number of Skylab subjects suggested that all nine subjects be treated as a single group. This approach was complicated by differences between missions, such as duration, subjects, average caloric intake, exercise levels, and degrees of motion sickness (see Chapter 3.3.1) On the first manned mission, a temporary malfunction of the spacecraft heat shield resulted in higher ambient temperatures for several days; this fact was used to explain apparent anomalies in the water balance analysis. In the final analysis, the treatment of data by subject ($N = 1$), by mission ($N = 3$), or by combining flights ($N = 9$) was dictated by the particular subsystem or response of interest. For example, the loss of red cell mass was progressively smaller on each subsequent mission for unknown reasons, and it became an important objective to explain these differences between flights. In this case, the data from each mission were treated separately. Alternatively, combining data for three missions was deemed permissible if there was reason to believe flight duration had little effect on a particular response. An illustration of the latter was the significant loss of body fluids and electrolytes, which appeared to be a common occurrence in all crewmembers on all three flights. Nine-

Table 3-10. Skylab Experiment Data Used for Integrated Systems Analysis

No.	Experiment Title	Data Used
M071	Mineral balance	Na^+, K^+, N, Ca^{++} in diet and excreta
M073	Bioassay of body fluids	H_2O intake and excreta Fluid volumes of total body, extracellular and plasma compartments Exchangeable body K^+ Biochemical assay of urine and plasma: Na^+, K^+, osmolarity, catecholamines, cortisol, angiotensin, aldosterone, and ADH Urine specific gravity
M074	Specimen mass measurement	Fecal weights Food residues
M092	Lower body negative pressure	Resting and stressed heart rates, systolic and diastolic pressures, and change in leg girth Leg blood flow Venous compliance Change in leg volume
M110	Hematology and immunology	Red cell mass Reticulocytes Inflight hemoglobin
M171	Metabolic activity	O_2 uptake Blood pressures Cardiac output Heart rate Pulmonary efficiencies Mechanical efficiencies
M172	Body mass measurement	Daily body mass Stereophotogrammetry Body volume Body density Change in leg volume

man averages were used, in this situation, to validate the fluid-electrolyte model. In most cases, the nine-man average was only appropriate for the period consisting of the first 28 days of flight; this was the period common to all flights. In other cases, a composite Skylab response was developed for a 3-month mission by averaging nine subjects for the first month, six subjects for the second month, and three subjects for the third month.

Another consideration that guided the data analysis was the number of variables considered as factors in a particular hypothesis. In general, as the number of observed variables available for comparison with a model's responses increased, the precision that we demanded in matching these responses decreased. This guideline usually meant that a larger number of subjects could be included in the pooled data, since it was not necessary to distinguish the more subtle changes between subjects or flights. Also, the group size was permitted to increase as the data became more

noisy (that is, trends with time were poorly delineated). Regardless of the grouping method employed, it was required that a consistent treatment be applied to all data used for testing a given hypothesis or set of hypotheses. This flexible approach to data grouping was necessary to enable the consideration of a maximum number of subjects for a particular hypothesis without neglecting important differences between subjects and flights.

3.3.5 Hypothesis Testing and Development
3.3.5.1 The Process. The analysis process, described earlier in Chapters 2.6 and 3.1, assisted the investigative team in rapidly scanning large quantities of time-dependent data for crew-men (individually or as a group), in detecting significant changes or trends in the measured variables, and in making statistical correlations between variables, flights, flight phases, and subjects. This process often suggested hypotheses regarding basic changes in physiological func-

tion that could be tested either statistically or by using the predictive capabilities of the simulation models.

The models, validated for preflight experiments, were used to simulate experiments during and following the mission. These "experiments" included not only well-defined stress tests such as LBNP and exercise but also the observations from the biochemical and biophysical analyses (that is, blood sample analyses, urine collections, and whole-body measurements). Because the models were validated for preflight experiments, the models, without any modifications for describing weightlessness, acted as a one-g control to the Skylab data. Any discrepancy between inflight data and inflight simulation predictions was assumed to be associated with adaptation to weightlessness or to other environmental, e.g., high ambient temperatures, dietary, metabolic, e.g., extravehicular activities or intense exercise periods, or medical, e.g., drug usage, factors. Candidate hypotheses that might account for these differences were then developed and incorporated into the mathematical model for testing.

Any hypothesis, to be acceptable, should meet specific criteria. The hypothesis should be physiologically plausible and should yield simulation results that exhibit the same trends observed in the Skylab data over the course of the mission. Furthermore, the hypothesis should also be consistent with other working hypotheses and with the results of other acceptable model simulations.

Often, more than one hypothesis or combination of model parameter values can lead to a given simulation response. The more plausible of these may be identified for further experimental examination. It may be quite possible to choose between competing hypotheses when the regulating system is easily defined and when the system variables can be measured directly. However, given the complexity of the physiological and modeling systems and the limited number of measurements available on Skylab, simulations were better suited for eliminating inappropriate hypotheses. The systems approach applied to hypothesis testing, therefore, usually resulted in a ranking of candidate hypotheses rather than in isolating one definitive conclusion.

Testing hypotheses using computer simulations of a mathematical model is not unlike performing experiments in the laboratory on an unknown system. The starting point is to ask simple and easily understood questions (based on a simple model) and progressing to the more complex world of reality. At each stage in this process, it was important to ensure that the model's response was appropriate. This objective was accomplished by validating the model for similar stresses for which the response mechanism was known (see Tables 3-2 and 3-7). In this way, it was possible to evaluate complex hypotheses involving multiple and competing stresses, each characterized by its own dynamic behavior. Figure 2-6 illustrates the steps in the use of models to test hypotheses.

As an example of how several models could be used as part of this hypothesis testing approach, consider the following hypotheses that involves three major body systems and three of the simulation models:

Hypothesis (A)
Total blood volume losses observed in spaceflight are a result of two separate occurrences:plasma volume losses and red cell mass losses.

Hypothesis (B)
Plasma volume is diminished in spaceflight as a result of headward fluid shifts activating renal excreting mechanisms.

Hypothesis (C)
Red cell mass is diminished in spaceflight as a result of hypovolemia-induced hemoconcentration which inhibits red cell production.

Hypothesis (D)
The higher heart rate observed in astronauts in space during LBNP testing (compared to the same LBNP tests on the ground) is a result of a decrease in total blood volume which causes enhanced signals from the baroreceptors.

Figure 3-52 is a pictorial representation of these hypotheses indicating the boundaries of interest for the appropriate simulation model. Hypothesis (B) can be tested in Guyton's circulatory-fluid-electrolyte model; hypothesis (C) can be tested in Leonard's erythropoiesis regulating model; and hypothesis (D) can be tested in Croston's cardiovascular system model. Alternatively, all the hypotheses can be tested in a single model – the combined Whole-Body Algorithm.

These hypotheses are only presented in abbreviated form; the complete spectrum of physiological pathways considered for each of these events is more complex and they are discussed in later chapters. Nevertheless, Fig. 3-52 indicates the systems concept used in this study. An integrated view of spaceflight physiology is achieved by segmenting the larger hypothesis into subsystem hypotheses, evaluating them separately on the individual subsystem models, and using the Whole-Body Algorithm to test the integrated total-body zero-g hypothesis.

3.3.5.2 Limitations. Although systems analysis techniques are useful in formulating and testing hypotheses, conclusions should be approached cautiously. One can conclude that a good simulation match with experimental data, even if only for one or two individuals, does support the hypothesis being tested, particularly when the inclusion of the hypothesis into the model changes the simulation results from a poor to a good match. However, successful simulation of the response to an experiment does not constitute proof that the hypotheses are valid. Alternatively, the failure to match the response of one or two crewmen is not proof that the hypotheses are invalid. Nevertheless, it must be considered encouraging when a complex process provides accurate simulations (in terms of magnitude and direction) of the dynamic response of a complicated physiological system to a wide range of stresses. Although the procedure is sound, the verification of any hypothesis involves a considerable amount of work, including verifying all data input to the models as well as experimental data, rechecking all calculations, estimates,
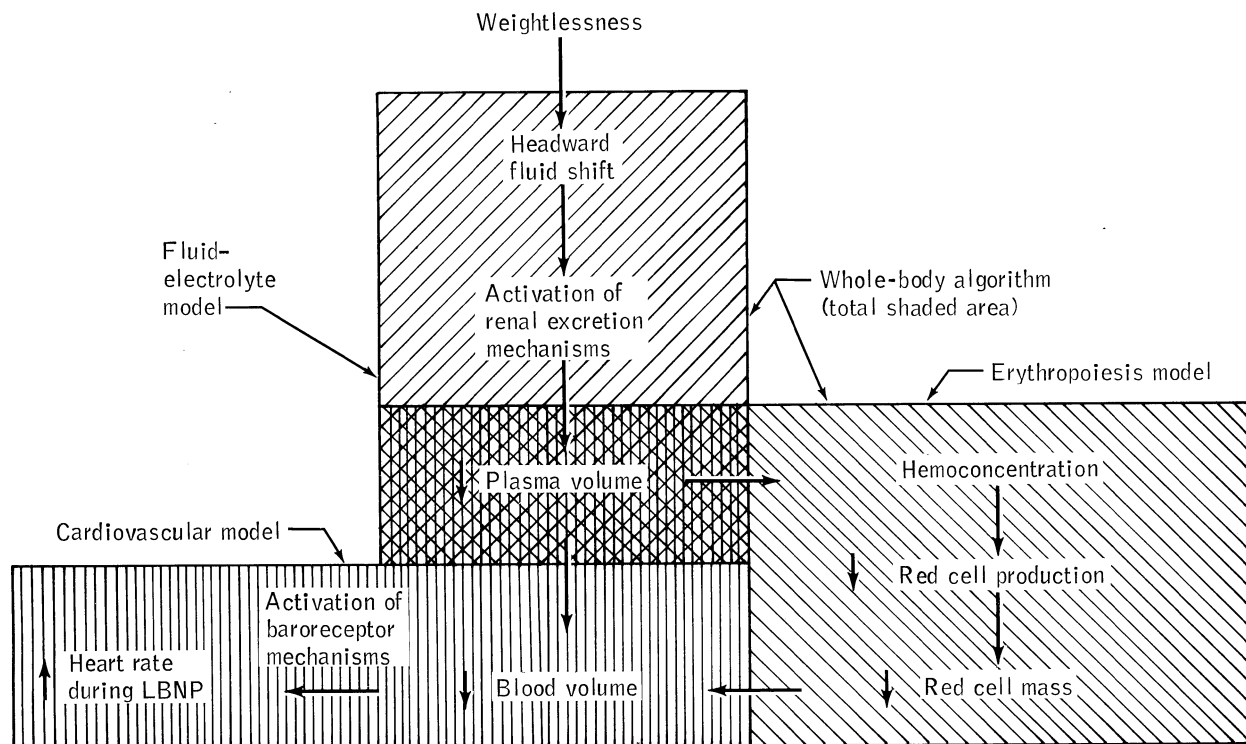
Figure 3-52. Example of subsystem and integrated hypothesis testing with simulation models. Shown here are three subsystem models that are contained in the Whole-Body Algorithm. The diagram illustrates how the effects of plasma volume disturbances can be studied in each model subsysem and integrated effects studied in the combined model.

and assumptions and supporting them with independent analyses or data from other sources, and comparing experimental data for different, but related, experiments for all crewmen with results from the model containing the hypotheses being tested.

Even with all of the precautions for assuring accuracy of the simulation, the model is only a representation of the real system and, as such, will probably never attain exact reproduction of that system. It is recognized that computer models cannot replace well-planned experimentation; it is also recognized that additional spaceflight studies are both infrequent and expensive. Ground-based studies, including both experimental and computer simulations of hypogravity, are viable alternatives in this situation. All conclusions drawn from the simulation models should be accepted cautiously and verified experimentally.

3.3.5.3 Relationship to Statistical Analysis. In conclusion, it would be appropriate to briefly discuss the relationship between statistical analysis and simulation analysis. Both approaches have been used in these studies to test hypotheses. Statistical tests of differences (i.e., t-tests), analysis of variances, can predict the likelihood that one group of data is different from another, and statistical correlation tests suggest causal relationships among variables. The simulation modeling process is capable of testing the significance of data and the relationships among

variables from a viewpoint other than that of a statistical approach. Also, the simulation models, because of their homology to the real system, can be useful in revealing the behavior of the real system and in formulating hypotheses. Statistical models are limited in this regard.

Statistical models suggest, but cannot prove, a casual relationship between measured quantities. This limitation is also characteristics of simulation models, but the simulated results have a more direct association with the measured quantities. Simulation algorithms already contain the basic feedback-regulating mechanisms that are believed to have produced the observed response. If the simulation model has gained a high degree of credibility and there is agreement between the observed and simulated responses for *several* variables, one can reasonable assume (but not prove) that the models' mathematical representation is basically correct and that the experimental findings are also real and internally consistent, even if the data do not achieve significance by conventional statistical tests. In many cases, changes in mean value or trends in experimental data do not achieve statistical significance merely because of an insufficient number of subjects of a low-resolution measuring device. These data would be ignored in more traditional methods of analysis.

Therefore, in using experimental data to evaluate and test hypotheses with simulation models, there was often little regard for the statistical significance of the observed

changes, especially in the earlier stages of the program. This approach was thought appropriate since the model simulation represents a high level of data and systems integration and it was likely that inconsistencies in the data, if present, would be revealed in the final analysis by comparison with the simulation responses. In this way, it was possible to use a greater diversity of data. Of course, at later stages of simulation applications, it was important to verify inconsistencies in the relationships by performing suitable statistical tests.

Although the emphasis in the study described here is on hypothesis testing using simulation rather than statistical models, it is recognized that both approaches are complementary and more powerful than either one alone.

References

1. Hoffler, G. W., Huntoon, C. L., Kimzey, S. L., and Rummel, J. A., *Skylab Selected Medical Experiments Data Summary, Skylab Medical Data Evaluation Program (SMEDEP)*, Contract NAS9-14523, NASA CR-160279, NASA, Johnson Space Center, Houston, TX, 1979.

2. Leonard, J. L., Grounds, D. J., and Fitzjerrel, D. G., *Final Report on Contract NAS 9-14523:Skylab Medical Data Evaluation Program*, Rep. TIR 74l-LSP-7020, General Electric Co., Houston, TX, 1977, pp. 1-32.

3. Srinivasan, S., Leonard, J. I., and White, R. J., Mathematical Modeling of Physiological States, in *Space Biology and Medicine:Humans in Spaceflight*, Vol. III, C. S. L. Huntoon, V. V. Antipov, and A. I. Grigoriev (Eds.), AIAA, Reston, VA, 1996, Chapter 26, pp. 559–594.

4. Starling, E. H., *The Linacre Lecture on the Law of the Heart*, Longmans, Green and Co., London, 1918.

5. Sagawa, K., Comparative Models of Overall Circulatory Mechanics, in *Advances in Biomedical Engineering*, Vol. 3, R. M. Kenedi (Ed.), Academic Press, New York, 1973, pp. 1–95.

6. Dick, D. E., *A Hybrid Computer Study of Major Transients in the Canine Cardiovascular System*, Ph.D. Dissertation, University of Wisconsin, 1968.

7. White, R. J., Croston, R. C., and Fitzjerrell, D. G., Cardiovascular Modeling:Simulating Human Response to Exercise, Lower-Body Negative Pressure, Zero Gravity and Clinical Conditions, *Adv. Cardiovasc. Phys.*, D.N. Ghista (Ed.), S. Karger, Basel, Switzerland, 1983, vol. 5 (Part I) 195–229.

8. Melchior, F. M., Srinivasan, R. S., and Charles, J. B., Mathematical Modeling of the Human Cardiovascular System for Simulation of Orthostatic Response, *Amer. J. Physiol.*, 262: H1920–H1933, 1992.

9. Croston, R. C., *A Cardiovascular Control System Simulation for Exercise*, Ph.D. Dissertation, University of Houston, Rep. TIR 741-MED-2010, General Electric Co., Houston, TX, 1972.

10. Guyton, A. C., Coleman, T. G., and Granger, H. J., Circulation Overall Regulation, *Ann. Rev. Physiol.*, 34: 13–46, 1972.

11. Rideout, V. C., and Dick, D. E., Difference-Differential Equations for Fluid Flow in Distensible Tubes, *IEEE Trans. Biomed. Eng.*, BME-14(3): 171–177, 1967.

12. Croston, R. C., Rummel, J. A., and Kay, F. J., Computer Model of Cardiovascular Control System Responses to Exercise, *Trans. ASME Ser. G:J. Dyn. Sys. Meas. & Cont.*, 95(3): 301–307, 1973.

13. Croston, R. C., and Fitzjerrell, D. G., Cardiovascular Model for the Simulation of Exercise, Lower Body Negative Pressure, and Tilt Experiments. Modeling and Simulation, vol. 5—*Proc. of the Fifth Annual Pittsburgh Conference*, W. G. Vogt and M. H. Mickle (Eds.), pt. 1, Instrument Society of America, Pittsburgh, 1974. pp. 471–476.

14. Altman, P. L., and Dittmer, D. S. (Eds.), *Respiration and Circulation, Federation of American Societies for Experimental Biology*, Bethesda, MD, 1971, pp. 391–395.

15. Korner, P. I., Integrative Neural Cardiovascular Control, *Physiol. Rev.*, 51(2): 312–367, 1971.

16. Bevegärd, B. S., and Shepherd, J. T., Circulatory Effects of Stimulating the Carotid Arterial Stretch Receptors in Man at Rest and During Exercise, *J. Clin. Invest.*, 45(1): 132–142, 1966.

17. Snyder, M. F., *A Study of the Human Venous System Using Hybrid Computer Modeling*, Ph. D. Dissertation, University of Wisconsin, 1969.

18. Ekblom, B., Åstrand, P.-O. B., *et al.*, Effect of Training on Circulatory Response to Exercise, *J. Appl. Physiol.*, 24(4): 518–528, 1968.

19. Musgrave, F. S., Zechman, F. W., and Mains, R. C., Comparison of the Effects of 70° Tilt and Several Levels of Lower Body Negative Pressure on Heart Rate and Blood Pressure in Man, *Aerosp. Med.*, 42(10): 1065–1069, 1971.

20. Wolthuis, R. A., Hoffler, G. W., and Johnson, R. L., Lower Body Negative Pressure as an Assay Technique for Orthostatic Tolerance, *Aerosp. Med.,* 41(1): 29–35, 1970.

21. Dietlein, L. F., and Judy, W. V., Experiment M-1, Cardiovascular Conditioning, in *Gemini Midprogram Conference Including Experiment Results*, Part II-B, Medical Science Experiments, Chapter 39, NASA SP-121, Washington, DC, 1966, pp. 381–391.

22. Segel, N., Dougherty, N. R., and Sackner, M. A., Effects of Tilting on Pulmonary Capillary Blood Flow in Normal Man, *J. Appl. Physiol.*, 35(2): 244–249, 1973.

23. Bartok, S. J., Carlson, L. D., Loren, D., and Walters, R. F., Cardiovascular Changes During Tilt and Leg Negative Pressure Tests, *Aerosp. Med.*, 39(11): 1157–1162, 1968.

24. Tuckman, J., and Shillingford, J., Effect of Different Degrees of Tilt on Cardiac Output, Heart Rate, and Blood Pressure in Normal Man, *British Heart J.*, 28(1): 32–39, 1966.

25. Wolthuis, R. A., Bergman, S. A., and Nicogossian, A. E., Physiological Effects of Locally Applied Reduced Pressure in Man, *Physiol. Rev.*, 54(3): 566–595, 1974.

26. Stolwijk, J. A. J., and Hardy, J. D., Temperature Regulation in Man: A Theoretical Study, *Pfluegers Arch.*, 291(2): 129–162, 1966.

27. Stolwijk, J. A. J., *Mathematical Model of Thermoregulation. Physiological and Behavioral Temperature Regulation*, ch. 48, James D. Hardy, A. Pharo Gagge, and Jan A. J. Stolwijk, (Eds.), Charles C. Thomas, Springfield, IL, 1970, pp. 703–721.

28. Stolwijk, J. A. J., *A Mathematical Model of Physiological*

Temperature Regulation in Man, Final Report, Contract NAS 9-9531, NASA CR-1855, NASA, Washington, DC, 1971.

29. Morgan, L. W., Collett, G., and Cook, D. W., *Computer Program Documentation:41-Node Transient Metabolic Man Program*, Rep. LEC/672-23-030031, Contract NAS 9-5384, Lockheed Electronics Co., Houston, TX, 1970.

30. Smith, S. M., *Simplification of 1108 Lockheed Version of Stolwijk Model and Incorporation of Improved Convective Heat Transfer Coefficient*, Rep. TIR 750-MED-2004, General Electric Co., Houston, TX, 1972.

31. Smith, S. M., *Simplified 41-Node Stolwijk Metabolic Man Model*, TIR 741-MED-3013, General Electric Co., Houston, TX, 1973.

32. Leonard, J. I., *Modifications to the Steady State 41-Node Thermoregulatory Model Including Validation of the Respiratory and Diffusional Water Loss Equations*, (TIR 741-MED-4014, General Electric Co., Houston, TX); NASA CR-160219, NASA, Washington, DC, 1974.

33. Leonard, J. I., *User's Instructions for the 41-Node Thermoregulatory Model (Steady State)*, (TIR 741-MED-4015, General Electric Co., Houston, TX); NASA CR-160220, NASA, Washington, DC, 1974.

34. Grounds, D. J., *Transient Thermoregulatory Model With Graphics Output*, (TIR 741-MED-4011, General Electric Co., Houston, TX); NASA CR-l60217, NASA, Washington, DC, 1974.

35. Fan, L.-T., Hsu, F.-T., and Hwang, C.-L., A Review on Mathematical Models of the Human Thermal System, *IEEE Trans. Biomed. Eng.*, BME-18(3): 218–234, 1971.

36. Leonard, J. I., *The Application of Sensitivity Analysis to Models of Large Scale Physiological Systems*, (TIR 741-MED-4028, Contract NAS 9-12932, General Electric Co., Houston, TX); NASA CR-160228, NASA, Washington, DC, 1974.

37. Waligora, J. M., *Thermal Comfort and Tolerance Design Criteria*, Rep. BRO DB-57-67, NASA Johnson Space Center, Houston, TX, 1967.

38. Webb, P., Thermal Exchanges and Temperature Stress, Foundations of Space Biology and Medicine, M. Calvin and O. G. Gazenko (Eds.), Vol. II, Book 1, *Ecological and Physiological Bases of Space Biology and Medicine*, pt. 1, Influence of an Artificial Gaseous Atmosphere of Spacecraft and Stations on the Organism, Ch. 3. NASA SP-374, 1975, pp. 94–126.

39. Weissman, M. H., *Respiratory-Thermal Modeling*, Research Report, Biomedical Research Division, Environmental Physiology Branch, NASA Johnson Space Center, Houston, TX, 1971.

40. Henane, R., Flandrois, R., and Charbonnier, J. P., Increase in Sweating Sensitivity by Endurance Conditioning in Man. *J. Appl. Physiol.*, 43(5): 822–828, 1977.

41. Yamamoto, W. S., and Raub, W. F., Models of the Regulation of External Respiration in Mannmals-Problems and Promises, *Comp & Biomed Res.*, 1(1): 65–104, 1967.

42. Bellville, J. W. , Fleischli, G., and Delares, J. G., A New Method of Studying Regulation of Respiration-The Response to Sinusoidally Varying CO_2 Inhalation, *Comp. & Biomed. Res.*, 2(4): 329–349, 1969.

43. Fry, D. L., A Preliminary Lung Model for Simulating the Aerodynamics of the Bronchial Tree, *Comp. & Biomed. Res.*, 2(2): 111–134, 1968.

44. Saidel, G. M., Militano, T. C., and Chester, E. H., Mass-Balance Model of Pulmonary Oxygen Transport, *IEEE Trans. Biomed. Eng.,* BME-19(3): 205–213, 1972.

45. Grodins, F. S., Buell, J., and Bart, A. J., Mathematical Analysis and Digital Simulation of the Respiratory Control System, *J. Appl. Physiol.*, 22(2): 260–276, 1967.

46. Milhorn, Jr.,, H. T., Benton, R., Ross, R., and Guyton, A. C., A Mathematical Model of the Human Respiratory Control System, *Biophys. J.* 5(1): 27–46, 1965.

47. Milhorn, Jr., H. T., Reynolds, W. L., and Holloman, Jr., G. H., Digital Simulation of the Ventilatory Response to CO_2 Inhalation and CSF Perfusion, *Comp. & Biomed. Res.*, 5(4): 301–314, 1972.

48. Milhorn, Jr., H. T., and Brown, D. R., Steady-State Simulation of the Human Respiratory System, *Comp. & Biomed. Res.*, 3(6): 604–619, 1971.

49. Gallagher, R. R., *Investigations of Respiratory Control Systems*, (TIR 741-MED-3047, General Electric Co., Houston, TX); NASA CR-160213, NASA, Washington, DC, 1973.

50. Gallagher, R. R., *Evaluation of Exercise-Respiratory System Modifications and Preliminary Respiratory Circulatory System Integration Scheme*, (TIR 741-MED-4018, General Electric Co., Houston, TX); NASA CR-160223, NASA, Washington, DC, 1974.

51. Gallagher, R. R., *Physiological System Integrations With Emphasis on the Respiratory-Cardiovascular System*, (TIR 741-MED-5001, General Electric Co., Houston, TX); NASA CR-160230, NASA, Washington, DC, 1975.

52. Astrand, P.-O., and Rodahl, K., *Textbook of Work Physiology*, McGraw-Hill Book Co., New York, 1970.

53. Whipp, B. J., Rate Constant for the Kinetics of Oxygen Uptake During Light Exercise, *J. Appl. Physiol.*, 30(2): 261–263, 1971.

54. D'Angelo, E., and Torelli, G., Neural Stimuli Increasing Respiration During Different Types of Exercise, *J. Appl. Physiol.*, 30(1): 116–121, 1971.

55. Dickinson, C. J., *A Computer Model of Human Respiration*, University Park Press, Baltimore, MD, 1977.

56. Fisher, J. W., Busuttil, R., et al., The Kidney and Erythropoietin Production: A Review, *Erythropoiesis Proc. 4th Intern. Conf. on Erythropoiesis*, K. Nakao, J. W. Fisher, and F. Takaku (Eds.), University Park Press, 1975, pp. 315–336.

57. Erslev, A. J., Erythropoietin in Clinical Medicine, *Erythropoiesis Proc. 4th Intern. Conf. on Erythropoiesis*, K. Nakao, J. W. Fisher, and F. Takaku (Eds.), University Park Press, 1975, pp. 425–433.

58. Hodgson, G., *Application of Control Theorv to the Study of Erythropoiesis. Regulation of Hematopoiesis*, Vol. 1, A. S. Gordon, (Ed.), Appleton-Century Crofts, New York, Chapter 15, 1970.

59. Mylrea, K. C., and Abbrecht, P.H., Mathematical Analysis and Digital Simulation of the Control of Erythropoiesis, *J. Theor. Biol.,* 33(2): 279–297, 1971.

60. Cavill, L., and Ricketts, C., The Kinetics of Iron Metabo-

lism. *Iron in Biochemistry and Medicine*, A. Jacobs and M. Worwood (Eds.), Academic Press, London, 1974, pp. 613–647.

61. Berzuini, C., Franzone, P. C., Stefanelli, M., and Viganotti, C., Iron Kinetics:Modelling and Parameter Estimation in Normal and Anemic States, *Comp. & Biomed. Res.*, 11(3): 209–228, 1978.

62. Mackey, M. C., Unified Hypothesis for the Origin of Aplastic Anemia and Periodic Hematopoiesis, *Blood*, 51: 941–956, 1978.

63. Lajtha, L. G., Oliver, R., and Gurney, C. W., Kinetic Model of a Bone-Marrow Stem-Cell Population, *British J. Hematol.*, 8: 442–460, 1962.

64. Kretchmar, L., Erythropoietin: Hypothesis of Action Tested by Analog Computer, *Science*, 152: 367–370, 1966.

65. Leonard, J. I., Kimzey, S. L. and Dunn, C. D. R., Dynamic Regulation of Erythropoiesis: A Computer Model of General Applicability. *Exper. Hematology*, 9: 355–378, 1981.

66. Krantz, S. B., and Jacobson, L. O., *Erythropoietin and the Regulation of Erythropoiesis*, University of Chicago Press, 1970.

67. Brewer, G. J., 2,3-DPG and Erythrocyte Oxygen Affinity, *Ann. Rev. Med.*, 25: 29–38, 1975.

68. Metcalfe, J., and Dhindsa, D. S., The Physiological Effects of Displacements of the Oxygen Dissociation Curve, in *Oxygen Affinity of Hemoglobin and Red Cell Acid-Base Status*, P. Astrup and M. Rorth (Eds.), Academic Press, New York, 1972, pp. 613–628.

69. Buderer, M. C., and Pace, N., Hemopoiesis in the Pig-Tailed Monkey Macaca Nemestrina During Chronic Altitude Exposure, *Amer. J. Physiol.*, 223(2): 346–352, 1972.

70. Abbrecht, P. H., and Littell, J. K., Plasma Erythropoietin in Men and Mice During Acclimatization to Different Altitudes, *J. Appl. Physiol.*, 32(1): 54–58, 1972.

71. Huff, R. L., Lawrence, J. H., et al., Effects of Changes in Altitude on Hematopoietic Activity, *Medicine,* 30(3): 197–217, 1951.

72. Faura, J., Ramos, J., et al., Effect of Altitude on Erythropoiesis, *Blood*, 33: 668–676, 1969.

73. Dunn, C. D. R., Jarvis, J. H., and Napier, J. A. F., Changes in Erythropoiesis and Renal Ultrastructure During Exposure of Mice to Hypoxia, *Exp. Hematol.,* 4(6): 365–381, 1976.

74. Finch, C. A., and Lenfant, C., Oxygen Transport in Man, *New England J. Med.*, 286(8): 407–415, 1972.

75. Dunn, C. D. R., Effect of Dehydration on Erythropoiesis in Mice: Relevance to the "Anemia" of Spaceflight, *Aviat. Space & Environ. Med.*, 49: 990–993, 1978.

76. Leonard, J. I., *System Parameters for Erythropoiesis Control Model: Comparison of Normal Values in Human and Mouse Model*, (TIR 741-LSP-8024, General Electric Co., Houston, TX); NASA CR-160401, NASA, Washington, DC, 1978.

77. Leonard, J. I., *Study Report-Improvements and Validation of the Erythropoiesis Control Model for the Simulation of Bedrest*, (TIR 741-LSP-7012, General Electric Co., Houston, TX); NASA CR-160187, NASA, Washington, DC, 1977.

78. Gurney, C. W., Wackman, N., and Filmanowicz, E., Studies on Erythropoiesis, XVII, Some Quantitative Aspects of the Erythropoietic Response to Erythropoietin, *Blood*, 17: 531–

79. Birkhill, F. R., Maloney, M. A., and Levenson, S. M., Effect of Transfusion Polyeythemia Upon Bone Marrow Activity and Erythrocyte Survival in Man, *Blood*, 6(11): 1021–1033, 1951.

80. Morse, B. S., Erythrokinetic Changes in Man Associated With Bedrest, *Lectures in Aerospace Medicine*, 6th Series, School of Aerospace Medicine, Brooks Air Force Base, TX, 1967, pp. 240–254.

81. Lancaster, M. C., Hematologic Aspects of Bedrest, in *Hypogravic and Hypodynamic Environments*, R. H. Murray and M. McCally, (Eds.), Sec. IV, Metabolic Effects of Bedrest, Chapter 23, NASA SP-269, NASA, Washington, DC, 1971, pp. 299–307.

82. Johnson, P. C. and Mitchell, C., (Eds.), *Report of 28-Day Bedrest Simulation of Skylab*, Vols I and II, The Methodist Hospital, Houston, TX; NASA CR-151354, NASA, Washington, DC, 1977.

83. Kimsey, S. L., The Effects of Extended Spaceflight on Hematologic and Immunologic Systems, *J. Amer. Med. Women's Assoc.*, 30(5): 218–232, 1975.

84. Harris, J.W., and Kellemeyer, R.W., *The Red Cell*, Harvard University Press, 1970.

85. Dunn, C. D. R., and Lange, R. D., Erythropoietic Effects of Spaceflight, *Acta Astronaut.*, 6: 725–732, 1979.

86. Dunn, C. D. R., and Lange, R. D., Erythropoietic Effects of Spaceflight Studied in a Potential Animal Model, *Proc. 50th Ann. Aero. Med. Assoc. Mtg.*, 1979, pp. 14–15.

87. Castle, W. B. and Jandle, T. H., Blood Viscosity and Blood Volume: Opposing Influences Upon Oxygen Transport in Polycythemia, *Seminars in Hematology*, 3, 1966, pp. 193–198.

88. Murphy, G. P., Johnston, G. S., and Scott, W. W., The Effect of Arterial Hematocrit Alteration on Renal Blood Flow and Resistance in Normotensive States, *J. Urol.*, 95: 453–464, 1966.

89. Petersen, L. H. (Chairman, Study Group on Circulatory Physiology), *Physiology in the Space Environment*, Vol. 1, Circulation, Publication 1485A, National Academy of Sciences, National Research Council, Washington, D.C., 1968.

90. White, R. J., *Summary Report on a Basic Model of Circulatory, Fluid, and Electrolyte Regulation in the Human System Based Upon the Model of Guyton*, (TIR 741-MED-3042, General Electric Co., Houston, TX); NASA CR-160212, NASA, Washington, DC, 1973.

91. Kuchar, N. R., and Sittel, K., *Modeling and Integration of Physiological Control Systems, Final Report,* Contract NAS 9-11657, General Electric Co., Houston, TX; NASA CR-160121, NASA, Washington, DC,1973.

92. Jacquez, J.A., Carnahan, B., and Abbrecht, P., A Model of the Renal Cortex and Medulla, *Math. Biosci.*, 1(2): 227–26l, 1967.

93. Alvi, Z. M., and Lyman, J. H., *Development of a Mathematical Model for the Nonequilibrium Kinetics of Major Electrolytes in the Human Body,* Tech. Rep, No, 45, Biotechnology Laboratory, Univ. of California-Los Angeles, 1969.

94. Levine, S. N., A Model for Renal-Electrolyte Regulation, *J. Theor. Biol.*, 11(2): 242–256, 1966.

95. DeHaven, J. C., and Shapiro, N. Z*., Intrinsic Control of*

Body Fluid and Electrolyte Distribution and Urine Formation, Rep. RM-4609-PR, The Rand Corp., Santa Monica, CA, 1965.

96. DeHaven, J. C., and Shapiro, N. Z., Simulation of the Renal Effects of Antidiuretic Hormone (ADH) in Man*, J. Theor. Biol.,* 28(2): 261–286, 1970.

97. Koshikawa, S., and Suzuki, K., Study of Osmo-Regulation as a Feedback System, *Med. & Biol, Eng*., 6(2): 149–158, 1968.

98. Reeve, E. B., and Kulhanek, L. J., Regulation of Body Water Content: A Preliminary Analysis, in *Physical Bases of Circulatory Transport: Regulation and Exchange*, E. B. Reeve and A. C. Guyton, (Eds.), W.B. Saunders Co., Philadelphia, 1967, pp. 151–177.

99. Cameron, W. H., A Model Framework for Computer Simulation of Overall Renal Function, *J. Theor. Biol.*, 66(3): 551–572, 1977.

100. Toates, F. M., and Oatley, K., Computer Simulation of Thirst and Water Balance, *Med. & Biol. Eng.*, 8(1): 71–87, 1970.

101. Badke, F., Further Development of a Model of Human Salt and Water Regulation, *Trans. ASME Ser. G: J. Dyn. Sys. Meas. & Cont.*, 95(3): 259–264, 1973.

102. Guyton, A. C., and Coleman, T. G., Quantitative Analysis of the Pathophysiology of Hypertension, *Circulation Res.*, 24, Suppl. 1, Hypertension—Vol. 17 Experimental Hypertension, May 1969, pp, I1–I20

103. Guyton, A. C., Coleman, T. G., *et al.*, Systems Analysis of Arterial Pressure Regulation and Hypertension, *Ann. Biomed. Eng.*, 1: 254–281, 1973.

104. Guyton, A. C., Coleman, T. G., *et al.*, *Relationship of Fluid and Electrolytes to Arterial Pressure Control and Hypertension: Quantitative Analysis of an Infinite Gain Feedback System, Hypertension: Mechanisms and Management*, G. Onesti, K. E. Kim, and J. H. Moyer (Eds.), Grune and Stratton, New York, 1973.

105. White, R. J., *A Long Term Model of Circulation: Final Report*, (TIR 741-MED-4021, General Electric Co., Houston, TX); NASA CR-147674, NASA, Washington, DC, 1974.

106. Guyton, A. C., Granger, H. J., and Taylor, A. E., Interstitial Fluid Pressure, *Physiol. Rev.*, 51(3): 527–561, 1971.

107. Hoffler, G. W., Cardiovascular Studies of U.S. Space Crews: An Overview and Perspective, in *Cardiovascular Flow Dynamics and Measurements*, N.H.C. Hwang and N.A. Normann, (Eds.), University Park Press, Baltimore, MD, 1977, pp. 335–363.

108. Thornton, W. E., and Hoffler, G. W., Hemodynamic Studies of the Legs Under Weightlessness, in *Biomedical Results From Skylab*, R. S. Johnston and L. F. Dietlein, (Eds.), Sec V, Cardiovascular and Metabolic Function, Chapter 31, NASA SP-377, 1977, pp. 324–329.

109. Greenleaf, J. E., Greenleaf, C. J., VanDerVeer, D., and Dorchak, K. J*., Adaptation to Prolonged Bedrest in Man: A Compendium of Research*, NASA TM X-3307, 1976.

110. Green, J. F., and Miller, N. C., A Model Describing the Response of the Circulatory System to Acceleration Stress, *Ann. Biomed. Eng.*, 1: 455–467, 1973.

111. Boyers, D. G., Cuthberison, J. G., and Luetscher, J. A., Simulation of the Human Cardiovascular System: A Model With Normal Responses to Change of Posture, Blood Loss, Transfusion, and Autonomic Blockade, *Simulation*, 18: 197–206, 1972.

112. Luetscher, J. A., Boyers, D. G., Cuthbertson, J. G., and McMahon, D. F., A Model of the Human Circulation: Regulation by Autonomic Nervous System and Renin-Angiotensin System, and Influence of Blood Volume on Cardiac Output and Blood Pressure, *Circulation Res.*, 32: Suppl. I, Hypertension—Vol. 21: Hypertension in Man and the Experimental Animal, pp. I84–I98, 1973.

113. Luetscher, J. A., Boyers, D., and Resnech, J., Control of the Renal Circulation and Kidney Functions, *Proc. of the Summer Comp. Simul. Conf.*, San Diego, CA, 1972, pp. 1099–1109.

114. Leonard, J. I., and Grounds, D. J., *Study Report Modification of the Long Term Circulatory Model for the Simulation of Bedrest*, (TIR 742-LSP-7011, General Electric Co., Houston, TX); NASA CR-160186, NASA, Washington, DC, 1977.

115. Ikeda, N., Marumo, F., Shirataka, W., and Sato, T., A Model of Overall Regulation of Body Fluids, *Ann. Biomed. Eng.*, 7: 135–166, 1979.

116. White, R. L., and Croston, R. C., Human Physiological Problems in Zero Gravity—An Attempt at Understanding Through Systems Analysis, *Proc. of the Summer Comp. Simul. Conf.*, vol. 2, AFIPS Press, Montvale, N.J., 1974, pp. 743–747.

117. Costill, D. L., and Sparks, K. E., Rapid Fluid Replacement Following Thermal Dehydration, *J. Appl, Physiol.*, 34(3): 299–303, 1973.

118. Guyton, A. C., *Textbook of Medical Physiology*, 5th ed., W.B. Saunders Co., Philadelphia, PA, 1976.

119. Bland, J. H., General Clinical Considerations in Water, Electrolyte and Hydrogen Ion Metabolism, *Clinical Metabolism of Body Water and Electrolytes*, Chapter 8, W.B. Saunders Co., Philadelphia, PA, 1963, pp. 165–224.

120. Dunn, F. L., Brennan, T. J., Nelson, A. F., and Robertson, G. L., The Role of Blood Osmolality and Volume in Regulating Vasopressin Secretion in the Rat, *J. Clin. Invest.*, 52(12): 3212–3219, 1973.

121. Leonard, J. I., and Abbrecht, P. H., Dynamics of Plasma-Interstitial Fluid Distribution Following Intravenous Infusions in Dogs—An Experimental and Computer Simulation Study, *Circulation Res.*, 33(6): 735–748, 1973.

122. Gauer, O. H., Henry, J. P., and Behn, C., The Regulation of Extracellular Fluid Volume, *Ann. Rev. Physiol.*, 32: 547–595, 1970.

123. Gann, D. S. and Pirkle, J. C., Role of Cortisol in the Restitution of Blood Volume After Hemorrhage, *Amer. J. Surg.*, 130(5): 565–569, 1975.

124. Fitzjerrell, D. G., *Design Specification for Whole-Body Algorithm*, (TIR 741-MED-4025, General Electric Co., Houston, TX); NASA CR-160226, NASA, Washington, DC, 1974.

125. Albergoni, V., Cobelli, C., and Torresin, G., Interaction Model Between the Circulatory and Respiratory Systems, *IEEE Trans. Biomed. Eng.*, BME-19(2): 108–113, 1972.

126. Atkins, R., and Mitchell, D., Simulating the Thermal Response of a Working Man With a Computer, *Int. J. Biometeorol.*, 15: 183–188, 1971.

127. Farrell, E. J., and Siegel, J. H., Investigation of Cardiorespiratory Abnormalities Through Computer Simulation, *Comp. & Biomed. Res.*, 6(2): 161–186, 1973.

128. Fujihara, Y., Hildebrandt, J., and Hildebrandt, J. R., Cardiorespiratory Transients in Exercising Man-II, Linear Models, *J. Appl. Physiol.*, 35(1): 68–76, 1973.

129. Fukui, Y., *A Study of the Human Cardiovascular-Respiratory System Using Hybrid Computer Modeling*, Ph.D. Dissertation, University of Wisconsin, 1972.

130. Mitchell, J. W., Stolwijk, J. A. J., and Nadel, E. R., Model Simulation of Blood Flow and Oxygen Uptake During Exercise, *Biophys, J.*, 12(11): 1452–1466, 1972.

131. Smith, Jr., P. E., and James, E. W., Human Responses to Heat Stress, *Arch. Environ. Health*, 9(3): 332–342 (1964).

132. Womack, B. F., and Hinderer, J. H., Modeling the Effect of Respiration on Heart Rate Through Analogue and Digital Computer Studies, *J. Assoc. Adv. Med. Instrum.*, 5: 38–43, 1971.

133. Miller, N. C., and Walters, R. F., Interactive Modeling as a Forcing Function for Research in the Physiology of Human Performance, *Simulation*, 22(1): 1–13, 1974.

134. Wissler, E. H., Mathematical Simulation of the Human Circulatory, Respiratory, and Thermal Systems in Exercise, *Proc. 26th ACEMB*, 8: 4–75, 1973.

135. Fitzjerrell, D. G., Grounds, D. J., and Leonard, J. I., *Study Report on Interfacing Major Physiological Subsystem Models: An Approach for Developing a Whole Body Algorithm*, (TIR 741-MED-5008, General Electric Co., Houston, TX); NASA CR-160232, NASA, Washington, DC, 1975.

136. Fitzjerrell, D.G., *Final Report-Automated System for Physiological Data,* (TIR 741-MED-5013, General Electric Co., Houston, TX); NASA CR-141933, NASA, Washington, DC, 1975.

137. Kay, F. J., *Study Report, The Development of a Whole-Body Algorithm*, (TIR 741-MED-3058, General Electric Co., Houston, TX); NASA CR-160214, NASA, Washington, DC, 1973.

138. White, R. J., *Study Report: Acid-Base Homeostasis in the Human System*, (TIR 741-MED-4017, General Electric Co., Houston, TX); NASA CR-160222, NASA, Washington, DC, 1974.

139. Gallagher, R. R., *Physiological System Integration with Emphasis on the Respiratory-Cardiovascular System,*, NASA CR-160230, NASA, Washington, DC, 1975.

140. Fitzjerrell, D. G., *User's Instructions for the G.E. Cardiovascular Model to Simulate LBNP and Tilt Experiments (With Graphic Capabilities)*, (TIR 741-MED-4008, General Electric Co., Houston, TX); NASA CR-160216, NASA, Washington, DC, 1974.

141. Fitzjerrell, D. G., *Comparison of GE Cardiovascular LBNP and Tilt Model Results With M.D. Anderson Model Results and Available Test Data*, TIR 741-MED-3054, General Electric Co., Houston, TX, 1973.

142. Leonard, J. I*., Validation of a Model for Investigating Red Cell Mass Changes During Weightlessness*, TIR 741-MED-6004, General Electric Co., Houston, TX, 1976.

143. Leonard, J. I., *Dynamic Regulation of Erythropoiesis: A Computer Model of General Applicability*, TIR 741-LSP-9005, General Electric Co., Houston, TX, 1979.

144. Hyatt, K. H., Smith, W. M., Kamenetsky, L. G., and Vogel, J. M., *A Study of Post-Recumbency Orthostasism and Prophylactic Measures for Prevention of This Phenomenon*, NASA CR-92178, pts, 1 and 2, 1968.

145. Murray, R. H., Thompson, L. J., Bowers, J. A., and Albright, C. D., Hemodynamic Effects of Graded Hypovolemia and Vasodepressor Syncope Induced by Lower Body Negative Pressure, *Amer. Heart J.*, 76(6): 799–811, 1968.

146. Murray, R. H., Thompson, L. J., et al., Hemodynamic Effects of Hypovolemia in Normal Subjects and Patients With Congestive Heart Failure, *Circulation*, 39(1): 55–63, 1969.

147. Kontos, H. A., Levasseur, J. F., et al., Comparative Circulatory Responses to Systemic Hypoxia in Man and in Unanesthetized Dogs, *J. Appl. Physiol.*, 23(3): 381–386, 1967.

148. Reynolds, W. J., and Milhorn, Jr., H. T., Transient Ventilatory Response to Hypoxia With and Without Controlled Alveolar P_{CO2} , *J. Appl. Physiol.*, 35(2): pp, 187–196, 1973.

149. Richardson, D. W., Wasserman, A. J., and Patterson, Jr., J. L., General and Regional Circulatory Responses to Change in Blood pH and Carbon Dioxide Tension, *J. Clin. Invest.*, 40, pp, 31–43, 1961.

150. Reynolds, W. J., Milhorn, Jr., H. T., and Holloman, Jr., G. H., Transient Ventilatory Response to Graded Hypercapnia in Man, *J. Appl. Physiol.*, 33(1): 47–54 (1972).

151. Stolwijk, J. A. J., and Hardy, J. D., Partitional Calorimetric Studies of Responses of Man to Thermal Transients, *J. Appl. Physiol.*, 21(3): 967–977, 1966.

152. Damato, N., Lau, S. H., et al., Cardiovascular Response to Acute Thermal Stress (Hot Dry Environment) in Unacclimatized Normal Subjects, *Amer. Heart J.*, 76(6): 769–774, 1968.

153. Saltin, B., Gagge, A. P., and Stolwijk, J. A. J., Body Temperatures and Sweating During Thermal Transients Caused by Exercise, *J. Appl. Physiol.*, 28(3): 318–327, 1970.

154. Johnson, J. M., Loring, L. B. R., and Brengelmann, G. L., Modification of the Skin Blood Flow-Body Temperature Relationship by Upright Exercise, *J. Appl. Physiol.*, 37(6): 880–886, 1974.

155. Wenger, C. B., Roberts, M. F., Stolwijk, J. A. J., and Nadel, E. R., Forearm Blood Flow During Body Temperature Transients Produced by Leg Exercise, *J. Appl. Physiol.*, 38(1): 58–63, 1975.

156. Rambaut, P. C., and Johnston, R. S., Prolonged Weightlessness and Calcium Loss in Man, *Acta Astronautica*, 6: 1113–1122, 1979.

157. Mack, P. B., LaChance, P. A., Vase, G. P., and Vogt, F. B., Bone Demineralization of Foot and Hand of Gemini-Titan IV, V and VII Astronauts During Orbital Flight, *Amer. J. Roentgenol. Radium Therapy & Nucl. Med.*, 100(3): 503–511, 1967.

158. Mack, P. B., and Vogt, F. B., Roentgenographic Bone Density Changes in Astronauts During Representative Apollo Spaceflight, *Amer. J. Roentgenol. Radium Therapy & Nucl. Med.*, 113(4): 621–633, 1971.

159. Johnston, R. S., and Dietlein, L. F., (Eds.), *Biomedical Results From Skylab*, NASA SP-377, 1971.

160. Aubert, J. P., Brunner, F., and Richelle, L. J., Quantitation of Calcium Metabolism, Theory*, J. Clin. Invest.*, 42(6): 885–897, 1963.

161. Cohn, S. H., Bozzo, S. R., et al., Formulation and Testing

of a Compartmental Model for Calcium Metabolism in Man, *Radiation Res.*, 26(3): 319–333, 1965.

162. Neer, R., Berman, M., Fisher, L., and Rosenberg, L. E., Multicompartmental Analysis of Calcium Kinetics in Normal Adult Males, *J. Clin. Invest.*, 46(8): 1364–1379, 1967.

163. Brand, S. N., *Preliminary Design Specifications of a Calcium Model*, (TIR 741-MED-8022, General Electric Co., Houston, TX); NASA CR-160199, NASA, Washington, DC, 1978.

164. Norman, W., Schaefer, K., et al., (Eds.), Third Workshop on Vitamin D*: Vitamin D Biochemical, Chemical and Clinical Aspects Related to Calcium Metabolism,* Walter de Gruyter Publ., 1977.

165. Parfitt, M., *Progress in Endocrinology and Metabolism-The Actions of Parathyroid Hormone on Bone: Relation to Bone Remodeling and Turnover, Calcium Homeostasis, and Metabolic Bone Disease*—Part I: Mechanisms of Calcium Transfer Between Blood and Bone and Their Cellular Basis: Morphological and Kinetic Approaches to Bone Turnover, *Metabolism*, 25(7): 809–844, 1976.

166. Parfitt, M., *Progress in Endocrinology and Metabolism-The Actions of Parathyroid Hormone on Bone: Relation to Bone Remodeling and Turnover, Calcium Homeostasis, and Metabolic Bone Disease*—Part II: PTH and Bone Cells: Bone Turnover and Plasma Calcium Regulation, *Metabolism*, 25(8): 909–955, 1976.

167. Parfitt, M., *Progress in Endocrinology and Metabolism-The Actions of Parathyroid Hormone on Bone: Relation to Bone Remodeling and Turnover, Calcium Homeostasis, and Metabolic Bone Disease*—Part III: PTH and Ostcoblasts, the Relationship Between Bone Turnover and Bone Loss, and the State of the Bones in Primary Hyperparathyrodism, *Metabolism*, 25(9): 1033–1069, 1976.

168. Parfitt, M., *Progress in Endocrinology and Metabolism-The Actions of Parathyroid Hormone on Bone: Relation to Bone Remodeling and Turnover, Calcium Homeostasis, and Metabolic Bone Disease*, Part IV: The State of the Bones in Uremic Hyperparat–hyroidism—The Mechanisms of Skeletal Resistance to PTH in Renal Failure and Pseudohypoparathyroidism and the Role of PTH in Osteoporosis, Osteopetrosis, and Osteofluorosis, *Metabolism*, 25(10): 1157–1188, 1976.

Update Endnotes

Update #1

Recent developments in Tgurktcvqt{ Eqpvqn'o qf gnu<

Another model of respiratory control superior to that of Grodins', became available in the late 1970's. Dickinson [55] developed his model known as "MACPUF" to simulate experimental and clinical conditions including exercise, hypocapnia and Cheyne-Stokes respiration. This model was tested by NASA but was not available in time to be incorporated into the Whole-Body Algorithm as a replacement for the Grodins model. Because there were no undesirable changes in pulmonary function noted during the Skylab missions, neither model was used on a stand-alone basis to help solve problems of spaceflight adaptation. A respiratory model was nevertheless, considered critical to the overall systems analysis planning effort because of the possibility of hypoxia or hypercapnia occuring in space capsules and because respiratory control is integral to models attempting to simulate exercise.

Chapter 4
Integrated Metabolic Balance and Body Composition During Spaceflight

4.1 Introduction

One of the most consistent findings in astronauts returning from spaceflight has been a loss in body weight. The Skylab biomedical findings provided the first detailed set of data designed to examine this loss of body weight, and allowed more definitive conclusions to be made about the metabolic and body composition changes that occur during zero-g. This chapter presents a comprehensive series of analytical studies designed to address the fundamental questions, "how does spaceflight alter the components of body fluid, mass and energy?" and "why do astronauts lose weight in space"? Figures 10-2 and 10-9 indicate the systematic approach used for characterizing the major routes of fluids and energy into and out of the body as well as the changing size of their storage compartments within the body. The extensive Skylab database was used to provide the information necessary to integrate the energy balance, mass balance, water balance, and body fluid volumes of the astronauts (Fig. 3-5).

4.1.1 Objectives

Although data gathered on the manned spaceflight missions through Apollo indicated that significant changes in human body fluid and mineral content were induced by hypogravity, it was not possible to follow these changes closely until the Skylab Program. Even in the workshop environment of Skylab, it was not feasible to measure whole-body composition directly, and only indirect analyses based on metabolic balances of minerals, nitrogen, and water losses have been performed [Refs. 1–9]. In the absence of direct data, these indirect methods have played a large role in the formulation of hypotheses related to the physiological effects of spaceflight.

In this section, the previous indirect analyses of the Skylab data are extended to include the following:

1. Integrate the most important Skylab findings related to the losses of body mass and biochemical constituents;
2. Process the metabolic balance data to obtain more meaningful interpretations regarding the dynamic behavior of metabolic changes and the relative influence and importance of the different avenues of metabolic losses;
3. Express body composition changes in a graphical format suitable for validating computer simulations using the fluid-electrolyte model;
4. Interpret body composition changes so that the influence of weightlessness can be distinguished from that of diet, exercise, and flight duration.

4.1.2 Approach

With these objectives in mind, procedures were developed to compute metabolic balances of water, minerals, mass, and energy in the common framework of a special-purpose algorithm called the Integrated Metabolic Analysis Program. This algorithmic approach is described in general terms in Chapter 3 and more fully in the next paragraphs.

The software developed for this analysis effort consisted of several specially designed subsystems (Fig. 4-1):
1. An extensive data base containing daily metabolic inputs and outputs for each of the nine subjects on each day of the preflight, inflight, and postflight periods;
2. Metabolic balance algorithms for computing daily balances and summarizing balance components (i.e., dietary inputs and urinary and fecal outputs);
3. A numerical time-integrating procedure for cumulating the sequential changes in daily balance;
4. An algorithm for using direct whole-body measurements to provide a check on the accuracy of the metabolic balance results and to minimize the errors inherent in conventional cumulative balance techniques;
5. A statistical algorithm for computing means and variances for each parameter by pooling results for each subject across a mission phase, by pooling results for each three-man crew, or by pooling all individual data on a daily basis;
6. A correlation analysis algorithm for determining relationships between variables and sources of errors in the balance method;
7. A plotting package that generates microfilm time-trend plots of any input or derived variable for any subject or for groups of subjects over any time interval. All results could be plotted as continuous daily values for convenience in displaying, scanning, and interpreting the data.

In general, metabolic balance techniques are based on the law of conservation requirement that, for a given substance, subtraction of the amount excreted (output) from the amount ingested (input) provides a measure of net retention or loss of that substance (so long as that substance is not created or destroyed within the body). Thus, cumulative sums of daily metabolic balances can be used to estimate continuous whole-body changes of the substance as a function of time. Direct total body measurements, obtained at intervals throughout the mission, provide a check on the results of the cumulative balances. The present analysis not only provides overall balances
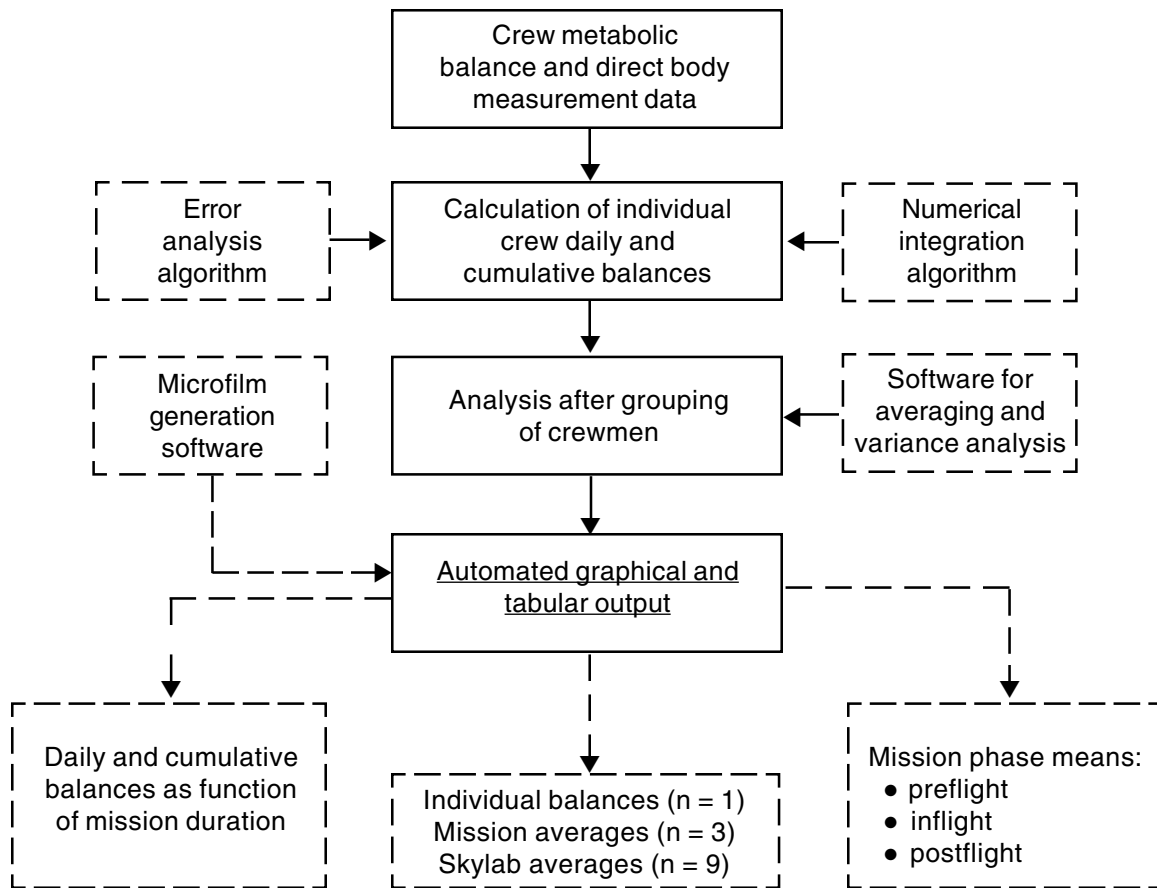
Figure 4-1. Flow diagram of the integrated metabolic balance analysis. Dashed boxes refer to specially designed software modules.

for water, tissue mass, minerals, and energy but allows these balances to be partitioned into components of input ingested from fluids or solids and of metabolic products and output (urinary, fecal, and sweat). Thus, a partitional water balance would describe the changes that result from water intake (free drinking water plus food water plus metabolic water) and water output (urine plus fecal water plus evaporative water loss). The input and output components of the various substances studied using the balance analysis described in this chapter, together with the available whole-body measurements, are shown in Table 4-1.

The data gathered during the Skylab Program that are relevant to the present analysis can be conveniently divided into the following categories.

1. Metabolic balances (intake, fecal, and urine analyses) for calories (bomb calorimetry), water, nitrogen, fats, carbohydrates, calcium, sodium, potassium, and other cellular electrolytes, which were performed each day of the preflight, inflight, and postflight periods [5,6,7,8, 9]. Dietary intake was controlled by pre-packaging meals. More than 900 man-days were included in these studies.
2. Total body weight/mass measurements, which were performed daily (before, during, and flight) using conventional scales in the terrestrial environment and using

the oscillation period of a spring-loaded balance in the zero-g environment [10,11].
3. Total body measurements of water (by tritium dilution), extracellular fluid (by ^{82}Br dilution), potassium (by ^{40}K dilution), and body volume (by stereophotogrammetry), which were performed only during the preflight and postflight phases; [4,12,13].

All these data used in the integrated metabolic balance analysis as summarized in Fig. 4-2.

4.1.3 Analytical Methods with Examples

The collection of metabolic data did not include losses associated with the skin (i.e., evaporative water loss, sweat secretions, nail and hair clippings, and skin flaking). Although neglect of these unmeasured losses usually does not represent serious errors in a daily balance (except for evaporative water loss in a water balance), errors do accumulate over time and can become quite large when computing cumulative balances. In our studies correction of daily balances by a term representing the unmeasured skin losses was accomplished by using the general procedure shown in Fig. 4-3. The correction factor is obtained by comparing the uncorrected cumulative daily balance dur-

Table 4-1. Components of Metabolic Balances Considered in Analysis

Type of balance	Input	Output	Direct total body measurement
Water	Drinking water Water bound in food Metabolic water*	Urine water Fecal water Evaporative water loss*	Total body water (tritium dilution)
Dry mass (gravimetric)	Dry food mass Metabolic oxygen mass*	Urine solids Dry fecal mass Metabolic carbon dioxide mass*	Total body mass/weight

Energy	Diet calories
	Energy from body protein
	  catabolism*
	Energy from body fat
	  catabolism*
		Urine calories
		Fecal calories
		Energy for body protein anabolism*
		Energy for body fat anabolism*
			No direct measurements;
			  assume total energy use constant
			  (work plus heat)*

Sodium	Diet sodium	Urine sodium
		Fecal sodium
		Sweat sodium
			Extracellular fluid times plasma
			  sodium concentration
			  = exchangeable body sodium

Potassium	Diet potassium	Urine potassium Fecal potassium Sweat potassium	Total exchangeable potassium (^{40}K dilution)

Nitrogen, calcium,
  phosphorus, and
  magnesium
	Diet	Urine
		Feces
			None

*Quantities not measured directly

ing a given time interval with the true body change as obtained by the direct whole-body measurement. The difference between these terms (shown graphically in the diagram of Fig. 4-3 as the "cumulative error") is expressed as a constant daily loss rate (calculated by dividing the net mission change by the number of days in the time interval), which is applied directly to the uncorrected metabolic balance. Use of this process ensures that the cumulative corrected balance agrees precisely with direct body measurements at the end-points of the time period being studied.

In terms of numerical analysis, this is a well-known parameter-estimation technique with known and restricted boundary conditions. The parameter being estimated in this case is the correction factor, and the boundary conditions are the measured total body changes. In addition to improving the accuracy of the cumulative balances, this method also enables estimation of unmeasured evaporative water loss, electrolyte sweat losses, and total dry skin losses. These derived quantities may be examined for their plausability bt comparing them with independently measured values from the literature.

The diagram in Fig. 4-3 represents only the inflight period, but similar calculations were performed for the preflight and postflight periods whenever wholebody measurements were available. In either case, CF is calculated as a cumulative error over the time interval of interest, divided by the number of days in the interval; the resulting daily value of CF is assumed constant throughout the time interval.

An example of a water balance study for a single crewman is presented in Fig. 4-4, in which the capability of these procedures in deriving and plotting daily and cumulative balances is shown. Subtle changes in the balance data (top graph) can lead to substantial total body changes as represented by the cumulative daily balance (bottom graph). These changes might not be fully appreciated by scanning daily balance data alone. The time-integrated analysis method (cumulative daily balance) challenges the accuracy of the experimental balance methods, since experimental errors become more apparent when cumulative balances are employed. An investigator may have more reason to be confident in the balance data if the results of the cumulative analysis appear reasonable, particularly when long time periods are involved. An example of the effect of the correction factor on the cumulative water balance is provided in Appendix F (Fig. F-1).

4.1.4 Reference Data for Crew and Skylab Environment

The physical characteristics of the Skylab crewmen, measured preflight, are presented in Table 4-2. The values
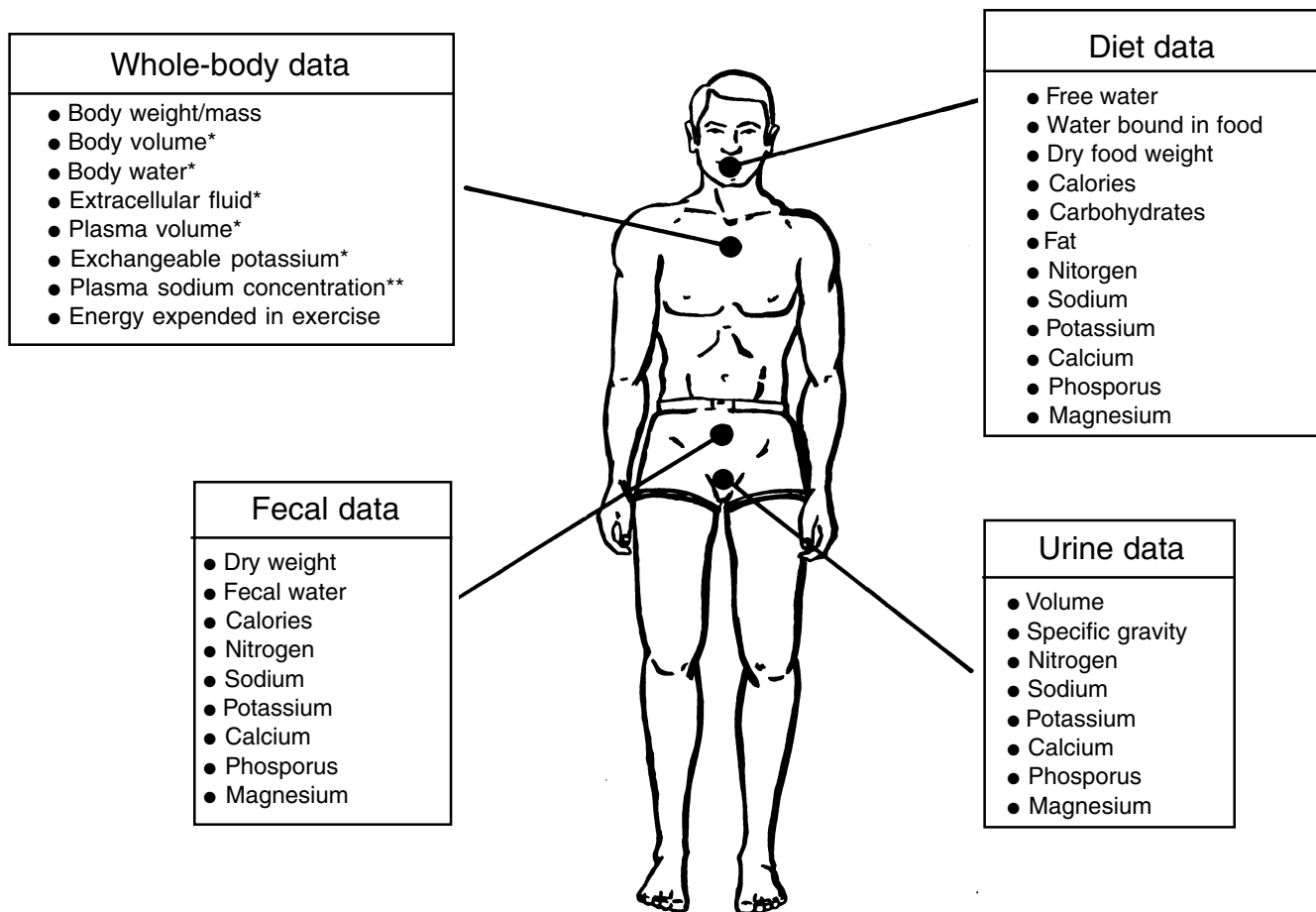
Figure 4-2. Data used in the integrated metabolic balance analysis. All date were obtained daily—before, during, and after flight—except as noted. (*) indicates pre- and post-flight measurements only; (**) indicates weekly inflight measurements.

Table 4-2. Physical Characteristics of Skylab Crew for Each Mission [N=3; Mean ± SD]

Mission duration, days	Age, yr	Height, cm	Surface area,* m²	Body wt., kg	Body fat,** percent	Oxygen uptake*** cm³/kg/min
28	42 ± 1	177 ± 7	1.85 ± 0.17	73.43 ± 9.81	11.2 ± 2.8	35.5 ± 1.0
59	40 ± 3	178 ± 5	1.81 ± 0.19	72.80 ± 13.60	15.0 ± 0.5	33.4 ± 4.7
84	40 ± 3	175 ± 0	1.77 ± 0.02	68.95 ± 2.22	12.1 ± 4.2	39.8 ± 6.6
Mean****	41 ± 2	177 ± 4	1.81 ± 0.13	71.73 ± 8.71	12.8 ± 3.1	36.2 ± 4.9

    * Determined by stereophotometric measurements
    ** Derived from water immersion technique
    *** Measured at 160-beat/min heart rate during bicycle ergometry exercise
    **** $n = 9$

Figure 4-3. Method of reducing errors in cumulative metabolic balances. Bar over quantities indicates average value over the time period of N days.

are grouped according to missions. The astronauts formed a fairly uniform population with regard to age, body size, body composition, and physical condition. The environmental parameters of the Skylab workshop (Table 4-3) were also very similar from flight to flight. Although each flight consisted of a small statistical sample, the uniformity of these environmental and physical characteristics reduces the probability that the differences between crewmen would obscure the effects of spaceflight on metabolic factors.

4.1.5 Summary of Analyses Performed

The integrated metabolic balance analysis resulted in several distinct studies, which are summarized in this section. The major type of results derived from these studies are listed here.

1. Daily inflight metabolic balances for
   a. Water
   b. Nitrogen
   c. Sodium
   d. Potassium
   e. Calcium
   f. Phosphorus
   g. Magnesium
2. Cumulative losses or gains of
   a. Body water
   b. Body tissue solids
   c. Body fat
   d. Body protein
   e. Body sodium
   f. Body potassium
3. Preflight body composition (lean body mass and percent fat) and net inflight changes using five independent methods based on
   a. Total body water
   b. Total body potassium
   c. Body density
   d. Nitrogen balance
   e. Potassium balance
4. Estimates of unaccountable metabolic losses representing
   a. Evaporative water loss (sensible plus insensible)
   b. Dry skin losses
   c. Sodium sweat losses
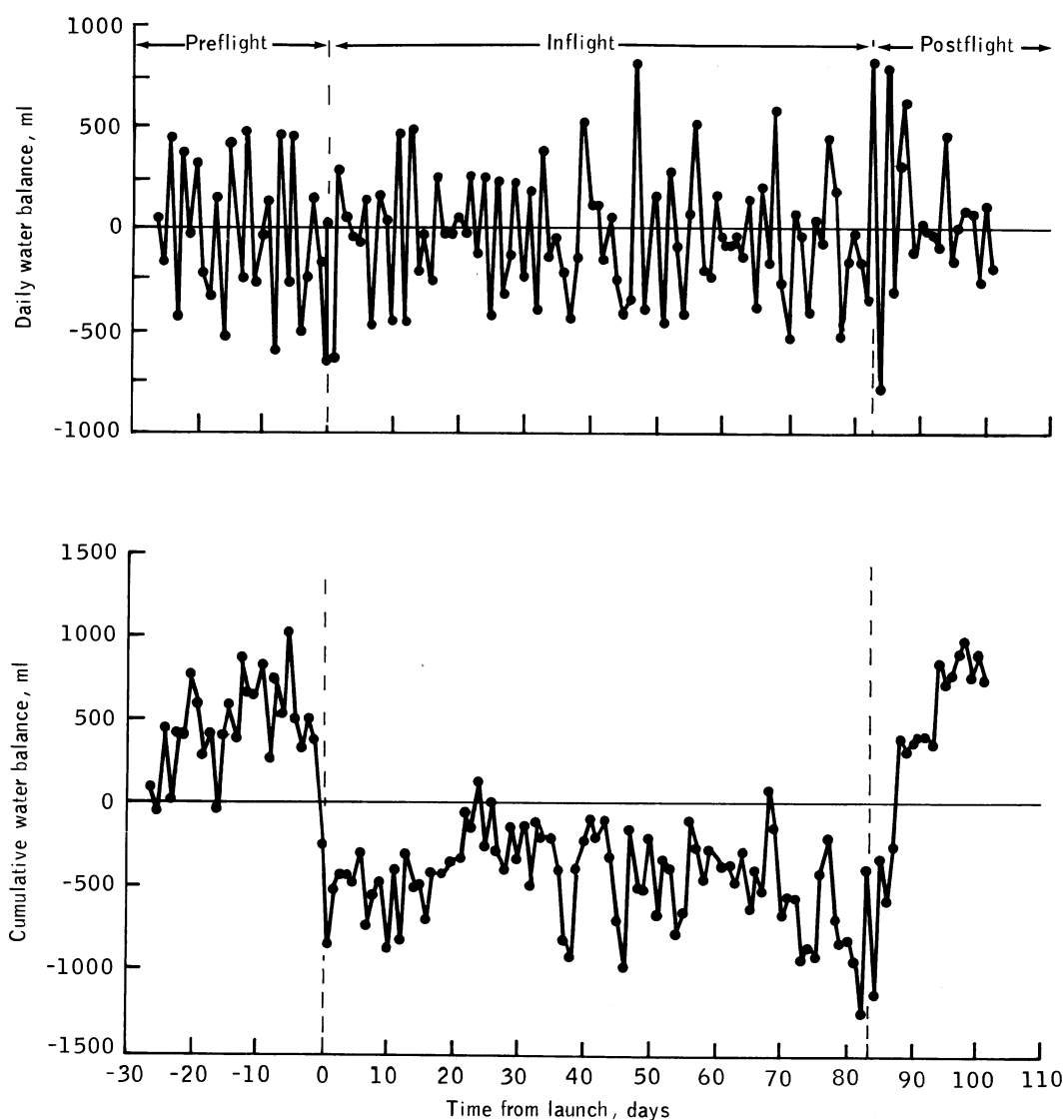
Figure 4-4. Daily water balance and cumulative water balance computed from water balance equation for a single Skylab crewman (subject 7). Cumulative water balance values represent changes from preflight baseline measured 1 day before liftoff.

Table 4-3. Skylab Environmental Parameters [Mean ± SE]

Mission duration, days	Temperature, °C	Pressure, mmHg			
		Ambient	pH$_2$O*	pO$_2$**	pCO$_2$***
28	24.3 ± 2.2	252 ± 0.04	8.9 ± 1.4	194 ± 0.5	3.7 ± 0.1
59	23.1 ± 1.1	263 ± 0.12	9.7 ± 0.7	185 ± 1.0	4.9 ± 0.1
84	24.1 ± 1.6	259 ± 0.11	9.8 ± 1.5	189 ± 0.5	5.1 ± 0.0

* Partial pressure of water vapor
** Partial pressure of oxygen
*** Partial pressure of carbon dioxide

Output   Input

Urine (dry) ←——— ←——— Food (dry)

Feces (dry) ←——— ←——— O_{2met}

CO_{2met} ←———

H_2O_{met} ←———

CF ←———

$$\Delta TBW = \Delta BWgt - \Delta Tis$$

$$\Delta Tis = \text{food (dry)} - \text{urine (dry)} - \text{feces (dry)} - IML + CF$$

where

IML = Insensible metabolic losses = $(H_2O + CO_2 - O_2)$ met
     = $\eta(Cho + Fat + 0.563 Pro)$
CF = correction factor = ΔTBW (direct) - ΔTBW (balance)
Cho = carbohydrate
Pro = protein
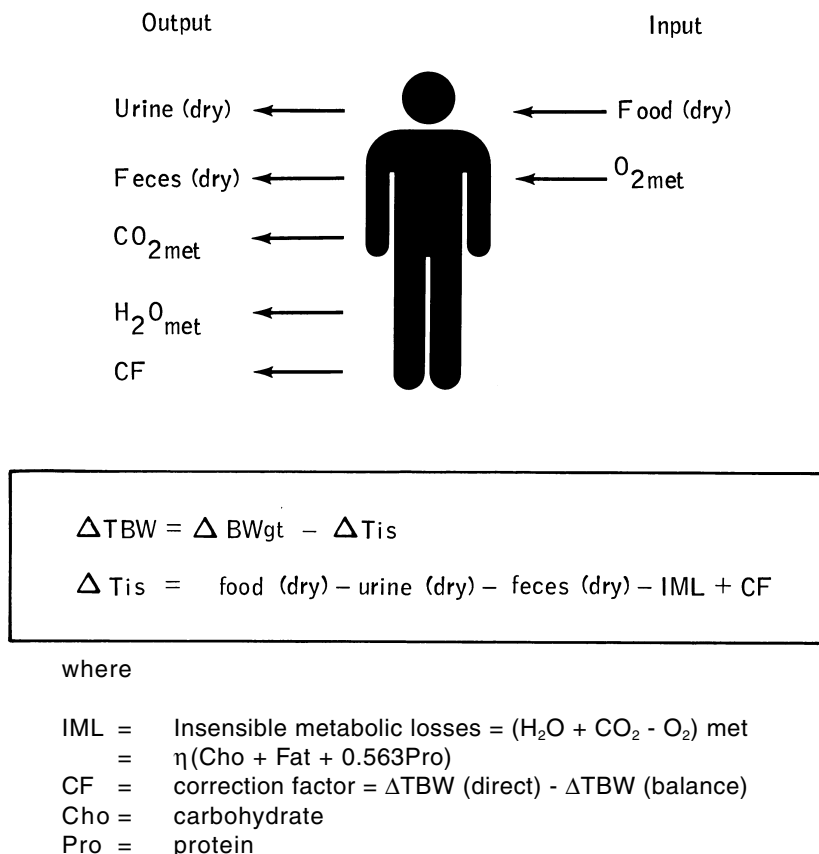
Figure 4-5. Method of computing daily changes in water balance using a solids balance. (Key: η = metabolic efficiency, TBW = total body water, BWgt = bodymass, Tis = dry tissue mass).

    d. Potassium sweat losses
5. Estimates of energy metabolism parameters
    a. Net energy use
    b. Metabolic efficiency
    c. Caloric intake requirements
    d. Exercise requirements

Complete reports of each analysis are available and are cited in the sections that follow. The methods of computation and associated assumptions that were used to obtain these results are provided in Appendix F.

4.2 Skylab Water Balance Analysis

A water balance analysis of the Skylab crewmen during the entire preflight, inflight, and postflight phases is summarized here. A knowledge of inflight changes in the fluid content of the body is essential for a complete understanding of the dynamics of body fluid shifts, renal function, electrolyte regulation, and hormonal regulation in response to extended periods of weightlessness. This infor-

mation will also be useful in interpreting other inflight experiments such as lower body negative pressure and exercise responses, in comparing weightlessness with bedrest, and in providing validation data for the simulation of weightlessness using mathematical models.

4.2.1 Approach

Daily changes in *total body water* (ΔTBW) are taken as the difference between changes in *body weight/mass* ($\Delta BWgt$) and *dry tissue* (ΔTIS) as shown in Fig. 4-5. Changes in the dry tissue were determined by a daily balance of solids on each crewmember. The amounts of dry food, urine, and feces were measured directly, whereas the values of *insensible metabolic loss* (IML) involved in food metabolism were obtained from dietary constituents, known stoichiometric relationships, and the metabolic efficiency η. A *correction factor* (CF) was employed to represent the unmeasured losses of sweat solids and skin flaking and the insensible metabolic losses from catabolism of body tissue. The correction factor was derived from the difference between the *directly measured losses of body water*

[$\Delta TBW(direct)$] and the losses over the same time interval obtained from an *uncorrected water balance* [ΔTBW (*balance*)](see Fig. 4-5). As mentioned earlier (see Fig. 4-3), the use of the correction factor in the balance equation ensures that the results from the indirect balance analysis agree with the total body water changes revealed by direct isotope-dilution methods. The water balance was computed as described in Fig. 4-5 and was expressed using the following definitions for water intake and output.

$$\text{Total water intake} = \text{water(drink)} + \text{water(food)} + \text{water(metabolic)} \quad (1)$$

$$\text{Total water output} = \text{urine volume} + \text{fecal(water)} + \text{evaporative water} \quad (2)$$

$$\text{Water balance} = \text{total water intake} - \text{total water output} \quad (3)$$

From the daily water balance equations, changes in total body water and *evaporative water loss* (EWL) can be calculated. Total body water changes between any two points in time were obtained from the accumulation of the daily water balances over that interval. The evaporative water loss was determined by using the two metabolic balance equations—the water balance and the mass balance—as shown in Fig. 4-6. In the mass balance equation, all the mass inputs and outputs of the body (liquid and solid) plus the changes in body mass are considered. In the water balance equation, only the fluid inputs and outputs of the body plus the changes in body water are considered. Metabolic oxygen, carbon dioxide, and water were determined from dietary components as shown in Fig. 4-6. Determination of evaporative water loss on a daily basis, using the water balance equation, was not possible since values of TBW were only known before and after flight – not on a daily or even weekly basis inflight. Therefore, the mass balance equation was used because all terms in the equation, including $\Delta BWgt$, were measured daily. Details of these methods are included in Appendices F(1) and F(2) or are available in technical reports [14,15].

4.2.2 Results and Discussion
4.2.2.1 Total Body Water Changes.
Average changes in total body water during the 2 weeks before and after launch and the 2 weeks after recovery are shown in Fig. 4-7 for all Skylab crewmen. The most notable feature of the total body water changes is the rapid change following launch and recovery. Immediately after launch, a significant loss of total body water occurs. The loss approaches a mean of 1400 ml and appears to be complete at the end of 2 days in flight. During recovery, nearly a week is required for the daily changes in total body water to equilibrate.

In the few days before launch, nearly a half liter of water was depleted from the body. This loss probably resulted from the busy workload during the period immediately before flight that may have precluded adequate hydration for the first few days in flight. For a variety of reasons, a diuresis was expected to occur the first day or two of the inflight period, but preflight dehydration can

partly suppress this diuretic response [16]. Thus, the loss of body water immediately before flight may partly help to explain why the expected early flight diuresis was not detected.

The mean inflight body water changes for the crews on each of the three Skylab missions are shown in Fig. 4-8. The largest losses occurred on the 59-day mission and the smallest on the 28-day mission. However, there appears to be a trend during the first 2 weeks in flight for the losses to converge toward a common value. Although not shown, the convergence continues for the following 2 weeks (see Fig. 4-27). The crew of the 59-day mission showed initial water losses that were more than twice as high as losses of either of the other crews. Half of this initial water loss is replenished by the end of the first month in flight. Data will be presented later in this section to suggest that the initial decrement in body water can be attributed to the large and persistent decrease in water intake, possibly as a result of motion sickness.

Throughout the manned spaceflight program prior to Skylab, there had been an unproven assumption that the large, rapid weight gain seen within the first few days after flight resulted from the recovery of body water that was lost in the first few days after launch. The rapid losses in body mass during the early inflight period, measured for the first time on Skylab, have been assumed to result from these body water losses. The results of this study tend to support that assumption. However, there is an increasing difference between body water and body weight change beginning almost immediately after launch and recovery as can be seen from Fig. 4-7. The computed change in total body water is always less than the change in body mass that is measured directly. The difference between body mass and body water is assumed to represent the change in body fat and body protein. This assumption implies a net loss of body tissue before and during flight and a net gain of body tissue after flight. Upon reentry, there appears to be a nearly linear rate of increase in body tissue that continues for the two weeks of measurment..

It is possible, using the present analysis, to obtain an estimate of the true total body water measurements between the morning of launch and the morning of recovery, rather than just between the days on which total body water was actually measured. These estimates are shown in Table 4-4. Total body water changes determined from direct measurements are lower than true inflight TBW changes by about 30%, possibly because direct measurements immediately before launch or reentry were not possible. The water balance approach may provide better estimates of the true responses of microgravity.

4.2.2.2 Water Loss.
The water balance charts of Figs. 4-9 and 4-10 illustrate the particular routes by which total body water is lost or gained following launch or recovery.[*] Figure 4-9 is a summary of the water balance data 14

---

[*] In Figs. 4-9 and 4-10, the scale of the water balance charts is negative below the zero line; therefore, a rise (i.e., a deflection toward the top of the page) in urine or total output signifies a decrease in that quantity. This is a traditional method of graphing metabolic balance data.

CREW MASS BALANCE

Evap H_2O ← ← Food (dry)

CO_{2met} ← ← H_2O (fluid + food)

Urine ← ΔW ← O_{2met}

Feces (wet) ←
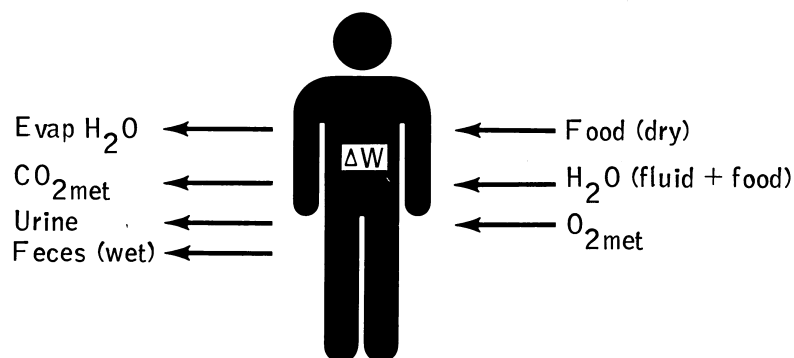
Evap H_2O = Food + H_2O in - Urine - Fecal + $(O_2 - CO_2)$met - ΔW_{body}

where

$(O_2 - CO_2)_{met} = -0.17Pro - 0.45Cho + 0.064fat$

CREW WATER BALANCE

Evap H_2O ← ← H_2O in (fluid + food)

Urine ← ΔW ← Met H_2O
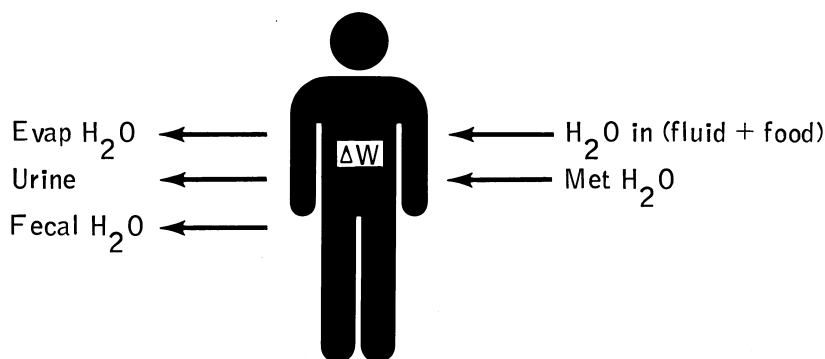
Fecal H_2O ←

Evap H_2O = H_2O in + met H_2O - Urine - Fecal H_2O - ΔW_{H20}

where
Met H2O = 0.41 Pro + 0.60Cho + 1.07Fat

Figure 4-6. Methods of calculating evaporative water loss using a total mass balance (top) and a water balance (bottom). (Key: met = metabolic, Pro = protein, Cho - carbohydrate, W_{body} = body mass, W_{H2O} = body water, Δ = change over time-period of balance).

days before and after launch of the Skylab crews, whereas Fig. 4-10 is a summary of the data 14 days before and after recovery. The major disturbance in the balance appears to occur during the first 2 days following launch and during the first week after recovery. It is evident that the body did not lose water after launch by either of the major output pathways: urine or evaporative water. Both urine and fecal water output, as well as evaporative water loss, were reduced during the first 2 mission days and therefore could not account for the decrement in water balance. The decrement appears to be due to changes in intake. An unex-

pected decrease in total water intake appears to account for the negative water balance observed in flight.

The mean decrease in total water intake reached a value as high as 40% of the preflight value by the second day. This decrease in total intake is highlighted in Fig. 4-11, which contains the average data from the crews of each Skylab mission. Total water intake in these charts represents the sum of free liquid intake plus food water plus metabolic water. In all three Skylab missions, total water intake was reduced at least the first 2 days in flight. A possible cause of the decreasing intake may be motion
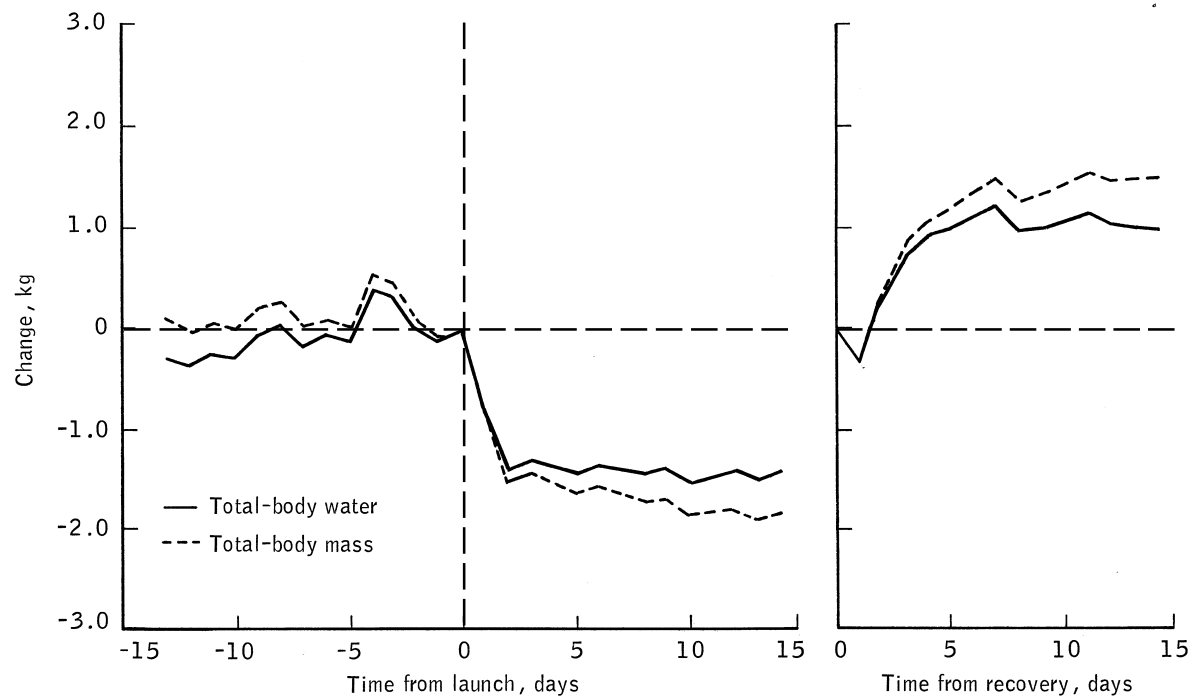
Figure 4-7. Daily changes in total body water and body mass at launch and recovery for all Skylab crewmen ($n = 9$). Values are shown as changes from morning of launch or recovery. The data for body mass was measured directly while that for body water was computed from the equation shown in Fig. 4-5.
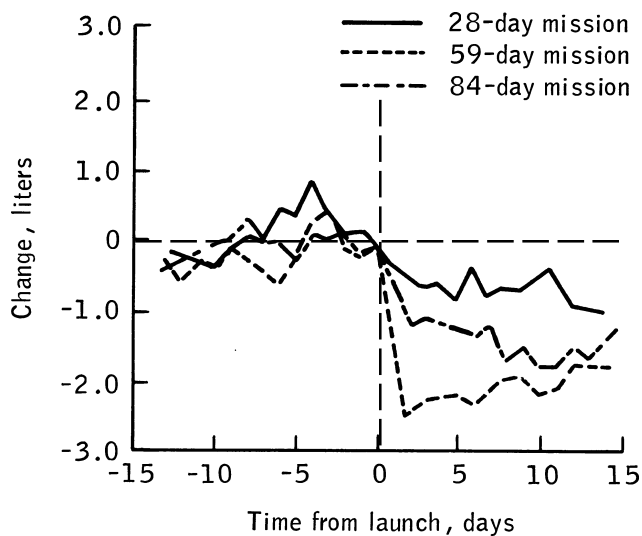
Figure 4-8. Daily changes in total body water of each Skylab crew ($n = 3$). Values are shown as changes from morning of launch.
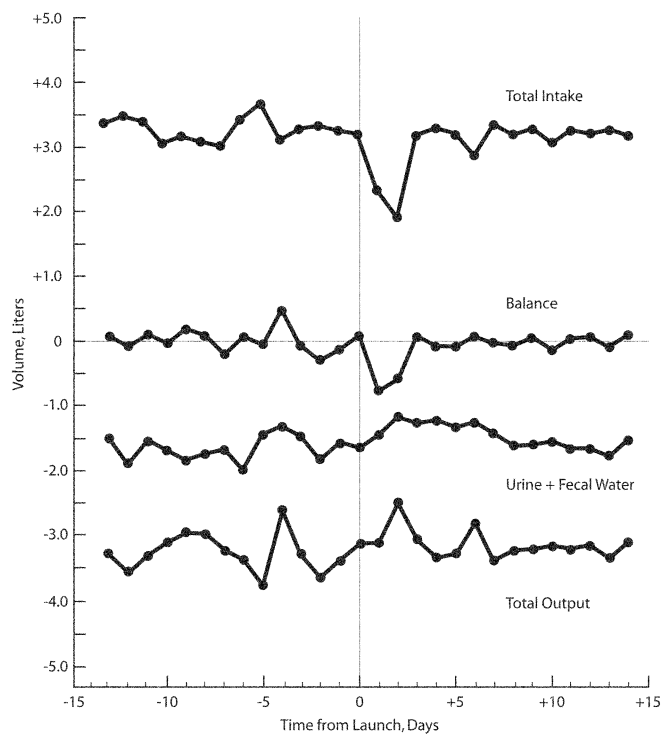
Figure 4-9. Average water balance for all Skylab crewmen ($n = 9$) 14 days before and after launch. The difference between the 'urine plus fecal' and 'total output' curves represents the evaporative water loss.

Table 4-4. Estimates of Changes in Body Weight and Body Water due to Weightless Flight: Comparison of Ground-Obtained Data with Those Obtained from the Water Balance Analysis

Flight duration, days	Water balance,* kg		Direct measurement, kg	
	ΔBWgt	ΔTBW	ΔBWgt**	ΔTBW***
28	–2.33	–0.89	–2.77	–1.22
59	–3.90	–1.53	–3.73	–0.60
84	–0.93	–1.00	–1.40	–0.63
Mean	–2.39	–1.14	–2.63	–0.82

* Measurement interval: morning of launch to morning of recovery day
** Measurement interval: morning of launch to first shipboard weight
*** Measurement interval: varies from 32 days before launch to recovery day
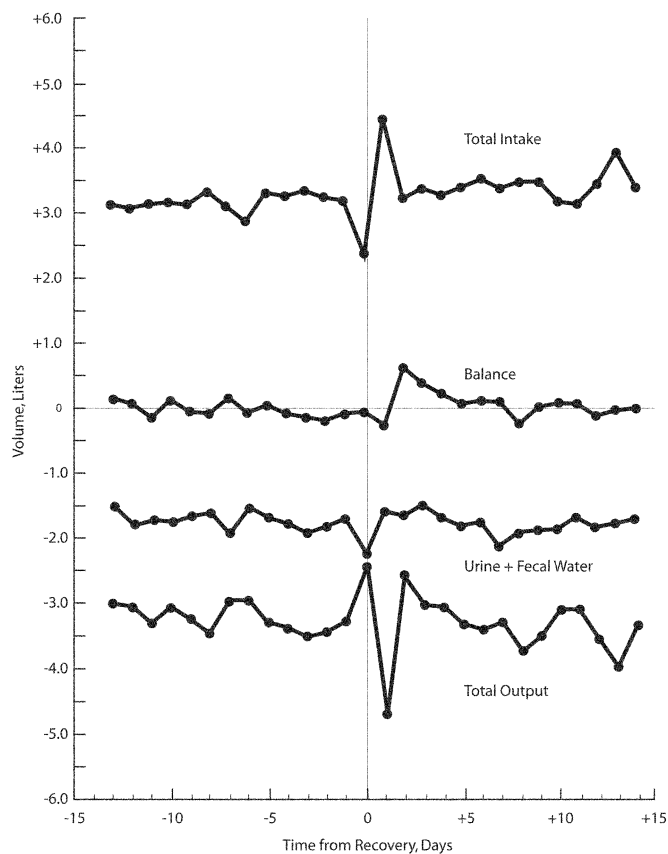
Figure 4-10. Average water balance for all Skylab crewmen ($n = 9$) 14 days before and after recovery. The difference between the 'urine plus fecal' and 'total output' curves represents the evaporative water loss.
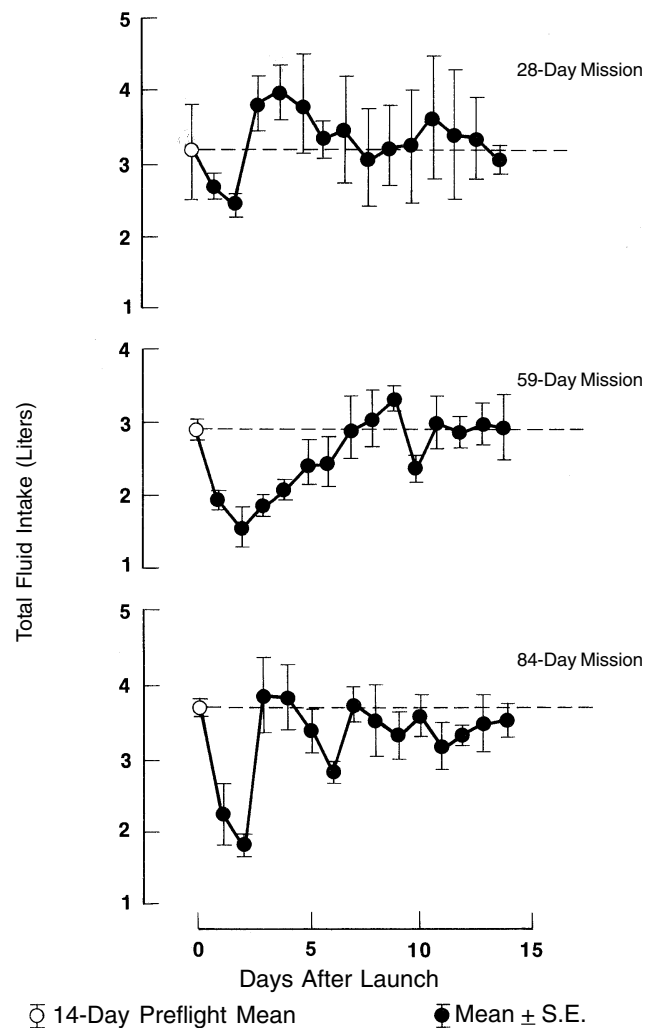
Figure 4-11. Total water intake (includes drinking water, fluid content of foods, and metabolic water) after launch of each Skylab mission ($N = 3$).

Table 4-5. Average Daily Evaporative Water Loss for the Three Skylab Missions

Flight duration, days	Subject	Preflight EWL			Inflight EWL		
		No. days Observed	ml/day	ml/day-m^2	No. days Observed*	ml/day	ml/day-m^2
28	1	30	1472	892	23	1206	731
	2		1814	926		1372	700
	3		<u>1664</u>	<u>862</u>		<u>1725</u>	<u>894</u>
Mean			1650	893		1434	775
SE			±99	±18		±153	±60
59	4	20	1124	646	54	1351	776
	5		1794	1081		1410	849
	6		<u>2036</u>	<u>1008</u>		<u>2170</u>	<u>1074</u>
Mean			1651	912		1644	900
SE			±273	±134		±264	±90
84	7	26	1378	787	79	1302	745
	8		2333	1311		1625	913
	9		<u>2104</u>	<u>1189</u>		<u>1862</u>	<u>1052</u>
Mean			1938	1096		1597	903
SE			±288	±158		±162	±89
SL mean			**1747**	**967**		**1558**	**859**
SE			**±127**	**±68**		**±105**	**±46**

* First 5 days excluded

sickness, since the first several days following launch were accompanied by motion sickness in most crewmembers. Motion sickness and/or anti-motion-sickness drugs probably was a factor in blunting appetite and thirst. However, it is possible that the decreased intake is a normal result of the weightlessness response (i.e., possibly by way of the angiotensin-thirst mechanism [17]) and would have occurred even in the absence of motion sickness.

Evaporative water loss was expected to increase during the flight because of the low barometric pressure (1/3 atmosphere) in the Skylab orbital workshop. However, evaporative water loss does not appear to be a major factor in the inflight changes in overall water balance. It does appear to be significant in the postflight changes in water balance (Fig. 4-10). The first day of recovery was characterized by large increases in evaporative water loss (perhaps because of the thermal stresses of entry) that were nearly counterbalanced by increases in water intake. It was of interest whether the evaporative water loss changed during flight and whether this change was marked by other components of the balance. This is the subject of the next section.

4.2.2.3 Evaporative Water Loss
4.2.2.3.1 *Evaporative Water Loss: Results.* *Evaporative water loss* (EWL) was computed from the mass balance formulas shown in Fig. 4-6 and in Appendix F(2).

Mean daily EWL results for all Skylab crewmen are shown in Table 4-5. Results are expressed in ml/day and ml/day per body surface area. Contrary to expectation, there was an average decrease in EWL of 10.8% (probability $p < 0.01$) for all subjects. There were significant changes from preflight values on the shortest (–13%, $p < 0.05$) and longest (–18%, $p < 0.01$) missions; the crew of the 59-day flight showed a negligible decrease. Two of the three crewmen who increased their inflight EWL were on the 59-day flight. In general, the effect of spaceflight on EWL was different in magnitude for each mission and was not related to any single variable such as mission length or exercise levels. The first 5 days of the inflight period was excluded from the statistical analysis performed for each crewman because, as will be shown below, this period was characterized by unusual variations in EWL and water balance.

When EWL is expressed in terms of body surface area, it is apparent that the mean of each successive crew increased during both the preflight and the inflight periods. This increase was qualitatively (but not quantitatively) related to the amount of exercise performed.

Although the results in Table 4-5 show a large variation in the different crewmen's inflight EWL response relative to preflight (a range of 70 to 120% of preflight value), these changes were significantly correlated with their preflight EWL values (correlation coefficient $r = –0.71$, $p <$
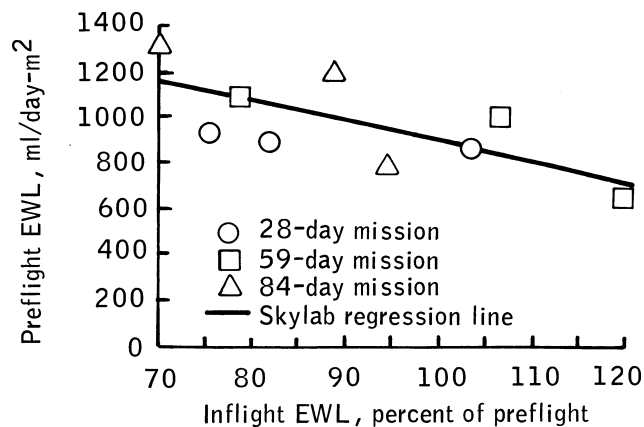
Figure 4-12. Correlation of inflight evaporative water loss (shown as percent of preflight mean) with preflight EWL values ($r = -0.71$, $p < 0.05$).

0.05). This first-order relationship, illustrated in Fig. 4-12, shows that the largest decrements of EWL during each mission occurred in those crewmen having the highest preflight EWL.

A comparison of the results of the two methods used to estimate EWL—mass balance and water balance (see Fig. 4-6)—is shown in Table 4-6. Inasmuch as TBW was measured strictly at the beginning and end of preflight and inflight periods in only six crewmen, the results from only these subjects could be computed. Values for the mass balance were averaged over the time-span coinciding with the indicated interval between TBW measurements. The results show a small but significant systematic difference ($< 3\%$, $p < 0.05$) between the two methods.

The average EWL for the first 10 days of each mission compared to preflight controls is presented in Fig. 4-13. There is an obvious difference between the EWL response for the 28-day crew and the other crews. In Figs. 4-13 and 4-14 the EWL changes could be qualitatively related to activity and ambient temperature loads, a testament to the accuracy of the methodology. The increase during the first week of the 28-day flight is related to the unusually high temperature (about 32°C) in the Skylab workshop during
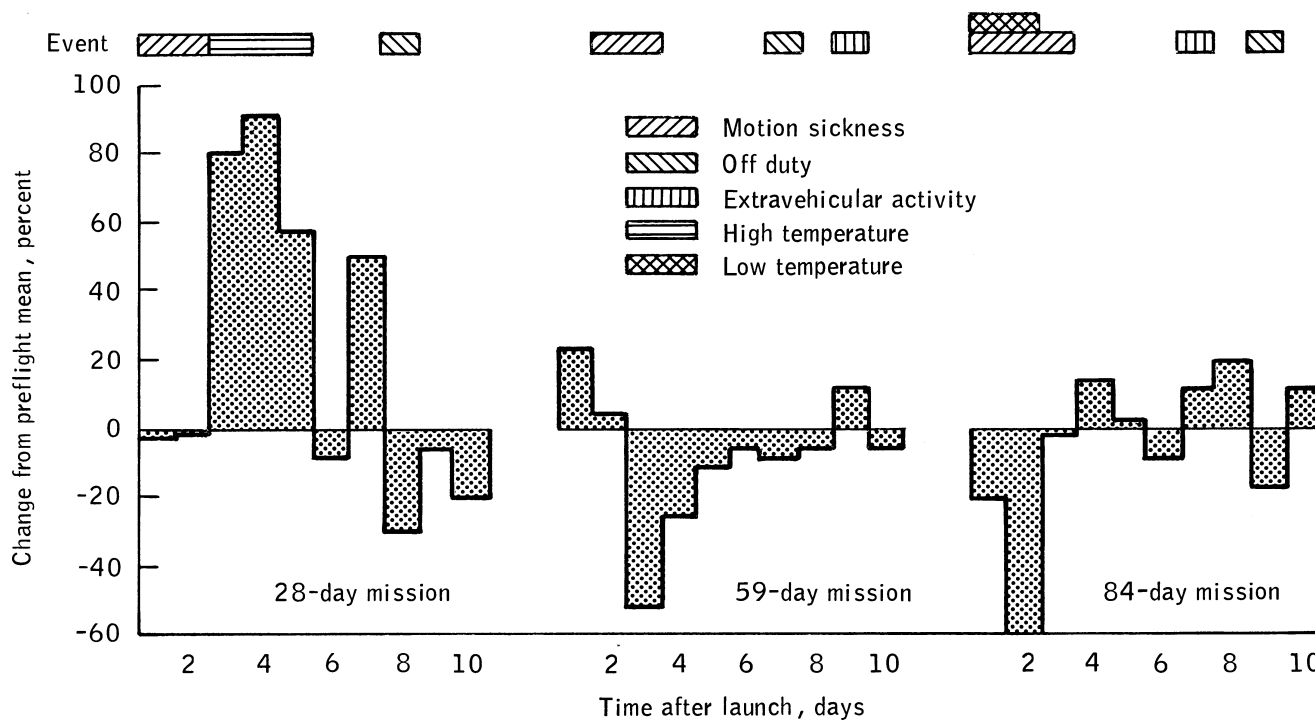
Figure 4-13. Average crew evaporative water loss during the first 10 days of each Skylab mission. The crew of the 28-day mission entered the Skylab workshop on the third day and encountered high ambient temperatures caused by a heat-shield malfunction. Crews on the other two flights may have been relatively inactive for several days because of space motion sickness.

Table 4-6. Comparison of Two Methods for Determining Evaporative Water Loss

Mission duration,	Subject	Δt,* days	ΔTBW, ml/day	Water Balance** ml/day	Mass Balance*** ml/day	Δ,**** ml/day
			Preflight			
28	1	20	−500	1307	1316	−9
	2	20	800	1726	1790	−64
	3	20	−300	1656	1702	−46
84	7	20	100	1390	1398	−8
	8	20	200	2253	2299	−46
	9	20	700	2050	2132	−82
Mean			**167**	**1730**	**1773**	**−43**
SD			**±520**	**±368**	**±390**	**±30**
			Inflight			
28	1	29	−500	1344	1390	−46
	2	30	−1200	1515	1620	−105
	3	29	−2000	1770	1824	−54
84	7	85	−900	1318	1326	−8
	8	85	−600	1604	1637	−33
	9	85	−900	1859	1858	−1
Mean			**−1017**	**1568**	**1609**	**−41**
SE			**±221**	**±90**	**±89**	**±16**

* Δt = time between TBW measurements
** *E*vaporative water loss from water balance
*** *E*vaporative water loss from mass balance
**** Δ = *Water Balance - Mass Balance*

this period, resulting from a temporary heat-shield malfunction. The first crew was able to restore cabin temperature to near normal after 5 days. Figure 4-13 also indicates a significant decrement in EWL during the first few inflight days of the longer missions, when the crew was relatively inactive because of motion sickness symptoms.

Daily EWL for a single crewman on the 84-day flight is plotted as a function of mission time in Fig. 4-14. In this subject, EWL was less on days when no planned exercise occurred and during periods when the workshop was at its lowest temperatures. Also, EWL increased during periods of extravehicular activity (EVA) and when environmental temperatures were increased. Otherwise, evaporative loss was usually lower in flight than before flight and showed no tendency to return to preflight levels. Although postflight values are also shown in this figure, they have not been included in the remainder of the analysis. No physical activity program was scheduled during the postflight period; therefore, it was unlike the preflight and inflight phases.

4.2.2.3.2 *Evaporative Water Loss: Discussion.* Evaporative water loss is affected by many factors, including environment, metabolic rate, physical activity, clothing, psychological stress, hydration, degree of heat acclimatization, and interactions in the physiological systems that are directly or indirectly involved in thermoregulation [18]. This study suggests, for the first time, that gravity or its absence may also influence EWL.

The preflight and inflight environments (the Skylab workshop and, on the ground, the buildings and trainers used by the crewmen) differed in only two major aspects: gravitational force and atmospheric pressure.‡ In seeking the reason that EWL did not increase during flight as expected (because of diminished ambient pressure), four possibilities were examined: the indirect method used to measure EWL was neither sufficiently accurate nor sufficiently sensitive to detect significant changes; the preflight environment in which the crew exercised could not be precisely controlled and acted to elevate preflight EWL, which masked the anticipated effect of the hypobaric environment; the effects of weightlessness, directly or indirectly, decreased one or more components of EWL; and specific biochemical effects. These possibilities will be discussed next and in doing a hypothesis to explain the inflight decrease in EWL will be advanced.

---

‡ The difference in atmospheric composition between preflight and inflight environments (i.e., 21% oxygen compared to 70% oxygen) is believed to have little influence on thermoregulatory processes [19].
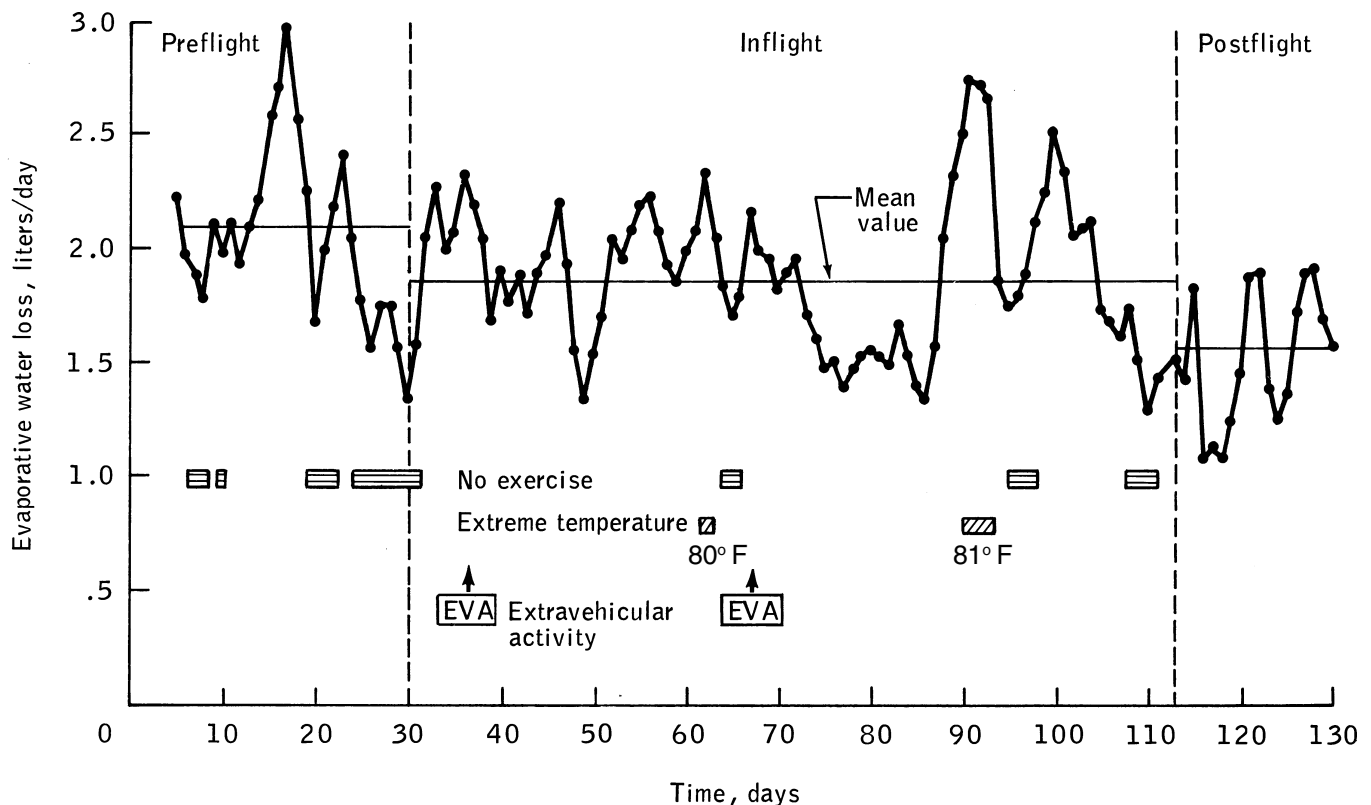
Figure 4-14. Example of evaporative water loss for a Skylab crewmember (subject 9).

a) Sensitivity of Indirect Method. For this study, it was estimated that the indirect method could detect real differences between preflight and inflight EWL that were greater than 8 to 12%. The method's sensitivity was enhanced because of the large number of consecutive daily observations, and instrument error was less than ±4% of EWL. The reader is referred to Leonard [20] and to Appendix F(1) and F(2) for a full discussion of balance technique errors.

It has been shown that EWL measurements obtained indirectly from mass and water balances do not always agree with more direct measurements [21]. However, in this study, the indirect method of calculation was sufficiently sensitive to reveal changes in daily EWL that could be correlated with ambient temperature variations and changing levels of metabolic activity (see Figs. 4-13 and 4-14). The day-to-day variation in EWL shown in Fig. 4-14 reflects similar fluctuations in water intake, urine loss, and body mass that were directly measured.

Variation of EWL between subjects was significant, but relatively small, and was similar to that noted in two previous studies employing the direct method of measurement [21,22]. Absolute levels of preflight EWL in the Skylab crew were similar to estimates of EWL for other astronauts at sea level who had comparable energy requirements [23]. A further indication of the precision of the analysis is the close agreement between the mass and water balance estimates of EWL (Table 4-6).

b) Effects of Environment and Metabolic Activity. Evaporative water loss consists of three components: respiratory losses, skin diffusion losses, and sweating. It is believed that reduced barometric pressure increases water diffusion from the skin, primarily as a result of enhanced vapor conductivity and, to a lesser extent, as a result of diminished heat convective loss [24,25]. Previous studies of inactive subjects in hypobaric chambers at (1/3 atmosphere) have demonstrated increases in skin diffusion ranging from 36 to 59% above that measured at sea level [26,27]. Others have found that diffusion loss across the incompletely wet skin membrane is inversely proportional to the square root of the pressure [25]. Respiratory water loss, although not measured directly on Skylab, probably increased, since resting minute volume increased in flight by nearly 20% [28]. Overall increases in insensible water loss (combined diffusion plus respiratory losses) of 15 to 38% have been reported for subjects in a one-g chamber at a pressure of 1/3 atmosphere [26,27].

Regarding sweat responses in high activity subjects, there have been no studies in hypobaric, normoxic environments that are comparable to the Skylab atmosphere, although it might be expected that this EWL component would also increase because of the reduced pressure, at least in one-g [29]. Therefore, the failure of inflight EWL to increase appears to involve a mechanism capable of causing major reductions of either in-

sensible or sensible water loss. The crew's environment and metabolic activity were examined to detect factors that may have affected EWL.

The Skylab medical experiments were designed to closely monitor and/or control the physical activity, diet, physiological condition, and environment of the crewmen before, during, and following the flights. During the 2- to 3-week isolation period preceding each flight, the crew was confined to environmentally controlled areas except for the time devoted to physical training outdoors. The mean temperatures of the preflight physical training environments were 22°C for the 28-day crew, 25°C for the 59-day crew, and 21°C for the 84-day crew. These temperatures were not very different from those of the Skylab workshop and appear uncorrelated with the preflight EWL levels for any of the crews.

Each successive crew exercised more frequently and vigorously during the preflight as well as the inflight periods. Starting with 30 minutes per day in the first mission, the crew of each succeeding mission was allowed an additional 30 minutes per day exercise. Whereas the preflight exercise regimen paralleled but did not exactly duplicate the flight program, routine daily activity was similar for all subjects throughout each mission. There is no indication that these tasks are different under zero-g conditions with regard to mean energy consumption.

Differences in EWL among the missions could result from variations in the sweat component caused by exercise. The average preflight plus inflight EWL rates of 834, 906, and 999 ml/day-m^2 for the 28-, 59-, and 84-day missions, respectively, are consistent with this assumption, although differences between flights were not statistically significant. But this, of course, does not explain the inflight decrease in EWL relative to preflight.

The crew and crewmen that performed the most inflight exercise showed the largest decrease in EWL. This fact suggests that, on the average, the inflight exercise protocol caused a much lower EWL than did the preflight exercise protocol. The decrease in EWL could be explained if the energy expenditure for exercise was less during flight. This lower energy expenditure may have occurred on the first mission, but there is indirect evidence, based on aerobic fitness, to show that there was a similar or higher energy expenditure on the two longest missions [30,31]. Energy balance considerations lead to the same conclusion [32]. It appears that the decrease in EWL inflight cannot be completely explained by uncontrolled environmental and metabolic activity factors.

c) Effects of Weightlessness on EWL. Several effects of weightlessness may directly or indirectly alter the absence of natural convective forces, a decrease in sweat drippage, an increasing influence of surface tension forces compared to gravity forces, and biochemical alterations. In weightlessness, both evaporation and heat transfer are reduced because natural convective forces are absent [26].

Since convective air flow assists in the evaporation of water from the skin, one must take into account the complete lack of natural convection in microgravity. Forced air movement in Skylab was not greater than in the preflight office and laboratory environment. Also in a normal gravity office or laboratory, natural convection may accounted for a significant proportion of total air movement [24]. The net effect of the Skylab environment on EWL is the result of a balance between the enhanced evaporative power of a hypobaric atmosphere and the reduced convective forces of a microgravity environment.

A clue to a possible mechanism for EWL reduction was provided by observations made by the Skylab crewmen. They observed that during zero-g, sweat generated during exercise does not readily drip from the body but rather tends to spread and to become evenly distributed on the skin surface, much like a film. One factor known to modify sweat rates is the degree of skin wettedness, which is determined by the balance between sweat production and evaporative loss rates. It has been demonstrated that as the wetted area increases, the buildup of surface water acts to inhibit the rate of sweating by nonthermal mechanisms that are poorly understood [34,35,36]. These studies have shown that this phenomenon (skin wettedness and hidromeiosis) can suppress sweat rates by as much as 80% and easily account for the discrepancy between expected and measured inflight EWL. It is tempting to speculate that during periods of high exercise activity, sweat rates were suppressed to an extent that masked the effect of an increased insensible water loss, which may have occurred during the remainder of the day with the net effect being a decrease in total daily EWL. The hidromeiosis hypothesis is consistent with the observation that crewmembers who performed the greatest amount of exercise also showed the largest decline in EWL from preflight levels. Also supporting this theory is the observation that the one crewman whose EWL was most markedly *increased* inflight consistently used a fan during his personal exercise period. A fan was not used by the other crewmen during exercise. It has been demonstrated that this maneuver can dramatically reverse a hidromeiotic effect by reducing skin wettedness [35], similar to the effects obtained by wiping the skin.

d) Biochemical Effects. There is a growing body of evidence indicating the ability of certain physiological parameters, other than those normally associated with environmental effects and metabolic activity, to influence evaporative loss rates. Factors that have been implicated in modifying thermal sweating during exercise in normal environments include the state of hydration [37], plasma sodium and calcium concentrations [38], body fluid osmolarity [36], and antidiuretic hormone levels [39]. These factors were altered in the Skylab crewmen [2]. However, when the direction and magnitude of these changes were evaluated, it seemed likely that the shifts would tend to increase rather than

Table 4-7. Estimates of Insensible and Sensible Evaporative Water Loss

EWL	Preflight[a]	Inflight[b]		
		Expected	Estimated	Difference
Insensible, ml	[c]850	[d]980 to 1170	[d]980 to 1170	
Rate, ml/day				
Expected vs. estimated, percent change				0
Sensible				
Rate, ml/day	[e]900	[f]900 to 1170	[e]390 to 580	
Skin wettedness[g]	1.10	0.69 to 0.90	0.30 to 0.45	
Expected vs. estimated, percent change				−35 to −67
Total[h]				
Rate, ml/day	[i]1750	[e]1800 to 2340	[i]1560	
Expected vs. estimated, percent change				−17 to −35
Change from preflight, Percent	0	7 to 34	−11	

[a] 1 atmosphere, one-g
[b] 1/3 atmosphere, zero-g
[c] Nominally accepted value for comfortable sea-level environment [27,40]
[d] Based on hypobaric chamber studies showing a 15- to 38% increase over sea-level values [22,26,27]
[e] Determined by subtraction or addition
[f] Based on hypoxic, hypobaric exercise studies showing increases as great as 30% over sea-level values [29]
[g] Skin wettedness = sensible EWL divided by maximum EWL
[h] Total EWL = insensible EWL plus sensible EWL
[i] Data from present study

decrease evaporative water loss. It may be speculated that these biochemical effects tended to increase early sweating [38], a condition known to favor overall sweat suppression [34].

4.2.2.3.3 *Analysis of Insensible and Sensible EWL.*
It is instructive to quantify the degree to which EWL would have been expected, on the basis of prior studies, to increase in the Skylab hypobaric environment, and to compare the expected EWL with the EWL actually observed. The estimates of sensible and insensible EWL for the preflight and inflight environments are summarized in Table 4-7. The expected inflight values are based on studies from one-g hypobaric environments. The assumptions and supportive studies for each of the values are indicated in footnotes to the table. In addition, the following assumptions were made: (1) inflight insensible water loss was assumed to be affected only by the reduced atmospheric pressure and unaffected by gravity, (2) other than differences in pressure and gravitational field, the preflight and inflight environments were considered identical, and (3) inflight metabolic activity was considered similar to preflight activity. Table 4-7 indicates that inflight values for total

losses were expected to be 7 to 34% higher than preflight values. However, a decrease of 11% in EWL was actually determined in these studies. Therefore, the total inflight EWL ranged from 17 to 33% below expected values. Similarly, it is estimated that actual inflight sweat losses ranged from 35 to 67% below expected values. This range is within acceptable limits of sweat suppression previously attributed to high degrees of skin wettedness [35].

Estimates of skin wettedness during sweating were also made [15] and are included in Table 4-7. The degree of skin wettedness is defined as sweating rate divided by maximal evaporative rate. It was assumed that the sweat losses were associated with an hour of daily exercise, and formulations from the literature were used to compute the evaporative loss rate for sea level and spaceflight environments [19,35,41]. Sweat begins dripping when skin wettedness is greater than 0.33 in terrestrial environments [42]. The results show that the potential for a buildup of skin surface water exists for all the cases considered, despite the hypobaric environment.

4.2.2.3.4 *Predictions of EWL Using the Thermoregulatory Model.* The mathematical model of the human ther-

Table 4-8. Values of Input Parameters for Human Thermoregulatory Model

	(a) Activity parameters					
Parameter	Activity					
	Sleep	Routine work	Ergometry		Gymnastics	EVA
			Leg	Arm		
Metabolic rate,* kcal/hr	75	109	630	405	405	230
Work efficiency, percent	0	5	22	22	10	10
Clothing resistance, clo	1.0	0.35	0.2	0.2	0.2	6.6
Position**	1	0.5	0	0	1	1

* Estimated from inflight records for subject 4
** 0 = seated; 1 = standing

(b) Environmental Parameters		
Ambient temperature	(°F)	73
Wall temperature	(°F)	73
Ambient dewpoint temp	(°F)	52
Ambient pressure	(psia)	5.1
Air velocity, m/sec	(ft/min)	40.0
Atmospheric specific heat	(kcal/kg-°C)	0.22
Body emissivity		0.95

moregulatory system, described in Chapter 3, can simulate responses to environmental and metabolic thermal disturbances. This model was of particular interest because of its capability to predict evaporative water loss from the three major pathways: respiration, skin diffusion, and sweating. As has been demonstrated, EWL was altered in spaceflight and has been responsible for secondary disturbances in fluid-electrolyte metabolism.

The model has been validated for one-g simulations at normal atmospheric pressure. Data are still lacking for testing the model under simulated hypobaric conditions at high metabolic rates. Since the environment of Skylab included both a zero-g and a hypobaric atmosphere, the Skylab simulations included in this section should be considered a preliminary study whose longer term objective is a validated model for weightlessness.

For this preliminary prototype simulation, the model was used to predict EWL for a single crewmember on the second Skylab mission. These results are compared to observed flight losses, as calculated from the metabolic technique discussed previously. Table 4-8 contains the input parameters to the model that were based on inflight records for the second Skylab mission. For purposes of computing daily EWL, each day was divided into 6 types of activities. Six separate simulations were performed for the basic activities shown. Metabolic rates for sleep and gymnastic activity were estimated

from average values found in the literature, whereas bicycle ergometry and EVA rates were measured directly inflight. The metabolic rate for "routine work" (which accounts for the largest fraction of daily evaporative loss) was based on a caloric balance of the nutrients consumed during the flight (see Chapter 4.6). Table 4-8 also indicates the capability of this model for considering a large number of input parameters and, thereby, for describing a given environmental and metabolic situation in considerable detail.

The evaporative losses predicted by the model are shown in Table 4-9 for two different ambient pressures — 760 and 264 torr — the latter case representing the Skylab environment. The model's output is in the form of an evaporative rate (grams per hour), which must be multiplied by the appropriate time period for each particular activity; these times are shown in the first two columns and are based on inflight records for the selected crewman. The average daily evaporative loss rate predicted by the model for the two ambient pressures is compared with the preflight and inflight values obtained from experimental data using the metabolic balance technique (last 2 rows of Table 4-9).

Agreement between the simulation and the data is excellent and well within several percentage points for both environmental conditions. (The crewmember chosen for this example was only one of two crewmen showing an increase in inflight EWL). However, the simulation was

Table 4-9. Evaporative Water Losses Predicted by Human Thermoregulatory Simulation Model for Inflight Activities at Two Ambient Pressures*

Activity	Time, Hr/day	No. of days	Predicted EWL				
			Rate,g/hr		Total, g/mission		Change, %
			760 torr	264 torr	760 torr	264 torr	
Sleep	8.0	58	17.7	20.1	8213	9326	14
Routine work	15.3	59	32.1	48.8	28977	44052	52
Leg ergometry	0.54	46	662	738	16444	18332	12
Arm ergometry	0.92	6	375	431	207	238	15
Gymnastics	0.38	40	368	420	5594	6384	14
EVA	2.68	1	173	213	464	571	23
Total mission EWL (59 days)					59899	78903	
Avg daily EWL, simulation model					1015	1337	32
Avg daily EWL, metabolic balance data*					**1056	***1275	21

* Estimated from inflight records for subject 4 (59-day mission)
** Preflight
*** Inflight

not designed to duplicate the preflight case. Unfortunately, physical activity and environmental conditions were not controlled variables during preflight activities, and data are insufficient to quantify these conditions as was done with the inflight period.

It must be remembered that these simulations only reflect the differences due to an altered ambient pressure and not the effects of weightlessness. Mechanisms for thermoregulation in zero-g are entered in the model to a limited extent (i.e., only a convective heat flow influence). Some of the influences of weightlessness that would be candidates for inclusion in a future model are: the lack of sweat dripping in a gravity-free environment, a high degree of skin wettedness, and a resultant suppression of thermal sweating [43]. It is significant that the astronaut logs indicated that the crewmember selected in this study was the only subject that invariably used a fan during bicycle ergometry workouts. An enhanced convective airflow during exercise has been shown to reduce sweat suppression on wetted skin. Therefore, if this mechanism is the major effect in weightlessness, and if it was only minimally present in this crewmember, comparison of this subject with the others could provide a means of distinguishing between the effects of low ambient pressure and zero-g. The simulation does reveal that the effect of the hypobaric environment is to increase evaporative loss by 32% (com-

pared to 21% for the measured change in the astronaut) for this particular metabolic protocol and environmental condition. Unfortunately, time restrictions prevented both a similar analysis for the other crewmembers and an evaluation of the sweat suppression effect in the model.

The metabolic balance studies have provided an overall estimate of daily evaporative losses. The model used is capable of revealing the components of this total loss. Table 4-10 contains the contribution to the total evaporative loss that may be assigned to each major activity and to each evaporative loss pathway. The values shown have been obtained from the simulation and predict that 32% of the total evaporative loss can be attributed to less than 1 hour of exercise per day. In addition, 57% of the total loss is derived from thermal sweating; half this amount occurs during routine work at reasonably low levels of metabolism.

In Fig. 4-15, these components of evaporative water loss as predicted by the model are graphically shown and the daily water loss rate is compared with that of a Skylab crewmember (the same subject whose data was used in Table 4-9) as well as with the mean value for all Skylab crewmen. The predictions of the model are in general agreement with one-g hypobaric chamber studies and with the single crewmember studied, but not with average zero-g data. This preliminary study, however, demonstrates the capability of using the model for predicting evaporative

Table 4-10. Relative Contribution of Major Activities and Evaporative Pathways to Total Simulated Evaporative Loss at 1/3 atm [Percent]

Activity	Respiration	Diffusion	Sweat	Total
Sleep (8 hr)	4.4	7.4	0.0	11.8
Routine work (25.7 hr)	12.5	15.4	27.9	55.8
Exercise (0.7 hr)	2.8	0.4	29.2	32.4
Totals	**19.7**	**23.2**	**57.1**	**100.0**
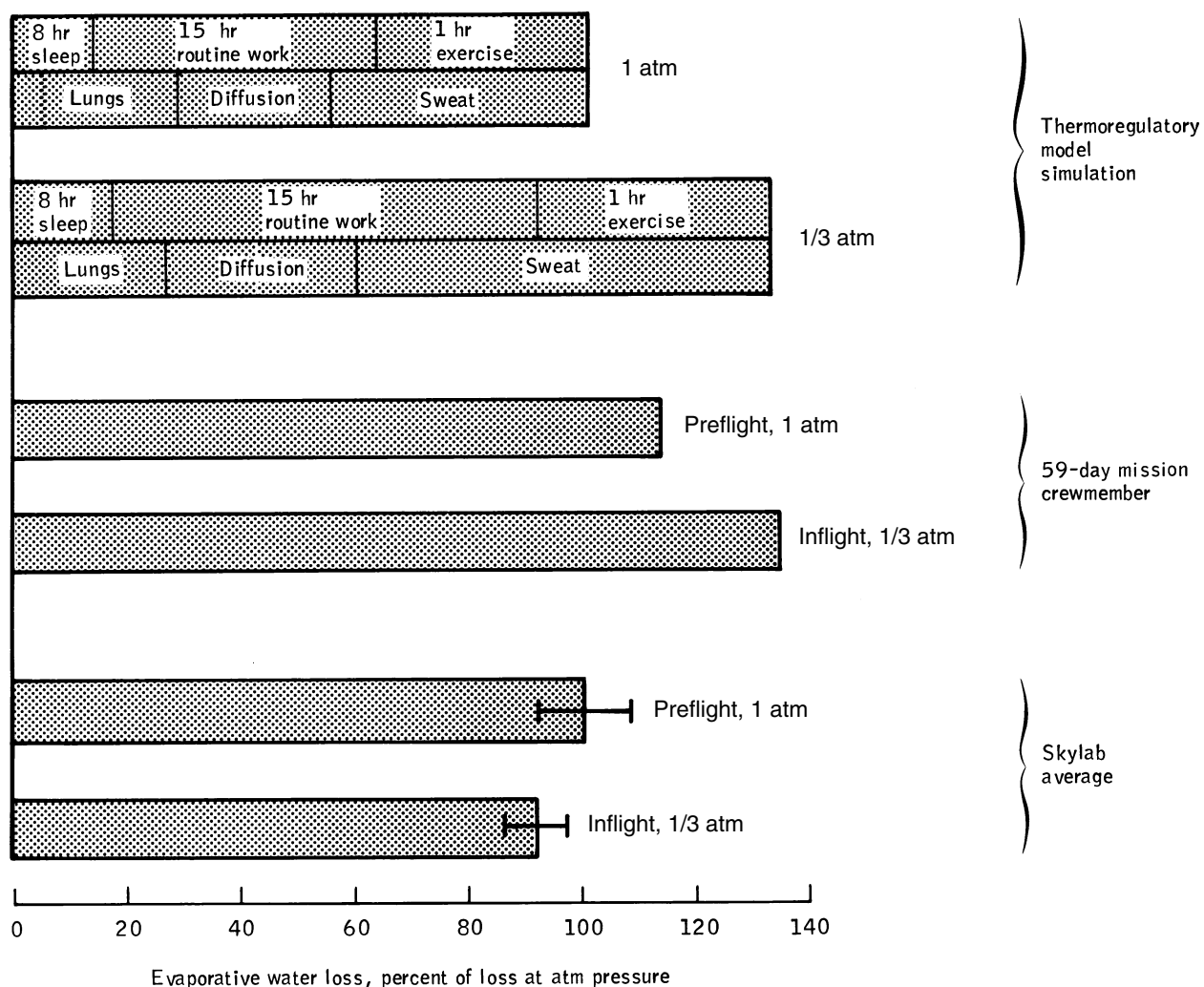
Figure 4-15. Predicted effect of ambient pressure on evaporative water loss compared to the measured Skylab crew results. (Preflight average = 100%).
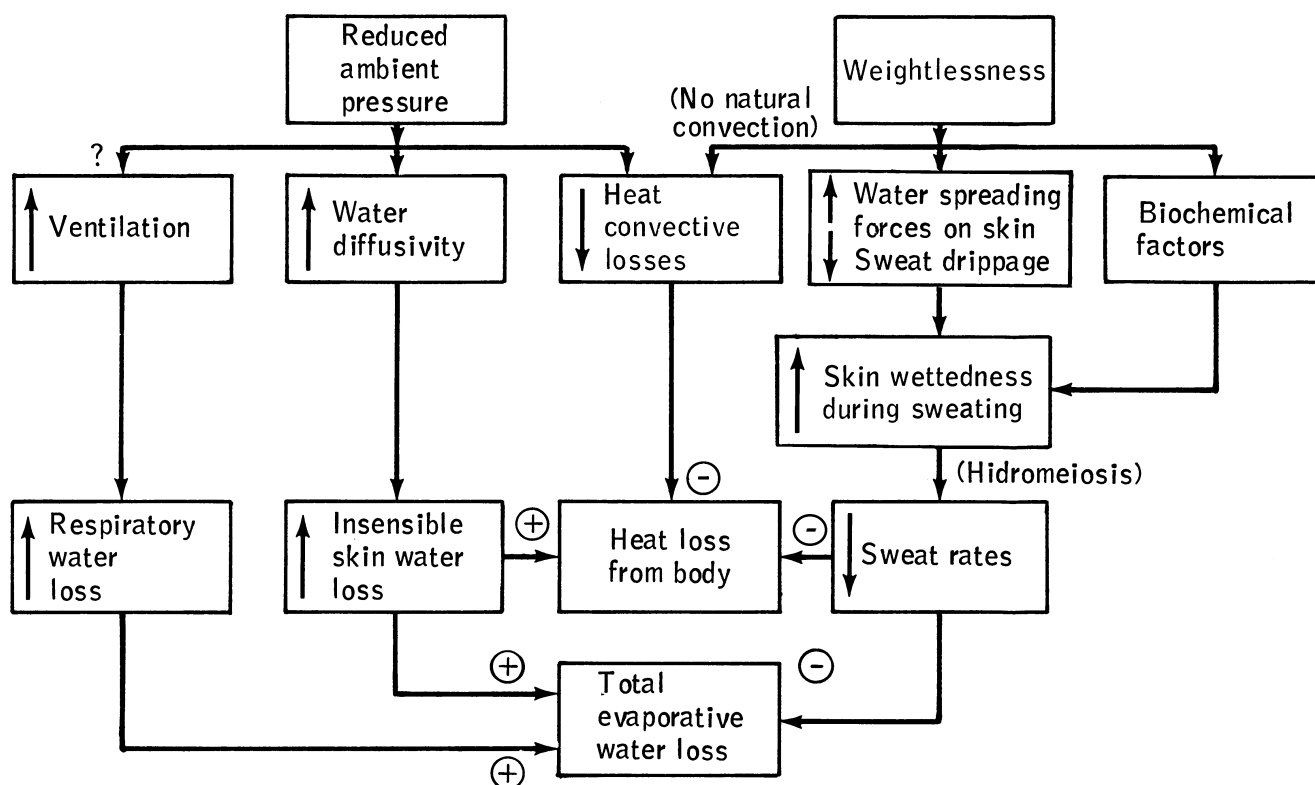
Figure 4-16. Hypothetical effects of Skylab environment on evaporative water and heat loss. Pluses signify increasing loss; minuses denote decreasing loss.

water losses and for incorporating specific hypotheses into the model to improve the fidelity of future simulations.

4.2.2.4 Water Balance Analysis—Summary and Conclusions

4.2.2.4.1 *Evaporative Water Loss.* Daily evaporative water losses during the three Skylab missions were computed using the indirect mass and water balance techniques. A mean inflight EWL (plus or minus standard error) of 859 ± 46 ml/day-m^2 was obtained for nine men who averaged 1 hour of daily exercise compared to a preflight value of 967 ± 68 ml/day-m^2. Although it was expected that EWL would increase in the reduced barometric pressure environment of Skylab, an average decrease of 11% from preflight sea level conditions was observed. Comparison of these results with previous studies in hypobaric chambers revealed that the effective decrease was probably higher than this value. The decrease in EWL cannot be explained by the various uncontrolled environmental and metabolic factors; therefore, weightlessness itself appears to have been a factor in modifying EWL.

Various factors that could explain the effects of the spaceflight environment on EWL are summarized in the hypothesis chart of Fig. 4-16. It is suggested that the two major environmental effects (reduced ambient pressure and zero-g) act to increase respiratory and skin diffusion losses but reduce sweat loss by hidromeiosis, leading to a net reduction in EWL. The absence of gravity may have contributed to the formation of a sheeting effect (a sweat film on the skin surface), which reduced sweat loss sufficiently to account for the discrepancy between the expected and measured EWL. It is more difficult to speculate on the net heat loss from the body because insensible evaporative effects act to increase heat loss, although the convective losses may be decreased. Although sweat rates may be reduced, additional study is required to determine whether evaporation of sweat from a fully wetted skin (and the accompanying heat loss) is decreased.

This conclusion is stated guardedly, because the evidence supporting it is indirect, and because there was a lack of strict controls. A wide range of EWL changes was seen, and the results may be peculiar to the nine astronauts involved in this study. This study does not support the argument that the reduction in body fluids found in Skylab astronauts after their return to Earth is due to an increase in EWL during flight. The importance of EWL in overall water balance and its influence on thermoregulatory processes indicates a need to study insensible water loss and sweating in upcoming space missions, using a specifically designed and rigorously controlled protocol.

4.2.2.4.2 *Water Balance.* This study supports the general belief that a major source of weight loss found in humans returning from spaceflight is a reduction in body water. The water balance analysis has demonstrated that the first 2 days following launch were characterized by negative water balance. This can be attributed primarily to a decreased water intake. This rapid fluid loss amounted to

about 1300 ml for the nine Skylab crewmembers, or about 2% of their body weight.

During periods of unusually high evaporative water loss (such as that which occurred during the first week of the 28-day mission), overall water balance was not significantly affected because of compensation of water intake. Contrary to prior expectation, evaporative water loss was generally lower inflight than before flight. Urine volume was reduced throughout the first week in zero-g, and the expected diuresis was not observed during the period in which body water decreased significantly. The urine response is tentatively attributed to a mild dehydration before launch and a severe reduction in fluid intake following launch.

The decrease in total body water measured directly by isotope dilution on recovery day can be attributed to losses that occurred immediately following launch. During the inflight phase, there appears to be a tendency for partial recovery of the initial water loss in the crewmen who lost the greatest volume of body water. On recovery day, the inflight water loss measured directly in the terrestrial environment (820 ml) amounted to about 33% of the total weight loss. However, the indirect water balance analysis indicated that the true mean water loss at the end of the zero-g phase might have been about 48% of the total weight loss (1100 ml). The difference may reflect partial fluid replenishment between the time of entry and the time of the ground-based measurement. During the postflight period, the gain in water was only slightly less than the original zero-g loss and required 5 or 6 days to reach completion.

To a large extent, the results reported in this study are supported by several other Skylab studies: the stereometric body volume measurement experiment performed before and after flight [12]; the lower body negative pressure study, in which calf girth was measured inflight and limb volume before and after flight [44]; and an experiment designed specifically to study inflight fluid shifts and anthropometric changes in the 84-day mission [45]. These Skylab experiments confirm the magnitude and time course of the water loss and subsequent recovery. Furthermore, they suggest that the zero-g fluid losses were derived from fluid losses in the legs. The shift of fluids from the legs toward the head begins within a few hours after launch, or even just before launch while the crew are strapped in their seats with their legs elevated. However, it is not possible to determine whether total body water begins to decrease that early.

Finally, these results help clarify the frequently poor correlation between weight loss and flight duration and between weight loss and water loss in men returning from space. Weight loss is the sum of fluid and tissue losses. Fluid losses occur early in flight and the volume lost is seemingly dependent on the leg fluid volume, which is shifted headward on exposure to weightlessness. Generally, fluid loss is independent of flight duration. Tissue loss, however, is dependent on caloric intake, exercise levels, and mission duration. On short-duration missions, close correlation of weight loss and fluid loss would be expected but correlation of fluid loss and flight duration would not be expected. Conversely, for longer duration missions in

which tissue loss may continue because of inadequate exercise or low caloric regimes, reasonable correlation between weight loss and flight duration, but not necessarily between weight and fluid losses, might be expected.

4.3 Skylab Sodium and Potassium Balance

The loss of significant quantities of body water during spaceflight strongly suggests that an equivalent loss of electrolytes may have occurred. Sodium and potassium represent the body's major cations in the extracellular fluids and intracellular fluids, respectively. Knowledge of total sodium and potassium losses and their rates of loss can provide important clues regarding the effects of weightlessness on tissue metabolism and on intracellular/extracellular fluid distribution. Sodium loss would be expected to accompany the zero-g loss of plasma, which is purported to result from headward fluid shifts. Potassium losses could arise from extracellular osmolarity changes and tissue atrophy, both expected phenomena in an environment in which postural muscles are not required. The whole-body fluid, mass and electrolyte ground-based measurements performed on each crewman before launch and on the day of recovery indicated an average inflight loss in exchangeable body potassium and extracellular sodium of 240 meq and 90 meq respectively as well as postflight gains of 164 meq of potassium and 100 meq of sodium.

4.3.1 Approach

Daily electrolyte balances and cumulative balances were calculated for both sodium and potassium using the following equations.

$$\text{Daily Electrolyte Balance} =$$
$$= \text{Diet} - \text{Urine} - \text{Fecal} - \text{CF} \qquad (4)$$
$$\text{Cumulative Electrolyte Balance} =$$
$$= \sum_{i=a}^{b} \text{Daily Electrolyte Balance} \qquad (5)$$

where CF is a *correction factor* which represents sweat losses, unaccounted losses, and error terms; a is the first day and b the last day of mission phase i. The correction factor was defined as follows:

$$\text{CF}_i = \overline{\text{Bal}}_i - \left(\frac{\Delta \text{TB}X_i}{N_i} \right) \qquad (6)$$

where $\overline{\text{Bal}}_i$ is the *uncorrected average balance* (that is, diet minus urine minus fecal values) for mission phase i (i = preflight, inflight, or postflight), $\Delta \text{TB}X_i$ represents the directly measured total body loss of that electrolyte in phase i, and N_i represents the number of days in phase i. Changes in total body potassium values were obtained from direct measurements of body ^{40}K. However, the changes in total body sodium were based on a calculation using directly measured extracellular fluid and plasma sodium concentration values. (For further details of the methods of com-

Table 4-11. Individual Electrolyte Balances for the Skylab Crewmen

Mission Duration, Days	Subject	Electrolyte balance, meq/day		
		Preflight	Inflight	Postflight
Sodium (uncorrected)				
28	1	46.7	35.5	54.8
	2	65.3	36.9	60.2
	3	44.1	28.9	42.2
59	4	48.1	38.1	56.6
	5	62.0	39.1	65.1
	6	70.0	60.6	77.2
84	7	57.3	51.4	69.4
	8	88.1	68.0	75.0
	9	82.3	59.4	54.0
Mean		**62.7**	**46.4**	**61.6**
SE		**±5.2**	**±4.6**	**±3.7**
Potassium (uncorrected)				
28	1	21.7	5.5	17.8
	2	24.9	5.0	22.3
	3	17.3	5.1	20.0
59	4	17.9	5.0	21.8
	5	14.0	6.4	24.9
	6	23.2	12.8	32.8
84	7	12.3	1.1	2.3
	8	13.6	6.9	15.5
	9	17.5	7.8	7.4
Mean		**18.0**	**6.2**	**18.3**
SE		**±1.5**	**±1.0**	**±3.0**

putation and the associated assumptions used in this section, see Appendix F(3)). Balances were computed for varying time periods corresponding to the first 2 weeks, the first month, the second month, and the third month in flight. These periods represented the period of the most significant changes with the first two periods containing nine crewmen and the third and fourth periods containing six crewmen and three crewmen, respectively. Since urine data from the first day of the 28-day mission were missing, urine sodium averages were computed using the data only from the 59- and 84-day missions.

4.3.2 Results and Discussion

The uncorrected sodium and potassium balances for individual Skylab crewmen are given in Table 4-11. The results of these uncorrected balances show a decrease of 16.3 meq for sodium from the preflight phase to the inflight phase and a decrease of 11.8 meq for potassium. Preflight and postflight balances were nearly identical for each electrolyte.

The average daily values for each term in the sodium balance equation corrected for skin losses are shown in Fig. 4-17 for the crewmen of the 59- and 84-day missions ($n = 6$). Dietary sodium is shown to decrease for 7 days following launch, but for the remainder of the first month

inflight, it is slightly increased over the preflight average (234 meq before flight and 244 meq for mission days 8 to 28). The 59-day mission is largely responsible for the decreased intake for the first 7 days, since the crewmen on the 84-day mission had regained preflight sodium intake levels on the third inflight day. A probable explanation for this decreased intake was the space sickness that occurred during the first week of the missions, with the 59-day crew suffering longer than the other crews.

Average urine sodium values also declined for the first 7 days in flight, with the exception of the value for the first inflight day, which actually exceeded preflight values. This elevation occurred despite the decreased diet and, therefore, can be considered a saluresis, probably accompanying the loss of extracellular fluid. After the initial decrease, average inflight urine values were elevated (169 meq before flight vs. 192 meq for mission days 8 to 28). This long-term increase in urine Na^+ can be partly explained by the increased dietary intake for the same period.

Fecal sodium appears slightly decreased during the first 28 days in flight. However, the magnitude of these changes (3.01 meq before flight and 1.44 meq for mission days 1 to 28) has little effect on the overall balance. Since fecal values did not change significantly, urinary and fe-
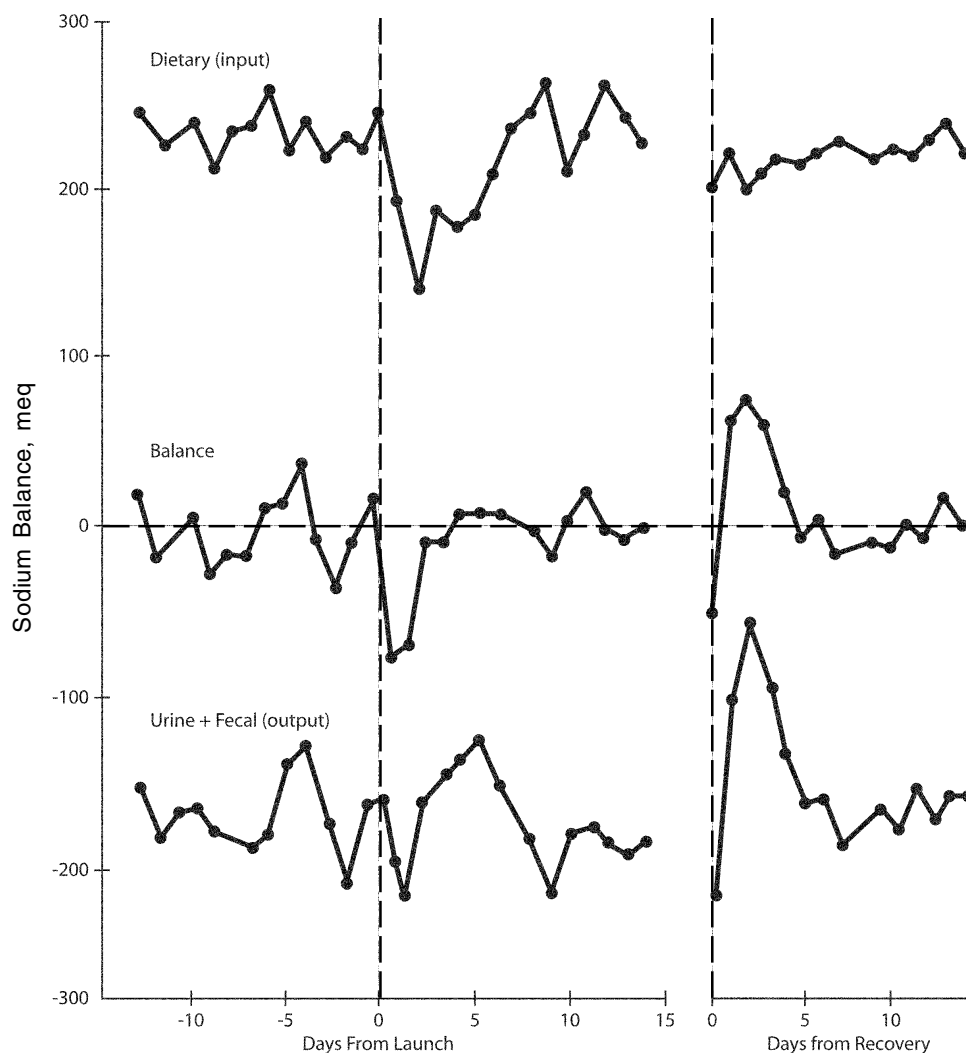
Figure 4-17. Corrected average sodium balance around launch and recovery for the 59-day and 84-day mission crews ($n = 6$). This is a traditional metabolic balance graph in which inputs are shown as increasing in the upward direction, while outputs are shown as increasing in a downward direction. The algebraic addition of the input and output is depicted as the "balance".

cal outputs are shown combined. The combined fecal and urine sodium values represent the directly measured outputs of sodium from the body.

Also shown in Fig. 4-17 is the corrected sodium balance for the six crewmen of the 59- and 84-day missions. The most prominent event in the balance occurs immediately after launch and consists of a large negative balance for the first 2 days in flight.

The corrected potassium balance and its components for all nine Skylab crewmen are shown in Fig. 4-18. Potassium intake was decreased for the early inflight phase, because of the anorexia of space sickness. The intake was at a minimum on the second inflight day and remained reduced for 10 days in flight. As in the case of sodium, the crew of the 59-day mission had the greatest influence on the mean dietary potassium changes during this period. During the remainder of the first month in flight, the po-

tassium intake remained relatively constant at slightly reduced levels compared to preflight values (102.9 meq before flight vs. 100.5 meq measured from mission day 11 to 28). Combined urine and fecal potassium excretion was elevated inflight from a preflight mean of 79.8 meq to 92.34 meq for mission days 1 to 28. Average fecal potassium was unchanged; therefore, any changes observed can be attributed to urine changes. The average potassium balance is negative for the first 10 inflight days. The balance is at a minimum the second inflight day and does not appear to reach an apparent inflight steady state until day 10, when the intake also appears to reach steady state.

Values of the terms in the sodium and potassium balances around recovery are also shown in Figs. 4-17 and 4-18, respectively. The composite graph includes the recovery of three men each from the 28-, 59-, and 84-day missions. Any conclusions from these data should account
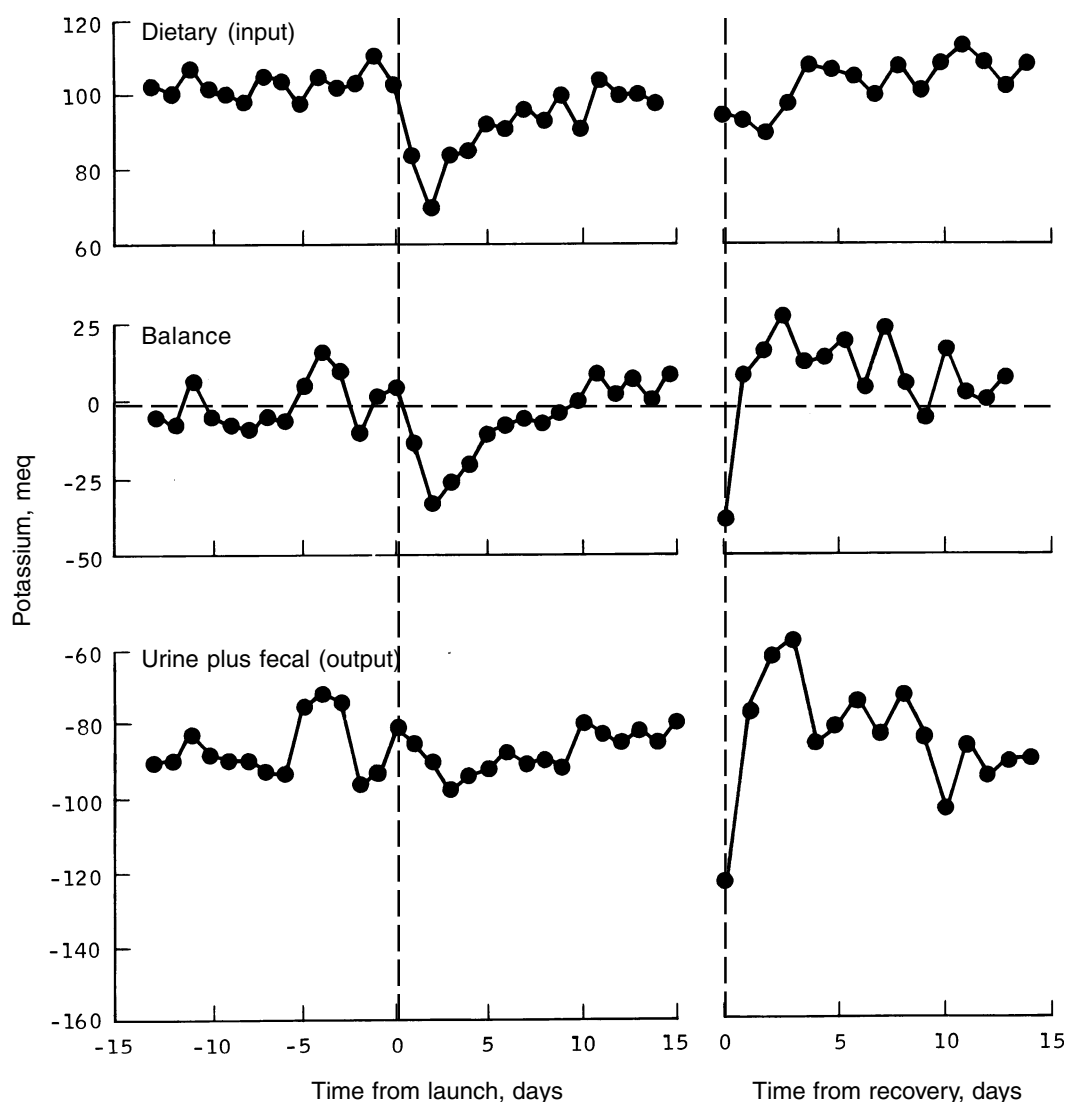
Figure 4-18. Corrected average potassium balance around launch and recovery for all Skylab crews ($n = 9$). See caption for Fig. 4-17.

for the fact that the average recovery values include data from subjects that resided in space for different periods of time. Recovery of both sodium and potassium during the postflight phase will be discussed next.

The mean diet sodium for all nine Skylab crewmen during recovery (Fig. 4-17) was 217.5 meq, which was less than preflight or inflight levels. Urinary sodium decreased markedly the first few days after flight. This decrease coincides with the retention of sodium as shown in the balance data for the same time frame. The sodium balance appeared to return to inflight levels for the remainder of the postflight period.

Postflight diet potassium (102.6 meq) appeared to change little from either preflight or inflight levels (Fig. 4-18). The potassium balance indicates retention of this electrolyte for the first postflight week, apparently as a result of diminished urinary excretion. The increased ex-

cretion on recovery day can be seen in all three missions, but the factors present during and immediately before re-entry prevent a clear explanation of this phenomenon.

When the corrected sodium and potassium balances are integrated (using Eq. (5)) from the reference day (day of launch), they illustrate the time course of change in the "total body" pools. The changes in total body sodium for the 59- and 84-day mission crews around launch and recovery are shown in Fig. 4-19. A rapid decrease in total body sodium of approximately 200 meq that occurred within 4 days of launch and remained essentially constant for the first month inflight, is shown. The greatest decreases occurred on the first and second inflight days.

The total body sodium changes around recovery appear to be opposite and of about the same magnitude as the changes immediately following launch. However, two other factors shown here should be considered. First, the day
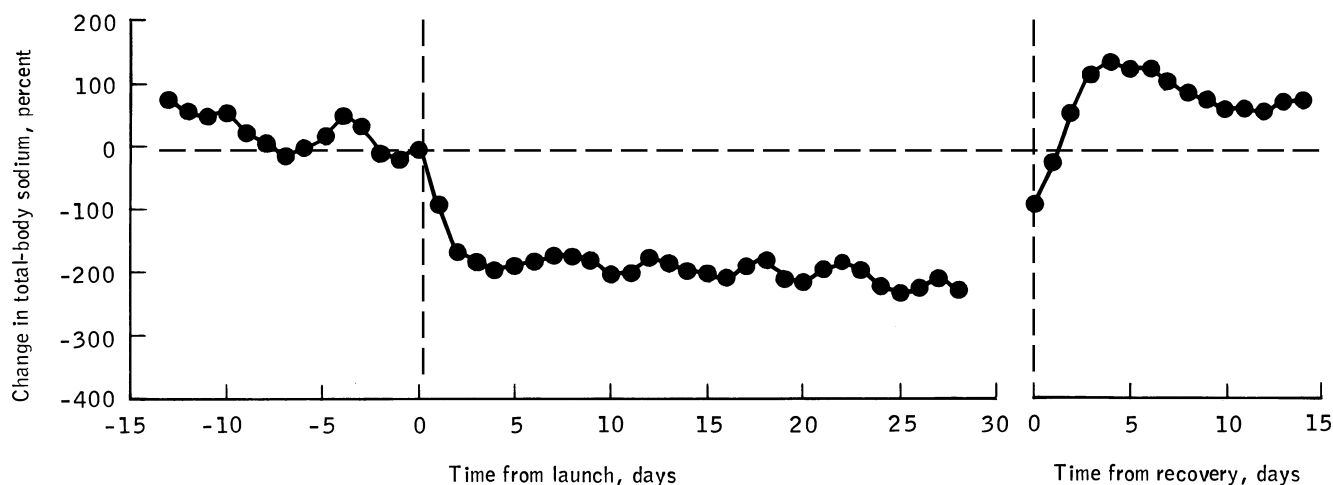
Figure 4-19. Average change in total body sodium from day of launch for the 59-day and 84-day mission crews ($n = 6$). This chart was computed from the cumulative sum of corrected daily sodium balance.

of recovery had a relatively large influence on the recovery changes, since 75 meq appeared to have been lost on that day. This influence could force the reference point on the day of recovery to be artificially low. Second, there seemed to be an overshoot in retaining total body sodium that was corrected within 10 days of recovery. This observation can be correlated to overshoots in extracellular fluid volumes and plasma volumes observed following bedrest [46,47]. These two factors, entry and overshoot, could make the net change in total body sodium by the end of the missions only about 100 meq. This change would be less than the initial change following launch and would suggest some inflight replacement of sodium or a reduction in the capacity of the extracellular fluid compartment.

Changes in total body potassium for 28 days in flight are shown in Fig. 4-20 for all nine Skylab crewmen. Acute potassium losses of about 100 to 150 meq appear to occur during the first 10 days of spaceflight. A further decline in total body potassium to about a 200 meq deficit appeared to occur after the second week inflight. Although not shown, the potassium losses level off after the first inflight month. Total losses measured were 240 meq for all nine subjects.

The change in total body potassium at recovery showed a much slower replacement (125 meq in 14 days) than that of sodium. The changes after recovery appeared to be much more linear with time, at least for the first 14 days, than the changes which occurred following launch.

4.3.3 Summary and Conclusions

A balance analysis was performed on the sodium and potassium data measured for the nine Skylab astronauts. The known terms of the balance equations were dietary intake and fecal and urinary losses. The remaining term, a correction factor, includes changes due to sweat losses,

unaccounted losses and measurement error. The results of an uncorrected balance analysis performed neglecting this last term showed the Skylab crewmen to be in positive sodium balance of slightly greater than 60 meq/day before and after flight and about 46 meq/day during inflight. Potassium analyses reflected a positive balance of about 18 meq/day before and after flight and about 6 meq/day inflight. Since a net loss was observed for both electrolytes by independent measurements, these balances demonstrate that the combined sweat, unaccounted, and error term, if neglected, would result in significant errors in computing the cumulative balances. This result suggests that notable changes had occurred in the correction factor term between mission phases.

The correction factors used to account for these unmeasured losses were based on matching the measured changes in the total body pools of sodium and potassium with the integrated balances. For sodium, this correction factor was based on plasma sodium concentrations and extracellular fluid volumes. The resulting changes in exchangable body sodium and total body potassium were computed with respect to the day of launch. An average of the 59- and 84-day mission crews showed a decrease in sodium of approximately 200 meq that occurred approximately exponentially with a time constant of about 1-1/4 days. The exchangable body pool appeared to remain constant for the remainder of the first month in flight. However, the change in exchangable body sodium as estimated from postflight measurements indicated a total inflight loss of only 90 meq. This result suggests that there was a recovery of approximately 100 meq of sodium during the remaining two inflight months.

Total body potassium decreased between 100 and 150 meq immediately following launch. The time course also appears to be approximately exponential with a time con-
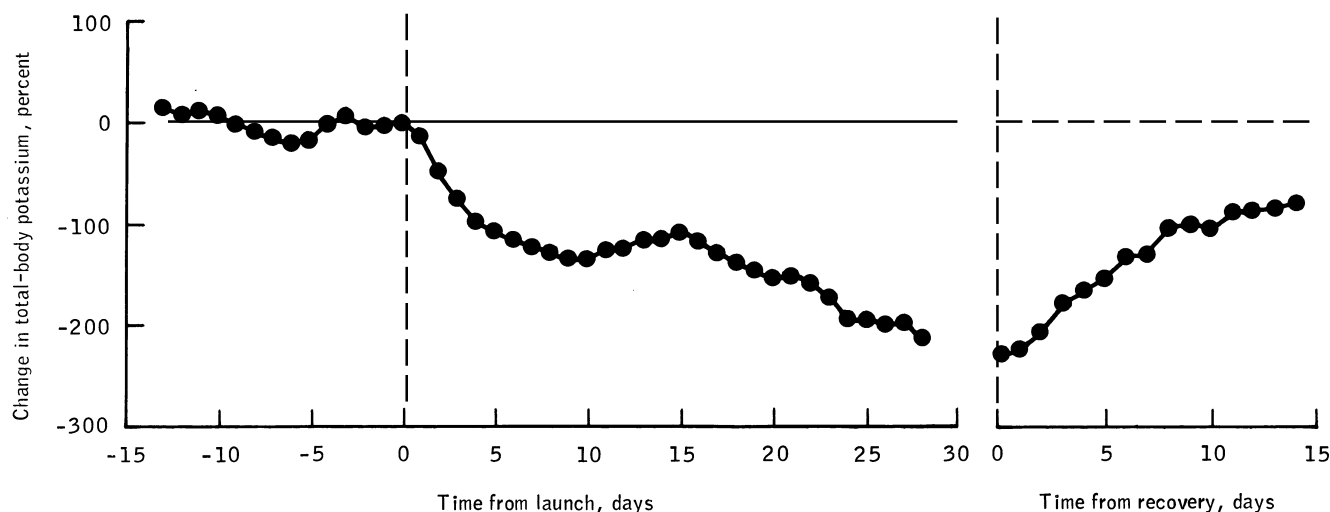
Figure 4-20. Average change in total body potassium from day of launch for all Skylab crews ($n = 9$). This chart was computed from the cumulative sum of corrected daily potassium balance.

stant of about 2 days. The initial decrease appeared to be complete by the tenth inflight day, but a further decline of 100 meq, which was more a linear function with respect to time, was seen by the end of the first inflight month. The average measured change in total exchangeable potassium of only 240 meq indicated that this trend could not continue at the observed rate for the remainder of the mission.

One revealing aspect of the analyses was that the diet had a strong influence on the time course of change in the balances for sodium and potassium early in the flight period. This result was surprising because the diet was designed to be basically constant for the duration of the missions. This change in intake levels of sodium and potassium was most likely the result of the anorexia associated with acute space sickness, since food and water intake was reduced by similar amounts.

The balances computed after recovery were a composite of recoveries of all three crews from missions of differing duration. During recovery, the balances indicated that the diet was relatively constant and, therefore, changes in urine and fecal amounts were more clearly responsible for the observed changes in the balances. The sodium balance for all nine Skylab crewmen was more positive after flight and appeared to level off after about 5 days of recovery with the most striking changes occurring within the first 2 days after flight. Potassium balance, however, did not appear to approach a new steady state even after 2 weeks following flight.

4.4 Integration of Fluid and Electrolyte Balance

The metabolic balance studies of the previous sections, indicated that the most dramatic disturbances to the body stores of water, sodium and potassium occurred during the first week of flight and the first few days of recovery. After these periods, a *relative* state of equilibrium in the body existed. During this inflight quasi-steady state period, which occupied most of the mission, the measured urine and fecal amounts were somewhat higher in general than during the preflight period. The purpose of this section is to develop a simplistic model that can help explain the increased urine and fecal water, sodium and potassium based on what is known or estimated about dietary intake and evaporative or sweat losses. This model is a gross representation of the metabolic inputs and outputs and assumes that after the first few days of flight, there is a relative state of metabolic equilibrium. The following analysis presents a different way of grouping the data discussed previously and examining them in terms of acute and chronic stages of flight. The simplified grouping of data developed here was also used as input forcing functions to perform simulations of the Skylab mission using the Guyton model (see Chapter 9.4).

4.4.1 Skin Losses

Summary estimates of total body and daily skin losses for all crewmen combined can be found in Table 4-12 for water, sodium, and potassium for each phase of the mission. These estimates as well as those presented in Table 4-13 discussed next, were based on the analysis presented earlier in this Chapter and in Appendix F. Reasonable values for skin losses were obtained for preflight control. Although sweating rates were not available for the Skylab crewmen, it was reasonable to assume that of the nearly 1700 ml/day of total preflight evaporative water loss, approximately 850 ml represents obligatory insensible water loss, and the remaining 850 ml was attributable to sweating. These figures agree with values obtained for normally active subjects [40]. At these sweat rates, the electrolyte skin

Table 4-12. Estimates of Total Body Balances and Skin Losses in Skylab Crews [*n* = 9]*

Quantity	Preflight	Inflight	Postflight
Measured total body change*			
Water, ml	170	−880	1120
Sodium, meq	0	−93	103
Potassium, meq	0	−236	128
Daily skin loss			
Water, ml/day	1675	1550	1641
Sodium, meq/day	63	48	54
Potassium, meq/day	18	10	7

* Change over entire mission phase

Table 4-13. Water and Electrolyte Balances During Prolonged Composite Spaceflight[a] [*n* = 9]

Quantity	Preflight (A)	Inflight		Difference[b]	
		First 5 days (B)	Remaining 52 days (C)	Change	Percent change
Water, ml/day					
Intake[c]	3320	2785	3200	−120	−4
Loss:					
Urine and fecal	1625	1290	1700	75	5
Evaporative	1675	1780	1495	−180	−11
Balance:					
Daily	[d]20	−285	5		
Cumulative, ml	[d]280	−1425	260		
Sodium, meq/day					
Diet	223	177	228	5	2
Loss:					
Urine and fecal	160	149	181	21	13
Sweat	63	48	48	−15	−24
Balance:					
Daily	[e]0	−20	−1		
Cumulative, meq	[e]0	−100	−52		
Potassium, meq/day					
Diet	103	83	101	−2	−2
Loss:					
Urine and fecal	85	93	93	8	9
Sweat	18	10	10	−8	−44
Balance:					
Daily	[d]0	−20	−2		
Cumulative, meq	[d]0	−100	−104		

a Average flight duration = 57 days
b Column (C) minus column (A)
c Includes liquid, food water, and metabolic water
d Based on direct total body measurements
e Assumed zero

losses are well within previously recorded ranges [48], although they are somewhat higher than mean values. It should be noted, however, that dietary intake of these electrolytes was higher than normal.

It can be observed from Table 4-12 that the estimates for inflight skin losses are less, in each case, than the corresponding preflight value. The water balance analysis of Chapter 4.2 supports the conclusion that, contrary to prior expectation, evaporative water losses were not greater in flight. In that analysis, it was postulated that overall evaporative water loss (sensible plus insensible loss) may have been reduced about 10% and the degree of sensible water loss during exercise could have decreased even more significantly (at least 30%). If it is assumed that electrolyte losses from the skin occur only during periods of metabolic sweating and if the concentrations of sodium and potassium in sweat are relatively constant for given levels of exercise in either one-g or zero-g, then it may be expected that the loss of body electrolytes attributed to sweating would decrease by amounts comparable to sensible water suppression; that is, about 30%. The results in Table 4-13 support this contention and indicate a decrease in inflight skin losses of 24 and 44% for sodium and potassium, respectively. A modeling technique for estimating inflight sweat losses was developed (see Appendix F.3.3) and was particularly useful in estimating sodium sweat losses for a spaceflight simulation (see Figs. 5.32 and 5.33).

4.4.2 Water and Electrolyte Balance

Most of the major losses in body fluids and electrolytes appeared to have occurred during the first several days in flight. Analysis of this early phase showed that these early decrements in fluids and electrolytes were not associated with increased excretion but rather with deficit intake. An additional analysis was performed for the much longer period following this initial disturbance to determine whether the body was in relative balance at these new homeostatic levels. The results of this analysis are shown in Table 4-13.

For convenience, a composite Skylab mission with an average duration of 57 days was assumed, and all nine crewmen were grouped together. In addition, the data from the first 5 days of flight (the acute stage) were considered separately from the remaining days. The values for urine and fecal excretion have been combined for convenient use in the Guyton model. However, it is known that fecal excretion represents only a small fraction of total excretion (i.e., 4% for water, 3% for sodium, and 12% for potassium).

Intake and excreta data were obtained by direct daily measurement of each crewmember for all flight phases. Preflight evaporative and sweat losses were obtained by subtracting the balance values from "Intake – Urine & Fecal". Body potassium was in balance during the preflight phase and water balance was slightly positive. In the case of sodium, there were insufficient preflight data to determine a direct balance and, for convenience, a zero balance was assumed.

Inflight electrolyte sweat losses were obtained as discussed in the previous Chapter 4.3 and Appendix F.3. It was assumed, because of limited information, that daily sweat losses of electrolytes were the same for the acute and chronic phases of flight. However, there were sufficient inflight data to calculate evaporative water loss for the two time periods. It was found that mean EWL for the first 5 days was about 6% higher than preflight EWL, whereas the EWL for the remainder of the flight was depressed by 11%. If electrolyte sweat losses followed a similar pattern, the values for sodium and potassium sweat losses would be somewhat higher than shown for the first 5 inflight days, whereas values for the remainder of the flight would be smaller than shown. This pattern would result in slightly more positive sodium and potassium balances for the longer inflight period. Simulation results lend support to this concept, especially for sodium.

Although the sodium balance of –1 meq/day (Table 4-13, column C) was close to a zero balance, it still represented a significant amount of sodium lost over 52 days (i.e., 52 meq). Only a negligible portion of sodium would be expected to be associated with observed losses of intracellular muscle and bone during the latter portion of the flights. Using the metabolic balance equations given earlier, small errors in estimated daily sodium sweat losses could result in large errors in cumulative sodium loss. These uncertainties are present because there was no direct measure of body sodium loss. On the other hand, the components of potassium metabolic balance shown in Table 4-13 were in more consistent agreement with the inflight losses of potassium as measured by tracer dilution methods. Taken as a whole, the results of this analysis suggested that for the portion of flight beyond the first few days, the daily water, sodium, and potassium balance was much closer to zero when compared to the acute phase.

4.4.3 Estimation of Excretion from Metabolic Balance Data

The analyses shown in Tables 4-12 and 4-13 revealed that the fluid and electrolyte losses from the body were not as severe as one would expect from an analysis of the excretion data alone. For example, renal excretion of water and electrolytes during the longer phase of the flight are slightly higher than preflight. If other elements of the balance equation were the same preflight and inflight, even these small renal increments would cause a large cumulative body loss over 57 days of flight. Therefore, the effect of renal excretion on body loss must only be evaluated in perspective with all other avenues of loss or gain from the body. For example, at steady state with fixed intake, the water excretion (renal and fecal excretion combined) can be derived as

$$\text{Water excretion} = \text{water intake} - \text{evaporative water loss} \quad (7)$$

Therefore, if evaporative water loss decreases, the body must excrete water to maintain a zero water balance. Under steady-state conditions, a decrease in urine volume would be predicted by the 120 ml/day decrease in water intake. (Refer to Table 4-13, next to last column, and to

Table 4-14. Combined Renal and Fecal Excretion of Water and Electrolytes During Skylab Missions

Quantity	Preflight (A)	Inflight		Difference[a]	
		First 5 days (B)	Remaining 52 days (C)	Change (C) - (A)	Percent change
Urine vol, ml/day	1625	1290	1700	75	5
Na$^+$, meq/day	160	149	181	21	13
[Na$^+$], meq/liter[b]	98.5	115.5	106.5	8	8
K$^+$, meq/day	85	93	93	8	9
[K$^+$], meq/liter[b]	52.3	72.1	54.7	2.4	5

a Column (C) minus column (A)

b Derived from other measured values shown

Eq. (7).) However, the estimated 180 ml/day decrease in evaporative water loss more than offsets the measured 120 ml/day decrease in water intake and results in an increased urine volume. The net result is a slightly positive balance rather than a large negative balance.

A similar argument can be applied to the sodium and potassium balances. The measured increase in urine and fecal sodium (21 meq/day) can be attributed almost entirely to a 25% decrease in sweat loss (1.6 meq/day) and a 2% increase in dietary sodium (5 meq/day). In the case of potassium, it is possible to account for half of the 8 meq/day increase in excretion because of changes in diet (–2 meq/day) and sweat losses (–6 meq/day). Despite a 44% decrease in estimated potassium sweat loss, the potassium balance still remains negative, representing continued loss from the tissues.

The postulated effects of decreased sweat losses on excretion are illustrated in Fig. 4-21. Double arrows indicate that the decrements in daily electrolyte sweat losses were greater than those of evaporative water losses. Therefore, excretion of electrolytes would be expected to be relatively greater than that of water. Consequently, the concentrations of potassium and sodium in excreted fluid would be predicted to increase in accordance with independent Skylab measurements. These renal effects are summarized in Table 4-14. It was possible to demonstrate these effects of sweat losses on renal excretion in the Guyton model (see Chapter 9.4).

The preceding analysis suggests the manner in which gross metabolic factors can account quantitatively for the increased excretion of fluids and electrolytes. The body appears to increase urinary and fecal excretion to compensate for decrements in sweat loss in a manner that maintains an overall body balance that is appropriate to prolonged spaceflight conditions. It cannot be overemphasized, however, that this analysis was based on indirect estimates of evaporative and sweat losses of fluids and electrolytes. Although the results were internally consistent and appeared to provide reasonable explanations for changes in renal excretion and maintenance of body balance, they have not been verified by direct measurement.

4.5 Quantitation of Tissue Loss Resulting from Prolonged Spaceflight

Prior to Skylab, the losses in body weight found after astronauts returned to Earth had been tentatively ascribed to a) alterations in water balance resulting from headward shifts of fluid; b) loss of musculoskeletal tissue as a result of gravity unloading deconditioning (i.e., postural disuse); and c) alterations in fat due to the imbalance between caloric intake and energy expenditure [4,10,49,50]. The Skylab experiments allowed confirmation of these early inferences, and much of the data describing mineral, tissue, and fluid losses in the Skylab astronauts have been reported in one form or another [2,3,4,9,32,51,52]. But there has been no systematic attempt to integrate all of the information directly related to the changes in body tissue (i.e., lean body mass and fat) that occur during spaceflight. The study summarized in this section (and in the original reports [53,54]) addresses this void. Direct measurements that were critical in this effort include preflight and postflight measurements of total body water, total body potassium, and body volume. In addition, daily inflight metabolic balance (potassium and nitrogen) and body mass measurements provided, for the first time, a description of the time course of change of the major components of weight loss. A number of different methods are available for equating changes in these quantities to changes in lean body mass. The purpose of the present analysis was to compare these various methods and to arrive at the best estimate of body composition change for the Skylab astronaut population.

4.5.1 Approach

A detailed discussion of the general approach used in this analysis and of the various methods employed can be found in Appendix F(4) as well as the original reports [53,54].

4.5.2 Results

A summary of the preflight and postflight values for the body composition parameters used to determine *lean body mass* (LBM) by the various methods is presented in
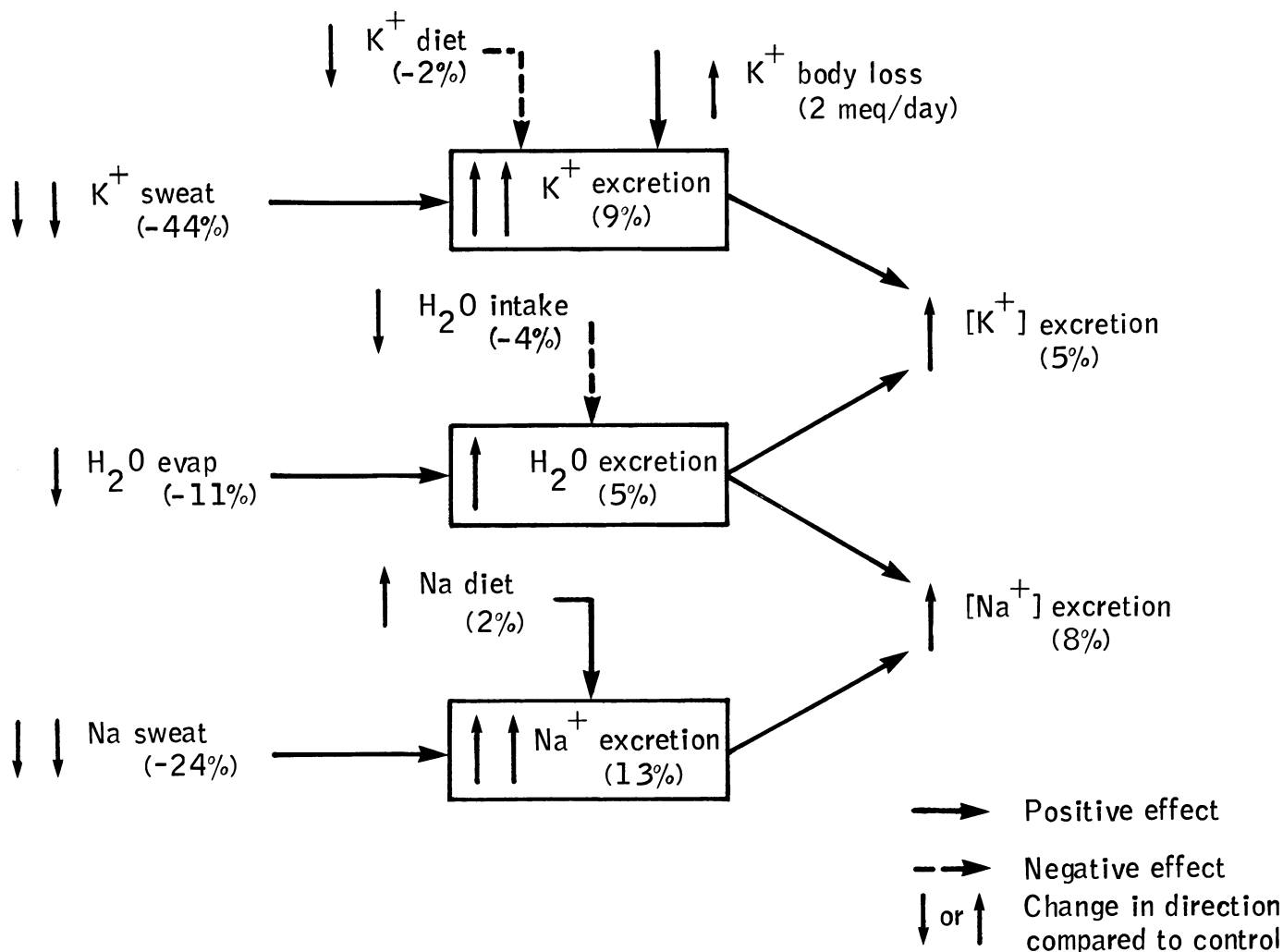
Figure 4-21. The effect of decreasing sweat and evaporative losses on renal excretion during the steady-state portion of spaceflight. See text for meaning of double arrow. [Na+] and [K+] refer to the concentration of sodium and potassium, respectively, in the urine.

Table 4-15. These data, shown as mean values for all nine Skylab subjects, were used to compute body composition changes resulting from spaceflight according to relationships shown in Table F-18, Appendix F(4). (Individual crew values corresponding to the data in Table 4-15 appear in Appendix F(4), Table F-19). A simple two-compartment model was assumed in which body mass was divided into lean and fat tissue. Body protein was assumed to be 19.4% of the lean body mass. Daily nitrogen and potassium metabolic balances were used to estimate the time course of the inflight changes. The values for nitrogen and potassium balances listed under the "postflight" column of Table 4-15, in fact, represents the average daily *inflight* balance.

Table 4-16 contains the preflight values and inflight changes of LBM and fat obtained using the various methods. Also shown for each method is the percent of body weight loss that is due to LBM or fat. The results are shown

for all crewmen pooled into a single group. Values have been normalized to an inflight weight loss of 2.63 ± 1.33 kgs (mean ± SD) measured from the morning of launch to the first shipboard weight measurement. Supportive calculations showing the results for each subject and for each method are given in Table 4-17 for preflight values and Table F-20 (Appendix F.4) for inflight changes in LBM.

The method for estimating lean body mass changes, based on TBK, gave results quite out of range from the other methods studied. These are shown on the line TBK (uncorrected) in Table 4-16 where inflight losses of lean body mass are computed as 3.63 kg, more than twice as large as with any of the other methods. This discrepancy was considered to be due to one of three possibilities: a) the formula used (LBM = TBK/65) does not apply to the astronaut population, b) the measured values of TBK are erroneous, or c) potassium loss from cell was not accompanied by other cellular components such as nitrogen and

Table 4-15. Body Composition Parameters Measured Before and After Skylab Missions [Mean ± SD; *n* = 9]

Parameter	Preflight	Postflight	Change
Body weight, kg	71.7 ± 8.7	68.9 ± 8.1	–2.8 ± 1.4[†]
Body volume, liters	67.6 ± 8.4	64.6 ± 7.6	–3.0 ± 1.7[†]
Body water, liters	45.6 ± 5.0	44.8 ± 4.4	–0.8 ± 0.8[†]
Body potassium, meq	3625 ± 480	3390 ± 470	–235 ± 125
Nitrogen balance, g/day	3.10 ± 2.50	–1.05 ± 0.62*	–4.15 ± 0.85[†]
Potassium balance, meq/day	18.05 ± 4	6.20 ± 3*	–11.86 ± 4

[†] p < 0.005
* Measured from inflight balance

Table 4-16. Preflight Body Composition and Inflight Changes for Skylab Crews Using Various Methods[a]
[Mean ± SD; *n* = 9]

Method	Preflight values		Inflight changes			
			ΔLBM		ΔFat	
	LBM, kg	Fat, percent body wt.	kg	%ΔBWgt	kg	%ΔBWgt
Total body water (TBW)	62.3 ± 6.8	12.8 ± 3.1	–1.18 ± 1.09[b]	45.0	–1.45 ± 1.83[c]	55.0
Total body potassium (TBK)						
a) Uncorrected	55.8 ± 7.4	22.3 ± 3.3	–3.63 ± 1.93	(d)	+0.94 ± 2.56	(d)
b) Corrected	55.8 ± 7.4	22.3 ± 3.3	–1.52 ± 1.92[c]	57.8	–1.11 ± 2.71	42.2
TBW and TBK						
a) Uncorrected	60.7 ± 6.9	15.3 ± 2.8	–1.53 ± 0.96[c]	59.3	–1.10 ± 1.63	43.0
b) Corrected	60.7 ± 6.9	15.3 ± 2.8	–1.12 ± 0.83[b]	42.6	–1.51 ± 1.59[c]	57.4
Body density	60.3 ± 9.3	16.0 ± 8.6	–1.51 ± 3.50	57.4	–1.12 ± 3.26	42.6
"Combined" method	61.3 ± 7.0	14.9 ± 4.5	–1.59 ± 1.09[b]	60.5	–1.04 ± 1.21[c]	39.5
Nitrogen balance	(d)	(d)	–1.63 ± 0.87[b]	62.0	–1.00 ± 1.82	38.0

a Inflight losses normalized to an inflight body weight loss of 2.63 ± 1.33 kg
b *p* < 0.01
c *p* < 0.05
d Cannot be determined

water. There are good arguments that favor the last of these possibilities [53,54]. In fact, a corrected LBM loss was calculated on the assumption that a significant amount of potassium leaves the cellular compartment independently of other cell constituents due to osmotic considerations. This correction yielded more reasonable inflight results for LBM and fat changes, but did not affect preflight values (see Table 4-16, TBK (corrected)). The "TBW and TBK" method shows a similar treatment in Table 4-16. A full discussion of these calculations and the assumptions on which they are based are provided in Appendix F(4)) (see "Errors in the TBK method"). In the remainder of this section only the *corrected* values for the TBK method will be considered.

As shown in Table 4-16 the inflight LBM losses calculated by the various methods ranged from 1.12 to 1.63 kg representing from 43 to 62% of the total body weight loss. Protein (solids) and fat losses were estimated to range from 0.22 to 0.36 kg and from 1.00 to 1.51 kg, respectively.

The confidence in the capability of these various methods to estimate *inflight changes* in LBM is enhanced by demonstrating their capability to predict *absolute values* of preflight LBM. With the exception of the "uncorrected" total body potassium method, there was close agreement between the estimates of preflight LBM obtained by the various methods employed (Table 4-16). The individual subject values of preflight LBM for each method are shown in Table 4-17(a) and as can be seen in Table 4-17(b) there is a significant degree of correlation between the methods. The nitrogen balance method was not suitable for determining absolute values of LBM.

Table 4-17. Preflight Lean Body Mass Using Different Methods

(a) Mass determined from all methods*

Subject	Method				
	TBW	TBK	TBW and TBK	Body density	Combined
1	56.8	50.3	55.2	52.2	55.3
2	66.7	60.3	65.1	54.8	63.7
3	71.3	59.5	68.2	66.7	69.1
4	58.1	51.4	56.4	62.7	58.0
5	53.4	47.1	51.8	59.8	53.8
6	73.2	71.5	72.9	81.7	75.4
7	57.2	49.7	55.3	57.3	56.3
8	62.0	56.5	60.7	52.7	59.7
9	62.4	55.6	60.7	55.3	60.3
Mean	**62.3**	**55.8**	**60.7**	**60.4**	**61.3**
±SD	**6.8**	**7.5**	**6.91**	**9.3**	**7.1**

* In kg

(b) Correlation coefficients for method-to-method comparison

Method	TBW	TBK	TBW plus TBK	Body density	Combined
TBW	—	—	—	—	—
TBK	0.94 [a]	—	—	—	—
TBW plus TBK	1.00 [a]	0.97 [a]	—	—	—
Body density	0.64	0.70 [b]	0.66 [b]	—	—
Combined	0.97 [a]	0.96 [a]	0.98 [a]	0.79 [a]	—

a $p < 0.01$
b $p < 0.05$

The results for inflight LBM and fat losses derived from each of the methods are grouped by mission and shown in Table 4-18. A corresponding presentation of individual subject data for LBM results is given in Table F-20 (Appendix F4)). A correlation analysis between the different methods was performed for the inflight tissue losses. Unlike the results shown in Table 4-17(b) for the preflight correlations, the inflight correlations between the methods were insignificant at the 95% level. The one exception was the expected strong correlation between the TBW method and the combined "TBW and TBK" method. However, weaker relationships ($p < 0.1$) are consistently found between the corrected TBK method and *all* other methods. The biostereometry-body density method, although on the average in agreement with the other methods, exhibited the poorest subject-to-subject correlation with other methods (both preflight and inflight), the highest coefficient of variation, and, consequently, the least statistically significant inflight losses.

No meaningful trends were observed between LBM loss and flight duration (Table 4-18). This observation supports the pooling of all subjects in estimating mean inflight losses. However, there was agreement with five of the six methods that the smallest fat loss occurred on the longest mission, the same flight on which the smallest weight loss occurred.

Daily metabolic balances (accounting for diet, urine, and feces but not sweat or skin losses) were determined for nitrogen and potassium. A comparison between these two balances is presented in Fig. 4-22 in terms of monthly averages. The inflight loss of potassium and nitrogen has been expressed as a shift from the preflight control value. The mean daily losses of nitrogen and potassium have been converted to the common units of grams of protein by using the factors 6.25 grams protein per gram nitrogen [55] and 2.23 grams muscle protein per meq potassium [48]. In Fig. 4-22, the entire population of nine subjects is represented in the first month's data, whereas the second and third month's data include six and three subjects, re-

Table 4-18. Lean Body Mass and Fat Losses for Each Skylab Mission (Kg) [*n* = 3]

Mission	TBW	TBK	TBW plus TBK	Nitrogen balance	Combined	Body density
			Method			
			Lean body mass loss			
28-day	−1.68	−2.27	−1.69	−1.47	−1.47	−2.16
59-day	−0.82	0.31	−0.54	−1.63	−4.72	−2.45
84-day	−0.86	−2.68	−1.18	−1.78	−0.96	−0.88
			Fat loss			
28-day	−1.52	−1.16	−1.74	−0.86	−2.37	−1.69
59-day	−2.58	−3.97	−3.12	−2.27	0.69	−1.58
84-day	−0.003	1.69	0.19	0.85	−2.16	−0.32

spectively. The control group followed the same pattern. This balance analysis demonstrated a similar time profile for both constituents. Both showed the largest losses during the first month with losses half as large thereafter. Similar losses during the last 2 months suggest an attainment of a constant loss rate.

4.5.3 Discussion and Conclusions

The estimates for preflight lean body mass and fat content (Table 4-16) all fall within the range previously reported for either active or athletic males [48,56,57]. In addition, the coefficient of variation for each of the different methods was considerably less than the values reported in a previous comparative study [57] attesting to the narrow variability in the combined population. There was less precision in the estimation of the *changes* in LBM during flight, although all methods indicated a loss of at least 1 kg. Even though these losses are large when compared to the overall losses observed in body weight, losses of this magnitude are not outside the error limits for these methods [13,58,59,60]. Since there was no suitable method available for directly measuring the true LBM losses, it was not possible to determine which of the methods studied was most accurate.

Certain methodological considerations with regard to the procedures used could have contributed toward method-to-method variations. The determination of body composition from the methods used in this study requires the assumption that the body tissues (fat and fat free) have a fixed density as well as an unvarying proportion of water or potassium. Furthermore, estimates of changes in body composition demand that water, potassium, and nitrogen be lost from the lean body in the same proportion as they exist in the normal intact individual. Agreement among the different methods may be limited by the degree to which these assumptions are correct.

More evidence is available to verify the accuracy of these methods in measuring *absolute values* in a control population than there are to validate the capability of the methods to estimate *changes* in body composition resulting from some disturbance. The strong correlations between total body water, total body potassium or nitrogen, and lean body mass may be invalidated in certain conditions [61]. For example, in starvation, infection, tissue ischemia, and anoxia, tissues are depleted of potassium and water in amounts proportionally greater than the protein loss [62,63]. Potassium loss from cells can occur not only from actual breakdown of protein but also from loss of intracellular fluid and the inefficiency of the energy metabolism process on which the maintenance of the transcellular membrane potassium gradients is dependent [62]. These factors undoubtedly had an influence on the TBK method and may have led to the large departure of this methods' results relative to the other methods. The reader is referred to Appendix F(4) for a discussion of errors in the TBK method.

A constancy of lean body density (the premise underlying these methods) demands proportional losses of tissue solids (protein and electrolytes) and water. In weightlessness the quantities of protein, electrolytes, and water are known to change and they appear to be depleted from the body at widely different rates. Water and sodium, for example, exhibit large reduction within the first several days of hypogravity because of internal fluid disturbances. Changes in the cell protein pool are influenced by slower acting metabolic processes [4]. Anorexia associated with space motion sickness early in flight would be expected to augment the loss of cell components, including fat [63]. These findings are supported by ground-based hypogravic stress studies such as water immersion [64] and bedrest [65,66]. Thus, the premise that the proportions between whole-body constituents observed during
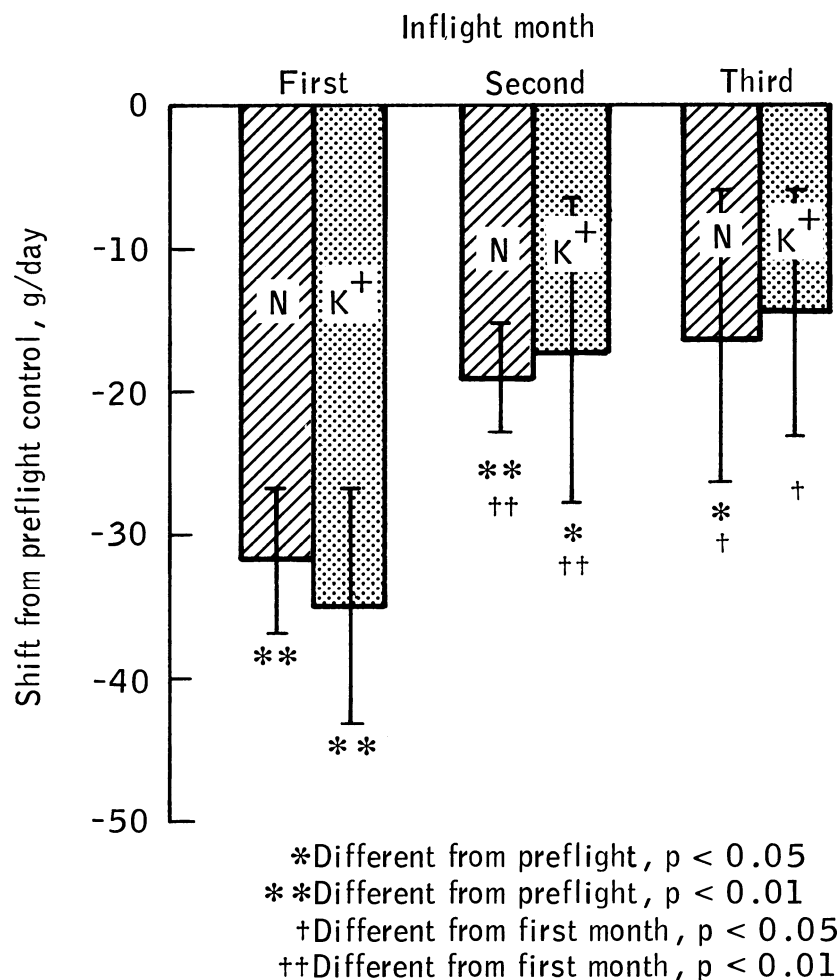
Figure 4-22. Mean (plus or minus standard deviation) monthly nitrogen (N) and potassium (K$^+$) balances expressed as inflight protein loss relative to preflight values.

preflight conditions are maintained during the *nonsteady-state* conditions of the inflight period is questionable. Whether or not the net results of these inflight changes are to establish a *new equilibrium level* appropriate to the zero-g state with the same proportions of body composition as in one-g is unknown. However, it should be pointed out that the data analyzed in this study were obtained after 1 to 3 months inflight, a period long enough to perhaps have achieved a new steady state. More direct measurements such as can be obtained from tissue biopsy samples may provide further information regarding the dynamic relationships among water, mineral, and protein at the cellular level.

Evidence that the inflight loss of two important cell constituents are depleted in proportion to their preflight composition ratios is provided by comparing the nitrogen and potassium metabolic balances (Table 4-19). There is good correlation between the nitrogen and potassium losses of the nine crewmembers ($r = 0.59$, $p < 0.01$) (see also Fig. 4-22). Just as important, the loss rates of nitrogen and potassium are

in a ratio consistent with normal skeletal muscle composition. The overall loss ratio, ΔK^+:ΔN = 11.9 meq/day: 4.2 g/day = 2.86, compared with 2.80 given for the normal potassium nitrogen content of skeletal muscle tissue [48].

In spite of these good correlations, the absolute value of inflight ΔLBM calculated from the ΔK^+ or ΔN values of Table 4-19 are both higher than is reasonable (i.e., three times the total body weight loss). Explanations for this discrepancy may be traced to general sources of error in the nitrogen balance method. For example, the nitrogen balance shows a net protein retention during the preflight period. This has often been observed and questioned by others [67], but sources of methodological errors in carefully controlled studies are not apparent [68]. A full discussion of errors in the nitrogen balance method are presented in Appendix F(4). Notwithstanding these errors, the inflight nitrogen balance without correction for sweat losses or preflight balances provides reasonable estimates of inflight loss and is the basis of one of the methods used for determining LBM loss in our analysis.

Table 4-19. Nitrogen and Potassium Balances of Skylab Crew*

Man	Nitrogen Balance (gm/d)			Potassium Balance (meq/d)		
	Preflight	Inflight	Δ	Preflight	Inflight	Δ
1	2.95	−0.96	−3.91	21.71	5.53	−16.18
2	3.12	−2.22	−5.34	24.94	5.04	−19.90
3	3.00	−1.71	−4.71	17.33	5.11	−12.22
4	3.07	−0.99	−4.06	17.84	5.01	−12.88
5	3.42	−0.78	−4.20	14.03	6.43	−7.60
6	4.05	−0.81	−4.86	23.19	12.79	−10.40
7	3.31	−1.24	−4.55	12.30	1.13	−11.17
8	2.20	−0.68	−2.88	13.62	6.93	−6.69
9	2.78	−0.06	−2.84	17.48	7.79	−9.69
Mean	**3.10**	**−1.05**	**−4.15**	**18.05**	**6.20**	**−11.86**
SD	**±0.50**	**±0.62**	**±0.85**	**± 4.43**	**±3.09**	**± 4.13**

Correlation coefficient: ΔN vs. ΔK = 0.59 ($p < 0.01$)

* No corrections for sweat losses

Avg. Protein Loss

From Nitrogen Balance: Avg ΔN Bal x Avg Mission Length x 6.25 = 1478 gm protein ÷ 19.4% = 7.6 Kg LBM

From Potassium Balance: Avg ΔK Bal x Avg Mission Length x 2.23 = 1508 gm protein ÷ 19.4% = 7.8 Kg LBM

The general conclusion of this study, obtained from averaging results of the six methods, is that a weight loss of 3.8% observed during the Skylab missions can be attributed to a 2.5% loss in lean body mass and a 10.4% loss in body fat corresponding to the following inflight losses: body weight, 2.7 ± 0.3 kg; LBM, 1.5 ± 0.3 kg; and body fat, 1.2 ± 0.3 kg. Using the relationships that protein is 19.4% of LBM and water is 73.2% of LBM, total body decrements of water and protein are found to be 1.1 kg and 0.3 kg, respectively. Supportive qualitative evidence for these whole-body losses comes from measurements of leg volume [44] and other body segments [52]; intracellular and extracellular fluid volumes [4,67]; urinary methylhistidine, cortisol creatinine, 17-ketosteroids, and hydroxyproline; plasma potassium concentrations [4]; metabolic balances for cellular electrolytes (i.e., magnesium, phosphorus, calcium) [32]; limb strength tests [69]; and skin-fold measurements [5]. No trend indicated that losses continued with increasing periods of weightlessness. In fact, the longest mission (84 days) was characterized by the smallest losses in weight and body fat. Interpretation of these losses and the degree to which diet, exercise, and the zero-g environment influences them is discussed in the next section.

4.6 Energy Balance and Composition of Weight Loss During Prolonged Spaceflight

In previous sections of this chapter the loss of body weight during spaceflight was analyzed from the perspective of a daily water balance, daily nitrogen balance, and certain whole-body measurements including total body potassium, total body water and body density made prior to and following the inflight phase. However, information was also obtained from the Skylab astronauts concerning the changes in energy balance, and analysis of this data can lead to inferences made on the composition of the weight lost, not just for the mission as a whole but for more discrete time periods. Interpretation of spaceflight related weight loss in terms of the major body elements and tissues (i.e., water, muscle, fat) is essential for understanding metabolic processes in weightlessness and predicting and minimizing weight losses in future missions. Also, since diet and activity affect lean and fat tissues differently, knowledge of expected changes will assist in establishing caloric and exercise requirements.

Before the Skylab missions, a definitive analysis of spaceflight-related body composition changes had been hampered by the difficulty in quantifying inflight physical activity and ensuring an adequate caloric intake. In addition, many operational constraints prevented direct measurements of tissue loss. On missions lasting less than one week (Mercury and some Gemini flights), a weight loss of several kg was ascribed almost completely to a negative water balance [71]. An analysis of the longer Apollo missions (about 12 days) indicated that of the total weight loss (average, 3.5 kg; range, 0.8 to 5.9 kg), only half could be attributed to water loss. The remainder consisted of tissue loss (both fat and fat-free solids). This result indicates the presence of a negative energy balance, which was caused by an estimated caloric deficiency of about 1000 kcal/day [50,63]. Among factors proposed to explain the weight loss were an inadequate dietary intake, reduced, or inappropriate, exercise level, adaptive metabolic effects possibly involving tissue catabolism and weightlessness itself. These earlier studies were inadequate

to either describe the effects of spaceflight on body composition changes nor to assign their causes.

During the Skylab missions, a major effort was directed at measuring, and partly controlling, the essential components of body weight including the daily collection of metabolic balance and body mass data. This was supplemented by pre- and postflight measurements of body composition. Weight loss, which results from tissue catabolism, must be consistent with metabolic balance findings for water and nitrogen, with energy balance data, and with evidence from directly measured body composition changes. Several previous studies have described the net changes in body composition of the Skylab astronauts, whose weight loss averaged 2.8 kg(range, 0.1 to 4.2 kg) [5,10,13,54]. The current study is a more comprehensive analysis because of the use of daily caloric balance (rather than water balance) to account for body fat changes, a determination of caloric and exercise requirements for spaceflight, and a superior computational approach. In this section, the energy balance of the Skylab crewmen is related to the observed changes in body composition. In particular, we describe, here and in Appendix F(5) separately for each of the three manned Skylab missions, the development of numerical procedures which allow: a) complete partitional metabolic balances for water, nitrogen and energy, b) time-continuous metabolic profiles on a daily basis, c) quantitative descriptions of the changes in the three major body components (fluid, protein, and fat) and d) estimates of caloric and exercise requirements necessary to maintain good health during spaceflight.

One important result of these analyses is a continuous-time profile of daily total body changes of water, protein and fat throughout the mission. Visualization of these changes facilitates an understanding of the gross metabolic disturbances which can occur in prolonged spaceflight. The overall conclusions, confirming an earlier, less detailed analyses [32,72], appear consistent with the concept of an acute obligatory loss of body water and a more gradual degradation of certain postural muscles. Changes in fat appear to depend on the gradual cumulative effects of a positive or negative energy balance. A more detailed account of this analysis is available [73].

4.6.1 Approach

Two basic formulations were used to analyze continuous body composition changes. First, an equation of body composition was used in which it was assumed that the changes in *total body weight* (ΔWGT) resulted from changes in *total body water* (ΔTBW), *total body protein* (ΔPRO), and *total body fat* (ΔFAT). Thus,

$$\Delta WGT = \Delta TBW + \Delta PRO + \Delta FAT \qquad (8)$$

Second, an energy balance equation was used in which *net energy utilization* (E_{util}) was computed as the sum of *energy intake from diet* (E_{diet}) minus *energy excreted in urine* (E_{urine}) *and feces* (E_{feces}) plus *energy available from body fat* (E_{fat}) *and body protein* (E_{pro}) catabolism.

$$E_{util}{}^* = \text{Work (internal + external)} + \text{Heat lost} \qquad (9)$$
$$= E_{diet} - E_{urine} - E_{feces} + E_{fat} + E_{pro}$$

As suggested by Eq. (9) the net energy available from food and tissue metabolism is utilized entirely to perform work and produce heat. $E_{util}{}^*$ could not be measured or estimated on a daily basis (i.e., by measuring work and heat lost or oxygen consumption) as were the other terms in the equation. It is designated with an asterick to indicate that it is estimated as an average constant quantity throughout each flight phase (preflight, inflight, postflight) and for each crewmember.

Equations (8) and (9) were used to compute daily changes in body composition, specifically, body water (ΔTBW) and body fat (ΔFAT). Daily values of all other terms in these two equations were measured directly in the crewmembers except for $E_{util}{}^*$. Specifically, this includes body mass measurements, protein changes from nitrogen balance, dietary energy from caloric values of foodstuffs, caloric value of urine from specific gravity, and bomb calorimetry of feces. While it was not possible to discern values of $E_{util}{}^*$ on a daily basis, it was assumed that this quantity (daily energy use) for each crewmember was reasonably constant during the inflight phase, since the astronauts adhered to a strict, standardized work and exercise schedule for each mission [5]. Accordingly, the values of the crewmembers energy use was computed by summing each term in Eq. (9) over the entire mission and then dividing the sum by the number of mission days. This calculation was possible because of the additional total body measurements of TBW and lean body mass (directly related to PRO) made prior to and following flight (see Chapters 4.2 and 4.5). See Appendix F(5) for a detailed discussion of the determination of each term in these mass and energy equations (Table F-22). Also in Appendix F(5) the reader will find tables for computed values of $E_{util}{}^*$ (Table F-23)as well as all other terms of these equations (Table F-26 to F-29).

As an example of these calculations refer to Fig. 4-23. The solid line on this graph illustrates the caloric value for net food intake (diet minus excreta) averaged for all nine crewmembers for each day of the preflight period and the first inflight month. The decline in food intake is associated with the onset of motion sickness symptoms in microgravity. The dashed line represents the average energy use, $E_{util}{}^*$, as computed by the method discussed previously. From Eq. (9) we note that if the body is in caloric balance and does not gain or lose tissue, $E_{util}{}^*$ is simply equal to the energy supplied in food less that excreted. Therefore, the difference between the dashed and solid lines is taken to be the energy deficit as supplied by fat and protein tissue catabolism. Or put another way, the deficit is the caloric equivalent of the tissue mass that was lost. If this difference is composed only of fat and protein, and if daily protein changes can be derived from the nitrogen balance, it should be possible to derive daily fat losses from Eq. (8). The difference between total weight loss and the sum of fat and protein losses was taken to be the daily

Table 4-20. Inflight Body Mass Changes in Each Skylab Mission [Mean ± SD]

Mission duration, days	Change in Body Element				
	ΔMass	ΔWater	ΔTissue	ΔProtein	ΔFat
(A) Total losses, g					
28 (n=3)	-2,330 ± 1100	-890 ± 1,040 (-1,020)[a]	-1,440 ± 960	-290 ± 110	-1,160 ± 860
59 (n=3)	-3,900 ± 300	-1,530 ± 1740 (-1,260)	-2,370 ± 1440	-320 ± 40	-2,060 ± 1440
84 (n=3)	-930 ± 810	-1,000 ± 530 (-910)	62 ± 790	-350 ± 310	-410 ± 940
Mean (n=9)	**-2,390 ± 1,460**	**-1,140 ± 1.090 (-1,160)**	**-1,250 ± 1,430**	**-320 ± 170**	**-940 ± 1,440**
(B) Average daily losses,[b] g/day-kg body wt.					
28 (n=3)	-1.10 ± 0.42	-0.42 ± 0.45	-0.68 ± 0.41	-0.14 ± 0.14	-0.55 ± 0.37
59 (n=3)	-0.93 ± 0.10	-0.32 ± 0.34	-0.60 ± 0.43	-0.08 ± 0.02	-0.53 ± 0.42
84 (n=3)	-0.16 ± 0.14	-0.17 ± 0.09	0.01 ± 0.13	-0.06 ± 0.05	0.07 ± 0.16
Mean (n=9)	**-0.73 ± 0.47**	**-0.30 ± 0.31**	**-0.43 ± 0.45**	**-0.09 ± 0.05**	**-0.33 ± 0.42**

[a] Values in parentheses are water losses calculated from protein and fat losses based on 74% water content of lean body mass and 15% water content of adipose tissue
[b] Values have been normalized with respect to mean body weight of the preflight period

change in body water as shown by Eq. (8). The cumulative losses of water, fat, and protein can then be computed as a function of flight duration by summing consecutive daily balances.

From Fig. 4-23, it is apparent that the Skylab crew was, on average, in negative energy balance during the first month of flight (and during the preflight period as well). The computed deficit averages 350 kcal/day during the first month inflight. Figure F-6 (Appendix F) shows this same graphical illustration for each of the three missions separately. While the first two missions show clearly that there was a caloric deficit, the third and longest mission appears to indicate that the crew was in approximate caloric balance.

Errors in the metabolic balances can produce seriously misleading results, especially if the balances are cumulative, as they are in this study. For this reason, considerable attention has been paid to addressing and minimizing these types of errors. An analytical approach, based on cumulative daily metabolic balance data, was developed to derive continuous changes in the major components of body weight loss (i.e., water, protein, and fat) for each crewmember exposed to weightlessness. The procedure avoided the large errors normally inherent in cumulative metabolic balances

by restricting the endpoints of the balance period (i.e., inflight phase) to values (say, of body water) determined directly by isotope dilution methods and by using daily body mass measurements to determine losses in tissues that were not measured directly. This technique of correct-
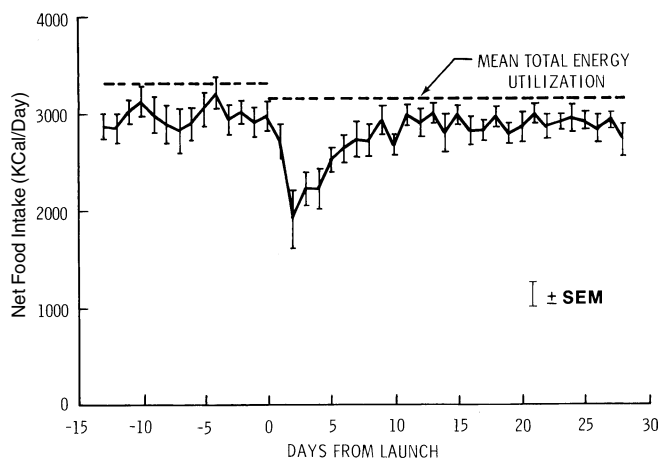
Figure 4-23. Average net food intake for the Skylab crews (*n* = 9).

Table 4-21. Energy Balance for Each Skylab Crew [Mean ± SD, N=3)]

Component	Energy rate, kcal/day		
	28-day mission	59-day mission	84-day mission
Preflight			
Total diet[a]	3086 ± 147	3354 ± 749	3214 ± 61
Excreta			
Urine[b]	107 ± 3	122 ± 38	124 ± 10
Feces	148 ± 9	135 ± 32	145 ± 15
Total	255 ± 8	257 ± 70	269 ± 6
Body tissue loss[c]			
Protein	-107 ± 3	-124 ± 18	-98 ± 20
Fat	512 ± 297	490 ± 226	413 ± 416
Total	405 ± 295	366 ± 238	315 ± 423
Net energy use[d]	3226 ± 434	3463 ± 480	3260 ± 462
Inflight			
Total diet[a]	2930 ± 88	3225 ± 608	3260 ± 106)
Excreta			
Urine[b]	139 ± 10	145 ± 38	153 ± 7
Feces	106 ± 2	141 ± 36	136 ± 31
Total	245 ± 11	286 ± 74	289 ± 36
Body tissue loss[c]			
Protein	58 ± 23	30 ± 4	23 ± 21
Fat	391 ± 289)	330 ± 231	-46 ± 105
Total	449 ± 309	360 ± 231	-23 ± 94
Net energy utilization[d]	3134 ± 383	3299 ± 338	2948 ± 97

a Diet calculated from 4.182 (carbohydrates) + 9.461 (fat) + 5.6 (protein)
b Urine energy = 8.32 (urine nitrogen)
c Energy available from body tissue loss: 5.65 kcal/g protein; 9.461 kcal/g fat. Minus sign indicates gain in body tissue
d Eq. (9)

Table 4-22. Skylab Inflight Exercise (Bicycle Ergometer) [Mean ± SD, N=3]

Mission Duration Days	Total mission useful exercise kW-min	Avg daily useful exercise, kW-min/day	Total avg daily work[*] kcal/day-kg body wgt
28	55 ± 9	1.951 ± 0.315	1.77 ± 0.52
59	276 ± 95	4.686 ± 1.615	4.12 ± 0.63
84	411 ± 60	4.894 ± 0.716	4.62 ± 0.56

* Bicycle work (in kilowatt-minutes per day) converted to total work expended (in kilocalories per day per kilogram of body weight) on exercise by dividing values in the center column (avg daily exercise) by 0.22 (mechanical efficiency of bicycle riding) and by the preflight body weight and then converting from watt-minutes to kilocalories by using the factor 1 kilocalories = 70 watt-minutes. Data from Michel (Ref. [28]).

ing cumulative errors in daily metabolic balances is described at the beginning of Chapter 4 (see Fig. 4-3). In the case of errors in the nitrogen balance, it has already been discussed in Chapter 4.5 and Appendix F(4) that the cumulative nitrogen balance method (without correction) is in agreement with other independent methods.

4.6.2 Results
4.6.2.1 Overall Mission Weight and Tissue Losses.
The tissue components of body mass that were lost on each mission as well as mean Skylab losses are summarized in Table 4-20 and Fig. 4-24. Data for the individual crewmembers are provided in Table F-24 (Appendix F).

Table 4-23. Inflight Energy Consumed in Diet, Expended on Exercise, and Available from Tissue Loss for the Three Skylab Missions [Mean ± SD, N=3]

Component	Energy balance, kcal/day-kg body wt.		
	28-day mission	59-day mission	84-day mission
Diet[a]	40.4 ± 5.5	44.3 ± 2.1	47.3 ± 3.0
Exercise[b]	1.77 ± 0.52	4.12 ± 0.63	4.62 ± 0.56
Diet minus exercise	38.6 ± 5.0	40.2 ± 2.1	42.7 ± 3.3
Body tissue loss[c]	5.94 ± 3.75	5.43 ± 4.01	-0.35 ± 1.36

a Calculated from caloric equivalent of carbohydrate, fat, and protein (Table 4-21)
b Based on bicycle exercise only assuming 22% efficiency in converting bicycle work to exercise energy expended (Table 4-21)
c Obtained from Table 4-21
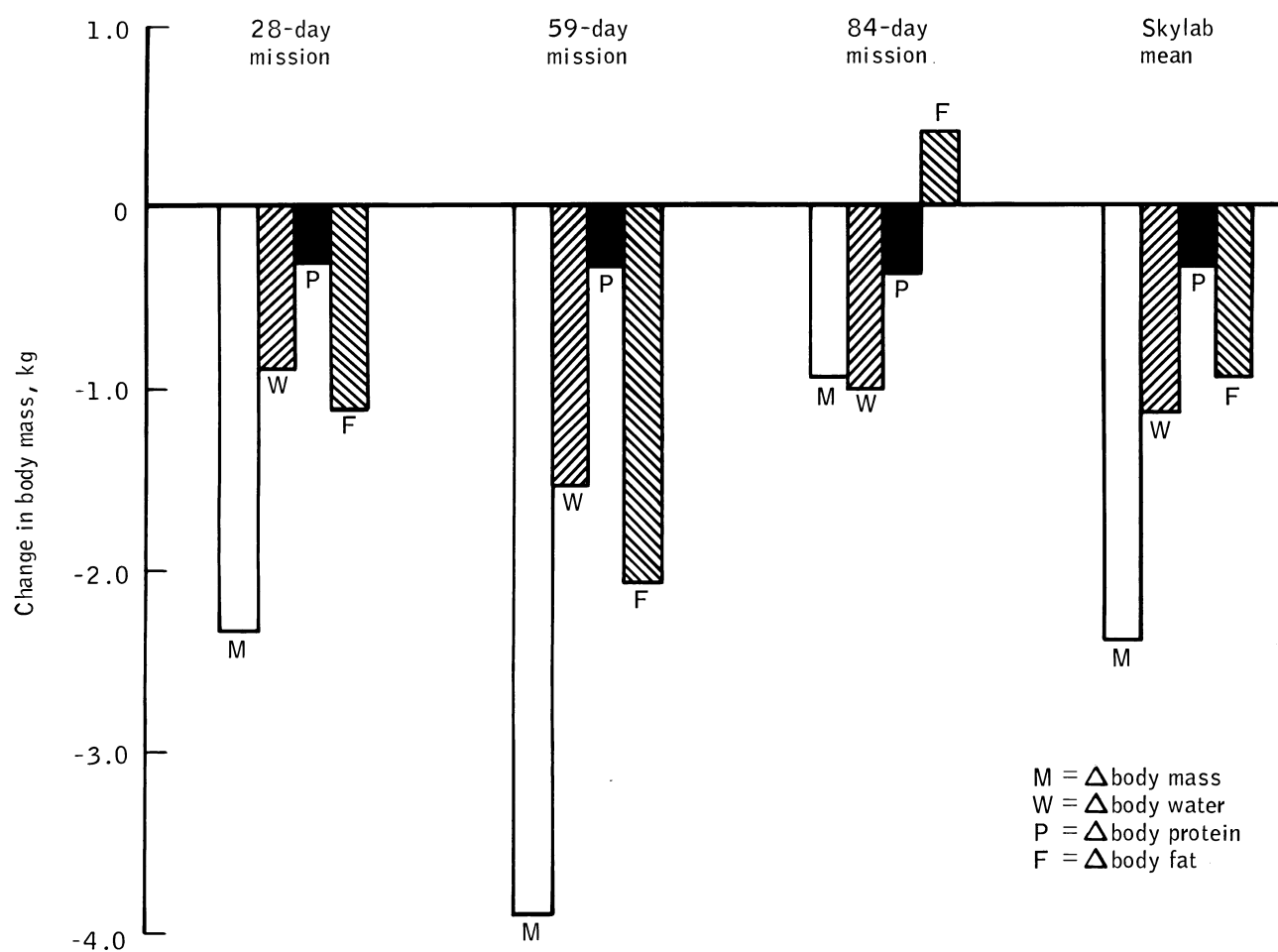
Figure 4-24. Inflight changes in body mass resulting from spaceflight.

The time period for these changes is computed from the morning of launch to the morning of the recovery day inclusive. Of the quantities shown in Table 4-20, body weight/mass was the only one measured directly. Total body water changes for this period were calculated from direct measurements obtained within one day after splashdown and corrected (for water replenishment and water lost) to reflect values on the morning of recovery day (see Table F-25 (Appendix F). Body protein, fat, and total tissue changes were estimated by using Eqs. (8) and (9).

The average loss of water, fat, and protein for the nine crewmen was found to be 48%, 39%, and 13%, respectively, of the total body mass loss of 2.4 kg. No statistically significant trends relating weight changes to mission duration were apparent from these data. Compared to the 28-day mission, the losses of all quantities were most severe during the 59-day mission but less severe (with the exception of body protein) during the 84-day mission. On the two shortest missions, body fat losses accounted for about one-half of the total weight loss, the remainder being attributed to lean body mass loss (i.e., the loss of water and protein). There was an apparent net increase in body fat on the longest mission. Protein losses were relatively similar on all missions and are, therefore, apparently independent of mission length. The computed water losses for all missions were found to be totally consistent with the estimated water losses derived from protein and fat losses (see footnote (a) in Table 4-20(A)).

When the data in Table 4-20(A) were converted to daily loss per kg body weight by division by the mission length and preflight body weight, the trend was towards smaller rates of loss as mission length was increased (Table 4-20(B)). That this trend was somewhat artificial and arose mainly because the major part of the changes occurred early in flight, rather than to several other possible causes, is explained below. In other words, dividing a relatively constant absolute loss by an increasing number of days gives the false impression of a decreasing rate of loss for longer missions. Improvements in diet and exercise during the longer missions could also be explanatory factors.

4.6.2.2 Energy Balance. The energy balance (Eq. (9)) for each mission is shown in Table 4-21; the two-week preflight phase and the inflight phase are shown separately. Corresponding data for each crewmember is provided in Tables F-26 to F-29 (Appendix F). Inflight dietary intake averaged 3138 ± 350 kcal/day (mean ± SD) for all nine subjects. This value was only slightly lower than the preflight average of 3218 ± 400 kcal/day. Although this difference was statistically insignificant, examination of the data for the individual crewmen provided a clue to the weight loss mechanism. Five of the nine crewmen decreased their mean caloric intake during flight; these subjects lost 75% more weight than the other crewmen, who increased or maintained their preflight intake. Small differences in caloric intake maintained for long periods are known to produce significant weight changes. Approximately 9% of the total calories consumed was excreted in
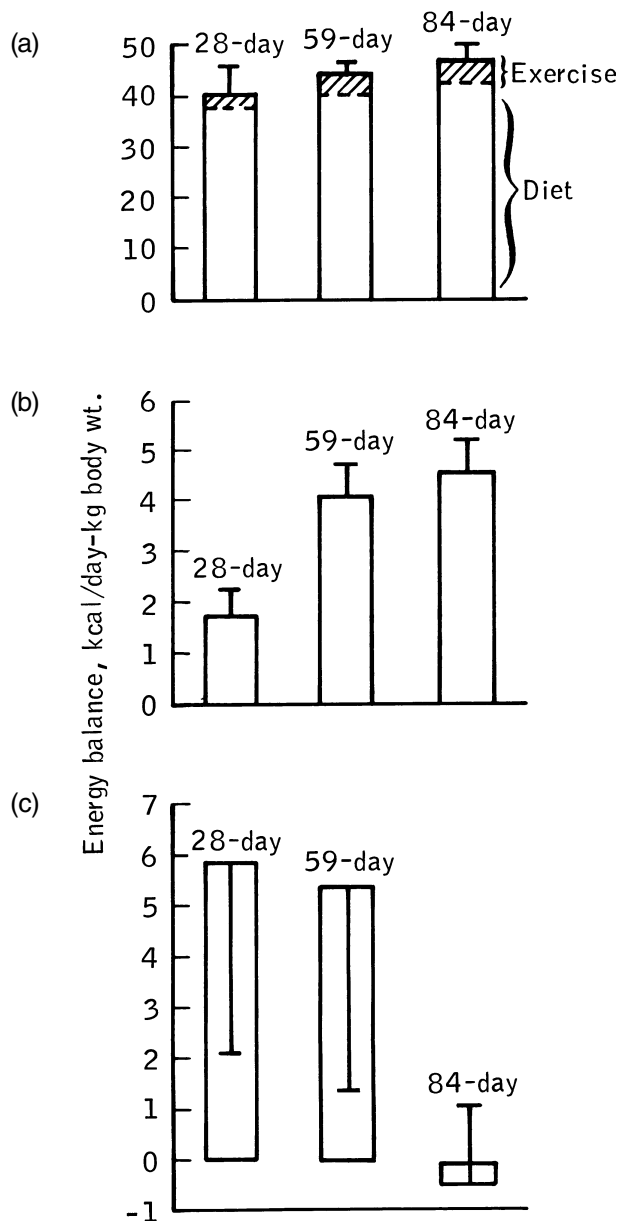
Figure 4-25. Energy balance (mean ± SD) during Skylab missions. (a) Energy from diet. (b) Energy expended on exercise, (c) Energy available from tissue loss.

urine and feces (Table F-27). This fraction was nearly constant for all crewmen during preflight and inflight phases.

A negative energy balance exists when energy intake is less than energy utilization; this condition is accompanied by loss of energy-bearing tissue (i.e., fat and muscle). The net caloric intake (dietary calories less urine and fecal calories) was less than the net energy utilization (estimated from Eq. (9)) for the 28-day mission (inflight phase), and this difference diminished for each longer mission.

These differences averaged over the inflight period, are –448 kcal/d, –360 kcal/d, and the +23 kcal/d for the 28-day, 59-day and 84-day missions, respectively. These deficits are reflected in the net loss of body tissue shown in Tables 4-20 and 4-21 and shown graphically in Fig. F-6 (Appendix F). On average there appears to have been an apparent loss in tissue on the two shortest flights but not on the longest flight.

Other investigators also concluded (without benefit of a complete energy balance) after examining data from earlier missions, e.g., Apollo, Gemini program, that the energetic cost of life in space was much higher than indicated by the actual total energy content of the food consumed [50,74]. It appears that for one reason or another it has been difficult for mission planners to predict the caloric value of the food supplied to astronauts needed to offset their energy expenditures in space and prevent body weight from declining. Alternatively, there may be obligatory tissue losses in a microgravity environment that are independent of caloric requirements. This matter will be discussed below.

4.6.2.3 Effects of Diet and Exercise. Both dietary caloric intake and the amount of daily exercise were intentionally increased on each subsequent mission in order to improve the crew's health parameters. The rigidly controlled diet provided for the crew on the first mission was based on an assumption (which has proved erroneous) that, without gravity to work against, the caloric expenditure for crews living in space is approximately 10% less than similar work expenditure on earth. (Although, astronauts can move around quite effortlessly in space it was not appreciated that they often require more energy to stabilize their body when performing a stationary task with their hands). After the crew on the first mission was observed to lose weight gradually and continuously over the course of 28 days inflight, the caloric content was increased for the next 3-man crew. Observation of that crew also showed continual weight loss and the dietary intake was again adjusted upward for the last crew. These adjustments in dietary kcal/day-kg BWgt are shown for all crewmen and missions in Appendix F, Table F-29, (i.e., E_{diet}); in general there was an increase of 3 to 4 kcal/day per kilogram of body weight on the inflight phase for each subsequent mission, while the caloric content of the preflight phase remained relatively constant. Specifically, the caloric content of food consumed by the crewmembers was 40.4 kcal/day-kg BWgt, 44.3 kcal/day-kg BWgt, and 47.3 kcal/day-kg BWgt for the 28-day, 59-day, and 84-day missions, respectively.

The time devoted to exercise and the number of exercise devices employed was also intentionally increased on each subsequent mission in an attempt to provide the crew with an optimal exercise program. The benefit of additional exercise was demonstrated by a superior postflight exercise and strength performance, as well as by an increased feeling of well-being during the flight [70].

All crewmembers exercised on the bicycle ergometer. In addition, a commercial mini-gym exerciser was used by the crews of the two longest missions, and a treadmill-type device was used on the longest mission. Quantitative estimates of exercise workload are available only for the bicycle ergometer [28]. However, these data, shown in Table 4-22, tend to reflect the time and intensity devoted to *total* exercise by each crew.

The relationship between diet, exercise, and body tissue loss for the three crews becomes more apparent when these quantities are expressed in the common units of kilocalories per day per kilogram of preflight body weight, as shown in Table 4-23 and Fig. 4-25. The increase in dietary intake for each subsequent mission more than offsets the increase in exercise expenditure, as indicated by the difference between diet and exercise ("Diet minus exercise" in Table 4-23), which also increases with mission duration. The crew that exercised the most (the 84-day mission) lost the least body fat, which would be paradoxical were it not for the fact that their caloric intake was also the highest. The data in Table 4-23, while not including *all* exercise, suggest that excess ingested calories may have been available to the crew on the longest mission to offset the increase in energy expended through exercise and to increase fat stores relative to the other two crews.

4.6.2.4 Continuous Changes During First Month: Skylab Mean. The dynamic profile for the changes in *weight/mass* (ΔBWgt), *total body water* (ΔTBW), *protein* (ΔPRO), and *fat* (ΔFAT) are shown in Fig. 4-26. These data represent the average response of all nine crewmen and include a preflight period, the first month in flight (the longest inflight interval common to all three missions), and a postflight period. Values for these quantites were computed as previously discussed in Chapter 4.6.1 and shown in Table F-22. The curve labeled "change in body tissue" is the sum of protein and fat losses. Protein losses were obtained directly from the nitrogen balance and represent loss of dry tissue. The sum of protein and water losses will be termed "lean body mass" losses.

The following information can be derived from the average responses shown in Fig. 4-26.
a) Body weight decreased significantly during the first few days following launch largely as a result of a body water loss of more than 1 liter. Body water remained relatively constant at this reduced level (with some replenishment), whereas body mass continued to decline gradually as body tissue (both fat and protein) were catabolized.
b) The time course of the body mass change can be explained by the losses of water, protein, and fat, each proceeding at different rates; water is lost most rapidly, followed by fat, and then by protein.
c) At the end of 28 days in flight, ΔBWgt ± SE was –2.2 ± 0.31 kg. The component losses were computed as: ΔTBW = –1.02 ± 0.21 kg, ΔFAT = –0.85 ± 0.30 kg, and ΔPRO = –0.34 ± 0.03 kg. Water accounts for 46% of the total mass loss, and the remainder is attributed to tissue loss. In analyzing for the muscle/fat ratio, we find that 62% of the total mass loss was attributed to lean body mass and 38% was attributed to fat. Lean body mass normally contains 75% water and 25% protein [75], which was the same ratio found in this analysis after 1 month in flight.
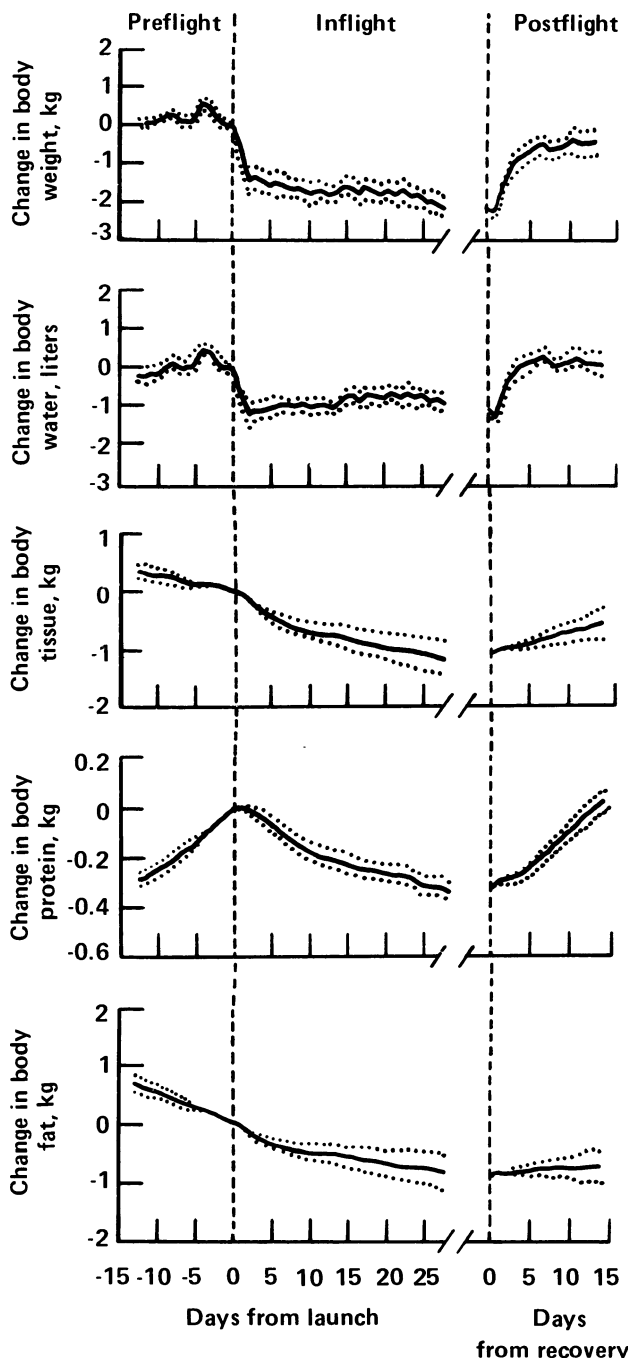
Figure 4-26. Mean (± standard error) changes in body composition during all mission phases for all Skylab crewmen (n = 9). Values are shown as changes from morning of launch.

d) The loss of protein and fat was consistent with an average inflight caloric deficiency of approximately 350 kcal/day, which was estimated to occur during this 28-day period, as illustrated in Fig. 4-23. The rate of tissue loss was much greater during the first week (where there was the highest caloric deficiency) than during the last 2 weeks of the first inflight month.

e) The preflight period was characterized by increases in protein mass and decreases in fat stores. This behavior could be expected for subjects on a high-protein, controlled diet, and who are engaged in physical conditioning [76].

f) During the postflight period, weight gain was nearly as rapid as the original inflight loss, and resulted primarily from changes in body water. Postflight recovery of protein was at rates similar to the preflight retention rates, whereas inflight fat losses did not show signs of postflight recovery.

4.6.2.5 Continuous Changes During First Month: Mission Differences. First-month inflight changes in diet and body composition for each of the three missions are presented in Fig. 4-27. The most remarkable intermission observation during the first month period is that the 59-day crew had, by far, the largest relative decrease in caloric (and water) intake (compared to their preflight level), as well as the sharpest and most sustained decline in body water and body fat. Most of these losses occurred during the first week after launch and could be attributed to symptoms of space motion sickness which were more severe in this crew than in the other two.[§] Therefore, it was not unexpected that the crew of the 59-day mission would exhibit the largest decreases and rates of decrease in total body weight, water, tissue, protein, and fat (Figs. 4-27(b) to 4-27(f)), especially during the first week in weightlessness, when intake of water and food was at a minimum. In contrast, the crew having the most adequate caloric intake (the 84-day mission) showed the least loss of fat and total tissue. By the end of the first month in flight, this crew showed the smallest losses in total body mass as well as a small gain in fat.

A caloric deficit by itself would be expected to result in fat loss and perhaps some muscle loss [74]. A deficit in water intake would deplete body water and further attenuate the total body mass loss. These differences in caloric and water intake between flight phases and between missions are offered as a possible explanation to account for many of the intramission differences of weight, fluid, and tissue loss.

4.6.2.6 Continuous Changes in Body Composition: Long-term Responses. The continuous changes in body composition for each mission are illustrated in Fig. 4-28(a) to 4-28(c). Long-term responses for the period beyond the first month are exemplified by the results of the 59-day and 84-day missions.

[§] Interestingly, the crew that was said to have essentially few symptoms of space motion sickness (i.e., the 28-day mission) also had a large dietary decrease for a week after launch. This crew may have eaten less because of a heavy activity schedule that included repair of a heat shield. The possibility also exists that the mechanisms which regulate caloric intake in proportion to energy expenditure are not always operative during weightlessness for reasons other than motion sickness. The hypothesis that a decrease in caloric intake is not always closely correlated with space motion sickness is supported by the data (Fig. 4-27) from the 84-day crew that showed the second highest incidence of motion sickness but had the least drop in caloric intake during the first few days inflight. A similar form of anorexia was described in the Apollo crew who generally ate less food than was provided and did not exhibit signs of motion sickness [63].
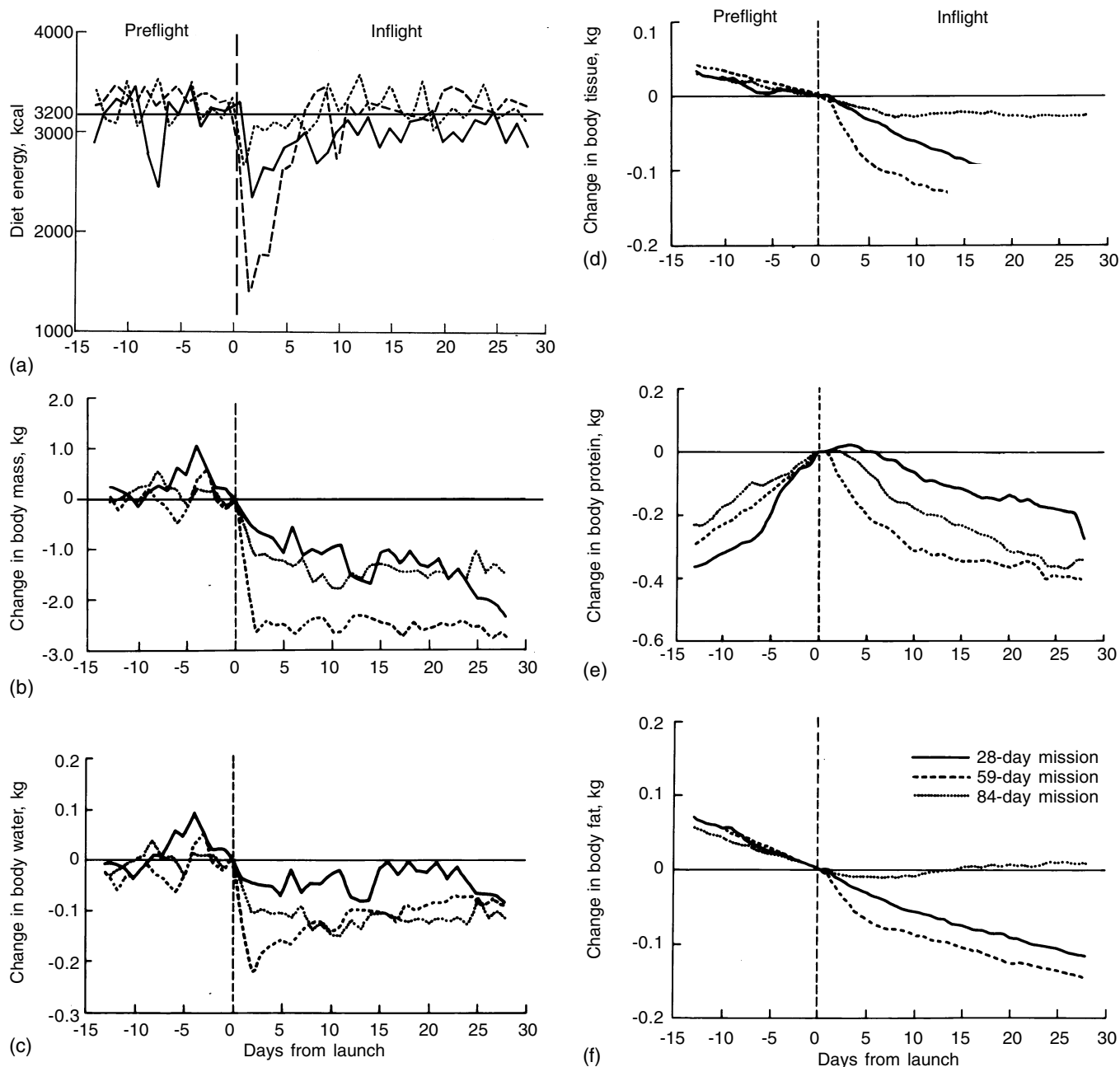
Figure 4-27. Changes in dietary intake and body composition before flight and during the first month of flight for each Skylab crew (*n* = 3). Values shown are referenced from the morning of launch. (a) Diet energy. (b) Change in body mass. (c) Change in body water. (d) Change in body tissue. (e) Change in body protein. (f) Change in body fat.

A small decline in body mass during the second month, reflecting a continuing loss of fat, was observed in the 59-day crew. Also, rehydration of body water continued to some extent. The 84-day mission was characterized by the greatest stability of body mass, water, and total body tissue. This was the only flight without a net change in tissue mass; in fact, a small degree of increased fat stores may have been observed. This stability reflected the combined adequacy of diet, exer-

cise, and general physical condition. By most accounts, this crew returned from space in better general health than any other crew [31]. The crew of the 84-day mission both exercised more and had a higher dietary intake than the crews of other missions. Because of this, it is difficult to separate the effects of flight duration, exercise, and diet.

The most important trend observed in this data that was not discernable in the first month's results, is the lev-

Table 4-24. Metabolic Balances of Intracellular Minerals

	Preflight	First Inflight month[a]	Second Inflight month[b]	Third Inflight month[c]
Nitrogen, g				
Diet	18.8	17.2	19.3	19.4
Urine	14.1	17.7	17.6	17.7
Fecal	1.5	1.3	1.5	1.5
Balance	3.2	1.8	0.2	0.2
Potassium (meq)				
Diet	103.3	96.3	101.7	98.1
Urine	74.4	81.6	79.9	78.6
Fecal	11.9	10.7	12.6	10.8
Balance	17.0	4.0	9.2	8.7
Calcium (mg)				
Diet	872.0	872.0	940.0	974.0
Urine	166.0	288.0	291.0	242.0
Fecal	699.0	602.0	819.0	900.0
Balance	7.0	-18.0	-170.0	-168.0
Phosphorus (mg)				
Diet	1749.0	1716.0	1861.0	1801.0
Urine	1055.0	1271.0	1202.0	1181.0
Fecal	514.0	469.0	596.0	601.0
Balance	180.0	-24.0	63.0	19.0
Magnesium (mg)				
Diet	311.0	302.0	333.0	310.0
Urine	109.0	131.0	116.0	120.0
Fecal	176.0	155.0	192.0	175.0
Balance	26.0	16.0	25.0	15.0

[a] $N = 9$
[b] $N = 6$
[c] $N = 3$

eling off of protein losses during the second and third months. This behavior could have been suspected from other Skylab data, such as the mineral balance [50] and leg volume measurements [10] that indicated a relative stability of lean body tissue during the last 2 months in flight. As in the analysis of the first month's data, these long-term trends in body protein appeared to be independent of the amount of exercise performed. Also remarkable is the overall uniformity of the body protein loss response among the three crews, especially in light of the potential error of the nitrogen balance method (see Appendix F). In all cases, the body protein increased during the preflight phase, decreased at variable rates during the inflight phase with an almost exponential decrease during the first month, followed by periods of relatively stable body protein mass, and then exhibited a complete recovery during the two week postflight phase.

The most severe *inflight* decline in protein mass among the three crews occurred on the 59-day mission and may be related to the fact that that crew had experienced the largest inflight caloric deficits relative to the other crews. However, the fact that the crew with the most

adequate intake (84-day mission), as well as performing the most exercise, did not show the smallest protein loss suggests that total body protein loss cannot be prevented by increasing caloric intake.

4.6.2.7 Electrolyte Losses. Metabolic balances were performed on a variety of electrolytes that are associated primarily with musculoskeletal tissue [6,7]. A summary of these analyses is presented in Table 4-24. The data were analyzed over four different time intervals: before flight, first month inflight, second month inflight, and third month inflight. These balances were uncorrected in the sense that losses from the skin and sources other than urine and fecal excreta were not measured. Normally, this procedure resulted in a positive balance during the control period. In all cases, the inflight balance was less than the preflight balance, suggesting a net loss during spaceflight.

The total of these mineral losses (excluding nitrogen) was estimated to be only 50 grams, which was insignificant relative to the total loss in body mass. Nevertheless, these results do support other findings that indicate a general loss of body tissue.
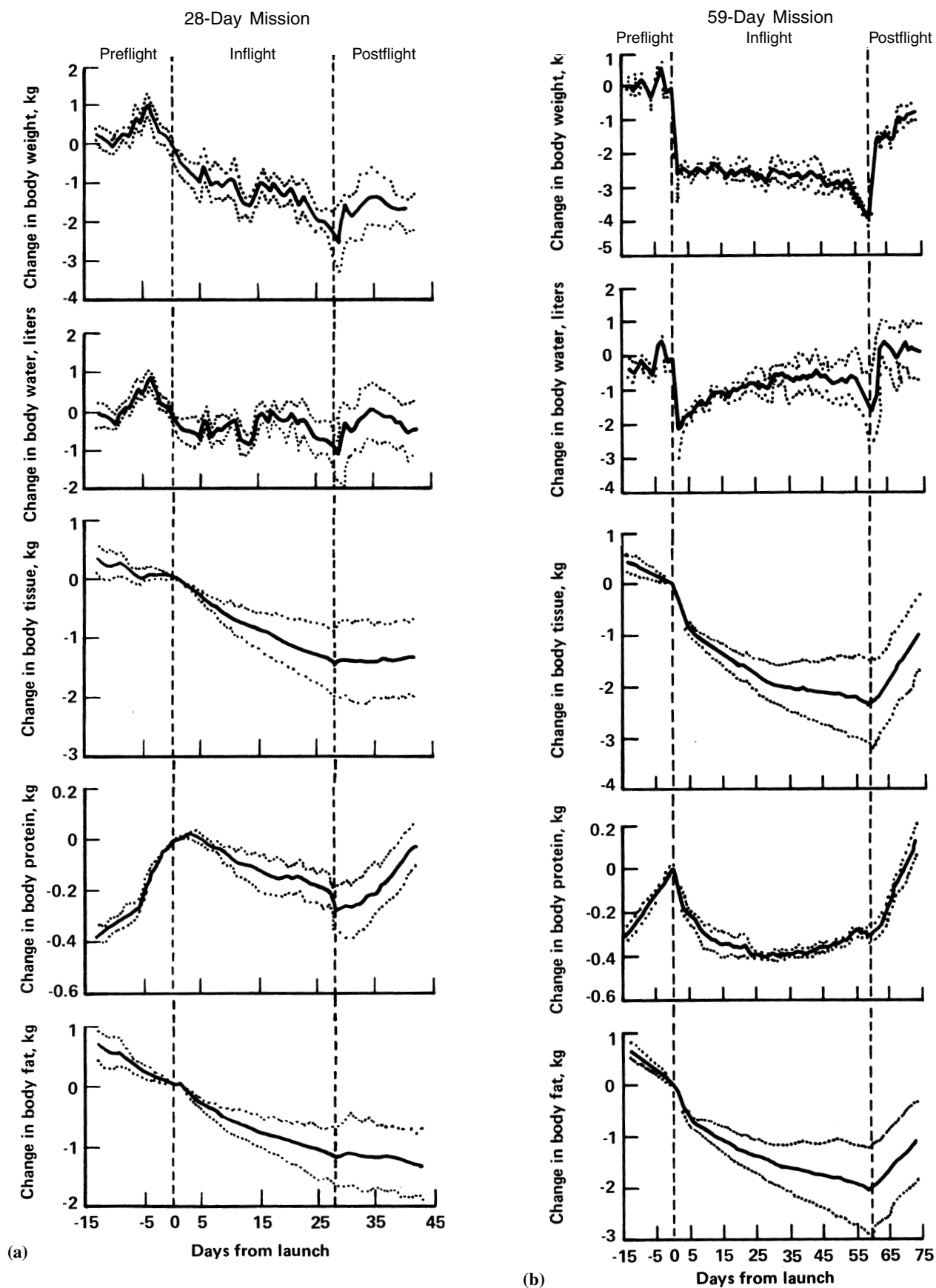
Figure 4-28. Body composition changes (mean ± SE) for each Skylab crew (*n* = 3). (a) 28-day mission. (b) 59-day mission.
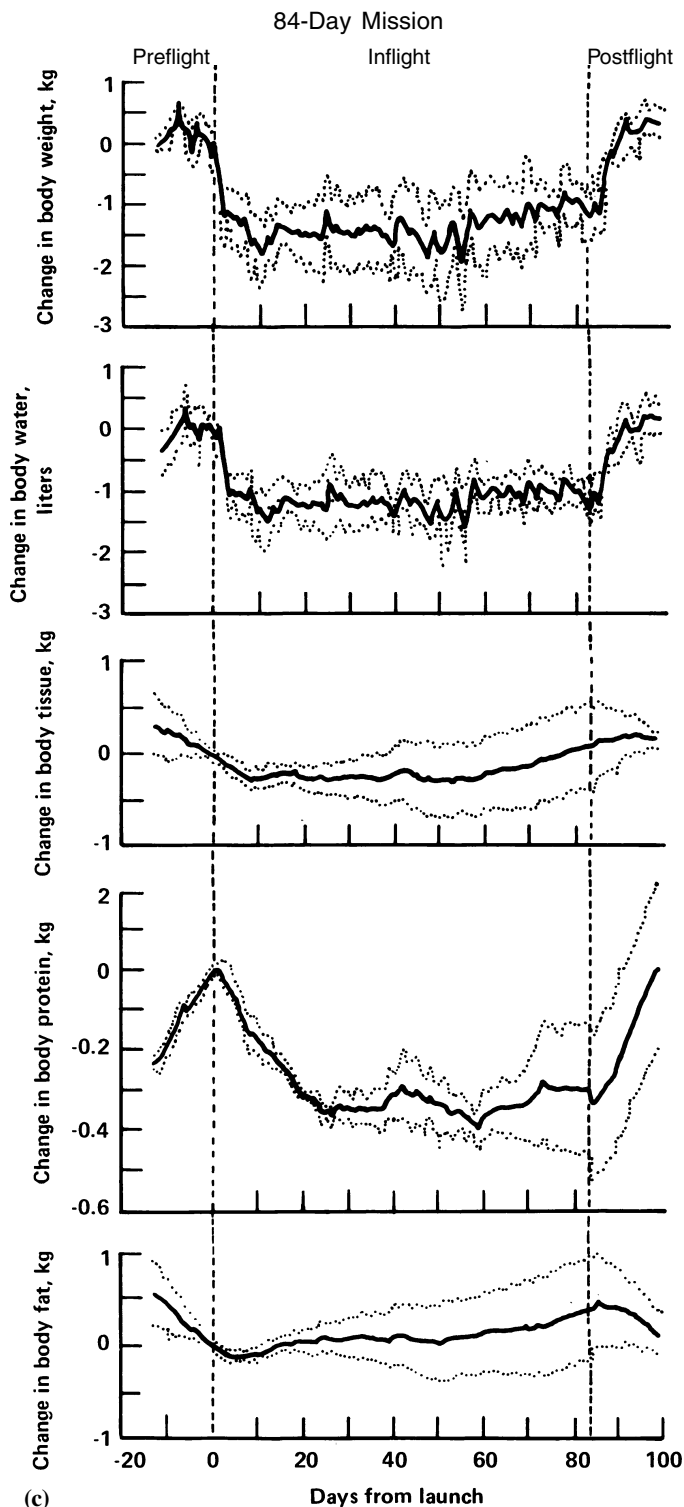
Figure 4-28(c). Body composition changes (mean ± SE) for each Skylab crew (*n* = 3). (c) 84-day mission.

Figure 4-29. Change in body weight as a function of dietary intake for all Skylab crewmen.

4.6.2.8 Estimates of Caloric and Exercise Requirements.

The three Skylab missions, by virtue of their wide variation in dietary intake, exercise expenditure, and weight loss, provided a basis for estimating the minimum caloric food content and exercise required to prevent significant loss of body mass. These estimates were derived by performing linear regression analyses on the inflight dietary intake or exercise levels as functions of the rate of body weight loss. The minimum required levels were estimated by determining the *x*-intercepts of the derived equations, which correspond to a zero change in body mass. Figure 4-29 is an example of the linear regression analyses performed; the normalized daily rate of body weight loss (determined by dividing total mission loss by mission duration) is plotted as a function of normalized daily dietary intake for each of the nine Skylab crewmembers. The line determined by least squares regression can be extrapolated to zero weight loss to determine the caloric intake required to maintain body weight; in this case, the necessary energy intake is 49.5 kcal/day-kg body weight. Additional analyses were performed using body fat and body protein losses as dependent variables and exercise as an independent variable. This analysis was similar to that reported by Whittle [52], who used biostereometrically determined regional body losses rather than whole-body losses to estimate caloric and exercise requirements for the Skylab crewmen.

The assumptions and regression equations used in the analysis are provided in Appendix F.5.1.4, The data used

Table 4-25. Food, Exercise, and Weight Loss Correlations

Variables	Entire mission		First month	
	Regression coefficient	Intercept,[a] kcal/day-kg body wgt.	Regression coefficient	Intercept,[a] kcal/day-kg body wgt.
Caloric intake[b] as a function of				
Change in body wgt.[c]	[d]0.82	49.5	[e]0.67	48.9
Change in fat[c]	0.49	45.7	0.56	44.7
Exercise[b] as a function of				
Change in body wgt.[c]	[e]0.70	4.97	-.018	2.97
Change in protein[c]	[d]0.85	5.67	-0.28	1.34

[a]Zero weight loss

[b]kilocalories per day per kilogram body weight

[c]Grams per day per kilogram body weight

[d] $p < 0.01$

[e]$p < 0.05$

to compute the overall mission regression coefficients are provided in Appendix F, Table F-30. A correlation analysis was also performed using similar data, but for only the first inflight month. This latter data was derived from the analysis that produced Figs. 4-26 and 4-27. Average daily exercise values for the first month were obtained from crew logs, and they are not significantly different from the daily whole-mission means.

The results of this study are summarized in Table 4-25. The first two columns of data are the regression coefficients and zero-weight-loss intercepts, respectively, for the entire mission analysis. The last two columns are the corresponding quantities for the first inflight month of the study.

The following interpretations were derived from this analysis.

a) Regressions using the data from the entire mission suggest that weight, fat and protein loss can be prevented if caloric intake is approximately 46 to 50 kcal/day-kg body weight and if exercise energy expenditure is approximately 5 to 6 kcal/day-kg body weight. By way of comparison, the highest level of caloric intake of any crewmember was 49.7 kcal/d-kg and the highest level of exercise was 5.1 kcal/d-kg. Regressions from the first month of data produce similar caloric requirements for the entire mission, but those for exercise are not statistically significant. These caloric and exercise requirements are similar to those obtained by Whittle [52] and Thornton [10].

Another method of estimating caloric requirements is from the net energy utilization data (Table 4-21 and Table F-23, Appendix F(5)). This quantity accounts for all calories needed for living in space whether derived from ingested food or via tissue catabolism. The average inflight value of this quantity for the nine crewmen is 3127 ± 300 kcal/day. Accounting for the 9% loss of diet calories in urine and feces, a value of 3127 kcal/day × 1.09 = 3410 kcal/day or 47.5 kcal/day body weight is obtained for an estimate of dietary intake with no tissue loss or gain. This value is well within the range of the estimates from the linear regression discussed previously.

b) The correlation coefficients using caloric intake as the independent variable were much larger for both time intervals examined when compared to those obtained using exercise as the independent variable. This result was interpreted to mean that on Skylab, tissue loss may have been dependent on caloric intake and independent of exercise.

c) The strong correlations for exercise obtained over the entire mission interval were probably a result of using data from different mission durations. Dividing tissue losses (the greatest percent of which occur during the first month) by an increasing number of days gives the erroneous impression that the daily rate of loss decreases as mission length increases.

d) The caloric intake requirement of 46 to 50 kcal/day-kg body weight found in this study may be too low. Five of the crewmen consumed diets that fell within this range, but only two showed no fat loss. No astronaut, however, reached the level of 50 kcal/day-kg) body weight. In establishing caloric requirements, the level of exercise and other activity as well as individual variation in basal metabolism and metabolic efficiency must be considered. Not all of these factors were accounted for in this study.

4.6.3 Discussion

4.6.3.1 Major Assumptions. In this study all of the relevant data (body mass, metabolic balance studies for en-

ergy, water, and nitrogen and postflight determinations of changes in body water, electrolytes and density) from the three Skylab missions have been integrated into a series of newly-developed numerical analyses. This has permitted a much greater in-depth answer, than has been heretofore possible to the question: "Why do astronauts lose weight in space"?. Such an analysis allows an interpretation of the weight loss in terms of the major body elements and tissues and is essential for understanding metabolic processes in space, for predicting energy requirements, and for ameliorating weight losses in future missions.

Two major assumptions were made in this analysis:

a) Changes in body protein for use in Eq. (8) were estimated from the cumulative nitrogen metabolic balance. This balance was uncorrected for the approximate 0.5 gm/day of nitrogen lost via shedding of cutaneous epithelium, hair, nails, and various skin secretions [73]. This cumulative uncorrected nitrogen balance has been used by others who have claimed meaningful results [77,78]. While errors in the nitrogen balance method have been hypothesized and discussed [67,79], sources of methodological errors in carefully controlled studies (the results of which are in agreement with the positive preflight nitrogen balances discussed in this report) are not apparent [68,76]. Other similar analyses ([54] and Chapter 4.5) in which body protein was estimated from whole-body exchangeable potassium, potassium balance, body density and body water yielded comparable conclusions to those detailed above and serve to enhance confidence in and to justify the use of uncorrected nitrogen metabolic balances as good indicators of changes in body protein.

b) The daily net energy utilization (Eq. (9)) for each crew member was constant during each phase of the mission. This assumption was justified on the basis that each subject adhered to a fairly strict work and exercise schedule especially throughout the inflight phase [32]. Although not subject to independent verfication, it does allow estimates to be calculated of time-varying changes in body composition which in turn can be subjected to confirmation or challenge by other related evidence.

It should also be noted that daily balances for water and fat were sequentially accumulated without increasing error. This was accomplished by combining daily balances with end-points restricted to whole-body measurements in accord with the suggestions of Hegsted [67]. For example, the sequential accumulation of the daily inflight water balance was forced to agree (by applying correction factors) with the direct measurements of total body water which were obtained at the beginning and end of each mission. Daily weight/mass measurements govern the maximum weight loss composed of the sum of all the body components. The inclusion of energy balance in the body composition analysis ensured that fat losses would be based on the degree of caloric intake deficit [63].

4.6.3.2 Interpretation of Body Composition Changes.

The considerable variability of body composition changes between the different crewmembers and their time course during prolonged spaceflight reflect the complex relationships between diet, exercise, physical condition, and energy balance that are normally observed in terrestrial conditions. In addition, other changes were observed that appear to be unique responses to the weightless environment. Interpretation of the Skylab data, with the view of identifying and isolating the zero-g factors, is made more difficult because each successive crew remained in flight a month longer, exercised longer and harder, and received a larger caloric intake per kilogram body weight. Furthermore, each crew comprised a very small statistical sample. Therefore, differences due to flight duration, exercise levels and caloric intake may be difficult to discern since they could be masked by differences among the particular subjects. Nevertheless, the data does lend itself to a reasonable interpretation which must eventually be verified by more direct measurements.

The results from these analyses can best be discussed in terms of the various body components:

4.6.3.2.1 *Body Water.*

There appears to be an obligatory and consistent loss of approximately 1 liter of *body water* which occurred within the first 2 days after insertion into microgravity. This water deficit was primarily a result of reduced fluid intake because urine and evaporative water losses were equal to or below control levels during this period [9,36]. Where decreased fluid intake and loss of body water was particularly severe in the first few days of flight, likely a consequence of space motion sickness (i.e., in the crew of the 59-day mission), some repletion of body water occurred during the days following resumption of normal drinking.

Over the entire period of 1 to 3 months of flight the body is very close to maintaining water equilibrium as shown by the partitional water balance of Table 4-26. Each major element of the water balance (see Fig. 4-6) can be examined in this format. These results suggest that a slightly negative mean inflight water balance was maintained by means of a decreased fluid intake (–5%) and in spite of a smaller decrease (–3%) in output. Net water output declined, although there was a small increase in urine volume (+2%), because of an estimated and unexpected decrease (–8%) in evaporative water loss (see Chapter 4.2 [14,15]). Table F-5 (Appendix F) provides details of this water balance analysis. Note that the values shown in Table 4-26 are averaged over the entire mission, and therefore, mask the dramatic changes in water balance that occur near launch and recovery.

The reduction in body water was maintained in spite of *ad libitum* drinking throughout a 1 to 3 month period. This observation supports the concept of fluid-regulating mechanisms which are continually responding to relieve an effective central hypervolemia created by the cephalad fluid shift induced by the reduction of gravitational influences [80,81,45]. Cephalad shifts of up to 2 liters of fluid have been reported [10] and could account for the total

Table 4-26. Partitional Water Balance in Skylab Crew

Water Balance, ml/day	Skylab Average	
	Preflight	Inflight
Input:		
Water ingested (food and drink)	2971	2822
Metabolic water	353	350
Output:		
Urine volume	1544	1577
Fecal water	82	68
Evaporative water	1677	1550
Net Water Balance	+21	−23

body water losses if, as seems reasonable, such a water load in the upper body was excessive for normal zero-g health and was eliminated from the body. (The physiology of this feedback pathway is fully described in Chapter 5). Confirmation of a one liter loss of body water was provided by measured inflight reductions in leg volume and postflight decreases in body water, blood volume and intracellular volume [4,45,69].

4.6.3.2.2 *Body Tissue.* *Body tissue* loss was directly related to the difference between net energy utilization and net caloric intake (Eq. (9) and Fig. 4-23). The results support the premise that body fat was the tissue component preferentially used to compensate for energy deficits due to inadequate caloric intake [63]. On average, approximately 3 times as much weight in body fat was consumed than in body protein and the fat provided nearly 6 times as much energy. The catabolism of fat and protein during spaceflight were sometimes, but not always, consistent with predictions of tissue loss based on previous metabolic studies in one-g. On one hand, the *preflight* period was characterized by an adequate diet during periods of exercise training; under these conditions one may have expected the loss of fat and increase in protein mass that was actually measured for the nine-man crew as shown Fig. 4-26 (preflight phase). Also, as expected protein loss was most severe when inflight dietary intake decreased the most from preflight levels. On the other hand, the *inflight* fat losses did not seem to correlate with the individual preflight body fat percentages (i.e., on earth the more fat one has the easier it is to lose) and whole body protein losses during flight did not appear to be related to the amount of exercise performed as they do in one-g (i.e., exercise promotes the build up of muscle mass).

4.6.3.2.3 *Body Fat.* Of all the components examined, the changes in *body fat* showed the most variability between the crews. This undoubtedly reflected the wide range of caloric intake as modified by the varying degrees of exercise performed. (As mentioned above, the plan for a similar rigidly controlled diet throughout all Skylab missions was altered in order to prevent the observed gradual loss of body mass during the flight phase and because of space

motion sickness induced anorexia during the first few days of flight). Based on the gradual decline of body fat, caloric intake was probably inadequate for the crews of the 28- and 59-day missions but sufficient for the crew of the 84-day flight whose fat stores were slightly increased despite their higher exercise levels. In general, there is little evidence to suggest that the body fat changes in spaceflight were influenced by weightlessness; they appear to be entirely explicable in terms of the balance between caloric intake and energy expenditure and were predictable from experiences in one-g [10].

4.6.3.2.4 *Body Protein.* It is well known that atrophy of the *body protein* embodied in skeletal muscle tissue will occur in response to disuse, inadequate functional load, insufficient food intake, and lack of exercise [82,83,84]. The crews of the 3 Skylab missions experienced, to varying levels and at various times, all of these conditions. The protein balance analysis dramatically indicates that protein loss occurred almost immediately after entering weightlessness, that it continued for most of the first month after launch, and thereafter stabilized. The inflight shift to a negative protein balance is supported by other Skylab data such as potassium balance (see Chapter 4.4), and leg volume and calf-girth measurements [44,45] and also finds support from investigations in animals whose hindlimbs were immobilized by casts [82] or suspended from their tails [85]. It is also in keeping with the concept that the large fraction of the body's musculature devoted to opposing gravity is virtually unused in space and disuse atrophy will rapidly occur [86].

The protein losses occurred in spite of a high-protein diet and in the presence of exercise training. This finding appears, at first, to be in conflict with the conclusions reached by other Skylab investigators [10,70] who suggested that exercise training during flight may have prevented even more loss of lean body mass. However, these researchers only measured *leg* volume and strength (as an indicator of whole body lean body mass) at the *end* of the mission. This obscures the result of the present study that the rate of *total body* protein loss during the *first month* was similar for *all* crews and was therefore independent of exercise. Also, by limiting the previous analysis to leg muscles for which exercises were specifically employed to strengthen, losses of body protein external to the legs were ignored. If, as seems likely, leg muscles were relatively better maintained through exercise [70] and the protein loss was from the unused postural muscles in the hips, back and neck, then an analysis based only on leg muscle would be incomplete.

Nevertheless, because each crew member performed some exercise it is not possible to quantitatively predict the zero-g effect of a total lack of exercise. Likewise, it cannot be determined that the exercise performed by the crews of the two longest missions contributed to the stabilization of protein losses after one month or if it was due to a gradual adaptive effect. Furthermore, while a reduced caloric intake appears to exacerbate the protein loss, the evidence does not allow such a firm conclusion that an

increased protein intake would ameliorate that loss. There is no reason to question, however, that exercise does maintain strength, muscle tone, and probably mass in the legs and improves circulation similar to exercise training in one-g [70].

4.7 Conclusions

The findings presented in this chapter suggest that the major components of body composition (water, protein, and fat) undergo significant changes in spaceflight. The kinetics and direction of these changes were different for each component, suggesting different influencing mechanisms. Losses of water and body tissues were significantly greater when temporary anorexia, observed early in flight, was present. Longer term, the body mass of each component appeared to converge toward new equilibrium levels appropriate for the weightless environment, which were modified by the caloric intake and level of activity. On average, the results of this study showed that about 60% of the weight loss measured during all three Skylab missions can be attributed to a loss of lean body mass, and the remainder is derived from fat stores. Since diet and exercise increased with mission length, it was difficult to completely separate the effects of these quantities from any adaptive effects of weightlessness that might have occurred over longer exposures to space. However, as a working hypothesis, the following scenarios are offered:

a) Water losses are obligatory as a result of a normal physiological response to acute cephalad fluid shifts in weightlessness; they occurred soon after launch and were independent of flight duration. They seem to be exacerbated by a short period of deficit fluid intake and may or may not be accompanied by a diuresis.

b) Protein losses are primarily a result of disuse atrophy of postural muscles and may be obligatory in weightlessness. Although overall body protein losses were independent of exercise levels on Skylab, some data indicate that locally applied exercise may have helped to maintain protein mass and muscle strength in specific areas, particularly the legs. Exercise may also have been a factor in causing protein losses to level off after the first month in flight, but this needs to be confirmed.

c) Fat losses are more variable and are probably dependent on the usual and well characterized one-g influences whereby fat stores increase with caloric intake and decrease with exercise. Also, changes in body fat depend on the cumulative effects of a positive or negative energy balance and are therefore, highly time dependent. In contrast to water loss related to cephlad fluid shifts and protein losses related to postural muscle atrophy, fat losses are probably preventable by dietary changes.

d) An anorexia of varying degrees and only partly caused by overt space motion sickness, appeared to be associated with the initial period of weightlessness. When present, the anorexia would augment tissue losses by virtue of a caloric deficiency and enhance water loss as a result of reduced fluid intake.

e) Contrary to earlier expectations, energy requirements for working in space do not appear to be significantly less than those needed to maintain body weight on the ground. The analysis suggest that a caloric intake of 46–50 kcal/day/kg body weight would have prevented significant tissue loss (primarily fat) in the Skylab crew. This conclusion needs to be confirmed in space using well-controlled workloads and a direct means of measuring energy expenditure.

The procedures used in this study to analyze the metabolic balance data admittedly provide only indirect estimates of inflight tissue and fluid loss behavior. This analysis was performed and is being reported because it is unlikely that direct inflight measurements of body composition changes will be accomplished in the near future. It was not originally envisioned by the Skylab researchers that the data used here would provide enough information or resolution to determine time-continuous profiles of changes in the major body constituents. The desire to express body composition changes in this format was driven by the need to validate computer simulations of the fluid-electrolyte model. However, we believe the data analysis portion of those modeling studies, contained in this chapter, represents a contribution in its own right.

References

1. Leach, C. S., and Rambaut, P. C., Biochemical Observations of Long Duration Manned Orbital Spaceflight, *J. American Med. Women's Assoc.*, 30(4): 153–172, 1975.

2. Leach, C. S., and Rambaut, P. C., Endocrine Responses in Long-Duration Manned Spaceflight, *Acta Astronaut.*, 2(1/2): 115–127, 1975.

3. Leach, C. S., Johnson, P. C., and Rambaut, P. C., Metabolic and Endocrine Studies: The Second Manned Skylab Mission, *Aviat. Space & Environ. Med.*, 47(4): 402–410, 1976.

4. Leach, C. S., and Rambaut, P. C., Biochemical Responses of the Skylab Crewmen: An Overview, in *Biomedical Results From Skylab*, Richard S. Johnston and Lawrence F. Dietlein, (Eds.), Sec. IV, *Biochemistry, Hematology, and Cytology*, ch. 23. NASA SP-377, NASA, Washington, DC, 204–216, 1977.

5. Rambaut, P. C., Leach, C. S., and Whedon, G. D., Metabolic Energy Requirements During Manned Orbital Skylab Missions. Life Sciences and Space Research XV, *Proceedings of the Open Meeting of the Working Group on Space Biology*, Pergamon Press, New York, 1977, 187–191.

6. Whedon, G. D., Lutwak, L., et al., Mineral and Nitrogen Metabolic Studies on Skylab Orbital Spaceflights, *Trans. Assoc. American Physicians*, 87, 95–110, 1974.

7. Whedon, G. Donald, Lutwak, L., et al., Mineral and Nitrogen Balance Study Observations: The Second Manned Skylab Mission, *Aviat. Space & Environ. Med.*, 47(4): 391–396, 1976.

8. Rambaut, P. C., Smith, M. C., and Stadler, C. R., Skylab Nutritional Studies, in *Life Sciences and Space Research*, Vol XV, R. Holmquist and A. C. Strickland (Eds.),

Pergamon Press, Oxford, 1977, pp. 193–197.

9. Rambaut, P. C., Smith, M. C., Jr., Leach, C. S., Whedon, G. D., and Reid, J., Nutrition and Responses to Zero Gravity, *Fed. Proc.*, 36(5): 1678–1682, 1977.

10. Thornton, W. E., Anthropornetric Changes in Weightlessness. *Anthropometric Source Book, Vol. 1, Anthropornetry for Designers,* NASA RP-1024, NASA, Washington, DC, 1978, p. 1024.

11. Thornton, W. E., and Ord, J., Physiological Mass Measurements in Skylab, in *Biomedical Results from Skylab*, NASA SP-377, Chapter 19, NASA, Washington, DC, 1977, pp. 175-182.

12. Whittle, M. W., Herron, R. E., and Cuzzi, J. R., Biostereometric Analysis of Body Form: The Second Manned Skylab Mission*, Aviat. Space & Environ. Med.,* 47(4): 410–412, 1976.

13. Whittle, M. W., *The Effects of Prolonged Spaceflight on Human Body Composition*, Ph. D. Thesis, University of Surrey, England, 1978, Available at Biostereometrics Laboratory, Texas Institute for Rehabilitation and Research, Houston, TX.

14. Leonard, J. I., *Skylab Water Balance Analysis*, (TIR 782-LSP-7003, General Electric Co., Houston, TX), NASA CR-167461, NASA, Washington, DC, 1977.

15. Leonard, J.I., *Analysis of Evaporative Water Loss in Skylab Astronauts,* (Rep. TIR 741LSP-7017, General Electric Co. Houston, TX), NASA CR-167462, NASA, Washington, DC, 1977.

16. Behn, C., Gauer, O. H., Kirsch, K., and Eckert, P., Effects of Sustained Intrathoracic Vascular Distension on Body Fluid Distribution and Renal Excretion in Man, *Pfluegers Arch.*, 313(2): 123–135, 1969.

17. Andersson, B., Regulation of Water Intake, *Physiol. Rev.*, 58(3): 582–603, 1978.

18. Hardy, J. D., Gagge., A. P., and Stolwijk, J. A. J., (Eds.), *Physiological and Behavioral Temperature Regulation*, Charles C. Thomas, Springfield, IL, 1970.

19. Berensen, P. J., and Robertson, W. G., Temperature, in *Bioastronautics Data Book*, 2nd ed., J. F. Parker, Jr., and V. R.West, (Eds.), NASA SP-3006, NASA, Washington, DC, 1973, pp. 65–148.

20. Leonard, J. I., *Water Balance Error Analysis*, (TIR 782-LSP-7006, General Electric Co., Houston, TX), NASA CR-160403, NASA, Washington, DC, 1977.

21. Carleton, W. M., and Welch, B. E., *Fluid Balance in Artificial Environments: Role of Environmental Variables*, NASA CR-114977, NASA, Washington, DC, 1971.

22. Hale, F. C., Westland, R. A., and Taylor, C. L., Barometric and Vapor Pressure Influences on Insensible Weight Loss*, J. Appl. Physiol.*, 12(1): 20–28, 1958.

23. Pecoraro, J. N., Aerospace Vehicle Water-Waste Management, in *Bioastronautics Data Book*, 2nd ed., J. F. Parker, Jr., and V. R. West, (Eds.), NASA SP-3006, NASA, Washington, DC, 1973, pp. 915–930.

24. Rapp, G. M., Convective Heat Transfer and Convective Coefficients of Nude Man, Cylinders and Spheres at Low Air Velocities, *ASHRAE Trans.*, 79, pt. 1, 1973, pp. 75–87.

25. Taylor, C. L., and Buettner, K., Influence of Evaporative Forces Upon Skin Temperature Dependency of Human Perspiration, *J. Appl. Physiol.*, 6(2): 113–123, 1953.

26. Carleton, W. M., and Welch, B. E., *Fluid Balance in Artificial Environments. 2: Influence of Physiological Changes Upon Rates of Skin Insensible Water Loss,* NASA CR-115024, NASA, Washington, DC, 1971.

27. Gee, G. F., Kronenberg, R. S., and Chapin, R. E., Insensible Weight and Water Loss During Simulated Spaceflight, *Aerosp. Med.*, **39**(9): 984–988, 1968.

28. Michel, E. L., Rummel, J. A., et al., Results of Skylab Medical Experiment M171-Metabolic Activity, in *Biomedical Results From Skylab*, Richard S. Johnston and Lawrence F. Dietlein, (Eds.), V: Cardiovascular and Metabolic Function, Chapter 36, NASA SP-377, NASA, Washington, DC, 1977, pp. 372–387.

29. Varene, P., Jacquemin, C., Durand, J., and Raynaud, J., Energy Balance During Moderate Exercise at Altitude, *J. Appl. Physiol.*, 34(5): 633–638, 1973.

30. Buderer, M. C., Rummel, J. A., et al., Exercise Cardiac Output Following Skylab Missions: The Second Manned Skylab Mission, *Aviat. Space & Environ. Med.*, 47(4), 365–372, 1976.

31. Rummel, J. A., Sawin, C. F., et al., Exercise and Long Duration Spaceflight Through 84 Days. *J. Amer. Med. Women's Assoc.*, 30(4): 173–187, 1975.

32. Rambaut, P. C., Leach, C. S., and Leonard, J. L., Observations in Energy Balance in Man During Spaceflight, *Amer. J. Physiol.*: *Regulatory, Integrative and Comparative Physiology*, 233: R208–R212, 1977.

33. Nishi, Y., and Gagge, A. P., Effective Temperature Scale Useful for Hypo- and Hyperbaric Environments, *Aviat. Space & Environ. Med.*, 48(2): 97–107, 1977.

34. Bernauer, E. M., Mole, P. A., and Johnson, R. E., Calculation of Metabolic Mixture and Water Balance Using Fortran Programs, *Metabolism,* 16(10): 899–909, 1967.

35. Nadel, Ethan R., and Stolwijk, Jan A. J., Effects of Skin Wettedness on Sweat Gland Response, *J. Appl. Physiol.*, 35(5): 689–694, 1973.

36. Sargent, F., II, Depression of Sweating in Man: So-Called "Sweat Gland Fatigue." *Advances in Biology of Skin*, Vol. III, Eccrine Sweat Glands and Eccrine Sweat, W. Montagna, R. A. Ellis, and A. F. Silver, (Eds.), Pergamon Press, New York, 1962, pp. 163–212.

37. Greenleaf, J. E., and Castle, B. L., Exercise Temperature Regulation in Man During Hypohydration and Hyperhydration. *J. Appl. Physiol.*, 30(6): 847–853, 1971.

38. Nielsen, B., Effect of Changes in Plasma Na^+ and Ca^{++} Ion Concentration on Body Temperature During Exercise, *Acta Physiol.*, Scandinavia, 91: 123–129, 1974.

39. Fasciolo, Juan Carlos, Total, Gregory L., and Johnson, Robert E., Antidiuretic Hormone and Human Eccrine Sweating, *J. Appl. Physiol.*, 27(3): 303–307, 1969.

40. Webb, Paul, Thermal Exchanges and Temperature Stress, *Foundations of Space Biology and Medicine*, M. Calvin and O. G. Gazenko, (Eds.), Vol. 11, Book 1, Ecological and Physiological Bases of Space Biology and Medicine, pt. 1, Influence of an Artificial Gaseous Atmosphere of Spacecraft and Stations on the Organism, Chapter 3. NASA SP-374,1975, pp. 94–126.

41. Saltin, B., Gagge, A. P., and Stolwijk, J. A. J., Body Tem-

peratures and Sweating During Thermal Transients Caused by Exercise, *J. Appl. Physiol.*, 28(3): 318–327, 1970.

42. Kerslake, D. McK., Errors Arising From the Use of Mean Heat Exchange Coefficients in the Calculation of the Heat Exchanges of a Cylindrical Body in a Transverse Wind. *Temperature: Its Measurement and Control in Science and Industry*, vol. 3, pt. 3, Biology and Medicine, J. D. Hardy, Ed., Sec. III, *Tissue Heating and Thermal Sensation*, Chapter 18, Reinhold New York, 1963, pp. 183–190.

43. Leach, C. S., Leonard, J. I., Rambaut, P. C., and Johnson, P. C., Evaporative Water Loss in Man in a Gravity-Free Environment, *J. Appl. Physiol.*, 45(3): 430–436, 1978.

44. Hoffler, G. W., Cardiovascular Studies of U. S. Space Crews: An Overview and Perspective. *Cardiovascular Flow Dynamics and Measurements*, N. H. C. Hwang and N. A. Normann, (Eds.), University Park Press, Baltimore, 1977, pp. 335–363.

45. Thornton, W. E., Hoffler, G. W., and Rummel, J. A., Anthropometric Changes and Fluid Shifts, in *Biomedical Results from Skylab,* Johnston, R. S. and Dietlein, L. F., (Eds.), Chapter 32, NASA SP-377, NASA, Washington, DC, 1977, pp. 330–339.

46. Bohn, B. J., Calder, B. E., et al., *A Study of the Role of Extravascular Dehydration in the Production of Cardiovascular Deconditioning by Simulated Weightlessness* (Bedrest), Part 1, Final Report, Public Health Service Hospital (San Fransisco, Calif.). NASA CR-114808, NASA, Washington, D.C., 1970.

47. Johnson, P. C., and Driscoll, T., *Red Cell Mass and Body Volume Changes After 28 Days of Bedrest*, Report of 28-Day Bedrest Simulation of Skylab, Vol. II, Philip C. Johnson and Cheryl Mitchell, (Eds.), The Methodist Hospital, Houston, TX; NASA CR-151354, NASA, Washington, DC, 1977, pp. E.1–E.29.

48 Snyder, W. S. (chairman): Report of the Task Group on Reference Man. Prepared by a Task Group of Committee 2 of the International Commission on Radiological Protection, Pergamon Press, Oxford, 1975.

49. Berry, C.A., Weightlessness, in *Bioastronautics Data Book*, 2nd ed., J. F. Parker, Jr., and V. R. West, (Eds.), Chapter 8, NASA SP-3006, NASA, Washington, DC, 1973, pp. 349–415.

50. Rambaut, P. C., Heidelbaugh, N. D., Reid, J. M., and Smith, M. C., Jr., Caloric Balance During Simulated and Actual Spaceflight, *Aerosp. Med.*, 44(11): 1264–1269, 1973.

51. Whedon, G. D., Lutwak, L., Rambaut, P. C., Whittle, M. W., Smith, M. C., Reid, J., Leach, C., Stadler, C. R., and Sanford, D. D., Mineral and Nitrogen Metabolic Studies, Experiment M071, in *Biomedical Results From Skylab*, Richard S. Johnston and Lawrence F. Dietlein, (Eds.), Sec. III, Musculoskeletal Function, Chapter 18, NASA SP-377, NASA, Washington, DC, 1977, pp. 164–174.

52. Whittle, M. W., Caloric and Exercise Requirements of Spaceflight: Biostereometric Results From Skylab, *Aviat. Space & Environ. Med.*, 50: 163–167, 1979.

53. Leonard, J. I., Quantitation of Tissue Loss During Prolonged Spaceflight. NASA CR-160402, NASA, Washington, D.C, Also Rep. TIR 741-LSP-9017, General Electric Co. Houston, TX, 1979.

54. Leonard, J. I., Leach, C. S., and Rambaut, P. C., Quantitation of Tissue Loss During Prolonged Spaceflight, *Amer. J. Clin. Nutr.* 38: 667–683, 1983.

55. Calloway, D. H., Basic Data for Planning Life-Support Systems, in *Foundations of Space Biology and Medicine*, M. Calvin and O. G. Gazenko, (Eds.), Vol. III, Space Medicine and Biotechnology, pt. 1, Methods of Providing Life Support for Astronauts, Chapter 1, NASA SP-374, NASA, Washington, DC, 1975, pp. 3–21.

56. Wood, P. D., Haskell, W. L., et al., Plasma Lipoprotein Distributions in Male and Female Runners, *Ann. New York Acad. Sci.*, 301, pp. 748–763, 1977.

57. Ward, G. M., Krzywicki, H. J., et al., Relationship of Anthropornetric Measurements to Body Fat as Determined by Densitometry, Potassium-40, and Body Water, *American J. Clin. Nutr.,* 28(2): 162–169, 1975.

58. Keys, A., and Brozek, J., Body Fat in Adult Man, *Physiol. Rev.*, 33(3): 245–325, 1953.

59. Krzywicki, H. J., Ward, G. M., et al., A Comparison of Methods for Estimating Human Body Composition, *American J. Clin. Nutr.*, 27(12), pp. 1380–1385, 1974.

60. Siri, William E., The Gross Composition of the Body, *Advances in Biological and Medical Physics*, Vol. IV, John H. Lawrence and Cornelius A. Tobias, (Eds.), Academic Press, New York, 1956, pp. 239–280.

61. Muldowney, F. P., and Healy, J. J., Lean Body Mass and Total Body Potassium, in *Compartments, Pools, and Spaces in Medical Physiology*, P.-E. E. Bergner, C. C. Lushbaugh, and Elizabeth B. Anderson, (Eds.), U. S. Atomic Energy Commission, Washington, DC, 1967, pp. 95–109.

62. Black, D. A. K., *Essentials of Fluid Balance*, 3rd ed. F. A. Davis Co., Philadephia, 1964.

63. Grande, F., Energy Balance in Body Composition Changes, *Ann. Intern. Med.,* 68: 467–480, 1968.

63. Johnson, P. C., Rambaut, P. C., and Leach, C. S., Apollo 16 Bioenergetic Considerations. *Nutr. Metab.*, 16: 119–126, 1974.

64. Kollias, J., VanDerVeer, D. V., Dorchak, K. J., and Greenleaf, J. E., *Physiological Responses to Water Immersion in Man, A Compendium of Research*, NASA TM X-3308, NASA, Washington, DC, 1978.

65. Greenleaf, J. E., Bernauer, E. M., et al., Effects of Exercise on Fluid Exchange and Body Composition in Man During 14-Day Bedrest, *J. Appl. Physiol.*, 43(1): 126–132, 1977.

66. Pace, N., Kodama, A. M., et al., Body Composition Changes in Men and Women After 2–3 Weeks of Bedrest, in *Life Sciences and Space Research XIV*, P. H. A. Sneath, (Ed.), Akademie-Verlag, Berlin, 1976, pp. 269–274.

67. Hegstead, D.M., Balance Studies, *J. of Nutrition,* 106(3): 307–311, 1976.

68. Steffee, W. P., Goldsmith, R. S., Pencharz, P. B., Scrimshaw, N. S., and Young, V. R., Dietary Protein Intake and Dynamic Aspects of Whole Body Nitrogen Metabolism in Adult Humans. *Metabolism,* 25: 281–297, 1976.

69. Johnson, P. C., Driscoll, T. B., and LeBlanc, A. D., Blood Volume Changes, in *Biomedical Results From Skylab*, R. S. Johnston and L. F. Dietlein, (Eds.), Chapter 26, NASA SP-377, NASA, Washington, DC, 1977, pp. 235–241.

70. Thornton, W. E., and Rummel, J. A., Muscular Decondi-

tioning and Its Prevention in Spaceflight, *Biomedical Results From Skylab*, R. S. Johnston and L. F. Dietlein, (Eds.), Chapter 21, NASA SP-377, NASA, Washington, DC, 1977, pp. 191–197.

71. Webb, P., Weight Loss in Men in Space, *Science*, 155(3762): 558–560, 1967.

72. Leonard, J. I., *Analysis of Metabolic Energy Utilization in the Skylab Astronauts*, (Report TIR 741-LSP-7018, General Electric Co., Houston, TX), NASA CR-160402, NASA, Washington, DC, 1977.

73. Leonard, J. I., *Energy Balance and the Composition of Weight Loss During Prolonged Spaceflight*, (Report TIR 2114-MED-2012, General Electric Co., Houston, TX); NASA CR-17145, NASA, Washington, DC, 1982.

74. Vanderveen, J. E., and Allen, T. H., Energy Requirements of Man Living in a Weightless Environment. Life Sciences and Space Research X, W. Vishniac, (Ed.), Akademie-Verlag, Berlin, 1972, pp. 105–112.

75. Pace, N., and Rathbun, E. N., Studies on Body Composition III: The Body Water and Chemically Combined Nitrogen Content in Relation to Fat Content, *J. Biol. Chem.*, 158: 685–691, 1945.

76. Krzywicki, H. J., Consolazio, C. F., Johnson, H. L., and Witt, N. F., Effects of Exercise and Dietary Protein Levels on Body Composition in Humans. Report AD-AO65 450/9GA, U.S. Dept of Commerce, Springfield, VA, available from National Technical Information Service, also Letterman Army Institute of Research, San Francisco, CA, 1978.

77. Calloway, D. H., Odell, A. C. F., and Margen, S., Sweat and Miscellaneous Nitrogen Losses in Human Balance Studies, *J. Nutr.* 101: 775–786, 1971.

78. Yang, M. and Van Itallie, T. B., Composition of Weight Lost During Short-Term Weight Reduction: Metabolic Responses of Obese Subjects to Starvation and Low-Calorie Ketogenic and Non-Ketogenic Diets, *J. of Clin. Invest.* 58: 722–730, 1976.

79. Forbes, G. B., Another Source of Error in the Metabolic Balance Method, *Nutr. Rev.* 31: 297–300, 1972.

80. Gauer, O. H., Recent Advances in the Physiology of Whole Body Immersion, *Acta Astronautica,* 2: 31–39, 1975.

81. Pace, N., Weightlessness: A Matter of Gravity, *New England J. Med.,* 297: 32–37, 1977.

82. Booth, F.W., Time Course of Muscular Atrophy During Immobilization of Hindlimbs in Rats. *J. Appl. Physiol.: Respirat. Environ. Exercise Physiol,* 43: 656–661, 1977.

83. Bourne, G. H., The Structure and Function of Muscle, 2nd ed., Academica Press, New York, 1972.

84. Edgerton, V. R., Roland, R. R., Response of Skeletal Muscle to Spaceflight, in *Fundamentals of Space Life Sciences*, Vol 1, S.E. Churchill, (Ed.), Kreiger Pub., Florida, 1997, Chapter 7, 1997, pp. 105–120.

85. Morey-Holton, E. R., and Wronkski, T. J., Animal Models for Simulating Weightlessness. *Physiologist,* 24, Suppl., pp. S45–48, 1981.

86. Jaweed, M. M., Muscle Structure and Function, in *Space Physiology and Medicine*, 3rd ed., Nicogossianm, A.E., Huntoon, C. L, and Pool, S. L., (Eds.), Chapter 16, Lea & Febiger, 1994, pp. 317–326.

Chapter 5
Fluid-Electrolyte Regulation During Long-Term Spaceflight

Throughout the manned space-flight program, there has been a continuous interest in response of the fluid regulating systems of the body to the exposure to weightlessness. In the context of NASA's biomedical program and, indeed, of an integrated view of physiology, the study of body fluid volumes demands the consideration of other related subsystems, including electrolyte regulation, circulatory and renal dynamics, endocrine function, body biochemistry, and metabolism. The Skylab program included the first comprehensive observations performed in space on these systems, and they were also carried out on the longest spaceflight that had been flown up to that time. The purpose of this section is to integrate and interpret the most significant findings of the Skylab studies in terms of the homeostatic relationships that govern body fluid volume and composition.

The Skylab data were evaluated on the basis of comparison with previous spaceflight results and ground-based studies such as bedrest and water immersion, especially in terms of the responses expected from the current understanding of fluid-electrolyte physiology. The data base analysis system (see Chapter 3), and the integrated metabolic balance analysis (see Chapter 4) permitted quantitative descriptions of body composition changes and established correlations between important variables. Preliminary model simulations were also valuable in formulating tentative hypotheses and guiding the data analysis.

One result of the preliminary analysis was identification of several groups of physiological quantities which changed significantly during spaceflight and which could be used to define the fluid-electrolyte status of the crewmen. These groups included body weight losses (total body water, lean body mass); body fluid volumes within the major compartments (blood, extracellular, intracellular, upper body, lower body); and major body electrolytes and their plasma concentrations (sodium and potassium). Another group consisted of hormones that control fluid electrolyte balance (angiotensin, aldosterone, ADH, cortisol); renal excretion of water and electrolytes (rates and concentrations); and water and electrolyte balances (intake, excretion, sweat). The ultimate goal of this analysis was to determine, insofar as possible, the mechanisms and physiological pathways that produced the observed changes in these quantities. A mathematical model that proved most important to this analysis was the modified Guyton model of fluid and electrolyte regulation (see Chapter 3). The capability of this model to simulate many of the responses to weightlessness provided a basis for identifying important regulatory mechanisms and testing hypotheses to explain selected Skylab findings and their apparent inconsistencies.

5.1 Review of Significant Findings

For convenience, the following review of significant findings in the area of fluid-electrolyte regulation will be divided into two categories: pre-Skylab and Skylab findings.

5.1.1 Pre-Skylab Findings

Prior to Skylab, a limited amount of information had been accumulated concerning the body's fluid and biochemical responses to spaceflight. These studies of the astronauts who participated in the Mercury, Gemini, and Apollo missions were designed to provide data relative to the maintenance of flight crew health and safety. The early flights were characterized by technological constraints that made the design of valid physiological experiments nearly impossible. With the exception of two missions, only preflight and postflight measurements were permitted, and there was limited opportunity to provide experimental controls for diet and activity. Therefore, most of the information collected was in the form of observations based on urine and blood analyses and some whole-body measurements, almost all of which were obtained on the ground. From these data, only gross changes could be revealed, and inflight aberrations could only be inferred. The investigation and elucidation of the basic physiological mechanisms responsible for these changes were to be performed on future flights, such as Skylab.

Sufficient data were obtained, however, to demonstrate that spaceflight is associated with significant weight loss, substantial deficits in fluid and electrolyte balance, a variety of endocrine responses, demineralization of bone, and cardiovascular deconditioning [1,2,3,4,5,6]. Water losses [7] were believed to occur principally on the first or second day of flight. On the basis of the rate of body weight recovery during the postflight phase (i.e., the most rapid gains in postflight weight are attributed to water replenishment) it was estimated that $50-85\%$ of the total weight loss during spaceflight could be attributed to water loss. The remaining loss was taken to be catabolism of tissue components (fat and protein), most likely a result of an inadequate diet [7]. In retrospect, it was suggested that a decrease in food consumption during the early period after launch may have been associated with low grade vestibular disturbances and space motion sickness symptoms [8]. Diminished urinary excretion in the immediate postflight period indicates efforts by the body to retain fluid and electrolytes lost inflight. Signs of musculoskeletal atrophy and loss of intracellular content was indicated by decreased total body potassium, a negative nitrogen balance, and reduced intracellular fluid volume. Preflight and postflight measurements of hormones related to fluid and

Table 5-1. Pre-Skylab Hypothesis Concerning Processes Involved in Man's Adaptation in Zero Gravity

Event		Response of Body
Entry into zero gravity. Redistribution of circulating blood volume.		Body attempts to reduce volume. ADH decreases, aldosterone production decreases.
Loss of water, sodium, potassium (loss of body weight).		Decrease in plasma volume. Aldosterone increases (secondary aldosteronism).
Increased sodium retention. Potassium loss continues. Cell: acidotic—extracellular fluid alkalotic		Intracellular exchange of potassium and hydrogen ions. Decrease in bone density, muscle cell potassium, and muscle mass; possibly including cardiac muscle.
Respiratory and renal compensation. Halt to weight loss trend.		Stabilizes with new effective circulating blood volume. New body fluid and electrolyte balance.

electrolyte balance were also consistent with inflight loss and postflight retention. In particular, elevated levels were noted postflight for urinary anti-diuretic hormone (ADH), aldosterone, catecholamines, and plasma angiotensin. These hormones are usually secreted when retention of water and salt is required. Also noted were moderate losses of blood volume (both plasma and red cells). Cardiovascular alterations were indicated by a postflight decrease in orthostatic tolerance and a reduction in exercise capacity.

Following Apollo and before Skylab, a working hypothesis was proposed which presumably accounted for the adaptive changes in the fluids, electrolytes, and hormones [9]. Table 5-1 outlines those parts of the proposed hypothesis related to fluid shifts within the body. Upon initial entry into the weightless environment, the circulating blood volume shifts from the legs and lower abdomen toward the central thoracic regions. This is interpreted by the body as an increase in total circulating blood volume (since "volume" receptors are located in the cardiopulmonary region), which the body attempts to reduce by a decrease in the production of ADH and aldosterone. The result is a loss of water, sodium, and potassium. The accompanying decrease in plasma volume may then produce a secondary aldosteronism. At this point, the body is believed to enter a phase of electrolyte and fluid imbalance, in which sodium retention increases, while potassium loss continues. The extracellular alkalosis that results from such a response may produce an intracellular exchange of potassium and hydrogen ions. At some point, it has been theorized, respiratory and renal compensation could halt the negative balance trend and produce a physiological system that is stabilized. This yields a new effective circulating blood volume and fluid and electrolyte balance.

Prior to Skylab, little was known about the detailed nature and time course of these changes during weightlessness. Also, it was uncertain as to whether the changes represented a new adaptive steady-state, or whether they would progress to the point of adaptive failure somewhere beyond the two to three weeks exposure to weightlessness

studied in previous flights [10]. Missing from the data collected on these early missions were data collected over a period of time sufficient to reflect a reliable baseline for quantitation of inflight urine excretion, inflight biochemical analysis of urine and blood, and sufficient postflight sampling to document the crew's return to normal. The Skylab experiments were designed to study, in greater detail, the aspects of biochemical and fluid regulation that had previously shown the most significant changes. The experiments were also designed to complete, where possible, the incomplete observations of the prior programs. Accordingly, the studies were designed to investigate the mechanisms involved in weight loss, bone demineralization, and altered endocrinological status. More specifically, evaluation of the endocrinological adaptation and other homeostatic mechanisms that control the volume and composition of the body fluids was needed. These objectives were accomplished under the Skylab Bioassay of Body Fluids Experiment by establishing controlled dietary conditions, collecting metabolic excreta and blood samples inflight, and by taking whole body measurements of fluid and electrolyte compartments prior to and after flights. Supporting this study were other related and overlapping experiments in which mineral balances, daily body mass, blood volumes, and leg volume measurements were performed.

5.1.2 Major Skylab Findings

The findings described below summarize the most important results of the Skylab studies related to fluid-electrolyte regulation. The original findings, as reported by the principal investigators, are available to the interested reader [Refs. 11–19]. New analyses of these data are presented here to permit a description of both the short and long-term responses to spaceflight. Obtaining a composite picture of these responses, based on the nine Skylab crewmen, was preferable in most instances to comparing each three-man crew to explain the differences between flights. This data analysis served as a starting point for defining the scope of the general systems analysis.
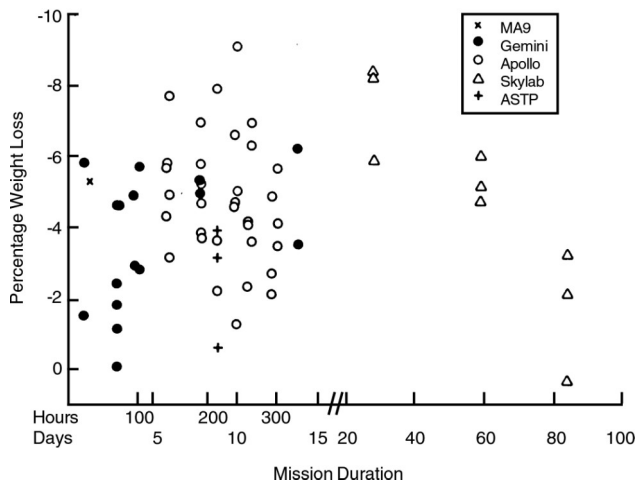
Figure 5-1. Percentage weight loss of U.S. space crewmen as a function of mission duration, based on preflight (usually the mean of multiple values) and immediate postflight weights [16]. No correlation exists between weight loss and mission length for flights up to two weeks. On the Skylab missions weight loss diminished with flight duration but this was likely caused by increased dietary intake rather than an effect of weightlessness. Data was collected in period 1963-1975.

5.1.2.1 Weight Loss. Weight loss has been one of the most commonly observed findings in astronauts returning from spaceflight, regardless of flight duration. Figure 5-1 shows the percentage weight loss compared to mission duration for all U.S. space crewmen through 1975 [16]. The average measured weight loss has been 2.8 kg, or 3.8% of preflight body weight. Although Fig. 5-1 suggests that weight loss may diminish for the longest flights, this is presumably not caused by any adaptive effects. Rather, it is caused by the fact that the dietary intake was increased on those flights; hence, fat loss was significantly reduced.

Skylab permitted the first inflight measurements of body mass. The analysis of the components of this weight loss (presented in Chapter 4.6), was based both on direct whole-body measurements and on indirect metabolic balance data. One of the conclusions from that analysis was that more than half of the weight loss was derived from lean body mass and the remainder from fat stores. Inasmuch as lean body mass contains the most significant amounts of water and electrolytes, the losses of this tissue component are of crucial interest in understanding the fluid-electrolyte disturbances which occur in spaceflight. Some of the major components of the lean body mass loss in the Skylab crew are summarized in Table 5-2.

About half the total weight loss occurred within the first two days of flight, and it was apparently due to water loss. The remaining loss occurred more gradually over the duration of the missions and was attributed to both fat and protein depletion. As demonstrated by inflight metabolic balances of nitrogen and potassium, the most significant losses of protein stores occurred during the first several weeks.

5.1.2.2 Body Fluids. The loss of body water was studied in considerable detail in Chapter 4, since it provides major clues to understanding the headward shift of fluids, the fate of electrolytes, renal function, and endocrine regulation. The dynamic behavior of body water was derived from consideration of water balance data and is shown in Fig. 5-2 for the first 28 days of flight. (This time period was examined closely for much of the data presented here, because it is the longest continuous period in which all crewmen from the three missions can be included.) A loss of between 1.0 and 1.4 liters occurred rapidly and then essentially stabilized at the reduced level with a tendency toward partial recovery. A greater initial loss of water was associated with the crewmen who exhibited space motion sickness and drank less fluid.

While body water changes could be estimated during flight, the fluid compartments of the body were measured only after the crewmen returned to earth. This information is summarized in the composite analysis of Table 5-2. Interpretation of these results is confounded by the fact that fluid compartments are labile and probably subject to rapid changes as a result of reentry forces. Therefore, these results, based primarily upon measurements performed on the first day of recovery may not truly reflect the magnitude of changes incurred inflight. This was exemplified in the detailed water balance analysis (see Table 4-4) that indicated that the inflight loss of water was probably closer to 1.1 liters rather than the 0.8 liter shown in Table 5-2. This discrepancy may be explained by assuming partial replenishment of water from drinking prior to the postflight isotope dilution studies.

Significant postflight decrements were found in blood volume (–590 ml), extracellular (–330 ml), and intracellular fluid (–480 ml). Interstitial fluid volume did not appear to change appreciably. Blood volume loss was caused by a combination of plasma volume and red cell mass loss. Hemoglobin concentration measurements, performed inflight, indicate that plasma volume losses of 10 to 15% occurred within the first few days and may have been rather stable thereafter. However, red cell mass appears to have been lost more gradually (–11%) over the course of the entire mission (see Chapter 6). During the two-week postflight period, blood volume and intracellular fluid volume recovered completely. Blood volume replenishment was primarily a result of over-recovery of plasma volume, since less than 20% of the red cells lost during spaceflight were regained during this time.

5.1.2.3 Fluid Redistribution. Headward shifts of fluid in weightlessness were documented for the first time by leg volume measurements performed on the crew of the 84-day Skylab mission. Most, if not all, of the body fluid deficit could be attributed to losses in the lower limbs.There is growing evidence from ground-based studies, such as water immersion, that a significant fraction of the fluid shifted headward from the legs is excreted from the body. Postural change is usually associated with an acute fluid volume shift of 600 to 800 ml. The fluid volume that shifted from the legs after several days of weightlessness appears to be

Table 5-2. Changes In Fluid and Electrolyte Compartments In Skylab Crew (N - 9)

Quantity	Inflight Losses*	Postflight Gains**
Leg Volume (ml)	-1500	+1500
Blood volume (ml)***	-590	+590
Red Cell Mass (ml)	-230	+240
Plasma Volume (ml)	-360	+550
Intracellular Water (ml)***	-480	+530
Extracellular Water (ml)***	-330	+590
Interstitial Water (ml)***	+30	+50
Total Body Water (ml)	−820	+1120
Exchangeable Body K^+ (meq)	-240	+164
Extracellular Na^+ (meq)***	-90	+100
Body Mass (gm)	-2630	+1840

  * Measured from preflight to recovery day (average mission length = 57 days)

  ** Measured from recovery day to two weeks postflight

*** Measured indirectly

much greater (about 1.8 liters). This implies that there are greater reserves of mobilized fluid than previously recognized. A mean leg volume loss of 1.5 liters for all nine crewmembers was found just after reentry, and this was almost completely regained within the first postflight week.

There are two important questions that were not completely resolved from these studies. The contribution of each major leg compartment (blood, interstitial, intracellular) to the initial loss of leg volume is still undetermined. It was also not determined how much of the fluid shifted was not excreted from the body and in which compartments of the upper body it may have been stored. The puffy tissues of the face and distended head and neck veins of the crewmen suggested that these regions were involved as storage depots. An expanded fluid volume in the upper body, if sustained and not accommodated, could have adverse consequences on pulmonary function, cardiac function, and volume receptor pathways.

5.1.2.4 Altered Water Balance. Body fluid loss was expected to result from increased renal excretion. However, a diuresis was not recorded in the 24-hour pooled urine samples obtained for each crewmember early in the mission (see Chapter 4.2). In fact, urinary excretion was diminished for the first ten days of the mission (see Fig. 5-3). The loss of body water during the first two days primarily resulted from a deficit intake of fluid. Evaporative water loss increased significantly for several days during the first week, mainly as a result of increased ambient temperatures in the orbital workshop when a heat shield malfunctioned on the first mission. However, due to a corresponding decrease in excretion this did not result in further body water losses. The three-month averages as shown in Fig. 5-3 indicates that essentially a zero water balance was achieved at new equilibrium levels for intake (slightly diminished compared to preflight), output (slightly increased), and evaporative water loss (decreased

10%). During the first few days of the postflight period, water was regained because of enhanced intake and diminished excretion, similar to results found in earlier flights.

5.1.2.5 Electrolyte Losses. Of all physiological changes seen during and after spaceflight, probably the most reliable clues to the mechanisms involved are offered by an examination of the electrolyte response. Loss of extracellular fluid is always accompanied by its major cation, sodium. Potassium, nitrogen, and magnesium are located primarily in the intracellular spaces. Loss of these quantities is assumed to reflect muscle degradation, a process known to occur during gravity unloading. Calcium and phosphorus losses are useful indicators of bone demineralization.

Of these substances, sodium and potassium were subjected to a more careful analysis (see Chapter 4.3). Exchangeable body potassium decreased about 240 meq (6.4%) from preflight levels, indicating a significant loss of cellular mass (see Table 5-2). A net loss of approximately 100 meq of sodium occurred from the extracellular space, and all of this was regained during the two-week postflight period. The time course of these changes is summarized in Fig. 5-2. There is an expected correspondence between total body water and sodium dynamics, since these quantities are believed to be associated with extracellular fluids, especially during periods of rapid changes. While body water and sodium appear to stabilize after the initial inflight disturbance, body tissue, as exemplified by potassium loss, continues to decline gradually. It was shown in Chapter 4.5 that potassium and nitrogen losses are essentially parallel. This might be expected for a generalized degradation of muscle tissue. Two quantities that were expected to be highly correlated, but were not, were cell water loss and potassium loss; more intracellular water should have accompanied potassium loss if their normal ratios were maintained.

Table 5-3. Average Daily Net Metabolic Balances of Intracellular Minerals [20]

	Preflight (N = 9)	1st Inflight Month (N = 9)	2nd Inflight Month (N = 6)	3rd Inflight Month (N = 3)
Nitrogen (g)	3.2	-1.7	0.2	0.2
Potassium (meq)	17.0	4.0	9.3	8.7
Calcium (mg)	8.0	-18.0	-170.0	-168.0
Phosphorus (mg)	180.0	-24.0	64.0	20.0
Magnesium (mg)	26.0	16.0	25.0	15.0
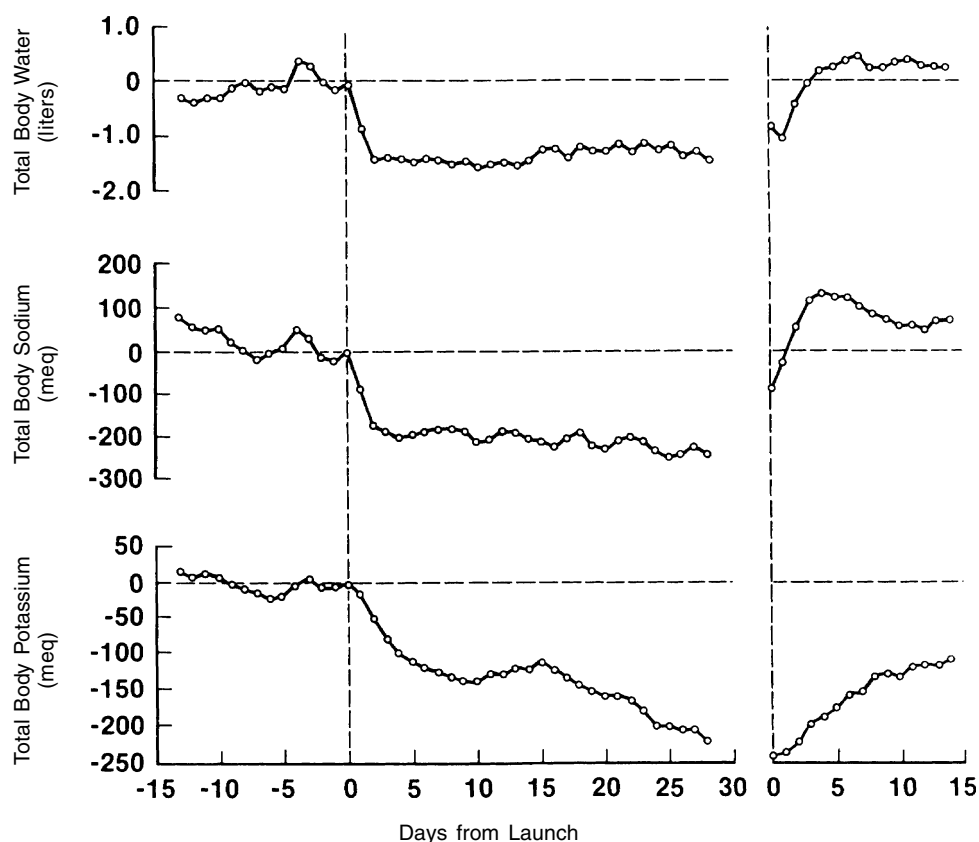
Figure 5-2. Changes in total body water, body sodium and body potassium for the entire Skylab crewmembers during preflight, the first inflight month, and recovery. Values shown are changes from morning of launch. Data was obtained by the indirect metabolic balance method (see Chapter 4).

The changes in metabolic balance (intake minus excreta) for the major intracellular electrolytes, calcium, phosphorus, nitrogen, and magnesium are shown in Table 5-3. While the loss of electrolytes represents significant changes in the body's physiology, it does not significantly contribute to the overall loss in body weight. Calcium metabolism and its loss in spaceflight will be treated in a separate section of this document (Chapter 4.4).

5.1.2.6 Plasma and Urine Analysis. Analysis of weekly blood samples and daily urine collections also reflected disturbances in the fluid-electrolyte system. These represent the first systematic collection of inflight body fluid specimens under somewhat controlled conditions during the space program. Plasma electrolyte concentrations are very useful in interpreting metabolic and hormonal alterations. Elevations in plasma levels were noted for potas-
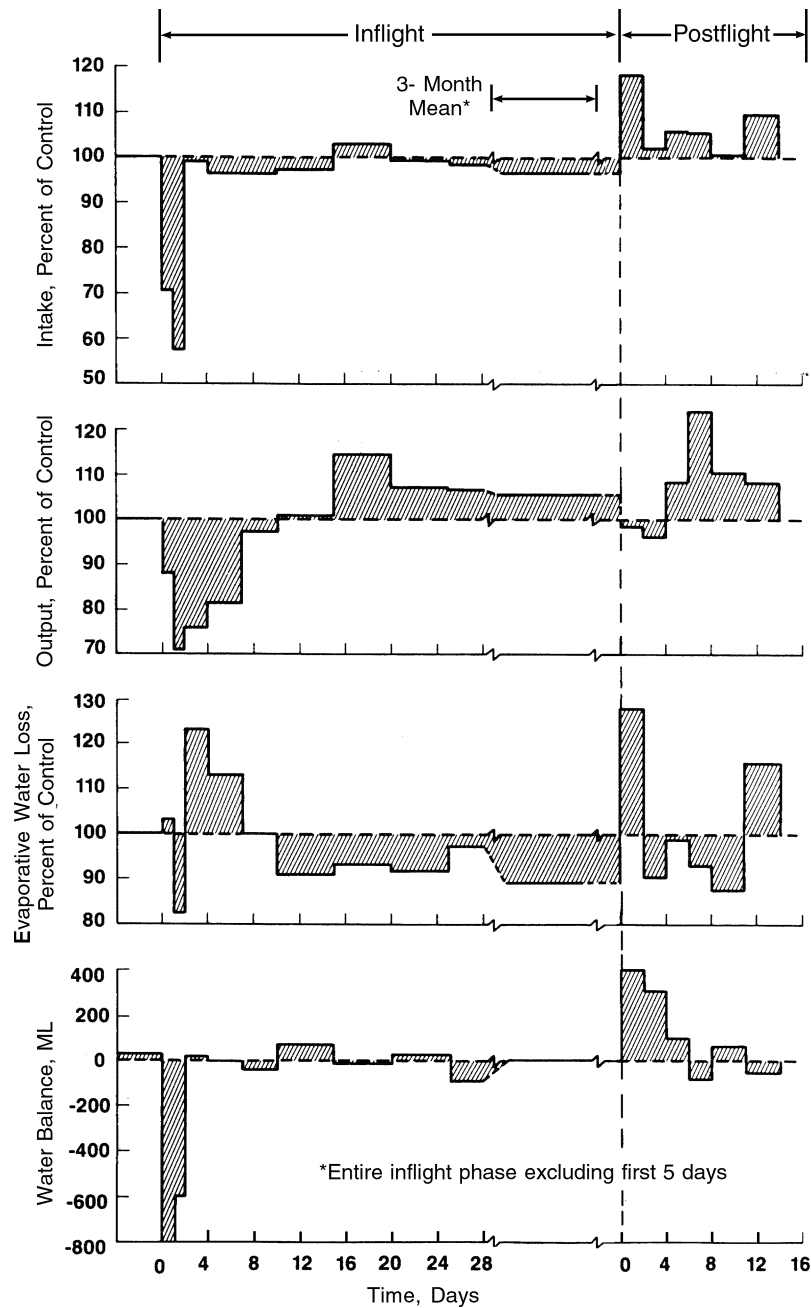
Figure 5-3. A composite water balance analysis of the Skylab crew ($N = 9$). Percent changes from control are indicated for the first 28 days and two weeks postflight. Also shown is the average three-month inflight mean that provides insight into long-term changes of intake, excreta and evaporative water loss during a time when the water balance is essentially zero. Intake includes drinking water, water in food and metabolically produced water. Output includes both urine and fecal water. Evaporative water loss was estimated indirectly (see Chapter 4.2).

Table 5-4. Changes In Plasma Electrolyte Concentrations In Skylab Crew (*N* = 9)*

Electrolyte	Preflight	Inflight
Na$^+$ (meq/l)	142.2 ± 2.6	137.7 ± 1.5**
K$^+$ (meq/l)	4.07 ± 0.13	4.23 ± 0.12**
Ca^{++} (meq/l)	9.52 ± 0.31	10.23 ± 0.23**
PO$_3^=$ (meq/l)	3.35 ± 0.54	3.96 ± 0.54
Cl$^-$ (meq/l)	100.3 ± 5.3	95.7 ± 1.7**
Osmolarity (mosm/l)	291.0 ± 2.8	286.4 ± 3.1**

* Means ± SD
**Inflight significantly different than preflight (p < 0.05)

sium, calcium, and phosphate, constituents that are normally associated with intracellular metabolism (see Table 5-4). The plasma concentration of the major extracellular salt, sodium chloride, was found to be reduced as was the plasma osmolarity. Elevated rates of renal excretion were found for all electrolytes (sodium, potassium, calcium, phosphates, and magnesium) during the flight period (see Fig. 5-4); all except calcium were reduced during the period following recovery. Loss of body protein is indicated by elevated urine creatinine and total urinary nitrogen. Uric acid was one of the few metabolites showing a decreased rate of renal excretion. Taken as a whole, these findings suggest loss of lean body mass constituents and degradation of tissues. However, unless all the routes of metabolism are examined, it is not possible to quantitatively estimate rates of loss by analyzing either plasma or urine composition alone.

5.1.2.7 Endocrine Function. Endocrine changes that reflected alterations in fluid-electrolyte status, physical stress, and tissue metabolism were observed in analyses of blood and urine. Examination of the data from the first month inflight (Fig. 5-5) revealed elevations in plasma angiotensin, urinary aldosterone, and urinary cortisal throughout this period; the highest levels were reached early inflight and on the first or second day of recovery. Urinary ADH was elevated during the first week inflight, but was depressed during the latter half of the first month. All the hormones shown in Fig. 5-5 reached maximum values on the first or second day of recovery. These substances are released during periods of general stress, but they are also sensitive to specific stressors, including plasma levels of electrolytes and blood pressures.

In many cases, the measured levels of these hormones can be plausibly correlated with other known changes. For example, increased angiotensin and aldosterone can account for the elevated renal potassium rates of excretion. Elevated cortisol levels undoubtedly contributed to muscle catabolism and increased nitrogen and potassium loss. The behavior of ADH qualitatively exhibits the expected inverse correlation with urine output during the inflight and postflight period (compare Figs. 5-3 and 5-5(a)). The elevation of the catecholamines (epinephrine

and norepinephrine) early in flight and on the day of recovery, together with cortisol changes, indicated acute stress responses.

Complete interpretation of these changes is impeded because of the multiple competing factors that influence hormonal secretion rates and the various target sites they affect. In some cases, paradoxical changes appear to exist with respect to known concepts of physiology and the working hypothesis discussed earlier. For example, angiotensin is a powerful vasoconstrictor in addition to its action as an aldosterone stimulator. It is usually released in response to hypovolemia, so it is not clear why angiotensin is elevated in microgravity (and also bedrest), at a time when there is a tendency for central blood volume expansion. ADH is also a potent pressor agent, in addition to its known effects on water excretion. However, this hormone is depressed, during periods when angiotensin is elevated. In addition, the behavior of ADH was quite different on the three missions, as indicated in Fig. 5-6. ADH levels were elevated on the shortest mission, but were reduced throughout the other two missions. In another case, aldosterone is a well-known promoter of renal sodium retention. Therefore, the elevated levels of aldosterone are inconsistent with the enhanced excretion of sodium. This is possibly evidence of a previously suggested natriuretic factor which may be operative in spaceflight.

5.1.2.8 Renal Function. Alterations in renal function during Skylab were indicated by minor changes in creatinine clearance, low levels of uric acid in urine and plasma, and increased secretion of angiotensin. As discussed above, the fluid-regulating hormones and the degree of water and salt excretion all were altered during the entire three-month period of study. However, there is no firm evidence at present to warrant the belief that renal function was impaired. Rather, renal function was probably responding to the demands of removing ordinary waste products from the body in addition to the extra demands of removing products created by the adaptive spaceflight processes. An understanding of renal function in the weightlessness environment is made more difficult by the necessity to study the large quantities of biochemical agents which control and are controlled by the kidneys as well as the complex-
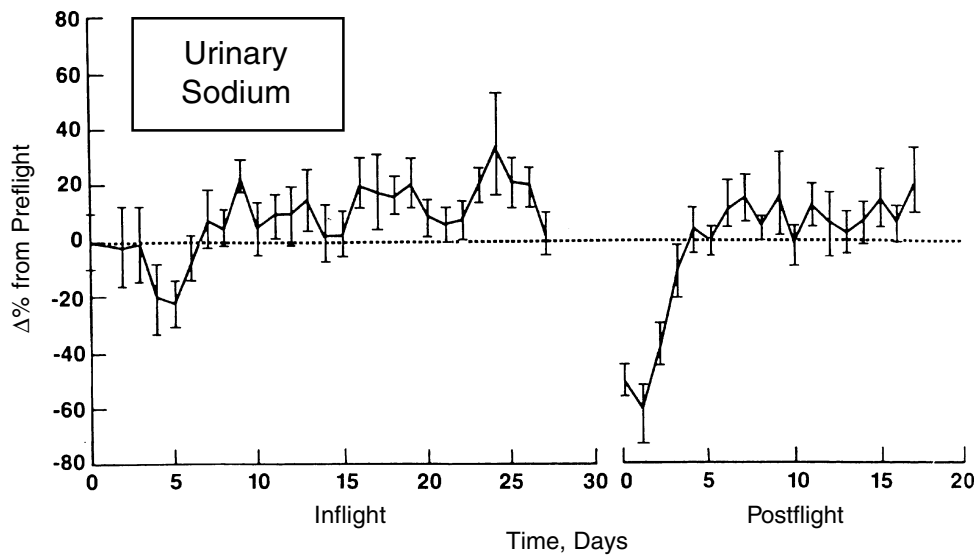
Figure 5-4 (a). Urinary sodium
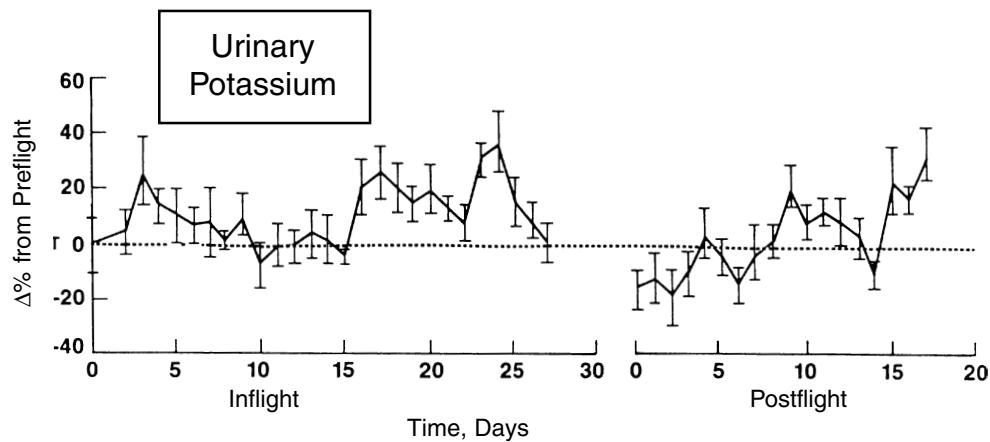
Figure 5-4(b). Urinary potassium
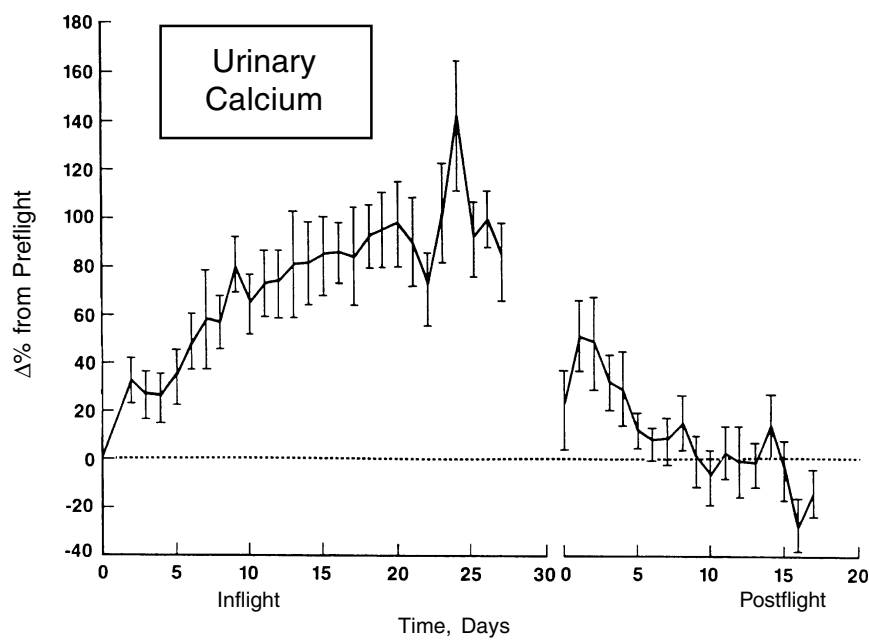
Figure 5-4(c). Urinary calcium

Figure 5-4. Daily changes in urine electrolytes as measured in 24-hr pooled specimen and expressed as percent change from preflight mean. Results for the mean (±SE) of the nine Skylab subjects are provided for the first 28 days inflight and two weeks of postflight recovery: (a) urinary sodium, (b) urinary potassium, (c) urinary calcium, (d) urinary magnesium, (e) urinary phosphate and (f) urinary osmolarity.
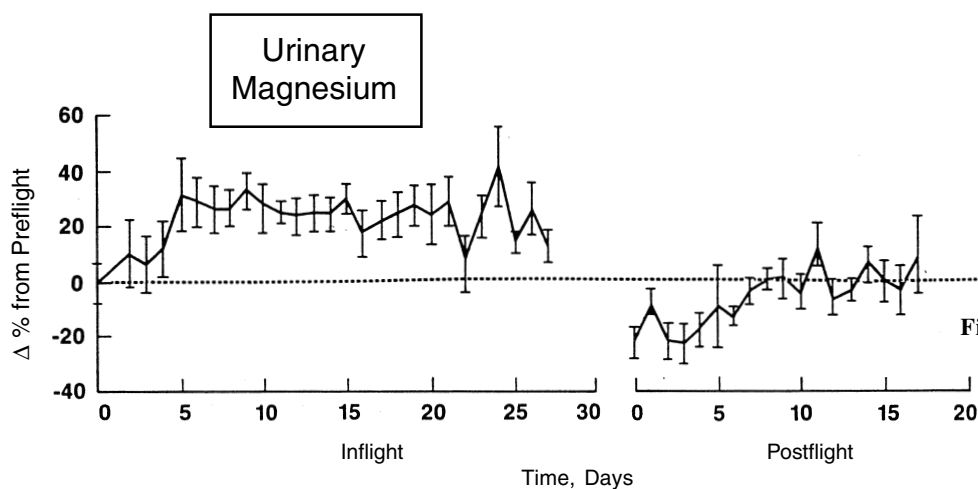
Figure 5-4(d). Urinary magnesium
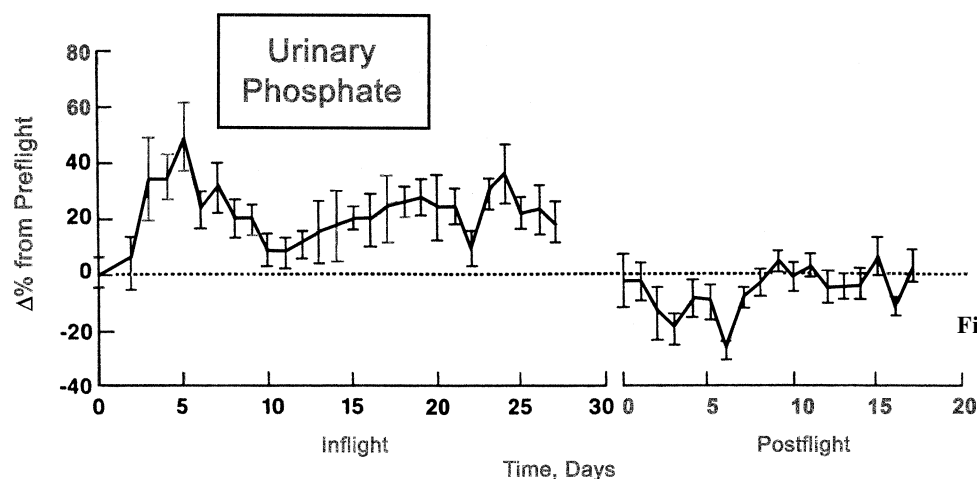
Figure 5-4(e). Urinary phosphate
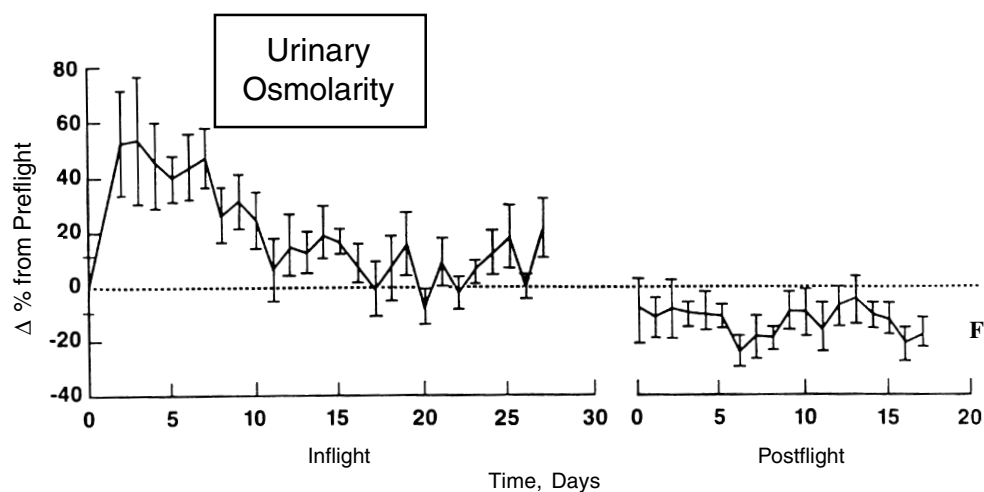
Figure 5-4(f). Urinary osmolarity

Figure 5-4 continued. Daily changes in urine electrolytes as measured in 24-hr pooled specimen and expressed as percent change from preflight mean. Results for the mean ($\pm$SE) of the nine Skylab subjects are provided for the first 28 days inflight and two weeks of postflight recovery: (a) urinary sodium, (b) urinary potassium, (c) urinary calcium, (d) urinary magnesium, (e) urinary phosphate and (f) urinary osmolarity.
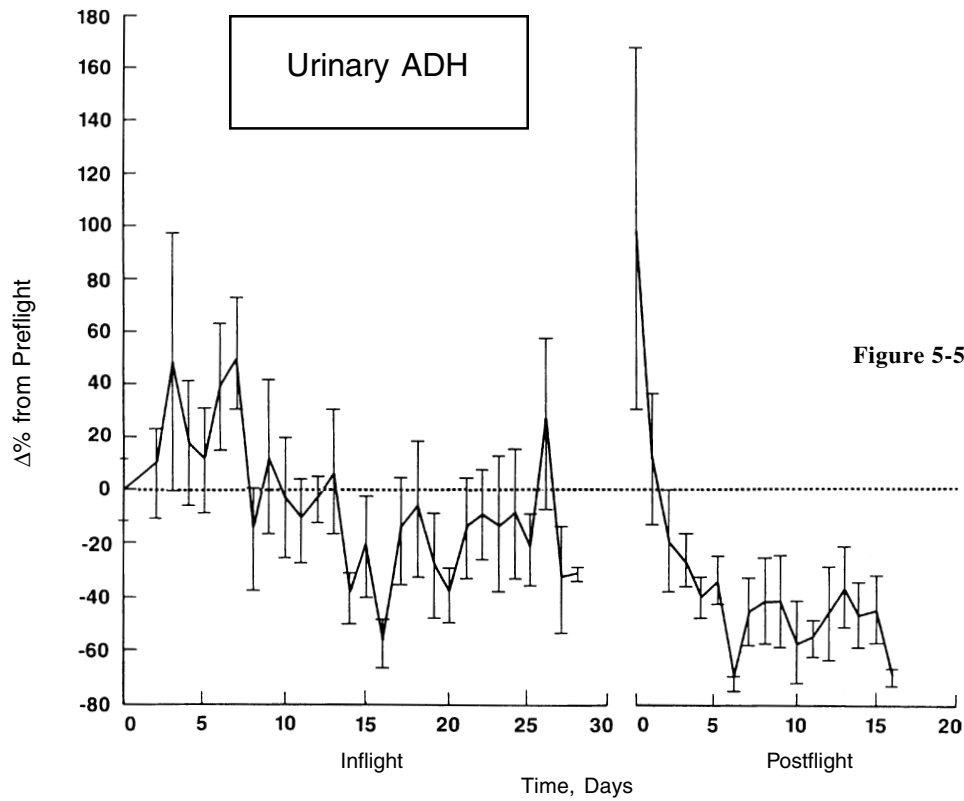
Figure 5-5(a). Urinary ADH
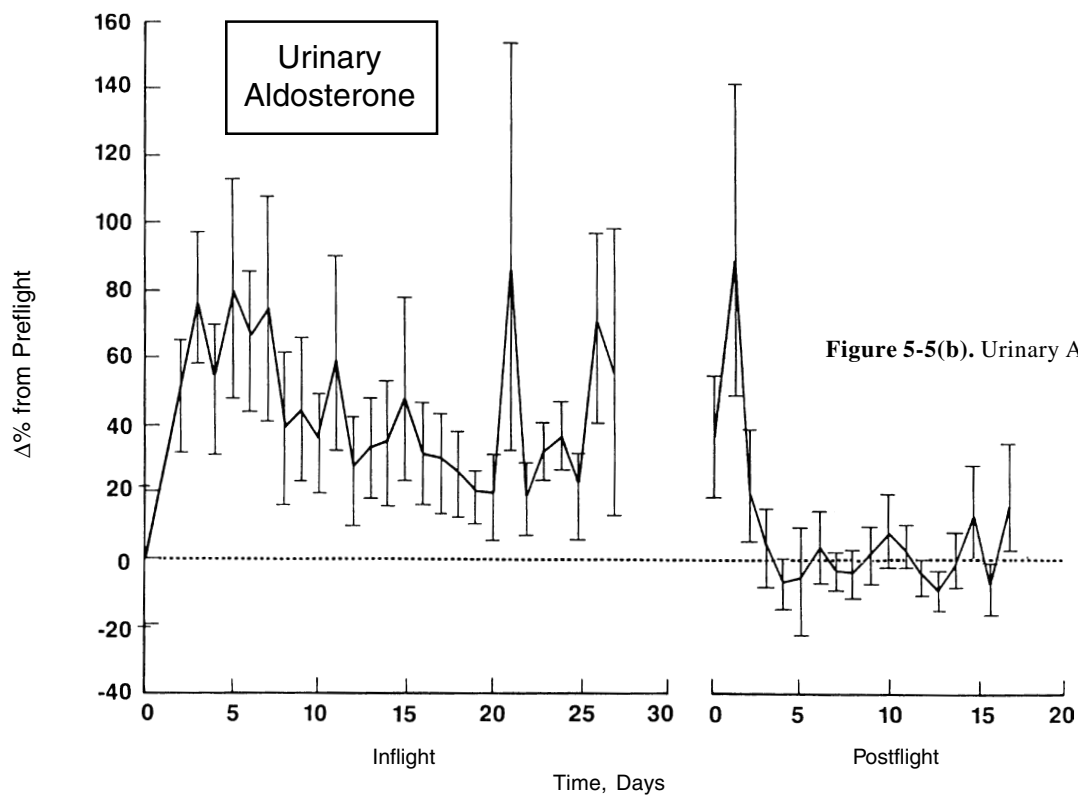
Figure 5-5(b). Urinary Aldosterone

Figure 5-5. Hormone changes in the Skylab crew ($N = 9$) for the first 28 days inflight and the two weeks of postflight recovery. Results are expressed as percent changes from the preflight mean: (a) urinary antidiuretic hormone; (b) urinary aldosterone; (c) urinary cortisol; (d) plasma angiotensin.

Figure 5-5(c). Urinary Cortisol

Figure 5-5(d). Plasma Angiotensin
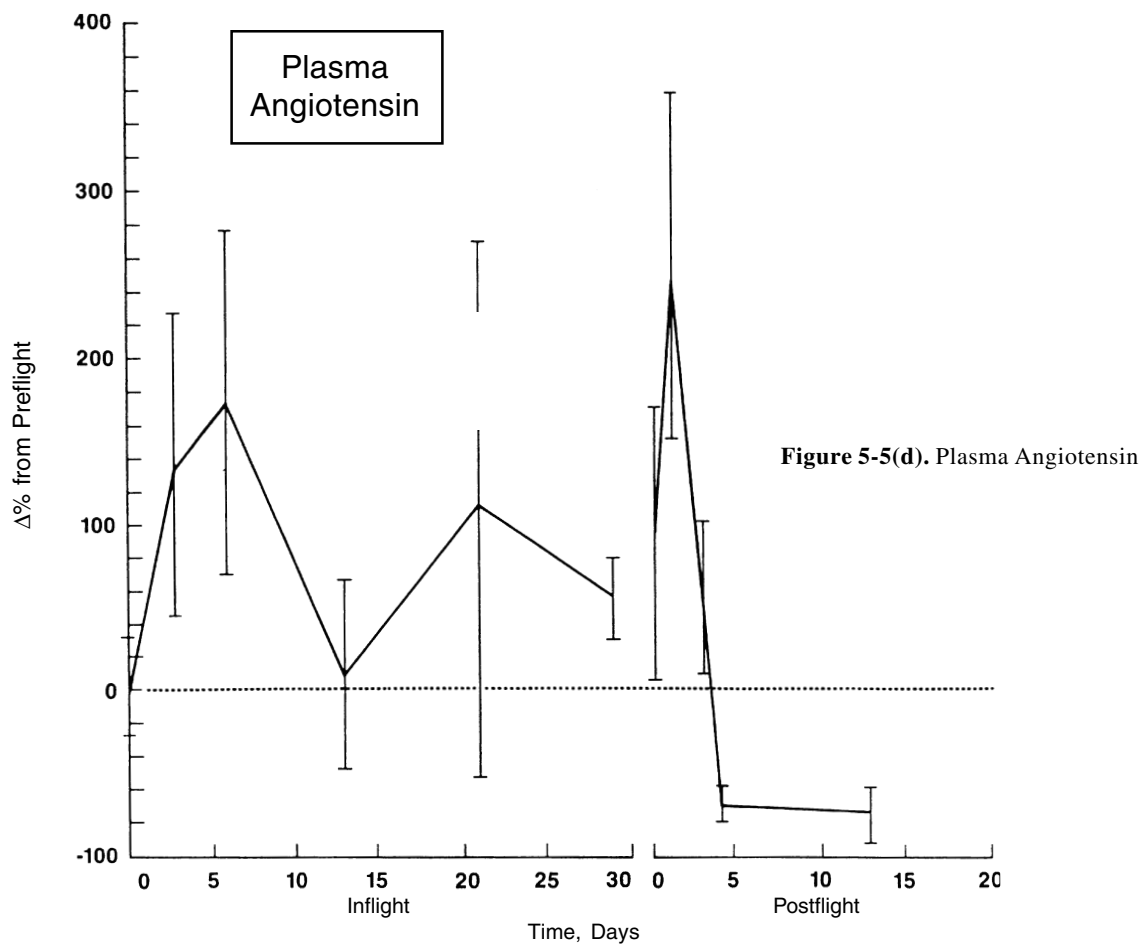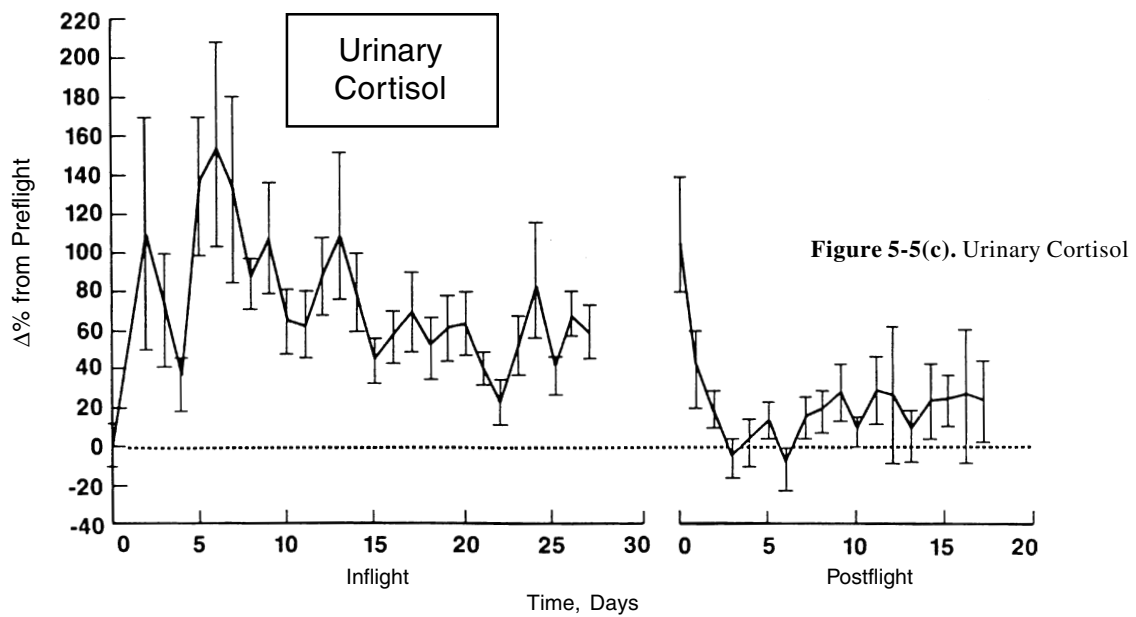
Figure 5-5 continued. Hormone changes in the Skylab crew ($N = 9$) for the first 28 days inflight and the two weeks of postflight recovery. Results are expressed as percent changes from the preflight mean: (a) urinary antidiuretic hormone; (b) urinary aldosterone; (c) urinary cortisol; (d) plasma angiotensin.

Figure 5-6. Comparison of variation of urinary ADH in the Skylab crew ($N = 3$) during first inflight month of each mission. Values are expressed as percent change from preflight mean.

hypothesized changes were indeed intensive enough to produce the expected response. The following section provides state-of-the-art descriptions of the general control systems involved. These are related to particular events that are known or suspected to have occurred during spaceflight. Finally, there will be a discussion of how conceptual and mathematical models were utilized in an attempt to answer the questions posed in Table 5-5, and to arrive at an integrated hypothesis for explaining the circulatory, fluid, and electrolyte responses during weightlessness.

5.2 Systems Analysis of Circulatory, Fluid, and Electrolyte Regulation

This section summarizes the major feedback control mechanisms involved in maintaining body fluid volume homeostasis. The purpose of this analysis was to identify the physiological pathways that should be considered in the interpretation of the Skylab data and to suggest which of those might predominate in the acute and longer-term responses. This analysis was also designed to suggest hypotheses that could be tested with the mathematical model and to reveal additional mechanisms that were not originally included in the simulation models. The following analysis discusses all of the assumptions of the regulatory system that were the basis for the zero-g hypotheses. The writings of Dr. A.C. Guyton and co-workers and detailed examination of the Guyton model were extremely useful in preparing this study [21,22,23]. However, other viewpoints of overall fluid volume control were included to provide a necessary balance to this still controversial subject [Refs. 24–32].

5.2.1 Overall Regulation of Water Balance

The water balance of the body depends on volume control in the several body fluid compartments (see Fig. 5-7) but most importantly, it depends on the control of blood volume. Blood volume regulation is accomplished by feedback control of three components: fluid intake, renal excretion, and transcapillary fluid movement between plasma and interstitial compartments. (Control of the red cell volume is deferred to a later chapter.) The interstitial fluid compartment has been regarded as an adjustable segment in the total water content of the body, capable of receiving large quantities of fluid in cases of blood volume overload or acting as a reservoir to transfer fluid to the circulation in cases of dehydration. Evidence for this regulatory role of interstitial fluid in the long-term control of overall body water is not as strong as it is in the acute case, since lymph flow, transcapillary forces, and the physio-chemical forces of the interstitium tend to return interstitial fluid to normal. The intracellular compartment appears to maintain a fairly constant volume. However, the requirement for osmotic equality between intracellular and extracellular fluid is often accomplished by volume adjustments between these two compartments. Increases in extracellular osmolarity, for example, will cause the osmotic transfer of intracellular fluid into the extracellular pool. Neither the volume, total electrolyte content, nor

ity of the regulatory processes associated with that organ. A major emphasis of the present study was directed toward the systematic study of these processes.

5.1.3 Identification of Problem Areas. Examination of the Skylab findings resulted in a comprehensive list of experimental observations some of which, on the surface, appeared paradoxical and whose etiology was not obvious. A representative portion of this list is summarized in Table 5-5. The subsequent analysis which was necessary to resolve the critical questions listed in the second column of Table 5-5 requires addressing various elements of the circulatory, fluid, electrolyte, hormonal, and renal systems. It is no longer adequate to answer any one of these questions without considering the effects on other related systems. A more specific analysis must include all the factors known to determine particular physiological responses and these factors must be put into the context of a total integrated control network. These pathways must be analyzed quantitatively to determine if certain observed or

Table 5-5. Important Observations and Critical Questions Identified In Analysis of Fluid-Electrolyte Systems

Observation	Questions for the Analysis
Significant losses of water, sodium, and potassium were measured directly or indirectly in the Skylab crew.	i) What was the overall magnitude and time course of the losses? ii) From what body compartments did these quantities originate? iii) What components of the metabolic balance were most significantly altered: intake, excretion, or sweat losses? iv) What regulatory mechanisms were predominantly involved in controlling the initial loss of fluids and electrolytes as well as in the final approach toward a new homeostatic level?
After the first several days of flight, the inflight phase was characterized by somewhat higher excretion rates of fluids and major electrolytes.	i) Does this imply continuous loss of fluids and electrolytes from the body, or does it reflect an alteration of intake or sweat components as suggested by metabolic balance studies? ii) What are the mechanisms required to accomplish this and are they consistent with observed biochemical changes?
Fluid losses from the legs occurred rapidly at the onset of zero-g and were unexpectedly large.	i) From what compartments does this fluid originate? ii) What are the forces which drive it from the legs? iii) Is this fluid eventually excreted from the body or is there a residual volume remaining? iv) If residual volume is stored in upper body as has been postulated, does this represent long-term stress with regard to volume receptors or do these receptors adapt?
Urine volumes were reduced during the first week inflight coincidence with a mean increase in ADH.	i) Is the Henry-Gauer reflex which predicts a diminished level of ADH and a diuresis during acute zero-g stress, not operative in this instance? ii) What factors are capable of modifying or reversing this reflex and can they quantitatively account for the observed renal excretion?
Urinary ADH was significantly depressed during the latter part of the inflight phase, while urine volume was only slightly elevated.	i) What are the factors causing the ADH response? ii) What other competing factors are present, including longer term adaptive mechanisms that maintain reduced ADH levels and that prevent urine volumes to be even higher than would be expected on earth?
The measured body loss ratio of potassium: intracellular water is not consistent with values expected from normal cell composition.	i) Does this reflect measurement error or are other factors such as altered extracellular osmolarity involved? ii) What are the factors which permit potassium extrusion from the intracellular compartment to occur.
Aldosterone was increased in spaceflight accompanied by an increased sodium excretion.	i) Is this paradoxical relationship (in terms of one-g physiology) explained by other factors which influence aldosterone release or sodium excretion? ii) Is this an instance of sodium escape from aldosterone? iii) What factors caused excess sodium excretion to occur in the face of hyponatremia and elevated aldosterone?
Angiotensin was apparently increased during spaceflight.	i) What mechanisms are responsible for the elevations in angiotensin in a situation where there is a tendency toward upper body fluid congestion and increases in central blood pressures which are usually associated with depressed angiotensin? ii) How is it possible to reconcile the increased angiotensin and aldosterone levels in spaceflight with the findings from water immersion studies, which show an opposite effect?
Plasma osmolarity and plasma sodium concentration were slightly reduced, while urine osmolarity was increased.	i) How can these findings be reconciled when it would be expected that a dilute urine would be associated with hypotonic plasma, decreased ADH and increased aldosterone? ii) What are the factors causing the hypotonic plasma and why does this phenomena persist when the renal-thirst reflexes are capable of exerting exquisite control of body fluid osmolarity?
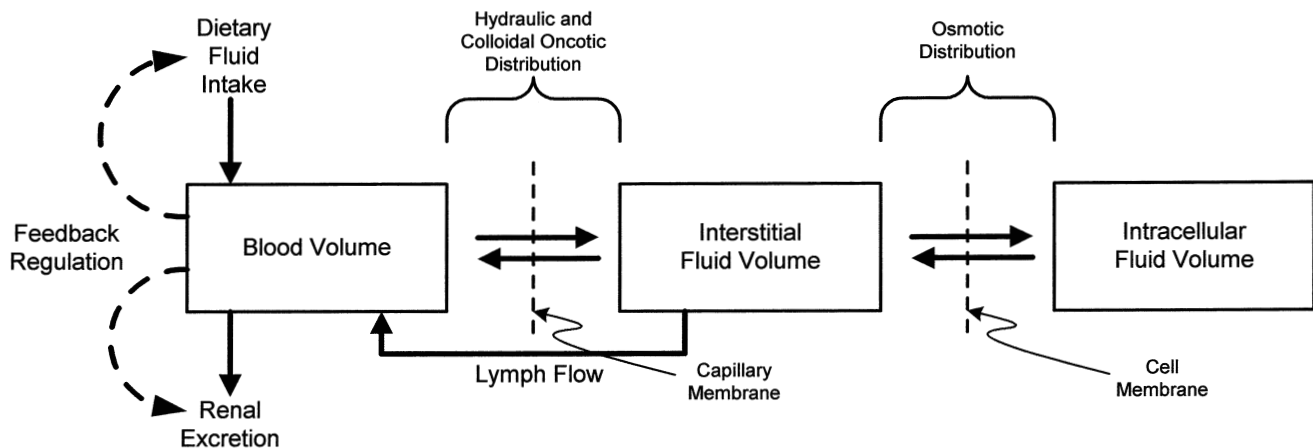
Figure 5-7. Regulation of body water balance showing factors that determine distribution between fluid compartments. Intracellular volume is ultimately regulated by feedback regulation of fluid intake and renal excretion. Cell membrane contains active pump which prevents sodium from entering intracellular compartment. Water moves freely across the cell membrane according to electrolyte osmotic distribution.

concentration of intracellular fluid is maintained independently of events occurring in extracellular fluid.

A normal total ionic concentration of body fluids is maintained by renal regulation. Loss of body fluid is always accompanied by a loss of electrolytes, although the proportion between these two quantities may vary widely. In the case of water deficit from inadequate intake, preservation of the normal ionic concentration of body fluids requires removal of a proportionally greater quantity of electrolytes than water (i.e., a hypertonic urine). Therefore, urine volume will be considerably reduced and hyperosmotic. On the other hand, when electrolytes are withheld in the diet, an accompanying elimination of hypotonic urine is necessary. If a therapeutic correction of water deficit occurs, it cannot be accomplished by water alone; the lost electrolyte must also be replaced.

These observations suggest that body fluid regulation cannot be separated from regulation of electrolytes, and a large part of the Skylab analysis was guided by this principle. A true understanding of fluid disturbances in any compartment in the body requires a basic knowledge of fluid volume and electrolyte content of intake, renal excretion, fecal excretion, sweat and evaporative water, and the major body fluid pools (see Fig. 10-2). This, of course, only provides the minimum information required to understand the extent of fluid disturbance. It does nothing to suggest the internal mechanisms by which the disturbances are ultimately corrected. These feedback homeostatic processes will be discussed next.

5.2.2 Control of Extracellular Fluid Volume

The control of extracellular fluid volume is under the influence of a variety of neural, humoral, and physical factors. There are no known receptors that respond to volume change, per se. However, volume changes are detected indirectly by sensors known to receive and respond to pressure, distention, or flow signals. While these sensors are located in various parts of the body, the pressure receptors in particular are found in the cardiopulmonary region, and they respond to circulatory pressures. Thus, the control of extracellular fluid volume, especially in cases of acute disturbances, can be understood best by examining the factors associated with blood volume changes.

The sensors for volume disturbances are very powerful in their ability to rapidly correct blood pressure by changing resistance and capacitance elements of the circulation, as well as in their ability to shift fluid between the vascular and interstitial segments. However, any disturbance of body fluid (i.e., dehydration, infusions, hemorrhage) cannot be fully corrected by these mechanisms, since the total amount of fluid deficit or gain still remains. The only mechanisms available for ultimate control of body fluid volume are those that affect drinking and renal volume excretion (Fig. 5-7). Figure 5-8 illustrates most of the known pathways by which acute and chronic disturbances of extracellular fluid volume are corrected. A more detailed examination of how these mechanisms affect renal function is shown in Fig. 5-9. References will be made to both of these illustrations, in order to discuss the most important thirst and renal mechanisms, as they are related to volume control.

5.2.2.1 Extrinsic Renal and Thirst Mechanisms. The body fluid control mechanisms have been divided into two major groups: a) extrinsic renal and thirst mechanisms, and b) intrinsic factors. In addition, the transcapillary fluid shift mechanism and other controllers of blood pressure are included. The extrinsic factors are discussed next.

(a) Arterial Pressure-Urinary Output Mechanism. In the view of Guyton [22], arterial blood pressure is the single most important influence on the long-term level

Figure 5-8. Regulation of extracellular fluid (ECF) volume and sodium by renal function. Control of this system is accomplished by hemodynamic, neural and hormonal factors that respond to blood volume, oxygen tension, and electrolyte concentration influences. (ADH = anti-diuretic hormone, EWL = evaporative water loss).

Figure 5-9. Regulation of renal blood flow (RBF) and urine excretion. Blood enters the renal artery and is partially filtered (red cells and plasma proteins remain in the blood) at the glomerular capillaries (Bowman's capsule). The remaining blood is passed through the efferent arterioles into the peritubular capillaries surrounding the renal tubules. Whereas net driving pressure across the glomeruli always favors a positive GFR (see equation for GFR where P_G = glomerular hydrostatic pressure, P_B = Bowman's capsule pressure, π_L = plasma colloidal oncotic pressure and K filtration coefficient) the net driving pressure across the peritubular capillaries always favors net reabsorption. The mechanisms that depend on hormonal and neural signals are described in the text.

of urinary volume excretion. An increase in blood volume is reflected by an increase in circulatory filling pressure, which has a direct hydraulic effect on the kidneys (via increased renal blood pressure and glomerular filtration rate) to increase urinary output until the pressure and volume have returned to normal. This mechanism (often called a pressure-diuresis) is a powerful controller of long-term blood volume regulation for several reasons. First, it is highly sensitive to small changes in arterial pressure, and secondly, the effect appears to be sustained indefinitely. This means that this mechanism is capable of 100% correction of any fluid volume disturbance, assuming all other factors return to normal.

(b) Volume Receptor-Renal Sympathetic Stimulation. Sympathetic stimulation, which may be evoked by even small decreases in blood volume by way of central arterial and atrial pressoceptors, has a powerful effect on constriction of the afferent renal arterioles. It acts rapidly to maintain blood pressure in the face of volume disturbances, and also works more gradually to correct the volume disturbance by altering transcapillary filtration in the kidneys and other tissues. Several features of this feedback system should be noted:

i) The mechanism for controlling urinary output may be primarily effective in hypovolemic disturbances rather than hypervolemia.
ii) Sympathetic activity to the kidney results in a decrease in renal blood flow, which is greater than the decrease in glomerular filtration rate (that is, an increase in filtration fraction occurs). As indicated in Fig. 5-9, this leads to an enhancement of peritubular capillary plasma, peritubular oncotic pressure, and increased fluid reabsorption from the tubules.
iii) The volume receptors initiating the sympathetic response are capable of adapting to a sustained pressure stimulus due to elastic creep of the receptor tissue. This suggests that the volume receptor element may be ineffective in correcting volume changes that are maintained longer than 24 to 48 hours duration. This has important implications in spaceflight where there is a constant tendency for body fluids to redistribute in a headward direction.

(c) Volume Receptor-ADH and Thirst Mechanism. Signals from volume receptors (particularly of the heart atria) are transmitted to hypothalmic centers that control both ADH secretion and thirst. Increases in blood volume lead to decreased ADH release, increased urinary excretion, and inhibition of the thirst drive. This corrective action decreases blood volume toward normal. The ADH-renal pathway is a potent short-term mechanism (Gauer–Henry reflex) for regulating water excretion in the face of moderate blood volume changes.

(d) Osmoreceptor-ADH and Thirst Mechanism. Plasma osmotic shifts have been observed to accompany

bedrest, water immersion, and spaceflight. Quantitative evidence recently obtained demonstrates the extreme sensitivity of ADH release to osmolar changes, compared to relative volume changes [33]. The feedback mechanism operates in this manner: increases in fluid osmolarity are sensed by hypothalamic receptors and ADH is released, causing renal water reabsorption and normalization of osmolarity. At the same time, the thirst drive is increased. Interpretation of disturbances in ADH levels must take into consideration the dual volume-osmoreceptor pathways affecting ADH, as well as the ability of the volume receptors to adapt.

(e) Aldosterone-Sodium and Water Reabsorption Mechanism. In the face of effective blood volume changes, aldosterone, a steroid secreted from the adrenal cortex, will appropriately respond in a direction to return fluid volumes toward normal. A primary effect of increased plasma aldosterone levels is an enhanced sodium renal reabsorption, accompanied by an osmotic reabsorption of water, thereby elevating blood volume levels. There are at least two pathways known where aldosterone secretion can be affected by blood volume changes. First, renin release and angiotensin formation are increased when blood volume is diminished to a moderate extent. This comes about either because of a direct effect of renal arterial pressure or reflexly by renal sympathetic activity. Angiotensin is a major factor affecting release of aldosterone. Second, there appears to be an inverse relationship between body fluid volumes and aldosterone secretion by some unknown mechanisms. Acute changes in plasma sodium concentration can also affect aldosterone secretion. Decreasing levels of plasma sodium concentration (hyponatremia) leads to increased aldosterone secretion that in turn promotes sodium retention and normalization of sodium concentration. Since hyponatremia is generally associated with low body fluid volumes, the aldosterone induced water and salt retention represents an appropriate feedback response. On the other hand, such situations as depressed sodium concentration resulting from dilutional overhydration (i.e., blood volume expansion), present competing stimuli (i.e., decreased sodium and increased blood pressure), and the net effect on aldosterone secretion is unclear.

(f) Aldosterone-Potassium Excretion Mechanism. Renal sodium reabsorption, under the influence of aldosterone, is an active process that exchanges sodium ions for other cations such as potassium, hydrogen, and magnesium ions. The aldosterone-potassium mechanism is the basis for a powerful feedback system for control of extracellular fluid potassium ion concentration. An increase in plasma potassium ion levels causes increased secretion of aldosterone, which in turn has a powerful effect toward promoting excess secretion of potassium into the renal tubule. Therefore, urinary output of potassium increases and

the plasma potassium ion concentration returns to normal. Of all the mechanisms that influence aldosterone secretion, none appear as powerful as changes in potassium ion concentration. An increase in plasma potassium of less than one meq/liter will triple the rate of aldosterone secretion [22].

(g) ***Renin-Angiotensin Mechanisms.*** Renin is released from the juxtaglomerular renal cells. The evidence suggests that renin secretion is inversely related to glomerular filtration rate, renal pressure, and sodium and angiotensin concentrations, and is directly related to renal sympathetic nerve activity. Renin is the precursor of angiotensin, which is a powerful vasoconstrictor of all arteriolar smooth muscle. Therefore, these substances are appropriately released in situations when arterial pressure falls (as in hypovolemia or standing). Its main effect on the kidney is probably associated with its ability to stimulate the adrenal secretion of aldosterone.

(h) ***Natriuretic Hormone and Third Factor.*** The concept of a "third factor" was originally postulated 20 years ago in order to explain experimental results that showed that excess sodium excretion could not always be accounted for by changes in aldosterone and glomerular filtration rate. It was postulated that the third factor might be a "natriuretic hormone" that acts on the renal tubules to turn off sodium reabsorption and increase renal sodium excretion in contrast to the action of aldosterone, which acts to increase sodium reabsorption and reduce renal excretion. Other "third factor" mechanisms that could theoretically explain the experimental observations have been either found or postulated. These other mechanisms include physical factors relating to peritubular capillary hydrostatic and oncotic pressures and intrarenal redistribution of blood flow. The precise contribution of each of the physical factors is still unclear. The natriuretic factor is of particular interest to space physiologists, since it is usually released in association with circulatory volume expansion. This is an active field of research. [UPDATE#1]

5.2.2.2 Intrinsic Factors Affecting Renal Function.
The extrarenal neural and hormonal control mechanisms previously discussed (i.e., sympathetic activity, ADH, and aldosterone) do not entirely explain why the kidney is able to reabsorb a very high percentage (about 99%) of the large quantity of plasma which is filtered through the glomerulus. This is basically accomplished by a number of intrinsic autoregulatory features of the kidney that control blood flow, plasma filtration and glomerulotubular balance. These mechanisms are briefly identified below:

i) Autoregulation of renal blood flow and glomerular filtration rate is thought to arise from changes in afferent arteriolar resistance by way of a local feedback circuit. This mechanism prevents large changes in glomerular filtration rate during daily variations in systemic blood pressure.

ii) Glomerulotubular balance insures that most of the glomerular filtrate is reabsorbed and does not pass into the urine.

iii) Peritubular capillary hydrostatic and oncotic pressures can have a marked effect on tubular reabsorption, and hence on urine volume excretion. Changes in plasma volume passively adjust peritubular pressures in directions that almost always insure appropriate feedback correction of the original volume disturbance.

iv) The well-known countercurrent multiplier mechanism permits the kidney to form a urine more concentrated than plasma. From a systems point of view, this mechanism seems to be important only in that it permits ADH to effectively concentrate the urine.

v) An intra-renal renin-angiotensin mechanism exists whereby angiotensin is produced within the juxtaglomerular cells (in distinction to the circulatory formation of angiotensin). It is postulated that by affecting the vasoactivity of the efferent renal arterioles, intrarenal angiotensin can conserve salt and water whenever arterial pressure falls, while still allowing normal excretion of metabolic waste products.

vi) Redistribution of blood flow between two groups of nephrons (cortical and medullary nephrons) that reabsorb sodium to different degrees may provide a mechanism for controlling sodium and water balance. Intrarenal blood flow redistribution may be under partial control of sympathetic activity.

These mechanisms are far from understood, and their importance has not been fully ascertained in certain cases. In general, their existence permits the basic renal function of eliminating wastes and conserving nutrients to take place, while allowing the major control of extracellular volume and ionic concentration to reside in other factors previously described such as aldosterone, ADH, and sympathetic stimulation. The spaceflight response involves controlling unusual volume disturbances as well as eliminating excess waste products from tissue degradation. Therefore, it was important to be cognizant of both intrinsic and extrinsic mechanisms when interpreting the biochemical and body fluid responses. Two very important non-renal mechanisms for controlling blood volume are discussed below.

5.2.3 Transcapillary Fluid Shift Mechanism
The fluid shift mechanism refers to the movement of plasma filtrate across the capillary membrane between the blood volume and the interstitial fluid compartment (see Fig. 5-7), and provides temporary and rapid correction of acute blood volume disturbances. This takes place in accordance with the so-called Starling forces, whereby transcapillary gradients of hydrostatic and colloidal oncotic pressures provide the driving force for fluid exchange. Disturbances in blood volume are reflected by changes in capillary pressure that can either drive plasma into the interstitium if pressure is increased, or reabsorb fluid into the vasculature from the interstitial reservoir if pressure is reduced. If hemodilution or hemoconcentra-

tion accompanies blood volume changes, colloidal osmotic gradients will occur which also serve to correct the volume disturbances. In addition to the transcapillary gradients, other factors that determine this distribution include compliance of the circulatory system, compliance of the interstitial compartment, the rate of lymph flow, and physiochemical relationships between gel and free fluid in the interstitial spaces [22].

The transcapillary fluid shift mechanism is also directly related to volume receptor pathways and sympathetic activity. For example, hypervolemia will result in elevation of capillary pressure, first by a direct effect on the volume-pressure relationships of the circulation, and second, by causing a decrease in the pre-/post-capillary resistance ratio by way of the pressoreceptor-sympathetic pathway. This ratio, along with arterial and venous pressures, is a major determinant of capillary pressure, and, in this case, leads to movement of fluid from the plasma into the interstitium.

5.2.4 Blood Pressure Control

Inasmuch as blood pressure changes are directly (but non-linearly) related to blood volume changes, the factors which control blood volume discussed above also play an important role in controlling blood pressure. However, there are additional mechanisms operative for blood pressure control that have only indirect effects on blood volume. These include both neural and local factors which control vascular resistance or capacitance. In general, the neural mechanisms (baroreceptor, chemoreceptor, central nervous system ischemic control) are sympathetically mediated and reach maximum effectiveness within seconds and minutes, while the local factors (stress relaxation, flow autoregulation, vascularization) act more gradually but maintain their effectiveness longer. A reduction in blood pressure at the cardiopulmonary pressoreceptors initiates a widespread increase in sympathetic activity that increases peripheral resistance by arteriolar constriction and decreases venous capacitance. These responses tend to restore mean blood pressure. Stress relaxation refers to the characteristic of vascular smooth muscle that allows it to slowly stretch when the pressure rises and to contract slowly (reverse stress relaxation) when the pressure falls. Vascularization refers to the opening of existing capillaries or the creation of new ones in the face of increased blood volumes and pressures; devascularization is a reverse process that accommodates reduced volumes and pressures. Since these processes (stress relaxation and vascularization) can take weeks to fully develop, they represent mechanisms that can profoundly alter the capacitance of the vasculature and accommodate long-term changes in blood volume (such as the reduced volumes observed in spaceflight) without significantly altering mean arterial blood pressure. The specifics of these adaptive processes, including their time course, are not well understood.

5.2.5 Fluid Volume Regulation in the Guyton Model

Many of the important pathways for fluid-electrolyte regulation identified in the overall systems analysis of the preceding discussion are contained in the modified Guyton model for circulatory, fluid, and electrolyte control. These include:

i) mechanisms related to fluid distribution among the major body compartments (transcapillary transport, transcellular osmotic diffusion and active transport, lymph flow and interstitial free fluid-gel equilibrium) (see Fig. 5-7);

ii) mechanisms related to circulatory control (cardiac control, blood volume distribution and autonomic, hormonal, and local control of blood flow) (see Fig. 5-8);

iii) mechanisms related to fluid-electrolyte controlling hormones (ADH, aldosterone, renin-angiotensin) (see Fig. 5-8); and

iv) mechanisms related to renal excretion of fluids and electrolytes (hormonal and neural control, autoregulation, glomerular tubular balance, colloidal oncotic forces) (see Fig. 5-9); and

v) mechanisms for the control of arterial blood pressure (see Fig. 5-10).

Figure 5-10 illustrates the response time and relative effectiveness for eight arterial pressure control mechanisms which are included in the model. All of these have been discussed above.

The most rapidly acting mechanisms are those involving neural feedback elements (baroreceptors, chemoreceptors, and ischemic response). While these mechanisms are capable of exerting a large degree of control for rapid disturbances such as postural changes, the effects are not long lasting, because of receptor adaptation. Control mechanisms of intermediate duration are represented by stress-relaxation of the vasculature, renin-angiotensin- vasoconstriction mechanisms, and the capillary fluid shift mechanism. These pathways do not become effective unless the disturbance persists for more than a minute or so, and they reach full development within a few hours. The aldosterone and renal-fluid pressure control mechanism often require hours or days to become fully effective; their activity is probably minimal in many disturbances which are effectively regulated by the short and intermediate term mechanisms. Note that the renal-blood volume pressure control mechanism, when it becomes fully activated, has infinite gain and insures that in the long run, renal volume excretion comes into balance with the net intake of fluid. In spite of the somewhat hypothetical nature of the gain curves, they are useful as a means of categorizing both the relative speed and effectiveness of the pressure regulating mechanisms of the body. It also suggests the application of the model to processes such as spaceflight that include long-term adaptation to significantly large fluid disturbances.

Figure 5-11 illustrates the particular mechanisms used in the Guyton model for regulating hormonal response and the mechanisms' effects on circulatory control and the renal excretion function. Comparison of Fig. 5-11 with Fig. 5-8 indicates the high level of detail that exists in the model (see Appendix G).

The renal subsystem of the Guyton model is depicted in Fig. 5-12. Just as in the real system (suggested by Fig.
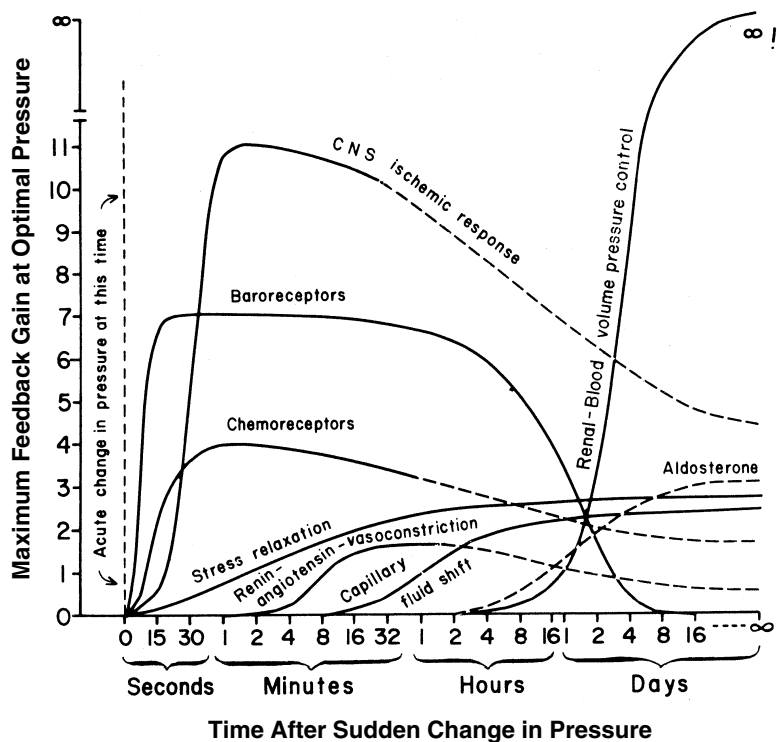
Figure 5-10. Response times and relative effectiveness of the arterial pressure control mechanisms. Maximum feedback gain is a measure of the effectiveness of the mechanisms and is defined as the ratio between initial and compensated pressure change. The greater the feedback gain, the more effective is the mechanism as a pressure (or blood volume) controller. The solid portions of these curves are based on experimental results while the dashed portions are extrapolations and are somewhat hypothetical. Each of these curves represents a single system result, that is, all systems except the one in question are presumably not responding to the stimulus. Note that the time base on the abcissa begins with seconds and then extends to minutes, hours, and days. (Reproduced from Guyton [34]).

5-9) angiotensin exerts its effects at the afferent and efferent renal arterioles, while ADH and aldosterone control water and salt tubule reabsorption. Glomerular filtration is realistically controlled by the transcapillary hydrostatic and oncotic forces.

While a majority of mechanisms affecting circulatory, fluid, and electrolyte control are included in the model, it is also apparent that some pathways that exist in the real system are absent in the model. For example, some of the intrinsic mechanisms such as peritubular effects, intrarenal blood redistribution and an intra-renal angiotensin mechanism are absent altogether, while others such as glomerulotubular balance are present only in a crude fashion. Third factor effects, including the postulated natriuretic hormone, are also missing. In the real system, active sodium reabsorption permits water to follow osmotically and this effect is absent. Therefore, this analysis has led to several specific recommendations for modifying the renal subsystem of the Guyton model (see Appendix G).

As will be demonstrated, however, the existing model is capable of predicting generally appropriate responses in many situations and of testing hypotheses of considerable complexity. It can be appreciated that the final integration of these pathways and feedback mechanisms are complex, particularly when the body is equipped with redundant and multiple interconnecting pathways. The dynamic characteristics of each pathway and their relative influence in correcting a particular volume, pressure, or osmolar disturbance are quite different. It is for these reasons that a careful systems analysis is required and that a large-scale quantitative simulation model becomes so useful.

5.3 Development of Hypothesis

This section will address the critical areas and questions identified in Table 5-5. Specifically, this involves accounting for the distribution, metabolism, and excretion of water, sodium, and potassium during acute and long-term spaceflight. While the study is limited in this manner, it does involve an extensive analysis of endocrine, autonomic, and local effects that participate in controlling the volumes and composition of each body fluid compartment via renal and blood pressure regulating pathways. The complexity of the fluid-electrolyte regulatory system summarized in the preceding section implies that any explanation of the spaceflight findings will not be an easy undertaking. Wherever possible, the hypotheses proposed in this project have been examined for their quantitative influence, either by a re-evaluation of the data or by computer simulation. In some cases, because of data, model, or
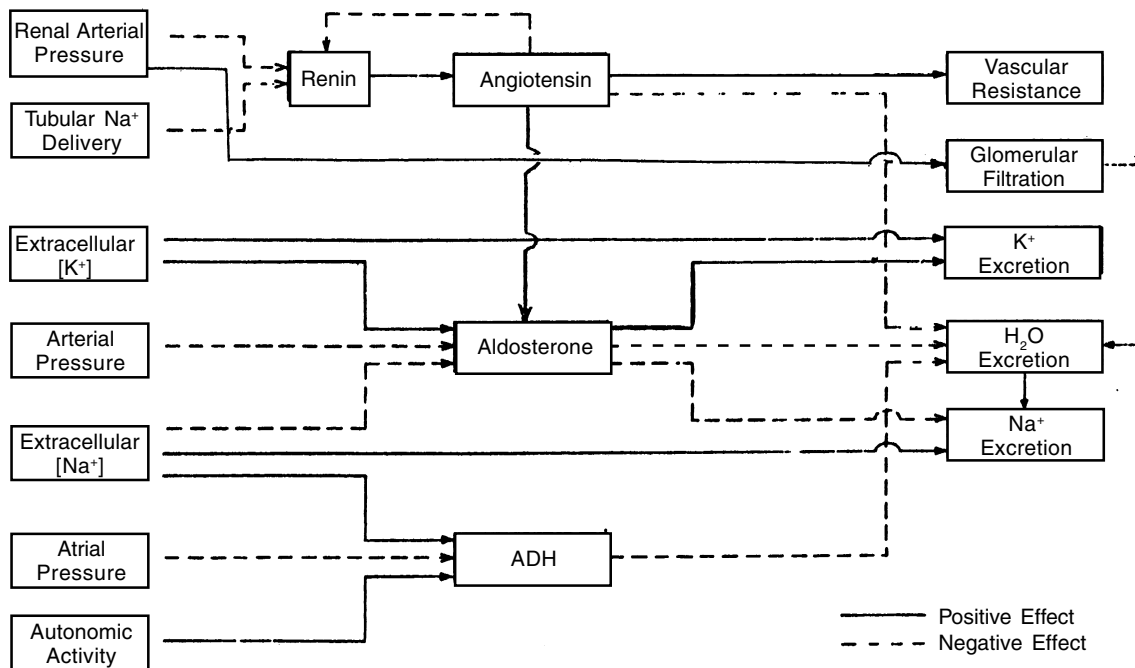
Figure 5-11. Hormonal control of fluid and electrolyte renal excretion as embodied in the Guyton model. All the factors that influence, and are influenced by, hormonal excretion are shown. The feedback circuit that permits renal excretion to regulate extracellular fluid volume nad ionic concentration are not shown here (see Fig. 5-8). Except for renin, all pathways shown are extra-renal. A more detailed description of the intra-renal subsystems are illustrated in the next figure.
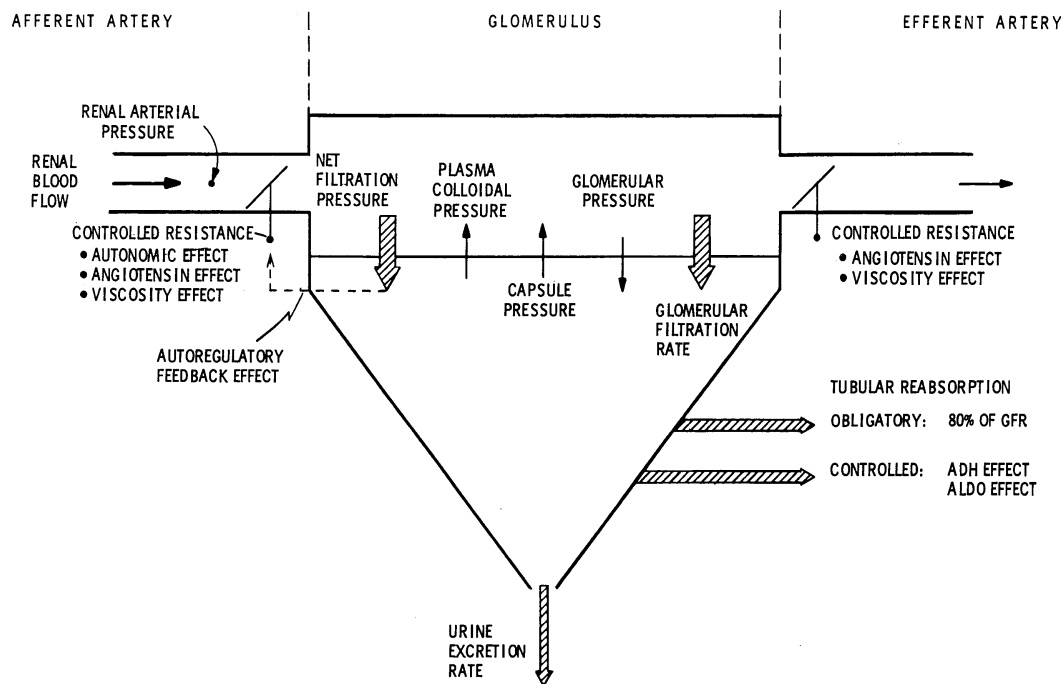
Figure 5-12. Renal regulation of urine volume excretion in the Guyton model. Renal blood flow and pressure (and hence glomerular pressure) is controlled by resistances in the afferent and efferent renal arteries that vary according to autonomic, angiotension, viscosity, and local feedback effects. Twenty percent of tubular reabsorption is under the influence of ADH and aldosterone. Urine exretion is determined by the difference between glomerular filtration rate and tubular reabsorption.

5.3.1 Acute Zero-G Response: Fluid Redistribution Hypothesis

Central to explanations of the physiological response to weightlessness is the frequently proposed fluid redistribution hypothesis (also known as the "headward fluid shift" hypothesis) [35,36,37,38]. Accordingly, exposure to weightless spaceflight or its ground-based analogs, bedrest and water immersion, results in a reduction of the hydrostatic gradients in the blood column (see Fig. 5-13). Fluid that is otherwise pooled in the lower extremities is redistributed headward by the elastic forces and tone of the tissues. While the proportions of leg intravascular and extravascular fluids involved in this translocation have not yet been established, it is believed that the resultant effect must be an increase in central blood volume (i.e., thoracic blood volume) and pressures. There is abundant evidence supporting this internal fluid shift. Reductions in leg volume have been observed in bedrest, water immersion, and spaceflight, and engorgement of neck veins and facial tissues and feelings of head fullness have been observed inflight [16]. In addition, significant increases in central blood volume and pressures have been measured directly during water immersion and head-down bedrest [39,40].

A second part of this hypothesis claims that the cephalad shifts of fluid from the legs is interpreted as an increase in effective blood volume which is appropriately corrected by neuro-humoral mechanisms or by more direct hemodynamic influences. These feedback pathways have been described in general terms in the last section and are illustrated in Fig. 5-14 to 5-17. The following discussion concerns the integration of these processes in order to relate them specifically to the regulation of fluid and sodium imbalance during the early phases of spaceflight. The hypotheses presented are consistent with conclusions previously reached by other investigators who have studied either blood volume expansion effects in general or the spaceflight responses in particular [22,36,38,41–44].

An expected inflight reduction in body water and plasma volume has often been explained by an acute diuresis via the volume receptor-ADH and thirst pathway (Fig. 5-14) [13,25,43,45]. The cephalad redistribution of fluid at the onset of weightlessness may be sufficient to reflexly suppress ADH and thereby contribute to a diuresis. These events have been demonstrated during acute water-immersion studies [46,47] and head-down tilt [48], both stresses causing headward fluid shifts. However, during the Skylab missions, no diuresis was observed in the first 24-hour pooled urine volumes, and ADH levels were elevated on the average during the first two weeks (ADH measurements could not be performed on the first day of flight). However, there was a considerable difference between the ADH response of the three missions; ADH increased on the shortest mission and decreased on the two longer missions (see Fig. 5-6). The differences between

these mission observations and the differences between the mean spaceflight and ground-based responses have not been explained, but several factors should be considered.

The absence of an early clear-cut diuresis during spaceflight must be considered in perspective with the known decrease in fluid intake on the first inflight day. The state of hydration has been shown to be a significant factor in eliciting a significant free-water diuresis during water immersion [49,50]. The depletion of over a liter of body water by the third day of the Skylab flights can be attributed almost entirely to deficit drinking. Therefore, it is possible that additional renal regulation was not required. The renal response at the onset of zero-g accompanied by a normal fluid intake is not yet known.[UPDATE#2]

Although volume receptor stimulation on the first day of weightlessness is a logical assumption, plasma osmolarity adjustments could have mitigated the ADH response. Increases in plasma osmolarity, a powerful activator of ADH, could have occured as a result of reduced fluid intake. However, plasma osmolarity was not measured until the third or fourth inflight day when it was found not to be elevated, but reduced.

Figure 5-13. Early effects of hypogravity on body fluids leads to headward fluid shifts and redistribution of leg fluids.

Modifying factors
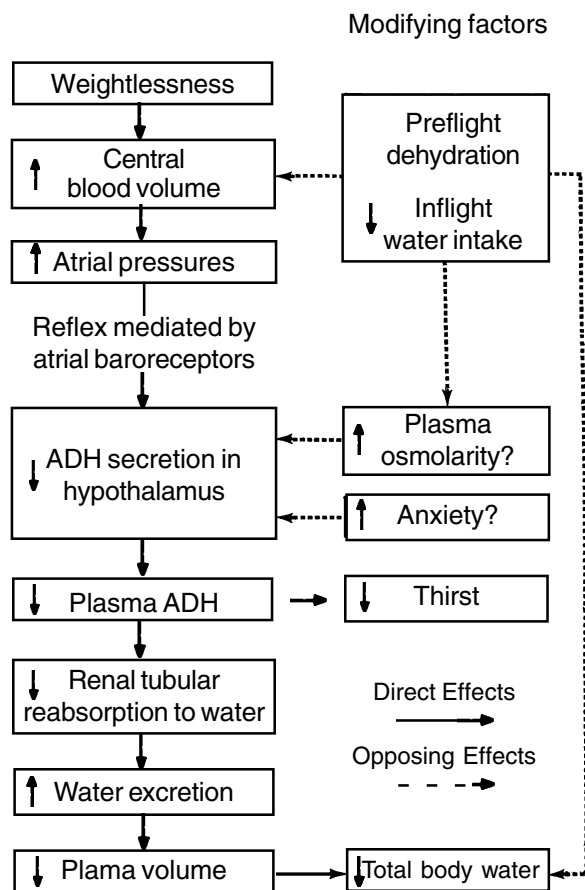
Figure 5-14. Reduction in plasma volume during exposure to weightlessness by activation of the volume receptor-ADH (Gauer–Henry) pathway [35]. Some of the factors that might interfere with this response include plasma osmolarity via dehydration, and anxiety stress.

An analysis of preflight water balance and body weight demonstrated that the crew of the 28-day mission lost nearly a liter of fluid during the several days prior to launch compared to a much more normal pre-launch water balance for the two other crews (see Chapter 4.6). In light of known effects of dehydration on the volume receptor-ADH-renal pathway, this observation might explain part of the early inflight difference in ADH response between the three Skylab crews (Fig. 5-6).

Space motion sickness, observed in a majority of Skylab crewmembers during the first week of flight [51] might account for the simultaneous reduction in fluid intake. In addition, anti-motion sickness drugs could have altered renal and hormonal function in a direction that contributed to a reduced urine volume [52].

Water immersion studies typically measure hourly urine excretion over a period of 4-6 hours. This is in contrast to the 24-hour pooled sample collected in Skylab. In addition, operational difficulties prevented total urine col-

lection in some crewmen on the first day inflight. It is conceivable that void-by-void urine sampling in future space missions will reveal an early diuresis component of the first day's water loss. In addition, ADH measurements performed during this time will complete the missing observation of Skylab; ADH would be expected to be reduced if hydration is normal.[UPDATE#2]

As will be shown later, many other pathways besides the ones shown in Fig. 5-14 may be involved in the renal response to headward fluid shifts. Their varied behavior during spaceflight or during water immersion may explain the different responses observed in these two stresses.

Correction of central blood volume expansion by renal excretion of water and salts may be accomplished by a multiplicity of pathways as suggested in Fig. 5-15. They may be conveniently categorized into volume receptor reflex pathways (shown on the right side of Fig. 5-15) consisting of neural and humoral controllers such as ADH, angiotensin and aldosterone, and direct hydraulic or hemodynamic effects involving intrarenal mechanisms such as renal arterial pressure, glomerular filtration and peritubular capillary pressures. Evidence suggests that the entire volume receptor component is probably ineffective in correcting volume changes for longer than 1–2 days due to adaptation or resetting of the elastic stretch receptors that exhibit creep and fatigue [22]. The direct hemodynamic effects, however, would not be expected to adapt as rapidly in this fashion. All of these mechanisms are known to alter urine excretion by adjustments in either glomerular filtration rate or tubular fluid reabsorption. By acting individually or in parallel, they can provide rapid short-term regulation of fluid and sodium imbalance.

A more complete analysis of the pathways that regulate sodium excretion following hypervolemic expansion is shown in Fig. 5-16. Factors influencing glomerular filtration rates and tubular reabsorption may be postulated. Glomerular filtration may be enhanced directly by increases in central blood pressures, or indirectly by reflex sympathetic mechanisms. A major factor in altering tubular sodium reabsorption in a direction favoring increased renal excretion is suppressed aldosterone secretion (via the renin-angiotensin pathway). Other mechanisms denoted in Fig. 5-16 as "third factor", are also theoretically capable of effecting tubular sodium reabsorption [42,53,54]. These include peritubular effects, intrarenal blood flow redistribution, and natriuretic factor. The presence of natriuretic activity in plasma is becoming an increasingly attractive hypothesis to explain acute renal sodium responses during the hypogravic-water immersion state and circulatory volume expansion [30,46,50]. Release of another humoral agent, renal prostaglandin, has also recently been implicated as contributing to the diuresis and natriuresis of volume expansion and water immersion [55]. On Skylab, data regarding natriuretic hormone or prostaglindin activity had not been collected.[UPDATE#1] A natriuresis was not observed early in the Skylab missions, but excess sodium excretion did occur following the first week of flight, even though aldosterone levels were high (Figs. 5-4 and 5-5). The considerations discussed above

Figure 5-15. Pathways that are postulated to increase urine water and sodium excretion following acute expansion of central blood volume. The degree of participation of each pathway is not well known, although it is believed that increases in glomerular filtration rate are not significant.

regarding restricted intake and drug usage may also be relevant to this situation as well and account for body sodium loss without excess renal excretion.

Although renal excretion is one of the best understood mechanisms for controlling plasma volume, other factors can be equally as important and undoubtedly played a part in the spaceflight response. As illustrated in Fig. 5-17, plasma volume control is under the influence of three major pathways consisting of renal excretion, thirst and transcapillary filtration. The factors that reduced fluid intake during the first days of spaceflight are not clear but have been related to space motion sickness. Also suggested in Fig. 5-17 is a secondary pathway by which a reduction in angiotensin may modify ADH release as well as thirst drive [24,56]. Transcapillary filtration into the interstitium would be favored during central blood volume expansion as a result of sympathetic, autoregulatory, and local pressure effects. In water immersion the diuresis is attenuated in favor of increased capillary filtration if the subjects are dehydrated, although the decrements in plasma volume are similar in magnitude to those found in well-hydrated subjects. However, a close inspection of the wa-

ter immersion studies suggests that removal of blood pooling forces augments *inward* filtration from lower limb capillary beds which leads to a transient elevation of plasma volume [57,58]. The subsequent rapid loss of plasma volume, by any of the routes available, including *outward* filtration in the upper body, can create a concentration of plasma colloids that limits loss of plasma into the tissues [59]. Therefore, the *net* plasma-intersitial exchange resulting from differing transcapillary forces in the upper *and* lower body is not apparent during a hypogravic maneuver. In this regard, it may be noteworthy that of all the fluid compartments measured or computed during the Skylab experiments, only the interstial compartment failed to exhibit a fluid loss (Table 5-2) as measured at the end of the mission.

In summary, the onset of weightlessness leads to volume expansion of the central vasculature. Several reactions may be predicted;
a) stimulation of the volume receptors and decreased sympathetic activity;
b) increased blood pressures and secondary decreases in peripheral resistance, promoting enhanced organ

Figure 5-16. Postulated early effects of spaceflight on sodium excretion pathways. Preflight dehydration and reduced dietary intake will modify the response as shown.

blood flow including that of the kidneys;

c) altered secretion of the fluid-electrolyte regulating hormones including, ADH, the renin-angiotensin-aldosterone triad, catecholamines, and possibly a natriuretic agent and renal prostaglandins;

d) enhanced renal excretion of fluid and electrolytes as a result of the alterations in sympathetic activity, hormone secretion and blood pressures and flows;

e) increased transcapillary filtration of plasma into the interstitium due to resetting of the pre-to postcapillary resistance ratio and elevated capillary pressures; and

f) a decrease in thirst following reduction in angiotensin levels and augmented by space motion sickness anorexia.

Most, if not all, of these rapidly acting mechanisms that serve to correct the original central hypervolemia would most likely be observed most readily during the first hours of a hypogravic stress. Therefore, it is not surprising that they have not been observed in actual spaceflight when operational constraints precluded early measurements. Nevertheless, the net result of these controlling mechanisms, that is, the loss of body fluids and

Figure 5-17. Direct and reflex mechanisms that can lead to the acute reduction of plasma volume following the loss of hydrostatic gradients during weightlessness.

electrolytes, has been observed frequently during and following weightless spaceflight.

It is not possible to predict from this analysis, or from the spaceflight findings, which pathways predominate. The utility of computer models, that incorporate representations of these mechanisms, can prove valuable in suggesting the relative importance of various pathways and in testing hypotheses and determining consistencies and discrepancies of measured results. Previously observed phenomena of "escape," adaptation, and resetting suggest that certain of these pathways change their effectiveness with time (see Fig. 5-10). Thus, long-term regulation of fluid-electrolyte balance, following correction of the initial disturbance, involves a similar but separate analysis. The greatest wealth of spaceflight data have been collected during the adaptive phase of fluid-electrolyte regulation where theoretical understanding is more limited. In contrast, spaceflight data are sparse during the acute stress stage where the conceptual understanding is much more extensive.

The roles of the major fluid-electrolyte regulating hormones (ADH, aldosterone, and angiotensin) in the long-term adaptive processes of weightlessness are far from clear [8,13]. For this reason, they have received special attention in the next discussion.

5.3.2 Long-term Regulation of Aldosterone and Potassium

Aldosterone secretion is influenced by a number of factors including plasma angiotensin levels, plasma sodium concentration, and plasma potassium concentration (see Fig. 5-8). The adrenocorticotrophic hormone (ACTH) also has a releasing effect on aldosterone. However, ACTH is activated during periods of emotional stress and its day-to-day influence on aldosterone has not been established. Other unknown factors appear to activate aldosterone during stresses related to circulatory insufficiency.

Aldosterone has potent effects on renal function, permitting potassium excretion and inhibiting sodium excretion. The effect on sodium results in an osmotically induced reduction of urine volume. Thus, aldosterone secretion appears to be controlled by, and has an effect on, factors related directly to changes in body water, sodium, and potassium. Due to this multiplicity of feedback pathways, in which aldosterone is a major control element, it is not surprising that the role this hormone plays in overall fluid-electrolyte regulation is not clear. [UPDATE#1]

Many investigators feel that aldosterone secretion is primarily under control of circulating angiotensin levels and that aldosterone plays a major role in the regulation of extracellular volume and sodium concentration. However, this may be true only in response to acute disturbances. Recent reports suggest that the whole question of the renin-angiotensin system in the long-term control of aldosterone and sodium metabolism must be reassessed [22]. For example, prolonged excess aldosterone secretion (primary aldosteronism) results in renal sodium retention of only a few percent above normal. Similarly, infusions of aldosterone eventually fail to exhibit their sodium retaining characteristics; that is, the renal tubules exhibit an "escape" phenomenon. Apparently, plasma sodium concentration is well regulated over the long-term by multiple non-aldosterone factors (see Fig. 5-16).

On the other hand, a functional aldosterone feedback system appears to be essential to maintain plasma potassium concentration within normal limits. Aldosterone control of renal potassium secretion is the only major mechanism known for controlling the extracellular fluid potassium ion concentration. In the absence of adequate aldosterone (that is, adrenocortical insufficiency), plasma potassium can rise to dangerously high levels. In the presence of chronic excesses of aldosterone (primary aldosteronism), a continued increase in potassium urinary excretion may result in hypokalemia and eventually muscle paralysis.

While the phenomenon of aldosterone "escape" mentioned previously has not been satisfactorily explained, the following schema offers one possible solution and also illustrates the complexity of water and salt regulation. Excess aldosterone (created experimentally by infusion, or in patients with primary aldosteronism) causes enhanced renal salt reabsorption that in turn leads to osmotic reabsorption of water. The immediate effect is to decrease urine volume and salt excretion markedly. Both extracellular volume and blood volume increase. At this point, other feedback mechanisms related to controlling excess fluid volumes come into play (for example, the pressure diuresis mechanism, the ADH circuit, or natriuretic factor), and overbalances the retention of fluid and salt by the kidneys. Consequently, both urine volume and sodium excretion rise until urinary output equals net body intake. At these new homeostatic levels, extracellular volume rarely rises more than 5-10%. Thus, aldosterone, working in concert with other feedback circuits, does not appear to have major long-term consequences on either fluid volumes or net sodium retention.

In the light of the previous discussion, it is not difficult to suggest mechanisms that contributed to the elevated aldosterone levels observed in the Skylab crew. According to the hypothesis diagram of Fig. 5-18, elevated cortisol and muscle disuse atrophy result in lean body tissue degradation and cellular release of potassium. These cell losses, together with an estimated decrease in potassium sweat losses (see Chapter 4.4) tend to raise plasma potassium concentration. Hyponatremic plasma and increased circulating catecholamines are factors known to augment renin-angiotensin activity. Accordingly, three of the four factors known to contribute to increased aldosterone secretion, (that is, elevated plasma potassium and angiotensin coupled with decreased plasma sodium levels) were all observed during the course of spaceflight. While decreases in ACTH were reported, these are reasons to believe that these measurements should be interpreted cautiously [13].

The increases in potassium renal excretion that would be expected to accompany excess aldosterone were also observed during spaceflight. Potassium renal excretion was elevated about 10% throughout the flight period (see Fig. 5-4(b)). As indicated in Fig. 5-2, most of the body potassium loss occurs during the first month and the major part of it during the first week of flight. However, why simultaneous decreases in sodium excretion, as suggested in Fig. 5-18, were not detected is unclear [13]. The elements of sodium "escape" from aldosterone seem to be present. Competing factors for sodium release, such as "third factor" natriuretic hormone or prostaglandins, could account for these results, but laboratory analysis of these agents was not performed. Future measurements of glomerular filtration may also reveal changes which are consistent with renal excretion of excess sodium in combination with elevated aldosterone.

5.3.3 Long-term Regulation of ADH, Extracellular Osmolarity, and Volume Control

The role of ADH in overall fluid-electrolyte regulation has not been satisfactorily defined. To a large extent, the difficulty stems from the occasionally opposing functions that ADH plays in two separate feedback pathways one of which controls blood volume and the other controlling plasma osmolarity. Gauer and colleagues [25] are proponents of the hypothesis that ADH is primarily involved in regulating extracellular fluid balance. They believe that ADH reliably responds to minor disturbances in central blood volume. Alternatively, Goetz and colleagues [60] claim that ADH secretion is not sensitive to small changes in blood volume and that the osmoreceptor-ADH pathway is sufficient to explain normal regulation of both extracellular volume and tonicity.

Guyton and co-workers [21,22] attempt to integrate both these points of view by proposing an integrative mechanism for fluid-electrolyte balance (see Fig. 5-19). The elements in this scheme include a volume receptor-ADH pathway that responds to acute, rather than prolonged, volume disturbances. The lack of long-term response is credited to receptor adaptation. Guyton's concept also includes a sensitive osmotic receptor-ADH pathway that can override

Plasma — ↑ Catecholamines

Renal tubule — ↓ Na^+ delivery

Plasma — ↓ $[Na^+]$

Cells — ↑ Tissue loss

Adrenals — ↑ Cortisol

CNS — ↑ Sympathetic activity

Renal JGA — ↑ Renin

Cells — ↓ K^+

Sweat — ↓ K^+

Pituitary — ↑ ACTH and other factor?

Plasma — ↑ $[Angiotensin]$

Plasma — ↑ $[K^+]$

Adrenals — ↑ Aldosterone secretion

Plasma — ↑ $[Aldosterone]$

Urine — ↓ Na^+ excretion

Urine — ↑ K^+ excretion

* Observed on Skylab

Figure 5-18. Long-term effects of spaceflight on aldosterone. This diagram represents an hypothesis for explaining the elevated plasma aldosterone levels observed in the Skylab crew.

inputs from the volume receptors, and an ADH-thirst drive that receives inputs from both volume and osmoreceptors. In this view, the osmo-receptor-ADH-thirst mechanism is primarily responsible for long-term control of plasma osmolarity. (Inasmuch as sodium contributes about 95% to total extracellular osmolarity, this pathway becomes essentially a means for controlling sodium concentration.) This concept is supported by recent animal studies that demonstrate that plasma osmolarity exerts a very sensitive effect on ADH secretion compared to the influence of blood volume changes [33]. The fact that volume receptors can adapt to sustained volume disturbances and that there are other more powerful mechanisms available for

long-term control of blood volume (see Fig. 5-10) supports the argument for a minor role of ADH in the long-term control of body fluid volume. The case for dual volume and electrolyte control of hormones is addressed more fully in Chapter 9.8.

As ADH secretion increases, reabsorption of water from the renal tubules and collecting ducts is enhanced and smaller volumes of increasingly concentrated urine are formed. Reduced ADH conversely forms large quantities of dilute urine. Some investigators feel that the ADH influence on the kidneys is a mechanism for partially dissociating water excretion from that of salt since a decreased ADH level may increase water excretion without altering

Figure 5-19. Scheme of osmoreceptor (A: upper portion) and volume receptor (B: lower portion) feedback regulation of thirst and ADH release. (Redrawn from Guyton, et al.[22]). Symbols are defined in Appendix A.

sodium excretion [24,50]. This separation of function may be crucial for renal regulation of extracellular osmolarity.

In the light of the previous discussions of ADH feedback regulation and the Skylab findings, it is possible to predict decreased secretion of ADH during spaceflight by two mechanisms: a) an observed mild decrease in plasma osmolarity and plasma sodium concentration by the third inflight day which continued throughout the weightless phase of the mission, and b) an elevation of central circulatory pressures which was not measured, but which may be postulated from such observations as distended neck veins and feelings of head fullness. The second of these influences on ADH would be expected to be operative early in flight if volume receptor adaptation takes place or if excess circulatory pressures do not persist. Nevertheless, ADH inexplicably did not decrease, on the average,

until after the second week inflight (Fig. 5-5(a)). If each mission is examined separately (Fig. 5-6), ADH exhibits the expected decrease throughout the two longer missions. The elevated ADH on the first mission is still paradoxical but may be related to preflight dehydration and large increases of inflight sweat losses of that crew.

The average urine excretion of nine men was decreased during the first week when ADH was elevated; after the second week of flight, both quantities reversed direction (Figs. 5-3 and 5-5(a)). The significant correlation between these quantities during the first month ($p < 0.05$) is in agreement with the expected influence of ADH on urinary volume, with regard to direction of response. However, based on the data summarized by DeHaven and Shapiro [61], suppression of ADH to the extent observed should have resulted in an increase of urine volume much larger

than that measured, and a urine more dilute than that measured, assuming all other factors did not change. For example, on the longest mission the mean urine volume was not different from preflight, the urine osomolarity was significantly increased, and yet ADH was approximately 30% below preflight levels.

It is likely that other factors that tend to limit and concentrate urine output were present. This may involve alterations in glomerular filtration rate (i.e., decreased renal pressure) or tubule water reabsorption (i.e., prostaglandins counteract the effect of ADH) [62]. Increased aldosterone, which can lead to renal sodium and water reabsorption may also have contributed to this result. A clearer understanding of acute and long-term control of ADH and urinary volume excretion should emerge by obtaining fluid samples earlier in flight, measuring the factors contributing to water retention, and recording indices of renal hemodynamics and circulatory pressures.

5.3.4 Long-Term Angiotensin Response

The elevated levels of angiotensin I, which have been observed during prolonged spaceflight, have not been satisfactorily explained [13]. The available evidence suggests that an increase in renin-angiotensin would be expected as a result of depressed glomerular filtration rate, renal pressure, extracellular sodium concentration, increased renal sympathetic nerve activity and elevated catecholamines (see Figs. 5-15 and 5-16) and Appendix A, Fig. A-3). Angiotensin is a powerful vasoconstrictor and is appropriately released in situations when arterial pressure or central blood volume falls [63,64,65,66,67]. If spaceflight is associated with chronic elevation of central or renal circulatory pressures, as some believe, then the angiotensin response is paradoxical unless other stimuli such as those discussed below in the following section, can be found which oppose that factor. Similar trends of angiotensin have also been unexpectedly observed in long-term bedrest (Chapter 9).

A major effect of angiotensin on renal function is its ability to stimulate the adrenal secretion of aldosterone. Elevated levels of aldosterone were apparent during the Skylab flights [13]. This hormone may also exert a specific intrarenal effect by conserving salt and water in the body while still allowing normal excretion of metabolic waste products [22]. Thus, the combination of elevated angiotensin and aldosterone can help restore depleted extracellular fluids and salts.

5.3.5 Effects of Altered Renal Hemodynamics

On earth, reflex adjustments in renal blood flow normally occur acutely with postural changes. During prolonged spaceflights, the major effects of weightlessness on the renal circulation are unknown and the consequences of an absence of these reflex adjustments may only be speculated. Astronauts exposed to long periods of weightlessness are likely to have decreased renal sympathetic nerve activity with a tendency toward vasodilation. In addition, changes in concentration of a variety of blood-borne humoral agents, such as angiotensin II, catecholamines, and certain other hormones and plasma electrolytes are likely to alter renal excretory function, renal blood flow, glomerular filtration rate, and renal endocrine function.

Measurements of renal pressure, renal blood flow, or glomerular filtration rate have not yet been made during spaceflight or after return to earth. Alterations in these parameters could have profound effects on renal excretion of fluids and sodium, renin release, prostaglandin release, and peritubular factors [22,62,67]. A number of observations and anticipated responses during spaceflight could therefore be attributed to an altered renal hemodynamic state. These observations include the postulated diuresis and natriuresis of the acute stress stage as well as the longer, persistent secretion of angiotensin and aldosterone. Excess renal excretion can occur as a result of a simple direct pressure effect at the glomerulus. While there is evidence to show that cephalad fluid shifts can increase renal flow appreciably [28,41], the long-term effects as observed in bedrest are unclear. This evidence will be reviewed in Chapter 9.

5.3.6 Dilution of Body Fluids: Implications for Fluid Regulation

The engorgement of fluid in the upper body during weightlessness is believed by some investigators to be sustained [68]. Reconciling this postulated hypertensive state with the enhanced renin-angiotensin and aldosterone secretion observed during spaceflight is difficult. These hormones are usually associated with hypotensive circulatory states [22]. On the other hand, ADH was decreased nearly throughout the three-month mission, which would be in accord with enhanced volume receptor activity [25]. It has been argued though, that the ADH pathway becomes insensitive to abnormal pressure changes that are sustained [21]. However, the whole question of a prolonged hypertensive state during spaceflight has not been experimentally confirmed. Pressures in the capacitance vessels and cardiopulmonary regions have not yet been measured directly, and the extent of upper body congestion has not been quantitated. (This also seems to be true with regard to prolonged water immersion and bedrest.) Resting mean arterial pressure in the Skylab crew was not above preflight levels.[UPDATE#3]

This study has evaluated another piece of evidence that has not received any attention to date and which may be related to these circumstances. The Skylab data show that plasma fluid was slightly hypotonic throughout the flight, with respect to sodium concentration (and total osmolarity) and in comparison to the preflight mean. As shown in Fig. 5-20, hyponatremic plasma has also been observed in several long-term bedrest studies and even in short-term water immersion [69]. This condition is puzzling for the following reasons: a) the body's thirst and renal mechanisms are capable of maintaining normal sodium levels within narrow limits; b) the hormones thought to regulate water and salt were at levels appropriate to correct decreased plasma sodium, (that is, sodium-retaining aldosterone was high and water-retaining ADH was low); and c) urine volume was nearly normal but sodium excretion was elevated above preflight levels in spite
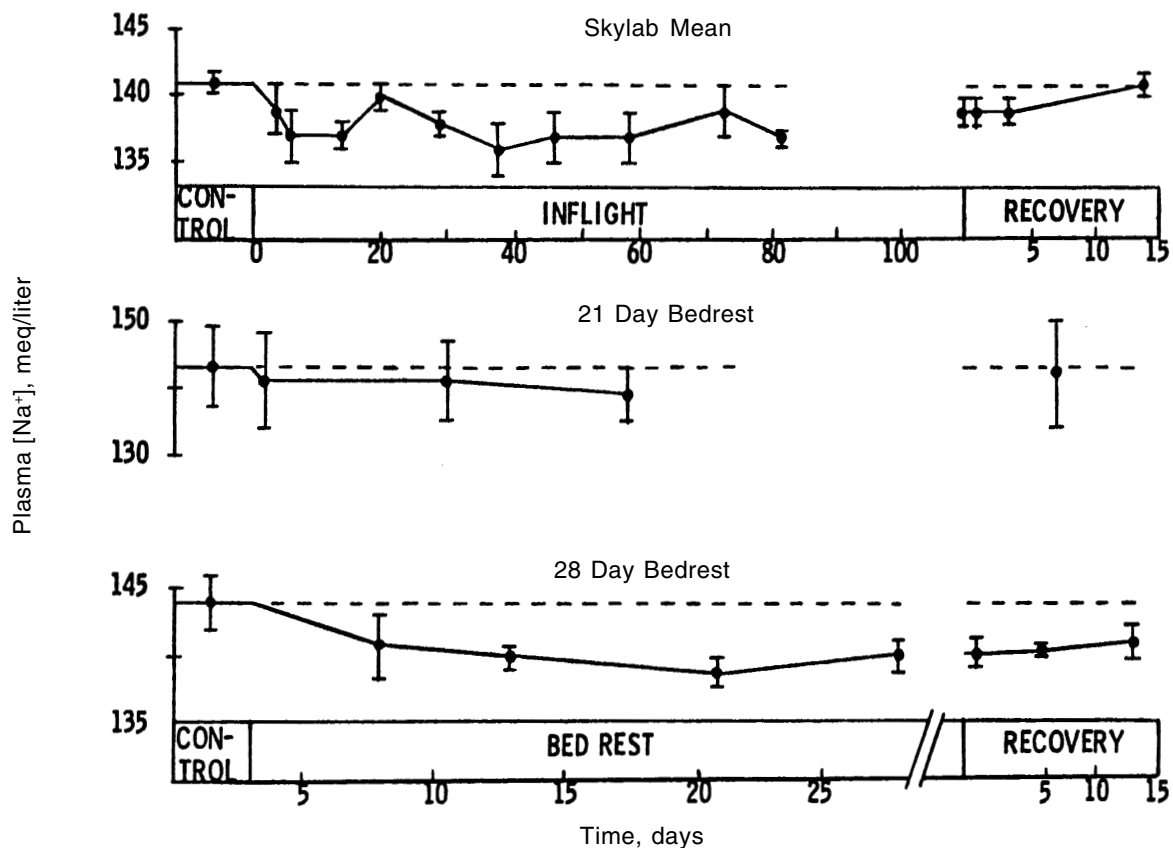
Figure 5-20. Effect of spaceflight and bedrest on plasma sodium concentration.

of enhanced aldosterone. An appropriate compensation for plasma hypotonicity would involve a hypertonic fluid intake and/or a hypotonic renal output. In fact, the Skylab data demonstrates quite the opposite for both of these pathways, thus indicating how the body fluids maintained their hypotonicity from a metabolic balance point of view.

Although the etiology of this phenomenon remains unresolved, the effects of hyponatremic extracellular fluids on fluid-electrolyte regulation must be considered. In particular, the sodium depleted, hyponatremic state has been shown to activate the renin-angiotensin system and induce hypersecretion of sodium-retaining aldosterone [56]. In addition, hyponatremia is known to depress thirst drive and ADH secretion, thus promoting renal excretion of water. All of these effects were noted to varying degrees on the Skylab crew. Whether or not they were induced by hyponatremic influences is unknown.

Hyponatremia also indicates that intracellular fluid is dilute and may be expanded unless accompanied by body losses of intracellular electrolytes [27]. This follows from the osmotic theory of water distribution across the cell membrane. The data from Skylab, taken as a whole (including measured losses in fluid volume and electrolytes), therefore indicates that all body fluids were dilute and hypovolemia existed (relative to preflight levels) in both intracellular and extracellular fluid. It is apparent that more electrolytes were lost from the body relative to the loss of fluid.

One can only speculate about the adaptive value of maintaining a hyponatremic body fluid. There appears to be an effect, similar to that found in chronic sodium depletion studies, in which extracellular volume is protected at the expense of extracellular osmolarity [31]. In other words, correction of hyponatremia in spaceflight would involve excretion of extracellular fluid volumes that are already significantly reduced. However, while sodium depletion in one-g invariably leads to both hyponatremia and hypotensive states, these events may be dissociated in zero-g, (that is, a hypertensive state of the upper body circulation may coexist with a condition of hyponatremia). It is unclear how the body is able to sense an absolute hypovolemia when fluid expansion seems to be prevalent in the regions of the cardiopulmonary mechanoreceptors. Thus, a study of the development of decreased serum sodium and measurement of the degree of upper body congestion on future flights may help reconcile the unusual combination of hormone levels (enhanced angiotensin and aldosterone and decreased ADH) encountered during hypogravic stress.

5.3.7 Fluid-Electrolyte Balance During Prolonged Spaceflight

Most of the major changes in body fluids (especially extracellular fluids) appear to occur during the first several days of flight. Observable losses of 1.8 liters of leg

volume and 1.5 kg of body weight were measured during that time. The physiological mechanisms that could have led to this result have been presented earlier in this section. An hypothesis which remains to be examined is whether the body establishes a new homeostatic level after these initial losses with respect to water, sodium, and potassium. There are several lines of evidence that suggest that water and sodium are in balance while potassium shows some continued loss. These data have been reviewed in Chapter 4 and will be re-examined and summarized in the following section.

A related question that has arisen is the following: if the body is in relative balance during the adaptive segment of the flight, why is it that excretion of fluids and electrolytes is elevated, on the average, during this period, compared to preflight? The answer should consider other metabolic avenues of loss and gain such as fluid intake and sweat losses. In the next section, the metabolic balance data will be re-examined to explain the altered pattern of fluid-electrolyte excretion on the basis of long-term disturbances in intake and sweat losses. The simulation model was valuable in helping to integrate the metabolic balance data and in determining not only its internal consistency but also in revealing the physiological mechanisms that play a role in establishing homeostatic levels.

5.4 Subsystems Evaluation of Hypotheses

The previous section discussed in qualitative terms, the factors that could potentially contribute to the loss of body water and major electrolytes during spaceflight. The purpose of this section is to discuss the evaluation of those hypotheses, in quantitative terms, by using actual flight data and predictions from the mathematical models. This effort represents the culmination of a wide spectrum of systems analysis activities, including data processing, qualitative analysis of physiological control mechanisms, hypotheses development, and quantitiative hypothesis testing.

5.4.1 Hypotheses Tested by Computer Simulation

The present analysis has been guided by the overall hypothesis that the observed changes in the renal, cardio-vascular, and endocrine subsystems of the Skylab crewmembers can be attributed, in large part, to the shifts in fluid volumes and electrolytes that occur as a result of weightlessness. This concept has been subjected to critical examination by breaking it into a smaller set of hypotheses. These hypotheses can be best understood by considering the types of fluid shifts that occur in microgravity and the approach used to simulate them.

The often described *acute cephalad intravascular shift of blood* from the lower extremities is only one of many types of fluid disturbances which must be considered (see Fig. 5-21). *Extravascular fluid in the legs* (i.e., filtrate) also must contribute to the initial rapid headward movement. *Longer-term migration of fluids from the legs* due to elastic tissue forces or tissue degradation does occur, but the significance of this effect has not yet been

established. Alterations in *plasma/interstitial* and *intracellular/extracellular* fluid exchange may also be expected, although quantitative documentation of these effects is sparse. In addition, the *overall water balance of the body* is dependent on factors that modify *fluid intake*, *evaporative water loss*, and *renal excretion*. In all cases, one or more of the major body electrolytes is associated with the movement of fluid; sodium is primarily associated with extracellular fluid and potassium with intracellular fluid.

The challenge to the computer simulation process was to ensure a correct representation of these diverse fluid disturbances. Given the mathematical representation of the stresses encountered in weightless spaceflight, the model's responses can be compared to the astronaut data obtained inflight or immediately postflight. During these studies, two types of questions were therefore addressed: a) what are the appropriate zero-g stresses to impose on the model in order to evoke the observed responses; and b) does the model contain a complete enough description of fluid-electrolyte control to allow it to produce a realistic response? In more than several instances, it was found that the model lacked certain features such as leg compartments and orthostatic mechanism. Other sections of this document describe the modifications that were performed on the models to correct the deficiencies so that appropriate responses to bedrest, water immersion, and postural change could be obtained. In this study of long-term spaceflight, the only additional effect needed was a natriuretic hormone; otherwise, the model modified with legs performed surprisingly well (see Chapter 3.2.5.2).

The stimulus for weightlessness that was ultimately used in the Guyton model for this study took advantage of the fact that the fluid-electrolyte model is extremely stable in a "supine" position. The hypogravic simulation was initiated from this reference state. In order to achieve the fluid shifts from the legs to the upper body in the supine position, it was necessary to artificially induce fluid movement from leg extracellular compartments where it was assumed that fluid was previously pooled. Just as standing has often been viewed as a functional hemorrhage of the central blood compartments into the leg vasculature, these stresses simulating hypogravity would be similar to an infusion of leg fluid into the upper body's circulation. While this approach resulted in successful simulations for many short-term responses, other acute and most long-term events observed during spaceflight could not be realistically simulated by headward fluid shifts alone. Therefore, other hypotheses were added as the simulation study proceeded, and as greater fidelity was required.

The specific hypotheses evaluated in this study were the following:

1) and 2) **Acute Headward Fluid Shifts:** Do the acute headward fluid shifts observed in such experiments as water immersion, head-down tilt, and infusions produce short-term responses typical of these stresses including volume receptor activation, plasma loss, interstitial/plasma redistribution, diuresis, and natriuresis? Can the model help distinguish between headward shifts of fluid arising from the leg vascula-
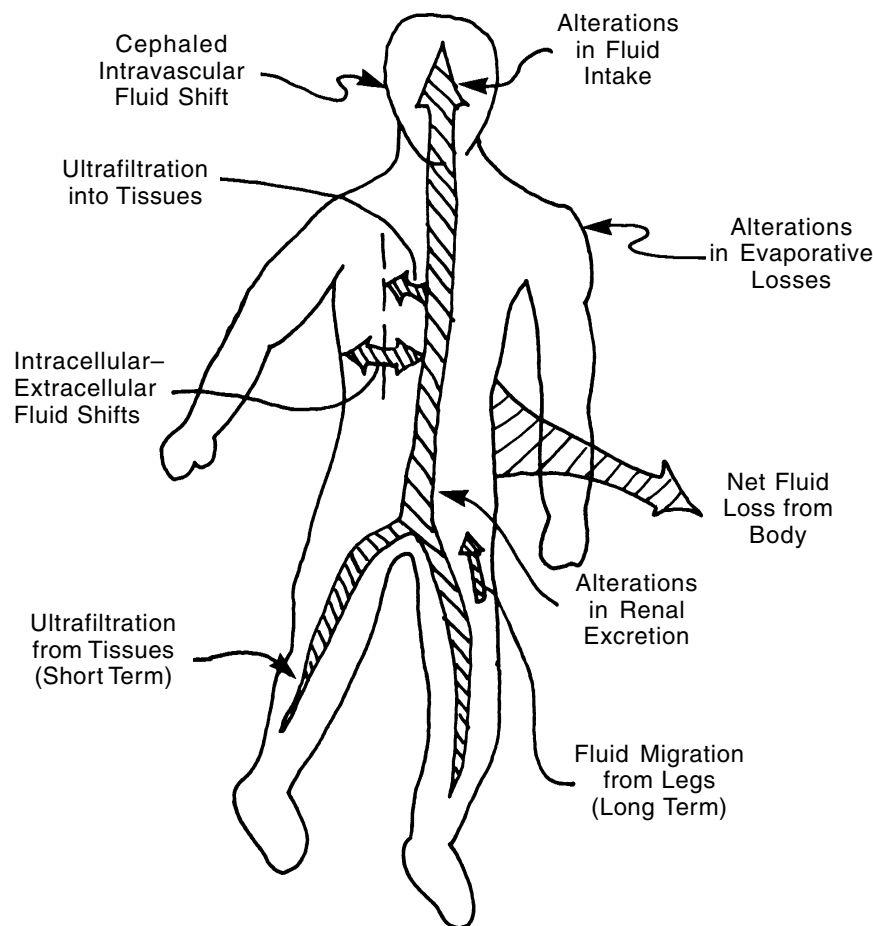
Figure 5-21. Types of fluid shifts during weightlessness. Consideration of each of these disturbances is necessary in order to realistically simulate the spaceflight fluid-electrolyte response.

ture (blood) (Hypothesis 1) in contrast to that from the leg tissues (plasma filtrate) (Hypothesis 2)?

3) **Potassium Release From Intracellular Compartment**. Can potassium release quantitatively explain the longer-term changes in loss of body potassium, elevated plasma potassium, intracellular/extracellular fluid redistribution, renal excretion of potassium, and altered endocrine behavior?

4) **Natriuretic Factor**. Can a natriuretic agent explain renal excretion of sodium not accounted for by other mechanisms in the model as well as production of hyponatremic body fluid?

5) **Alteration in Sweat Component**. Are sweat components altered from control conditions and does this contribute to observed changes in renal excretion and electrolyte concentrations in plasma and urine?

6) **Alterations in Metabolic Intake**. Does the early reduction in intake observed in the astronauts modify the diuresis and natriuresis that are otherwise expected to occur?

An important concept that guided the simulation analysis was that the mechanisms that participate in the short-term response (the time during which the most promi-

nent fluid-electrolyte disturbances occur) are different from those that lead to adaptation during prolonged spaceflight. Therefore, the hypotheses evaluation study was divided into acute and chronic phases as a convenient method of examining the spaceflight data and performing computer simulations. The circulatory, fluid, and electrolyte model is capable of simulating both short and long-term responses. This is not unlike investigators who are interested in the 2 to 4 hour response to water immersion in contrast to other researchers who perform a 5-day bedrest study.

Two sets of data were most crucial for the simulation analysis. One of these was related to describing the magnitude and time course of the headward shift of fluids. The second group of data was that related to the metabolic balance of water, sodium, and potassium and the related measurements reflecting whole body changes in these quantities. It was discovered early in the investigation that the amounts and ratios of water and electrolytes for the intake, excreta (including sweat losses), and, body fluids must be specified in order to produce a realistic simulation for prolonged adaptation.

The final integrative simulation utilized headward fluid shifts, metabolic intake, and sweat loss as major forcing func-

tions for the model. A critical analysis, summarized in this section, was performed on each of these groups of data.

For convenience, the hypotheses evaluation discussion has been divided into two parts: a) hypotheses related to altered fluid distribution including acute headward shifts, extracellular and intracellular, as well as interstitial and plasm fluid distribution; and b) hypotheses related to altered metabolic balance, including altered intake, excretion and sweat losses. Both groups of hypotheses were found to be necessary to account for the dynamic behavior of the fluid-electrolyte regulation during the Skylab missions.

5.4.2 Hypotheses Related to Altered Fluid Distribution

The redistribution of fluid within the body during weightlessness includes headward shifts, dehydration of the legs, extracellular/intracellular shifts, and interstitial plasma exchange. Spaceflight data related to these effects are quite sparse and have been summarized in Table 5-2. This next section begins with a critical examination of the headward shift phenomenon, which is perhaps the singular most important physiological event characterizing weightlessness. This analysis forms the foundation for the subsequent computer simulations of altered fluid distribution.

5.4.2.1 Analysis of Altered Fluid Distribution.
For convenience, this physiological disturbance has been segmented into three phases: a short-term (acute) phase, lasting several hours to one day; an intermediate phase, which appears to stabilize after several days; and a long-term phase, lasting the remainder of the mission.

5.4.2.1.1 *Short-term Fluid Shifts*.
In one-g, a critical factor affecting blood distribution is the hydrostatic gravity load on vertical columns of blood causing pooling of fluid in the legs.. The immediate effect of a reduction in hydrostatic forces is a rapid shift of blood from the legs toward the head. Blood volumes are distributed in zero-g in accordance with any net extravascular tissue forces and compliances of the blood vessels throughout the body.

Leg volume measurements during acute postural changes or leg negative pressure studies suggest that 400 to 600 ml of blood is highly mobile and is immediately transferred between legs and upper body (primarily thoracic volume) [71,72]. Muscular contraction during standing can reduce this amount somewhat [73]. Immersion studies have demonstrated immediate expansion of central blood volume by 700 ml [74] at the expense of pooled blood in the lower extremeties. During weightlessness, it would be expected that this pooled blood is the first reservoir to be mobilized and shifts rapidly headward. In addition, there is another approximately 500 ml of plasma that is normally pooled extravascularly in the leg tissues upon standing. Tilt studies suggest that this extravasation is complete within 30 minutes. This fluid is probably returned to the leg vasculature and eventually to the upper body in a hypogravic environment, and probably moves headward more slowly than the blood pooled in the leg. Thus, at least a liter of fluid is normally pooled in the legs

Table 5-6. Leg Volume Changes During Skylab [16]*

Time	Leg Volume
0	0
6 hr.	-1 liter
1 day	-1.3 liters
4 day	-1.8 liters
84 day	-2.2 liters
R + 0	-1.5 liters
R + 7	-0.2 liters

* See Fig. 9-10 for a graphical representation of this data

R = Recovery Date

when standing and is available to shift toward the head during zero-g.

In zero-g, a portion of this volume enters the normally collapsed head and neck veins until they are full. Any additional volume beyond this zone of free distensibility in the upper part of the body contributes toward increasing blood pressures and will initiate renal mechanisms, which act to reduce the excess volume. In addition, the increase in circulatory pressures may increase capillary pressures and provide a driving force for filtration into the interstitium.

A composite picture of the data obtained from the Skylab and Apollo–Soyez Test Project crews suggests a time course of leg volume changes shown in Table 5-6 [16]. Examination of these data suggests that there is an acute fluid shift of about 0.7 to 1.0 liters from the legs when entering zero-g, which is quickly returned when leaving zero-g. This shift is complete within several hours and appears to be consistent with the quantity of leg interstitial and vascular fluid mobilized during orthostatic stress tests.

Determining the sources of the leg fluid changes is made more difficult because of the uncertainty of the preflight reference leg volume measurement. If the reference position in one-g was the upright state, then the loss of a liter of fluid from the legs (during the first few hours inflight) can be easily explained as noted above. However, the actual reference (control) position was not upright, but was supine for perhaps one-half hour after ambulation. Thus, an unknown portion of previously pooled fluid (approximately 0.5 to 1.0 liters based on tilt studies in one-g) was probably removed from the legs by the time the reference measurement was performed. This makes the changes observed during spaceflight even more dramatic when compared to ordinary postural changes in one-g [68].

It is possible that the interstitial tissues in the legs contain a larger amount of readily mobilized fluid than has been previously recognized. Estimates of fluid pooling in the tissues during one-g orthostasis have come, in part, indirectly from plasma volume measurements before and after tilt. There is some indication that, during these postural changes, outward filtration of plasma in the legs is accompanied by some inward filtration in the upper

Table 5-7. Properties of the Upper And Lower Body Compartments*

	I. Weights, Volumes, and Water					
	Weight		Volume		Water	
Body Segment	Kg	%	Liters	%	Liters	%
Upper Body	45.8	65.5	50.5	76.6	32	48.8
Legs	24.2	34.5	15.4	23.4	10	14.9
Total	**70.0**	**100.0**	**65.9**	**100.0**	**42**	**63.7**

II. Fluid Compartments		
Compartment	Body Fluid Volume (liters)	Leg Fluid Volume (liters)
Plasma	3.0	0.75
Interstitial	16.0	3.75
Intracellular	23.0	5.50
Total	**42.0**	**10.0**

(1) Based on 70 kg man, whole body sp. gr. = 1.062

(2) Weight distribution from Bioastronautics Data Book [9]

(3) Leg fluid volumes based on total body proportions.

body [75]. If this is true, then the tissue fluid accumulation in the legs could be the sum of the net change in plasma volume plus this reabsorbed fluid.

5.4.2.1.2 *Intemediate-term Fluid Shifts.* At the end of several days inflight, a total of 1.8 liters of fluid may be lost from the legs. The idea that this fluid is transferred to the upper body and then excreted through the kidneys in accordance with the volume reflex pathway gains credence from the finding of nearly 1.5 liters reduction in computed total body water by the third or fourth day inflight. This shift of nearly two liters from the legs is a much larger volume than is usually associated with acute postural changes in one-g. This suggests a gradual loss of blood, interstitial, and perhaps intracellular fluid from the lower extremities, which is essentially complete within several days. An attempt was made to estimate the contribution of each major fluid compartment to this total loss. Volumes of leg compartments are not known precisely but were approximated from available data on upper and lower body weight distributions (see Table 5-7). Accordingly, a loss of two liters from the legs represents a 13% of total leg volume, 20% of leg fluid volume, and 45% of leg extracellular volume. Certainly, there is not enough blood in the legs to account for the total changes observed.

5.4.2.1.3 *Long-term Fluid Shifts.* Prolonged absence of hydrostatic forces may result in further depletion of the leg fluid volumes. By the second and third month inflight, leg volume decreased by a total of more than two liters. Eighty percent of this is completed during the first week, as previously discussed. Beyond the first week inflight, the data become more difficult to interpret. Loss in leg volume during this period can be ascribed to further dehy-

dration of the legs (plasma, interstitial, or intracellular fluid), but most assuredly there is a significant component due to loss of muscle tissue. Calf girth measurements indicate a clear trend toward decreasing circumference throughout the entire three-month mission of the 84-day mission [16]. In addition, nitrogen and potassium balances are strongly negative during the flight, particularly during the first month, although it is not possible to determine from which part of the body these elements are derived (see Fig. 4-22). Biosteriometric measurements, however, confirm that at recovery day the greatest relative volume losses in the body occurred in the calves [76,77]. Loss of leg strength was also noted following reentry. Perhaps half of the long-term volume loss in the legs, or approximately 200 ml, was due to increased fluid drainage involving interstitial, lymphatic, vascular, and intracellular compartments and the other half may represent cell solids.

The inflight water balance suggests that after an early loss of 1.5 liters of body water, total body water did not decrease further, but remained approximately constant with a tendency to return toward control (see Fig. 4-26). At recovery, the data suggest a deficit of 0.8 to 1.1 liters in total body water. This is smaller than the loss of leg volume (–1.5 liters at recovery), and suggests that of the total fluid shifted from the legs, a large segment is removed from the body, and a smaller, but significant portion (perhaps several hundred ml) may be stored in the upper body. The upper body pooling during zero-g may be considered the reverse of fluid pooling in the legs during standing. If upper body fluid storage does occur, it can account for the almost universal inflight symptoms of head fullness and nasal stuffiness, facial plethora, and distended neck and scalp veins [16]. It is not clear whether the excess fluid was accepted by the vascular or extravascular compartments.

In the face of an expanded central blood volume during spaceflight, the circulatory components are capable of permitting a portion of the excess volume to be accepted without proportional increases in blood pressures. This is accomplished by processes such as vascular stress relaxation and vascularization (i.e., increases in number of capillaries). There is a possibility that these processes occurred in the upper body during the prolonged inflight phase of Skylab, when venous distention and head fullness were noted. During the two-week postflight period, the plasma volume of most all crewmen showed a tendency to increase several hundred ml above preflight control. Similar overshoot effects have been noted following bedrest. These effects remain unexplained. However, if stress relaxation of the veins or vascularization in the upper body occurred during prolonged spaceflight, it would be expected that upon return to one-g, the return of vascular volume to normal size would take several weeks to be complete. Until this occurs, the capacitance of the circulation would be expected to be higher than normal. A similar volume compensatory process, but in reverse (i.e., reverse stress relaxation and devascularization) could have occurred in the legs during zero-g exposure, thus tending to keep vascular capacity constant or reduced [45]. Little is known, however, regarding the relative differences in vascular reactivity between upper and lower body circulatory vessels. The possibility exists that leg vessels can resist high pressures (as in one-g orthostasis) more easily than the upper body vasculature and that stress relaxation effects may be more prevalent in the latter region.

5.4.2.1.4 *Recovery.*

The average deficit in leg volume for the nine crewmen at recovery was 1.5 liters (see Table 5-6). However, inflight data from the 84-day mission suggest this may have been actually as much as 2.2 liters, if measured immediately prior to reentry. Therefore, nearly 700 ml of fluid enters the legs between the start of reentry and first recovery measurement, despite the fact that the crewmen wore leg pressure garments during this interval.

This is approximately the amount of fluid that shifts toward the head immediately after launch and confirms the quantity of easily mobilized fluid recorded during postural changes and water immersion. By the end of the first week of the postflight period, the leg volume has nearly returned to normal.

5.4.2.2 Simulation and Hypothesis Testing of Altered Fluid Distribution.

Having developed a quantitative scenario for the progression of headward fluid shifts in microgravity, it was then possible to simulate these fluid disturbances and to examine their physiological consequences with computer models. Specifically, the purpose of these simulations was to test the six hypotheses listed in Chapter 5.4.1. Spaceflight data during the acute phase are incomplete, and reference will therefore be made to ground-based zero-g analog experiments for determining the veracity of the computer predictions. A more detailed description and simulation of these ground-based studies will be found in Chapter 9.

Hypotheses #1 and #2: Acute Headward Shift of Leg Blood and Tissue Fluid.

One of the most significant acute responses to exposure to zero-g is a shift of pooled fluid from the legs to the upper body. The fluid shifted headward is assumed to consist of two components: a) blood originally pooled in the vessels (primarily veins) of the legs, and b) plasma filtrate pooled in the interstitial spaces of the legs. This hypothesis was examined in the model by forcing both blood and tissue fluid from the leg compartments and recording the simulated response. The quantity of mobilized fluid from each compartment is imprecisely known, but for convenience, it was assumed that one liter of fluid was shifted rapidly from the extracellular fluid of the legs. Further, it was assumed that half of this (500 ml blood) was derived from the leg vascular compartment and the other half from the leg interstitial compartment (500 ml plasma filtrate). These agree in general with changes in leg volume measured during the first few hours after launch into zero-g and with changes in blood volume measured during one-g tilt and immersion studies (see Table 5-6 and Chapter 9).

Although these two volume shifts occur simultaneously, it is possible to evaluate their effects separately using the modified Guyton simulation model, an analysis not possible by experimental means. The results of this analysis are shown in Fig. 5-22. The predicted responses to the simultaneous movement of *both* blood and filtrate from the legs are shown in Fig. 5-23. In this figure, the response has been extended from two days to two weeks to study long-term behavior.

The simulation of a 500 ml shift of blood (solid line, in Fig. 5-22) from the leg vasculature was accomplished by reducing the unstressed volume of the leg venous compartment. The other simulation of a 500 ml shift of plasma filtrate (dashed line in Fig. 5-22) was achieved by increasing the tissue pressure in the legs and allowing tissue fluid to be reabsorbed into the vasculature through the ordinary routes of capillary exchange. Both of these fluid volumes are, therefore, initially conserved intravascularly, where they are redistributed according to the compliances in the seven blood containing compartments of the model.

As the fluid enters the central blood compartments, there is an increase in blood pressure which initiates the complex sequence of events suggested in Figs. 5-15 and 5-17. This scenario is reproduced by the simulations shown in Fig. 5-22 and 5-23. The expected transient diuresis and natriuresis can be observed, as can be the final reduction in total body water and body sodium. Figure 5-24 is an attempt to depict the causal events in these two simulations and to contrast their differences. Accordingly, Fig. 5-24 indicates that during both simulation cases there is a reduction in leg volume and body water and salts, and increases in circulatory pressures and urine excretion. However, other factors, such as the blood volume, interstitial fluid volume, and hemoconcentration responses are quite different. These differences, which arise primarily because whole blood contains colloids and red cells while the plasma filtrate does not, may be summarized as follows:
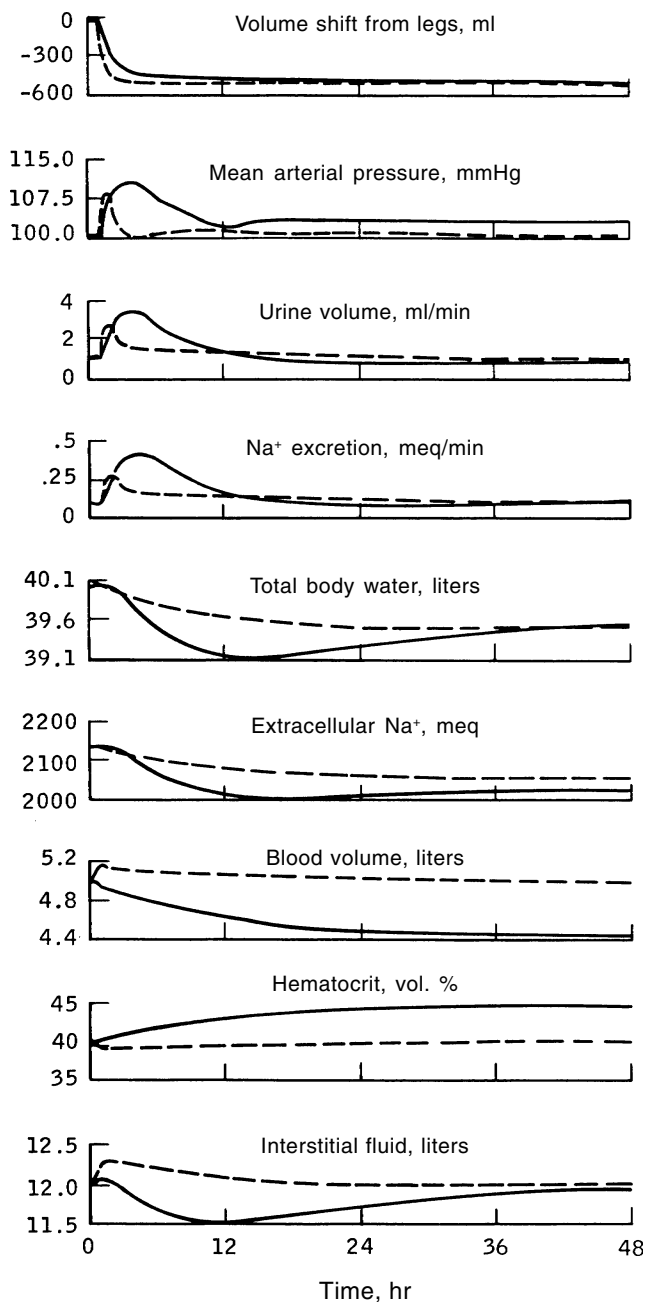
Figure 5-22. Simulation of circulatory, fluid, electrolyte and renal responses to fluid shifts from the legs: (a) 500 ml blood shift from legs (solid line), and (b) 500 ml filtrate shift from legs (dashed line). The bottom graph refers to the upper body interstitial fluid.

Figure 5-23. Simulation of circulatory, fluid, electrolyte and renal responses to combined blood (500 ml) and filtrate (500 ml) shifts from the legs. Note that the timescale is different from Fig. 5-22.

a)   In the case of the filtrate shift, the original blood volume is initially expanded as leg tissue fluid enters the circulation. Intravascular red cells and plasma colloids are diluted by this filtrate. On the other hand, the translocation of blood from the legs expands the central blood volume but the total blood volume does not initially change; neither does hematocrit, nor colloidal osmotic pressure. The eventual reduction in

blood volume occurs only in the case of a blood shift inasmuch as blood volume (transiently increased) is restored to normal following the filtrate shift.

b)   In both cases there is a tendency for the excess central blood volume to be eliminated via transcapillary filtration into the upper body and into the renal tubules. However, in the case of the whole blood shift, this results in hemoconcentration and an increase in the concentration of plasma colloids, but in the case of the filtrate shift, there is no net increase in red cell or colloidal concentration because the original inward shift from the legs did not contain these components.
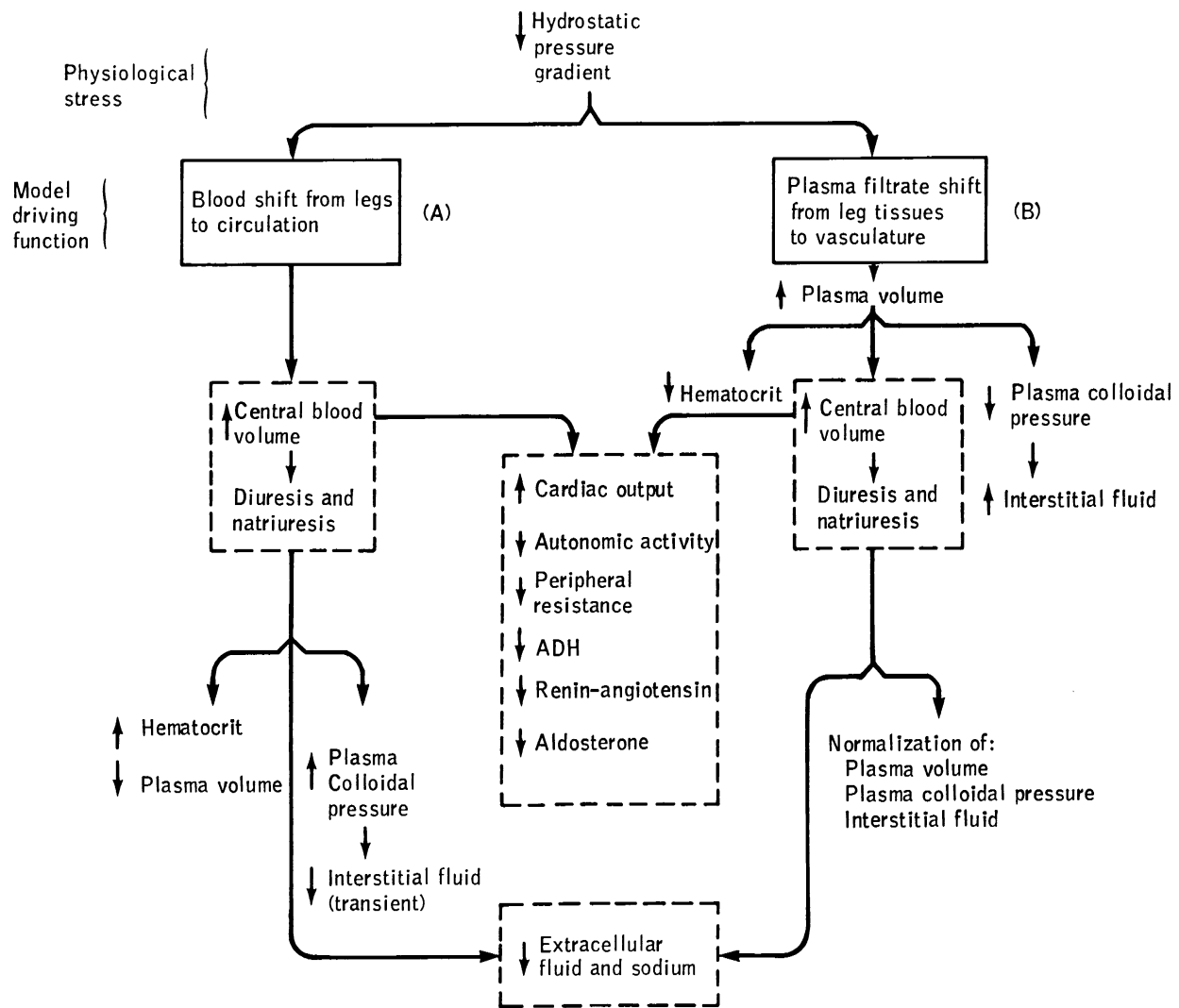
Figure 5-24. Hypotheses for simulation of fluid shifts during the first day of weightlessness. This diagram considers two type of headward fluid transport: (A) a blood shift from the legs to the central circulation, and (B) a plasma filtrate shift from leg tissues to the vasculature. The dashed boxes contain the events which are common to both events. These pathways were determined from the simulated behavior of the model during the responses illustrated in the previous two figures.

Thus, the hematocrit increases for the blood shift but not for the filtrate shift.

c) Although the total amount of fluid shifted in both cases is identical, the magnitude of the pressure and renal response is more dramatic for the shift in blood than for the shift in filtrate. In these simulations, the entire blood shift is forced into the upper body vessels and thereby increases central pressures more than in the case of the filtrate shift, the latter of which has been allowed to distribute between both upper and lower body compartments.

d) Outward filtration from the central circulation to the surrounding tissues of the upper body is enhanced by the dilution of plasma colloids in the case of the filtrate shift and attenuated by hemoconcentration in the case of the blood shift. Thus, in the former case,

upper body interstitial volume increases, but in the latter case there is a net decrease in interstitial fluid. This excess fluid is immediately excreted by the kidneys, and therefore, contributes to the diuresis. Thus, for this reason as well as the one mentioned above, the magnitude of the blood pressure and renal responses may be more dramatic for the shift in whole blood compared to the shift in filtrate. Similar changes have been reported in infusion studies of blood and saline in experimental animals [78,79].

These studies have suggested that the total response will depend in large measure on the total volume of fluid shifted as well as the ratio of filtrate/whole blood that is shifted. These factors are undoubtedly different for the various hypogravic maneuvers in use today, including

water immersion, head-down tilt, bedrest and spaceflight, because the initial stress on the legs is different. For example, total leg volume decrements have been reported to vary from about 500 ml during supine bedrest, to 900 ml during head-down tilt, to more than 1500 ml during spaceflight. Therefore, the acute responses of each of these stresses may be different, not because of some fundamentally different reaction, but merely because of the difference in tissue fluid volume mobilized compared to that for whole blood. Unfortunately, there is no practical means of measuring these differences directly. It may be possible, however, using parameter estimation techniques, to assess the filtrate/whole blood shift ratio by comparing model and experimental responses.

How do these simulations compare with spaceflight related experiments? The initial simulation responses of pressure, urine excretion, changes in fluid volumes, electrolyte quantities, and hematocrit, (Fig. 5-22) are quite similar to those observed during a typical 4 to 6 hour water immersion experiment [43,44,57]. The long-term effects predicted by the model (Fig. 5-23) indicate that all quantities return toward normal except for total body water and sodium, leg fluid volume, and blood volume. This is similar to observations in prolonged bedrest and spaceflight.

The transient changes in total body water and interstitial fluid, which are predicted to occur the first day (Fig. 5-23) have not been reported in space. Special measurement techniques would be required to evaluate the rapid changes of these quantities (including over- and under-shoots) noted in the simulation. While it has been previously postulated that the reduction in blood volume secondary to hypogravic exposure is accomplished both by renal excretion and transport into the interstitial reservoir [45], the role of colloidal oncotic forces has not heretofore been seriously considered. The simulation suggests that the colloidal oncotic forces could be an important factor in the short-term response, since changes in colloidal forces are equivalent to hydraulic forces with respect to transcapillary movement. This aspect has been studied in greater detail as reported in Chapter 9.

This analysis demonstrated that fluid shifts from the legs could indeed account for some of the important short and long-term circulatory, renal, hormonal, neural, and fluid-electrolyte disturbances observed in various studies of hypogravity. However, many of the responses that were found in Skylab subjects could not be achieved with the model by a simple internal shift of fluids. In particular, the diuresis and natriuresis predicted by ground-based studies and supported by model results have not been observed in space, nor can this hypothesis account for intracellular losses of fluids and electrolytes. For that reason, other hypotheses were tested.

Hypothesis #3: Release of Potassium and Water From Cells. Losses of cellular constituents (including water, electrolytes, and nitrogen) were observed in the Skylab crewmembers as well as in subjects undergoing prolonged bedrest. While these losses may contribute to decrements in musculoskeletal function (i.e., calcium loss

and loss of strength), the full significance of these changes has not yet been ascertained. However, secondary effects may be expected from the biochemical products of tissue catabolism, which are released into extracellular fluids and the circulation, thereby increasing the excretory load of the kidneys. These biochemical effects were examined in this study, and a more realistic simulation of fluid and electrolyte loss was obtained.

The cell compartment is represented in the fluid-electrolyte model by a simplified formulation; potassium and water are its only constituents. However, transfer of water is permitted to take place across the cell membrane according the osmotic gradient between potassium rich fluid on one side and sodium rich fluid on the other. In addition, the membrane is impermeable to sodium, while a pump mechanism maintains potassium in the cells. Excess extracellular potassium can be regulated by either active transport into the cells or excretion by the kidneys under control of aldosterone.

Figure 5-25 shows the results of a simulation, in which 70 meq of potassium was artificially forced from the cells in an exponential manner, over a four-week period. As potassium leaves the cells, plasma potassium concentration is elevated and renal potassium excretion increases by approximately 20% before gradually returning to normal. As expected, water follows potassium from the cells and extracellular volume expands temporarily at the expense of intracellular fluid. Renal potassium excretion increases as a result of plasma potassium stimulation of aldosterone secretion. However, aldosterone's sodium retaining properties reduce renal sodium excretion and the extracellular sodium concentration increases. This creates an additional osmotic effect in depleting cellular fluid. Notice that the decrease in sodium excretion is only temporary, and within several days, it rises slightly above control. This occurs at a time when aldosterone is still elevated. Thus, the model exhibits an "escape" phenomenon. The increase in aldosterone is due to the elevated potassium level in plasma and not due to angiotensin. In the model angiotensin is shown to be suppressed. These effects of the potassium release mechanism are summarized in the hypothesis diagram of Fig. 5-26.

The combination of hypotheses #1, #2, and #3 is illustrated in the simulation results of Fig. 5-27. The loss of cell potassium leads to a more realistic prediction of body water loss, intracellular water loss, plasma potassium concentration, angiotensin, and aldosterone levels. One quantity that is not in agreement with experimental findings is plasma sodium concentration, which is transiently increased before returning to normal. As a result, ADH is predicted to increase. However, observations on Skylab indicated that sodium concentration in fact decreases by about 3% and ADH significantly decreases.

The relative quantities of potassium and water that are derived from the cell compartment of the model is another apparently questionable result. The simulation study, shown here, required a release of only 70 meq potassium in order to effect the transfer of 500 ml intracellular fluid. In contrast, more than three times this quantity of body
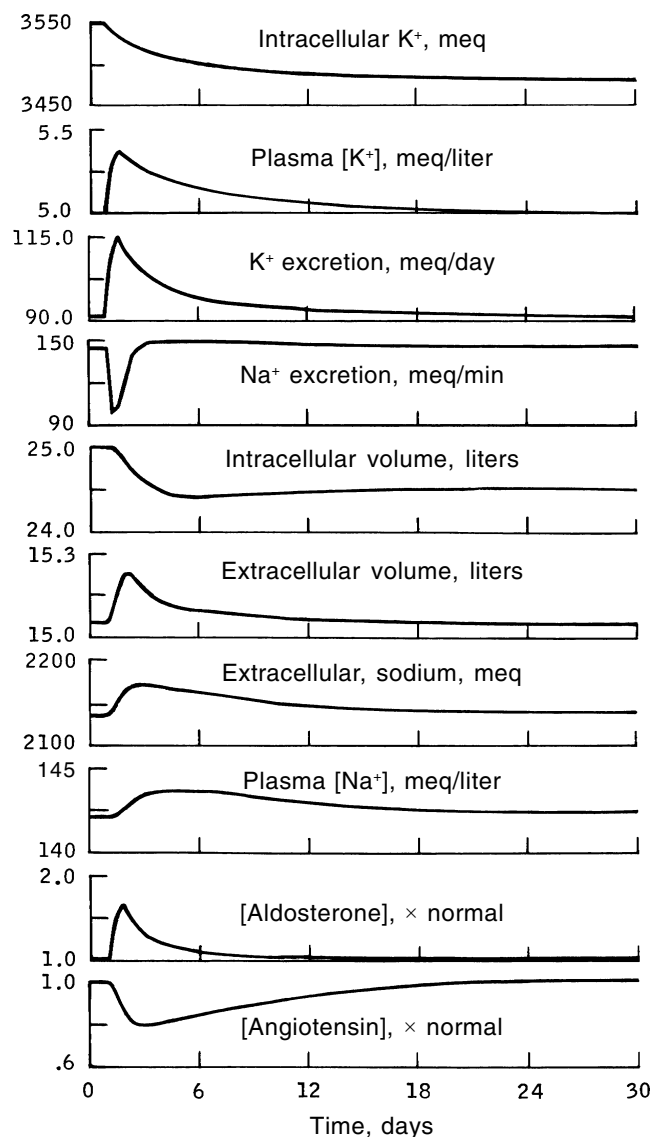
Figure 5-25. Simulated fluid, electrolyte, hormonal and renal responses to the release of cell potassium.

Figure 5-26. Hypothesis derived from simulation showing the events leading to reduction of lean body mass (cell water and potassium) during prolonged weightlessness.

potassium was lost from the Skylab crew, although the cell water loss was the same as with the model (see Table 5-2). Another way of looking at this is to assume a nominal cell potassium concentration of 150 meq/1; then the loss of 240 meq potassium measured in the human subjects would be expected to result in an iso-osmotic loss of 240/150 = 1.6 liters of water, or three times that measured.

In order to account for the measured losses of cellular water and potassium, it is necessary to hypothesize that cell fluid tonicity is below normal. A method of quantifying these losses is presented in Fig. 5-28. This graph predicts the amount of cell water (or extracellular water) that osmotically follows a given potassium loss (or sodium loss) as a function of tonicity of body water. The analysis is based on the Guyton model formulation of intracellu-

lar/extracellular fluid exchange as well as the osmotic theories originally proposed by Darrow-Yannet [27]. The assumptions in this model are: a) the osmotic gradient across the cell membrane is created by a sodium concentration on the one side and a potassium concentration on the other; b) any imbalance in osmotic gradient is relieved by water transfer toward the compartment of greatest electrolyte concentration so that in the steady-state, the concentrations of extracellular sodium and intracellular potassium are identical; and c) the normal extracellular (intracellular) concentration is 142 meq sodium (potassium) per liter. At the measured loss of 6% potassium, the graph predicts an intracellular water loss of 1.6 liters if performed isotonically at 142 meq./l., and only about 0.5 liters (the loss observed in the Skylab crew) if performed hypotonically at 136 meq./l. It was, therefore, not surprising to find that the plasma of the Skylab crew was mildly hypotonic and hyponatremic (see Fig. 5-20), to an extent that the observed potassium to cell water loss ratio is in almost perfect agreement with this analysis. The factors that produce this tonicity effect and its consequences are the subject of the next hypothesis.

Hypothesis #4: Natriuretic Factor. One of the more intriguing experimental observations that was closely examined was the mild hyponatremia and plasma hypo-osmolarity which developed early in the missions and continued
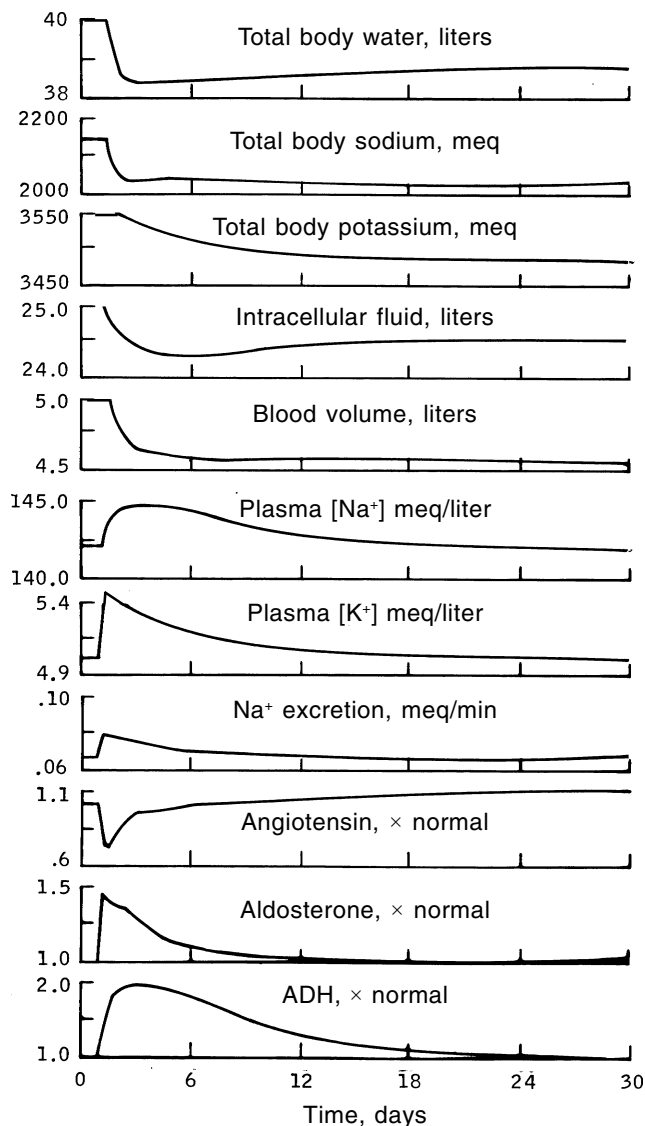
Figure 5-27. Simulation of fluid-electrolyte response showing the combined effect of three hypotheses: (a) blood shift from legs, (b) filtrate shift from leg tissues, and (c) potassium release from cells. Qualitatively, all the responses are appropriate compared to the spaceflight data except those of plasma sodium concentration and ADH.

throughout the three Skylab flights [11]. These observations are puzzling, because few physiological parameters appear to be as well controlled as plasma sodium concentration, especially in healthy subjects who have free access to water. In view of the known effects of hyponatremia on hormonal secretion levels (see previous section), it was necessary to consider this phenomenon in the simulation.

Plasma hyponatremia turned out to be a difficult response to reproduce with the fluid-electrolyte model, unless the net intake of fluids was also hyponatremic. However, this was not the case on Skylab. While not shown in the previous simulations of Hypotheses #1 and #2, the

headward shift of fluids resulted in a slight transient increase in plasma sodium concentration before returning to normal values within 24 hours. In the original version of the model, several factors affected sodium excretion: aldosterone, extracellular sodium concentration, and the volume rate of urine (see Fig. 5-11). These factors did contribute to a simulated natriuresis in response to headward fluid shifts. However, the natriuresis was not strong enough to reduce plasma sodium. It became obvious that a factor, not presently included in the model, was required, which would cause the ratio of sodium to water in urine to increase, resulting in reduced plasma sodium concentration.

Other so-called "third factors" have been recently identified (see Fig. 5-16), which can also affect the renal handling of sodium. Therefore, a natriuretic factor was postulated that would become activated by increases in upper circulatory pressures, as in the case of expansion of central blood volume in zero-g. As a result of adding this modification to the model, a mild hyponatremic plasma was produced in response to headward shifts of leg fluid. The reduced extracellular sodium concentrations also produced secondary effects (Fig. 5-29) that resulted in more realistic responses including elevated renin-angiotensin secretion, elevated aldosterone secretion, suppressed ADH secretion, and osmotic transfer of water into the intracellular compartment. The hormonal effects are consistent with the previous analysis of the model's pathways (Fig. 5-11), that revealed these direct effects of sodium concentration. The volume expansion of the intracellular compartment is beneficial to the zero-g simulation in that it permits a larger quantity of cell potassium release to be postulated without drastically reducing cell water. This volume effect also could have been predicted as discussed in the previous section (see Fig. 5-28).

The effect of the natriuretic factor on a zero-g simulation is illustrated in Fig. 5-30. The simulation shown in Fig. 5-27 was rerun with a natriuretic factor included in the model, and the results of the two simulations were compared. The simulation shown in Fig. 5-30, therefore, includes all of the four hypotheses thus far discussed: blood shift from the legs; tissue fluid shift from legs; potassium release from cells; and a natriuretic factor. The reduction in plasma sodium concentration increased the realism of the simulated response with respect to the effects mentioned in the previous paragraph. The decrease in intracellular water loss is also apparent. Other quantities such as body water, body sodium, and blood volume did not appear to be affected by the natriuretic factor, especially in the long-term period. Hormonal responses, however, were significantly affected, particularly the elevations in angiotensin and ADH.

It is important to note that all variables predicted by the model exhibited improved agreement with the Skylab data when the natriuretic factor was added to the model. This is unusual in a model as complex as the one employed here, and supports the belief that a natriuretic factor should be incorporated on a permanent basis. The present formulation, however, does not appear to be totally satisfactory. It was difficult, for example, to suppress
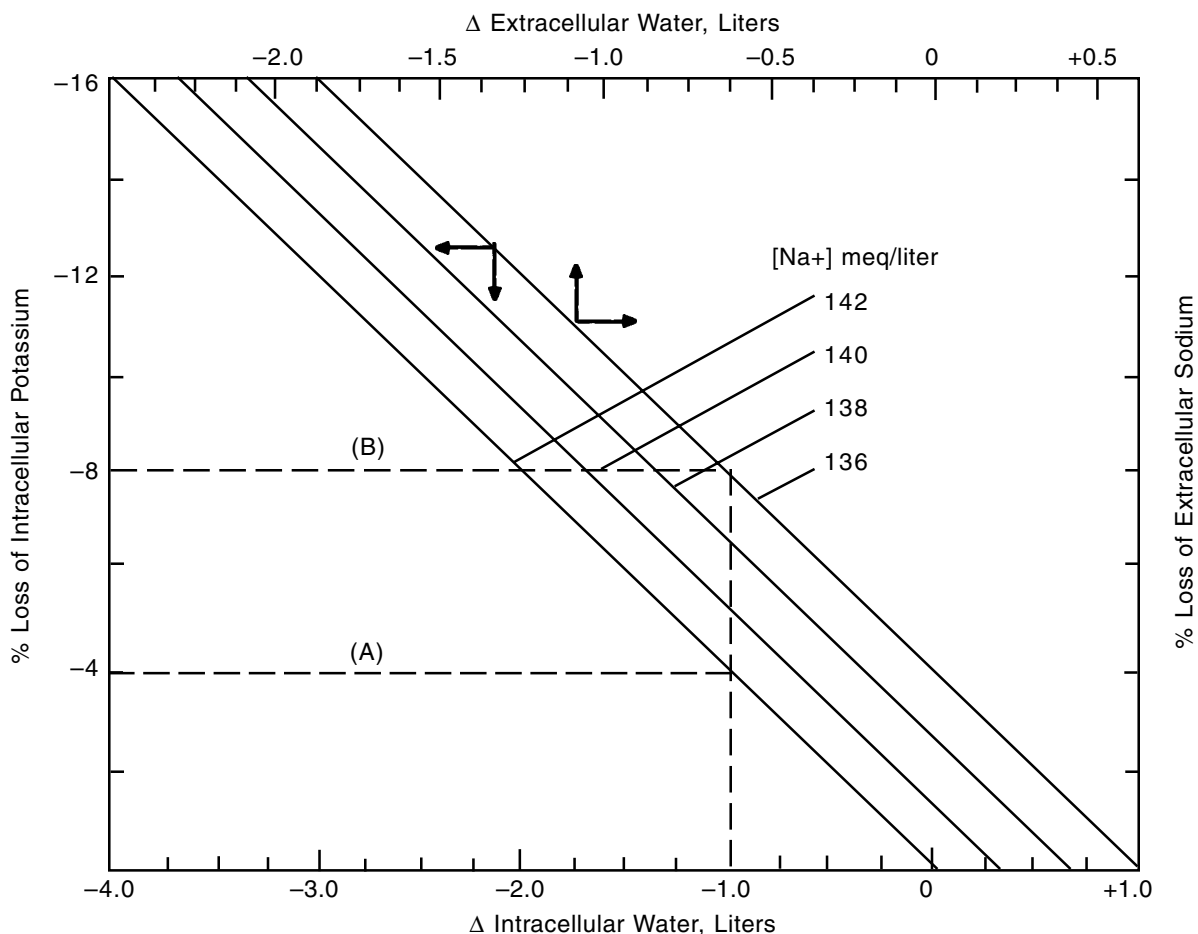
Figure 5-28. Equilibrium relationships between changes in fluid volume and electrolytes for the extracellular and intracellular compartments. In this simple model the intracellular concentration of potassium is considered identical to the extracellular concentration of sodium so as to maintain osmotic balance in the two pools. (Other assumptions are given in text.) In the example shown (dashed line) a one liter decrease in intracellular water must be accompanied by a 4% reduction in intracellular potassium in order to maintain isosmotic equilibrim with the extracellular compartment (case A). If body fluids became diluted from the nominal value of 142 meq/liter to 136 meq/liter then the potassium loss must increased to 8% (a doubling of the loss in the previous example) to sustain the same volume loss and remain in equilibrium in the hypotonic environment (case B). A similar analysis can be performed for changes in extracellular volume and extracellular sodium.

5.4.3 Hypotheses Related to Altered Metabolic Balances

The response to fluid-electrolyte disturbances, such as headward fluid shifts or intracellular/extracellular exchange, can be modified by changes in the components of metabolic balance. In Skylab, there were measured decrements in dietary intake, particularly during the acute period following launch. Increased sweat losses would be expected to affect the net metabolic balance and renal behavior in the same manner as decreased intake. These considerations led to a composite metabolic balance analysis of the Skylab crew (see Chapter 4.4). Two general conclusions were reached from that study: during the acute stress stage early in flight, the fluid and electrolyte losses from the body could best be explained by a reduced dietary intake of those substances, and during the steady-state portion of the flight, the volume and electrolyte concentrations of renal excretion could logically be explained only by a decrease in sweat losses. However, a traditional metabolic balance analysis alone cannot account for the alterations in body fluid volumes and composition, nor can it specify the mechanisms responsible for these changes. For this reason, the modified Guyton model was used to verify the results of the metabolic analysis and extend them to include an analysis of dynamic regulation in the face of metabolic disturbances. Hypotheses #5 and #6,

the plasma sodium concentration to the full extent observed in subjects exposed to hypogravity. A more appropriate suppression of plasma sodium would have resulted in even more realistic responses. Further design and validation studies are therefore recommended.

Hydrostqatic
Pressure
Gradient

Central Blood
Volume & Pressures

Natriuretic
Factor

Na⁺
Excretion

Extracellular [Na⁺]

Renin–Angiotensin

Aldosterone

ADH

Intracellular Water

Figure 5-29. Hypotheses derived from the simulation showing the effect of a postulated natriuretic factor on sodium excretion during expansion of the central blood volume.

Total body water, liters

Total body sodium, meq

Total body potassium, meq

Intracellular fluid, liters

Blood volume, liters

Plasma [Na⁺] meq/liter

Plasma [K⁺] meq/liter

Na⁺ excretion, meq/min

Angiotensin, × normal

Aldosterone, × normal

ADH, × normal

Time, days

Figure 5-30. The simulated effect of a postulated natriuretic factor on a zero-g simulation. The solid curves are taken directly from Fig. 5-27, whereby the combined effects of blood and filtrate headward shifts and potassium release from cells were simulated. The dashed curves represent the simulation of the same combined effects with the addition of a natriuretic factor in the model. The primary effect of natriuretic factor in the model is to reduce plasma sodium concentration and ADH levels.

evaluated below, concern the acute and long-term effects of decrements in dietary intake and sweat.

Hypothesis #5: Chronic Decrease in Sweat Losses.

Sweat components were not originally incorporated in the Guyton model. The model was modified by simply including a parameter representing the sweat rate in the equation that determines the rate of change of extracellular water, extracellular sodium, or extracellular potassium. During the control period of the simulation (i.e., preflight phase) these parameters were assigned (normalized) values similar to those obtained for the Skylab crewmen during the preflight period (see Table 5-8). In computing these values, the model's dietary intakes for water, sodium, and potassium were increased by exactly the same amounts as the sweat losses so that renal excretion and the net body balance was not changed during the control period.

The effect of decreasing sweat losses on fluid-electrolyte balance during the "inflight" phase was evaluated merely by reducing these sweat parameters by 10% for evaporative water loss and 30% for electrolyte sweat losses while holding intake at control values. These changes are in general accord with the Skylab estimates for the

long-term portion of spaceflight as derived in Chapter 4.4 and shown in Table 5-9. The results of this simulation are shown in Fig. 5-31.

Only small or insignificant changes occurred in the fluid-electrolyte compartments. Aldosterone concentration rose nearly 10% in response to the small increase in plasma potassium concentration. However, more significant changes occurred, as expected, in the quantities and con-

Table 5-8. Control Values for Modified Guyton Model

	Water	Sodium	Potassium
Intake	2.88 liters/d	200 meq/d	100 meq/d
Excreta	1.44 liters/d	144 meq/d	90 meq/d
Sweat	1.44 liters/d	56 meq/d	10 meq/d
Total Body Amounts	40 liters	2150 meq	3550 meq

Table 5-9. Alterations in Components of Metabolic Balance of the Skylab Crew*

	First 5 Days					Remainder of Mission			
	Cumulative Body Losses	Diet	Excretion	Sweat		Cumulative Body Losses	Diet	Excretion	Sweat
Water	-1400 liters	-16%	-21%	+6%		-1170 liters	-4%	+ 5%	-11%
Sodium	- 100 meq	-32%	- 7%	–24%		- 143 meq	+2%	+13%	-25%
Potassium	- 100 meq	-19%	+ 9%	–44%		- 234 meq	-2%	+ 5%	-44%

*Summarized from Chapter 4 (Tables 4-12, 4-13, 4-14, Fig. 4-21)

centrations excreted. The steady-state increases for water, sodium, and potassium renal excretion were 10% (144 ml/day), 12% (17 meq/d), and 3.5% (3 meq/d), respectively. These are in basic agreement with the values estimated for the Skylab crew (see Table 5-9). Predicted water excretion is nearly double the observed Skylab value because the long-term reduction in water intake was not accounted for in this simulation. Similarly, the simulated potassium excretion is about half of that expected because the cell potassium release hypothesis was not used. In other words, the effects shown in Fig. 5-31 are the result of sweat suppression only. It is interesting to note that these responses do not reach their equilibrium levels immediately and the dynamics of each constituent are somewhat different.

Hypothesis #6: Anorexia and Increased Sweating Early in Flight. It was postulated that the anorexia of space motion sickness together with a marked increase in mean evaporative water loss could account for a large part of the observed changes in renal excretory patterns early in flight. In particular, it was anticipated that there would be a partial suppression of the expected diuresis and natriuresis during the early period when the largest losses of body water, sodium, and potassium occurred. It was reasoned that loss of any body constituent could occur by either increased renal excretion in the face of constant intake and sweat or, on the other hand, by decreased intake and/or increased sweat accompanied by normal or even reduced renal loss. Water intake was severely reduced (up to 40%) during the first several days on the second and third mission, and electrolyte intake did not return to normal on the second mission until the end of the first week. Evaporative water loss was near normal or reduced during the first few days of the last two missions, but on

the first mission (where there was a temporary heat shield malfunction) sweating rates increased by almost 80% above control during inflight days 3-5. The average intake and sweat components for the nine crewmen are shown in Fig. 5-32 for the first ten mission days. Some of the data were averaged over several days for convenience in simulation. This data was obtained largely from the analysis of Chapters 4.2 and 4.4. Sodium sweat losses were computed by a compartmental analysis technique described in Appendix F (see Fig. F-3). This method permitted a more accurate assessment of these losses compared to the results obtained in the metabolic balance analysis of Chapter 4.4. Accordingly, sodium sweat losses, averaged over the first five days, exhibited an increase similar to the trend shown for evaporative water losses.

The decrements of body water, sodium, and potassium as well as the rates of renal excretion predicted by the model are shown in Fig. 5-33 for two cases: no change in intake or sweat from preflight control, and changes in intake and sweat as shown in Fig. 5-32. In both cases, the combined hypotheses #1 to #4 were used to provide a more realistic simulation of weightlessness. The decreases in body composition were similar in both cases after ten days, although the shorter term dynamics are somewhat different. Also, the renal losses of water and sodium in the case of altered intake and sweat were markedly reduced for the first several days, following a brief increase in excretion. Renal potassium was increased above control in both cases, but the increase was more dramatic when intake and sweat were normal. In the simulation, renal potassium increased because of the large loss of cellular potassium and in spite of alterations in potassium intake and sweat loss. The model prediction with respect to body water and electrolyte losses and renal excretion (after the
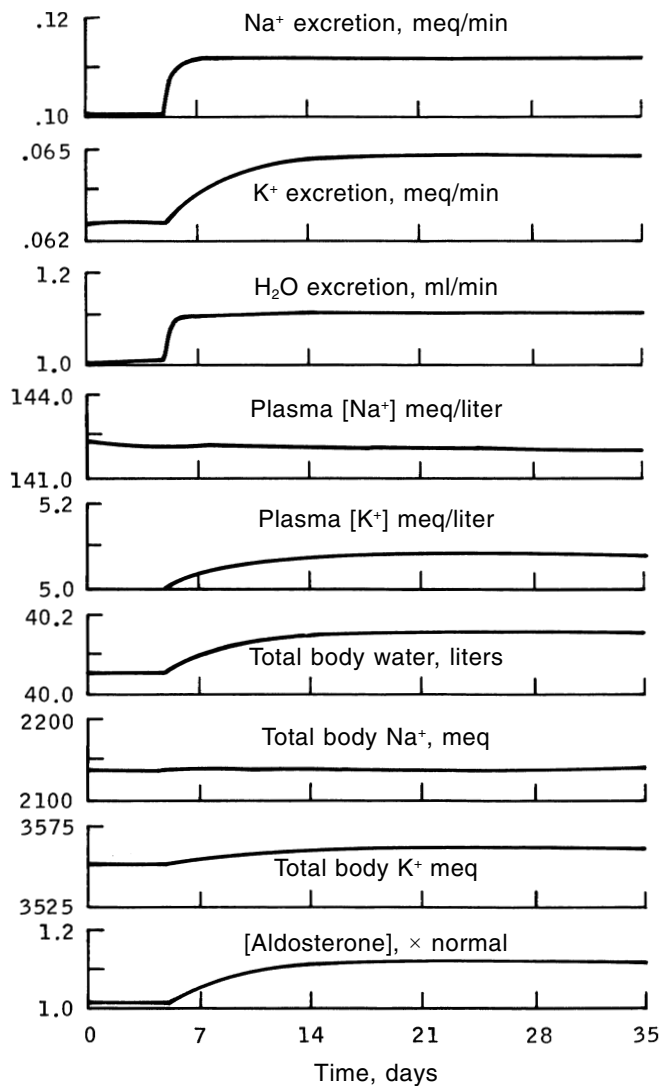
Figure 5-31. Simulated effect of reducing evaporative water loss (−10%), sweat sodium (−30%) and sweat potassium (−30%) on body composition and renal function.

Figure 5-32. Mean changes in dietary intake and sweat losses of the Skylab crew during the first 10 days of weightlessness. These normalized values, obtained from crew data, were used directly as forcing functions in the model to obtain the simulations illustrated in the next figure.

1st 12 hours) are in basic agreement with the observed Skylab results (i.e., see Table 5-9, Figs. 5-2, 5-3, and 5-4).

The renal water loss predicted on the first half-day of the simulated mission, as shown in Fig. 5-33, is much higher than control, while the 24-hour pooled samples of Skylab indicate a depressed excretion. Although these studies have demonstrated that the state of hydration and intake/sweat levels can greatly modify the basic renal response, the model has consistently demonstrated that a diuresis and natriuresis is expected for at least the first few hours during which time 0.5 to 1.0 liters of fluid shifts rapidly headward. This is predicted to occur whether or not intake is reduced, and is in agreement with the studies of Behn and colleagues [49] who showed that dehydration will attenuate but not abolish the diuresis of water immersion. However, the model predicts a significant de-

crease below control in renal excretion the latter half of the first day when intake and sweat were altered. In the model, renal excretion never diminishes below control when intake and sweat are normal. Thus, these simulations provide a rational explanation for why a 24-hour pooled urine sample for the first day inflight would show little net change from control.

The last two hypotheses, related to long-term effects of altered sweating (hypothesis #5) and short-term effects of intake and sweat changes (hypothesis #6) are summarized in Fig. 5-34. The early decrease in intake and the accompanying increase in sweat losses are postulated to contribute to the reduction of body fluids and electrolytes. However, later in the mission, when dietary intake is relatively normal, renal excretion must increase in order to maintain body fluid and electrolyte balance in the face of decreased sweat losses.

The simulations presented above were devoted to developing and testing individual hypotheses. A simulation of the combined set of hypotheses (#1 to #6) will be presented in Chapter 9.4.
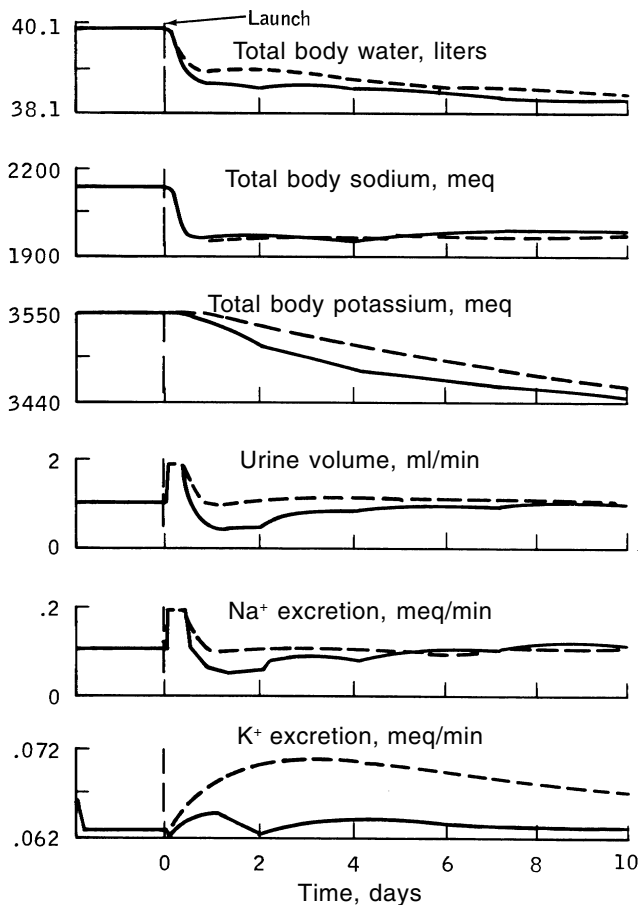
Figure 5-33. Effect of space sickness anorexia and sweat changes on body composition and renal function during simulated space-flight. The combined effects of Hypotheses #1 and 4 (that is, blood shift, filtrate shift, potassium release, natriuretic factor) were employed in both simulations shown. Dashed curves represent response using normal intake and sweat losses. Solid curves represent response using altered intake and sweat losses of the Skylab crew as shown in the previous figure.

5.5 Conclusions

Overall, this analysis has identified and quantified a number of physiological events important to an accurate assessment of fluid-electrolyte disturbances during spaceflight. These included: a) the redistribution of fluids between various compartments and locations such as intracellular/extracellular, plasma/interstitium, lower body/upper body; b) the changes in quantity and concentrations of the body electrolytes as they affect the loss of fluids from the body and osmotic shifts within the body; c) the separate effects of short- and long-term neural, hormonal and hemodynamic regulators of the circulatory-renal system as they influence the above processes; and d) the changes in intake, sweat losses and body tissue metabolism of not only water, but of the major electrolytes as they effect the transient and steady-state renal and plasma concentration responses. The simulation model of Guyton, as modified by us, demonstrated its usefulness in integrating these factors and predicting responses that were generally in accord with observation. Other predictions must await confirmation by the experimental results of future studies.

The analysis provided an interpretation of many of the biochemical and fluid changes observed during spaceflight. These are summarized in Table 5-10, and are discussed more fully in the preceding pages. Measurements made on the Skylab crew are listed in the middle column ("observation"). The last column summarizes suggested physiological pathways to explain the observations based on the systems analysis. In a sense the analysis summarized in Table 5-10 is a partial answer to the critical questions posed at the beginning of this chapter in Table 5-5.

Briefly, it was demonstrated that most of the water and sodium losses occur during the first few days of flight while potassium was lost more gradually. The acute losses could have been expected on the basis of known regulatory mechanisms responding to headward fluid shifts observed in zero-g. These mechanisms predicted an early

Figure 5-34. Hypotheses for simulation of disturbances in intake and sweating during Skylab missions.

Table 5-10. Indices of Fluid-Electrolyte Status Observed in Skylab Crew with Interpretations from Present Analysis

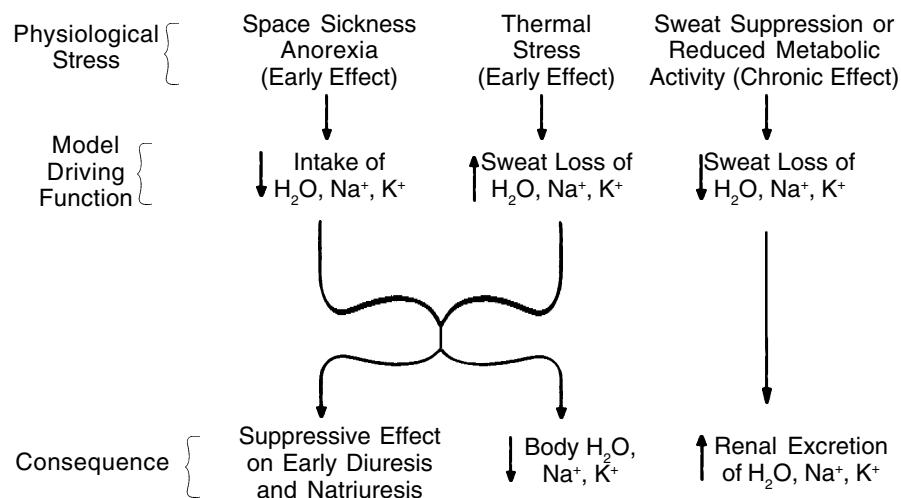| VARIABLE	OBSERVATION	SUGGESTED ETIOLOGY
Leg Volume	Decreased 1.5 liters in two days and smaller losses thereafter	Fluid loss derived from vascular, interstitial and possibly intracellular compartments
Total Body Water	Decreased 1.1 - 1.4 liters in 2 days. Tendency to partially recover in crews that were most dehydrated	Fluid lost appears to be derived from legs. Body water falls by combination of short-term diuresis (not observed) and decreased intake
Extracellular Sodium	Decreased about 100 meq in two days and stable thereafter	Sodium loss accompanies extracellular water loss. Natriuresis may occur, but primary loss results from decrease in intake
Exchangeable Body Potassium	Decreases more gradually than sodium; 240 meq lost throughout mission	Loss occurs primarily over first month; derived from intracellular fluids; early decreased intake and prolonged elevation of renal potassium identified as avenues of loss
Intracellular Water	Decreased about 0.5 liters	Cell fluids and potassium loss associated with gravity unloading and muscle disuse atrophy; fluid loss proportionally less than potassium, but can be explained on basis of hypotonic extracellular fluid
Interstitial Fluid	No change	Lymph flow and tissue gel tend to return interstitium to original state after initial loading
Plasma volume	Decreases 10-15%	Initial loss associated with decrements in total body water; loss is maintained by mechanisms which regulate hypervolemia; plasma volume losses may represent nearly half of body water losses
Hematocrit	Increased 10% acutely and diminishes slowly	Results from early loss of plasma volume followed by more gradual decrements of red cell mass
Intake of Fluids and Electrolytes	Decreased early in flight; otherwise similar to pre-flight.	Space sickness anorexia may be responsible for intake reductions up to 40% persisting up to a week in a few crewmembers. Responsible in large part for fluids and electrolytes lost early in flight
Urine Volume	Decreased about 20% first week; slightly above control thereafter.	No diuresis observed first day, possibly due to lack of void-by-void sampling. Decrease associated with reduced intake of fluids. Long-term response associated with decreased evaporative water loss
Sodium Excretion	Decreased about 10% early inflight and increased about 12% above control thereafter	Early decrease associated with reduced intake and aldosterone levels; later increase reflects reduced sweat losses rather than continuous body loss. Not clear how excretion increases when aldosterone is elevated; this "escape from aldosterone" may be mediated by a natriuretic factor
Potassium Excretion	Increased about 10% throughout flight	Reflects both cellular loss and perhaps decreased sweat losses. Governed primarily by increased aldosterone and increased plasma potassium
Evaporative Water Loss	Decreased about 10%	Unexpected decrease measured indirectly; possibly resulting from suppressed sweating
Sodium and Potassium Sweat Losses	Decreased	Measured indirectly; perhaps due to suppressed sweat water losses and believed to be of same magnitude (about -30%)
Urine [Na^+]	Increased about 10%	Paradoxical for reduced ADH and elevated aldosterone combination; however, expected on basis of steady-state analysis showing net change in sodium intake (diet - sweat) greater than change in net fluid intake
Plasma [Na^+]	Decreased about 3% throughout flight	Total osmolarity also decreased; cause not known. Natriuretic factor may be involved in excretion of sodium
Plasma [K^+]	Increased 2 - 4%	Intracellular potassium loss and possibly decreased sweat losses contribute to these results
Angiotensin	Increases about 100% in plasma	Etiology not clear in light of suspected hypervolemia of upper body; decreased plasma sodium concentration can explain part of increase
Aldosterone	Increased about 100% in urine	Several factors can explain change: increased plasma potassium, increased angiotensin, decreased plasma sodium
Anti-diuretic Hormone (ADH)	Increased on first mission, decreased on last two missions	Decreased ADH explained on basis of decreased plasma osmolarity; role of volume receptors not clear, but hypervolemia could have also contributed. Results of first mission are paradoxical

diuresis and natriuresis, although neither was observed on Skylab. The model confirmed that the acute losses could alternatively be accounted for by an observed decreased intake of fluid and electrolytes in the early flight period. However, the model also indicated that with a diminished intake, the diuresis response during the first few hours of weightlessness would be attenuated and this would be followed by a reduction of urine excretion below control. Thus, a 24-hour pooled urine sample, the mode of collection on Skylab, might show little (volume) change from control. Whatever the mechanism, most of these early whole-body losses were probably ultimately derived from observed decrements in leg volume involving a contraction of the plasma, interstitial, and possibly intracellular fluid spaces of the lower limbs. At the end of the acute stress stage (1 – 5 days), there was a significant reduction in body water, body sodium, and body potassium. About half the loss in body water was derived from plasma volume.

The more prolonged adaptive phase was characterized by a new steady-state with respect to water and sodium and a slightly negative balance of potassium. The increased urine and fecal excretion of water and sodium throughout the adaptive phase did not necessarily reflect continued body loss inasmuch as the model predicted that excretion could have been offset by a decreased sweat component. A steady-state metabolic analysis verified that the long-term renal losses were consistent with known alterations in intake and postulated changes in sweating for both water and electrolytes.

The regulatory mechanisms that contributed to these changes were also examined. The failure of the plasma volume to eventually return to normal in zero-g presumably reflects the presence of blood volume controllers responding to the tendency of fluids to move headward. The importance of autonomic, hemodynamic and hormonal regulators of circulatory and renal function was ascertained by model simulation. These pathways were influenced by various types of fluid shifts, potassium loss from the cells, and plasma electrolyte concentrations. A natriuretic factor was introduced into the model to explain the otherwise inexplicable responses of sodium excretion, plasma sodium concentration, the secretion of other hormones, and intracellular volume. The model correctly predicted the observed direction of the long-term response for ADH, angiotensin and aldosterone. Upon further analysis it appeared that the stimulating factors for these renal-regulating hormones are likely different for the acute fluid-shift phase compared to the adaptive phase of flight. Volume controllers appear to dominate in the former case, while osmo-controllers (i.e., plasma sodium and potassium concentrations) take over control in the latter case. This dual concept of hormone control is discussed fully in Chapter 9.8. More advanced simulation studies along the lines discussed here are presented in Chapter 9 and further conclusions are discussed in Chapter 10.

References

1. Link, M.M., *Space Medicine in Project Mercury*, NASA SP-4003, NASA, Washington, DC, 1965.
2. National Aeronautics and Space Administration, *Gemini Midprogram Conference, Including Experimental Results*, NASA SP-121, Manned Spacecraft Center, Houston, TX, 1966.
3. Berry, C.A., Space Medicine in Perspective – A critical review of the manned space program, *J. Amer. Med. Assoc.*, 201(4): 232–241, 1967.
4. Berry, C.A., Summary of Medical Experience in the Apollo 7 through 11 manned spaceflights, *Aerospace Med.*, 41(5): 500–519, 1970.
5. Berry, C.A. The medical legacy of Apollo, *Aerospace Med.*, 45(9): 1046–1057, 1974.
6. Johnston, R.S., Dietlein, L.F., and Berry, C.A. (Eds.), *Biomedical Results of Apollo*, NASA SP-368, NASA, Washington, D.C., 1975.
7. Rambaut, P. C., Smith, M. C., and Wheeler, H. O., Nutritional Studies, in *Biomedical Results of Apollo*, NASA SP-368, Chapter 6, NASA, Washington, DC, 1975, pp. 277-302.
8. Dietlein, L. F., Skylab: A Beginning, in *Biomedical Results from Skylab*, R. S. Johnston and L. F. Dietlein, Eds., NASA SP-377, NASA, Washington, DC, 1977, pp. 408-418.
9. Berry, C.A., Weightlessness, *Bioastronautics Data Book*, Second ed., J. F. Parker, Jr. and V. R. West, Eds., NASA SP-3006, NASA, Washington, DC, 1973, pp. 349-415.
10. Pace, N., Electrolyte and metabolic Problems of Weightlessness, *The Physiologist*, 16: 212-224, 1973.
11. Leach, C.S., and P. C. Rambaut, Biochemical Observations of Long Duration Manned Orbital Spaceflight, *J. Amer. Med. Women's Assn.*, 30: 153-172, 1975.
12. Leach, C.S. and P. C. Rambaut, Endocrine Responses in Long-Duration Manned Spaceflight, *Acta Astronautica*, Vol. 2, 115-127, 1975.
13. Leach, C.S. and P. C. Rambaut, Biochemical Responses of the Skylab Crewmen: An Overview, in *Biomedical Results from Skylab*, R. S. Johnston and L. F. Dietlein, Eds., NASA SP-377, NASA, Washington, DC, 1977, pp. 204-216.
14. Leach, C.S., Johnson, P. C., and Rambaut, P. C., Metabolic and Endocrine Studies: The Second Manned Skylab Mission, *Aviat. Space Environ. Med.*, 47: 402-410, 1976.
15. Leach,C.S., J. I. Leonard, P. C. Rambaut, and P. C. Johnson, Evaporative water Loss in man in a Gravity-Free Environment, *J. Appl. Physiol.- Respir. Environ. Exercise Physiol.*, 45: 430-436, 1978.
16. Hoffler,G.W., Cardiovascular Studies of U.S. Space Crews: An Overview and Perspective, *Cardiovascular Flow Dynamics and Measurements*, N. H. C. Hwang and N. A. Normann, Eds., University Park Press, 1977, pp. 335-363.
17. Kimzey, S.L., The Effects of Extended Spaceflight on Hematologica and Immunologic Systems, *J. Amer. Med. Women's Assn.*, 30: 218-232, 1975.
18. Rambaut, P.C., M. C. Smith, C. S. Leach, G. D. Whedon, and J. Reid, Nutrition and Responses to Zero Gravity, *Fed. Proc.*, 36: 1678-1682, 1977.
19. Whedon, G. D., Lutwak, L., Rambaut, P. C., Whittle, M. W., Smith, M. C., Reid, J., Leach, C., Stadler, C. R., and

Stanford, D. D., Mineral and Nitrogen Metabolic Studies: Experiment M071, in *Biomedical Results from Skylab*, R.S. Johnston and L. F. Dietlein, (Eds.), NASA SP-377, NASA, Washington, DC, 1977, pp. 164-174.

20. Leonard, J.I., *Analysis of Metabolic Energy Utilization in the Skylab Astronauts*, (Report TIR 741-LSP-7018, General Electric Co., Houston, TX), NASA CR-160402, NASA, Washington, DC, 1977.

21. Guyton,A.C., T. G. Coleman and H. J. Granger, Circulation: Overall Regulation, *Annual Review Physiology,* 34: Comroe, Jr., J. H., Giese, A. C., and Sonnenschien, R. P., (Eds.), 1972, pp. 13-46.

22. Guyton, A.C., Taylor, A. E., and Granger, H. J., *Circulatory Physiology II: Dynamics and Control of the Body Fluids*, W. B. Saunders Company, 1975.

23. Guyton, A. C., *Textbook of Medical Physiology*, 5th ed., W. B. Saunders Company, 1976.

24. Vander, A. J., *Renal Physiology,* McGraw-Hill Book Co., 1975.

25. Gauer, O. H., Henry, J. P., and Behn, C., The Regulation of Extracellular Fluid Volume, *Ann. Rev. Physiol.*, 32: 547-595, 1970.

26. Gamble, J. L., Chemical Anatomy Physiology and Pathology of Extracellular Fluid, 6th ed., Harvard University Press, 1960.

27. Bland, J. H., *Clinical Metabolism of Body Water and Electrolytes*, W. B. Saudners Company, 1963.

28. Pitts, R. F., *Physiology of the Kidney and Body Fluids*, 2nd ed., Yearbook Medical Publishers, 1968.

29. Black, D. A. K., *Essentials of Fluid Balance*, 3rd ed., F. A. Davis Company, 1964.

30. Cort, J. H. and Lichardus, B., Eds., *Regulation of Body Fluid Volumes by the Kidney*, S. Karger, 1970.

31. Andreoli, T. E., Grantham, J. J., and Rector, Jr., F. C., Eds., *Disturbances in Body Fluid Osmolality*, American Physiological Society, 1977.

32. Haddy, F. J., and Overbeck, H. W., Minireview: The Role of Humoral Agents in Volume Expanded Hypertension, *Life Sciences*, 19: 935-948, 1976.

33. Dunn, F. L., Brennan, T. J., Nelson, A. E., and Robertson, G. L., The Role of Blood Osmolality and Volume Regulating Vasopressin Secretion in the Rat, *J. Clin. Invest.*, 52: 3212-3219, 1973.

34. Guyton, A. C., *Circulatory Physiology III: Arterial Pressure and Hypertension*, W. B. Saunders Co., Philadelphia, 1980.

35. Gauer, O. H., and Henry, J. P., Circulatory Basis of Fluid Volume Control, *Physiol. Rev.*, 43: 423-481, 1963.

36. McCalley, M. and Graveline, D. E., Physiologic Aspects of Prolonged Weightlessness: Body Fluid Distribution and the Cardiovascular System, *N. Engl. J. Med.*, 269: 508-516, 1963.

37. Leach, C. S., Alexander, W. C., and Fischer, C. L., Compensatory Changes During Adaptation to the Weightlessness Environment, *The Physiologist.*, 246: 1972.

38. Pace, N., Weightlessness: A Matter of Gravity, *New Engl. J. Med.*, 297: 32-37, 1977.

39. Echt, M., Lange, L., and Gauer, O. H., Changes of Peripheral Venous Tone and Central Transmural Venous Pressure During Immersion in a Thermo-Neutral Bath, *Pflugers Arch.*, 352: 211-217, 1974.

40. Murray, R.G., Nixon, J. V., Bryant, C., Dowdey, A. B. C., Holland, O. B., Johnson, R. L., Mitchell, J. H., Vergne-Marini, P., and Blomqvist, C. G., Adaptations to Simulated Zero Gravity: Control of Blood Volume, *Clin. Res.*, 24: A4, 1976.

41. Plemme, T. E., Body Fluid Volume and Renal Relationships to Gravity in *Hypodynamics and Hypogravics - The Physiology of Inactivity and Weightlessness*, M. McCalley, (Ed.), Academic Press, 1968, pp. 133-161.

42. Earley, L. E. and Daugharty, T. M., Sodium Metabolism, *N. Engl. J. Med.*, 281, 72-86, 1969.

43. Gauer, O. H., Recent Advances in the Physiology of Whole Body Immersion, *Acta Astronautica*, 2: 31-39, 1975.

44. Epstein, M., Cardiovascular and Renal Effects of Head-out Water Immersion in Man, *Circ. Res.*, 39: 619-628, 1976.

45. Gauer, O. H., Body Fluid Regulation During Immersion, *Hypogravic and Hypodynamic Environments*, NASA SP-269, 1971, NASA, Washington, DC, pp. 345-355.

46. Epstein, M., Levinson, R., and Loutzenhiser, R., Effects of Water Immersion on Renal Hemodynamics in Normal Man, *J. Appl. Physiol.*, 41: 230-233, 1976.

47. Greenleaf, J. E., Shvartz, E. Kravik, S. and Keil, L. C. Fluid Shifts and Endocrine Responses During Chair-Rest and Water Immersion in Man, *J. Appl. Physiol. - Respir. Environ.*, 48: 79-68, 1980.

48. Nixon, J. V., Murray, R. G., Bryant, C., Johnson, Jr., R. L., Mitchell, J. H., Holland, O. B., Gomez-Sanchez, C. Vergne-Marini, P., and Blomqvist, C. G., Early Cardiovascular Adaptation to Simulated Zero Gravity, *J. Appl. Physiol. Respir. Environ.*, 46: 548-548, 1979.

49. Behn, C., Gauer, O. H., Kirsch, K., and Eckert, P., Effects of Sustained Intrathoracic Vascular Distention on Body Fluid Distribution and Renal Excretion in Man, *Pflugers Arch.*, 313: 123, 1969.

50. Epstein, M., Renal Effects of Head-out Water Immersion in Man: Implications for an Understanding of Volume Homeostasis, *Physiol. Reviews*, 58: 529-581, 1978.

51. Graybiel, A., Miller, II, E. F., and Homick, J. L., Individual Differences in Susceptibility to Motion Sickness Among Six Skylab Astronauts, *Acta Astronautica*, 2: 155-174, 1975.

52. Vernikos-Danellis, J., Winget, C. M., Leach, C. S. Rosenblatt, L. S., Lyman, J., and Beljan, J. R., Space Motion Sickness Medications interference with Biomedical Parameters, *XXVII Congress International Astronautical Federation*, Preprint #IAF-76-036, 1976.

53. Bricker, N.S., The Control of Sodium Excretion with Normal and Reduced Nephron Populations: The Pre-eminance of Third Factor, *Amer. J. Med.*, 43: 313-321, 1967.

54. Schrier, R. W. and DeWardener, H. E., Tubular Reabsorption of Sodium Ion: Influence of Factors Other Than Aldosterone and Glomerular Filtration Rate, *N. Engl. J. Med.*, 285: 1231-1243, 1293-1303, 1971.

55. Epstein, M., Bricker, N.S., and Bourgoignie, J.J., Presence of a Natriuretic Factor in Urine of Normal Men Undergoing Water Immersion, *Kidney Int*., 13: 152-158, 1978.

56. Andersson, B., Regulation of Body Fluids, *Ann. Rev. Physiol.*, 39: 185-200, 1977.

57. McCally, M., Plasma Volume Response to Water Immer-

sion; Implications for Spaceflight, *Aerospace Med.*, 35: 130-132, 1964.

58. Davis, J. T. and DuBois, A., Immersion Diuresis in Dogs, *J. Appl. Physiol: Respir. Environ. Exercise Physiol.*, 42: 915-922, 1977.

59. Wiederhielm, C. A., Dynamics of Transcapillary Fluid Exchange, *J. Gen. Physiol.*, 52: 29s-63s, 1968.

60. Goetz, K.L., Bond, G. C., and Bloxham, D. D., Atrial Receptors and Renal Function, *Physiol. Rev.,* 55: 157-205, 1975.

61. DeHaven, J. C. and Shapiro, N. Z. Simulation of the Renal Effects of Antidiuretic Hormone (ADH) in Man, *J. Theor. Biol.*, 28: 261-286, 1970.

62. Dunn, M. J. and Hood, V. L. Prostaglandins and the Kidney, *Amer. J. Physiol.*, 233: F169-F184, 1977.

63. Bunag, R.D., Page, I. H. and McCubbin, J. W., Neural Stimulation of Release of Renin, *Circ. Res.*, 19: 851-858, 1966.

64. Oparil, S., Vassaux, C., Sanders, C. A., and Haber, E., Role of Renin in Acute Postural Homeostasis, *Circulation*, 41: 89-95, 1970.

65. Vander, A. J., Control of Renin Release, *Physiol. Review*, 47: 359-381, 1967.

66. Oparil, S. and Haber, E. The Renin-Angiotensin System, *N. Engl. J. Med.,* 291: 389-401 and 446-457, 1974.

67. Davis, J. O. and Freeman, R. H., Mechanisms Regulating Renin Release, *Physiol. Rev.*, 56: 1-56, 1976.

68. Gauer, O. H., Moderator's Introduction to International Symposium on Neural Control of the Cardiovascular System and Orthostatic Regulation, *Cardiology,* 61: Suppl. 1, 2-6, 1976.

69. Epstein, M., Pins, D. S., and Miller, M., Suppression of ADH During Water Immersion in Normal Man – Antidiuretic Hormone, *J. Appl. Physiol.*, 38: 1038-**104**, 1975.

70. Leonard, J. I. and Grounds, D. J., *Study Report: Modification of the Long Term Circulatory Model for the Simulation of Bedrest*, (TIR 782-LSP-7011, General Electric Co., Houston, TX.) CR-160186, NASA, Washington, DC, 1977.

71. Rushmer, R. F., Effects of Posture, Cardiovascular Dynamics, Third ed., W. B. Saunders Company, 1970, pp. 210-219.

72. Sjostrand, T., Volume and Distribution of Blood and Their Significance in Regulating the Circulation, *Physiol. Review*, 33: 202-228, 1953.

73. Guyton, A. C., Jones, C. E., and Coleman, T. G., *Circulatory Physiology: Cardiac Output and Its Regulation*, 2nd ed., W. B. Saunders Co., Philadelphia, 1973.

74. Arborelius, Jr., M., Balldin, U. I., Lilja, B., and Lundgren, C. E. G., Hemodynamic Changes in Man During Immersion with the Head Above Water, *Aerospace Med.*, 43: 592-598, 1972.

75. Foux, A., Seliktar, R., and Valero, A., Effects of Lower Body Negative Pressure (LBNP) on the Distribution of Body Fluids, *J. Appl. Physiol.*, 41: 719-726, 1976.

76. Whittle, M. W., Caloric and Exercise Requirements of

Spaceflight: Biostereometric Results From Skylab, *Aviat. Space Environ. Med.*, 50: 163-167, 1979.

77. Thornton, W. E. and Rummel, J. A., Muscular Deconditioning and Its Prevention in Spaceflight in *Biomedical Results from Skylab*, NASA SP-377, Chapter 21, NASA, Washington, DC, 1977.

78. Leonard, J. I. and Abbrecht, P. H., Dynamics of Plasma-Interstitial Fluid Distribution Following Intravenous Infusions in Dogs - An Experimental and Computer Simulation Study, *Circ. Res.*, 33: 735-748, 1973.

79. Prather, J. W., Taylor, A. E. and Guyton, A. C., Effects of Blood Volume, Mean Circulatory Pressure, and Stress Relaxation on Cardiac Output, *Amer. J. Physiol.*, 216: 467, 1969.

80. Leach, C. S., Alfrey, C. P., Suki, W. N., Leonard, J. I., Rambaut, P. C., Inners, L. D., Smith, S. M., Lane, H. W., and Krauhs, J. M., Regulation of Body Fluid Compartments During Short-Term Spaceflight, *J. Appl. Physiol.*, 81: 105–116, 1996.

81. Buckey, J. C., Jr., Central Venous Pressure, in *Gravity and the Lung: Lessons from Microgravity*, Prisk, G. K., Paiva, M., and West, J. B., (Eds.), Marcel Dekker, Inc., N.Y., 2001, pp. 225–253.

Update Endnotes

Update #1. Renal-Regulating Hormones (TBD)

Recent research regarding renal-regulating hormones, including aldosterone, natriuretic factor, and prostaglandin activity, how they participate in regulating fluid-electrolyte metabolism and what has been found from spaceflight experiments.

Update #2. Diuresis in Spaceflight

The concepts and hypotheses developed in this chapter formed the basis for a major spaceflight experiments which was conducted more recently on the Shuttle Spacelab. An important aspect of this experiment was an attempt to detect a spaceflight diuresis by measuring each urine void and attempting to ensure that astronaut subjects were well hydrated prior to launch. Early measurements of renal-regulating hormones were also obtained. This experiment was designed in part to confirm or disprove the existence of the Gauer–Henry pathway during acute adjustment to spaceflight. The results of this experiment [80] and other related studies are summarized in the Update section of Chapter 9.

Update #3. Venous Pressure in Spaceflight

Measurement of venous pressure during spaceflight have been made since the time of the analyses summarized in this chapter [81]. The results of these unexpected findings are summarized in the Update section of Chapter 9.

Chapter 6
Erythropoiesis Regulation and the Anemia of Spaceflight

6.1 Introduction

The most obvious and consistent manisfestation of spaceflight on the human hematologic system is a reduction in the circulating blood volume—including both plasma and red cell components—during flight. The previous chapter reviewed the mechanisms by which the plasma volume decrement may have occurred. In this chapter, the emphasis will be on the important factors that may have led to changes in the red cell component of blood. Inasmuch as the red cells play a dominant role in the oxygen transport functions of the body, the importance of tissue oxygenation will also be considered.

Explanations for the reduction in red cell mass (RCM) have been proposed, but confirmatory evidence was still lacking until the Shuttle Spacelab era. At the time of the first Skylab mission, the so-called "anemia of spaceflight" had been variously ascribed to weightlessness, the relative immobility of the crew, lack of atmospheric nitrogen, and a high oxygen partial pressure within the space vehicle. With the exception of weightlessness, these factors were known to alter rates of red cell production and destruction in ground-based experiments using human and animal subjects and were thought to be operative in spaceflight as well. On Skylab, however, in contrast to previous space missions, crews moved about freely in gaseous atmospheres of oxygen and nitrogen much as on earth. Nevertheless, each of the nine crewmembers exhibited significant red blood cell loss. This unexpected result provided the motivation to reexamine the data and current hypotheses through the lens of systems analysis and computer simulation models.

In support of NASA hematology research, the findings and hypotheses of previous spaceflight and experimental studies were integrated within the framework of a theoretical model of erythropoiesis regulation. This model, described in Chapter 3 and Appendix C, was developed by the GE/NASA team, especially to investigate the agents responsible for the loss of circulating red blood cells observed in crewmen returning from space missions. The studies described in this section, based on simulations of the mathematical model, provided new insights into this phenomenon, which is still under investigation.

The general approach for providing systems analysis support of the hematology program is illustrated in Fig. 6-1. The major achievements of the analyses are indicated, as are the reports and publications that describe them. At the outset of the study, a suitable model of erythropoiesis regulation did not exist. In addition, it was uncertain if the systems analysis approach would be of value in this particular investigative area. Therefore, a feasibility study was performed which consisted of a review of the essential physiology describing erythropoiesis regulation, a sur-

vey of available models of this system, the formulation and implementation of a preliminary version of a new mathematical model, a review of the spaceflight findings, and finally, the development of several simple hypotheses based on the model's behavior, which could explain these findings. This initial study indicated that the modeling approach might be limited as an investigative tool in the Skylab hematological experiments because of the paucity of inflight data, and because of an incomplete understanding of the mechanisms affecting erythropoiesis in general. Nevertheless, it was concluded that a more advanced model could assist investigators in several ways that have been previously enumerated in Chapter 3, that is, it could identify important parameters, provide a method by which to test hypotheses rapidly, define areas requiring further study, and predict the time course of difficult-to-measure parameters.

The development of the model proceeded in a systematic fashion, as indicated in Fig. 6-1. Verification and validation of the model are described in Chapter 3, Appendix B and by Leonard and co-workers [1,2,3,4,5]. Simulations were performed for experimental stresses related to spaceflight such as red blood cell infusions, descent from altitude, and bedrest. Experimental data for these studies were taken from the available literature. In addition, collaborations with NASA investigators of bedrest and other zero-g analogs provided specific data that were needed to define model parameters and confirm model predictions. Major improvements were made in the model in order to provide more realistic simulations of these experiments. These included the addition of explicit elements representing erythropoietin and red blood cell production, bone marrow time delays, variations in the oxy-hemoglobin dissociation function curves, and an algorithm for entering experimental data as time-varying driving functions. Other more generalized simulation analyses, including sensitivity analysis provided information regarding the relative importance of model parameters and some basic quantitative relationships between model parameters that would be difficult to obtain experimentally. A species-specific model for the mouse was developed to perform simulations of dehydration and infusion based on animal experiments that were currently in progress. At each step of the program, additional hypotheses were conceived, expressed mathematically, tested in the model against experimental data, then tested once again for their validity in spaceflight simulations. The most promising hypotheses were then considered for evaluation in the laboratory or for future space missions.

More than in any other investigative area considered in this book, the modeling approach served to coordinate data from various ongoing ground-based experimental programs, and helped maximize the utilization of the acquired information.
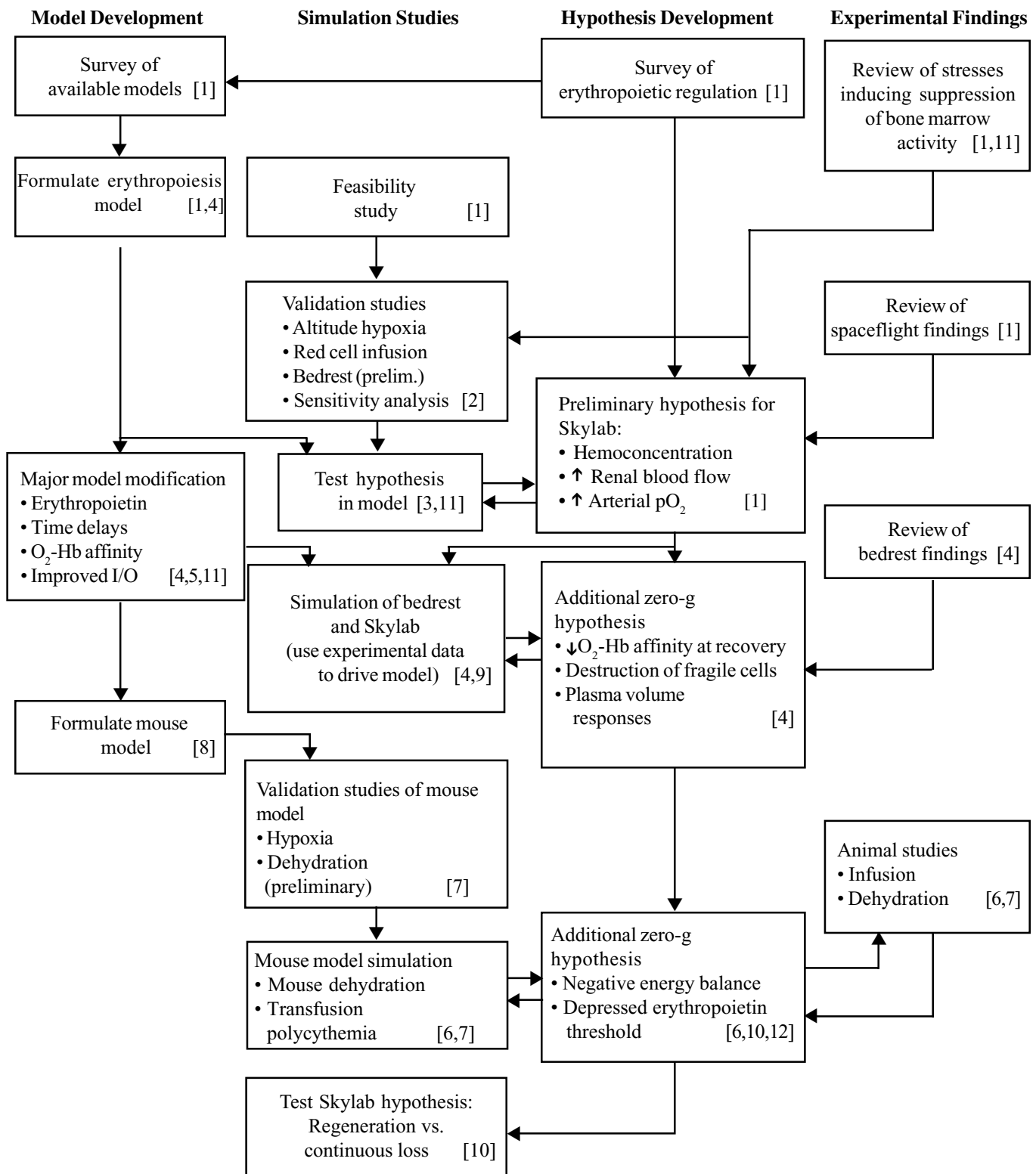
Figure 6-1. Approach for studying erythropoietic regulation during spaceflight. The progressive development in each systems analysis area such as model development is in the downward direction of the diagram while the horizontal lines indicate the high degree of interaction between all phases of the study. Hypotheses were formulated based on new insights from the different experimental studies and ultimately the most promising of these were tested agains the Skylab data. The numbers refer to published reports by the GE/NASA team (see References).

6.2 Review of Spaceflight Studies

The hematology experiments performed on Skylab encompassed a wide range of objectives, including assessment of man's immunological integrity, cytogenetic studies, red cell metabolism, topographical alterations of red cells, and blood volume changes. Only a small portion of these data were deemed directly applicable to describing and explaining overall disturbances in circulating red cell mass. The most relevant data obtained from human spaceflight studies, including that from pre-Skylab missions, will be briefly reviewed here. This information formed the basis for developing specific hypotheses that guided the systems analysis study.

6.2.1 Gemini Findings

The loss of red cell mass during spaceflight was first observed on the Gemini 4 mission. The measured loss (12% in 4 days) was much higher than could be accounted for by natural attrition of cells (i.e., about 1% per day), even if production rates were completely inhibited. This suggested increased red cell destruction as a causative factor. Subsequent studies on other flights confirmed a decrease in red cell survival (based on ^{51}Cr half-times), and suggested that a hemolytic process was responsible for the observed red cell loss. Also noted were increases in cell membrane fragility and biochemical alterations that are known to influence red cell integrity [13].

An hypothesis was advanced that was consistent with most of these observations; it was based on the 100% breathable oxygen atmosphere of the Gemini space capsules. Compared to a normal earth oxygen partial pressure of 150 to 160 mmHg, the astronauts of the Gemini (and later Apollo flights) were exposed to about 260 mmHg (100% oxygen at 1/3 normal atmospheric pressure). This atmosphere was found to have a toxic effect on the membranes of red cells and could have accounted for the increased destruction and reduced magnitude of the circulating red cell mass [14].

A normal feedback compensation for destruction of cells is a compensatory increase in production rates. Reticulocyte counts are generally good indicators of bone marrow production rates. For reasons not understood at the time, compensatory erythropoiesis was not evident in these early flights, as reflected by the lack of reticulocytosis until several days after the day of recovery.

6.2.2 Apollo Findings

The Apollo missions were also characterized by a significant loss of red cell mass, although its severity was less than that observed during the Gemini flights. In contrast to the Gemini missions, red cell survival was not significantly altered during the inflight or postflight phases of all of the Apollo missions. This indicated that hemolysis either did not occur or was very slight [15]. Like the Gemini crewmen, the Apollo astronauts breathed an atmosphere that was primarily hypobaric oxygen. However, on Apollo, the atmospheres contained small, but varying amounts of nitrogen with extended periods of nearly 100% oxygen. A qualitative analysis of all space and ground-based chamber studies performed up to that time revealed that the most severe losses in red cell mass occurred when a 100% oxygen atmosphere was used (compared to those situations in which a diluent gas was present) [14,16].

It was proposed that the hyperoxic atmosphere was not only capable of initiating red cell destruction, but it was also capable of inhibiting the production of red cells as well [17]. Hyperoxia is thought to limit erythropoiesis (even in atmospheres with a diluent gas) by the same feedback pathways (operating in an inverse manner) that cause enhanced production during hypoxia [18]. In order to account for the losses observed in some of the Apollo flights, red cell production would have to be totally inhibited for the duration of the flight, assuming a normal loss of approximately 1% per day. Taken as a whole, the data suggested that the decrements during Apollo may result not only from diminished production of red cells, but also from an increased red cell destruction, as was the case on Gemini.

Suppression of red cell production on the Apollo flights was not only inferred by normal red cell survival times, but also by a reduced reticulocytosis immediately upon return to earth. In light of the Apollo findings, it appears that suppressed production may have also occurred in the Gemini crew. This may be inferred from their reticulocyte counts at recovery, which, while normal, should have been much higher, based on the amount of hemolysis measured.

Table 6-1 shows a comparison of the percent changes in red cell mass and plasma volume in all spaceflight crews (through the 1975 Apollo–Soyez Test Project) in which these parameters were measured. For comparison, data for the ground control subjects are also included. Of these control studies, the subjects in all except the Skylab Metabolic Experiment Altitude Test (SMEAT) and the Brooks Air Force studies (both done in hypobaric chambers) were exposed to a normal earth atmosphere. The SMEAT study used an atmosphere (pressure and composition) similar to that of Skylab, and Brooks used an atmosphere similar to that of the Gemini atmospheres. The atmospheres of the Gemini missions were 100% oxygen, and the crewmen were de-nitrogenated prior to launch. The Apollo 14 to 17 flights were lunar missions, so that only partial degrees of weightlessness were encountered. No indications of hemolysis were observed on these latter Apollo flights. A significant conclusion that can be drawn from Table 6-1 is that there was a variable decrease in all astronauts, the severity of which was not seemingly related to the duration of flight.

The limited amount of data collected on these missions, and the complete lack of inflight observations on the indices that measured oxygen transport, red cell production, and red cell lifespan precluded establishing the exact mechanisms of the red cell mass loss. Atmospheric oxygen undoubtedly was a contributory agent, but it was probably not the only one [15,19]. To confound the issue, bedrest studies (used as ground-based analogs of weightless spaceflight) had demonstrated that significant decrements in red cell mass could occur in a normoxic terrestrial atmo-

Table 6-1. Changes in Vascular Compartments During Spaceflight*

Mission	Duration (Days)	Red Cell Mass (%Change)	Plasma Volume (%Change)
Gemini 4	4	−12	−9
Gemini 5	8	−21	−7
Gemini 7	14	−14	+11
Apollo 7-8	6–11	−2	−8
Apollo 9	10	−8	−9
Apollo 14-17	9–13	−10	−4
Skylab 2	28	−14	−8
Skylab 3	59	−12	−13
Skylab 4	84	−7	−16
Apollo–Soyuz	9	−7	−11
Ground Controls			
Apollo 14-17**	9–13	−1.1	+10
Skylab 2**	28	+0.4	+ 8
Skylab 3**	59	+0.8	−2
Skylab 4**	84	0	−3
SMEAT	60	−3	+2
Brooks***	30	−12	—
Apollo–Soyuz	9	+1	+6

* Ref [19]
** Subjects exposed to normal earth atmosphere
***Subjects exposed to 1/3 atm, 100% oxygen

Table 6-2. Comparison of Major Hematological Findings on U.S. Manned Spaceflights

	Gemini	Apollo	Skylab
• 100% oxygen atmosphere	Yes	No	No
• Red Cell mass decrease	Yes	Yes	Yes
• Plasma volume decrease	Yes	Yes	Yes
• Inflight Hb increase	ND	ND	Yes
• RBC survival decrease	Yes	Slight	Only 28-day mission
• Reticulocytes on recovery day	No Change	Reduced	Reduced
• Delayed recovery of red cell mass	Yes	Yes	Only 28-day mission
• Flight Duration	4d-14d	l0d-16d	28d-84d

ND = Not Determined

tion were obtained from the published accounts of the principal investigators [15,19,23-27].

6.2.3.1 Red Cell Mass and Plasma Volume. The red cell mass losses on the 28-, 59-, and 84-day missions averaged 14.3, 12.3, and 6.8% respectively, as measured on the first day of recovery (see Fig. 6-2). Although the mean change of the second flight was not statistically different from that of the first flight, the general trend would seem to imply that the red cell mass loss decreases in severity with increasing mission duration beyond one to two months and may thereby be said to be self-limiting.

No inflight plasma volume determinations were performed. The first postflight measurements demonstrated losses of 8, 13, and 16% in plasma volume for the 28-, 59-, and 84-day crews, respectively, or an average loss of 360 ml for all crewmen (see Fig. 6-2). However, plasma volume is known to change rapidly (i.e., 10% variations are seen during brief postural changes) and the value measured shipboard on recovery day may not reflect the true volume in zero-g prior to reentry. (This is in contrast to red cell mass measurements that in the absence of hemolysis, are relatively constant during acute plasma volume changes).

6.2.3.2 Hemoglobin Concentration. Hemoglobin concentrations were measured inflight using a hemoglobinometer in conjunction with each inflight venipuncture. Postflight, hemoglobin measurements of inflight blood were made by biochemical analysis of the returned frozen samples [24]. Inflight data were obtained by these two procedures only on the crews of the 59- and 84-day mis-

sphere, thereby implicating factors such as immobilization or weightlessness itself [20,21]. Nevertheless, the general belief was that the Skylab astronauts would be protected from red cell mass losses because the oxygen partial pressure would be much more similar to earth's atmosphere than in previous flights and because of the use of nitrogen as a diluent in concentrations higher than that used in any previous flight [22]. The cabin atmosphere of the Skylab missions differed from that of Apollo flights by having an oxygen:nitrogen ratio of 70%: 30% (at 1/3 atmospheric pressure). Therefore, it was totally unexpected when the crew of the first Skylab mission returned with red cell losses as great as those seen in the Gemini astronauts.

6.2.3 Skylab Findings

Although the common characteristic of all space missions has been the reduction of red cell mass and plasma volume, other hematological parameters and influencing factors did not necessarily exhibit the same uniformity, as is illustrated in Table 6-2. Thus, measurements of red cell survival, reticulocytosis, and postflight recovery differed not only among the Gemini, Apollo, and Skylab series, but, as the following discussion reveals, among the three Skylab missions as well. The data summarized in this sec-

___

* Hb concentration values were higher when measured inflight, compared to the postflight measurements on samples obtained inflight. This difference was noted [25], but no cause could be found. However, it is possible that the somewhat hyperoxic atmosphere (190 mmHg oxygen partial pressure) may have been responsible for increasing oxygen saturation of blood samples (and thus Hb concentration) measured *in vitro* by the hemoglobinometer technique.
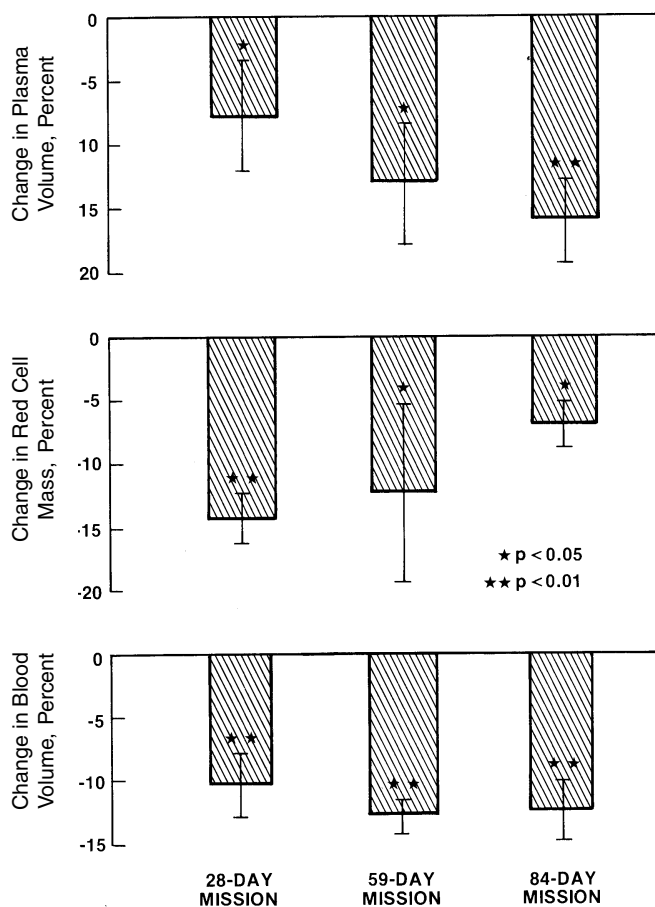
Figure 6-2. Changes in plasma volume, red cell mass, and total blood volume of the Skylab crew. Each bar represents the mean (±SD) difference between preflight and postflight measurements for each three-man mission. The postflight value was obtained on the day of recovery.

Figure 6-3. Hematological parameters measured as a function of time from launch for the inflight and postflight phases of the 28-day mission. Mean (±SD) values for the three crewmen are expressed as percent change from preflight control levels. No inflight measurements were obtained for red cell mass and plasma volume on any Skylab mission. Plasma hemoglobin was not measured during the inflight phase on the 28-day mission.

sions; hemoglobin alterations during the 28-day mission are, therefore, unknown. The precision of the inflight data is admittedly less than that associated with pre- and postflight determinations.*

Consistent in all the inflight Hb determinations was an elevated value in the first inflight sample, presumably due to a loss of plasma volume. If hemoglobin concentration disturbances are used as an index of plasma volume changes [28], it would appear that the rate of change of plasma volume during spaceflight is extremely rapid. The earliest Hb measurement was obtained on the third inflight day, and showed an average ($N = 6$) increase of about 11%. Assuming red cell mass did not change during this time (which is not certain), this translates into a plasma volume decrease of approximately 500 ml, or 18% below control. It is not valid to use hemoglobin measurements after this point to estimate plasma volume, since red cell mass is undoubtedly also changing at an unknown rate.

As the mission progressed, Hb concentration remained elevated but there was a gradual reduction in their values

toward normal. The latter trend would indicate a gradual drop in red cell mass if plasma volumes were stable at a reduced level. However, plasma volume determinations were not performed inflight. Figures 6-3, 6-4, and 6-5 summarize all the known Skylab data with respect to Hb concentrations, red cell mass, and plasma volume.

6.2.3.3 Lifespan Studies. Indicators of intravascular hemolysis were provided by both ^{51}Cr red cell halftimes and ^{14}C-glycine red cell mean lifespans. Treating the entire population of nine crewmembers as a single group, there were no statistically significant differences between the preflight and postflight mean values, or between the
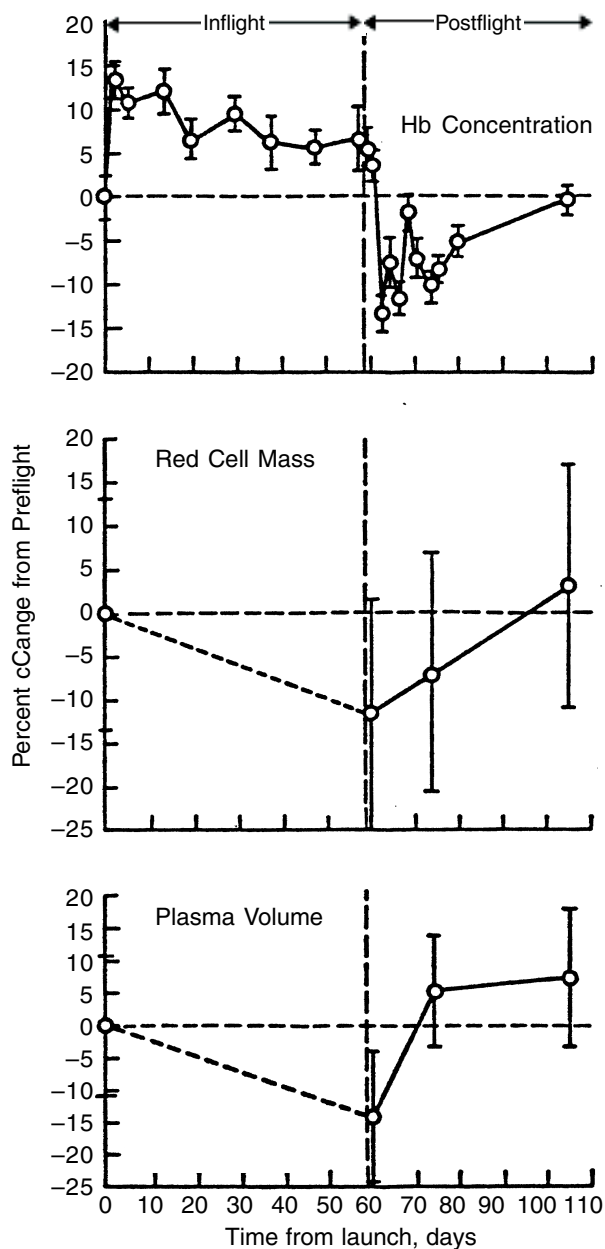
Figure 6-4. Hematological parameters measured as a function of time from launch for the inflight and postflight phases of the 59-day mission. See caption for Fig. 6-3.

Figure 6-5. Hematological parameters measured as a function of time from launch for the inflight and postflight phases of the 84-day mission. See caption for Fig. 6-3.
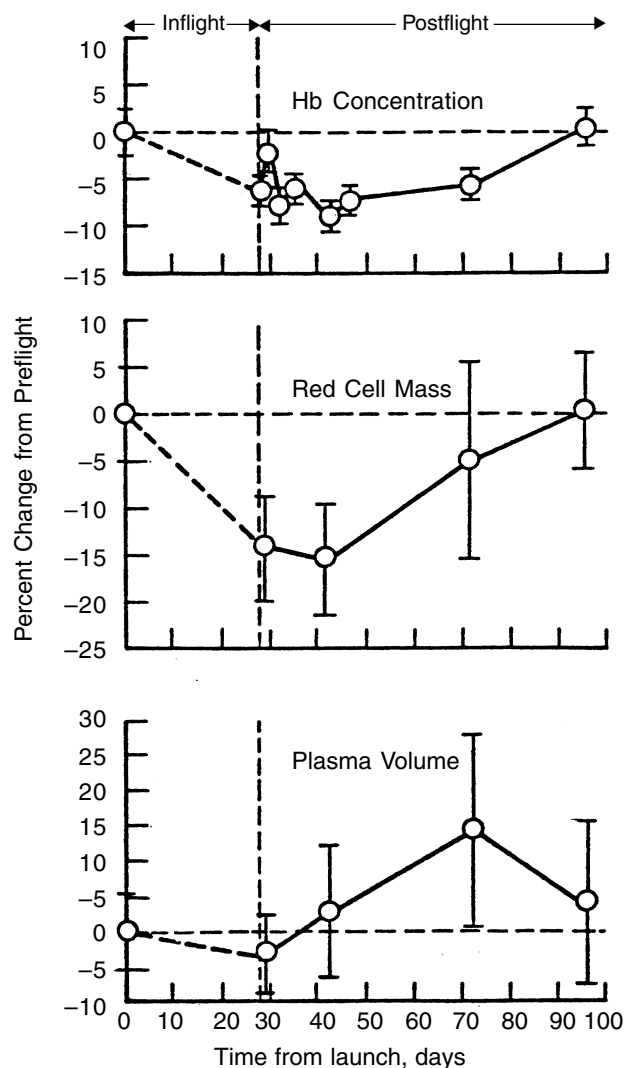
6.2.3.4 Reticulocyte Counts. Postflight reticulocyte counts from all three missions are shown in Table 6-4. Increases in reticulocytes can be taken as an index of red cell production. The low values on the first recovery day suggest suppressed red cell production, and imply that this is a carry-over from the previous days spent in zero-g. The general tendency of reticulocyte counts to rise toward and above normal during the following weeks indicates augmented production and regeneration of red cell mass. The differences between the first crew and the last two are noteworthy. The postflight reticulocyte counts of the crew of the 28-day mission rose much more slowly than those of the two longer missions, and they never rose above preflight values. Also, each subsequent crew exhibited higher reticulocyte counts on the first day of recovery and the counts rose fastest for crews that remained in space longer. These results are generally consistent with the pattern of inflight red cell mass loss and postflight recovery reflecting zero-g suppression followed by enhanced production of erythrocytes in one-g.

flight crew and a one-g control group for either of the two measurement methods [26]. However, the postflight ^{51}Cr halftimes for the crewmen of the 28-day mission were 18% less than their preflight values ($p < 0.05$). If their ground control effects are removed, the net effect due to spaceflight is a 12% decrease ($p < 0.05$) in red cell halftime (see Table 6-3). This indicates that hemolysis may have been a factor on that mission. The red cell mass loss of this particular flight was also the largest of the three missions.

Table 6-3. Percent Change in ^{51}Cr Red Cell Half-Times of Skylab Crewmembers and Control Subjects [26]

Mission	N	Skylab Crewmembers	Ground Controls	Difference Due To Spaceflight
28-day	3	-17.8 ± 5.0*+	-6.0 ± 3.6	(*p* < 0.05)
59-day	3	-6.6 ± 1.1*	-5.9 ± 9.8	(NS)
84-day	3	+4.3 ± 10.3	-3.5 ± 4.2	(NS)
Skylab Mean	**9**	**-7.3 ± 11.1**	**-5.4 ± 6.4**	**(NS)**

*   Different from preflight (*p* < 0.05)
+   Different from control group (*p* < 0.05)
NS Not Significant

Table 6-4. Skylab Crews Postflight Reticuloctye Counts (Percentage of Premission Mean) [26]

	Mission		
Day	28 day mission	59 day mission	84 day mission
R + 0	44	69	88
R + 1	53	—	117
R + 3	67	87	87
R + 7	80	184	143
R + 14	86	227	184
R + 21	93	234	180

6.2.3.5 Change in Red Cell Shape. Special hematological studies of the inflight blood samples showed that during extended exposure to spac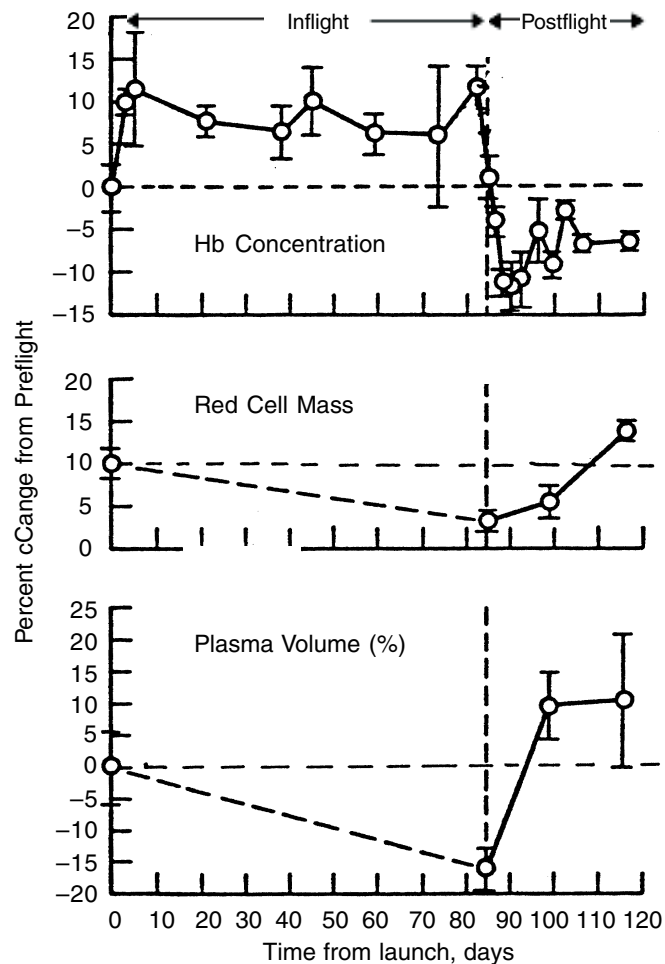eflight, significant alterations occur in the distribution of red cell shapes in the peripheral circulation [15,25]. Severe deformation of circulating red cells can result in their premature sequestration by the reticuloendothelial system (RES). The alteration in red cell shape during spaceflight might provide a sufficient stimulus to the RES to initiate trapping and eventual removal of these cells from the circulating red cell mass. Maintenance of normal red cell shape and normal deformability are essential to survival of the cell in vivo. A major function of the RES is to remove from circulation, those cells whose structure is abnormal or whose membrane is too rigid. It was not possible to substantiate a direct relationship between the red cell shape alterations during the Skylab missions and the concomitant loss in red cell mass, but this is an area that merits further investigation.

6.2.4 Bedrest Findings

Experimental bedrest involving healthy subjects has been considered an analogous stress to weightlessness because it minimizes certain effects of gravity (particularly hydrostatic and load-bearing effects in the longitudinal direction). The earliest of these studies [29], as well as those
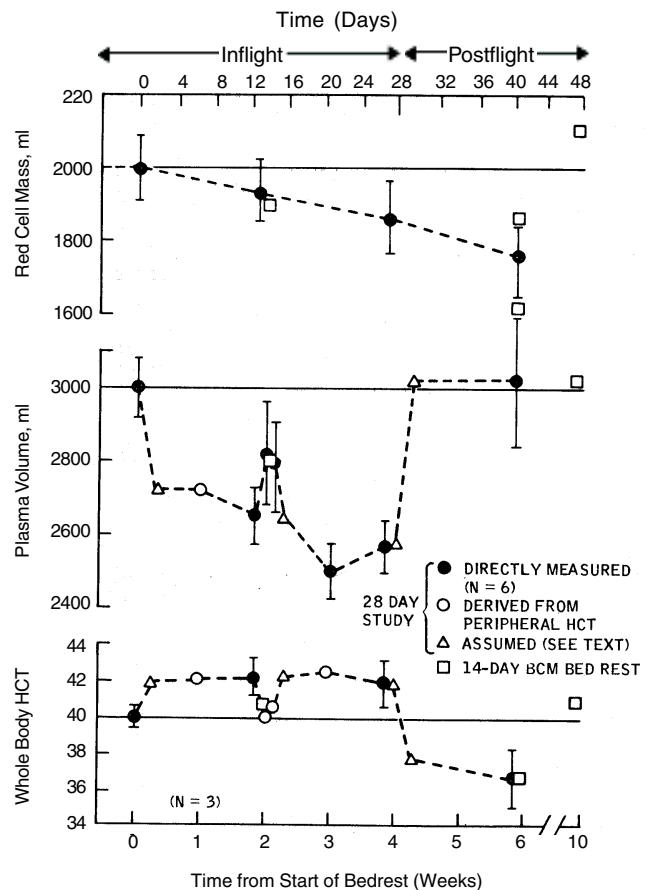
Figure 6-6. Hematological measurements from a two-week and four-week bedrest study [30,32]. The data are normalized with respect to the computer model's control values (indicated by the solid horizontal lines). The symbols designated as "assumed" provide the most realistic estimates of plasma volume where large fluid shifts are believed to occur, but were not measured. These assumptions were necessary to obtain accurate simulations with the computer model (see Chapter 6.5.3). The rationale for these assumptions is available elsewhere [9]. During days 13, 14, and 15, each subject received a one-liter saline solution administered orally as part of an experiment to test its efficacy against orthostatic intolerance.

conducted more recently [30] (see Fig. 6-6) have invariably reported blood volume decrements both in the plasma and red cell components. Typically, for studies lasting less than one month, red cell mass losses are greater during spaceflight and plasma volume losses are greater during bedrest [31].

Unlike spaceflight, the time-varying behavior of these blood volume components is more easily examined during bedrest. Figure 6-6 illustrates several responses that are typical of many bedrest studies. As shown in the figure , red cell mass declines linearly as a function of time [30], while plasma volume declines in roughly exponential fashion with half the total loss occurring the first few days and the remainder lost over several weeks [32,33]. Hematocrit and hemoglobin concentration increases within several days by 5-10% and remains elevated despite the loss in red cell mass because

Table 6-5. Summary of Spaceflight Findings

- Red cell mass consistently reduced during spaceflight

- Evidence of hemolysis on Gemini flights

- No consistent evidence of hemolysis on Apollo and Skylab flights

- Rate of red cell loss in Skylab greater than observed during bedrest studies of comparable duration

- Reticulocytes reduced immediately after mission recovery

- Postflight reticulocytosis is often delayed several days

- Hemoconcentration occurs early in spaceflight

- Hemodilution occurs during postflight period

- Plasma volume reduction measured postflight

- Significant alterations in red cell shape

- Hematological responses of the first Skylab mission different than for second and third missions (see Table 6-6)

Table 6-6. Observations from the 28-Day Skylab Flight that Differed from the 59- and 84-Day Missions

- Red cell loss was the greatest of the three Skylab missions

- Only crew in which reticulocytosis did not occur postflight

- Rate of postflight recovery of RCM was delayed until after two weeks from reentry; other Skylab crews did not show delay

- Plasma volume losses were the smallest, as measured postflight

- Only crew to have statistically different ^{51}Cr halftimes

- Hematocrits and hemoglobin decreased during postflight period (resulting from plasma refilling) as on other flights, but was decreased the least (half as much) on the 28-day flight

- Diet and exercise were the least adequate during the mission

- Crew lost the most weight, suggestive of negative energy balance

plasma volume is also disappearing from the circulation [20]. Following bedrest, plasma volume increases rapidly (resulting in hemodilution), but red cell mass does not begin to regenerate until after one or two weeks [4].

The fact that these changes are qualitatively similar to those that are found after spaceflight suggests that similar mechanisms may be operative in these two hypogravic stresses. The validity of this assumption has not been firmly established. Unfortunately, most bedrest studies have not been directed toward examining the erythropoietic system in detail. Evidence for suppression of erythropoietic activity is somewhat stronger for bedrest than it is for spaceflight, although indications of mild hemolysis have also been reported in bedrest [20]. Reductions in reticulocyte counts and erythropoietin levels have been observed [20,34] but not consistently [35].

Taken together, these data indicate erythro-suppression, possibly mediated by an excess of oxygen supply over demand. However, the hypo-metabolism of bedrest subjects in comparison to the more normal metabolic activity of the Skylab subjects makes comparison of these stresses difficult. Likewise, the normoxic environment in which bedrest is usually studied is not comparable to the hyperoxic atmosphere of the earlier Gemini and Apollo missions. In addition, losses of red cell mass have only been measured for up to 35 days during bedrest, which provides few clues to the regenerative behavior suggested in spaceflights beyond 60 days. These considerations were examined systematically in the studies described in this section.

6.2.5 Preliminary Hypotheses

A summary of the major spaceflight findings related to red cell loss are shown in Table 6-5. Any interpretation of these observations should be consistent with the fact that, qualitatively and quantitatively, the first Skylab mission had a somewhat different response than the two longer missions (see Table 6-6). In their primary Skylab reports, Kimzey [25], Johnson et al. [26], and Dietlein [36] offered several hypotheses to explain the hematological findings; these are summarized in Table 6-7.

The etiology of the drop in red cell mass and lowered reticulocyte counts at recovery is unknown. The red cell mass is the most stable of the various blood constituents, and rapid changes are only possible in hemorrhaging or hemolysis. Gradual decreases may be produced by inhibition of bone marrow activity, ineffective erythropoiesis, hemolysis, chronic hemorrhage, or sequestration of cells. The spaceflight experiments appear to rule out all but the first of these factors. There was no clinical indication of hemorrhage among the crews, and data collected during the mission did not support the concept of intravascular hemolysis as reflected by normal ^{51}Cr halftimes, normal ^{14}C-glycine lifespans, and normal haptoglobins. Iron kinetic studies (serum iron, iron turnover, and iron reappearance) tended to rule out ineffective erythropoiesis [15], a conclusion also reached in bedrest studies [30]. The low reticulocyte counts at recovery are additional evidence against ineffective erythropoiesisis. A proposed splenic trapping of circulating cells was unconfirmed by spleen and liver scans during the Apollo-Soyuz flight, the first U.S. manned space mission to be performed after Skylab [37]. Finally, the one-g control subjects showed little change in either red cell mass or reticulocyte counts, ruling out effects resulting from the blood drawing schedule. Taken as a whole, these data suggest, by inference, that the Skylab red cell mass losses were a result of decreased production rather than an increase in red cell destruction.

Table 6-7. Preliminary Hypotheses to Explain Spaceflight Hematological Findings [25, 26, 36]

- Erythropoiesis is suppressed during exposure to weightlessness

- Red cell destruction contributed to Gemini red cell losses and possibly to a smaller extent during Apollo, while red cell life span was normal on the average in Skylab

- Hyperoxic atmosphere contributory to red cell loss in Gemini and Apollo

- Red cell mass loss is self-limiting and eventually regenerative

- Kinetics of red cell mass recovery (postflight) independent of duration of weightlessness exposure

- Hemoconcentration during spaceflight and bedrest a result of rapid and sustained reduction in plasma volume

- Hemodilution during postflight phase a result of plasma volume rapidly returning to normal

- Red cell mass loss may be due to splenic trapping of red cells promoted by alterations in red cell shape

- Rule out hemolysis, splenic trapping of red cells, ineffective erythropoiesis, blood sampling effects, hemorrhage

- Hemoconcentration and increased O_2-Hb affinity contributed to inadequate erythropoietic response to the loss of red blood cells during the first month

- Insufficient caloric intake, especially on the 28-day mission, leads to loss of red cells

The initial published accounts of the Skylab experiments left the etiology of the probable decrease in bone marrow activity unanswered. Johnson *et al* [26], addressed the question of why the bone marrow failed to deplete red cells in spaceflight. They proposed that hemoconcentration or rightward shifts in the oxy-hemoglobin equilibrium curve may have maintained oxygen flow to the kidney and prevented erythropoietin secretion. A later paper by Johnson [27] summarized all the current hypotheses including results from more advanced analyses of Skylab data and post-Skylab animal investigations. Also, during this post-Skylab, pre-Space Shuttle period, the first of the systems analysis and modeling studies of the erythropoiesis system in spaceflight conducted by Leonard and associates were published [1,2,3,4,6,8].

Whatever the cause of the decreased red cell mass, it appeared that the losses were self-limiting, since increased time spent in space did not result in additional loss. Furthermore, the smaller losses of red cell mass on each longer mission gave rise to a "regeneration" theory by the Skylab researchers. Accordingly, red cell mass initially decreases during the first 30 days of flight and this is followed by a gradual recovery of red cells which begins approximately 60 days after launch [25,26,36,38]. Although no measure-

ments of red cell mass were made inflight, this theory has a basis of support from a composite time profile of the postflight red cell mass measurements (Fig. 6-7).

The primary objective of the hematology systems analysis was to assist in the interpretation of the Skylab findings. One of the more important post-Skylab summaries [38] emphasized the need to better understand the erythropoiesis "governor" that prevents the red cell mass from falling below a certain level; it was suggested such insight into a previously unknown mechanism may apply to other disease situations on the ground. Accordingly, an specific approach was chosen to develop and test hypotheses, using computer simulation techniques, to explain the loss of red cell mass during spaceflight, and the self-limiting nature of the Skylab crew's red cell mass loss, as well as the difference in recovery kinetics between the first flight and the last two flights.

Ground-based studies, sponsored by NASA, were performed on human and animal subjects and carried out with the view of explaining these findings on an experimental basis. An additional objective of the present analysis was to colloborate with the ground-based investigators by suggesting experimental objectives, assisting in data interpretation, and using the newly acquired data to modify the model, if necessary.

6.3 Theoretical Considerations of Erythropoiesis: Tissue Oxygenation

An important assumption in this study was that the basic relationship between tissue oxygenation and erythropoiesis would provide clues for understanding the loss of red cell mass during spaceflight.. This assumption was derived from the accepted physiological concept that the balance between oxygen supply and demand at the tissue level is the major determinant of bone marrow erythropoiesis. Some of the important considerations regarding tissue oxygenation will be reviewed here to provide a theoretical foundation for developing specific hypotheses relevant to the spaceflight findings. A mathematical model embodying the essential elements of tissue oxygenation and erythrocyte production is also summarized. This model, especially its physiological basis and its simulated behavior, was the basis for interpreting the spaceflight events.

6.3.1 Physiology of Tissue Oxygenation

An adequate supply of oxygen to individual tissues is dependent on a circulatory system that transports oxygen, bound reversibly to hemoglobin, from an oxygen-loading organ (i.e., lungs) to the capillaries of an oxygen-consuming organ. Oxygen enters the cellular space by diffusion along an oxygen tension gradient between the capillary and the cell. Normally, a steady-state exists between the rate of oxygen consumed by the tissues and the rate of oxygen delivered to the tissues. The amount of oxygen delivered to a tissue depends on a number of factors, the most obvious of which are oxygen tension of inspired air, pulmonary function, hemoglobin concentration [Hb], affinity of hemoglobin for oxygen, speed of dissociation of oxygen
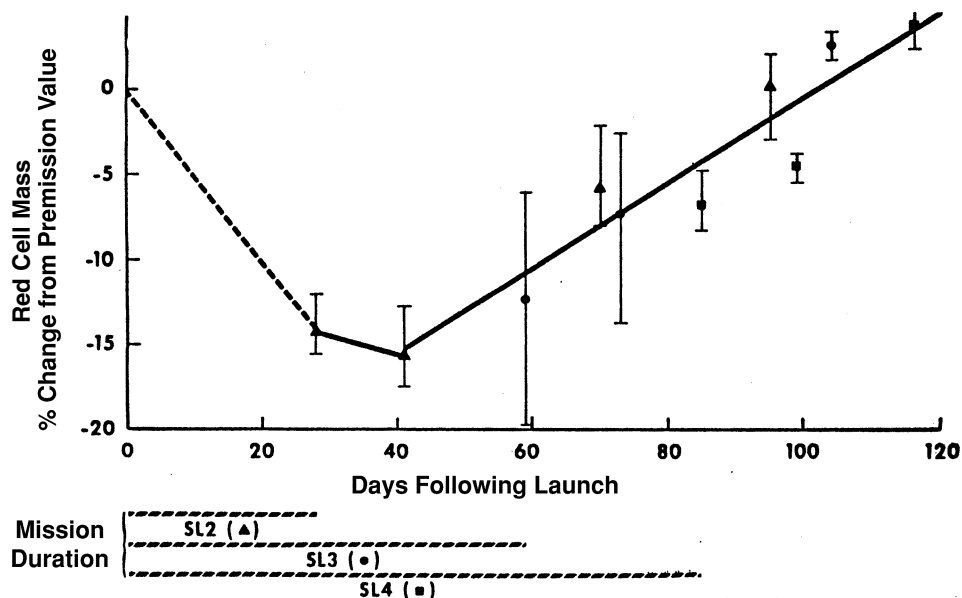
Figure 6-7. Changes in red cell mass in the Skylab crew measured from the day of the launch. Each point represents the mean (±SD) changes of the three-man crews as measured on subsequent days of the postflight period. The first measurement for each crew was obtained on the day of recovery. The solid line through the points (calculated by least squares method) support the hypothesis that regeneration of red cell mass begins after 40 days from launch (Figure reproduced from Dietlein [36]).

from hemoglobin, cardiac output, and the vascular distribution of circulating blood among the various tissues [39,40]. A disturbance in any of these factors, or in the rate of metabolism, will cause a temporary imbalance between tissue oxygen supply and demand and, thereby, will change tissue oxygenation.

At the tissue level, the rate of arterial oxygen supply can be expressed as follows:

Oxygen flow rate = blood flow rate to tissue
                x fraction of Hb saturated with oxygen
                x Hb concentration in blood
                x O_2 carrying capacity of Hb
                 (normally constant)

The bone marrow elements of the erythropoiesis system primarily regulate only one of these factors, the hemoglobin concentration. Control of blood flow and hemoglobin saturation may be considered to be under the domain of the circulatory, respiratory, and blood biochemical regulatory systems (see Fig. 6-8). These latter systems are capable of rapid compensatory adjustments in the face of small changes in the oxygen supply-demand balance. For example, changes in the number of active tissue capillaries and blood flow adjustments are common circulatory responses to minor local fluctuations in the degree of tissue oxygenation. Under these conditions, the rate of red cell production and the circulating red cell mass are essentially invariant. However, in more extreme and chronic situations such as hemorrhage, altitude hypoxia, or pulmonary disorders, an increase in red cell production and circulating red cell mass appears to be a major pathway by

which the body compensates for an insufficient tissue oxygen supply [41]. Similarly, conditions that lead to chronic levels of tissue hyperoxia, such as breathing from an hyperoxic atmosphere, transfusion-induced polycythemia, or when the tissue demand for oxygen is decreased as in hypothyroidism, hypophysectomy, and starvation, there is a significant decrease in erythropoiesis [42].

In assessing the etiology of the loss of red cells during spaceflight, it is plausible to look for factors that chronically disturb the delicate balance between tissue oxygen supply and demand. Since short-term alterations in tissue oxygenation can theoretically be corrected by the circulatory, respiratory and biochemical systems, it is likely that disturbances in the erythropoiesis system itself are responsible for the longer-term spaceflight findings. However, the behavior of the erythropoietic processes must ultimately be judged in the context of the total oxygen transport system.

6.3.2 Concept of a Renal pO$_2$ Sensor

A majority of experimental evidence supports the hypothesis that oxygen supply to a renal "detector" site in relation to the oxygen demand of that region is the primary stimulus for erythrocyte production via the release of a renal erythropoietic hormone, erythropoietin [39,42,43]. Erythropoietin production is believed to be dependent on renal tissue oxygen tension, a variable reflecting the summation of renal oxygen supply and oxygen consumption.

The location of the renal sensing site for monitoring oxygen tension and releasing erythropoietin has still not been isolated. However, anatomical and physiological con-
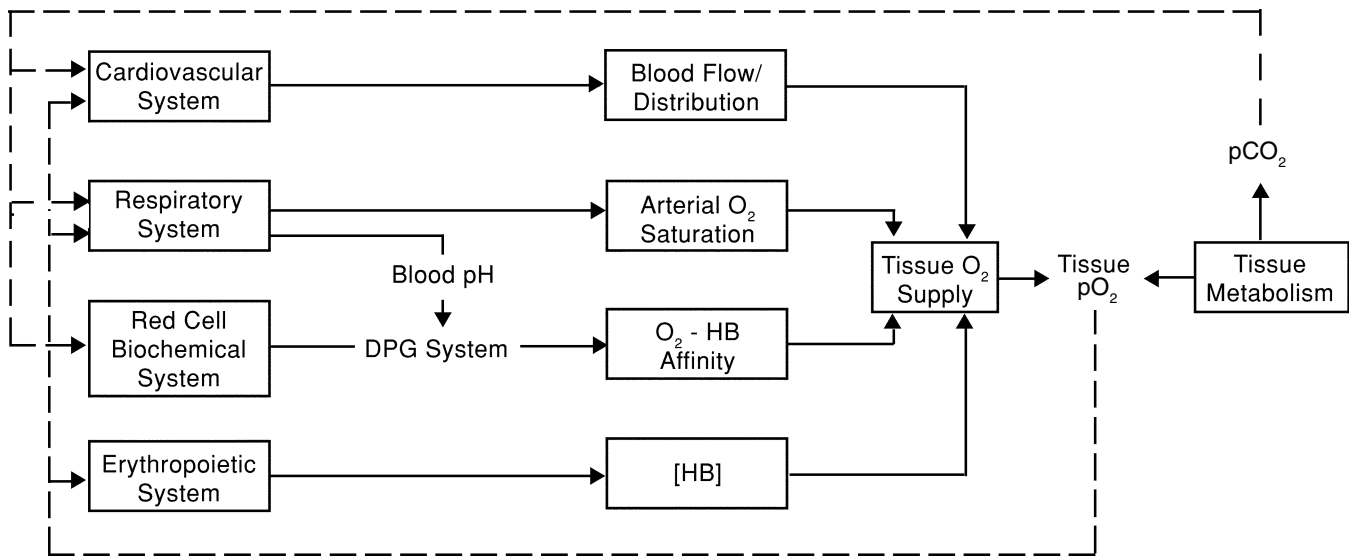
Figure 6-8. Regulation of tissue oxygen tension showing the contributions of the cardiovascular, respiratory, biochemical, and erythropoietic systems.

siderations suggest that the kidney tissue has developed a specialization that enables it to function as a sensitive oxygen chemoreceptor. Several important characteristics of the sensing site have been identified, and they are discussed in the next paragraphs:

a) While most organs in the body exhibit a blood distribution pattern that results in an even release of blood oxygen into the tissues, the kidney has a peculiar microcirculation that favors a reduced hematocrit in the smaller vessels and a steep gradient of tissue oxygen tension along the cortico-medullary axis [42,44]. Thus, a relative hypoxia is present which may act as a continual stimulus for daily erythropoietin production.

b) The kidney, and especially the renal cortex, has a uniquely low arteriovenous oxygen difference. Its capillaries differ from the rest of the capillaries of the body in that they lie along the flat upper part of the blood oxygen dissociation curve, where small changes in oxygen concentration are associated with large changes in pO_2. This characteristic amplifies the signal for erythropoietin production [45,46].

c) The sensors which regulate erythropoietin production appear to monitor venous or tissue pO_2, rather than arterial pO_2 [47,48,49].

d) Evidence suggests that the sensing sites are located in areas where blood flow and oxygen consumption are held stable over a wide range of oxygen tensions [50] Autoregulation of blood flow is a recognized feature of the kidney [46]. In addition, changes in blood flow, if they did occur, would be expected to have a dampened effect on tissue pO_2 because of the unique coupling in the kidney of blood flow and oxygen consumption [51].

These characteristics effectively make these renal sites a sensor of blood hemoglobin levels (or hematocrit).[†] Since oxygen delivery to tissue is dependent essentially on blood flow rate, oxygen hemoglobin affinity, and hemoglobin concentration (see previous equation), a system that can keep blood flow and oxyhemoglobin affinity constant will deliver oxygen at a rate proportional only to hemoglobin concentration. In addition, by requiring a constant rate of oxygen consumption, the tissue pO_2 will vary in direct proportion to hemoglobin concentration. Therefore, the renal oxygen sensor can be construed, under the specified conditions, as a highly sensitive, high gain hemoglobinometer of the body [52]. When combined with a controller that can vary the rate of hemoglobin production, this system may be capable of regulating hemoglobin levels and tissue oxygen tension. This view of the erythropoiesis controller has not been fully recognized in the past and may provide important clues to bedrest and spaceflight hematological changes, inasmuch as these stresses are often accompanied by alterations in hematocrit.[UPDATE #1]

6.3.3 Effect of Hematocrit Levels on Oxygen Transport

The influence of plasma hemoglobin concentration on oxygen delivery to the tissues, discussed in the preceding paragraphs, is more complex than the simple linear effect suggested by the oxygen flow rate equation. This is true because two of the factors that determine blood oxygen delivery (blood flow and hematocrit) have an interdependent relationship. Blood viscosity increases as the proportion of red cells in blood increases [53] and blood

---

[†] Hematocrit is directly related to the blood Hb concentration by the mean corpuscular Hb concentration, MCHC, which is normally quite constant.

flow is inversely related to blood viscosity. Thus, a changing hematocrit can have two opposing effects on oxygen transportability. First, as the hematocrit is increased, the oxygen content of the blood is increased. Second, as the hematocrit is increased, the rate of blood flow to the tissues is decreased because of the increased blood viscosity.

Therefore, it is not apparent in this situation whether there will be an actual improvement in oxygen supply to the tissues. In fact, these opposing effects would be expected to produce a maximum level of oxygen transport at a specific hematocrit, (i.e., the "optimal" hematocrit). Oxygen transport would be reduced below the optimal level if hematocrit were reduced (i.e., oxygen concentration effect) or if hematocrits were increased (i.e., viscosity-flow effect) away from the optimum. The concept of an "optimum hematocrit" for oxygen transport is supported by studies of experimentally-induced anemia and polycythemia in both normovolemic and hypervolemic animals and in man [54,55].

These relationships are shown graphically in Fig. 6-9 (solid lines). The influence of hematocrit on blood oxygen concentration and blood flow are shown in Fig. 6-9(a). Both of these relationships are essentially linear over a wide hematocrit range. Oxygen transport, shown in Fig. 6-9(b) is taken as the product of blood flow and oxygen concentration. The inverse linear relationship between blood flow and hematocrit has been cited on numerous occasions [55,56,57,58,59]. Thus, blood with a high hematocrit may have a rheologic disadvantage with respect to oxygen transport in spite of the advantages of an increased oxygen capacity.

An additional effect (shown in Fig. 6-9) is that of blood volume on blood flow (dashed lines). One effect of an increased blood volume is a decrease in geometric vascular resistance (i.e., due to passive distension of blood vessels), and an increase in cardiac output at any given hematocrit level. The relationships for normo- and hyper-volemia are shown. The family of parabolic shaped curves, shown in Fig. 6-9(b), representing the effects of blood volume, theoretically shifts the optimum hematocrit to higher levels as blood volume increases. More important, however, is the fact that hematocrits higher than the normal optimum do not necessarily result in reduced oxygen transport when accompanied by hypervolemia. This upward shift of the oxygen transport-hematocrit relationship helps explain why, in cases of acute hypertransfusion or chronic cases of polycythemia vera (i.e., expanded red cell mass and blood volume), oxygen transport is not depressed, but may in fact, be enhanced [59,60]. Also, some important differences between the hemoconcentrating stresses of either an absolute erythrocytosis (i.e., there is an increase in red cell mass such as occurs with red cell infusion) and a relative erythrocytosis (i.e., there is no increase in red cell mass but rather a decrease in plasma volume such as occurs with dehydration) are more readily appreciated in light of this analysis (see Chapter 6.5.4 and Fig. 6-32).

The preceding discussion serves to emphasize that predicting the level of oxygen transport requires consid-
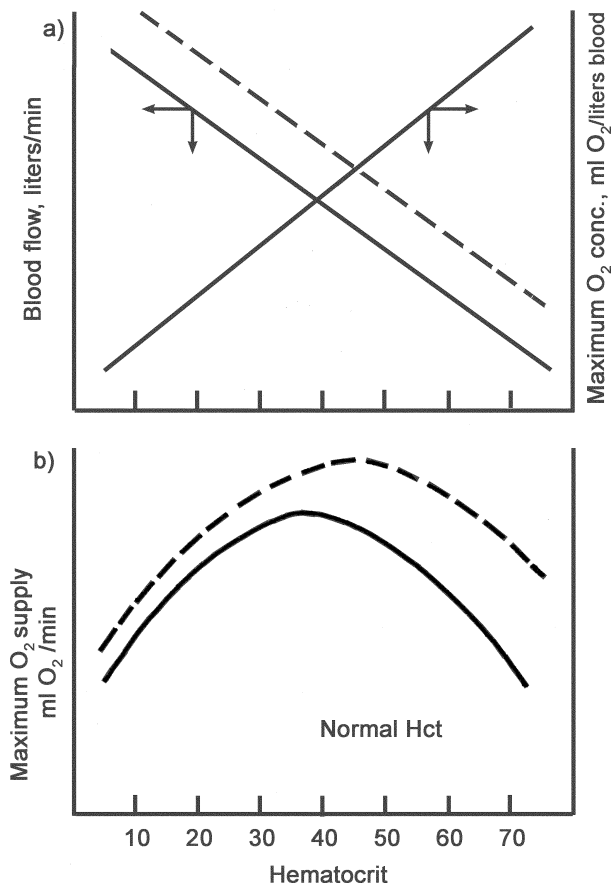
Figure 6-9. Effect of hematocrit on oxygen transport: (a) maximum blood oxygen concentration varies directly and blood flow varies inversely with hematocrit, (b) maximum oxygen transport, calculated as the product of blood flow and maximum oxygen concentration, is a parabolic shaped curve when related to hematocrit, with an optimum occurring in the normal hematocrit range for humans. As hematocrit increases, the maximum amount of oxygen that can be transported to the tissues also increases initially, but declines at very high hematocrits due to the effects of viscous flow resistance. The solid line indicates normovolemia; hypervolemia, indicated by the dashed line, causes the optimum levels to shift as shown. (Redrawn from Ref. [53] and [60])

eration of the independent and opposite influences of blood viscosity and blood volume on blood flow. During exposure to weightlessness and in ground-based studies related to spaceflight hematology (i.e., bedrest, dehydration, and infusions), both the viscosity and volume of blood are known to change to modest extents. With regard to erythropoiesis regulation, any disturbance of oxygen transport needs to be examined in the region of the renal oxygen sensors. These tissues, which release the erythrocyte-stimulating factor, are a crucial part of the feedback control system that corrects long-term changes in oxygen transport. Unfortunately, the effects of viscous resistance and passive distention on renal blood flow are not well established, particularly for this organ, which has unique
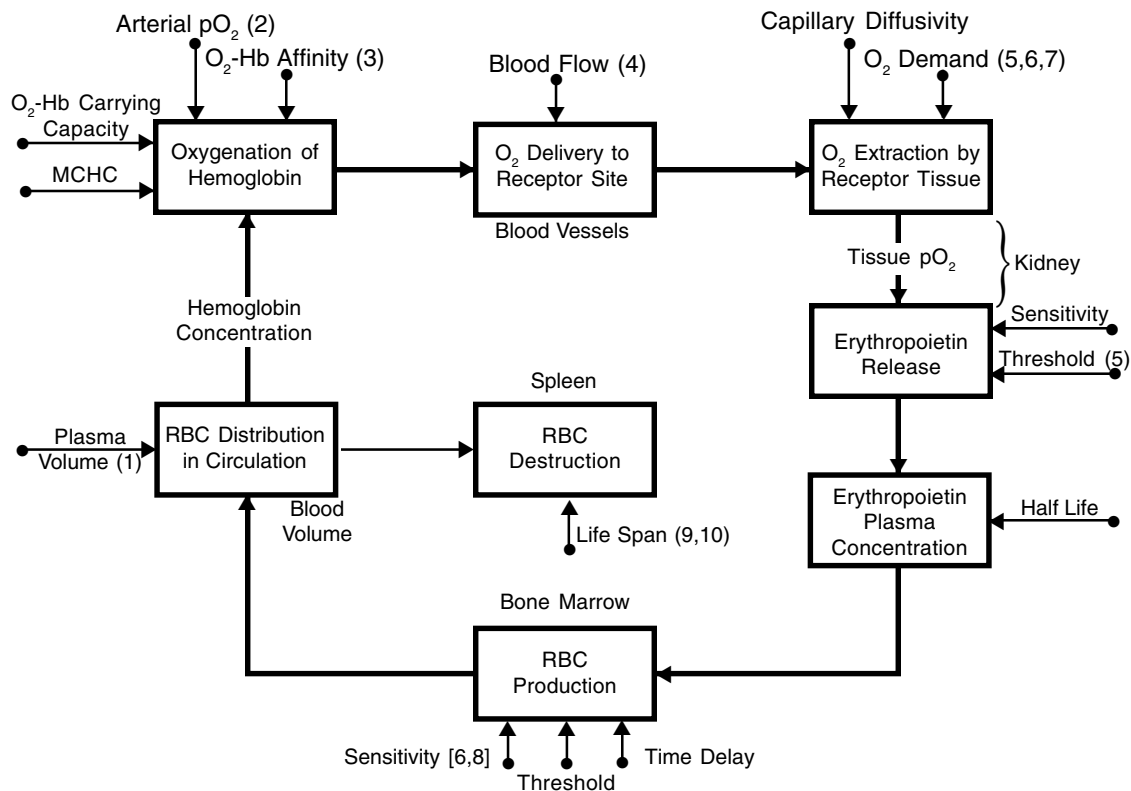
Figure 6-10. Systems diagram of the mmodel for control of erythropoiesis. Fixed parameters of the model are designated by the bullet-ended arrows. Numbers in parenthesis refer to the parameters that were used to evaluate hypotheses explaining red cell mass loss during spaceflight (see Fig. 6-14).

autoregulatory flow capabilities. Nevertheless, the relationship between the factors determining oxygen transport, exemplified in part by the oxygen flow rate equation and Fig. 6-8), have contributed to formulating a consistent and unified interpretation of many diverse studies, both in human and in animal subjects.

6.3.4 Tissue Oxygenation and Erythropoiesis: A Model

The physiologic role of the erythron is to provide an adequate amount of available oxygen in arterial blood at a suitable oxygen tension. Therefore, a complete characterization of erythropoiesis must consider the relationship between tissue oxygenation and the red cell producing mechanisms. It is generally accepted that this relationship can be described in terms of a negative feedback control circuit. Figure 6-10 illustrates the essential physiological and anatomical elements of such a control system, showing the relationship between blood oxygenation, tissue oxygenation, erythropoietin, red cell production, and hemoglobin concentration.

The concept shown in Fig. 6-10 was translated into a mathematical model for the purposes of quantitatively simulating the responses to erythropoietic disturbances. This model, including its mathematical description and validation, has been fully described elsewhere [5,9] (also see Chapter 3 and Appendix B). For convenience, the major assumptions that were used in formulating the model are summarized in Table 6-8.

In order to compare the performance of the model to real-world behavior, an understanding of the model's limitations is essential. Many of these limitations are discussed in the sections describing the details of the model. In the context of the present discussion, several aspects of tissue oxygenation that have just been described but are not represented in the model will be discussed next.

The model is restricted to control of the erythropoiesis system. It represents a system for controlling levels of circulating red cell mass, but does not have circulatory, respiratory, or biochemical feedback elements which describe the other aspects of tissue oxygenation that are suggested in Fig. 6-8. While user-controlled parameters that represent these functions are included in the model (i.e., blood flow, arterial oxygenation, oxy-hemoglobin affinity), they are not automatically adjusted in closed-loop autoregulatory fashion.

The anatomical representation of the kidney structure with respect to intrarenal gradients of oxygen tension are not included in the model (see Chapter 6.3.2). This formulation must await further experimental description of the

Table 6-8. Major Assumptions of Computer Model of Erythropoiesis Control

- Erythropoiesis governed by level of renal tissue oxygen tension

- Decreasing renal oxygen supply in relation to renal oxygen demand results in reduced oxygen tension and increasing rates of erythropoiesis (and the reverse as well).

- Renal tissue oxygenation is a function of hemoglobin concentration, blood flow, mean corpuscular hemoglobin concentration, oxygen saturation of arterial hemoglobin, diffusivity of oxygen at renal capillaries, and oxygen uptake of renal tissues

- The hormone, erythropoietin, is released by the kidneys into the blood at a rate inversely related to the renal tissue oxygen tension

- The rate of red cell production is directly related to the log of the log of the erythropoietin plasma concentration

- The rate of red cell destruction is based on the life span of the cell and is a fixed percentage of the circulating red cell mass

- Changes in circulating red cell mass are determined by the time integral of the production rate minus the destruction rate

renal oxygen sensing sites. At present, this does not seem to be a serious limitation, either in simulating spaceflight or related experiments.

The effects of viscosity and blood volume on blood flow and erythropoiesis are not included in the model (see Chapter 6.3.3). The conditions under which these omissions would lead to serious error are not usually encountered in hypogravic simulations. However, since blood flow is an explicit parameter in the model, hypotheses concerning viscosity and volume effects were evaluated.

Development of the model and a study of its simulated behavior led to identification of several important features of the control system that are not generally recognized. These properties, derived from a theoretical model, were especially useful in interpreting the experimental results examined in this study, and are summarized as follows:

a) The variable that is under primary control is the renal tissue oxygen tension. Other time-varying quantities, including hemoglobin concentration (or hematocrit) and red cell production rate can be considered feedback variables that are adjusted to return tissue pO_2 toward normal. Erythropoietin acts as a simple messenger conveying information regarding the changing state of renal tissue pO_2 to the bone marrow.

b) It is assumed that the renal tissue functions as an oxygen sensor that is located at the venous capillaries in a region of constant blood flow and constant oxygen uptake. If other parameters affecting oxygen transport (such as arterial pO_2 and hemoglobin saturation) are non-varying, the sensor may be considered to function as a hemoglobinometer. In this mode, hemoglobin concentration is the major variable to influence, and ultimately to be controlled by, the oxygen sensor.

c) The quantity d(RCM)/dt (i.e., the change of red cell mass with respect to time) operates as if it were under integral control so that it always returns to a value of zero at steady-state, regardless of the type of disturbance. This is accomplished by changes in both production and destruction rates.

d) The combined renal-bone marrow controller operates

according to the principles of proportional control, at least in its normal operating range. Under this type of control, the tissue oxygen tension, if disturbed away from its control value, will always tend to return to normal, and in most all cases there will be some steady-state error (i.e., 100% compensation in the face of a load disturbance is normally not possible). Increasing controller gain (i.e., the sensitivity to tissue pO_2) will decrease the time at which maximum compensation is reached and will decrease the steady-state error at the sacrifice of some dynamic stability in the formation of erythrocytes.

e) Disappearance of red cells during spaceflight may be expected to occur under certain conditions at much slower rates than their subsequent replenishment. The maximum rate of red cell mass loss (assuming production is completely inhibited) is limited by the natural attrition rate of red cells, which in the human, is 1% per day or about 20 ml packed red cells per day. In contrast, the maximum rate of red cell production is governed by the bone marrow production capacity, usually said to be about six times normal or about 120 ml packed red cells per day.[‡]

One of the first, and potentially the most important, uses to which the model was applied concerned identification of factors which could lead to suppression of circulating red cell mass. In keeping with the emphasis of the previous discussion on tissue oxygenation, and in accord with the model shown in Fig. 6-10, it was obvious that increasing levels of tissue oxygen tension would provide a diminished stimulus for erythropoietin production. The steady-state relationship between tissue pO_2 and red cell production may be derived by reducing the formulation of the model's erythropoietin and erythrocyte controllers (Fig. 6-11(a)) to the more compact form of Fig. 6-11(b). This relationship is shown in detail in Fig. 6-12, in which

---

[‡] A number of factors that could have caused rates of red cell destruction in excess of normal during spaceflight are discussed in Chapter 6.4.10.

(a)

(b)
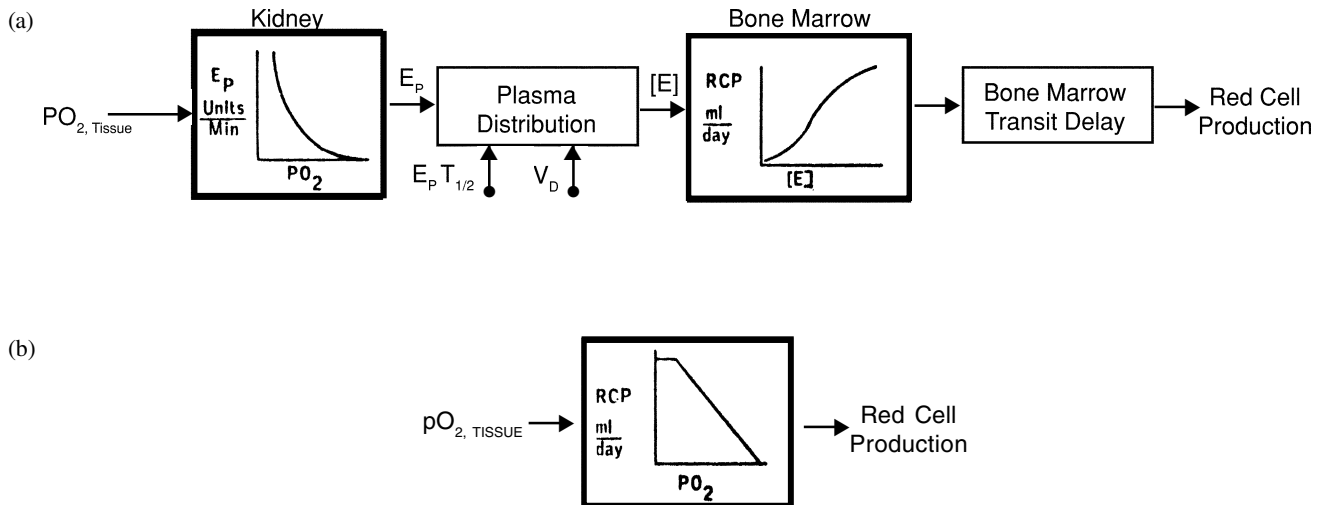
Figure 6-11. Relationship between tissue oxygenation and red cell production. (a) Elements, contained in the computer model showing the renal-bone marrow controllers which has been simplified in (b) by eliminating the effect of erythropoietin which acts merely as a signal transmitter of tissue oxygen content. The portion of the graph shown in (b) is presented in detail in Fig. 6-12. (Ep = rate of erythropoietin release, $E_p T_{1/2}$ = plasma half-life of erythropoietin, [E] = erythropoietin plasma concentration, PO_2 = tissue oxygen tension, V_D = volume of distribution of erythropoietin, RCP = red cell production rate).
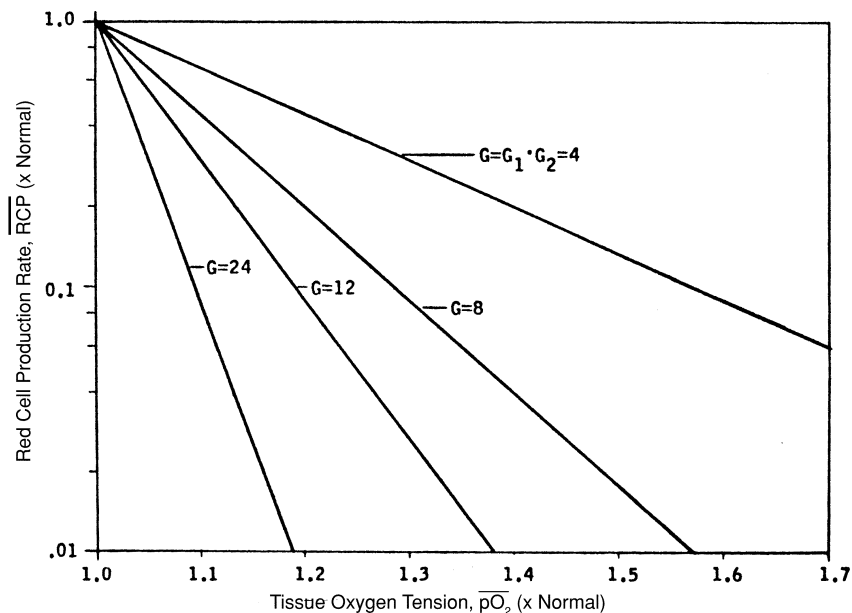
Figure 6-12. Combined renal-bone marrow controller function curves (semi-logarithmic plot) showing depressed erythropoiesis at high tissue oxygen tensions. Curves are shown for different assumed values of overall controller gain (G) are shown. A detailed discussion of the renal gain, G_1, and the bone marrow gain, G_2, can be found in Appendix B. Scale indicates normalized values (Normal = 1.0).

only the hyperoxic range of tissue pO_2 is shown. It is in this region that suppression of red cell production is predicted to occur to a degree dependent not only on tissue pO_2, but also on the overall controller gain, G. Although neither tissue pO_2 nor controller gain is normally measured directly, these quantities can be determined by parameter estimation techniques. Using the theoretical analysis of Fig. 6-12, it is possible to predict a significant suppression of erythropoiesis due to moderate increases in tissue oxygen tension.

The factors that are capable of altering tissue oxygen may also be assessed for their quantitative and dynamic influence an erythropoiesis using the model. The simulated model behavior resulting from step changes for six normally

fixed parameters is shown in the sensitivity analysis of Fig. 6-13. Alterations in the following parameters were evaluated: oxygen uptake of renal tissue, oxy-hemoglobin affinity (expressed as P_{50}), renal blood flow, arterial oxygenation, total plasma volume, and size of the marrow pool (indicated in Fig. 6-13 as bone marrow responsiveness). The values of these quantities were changed prior to simulation by a magnitude of 20% from control and in a direction that led to a suppression of erythropoiesis and red cell mass.

The sensitivity analysis provided a basis for determining the relative importance of parameters and for identifying likely causal factors for the decrease in red cell mass observed in spaceflight. These assessments were considered in the light of known physiological function. For example, while renal oxygen demand demonstrated the most significant effect on tissue pO_2 and erythrocyte production, there was no reason to initially believe that this parameter was altered during exposure to weightlessness. On the other hand, decreases in plasma volume are a well-known occurrence in hypogravity, and the resulting hemoconcentration is capable, at least according to the model's predictions, of producing tissue hyperoxia, suppression of erythropoietin, reduction in erythrocyte production, and gradually diminished red cell mass. In this manner, each of the parameters identified by the systems analysis were evaluated to determine whether a reduced gravity environment could cause a change from its pre-flight value. The results of manned spaceflight experiments were reviewed as well as experimental analogs of long-term weightlessness, such as human bedrest and animal dehydration studies. Factors other than those directly contributing to tissue oxygenation were also considered, such as increased red cell destruction and altered controller sensitivity. Ground-based experiments, such as descent from altitude and red cell transfusions, were also examined by computer simulation and found to have unexpected relevance to the spaceflight situation. This systematic approach (see Fig. 6-1) led to the formulation of a series of hypotheses that could explain zero-g induced red cell loss, not as some pathological event, but in terms of a normal response to disturbances in a feedback control system. These hypotheses and their evaluation using model simulation are discussed in the next section.

6.4 Development of Hypotheses

The most attractive candidate hypotheses for reconciling the experimental findings can be conveniently grouped into three categories: a) those relating to disturbances in the oxygen-supply demand balance and which are expressed via diminished levels of erythropoietin; b)those having a direct effect on the bone marrow and thereby by-passing the erythropoietin mechanism; and c) those which have an influence on removing red cells from the circulation. These three groups of hypotheses, illustrated in Fig. 6-14, attempt to explain the disappearance of circulating erythrocytes by either a decrease in production or an increase in destruction.
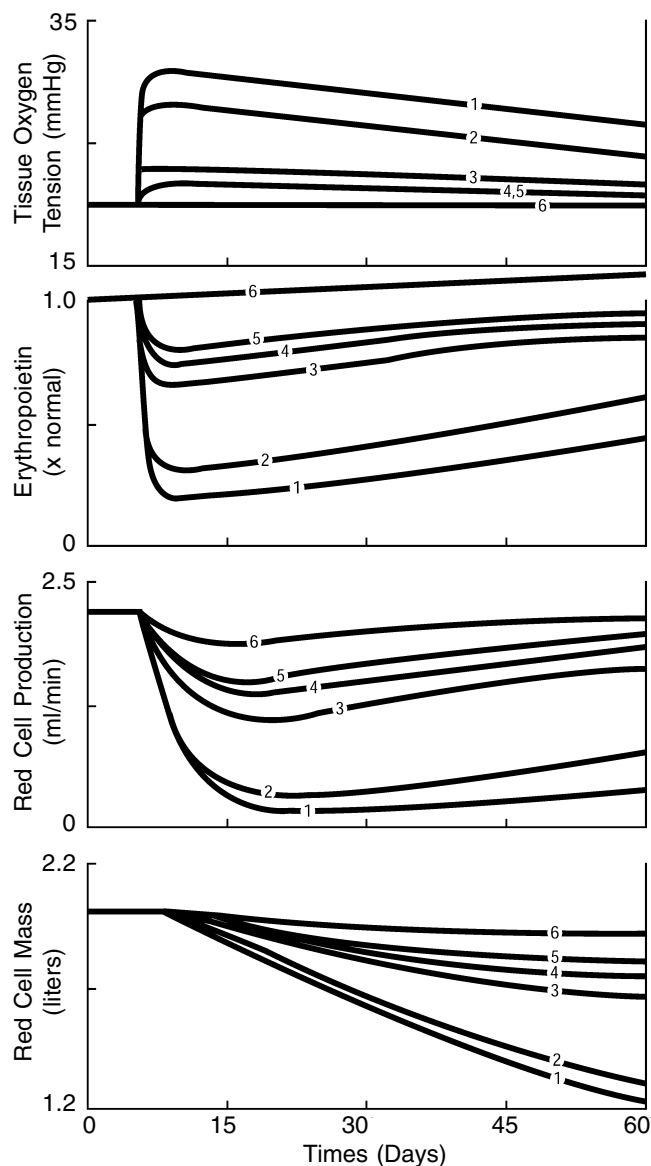
Figure 6-13. A sensitivity analysis showing the behavior of the computer model resulting from disturbances that lead to suppression of red cell production. The model's response is illustrated for a 20% constant load disturbance (that is, step change) of six parameters.

Curve 1 = renal oxygen uptake (–);
Curve 2 = oxy-hemoglobin affinity, P50 (+);
Curve 3 = blood flow (+);
Curve 4 = plasma volume (-);
Curve 5 = arterial oxygen tension (+);
Curve 6 = bone marrow responsiveness, P1 (-).

Algebraic sign refers to direction in change of each parameter ((+) = increase, (–) = decrease) from its normal control value in order to suppress red cell production.
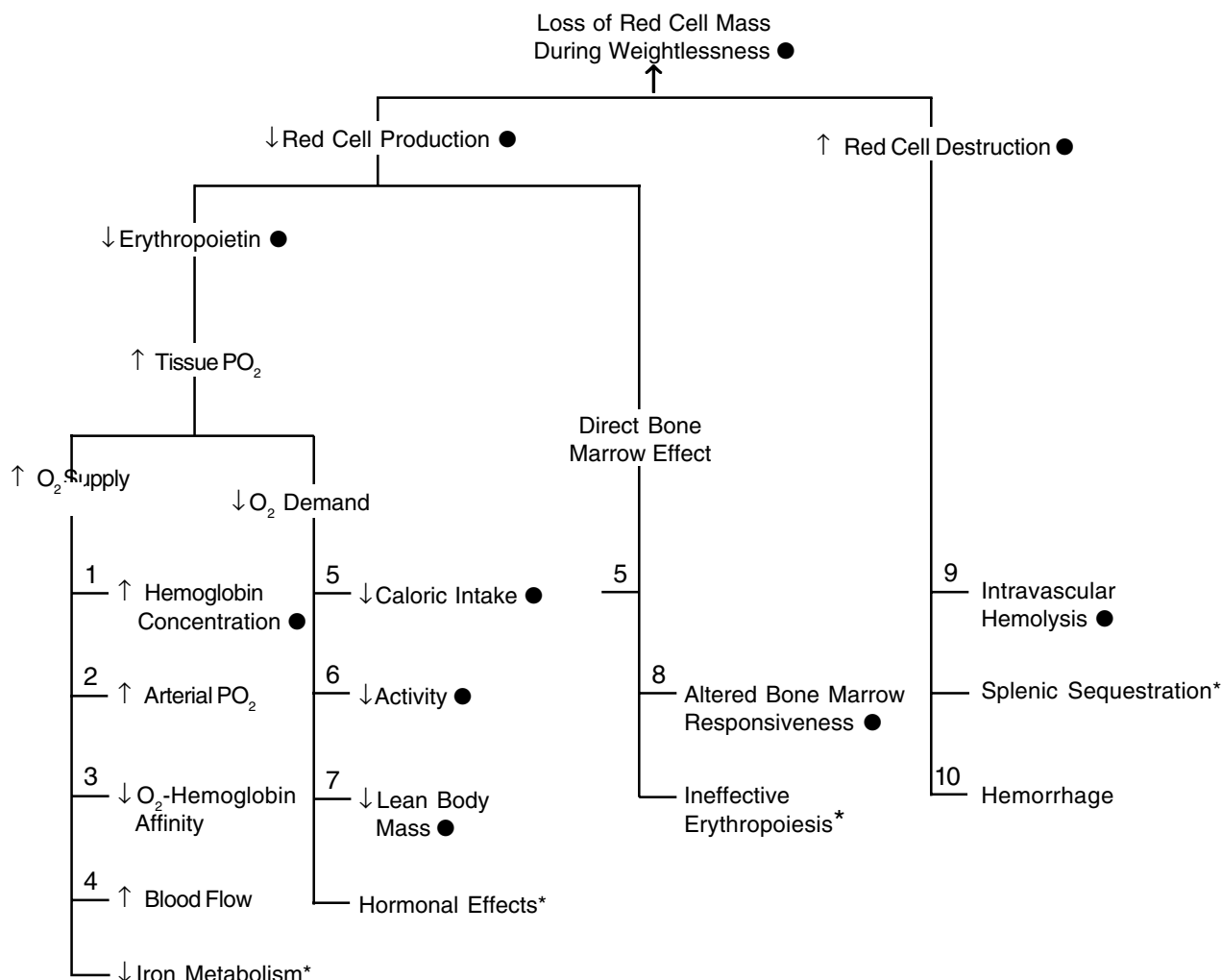
Figure 6-14. Hypothesis diagram showing the various factors considered in the present study to account for red cell mass loss during weightlessness. The numbers adjacent to each factor indicates the model parameter that was altered (see Fig. 6-10) in order to evaluate the influence of that factor by simulation techniques. (*) indicates that the designated pathway is not testable in the current model. (●) indicates that evidence is available supporting the event shown. (BM = bone marrow, Hb = hemoglobin).

The mathematical model is particularly well-suited for identifying and evaluating factors relating to oxygen supply. These factors included alteration in Hb concentration, arterial pO_2, oxy-hemoglobin affinity (i.e., P_{50}), and blood flow. Other factors that may influence oxygen demand (i.e., diminished caloric intake, activity, and lean body mass), or the bone marrow (i.e., ineffective erythropoiesis and altered marrow responsiveness), or red cell destruction (i.e., intravascular hemolysis, hemorrhage, and splenic sequestration) are not explicitly represented in the model. Therefore, inferences regarding these mechanisms were made and tested in the model by adjustments in the oxygen uptake, bone marrow control function and red cell lifespan parameters. Most of the hypotheses in Fig. 6-14 are indexed with a number that corresponds to a model parameter (shown in Fig. 6-10) by which the hypothesis could be evaluated.

The following discussion will address each major hypothesis in turn, with particular emphasis on the physiological pathways involved, the evidence that supports the hypothesis, and its plausibility in the context of weightless spaceflight. Wherever possible, this discussion will be supplemented by computer simulations in an attempt to provide some notion as to the quantitative importance of each proposed mechanism. Only simple model disturbances (such as step changes in parameter values) will be used in this discussion. More complex challenges to the model, including multiple, sequential, and time-varying driving functions will be described later when simulations of laboratory experiments are presented.

6.4.1 Hemoconcentration

Of all the factors which can contribute to an increase in oxygen delivery to tissues, there appears to be only one

which has been observed consistently in hypogravic maneuvers in association with loss of red cell mass. That factor is hemoconcentration and results from an apparently rapid reduction in plasma volume. Modest elevations in hematocrits up to 15% have been observed during spaceflight, bedrest, and water immersion [25,61,62].

The idea that hemoconcentration was implicated in the hypogravic response was first proposed in the interpretation of bedrest data [20,63]. This concept was not related to the spaceflight situation until much later [1,25]. Other than in bedrest, information relating to the long-term effects of decreased plasma volume on erythropoiesis is sparse. However, there is considerable evidence to suggest that the erythropoietic system is very sensitive to hematocrit changes in either direction. Significant reductions in erythropoietic activity have been observed following the increases in hematocrit induced by red cell infusion in humans [64] and animals [65,66] thirst dehydration [67,68] and altitude hypoxia followed by descent to sea level [69,70]. As for decreased hematocrit changes, the enhanced erythropoietic response of many types of acute and chronic anemia are well known [71,72]. The studies cited were concerned with changes lasting several days to many weeks, and they represent stresses for which the model has been validated (see Table 3-7). These simulation studies will be summarized later in this section.

Hemoconcentration is not only associated with an increase in viscosity, but it invariably is produced by events which alter the blood volume. An increase in hemoglobin levels can be experimentally or clinically obtained by reduction in plasma volume (relative erythrocytosis) or transfusions of red cells (absolute erythrocytosis). The former case is a hypovolemic maneuver, while the latter case is hypervolemic, but hemoconcentration is a characteristic of both.

Both blood volume and viscosity are capable of influencing tissue oxygenation and erythropoiesis independent of hemoconcentration effects, as discussed previously (see Fig. 6-9). It was necessary to account for these viscous and volume effects to explain some short-term hematological observations involving hypovolemic and hypervolemic hemocentration (see Chapter 6.5.4). However, the analysis presented in the following pages as well as by others [67] suggest that in long-term studies, blood volume or red cell mass changes by themselves, have much less influence on erythropoiesis than do moderate changes in hematocrit.

According to the regulatory concepts outlined previously, hemoconcentration is capable of reducing bone marrow erythropoietic activity via tissue hyperoxia and suppression of erythropoietin release. This effect was illustrated by model simulations already presented (Fig. 6-13), and is further demonstrated by the parametric analysis of Fig. 6-15. In this latter study, the plasma volume parameter was reduced incrementally and simulations were performed at each level for sixty-day periods. As shown in Fig. 6-15, the rapid rise in hematocrit initiated, in turn, the more gradual responses in erythropoietin, erythrocyte production and red cell mass. The falling red cell mass eventually lowered the
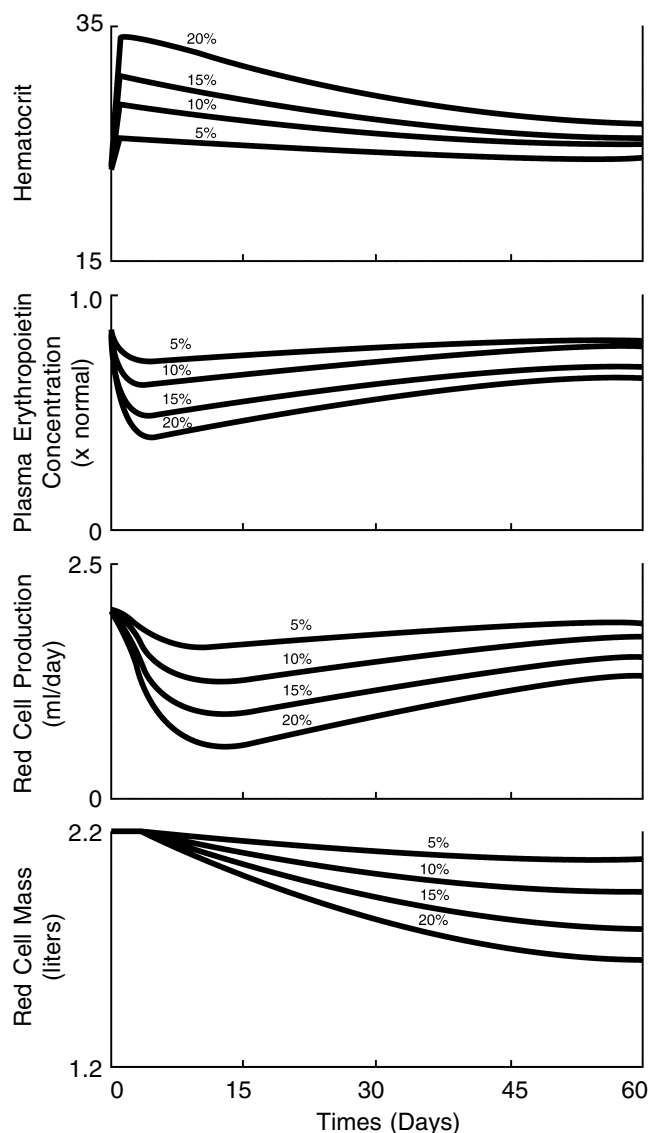
Figure 6-15. The simulated effect of hemoconcentration on erythropoiesis regulation illustrating the sensitivity of the model to changes in plasma volume. The plasma volume parameter was diminished at zero time by the percentage indicated and held at that level for the entire period shown. Gain of the feedback controller was set to G = 6 for this and all other simulations in this section unless otherwise indicated. Increasing the gain value would cause a similar but more intense response leading to even larger losses of red cell mass. The effect of gain on erythropoiesis is indicated in Fig. 6-12.

hematocrit toward control levels, thus diminishing the stimulus for erythropoiesis suppression.

An idealized simulation of spaceflight or bedrest is illustrated in Fig. 6-16. The two-phase sequence of hypogravity and recovery is characterized, in this case, solely by a period of hemoconcentration, followed by a period of hemodilution. This simulation was driven by an idealized plasma volume behavior (derived from a bedrest
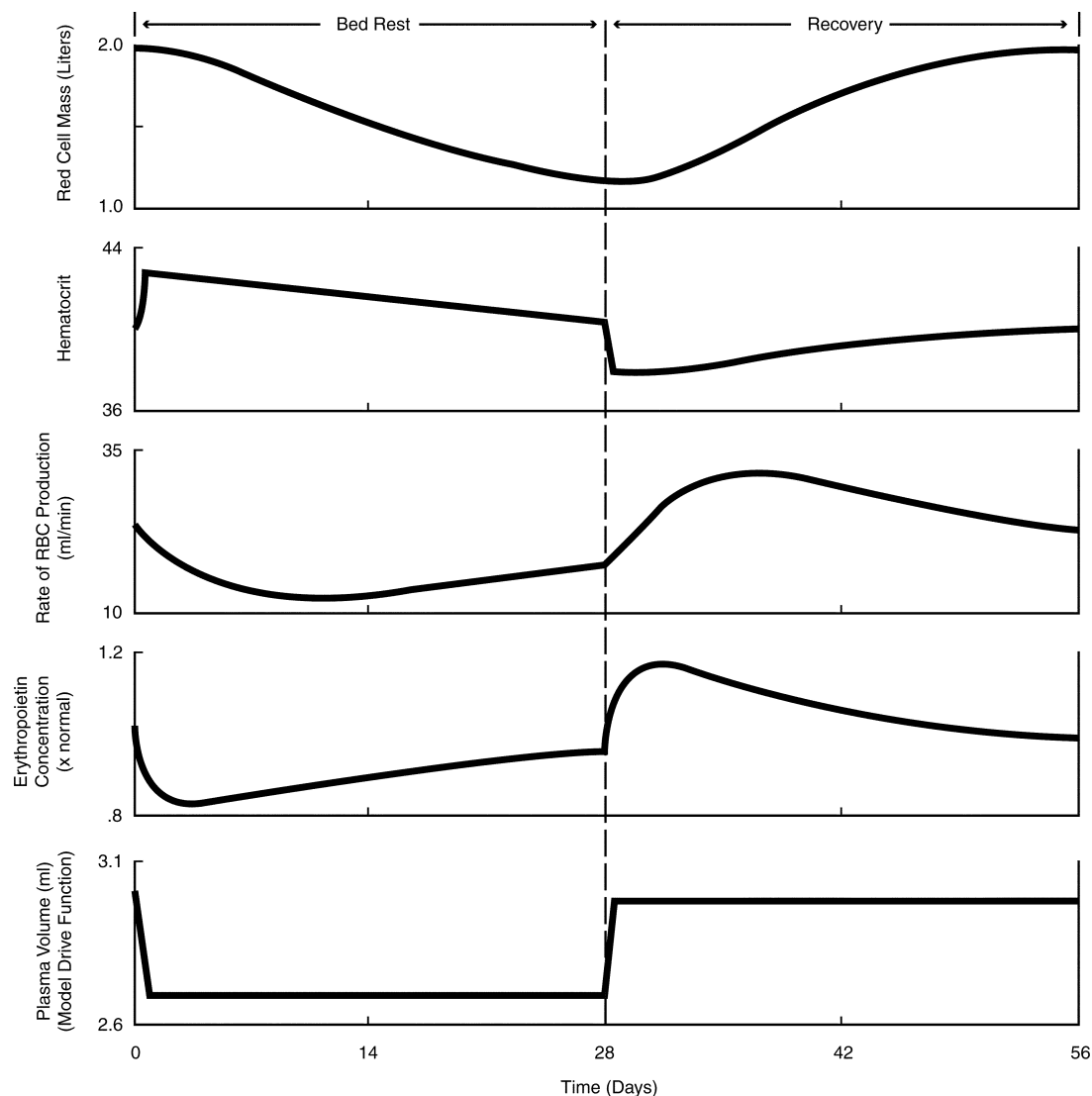
Figure 6-16. Simulation of a hypothetical bedrest study in which plasma volume (bottom panel) is reduced 300 ml (−10%) and then returned to normal after 28 days.

study [20]. Although hemoconcentration causes red cell mass to fall and hemodilution restores red cell mass, the recovery period is not an exact mirror image of the treatment (bedrest) phase. Many factors contribute to this non-symmetrical effect, including non-linear controller functions, time delays in renal and bone marrow elements, and the fact that the hemodilution event is initiated from an erythro-suppressive state in contrast to the normal state preceding hemoconcentration.

If hemoconcentration is a major factor to consider in explaining losses in red cell mass, then it is important to examine the degree and dynamic behavior of the hemoconcentrating event. In bedrest, hemoglobin levels tend to rise slowly and then stabilize, while in spaceflight the rise is relatively more rapid and extreme in magnitude,

and a subsequent prolonged downward trend toward control is observed (see Figs. 6-4 to 6-6). Comparable changes in plasma volume losses (10 - 20%) can occur in both spaceflight and bedrest, but the reduction in volume proceeds more rapidly in spaceflight. This difference in rate of plasma loss will, of course, be reflected in the dynamic behavior of hemoglobin levels, so that the hemoconcentrating ability of spaceflight is initially greater than that for bedrest. The long-term behavior of hemoglobin levels depends entirely on the relative rates at which plasma volume and red cell mass disappear. As will be shown later, the computer model proved to be an ideal tool to explain these complex dynamics and to examine the erythrokinetic differences between bedrest and spaceflight.

Table 6-9. Estimates of Partial Pressure of Oxygen in Arterial Blood of the Skylab Crew*

Quantity	Preflight	Inflight 28-Day Mission	59-Day Mission	84-Day Mission	Skylab Avg
**B	760	252	263	259	258
**P_IO_2	158	194	185	189	189
**P_ICO_2	0	3.7	5.0	5.1	4.6
P_ACO_2	40	43.7	45.0	45.1	44.6
**RQ	0.87	0.91	0.90	0.88	0.90
*P_aO_2	109.50	117.5	110.4	114.1	113.1
ΔP_aO_2	0	8.0	0.9	4.6	3.6

$$*P_aO_2 = (B - PH_2O) \times \frac{P_IO_2}{B} - P_ACO_2\left(1 - \frac{P_IO_2}{B}\left(\frac{1-RQ}{RQ}\right)\right)$$

where B = total ambient pressure, mmHg [75]

PH_2O = partial pressure of water vapor in lungs (at body temperature of 37°C, PH_2O = 47 mmHg)
P_IO_2 = ambient partial pressure of oxygen, mmHg
P_ACO_2 = partial pressure of CO_2 in alveolar air, mmHg (assumed that P_ACO_2 = 40 + P_ICO_2)
RQ = respiratory quotient
P_aO_2 = partial pressure of oxygen in arterial blood, mmHg
ΔP_aO_2 = difference in P_aO_2 between inflight and preflight
** measured

6.4.2 Arterial Oxygen Tension

While the atmosphere of the Skylab workshop did not contain oxygen in high enough concentrations to produce toxic effects on red cells, it did exert a higher than normal oxygen partial pressure (189 mmHg compared to 160 mmHg). If this resulted in even modest increases in blood pO_2, the possibility exists that red cell production was partially suppressed because of decreased levels of erythropoietin secondary to tissue hyperoxia [18,73]. A second factor present that could contribute toward a higher than normal oxygen partial pressure in the blood was an observed resting ventilatory rate (minute volume) that was about 20% higher inflight compared to preflight [74].

While the inflight pO_2 of Skylab's atmosphere was approximately 30 mmHg higher than preflight levels, the effective increase in blood pO_2 would be expected to be much less because of a modulating effect in lung oxygenation. In the absence of direct blood measurements, a formulation for predicting blood pO_2 from ambient oxygen concentrations was employed [75]. The results of applying this equation to the three Skylab crews are shown in Table 6-9. On the average, there was an estimated increase of only 3-4 mmHg in blood pO_2 during the flight phase in comparison to the preflight phase. The crew of the 28-day mission showed the highest estimated arterial pO_2. The fact that this crew also exhibited the largest losses in red cell mass may be more than coincidental.

The effect of even small changes in arterial blood oxygenation can accumulate over time and eventually lead to significant changes in total circulating red cell mass, as suggested by the simulations of Fig. 6-17. If atmospheric hyperoxia is combined with bedrest or spaceflight, a larger decrement in red cell mass may, therefore, be expected than for bedrest or spaceflight alone. This has not been confirmed experimentally, but the reverse case—altitude hypoxia during bedrest—demonstrated that hypoxia can abolish the erythro-suppressive effects of hemoconcentration [76].

The evidence reviewed here is indirect and suggestive, so that a strong conclusion regarding the effect of enhanced arterial pO_2 is not warranted. However, it may have been a contributory factor, especially in the largest red cell mass losses observed on the first Skylab mission.

6.4.3 Oxy-Hemoglobin Affinity

Displacements of the oxygen-hemoglobin equilibrium curve (OEC) to the right or left (conventionally characterized by the value of P_{50}) reflect decreasing and increasing affinity, respectively, between oxygen and hemoglobin (see Fig. B-5). Because of the shape of the curve, any change in it's position profoundly affects the amount of oxygen available at normal tissue oxygen tensions, whereas oxygen uptake by hemoglobin is little affected [40]. The capability to alter O_2-Hb affinity and oxygen unloading at the tissue level in response to environmental changes and ultimately influence erythropoiesis regulation has only recently been appreciated [52,77,78].

Quantitatively, a decrease in oxygen-hemoglobin affinity can be considered comparable to increases in blood flow, hemoglobin concentration, or arterial pO_2 in promoting the supply of oxygen to tissues. Changes leading to a shift to the right (increasing values of P_{50}) have been observed in sub-
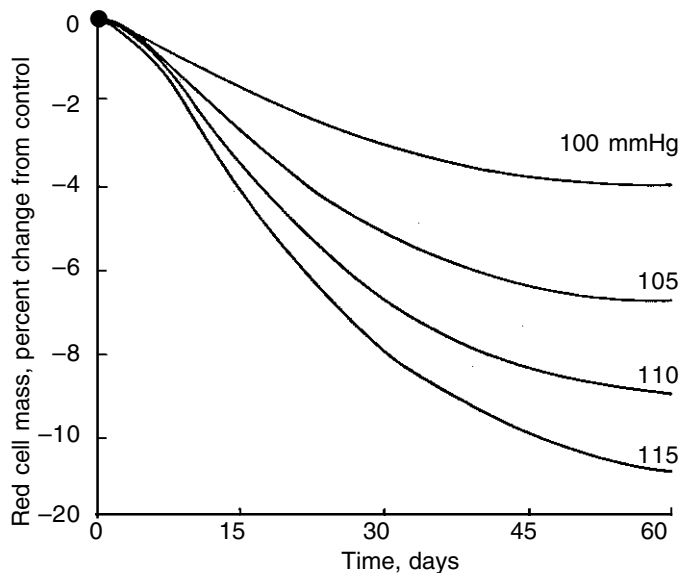
Figure 6-17. The simulated effect of increasing arterial blood oxygen tension (P_aO_2) on reducing red cell mass. At zero time the value of P_aO_2 was increased from its normal value of 95 mmHg to the value shown in the graph and it was held at that level for the entire period shown. The behavior of other model variables during this simulation is indicated in Fig. 6-13 (Curve 5).

jects exposed to hypoxic conditions at high altitude, exercising individuals, and patients with anemic and cardiac impairment [79,80,81,82]. The reverse situation, leftward shifts in the OEC in response to hyperoxia, may be expected on theoretical grounds, but supportive evidence is scant. The outward appearance of a feedback control circuit is, therefore, present, whereby tissue hypoxia increases blood P_{50} that facilitates oxygen unloading from blood hemoglobin. This tends to correct the hypoxic disturbance.

The influence of shifts in the OEC on erythrocyte production has not been well studied, but this relationship is suggested from reports relating P_{50} levels to erythropoietin production [48,78,83]. A pathologically or experimentally induced shift of the equilibrium curve could conceivably result in anemic or polycythemic conditions [52]. Simulations using the computer model support the view that small shifts in P_{50} cause dramatic short-term changes in tissue oxygenation and long-term changes in red cell mass (see Fig. 6-13; Curve 2). Normally, however, changes in P_{50} appear to be a response to an hypoxic situation in a direction that favors oxygen unloading, rather than a cause of the hypoxia.

It is well known that the position of the OEC is governed by such blood factors as pH, CO_2, and temperature. An additional factor that has more recently been implicated in alterations in oxygen-hemoglobin affinity are intracellular phosphate compounds, particularly 2,3-diphosphoglycerate (2,3-DPG) [84]. The dissociation of oxygen appears to be facilitated by 2,3-DPG because it preferentially and reversibly binds to deoxyhemoglobin.

The shifts in P_{50} discussed here in relation to hypoxic situations are believed to be a result of increasing levels of 2,3-DPG [85,86].

There is no conclusive evidence that hemoglobin changes of this nature can account for the loss of red cell mass during spaceflight or bedrest. Values of P_{50} during ground-based hypogravity maneuvers have not been reported. Skylab measurements were performed on 2,3-DPG and indicated no significant change inflight [87]. However, plasma hyperphosphotemia was observed during spaceflight [88] and the possibility exists that blood pCO_2 levels were increased because ambient levels of carbon dioxide were many times normal concentrations in the artificial gaseous atmosphere (see Table 6-9). Both of these may contribute toward a *decrease* in O_2-Hb affinity and a tendency for unloading additional oxygen at the tissue level.[§] On the other hand, if the feedback concept outlined above is valid, the modest degree of predicted inflight tissue hyperoxia (caused by hemoconcentration) would have contributed toward an *increased* O_2-Hb affinity. These opposing factors prevent one from reaching a conclusive prediction regarding alterations of inflight oxyhemoglobin affinity. However, during the postflight recovery phase, it seems more likely that the hemodilutional anemia would result in an increase in P_{50}; this is consistent with the relatively large but non-significant increase in 2,3-DPG measured during the recovery phase [87]. This latter hypothesis was tested by computer simulation and appears to be a fruitful area for experimental investigation.

6.4.4 Renal Blood Flow

Renal blood flow could markedly affect the amount of oxygen delivered to the special oxygen sensing sites. If tissue oxygenation of renal tissue is similar to that of other tissues, a reduction of renal flow would decrease tissue oxygen tension [89]. Moreover, since erythropoietin release is supposedly a sensitive indicator of renal tissue oxygenation, increasing amounts of erythropoietin should be observed in tissue made hypoxic by reductions in renal arterial flow. (This is a prediction of the computer model as shown previously in Fig. 3-28. Some experimental studies using renal artery occlusion support this hypothesis [90,91] while others do not [42,44,92].

Two factors in particular support a relative insensitivity of the erythropoietin producing apparatus to renal blood flow. First, in contrast to all other body organs and tissues, the oxygen demand or consumption in the kidney is more or less proportional to blood flow rather than remaining relatively constant at rest [51]. Thus, although moderate reduc-

---

[§] Johnson, et al [26] postulated that such a decrease in O_2-Hb affinity could, in fact, be responsible for an *hyperoxic* condition and thence a suppression of erythropoiesis. Our interpretation of the existing literature rejects this notion on the grounds that the decrease in O_2-Hb affinity, if it occurred, would be in response to an hypoxic condition and would not overcompensate by creating hyperoxia. It is more likely that inflight hemoconcentration would favor an increase in O_2-Hb affinity.

tions in renal blood flow do affect oxygen delivery, they may not alter tissue pO_2 and erythropoietin production, presumably because renal oxygen consumption is also decreased. Secondly, renal blood flow is known to be under a high degree of autoregulatory control [46]. Both of these considerations suggest that the balance between tissue oxygen supply and demand is not markedly influenced by moderate blood flow changes in the kidney. Whether the renal oxygen detector sites exhibit these same characteristics that may exist for the kidney as a whole is not known.

In order to explain the spaceflight decrease in red cell production on the basis of blood flow, an increase in renal blood flow must be postulated. There is some evidence, based on postural change studies, which suggests an increase in renal blood flow during the acute stress phase of weightlessness [51,93]. The headward shift of fluid in microgravity is a volume-expanding event with respect to the upper body circulation and may enhance renal flow, at least temporarily. However, there is some indirect evidence that does not support an increased renal blood flow, or at best confuses the issue. First, an increased renal blood flow is not a consistent finding in acute water immersion studies [94], and second, longer term bedrest studies show equivocal results with respect to changes in renal blood flow [95,96], although none of these studies measured erythropoietin or the direct effect on erythropoiesis. Third, exercise is known to decrease renal blood flow [46] and daily exercise of varying levels of intensity was used as a deconditioning countermeasure on Skylab flights. Fourth, the hemoconcentration accompanying spaceflight may be responsible for altering intrarenal blood flow [97] and, therefore, may affect the renal oxygen sensors in a yet unknown manner.

In view of the inconclusive evidence relating blood flow to erythropoiesis and the lack of data describing renal blood flow change during spaceflight, it would seem prudent to await new experimental evidence before invoking this mechanism as a long-term causative factor in the reduction of red cell production. UPDATE #1

6.4.5 Altered Oxygen Demand

A decrease in red cell mass could conceivably result from decreased oxygen consumption of the renal tissue because erythropoietin is supposedly responsive to the oxygen supply-demand relationship in that tissue. The major portion of renal oxygen demand is directed toward active transport processes related to eliminating wastes and conserving nutrients [51]. Any event that decreases waste product or nutrient supply to the kidney may be expected to reduce renal oxygen uptake. Such events might include the restrictions in dietary intake and reduced metabolic activity in bedrest subjects and in astronauts in physically confining spacecraft. Although a reduced level of activity was not believed to have been present during Skylab, dietary levels were inadequate throughout the 28-day mission, and possibly the 59-day mission, and particularly for the first week of flight on most other prior missions because of space sickness [98]. On the other hand, loss of cellular material resulting from musculoskeletal

atrophy, a common occurrence in both bedrest and spaceflight, might lead to greater demand for renal oxygen uptake in ridding the body of this waste material. Therefore, the net effect on renal oxygen consumption is difficult to predict.

It is also reasonable to examine possible changes in whole-body oxygen demand, since this parameter is more easily measured and has been linked to changes in erythropoietic activity. For example, the decreases in metabolic rate seen with hypophysectomy, starvation, and hypothyroidism reduced the need for oxygen in relation to an unaltered oxygen supply and were followed by decreased erythropoiesis until a new steady-state was established [42]. Decreases in basal metabolism of about 7% have been noted in bedrest subjects, and even larger decrements would be expected in total energy metabolism [99].

Weightless spaceflight was thought at one time to promote effortless activity in performing tasks with an accompanying reduction in metabolic demand [100]. Consequently, recommended dietary intake during flight was usually reduced below preflight levels. However, this concept has not been borne out and it is now believed that in a high activity mission like Skylab, total metabolic expenditure is similar to that on the ground [101]. The tentative conclusion one draws is that total oxygen consumption is reduced during bedrest and during flights in small space capsules, but there is probably little change for subjects in larger space workshops.

Hypotheses regarding altered oxygen demand on spaceflight erythropoiesis activity were only evaluated to a limited extent in the present study because there is scant quantitative information available for statistical analysis, and there is no information available regarding renal oxygen consumption. Likewise, there is no information presently available that suggests a mechanism by which whole-body oxygen demand can influence erythropoiesis by pathways not related to renal oxygen demand. However, it was desirable to consider changes in oxygen demand in the particular instance of evaluating the wide variation in exercise levels recorded by the Skylab crew (see Chapter 6.4.7).

6.4.6 Reduced Lean Body Mass

Hypogravity, whether induced by bedrest or by spaceflight, often results in a decreased lean body mass, even in the presence of periodic exercise [33] (also see Chapter 4.5). Among a normal population, there is an excellent correlation between lean body mass and red cell mass [102]. It is reasonable to speculate that this correlation may be based on the size of the oxygen-supplying erythron conforming to the size of the metabolically active tissue mass of the body. If this is true, a decrease in lean body mass may be a causal factor in a reduction in red cell mass. This influence was statistically evaluated in the Skylab crewmen (see next section). One might also conjecture that it is not the size of the lean body mass that is important, but rather the total amount of oxygen consumption by this tissue. Since the limited data available suggests that, total body metabolism is not different in space than on Earth,

an alternative hypothesis is that proportionately, more work was being demanded of a diminishing muscle mass [101] and hence, no change in erythron mass would be expected as a result of a reduction in lean body mass.

6.4.7 Effect of Physical Activity

Exercise conditioning is known to have major long- and short-term effects on the oxygen transport systems [103]. Therefore, it is certainly conceivable that exercise, or the lack of it, would affect the erythropoietic process and modify the red cell mass response to both bedrest and spaceflight. However, the effects of exercise on erythropoietic activity and circulating red cell mass are complex and poorly understood.

No clear picture emerges regarding an exercise effect from a review of spaceflight and bedrest studies. Simple bedrest, characterized by a complete absence of physical activity, is associated with a loss of red cell mass. When intermittent daily supine exercise was added to a bedrest protocol, the loss of red cells became more severe, at least in one study [104]. Spaceflight has been characterized by varying degrees of metabolic activity ranging from partial immobility during the earliest suborbital flights to the shirt-sleeve 90-minute daily workouts on treadmill and bicycle during the 84-day Skylab mission. In Skylab (and in apparent contrast to the bedrest study cited above) increasing levels of exercise were correlated with smaller decreases of red cell mass. However, this result is not conclusive because of the lack of suitable controls.

The possibility exists that exercise may have an effect not only during bedrest or spaceflight, but during the recovery period as well. During recovery from bedrest and during the first (28-day) Skylab mission, repletion of red cell mass was observed to be delayed for up to two weeks. A delay was not observed after the 59-day and 84-day missions. These observations may be attributed to the increase in physical activity following bedrest [30,104] in contrast to a reduction in activity following the 59-day and 84-day Skylab missions.

While most investigators find an increase in blood volume during simple exercise conditioning, there is as yet no clear agreement whether this is accompanied by an increase or decrease in red cell mass [103,105-108]. These inconclusive results pertain to both comparisons between athletic versus non-athletic populations and to longitudinal training program studies in the same individual. Most often, an increase in plasma volume at rest is observed with exercise training associated with a concomitant decrease in hematocrit.

Physiologically, it appears that exercise may have two opposing effects on the circulating red cell mass that can account for the varied results. On the one hand, sustained physical training regimens may be associated with an increase in blood destruction rates manifested by an observed drop in red cell mass and hematocrit. This phenomenon, first observed in dogs [109] was recently termed "sports anemia" and has been attributed to mechanical hemolysis resulting from heavy muscular work. It has been observed in both fit and unfit populations, although the results seem to be exaggerated after prolonged confinement or sedentary activity. On the other hand, exercise may act as a bone marrow stimulant and increase the production of red cells. This phenomenon has not been well described, but possibly is a result of the stimulus of blood loss arising from the hemolysis effect [109]. It is also plausible to consider the increased need for oxygen as a causative factor.

Tests with the erythropoiesis model have shown that increased destruction of cells will reduce the hematocrit, and this slight anemic condition will, in turn, increase red cell production. The net result, however, is still a slightly reduced hematocrit; that is, over-compensation and net increases in red cell mass do not occur in the model system, contrary to the implication by Broun [109]. The simulation analysis, illustrated in Fig. 6-18, confirmed the conclusions of Hodgson [47] who showed on theoretical grounds that large increases in destruction rates will result in relatively small decreases in red cell mass because of an effective and sensitive controller of bone marrow production.

If exercise, per se, can influence both destruction and production rates of red cells, then any resulting changes in red cell mass would be dependent on the delicate balance between these two rates. Any imbalance would have a cumulative effect during prolonged training periods. Mechanical destruction of cells would likely be affected by the type of exercise, whether it be jogging, skiing, or swimming. Similarly, if production is based on long-term oxygen demand, the intensity and duration of exercise would be crucial factors affecting steady-state rates of erythropoiesis. These considerations could, in part, explain why different investigators obtain different results. Unfortunately, the most precise methods available to measure rates of red cell production and destruction have yet to be applied to exercise studies.[UPDATE #2]

The effect of complete cessation of exercise in previously athletic individuals, as exemplified in some bedrest studies and pre-Skylab spaceflights, may lead to effects opposite to those of exercise training. A decreased metabolic rate, a decrease in lean body mass (see Chapter 6.4.5 and Chapter 6.4.6) and minimal mechanical stress could increase red cell lifespan (by reducing the rate of hemolysis in previously athletic subjects), and increase the tendency for lower red cell production rates. Without precise determinations of these opposing factors that influence red cell mass, it would be difficult to predict the final effect.

Any theory that exercise, or the lack of it, influences hematological behavior during hypogravic maneuvers must be consistent with the following facts: bedrest is characterized by a cessation of exercise and loss of red cell mass; the Skylab missions were characterized by a loss of red cell mass that was less severe on each subsequent mission in association with increasing amounts of exercise; the degree of exercise on the shortest Skylab flight was probably less than was performed preflight, and this crew lost the largest amount of red cells compared to any subsequent crew and also exhibited a possible shortening of red cell lifespan at recovery; and, recovery from bedrest
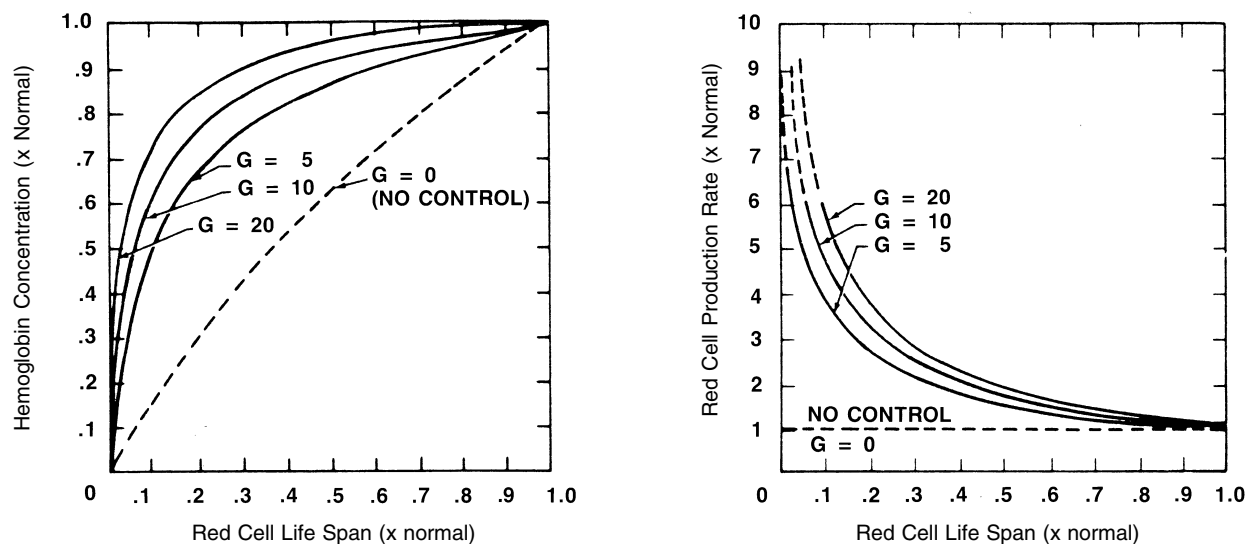
Figure 6-18. Simulated steady-state response to a shortened red blood cell lifespan (hemolytic anemia). Predicted hemoglobin levels and red cell production rates are shown as a function of red cell lifespan and controller gain (G). Dashed line (G = 0) indicates no feedback control. Results suggest that hemoglobin levels are always below control, but they can be maintained near normal for a large range of reduced lifespan provided that controller gain is high.

(ambulation) and from the 28-day Skylab mission was characterized by increased activity and a delayed recovery of red cell mass.

The following hypotheses are proposed to account for these observations:

a) some factor other than exercise, possibly hemoconcentration, is responsible for the primary fall in red cell mass during hypogravity maneuvers, but exercise could modify this response;

b) oxygen demand, as reflected by the degree of activity performed over a long time span during bedrest or spaceflight, ultimately has a controlling influence on promoting red cell production by an unknown mechanism;

c) the type and intensity of exercise performed during weightlessness does not lend itself to significant levels of red cell destruction; and

d) a lack of exercise in certain hypogravic studies may conserve fragile red cells (i.e., increased lifespan) which are more vulnerable to destruction during the early ambulation period (i.e., decreased lifespan postflight) [30].

These hypotheses are aimed primarily at explaining differences between studies in which exercise levels are varied. Accordingly, the increasing degree of exercise on each longer Skylab mission may have limited the severity of the red cell loss. Also, assuming that a period of high activity precedes and follows a minimal activity bedrest phase or a high activity spaceflight phase, the exercise effect, as such, could cause red cell loss to be more severe after bedrest than after spaceflight. Finally, the delay in replenishment of red cells during the recovery period of both bedrest and low activity spaceflights is in accord with hypothesis (d).

There are some grounds for questioning this set of hypotheses. The postulated effect of long-term oxygen demand on red cell production is not known, but cannot be ruled out. Such an effect may exist under conditions of reduced red cell mass (that is, weightlessness), but not when red cell mass is normal (as in terrestrial studies of exercise conditioning). Also, evidence for significant destruction of red cells during or following bedrest or spaceflight is not strong (except under conditions of pure atmospheric oxygen). However, only limited data are available and quantitative techniques for testing these hypotheses suffer from lack of precision.

This discussion of potential exercise effects is presented, in spite of its speculative nature, because it is one of three factors that have been identified which might explain the differences between the red cell losses on each of three Skylab missions. The other two factors are diet and mission duration. These will be considered next in the recent findings on the effect of exercise on erythropoiesis and red cell destruction.

6.4.8 Effect of Diet

It has been established that animals deprived of food, protein, or water exhibit a significant suppression of red cell production [111,112,113,114,115]. The implication of this finding as a causal factor of the "anemia" of spaceflight was recently suggested on the basis of hematological findings in dehydrated mice [66,68]. Restriction of food and water intake was frequently noted on the Skylab mission during the first week of flight (see Chapter 4.6). Also, on at least one Skylab flight and on numerous

pre-Skylab missions, the diet was considered significantly inadequate [100,116]. These factors contributed toward a negative energy balance and negative water balance in spaceflight [101,117] both of which are characteristic findings of the original animal studies.

The actual mechanisms whereby food restriction or dehydration in animals reduce red cell production is not entirely clear. A resolution of the processes involved is complicated by the fact that starved mice or rats refuse water and dehydrated animals refuse food. There appear to be two components to the erythroid suppression which follows either food or water restriction: a) a component related to dehydration and the resulting increase in hematocrit, and b) an energy-balance factor related to the reduced food consumption (see Fig. 6-19).

With regard to the first component, water deprivation induces a state of relative polycythemia that, by increasing oxygen capacity per unit of blood, could lead to tissue hyperoxia and suppression of erythropoietin [66,115]. This is similar to the pathway previously described by which polycythemia, induced by red cell infusion or bedrest, reduces erythropoietic activity (see Chapter 6.4.1).

The energy balance component of red cell loss is more complex and not as well understood. Deprivation of water and food was shown to result in a depression of oxygen uptake, reduced radio-iron uptake by red cells, decreased erythropoietin formation in hypoxia and reduced erythroid responsiveness to exogenous erythropoietin [115,116,117,118]. In terms of the mathematical model of erythropoiesis, these findings can be interpreted to mean that food restriction leads to decreased red cell production by at least three separate pathways (see Fig. 6-19):
a) a reduction in oxygen demand, which leads to tissue hyperoxia if oxygen supply is constant;
b) a direct effect on the erythropoietin producing tissues, which reduces their sensitivity to changes in oxygen supply; and
c) a direct effect on the erythrocyte-producing tissues, which reduces their sensitivity to changes in erythropoietin.

The latter two direct effects on the erythropoietic controllers may be a result of deprivation of critical proteins [112]. The possibility that a disturbance of food intake can affect the erythropoietic regulatory process at several distinct entry points as shown in Fig. 6-19 makes the negative energy balance mechanism a potentially powerful one. In an effort to distinguish between these different effects, it has been concluded that both the hematocrit and the negative energy balance effects are each significantly important, at least in short-term studies [118].

It is not clear whether the food deprivation mechanism is operative in humans as it is in animals, and if it is, whether the magnitudes of dietary intake restriction observed in astronauts can produce a similar erythroid-suppression behavior. Also, it is not likely that a dietary effect can explain the entire loss of red cell mass in the Skylab astronauts because a significant loss was noted in the one crew (84-day flight) that was known to have an entirely adequate diet. However, this
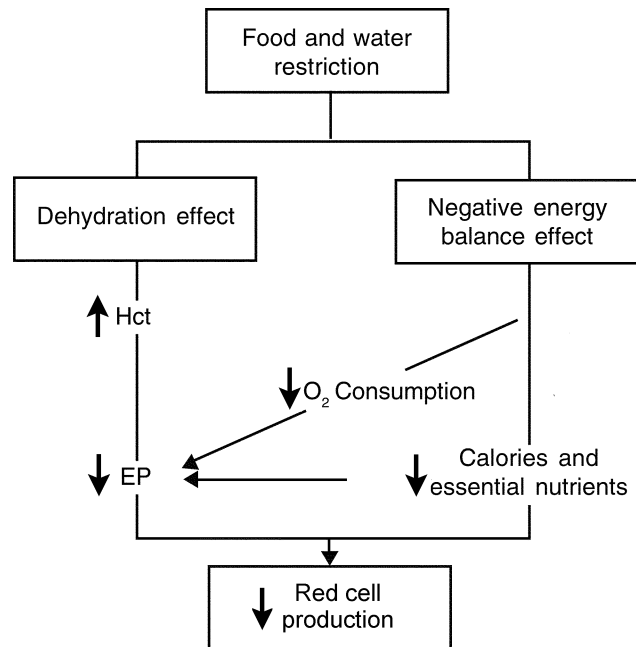
Figure 6-19. Hypotheses that can account for reduced erythropoiesis following food and water restriction. These pathways are based on animal studies. (Hct = hematocrit; EP = erythropoietin)

pathway may explain differences in red cell loss between the different crews inasmuch as the astronauts having the largest negative energy balance (see Chapter 4.6) also showed the largest decrease in red cell mass.

6.4.9 Altered Controller Function

The shape and position of the renal and bone marrow tissue function curves (see Figs. 6-11 and 6-12) have been found to be crucial elements in the control of erythropoiesis. Each curve (which is essentially a dose-response curve describing erythropoietin or erythrocyte production rates) may be roughly characterized by its slope (sensitivity or gain) and by its normal operating point (i.e., the basal or threshold level of production rate**). The effects of changes in sensitivity on controller response have been previously illustrated (see Fig. 6-12 and Appendix B, Figs. B-2, B-3, and B-4). Figure 6-20 shows the effects on the bone marrow when both sensitivity (curve A) and operating point (curve B) are decreased from normal. Combinations of these cases, in which both sensitivity and operating points change simultaneously, can also be postulated. Dramatic changes in erythrocyte production and erythropoietin sensitivity of the marrow are possible by altering the shapes and position of the controller function. Erythropoietin production (as a function of tissue pO_2) is controlled in a similar manner.

** A linear function curve may be simply defined by its slope and intercept; a non-linear function curve requires other parameters for its characterization (as illustrated in Appendix B, Fig. B-3).
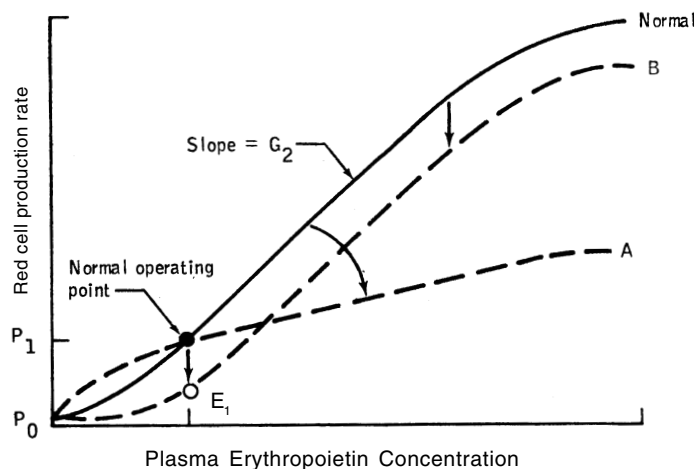
Figure 6-20. The erythropoiesis controller illustrating hypothetical alterations in bone marrow responsiveness. The normal function relating erythropoietin concentration to red cell production is shown as the solid curve. Two distinct types of controller shifts are indicated by the dashed curves. Curve (A): a simple reduction in slope (by rotation about the normal operating point) reduces the sensitivity (gain) of the bone marrow to erythropoietin while maintaining normal operating levels of red cell production. Curve (B): a downward shift in the normal function curve results in reduced erythrocyte producing activity for any given level of erythropoietin, although the sensitivity of the bone marrow to changes in erythropoietin are not significantly altered. (P_1 = normal red cell production, P_o = basal production rate, E_1 = normal erythropoietin levels).

Figure 6-21. The simulated response to alterations in the operating point, P_1. At zero time, P_1 was adjusted from its normal level (1.0) to the value shown.

The effect of a change in the bone marrow's normal operating point on erythropoietic activity was evaluated by model simulation (Fig. 6-21). In this study, the parameter controlling the position of the basal production rate of red cells (P1) was altered (see also Appendix B, Fig. B-3 for parameter definitions). A decrease in P1 would be analogous to a primary anemia of bone marrow failure. The initial effect on production rate is dampened by the bone marrow transit time delay. The reduction in red cell mass (and hematocrit) accompanying this case produces a secondary response of erythropoietin release (not shown), which tends to partially restore production rate to a new, sub-basal, steady-state level. This process causes the undershoot of the simulated production rate. A long-term effect of this stress is also demonstrated, inasmuch as red cell mass does not appear to have stabilized even by sixty days.

The controller functions have not been well described in the human, and it is mostly from animal studies that their general characteristics are known. Comparison of simulation responses with experimental responses has verified the accuracy of the functions used in the model, and has permitted estimation of the parameters that characterize their shape and position. If these control functions behave similarly to those of other physiological systems, it may be assumed that their characteristic parameters may be altered during certain stressful conditions, particularly

if the stress is maintained chronically. In fact, shifts in control function are one important way in which the body adapts to unusual conditions. There is a growing body of literature reporting specific instances of these types of adaptive changes. These reports have been reviewed in Appendix B, and some are particularly relevant to the present study of spaceflight anemia accompanied by hemoconcentration. It has been noted, for example, that hypertransfused animals become progressively more sensitive to erythropoietin within one to two days after transfusion of red cells [119,120]. There is indirect evidence to suggest that prolonged decreases in erythropoietin concentration may lead to decreases in bone marrow sensitivity to erythropoietin [121,122]. Others have shown that bone marrow responsiveness to exogenous erythropoietin decreases during restriction of food and water [66,115]. If the size of the stem cell pool increases, as suggested during the response to hemolytic anemia [72], this can be expressed in the model as an upward shift in operating point and an increase in sensitivity.

These findings, while limited, provide a rationale for testing the hypothesis that the renal or bone-marrow function curves are altered during simulations related to spaceflight studies. One preliminary model analysis suggested that spaceflight is accompanied by decreases and then increases in the controller operating point [3], although the mechanism for inducing this change could not be postulated at the time. Since then, evidence has become available suggesting that negative energy and water balances (both characteristics of most spaceflights) could reduce

236

bone marrow sensitivity and responsiveness to erythropoietin and thereby be responsible for a reduction in erythrocyte production. Evaluation of this hypothesis is discussed later in this chapter (6.5.5.1).

6.4.10 Red Cell Destruction

Red cell death normally occurs after about 120 days by extravascular hemolysis (i.e., sequestration and destruction of senescent red cells in the reticuloendothelial system of the spleen and liver), and, less commonly, by intravascular hemolysis. These pathways account for the normal attrition of about 1% of the circulating red cell mass per day. Abnormal loss of circulating red cells can occur by increasing the degree of hemolysis, and also by such factors as hemorrhage (including blood sampling losses) and splenic trapping. Radio-labeling techniques and analysis of body fluids for cell breakdown products are useful for determining if cell death is occurring prematurely.

Using these methods, a shortened red cell lifespan was detected for Gemini crewmen and astronauts on the 28-day Skylab mission. Toxicity resulting from a high pO_2 cabin atmosphere was probably responsible for the Gemini findings, but as yet, no cause for the Skylab results has been found. Table 6-10 lists a number of factors that have been examined to account for unusual red cell destruction.[††]

Factors that have been considered and ruled out include blood sampling, splenic trapping, exercise, and increases in cell membrane fragility. It is conceivable that excess hemolysis can be attributed to the stress of launch and reentry (high G forces and vibration), but a shortened post-flight lifespan is not a consistent finding on all missions. Changes in red cell shape have been reported [25] but they have not been well correlated with the rates of red cell disappearance. However, since cell surface and shape changes are known to influence red cell survival, this mechanism probably deserves further attention. At present, it is not possible to distinguish between these various mechanisms of red cell disappearance using the computer model. A single parameter, the red cell lifespan, can however, be used to test various hypotheses related to the rate, degree, and time course of destruction, whatever its origin.

It can be argued that the failure to measure a shortened lifespan does not rule out the possibility that excess hemolysis or removal of cells did occur to an extent that was beyond the resolution of the techniques employed. There are two such types of losses to consider: an acute loss, which may occur soon after launch, and a chronic, but low level loss which may continue for longer periods of time. With regard to the first of these, it has been pro-

posed that an age-dependent loss of red cells cannot be ruled out [26]. In particular, the ^{14}C-glycine lifespan tests are based on a radio-label injected 30 days prior to flight, with subsequent measurement during the postflight period. Therefore, if red cells greater than 30 days of age at the time of launch were sequestrated and destroyed selectively during the first few mission days, this event would not be seen in the ^{14}C-glycine survival curves. While such a process is conceivable, it must be consistent with observed levels of inflight hemoglobin concentration, inasmuch as any acute loss would lower those levels. Computer simulations that quantitatively evaluate this hypothesized route of loss will be presented later in this chapter.

The effect on red cell mass of chronic shortening of red cell lifespan is illustrated by the computer simulation of Fig. 6-22 (solid line). In this study the normal lifespan was reduced by 10% (i.e., the approximate corrected change found for the crew of the 28-day mission as shown in Table 6-3), and the predicted effects during the subsequent 60 days were recorded. The model predicts a decrement in red cell mass of only several percent, reflecting the sensitivity of feedback compensation which limits red cell loss by increasing erythropoiesis (see also Fig. 6-18). However, if production rates had not increased in response to abnormal hemolysis, losses of red cell mass greater than 6% are predicted (see Fig. 6-22 (dashed line)). This latter case may have been closer to the spaceflight situation since erythropoiesis is believed to be inhibited in weightlessness. These simulations suggest that a large fraction of the total red cell mass loss observed an the 28-day mission may be attributed to a measured 10% decrease in lifespan assuming there is no compensatory increase in erythropoiesis. Smaller changes in lifespan may not be detectable (i.e., see control group in Table 6-3), but could still contribute significantly to the overall loss if the condition is maintained.

Despite of the lack of extensive spaceflight data, it appears reasonable to conclude that red cell destruction was not responsible for all of the measured losses of red cell mass, even on those missions where a decrease in lifespan was observed.

6.4.11 Differences Between Missions

Regardless of the cause of red cell mass loss during spaceflight, the problem of explaining the unexpected differences of these losses among the three Skylab missions remains. Figure 6-2 showed that the severity of red cell mass loss (as determined on the first recovery day after flight) was progressively smaller for each subsequent flight of longer duration. Since red cell mass was not measured inflight, it is only possible to speculate on inflight behavior. Two alternative hypotheses will be considered here; they will be termed the "regeneration theory" and the "continuous loss theory".

Regeneration Theory. One hypothesis that was offered to explain red cell mass behavior on Skylab claimed that regeneration of erythropoiesis occurs during prolonged spaceflight [15,25,124]. Accordingly, if the three missions

---

[††] In the most significant spaceflight findings since this chapter was originally written, Alfrey and co-workers [123], have concluded from experiments performed on Spacelab crews that a newly revealed process of red cell destruction is taking place during the first week of spaceflight. Dubbed "neocytolysis", the red cells most recently released from the bone marrow are selectively targeted for destruction apparently in response to the previously noted hemoconcentration. The Spacelab results and neocytolysis is discussed more fully at the end of this chapter.[UPDATE#3]

Table 6-10. Factors Proposed For Explaining Increased Red Cell Destruction During Spaceflight

Factor	Evaluation
Blood sampling	Ruled out on basis of ground control studies.
Mechanical stress of launch and reentry	Cannot be ruled out; may be responsible for postulated age-dependent loss early in flight or decreased life span measured on 28-day mission.
Change in red cell shape	Morphological changes were observed but were not correlated with red cell loss; may require further attention.
Increased cell membrane fragility	Ruled out on basis of osmotic fragility tests
Exercise hemolysis	Ruled out on basis that increasing exercise in space was associated with less RCM loss.
Splenic trapping	Ruled out on basis of spleen and liver scans on Apollo-Soyuz mission.
Oxygen toxicity	Probable cause of hemolysis on Gemini and Apollo but not on Skylab.

are considered as a composite, a time-relationship between the red cell mass change and the time following launch becomes apparent (Fig. 6-7). This relationship suggests that "following some initial insult, during the first 2 or 3 weeks of flight, the red cell mass begins to recover, after a refractory period, at about day 60" [25].

In order for the "regeneration hypothesis" to be credible, it must include an explanation for three events: the initial loss of red cells, the refractory period, and the inflight red cell mass-repletion process. With regard to the initial loss of cells, the preliminary belief was that it took place early in the flight due to either hemoconcentration-induced-hyperoxia [1,25] or to splenic trapping of red cells older than 30 days [26]. The former mechanism is based on suppressed erythrocyte production, while the latter mechanism is effectively a form of red cell destruction. A refractory period, supposedly characterized by a red cell mass that temporarily stabilized at reduced levels prior to regeneration, was believed to be a result of continued hemoconcentration and decreased oxy-hemoglobin affinity. The mechanism originally proposed for inflight regeneration of red cell mass was a transient hemodilution at about the same time (about 60 days after launch) that the red cell mass is theorized to begin rising toward control (Fig. 6-23). The sudden drop in hemoglobin, if real, may have been due to a rise in plasma volume. It was hypothesized that this event may have triggered the production of erythropoietin and red cells and provide the basis for a regeneration phenomenon [25]. The liklihood of regeneration late in flight was said to be supported by a post-mission reticulocytosis, that was apparent soon after recovery of the longest mission, but which did not appear after the shortest mission (see Table 6-4).

In spite of the attractiveness of the regeneration theory, it was based on assumptions that must be critically examined, particularly in the light of new analyses conducted in the interim period. The theory might be challenged on the following grounds:

a) The regeneration curve of Fig. 6-7 was constructed entirely from postflight measurements, but the implication is that they reflect the time course of inflight red cell mass changes. Shipboard data collected on the first postflight day presumably reflects red cell mass prior to reentry. However, there is reason to believe that postflight recovery is not an accurate indicator of a postulated inflight recovery (see (b)).

b) The kinetics of the postflight repletion response appears similar to that which occurs following any usual blood loss (i.e., hemorrhage, acute hemolysis, blood donation), and is likely controlled by similar mechanisms. Although these mechanisms are not completely understood, there is a good reason to suspect that hemodilutional anemia (caused by plasma refilling after blood loss) is a major causative factor in stimulating erythropoiesis [71]. Figure 6-7 suggests that regeneration during spaceflight is controlled by the same mechanisms that control postflight recovery. However, the in-flight period is characterized (with the exception of one datum) by hemoconcentration (erythro-suppressing) in contrast to the hemodilution (erythro-activating) of the postflight period.

c) Splenic trapping, a mechanism advanced in preliminary analysis to explain the original red cell mass loss, cannot be supported on the basis of spleen and liver radio-scans performed on the subsequent Apollo-Soyuz crew [37]. An age-dependent destruction of cells by other means cannot, however, be ruled out.

d) While it is possible that a decreased oxy-hemoglobin affinity could contribute to oxygen unloading at the tissues and suppression of erythrocyte production, as proposed [26], there is no strong evidence of this occurring either during spaceflight or bedrest. Furthermore, it is the conventional wisdom that a decreased oxy-hemoglobin affinity arises in response to tissue hypoxia and not the hyperoxia that was thought to be present [125].
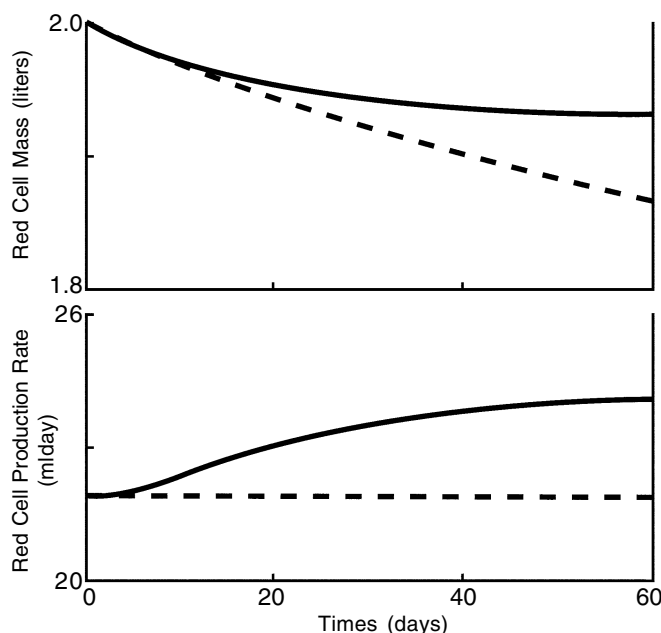
Figure 6-22. Simulation of the effects of hemoysis caused by reducing the red cell lifespan by 10% in the intact model (solid curves) and in the case where compensatory increases in red cell production are prohibited (dashed curves). The model predicts red cell loss of about 3% at the end of 60 days due to a 10% shortened lifespan, but a loss twice as great if erythropoiesis is completely suppressed.

Figure 6-23. Inflight hemoglobin concentration during the 59-day and 84-day missions expressed as percent of preflight mean. The first determinations at Day 4 after launch show a 10% hemoconcentration reflecting plasma loss. Thereafter, hemoglobin levels decline slowly, presumably due to red cell mass loss. Each point is the mean of three crewmen. All data, except those marked (*) were determined by averaging measurements from two different methods (see Chapter 6.2.3.2). The (*) data was obtained by the finger stick-hemoglobinometer technique only and its accuracy and meaningfulness is being reassessed (see text). The data in question were omitted from Fig. 6-5. (Reproduced from Kimzey [25]).

e) A postflight refractory period in the recovery curves of the crew of the 28-day mission may have been caused by a lack of hemodilution as suggested by Kimzey [25]. However, an in-flight refractory period cannot realistically be postulated based on postflight recovery kinetics. If, on the other hand, inflight hemoconcentration and a decreased oxy-hemoglobin affinity contribute to the postulated refractory period by inhibition of erythrocyte production, it is difficult to understand why the red cell mass does not continue to fall during this inflight period rather than stabilize.

f) The mechanism by which regeneration was thought to take place centered on a single datum showing a sudden fall in hemoglobin concentration on day 60 of the 84-day mission (Fig. 6-23). Closer inspection revealed that this value was heavily biased by measurements on one individual on a day when his water intake was unusually high. Also, an in-flight technique of questionable accuracy was used (finger stick-hemoglobinometer method) to obtain that day's value in contrast to the other data of Fig. 6-23, in which results from two techniques have been combined. It is unlikely that a short period of hemodilution, if it was real, could have caused a sustained period of erythropoietic activity leading to a 10% increase in red cell mass as suggested by Fig. 6-7. In sum, it is questionable that hemodilution is a general occurrence (or occurs at all) during spaceflight and that it was re-

sponsible for inflight regeneration in Skylab.

g) A consequence of the regeneration theory is that initiation of red cell production is apparently independent of the presence or absence of gravity, but rather is a function of the time after first exposure to weightlessness [25]. Absent from the hypothesis, if hemodilution is discounted for the reasons discussed above, is a suitable explanation of the processes which underlie these unusual kinetics, particularly the stimulus that causes regeneration to occur.

h) The legitimacy of using data from different missions in the composite diagram of Fig. 6-7 derives in part from the assumption that the conditions present during spaceflight that affect erythropoiesis were identical on each flight and that the primary difference between flights was their duration. However, it is known that at least two factors were present, diet and exercise, that were augmented on each subsequent flight. That is, the increasing duration of weightlessness was accompanied by increasing levels of diet and exercise; also, the level of diet on the first mission was inadequate to prevent weight loss. Both of these factors are known to affect erythropoiesis, as discussed earlier in this section. They also had a demonstrated effect on other tissues. It is generally agreed that the crew of the 84-day mission (on which red cell mass loss dimin-

ished the least) was successful in preventing significant muscular and circulatory deconditioning and weight loss by their superior exercise program and relatively hypercaloric diet (see Chapter 4.6) [126,127].

The preceding comments are not meant to suggest that regeneration of red cells in space did not occur. However, a plausible explanation for its occurence is still lacking. While hemoconcentration is still highly attractive as a mechanism contributing to reducing red cell mass, it is not likely that the transient alterations in inflight hemoglobin levels can be invoked as a causative factor for regeneration. In summary, the available evidence does not appear to support regeneration as a general theory for erythropoietic activity during weightlessness.

Continuous Loss Theory. An alternative, and more conservative, hypothesis that avoids most of the objections to the regeneration theory, is illustrated in Fig. 6-24. It takes into account the idea that all missions were not identical. Therefore, a composite of flight data based on end-point determinations should not be used to describe inflight kinetics. The dashed lines in Fig. 6-24 represent the decline in red cell mass during the inflight phase. While it is not possible to conclusively define the kinetics of this period, ground-based bedrest studies suggest that a linear decline (as shown) may, in fact, have occurred.

If true, the rate of decline of red cell mass would be seen as inversely related to the duration of flight. This is in contrast to the postflight recovery of red cells (denoted by solid lines in Fig. 6-24), which appears to have been achieved at similar rates for all crews, except for the first two weeks of the shortest mission. This alternative theory can be termed the "continuous loss" hypothesis because it proposes that the loss of red cells is primarily a monotonic function throughout the in-flight phase. While some regeneration cannot be ruled out, it would not have thought to occur to the extent predicted by the regeneration theory as illustrated in Fig. 6-7.

The challenge of the continuous loss theory is to explain how the loss rates of red cell mass could be different on each flight. Hemoconcentration is currently the most plausible factor implicated in suppressing red cell production and, as suggested in Fig. 6-23, was presumably similar on each flight. With this in mind, a rationale for the behavior described by the three curves of Fig. 6-24 can be hypothesized. Specifically, it can be hypothesized that some erythro-suppressive phenomenon, common to all flights and a direct function of the weightless environment (perhaps hemoconcentration), acts to reduce red cell mass by inhibiting production, and that other factors that are different on each mission, e.g., level of caloric intake and/or exercise, modifies erythropoietic activity. Therefore, a varying behavior of erythrokinetics would be expected for each mission. In support of the continuous loss theory, are several recent findings that were not available during the immediate post-Skylab period:

a) A composite of bedrest studies indicate a clear linear decline in red cell mass with no observable regenera-

tion [30]. However, the regeneration theory of spaceflight requires the period of repletion to be delayed for up to two months after the hypogravic stimuli, and the bedrest data includes measurements only up to 5 weeks.

b) The studies reviewed in association with Fig. 6-19 showed that both hemoconcentration and negative energy balance can be responsible for significant erythro-suppressive effects in mice. These animal studies are admittedly short-term experiments, but nevertheless, a negative energy balance was reported for the three crews, and this balance varied directly with red cell mass loss (see Chapter 4.6).

c) A similar trend for red cell mass among the three crews was reported for solid tissue loss (see Chapter 4, Fig. 4-24), and this was not thought to result from any adaptive or regenerative effects of zero-g exposure time, but rather from diet and exercise differences between the crews superimposed upon a common loss due to direct effects of weightlessness. The continuous loss theory becomes more attractive if it can be assumed that the mass of red cells in space behaves similarly to other body tissues.

Both theories can explain the different losses of red cell mass for the three missions; their basic dissimilarity lies in the postulated in-flight kinetic behavior (monotonic vs. biphasic) of red cell mass and red cell production. Repletion of red cell mass would begin, according to the regeneration hypothesis, approximately two months after launch, whether or not the crew has returned to earth. In contrast, the continuous loss hypothesis postulates that red cell mass begins recovery only after the crew returns to earth and hemodilution accompanied by normal activity and diet occurs. The differences among the recovery rates of the three crews can perhaps be explained by the relative degree of hemodilution of these crews, in accord with the suggestion of Kimzey [25]. These and other important differences between the two theories are summarized in Table 6-11. Both theories were evaluated by computer simulation as discussed in the Chapter 6.5.

6.4.12 Data Limitations and Experimental Error

The credibility of any hypothesis or set of hypotheses is only as good as the data on which the interpretations are based. Most of the experimental studies reviewed in this section, whether they be spaceflight or groundbased, are relatively sparse with regard to the type of data collected compared to the number of important hematological indices available for examination. For example, the computer model has identified the following parameters as being potentially critical to characterizing and interpreting the spaceflight findings: hemoglobin concentration (or hematocrit), red cell mass, plasma volume, red cell production rate, red cell destruction rate, plasma erythropoietin levels, and blood P_{50}. Of less importance but equally as pertinent are arterial pO_2, bone marrow sensitivity to erythropoietin, metabolic rate, and adequate control or monitoring of diet and exercise. Although techniques are available for their mea-
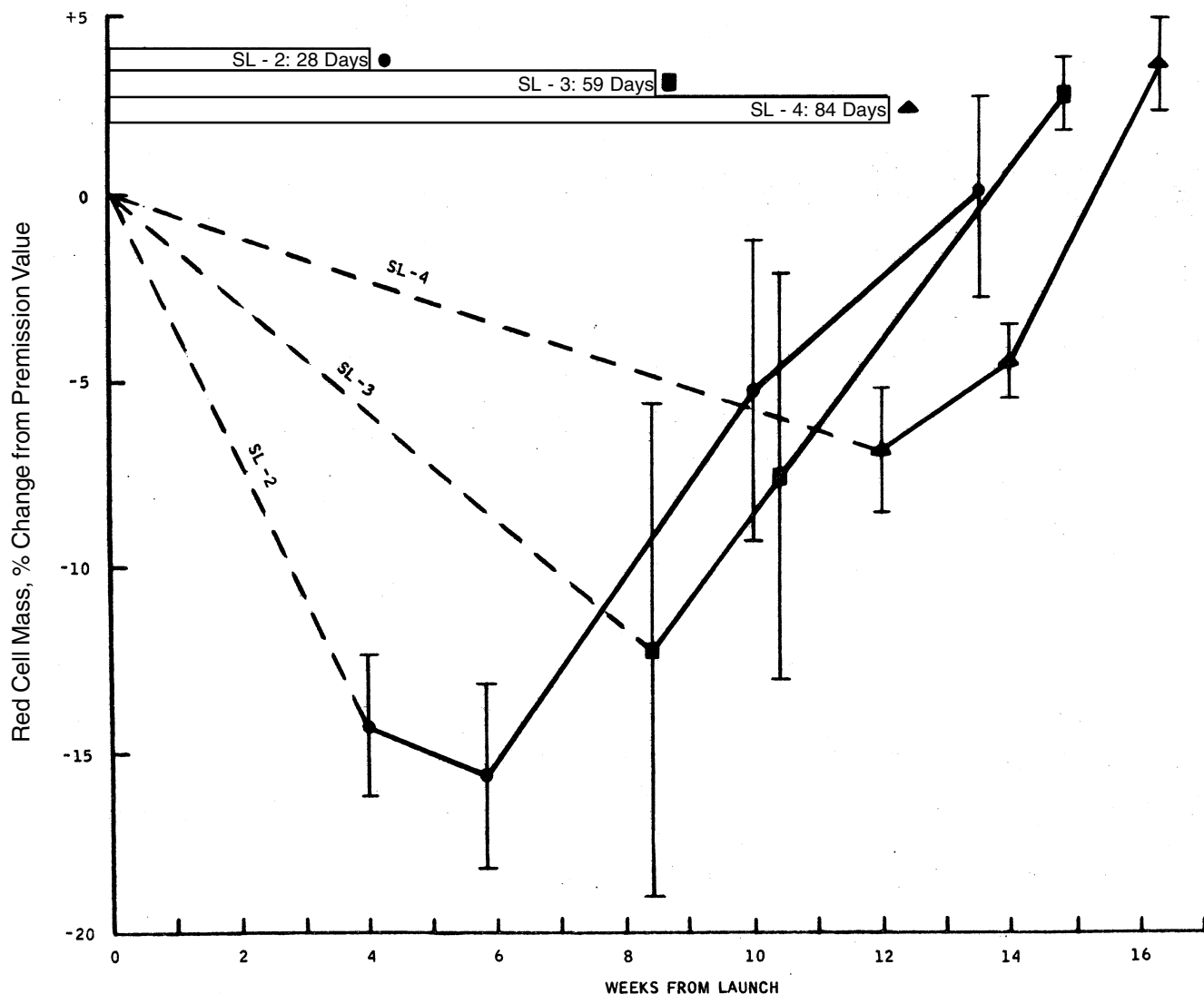
Figure 6-24. Changes in red cell mass in the Skylab crew measured from the day of launch. Each point represents the mean (±SD) change of the three-man crew as measured on the first day of recovery and during the subsequent postflight period. The dashed lines roughly suggest the time course of inflight behavior while the solid lines connect the measured postflight values. The data shown here are identical to that shown in Fig. 6-7. Only the lines connecting the points have been altered to emphasize that each mission could be treated as a separate event rather than as points on a continuum. This representation of the data is termed the "continuous loss theory" in contrast to the "regeneration theory" of Fig. 6-7.

surement in humans and animals, it is rare that more than several of these parameters are determined in any single study. In the Skylab program, for example, data for hemoglobin concentrations and monitoring of dietary intake were the only critical inflight measurements performed. Human bedrest studies and animal studies include additional measurements, but an overall description of the erythropoietic response to hypogravity must still be based on a composite of many studies performed by different investigators under diverse conditions and on different animal species. The simulation model is ideally suited to integrate these data, but without additional experimentation, hypotheses cannot be suitably evaluated.

In addition to the lack of data, the job of interpreting and utilizing the data that are available is made difficult because of some inherent inaccuracies in traditional measurement techniques. Reference is made in particular to determination of erythropoietin, red cell production rates, and red cell lifespan studies; these are discussed next.

It is the current belief that red cell production is suppressed in association with reduced erythropoietin levels. An *in vitro* fetal mouse liver cell assay has recently been developed [128] that does claim to have the required sensitivity for measuring low level erythropoietin, and results using this technique are summarized later in this section. However, this technique is not yet in wide use,

Table 6-11. Comparison of Two Theories To Explain Behavior of Red Cell Loss During Skylab Missions

	Regeneration Theory	Continuous Loss Theory
1. Behavior of RCM Response	Loss curve of RCM is biphasic and proposes inflight recovery.	Loss curve of RCM is monotonic
2. Comparison Between Missions	All Skylab missions considered identical except for duration.	Hemoconcentration behavior assumed similar on all missions, but other modifying factors such as diet and exercise were different.
3. Hemoconcentration	Hemoconcentration proposed as a causal factor in loss of RCM	Same
4. Inflight Hemodilution	Temporary inflight hemodilution responsible for regeneration	Temporary inflight hemodilution has little effect on long-term erythrokinetics.
5. Refractory Period	Refractory period exists during second month in flight.	No inflight refractory period proposed; delayed recovery of 28-day flight due to minimal postflight hemodilution.
6. Recovery of RCM	Recovery of RCM initiated after two months from launch irrespective of time spent in space.	Recovery of RCM initiated only after return from space.

and other bioassay techniques currently available are generally not accurate for measuring sub-basal erythropoietin levels. Data are, therefore, extremely limited in this regard.[UPDATE #4]

Red cell production rates are most accurately determined by the indirect method of radio-iron incorporation into the erythron. However, this method is often neglected in favor of the more popular use of the reticulocyte index. Confusing results have been obtained during the post-spaceflight and post-bedrest periods in which high rates of reticulocytosis were not accompanied by simultaneous increases in red cell mass [20,35]. However, reticulocytes are not a reliable index of red cell production during periods of strong erythropoietic activity [39], so these data should be viewed with skepticism.

Red cell lifespan studies are used to determine red cell destruction rates and to ascertain the presence and degree of any hemolysis. Most of the procedures involve following the time course of disappearance of radio-labelled cells. Normally the tracking of these cells requires many days and if the subject is not in a hematologically stable state (production of cells balancing destruction), or if sequestration of cells occurs, the method yields inaccurate results. The changing red cell mass accompanying spaceflight and bedrest studies indicates a non-stable state and, therefore, caution must be used in interpreting the findings.

The simulation model can assist in identifying the accuracy with which various parameters should be determined. Sensitivity analyses and parameter variation studies indicate the relative importance of parameters and the degree to which changes in their values can influence overall hematological behavior. It has been found, for example, that shifts of oxygen-hemoglobin affinity can produce dra-

matic changes in tissue oxygenation and that measurements of P_{50} should be made with accuracy better than ±1 mmHg.

Comparison of model behavior with experimental observations and any resulting interpretation, as discussed in the next section, should take into account the limited data available and the experimental error associated with these data.

6.5 Simulations of Ground-Based and Spaceflight Studies

The model simulations that have been thus far presented have exemplified the behavior of the model of erythropoiesis regulation. However, they did not demonstrate the greater capabilities of the modeling approach that arise out of a more direct involvement with experimentation or experimental data. Model-to-data comparison is a much more challenging test of model credibility, and it affords the opportunity to interpret data, evaluate the relative effectiveness of different control mechanisms and guide the experimental process. In this section, a number of experimental studies that have been subjected to simulation analyses will be described.

These studies were performed using both human and animal subjects and involved both long- and short-term events. Both the human and mouse versions of the erythropoietic control model were employed. The types of stresses which were examined can be divided into two major categories: a) stresses which resulted in a relative erythrocytosis (or polycythemia) such as thirst, dehydration, bedrest and spaceflight where there is an increase in [Hb] but no increase in red cell mass and b) stresses which result in an absolute erythrocytosis (or polycythemia) such as hypoxia

and red cell infusions where there is an increase in [Hb] as well as an increase in red cell mass. Because of the scarcity of data concerning long-term relative erythrocytosis (which is directly relevant to spaceflight), it was believed that useful insights could be obtained by studying cases of absolute erythrocytosis for which a larger body of literature existed. All of these experimental maneuvers result in hemoconcentration and erythro-suppression, factors identified early in this study as possibly being responsible for the red cell mass loss in spaceflight.

As the study progressed and the number of experiments that were simulated were increased, it became clear that factors other than hemoconcentration were involved, to an extent that remains to be determined. Additional hypotheses were therefore formulated, and these have been described individually in the previous section. In the following pages, the results of applying these hypotheses, both singularly and in combination, to produce realistic simulations of human and animal responses will be described.

6.5.1 Simulation of Altitude Hypoxia

A simulation analysis of altitude hypoxia was presented earlier in this volume to demonstrate validity of the erythropoietic control model (see Chapter 3, Fig. 3-29 and Ref. [5]). One of the more interesting aspects of this simulation study turned out to be, not the ascent to altitude, but rather the descent back to sea level. Subjects returning from prolonged stays at high altitude breathe air at ordinary oxygen levels, but their red cell mass and hematocrit are considerably elevated. In the absence of other changes that influence oxygen supply and demand, the model predicted that hemoconcentration would suppress erythropoietin and red cell production until the red cell mass and hematocrit returned to the original prealtitude levels. Experimental data confirms the overall changes that the model predicts in ex-hypoxic subjects as illustrated in Fig. 3-29 [69,129-131]. However, it should be emphasized that a direct cause and effect between hemoconcentration and erythro-suppression has not yet been firmly established, although this seems to be a plausible mechanism. If an increase in hematocrit resulting from a previous hypoxic exposure could lead to suppression of red cell production, it seemed reasonable to presume that the same type of suppression should occur if hematocrits were increased merely by infusing additional red cells. Analysis of this latter stress condition is described next.

6.5.2 Simulation of Red Cell Infusion

Polycythemia, induced by infusing red cells from a donor, has long been known to suppress erythropoietin and red cell production of the recipient [65]. Induction of the erythroid-suppressed state by this procedure in the mouse forms the basis of an erythropoietin bioassay. One of the few available studies of the long-term effects of red cell infusion in humans was reported by Birkhill [64] who showed that the suppression of red cell production was directly related to the amount of red cells infused.

A simulation of this experiment is illustrated in Fig. 6-25. At the start of the simulation, 800 ml red cells were infused. The model was modified so that the infused red cells could be distinguished from the original circulating red cell mass and could disappear at a linear rate over a period of 126 days. Analysis of the model's response showed that the increased hematocrit leads to tissue hyperoxia, decreased release of erythropoietin, and suppression of red cell production. Loss of the recipient's red cell mass continues until the hematocrit decreases to a point where erythropoiesis returns toward normal and is equal to the destruction of recipient cells. As production rates continue to rise slightly (due to an hematocrit which is just below normal), the recipient's red cell mass reaches a minimum value and then rises toward its control level. The results suggest that erythropoiesis is under the control of hematocrit levels, and the renal oxygen sensor in this instance is behaving as the "hemoglobinometer" described by Beutler [52].

The simulation results compare favorably with the experimental results, both with regard to magnitude and time course of the changes in hematocrit, disappearance of infused blood cells, and suppression and recovery of the recipient's red cell mass. Allowance should be made for the fact that the experimental study used only two subjects, did not have the accuracy that radio-labeled cells would have afforded, and was performed at a time prior to the identification of erythropoietin.

The similarity between the infusion response and the descent-from-altitude response of the previously described simulation should be apparent. In both cases, the increased hematocrit contributed to tissue hyperoxia and erythro-suppression. The degree of suppression was much greater for the descent phase than for red cell infusion, primarily because the hematocrit levels were higher in the former case. In both simulations, a similar value of controller gain (G = 12) was used to obtain the best fit with experimental data. This also compared favorably with the controller gain value obtained from mice data previously reported by Hodgson [47].

6.5.3 Simulation of Bedrest

Bedrest and spaceflight are the only experimental maneuvers available at present for studying relative polycythemia in healthy subjects over long periods of time. As we have discussed, in these situations "down-regulation" of the erythron (i.e., erythrosuppression) is a potential powerful route for restoring hemoglobin concentration to normal. However, these stresses have received comparatively little research attention compared to the situations that lead to "up-regulation", such as hypoxia and anemia. This is undoubtedly a major factor contributing to the lack of understanding of the present problem. Some of the general conclusions from bedrest and their relationship to spaceflight hematology have been presented earlier (see Chapter 6.2.4). In the following pages a detailed analysis will be presented in which the mathematical model of erythropoiesis control was used to simulate and interpret findings from a 28-day bedrest study [4,9,30].

The results of the Baylor College of Medicine (BCM) study have been presented previously in Fig. 6-6. As in
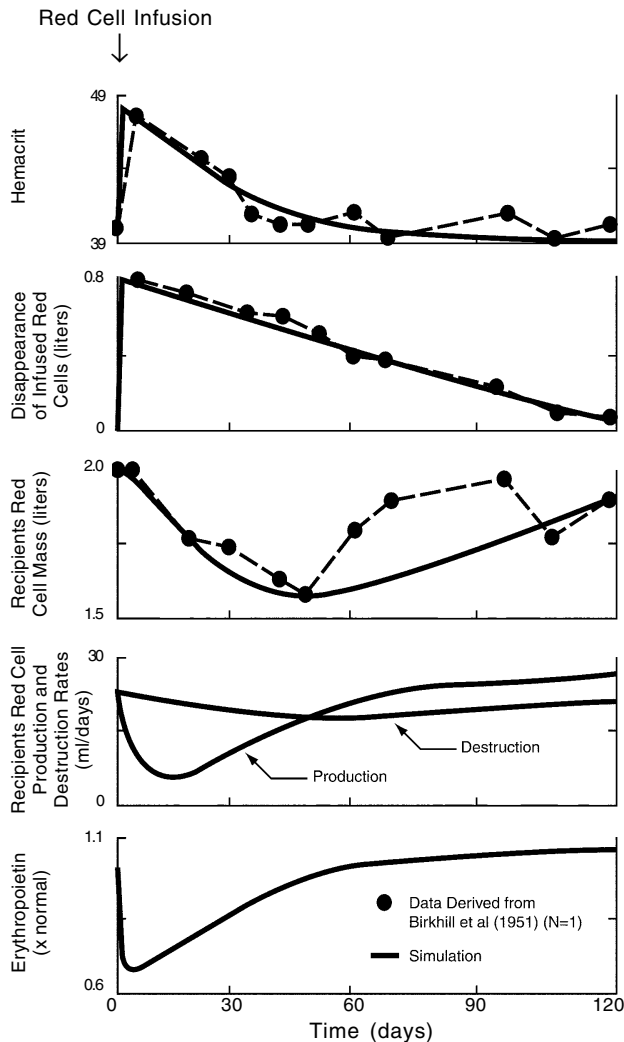
Red Cell Infusion
↓

Figure 6-25. Simulated response to sudden infusion of 800 ml red blood cells (solid lines). Experimental data from a single subject are shown as filled circles and dashed lines [64]. Infused cells disappear completely at a constant rate, while the recipients red cell mass decreases to a minimum value as erythropoiesis is temporarily inhibited. Controller gain, G, was set to a value of 12 throughout the simulation.

previous studies of this type, a small but significant decline of red cell mass (-7%) was observed. Using the mathematical model, various hypotheses were tested to provide insight into the response of the erythropoiesis system to bedrest. The principal hypothesis under consideration was that the red cell mass decrease during bedrest could be accounted for, in large part, by the observed downward shift in plasma volume. It was believed that the resulting hypovolemic polycythemia (i.e., relative erythrocytosis) would lead secondarily to suppression of erythrocyte production in the same manner as was suggested for the hypervolemic polycythemia (i.e., absolute erythrocytosis) of red cell infusion and post-altitude hypoxia.

The 28-day BCM study is particularly worthy of close scrutiny for several reasons. First, it was of the same length as the first Skylab mission during which a 14% decrease in red cell mass *was* observed. Secondly, the procedures used were nearly identical to those for the Skylab hematologic experiments and were conducted by the same principal investigator. Furthermore, several important hematologic measurements were made which were not available from spaceflight studies. These data are crucial for maximum utilization of the erythropoiesis model.

A preliminary simulation, performed with an earlier version of the computer model, showed reasonable agreement with a 35-day bedrest study [2]. However, the data analyzed since that time, including the BCM studies, revealed two important facets of the red cell loss that previously were not fully appreciated. First, the combined results from a number of bedrest studies demonstrate that the red cell loss is a linear function with time (rather than the exponential disappearance predicted originally by the model or the biphasic regenerative behavior as suggested by Skylab data) [30]. Secondly, the earlier observation by some investigators that red cell mass continues to decline following bedrest was confirmed during the 14-day and 28-day BCM studies (Fig. 6-6). It appears that this "refractory" period can last for up to two weeks after bedrest is ended [28,29,132,133]. The red cell mass eventually returns to normal during the recovery phase, but the precise dynamics of this event are not clear because of the sparsity of data. The ability to mathematically simulate both of these phenomena, operative during the supine phase and the recovery phase of bedrest, was singled out as particularly desirable for the simulation study.

Details of the bedrest study and of treatment of the data prior to simulation are provided elsewhere [9,30] Simulations were performed using either the bedrest hematocrit data as a driving function, or in some cases, using an idealized plasma volume function as a driver. Where possible, the simulation responses (i.e., red cell mass, plasma volume, erythropoietin, red cell production) were compared directly with other experimental data. In addition, parameters were adjusted as necessary, in accord with postulated events in order to obtain closer agreement between model and observed responses. For convenience, the results will be divided into those related to the supine phase of bedrest, and the ambulatory recovery phase of bedrest.

6.5.3.1 Supine Phase of Bedrest. Figure 6-26 shows the results obtained using the experimentally determined hematocrit as the only driving function (from Fig. 6-6). The open loop gain of the feedback elements (i.e., G) was adjusted prior to the simulation until the predicted red cell mass at day 28 was equal to the measured value on that day. (The gain factor is described fully in Chapter 3 and in Appendix B, Fig. B-4). The gain was assumed constant throughout the supine and ambulatory phases, and its value was consistent with prior validation studies of the model involving descent from altitude and red cell infusions. The linear change in red cell mass and alterations in plasma volume predicted by the model are in
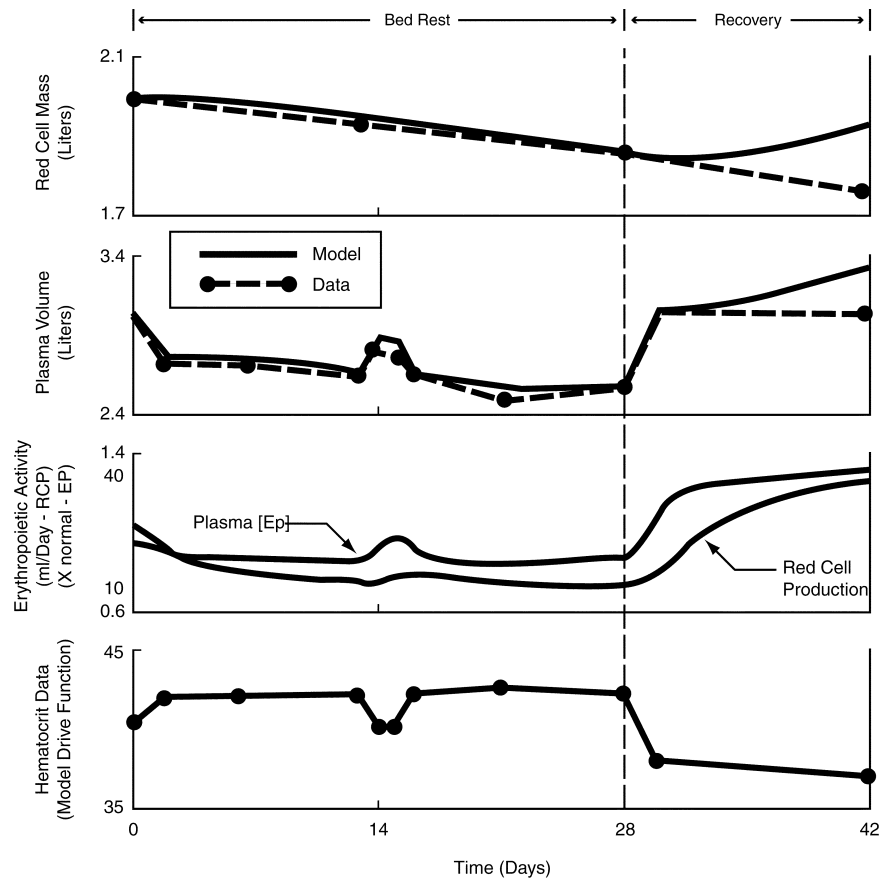
Figure 6-26. Simulation of a 28-day bedrest study. Hematocrit data was used to drive the model during bedrest and recovery phases. Dashed lines and solid circles represent experimental data [30]. The off-normal transient at 14 days is a result of ingestion of saline (see caption in Fig. 6-6). It appears to have affected erythropoietic activity to a small extent but the long term effect on red cell mass seems negligible. Controller gain, G, was set to a value of 10 throughout the simulation.

excellent agreement with the measured values during the supine phase.

The model predicts an average fall in plasma erythropoietin levels of about 15% and in red cell production rate of about 27% during the first 28 days. During the subsequent recovery phase, both of these indices of erythropoietic activity increased above baseline levels. These model predictions are generally, but not totally, consistent with bedrest data with respect to direction, magnitude, and time course of change [20,30,34]. Reticulocyte counts (taken as a measure of red cell production rate) observed during bedrest, show either a 20% reduction [20], or no significant change [35]. The only measurements of erythropoietin made during bedrest with supposedly accurate assays for sub-basal levels unexpectedly failed to confirm a decline in erythropoietin [35]. However, post-bedrest elevations in erythropoietin and reticulocytes have been reported and were generally consistent with the model results of Fig. 6-26.^{UPDATE #5}

This portion of the simulation suggests very strongly that hematocrit changes alone (via erythrosuppression) can account for the magnitude and time course of the red cell mass decrements observed during the bedrest study. In addition, the non-linear plasma volume loss and the time delays in bone marrow production were important contributory factors in producing the linear nature of the red cell mass decrease in the model and possibly in the human subjects as well. The effects of these factors on the dynamics of red cell loss are shown more clearly in Fig. 6-27. The three simulations in that figure were accomplished by reducing plasma volume to the same extent in each case. Using only an idealized step decrease in plasma volume and no time delays, the exponential decline of curve A is generated. The addition of the four day bone marrow transit time delay increases the linearity of the red cell mass response as shown in curve B. Curve C was produced by assuming a more realistic exponential decline of plasma volume and leaving the time delay function intact. Curve C represents the optimal predicted response. Therefore, the only difference between curves B and C is the dynamic behavior of plasma volume loss. In case C, the hematocrit declines relatively slowly compared to the other
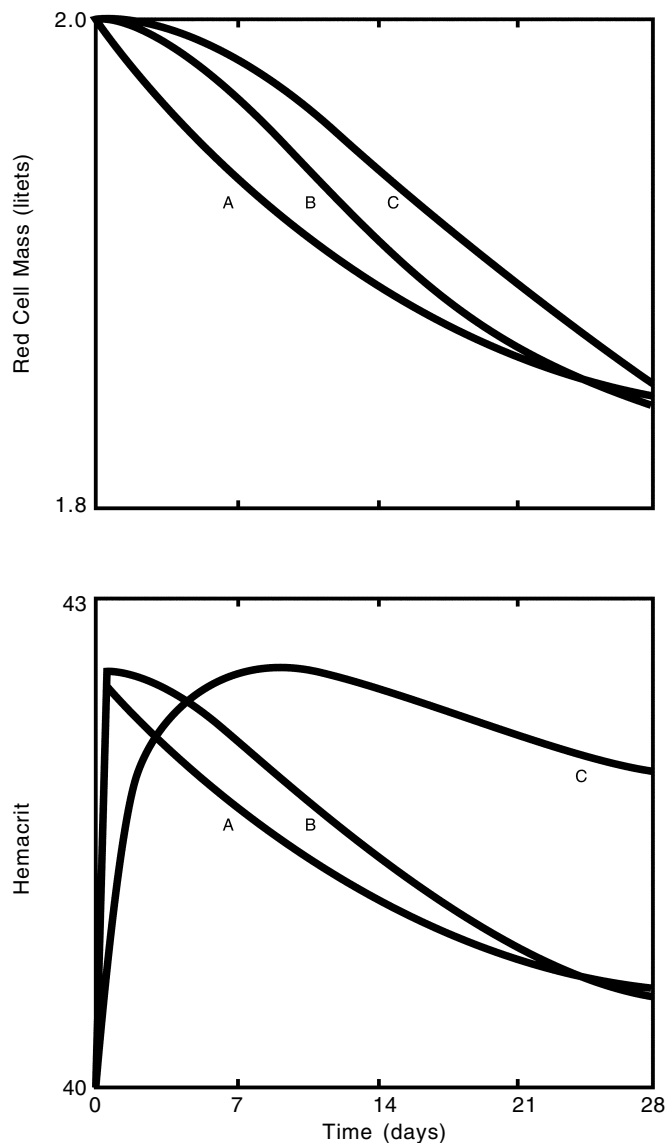
Figure 6-27. Effect of bone marrow time delay and dynamics of plasma volume (PV) disappearance on red cell mass and hematocrit behavior during a bedrest simulation. (A) 300 ml PV step decrease using model with time delays set to zero, (B) 300 ml PV step decrease using model with normal first order time delay of 4 days, (C) PV decreases exponentially with 300 ml depleted at end of two days and 200 ml additional loss thereafter, using model with normal time delay. Gain of model adjusted in each case to provide the same total red cell loss at the end of 28 days. Curve C most closely approximates the experimental data shown in Fig. 6-26.

Figure 6-28. Simulation response to a step decrease (300 ml) of plasma volume showing approach toward equilibrium. The entire response is due to a hemoconcentration-erythrosuppression effect. The simulation suggests the self-limiting nature of red cell loss when plasma volume loss stablizes. Equilibrium is realized when rates of red cell production and destruction converge.

cases, in spite of an equivalent decrement in red cell mass. This occurs because the plasma volume continues to decrease throughout the four-week period in case C in accord with the data shown in Fig. 6-6. It is noteworthy that the model's responses became more accurate as more realistic features were added.

Bedrest studies to date have shown that red cell mass decreases linearly, without apparent limit, up to at least 35 days. These simulations have replicated this phenomenon and in the process, have revealed that this is true only as long as plasma volume continues to decline. If the plasma volume stabilizes at a reduced level (Figs. 6-16 and 6-28), the hematocrit will fall with continued red cell loss and the depressant effect on erythropoiesis will be diminished. This process will continue until red cell production converges toward the now slightly, reduced destruction rate. (If the lifespan of red cells are assumed constant, destruction rates in the model are proportional to the total mass of circulating red cell mass). A new equilibrium will be established at which time the red cell mass will be reduced and hematocrit will be slightly above normal. A steady-state error of this type is expected for proportional control systems. This down-regulation of red cell mass represents a normal physiological feedback process. As can be visualized from Fig. 6-28, this process can take a considerable length of time for perfect equilibrium to be established.

6.5.3.2 Recovery Phase of Bedrest. The initial model simulation, driven by experimental hematocrit data, failed to predict the continued decline in red cell mass for the 14 days following the end of bedrest. Instead, the post-bedrest simulation (as shown in Fig. 6-26 and repeated in Fig. 6-29 (panel A)), exhibits a delay in red cell mass recovery for
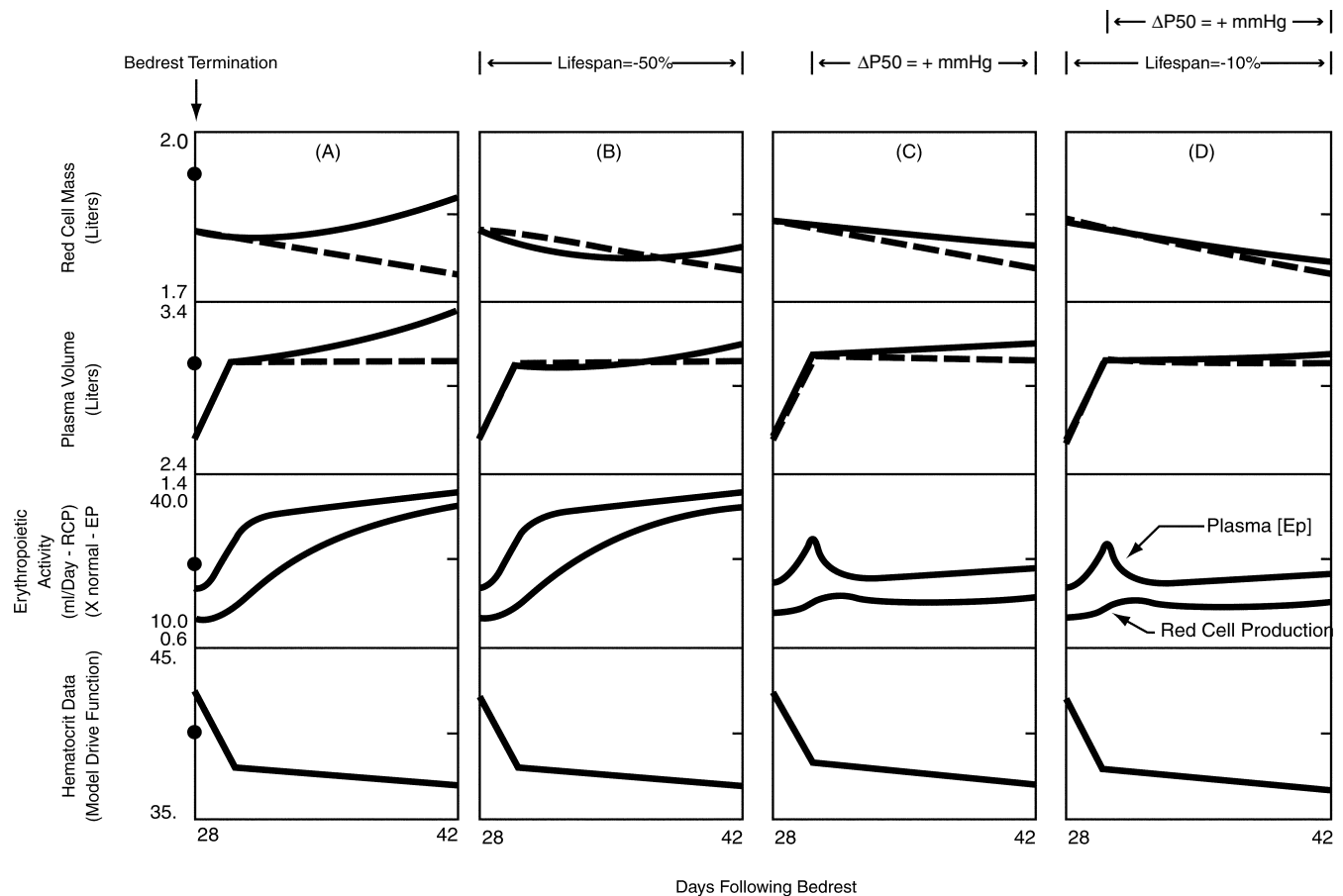
Figure 6-29. Simulation (solid line) of various hypotheses to account for delayed recovery of red cell mass during post-bedrest period. The prebedrest control values are shown by solid circles in panel (A). The supine phase of bedrest which precedes the recovery period is given in Fig. 6-26. The hematocrit data were used to drive the simulation in all cases shown. (A) effect of hematocrit drive alone, (B) effect of hematocrit and 50% reduction in RBC lifespan, (C) effect of hematocrit and P_{50} shift, (D) effect of hematocrit, lifespan reduction and P_{50} shift combined. Dashed lines are experimental data [30].

only several days, a result of the bone marrow delay factor, which is included in the model. The model was used to examine hypotheses that could account for the delayed recovery of red cell mass for the remaining post-bedrest period. Three specific post-bedrest hypotheses were tested:

a) that plasma volume returns toward control levels more slowly than was assumed (not shown),

b) that there was a temporary increase in the rate of red cell destruction (Fig. 6-29, panel B), and

c) that there was a shift in oxygen-hemoglobin affinity in response to the modest hemodilution at recovery (panel C).

These will be discussed next.

The sparsity of data for the period immediately following bedrest brings into question the true rate of recovery of the post-bedrest plasma volume and hematocrit. No measurements of plasma volume or hematocrit were determined until two weeks after the BCM bedrest study. Since red cell production has been shown to be sensitive to hematocrit shifts, it was reasonable to test the hypothesis that plasma values at recovery do not return toward normal as rapidly as had been assumed in the simulation of Fig. 6-29(A). When the assumption that two weeks were required to return plasma volume to normal (instead of the two days previously assumed) was tested, the simulated red cell mass response during the first recovery week was substantially improved (not shown) in comparison to the data; that is, there was a slower replacement of red cell mass. While it is improbable that plasma volume recovery was this slow [20,32], this simulation suggests that a more complete experimental determination of the recovery response is desirable. Further demonstration of the importance of plasma volume and hematocrit on recovery dynamics will be found in the section devoted to space-flight simulations.

The model was used to test the hypothesis that decreased exercise levels during bedrest conserves fragile

red cells which are more vulnerable to destruction during the early ambulatory period. This hypothesis was tested by reducing the mean red cell lifespan in the model during the recovery period in order to represent the more rapid destruction of fragile cells. The results (see Fig. 6-29, panel (B)) indicated that in order to completely account for the recovery response, the mean cell lifespan had to be increased to values that appear to be unrealistically high (i.e., 50% reduction in lifespan throughout a 2-week period).

Although evidence is not available to confirm changes in blood P_{50} during bedrest or spaceflight, it is interesting to speculate what effect such a shift might have had on the time course of red cell mass recovery from these stresses. Based on findings showing decreased oxy-hemoglobin affinity associated with many forms of hypoxic disturbances [85], it was postulated that increases in P_{50} could have occurred during the recovery from bedrest in compensation for the observed hemodilutional anemia. The simulation results suggested that only a very small increase in P_{50} of about 1 mmHg would account for a large part of the decreased red cell mass during the two weeks of recovery (i.e., compare panels (A) and (C) in Fig. 6-29). With the change in P_{50} (panel C) erythropoietin release is suppressed along with red cell production in comparison to the base case (panel A). The transient increase in erythropoietin concentration shown in Fig. 6-29 (C) at the time the P_{50} shift was activated corresponds to a similar event reported during the 28-day bedrest [35]. The profound influence that small changes of P_{50} had on the response was surprising, although suppressed erythropoietin is not an unexpected result [52].

The possibility was considered that more than one mechanism might be simultaneously operative during the recovery phase. For example, reductions in red cell lifespan and increases in P_{50} could have occurred which were small enough to be experimentally undetectable, but which could produce measurable effects on red cell mass over a long enough period. This hypothesis was used in the simulation shown in Fig. 6-29 (D) where the lifespan was decreased 10% in combination with a +1 mmHg shift in P_{50}. This resulted in improved agreement with red cell mass response although red cell production levels failed to rise above control.

A peculiarity noted in at least two bedrest studies [20,30] was a sharp increase in reticulocyte index after bedrest, in the face of a continued decline of red cell mass. Morse [20] speculated that this paradox could be accounted for by a "compensated hemolytic syndrome in which in the rate of production balances the rate of hemolysis." This is in accord with the recovery simulation of Fig. 6-29(B), if one accepts large values of red cell destruction. Ineffective erythropoiesis, a mechanism not included in the model, will also produce reticulocytosis while circulating red cell mass is reduced. However, there is no strong evidence to suggest significant incidences of ineffective erythropoiesis [30], and only sparse data exist supporting hemolytic events [20]. A possibility that remains to be examined is that red cell production during recovery is much lower than the reticulocyte index indicates. Under conditions of strong erythropoietic stimuli, it is known

that reticulocytes appear much earlier than usual and are not a reliable index of red cell production [39]. This effect is not accounted for in the model. Other hypotheses for the delay in recovery of red cell mass include hemorrhage, splenic sequestering, and effects of blood sampling, but as discussed in Chapter 6.4.10, these have tended to be ruled out [15,30].

The results presented thus far support the hypothesis that red cell losses during long-term supine bedrest, red cell infusions, and descent from high altitude are all normal physiological feedback processes in response to the sequence: hemoconcentration → enhanced tissue-oxygenation →suppression of red cell production. This is not to suggest that other mechanisms do not play a contributory role, but merely that the data available do not permit one to distinguish between alternate theories. There have been other hypotheses proposed to account for the suppression of the erythropoietic system during bedrest. These have included: a reduction in oxygen requirements [20,34,134]; age dependent loss of red cells [15]; an increase in plasma phosphates [26]; increased renal blood flow [1,34,95]; changes in gain and thresholds of the kidney-bone marrow controller [3]; and changes in energy balance [66]. Some of these factors will be evaluated in the following simulations of ground-based animal studies and human spaceflight studies.

6.5.4 Simulation of the Dehydrated Mouse

In the previous simulation studies, similar responses were demonstrated for cases involving both an absolute as well as a relative polycythemia. That is, the model was unable to distinguish between a hemoconcentration-induced erythrosuppression caused, on the one hand by an excess of red cells, or on the other hand by a loss of plasma volume. Also, this similarity was not in opposition to the available experimental data. However, recent studies using dehydrated mice as a potential experimental model of spaceflight, have suggested some previously unrecognized differences between absolute and relative polycythemia. Because of the potential importance of these findings to the simulation analysis task, a collaborative effort was initiated between the scientific investigators of the animal experiments and the systems analysis team. The results of this integrative approach provided clues that factors in addition to hemoconcentration may be involved in the spaceflight and bedrest responses.

The experiments which will be discussed have been described in detail elsewhere [6,7,66,68,118] and the results are summarized in Fig. 6-30. Briefly, dehydration in mice by water restriction produces a 22% reduction in plasma volume within the first 24 hours, and a 39% reduction within 72 hours. The proportional elevation in hematocrit was accompanied by suppression of erythrocyte production rates, and by the end of three days, a noticeable reduction in red cell mass. A decrease in red cell production (determined by radio-iron incorporation into newly formed cells) was measured on each of the first three days of dehydration, with suppression becoming progressively more severe with time. This trend was also evidenced by a decrease in cellularity of hemopoietic tissue.

These findings could have been expected in light of the mechanisms previously discussed, involving tissue hyperoxia and suppression of a humoral regulator, erythropoietin. Erythropoietin titers were reduced, as expected on the second and third days of dehydration, but surprisingly, erythropoietin levels were normal on the first day. This apparent temporary dissociation between erythropoietin and red cell production was partially resolved by the finding that the splenic tissue became less sensitive to erythropoietin within 24 hours after dehydration. (In mice, the spleen is an important erythropoietic organ). The reduced sensitivity was attributed to a reduced food intake which is found to be a voluntary response to water restriction. In addition, a small reduction in oxygen consumption was noted by the third day of dehydration, which may have been related to the loss in body weight. It was, therefore, hypothesized that a food restriction induced-negative energy balance can suppress erythropoiesis by direct effects on the hemopoietic tissue and independent of the hemoconcentrating effects of dehydration (see Chapter 6.4.8).

By comparing the responses of dehydrated, food-restricted mice to those of red cell-transfused mice, it was possible to separate the effects of hemoconcentration (which occurs in both groups) from that of food restriction (which occurs only in the former group). This is indicated in Fig. 6-31 where suppression of red cell production is observed for both dehydrated mice and mice transfused to a hematocrit similar to that observed in dehydrated animals. Assuming that the hemoconcentration-related effect is similar for both groups, the differences between the two responses can be taken as a reflection of the energy related (i.e., food restricted) effect. These results suggest that the initial suppression of erythropoiesis in dehydrated mice, e.g., within the first 24 hours, is entirely due to a reduced food intake (because erythropoietin did not change during that period). Thereafter, suppression can be attributed equally to the hemoconcentration and negative energy balance.

These findings, while demonstrating that factors other than hemoconcentration are important, did not reveal the precise pathways that are operative. For example, the failure of erythropoietin to become suppressed for the first day in spite of significant hemoconcentration was not explained. Other studies suggested that hemoconcentration (of ex-hypoxic mice) is capable of suppressing erythropoietin within several hours [129]. In addition, other important factors were not considered in interpreting the results, such as the effect of hypovolemia and hypervolemia during relative and absolute polycythemia, respectively. Blood volume is an indirect modifying influence on oxygen transport as described earlier (see Chapter 6.3.3). Nevertheless, the wealth of data from animal experiments such as these suggested that a more rigorous examination of the data using systems analysis techniques could help resolve these issues.

An understanding of the experimental results is facilitated by a theoretical analysis of the differing effects of hemoconcentration by either increasing the red cell mass, for example, by hypertransfusion, or by reducing the plasma volume, for example, by dehydration (see Fig. 6-32). Both conditions are characterized by hemoconcentration with resulting increases in oxygen delivery, e.g., tissue PO_2, decreased erythropoietin, and suppressed erythropoiesis. The increased viscosity accompanying hemoconcentration provides a resistance to blood flows and leads to a force that opposes, but apparently does not overwhelm the direct hemoconcentration effect. Several important differences also exist between the two hemoconcentration stresses: a) dehydration is hypovolemic while transfusion is hypervolemic; therefore, the effect of blood volume on blood flow (i.e., the oxygen delivery rate) is additive to the viscosity effect during dehydration, but in opposition during transfusion; b) dehydration in mice results in a decreased oxygen demand which could have a significant effect if manifested at the renal oxygen sensing site; c) dehydration in mice also has been found to be accompanied by reduced *ad libitum* dietary intake, and this may be responsible for the reduced responsiveness and a decreased time delay in cell maturation observed in hemopoietic tissue. The pathways by which diet, and especially a negative energy balance, might affect erythrocyte production was previously discussed in detail (see Chapter 6.4.8 and Fig. 6-19). The crucial fact here is that diet restriction can suppress erythrocytes directly, without altering erythropoietin. The individual effects of these pathways have been studied by model simulation techniques and those analyses suggest that red cell mass would be expected to decrease more rapidly and to a larger extent with dehydration (accompanied by food restriction), than with transfusion.

Simulations of the three-day dehydration experiments were performed in a version of the erythropoietic control model that was specifically adapted to the mouse. This version of the model is described in Chapter 3 and Appendix B. The elements of the original human model which were modified to formulate a mouse model included parameters that were based on size (i.e., blood volume, plasma volume, red cell mass) and total oxygen uptake, and parameters that were based on values which are known to be species-specific, irrespective of size, e.g., red cell lifespan and the oxygen-hemoglobin equilibrium curve. In addition, validation studies were required to ascertain if the model could realistically respond to short-term stress conditions as it does to longer-term disturbances. One such validation study is shown in Fig. 6-33, in which erythrocyte production responses to single and multiple injections of erythropoietin are illustrated. These results compare favorably to the dynamic behavior of reticulocytosis following erythropoietin injections, as measured some years ago in the mouse [121]. These and other short-term validation studies [68,118] provided the basis for utilizing the model for simulating dehydration and infusion experiments.

Two simulations based on the analysis of Fig. 6-32 are shown in Fig. 6-34. Identical increases in hematocrit were accomplished by either step increases in red cell mass simulating transfusion or by more gradual reductions in plasma volume similar to the dehydration maneuver. The transfusion response, which agrees with animal (Fig. 6-31) and
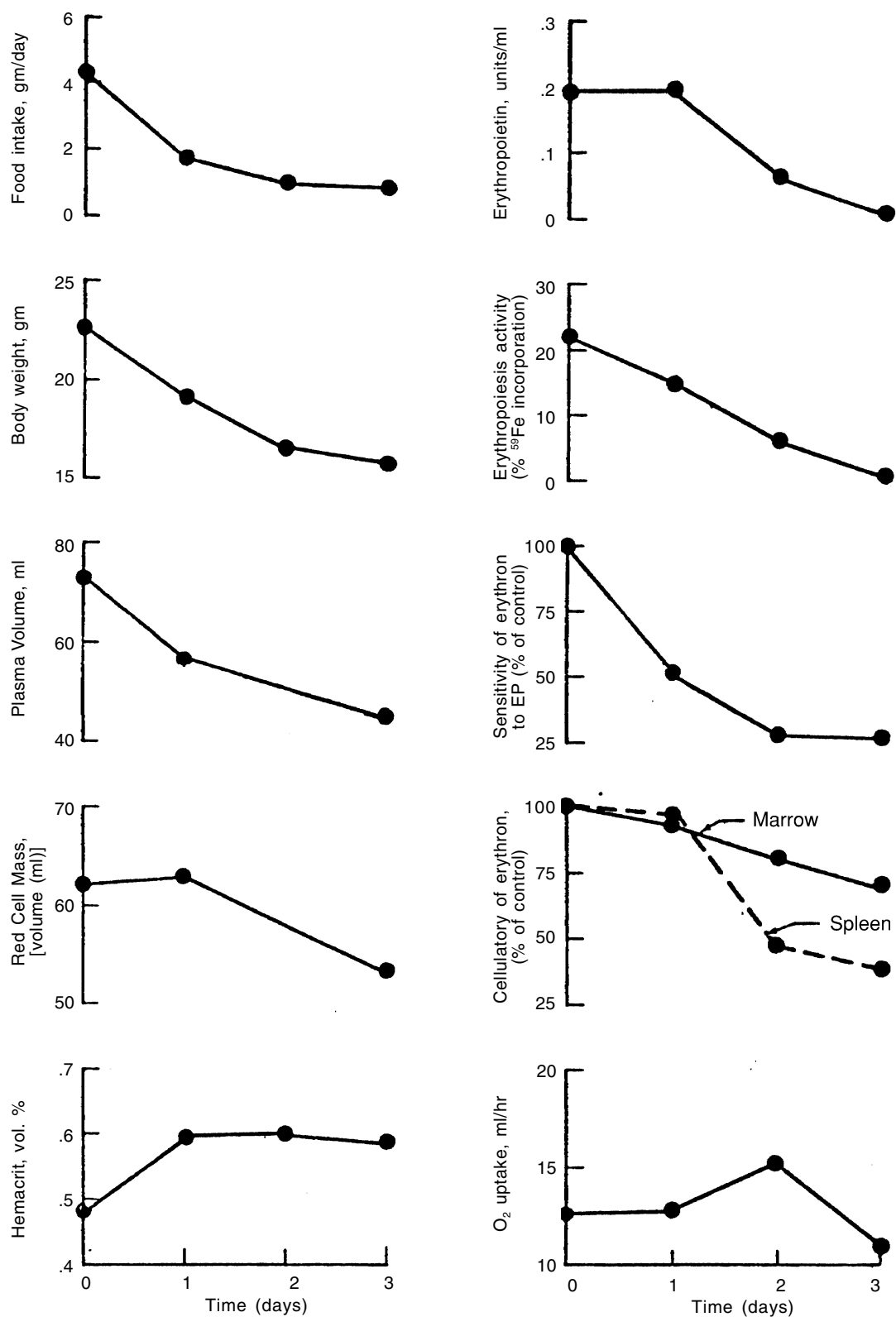
Figure 6-30. Dehydration response in mice restricted from water for 3 days. Loss of body water is reflected in reduced body weight, plasma volume and increased hematocrit. The voluntary food restriction that always accompanies water restriction in mice results in further weight loss and presumably influences changes in splenic sensitivity to erythropoietin, cellularity of the erythron, and oxygen uptake. A reduction in erythropoietin, erythropoiesis, and red cell mass are the secondary hematological responses to food and water restriction as suggested by the hypothesis chart of Fig. 6-19. (Data obtained from Dunn and coworkers [66,68,118]).
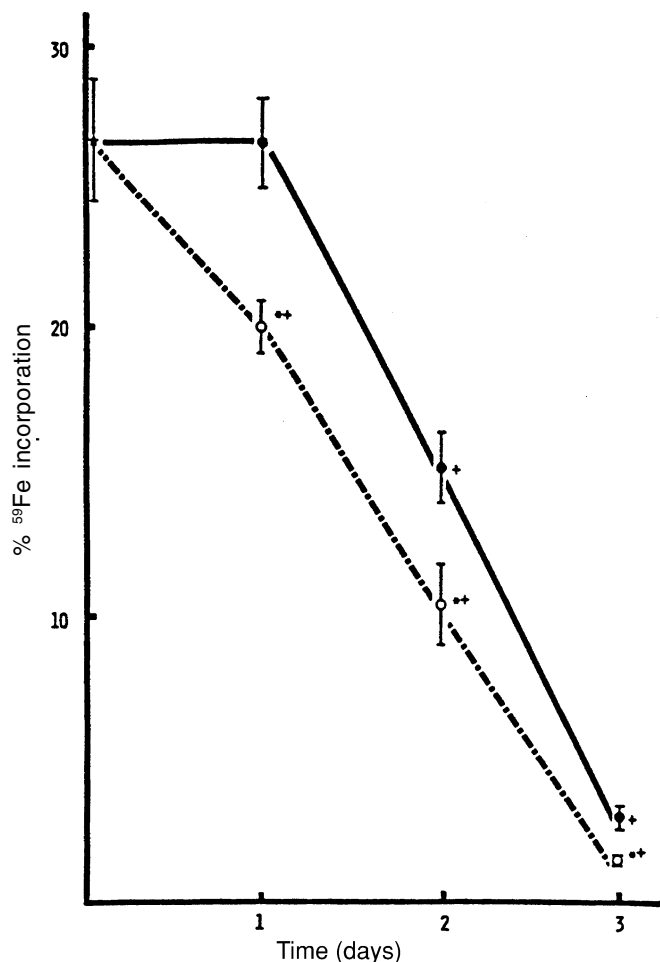
Figure 6-31. Rates of erythropoiesis as measured by radio-iron incorporation in newly formed cells. Dehydrated mice are shown by open circles and dashed line and transfused mice are shown by filled circles and solid line. Vertical bars indicated ±SEM. (* = P < 0.05 from controls; + = P < 0.05 of dehydrated mice compared to transfused animals). Since the transfused mice ate and drank normally and the dehydrated mice were also food restricted, it is assumed that the difference between the two curves reflect the erythroid suppression of the energy related component.

first day which, by an assumed renal autoregulatory effect, returns to normal thereafter), reduction in maturation time to 25% of that used in the transfusion case, and a decreased responsiveness of hemopoietic tissue as dictated by experimental results (Fig. 6-30).

With the addition of these hypotheses, the model demonstrated the capability of simulating different responses for dehydration and transfusions and the model responses compare favorably with those found experimentally. Physiologically, the two most important aspects of this simulation are a delay in erythropoietin suppression during dehydration, but not after transfusion, and a delay in suppression of red cell production after transfusion, but not during dehydration. Thus, the dissociation between erythropoietin and red cell production during dehydration, explained by direct action of diet restriction on hemopoietic tissue which bypasses the erythropoietin pathway, coupled with a transient decrease in blood flow, was successfully reproduced in the simulation (see Fig. 6-34).

Simulations that are more detailed were also performed of the dehydration experiments. Figure 6-35 shows the response both for the mouse and for the mathematical model for 3 days of dehydration and 7 subsequent days of rehydration. The suppression of erythropoietin and red cell production is similar to that shown in Fig. 6-34. During dehydration, the following parameters were adjusted in a direction in accord with the hypotheses presented in Fig. 6-32 and, where possible, in a magnitude dictated by the experimental results: a) a decrease in plasma volume as shown; b) a transient decrease in blood flow (-10%) for the first 24 hours; c) a gradual decrease in responsiveness of hemopoietic tissue to erythropoietin to 20% of control; d) a gradual decrease in oxygen uptake to 80% of control; and e) a reduction of the time (i.e., maturation time) required for erythrocyte production to respond to influencing factors. During rehydration, these parameters were returned to normal and only the plasma volume influence was used to drive the simulation. These choices of parameter adjustments were established by a trial-and-error procedure, continually testing the model response against the experimental data.

Once a reasonable simulation is achieved, as demonstrated in Fig. 6-35, it is then possible and instructive to determine the relative influence of each major factor on the final response. This is accomplished easily with a model by first performing the optimal simulation with all the required hypotheses and then selectively removing one or more of the effects (i.e., setting the model parameter at its control value) and performing the simulation again. In this particular case, it is convenient to think of the dehydration response as being under the influence of both a negative water balance effect and a negative energy balance effect. Of the five hypotheses described in the paragraph above, the first two (plasma volume and blood flow effects) are related to water balance and the remaining hypotheses (hemopoietic responsiveness, oxygen uptake, and transit time) are related to energy balance effects. Two simulations were performed, as shown in Fig. 6-36, to examine the separate influences of these water

human studies (Fig. 6-25) was produced by using only the influence of hemoconcentration. If hematocrit changes alone were the only factors considered in the dehydration case, its responses would be extremely similar to the transfusion responses because the model responds to the magnitudes of the hematocrit disturbances, regardless of their causes. However, the analysis discussed above demonstrates important differences in the erythropoietin and red blood cell production responses for these two cases. In order to achieve closer agreement with the animal data and produce the results shown here, it was necessary to include the additional factors addressed in Fig. 6-32 in simulating the dehydration case. These factors included alterations in blood flow (a decrease of 10% during the

Hypervolemic Polycythemia (Transfusion)

⇑RCM —— ⇑HCT ———————— ⇑PO₂ —— ⇓⇓ EP ⇒ ⊖
⇑ Viscosity —— ⇓⇓BF —— ⇓PO₂ —— ⇑ EP ⇒ ⊕ → Red Cell Production
⇑⇑BV ———— ⇑BF —— ⇑⇑PO₂ —— ⇓ EP ⇒ ⊖

Hypovolemic Polycythemia (Dehydration)

⇓⇓PV ———— ⇑ HCT ———————— ⇑⇑PO₂ —— ⇓ EP ⇒ ⊖
⇑ Viscosity — ⇓⇓BF —— ⇓PO₂ —— ⇑ EP ⇒ ⊕ → Red Cell Production
⇓⇓ BV
⇓ O₂ Demand ———————— ⇑PO₂ —— ⇓ EP ⇒ ⊖ ⊖
⇓ Caloric Intake ———————— ⇓ Erythron Sensitivity Threshold & Time Delay

Figure 6-32. Hypotheses that explain differences between transfusion and dehydration polycythemia. (PV=plasma volume, RCM=red cell mass, HCT=hematocrit, BV=blood volume, BF=blood flow, PO₂=renal tissue oxygen tension, EP=plasma erythropoietin concentration).

balance and energy balance factors on the red cell mass, red cell production rate, and erythropoietin levels.

It is clear that the effect of the hypotheses related to a negative energy balance has a more profound influence on erythro-suppression than the hypotheses related to a negative water balance. However, it should be noted that the suppression of erythrocyte production during the water balance simulation, while less acute, is quite similar in magnitude to that predicted for bedrest (see Fig. 6-26). And while in the case of bedrest, a negative water balance is a sufficient stimulus to decrease the red cell mass significantly given sufficient time, the three-day dehydration experiment is far too short to produce a noticeable effect on red cell mass in this simulation. Most of the decrease in red cell mass during short-term dehydration is, therefore, attributed to the dramatic inhibition of red cell production as induced by energy balance factors. Also of interest is the fact that erythropoietin levels for the two cases considered are similar, when compared to their quite dissimilar effects on red cell production and red cell mass. The entire erythropoietin effect in the energy balance simulation is due to the reduction in oxygen uptake.

The computer simulations were particularly valuable in revealing unusual trends in the data and suggesting clarifying experiments. A summary of the major problem areas that were resolved with the assistance of the model are listed in Table 6-12. The first column represents the trends in the data that were not easily explained by the original computer analysis or by intuition. One or more hypotheses that could resolve the descrepancy, as suggested by the simulation approach, are shown in the second column. The last column indicates the results of

second generation experiments which were performed to test the hypotheses in the laboratory. The model behavior suggested that all of the hypotheses listed in Table 6-12 were theoretically credible, but, as shown, the experimental evaluation proved that some of them were "ruled out" because they were not biologically plausible. The interaction between modeling and animal testing demonstrated that the hemoconcentration effect (i.e., plasma volume changes) and negative energy balance effects (i.e., reductions in tissue sensitivity to erythropoietin and metabolic rate) were the most influential in accounting for the experimental findings, e.g., Items 1,2 and 6 in Table 6-12. However, in order to bring all of the simulated variables into agreement with the experimental findings, several additional factors need to be considered, which eventually produced the simulations presented in Fig. 6-35. These factors, shown in Table 6-12 (Items 3,4 and 5), are discussed in the next three paragraphs.

The red cell mass decreased more rapidly *in vivo* than was predicted by the computer model. The animal data could be simulated by assuming a 50% increase in the rate of red cell hemolysis during dehydration. Estimation of serum bilirubin levels failed to support this concept. Survival of ^{51}Cr-labelled red cells also failed to support the concept of increased hemolysis during dehydration. However, these measurements demonstrated that the normal red cell lifespan in the particular strain of mice used to study dehydration was about half the value used initially in the computer model (which was based on accepted literature data [135]). Adjustment of the computer parameter for red cell destruction to 5.3% per day (corresponding to a life span of 20 days rather than the original value of 40
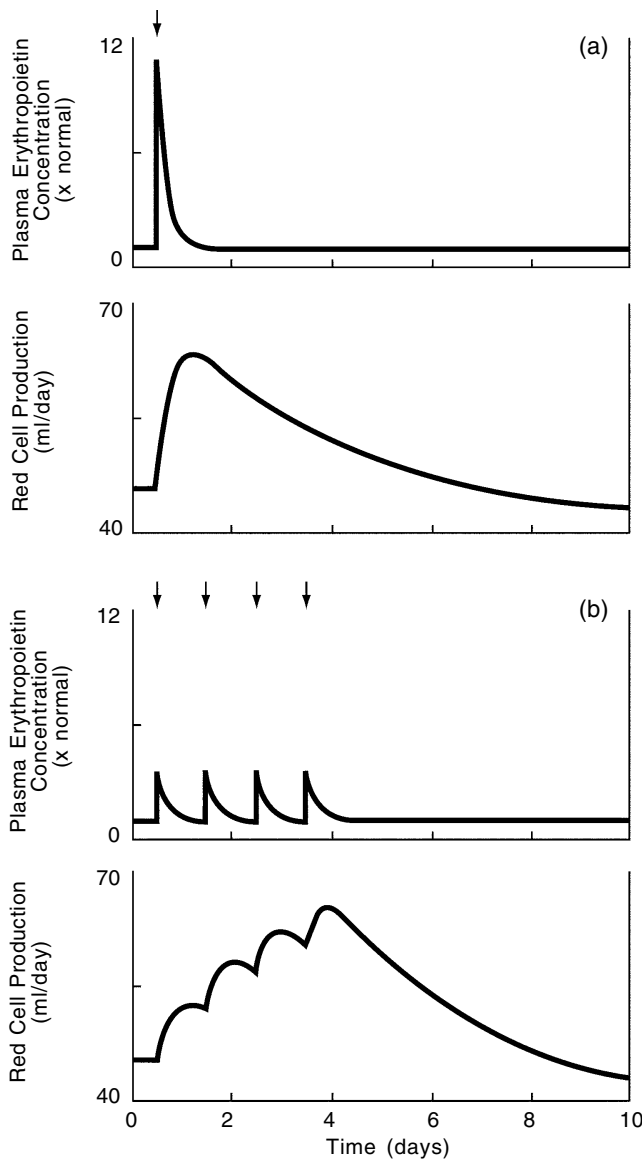
Figure 6-33. Simulated responses of mouse model to erythropoietin injections: (a) bone marrow response to single dose of erythropoietin. (b) bone marrow resonse to multiple doses of erythropoietin. Arrows indicate time of injections.

Figure 6-34. Simulated responses to red cell transfusion (solid line) and dehydration (dashed line) using the mouse model. For the case of dehydration, the plasma volume was reduced over a period of one day while in the case of transfusion, red cells were infused instantaneously, resulting in a similar degree of hemoconcentration for both cases. In addition, the following parameter adjustments were made during the dehydration simulation only to reflect energy balance effects: red cell maturation time reduced from 2 days to 0.5 days; controller operating point, P1, reduced from 1.0 to 0.2; blood flow reduced to 90% of control for the first day and then returned to normal. Controller gain was set at G = 18 for both simulations.

days) resulted in a good simulation of the experimentally determined changes in red cell mass not only during dehydration but also during rehydration.

Even when appropriate changes in metabolic rate and tissue sensitivity to erythropoietin were incorporated into the computer simulation, the rate of red cell production did not fall as rapidly as was determined experimentally. Therefore, the computer simulation shown was obtained by reducing the transit time for red cell precursors through hematopoietic tissue to one day from its nominal value of 3 to 5 days [121,136]. Experimental justification for this maneuver is based on the following evidence: spleen and, particularly bone marrow cellularities show marked de-

creases within 24 hours of commencing dehydration (see Fig. 6-30), and proliferation of normal marrow stem cells *in vitro* is more rapid for the strains of mice used in these experiments than in other strains, suggesting a normally shorter transit delay in red cell production (C.D.R. Dunn, unpublished observation).

In the computer simulations, an increase in hematocrit, whether induced by red cell transfusion or a reduction in plasma volume, resulted in an immediate decrease in serum titers of erythropoietin (i.e.. see Figs. 6-25 and 6-26). In contrast, in the dehydrated animal studies, erythropoietin remained normal for at least the first 24 hours of dehydration. Four factors were considered to bring the computer simulations into agreement with the experimental findings:

a) a change in the sensitivity of the erythropoietin producing system; if the hormone producing system became less sensitive to increases in tissue oxygen then, theoretically, this might be expected to maintain erythropoietin titers near normal;

b) a change in erythropoietin half-life ($t_{1/2}$); if erythropoietin $t_{1/2}$ is related to marrow erythroid activity [137]
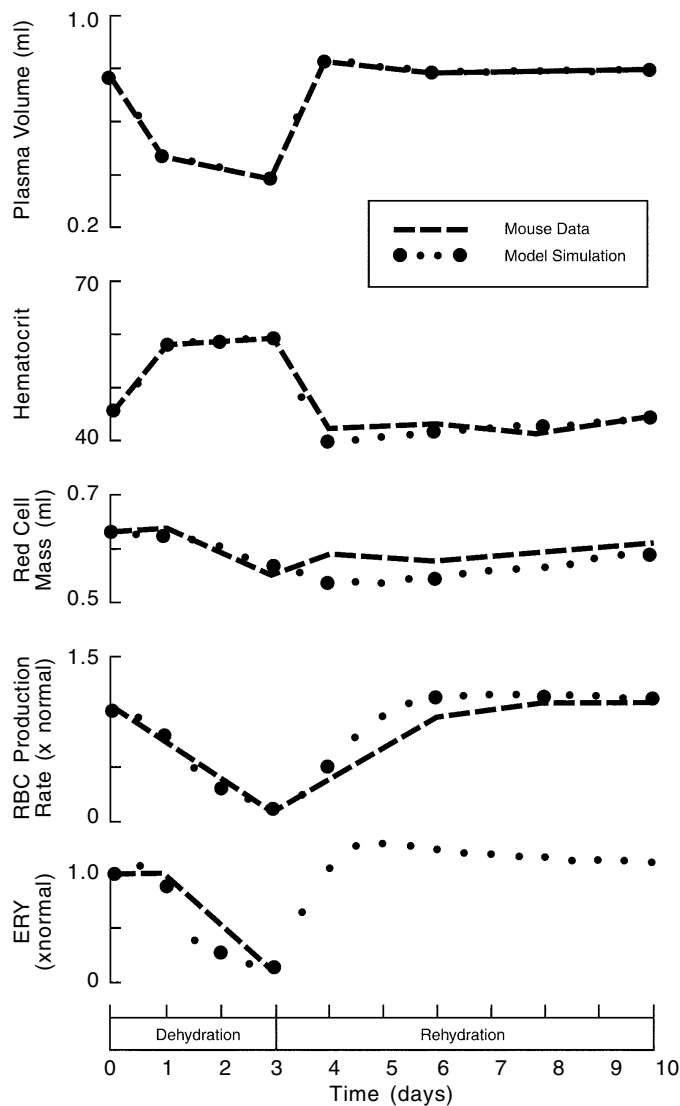
Figure 6-35. Simulation and experimental murine hematological responses to 3 days of dehydration and 7 subsequent days of rehydration. The mouse data was taken from a composite of several different experiments reported by Dunn and co-workers [7,66,68,118].

Figure 6-36. Simulated responses of mouse model showing the separate effects of water balance factors (solid line) and energy balance factors (dashed line) in producing the combined response illustrated in the previous figure. Water balance factors consist of reductions in plasma volume and blood flow. Energy balance factors include decreases in oxygen demand, marrow responsiveness, and cell maturation time. See text for description of parameter adjustments during each simulation.

then suppressed erythropoiesis might be expected to extend $t_{1/2}$ which, in turn, would act to maintain serum erythropoietin titers near normal;

c) a shift in blood P_{50}; a decrease in P_{50} would diminish oxy-hemoglobin affinity and the degree of oxygen unloading at the tissue level, thus tending to increase erythropoietin levels;

d) a change in renal blood flow; theoretically, the reduced plasma volume would be expected to increase blood viscosity and passively blood vessels to shrink in diameter. Both of these effects would reduce blood flow and oxygen transport.

The first three assumptions were examined experimentally [7] and found not to change. However, other investigators have shown a reduction in the sensitivity of erythropoietin release to hypoxia following dehydration [115]. As far as blood flow is concerned, it was assumed that a reduction in renal blood flow could occur only during the first day in the light of the excellent flow autoregulatory capability of the kidney. This remains a hypothetical but perhaps logical explanation for the maintenance of normal erythropoietin titers, despite an increased hematocrit. It was not possible, at the time, to experimentally test this hypothesis.

These studies illustrate the potential usefulness of the interaction of experimental and computer studies in the systematic analysis of alterations in the control systems of specific biological processes. Thus, the red cell lifespan, oxygen uptake, sensitivity of the erythropoietin producing system, erythropoietin half-life, and blood P_{50} would probably not have been measured if experimental and computer studies had originally been in agreement. Also, certain concepts such as the effects of total blood volume and blood flow on tissue oxygenation, and of red cell marrow transit times on erythropoietic dynamics would probably not have been considered to explain the data obtained in the dehydrated mouse if computer simulations had not been undertaken.

Table 6-12. Dehydrated Mouse Study: Hypotheses Formulated and Tested To Explain Discrepancy Between Experimental and Simulation Responses

Problem	Hypothesis Revealed by Simulation	Experimental Evaluation
1. Explain reduction in red cell production during dehydration	Erythropoietin suppression induced by tissue hyperoxia secondary to hemoconcentration.	Hemoconcentration confirmed; tissue oxygenation not measured; EP not suppressed on first day.
2. Explain reduction of erythrocyte production despite normal EP titers on first day of dehydration.	Reduction in sensitivity of hemopoietic tissue to EP	Confirmed for spleen, but not for bone marrow
3. Explain normal EP titers on first day despite hemoconcentration and reduced erythrocyte production rates.	a) Reduced sensitivity of renal tissue to tissue oxygenation. b) Increased EP half-life c) Increased oxy-hermoglobin affinity d) Reduced blood flow	a) Ruled out b) Ruled out c) Ruled out d) Not measured; cannot be ruled out
4. Explain larger decrement in red cell mass during dehydration than is predicted by model.	Reduction in red cell lifespan	Hemolysis ruled out, but normal life span found to be shorter than originally believed.
5. Explain rapid fall in erythrocyte production on first day of dehydration despite maturation time delay	Reduced response time of hemopoietic tissue to EP, i.e., shorter time delay,	Confirmed for splenic tissue
6. Explain more rapid and extreme fall in EP titers after first day of dehydration than is predicted by model on basis of hemoconcentration.	Delayed reduction in oxygen uptake	Confirmed

In summary, these animal and computer studies have shown that hemoconcentration is a major factor in producing erythro-suppression in both absolute and relative erythrocytosis. However, when hemoconcentration is caused by water-restriction, an additional factor is present that reduces the responsiveness of hemopoietic tissue to erythropoietin. The negative energy balance that accompanies dehydration in mice was implicated as a causative agent in this mechanism. The hypovolemia of dehydration may have contributed to a transient decrease in blood flow, which together with the reduced insensitivity of hemopoietic tissue accounts for a temporary dissociation between erythropoietic activity and its hormone regulator. Extrapolating to the spaceflight situation, it is suggested that the negative energy balance may contribute to the loss in red cell mass to a degree that had heretofore not been appreciated. Food intakes that are lower than necessary to maintain energy balance and body mass have often been observed in astronauts (see Chapter 4.6).

From the point of view that dehydrated mice and space travelers have both been observed to experience a negative water and negative energy balance which leads to hemoconcentration and reduction in erythropoietic activity, the dehydrated mouse may be considered to be a suitable ground-based analog of the hematological response to weightlessness. However, there are several important differences between the humans exposed to zero-g and their dehydrated animal counterparts:

a) hemoconcentration of astronauts may not necessarily occur by fluid restriction, but rather by excess renal excretion secondary to headward fluid shifts;
b) the reduced body fluid volume of space travelers is believed to be appropriate for health in zero-g while dehydrated mice cannot be maintained for more than several days because of water and nutritional deficiency;
c) the body fluid composition of astronauts are more likely to be normal compared to dehydrated mice; and
d) food restriction in human space travelers have typically been observed in conjunction with space sickness, which is not always present, while food restriction in mice always accompanies fluid restriction.

Therefore, these animals can, at best, represent the human condition in zero-g for only a brief period of time and only when both food and water restriction is evident.

6.5.5 Spaceflight Simulations

Many factors have been discussed which could have contributed to the anemia of spaceflight. The available inflight data, as sparse as it is, together with the analysis of human and groundbased studies, does permit speculation to center on several probable pathways. It seems plausible to suggest that the enhanced oxygen carrying capability of hemoconcentrated blood and the decreased energy balance of a restricted diet may have limited the production of erythrocytes. Other factors which cannot

presently be ruled out, but which are believed to be capable of exerting a secondary influence, include the possibility of some red cell destruction, the influence of a slightly hyperoxic environment, shifts in oxygen-hemoglobin affinity, changes in total blood volume, blood flow alterations, and the varying levels of exercise performed by the space crews.

The problem which remains is to relate these factors not only to the absolute fall in red cell mass, but to the varying degrees to which red cells disappeared in the different Skylab missions as well as to the non-uniform kinetics of postflight recovery. Within limits, the techniques of computer simulation have proved valuable in integrating the available data with current concepts of erythropoietic regulation and choosing between alternative zero-g hypotheses. Simulation studies will be presented in this section in three broad areas: suppression of red cell mass during spaceflight; postflight recovery of red cell mass; and comparison between bedrest and spaceflight erythrokinetics.

6.5.5.1 Suppression of Red Cell Mass During Spaceflight.
The kinetics of red cell mass disappearance during flight is unknown because of the lack of measurements. Two theories have been advanced to explain inflight erythrodynamics and to account for the different net red cell mass losses observed on the three flights (see Chapter 6.4.11). Evaluation of these two divergent concepts, termed the "regeneration theory" and the "continuous loss theory" will be described below.

6.5.5.1.1 *Evaluation of Regeneration Theory.*
The regeneration theory hypothesizes that red cell mass decrements occur within the first month of flight and that repletion of cells begins shortly thereafter whether or not the human subjects return from space. In the previous discussion of this theory, it was argued that while regeneration is theoretically a possibility, the supporting data are weak and inconclusive. In particular, the suggestion by Kimzey [15,25] that a temporary hemodilution (observed during a single inflight day) could trigger the regeneration of red cells over the next month was deemed unlikely. The improbability of this event received support, inadvertently, from a bedrest study in which a large amount of ingested saline was tested as a countermeasure for orthostatic intolerance (see Fig. 6-6). The resulting temporary hemodilution did not appear to alter the course of red cell disappearance. This conclusion was supported by computer simulation studies, although a small effect on erythrokinetics of the bone marrow was demonstrated (see Fig. 6-26).

There are factors other than inflight hemodilution which can be conceived to be responsible for regeneration of red cell mass. Simulation analysis has suggested several guidelines which can be used in formulating hypotheses, for example:

a) regeneration is only possible if production rates of red cells increase above destruction rates;
b) a biphasic regeneration response (see Fig. 6-7) is not

likely to occur when two competing stimuli, one erythro-suppressive and the other erythro-active, are initiated simultaneously, and are maintained for the same length of time; and
c) a biphasic red cell mass recovery curve becomes more credible by assuming that an early erythro-suppressive influence is followed by an erythro-active stimuli.

It can be assumed that one suppressive influence on red cell production is that of hemoconcentration, which appears to persist at progressively diminished levels throughout three months of spaceflight (Fig. 6-23). However, experimental and simulation studies have shown that a chronically maintained relative polycythemic condition will not, by itself, allow production rates to rise to levels which promote red cell mass regeneration (see Fig. 6-26 and 6-28). Therefore, it is likely that additional factors or events must be postulated to account for regeneration. Two scenarios have been postulated. First, a stressor acting early in flight reduces the red cell mass within the first few days or weeks and thereafter its influence is greatly diminished or entirely disappears, thereby permitting normal or enhanced erythropoiesis. Examples of such a stressor which would be compatible with spaceflight data may include hemolytic destruction of cells early in flight or restricted dietary intake early in flight. Secondly, some stimuli not previously present could increase production rates late in flight. Such an effect could be induced by some as yet unknown adaptive influence of zero-g on oxygen transport (i.e., shifts in oxy-hemoglobin affinity) renal blood flow, or the bone marrow. However, there is currently no evidence of any kind for such a late acting mechanism during spaceflight or bedrest, and this possibility will not be considered further.

With regard to the first scenario of an early acting stressor, two hypotheses were examined by simulating the 59-day Skylab mission. In the study illustrated in Fig. 6-37, it was assumed that the renal-bone marrow controller exhibited a reduction in responsiveness (i.e., change in sensitivity and threshold) during the first month in space. The suppression was removed during the second month and a small enhancement in responsiveness was assumed thereafter. A concomitant reduction in plasma volume was imposed for the first two months before returning to normal as suggested by hematocrit changes and bedrest studies. The rationale behind the change in controller sensitivity was not well formulated at the time this simulation was first performed [3]. Subsequently, the work with dehydrated mice (see Chapter 6.5.4) suggested that such a parameter alteration is a somewhat plausible representation of the influence of the negative energy balance observed in the 59-day Skylab mission [101] (also see Chapter 4.6). In that flight, the severe symptoms of space motion sickness impaired normal dietary intake for the first mission week. Thus, an early reduction in red cell mass could have occurred on two accounts: hemoconcentration, and reduced dietary intake. Later in flight, the dietary intake increases toward normal while the hemoconcentration effect diminishes somewhat, as red cell mass
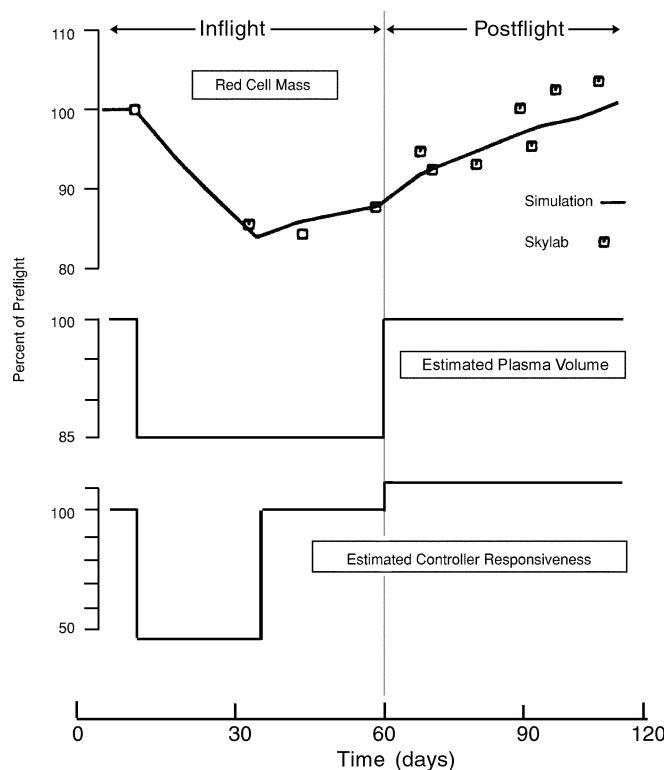
Figure 6-37. Simulation of the 59-day Skylab mission illustrating the hypothetical conditions under which regeneration of red cell mass may take place. Plasma volume was assumed to decrease during the entire inflight phase and controller responsiveness was assumed to decrease only during the first month. This resulted in the decline of red cell mass. Regeneration took place following postflight hemodilution (return of plasma volume to normal) and a postulated increase in controller responsiveness. The experimental red cell mass is a composite of postflight measurements obtained from the nine Skylab crewmen [3,124].

Figure 6-38. Simulation analysis comparing loss of red cell mass by either hemolysis of 10% of the circulating red cells during the first 3 days (solid line) or plasma volume reduction of 500 ml maintained throughout the period studied (dashed line). Acute hemolysis produces a biphasic regneration response but the hematocrit and red cell production are opposite to the responses expected for hemoconcentration alone. The effect of both stresses, hemolysis plus hemoconcentration, acting together are shown in the next figure.

is lost. This might favor increases in bone marrow production and a partial restoration of red cell mass.

While this simulation of the 59-day mission agrees with the regeneration curve composed of data from all 3 flight crews, corresponding simulations of the 28-day and 84-day missions did not show similar agreement for two reasons. First, dietary restriction was not severe on the shortest flight and almost non-existent on the longest flight, so that the controller parameters would not be expected to change to the same extent as shown in Fig. 6-37. Secondly, plasma volume levels should return one month sooner than shown for the 28-day flight and one month later than shown for the 84-day flight. When these changes were instituted, the inflight red cell mass response curve departed widely from the regeneration curve based on postflight crew data.

A second hypothesis to explain regeneration was examined in which it was assumed that a loss of red cells took place during the first several days of the mission. Such a loss could be explained by intravascular hemolysis or splenic sequestration and destruction of cells.

Johnson [26] speculated that if this loss occurred selectively in older cells, it would not necessarily be detected by lifespan measurements (see Chapter 6.4.10). Figure 6-38 illustrates the simulated responses for two cases:

a) a short period of hemolysis (10% of cells destroyed in 3 days), and

b) hemoconcentration produced by a sustained reduction in plasma volume leading to erythrosuppression.

The latter case is similar to previous illustrations of hemoconcentration (see Fig. 6-28). Hemolysis (solid line) results in a biphasic regeneration response of red cell mass, but since hematocrit and erythrocyte production rate responses are opposite to expected or measured values, it is not likely that hemolysis by itself can account for either the entire spaceflight loss of red cell mass or its regeneration. Hemoconcentration alone (dashed line) does account for loss in red cell mass, but as suggested earlier, a regeneration response is not possible by this mechanism.

The simultaneous occurrence of hemoconcentration and hemolysis is illustrated in Fig. 6-39. Two responses are shown, the solid line representing the case where hemolysis destroys 10% of the cells, and the dashed line representing 20% of cell destruction. A plasma volume reduction of 500 ml was imposed on both simulations. If

cell destruction is large (dashed line), a biphasic regeneration curve of red cell mass is apparent, as in the case of hemolysis by itself. However, the accompanying hematocrit response is triphasic, quite unlike the observed inflight data. On the other hand, for smaller degrees of hemolysis that are not large enough to reduce hematocrit to below control levels (solid line), hemoconcentration is evident throughout the response period and production rates are below control as expected. On the other hand, the red cell mass no longer exhibits regeneration characteristics. In fact, the simulation predicts that the long-term reduction in red cell mass is the same whether or not hemolysis occurs; it is only the short-term response which results in enhanced red cell mass loss due to the addition of hemolysis.

It becomes apparent that alterations in hemoglobin levels consistent with those observed during Skylab could not by themselves generate computer simulation responses comparable to the observed changes in red cell mass, if one accepts a composite (multi-mission) view of the postflight data. These analyses suggest that some degree of regeneration of red cell mass may have occurred in isolated instances such as during the 59-day mission when severe space motion sickness resulted in large temporary decrements in food intake. But it is difficult to demonstrate, on the basis of plausible hypotheses, that regeneration is a universal phenomenon of space travelers as originally suggested [25]. The simulation and experimental studies have tended to rule out inflight hemodilution, negative energy balance, or hemolysis as causative factors in the regeneration phenomenon. However, it has been impossible to rule out a modest early inflight hemolysis event as a contributory factor to red cell mass loss (without regeneration) during spaceflight.UPDATE #3

6.5.5.1.2 *Evaluation of Continuous Loss Theory.* The continuous loss theory specifies that red cell mass depletes gradually as a function of time in weightlessness, similar to the behavior seen in bedrest. Furthermore, the differences in red cell mass loss among the Skylab crewmembers who remained in space for varying time periods is assumed not to result from any adaptive or regenerative process. Rather, it is proposed that factors that influence erythropoietic activity are present in different degrees in the three missions. The net result of these factors is presumed to be a suppression of erythropoiesis that is greatest during the shortest Skylab flight and least during the longest flight.

The most promising candidates which have been identified as erythrosuppressive factors and which were known to be present during spaceflight are those related to hemoconcentration and negative energy balance. Energy balance is determined by diet and physical activity, and it appears that both of these were adequate on the longest flight and grossly inadequate on the shortest flight [116; see Chapter 4.6]. It is known that dietary restriction suppresses erythrocyte production, and it will be assumed that a reduced amount of activity has the same effect (see Chapters 6.4.7 and 6.4.8). These three factors, hemoconcentration, diet, and activity, and an estimate of their varying
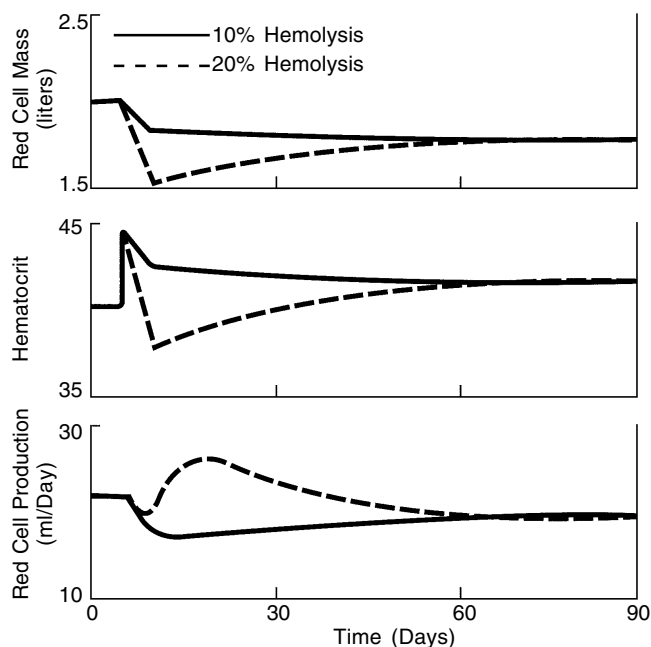
Figure 6-39. Simulated analysis of hemolysis as a possible causative factor of regeneration. In both cases shown, the plasma volume was reduced stepwise by 500 ml and this was combined with an acute 3-day hemolysis simulated by transiently reducing the red cell lifespan. Qualitatively different responses are seen when either 10% (solid line) or 20% (dashed line) of the circulating red cell mass is destroyed by hemolysis. Note that after hemolysis, the loss of red cells continues in the case of 10% loss, due to hemocentration effects.

presence on the Skylab missions are given in Table 6-13. Two other factors are also listed, hemolysis and hyperoxic blood, which could have been present on the 28-day mission to a modest extent (see Table 6-3 and Table 6-9). The analysis of Table 6-13 provides a rational basis for qualitatively predicting that the greatest red cell mass loss occurred on the shortest mission and the smallest loss occurred on the longest mission. These factors were subjected to further quantitative examination using simulation and statistical analysis.

Evaluation of the continuous loss theory was accomplished in two stages. First, the influence of hemoconcentration (negative water balance) on red cell mass was ascertained by computer simulation. Secondly, the differences in energy balance factors were described and tested.

The hematological responses of the Skylab crew that resulted only from the influence of hematocrit alterations were estimated by computer simulation. Figures 6-40 and 6-41 illustrate the computer-generated responses for the 59-day and 84-day missions, respectively, using only the mean inflight plasma hemoglobin concentration data to drive the model. (The 28-day mission was not simulated because no inflight hemoglobin data were obtained on that flight). This procedure is identical to that used in the bedrest analysis (Fig. 6-26). The postflight values of plasma volume and red cell mass (no inflight measure-

Table 6-13. Relative Importance of Factors Proposed To Be Responsible For Reduced Red Cell Mass On Skylab*

Factor	28-Day Mission	59-Day Mission	84-Day Mission
Hemoconcentration**	1	1	1
Reduced Dietary Intake	2	1	0
Reduced Physical Activity	2	1	0
Hemolysis	1	0	0
Increased Arterial pO_2	1	0	0
Relative Erythrosuppression Effect on Red Cell Mass	3	2	1

* The numbers indicate the estimated effect of reducing RCM due to each factor based on its relative intensity on the three flights. Factors are ranked horizontally only. A higher number indicates a greater erythrosuppressive effect for that factor relative to the other missions. "0" indicates no presumed effect.

** Inflight hemoglobin concentration was not measured on the 28-day mission, but it is assumed that hemoconcentration was similar to the other flights.

ments were determined for these quantities) are indicated by solid circles. The gain factor, G, was adjusted (and held constant throughout the simulation) so that the simulated total inflight red cell mass loss agreed with the measured value obtained on recovery day. No further gain adjustments were made to simulate the postflight period. Agreement between model and data during the postflight period for red cell mass and plasma volume is considered good.

These simulations represent the first systematic attempt to predict, on a continuous basis, inflight red cell mass and quantities associated with its regulation using actual flight data. The regulatory basis by which decrements in erythropoietin, red cell production, red cell mass, and plasma volume are produced in the zero-g phase of the mission are quite similar to that described for the bedrest study previously discussed. The inflight response is essentially a response to a relative polycythemia-induced-hyperoxia, and the postflight recovery response results from the dilutional anemia-induced-tissue hypoxia.

These simulations suggest, at first glance, that the loss of plasma volume during spaceflight can account for many of the changes in erythropoietic activity during flight and recovery. The similarity between these spaceflight simulations and previously discussed bedrest simulations, all in basic agreement with measured values, suggests a common etiology based on normal feedback regulation of erythropoiesis. It is encouraging that the two spaceflight simulations exhibited similar trends and that both inflight and recovery phases could be estimated successfully using a single parameter adjustment for overall gain.

There was, however, one disturbing aspect of these simulations. The model, operating as a hemoglobinometer, predicts that the degree of erythro-suppression is proportional to the degree of hemoconcentration. It would, therefore, be expected that the similar levels of hemoglobin concentrations measured on the 59-day and 84-day

missions (see Fig. 6-23) would result in equal rates of loss of red cell mass on both flights and that there would be greater losses at the end of 84 days in space than after 59 days in space. However, the measured red cell mass loss was almost twice as great for the 59-day mission than for the 84-day mission. This discrepancy was empirically resolved during the simulations shown in Figs. 6-40 and 6-41 by assuming that the sensitivity of red cell production to hemoglobin concentration (overall open loop gain, G) was two and one-half times higher for the longer flight compared to that of the 59-day flight. The gain factors required to obtain successful spaceflight simulations was also quite different for those determined for other stresses examined, all of which were characterized by hemoconcentration (Table 6-14). The fact that the spaceflight values differ by up to 600% compared to bedrest, infusions, or descent from high altitude, suggests that other factors, in addition to hemoconcentration, are most likely present during spaceflight and have not been taken into account in the modeling analysis. In simulation, it is often possible to use changes in gain to mimic some other effect that is not considered explicitly in the model.

Other than hemoconcentration, energy balance factors appear to offer the most plausible explanation for red cell mass decrements. Using the results of a previous Skylab energy balance analysis [101,117] (see Chapter 4.6), it was found that the largest losses of red cell mass were associated with the crews who consumed the fewest calories ($r = 0.71$, $p < 0.05$), exercised the least ($r = 0.63$, $p < 0.1$) and lost the most tissue mass ($r = 0.66$; $p < 0.05$) (see Tables 6-15 and 6-16). A negative energy balance is a reflection of decreased intake of calories and/or increased exercise expenditures, resulting in increasing amounts of endogenous tissue loss. On Skylab, it was believed that the increase in diet provided to the crewmen on the longer missions was greater than the accompanying increase in exercise, so that net energy balance became less negative, or even positive, for those crewmen (see Table 4-23). Taken as a whole, the correlations of Table 6-16 suggest that energy balance factors may indeed have been a factor in reducing red cell mass during spaceflight.

These statistical findings must be tempered, however, by the realization that the experimental design was not intended to reveal the caloric factors involved in erythropoiesis regulation. For example, the fact that diet and exercise both increased with increasing mission duration calls for caution in interpreting these results. (A regression of red cell mass loss vs. mission duration shows as strong a correlation ($r = 0.75$, $p < 0.05$) as that for red cell mass loss versus diet).

Diet and exercise factors are not included implicitly in the computer model of erythropoiesis regulation. It was assumed that alteration of these quantities could be simulated by adjusting either of two model parameters: oxygen uptake (an exercise effect), and the operating position of the bone marrow controller function curve (possibly an exercise and dietary effect). Simulations of the three Skylab missions were accomplished using the influencing factors in Table 6-13 as a guide in the following manner:
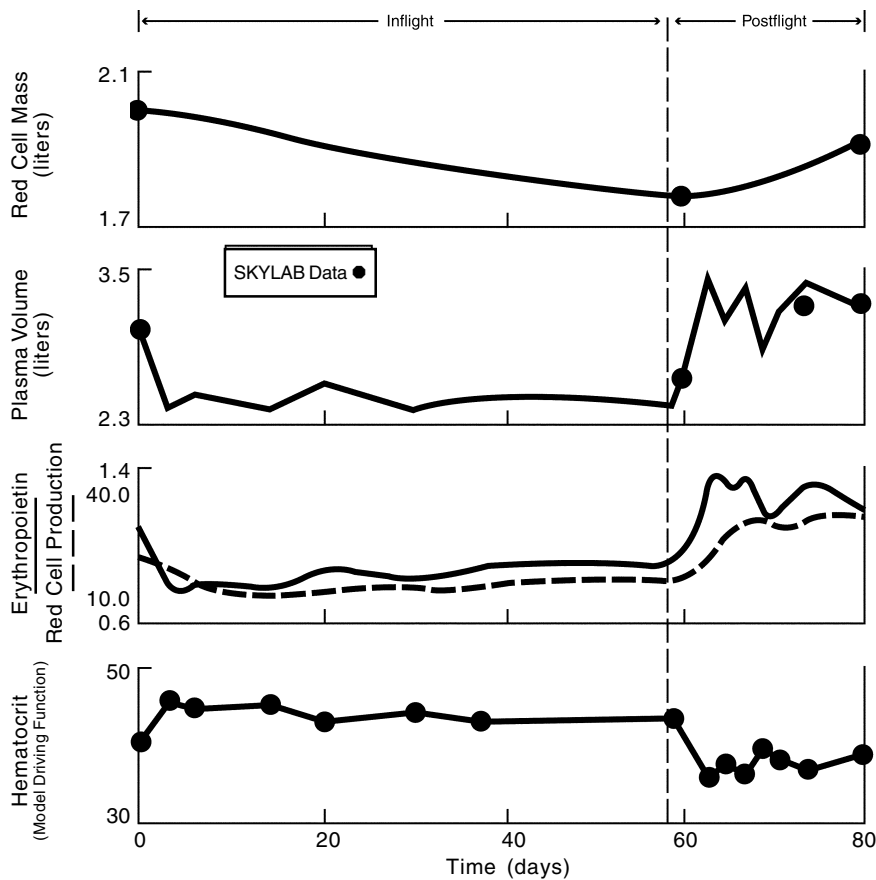
Figure 6-40. Simulated hematological response of the crew of the 59-day mission. The response of the erythropoietic model was generated by using the measured hematocrit-time profile as the primary driving function. In addition to a gradual loss in red cell mass, the model predicts even more rapid decreases in plasma volume, erythropoietin and red cell production. Red cell mass and plasma volume data obtained postflight compares favorably with the simulated response. Contoller gain, G, was set to 5 throughout the simulation.

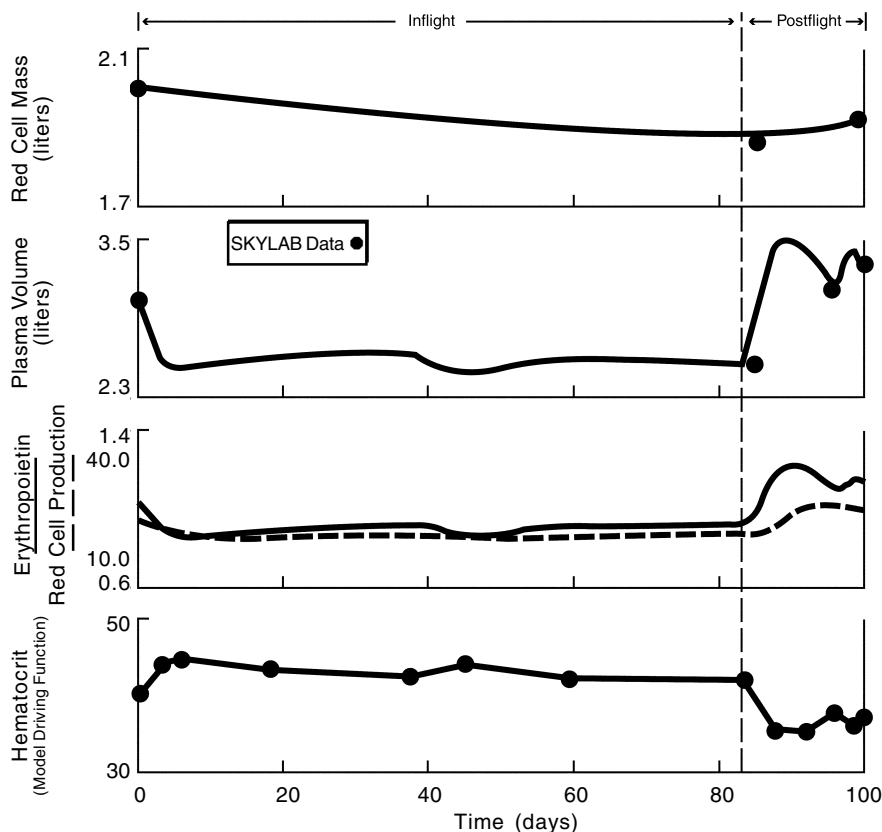**Figure 6-41.** Simulated hematological response of the crew of the 84-day mission. See caption of previous figure. Controller gain, G set to 2 throughout the simulation. Because G was set to different values in the simulations of this and the last figure, controller gain should be thought of as a secondary driving function perhaps reflecting the different energy balances between the two missions.

Table 6-14. Gain Factors Used In Simulations When Hemoconcentration Was The Only Driver

Condition	Gain Value Required For Optimal Fit With Data*
Descent from Altitude	12
Red Cell Infusions	12
Bedrest	10
Skylab: 59-day mission	5
Skylab: 84-day mission	2

*Gain refers to overall renal-bone marrow controller sensitivity relating tissue oxygenation to erythrocyte production rate (see Fig. 6-12).

a) an inflight plasma hemoglobin concentration vs. time function was constructed from the average of the two flights for which data were available, and this single function was used to drive each of the three mission simulations (i.e., it was assumed that there was no difference in hemoconcentration among the three missions);
b) differences in dietary and metabolic activity were simulated by adjusting the controller operating point to values that provided a reasonable agreement between experimental and predicted red cell mass;
c) a 10% decrease in red blood cell (RBC) lifespan was assumed for the 28-day flight in accord with the estimates presented in Table 6-3;
d) a 7% increase in arterial oxygen tension was assumed for the 28-day flight in accord with the estimates presented in Table 6-9; and
e) controller gain factors were held constant for all simulations (G = 10) in accord with previous estimates for bedrest shown in Table 6-14.

These parameter adjustments are listed in Table 6-17 (case 1) and the results of the simulations are shown in Fig. 6-42, which includes the hemoglobin drive function employed.

Additional simulations were performed, for comparative purposes, that used different parameter combinations and values. For simplicity, changes in arterial oxygen tension and red cell lifespan were ignored in these other cases, which are listed in Table 6-17. Instead, in cases 2 to 4, overall gain was chosen to be either 10 or 5, and optimal fits with the data were obtained by adjusting the operating point and oxygen uptake (case 4). A final simulation was performed (case 5) in which only the overall gain was adjusted. The simulated responses of these additional cases were essentially all similar to case 1, which is illustrated in Fig. 6-42.

These simulations demonstrate the plausibility of the continuous loss theory. In order to account for the observed differences between Skylab missions, it was not necessary to consider inflight regenerative behavior, nor a variable controller sensitivity (i.e., G was identical in all missions for cases (1) to (4)), thus overcoming certain restrictions and discrepancies of earlier simulations (see

Table 6-14). Hemoconcentration can explain part of the loss of red cell mass, but it cannot explain the differences between missions. These differences may, however, be explained by other factors such as changes in controller function, oxygen uptake, arterial oxygen tension, and red cell lifespan. In each of the cases (2), (3), and (4), the values of P1 and oxygen uptake which provided good agreement between model response and data are in ascending order for the 28-day, 59-day, and 84-day missions, respectively. This would be expected if their values were somewhat proportional to average dietary and exercise levels of those crews. These simulations also indicate that more than one computer solution (i.e., combination of parameter values) can account for the observed losses in red cell mass. The predictive value of the simulation technique is thus limited by the lack of inflight data. Nevertheless, the additional information that must be obtained in order to distinguish between the alternative scenarios is suggested directly by this study.

6.5.5.2 Postflight Recovery of Red Cell Mass. An observation, selected for closer examination, was that after leaving the space environment, replacement of red cells in the crew of the 28-day mission was delayed for about two weeks. This "refractory" phenomenon was different from the more rapid recovery exhibited by the crews of the two longer missions as evidenced by a reticulocytosis and measured rise in red cell mass (Table 6-4 and Fig. 6-24). It was shown previously that bedrest is characterized by a similar delay in red cell mass recovery as that seen after the 28-day spaceflight (Fig. 6-6). However, a reticulocytosis was observed much earlier after bedrest than after spaceflights of similar duration [35] even though red cell mass failed to show demonstrable repletion in both cases.

In the case of bedrest, the simulation analysis suggested the delay in red cell mass recovery may have resulted from a combination of factors which included a normal bone marrow transit time delay of several days, increased destruction of cells, decreased oxy-hemoglobin affinity, and a delay in plasma volume repletion [9] (see Chapter 6.5.3). The last of these factors could not be adequately examined because of the sparsity of data relating to plasma volume recovery. In Skylab, however, a much more complete description of plasma hemoglobin concentration changes (from which plasma volume could be inferred) was available during the postflight period. These data were presented in Figs. 6-3 to 6-5 and have been redrawn in Fig. 6-43 for convenience in comparing mission differences.

Accordingly, it appears that the hemodilution arising from plasma refilling was much greater following recovery day of the two longer missions, compared to the 28-day mission. This is confirmed, in part, by the less frequent plasma volume measurements which indicates that maximum repletion of plasma took place almost 6 weeks following recovery for the 28-day crew compared to two weeks for maximum recovery for the 59-day and 84-day crews (Figs. 6-3, 6-4, and 6-5). No explanation for this difference in plasma refilling behavior has yet been advanced, but a tentative hypothesis is provided in the paragraph below.

Table 6-15. Summary of Inflight Energy Balance Components On Skylab (*N* = 3)*

	28-Day Mission	59-Day Mission	84-Day Mission
Red Cell Mass Loss:			
(total ml)	311 ± 19	247 ± 123	134 ± 39
(ml/day)	11.1 ± 0.6	4.2 ± 2.1	1.6 ± 0.5
Diet (Kcal/d)	2930 ± 90	3225 ± 610	3260 ± 105
Exercise (W-m/d)	1950 ± 315	4690 ± 1620	4890 ± 715
Lean Body Loss (gm/d)	−60 ± 40	−14 ± 26	−10 ± 3
Fat Loss (gm/d)	−41 ± 31	−35 ± 24	+ 5 ± 11
Solid Tissue Loss (gm/d)	−52 ± 34	−40 ± 24	+ 0.7 ± 9

* Data derived from Chapter 4.6
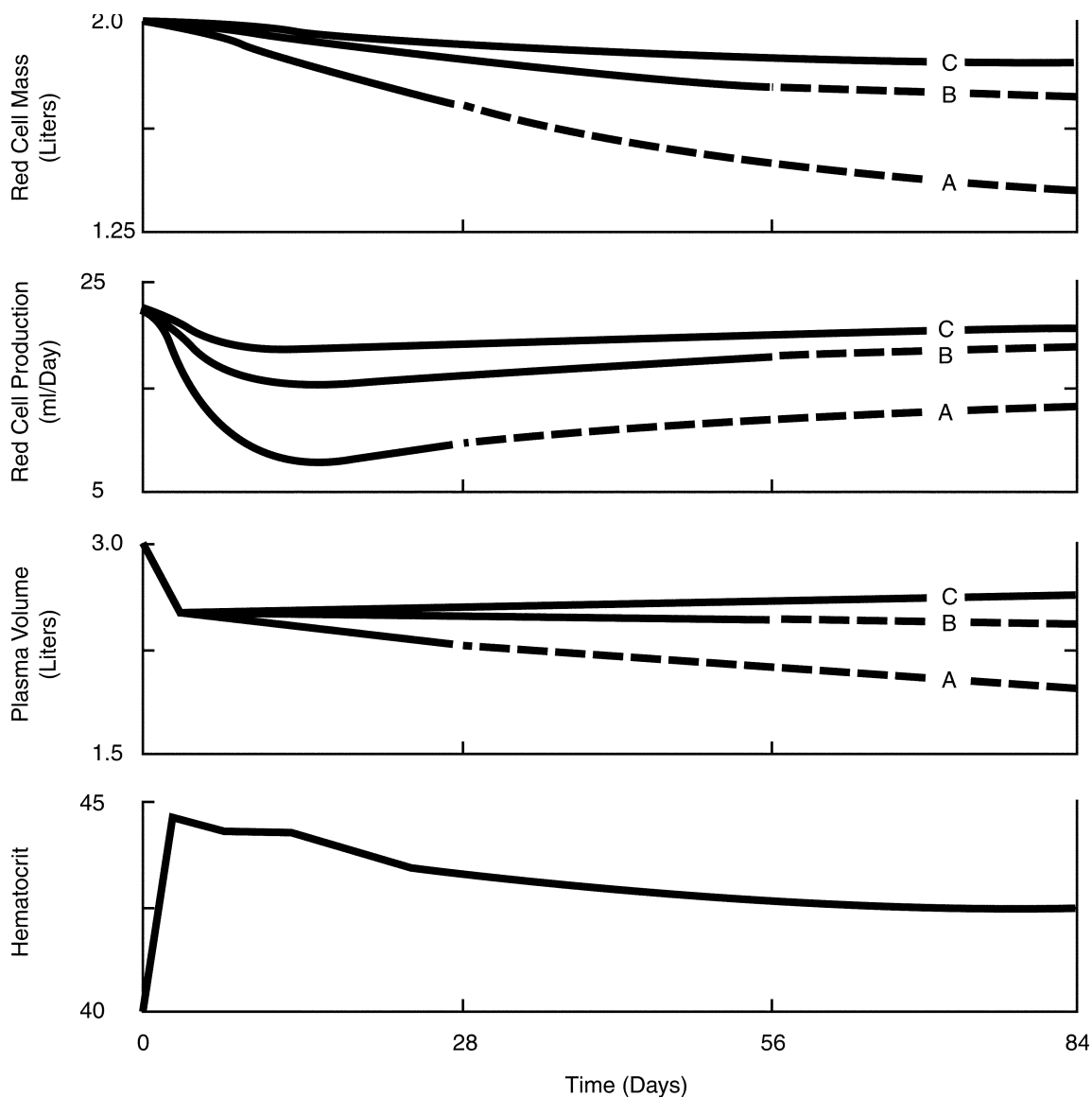
Figure 6-42. Simulation of the three Skylab missions: A = 28-day mission, B = 59-day mission, and C = 84-day mission. The hematocrit-time profile shown in the bottom panel was based on a composite of inflight data and was used to drive the model for the three simulations. In addition, the parameter adjustments shown in Table 6-17 (Case 1) were used. The dashed portion of the curves are predicted responses if all missions had continued for 84 days. The predicted end-of-mission values for red cell mass and red cell production are in good agreement with measured values. The predicted plasma volumes losses are greater than measured at recovery for the two shorter missions. However, plasma volume measurements could be expected to be quite erratic at the end of space missions.

Table 6-16. Energy Balance Factors Tested for Their Influence on RCM Change (*N* = 9)

Factor	Correlation Coefficient
Diet[1]	–0.71***
Bicycle Work[1]	–0.63**
ΔLean Body Mass[2]	+0.61**
ΔBody Fat[2]	+0.61**
ΔSolid Body Tissue[2]	+0.66***

1. Total mission calories vs. total mission red cell mass loss
2. Mass of tissue lost per day vs. red cell mass loss per day
** $p < 0.10$; *** $p < 0.05$

If plasma volume changes were similar on all flights, it would be expected that the crewmembers with the largest decrements in red cell mass (i.e., the 28-day crew) would exhibit the greatest amount of postflight plasma volume refilling in order to return blood volume to the preflight level. However, inflight plasma volume changes were apparently not the same, but rather the least losses occurred on the 28-day flight and the greatest losses occurred on the 84-day flight. Also, the amount of postflight plasma volume refilling (by the end of two weeks postflight) was directly related to the amount of plasma lost inflight. The overshoot of plasma volume above control levels, often seen after bedrest and spaceflight, may be ascribed as a compensation for the previous losses in red cell mass. From the point of view that plasma volume is regulated both inflight and postflight to maintain blood volume appropriate to the respective gravity environments, the smaller degree of refilling on the 28-day mission seems more understandable.

The observation that the greatest losses in red cell mass were accompanied by the least losses in plasma volume resulted in a blood volume loss that was essentially constant regardless of mission duration (Fig. 6-2). This suggests a regulatory process whereby blood volume is maintained at reduced levels, appropriate for zero-g, by control of plasma volume. Accordingly it can be presumed that downward plasma volume adjustments are required for the acute upper circulatory overload upon entering zero-g, and longer term upward adjustments take place in compensation for the more gradual red cell mass changes which would otherwise reduce blood volume further (see Fig. 10-15). Long-term plasma volume regulations in response to a primary disturbance in circulating red cell mass has also been noted in erythremic states such as polycythemia vera [138] and altitude hypoxia [139].

The effect of plasma volume refilling following spaceflight was studied by computer simulation. An idealized spaceflight simulation was performed by reducing the plasma volume 500 ml below control and permitting the model to achieve a new steady-state, at which time 250 ml of red cell mass had disappeared (see Fig. 6-28). Thereafter, three idealized postflight cases were examined: a) plasma volume refilling of 250 ml (undershoot); b) plasma

volume refilling of 500 ml (return to control); and c) plasma volume refilling of 750 ml (overshoot). The responses to these volume adjustments are shown in Fig. 6-44. In each case, the model is responding to the simulated postflight hemodilution that has different levels of severity, depending upon the degree of plasma refilling. After 30 simulated days, the red cell mass had only returned to normal for the case where a plasma refilling overshoot was postulated (case C). For case A, where plasma refilling was incomplete but hematocrit was depressed 6% from the last inflight day (similar to the 28-day mission), recovery of red cell mass was essentially negligible after two weeks, and after 30 days, only 33% of the lost red cells had reappeared in the circulation. Thus, when combined with the normal 4-day transit delay for bone marrow production (included in the model), the diminished recovery of plasma volume on the 28-day mission compared to that observed on the other flights seems sufficient to account for the differences in postflight recovery kinetics of red cell mass among crewmen. In addition, a small degree of hemolysis cannot be ruled out following the shortest mission (see Table 6-3). The available data do not permit any speculation regarding shifts in oxy-hemoglobin affinity, as was postulated in the bedrest study (see Chapter 6.5.3).

6.5.6 Comparison Between Bedrest and Spaceflight Erythrokinetics

Comparison of the hematological responses between bedrest subjects and the crews of Skylab reveals many similarities including: a) a seemingly gradual decrease in red cell mass, b) a more rapid decrease in plasma volume, c) hemoconcentration throughout the stress period, d) destruction rates of red cells which are either normal or not high enough to account for the total red cell mass loss, e) a depressed reticulocyte count immediately following the hypogravic stress which subsequently increases to supra-normal levels upon return to a one-g ambulatory environment, and f) a return-to-normal of red cell mass requiring 3-7 weeks. In addition, and as just discussed, a delay in red cell mass recovery has been found in bedrest and spaceflights which last less than a month.

Blood volume losses for the first 30 days of spaceflight and bedrest are compared in Fig. 6-45. The bedrest results are based on two empirical formulations, which were derived from a large number of studies of different lengths. First, a predictive equation describing red cell mass (RCM) loss was given as [30]:

$$\text{RCM Loss (percent decrease)} = 0.24 \times \text{Days of Bedrest} + 0.90$$

This formulation is based on bedrest studies whose length varied from 2 to 35 days and should not be extrapolated outside this range. Secondly, plasma volume (PV) losses were fitted by a regression equation which appears accurate for about 30 days of bedrest [33]:

$$\text{PV Loss (percent decrease)} = \text{Days of Bedrest}/(0.33 + 0.039 \times \text{Days of Bedrest})$$

TABLE 6-17. Alternative Scenarios which Produce Nearly Equivalent Simulations of the Three Skylab Missions

	28-Day Mission	59-Day Mission	84-Day Mission
Case 1			
Overall Gain, G	10	10	10
*Operating Point, P1	+ 20%	+ 20%	+ 30%
Arterial Oxygen Tension	+ 7%	0%	0%
RBC Life Span	- 10%	0%	0%
Case 2			
Overall Gain, G	10	10	10
*Operating Point, P1	-10%	+ 20%	+ 30%
Case 3			
Overall Gain, G	5	5	5
*Operating Point, P1	-20%	0%	+10%
Case 4			
Overall Gain, G	5	5	5
*Operating Point, pi	- 2.5%	0%	+ 1.5%
*Oxygen Uptake	- 2.5%	0%	+ 1.5%
Case 5			
*Overall Gain, G	14	5	2.5

Note 1: Percentages in Table refer to changes with respect to normal model parameter value. A value of zero means that the normal value was used.
Note 2: The hematocrit vs. time function that was used in these simulations is a composite of the 59-day and 84-day mission inflight data.
Note 3: (*) designates parameters which were adjusted to obtain optimal fit with data.

The results from Apollo and the 28-day Skylab missions shown in Fig. 6-45 are taken from direct measurements on crewmen obtained during the first day of recovery. The other curves, representing the 59-day and 84-day Skylab missions, are taken from the computer simulations of Figs. 6-40 and 6-41. These should be considered unconfirmed estimates, since no direct measurements of red cell mass and plasma volume are available in this time period. The 28-day Skylab mission could not be accurately simulated since no inflight hemoglobin data were obtained.

It is difficult to discern specific differences between spaceflight and bedrest from the data presented in Fig. 6-45. Based on a strict interpretation of hard data (i.e., excluding simulation predictions by Johnson [31]) claims that in spaceflight, losses of red cell mass are greater, and plasma volume losses are smaller, compared to bedrest. However, these conclusions should be stated guardedly for the following reasons. First, it is believed that some of the Apollo results included a significant red cell loss due to oxygen toxicity, a factor that was not present in the Skylab and bedrest situations. Secondly, if the simulation results of the 59-day and 84-day missions (i.e., those consistent with the "continuous loss" hypothesis) are tentatively acceptable in place of non-existent data for the first 30 days in space, the red cell mass losses of the two longest Skylab missions appear to be less than that of bedrest, as illustrated in Fig. 6-45. Thirdly, with regard to plasma volume, measurements of this labile fluid compartment on the day of recovery are not necessarily representative of the true inflight loss because of the body's capacity to

rapidly replenish plasma deficits prior to their measurements in one-g. Also, the possibility exists that measured spaceflight plasma volume losses were under-estimated because of a diurnal variation [31].

The plasma volume values shown in Fig. 6-45 for bedrest were obtained by direct measurement while the simulation results for the two longer Skylab missions were inferred from inflight hemoglobin measurements. Thus, these latter data, although indirect may be more reflective of the hypogravic state than measurements made after the mission because the complicating factors of recovery are not present. If this is true, than plasma volume may decline more rapidly in spaceflight than in bedrest. This is supported by the evidence that hemoconcentration is more extreme in spaceflight than in bedrest (see Figs. 6-6 and 6-23).

Proponents of the theory that a significant loss of red cells are destroyed early in a spaceflight mission could argue that the Skylab simulations for red cell mass shown in Fig. 6-45 are in error and should diminish more in-line with the other spaceflight data shown (solid line). If we assume that a rapid loss of 7% red cells (similar in magnitude to that seen in Apollo), then using the observed acute increase in inflight hematocrit as a guide (10%; see Fig. 6-23), it is easy to calculate the plasma volume would have decreased more than 25%. This is thought to be unlikely. See also the discussion of an acute hemolysis in Chapter 6.5.5.1.1.

One of the more intriguing patterns that emerge from Fig. 6-45 is that associated with the blood volume data. Compared to the results of red cell mass and plasma vol-
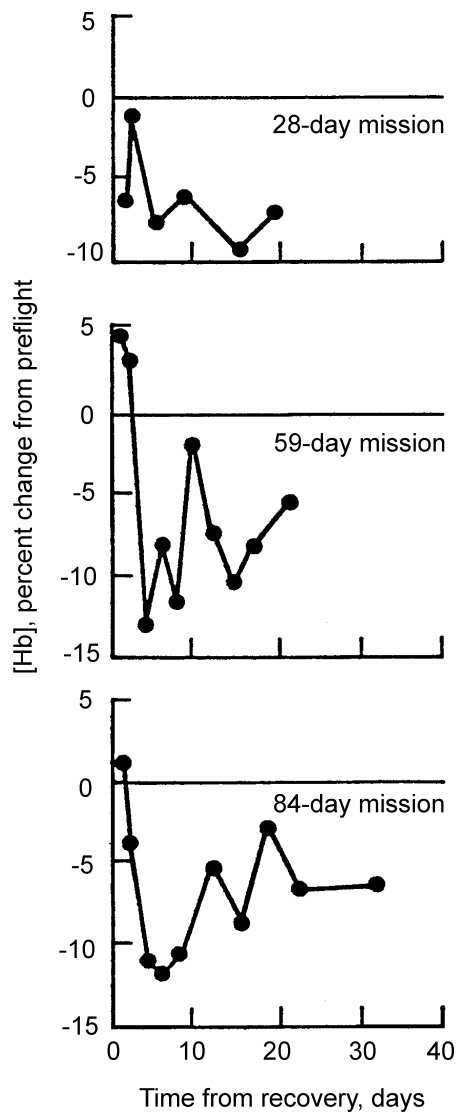
Figure 6-43. Postflight blood hemoglobin concentrations of each Skylab crew expressed as percent of preflight control.

Figure 6-44. Simulation analysis of postflight recovery of red cell mass showing the influence of different degrees of hemodilution. The responses shown in this figure were preceded by a 120 day idealized spaceflight simulation (similar to Fig. 6-28), which was accomplished by reducing plasma volume by 500 ml. The pre-spaceflight control values are shown by the solid circles on the left. At 120 days, recovery was initiated by refilling plasma volume to varying degrees: 250 ml added (......), 500 ml added (- - - -) or 750 ml added (———). The resulting hemodilution (indicated by the hematocrit response) then served as the stimulus for red cell mass recovery.

ume, the blood volume losses appear to be more uniform (i.e., less scatter) for all bedrest and spaceflights examined. This observation lends support to the concept, stated in the previous section, that total blood volume is closely regulated and tends to stabilize in hypogravic environments at levels approximately 90% of control. Also see supporting simulation with Guyton model in Chapter 10 (Fig. 10-15).

If hemoconcentration resulting from plasma volume depletion was the sole cause of red cell mass changes, it would be expected that those situations in which plasma volume dropped more rapidly (i.e., 59-day and 84-day Skylab missions) would be associated with the most rapid drop in red cell mass. This hypothesis is supported by the idealized simulation shown in Fig. 6-46 in which plasma volume decreases either rapidly (as in spaceflight) to a constant level, or falls more gradually (as in bedrest) to the same level. However, the contrary situation seems to be present in Fig. 6-45; i.e, those studies in which plasma volume decreased most rapidly were accompanied by the least changes in red cell mass. This does not negate hemoconcentration as a causative agent in red cell loss, but suggests that other factors were present to varying degrees in the cases examined in Fig. 6-45. In this regard, and in the light of the previous discussions on the role of energy balance, the differences between diet and overall metabolic rate between spaceflight and bedrest merits further attention. Bedrest subjects are often given a decreased dietary intake thought to be commensurate with the decreased metabolic rate. Twenty-four hour metabolic rates during spaceflight have not been measured, but they undoubtedly have varied widely as a result of nearly total confinement in the earlier missions and the free-ranging movement in the lunar environment and the Skylab workshop. This has been accompanied by a nearly universal occurrence of inadequate dietary intake in spaceflight, with the single exception of the 84-day mission.
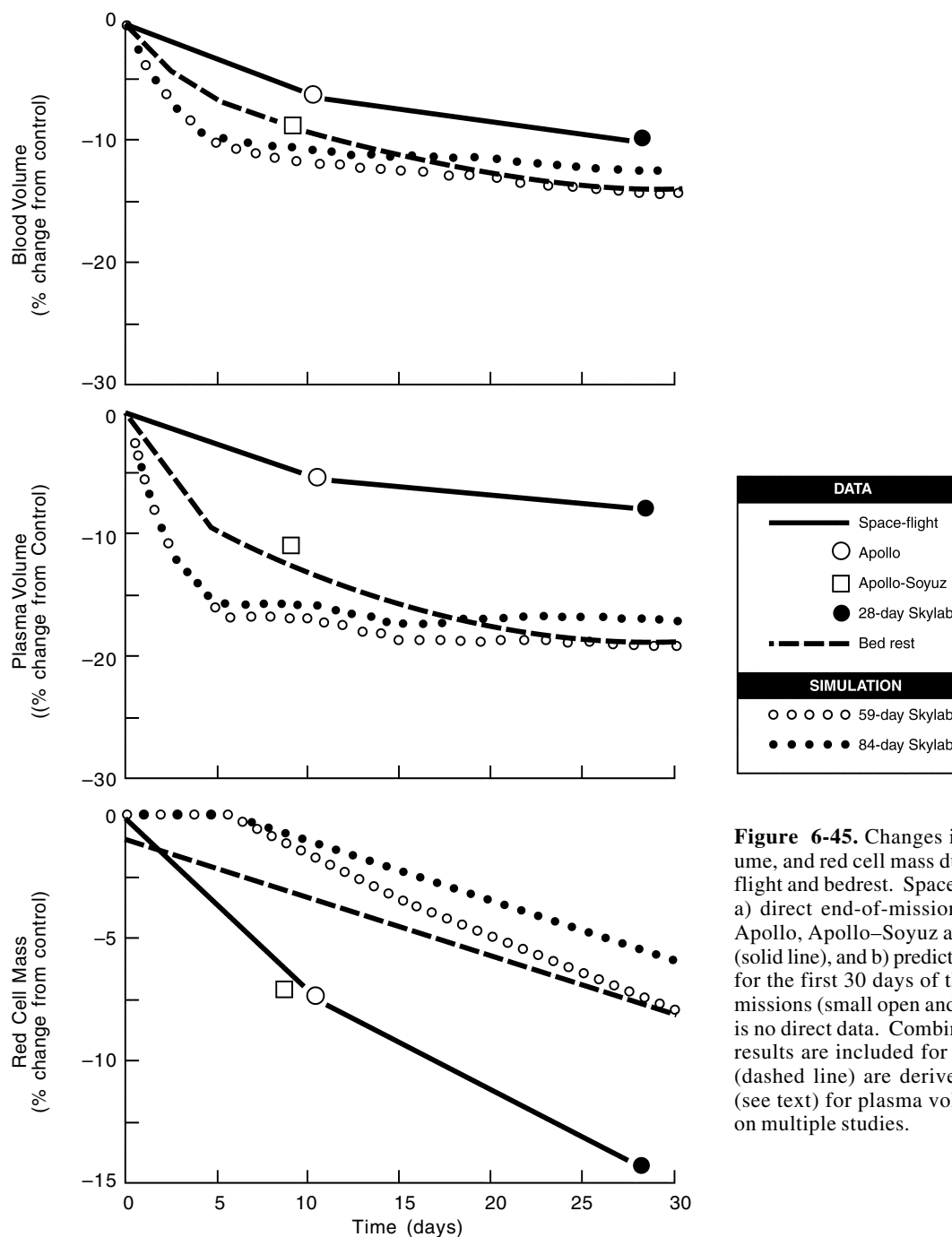
Figure 6-45. Changes in blood volume, plasma volume, and red cell mass during the first month of spaceflight and bedrest. Spaceflight results are of two types: a) direct end-of-mission data [19] from combined-Apollo, Apollo–Soyuz and the 28-day Skylab mission (solid line), and b) predictions from the simulation model for the first 30 days of the 59-day and 84-day Skylab missions (small open and filled circles) for which there is no direct data. Combined Apollo and Apollo–Soyez results are included for reference only. Bedrest data (dashed line) are derived from regression equations (see text) for plasma volume and red cell mass based on multiple studies.

The general conclusion appears inescapable that bedrest and spaceflight have more similarities than differences with regard to the erythropoietic response. However, a more complete description of the disturbances in oxygen transport, bone marrow activity, and red cell lifespan are required in both situations. Differences between bedrest and spaceflight may ultimately be explained by the energy balance factors of diet and metabolic rate, by the dynamics of plasma volume shifts, and possibly by selective destruction of an age-related cohort of red cells.

6.5.6 Simulation of Spaceflight Experiment

A very useful application of computer models is to help define and refine experimental designs and protocols (see Chapter 11.2). The ability of the model to predict experiment outcomes allows the researcher to determine such information as the most important variables for measurement, the frequency of measurement, and the types of interventions that could test alternative hypotheses. An important hematology experiment, one that was designed to address unanswered questions from the Skylab program,
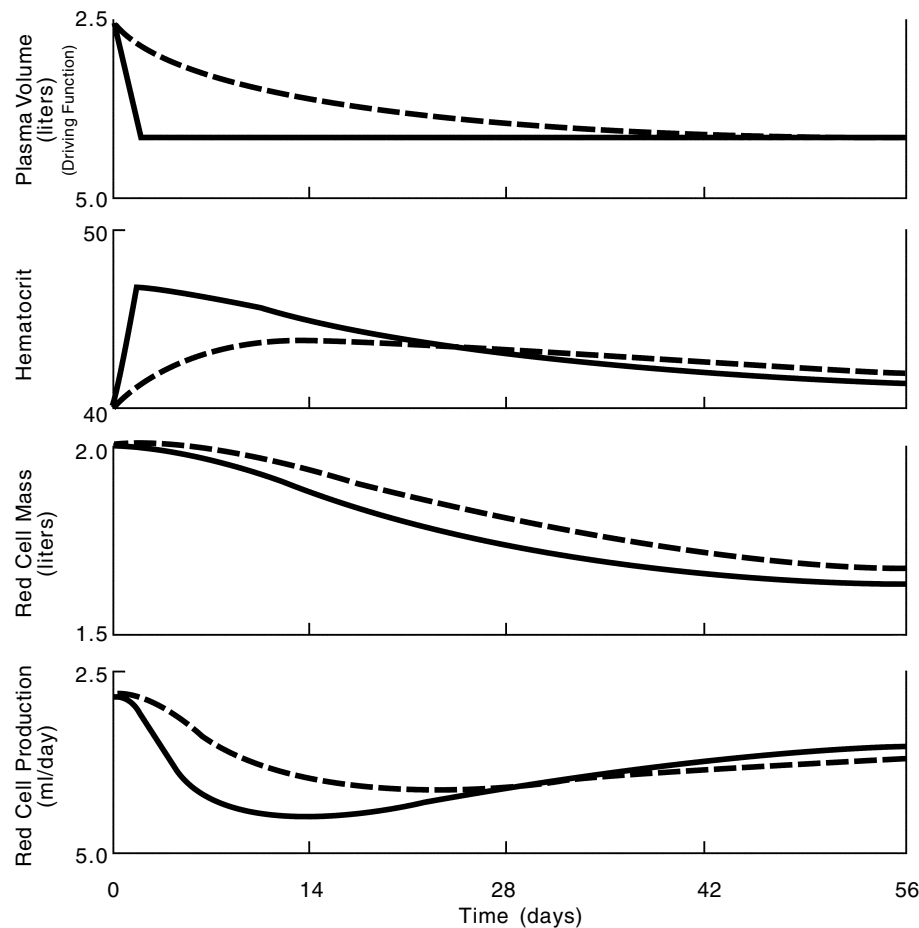
Figure 6-46. Simulation of an acute drop in plasma volume (representing spaceflight) in comparison to an exponential fall in plasma volume (representing bedrest). Erythropoiesis is controlled by the hematocrit-time profile. On the basis of a hemoconcentration influence alone, the model predicts a greater erythro-suppression for spaceflight than for bedrest during the first four weeks. Because plasma volume decreases to the same level in both cases, convergence of all corresponding variables to the same steady-state value is predicted by eight weeks.

was conducted on the first Shuttle Spacelab mission (SL-1). The same model discussed throughout this chapter was applied to help predict possible outcomes of this experiment with the goal of understanding whether the blood sampling from the human subjects would obscure the effects of spaceflight that the experiment was designed to measure [140]. Simply put, the hypothesis of the flight experiment was that weightless spaceflight would induce a *decrease* in red cell production and eventually a measured reduction in red cell mass. On the other hand, drawing blood for analysis, would also be expected to reduce blood volume but could also cause a measurable feedback *increase* in red cell production. Would the effects of blood sampling be large enough to oscure the expected effects of spaceflight on erythropoiesis?

The experiment, conducted on a 10-day mission, would measure factors involved in the control of erythropoiesis, including red blood cell mass and plasma volume (pre and postflight) as well as inflight hematocrit, red cell production and erythropoietin, all variables which are ac-

counted for by the model. Erythropoietin would be measured for the first time in space; the model had previously predicted a decrease in erythropoietin for the Skylab astronauts of about 20% (see Figs. 6-40 and 6-41), so it would be very interesting to test this prediction. Just as important, however, was to assess the influence on erythropoiesis of the blood sampling protocol. The original plan for drawing blood consisted of 10 blood draws (from each of 2 crewmen) during the preflight, inflight and postflight periods, each draw averaging approximately 93 ml blood, or a total of about 0.93 liter blood during an 8 week period. (The blood samples were required for several different experiments in addition to the hematology experiment).

A series of computer simulations, shown in Fig. 6-47, was conducted using the above information to test the effect of blood draws on erythropoiesis. All simulations included a 30-day preflight period, a 10-day inflight period and a 2-week postflight period. The first simulation (dotted line) was a simulation of weightless spaceflight
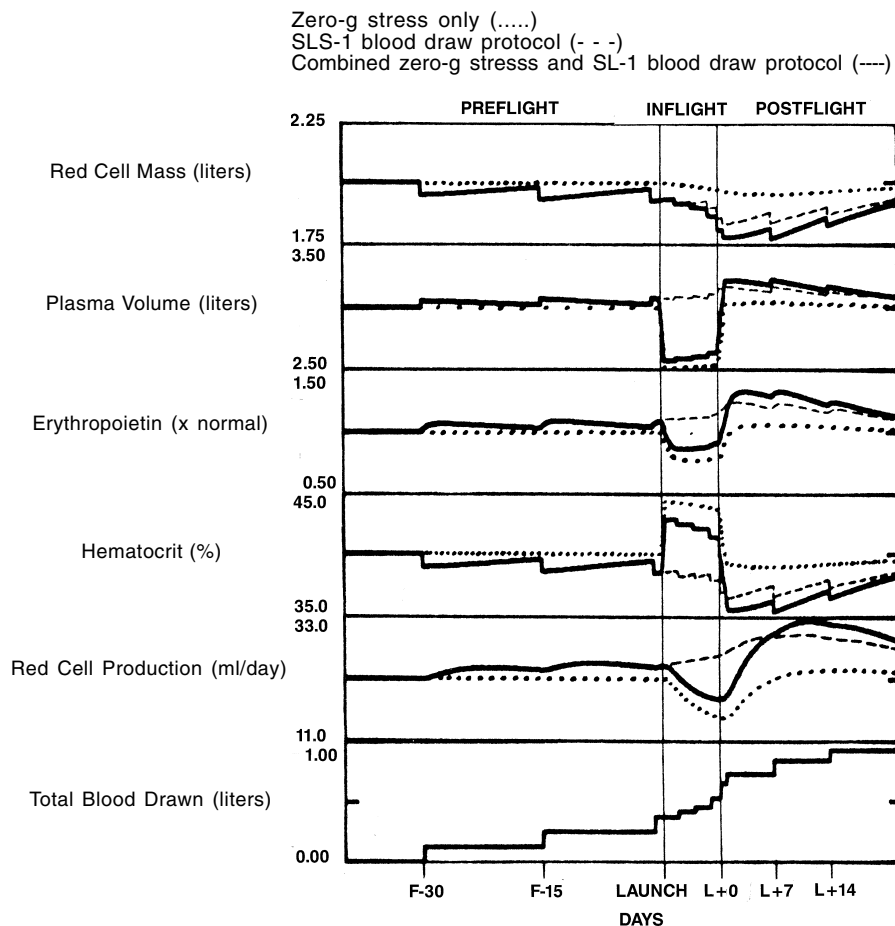
Figure 6-47. Simulated results of the Spacelab-1 (SL-1) hematology investigation using the model of erythropoiesis regulation.

without any blood draws. This simulation is similar to that shown in Fig. 6-16 for the case where the initializing stimulus (onset of weightlessness) is a sudden decrease in plasma volume of 10% that is returned to normal 10 days later. A second simulation (dashed line) was performed using only the blood draw protocol as the driving function. Appropriate amounts of red cell mass and plasma were removed on the days specified in the protocol. A third simulation (solid line) was simply a combination of the first two; a simulation of weightlessness combined with a simulated blood draw protocol. These three simulations provided a visual assessment of the consequences of spaceflight on erythropoiesis and of a concomitant blood-draw schedule. The bottom curve of Fig. 9-47 indicates the cumulative blood drawn for sampling.

The overall result indicated that the blood draw protocol does have a significant impact on the erythropoietic system, but that in most cases the changes due to spaceflight are much greater. Even with the large blood samples considered here, the response of the important variables of the erythropoiesis system in a spaceflight environment were qualitatively similar whether or not blood is sampled. Thus, weightlessness is the dominant stress during the inflight phase. However, during the important early post-

flight period blood sampling appears to obscure two specific measurements, that of erythropoietin and red cell mass. Erythropoietin is predicted to remain below control as a result of weightlessness but may rise above control on the first or second postflight day as a result of the blood draws. Similarly, the predicted loss in red cell mass is barely significant after only 10 days in space but may exhibit a 10% loss due to the cumulative effects of blood sampling. Also, a distinctive "overshoot" is apparent in both cases that involved blood being sampled but not in the case of a "pure" weightlessness response.

As a result of this analysis and other ground-based testing, it was decided to reduce the amount of blood drawn for sampling purposes to about half of that originally proposed. When the results of the flight experiment became known, they were compared to the predictions made by the simulation. The correspondence between simulated and experimental results were qualitatively and quantitatively acceptable as shown in Table 6-18.

An interesting side-note to this analysis was that the principal investigators of the flight study originally reported a much greater inflight and postflight reduction of erythropoietin than the values predicted by the model (−75% vs. −14% inflight; −44% vs. +2% postflight) [141].

Table 6-18. Comparison of Predictions of the Erythropoiesis Regulatory Model and Experimental Results from SL-1 [% change from baseline]

Measured Variable	Predicted	Measured*
RBC mass (landing day)	−6	−10
Plasma volume (landing day)	−10	−6
Erythropoietin (FD7)	−14	−20
Erythropoietin (R+1)	+2	+10
Hematocrit (FD7)	+8	+7
Hematocrit (R+1)	−6	0
RBC Production (FD7)	−19	−25
RBC Production (R+8)	+50	+50

* Ref. [143]
FD = flight day; R+ = number of days after landing

Also, the model predicted a postflight overshoot of erythropoietin although this was not measured. Those authors made a point of faulting the model's capability to predict the observed changes (even though they were not statistically significant) and suggested "a need for continued refinement of the computer model" [142]. However, in a subsequent publication, the same authors reported the results of a re-analysis of the flight blood samples using a more sensitive erythropoietin assay [143]. The corrected results agreed very closely with the simulation results (see Table 6-18), although the authors failed to mention the model's veracity. However, gratifying confirmation of model predictions might be, it is worth remembering that the ultimate usefulness of a model is not in the accuracy of its predictions but in the power of a model to force the user to ask critical questions and to turn model predictions (good or bad) into ideas for more probing experiments.

6.6 Summary

The regulation of erythropoiesis during weightless spaceflight was studied using a theoretical model. The model incorporates the best current understanding of the dynamics of red cell production and the associated feedback regulation based on knowledge current at the time of model development. Using the techniques of computer simulations, it was possible to apply the model to study candidate hypotheses that might explain the loss of circulating red cell mass during spaceflight.

Both ground-based and spaceflight experiments have suggested that, in the normoxic environment of Skylab, this loss was likely a result of suppressed erythropoietic activity rather than elevated destruction of red cells, although occurrence of the latter to some extent cannot presently be ruled out. According to current concepts embodied in the theoretical model, a reduced erythropoietic state can be caused indirectly by hyperoxia of a renal oxygen sensor via the humoral regulator, erythropoietin, acting on the bone marrow, or by direct alteration of stem cell kinetics at the marrow controller. (The presence of

erythropoietin inhibitors was not considered in this analysis). Tissue hyperoxia may be caused by factors that increase oxygen supply (i.e., hemoconcentration, enhanced blood flow, decreased oxy-hemoglobin affinity and increased arterial oxygen loading) or by factors that decrease oxygen demand. Proliferation of erythrocytes at the bone marrow level is affected, not only by erythropoietin, but also by dietary factors. One can reasonably postulate that all of these various influences were present to various degrees during spaceflight and bedrest, and they contributed to the eventual reduction in red cell mass.

Evaluation of these hypotheses was accomplished by several means including: sensitivity analyses of mathematical models which revealed the relative influence of each major hematological parameter on circulating red cell mass; dynamic simulation of human and animal studies, whereby the effects of single, multiple, or time-varying stresses were assessed for their potential to generate computer responses similar to those observed experimentally; and, collaboration with investigators performing animal studies to test, in the biological system, those hypotheses suggested by the computer model. Results from a number of experimental studies, each characterized by a reduced red cell mass or suppressed erythropoietic activity, were examined. These included not only spaceflight investigations, but also those of bedrest, red cell infusions, dehydration and descent-from-altitude. The simulation model was valuable in revealing the pathways which were common to all of these situations and provided a quantitative basis for testing whether the same mechanisms were operative in spaceflight.

This hypothesis testing approach led to the following conclusions:

a) The shifts in plasma volume accompanying hypogravic maneuvers results in an observed mild hemoconcentration which can eventually lead to significant decrements in circulating red cell mass. The model predicts that moderate increases in hematocrit, if unopposed by other factors involving oxygen delivery to tissues, can proportionately increase oxygen tension at a renal sensing site and exert a sensitive suppressant effect on erythropoietin and red cell production. The erythropoietic regulatory system may be viewed, when operating in this fashion, as a hemoglobinometer (i.e., red cell production decreases so as to eventually relieve the hyperoxic condition). The final predicted result is a nearly complete restoration of hemoglobin concentration (or hematocrit) accompanied by a diminished red cell mass. 'The simulation of bedrest, using the observed non-linear plasma volume changes as model driving functions, predicted a qualitatively accurate linear rate of fall in red cell mass. The model suggests that red cell mass will stabilize as hematocrits normalize; this has not yet been confirmed experimentally, either in space or on the ground. Therefore, this overall process can be explained in large part, in terms of normal feedback regulation of the erythropoietic system in the face of sustained decreases in plasma volume.

b) Other factors which may have enhanced oxygen delivery and produced the same effects as hemoconcentration cannot be ruled out (i.e., shifts in blood flow, P_{50} and arterial pO_2), but direct data are only available to support the hemoconcentration effect. In any event, the model system predicts that even small changes in a variety of parameters (perhaps smaller than can be measured experimentally), if sustained for long enough periods of time, could lead to a progressive and significant degeneration of red cell mass.

c) The ability of hemoconcentrated blood to suppress erythropoietic activity was qualitatively similar in all situations studied, whether it involved red cell infusion, descent from altitude, water deprived dehydration, bedrest, or spaceflight. However, as revealed by computer simulation, the quantitative effect was not always the same. That is, equal degrees of hemoconcentration did not result in the same degree of erythro-suppression for bedrest and spaceflight, nor for the 59-day and 84-day Skylab missions. This suggested that other factors may have been present which either augmented or opposed the hemoconcentration effect.

d) Two additional factors were examined in some detail: diet and exercise. The hypotheses that dietary restriction can reduce, and exercise can enhance, erythropoiesis (as reported in animal studies) appeared to account for the discrepancies noted in (c). An inadequate diet, in particular, has been shown to lead to suppressed erythropoiesis by mechanisms which may bypass the hormone regulator and act directly on the bone marrow controller. This could explain the occasional findings that erythropoietic activity decreases in the presence of normal levels of erythropoietin. However, both dietary and exercise effects have not been well defined in the human subject and the lack of appropriate controls during spaceflight studies does not permit a definitive conclusion.

e) The simulation analysis failed to rule out some small degree of acute red cell destruction as contributing to either the reduced red cell mass during hypogravity or the delayed recovery of red cells following some spaceflights and bedrest. Unusual removal of cells from the circulation could possibly arise from the mechanical stresses of launch, splenic sequestration, exercise hemolysis during flight, or postflight hemolysis of cells made more fragile by weightlessness or bedrest. However, a major role of inflight cell destruction is unlikely, because this would contradict the observations that hemoglobin concentrations are significantly elevated and that overt signs of hemolysis were seldom found.

f) The model erroneously predicts an identical hematological response to both relative and absolute polycythemia (produced by plasma volume decreases or red cell mass increases, respectively). While both cases result in hemoconcentration and reduced erythropoietic activity, the influences of blood volume (i.e., relative polycythemia is hypovolemic and absolute polycythemia is hypervolemic) on blood flow, which is not accounted for in the model, may partially explain the different experimental responses to these two stresses.

g) Two theories were examined to explain the Skylab findings that demonstrated decreasing red cell mass losses with increased exposure to weightlessness. According to the so-called "regeneration theory," this behavior represents an adaptive influence to an initial insult of weightlessness. Treating the Skylab crew data from three separate missions as a composite suggested that an early loss of red cells is followed by regeneration which begins two months after launch. Acceptance of this hypothesis as a generalized theory of erythropoietic regulation in weightlessness is confounded by the fact that decreasing losses of red cell mass were associated, not only with longer duration flights, but also with increasing levels of diet and exercise. These latter factors had demonstrable effects on maintenance of body tissue and cardiovascular condition, and their further involvement in the oxygen transport-erythropoietic system was postulated herein. As a result, an alternative and more plausible ("continuous loss") theory was proposed which suggested that there were two components to the suppression of red cell production: one related to energy balance and one related to water balance. Differences among the crewmen's red cell mass losses were thereby considered to be a result of different levels of dietary intake and exercise, superimposed on a common loss due to hemoconcentration. According to this concept, the kinetics of red cell mass disappearance would not include regenerative behavior, but would be more similar to the continuous, linear losses observed in bedrest. Experimental animal studies support this theory.

h) Computer simulation predicted that in most cases the observed repletion of red cells during the recovery period from hypogravity can be attributed to hemodilution-induced hypoxia (i.e., an effective anemia resulting from inflight red cell mass depletion and followed by postflight plasma refilling). The delayed recovery of red cell mass during the 28-day Skylab mission and the 28-day bedrest simulation of that mission was attributed in part to a normal 3-4 day bone marrow transit time and a time-lag in plasma volume recovery. The presence of an acute reticulocytosis following bedrest and its absence after a Skylab mission of the same length, suggests somewhat different mechanisms were operative in each case. The involvement of shifts in oxy-hemoglobin affinity, mild hemolysis, or ineffective erythropoiesis were suggested as areas of future study.

i) The hematological responses to bedrest and spaceflight were found to be more similar than different. Common characteristics of both stresses include the loss of red cell mass, loss of plasma volume, hemoconcentration, and, in some cases, the kinetics of recovery. In addition, the restricted dietary intake and diminished metabolic demands of bedrest are qualita-

tively similar to that exhibited on the shorter space-flights. However, the plasma volume losses may not occur in bedrest as rapidly as observed in spaceflight and the dynamics of hemoconcentration are somewhat different. Also, it is possible that the history of exercise during spaceflight compared to the history of inactivity during bedrest may be partly responsible for different kinetics of the recovery response. It is probable that at least two elements, a negative energy balance and negative water balance, may be important causative factors in both bedrest and spaceflight.

j) The red cell mass losses on the earlier spaceflights were attributed to the toxic effects of 100% oxygen atmosphere and a resulting intravascular hemolysis. The results of the present study suggest that many of the factors considered to explain the Skylab and bedrest observations, particularly, hemoconcentration, negative energy balance, and decreased physical activity undoubtedly also played a contributory role in the Gemini and Apollo flights. This helps to explain the large red cell mass losses observed during those relatively short flights.

The discussion in this section extends the analysis of the hematological responses originally presented in the Skylab postflight reports [25,26]. The lack of additional spaceflight experimentation in the intervening period precluded testing of newly developed hypotheses in a true weightless environment. Some of the experimental discrepancies revealed by the quantitative nature of model simulation analysis suggest approaches for future experimentation. For example, it is crucial to obtain direct in-flight measurements of erythropoietin and bone marrow activity. If reduced erythropoietin levels cannot be demonstrated during spaceflight, then the hemoconcentration theory may have to be abandoned. Also, the importance of diet and exercise on erythropoiesis needs to be studied more carefully in humans with and without accompanying hypogravity. The question has been raised whether moderate and relatively short periods of dietary or exercise restriction by themselves could alter red cell production in humans. At the very least, diet and exercise should be controlled more carefully on future missions in which the hematological system is under investigation. Another area that needs clarification is the possibility of some degree of cell destruction greater than the normal attrition rate, possibly related to the age of the red cell. This would require improved techniques to measure cell life span and biochemical products of cell destruction as well as inflight red cell mass measurements. The present analysis has also questioned the occurrence of inflight regeneration of red cell mass. Testing the regeneration hypothesis will require inflight measurements of red cell mass on flights lasting several months. While no U.S. manned flights of this duration are planned for the near future, data from the long-term Soviet mission might help to resolve this issue. In addition to inflight studies, the question of postflight kinetics was not entirely resolved. For example, it would be desirable to explain the presence of a reticulocytosis during the immediate post-bedrest period in contrast to a delayed reticulocytosis in a space-flight of comparable duration. Also, the profound influence that oxygen-hemoglobin affinity might exert on inflight and postflight tissue oxygenation as predicted by the model merits additional attention. The reader is referred to more recent research[‡‡] as well as to additional conclusions in Chapter 10.3.2 and recommendations in Appendix G.

References

1. Leonard, J. I., *The Applications of Systems Analysis and Mathematical Models to the Study of Erythropoiesis During Spaceflight*, (Rep. TIR 741-MED-4012, General Electric Co., Houston, TX), NASA CR-160218, Washington, DC, 1974.

2. Leonard, J. I., *Validation of a Model for Investigation Red Cell Mass Changes During Weightlessness*, (Rep. TIR 782-MED-6004, General Electric Co., Houston, TX), NASA CR-160188, NASA, Washington, DC, 1976.

3. Kimzey, S. L., Leonard, J. I., Buderer, M. C., and Johnson, P. C., A Computer Simulation of the Regulation of Erythropoiesis During Spaceflight, *Proc. 49th Ann. Aerospace Med. Assoc. Mtg*. pp 32, 1976.

4. Leonard, J. I., *Improvements and Validation of the Erythropoiesis Control Model for Bedrest Simulation*, (Rep. TIR 782-LSP-7012, General Electric Co., Houston, TX), NASA CR-160187, NASA, Washington, DC, 1977.

5. Leonard, J. I., Kimzey, S. L., and Dunn, C. D. R., Dynamic Regulation of Erythropoiesis: A Computer Model of General Applicability, *Exper. Hematology* vol. 9, pp. 355–378, 1981.

6. Leonard, J. I., Dunn, C. D. R. and Kimzey, S. L., Computer Simulation of Erythropoietic Suppression in a Potential Animal Model for Spaceflight. *Proc. 40th Ann. Aerospace Med. Assoc. Mtg.*, pp 16, 1979.

7. Dunn, C. D. R., Leonard, J. I., and Kimzey, S. L., Interaction of Animal and Computer Models in Investigation of the Anemia of Spaceflight. *Aviat. Space Environ. Med.* 52: 683–690, 1981.

8. Leonard, J. I., *Systems Parameters for Erythropoiesis Control Model: Comparison of Normal Values in Human and Mouse Model*, (Rep. TIR 741-LSP-8024, General Electric Co., Houston, TX), NASA CR-160401, NASA, Washington, DC,1978.

9. Kimzey, S. L., Leonard, J. I., and Johnson, P. C., A Mathematical and Experimental Simulation of the Hematological Response to Weightlessness. *Acta Astonautica*, 6: 1289–1303, 1979.

10. Leonard, J. I., *A Systems Analysis of the Erythropoietic Responses to Weightlessness*, Rep. TIR 2114-MED-5003, General Electric Co., Houston, TX, 1985.

[‡‡] This chapter summary was left intact from its original version, written in the early 1980's. Since that time some of the questions that were raised by the systems analysis have been addressed, although few new conclusive findings are available. The reader is referred to the Update Endnotes of this chapter.

11. Leonard, J.I., *Users Instructions for the Erythropoiesis Regulatory Model,* (TIR-741-LSP-8004, General Electric, Houston, TX), NASA CR-1690193, NASA, Washington, DC, 1978.

12. Dunn, C. D. R., Johnson, P. C., and Leonard, J. I., Erythropoietic Effects of Spaceflight Re-evaluated. *The Physiologist* 24: S5–S6, 1981.

13. Fischer, C. L., Johnson, P. C., and Berry, C. A., Red Blood Cell Mass and Plasma Volume Changes in Manned Spaceflight, *JAMA*, 200: 579–583, 1967.

14. Fischer, C. L., and Kimzey, S. L*., Effects of Oxygen on Blood Formation and Destruction. In: Underwater Physiology*, C.J. Lambertsen, Ed., Academic Press, New York, 1971, pp. 41–47.

15. Kimzey, S. L., The Effects of Extended Spaceflight on Hematologic and Immunologic Systems, *J. Amer. Med. Women's Assn*., 30: 218–232, 1975

16. Kimzey, S. L., Fischer, C. L., Johnson, P. C., Ritzmann, S. E., and Mengel, C. E., Hematology and Immunologies Studies, in *Biomedical Results of Apollo*, R. S. Johnston, L. F. Dietlein, and C. A. Berry, (Eds.), NASA SP-368, NASA, Washington, DC, 1975, pp. 197–266.

17. Larkin, E. C., Adams, J. D., Williams, W. T., and Duncan, D.M., The Hematologic Response to Hypobaric Hyperoxia. *Amer. J. Physiol*., 223: 431–437, 1972

18. Jaskunas, S. R., Stork, E. J., and Richardson, B., Effects of a Hyperoxic Environment on Erythropoietin Production, *Aerospace Med*., 44: 1112–1116, 1973,

19. Kimzey, S. L., A Review of Hematology Studies Associated with Spaceflight, *Third International Congress of Biorheology: Symposium on Hemorheology in Astronautics. Biorheology*, Vol. 16, 1979, Pergamon Press Ltd, pp. 13–21.

20. Morse, B. S., Erythrokinetic Changes in Man Associated with Bedrest, *Lectures in Aerospace Medicine*, 6th Series, School of Aerospace Medicine, Brooks AFB, TX, 1967, pp. 240–254.

21. Jensen, W. H., Contribution of Spaceflight to our Knowledge of Hematology, *Acta Astronautica*, 17: 223–227, 1972.

22. Berry, C. A., Medical Legacy of Skylab as of May 9, 1974: The Manned Skylab Missions, *Aviat. Space Environ. Med*., 47: 418–424, 1976

23. Kimzey, S. L., Ritzman, S. E., Mengel, C. E., and Fischer, C. L., Skylab Experiment Results: Hematology Studies, *Acta Astronautica*, 2: 141–154, 1975.

24. Kimzey, S. L., Johnson, P. C., Ritzman, S. E., and Mengel, C. E., Hematology and Immunology Studies: The Second Manned Skylab Mission, *Aviat. Space Environ. Med*. 47(4): 383–390, 1976.

25. Kimzey, S. L., Hematology and Immunology Studies, in *Biomedical Results from Skylab*, R.S. Johnston and L.F. Dietlein (Eds.), SP-377, NASA, Washington, DC 1977, pp. 249–281.

26. Johnson, P. C., Driscoll, T. B., and LeBlanc, A. D., Blood Volume Changes, in *Biomedical Results from Skylab*, R. S. Johnston and L. F. Dietlein (Eds.), SP-377, NASA, Washington, DC 1977, pp. 235–241.

27. Johnson, P. C., *The Erythropietic Effects of Weightlessness, in Current Concepts in Erythropoiesis*, C.D.R. Dunn (Ed.), John Wiley & Sons, Inc., 1983, pp. 279–300.

28. Van Beaumont, W., Greenleaf, J. E., and Juhos, L. J., Disproportional Changes in Hematocrit, Plasma Volume, and Proteins During Exercise and Bedrest, *J. Appl. Physiol.*, 3: 55–61, 1972.

29. Taylor, H. L., Erickson, L., Henschel, A., and Keys, A., The Effects of Bedrest on the Blood Volume of Normal Young Men, *Am. J. Physiol*., 144: 227–232, 1945.

30. Johnson, P. C., and Driscoll, T., Red Cell Mass and Body Volume Changes After 28 Days of Bedrest, *Report of 28-Day Bedrest Simulation of Skylab*, Vol. II, P.C. Johnson and C. Mitchell, (Eds.), NASA CR-151353, 1977.

31. Johnson, P. C., Fluid Volumes Changes Induced by Spaceflight, *Acta Astronautica*, 6: 1335–1341, 1979.

32. Johnson, P. C., Fisher, C. L., and Leach, C. S., Hematologic Implications of Hypodynamic States, in *Hypogravic and Hypodynamic Environments*, NASA SP-269, 1971, pp. 27–34.

33. Greenleaf, J. E., Bernauer, E. M., Juhos, L. T., Young, H. L., Morse, J. T., and Staley, R. W., Effects of Exercise on Fluid Balance and Body Composition in Man During 14-Day Bedrest*, J. Appl. Physiol*., *Respir. Environ. Exercise Physiol.,* 43: 126–132, 1977.

34. Shcherba, M. M., Moiseyeva, O. I., Volzhskaya, A. M., and Glazunov, Ye. N., Erythropoietic Properties of Plasma in Hypodynamia, *Fiziologicheskiy Zhurnal, SSSR im. N.M. Sechenova*, Vol. LXI, 1975, pp. 1625–1830, (in Russian); NASA Technical Translation, NASA TTF-17, 019, 1976.

35. Dunn, C. D., Lange, R. D., Kimzey, S. L., Johnson, P. C., and Leach C. S., Serum Erythropoietin Titers During Prolonged Bedrest: Relevance to the "Anaemia" of Spaceflight, *Eur. J. Appl. Physiol. Occup. Physiol*., 52(2): 178–182, 1984.

36. Dietlein, L. F., Skylab: A Beginning, in *Biomedical Results from Skylab*. R.S. Johnston and L. F. Dietlein, (Eds.), NASA SP-377, 1977, pp. 408–418.

37. Kimzey, S. L. and Johnson, P. C., Hematological and Immunological Studies, in *The Apollo–Soyez Test Project Medical Report*, NASA SP-411, Nicogossian, A.E. (Ed.), Washington, DC, U.S. Government Printing Office, 1977, pp. 101–118.

38. Berry, C. A., Medical Legacy of Skylab as of May 9, 1974: The Manned Skylab Missions, *Aviat. Space. Environ. Med* 47(4): 418–424, 1976.

39. Harris, J. W. and Kellermeyer, R. W. *The Red Cell*, Harvard University Press, Cambridge, MA, 1970.

40. Finch, C. A. and Lenfant, C., Oxygen Transport in Man, *N. Engl. J. Med*., 286: 407–415, 1972.

41. Hannon, J. P. and Vogel, J. A., Oxygen Transport During Early Altitude Acclimitization: A Perspective Study, *Europ. J. Appl. Physiol.*, 36: 285–297, 1977.

42. Krantz, S. B. and Jacobson, L. O., *Erythropoietin and the Regulation of Erythropoiesis,* Univ. of Chicago Press, Chicago, IL, 1970.

43. Wintrobe, M. M., *Clinical Hematology*, 6th ed., Lea and Febiger, 1973.

44. Gordon, A. S. and Zanjani, E. D., Some Aspects of Erythropoietin Physiology, in *Regulation of Hematopoiesis*, Chap. 19, A. S. Gordon (Ed.), Appleton-Century-Crofts, 1970.

45. Metcalf, J., and Dhindsa, D. S., The Physiological Effects of Displacement of the Oxygen Dissociation Curve, in *Oxy-*

gen Affinity of Hemoglobin and Red Cell Acid-Base Status, P. Astrup and M. Roth (Eds.), Academic Press, 1972, pp. 613–628.

46. Selkurt, E. E., The Renal Circulation, in *Handbook of Physiology*, Section 2: Circulation, Vol. II, Chap. 43, W. F. Hamilton and P. Dow (Eds.), 1963.

47. Hodgson, G., Application of Control Theory to the Study of Erythropoiesis, in *Regulation of Hematopoiesis*, Chapter 15. A. S. Gordon, (Ed.), Appleton-Century-Crofts, 1970.

48. Adamson, J. W., Parer, J. T. and Stamatoyannopoulous, G., Erythrocytosis Associated with Hemoglobin Rainier: Oxygen Equilibria and Marrow Regulation, *J. Clin. Invest.*, 48: 1376–1386, 1969.

49. Weil, J. V., Jamieson, G., Brown, D. W., Grover, R. F., Balchum, O. J. and Murry, J. F., The Red Cell Mass-Arterial Oxygen Relationship in Normal Man: Application to Patients with Chronic Obstructive Airway Disease, *J. Clin. Invest.*, 47: 1627–1639, 1968.

50. Aperia, A. C., Liebow, A. A., and Roberts, L. E., Renal Adaptation to Anemia, *Circ. Res.*, 22: 489–500, 1968.

51. Pitts, R. F., Physiology of the Kidney and Body Fluids, 2nd ed., Year Book Medical Pub., 1968.

52. Beutler, E., A Shift to the Left or a Shift to the Right in the Regulation of Erythropoiesis, *Blood*, 33: 496, 1969.

53. Guyton, A. C., Jones, C. E. and Coleman, T. G., *Circulatory Physiology: Cardiac Output and Its Regulation*, 2nd ed., W. B. Saunders, 1973.

54. Murray, J. F., Escobar, E. and Rapaport, E., Effects of Blood Viscosity on Hemodynamic Responses in Acute Normovolemic Anemia, *Amer. J. Physiol.*, 216(3): 638–642, 1969.

55. Repalogle, R. L. and Merrill, E. W., Experimental Polycythemia and Hemodilution, *J. Thor. Cardiov. Surg.*, 60: 582–588, 1970.

56. Richardson, T. Q. and Guyton, A. C., Effect of Polycythemia and Anemia on Cardiac Output and Other Circulatory Factors, *Amer. J. Physiol.*, 197(6): 1167–1170, 1954.

57. Fowler, N. O. and Holmes, T. C., Blood Viscosity and Cardiac Output in Acute Experimental Anemia, *J. Appl. Physiol.*, 39: 453–456, 1975.

58. Weisse, A. B., Regan, T. J., Nadimi, N., and Hellems, H. K., Late Circulatory Adjustments to Acute Normovolemic Polycythemia, *Amer. J. Physiol.*, 211(6): 1413–1416, 1966.

59. Thorling, E. B. and Erslev, A. J., The Tissue Tension of Oxygen and its Relation to Hematocrit and Erythropoiesis, *Blood*, 31: 332–343, 1968.

60. Castle, W. B. and Jandl, J. H., Blood Viscosity and Blood Volume: Opposing Influences Upon Oxygen Transport in Polycythemia, *Seminars Hemat.*, 3: 193–198, 1966

61. Kollias, J., Van Derveer, D., Dorchak, K. J. and Greenleaf, J.E., *Physiologic Responses to Water Immersion in Man: A Compendium of Research*, NASA TM-X 3308, 1976.

62. McCally, M., Plasma Volume Response to Water Immersion: Implications for Spaceflight, *Aerospace Med.*, 35: 130–132, 1964.

63. Lancaster, M., Hematologic Aspects of Bedrest, in *Hypogravic and Hypodynamic Environments*, NASA SP-269, NASA, Washington, DC, 1971, pp. 299–308.

64. Birkhill, F. R., Maloney, M. A., and Levenson, S. M., Effect of Transfusion Polycythemia Upon Bone Marrow Activity and Erythrocyte Survival in Man, *Blood*, 6: 1021–1023, 1951.

65. Gurney, C. W., and Pan, C., Studies on Erythropoiesis, IX: Mechanism of Decreased Erythropoiesis in Experimental Polycythemia, *Soc. Exp. Biol. Med. Proc.*, Vol. 98, pp. 789–793, 1958.

66. Dunn, C. D. R., and Lange, R. D., Erythropoietic Effects of Spaceflight: Further Studies in a Potential Animal Model, *Acta Astronautica*, 6: 725–732, 1979.

67. Kilbridge, T. M., Fried, W. and Heller, P., The Mechanism by Which Plethora Suppresses Erythropoiesis, *Blood*, 33, 104–113, 1969.

68. Dunn, C. D. R., Effect of Dehydration on Erythropoiesis in Mice: Relevance to the "Anemia" of Spaceflight, *Aviat. Space Environ. Med.* 49: 990–993, 1978.

69. Buderer, M. C. and Pace, N., Hemopoiesis in the Pig-Tailed Monkey Macaca Nemestrina During Chronic Altitude Exposure, *Amer. J. Physiol.*, 223: 346–352, 1972.

70. Huff, R. L., Lawrence, J. H., Siri, W. E., Wasserman, L. R., and Hennessy, T. G., Effects of Changes in Altitude on Hematopoietic Activity, *Medicine*, 30: 197–217, 1951.

71. Adamson, J. W., The Erythropoietin Hematocrit Relationship in Normal and Polycythemic Man: Implications of Marrow Regulation. *Blood, 32*: 597, 1968.

72. Erslev, A. J., and Silver, R. K., Compensated Hemolytic Anemia, in *Blood Cells*, Vol. 1, pp. 509–525, 1975.

73. Larkin, E. C., Adams, J. D., Williams, W. T. and Duncan, D. M., The Hematologic Response to Hypobaric Hyperoxia, *Amer. J. Physiol.*, 223: 431–437, 1972.

74. Michel, E. L., Rummel, J. A., Sawin, C. F., Buderer, M. C., and Lem, J. D., Results of Skylab Medical Experiment M171 – Metabolic Activity, in *Biomedical Results of Skylab*, R. S. Johnston and L. F. Dietlein (Eds.), NASA SP-377, NASA, Washington, DC, 1977, pp. 372–387.

75. Malkin, V. B., *Foundations of Space Biology and Medicine*, Vol. II, Book 1, Chapter 1, M. Calvin and O.G. Gazenko (Eds.), NASA, Washington, DC, 1975.

76. Stevens, P. M., Miller, P. B., Lynch, T. N., Gilbert, C., Johnson, R. L., and Lamb, L. E., Effects of LBNP on Physiologic Changes Due to Four Weeks of Hypoxic Bedrest, *Aerospace Med.*, 37: 466–474, 1966.

77. Astrup, P., Garby, L., and deVerdier, C. H., Displacement of the Oxyhemoglobin Dissociation Curve, *Scand. J. Clin. Lab. Invest.*, 22: 171–176, 1968.

78. Parer, J. T., Oxygen Transport in Human Subjects with Hemoglobin Variants Having Altered Oxygen Affinity. *Resp. Physiol.*, 9: 43–49, 1970.

79. Brewer, G. J., and Eaton, J. W., Erythrocyte Metabolism: Interaction with Oxygen Transport, *Science*, 171: 1205–1211, 1971.

80. Lenfant, C., Torrance, J. D., and Reynafarje, C., Shift of the O_2-Hb Dissociation Curve at Altitude: Mechanism and Effect, *J. Appl. Physiol.*, 30(5): 625, 1971.

81. Kennedy, A. C. and Valtes, D. J., The Oxygen Dissociation Curve in Anemia of Various Types, *J. Clin. Invest.*, 33: 1372–1381, 1954.

82. Woodson, R. D., Torrance, J. D., Shappell, S. D., and Lenfant, C., The Effects of Cardiac Disease on

Hemoglobin-Oxygen Binding, *J. Clin. Invest.*, 49: 1349–1356, 1970.

83. Hillman, R. S., and Finch, C. A., *Red Cell Manual*, Fourth ed., F.A. Davis Co., 1974.

84. Duc, G., and Engel, K., Effect of 2,3-DPG Concentration on Hemoglobin Oxygen Affinity of Whole Blood, *Scand. J. Clin. Lab. Invest.*, 24: 405–412, 1969.

85. Brewer, G. J., 2,3-DPG and Erythrocyte Oxygen Affinity, *Ann. Rev. Med.*, 25: pp. 29–38, 1974.

86. Bunn, H. F., and Jandl, J. H., Control of Hemoglobin Function Within the Red Cell, *N. Engl. J. Med.*, 282: 1414–1470, 1970.

87. Mengel, C. E., Red Cell Metabolism Studies on Skylab, in *Biomedical Results from Skylab*, R.S. Johnston and L. F. Dietlein (Eds.), SP-377, NASA, Washington, DC 1977, Chap. 27, pp. 242–248.

88. Leach, C. S., and Rambaut, P. C., Biochemical Responses of the Skylab Crewmen: An Overview, in *Biomedical Results from Skylab*, R. S. Johnston and L. F. Dietlein (Eds.), SP-377, NASA, Washington, DC 1977, Chap. 27, pp. 204–216.

89. Granger, H. J., Goodman, A. H. and Cook, B. H., Metabolic Models of Microcirculatory Regulation, *Fed. Proc.*, Vol. 34, pp. 2025–2030, 1975.

90. Takaku, F., Hirashima, K., and Nakao, K., Studies on the Mechanism of Erythropoietin Production. I. Effects of Unilateral Construction of the Left Renal Artery, *J. Lab. Clin. Med.*, 59: 815–820, 1962.

91. Fisher, J. W., and Samuels, A. I., Relationship Between Renal Blood Flow and Erythropoietin Production in Dogs, *Proc. Soc. Exp. Biol. Med.*, Vol. 125, pp. 482–485, 1967.

92. Adamson, J. W., and Finch, C. A., Hemoglobin Function, Oxygen Affinity, and Erythropoietin, *Ann. Rev. Physiol.*, 37: p. 351, 1975.

93. Pimme, T. E., Body Fluid Volume and Renal Relationships to Gravity, in *Hypodynamics and Hypogravics—The Physiology of Inactivity and Weightlessness*, M. McCally, (Ed.), Academic Press, 1968.

94. Epstein, M. Renal Effects of Head-Out Water Immersion in Man: Implications for an Understanding of Volume Homeostasis, *Physiol. Rev.*, 58: 529–81, 1978.

95. Fuller, J. H., Bernauer, E. M. and Adams, W. C., Renal Function, Water, and Electrolyte Exchange During Bedrest With Daily Exercise, *Aerospace Med.*, 41: 60–72, 1970.

96. Melada, G. A., Goldman, R. H., Luetscher, J. A., and Zager, P. G., Hemodynamics, Renal Function, Plasma Renin, and Aldosterone in Man After 5–14 days of Bedrest, *Aviat. Space and Environ. Med.,* 46: 1049–1055, 1975.

97. Migdal, S., Alexander, E. A., Burns, F. J., Riley, A. L., and Levinsky, N. G., Effect of Hemodilution of the Distribution of Renal Blood Flow, *Circ. Res.*, 36: 71–74, 1975.

98. Graybiel, A., Miller II, E. F., and Homick, J. L., Experiment M131. Human Vestibular Function, I. Susceptibility to Motion Sickness, in *Biomedical Results from Skylab*, R. S. Johnston and L. F. Dietlein (Eds.), SP-377, NASA, Washington, DC 1977, Chap. 11, pp. 74–91.

99. Dietrick, J. E., Whedon, G. D., and Shorr, E., Effects of Immobilization Upon Various Metabolic and Physiological Functions of Normal Men, *Am. J. Med.,* 4(3), 1948.

100. Rambaut, P. C., Heidelbaugh, N. D., Reid, J. M. and Smith, M. C., Caloric Balance During Simulated and Actual Flight, *Aerospace Med.*, 44: 1264–1269, 1973.

101. Rambaut, P. C., Leach, C. S., and Leonard, J. I., Observations in Energy Balance in Man During Spaceflight. *Amer. J. Physiol.*, 233: R208–R212, 1977.

102. Muldowney, F. P., and Healy, J. J., Lean Body Mass and Total Body Potassium, in *Compartments, Pools, and Spaces in Medical Physiology*, Per-Erik E. Bergner, C. C. Lushbauch and E. Anderson (Eds.), 1967, pp. 95–110.

103. Scheuer, J., and Tipton, C., Cardiovascular Adaptations to Physical Training, *Ann. Rev. Physiol.,* 39: 221–251, 1977.

104. Miller, P. B., Johnson, R. L., and Lamb, L. E., Effects of Moderate Physical Exercise During Four Weeks of Bedrest on Circulatory Functions in Man, *Aerospace Med.*, 36: 1077–1082, 1965.

105. Sjostrand, T., Blood Volume, Handbook of Physiology, Section 2: Circulation, *Amer. Physiol. Soc.*, Vol. 1, Chap. 4, 1962, p. 51.

106. Rocker, L., Kirsh, K. A., and Stoboy, H., Plasma Volume, Albumin and Globulin Concentrations and Their Intravascular Masses, *Eur. J. Appl. Physiol.*, 36: 57–64, 1976.

107. Holmgren, A., Effect of Training on Work Capacity, Total Hemoglobin, Blood Volume, Heart Volume, and Pulse Rate in Recumbent and Upright Positions, *Acta Physiol. Scand.*, 50: 72–83, 1960.

108. Bruce, R. A., Kusumi, F., Culver, B. H. and Buttler, J., Cardiac Limitations to Maximal Oxygen Transport and Changes in Components After Jogging Across the U.S., *J. Appl. Physiol.*, 39: 958–964, 1975.

109. Broun, G. O., Blood Destruction During Exercise: III. Exercise as a Bone Marrow Stimulus, and IV. The Development of Equilibrium Between Blood Destruction and Regeneration After a Period of Training, *J. Exp. Med.*, 37: 187–220, 1923.

110. Radomski, M. W., Sabiston, B. H., and Isoard, P., Development of Sports Anemia in Physically Fit Men After Daily Sustained Submaximal Physical Exercise, *Aviat. Space Environ. Med.*, 51: 41–45, 1960.

111. Reissmann, K. R., Protein Metabolism and Erythropoiesis, II. Erythropoietin Formation and Erythroid Responsiveness in Protein-Deprived Rats, *Blood*, 23, 146–153, 1964.

112. Anagnostou, A., Schade, S., Ashkinaz, M., Barone, J. and Fried, W., Effect of Protein Deprivation on Erythropoiesis, *Blood*, 50: 1093–1097, 1977.

113. Fried, W., Vlzak, L. F., Jacobson, L. O. and Goldwasser, E., Studies on Erythropoiesis III. Factors Controlling Erythropoietin Production, *Proc. Soc. Exp. Biol. Med.*, 94: 237–241, 1957.

114. Naets, J. P., and Wittek, M., Effect of Starvation on the Response to Erythropoietin in the Rat, *Acta Haematol.* 52(3): 141–150, 1974.

115. Giglio, J. M., Alippi, R. M., Barcelo, A. C., and Bozzini, C. E., Mechanism of the Decreased Erythropoiesis in the Water Deprived Rat, *Brit. J. Hematol.*, 42: 93–99, 1979.

116. Thornton, W. W., Anthropometric Changes in Weightlessness, in *Anthropometric Source Book*, Vol. 1, *Anthropometry for Designers*, Reference Publication NASA RP-1024, NASA, Washington, DC, 1978.

117. Leonard, J. I., *Energy Balance and the Composition of*

Weight Loss During Prolonged Spaceflight, (Report TIR 2114-MED-2012, General Electric Co., Houston, TX), NASA CR-17145, NASA, Washington, DC, 1982.

118. Dunn, C. D. R., Effect of Food or Water Restriction on Erythropoiesis in Mice: Relevance to the Anemia of Space-flight, *Amer. J. Physiol.*, 238(5): R301–305, 1980.

119. Schooley, J. C., Responsiveness of Hematopoietic Tissue to Erythropoietin in Relation to the Time of Administration and Duration of Action of the Hormone, *Blood*, Vol. 25**,** pp. 795, 1965.

120. Kretchmar, A. L., Erythropoietin: Hypothesis of Action Tested by Analog Computer, *Science*, Vol. 152, pp. 367–370, 1966.

121. Gurney, C. W., Wackman, N., and Filmanowicz, E., Studies on Erythropoiesis, XVII. Some Quantitative Aspects of the Erythropoietic Response to Erythropoietin, *Blood*, 17: pp. 531, 1961.

122. Mylrea, K. C., and Abbrecht, P. H., Use of Systems Tech-niques in the Analysis of the Control of Erythropoiesis, Chemical Engineering in Medicine, *American Chemical Society Advances in Chemistry Series*, Vol. **118,** 1973, pp. 218–235.

123. Alfrey, C. P., Rice, L., Udden, M. M., Driscoll, T.B., Neocytolysis: Physiological Down-Regulator of Red-Cell Mass, *Lancet*, 349(9062): 1389–1390, 1997.

124. Dietlein, L. F., Skylab: A Beginning, in *Biomedical Results from Skylab*, R. S. Johnston and L. F. Dietlein (Eds.), SP-377, NASA, Washington, DC, 1977, pp. 408–418.

125. Swisher, S. N., *Proceedings of the Skylab Life Sciences Symposium*, Vol. II. NASA TMX-58154, Johnson Space Center, Houston, TX, 1974, pp. 837–839.

126. Thornton, W. T., and Rummel, J. A., Muscular Deconditioning and Its Prevention in Spaceflight, in *Biomedical Results from Skylab* (NASA SP-377), R. S. Johnston, and L. F. Dietlein (Eds.), NASA, Washington, DC, 1977, pp. 191–197.

127. Rummel, J. A., Sawin, C. F., Michel, E. L., Buderer, M.C. and Thornton, W.T., Exercise and Long Duration Space-flight through 84 days. *J. Am. Med. Womens Assoc.*, 30(4): 173–187, 1975.

128. Napier, J. A. F., Dunn, C. D. R., Ford, T. W., and Price, V., Pathophysiological Changes in Serum Erythropoiesis Stimulating Activity, *Brit. J. Hematol.* 35: 403–409, 1977.

129. Dunn, C. D. R., Jarvis, J. H., and Napier, J. A. F., Changes in Erythropoiesis and Renal Ultrastructure During Expo-sure of Mice to Hypoxia, *Exp. Hemat.*, 4: 365–381, 1976.

130. Jain, S. C., Malhotra, M. S., Krishna, B., Bardhan, J., and Grover, A., Hematologic Changes in Rabbits During Ac-climatization, and Reinduction to Hypoxia, *Aviat. Space, Environ. Med.*, 49: 952–958, 1978.

131. Huff, J. E., Kaufman, G. E., and Ingram, M., Hematologic Changes in Mice During and After Exposure to Severe Hypobaric Hypoxia, *Aviat. Space Environ. Med.*, 46(9): 1147–1151, 1975.

132. Miller, P. B., Johnson, R. L., and Lamb, L. E., Effects of Four Weeks of Absolute Bedrest on Circulatory Functions in *Man. Aerospace Med.*, 35: 1194–1200, 1964.

133. Hyatt, K. H., Hemodynamic and Body Fluid Alterations Induced by Bedrest, in *Hypogravic and Hypodynamic En-vironments*. R.H. Murray and M. McCally, (Eds.), NASA SP-269, 1971.

134. Shvets, V. N., and Portugalov, V. V., Spaceflight Effects on the Hemopoietic Function of Bone Marrow of the Rat, *Aviat. Space Environ. Med.*, 47: 746–749, 1976.

135. Abbrecht, P. H., and Littell, J. K., Erythrocyte life-span in mice acclimatized to different degrees of hypoxia. *J. Appl Physiol*. Apr; 32(4): 443–445, 1972.

136. Kirk, T., Orr, J. S., and Hope, C. S., A Mathematical Analy-sis of Red Blood Cell and Bone Marrow Stem Cell Control Mechanisms, *Brit. J. Hematol.*, 15: 35–46, 1968.

137. Stohlman, Jr., F., Erythropoiesis, *N. Engl. J. Med.*, 167: 392–399, 1962.

138. Nusynowitz, M. L., Blumhardt, R., and Volve, J., Plasma Volume in Erythemic States, *Amer. J. Med. Sci.*, 267(1): 31–34, 1974.

139. Sanchez, C., Merino, C., and Figallo, M., Simultaneous Measurement of Plasma Volume and Cell Mass in Poly-cythemia of High Altitude, *J. Appl. Physiol.*, 28(6): 775–778, 1970.

140. Nordheim, A.W. and Leach, C.S., A computer simulation of the effect of the proposed Spacelab-1 blood draw proto-col on the human red cell system, *Proc. Aerospace Med. Assoc.,* 1983.

141. Leach, C.S. and Johnson, P.C., Influence of spaceflight on erythrokinetics in man, *Science, 225:* 216–218, 1984.

142. Leach, C.S., Chen, J.P., Crosby, W., Johnson, P.C., Lange, R.D., Larkin, E., and Tavassoli, M., Hematology and bio-chemical findings of Spacelab-1 flight, *Regulation of Erythro-poiesis,* Zanjani, E.D., Tavassoli, M., and Ascensao, J.L (Eds), PMA Publishing Corp., New York, 1988, pp. 415–453.

143. Leach, C.S., Johnson, P.C., and Cintron, N.M., The endocrine system in spaceflight, *Acta Astronautica,* 18:161–166, 1988.

Update Endnotes

UPDATE #1. Renal Oxygen Sensing Site (TBD)

Recent research regarding the renal oxygen sensing site including the influence of renal blood flow.

UPDATE #2. Effect of Exercise (TBD)

Recent findings on the effects of exercise on erythro-poiesis and red cell destruction.

UPDATE #3. Neocytolysis in Spaceflight (TBD)

Recent findings on SLS-1 (1991 and 1993) have sug-gested a newly identified process, called "neocytolysis" by which newly formed red cells are selectively destroyed in response to a sustained hyperoxic stimulus such as spaceflight hemoconcentration or descent from altitude of high altitude dwellers [123].

UPDATE #4. Erythropoietin Assays (TBD)

Recent progress on assays for erythropoietin and their use in spaceflight research.

UPDATE #5. Recent Bedrest Findings (TBD)

Recent measurements of red cell production and eryth-ropoietin during bedrest.

Chapter 7
Cardiovascular Regulation During Spaceflight*

7.1 Introduction

One of the well-known effects of spaceflight in humans is cardiovascular deconditioning that manifests itself as reductions in orthostatic tolerance and postflight exercise capacity [1,2]. The alterations are significant and have consistently been observed in several studies from the early days of spaceflight in both the US and Russia [3]. A number of changes in cardiovascular parameters contribute to these decrements, the loss of blood volume being perhaps the most central among them [4].

Prior to extensive studies conducted during the Skylab missions, the assessment of space cardiovascular changes were inferred mostly from pre- and post-flight measurements. The three manned Skylab missions were the first attempt to evaluate both acute and adaptive changes that occur under hypogravic conditions and to understand the underlying physiologic mechanisms. The constraints of spaceflight and concern over possible risks in using invasive procedures in a space environment limited the measurements to those that could be readily obtained by non-invasive means. Still, a wealth of information was gathered from which a composite picture could be pieced together and plausible hypotheses could be formulated. After 30 years the Skylab experiments still stand as the best long-duration (90-day) space-based study of exercise and orthostatic tolerance.

The exercise stress test using bicycle ergometry and the orthostatic stress test with application of pressures below the ambient level to the lower extremities of the body (known as lower body negative pressure or LBNP) were two important Skylab tests designed for examining the ability of the cardiovascular system to cope with the physiological challenges of spaceflight. The results of these tests were not always easy to interpret because of the narrow breadth of measured variables and led to hypotheses for explanation rather than definitive conclusions. With inflight studies for obtaining needed additional data at least a decade away, the researchers thought that mathematical models could be helpful for testing the validity of various candidate hypotheses through computer simulation.

This chapter describes the effort of the systems analysis project to interpret the data from Skylab cardiovascular experiments in the context of mathematical modeling and computer simulation. As in other chapters of this book, the emphasis is on the utility of mathematical models in discerning physiologic mechanisms that would lead to the observed results. In addition to analyses pertaining to the Skylab results, this study examined orthostatic intol-erance during the reentry phase of the, then, new Space Shuttle, and is an example of the systems analysis methodology to help resolve an ongoing medical operational problem. Also discussed are improvements in cardiovascular modeling needed for testing other candidate mechanisms and more recent model developments aimed at simplifying the model specifically for simulating orthostatic stress responses.

7.2 Model of Cardiovascular System

The cardiovascular model used in the analyses discussed in this chapter is a multi-compartment representation of the cardiovascular system with lumped parameters that consist mostly of resistances and compliances. It is a beat-to-beat model built on the assumption of a closed vascular system, with no provision for fluid filtration into the extravascular space. The omission of capillary filtration and endocrine control were justified on the basis that it is a short-term model intended to simulate responses lasting less than 30 minutes. The pressure-volume relationships in many (but not all) of the compartments are non-linear; this feature will be important in the analysis of LBNP findings. Chapter 3.2.1 contains a detailed description of the model which was originally developed by Croston [5] for simulating exercise responses (EXER model). It was later simplified for simulating responses to head-up tilt and lower body negative pressure (LBNP model) by excluding the metabolic control elements and adding the capability to respond to different compression and gravitational forces [6]. Thus, the two versions of the model differ mostly in the way the cardiovascular control is represented.

Figure 3-15 shows the cardiovascular control system for the EXER model while Fig. 7-1 shows the simplified cardiovascular control representation associated with the LBNP model. The latter model consists essentially of the baroreceptor system with control signals derived from carotid and aortic pressures for acute regulation of heart rate, strength of cardiac contraction, venous tone, and some peripheral resistances. Although admittedly incomplete in many respects, the pulsatile cardiovascular model has proven to be an excellent tool to systematically explore and analyze conceivable underlying physiologic mechanisms and to provide an integrated picture of the observed cardiovascular changes in microgravity.

The Skylab studies on metabolic activity and LBNP were specifically aimed at elucidating cardiovascular adaptation to weightlessness. The adaptive changes include reductions in orthostatic tolerance and postflight exercise
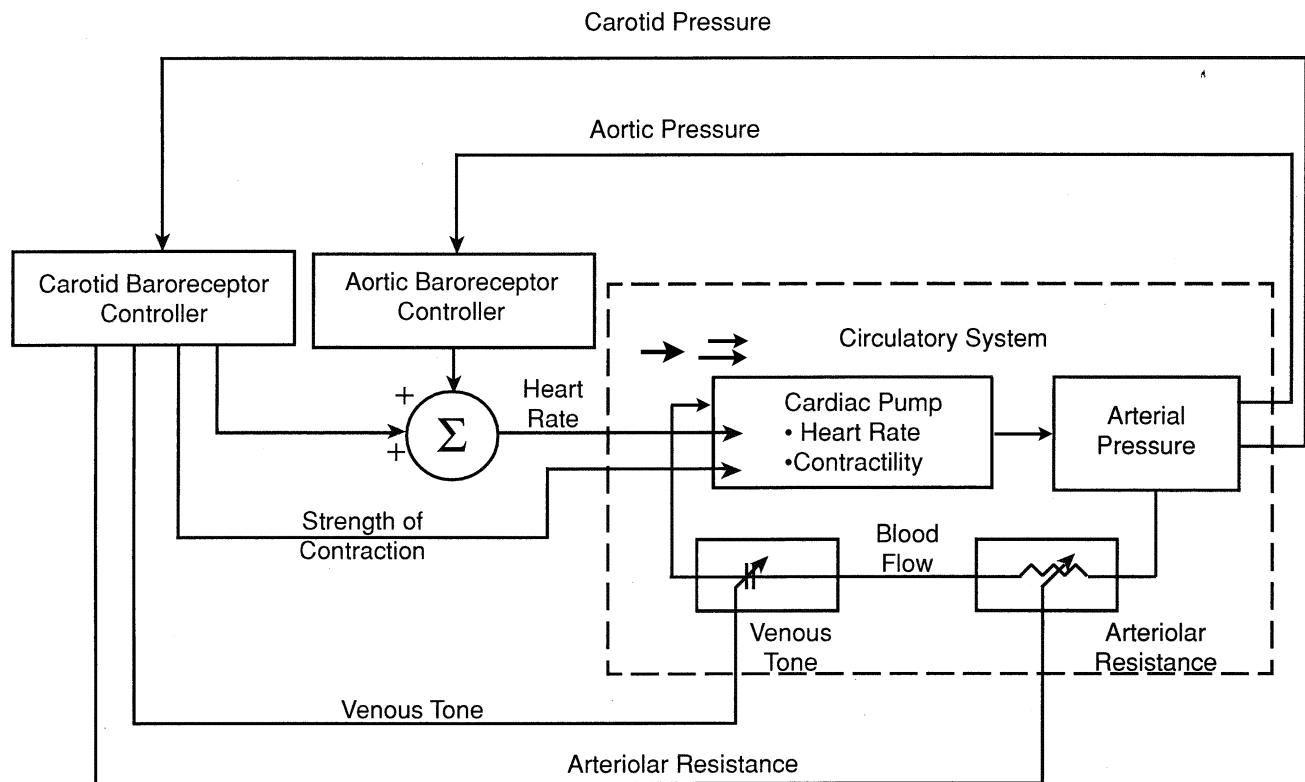
Figure 7-1. Simplified controlling system associated with the LBNP model of the cardiovascular system.

capacity, weight loss, decrements in blood and leg volumes, changes in leg venous compliance, and a reduction of heart size, among others. We describe below the two Skylab experiments and discuss the analyses that were performed using these mathematical models of the cardiovascular system to explain some of the observations.

7.3 Skylab Metabolic Activity (Exercise) Studies

7.3.1 Experimental Observations

The alterations in metabolic activity caused by exposure to weightlessness were assessed with graded levels of exercise performed by Skylab crewmen while seated on a bicycle ergometer. In addition to heart rate and blood pressure, oxygen consumption and carbon dioxide output were monitored with measurements of flow and gas concentrations of inspired and expired breathing mixtures. The protocol consisted of rest, exercise at 25%, 50%, and 75% of maximal oxygen consumption, and recovery, each test segment lasting for 5 min with a total test period of 25 min. Inflight tests were performed 6 times on Skylab-2 (28-day mission), 9 times on Skylab-3 (59-day mission), and 12 times on Skylab-4 (84-day mission) on each astronaut at regular intervals during the mission [7]. Pre- and postflight tests included exercise in both supine and sitting positions for comparison with inflight results.

The cardiovascular response to exercise [7,8,9,10] showed no change or a slight decrease in inflight heart rate for a given workload compared to preflight. Also, there was no change in mean arterial pressure and oxygen uptake inflight compared to preflight. However, physical deconditioning was particularly apparent during postflight testing. Early postflight measurements showed a significant increase in heart rate and a decrease in cardiac output during exercise. The degradation of cardiovascular performance immediately upon return was consistent with observations from all earlier spaceflights [3].

Thus, an important finding from the metabolic activity studies was that exercise capacity, observed to be diminished postflight in all spaceflight studies, showed no appreciable decrease inflight. In addition, the postflight reduction in exercise capacity was smaller in the crewmen of Skylab-4 than in those of Skylab-2 and Skylab-3 [2,7]. Skylab-4 astronauts engaged in longer and more strenuous personal exercise throughout their entire mission, between 150% to 300% greater than on Skylab-2 or Sklylab-3 [10]. Two hypotheses were suggested to explain these findings:

a) The resting blood volume, although reduced in weightlessness, might still be adequate to meet the inflight metabolic needs, perhaps because plasma hemoglobin concentration was higher and tissue oxy-

gen delivery was not greatly altered (see Chapter 6).

b) Crewmen of Skylab-4 might have undergone some physical conditioning during their spaceflight due to increased levels of exercise, and this training effect could be the reason for the observed improvement in their postflight exercise capacity.

7.3.2 Model Analysis

An analysis of the exercise findings was performed to determine if the effects of training could account for the lesser reduction in postflight exercise capacity exhibited by Skylab-4 crewmen. The approach for accomplishing this was as follows:

a) identify the physiological effects of one-g exercise training (conditioning) that could be responsible for a possible training effect in Skylab-4;

b) identify the physiological effects of zero-g adaptation (deconditioning) that would be expected to influence the inflight and postflight exercise response if there were no training effect, i.e., Skylab-2 and –3;

c) determine, through model simulation if there is some combination of deconditioning and conditioning effects that can explain the overall Skylab results.

7.3.2.1 Model Validation and Exercise Conditioning.
Validation of the EXER model for simulating simple exercise, uncomplicated by training effects, was accomplished as part of the model development procedure and was described in Chapter 3 (Chapter 3.2.1.4 and Fig. 3-16). As part of the Whole-Body Algorithm, the EXER model subsystem was validated for simulating simple exercise (Fig. 3-47) and for simulating supine exercise before and after 28 days of bedrest (see Chapter 9, Fig 9-9).

A special validation study was conducted to determine if known training effects could be introduced into the model in order that a simulation of the exercise response of trained athletes could be accomplished. The following changes, supported by the data of Ekblom et al. [11], were introduced in the EXER model by adjusting the values of appropriate parameters to account for the effects of exercise training observed in athletes (at rest unless otherwise stated):

(a) reduced sympathetic activity;
(b) decreased arteriolar vasodilation (neurogenic term) during exercise, and hence increased peripheral resistance;
(c) a larger heart with increased contractility;
(d) increased leg capillary density, and
(e) increased vagal activity at rest to account for lower resting heart rate due to training.

Figure 7-2 illustrates the effects of training on oxygen uptake, blood pressure, arterio-venous oxygen difference, heart rate, stroke volume, and cardiac output. The simulated results agree reasonably well with experimental data, showing the ability of the model to reproduce changes in cardiovascular response due to the physical conditioning effects which have been listed above.

7.3.2.2 Hypogravic Deconditioning.
Although it is known that spaceflight induced-cardiovascular deconditioning manifests itself in terms of orthostatic intolerance and decreased exercise performance, the fundamental physiological mechanisms that bring about these changes in microgravity are not well understood and are the subject of ongoing research, including the current systems analysis effort. Accordingly, a set of hypotheses was formulated that represents the effects of spaceflight on the circulatory system, and that could help account for observations of cardiovascular performance. The following four hypotheses were identified as occurring during or following bedrest or spaceflight:

a) Increased sympathetic activity,
b) Increased peripheral resistance,
c) Decreased total blood volume, and
d) Decreased leg capillary density.

Some of these hypothesis have an experimental basis, such as a decreased blood volume (Chapter 6); some of them are inferred from other measurements, such as elevated catecholamine and angiotensin levels found in long-duration spaceflight [12,13] (see Fig. 9-5) suggesting increased sympathetic activity and peripheral resistance, respectively. Changes in vascularization (leg capillary density) are more speculative because they are difficult to measure, but are known to increase in individuals undergoing long-term training [11]. Mathematically, this would be represented in the model in a similar fashion to the phenomenon of venous stress relaxation, i.e., an increase in unstressed volume. In exercise training such as running or bicycling, the demand of the leg muscle tissues to increased blood supply causes an adaptive increase in vascularization (increased number of capillaries). For spaceflight, reverse stress relaxation and devascularization is postulated for the leg circulatory system because veins are collapsed at rest in space and leg postural muscles do not require as robust a circulation as they do on the ground. Chapter 7.4.3.6.2 describes the stress relaxation phenomenon with regard to interpreting LBNP results. These hypotheses for hypogravity deconditioning can be thought of as a companion set of hypotheses to those postulated for exercise conditioning (identified above); so they parallel each other in a sense, often having opposite effects.

7.3.2.3 Simulation of Conditioning versus Deconditioning.
Model simulations were performed for one-g exercise (50W) for three cases using the appropriate set of hypotheses as described above: a) Normal EXER model representing Preflight exercise, b) EXER model with "deconditioning" hypotheses representing an immediate postflight exercise test following a long-duration spaceflight, and c) EXER model with "conditioning" hypotheses representing an exercise test following a long-term training regimen. These model results were then compared to responses of the Skylab crew during their immediate post-
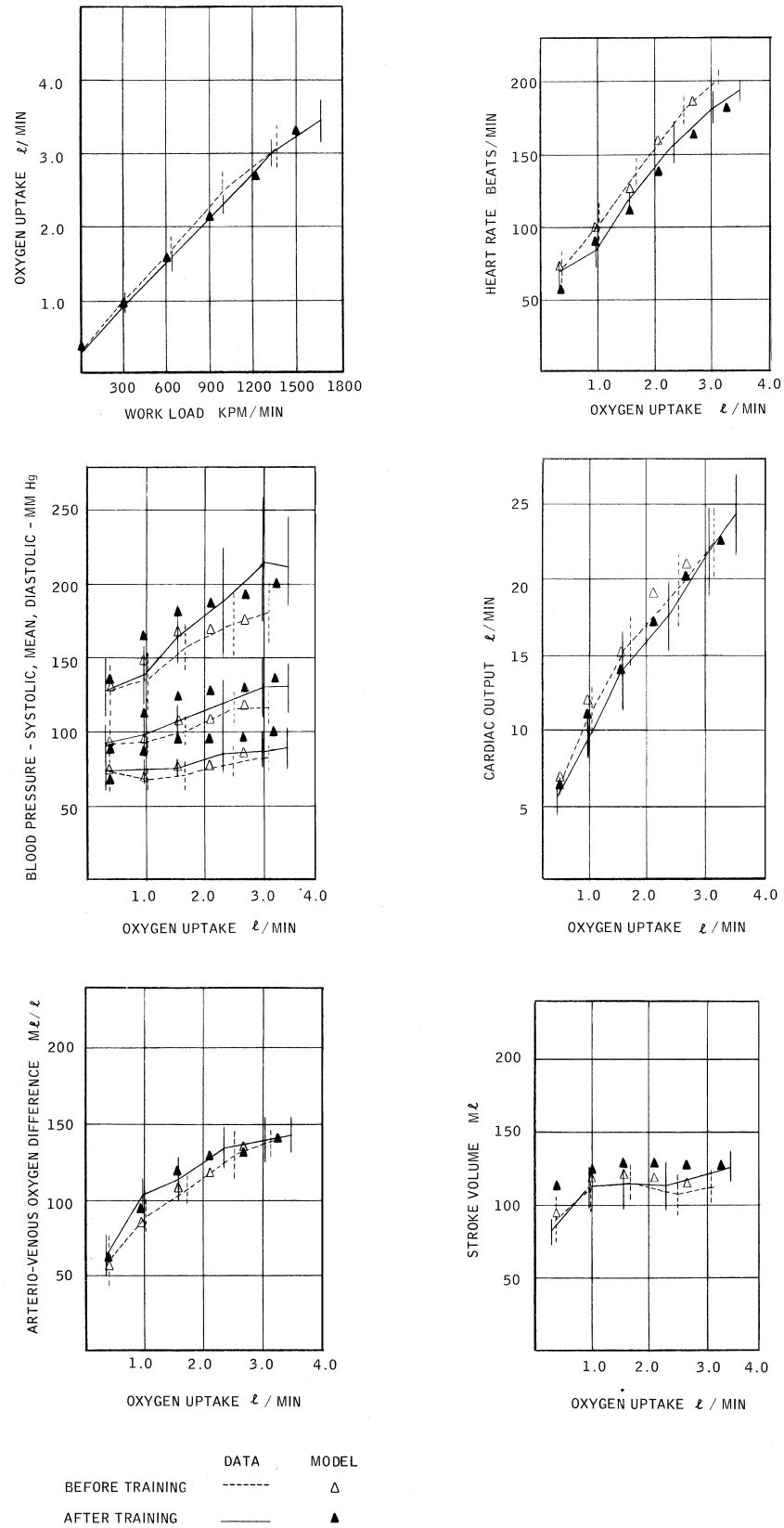
Figure 7-2. Comparison of trained and untrained steady-state exercise responses generated by the EXER model with experimental data [11].
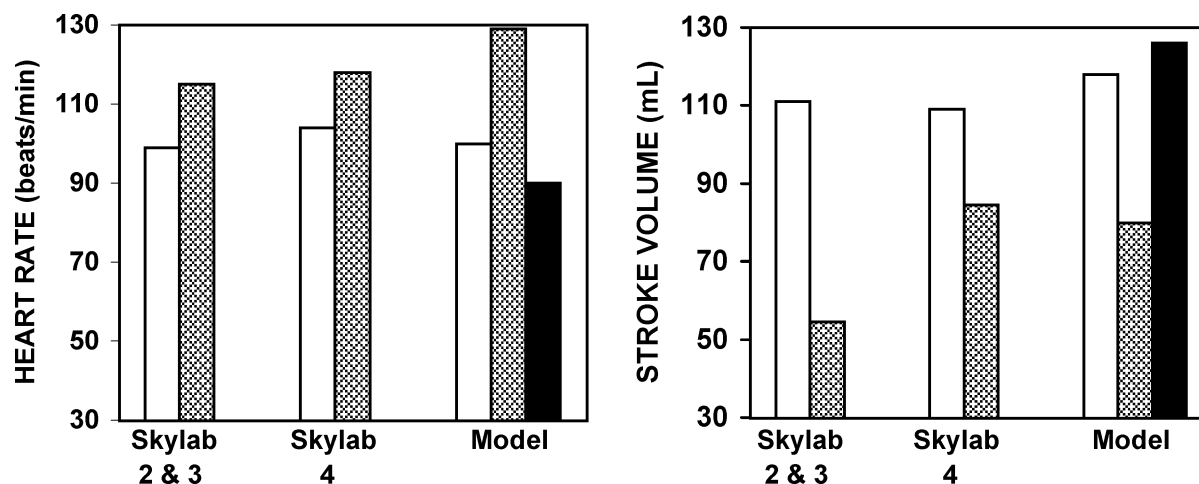
Figure 7-3. Comparison of hemodynamic variables, heart rate and stroke volume, for Skylab astronauts with EXER model responses resulting from exercise at 50 watts. The Skylab data for the first two missions (Skylab-2 and -3) are grouped together (see text). The first two pairs of columns in each panel compare preflight (clear bars) with postflight (shaded bars) measurements. The model responses includes the normal condition representing preflight (clear bars), weightlessness conditions (shaded bars), and training effects (filled bars).

flight tests. All tests and simulations were performed in the sitting position.

Figure 7-3 compares the pre- and postflight Skylab measurements of heart rate and stroke volume in response to exercise at 50W with simulated responses using the EXER model. The data from Skylab-2 and Skylab-3 crews were combined because they were similar compared to the Skylab-4 crew. Although the increase in heart rate between preflight and postflight was similar for all crewmembers, the postflight-to-preflight decrease in stroke volume is significantly smaller in Skylab-4 astronauts possibly due to the influence of exercise training. The larger stroke volume decrease for the Skylab 2 & 3 crews is an indication of cardiovascular deconditioning. The simulated "model" responses for weightlessness (hatched bar) and training effects (filled bar) are also shown separately and can be compared to the simulation without either weightlessness or training effects (clear bar).[*]

As indicated by the simulation results in Fig. 7-3, hypogravic deconditioning (model: hatched bar) increases the heart rate and decreases the stroke volume from the normal levels, while the opposite is the case with exercise training (model: filled bar). Thus, the model appears to confirm that training effects could have been responsible for the improved Skylab-4 crews postflight response to exercise. An appropriate combination of conditioning and deconditioning effects should yield results close to those observed in Skylab-4 mission, if indeed inflight exercise training is the reason for the improved postflight exercise capacity.

Accordingly, several hypotheses were formulated that were designed to test the deconditioning or conditioning hypotheses or some combination of the two. These hypotheses were the basis of a series of simulations, the results of which were compared to responses of the Skylab-4 crewmembers. The following hypotheses were formulated and tested:

0. Normal model (1-g mode)
1. Increased sympathetic activity affecting heart rate only,
2. Reduced blood volume only (250 ml),
3. Combination of 1 and 2 above,
4. Increased peripheral resistance only, and
5. Increased sympathetic activity on heart rate, increased peripheral resistance, increased heart contractility, and 100 ml of blood volume loss uncompensated by vascular changes.

The first item on the list is the control hypothesis representing preflight; #1 through #4 are relatively simple hypotheses; #5 is a selected complex hypothesis. The uncompensated blood volume loss in hypothesis #5 refers to the net blood volume loss (250 ml) less the quantity of estimated reverse stress relaxation in the legs (150 ml).

Figures 7-4(a) and 7-4(b) compare the average data from Skylab-4 astronauts with simulation results obtained by incorporating each hypothesis in the EXER model through appropriate changes of model parameter values. Preflight data (A) should be compared with the simulation with no special effects (0), i.e., the normal 1-g model. Clearly, a reduction in blood volume, which is known to occur in spaceflight (hypothesis #2), cannot by itself explain the observed pattern of changes between preflight and postflight for stroke volume, systolic blood pressure, and diastolic blood pressure (supine vs. sitting). This simulation result is consistent with the suggestion noted earlier that a reduced blood volume might not compromise the inflight metabolic needs. The model and experimental

---

[*]Unless otherwise noted, the Skylab data shown in this chapter was provided by the Skylab investigators J. A. Rummel (Exercise) and G. W. Hoffler (LBNP).
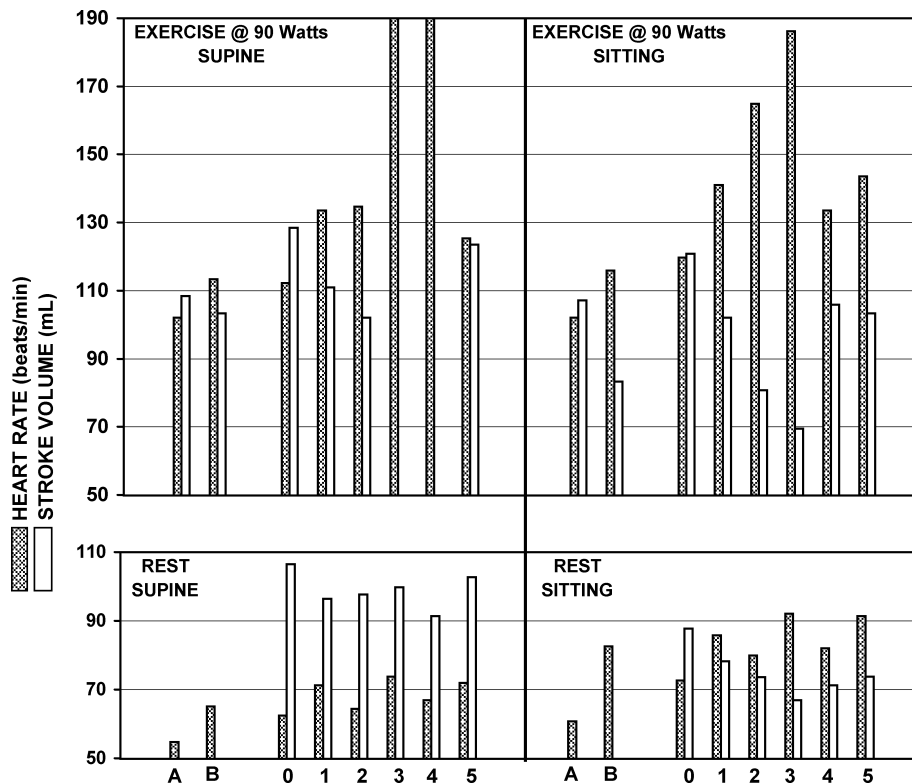
Figure 7-4(a). Simulated values of heart rate and stroke volume compared to average data from the crewmen of the 84-day Skylab-4 mission for both rest and exercise in supine and sitting positions. Comparisons should be made of preflight data (A) with simulated values (0) and immediate post-flight data (B) with simulated results obtained with each hypothesis tested (1 through 5). See text for hypothesis description and interpretation.

Figure 7-4(b). Simulated values of blood pressure compared to average data from the crewmen of the 84-day Skylab-4 mission for both rest and exercise in supine and sitting positions. Comparisons should be made of preflight data (A) with simulated values (0) and immediate post-flight data (B) with simulated results obtained with each hypothesis tested (1 through 5). See text for hypothesis description and interpretation.

	SYMPATHETIC ACTIVITY	PERIPHERAL RESISTANCE	HEART RATE CONTRACTILITY	BLOOD VOLUME	LEG CAPILLARY DENSITY
BED REST	↑	↑	−	↓	↓
TRAINING	↓	↑	↑	−	↑
HYPOTHESIS # 5	↑	↑	↑	↓	↓

Figure 7-5. Comparison of changes in cardiovascular control parameters needed to simulate weightlessness (bedrest) and one-g training effects with those of hypothesis #5 (see text) that best reproduced the average data of Skylab-4 astronauts.

responses match most closely for hypothesis #5, indicating this to be the most likely explanation. However, it is by no means unique, and further theoretical and experimental results are needed to identify the causes of the altered postflight exercise response.

7.3.2.4 Skylab Exercise Hypotheses. Hypothesis #5, which gave the best results in terms of matching the observed and simulated values, is in fact a combination of the changes in cardiovascular parameters brought about by weightlessness and exercise training. The postflight increase in blood pressure (Fig 7-4(b)) is possibly due to increased peripheral resistance as a result of change in the leg capillary bed; these are features of hypothesis #5. As suggested in Fig. 7-5, conditioning and deconditioning effects, according to this analysis, are not complete opposites; they include some quantities that move in opposite directions, but some that induce changes in the same direction. It is questionable if all effects of exercise training occur in space, but the broad assumption here is that they do but are mitigated by the deconditioning of spaceflight. Clearly, we need much more data to identify the presence or absence of these changes and their relative significance, but the point we emphasize here is the useful role of mathematical modeling in suggesting possible combinations of mechanisms that would explain the observed changes.

7.4 Skylab Lower Body Negative Pressure (LBNP) Studies

7.4.1 Introduction

The LBNP stress test consists of applying pressures below ambient level to the lower part of the body in graded steps and measuring the resulting changes in cardiovascular response. Many investigators have used the test in ground-based studies and have shown it to provide sensitive indices of cardiovascular performance [14,15,16,17,18]. It has also been suggested for simulating the effects of hemorrhage by shifting blood from upper to lower parts of the body [19]. It is a highly reproducible test with a safer methodology compared to clinical stand and tilt tests for evaluating orthostatic tolerance.

The primary effect of LBNP is a transfer of blood from the central circulation to the blood vessels in the legs, reducing effective circulating blood volume. The ensuing central hypovolemia results in a reduction of central venous pressure and cardiac output. The decrease in cardiac output is associated with a decrease in stroke volume caused by decreased venous return and insufficient cardiac filling. Heart rate and peripheral resistance are increased by the baroreceptor reflex mechanism to restore cardiac output and mean arterial pressure. The magnitude of cardiovascular changes induced by LBNP increases as the negative pressure applied to the lower limbs increases because more blood is shifted legward and out of the central circulation. Thus, the degree of stress produced depends in large part on the total amount of circulating blood volume and the pressure-volume (P-V) relationship of the leg veins, both of which could be significantly affected by spaceflight. Because in spaceflight there is a well-known reduction of blood volume (10%-15% loss), inflight LBNP starts with an already reduced blood volume.

7.4.2 Skylab Observations

The Skylab equipment for performing LBNP tests consisted of a rigid container with an air-tight waist seal that provided a reduced pressure (maximum of 50 mmHg below ambient or –-50 mmHg) around the legs and lower torso while the rest of the body remained at ambient pressure [20]. The test protocol included resting supine control for 5 minutes, five graded levels of LBNP (1 minute at –-8 mmHg, 1 minute at -16 mmHg, 3 minutes at -30 mmHg, 5 minutes at -40 mmHg, 5 minutes at -50 mmHg), and a final 5 minutes of recovery at ambient pressure. The number of daily inflight tests on each crewmember was 7 in the 28-day Skylab mission, 16 in the 59-day mission, and 22 in the 84-day mission. The tests were performed at regular intervals during the mission but not on the same day as the exercise tests. The measurements included vectorcardiogram from which heart rate was determined, systolic and diastolic blood pressure, and percent changes in leg volume using a special leg volume measuring system [21]. Thus, changes in both hemodynamic and electrocardiographic responses to LBNP were assessed. Hoffler [4], Johnson et al. [22], and Sandler [23] have reviewed in detail the results of the Skylab LBNP experiment. The major findings comparing inflight LBNP with preflight LBNP responses pertinent to analyses discussed here (and which will be shown later in Figs. 7-6, 7-7 and 7-11) include the following:

- Inflight elevation of *resting* heart rate, which tended to be slightly higher early in flight compared to increases noted later in flight.
- Increased systolic and pulse pressures and decreased diastolic and mean pressures at rest compared to preflight measurements of the same.
- Decreased orthostatic tolerance as indicated by sig-

Table 7-1. Simulation studies and analyses performed using the pulsatile cardiovascular model and cardiovascular data from the Skylab LBNP experiment

| Description of Analysis	Experimental Data Used	Results
Simulation of Preflight LBNP Response – Model Validation	Average data from 6 crewmen of Skylab missions 2 and 3 and Average data from crewmen of Apollo missions 7, 8, 9, and 15	Favorable comparison of simulated and observed changes in heart rate and pulse pressure
Measured heart rate and blood pressure responses to LBNP*	Average data from all Skylab crewmen for the first month inflight.	Significant increase in orthostatic intolerance after one week in space.
Influence of Blood Volume Loss on LBNP Response · Parametric Analysis Using the Model · Comparison with Experimental Results	None Average data from all Skylab crewmen for the first month inflight.	Significant changes in heart rate compared to only moderate changes in blood pressure A large fraction of inflight changes in heart rate and pulse pressure explained on the basis of decreased blood volume
Leg Volume Response to LBNP*	Average data from all Skylab crewmen	Significant inflight increases in percent leg volume change (PLVC) at lower levels of LBNP.
Effect of Changes in Leg Venous Compliance	None	Leg volume changes in weightlessness cannot be explained based on increased leg venous compliance alone.
Effect of blood volume loss, fluid shift from legs and delayed compliance on LBNP response	Data from a single Skylab crewman from early and late in the mission.	Delayed compliance change (reverse stress relaxation) can partly explain difference between early and late mission LBNP results.

* No simulation involved
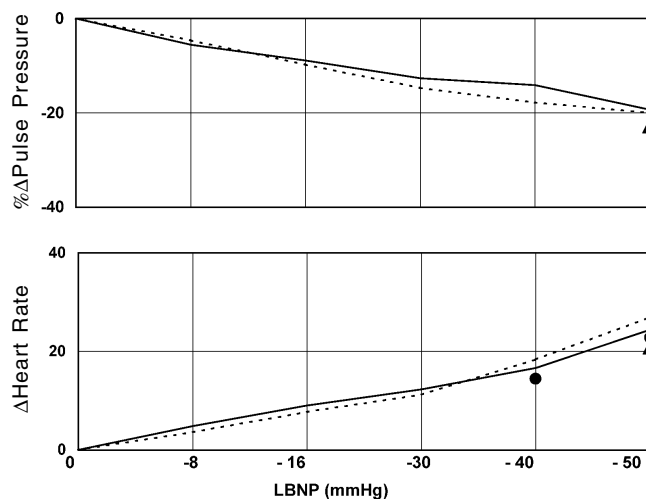
Figure 7-6. LBNP model validation study showing preflight responses from spaceflight crews. Simulation results (———) compared with averages of 6 runs from each of 3 subjects in typical space crews (- - - -). ● Averages of Apollo 7, 8, 9, and 15 crews, 3 runs each; ▲ Average of Skylab crews, 6 runs each. Redrawn from Ref [25].

nificant increases in heart rate at -50 mmHg LBNP compared to preflight. This occurred as early as the first inflight measurements 4 to 6 days after launch.

- Significant correlations between orthostatically stressed heart rates (change from rest to -50 mmHg LBNP) and decrements in blood volume, the latter measured on recovery day.
- Greater LBNP-induced leg volume increases inflight compared to those seen in preflight tests.
- More stable cardiovascular response to LBNP and relatively improving orthostatic tolerance after 5 - 7 weeks of flight tending toward preflight normals.

7.4.3 Model Analysis

7.4.3.1 Simulation Approach. Hoffler [4] and Johnson et al. [22] identified a number of possible contributory factors that would explain the observed changes in cardiovascular response to LBNP in weightlessness. The most dominant among these factors was the reduction in blood volume, and accordingly, our initial analysis focused on the influence of blood volume loss on LBNP response. The analysis utilized the LBNP model, a simplified version of the EXER model as noted earlier. In addition, the data on leg volume response to LBNP were examined in detail to find plausible explanations for the observed inflight changes. Specifically, the LBNP model was used to discern the role of leg venous compliance in LBNP-
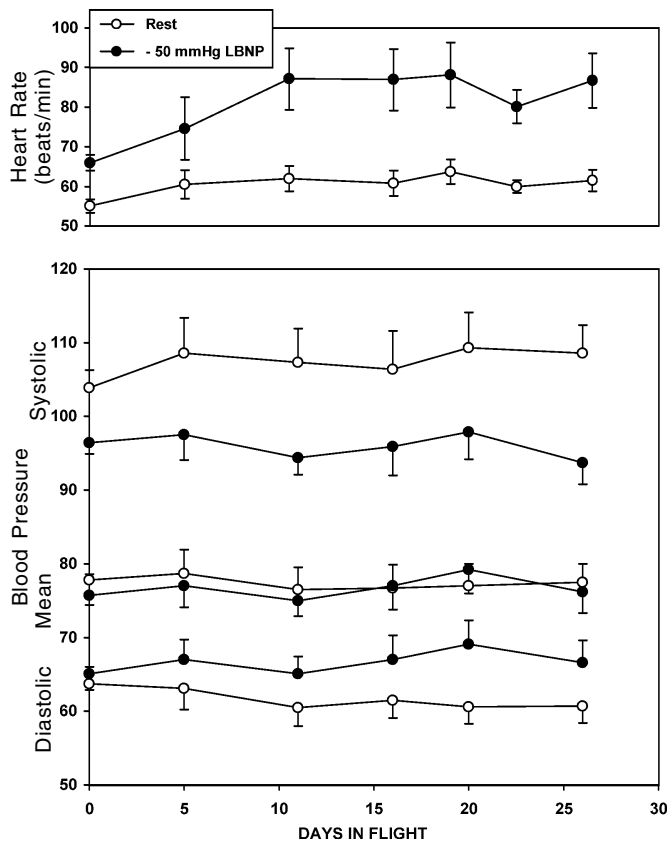
Figure 7-7. Mean Skylab heart rate (top panel) and blood pressure (systolic, diastolic, and mean; bottom panel) responses to LBNP during the first month inflight (N=9; mean ± SE)). The values at rest (pre-test) are shown by open circles and the values at maximum LBNP of -50 mmHg are shown by filled circles. The values at zero time are the preflight means.

induced leg volume changes, based on the suggestion of increased leg compliance as a significant factor of leg volume response in weightlessness [4,24]. Finally, in order to understand why the LBNP responses that were obtained early inflight differed so dramatically from those administered late in the mission, hypotheses were tested associated with long-term circulatory adaptive changes, such as delayed compliance. Table 7-1 lists the simulation studies and data analyses performed and the results obtained.

Prior to these studies the LBNP model was validated using data obtained in one-g (see next section). For the analysis of inflight Skylab data, various hypotheses were tested with the model as described above. These simulation results were compared with the average LBNP data from the three manned Skylab missions for the common flight duration of the first 28 days after launch, a period corresponding to the shortest mission, and where the data for all nine crewman could be included. Despite the considerable differences among the three missions regarding diet, exercise, and other crew activities (see Chapter 4.6), it was deemed reasonable to assume that the overwhelm-

ing effect of weightlessness would tend to minimize other sources of variability in the measured quantities.

7.4.3.2 Simulation of Preflight LBNP Response — Model Validation. Validation tests were performed to demonstrate that the LBNP model could reproduce observed changes under one-g conditions without the unknown and confounding effects of weightlessness. Preliminary LBNP validation studies were presented in Chapter 3.2.1.4 using data from NASA and non-NASA earth-based laboratories. The techniques for simulating LBNP were also described as well as a model comparison between a tilt test and LBNP test for measuring orthostatic intolerance. The results demonstrated that the model was able to simulate plausible cardiac and circulatory changes expected from these maneuvers.

A validation study more relevant to the current analysis was conducted using preflight LBNP tests on the astronauts who flew missions in the Apollo and Skylab programs (Fig. 7-6). Steady state heart rate and pulse pressure changes due to applied LBNP were computed and compared with those obtained in preflight LBNP tests. Values are presented as percent changes in heart rate and pulse pressure. Normalized parameters are used to provide a basis of comparison because of the wide range of resting normal values of blood pressure and heart rate that existed among the Skylab and Apollo crewmembers. The favorable comparison of simulated and observed changes indicated that the model was sufficiently accurate for simulating inflight data and comparing the results with experimental observations.

7.4.3.3 Influence of Blood Volume Loss on LBNP Response

7.4.3.3.1 *Skylab Measurements.* Figure 7-7 shows the average Skylab heart rate and blood pressure responses in the resting state and during steady-state LBNP of -50 mmHg. Clearly, the inflight increase in heart rate at -50 mmHg LBNP from the resting level is much larger compared to the corresponding increase prior to flight. On the other hand, the mean arterial pressure does not appear to change significantly either from preflight to inflight or from resting to -50 mmHg LBNP. There is also a slight tendency for the pulse pressure (systolic minus diastolic) at rest to increase while the stressed pulse pressure decreases slightly over time and compared to preflight.

7.4.3.3.2 *Parametric Analysis Using the Model.* The reduction in blood volume as a result of spaceflight is believed to have a critical influence on the inflight response to LBNP as well as on the immediate postflight response to standing [26]. In order to assess the contribution of blood volume loss to LBNP response, a parametric analysis was performed using the LBNP model. Figure 7-8 (top panel) shows the heart rate responses at rest and at the maximum LBNP level of -50 mmHg produced by the model over a range of blood volume losses. The response to maximal LBNP shows that a 20% blood volume loss (approximately a liter in an average subject) represents a severe stress. The steep increase in heart rates and decrease in systolic and
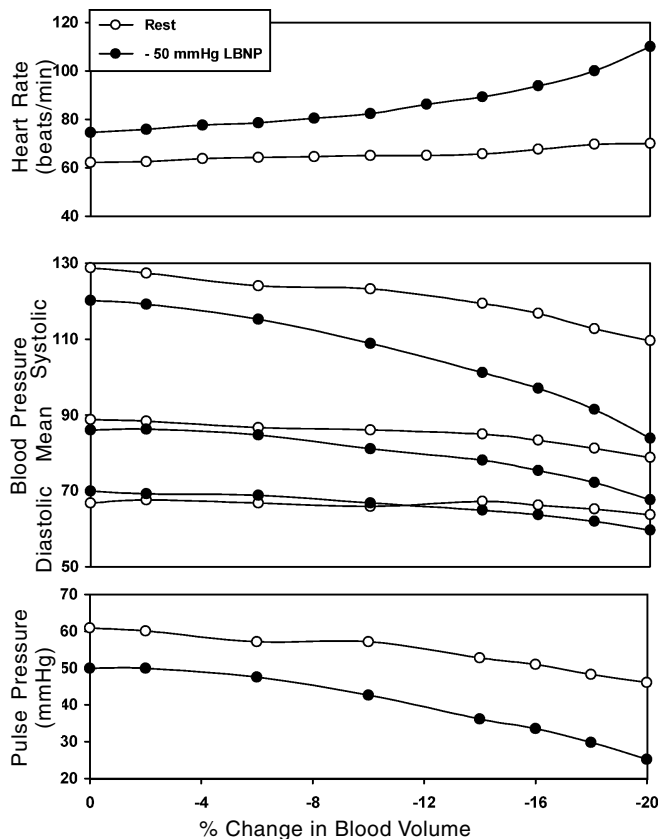
Figure 7-8. Model-simulated heart rate and blood pressure responses to LBNP as a function of decreases in blood volume. The values at rest are shown by open circles and the values at maximum LBNP of -50 mmHg by filled circles.
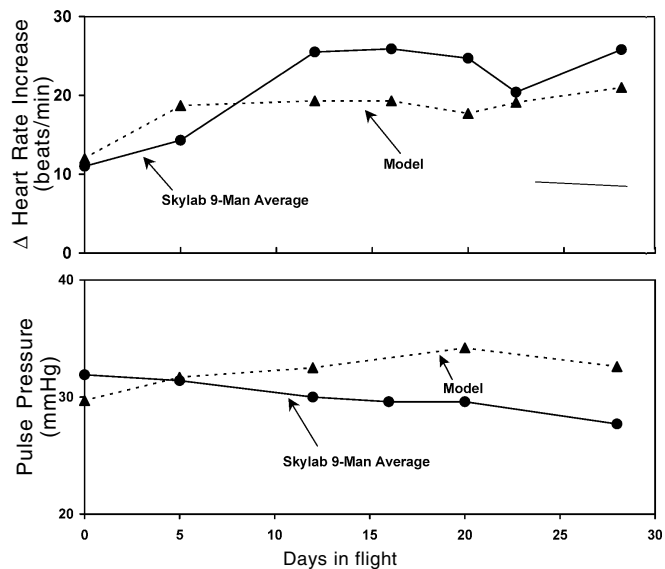

Figure 7-9. Comparison of measured and simulated values of heart rate (increases from resting levels) and pulse pressure (PP) at maximum LBNP of -50 mmHg during the first month of the Skylab missions. Experimental values were obtained from data in Fig. 7-7. Simulated values were calculated from Fig. 7-8 using estimated inflight blood volume changes from Fig. 7-10. Simulated PP values were further normalized by adding the difference between the experimental resting PP (Fig. 7-7) and the model's resting PP (Fig. 7-8) to the model's PP at –50 mmHg.

pulse pressures at the larger blood volume losses may be indicative of initiation of syncope that has been observed at high LBNP levels. For example, in normal subjects syncope occurs at approximately –70 mmHg LBNP [19], while it occasionally took place at –50 mmHg during the inflight phase of Skylab [22]. (No episodes were reported preflight). At lower levels of blood volume loss, the heart rate increases predicted by the model (Fig. 7-8) are lower compared to available experimental measurements [14].

Figure 7-8 (middle panel) shows the effects of decreased blood volumes on the blood pressure response to LBNP. Significant decrements occur in systolic pressures, especially at larger blood volume losses. On the other hand, the changes in diastolic and mean pressures are relatively small amounting to less than 10%. Most of the changes in mean arterial pressure results from a decreased systolic pressure. Also, decreases in systolic pressure result in a diminished pulse pressure response to LBNP with blood volume reductions (Fig. 7-8, bottom panel). The difference between resting and stressed pulse pressures increases with blood volume loss.

7.4.3.3.3 *Comparison with Experimental Results.* Referring to experimental data in Fig. 7-7 (top panel), inflight

heart rates at rest are elevated above preflight control values and exhibit a tendency to plateau for the duration of the mission. The factors causing the elevated resting heart rates, also noted in bedrest studies (see Fig 9-4), whether mediated by mechanical, neural, hormonal, or local mechanisms are not understood. Because the model was not able to reproduce this heart rate effect, it is difficult to make direct comparison between data and model with regard to absolute values. However, the *change* in heart rates from rest to stressed levels can be compared between model and data. When this is done, the parametric study of Fig. 7-8 can be analyzed and some inferences can be drawn regarding the effect of blood volume.

Using the data from Fig. 7-7, the average change in heart rate from resting to stress level at -50 mmHg LBNP for the nine Skylab astronauts was computed as shown in Fig. 7-9. The change increases from a little over 10 beats/minute preflight to approximately 25 beats/minute by the eleventh inflight day and remains elevated throughout the remaining days of the mission. This implies that, if we assume blood volume loss as the only causative factor for the increased heart rate response, the loss is mostly complete by the eleventh day of the flight. Based on the model analysis shown in Fig. 7-8, an increase of 25 beats/minute corresponds to a 15% blood volume deficit or approximately 750 ml for a normal subject. This is comparable to that reported by Murray et al. [18] who found a heart rate increase of 25 beats/minute with a blood loss of 500 ml
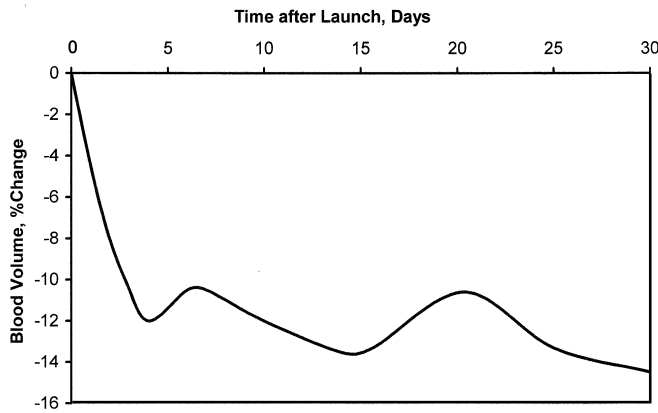
Figure 7-10. Blood volume changes during the first month of Skylab predicted by the erythropoiesis regulatory model (Chapter 6) using measured plasma hemoglobin concentration as a model driving function.

Figure 7-11. Skylab mean percent leg volume change (PLVC) response to LBNP ($N = 9$; mean ±SE). The data at zero time are mean preflight values.

(acute venesection) at -40 mmHg LBNP. Blood volume loss for the Skylab crew was measured postflight as 590 ml (see Table 5-2), an amount sufficient to explain the early increase in stressed heart rate.

A different type of comparison of the experimental LBNP responses (Fig. 7-7) with simulation results over the course of the first month can be made by estimating the inflight changes in blood volume and by assuming blood volume to be solely responsible for the observed response to LBNP. No measurements of blood volume were performed during flight but it had become possible to compute this variable from the erythropoiesis model (see Chapter 6). Specifically, the model was programmed with the measured changes in plasma hemoglobin concentration measured in the Skylab crew and was able to predict plasma volume, red cell mass and total blood volume during the course of the mission. Although superior methods of simulating the effects of spaceflight on blood volume were developed later in the project (see Figs. 6-40, 6-45 and 9-19), Fig. 7-10 shows the blood volume estimate that was available at the time of these LBNP studies based on hemoglobin data from the Skylab missions. This data was used in each of the inflight simulations for Figs. 7-9, 7-14 and 7-15.

Figure 7-9 includes the simulated values of the change in heart rate from resting control levels to -50 mmHg LBNP plotted as a function of mission time for comparison with experimental results. Figure 7-8 was used to determine the delta heart rate response predicted by the model for the particular mission day using blood volume estimates from Fig. 7-10. The comparison between model and delta heart rate data in Fig. 7-9 indicates that approximately 75% of the observed increase in stressed heart rate from resting levels can be accounted for by decrements in blood volume resulting from exposure to weightlessness. The bottom panel of Fig. 7-9 shows a similar comparison of the pulse pressure at –50 mmHg LBNP. The model values show a slight increase (less than 7 mmHg), while the observed values
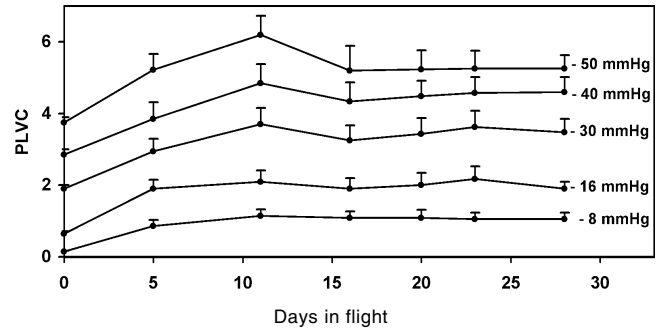
exhibit a slight decrease throughout the mission. Although the trend in the human data does not seem to be reflected in the model predictions, the data and model agree fairly closely early in the mission and on an absolute mean basis. The basic conclusion is the same as for the heart rate comparison – most of the LBNP response can be associated with direct effects of a reduced blood volume.

7.4.3.4 Leg Volume Response to LBNP

7.4.3.4.1 *Experimental Measurements.* The leg volume was determined both at rest and during LBNP tests in the Skylab missions by measuring the circumference at a number of points along the leg and calculating the total volume as the summation of multiple truncated conical volumes [21]. The application of LBNP results in an increase in leg volume due to fluid pooling in the lower half of the body caused by the pressure gradient. Figure 7-11 shows the plot of average percent leg volume change (PLVC), i.e., deviation from resting control levels during any session, as a function of mission time for the nine Skylab astronauts for all five levels of Skylab LBNP protocol.

7.4.3.4.2 *Analysis of Data.* The data shows that the percentage increase in leg volume during inflight LBNP, i.e., PLVC, was greater than the preflight value for any given level of LBNP. In addition, the difference between inflight and preflight, as measured by the percent increase in PLVC, i.e., ΔPLVC, is greater for the lower levels of LBNP. (For example, for –16 mmHg, the mean inflight change in PLVC compared to preflight is over 200%, while the corresponding value for –50 mmHg is only 45%). This is consistent with the observations of the Skylab researchers who noted that the rate and magnitude of leg volume increase measured during inflight tests were especially pronounced at the lower levels LBNP of –8, –16 and –30 mmHg [22]. Presumably, a given increment of negative pressure has a greater effect in forcing fluids into the legs at lower LBNP levels.
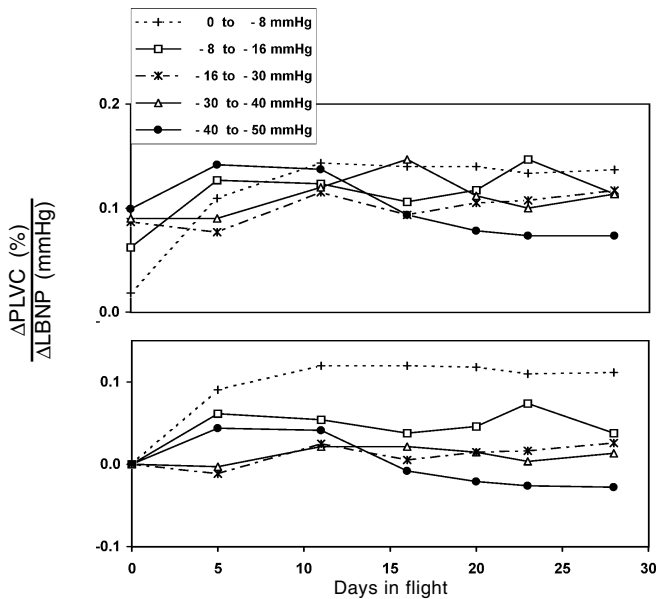
Figure 7-12. Analysis of Skylab leg volume changes during LBNP. The upper panel shows the ratio of change in leg volume to change in pressure level during LBNP using Skylab data, and the lower panel shows the same referenced to the preflight mean

The above observation is more readily seen by calculating the change in PLVC per unit of applied negative pressure between protocol levels (ΔPLVC/ΔLBNP). The resulting ratio can be taken to represent the volume response of the leg to a unit of negative pressure applied. As such, ΔPLVC /ΔLBNP, is an index of leg compliance. Figure 7-12 shows the results of this transformation for each level of LBNP protocol. The inflight changes are remarkably similar (Fig 7-12, top panel) with the exception of the values for the maximum stress levels of LBNP, i.e., -40 to -50 mmHg, which show a decrease in leg volume response to pressure after two weeks of flight. The interpretation of this finding remains speculative. It could be due to a decrease in leg vascular capacity (reverse stress relaxation or devascularization) or a stronger sympathetic response to the stress than during preflight; the effect has a greater influence later in the mission and at higher stress levels.

Another observation of interest is that during preflight, the compliance indices for the two lowest LBNP levels are less than the indices at higher levels of LBNP stress (see Fig. 7-12 for zero time). This becomes evident by replotting the indices with the preflight levels at the origin as indicated in the lower panel of Fig. 7-12. This plot clearly shows the compliance index is highest at the lowest levels of LBNP as well as the dramatic divergence between the index at the highest and lowest levels of LBNP.

7.4.3.4.3 *Hypothesis for Leg Volume Findings.*
Several hypotheses are offered to explain these findings related to changes in leg volume.
a) **Effect of a Diminished Resting Leg Volume.** A partial explanation for this phenomena resides in the

Table 7-2. ΔPLVC/ΔLBNP Ratios for LBNP Steps of Skylab Protocol

Increase in Compliance	ΔLBNP Level (mmHg)				
	0-8	8-16	16-30	30-40	40-50
20	0.23	0.28	0.25	0.26	0.24
40	0.44	0.55	0.49	0.51	0.47
100	1.07	1.32	1.18	1.22	1.13

Note: Ratios were calculated using the leg blood volume changes produced by the LBNP model with increase in leg venous compliance. The indicated ratios are referenced to that obtained with no change in compliance corresponding to preflight, as in Fig. 7-12 (bottom).

recognition that resting leg volume gradually diminishes over the course of the mission. Because PLVC is defined as the ratio of leg volume change to the resting leg volume, then for the same absolute change in leg volume, the inflight PLVC would be greater than the corresponding preflight value. Direct measurements aboard the 84-day mission showed that the resting leg volume decreased early inflight and continued to decline very gradually for exposures to microgravity up to 3-months (see Fig. 9-10). The average resting leg volume decrement in Skylab was 2.2 liters by the end of the longest mission. For an average 70 kg man, the combined total leg volume is approximately 16 liters. Thus, for an identical increase of 500 ml in leg volume due to LBNP, the PLVC would be 3.60% inflight compared to 3.13% preflight. This effect of a gradually diminished resting leg volume can account for a 15% increase in PLVC inflight assuming the same volume of fluid shifted at all levels of LBNP, but it is not sufficient to explain the observed inflight increases in PLVC obtained at the highest LBNP levels, e.g., increase from 3.8 to 5.4 at -50 mmHg LBNP, which is an increase of over 40%.
b) **Partial Collapse of Leg Veins.** A more complete explanation for the greater inflight leg volume changes at lower LBNP levels is based on the partial collapse of leg veins prior to the beginning of the LBNP tests. The leg veins are relatively empty in a supine, resting one-g state but more so during inflight than preflight because of the tendency for fluids to move headward and the legs to dehydrate. Therefore, the legs, being less full during flight, can accommodate more blood volume with the application of small increases in LBNP. Calculations indicate that only 135 ml to 200 ml of fluid would need to be removed from the one-g supine leg blood volume to completely account for the effects shown in Figs. 7-11 and 7-12. This hypothesis has been advanced by Skylab investigators [22]; it has also been used in previous modeling studies [25]; and will be discussed later in this chapter as part of an overall hypothesis for LBNP response.
c) **Increase in Leg Venous Compliance.** Another, equally plausible hypotheses for inflight increases in leg volume change is a simple increase in leg compli-
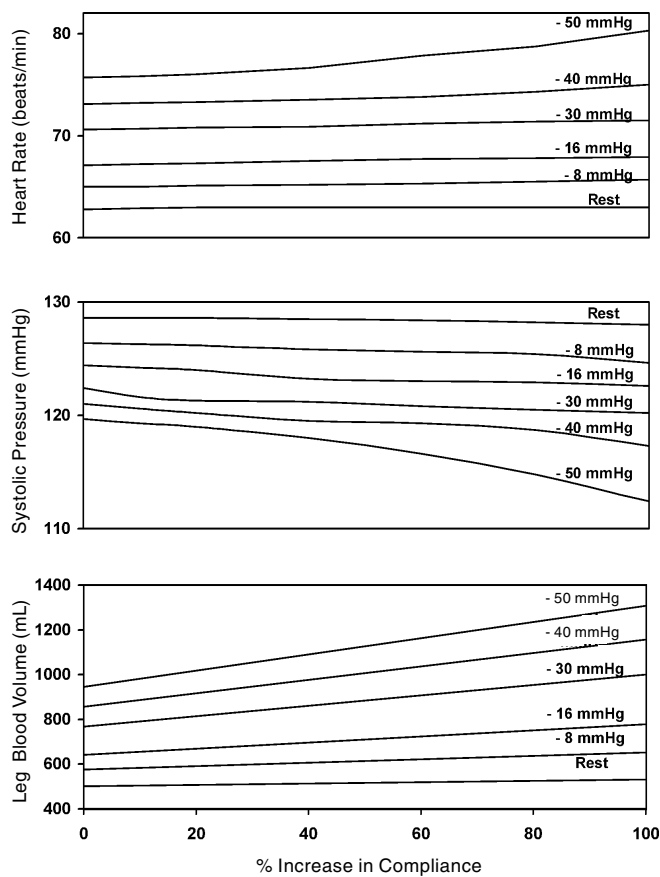
Figure 7-13. Model responses to LBNP with increased leg venous compliance.

ance. This could be caused by the reduction in force exerted transversely on the leg veins by the surrounding muscle and other tissues under weightless conditions. Normally, the weight of tissues acting transversely on the leg veins must be opposed by accumulating venous pressure or by external LBNP forces in one-g before leg veins can fill. In zero-g the overlying tissues are weightless, tissues are dehydrated and muscles have atrophied; there is good reason to believe that under these conditions LBNP is transmitted more directly to leg veins. In addition, prolonged spaceflight may act directly to increase compliance of the leg veins, reduce tone of supporting muscle and diminish tissue pressue, all of which may enhance the leg fluid pooling during LBNP. Thus, the same increment of LBNP could be more effective in spaceflight in filling the veins. This translates into an increase of leg venous compliance (larger change in volume for a given change in transmural pressure).

Such an altered compliance has been suggested as the cause of increased leg volume in weightlessness during LBNP tests [24]. There is no doubt that overall resting leg compliance increases in spaceflight [27]. The real practical question is to what extent an increased leg venous compliance and the consequent

increase in leg blood volumes under LBNP can account for the observed changes in total leg volume and other physiological responses.

The LBNP model was used to evaluate the effect of changes in leg venous compliance on LBNP response. A parametric analysis of the model response was performed by increasing the compliance of small veins and venules of the legs up to 100%. The top two panels in Fig. 7-13 show the results on heart rate and systolic pressure. The latter was used to represent blood pressure response because simulation results showed no appreciable effects on diastolic pressure. Accordingly, changes in systolic pressure reflect all changes in mean arterial pressure and the pulse pressure. Although these simulations indicate that an increase of leg venous compliance has no effect on resting heart rate and systolic pressure, the model predicts elevations of stressed heart rate and decrements in systolic blood pressure at all levels of an LBNP protocol.

The bottom panel in Fig. 7-13 shows the simulated results on leg blood volume, which increases linearly with leg venous compliance at each level of LBNP. (Note that the model can only predict increases in leg blood volume rather than total leg volume. For the purposes of this analysis we assume that changes in leg blood volume are similar in nature to leg volume, the latter being the measured variable). At any venous compliance, leg blood volume increases progressively from rest to higher LBNP levels. Table 7-2 shows the ΔPLVC/ΔLBNP ratios calculated as described earlier, but using the simulated leg blood volume (from Fig. 7-13) in place of leg volume and the preflight value corresponding to zero change in compliance as reference. The ratios are not significantly different at any one compliance level, except for the slightly larger value for the LBNP step from –8 to –16 mmHg. With this exception, they do not exhibit larger leg volume increases observed at lower levels of LBNP as was observed in the Skylab experiment. Also, they increase with increasing levels of compliance. We cannot associate increasing compliance with mission duration, because ΔPLVC/ΔLBNP, based on measurements, showed little change through the mission (Fig. 7-12).

Thus, (within the limitations of the model's inability to distinguish between *leg volume* and *leg blood volume* changes) the results on leg volume changes during LBNP from the Skylab experiment cannot be explained based on increased leg venous compliance alone. This analysis, however, does not test other factors that could have contributed to the observed changes in the overall leg pressure/volume relationship. Both the changes in the leg tissues which surround and support the leg veins and diminished tissue pressure that accompanies leg dehydration may participate to varying degrees in this relationship and help explain the large inflight leg volumes observed inflight compared to preflight, especially at the higher levels of LBNP. (Additional comments about this analysis are found at the end of the next section).
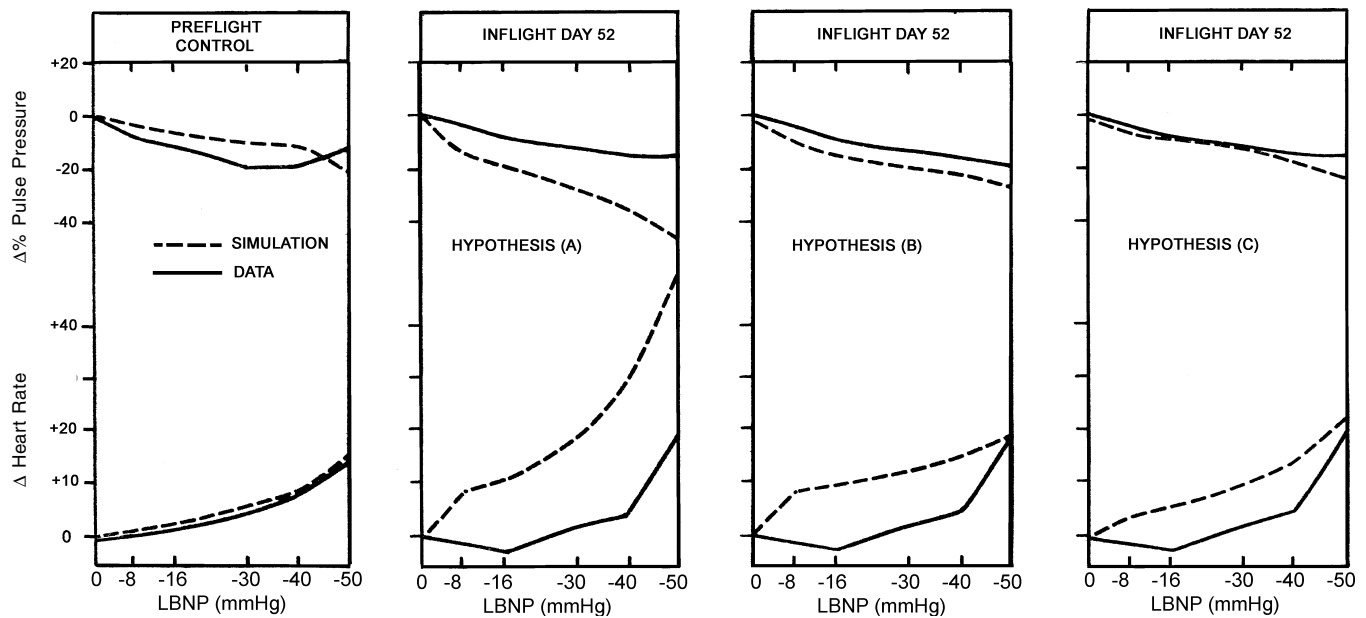
Figure 7-14. Comparison of experimental and model responses to LBNP response for a single Skylab crewman. Three hypotheses were used in the model to account for inflight changes in heart rate and pulse pressure on Inflight Day 52. See text for explanation of hypotheses (A), (B) and (C). See Fig. 7-15 for a similar comparison on Inflight Day 20 using a simulation of Hypothesis (A) and data from the same subject.

7.4.3.6 Hypotheses For LBNP Response In Weightlessness.
The following key factors emerge from the foregoing discussion to explain the experimental results: a) blood volume loss during spaceflight, b) headward fluid shifts accompanied by blood leaving the legs, resulting in a partial collapse of leg veins, and a relatively empty venous system in the legs at the beginning of the LBNP test, and c) delayed retoning of the legs blood vessels to accommodate the reduced inflight leg blood volume. The first two of these may help explain the difference between preflight and early inflight responses to LBNP while the third factor may explain the difference between early and later mission results.

7.4.3.6.1 *Hypotheses to Explain Early and Late Responses*.
It was clear that LBNP tests soon after launch were quite different than preflight (see Figs. 7-7 and 7-11). Model simulations also indicated that the loss of blood volume could be a major factor in explaining the LBNP results, at least early inflight (see Figs. 7-8 and 7-9). However, blood volume changes alone could not explain the LBNP results later in the missions. A comparison of model response with inflight data (Fig. 7-9), using blood volume loss as the only model hypothesis to distinguish between preflight and inflight conditions, showed the differences became greater during tests in the later portion of spaceflight. In addition, Skylab findings revealed that the greatest decrements in orthostatic intolerance occurred during the first several weeks of flight, but after approximately 5-7 weeks, cardiovascular responses became more stable and tended towards preflight normals [22]. A simulation study

was undertaken to answer the question "what hypotheses are required in the model to obtain reasonable agreement between model results and Skylab data for both early and late responses?" Although only a single crewman's data was used in this analysis (originally a pilot study) it is a convenient means of demonstrating an important concept of cardiovascular adaptation – that of stress relaxation. Using the data for the selected crewman, Figs. 7-14 and 7-15 compares experimental and model responses to LBNP at three phases of the mission: Preflight control (Fig. 7-14); Inflight Day 20, representing an early mission LBNP test (Fig. 7-15); and Inflight Day 52, representing a late mission test (Fig 7-14). Figure 7-14 also summarizes three hypotheses that were used to improve the agreement between model and data for the Inflight Day 52 test. The following hypotheses were evaluated:

The overriding hypothesis tested was that blood volume changes were responsible for the differences between inflight and preflight LBNP responses. Blood volume changes during the mission were estimated from the model as noted in Chapter 7.4.3.3 and Fig. 7-10. These changes were introduced in each of the inflight simulations in Figs. 7-14 and 7-15 in addition to one of the following secondary hypotheses.

Hypothesis (A): Blood Migration from the Legs
The absence of gravity allows headward migration of blood from the legs. In the absence of a hypothesis for the physiological mechanism involved, a pressure bias term was added to the leg vasculature in the model to force blood from the legs into the upper body prior to initiating
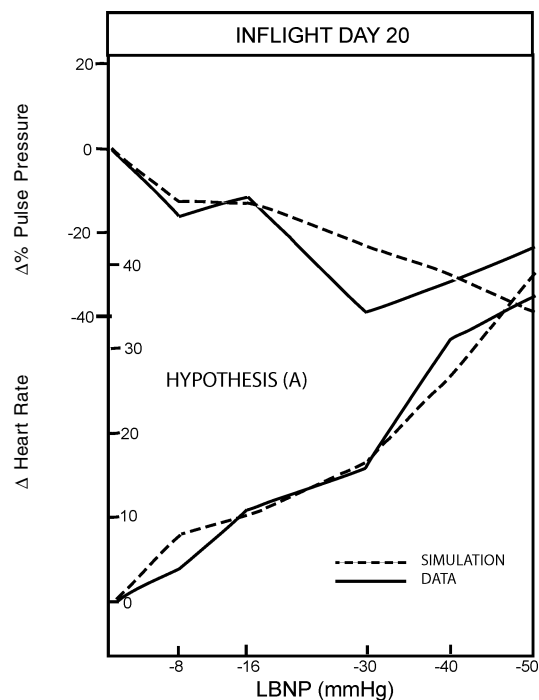
Figure 7-15. LBNP response on Inflight Day 20 for the selected crewman (solid line) compared to the simulated response (dashed line). This graph is from the same series of simulations shown in Fig. 7-14. As a means of representing the inflight physiological condition, the model was initialized with a reduced total blood volume and reduced leg blood volume (see Hypothesis (A) in text). Although comparison between model and data was reasonable on Inflight Day 20, the same hypotheses produced a poor fit on Inflight Day 52 (see Fig. 7-14, Hypothesis (A)).

the LBNP test. The exact quantity of blood that was shifted was derived from the resting leg volume measurements made at rest prior to LBNP. Thus, it was possible to compute from these inflight leg volume measurements, a time-varying estimate of fluid shifts during the mission. The test of this hypothesis, together with the overriding hypothesis of blood volume loss, is shown in Fig. 7-15 for Inflight Day 20 and in the second panel of Fig. 7-14 for Inflight Day 52 (Hypothesis A). Hypothesis (A) resulted in good agreement for the test early in the flight, but poor agreement for the later test.

Hypothesis (B): Partial Collapse of Leg Veins Followed by Reverse Stress Relaxation

The failure of the model to simulate the later mission LBNP experiments resulted in the generation of another hypothesis to account for a long-term change in the cardiovascular system. This hypothesis postulates a retoning of the partially collapsed leg veins after a headward migration of blood from the legs has occurred. The long-term change postulated is called reverse stress relaxation and has the characteristics of retoning the vasculature to accommodate the reduced blood volume in the legs and returning venous pressure toward normal. This hypothesis was included in the LBNP simulation model by shifting the leg compliance curve (effectively reducing the unstressed volume in the vein). Reverse stress relaxation will be further explained in a section below. The test of this hypothesis, together with the overriding hypothesis of blood volume loss, is shown in the third panel of Fig. 7-14 for Inflight Day 52 (Hypothesis B).

Hypothesis (C): Leg Blood Volume Loss Equal to Total Blood Volume Loss:

Another hypothesis considered is that the eventual reduction in total blood volume is equal to the amount that migrated from the legs to the upper body. In other words, the upper body somehow sensed the influx of blood from the legs as excess and moved to reduce the total blood volume by that amount. This hypothesis was tested by setting the history of leg blood volume reduction equal to the history of model-estimated total blood volume reduction and rerunning the LBNP simulations for the later mission days. The test of this hypothesis, together with the overriding hypothesis of blood volume loss and including Hypothesis (B) is shown in the fourth panel of Fig. 7-14 for Inflight Day 52 (Hypothesis C).

In summary, as shown in Fig. 7-15, the loss of blood volume can account for most of the LBNP response early in the mission. However, the difference between simulated and measured responses for a mission day test late in the flight was poor (Fig. 7-14) if one considered only blood volume losses and migration of blood from the legs (Hypothesis A), simulated by forcing blood out of the leg compartments with a pressure bias term. The agreement improved considerably by allowing the leg venous compartments to retone after partial collapse (Hypothesis B), or assuming that the migrated blood from the legs was lost from the circulation so that it was not available to move to the legs during LBNP (Hypothesis C).[†] The best agreement of Hypothesis (C) was achieved without sacrificing the good agreement for early tests (e.g., Fig. 7-15). In almost every case the model simulation of late mission tests was improved by the addition of the hypothesis to the model, giving credence but not conclusiveness to the hypothesis. By far the greatest improvement was realized by the addition of the long-term reverse stress relaxation hypothesis.

7.4.3.6.2 Reverse Stress Relaxation and the Importance of the Compliance Curve. Figure 7-16 illustrates the concept of reverse stress relaxation with a typical P-V relationship of a venous segment (representative of data on vena cava; see Fig. 3-14) with an unstressed volume V_o. A sudden drop in volume causes point A to shift to point B on the normal P-V curve (solid line) with a concomitant drop in transmural pressure. Re-toning of the veins re-

---

[†] Whether fluids that shift headward in spaceflight leave the circulation or are available to supplement circulating blood volume during LBNP was considered an unanswered question of great importance by the Skylab investigators [22]. The present analysis preliminarily indicates that the headward shifted blood is not available.
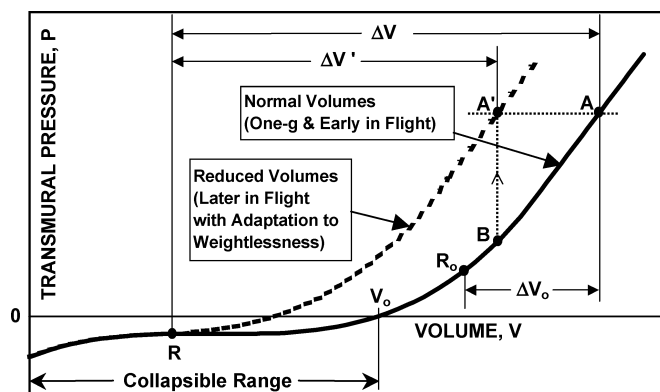
Figure 7-16. Normal pressure-volume (P-V) relationship in a venous segment of the cardiovascular system (solid curve) showing the effect of reverse stress relaxation (dashed curve), by which reduced transmural pressure due to a reduction in volume (from A to B) is restored to its original value (from B to A', as indicated by the dotted line with an arrow). The normal (one-g) unstressed volume is V_o, and the symbols R_o and R refer to the resting operating points in one-g and weightlessness, respectively. Volume and pressure are small at R due to partial collapse of the vein and migration of blood out of the vein in zero-g. The volume increase due to LBNP is ΔV_o (from R_o to A) in one-g, ΔV (from R to A) early in flight, and $\Delta V'$ (from R to A') later in flight with adaptation to weightlessness. Both ΔV and $\Delta V'$ are greater than ΔV_o, and $\Delta V'$ is less than ΔV. Compliance is defined as the inverse of the slope of these curves at any point.

stores the pressure to its original level as indicated by point A' on a P-V curve with a reduced unstressed volume (dashed line). Movement from point B to point A' (indicated by a broken line with an arrow) for restoring the transmural pressure to its original level is not immediate. In the model simulation described above, the compliance curve was allowed to shift as a function of the history of the reduction in leg blood volume (obtained from inflight measurements) and with a time constant of 14 days, i.e., 63% of the change occurs in one time constant [Guyton, A.C., private communication].

Stress relaxation (or delayed compliance) refers to the additional increase in volume that occurs in response to continued pressure of the same amount over a long period of time, this additional volume occurring by slow accretion. Delayed compliance is caused by progressive plastic stretching of the vasculature with time. During the early period of spaceflight, there is a large influx of blood from the legs to the central circulation, which undoubtedly is accommodated by some degree of stress relaxation in the large central veins. On the other hand, the venous system of the legs may experience reverse stress relaxation as the vessels attempt to accommodate the partially collapsed veins. A description of this mechanism can also be found in Chapter 9.7.3.1 and in Guyton [28]. Clearly, stress relaxation in the upper body, and reverse stress relaxation in the legs, is imperfect and does not completely accommodate the shifting of blood volume or the net losses of blood

volume that occur in spaceflight. If there was perfect and instantaneous compensation, i.e., the operating point shifted from A to A' in Fig. 7-16, there would be no change in mean circulatory pressure and provocative stresses such as LBNP would likely reveal little change from preflight to inflight as a result of blood volume loss.

The effect of reverse stress relaxation (which will partially reduce the capacitance of the veins) and/or devascularization of the tissues (which accomplishes the same thing by reducing capillary capacity) is to reduce blood pooling during LBNP. This is clear from Fig. 7-16 by comparing the increases in volume from rest to LBNP early in flight (from R to A) and later in flight (from R to A'), both of which are larger than the preflight increase (from R_o to A). Because the effect has a long time-constant of action, this mechanism may explain the fact that after 5-7 weeks of flight, the cardiovascular response became more stable and evidence of improved orthostatic tolerance appeared. Another effect that may have aided the partial recovery of inflight tolerance is a gradual increase in baroreceptors sensitivity that could lead to more intense vasoconstriction and venomotor function during LBNP [29].

It should be noted that the P-V curves depicted in Fig. 7-16 have a similar compliance, i.e., inverse slope, in the linear elastic region at high transmural pressures. However, this may not be true, and the inflight changes in P-V relationship may be more complex than a simple shift with reduced volumes, especially with prolonged exposure to weightlessness.[‡] A more rigorous analysis of simulated leg volume responses during LBNP, i.e., Fig. 7-13, and comparison of Skylab data, should take into account changes in leg compliance due to changes in vasculature, muscle, and connective tissues of the leg, all of which are influenced in weightlessness by hormonal and neural activities that control fluid volumes.

The P-V relationships shown in Fig. 7-16 indicate a non-linear region at transmural pressures slightly above and below zero, in the vicinity of the collapsible range. The LBNP model includes this non-linear representation for the large veins of the upper body (see Fig. 3-14) but a linear representation has been chosen for the leg veins (see Fig. 9-32). The linear approximation is adequate if the transmural pressures stay in the elastic region of low compliance, but the nonlinearity should not be ignored if the veins become partially collapsed with pressures close to or below zero. Specifically, the analysis of compliance in Chapter 7.4.3.5 revealed a linear relationship between leg blood volume and compliance (Fig. 7-13 bottom panel) and was not able to account for the differences in leg volume increments with successive LBNP steps. We now suspect that the use of a more realistic linear compliance for leg veins may have changed these results, so that this should be considered only a preliminary analysis.

[‡] Increases in leg compliance at rest during spaceflight are no longer in dispute but there is a question of how much this factor contributes to postflight standing intolerance [27].
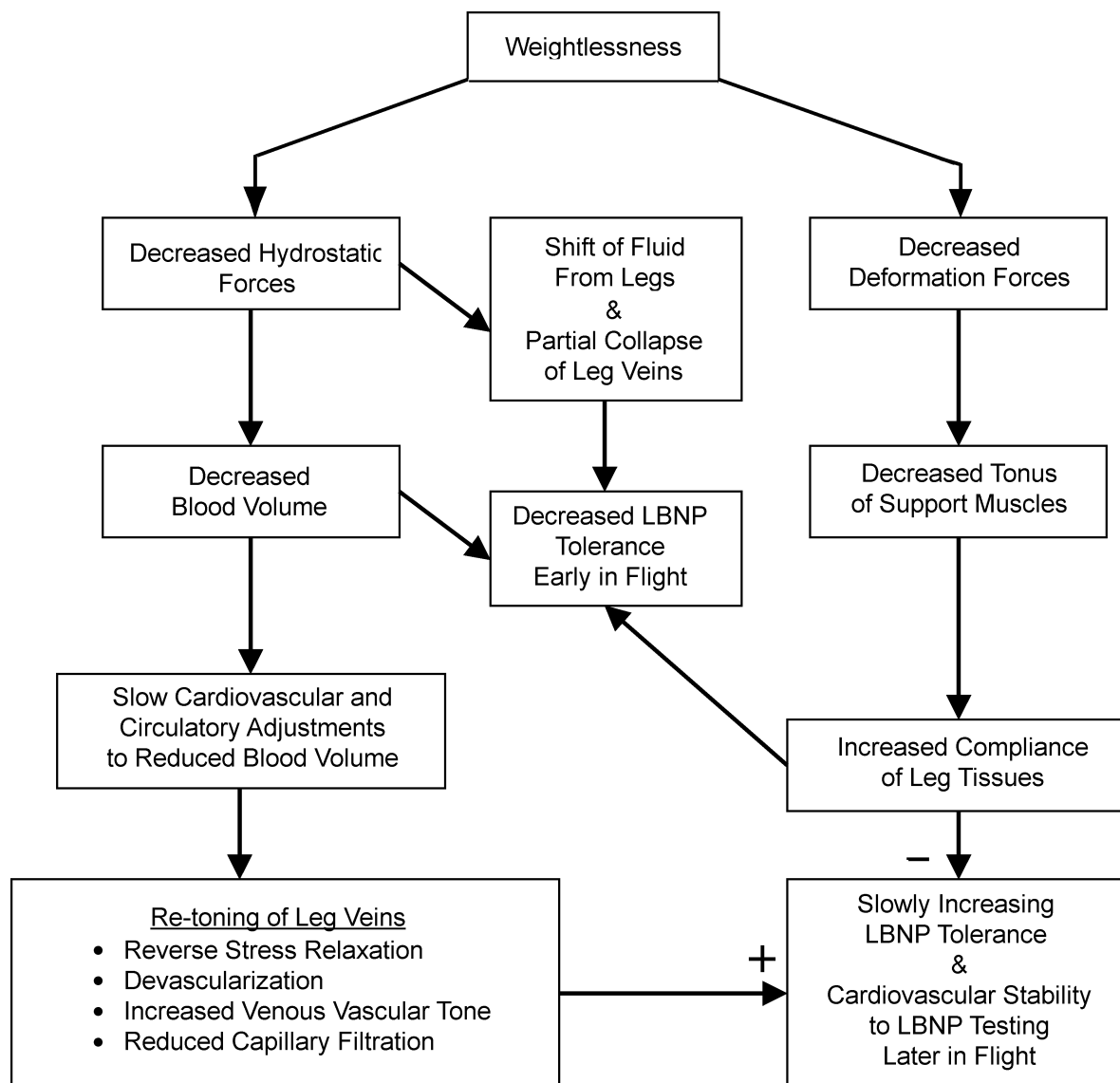
Figure 7-17. Hypotheses for cardiovascular changes that explain the LBNP findings during the early (acute) and late (adaptive) phases of spaceflight. Late mission results are influenced by factors that either promote greater orthostatic tolerance (+) or oppose it (-).

7.4.3.7 Summary

In summary, the modeling analysis has confirmed the belief of the importance of blood volume loss in affecting cardiovascular performance and orthostatic intolerance in spaceflight. Heart rate and pulse pressure responses to LBNP can be largely, but not wholly, attributed to this factor. The increased leg volume pooling during LBNP (compared to preflight) can be primarily explained by the partial collapse of leg veins and a reduced leg blood volume at rest prior to the test. The ability of legs veins to collapse in space, led to the study of a mechanism (reverse stress relaxation) that allows the leg vessels to gradually retone, thus perhaps explaining the improvement in orthostatic tolerance as the mission progressed. Simple passive increases in leg compliance, while theoretically attractive, did not appear to explain LPNP response but the analysis may have been flawed by the assumption of a linear leg vein compliance curve. Leg compliance is influenced by a number of factors and measurements strongly suggest that compliance increases in flight at rest. Figure 7-17 shows the possible sequence of these mechanisms that could lead to the observed changes in the cardiovascular response, both in the near-term and in the long-term.

7.5 Orthostatic Intolerance During Shuttle Landings

In contrast to all previous manned spaceflights, the upright sitting posture of the Shuttle crew during reentry
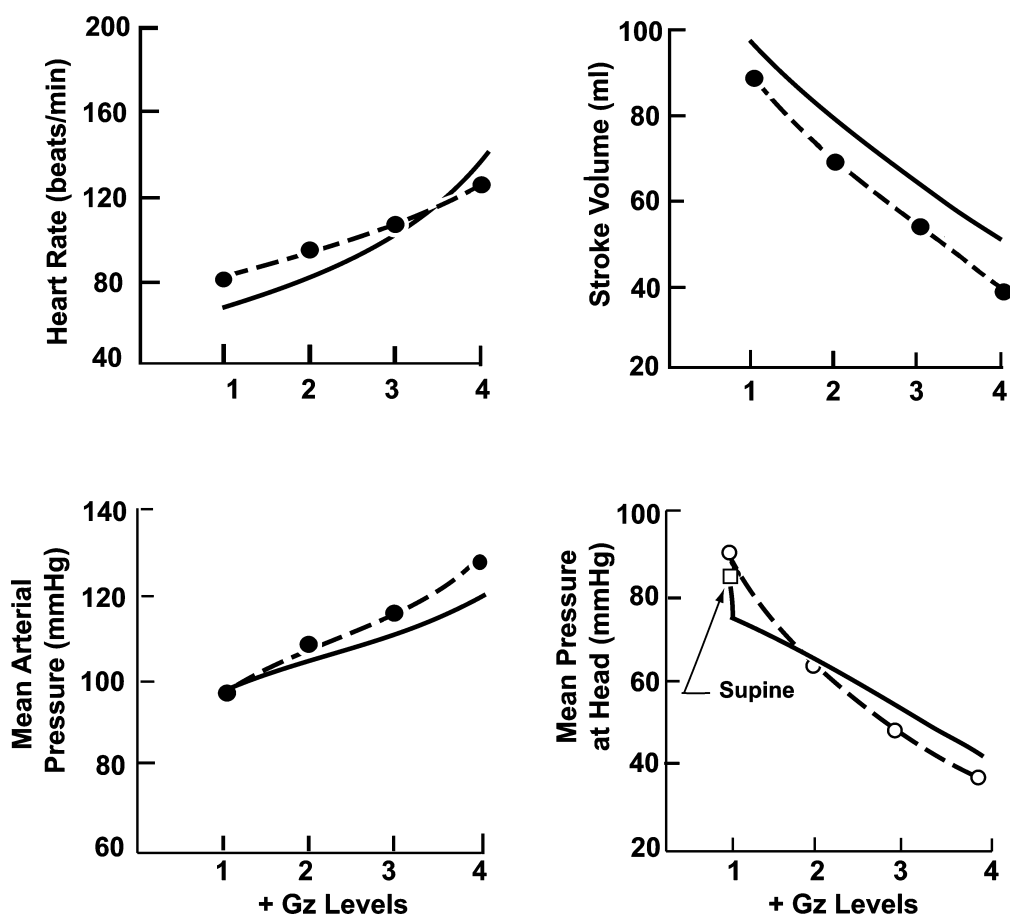
Figure 7-18. Comparison of steady-state cardiovascular response to +G$_z$ acceleration produced by the LBNP model with experimental data obtained from centrifugation studies. Simulation (solid line); Lindberg and Wood [30,32] (dashed lines, filled circles); Henry, et al. [31] (dashed lines, open circles).

into the Earth's atmosphere exposes them to +G$_z$ acceleration that would reach a maximum of twice the normal acceleration due to gravity at sea level. The pooling of fluid in the legs at such high g-forces combined with the loss of blood volume caused by exposure to weightlessness, had the potential of rendering the crew orthostatically intolerant at a time when their performance level needed to remain high. Experimental data showing the combined effect of the two stresses (blood loss and blood pooling) on cardiovascular performance were limited, and therefore, the computer simulation approach was used to generate the needed results.

In this section, we summarize the results of a study using the LBNP model that examined the combined effect of blood volume loss and head-to-foot (+Gz) acceleration on cardiovascular response. The simulation study was initiated during the early testing phase of the Space Shuttle program. It was the first attempt in this project to use a mathematical model to analyze an ongoing operational problem concerning astronaut health and safety. The simulations were first designed to explain the high heart rates that were observed in the crewman returning on the early

shuttle flights. A second goal was to determine the maximum tolerable +G$_z$ acceleration at any given level of blood volume loss. Finally, the simulations were extended to assess the effectiveness of an anti-g garment as a countermeasure to orthostatic intolerance.

7.5.1 Simulated Response to +G$_z$: Model Validation

The LBNP model was validated for simulating responses to +G$_z$ acceleration, which is an orthostatic stress that produces blood pooling in the legs not unlike LBNP. Accelerations greater than one-g are obtained in the laboratory by using man-rated centrifuges to obtain forces along whichever axis of the body is of interest. The results of a validation study, using data from both steady-state and dynamic behavior of the cardiovascular system during centrifugation of normal human subjects [30,31,32], showed that the model was capable of producing correct responses.

Figure 7-18 compares the steady-state responses, showing favorable agreement between simulated results and experimental observations. Figures 7-19(a) and 7-19(b) compare experimental and simulated pressure waveforms obtained with a force of 4.5-g lasting for 15 seconds. Re-
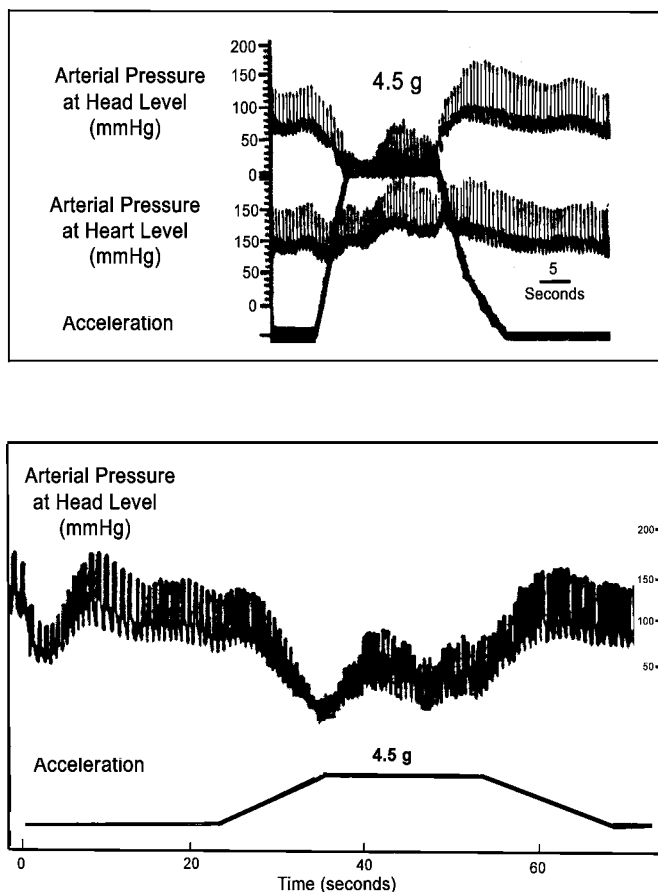
Figure 7-19(a). Blood pressure waveforms in response to +G$_z$ acceleration of 4.5 g in normal subjects from two separate centrifugation experiments: Top panel: Lindberg & Wood [32]; Bottom panel: Henry, et al. [31]. Both studies indicate that arterial pressure at the head level diminishes to about zero. Brain circulation fails when arterial pressure at that point becomes subzero, the carotid vessels collapse, and blood flow ceases.

Figure 7-19(b). Blood pressure waveforms in response to +G$_z$ acceleration of 4.5 g produced by the LBNP model. The unique pulsatile waveform pattern measured in human subjects and shown in Fig. 7-19(a) is reproduced by the model.

ferring to the experimental waveforms (Fig. 7-19(a)), the pressure measured at the head level decreases rapidly to very nearly zero with increasing g-force as blood is being forced away from the heart. Reflex action partially restores head pressure at the peak acceleration level. There is an increase in waveform frequency during the centrifugation reflecting an increase in heart rate. While the pressure at the head level falls, the pressure at the heart level rises. This latter elevation is both due to baroreceptor reflex action and due to the measured pressure being just below the hydrostatic indifference point, below which pressures increase during standing. The simulated pressure waveforms produced by the model (Fig. 7-19(b)) reflect all the features of the highly dynamic measured waveforms just mentioned.

Thus, the LBNP model was verified to be capable of accurately reproducing both steady-state and dynamic characteristics of the cardiovascular response to centrifugation, and thus, its potential for use in the Shuttle reentry

study. No modification was necessary to extend the model's capability, which is attributable to the fact that the model is based on established physiological concepts and general physical principles governing flow of incompressible fluid in a closed elastic system.

7.5.2 Response to Combined +G$_z$ and Blood Volume Loss

The validated model was used to evaluate the sensitivity of the response to g-level and blood volume loss. Figure 7-20 shows the simulated systolic carotid pressure response to combined +G$_z$ acceleration as a function of blood volume loss produced by the model. Model responses are shown for g-forces of 1.0, 1.5 and 2.0-g's. The dashed lines represent the threshold pressure levels for blackout and two types of vision impairment based on data obtained during centrifugation in normal subjects [32]. Compared to results in normal subjects at one-g, the systolic carotid pressure at 2-g's is about 15% lower with no blood volume loss, but the decrement increases to nearly 50% at a blood volume loss of 10%. These simulations predicted that at one-g, blood volume losses somewhat greater than 15% can be tolerated without any vision impairment. However, the tolerable amount of blood volume loss is less at higher g-levels. Thus, the model predicts that with a blood volume loss of 10-15%, the Shuttle crew could be at some risk during reentry because maximum g-forces are in the range between 1.5 and 2.0 g's. This conclusion, not verifiable with currently available
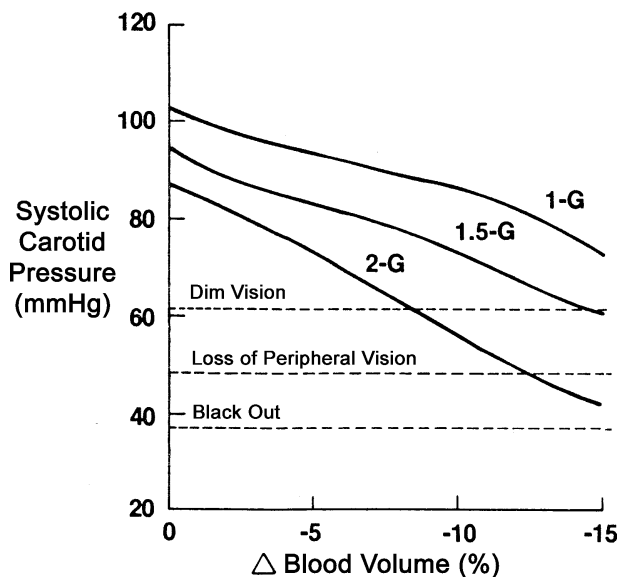
Figure 7-20. Combined effect of $+G_z$ acceleration and blood volume loss on vision. Solid curves are generated by the model. Horizontal dashed lines are obtained from data reported in Lindberg and Wood [32].

ground-based data, was substantiated by comparing data from Shuttle pilots as discussed next.

7.5.3 Simulation of Responses from Shuttle Flight

The model was used to analyze heart rate and blood pressure data from the crew of the first Shuttle flight, STS-1. Figure 7-21 shows heart rate data recorded from the two crewmen of STS-1 during reentry [33] (top panel, dashed lines). Also shown are the heart rate responses for three different simulations, using three levels of blood volume loss (top panel, solid lines). (During the reentry phase, the only biomedical data measured were the continuously-monitored values of the crew's heart rate). Each of the simulations incorporated the time-varying reentry g-force profile encountered by the crew as input into the model (bottom panel). Peak g-forces occur at about 12 minutes prior to touchdown. The effect of these peak g-forces on orthostatic tolerance is suggested by the simulated response of the carotid blood pressure during reentry (Fig. 7-21, middle panel). Accordingly, the threshold of vision impairment (62 mmHg) may have been exceeded if the blood volume loss was as high as 16%.

The sensitivity of the model to both blood volume loss and g-forces is evident from these results. For a blood volume loss of –16% the heart rate curve reflects the g-profile. Response with a blood volume loss of 8% closely approximates the measured heart rates, except during the last 5 minutes of reentry. This discrepancy in the waning minutes of the flight could be the result of factors not built into the model, i.e., anticipation and anxiety when the crew gets ready to assume manual control of the spacecraft. An equally plausible explanation is an increased blood volume loss due to excess capillary filtration of plasma into leg tissues during the latter phase of reentry,

as indicated by better agreement between measured and simulated responses at a blood volume loss of 16% in the last few minutes before landing. The limited data do not permit a resolution of these two explanations.

Thus, taking into account the differences between measured and simulated heart rate responses toward the end of reentry, the simulation results indicate a blood volume of loss of 8-16%. This was corroborated during a stand test that was administered soon after Shuttle landing. The comparison of the preflight and postflight stand tests in the two Shuttle crewmen is shown in Fig. 7-22. Blood pressure and heart rate responses are shown before (supine) and after (standing) approximately 1 minute of standing. Figure 7-23(left side) repeats this data from Crewman A which is compared to the results of four simulations of the stand test, performed using the LBNP model. Each simulated stand test was performed with a different blood volume: a normal blood volume (0%) and a 5%, 10% and 15% reduction in blood volume. (The ability of the LBNP model to reproduce an orthostatic tolerance test using upright tilt, with a normal blood volume, was validated as described in Chapter 3.2.1.4).

The first simulation with a normal blood volume, in Fig. 7-23 represents the preflight condition, while the others showing different degrees of blood volume loss are alternative simulations for the postflight condition. The simulated data that best approximates the patterns measured in the human subject are those corresponding to a blood volume loss of 10-15%; this is consistent with the tentative conclusions from the analysis of heart rate measurements during reentry (see Fig. 7-21). These results assume that blood volume loss alone can account for the differences between pre-and postflight. Interestingly, the postflight response of the two crewman, shown in Fig. 7-22, are quite different from one another. The response of Crewman B does not match the simulation response at any blood volume level. In particular, Crewman A exhibits postflight diastolic hypotension (similar to the model response) as opposed to diastolic hypertension in Crewman B.

Nevertheless, there are some important common features to both crewmen's responses. Specifically, relative to preflight, (i) the measured pulse pressure is narrower postflight, especially in the standing position, and (ii) the measured changes between supine and standing show an increase in heart rate, a lowering of systolic pressure, and a flattening of diastolic pressure. These differences are reproduced by the model. The differences in the responses of the two crewman may be explained by considering changes in factors other than blood volume (i.e., baroreceptor sensitivity, venous tone, catecholamine release and sympathetic activity), that are presumably different in the two crewmen.§ Although these factors were not tested in the current model analysis, the ability to discriminate between individual responses undergoing similar treatments is a sought-after goal of modeling.

---

§ Orthostatic intolerance with losses of both blood volume and baroreceptor sensitivity has been addressed in a subsequent simulation study using the LBNP model [29].
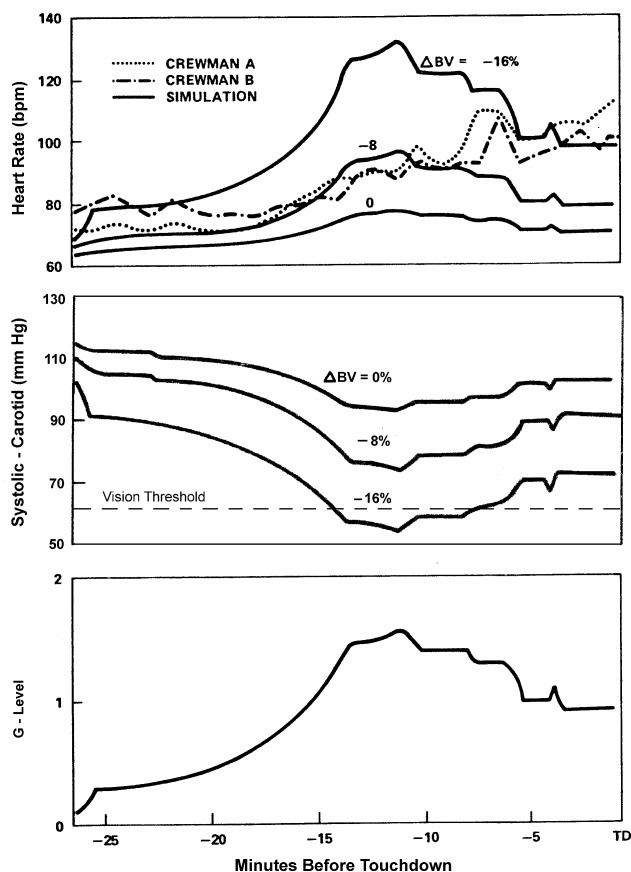
Figure 7-21. Comparison of heart rate responses of crewmen from the first Shuttle flight (STS-1) during re-entry with data generated using the LBNP model with different amounts of blood volume loss (top panel). The fall in carotid blood pressure (middle panel) could have exceeded the vision impairment threshold (dashed line). The g-force profile experienced by the crew is shown (bottom panel) and was used to drive the model. TD = Shuttle touchdown.

The simulation study, using the LBNP model, helped substantiate the conclusion based on available data from bedrest studies [34] (i.e., depending on the severity of blood volume loss), the reentry acceleration might be detrimental to physiologic function and may place the physiologic status of the Shuttle crew near the borderline of some form of impairment. Model results suggest that moderate blood volume losses (10-15%) may be reason for medical concern in this situation. It has been emphasized that the major assumption is that blood volume losses could account for the observed changes. We have failed to locate experimental data showing how simple blood volume loss uncomplicated by weightlessness or similar conditions can modify the normal circulatory response to centrifugation. Such data would be highly useful to separate the effects of blood volume loss from other aspects of cardiovascular deconditioning alluded to above.
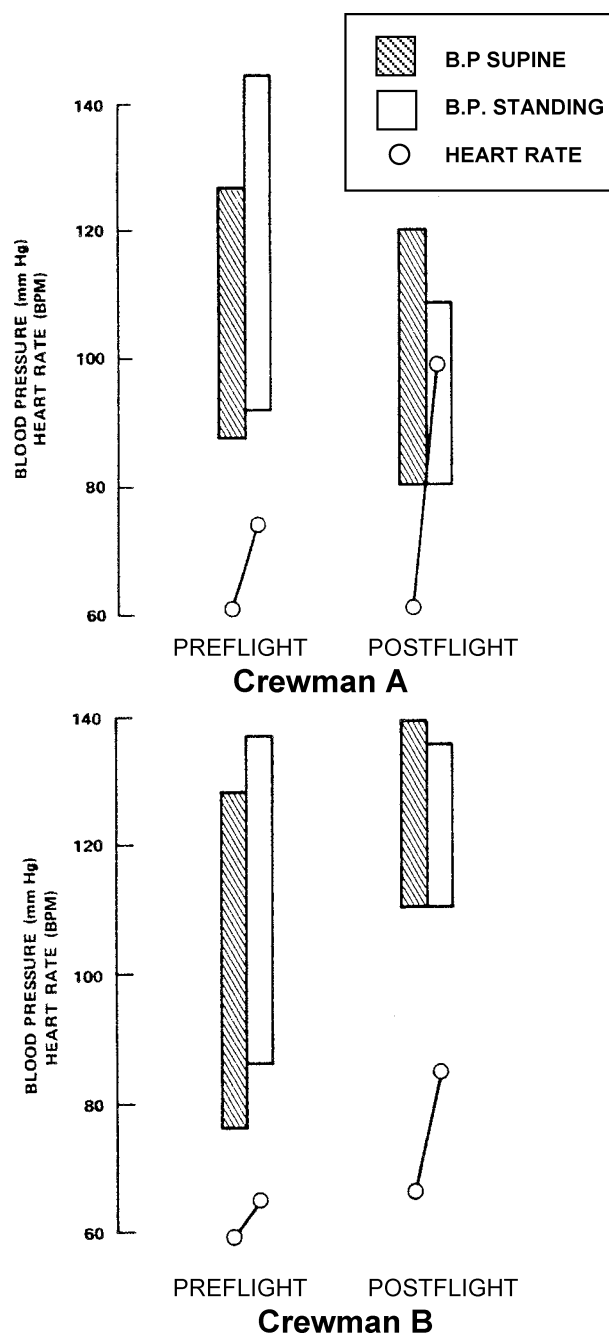
Figure 7-22. Blood pressure and heart rate responses for the two STS-1 crewmen during a one-minute stand test administered preflight and immediately after return from space. Blood pressure is represented by a bar showing systolic and diastolic levels; the height of the bar is the pulse pressure. Each stand test consists of a supine phase (hatched bar) and a stand phase (white bar).
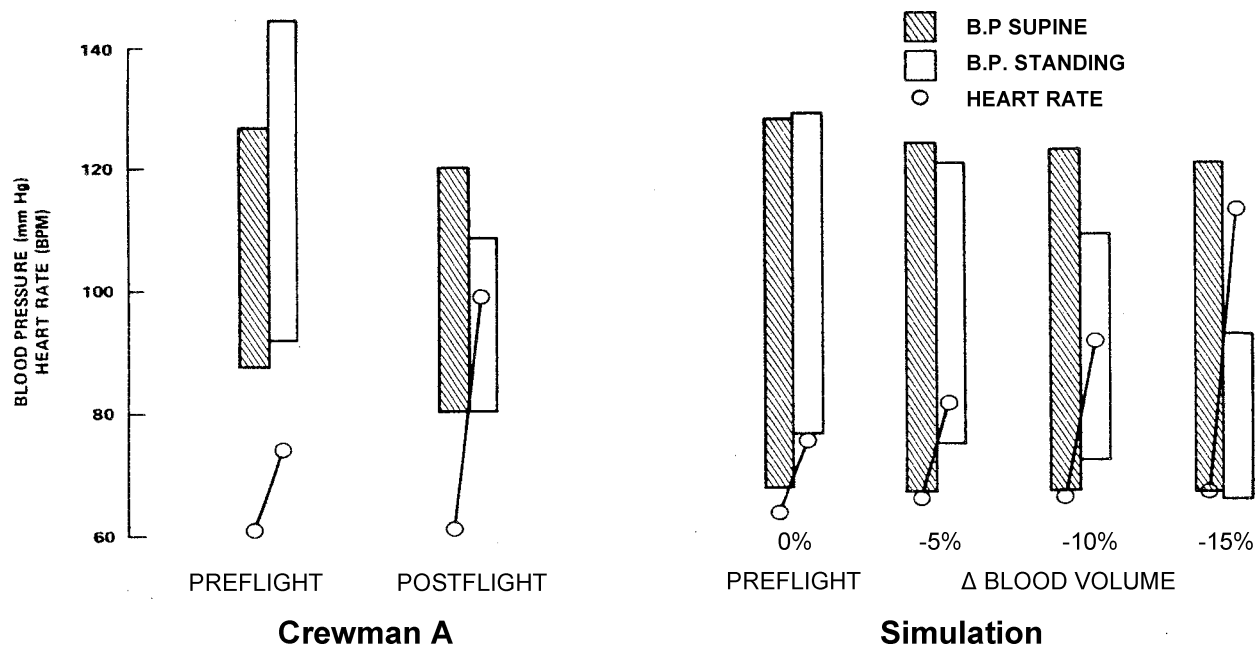
Figure 7-23. Measured (left side) versus simulated responses (right side) of crewmen from the first Shuttle flight (STS-1) to stand test administered preflight and immediately after return from space. Only the data from Crewman A is shown (repeated from Fig. 7-22). The first simulated stand test (at normal blood volume) represents preflight condition while the other 3 three simulated tests (at –5%, -10% and –15% blood volume loss) are alternatives for the postflight condition.

All of these factors taken together increase the likelihood of impaired performance during and after Shuttle landing. Therefore, it was deemed prudent to initiate some form of corrective measures prior to or during reentry (fluid loading, for example) that would increase the margin of safety, or at the very least, provide emergency countermeasures (anti-g suit, for example) that could be used at the first sign of impairment. It should be pointed out that both fluid loading and donning of anti-g garment are now part of standard operating procedures to be followed during the return of the Shuttle from space. An analysis of the anti-g suit is presented next.

7.5.4 Response with Anti-g Suit as a Countermeasure

The anti-g suit is one of the countermeasures used by the Shuttle crew for improving tolerance to headward acceleration during the reentry phase of the flight.[**] The crew would inflate the suit at the first sign of acceleration intolerance such as difficulty in vision. The positive pressure of the anti-g suit forces blood and other fluids from the legs into the central circulation. The resulting increase in venous return, cardiac output, and total peripheral resistance improves cerebral perfusion. The use of anti-g suit for improving tolerance to $+G_z$ has long been recognized for high performance jet fighter pilots [32]. However, its effectiveness may be reduced in Shuttle flights because of cardiovascular deconditioning resulting from weightless

exposure. For example, the minimum suit pressure required for a given level of protection (as judged by the carotid systolic pressure) may be expected to be higher with increasing loss of blood volume.

The dependency of minimum suit pressure on blood volume loss was examined using the LBNP model. No model modification was necessary for this study; application of anti-g suit pressure required only assigning a positive value for the LBNP parameter. Figure 7-24 shows the results of a sensitivity analysis of the effect of anti-g suit pressure on systolic carotid pressure. Results were obtained at normal blood volume and 3 levels of reduced blood volume. Operating points below a systolic carotid pressure of 62 mmHg are in a danger zone. All simulations were conducted using a g-level of 2.0. At g-levels less than 2.0 the four curves of Fig. 7-24 would shift upwards to a safer zone (not shown).

The results indicate that, a 10% BV loss can be tolerated only up to 2-g without anti-g garment protection. With a loss of 15%, the suit pressure must be at least 46 mmHg in order for the carotid systolic pressure to stay above 62 mmHg, and thus above all threshold levels. The available data from Shuttle flights showed that approximately 50% of astronauts chose to inflate the anti-g suit during reentry. The inflation pressure ranged from 26 to 78 mmHg with an average of 52 mmHg, which is close agreement with the minimum suit pressure determined from the simulation results.

Figure 7-25 shows the effects of anti-g suit pressure on cardiovascular response during Shuttle re-entry, using the STS-1 re-entry g-profile. A high value of 16% was

---

[**] Fluid loading is another countermeasure used by the Shuttle crew, discussed in Chapter 9.7.6.
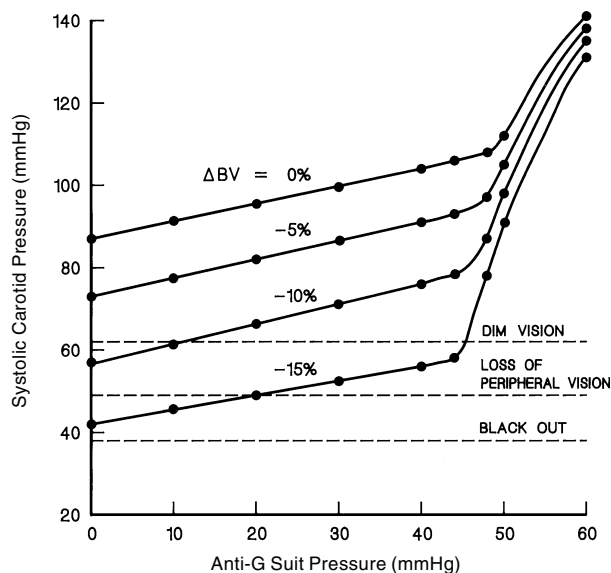
Figure 7-24. Changes in systolic carotid pressure with increase of anti-g suit pressure at different blood volume losses. Results (solid line) were obtained from the LBNP model with g-level set at 2.0. The threshold levels for visual symptoms (dashed lines) are the same as in Fig. 7-20.

Figure 7-25. Simulation of the effect of inflating the anti-g suit on cardiovascular response during re-entry, assuming a blood volume loss of 16% and the STS-1 reentry g-profile. The suit was inflated to 30 mmHg when the systolic carotid pressure reached 60 mmHg.

assumed for blood volume loss, since incidence of vision impairment are highly likely for losses of this magnitude especially if the peak g-force exceeds 2-g. The anti-g suit inflation to 30 mmHg was assumed to begin at a declining systolic carotid pressure of 60 mmHg. The simulation results indicate considerable improvement in cardiovascular response even at this low inflation pressure. These results are in basic agreement with a related pressure suit study [35] with the major exception that the peripheral resistance decreased in the simulation (not shown) but increased in the human subject. One explanation for this difference is that the simulations discussed above did not take into consideration possible mechanical compression of blood vessels below the trunk with application of lower body positive pressure. Another possibility is that the baroreceptor control included in the model is not strong enough. Nevertheless, the model was sufficiently accurate to yield plausible lower bounds of suit pressure for given levels of g-force and blood volume loss.

More detailed discussion of the Shuttle reentry problem and g-suit analysis using the LBNP model may be found in previous publications [29,36,37]. These studies demonstrate the utility of mathematical models in explaining observed responses and formulating hypotheses that lead to further experimentation, a theme emphasized throughout this book.

7.6 Cardiovascular Modeling Considerations

7.6.1 Strengths and Drawbacks of the Present Model

Analyses and simulation results presented in the foregoing sections amply demonstrate the beneficial role of mathematical models in assessing the effects of possible changes to the cardiovascular system brought about by an exposure to weightlessness. The application of mechanistic models provides a complimentary approach to traditional statistical analysis. The model may be viewed as the common background against which data from different experiments obtained under varied experimental conditions could be analyzed. However, this requires the model to be comprehensive and representative of the human system. Accordingly, our model of the cardiovascular system is large-scale in its scope with the controlled system represented by as many as 28 compartments (see Fig. 3-12). It should be noted that the systemic circulation may be modeled as elaborately as desired based on anatomical structure. Models of the arterial tree much more detailed than the representation in our model have appeared in the literature [38,39,40].

While the *controlled* system is modeled with a large number of compartments to retain close correspondence to the real system, it was not always necessary to consider the myriad of physiological factors involved in cardiovascular *control* [41]. For simulating both exercise and LBNP responses, it was sufficient to consider only the *acute* controls exerted by the autonomic nervous system. In the case of only LBNP responses, the controlling system could be further simplified by excluding the metabolic control exerted by oxygen requirements. The *more gradual* changes in cardiovascular variables, such as blood volume, brought about by the influence of long-term control mechanisms

are readily introduced into the simulation by manual changes in appropriate fixed model parameters. It is precisely these changes in model parameters that we seek when we use the model to explain the observed changes in LBNP and exercise responses during spaceflight.

The autonomic function is represented in our cardiovascular model by a proportional controller that operates on signals sensed by the baroreceptors located in the aortic arch and the carotid sinuses. No adaptation of the baroreceptors is considered such as changes in gain or threshold levels. The effects of sympathetic and parasympathetic neural components are combined into a single autonomic signal and is used to control flow resistances, compartmental compliances, and both the strength and the frequency of cardiac contractions. This representation of autonomic function was deemed adequate when the model was developed originally for simulating responses to submaximal exercise. Its inadequacy is apparent when one considers simulation of equivalent changes in heart rate controlled by different proportions of sympathetic and parasympathetic signals. The poor results of some simulations are attributable at least in part to this deficiency in the present model. Inclusion of dual autonomic control in the controlling system will certainly improve the model's capabilities.

7.6.2 Model Simplification for Simulating Orthostatic Stress Response

The approach to building the simplified cardiovascular models described here is to begin with a detailed large-scale representation and to remove elements and mechanisms that are not needed for accurate representation of the simulations of interest (top-down approach). In contrast, we can construct a simple model with only the essential elements that are necessary for simulating the data on hand and expand the model to satisfactorily simulate additional data as they become available (bottoms-up approach). We can develop a simple model of the cardiovascular system starting with our present model by reducing the number of vascular compartments and 'fine-tuning' the controlling system. We describe below such a minimal representation developed for simulating cardiovascular responses to orthostatic stress over a wide range.

The effort began with a review of the principles and data requirements for modeling the cardiovascular system to simulate its short-term response to orthostatic stresses [41]. A survey of published models showed that the existing models could be improved based on current knowledge of the cardiovascular system and recent experimental data. Three different overall models of the cardiovascular system, including the one described in the preceding sections, were compared for their capabilities in reproducing responses to different stimuli that result in an orthostatic stress (i.e., LBNP, head-up tilt, and blood volume loss [42]). These models had a similar structural skeleton, but differed in the number of compartments, assumptions for solving the equations relating pressure and flow in the arterial segments, and representations of the venous system and the cardiac function. The orthostatic responses simulated by the models were in qualitative agreement with available experimental data, but the differences were quantitatively significant. Each model produced best agreement for the stress for which it was designed.

The review and the comparison study brought to light the considerable variabilities in the observed cardiovascular responses, and pointed to the need for a simple cardiovascular model with a minimal number of elements, which would allow one to fit the experimental data from each individual subject and thus explain the observations. Such a model has been developed and applied to LBNP data [43]. It is a steady-state model aimed at simulating the pulsatile pressure and flow in the cardiovascular system following application of LBNP. The model equations are based on the following processes involved in eliciting the orthostatic response: (a) blood volume redistribution, (b) left-ventricular end-diastolic filling, (c) interaction between left ventricle and peripheral circulation, and (d) modulation of heart rate and peripheral resistances by arterial and cardiopulmonary baroreflexes.

The simple cardiovascular model and its variants have been used to simulate LBNP response up to presyncopal levels [44] as well as LBNP response modified by decreased blood volume [45]. Figure 7-26 shows comparison of experimental data compiled from a large number of LBNP studies [46] with model-generated data up to -40 mmHg LBNP. The model has also been shown to reproduce well the effects of autonomic blockade [43]. The model has far fewer number of sensitive parameters than large overall models of the cardiovascular system. Along similar lines, a ten-compartment model has been reported recently [47]. Such simple representations that contain the essential features of the cardiovascular system, but are parsimonious in the number of parameters, have the potential for simulating and comparing data from individual subjects with optimization of parameter values, and deriving indicators of cardiovascular performance under or following altered environmental conditions such as exposure to weightlessness.

7.7 Summary

The pulsatile cardiovascular model, although deficient in some respects, has proven to be a very useful tool for simulating orthostatic intolerance and exercise responses associated with spaceflight. This approach is especially convenient because of the difficulties involved in obtaining measurements during the critical periods of flight. The simulation results using the model corroborate the findings by other investigators of Skylab data. An extended analysis demonstrated the capability of the model to predict physiological responses that were not amenable to measurement and to generate and evaluate hypotheses to explain the results. Thus, it was possible to quantitatively evaluate how exercise conditioning could oppose zero-g deconditioning, to show how acute headward fluid shifts, collapsing leg veins and eventual reverse stress relaxation can help explain short and long-term changes in the cardiovascular system, and to demonstrate how blood vol-
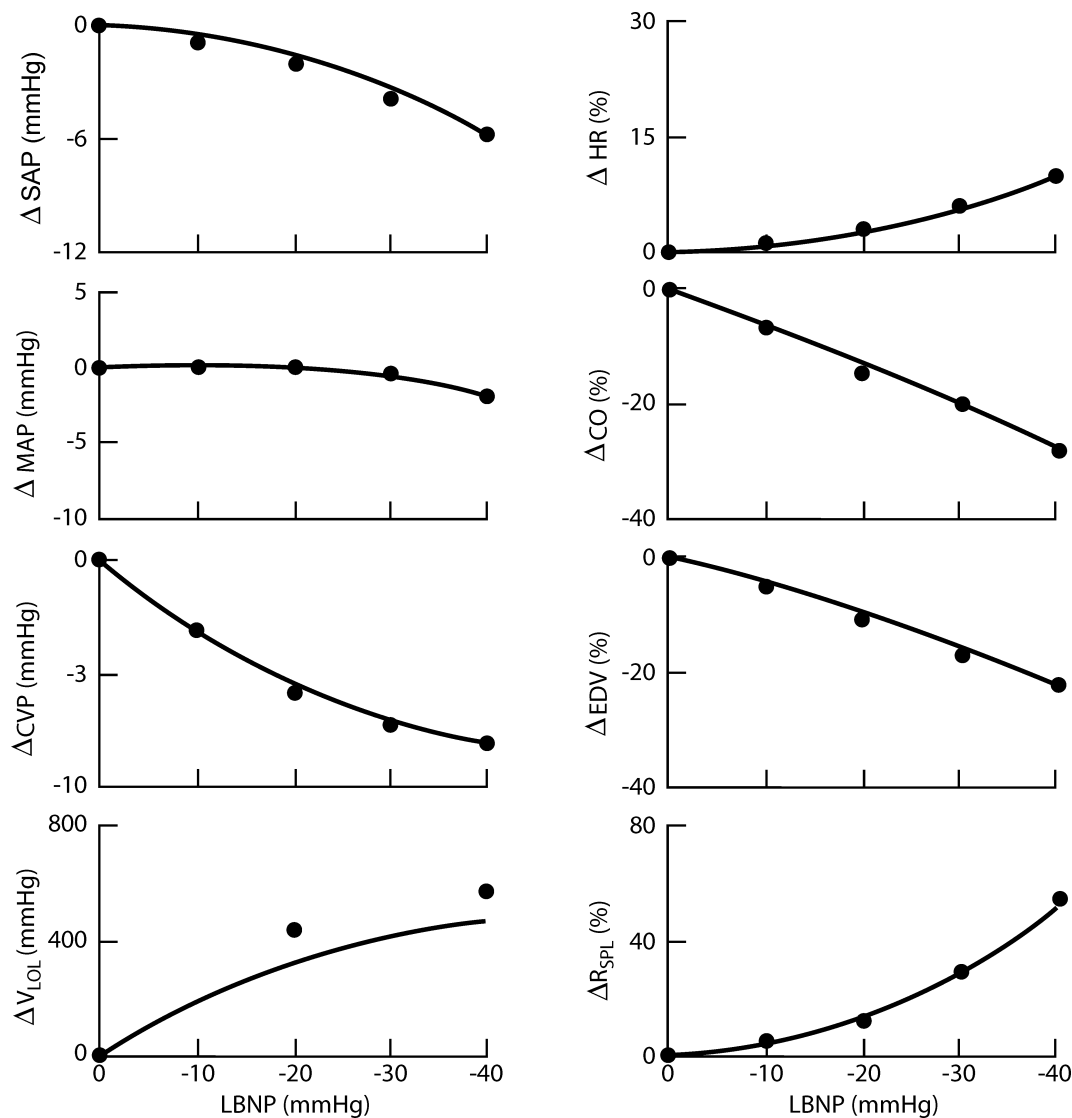
Figure 7-26. Results of the model response (solid line) to LBNP up to -40 mmHg compared to experimental data [46] (filled circles). D denotes change from baseline value at zero LBNP. SAP = systolic arterial pressure; MAP = mean arterial pressure; CVP = central venous pressure; V_{LOL} = leg volume (compartment representing the lower limbs); HR = heart rate; CO = cardiac output; EDV = end diastolic volume; R_{SPL} = splanchnic resistance.

ume loss accounts for much, but not all, of the orthostatic intolerance seen during LBNP and during Shuttle reentry from space. Other factors, including autonomic control, catecholamine release, baroreflex adaptation, and venous tone were identified for future study. An example of countermeasure development to ameliorate orthostatic intolerance, using model analysis, was also described.

In the process, a number of inadequacies of the computer models were identified, including the lack of separate sympathetic and parasympathetic pathways, a need for non-linear compliances for the leg veins modeled after the upper body veins, representation of adaptive mechanisms for baroreceptors, delayed vessel compliance and the desirability of an "open" circulation that can filter

plasma into tissues. With appropriate representation of cardiovascular control, a simplified version of the model can acceptably reproduce cardiovascular responses to orthostatic stress. Further expansion of the simplified model is the next step in the evolutionary development toward a more comprehensive (albeit minimal) model of the cardiovascular system, one that can simulate with fidelity, results from various experiments. Such a model can serve as a framework within which the results can be explained without inconsistencies and the underlying physiologic mechanisms can be elucidated.

In this chapter, the cardiovascular system has been examined during provocative maneuvers (exercise, LBNP, Shuttle reentry). The manner in which weightless space-

flight effects the cardiovascular system at rest is also of great interest. This subject is addressed in Chapter 5 and 9 as part of the response to headward fluid shifts during spaceflight and ground-based maneuvers such as water immersion and head-down tilt. The Guyton model of circulatory control has been very useful in this regard. A summary of the resting cardiovascular response to weightlessness is provided in Chapter 10.3.3.

References

1. Buckey, J. C., Lane, L. D., Levine, B. D., Watenpaugh, D. E., Wright, S. J., Moore, W. E., Gaffney, F. A., and Blomquist, C. G., Orthostatic Intolerance After Spaceflight. *J. Appl. Physiol.*, 81: 7-18,1996.

2. Convertino, V. A., Exercise and Adaptation to Microgravity Environments, in *Handbook of Physiology: Environmental Physiology III. The Gravitational Environment*, M. J. Fregly and C. M. Blatteis (Eds.), New York, NY, Oxford University Press, 1995, vol. II, chap. 36, pp. 815-843.

3. Charles, J. B., Bungo, M. W., and Fortner G. W., Cadiopulmonary Function, in *Space Physiology and Medicine*, Third Edition, A.E. Nicogossian, C.L. Huntoon and S. L. Pool, (Eds.), Lea & Febiger, Philadelphia, PA, 1994, pp. 286-304.

4. Hoffler, G. W., Cardiovascular Studies in U.S. Space Crews: An Overview and Perspective, in *Cardiovascular Flow Dynamics and Measurements,* N. H. C. Hwang and H. A. Normann (Eds.), University Park Press, 1977. pp. 335-363.

5. Croston R. C., Rummel, J. A., and Kay, F. J., Computer Model of Cardiovascular Control System Responses to Exercise. *J. Dynamic Systems, Measurement, and Control,* 95: 301-307, 1973.

6. Croston, R. C., and Fitzjerrell, D. G., Cardiovascular Model for the Simulation of Exercise, Lower Body Negative Pressure, and Tilt Experiments, *Modeling and Simulation,* 5: 471-476, 1974.

7. Michel. E. L, Rummel, J. A., Sawin, C. F., Buderer, M. C., and Lem, J. D., Results of Skylab Experiment M171 - Metabolic Activity, in *Biomedical Results of Skylab*, R. S. Johnston and L. F. Dietlien (Eds.), SP-377, NASA, Washington DC, pp. 372-387, 1977.

8. Michel, E. L., Rummel, J. A., and Sawin C. F., Skylab Experiment M-171 "Metabolic Activity": Results of the First Manned Mission. *Acta Astronautica* 2: 351-365, 1975.

9. Rummel, J. A., Michel, E. L., Sawin, C. F., and Buderer, M. C., Metabolic Studies During Exercise: The Second Manned Mission, *Aviat. Space Environ. Med.* 47: 1056-1060, 1976.

10. Rummel, J. A., Sawin, C. F., Michel, E. L., Buderer, M. C., and Thornton, W. T., Exercise and Long Duration Spaceflight Through 84 Days, *J. Am. Med. Women's Assoc.* 30: 173-187, 1974.

11. Ekbolm, B., Astrand, P., Saltin, B., Stenberg, J., and Wallstrom, B., The Effect of Training on the Circulatory Response to Exercise. *J. Appl. Physiol.* 24: 518-528, 1968.

12. Leach, C.S. and Rambaut, P.C., Biochemical Responses of the Skylab Crewmen: An Overview, in *Biomedical Results from Skylab*, R. S. Johnston and L. F. Dietlein, (Eds.), NASA SP-377, NASA, Washington, DC, 1977, pp. 204-216.

13. Frey, M.A.B., Charles, J.B. and Houston, D.E., Weightlessness and Response to Orthostatic Stress, in *Circulatory Response to the Upright Posture*, J.J. Smith (Ed.), CRC Press, Boca Raton, FL, 1990, pp. 65-120.

14. Shimizu, M., Ghista, D., and Sandler, H., Cardiovascular Regulatory Response to Lower Body Negative Pressure Following Blood Loss, *Aviat. Sp. Environ. Med.* 50: 24-33, 1979.

15. Montgomery, L. D., Kirk, P. J., Payne, P. A., Gerber, R. L., Newton, S. D., and Williams, B. A., Cardiovascular Responses of Men and Women to Lower Body Negative Pressure*, Aviat. Space. Environ. Med.* 48(2): 138-145, 1977.

16. Wothuis, R. A., Bergman, S. A., and Nicogossian, A. E., Physiological Effects of Locally Applied Reduced Pressure in Man, *Physiol. Rev.* 54: 566, 1974.

17. Murray, R. H., Bowers, J., and Albright, C., Hemodynamic Effects Of Graded Hypovolumia and Vasodepressor Syncope Induced by Lower Body Negative Pressure, *Am. Heart J.* 76: 799-811, 1968.

18. Murray, R. H., Krog, J., Carlson, L. D., and Bowers, J., Cumulative Effects of Venesection and Lower Body Negative Pressure, *Aerosp. Med.* 38: 243, 1967.

19. Convertino, V. A., Lower Body Negative Pressure as a Tool for Research in Aerospace Physiology and Military Medicine, *J. Grav. Physiol.* 8(2):1-14, 2001.

20. Nolte RW. Lower Body Negative Pressure Device (M092), in *Biomedical Results of Skylab*, R. S. Johnston and L. F. Dietlien (Eds.), NASA SP-377, NASA, Washington DC, 1977, pp. 421-423.

21. Nolte, R. W., Leg Volume Measuring System (M092), in *Biomedical Results of Skylab*, R. S. Johnston and L. F. Dietlien, (Eds.), NASA SP-377, NASA, Washington DC, 1977, pp. 424-427.

22. Johnson, R. L., Hoffler, G. W., Nicogossian, A. E., Bergman, S. A., and Jackson, M. M., Lower Body Negative Pressure: Third Manned Skylab Mission, in *Biomedical Results of Skylab*, R. S. Johnston and L. F. Dietlien, (Eds.), NASA SP-377, NASA, Washington DC, 1977, pp. 284-312.

23. Sandler, H., Cardiovascular Effects of Weightlessness, *Progress in Cardiology* 5: 227-270, 1976.

24. Thornton, W. T., and Hoffler, G. W., Hemodynamic Studies Of Legs Under Weightlessness, in *Biomedical Results of Skylab*, R. S. Johnston and L. F. Dietlien, (Eds.), NASA SP-377, NASA, Washington DC, 1977, pp. 324-329.

25. White R. J., Croston, R. C., and Fitzjerrell, D. G., Cardiovascular Modeling: Simulating the Human Response to Exercise, Lower Body Negative Pressure, Zero Gravity and Clinical Conditions, in *Advances in Cardiovascular Physics*, G. N. Ghista, (Ed.), S. Karger, Basel, Switzerland, 1983, Vol. 5, (Part I), pp. 195-229.

26. Convertino, V. A., Mechanisms of Microgravity Induced Orthostatic Intolerance: Implications for Effective Countermeasures - Overview And Future Directions, *J. Grav. Physiol.* 9:1-12, 2002.

27. Watenpaugh, D. E., and Hargens, A. R., The Cardiovascular System in Microgravity, in *Handbook of Physiology*, Section 4, Vol. 1, M. E. Fregly and C. M. Blatteis (Eds.), Amer. Physiol. Soc., Oxford University Press, New York, NY, 1996, pp. 631-674.

28. Guyton, A. C., Circulatory Physiology III: Arterial Pressure

and Hypertension, W. B. Saunders Co., 1980, pp. 61-64.

29. Srinivasan, R. S., Leonard, J. I., and White, R. J., Mathematical Modeling of Physiological States, in *Space Physiology and Medicine*, A. E. Nicogossian, S. R. Mohler, O. G. Gazenco, and A. I. Grigoriev, (Eds.), VA Reston. Reston, VA, American Institute of Aeronautics and Astronautics and Moscow, Russia, Nauka Presss, 1996, Vol. III, Chap. 26, pp. 559- 594.

30. Wood, E. H., Acceleration, in *Bioastonautics Data Book*, P. Webb, (Ed.), NASA SP-3006, 1st ed., NASA, Washington, D.C., 1964.

31. Henry J. P., Gauer O. H., Kety, S. S., and Kramer, K., Factors Maintaining Cerebral Circulation During Gravitational Stress, *J. Clin. Invest.* 30: 292-300, 1950.

32. Lindberg, E. F., and Wood, E. H., Acceleration, in *Physiology of Man in Space*, J. M. U. Brown, (Ed.), Academic Press, NY, 1963, pp. 61-111.

33. Bungo, M. W., Crew Cardiovascular Profile, *STS-1 Medical Report*, S. L. Pool, P. C. Johnson and J. A. Mason, (Eds.), NASA TM-58240, NASA, Washington, DC, 1981.

34. Greenleaf, J. E., Van Beaumont, W., Bernauer, E. M., Haines, R. F., Sandler, H., Staley, R. W., Young, H. L., and Yusken, J. W., Effects of Rehydration on +G_z Tolerance After 14-Days Bedrest, *Aerospace Med.,* 44: 715-722, 1973.

35. Gaffney, F. A., Thal, E. R., and Taylor, W. F., Hemodynamic Effect of Medical Anti-Shock Trousers (MAST Garments). *J. Trauma* 21: 931-935, 1981.

36. Leonard J. I., and Srinivasan, R., Predictions Of Cardiovascular Responses During STS Reentry Using Mathematical Models, *Technical Information Release*, 2114-MED-4002, General Electric Company, NASA Contract NAS9-17151, NASA, Washington DC, 1984.

37. Srinivasan, R. S., and Leonard, J. I., Simulation of Cardiovascular Response to Acceleration Stress Following Weightless Exposure, *Proc. Summer Simulation Conf.*, Vancouver, Canada, July 11-13, 1983, Society for Computer Simulation, San Diego, CA, 1983, vol. 1, pp. 598-603.

38. Sheng, C., Sarwal, S. N., Watts, K. C., and Marble, A. E., Computational Simulation of Blood Flow in Human Systemic Circulation Incorporating an External Force Field, *Med. & Biol. Eng. & Comput.* 33: 8-17, 1995.

39. Sud, V. K., Srinivasan, R. S., Charles, J. B., and Bungo, M. W., Effects of Lower Body Negative Pressure on Blood Flow With Applications to the Human Cardiovascular System, *Med. & Biol. Eng. & Comput.,* 31: 569-575, 1993.

40. Avolio, A. P., Multi-Branched Model of the Human Arterial System, *Med. Biol. Eng. Comput.,* 18: 709-718, 1980.

41. Melçhior, F. M., Srinivasan, R. S., and Charles, J. B., Mathematical Modeling of Human Cardiovascular System for Simulation of Orthostatic Response, *Am. J. Physiol.* 262(31): H1920-H1933, 1992.

42. Karam, E. H., Srinivasan, R. S., and Charles, J. B., A Comparison of Overall Mathematical Models of the Cardiovascular System for Simulating Response to Orthostatic Stress, *The Physiologist* 35 (Suppl.): S164-S165, 1993.

43. Melçhior, F. M., Srinivasan, R. S., Thullier, P., and Clere, J. M., Simulation of Cardiovascular Response to Lower Body Negative Pressure from 0 to –40 mmhg, *J. Appl. Physiol.* 77(2): 630-630, 1994.

44. Karam, E. H., Srinivasan, R. S., and Charles, J. B., Simulation of Cardiovascular Response to Lower Body Negative Pressure up to Presyncopal Levels, *Mathematical Modeling And Scientific Computing* 4: 327-332, 1994.

45. Karam, E. H., Srinivasan, R. S., Charles, J. B., and Fortney, S. M., The Effect of Blood Volume Loss on Cardiovascular Response to Lower Body Negative Pressure Using a Mathematical Model, In *Proc. Ann. Meet. Internat. Soc. Grav. Physiol.*, Barcelona, Spain, Oct. 3-8, 1993, pp. P96-P97.

46. Blomqvist, C. G., and Stone, H. L., Cardiovascular Adjustment to Gravitational Stress, In *Handbook of Physiology. The Cardiovascular System. Peripheral Circulation and Organ Blood Flow*, Am. Physiol. Soc., Bethesda, MD, 1983, Sect. 2, Vol. III, Pt. 2, Chap. 28, pp. 1025-1063.

47. Heldt, T., Shim, E. B., Kamm, R. D., and Mark, R. G., Computational Modeling of Cardiovascular Response to Orthostatic Stress, *J. Appl. Physiol* 92: 1239-1254, 2002.

Chapter 8
Musculoskeletal System and Calcium Regulation

Losses in bone and muscle mass were among the many physiological changes seen in Skylab crewmen during spaceflight. The losses, first observed in the Gemini and Apollo crews, [1,2] were not studied extensively until the Skylab missions. Deficiencies identified in the musculoskeletal system during hypogravity include: a) muscle and connective tissue atrophy and localized bone loss; b) reductions in motor performance; and c) increased susceptibility to injury (fracture, sprains). In addition, muscle atrophy undoubtedly contributes to (but is not normally implicated in) the occurrence of orthostatic intolerance observed upon immediate return from spaceflight. Because the systems analysis tools that were used to investigate the hypotheses have not yet been as fully developed as in other disciplines (i.e., Chapters 4 to 7), the analysis presented here concerning musculoskeletal adaptation in zero-g should be considered as a preliminary one. If these losses are understood, perhaps they can be prevented or reversed by taking the appropriate measures in future missions.

The main emphasis in this chapter will be on calcium regulation with the aim of using knowledge of this complex feedback system to better understand bone demineralization in spaceflight. A unique contribution to this area is the application of a mathematical model to simulate the hypogravity environment. Analysis of muscle atrophy using metabolic balance techniques has been reported in Chapter 4. In this chapter there is a brief summary of other experimental evidence (mostly obtained from Skylab) supporting the findings of muscle atrophy and a discussion of the underlying mechanisms. Finally, there is a short discussion of the benefits of exercise and other countermeasures to both of these tissue systems.

8.1 Bone and Calcium Regulation

8.1.1 Introduction

Loss of calcium from the body had been observed during bedrest studies and in short-term spaceflight missions prior to Skylab [3,4]. One of the most important contributions of the Skylab missions was to show the extent of calcium loss in a relatively long 3-month mission and to document biochemical changes related to calcium loss during flight [5]. In the post-Skylab era, calcium losses have been noted consistently in both U.S. and Russian space missions, some of which have lasted more than a year [6]. At the time of Skylab the prevailing hypothesis to explain calcium loss was that it was related to the removal of mechanical loading as the originating event. But it was not clear just how this occurred nor whether there were some other primary events that originate in the kidneys, intestines, or hormonal secretion organs and have secondary effects on bone demineralization.

The systems analysis of bone loss in space, including the use of a mathematical model of calcium regulation, addressed the various hypotheses and interpretations of spaceflight and bedrest findings. A summary of the analysis will include the following topics: a) a brief review of physiological considerations that are needed to interpret the experimental findings and to create a model of calcium regulation; b) the most significant results from the Skylab missions; c) a summary of a bedrest study not previously published with comparison to spaceflight results; d) a description of the computer model and simulations of hypogravity; and e) development of hypotheses to explain the spaceflight and bedrest findings. Results from spaceflight, bedrest and mathematical modeling studies will be combined to help formulate an overall hypothesis of calcium metabolism adaptation to long-term spaceflight.

In order to better understand the experimental findings and their role in overall calcium metabolism, a brief review of the components of the calcium regulating system is provided below.

8.1.2 Physiology of Calcium Metabolism

Calcium is a critical element in the composition of bone, as is suggested from the fact that 98% of the total body calcium is contained in the skeletal tissue. Calcium metabolism centers on maintenance of the integrity of the bone and homeostatic control of extracellular (or plasma) calcium concentration. There are three major organs responsible for calcium regulation: bone, kidneys and intestines (see Fig. 8-1). Bone can be thought of as a calcium reservoir for the maintenance of plasma calcium. The intestines act as both a source of external calcium via dietary intake as well as a means of (fecal) excretion. Blood calcium is filtered into the kidneys at high rates and most is reabsorbed back into the circulating plasma; thus small changes in reabsorption will produce large changes in urinary excretion of calcium. Similarly, there is a great turnover of bone calcium under normal conditions; bone formation and bone reabsorption are both naturally high flux processes.

Calcium concentration in plasma is exquisitely controlled. The pathways available to correct increases or decreases in extracellular calcium concentration are indicated in Fig. 8-2. Accordingly, if calcium concentration rises above normal, the excess calcium can be excreted through the kidneys or intestines or can incorporated into new or existing bone (known as accretion, deposition, formation, or mineralization). Conversely, if calcium concentration falls below normal, calcium sources are activated by increasing the fluxes into the extracellular pool. These sources include bone resorption (i.e., demineralization), renal reabsorption and intestinal absorption. Also shown
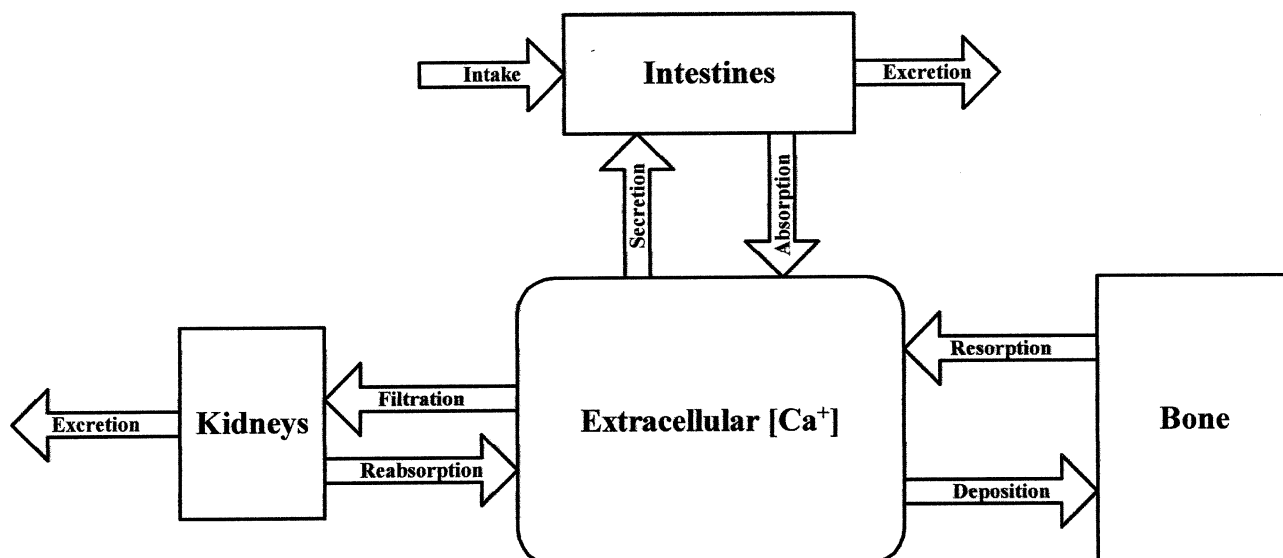
Figure 8-1. Simple model of the organ compartments that participate in regulation of extracellular calcium concentration. The calcium fluxes connecting the Extracellular compartment are under control of the calcitropic hormones (not shown here). Note the confusing similarities of some of the terms often used to describe "inward" calcium flux: *resorption* from bone, *reabsorption* from kidneys, and *absorption* from the intestines.
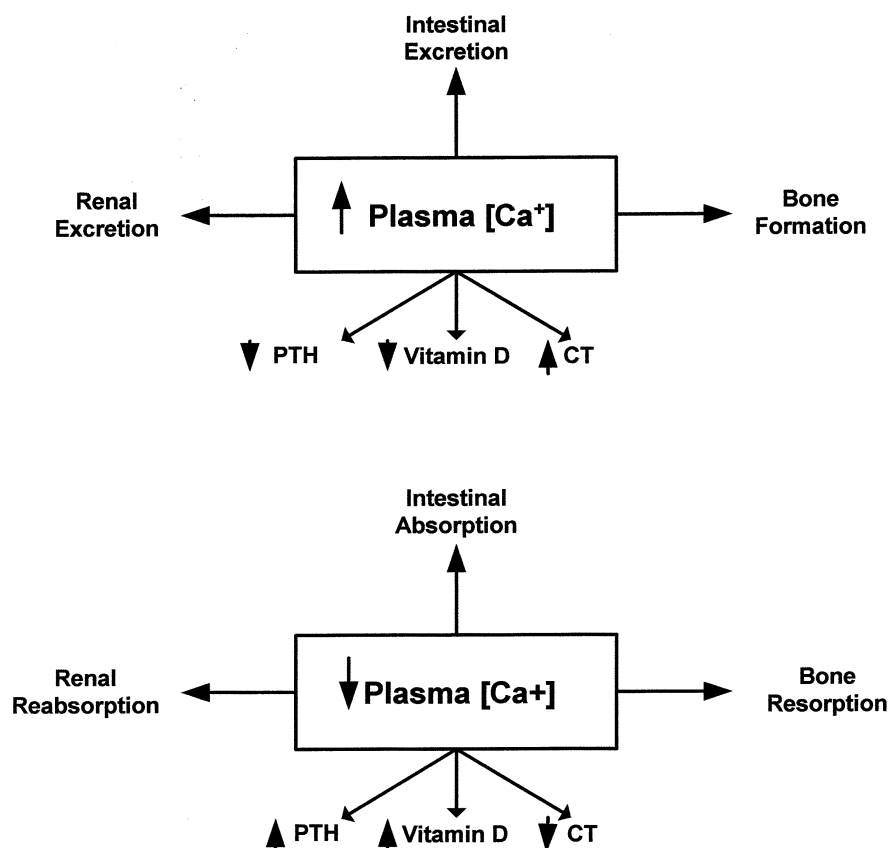
Figure 8-2. Basic physiological responses to a decrease (top figure) or increase (bottom figure) in plasma calcium concentration. Changes in plasma calcium can be corrected by fluxes into or out of bone, or increases and decreases in renal and intestinal excretion. The hormone controllers will theoretically change in the directions shown. The relationships between the hormones and their actions on bone, kidney and intestines are shown in Fig. 8-3. See text and Fig. 8-7 for further clarification. (PTH = parathyroid hormone; CT = calcitonin).
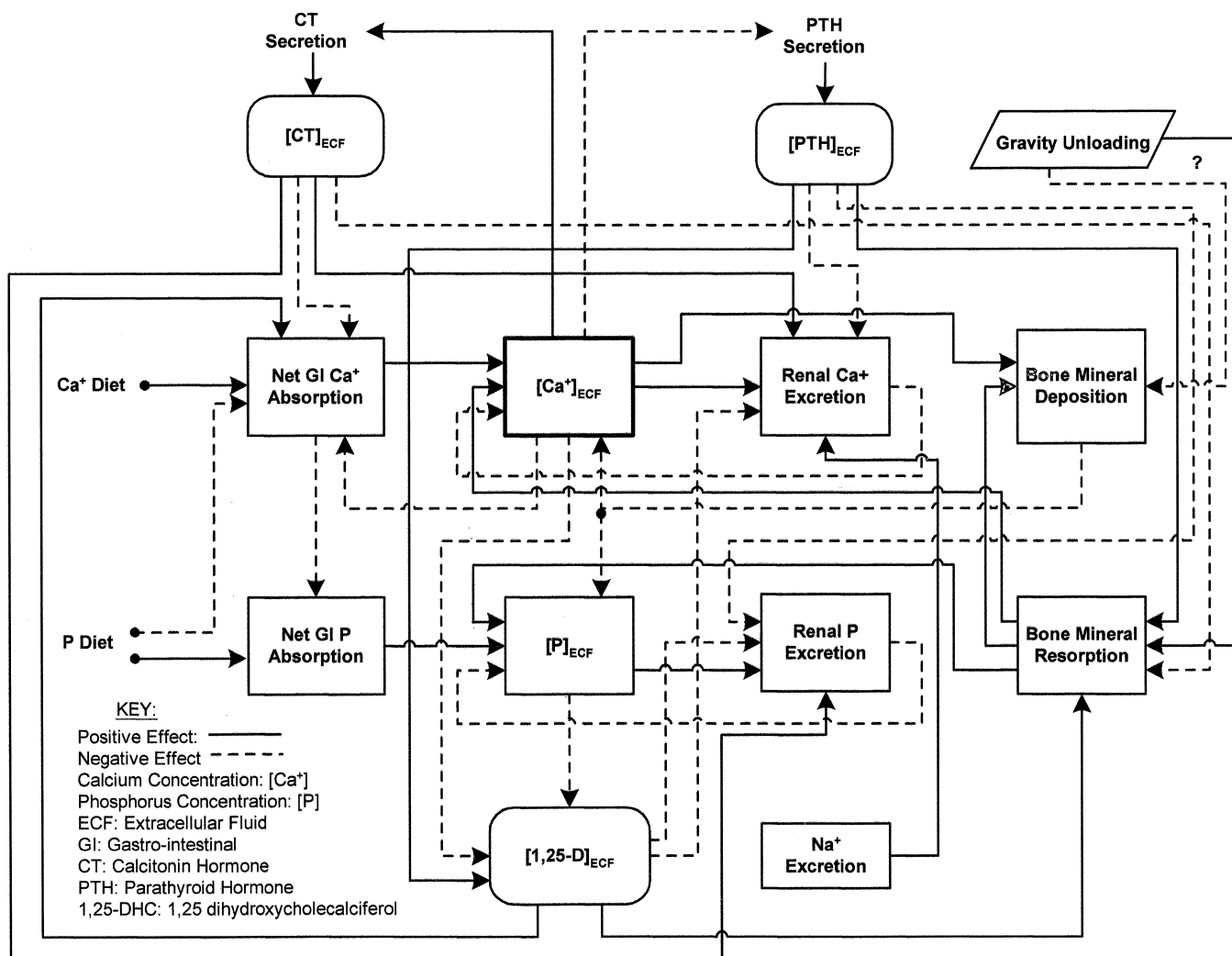
Figure 8-3. Model of calcium metabolism showing the interrelationships between the three major organ systems involved with calcium homeostasis: intestines, kidneys, and bone tissue. The three calcitropic regulatory hormones, parathyroid hormone (PTH), calcitonin (CT), and vitamin D (1,25-DHC) are included. Phosphorus (P) is also included because it is a critical element in both bone composition and calcium regulation. The system functions to regulate extracellular (ECF) calcium concentration. Suggested pathways for gravity effects are shown. The computer model shown in Fig. 8-7 uses a subset of these pathways. Suggested pathways for gravity effects are shown.

in Fig. 8-2 are the expected changes in the three major calcitropic hormones (parathyroid hormone, metabolites of vitamin D, and calcitonin) that participate in the feedback regulation. (Their modes of action are described below). In experimental studies, including those of bedrest and spaceflight, the expected changes of these theoretical pathways are not always observed. The preferred pathways and the actions of hormone controllers and other possible regulators under many experimental and clinical conditions are still actively being researched and are not well understood. Two pathways in particular, filtration into the kidneys and secretion into the intestines are often considered to be relatively constant and not under regulatory control. With little evidence to the contrary, that is the assumption that was used in the mathematical model.

Figure 8-3 is a rather intricate diagram of the (mostly) accepted relationships of calcium metabolism as they occur in the major organs depicted in Fig. 8-1. The interaction of phosphorus, another critical bone mineral, is also shown. The regulation of calcium metabolism is largely under the control of three hormones mentioned above: one secreted by the parathyroid glands (parathyroid hormone; PTH), one from the thyroid gland (calcitonin; CT), and one derived from vitamin D through activation processes by the skin, liver, and kidney (1,25 dihydroxycholecalciferol; 1,25-DHC). 1,25-DHC is the most biologically active metabolite of vitamin D3 [7]. PTH and CT have opposing effects and are thought to be primarily responsible for regulation of extracellular calcium levels; PTH mobilizes calcium from the bone and increases

renal tubular reabsorption in response to a decreased plasma calcium; CT depresses bone resorption transiently and thus inhibits the flow of calcium from bone to blood in response to elevated serum calcium. Less is known about all the forms and functions of vitamin D, but it has a major role in enhancing intestinal absorption of calcium and a lesser role in enhancing renal calcium reabsorption; both these effects thus tend to raise plasma calcium levels. The action of Vitamin D on the bone is more complex, because it appears to both promote bone formation and calcium mobilization (reabsorption). The actions of these hormones are complex and interrelated as the overlapping feedback loops in Fig. 8-3 illustrate.

Although complex, the information in Fig. 8-3 is very compact and efficiently presented and can be viewed in various ways. For example, examining the inputs and outputs to the box representing the extracellular calcium concentration, $[Ca^+]_{ECF}$, indicates that there are four pathways that can change $[Ca^+]_{EFC}$ (GI absorption, renal excretion, bone resorption, and bone formation) and there are six different quantities that $[Ca^+]_{ECF}$ can influence (PTH, CT and 1,25-DHC, bone deposition, renal excretion, and intestinal absorption). The known affects of each of the calcitropic hormones are explicitly shown. Also shown are the postulated direct effects of gravity unloading (weightlessness) on bone formation and resorption. All of these are gross effects, only indicating whether one quantity has a positive or negative influence on another. It does not portray the magnitude of the effects, thresholds, adaptation to prolonged effects, etc. Many of these relationships and effects, if well described (and many are not) are incorporated into the mathematical model that is presented later in this chapter.

With this rudimentary physiological schema as a context, the primary findings of spaceflight and bedrest studies will be presented next.

8.1.3 Skylab Mission Results

The Skylab missions presented the first opportunity to study calcium metabolism and bone demineralization during spaceflight. Assumptions of human bone degradation in space, which are today well accepted, have been based on several types of Skylab findings: a) negative calcium balances including excess excretion of calcium in urine and feces, b) reduction in mineral density of load-bearing bones, c) increased rates of hydroxyproline excretion rates, and d) analysis of plasma and urine samples for bone minerals and hormones known to regulate calcium metabolism [5,8]. These findings will be summarized briefly below:

a) **An Increase in Urine and Fecal Calcium.** The first indication of a disturbance in calcium metabolism in microgravity was the immediate increase in urine calcium excretion rates. Levels of urinary calcium increased progressively the first 18 to 24 days inflight, after which time they appeared to stabilize at a new excretory rate (see Fig. 8-4). The plateau occurred at a value approximately 60% higher than the preflight mean. Excretion of calcium in the feces also exceeded preflight norms but not until 2-3 weeks af-

ter launch and then the loss became more progressive (did not plateau) and continued to increase with flight duration.

b) **A Negative Calcium Metabolic Balance.** The calcium balances, computed by subtracting renal and fecal excretion rates from dietary intake, confirmed a consistent and progressive loss in total body calcium (see Table 4-24 and Fig. 8-5). The inflight calcium balances during the first month were slightly more negative than the preflight balances and they became increasingly more negative with each successive month in space. The early (first month) losses in total body calcium can be attributed to the higher urinary losses of calcium (Fig. 8-4), while losses later in the mission are a combined result of renal and fecal losses. The total losses of calcium derived from these studies (uncorrected for the small amount of losses in perspiration) indicate that an average 20 g of calcium, or about 0.8% of the total body pool, was lost from each of the three Skylab crewman on the 84-day mission.

c) **A Reduction in Bone Density.** Inflight losses of bone mass were detected by bone density changes in the heel (calcaneus) which were measured by photon absorptiometric techniques (x-ray densitomography) during both the Apollo and Skylab programs [5,9]. On Skylab, calcaneous losses were not significant during the 28-day mission; the losses averaged about 2% of the preflight density on the 59-day mission; on the 84-day mission the losses averaged 4% of preflight density. Apparently, a slow but consistent loss in calcaneus bone density occurs with extended durations in space.

Calcaneal loss of calcium was found to be proportional to that calculated from calcium balance studies in the Skylab crewmembers (correlation coefficient = 0.8), strongly suggesting that loading bearing bones are preferentially losing calcium and are responsible for the negative calcium metabolic balance [10]. This conclusion is supported by bone density measurements of the radius and the ulna bones (of the arm) which showed no appreciable loss during any of the Skylab missions. Because the calcaneus only contains about 0.2% of the total body calcium, other weight-bearing bones likely contribute to the estimated total whole-body losses of calcium.

d) **Excretion of Hydroxyproline.** Indirect support for bone mass changes were derived from urinary losses of hydroxyproline and hydroxylycine. These substances are components of the collagen matrix of the bone, and their presence in the urine is assumed to be related to collagen break down, a tissue present in bone joints and a source of calcium. On Skylab, both these substances were measured in urine and showed a gradual increase on each mission [5,11]. Urinary hydroxyproline increases progressively the first month and plateaus at a value 34% higher than the preflight mean.

e) **Blood and Urine Biochemistry.** Analysis of plasma and urine revealed inflight increases in calcium and phosphate that were significant throughout the 3-month duration in space [12]. Plasma PTH was more
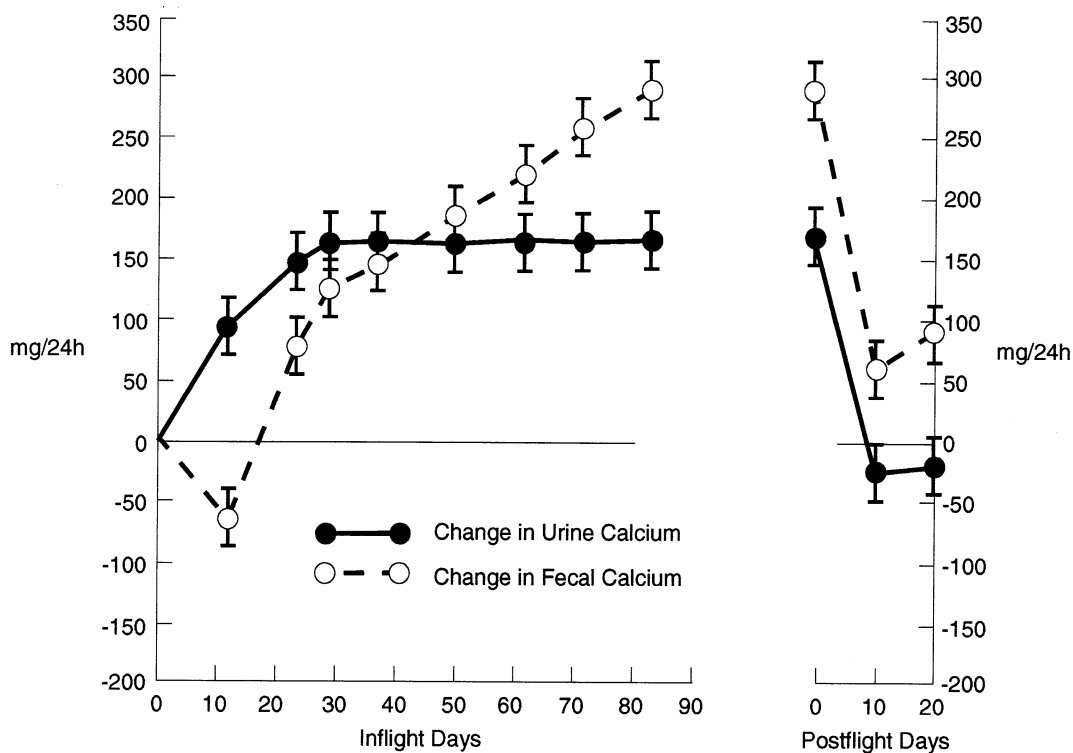
Figure 8-4. Urine and fecal calcium excretion during the 84-day Skylab mission (mean ± SE). From Rambaut and Johnston [5].
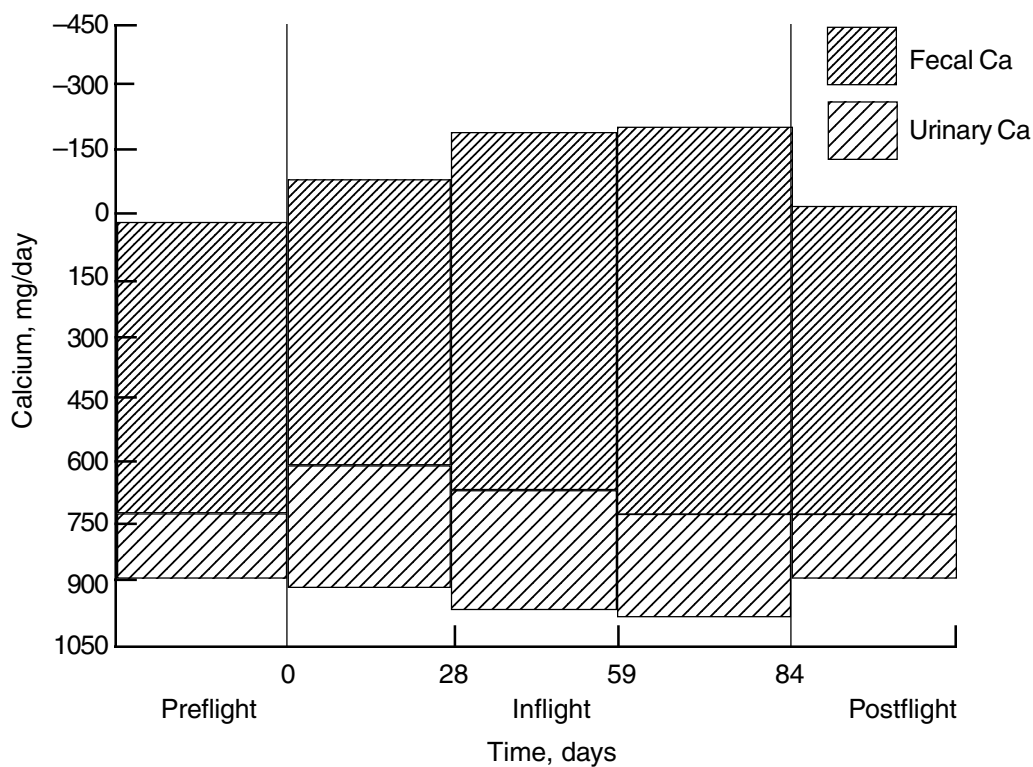
Figure 8-5. Average calcium balance of the three Skylab crews. The preflight, postflight, and first month inflight averages are of nine crewmembers. The second and third inflight month averages were calculated from six and three subjects, respectively. The data are plotted in the conventional Albright–Reifenstein style: from the zero baseline, dietary intake is plotted downward. Urinary excretion is plotted upward from the intake value and fecal excretion is plotted upward from the urinary value. The top of the fecal value indicates the balance. Values below the zero baseline are positive balances; above are negative balances.

difficult to interpret; one report showed higher mean values inflight for all nine crewmembers while another showed a decrease in mean value for crewmembers on the 84-day mission. None of these results were statistically significant. Plasma vitamin D, measured only after the missions, showed no change. Calcitonin was below the level required for detection. Another hormone that is capable of influencing calcium metabolism is cortisol, a substance that was found to be elevated on all Skylab flights [12]. High levels of cortisol are known to cause bone mineral loss in humans and may have contributed to the changes in calcium regulation in spaceflight [13].

In summary, the results collected from the Skylab crews suggested that the integrity of particular bones began to decay upon long-term exposure to spaceflight. Most of the Skylab measurements of calcium metabolism indicated negligible calcium losses after the first month inflight; they showed considerable losses the second month and some of the indicators showed progressive losses carrying into the third month in space.

8.1.4 Bedrest

Bedrest is frequently used as a ground-based analog of the microgravity of spaceflight; it provides a means of testing and examining microgravity physiology in a one-g environment. By removing the downward gravitational forces that occur during erect ambulation, a degradation effect of bone is produced that may be similar to that encountered in weightlessness. (In the next chapter it will be shown how bedrest is used to emulate the circulatory, fluid and electrolyte responses of microgravity). However, bedrest does not *remove* the effects of the gravity vector completely, it merely *reduces* the effect of gravity, so the analogy is imperfect. Because bedrest is ground-based, it is possible to conduct studies in a laboratory setting, using superior measurement techniques that would not be suited for a remote space cabin, with a higher statistical subject population.

8.1.4.1 Analysis of Results. A collection of bedrest data, never previously published, was made available to the systems analysis project for examination [14]. The data was collected over a 10-year period and included strict supine bedrest periods lasting up to 36 weeks. During the analysis, comparisons were made between bedrest and spaceflight using the Skylab microgravity data. A summary of the main conclusions of this analysis is provided below from the original report [15].

a) **Comparison of Bedrest and Spaceflight.** Figure 8-6 shows a selected portion of the bedrest data in comparison with Skylab data over a period of 3 months of hypogravic testing. Many of the bedrest responses are similar to the spaceflight responses reported by
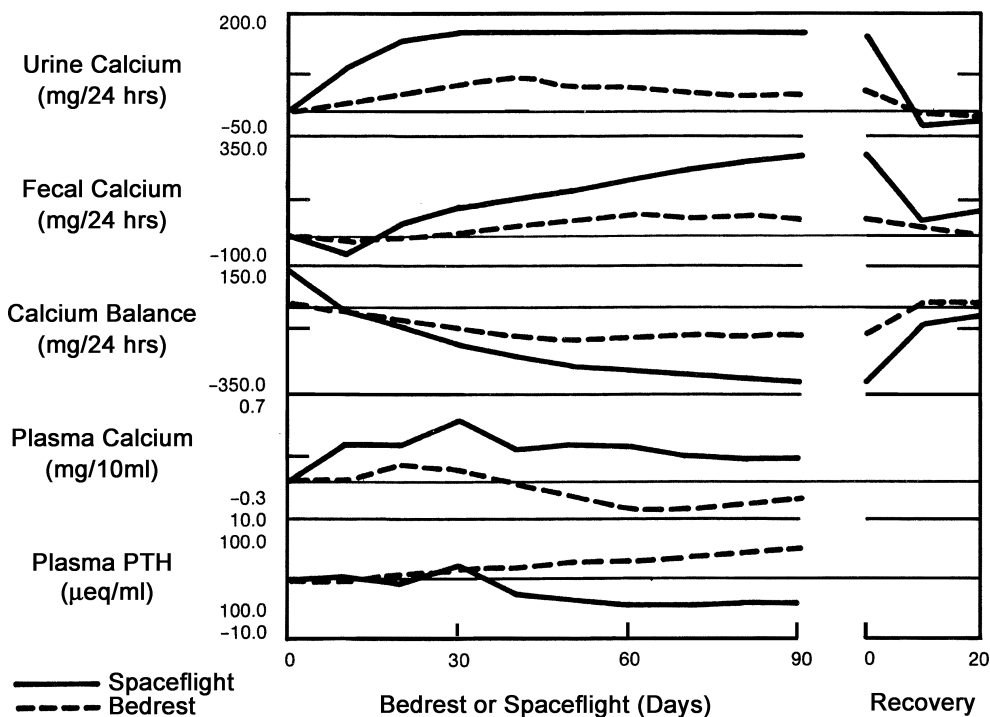
Figure 8-6. Comparison of bedrest and spaceflight data. Spaceflight is represented by the data from Skylab [5,8,12] while the bedrest data is taken from a collection of clinical hospital studies [14,15]. Values are shown as mean change from ambulatory control.

Skylab investigators [5,8,12]. The main differences are quantitative, and these may be due to the nature of the mechanical stress forces present during bedrest vs. spaceflight. Another explanation is the differences in experimental protocol. For example, during spaceflight there was an increase in dietary calcium both within a single mission as a function of time and between successive missions. Dietary calcium was increased on Skylab because of the belief that it might inhibit some of the calcium loss; thus, an increase in dietary calcium may be expected to affect the spaceflight data shown in Fig. 8-6 and confound the analysis.

**b)** **Kidney Excretion.** Urine excretion of calcium began to increase almost immediately in both bedrest and spaceflight. In bedrest, phosphorus excretion followed calcium excretion very closely, both elements probably coming from the same source – skeletal tissue. After several weeks of bedrest, the renal excretion rates of calcium decline (although still remaining above baseline), but during spaceflight they remain stable at an elevated level (Fig. 8-6).

c) **Hormonal Regulation.** PTH is known to cause a decrease in renal calcium excretion by virtue of its ability to enhance tubular reabsorption (see Fig. 8-3). In bedrest, this hormone gradually increased significantly after a month, helping to explain the longer term renal calcium excretion behavior noted above. Although the graph in Fig. 8-6 suggests that PTH becomes elevated in bedrest and reduced in spaceflight, the statistical significance of the data in both cases is rather low. However, based merely on the average long-term changes (longer than 6 weeks) it is likely that the reduced plasma calcium levels observed in bedrest were responsible for the increased PTH levels and long-term decline of the urine calcium excretion toward control. The reverse process may occur in spaceflight. Although this scenario is consistent with current theory, it is not clear why bedrest and spaceflight should exhibit these quite different effects. More specifically, why is calcium plasma concentration found to be below control in bedrest and above control in spaceflight? The experimental results should be confirmed in both situations before searching for alternative explanations. One alternative, for example, is that in this bedrest study, the correlation of the reduction in plasma magnesium and increasing PTH levels is quite high, suggesting a possible causal effect.

The vitamin D data are scant and inconclusive in this bedrest study and there seems to be little agreement regarding trends in hypogravity [6]. Calcitonin was not measured during the bedrest study nor has it been measured in spaceflight[UPDATE #1].

d) **Intestinal Absorption and Excretion.** During bedrest, the intestinal absorption of calcium gradually decreases to rates as low as 75% below control. There is also a more subtle decrease in phosphorus absorption. These changes are directly related to the increase in fecal calcium excretion. Similar alterations in intestinal absorption and fecal loss are apparent in the Skylab results (Fig 8-4 and 8-6). These changes are long-term, requiring five or six weeks to be maximally effective, and are presumably mediated by decreases in 1,25-DHC. In Skylab, the effect of 1,25-DHC on absorption may be partially countered by the increasing dietary intake of calcium over time, which can cause intestinal absorption to increase by passive diffusion.

e) **Bone Resorption.** In these bedrest studies, no direct bone measurements were made, (i.e., bone density or osteoclastic activity), but the urine excretion of hydroxyproline showed that it paralleled urinary calcium excretion for the first several weeks. This can indicate that bone resorption is elevated and the products of bone demineralization are being excreted by the kidneys. An increase in resorption is consistent with the hypothesis that this is the initiating event in bone demineralization because of an unknown mechanical stress factor. In this regard, bedrest and spaceflight may be similar.

8.1.4.2 Summary of Bedrest. The response to bedrest is difficult to typify with the existing data, but it can be categorized as occurring in three distinct time periods: short, intermediate and long term. The *short-term period* (up to two weeks) is characterized by small, recordable changes in urine excretion rates. Calcium efflux from bone commences at the onset of hypogravity, but the bone has such large quantities of calcium, and the calcium regulatory system is so effective, that these changes in calcium efflux may be too small to detect as increases in plasma calcium concentration. *The intermediate period* (from 4 to 6 weeks after onset) is characterized by increasing urine excretion rates of calcium, phosphorus, magnesium, and hydroxyproline presumably reflecting osteoclastic bone resorption activity. The kidney filters the excess load of each substance from the plasma by means of normal renal regulation (modulated by PTH in the case of calcium) maintaining the plasma calcium and phosphorus concentrations within a few percent of normal. This period may also be characterized by the changes in the production and secretion rates of the calcitropic hormones. The *long-term period* (beyond 6 weeks) is characterized by renal excretion rates decreasing toward baseline during bedrest. Net intestinal absorption rates decrease also, allowing the calcium load to be eliminated preferentially through intestinal excretion. Eventually, the system balances at a new steady state, with slightly different calcium fluxes into and out of each compartment. New plasma concentrations of calcium, phosphorus, PTH and 1,25-DHC are also established.

8.1.5 Simulations Studies with the Calcium Regulatory Model

The Skylab data confirmed the total body losses of calcium, but did little to expand our understanding of the physiological processes involved with the altered calcium state. What are the fundamental drivers for body calcium

loss in space? What is the behavior of osteoblastic and osteoclastic activity during long-term adaptation to space-flight? Is it possible to predict the magnitude and direction of the calcitropic hormone regulators for long-term exposure to microgravity? Addressing these types of calcium regulatory issues can sometimes be best addressed using a model that contains the appropriate calcium pathways and the (hormonal) feedback regulatory elements.

As we have shown in earlier chapters mathematical models can be used to extend the predictive powers of the physiologist and, by means of simulation, to define hypotheses and check them against experimental results, thus gaining insights into processes that are not amenable to measurement. At the very least, the modeling process permits the researcher to organize in a systematic way all of the relationships of this very complex system; the model then provides a framework to identify gaps in knowledge and to add new information as it becomes available.

Modeling efforts of calcium metabolism that incorporated representations of physiological processes did not begin until the late 1970's. It was only at that time that the role of the excretory organs, regulatory agents and bone biochemistry had become defined. To further our understanding of the alterations of whole-body calcium metabolism upon exposure to reduced gravity conditions, a mathematical model of calcium metabolism was developed as part of this project.

8.1.5.1 Model Description. The model is based upon the interactive and logical characteristics of biological homeostatic feedback theory and the mathematical representation of calcium-related control systems. The central purpose of the model, as well as the physiological system that it represents, is the control of extracellular calcium-ion concentration, $[Ca^+]_{ECF}$ which is the controlled variable in the model. Model regulation is achieved using subsystems that describe urinary excretion, intestinal absorption, and skeletal handling of calcium. The calcitropic hormones are included as regulatory agents. Many of the relationships in the model were discussed earlier in Chapter 8.1.2 (see Fig. 8-3) and an overview of the model was presented in Chapter 3.2.7.

A schematic form of the basic model is shown in Fig. 8-7. The model consists of four compartments, a central *extracellular fluid* compartment, in which the concentration of calcium is regulated by fluxes to and from the *renal, intestinal, and skeletal* compartments. The renal compartment removes calcium from the central compartments, the intestinal compartment adds dietary calcium to the central compartment, and the bone compartment stores calcium in an internal reservoir and acts as a buffer to the central compartment. Calcium enters the intestines in dietary form as well as in the secreted digestive juices; part of the calcium in the intestines is absorbed into the plasma while the rest is lost in the excreta. In the kidneys, calcium is filtered; part of it is reabsorbed, the rest excreted.

The routes of calcium in and out of the bone compartment represent net changes that are related to specific cellular and biochemical activity rates. Referring to Fig. 8-7,

the term *resorption* represents a general degradation, or loss of calcium out of the solid bone that is assumed to be caused primarily by cellular osteoclastic activity (or bone demineralization); *accretion* represents the buildup, or increase of calcium into the solid bone mineral by osteoblastic activity (or bone formation); *influx* and *efflux* represent general gains and losses, respectively, from the bone fluid. Bone fluid is the fluid between the cells just exterior to the bone surface and the bone surface itself (osteocytic lining) and contains recently deposited amorphous calcium phosphate. Through the osteocytic lining, calcium can be rapidly added to or removed from the extracellular fluid. Thus, the bone fluid is the most important short-term buffer system for calcium in the body [16]. The solid bone compartment contains crystallized matrices of calcium (hydroxyapitate) to form the skeletal structure and probably plays an important role in long-term regulation. The solid bone may be thought of as providing a calcium pool for the bone fluid, which, in turn, provides a calcium pool for the extracellular fluid. The soft tissue system, particularly the kidneys and bone fluid, and hormonal glands are capable of rapid response, but the solid bone system responds much more slowly.

Regulation of calcium homeostasis is under the control of three hormones that are also shown in Fig. 8-7. These hormone regulators (parathyroid hormone (PTH), Vitamin D (1,25-DHC), and calcitonin (CT)) stimulate or inhibit the calcium fluxes between compartments via negative feedback control. The secretion rate of these hormones depends on the amount of calcium in the extracellular fluid (the model's controlled variable) and sometimes its rate of change. The action of these hormones have been described earlier in this chapter (see Figs. 8-2 and 8-3) and their influence in the model is indicated in Fig. 8-7. Basically, intestinal calcium absorption is under the direct control of 1,25-DHC, renal excretion is inversely regulated by PTH, and bone compartment osteoclastic activity (resorption or destruction) is stimulated by PTH and 1,25-DHC, and is inhibited by CT.

The first version of this model was proposed by Jaros, Coleman, and Guyton [17] and, after conducting preliminary simulations, was modified in this project, to include detailed representations of some of the subsystems [18,19,20]. Because of inadequacies in the renal subsystem, temporary modifications were included in the simulations as described below. A gravitational term was included in order to represent the effect of gravity unloading on the release of calcium from the bone compartment.

Jaros and co-workers demonstrated that their model was designed for short-term (hours) calcium homeostasis. For example, the model appears to respond properly to repeated calcium removal from plasma, to short-term calcium infusion, to injection of calcitonin and parathyroid hormone and to parathyroidectomy [16]. But clearly the model has not been tested, until now, for the weeks and months of bone demineralization that is seen during prolonged bedrest and spaceflight. While most of the elements of long-term calcium homeostasis are grossly contained in the model, they are being validated for the first

time in the current project. The model's original authors have presented their results in two reports [16,17], the latter containing a more detailed description of major subsystems, particularly the role of the bone in calcium homeostasis, and the addition of a phosphate metabolism subsystem. Because of the unavailability of the second publication at the time this project was initiated, the model and its simulations shown below are based on the original description. Unfortunately the project was terminated before the model could be updated and before it could be fully tested and explored in an equivalent manner to the other modeling studies described in this volume.

8.1.5.2 Simulation of Gravity Unloading.
Simulation of gravity unloading in hypogravic environments was accomplished in the calcium model by making the following initialization parameter adjustments:

a) The value of a hypothetical gravitational term, representing mechanical loading of the bone, was reduced (see Figs. 8-3 and 8-7). This in turn allowed a rise in calcium loss from the bone compartment. This initialization factor permits a slow, consistent, gravity-induced, mineral loss from bone during the entire simulation. (This loss is not explicitly represented in the tables or figures below).

b) Extracellular fluid volume was reduced by one liter in accord with Skylab measurements, presumably due to the acute regulatory response to headward fluid shifts. This will affect the plasma concentration of electrolytes and regulatory hormones.

c) A forced increase in urinary calcium excretion presumably in response to elevated concentrations of calcium in the extracellular fluid. This is an added renal stimulation to the original model's renal calcium excretion algorithm and was necessary to prevent plasma calcium from rising unrealistically high (see below).

In addition to these initializing parameter changes that drive the simulation, the following assumptions were made:

i. Calcium sources from the muscle and collagen are assumed to be negligible during exposure to hypogravic
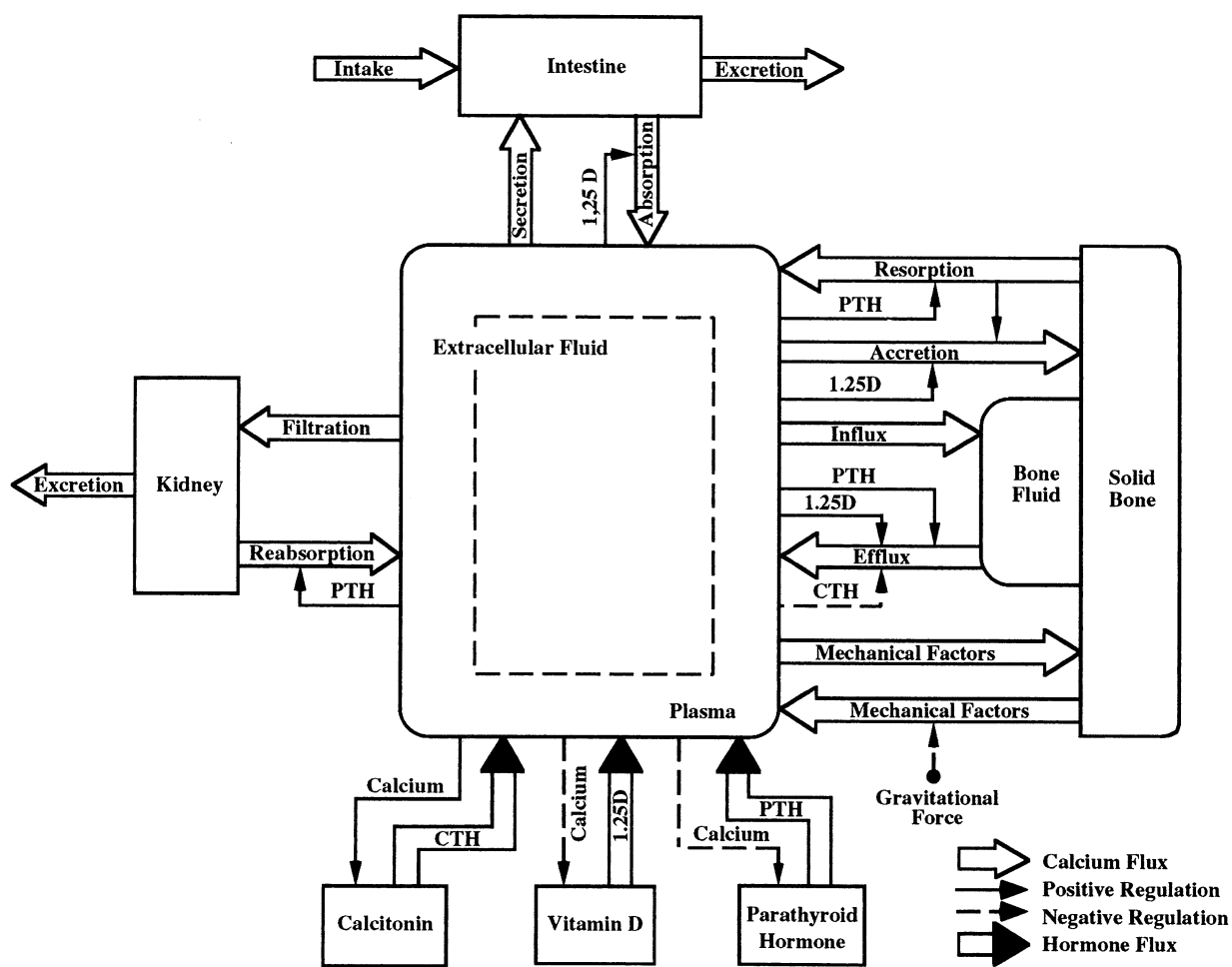

Figure 8-7. Scheme of the calcium regulatory computer model showing major compartments, fluxes and regulatory influences. (CTH = calcitonin; PTH = parathyroid hormone; 1,25D = active Vitamin D metabolite).

environments. Therefore, calcium removed from the body is ultimately derived solely from the bone.

ii. Intestinal secretion rates (calcium flow into the gut) are assumed to remain constant at the control value. This is also a common assumption in measuring intestinal calcium fluxes [21].

iii. Dietary calcium is constant and set to its control value.

The initializing parameter adjustment that altered urinary calcium excretion (item (c) above) was required to maintain plasma calcium levels at realistic levels. Urine calcium excretion, in the original model, is a controlled variable responding to PTH and $[Ca^+]_{PLASMA}$. However, initial simulation trials indicated an apparent deficiency in the renal subsystem, in that calcium excretion rates were much lower than bedrest findings and too low to prevent $[Ca^+]_{PLASMA}$ from becoming unrealistically high in response to the stimulus of calcium efflux from the bone (item(a) above). The model's original creators indicated that the renal subsystem was not fully functional [16]. Until new research provides a basis to improve the renal subsystem, it was decided to artificially increase the urine excretion rate by a fixed amount that is maintained throughout the hypogravic stress. Accordingly, the renal subsystem provides regulation of calcium excretion, according to the model's original formulation, around this "bias". The bias was set to one of two values comparable to the experimentally measured excretion rate: 45% above control based on bedrest findings or 80% above control based on spaceflight findings. Unless otherwise stated, the computer studies below are simulations of bedrest. Validation data with which to compare model results came from two sources, bedrest and spaceflight (see Fig. 8-6).

8.1.5.2.1 *Bedrest Simulation.* Figure 8-8(a) and 8-8(b) presents a group of selected variables from the bedrest simulation performed as described above. The variables in Fig. 8-8(a) are related to the soft tissue compartments (kidney, intestines, and plasma) and hormones, while those in Fig. 8-8(b) relate primarily to the fluxes of calcium into and out of the solid and fluid bone compartments. The step increase in urine calcium and release of skeletal calcium efflux at the beginning of simulated bedrest are responsible for the step decrease in simulated calcium balance. In this preliminary model simulation, the sudden onset of these variables is not physiologically correct, and changes around the onset of bedrest should be ignored since they reflect the artificially imposed initial conditions. But the longer-term changes of these and other quantities are more reasonable. The results of each figure will be discussed in sequence.

Many of the variables in Fig. 8-8(a) agree with the experimental bedrest data of Fig. 8-6 both qualitatively and quantitatively. In both the model and actual physiological system, rapid renal calcium filtration tends to compensate for the skeletal unloading of calcium into the plasma, resulting in the maintenance of relatively stable plasma calcium levels in spite of the input load. Plasma calcium is only 4% above control in the simulation while

it fluctuates closely around control value in bedrest. Only in spaceflight is the plasma calcium level well above control values (+7%). In the simulation, urine calcium excretion increases immediately to about 41% above control, and remains at a high level. However, in bedrest, calcium excretion rises much more gradually over a 3-week period to a maximum level (45% above control) and then decreases for the duration of the study to about 10% above the ambulatory mean (see Fig. 8-6). This discrepancy between simulation and experimental results is attributed to the deficiencies in the renal subsystem noted above and the imposed initialization adjustment

The intestinal calcium absorption rate does not change significantly for the first 5 weeks of simulated bedrest. But after 5 weeks, it decreases below the ambulatory baseline value to a rate that is very close to that calculated from bedrest data [15]. (The data graphed in Fig. 8-6 does not include intestinal absorption but rather fecal excretion which is inversely related to intestinal absorption). In the model, the intestinal absorption rate is regulated by the plasma level of 1,25-DHC. This vitamin is decreased modestly both in the simulation and in the bedrest study. Because the calcium levels in the extracellular pool are higher than normal, the model is apparently reducing the amount of intestinal calcium secretions that are returned to the extracellular fluid pool as well as reducing the amount of dietary calcium absorbed. This reduction in intestinal absorption is an appropriate regulatory response in the face of high plasma calcium levels.

Body calcium decreases after about 20 days of bedrest (Fig. 8-6). The simulation of Fig. 8-8(b) suggests the changes in unmeasured calcium fluxes into and out of bone. Although the rate of calcium resorption decreases slightly (a maximum of 5%), and thereby reduces the rate of bone mineral removal, the rate of accretion, by which new collagen for new mineral formation is deposited, decreases by 20%. In addition, the rate of calcium efflux is eventually inhibited by a maximum of 18% while the rate of influx is stimulated by 6%. This suggests that the bone fluid is buffering the amount of calcium being lost from the solid bone mineral and being dumped into the plasma compartment. These skeletal results contribute significantly to the negative calcium balance shown in Fig. 8-8(a).

The relationship of these long-term bone changes to the hormone regulators provides some insight into physiological processes. For example, the gradual decline of skeletal calcium efflux from bone fluid below control is a response to the simulated rise in calcitonin and decrease in 1,25-DHC. The decline of bone resorption and the greater decline in bone formation (accretion) is in part due to the reduced secretion of PTH in the former case and 1,25-DHC in the latter case.

8.1.5.2.2 *Sensitivity Analysis: Effect of PTH on Calcium Metabolism.* As a result of a primary increase in calcium release from bone in hypogravity environments the model predicts an increase in plasma calcium and this is supported by a number of studies. In theory this should cause a suppression in plasma PTH, as is demonstrated
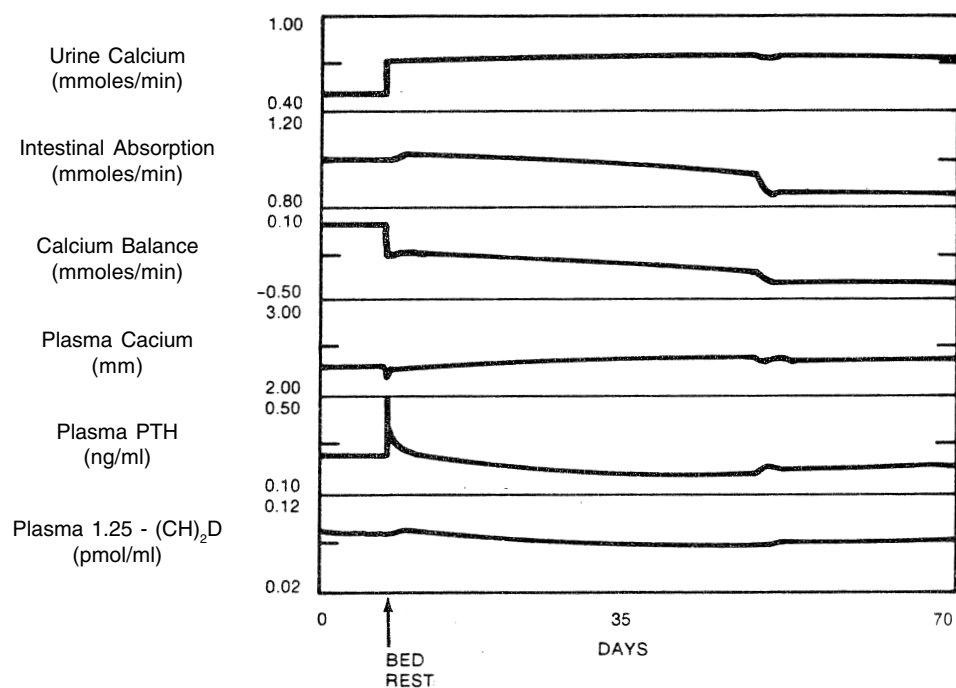
Figure 8-8 (a). Selected variables from the computer model simulation of bedrest: Non-skeletal tissue quantities.
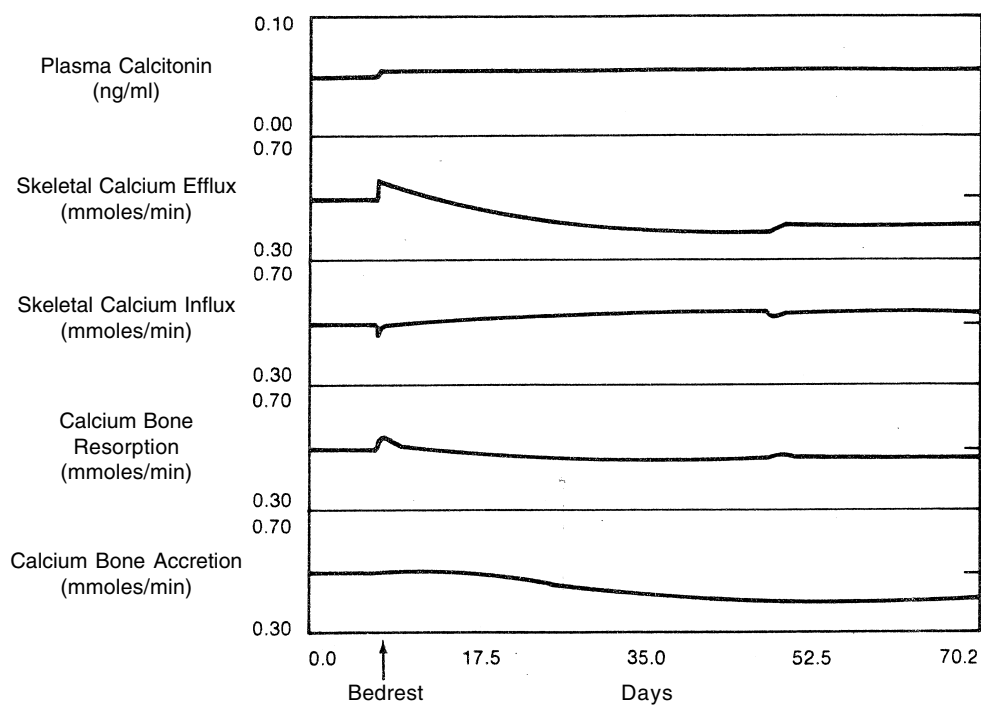

Figure 8-8 (b). Selected variables from the computer model simulation of bedrest: Skeletal tissue fluxes.

Table 8-1. Influence of Varying Levels of Plasma PTH on Selected Model Variables during Bedrest Simulations (percent change from baseline).

Selected Variable	Plasma PTH Level		
	−30%	0%	+30%
Urine Excretion	45	47	49
Plasma Calcium	4	5	6
Intestinal Absorption	−13	−16	−20
Bone Fluid Calcium Efflux	−18	−17	−15
Bone Fluid Calcium Influx	6	7	9
Solid Bone Calcium Reabsorption	− 5	0	+7
Solid Bone Calcium Accretion	−20	−17	−18
Plasma 1,25-DHC	−12	−17	− 22

during the simulations of bedrest (see Fig. 8-8(a). However, findings of depressed PTH are not universal in either bedrest or spaceflight as Fig. 8-6 demonstrates. Alternatively, PTH is reported increased, decreased or not changed, with no particular trend over time [6,13] although one reviewer suggests that PTH is normally suppressed in spaceflight, at least for the short-term [21].

Inasmuch as the direction and magnitude of the plasma PTH response to hypogravity is not clear, the model was used to show the influence of this hormone on calcium metabolism for a range of PTH levels. A sensitivity analysis of PTH was performed by severing the feedback control loop of PTH and assigning the following values to PTH plasma concentration: a 30% increase, a 30% decrease or no change. (Note: This analysis is similar, in the case of an increase in PTH, to a thyroidectomy which eliminates PTH secretion followed by an infusion of PTH). Otherwise the model adjustments were the same as for the bedrest simulation described above. The results of this open-loop analysis are shown in Table 8-1.

The results suggest that PTH exerts little influence on several important calcium metabolic variables. A ± 30% change from normal in plasma PTH concentration only slightly affects the urine calcium excretion rate and plasma calcium concentration. (Reminder: the value for urine calcium has a 45% bias because of the initialization adjustments). The effect on the intestinal absorption rate is more pronounced because of the increasing influence of 1,25-DHC. This hormone is inversely related to plasma calcium.

There is also a PTH effect on the four calcium flow paths into and out of bone. The most dramatic influence is on calcium reabsorption which, in the model, is regulated directly, and solely, by the plasma concentration of PTH. Thus, as PTH increases, bone resorption rates increases. And as PTH concentration changes from below control to above control, bone resorption changes in the same manner, leading to an elevated bone loss and negative calcium balance.

In the model, as is believed to exist in the human, bone formation is influenced by a direct effect of bone resorption (Fig. 8-7). Thus, as bone resorption increases, bone formation also increases; apparently bone is con-

stantly losing and gaining mineral – a biological turnover of bone calcium. However, in the bedrest sensitivity simulation, as resorption increases (with higher levels of PTH), accretion rates do not continue to increase (or become less negative) as expected. Rather, there is a disassociation between resorption and accretion which is due to a second influence on bone accretion, that of 1,25-DHC. The long-term decrements in 1,25-DHC (with increasing levels of PTH) are great enough to slow down the rate of bone formation even further.

In the simulations whose results are shown in Table 8-1, it appears that the skeletal system attempts to maintain bone integrity in the face of the slow, consistent, gravity-induced, mineral loss from the solid bone compartment. A careful examination of the values for the four bone fluxes suggests that there is a diminished ability to rebuild mineral mass despite maintenance of calcium concentrations in the surrounding bone fluid. Nevertheless, for the case where PTH is below control (the case most representative of bedrest) there is an improvement in this diminished ability. That is, due to changes in the three bone fluxes where there is active regulatory control, there remains a net loss of bone, but there is a reduction in the rate of loss.

8.1.5.3 Summary of Model Analysis. Because this project was forced to end prematurely, the simulation studies described above are only suggestive of the type of results that can be achieved with this model, but are not indicative of the more powerful uses of the model, specifically the testing of alternative hypotheses, identifying gaps in knowledge, and designing critical experiments. The model could also help understand the consequences of certain countermeasures or disturbances in the feedback circuitry. For example, what happens if calcium or vitamin D is increased in the diet? Will this reverse the decline in intestinal absorption and if so will it worsen the hypercalcemia that already exists? Will alterations of hormonal substances be able to reverse the bone loss?

Although model development was not completed, it was determined that the model did work as expected according to accepted feedback relationships and simulations that included plausible responses to parameter

disturbances. Deficiencies in the model and recommended corrections will be discussed in the concluding section below (see Chapter 8.1.7.2). Most of the insights gleaned from working with the model were related to the function and behavior of the soft-tissue elements, the kidney, intestines, and the extracellular fluid. It was found, for example, that (in spite of the fact that calcium is preferentially excreted via the intestines compared to the kidneys) the kidney was the fastest acting and most influential controller responsible for the maintenance of short-term plasma calcium homeostasis. This conclusion is strengthened by the fact that fecal calcium in both bedrest and spaceflight does not participate with increased calcium excretion until almost a month after initiation of hypogravity. Thus, while there is decreased intestinal absorption of calcium during hypogravity in both the human and model, the model includes a built-in delay [16]. This may underlie the observation that in the Skylab astronauts, gastrointestinal absorption appears to be relatively insensitive to changes in bone calcium [5]. In this study, the change in plasma calcium concentration was found to be much higher during spaceflight than during bedrest. This suggests that the rate of skeletal calcium efflux is greater and is less compensated by the urine calcium excretion rate during spaceflight than during bedrest. Since the concentration of plasma calcium is the main regulator in most of the subsystems of the calcium model, the changes of the simulation variables would be expected to be more dramatic during spaceflight than bedrest, as seems to be true in the human subjects (see Fig. 8-6).

8.1.6 Hypothesis Development

What initiates bone loss in microgravity? Any hypothesis attempting to explain the spaceflight observations of bone loss should first address the primary event in the process. While there is a general consensus that the mechanical unloading of stress acting directly on the bone is a *causa ultimata* of bone demineralization, the specific pathways and processes have not been revealed; certainly nothing definitive was known at the time of the early Skylab missions. Thus, other alternative hypotheses should be explored and the most promising of these will be examined below. The appearance of large quantities of calcium in the urine immediately upon entering microgravity needs to be explained either as an initiating event or as a feedback response. In addition, if fecal calcium excretion really increases progressively as the Skylab data suggests, then the health of the skeletal system during long-term spaceflight may be in question. Could some primary disturbance in the calcitropic hormones cause renal excretion and bone loss? Finally, what can be postulated about biological activity in bone tissue, e.g., osteoclastic and osteoblastic activity, processes which were not measured directly.

8.1.6.1 Initating and Continuation of Calcium Loss.
The initiation of the bone loss in spaceflight may be due to a property of the bone itself, as it relates to mechanical factors, or the loss may be a result of physiological changes

of calcium metabolism external to skeletal tissue (non-skeletal factors) or to both of these. Mechanical factors refer to stress induced by gravitational loading and/or musculoskeletal interactions. They can include piezoelectric, compression, tensile, and shearing forces that may be very important to bone maintenance as well as to the repair of bone. However, the effect of the absence of these specific forces or their absence on bone mineralization had not been experimentally ascertained during the Skylab era and has only begun to be addressed more recently[UPDATE#2]. Non-skeletal factors refer to physiological changes in the excretory organs or fluid compartments and include hormonally induced stresses. For example headward fluid shifts are one of the most notable changes seen upon exposure to zero-g (see Chapter 5). They are thought to produce diuresis, natriuresis, and have a large dehydration effect upon the legs. Scenarios that are consistent with the two main alternative approaches suggested above, a primary renal calcium leak or a primary bone response, are provided below:

a) *Primary Renal Calcium Leak.* In this scenario the kidneys begin to excrete excess calcium early in spaceflight, perhaps in response to a sodium diuresis (which is known to promote hypercalciuria) or because of a primary defect in hormones that lead to the same result, (i.e., decrease in PTH or increase in calcitonin). According to Cann [21], the following scenario has not been definitively ruled out and can theoretically explain some of the spaceflight findings.

As a result of hypercalcuria, such as is observed in spaceflight and bedrest, the extracellular fluid compartment loses calcium via excretory pathways, and to compensate, calcium flows from the bone compartment to the extracellular fluid compartment and restores the extracellular fluid calcium concentration (see Fig. 8-2 bottom). If the intestine does not respond to the demand for increased calcium input, then the bone continues to compensate for the calcium losses by drawing upon normally inaccessible calcium reserves and the system becomes negatively balanced. This theory seems flawed because the kidney does not appear to initiate these changes but rather seems to respond to excesses in extracellular fluid. In spaceflight there is an increase, not a decrease in plasma calcium as would be expected under this scenario. In addition, PTH seems to decrease in spaceflight, which inhibits net bone resorption. The decrease in intestinal absorption coupled with the reduced levels of plasma 1,25-DHC, further support the notion that the calcium metabolic system is attempting to remove, rather than restore, calcium from the extracellular fluid.

b) *Primary Bone Response to Gravity Unloading.* As noted above, bone is known to be highly sensitive to changes in its customary amount of intermittent loading and deformation. Although not completely understood, mechanical stress and loading generates increased skeletal mineral content and the removal of such forces can cause a reversal of this process and an

increase in skeletal calcium efflux. This has become the central idea for bone demineralization in hypogravity environments. Upon entry into an hypogravic environment, the skeletal system is assumed to dump, in some undefined manner, calcium into the extracellular fluid [5,15]. The rise in extracellular calcium concentration, in turn, will force calcium through the kidneys at a higher rate. The calcium metabolic system then attempts to restore homeostasis to the extracellular fluid with a series of compensatory and hormonal feedback responses. These series of responses were examined in the calcium model, described in the previous section.

Of these two hypotheses, the first is shown to be theoretically possible but likely invalid when compared to observations. Therefore, the second hypothesis, changes in gravitational stresses and musculoskeletal interactions, continue to be the prevailing theory for initiating the observed bone losses, although experimental support is lacking. Not only is a primary effect on the bone thought to initiate the bone loss, but it is believed that the loss will continue as long as gravity unloading occurs.

8.1.6.2 Mechanical Forces on the Bone.

The nature of the reduction in the gravitational force on weight-bearing bones is different during bedrest and spaceflight. One should be cognizant of the differences in mechanical forces on the different body tissues during bedrest, spaceflight, and the erect ambulatory position. These differences can be described in terms of externally applied compression from gravity, and internally-applied torsion, tension, compression, and shear from muscle-bone interactions. In a one-g upright environment, the gravitational vector concentrates the force of body weight towards the feet and provides compression to the long bones. When the individual is in the horizontal (bedrested) position, the gravity vector is distributed along the entire length of the body. In space, the skeletal system is completely relieved of gravitational forces, and therefore, of body weight loads and impact forces. Consequently, the difference between bedrest and spaceflight calcium responses may be due to a different distribution of forces. In this report, the primary mechanical force is considered to be externally applied compression from gravity. However, the relationship of internally applied forces to bone degradation and integrity are poorly understood. The current hypothesis is that the greater skeletal loss of spaceflight, in comparison to bedrest, is due to differences in mechanical factors applied to the bone.

8.1.6.3 Control of Renal Calcium Excretion

Urine excretion of calcium begins immediately upon entering microgravity [5]. As shown in Fig. 8-3, the renal excretion of calcium can be affected by the plasma concentration of calcium, calcitonin, parathyroid hormone, 1,25-DHC, and the rate of sodium excretion during diuresis. Plasma calcium levels were elevated slightly throughout the Skylab flights, significantly so for the first month [12]. Although

urinary sodium excretion was elevated also for the duration of the flight, a diuresis was never observed (see Chapter 5). PTH may have been reduced [5]. The rise in renal calcium excretion can be explained by those factors. Part of the reason for the plateau of renal calcium excretion in spaceflight or the decline of calcium excretion toward baseline during bedrest, after a month or more, (see Fig. 8-6) is because the intestines are excreting progressively greater amounts of calcium; this relieves the filtered loads at the kidney.

8.1.6.4 Control of Intestinal Calcium Excretion.

The intestinal absorption of calcium is primarily a function of the dietary intake of calcium, the plasma concentrations of calcium, and 1,25-DHC (Fig. 8-3). Dietary levels of phosphate may also have an effect on the absorption of calcium. The secretion of calcium into the intestinal tract does not appear to be a regulated process, although it does seem to increase slightly as the dietary absorption of calcium increases [22].

The spaceflight measurements indicate that the fecal excretion continually rose (Fig. 8-4). Based on the simple diagram of Fig. 8-1 a change in one or more of three pathways could explain the fecal increase: increased intestinal calcium secretion, decreased intestinal calcium absorption, or an increase in dietary calcium. Within each Skylab mission, as the duration of the flight increased, both the dietary intake, and the fecal excretion of calcium increased [8]; (see Table 4-24). If the changes in dietary loads are subtracted from the quantities of fecal calcium, no change in fecal calcium excretion, from the preflight norms, are observed. These results suggest that the progressive fecal increases result from increases in dietary calcium intake that are not absorbed through the intestines. (This assumes the intestinal secretion of calcium is basically the same throughout preflight and inflight periods). If the excess dietary calcium is not being absorbed, the most likely reason is that the active transport of intestinal calcium is not being stimulated by 1,25-DHC. The decrease in intestinal calcium absorption also suggested that the inflight crew members were in an adequate calcium state, that is, the body was not in need of calcium.

8.1.6.5 Biological Activity in Skeletal Tissue.

The most important organ in the calcium regulatory system is skeletal tissue (bone), and it is the most difficult to study in humans. Little is known about the response of bone to microgravity at the organ level nor about the fundamental processes of bone remodeling and resorption at the tissue level [21]. Other than bone density, no direct measurements have been done on humans during spaceflight because of the invasive nature of these methods. Animal studies in the late 70's on Russian biosatellites and U.S. Spacelabs have formed the basis of our knowledge. These flights were less than 3 weeks in length. The primary advantage of using animals as human surrogates is that they permit the use of invasive and destructive techniques and provide a true response to microgravity without the confounding effects of countermeasures.

Accordingly, research on rodents and primates in space have shown decreased bone growth, decreased mineralization, decreased bending strength, and decreased mass [10,23]. In short-term spaceflights, primates have been shown to not only increase bone resorption but to decrease bone formation, amplifying the loss of bone material compared to increased bone resorption alone [10,21]. Similar results of the effects of microgravity on the bone remodeling system that were found in the primate were also found in rodents. However, in rodents resorption is not affected significantly [24].

8.1.6.6 Summary: Hypothesis of Spaceflight Bone Demineralization. The hypothesis that has emerged from this analysis for bone demineralization and calcium regulation during spaceflight is illustrated in Fig. 8-9. It is assumed that gravity or mechanical unloading initiates skeletal degradation in some as yet undefined manner and causes bone mineral to be released into the plasma, resulting in an increase in plasma calcium concentration and increased appearance in the urine of products of bone resorption, such as hydroxyproline. This is interpreted by the soft tissue regulatory system as an excess of extracellular calcium which must be eliminated. There are normally three major routes for reversing a rise in plasma calcium, via renal excretion, intestinal excretion and bone formation (see Fig. 8-2). If bone is being degraded in spaceflight, the latter route is no longer available for calcium regulation, so that it falls on renal and intestinal routes to control blood calcium levels. The calcium control system, therefore, behaves as if were attempting to reduce the rise in plasma calcium by excreting calcium, first by the kidneys and later by the intestines. Thus, renal and fecal excretion of calcium eventually rise to high levels resulting in whole-body loss of calcium, which is reflected as a negative calcium balance and eventually, as a measured decrease in bone density. These actions are mediated by two hormone regulators (PTH and 1,25-DHC) whose production is inversely related to plasma calcium concentration (the controlled variable). Both of these hormones would be expected to be depressed at least during the early portion of spaceflight, leading to, in the case of PTH, decreased renal reabsorption and enhanced renal excretion of calcium, and, in the case of 1,25-DHC, a decreased intestinal calcium absorption and enhanced fecal calcium excretion. PTH and 1,25-DHC, if reduced as expected, are capable of producing secondary feedback effects on the bone itself, possibly limiting net resorption. A third calcitropic hormone, calcitonin, is known to be secreted in response to elevated plasma calcium and can decrease blood calcium also by blocking bone resorption. However, calcitonin appears relatively unaffected by either bedrest or small changes in plasma calcium. In addition there is a question whether any of these hormones are capable of reducing or reversing bone resorption in the face of gravity unloading.

The entire regulatory system functions as if to maintain plasma calcium at constant levels. Gravity unloading apparently creates a defect in the system by interfering with the normal processes of bone remodeling in weight-bearing bone sites. Until this defect is corrected (by entering a gravitational field, for example), feedback regulators are not able to cause a net increase in bone formation and counteract demineralization. However, all other elements of the control system appear to respond appropriately to this stress. This scenario appears to account for the known responses to spaceflight and is consistent with the preliminary computer modeling studies described above.

8.1.7 Conclusions: Calcium Regulation
8.1.7.1 Critical Questions for Future Research. From these analyses, a number of critical questions arise related to what is actually known about the physiological process of bone demineralization in spaceflight. How does a reduction in mechanical loading lead to net bone loss? How do the weight-bearing bones detect the lack of gravity? Is mechanical unloading the sole cause of zero-g induced bone loss? Is the rate of skeletal calcium efflux, in fact, greater during spaceflight than during bedrest? What is the nature of the skeletal loss? That is, does it arise from an increase in bone resorption or calcium efflux in contast to a decrease in bone formation or calcium influx? Is the skeleton the only source of calcium elimination from the body or do soft tissue calcium pools also contribute, and if so, to what extent? In the study of calcium homeostasis in microgravity, two effects must be considered: the acute homeostatic response to the microgravity unloading, and the adaptation which results from long-term maintenance of the microgravity stimulus. If bone resorption or formation is under the influence of gravity unloading, can the hormone regulators, PTH, calcitonin or 1,25-DHC, still function in such a way as to reduce or buffer bone loss or are those routes blocked from hormonal intervention? In attempting to adapt to continued gravity unloading, does bone demineralization eventually cease? Does the seemingly progressive elevation of fecal calcium continue unabated? What type of countermeasures are available for reversing the unloading effect on bone? Because of the lack of controls, the ethical requirement for countermeasure use in humans, and the unavailability (until recently) of a long-term space platform to perform careful scientific study, no definitive statements can be made about the effect of microgravity (as opposed to spaceflight) on bone resorption, intestinal calcium absorption, bone cell regulatory factors, or the transduction mechanism by which microgravity signals bone tissue [21].

8.1.7.2 Future Work with Model. The results of the bedrest and spaceflight simulations using the Jaros, Coleman, and Guyton calcium model [16] demonstrate that the model is capable of simulating calcium metabolic responses to hypogravic environments. Although not completely realistic, and unable at this time to distinguish properly between bedrest and spaceflight, the model is expected to improve with future modifications. The exact manner in which bone contributes to the homeostasis of calcium ions has not yet been agreed upon; therefore sig-
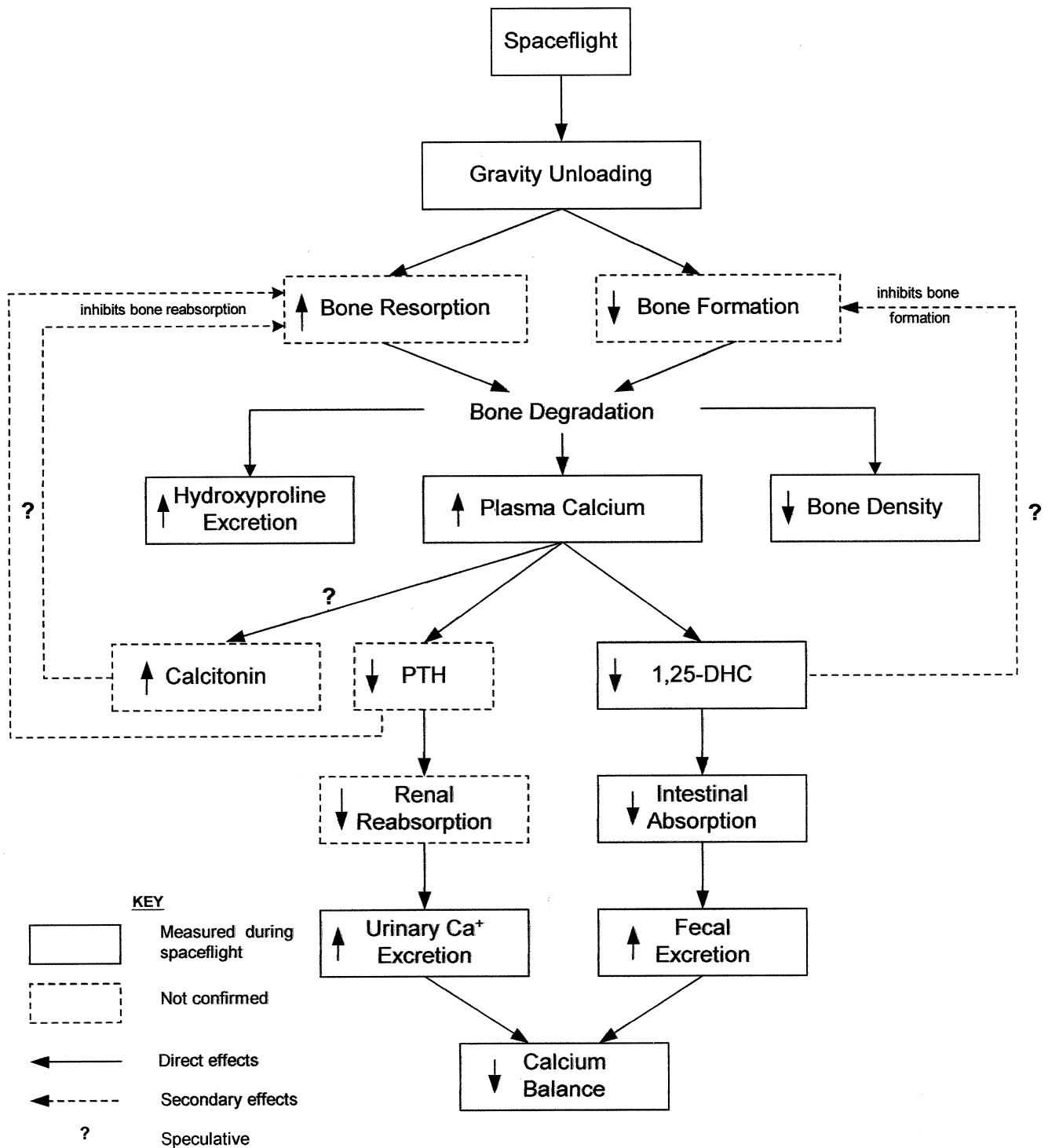
Figure 8-9. Hypothesis for the physiological responses of the calcium metabolic system to the weightless environment. The events that have been confirmed experimentally in humans at the time that these modeling studies were performed (early 1980's) are shown with solid boxes.

nificant experimental research will be required to improve the model sufficiently to represent long-term physiological adaptation to spaceflight. Regarding specific improvements to the current version of the model, the renal subsystem must be modified to respond more appropriately to plasma calcium loads and the relationship between mechanical loads and bone demineralization must be better understood. Bone regulatory forces, such as piezoelectric and mechanical stresses, are eventually expected to also be included. The more advanced model of the original authors contains modifications and expansions of their skeletal subsystem so that it is more representative of the actual physiology and biochemistry of the bone [17]. These modifications were in the process of being incorporated into the existing model when the project concluded. Thus, continued development and testing with this model has become a future goal.

As it is being developed, the model will be validated for a variety of normal and pathological stresses and used, as with all the other models, as a test bed for identifying and testing important hypotheses. This should naturally lead to predict changes which may occur in different, as yet untested situations, and to design critical experiments. The model should be developed to the extent that it can be used to evaluate countermeasures to prevent significant bone loss in long-duration spaceflight. This will require a thorough understanding of the mechanistic and regulatory factors related to zero-g calcium metabolism.

8.2 Muscle and Lean Body Mass

8.2.1 Spaceflight Findings

Several experimental techniques used in the Skylab missions supported, either directly or indirectly, the hypothesis of decreased muscle integrity in persons exposed to long-term zero-gravity. In addition to the losses of protein documented by metabolic balances (see Chapter 4.5 and 4.6), increases in the concentration of particular urinary amino acids, decreases in muscle mass and strength, and changes in electromyographic responses all suggested that muscle mass was lost, and muscle tissue biochemistry was altered, during spaceflight. Metabolic balance techniques are only an indirect measure of muscle loss because protein is a molecule found in most other body tissues. These analyses of the Skylab experiments showed losses in lean body mass of approximately 1.5 kg on average for each astronaut [25]. Lean body mass is assumed to be 19.4% protein; using this percentage and the lean body mass losses, the total body decrements of protein after three months were calculated to be 0.3 kg. The losses in total body protein have been assumed to be derived, primarily, from losses in muscle mass.

A more direct indicator of muscle loss, however, may lie in the measurements of the urinary excretion of 3-methyl-histidine. Muscle is composed of two main proteins, actin and myosin, each of which contains the unusual amino acid, 3-methylhidstidine. Consequently, when muscle is broken down, this substance is released into the blood and is subsequently excreted through the kid-

neys. The monthly pattern of the protein losses, as indicated by the urinary excretion of 3-methylhistidine in the Skylab astronauts, was 60% above control the first month, 32% the second month, and 21% the third month [11].

The major type of muscle lost during spaceflight is assumed to be skeletal and is assumed to be lost primarily from the legs. Muscular strength was assessed preflight and postflight on all of the Skylab crewmen through use of the Cyber Isokinetic Dynamometer which recorded the muscle forces of the limb by repetitive testing. Average muscle strength was reduced during each of the missions, with the crew of the 28-day flight showing the greatest losses in muscle strength [26,27]. This crew showed losses of muscle strength in the arms and the legs, approximately 8% and 26% of the preflight means, respectively. This same crew also exhibited a 5% loss in leg volume and a 4% loss in body weight. The 59-day mission crew eliminated most of the muscle strength losses in the arms by increasing the intensity, duration, and type of exercise to the arms. No such improvement was seen in the legs. There were fewer changes in leg muscle strength and volume observed in the crew of the 84-day mission than in the crews of the two shorter missions although the loss of strength averaged 8%. This was assumed to be attributable to exercise since additional exercise devices were included in this mission specifically for improving muscle strength in the legs [27].

Electromyographic responses of skeletal muscles were obtained for the legs of the crew members on both the 59-day and 84-day mission [28,29]. The duration and muscle potential interval of the Achilles reflex was measured pre- and post-flight. Measurements of the Achilles reflex may yield indications of muscle fatigue and the type of muscle fiber affected during spaceflight [30]. The changes in the duration of the Achilles reflex followed the same qualitative pattern, as the leg strength measurements; they decreased after two months inflight compared to preflight, and improved after three months, compared to the first two months.

Muscles contain two types of fibers, red fibers (type I) and white fibers (type II). Red fibers are slow-twitch, fatigue resistant fibers that normally control anti-gravity or postural functions, and white fibers are fast-twitch, easily fatigable fibers which control movements. Skeletal muscles are composed of a combination of these two fibers, and their relative proportions depend upon the use of the muscle, as well as the subject's diet. Simple disuse and high intensity exercise preferentially affects red fibers, while starvation appears to degrade mainly the white fibers. Crucial to the understanding of muscle losses during spaceflight is the question of whether particular muscle fibers, either the red or the white, are preferentially affected by spaceflight, or whether the losses are generalized system losses.

Muscle biopsies from the Skylab crews were not collected; however, more recent studies of 5- to 11-day Space Shuttle flights revealed significant muscle atrophy of both fiber types [31]. Bedrest studies also revealed a decline in both fiber types; but after 2 months the Type II fast-twitch

fibers reached a plateau while atrophy of the Type I slow-twitch fibers continued [32].

Spaceflight studies of muscular adaptation in rats have allowed biochemical and histological examination of the muscle fibers collected through biopsies. Although care must be taken in relating the animal studies to human studies (since the muscle groups and fibers between humans and rats are different), the studies do confirm that the muscles are affected by exposure to hypogravity. The animal studies demonstrated that muscle mass diminished significantly during spaceflight, and the rate of red fiber break-down especially increased [33,34,35] as one would expect from a preferential atrophy of postural muscles. Such consistency with expectations is not universal; in more than a few studies both red and white fibers showed the same decrements or greater losses of white fibers. More recent studies in hind-limb suspended rats and in space-flown rats and primates indicate that there is a transformation of slow fibers into fast fibers in leg postural muscles, especially in the soleus [32]. Another line of recent evidence also suggests that neuromuscular changes (altered recruitment, fiber type composition) occur in space-flown rats which may help explain the changes in lean body mass.

8.2.2 Hypotheses of Muscle Atrophy

Muscle atrophy is hypothesized to explain the protein losses and muscular changes observed in the Skylab crews. It is well known that atrophy of skeletal muscle occurs in response to disuse, inadequate functional load, and insufficient dietary intake [36,37,38], and spaceflight may be associated with more than one of these conditions. The absence of gravity resulted in diminished use of the lower limbs for postural support and locomotion, reduced body weight on weight-bearing tissues, and interference with proprioreceptor reflexes which can influence muscle metabolism and function [39,40]. Data from the first month of Skylab reflect dietary insufficiency, since dietary intake was reduced considerably during periods of space motion sickness [41]. The Skylab data support the hypothesis of muscle atrophy by demonstrating a consistent loss of lean body mass, a consistent loss of urinary 3-methylhistldine, and decreases in muscular strength.

Although there are several known causes of atrophy, it is thought to result primarily from disuse rather than dietary insufficiency. The dietary insufficiency in Skylab crewmen probably lasted about one week (see Chapter 4, Fig. 4-23), which was the maximum duration of the motion sickness. In contrast, the reduced loading and functional disuse lasted potentially for the duration of the flight, except during the short periods of exercise. The amount of exercise varied among the three Skylab crews, ranging from what could be considered minimal to intensive work [42]. However, while leg muscle strength decreased less with leg exercise, the losses of whole-body protein (which is derived from both postural and non-postural muscles) were not reversed, but neither did they get worse.

Disuse muscle atrophy is associated with diminished muscle mass and contractile strength, as well as with increased muscle stiffness and fatigability. Histologically, disuse atrophy is characterized by shrinkage of the connective tissue; increase in collagen in the connective tissues; decrease in the cross-sectional size and size of the individual muscle fibers; increase in the extracellular space in the muscle; and decrease in the water and solid components of muscle tissue [43]. Consequently, muscles subjected to disuse atrophy appear histologically normal. The fibers are simply smaller and further apart than normal fibers and the muscle is stiffer and cross-sectionally smaller. Spaceflight adaptation in rats reflected such changes. Consequently, the hypothesis of disuse atrophy appears to be supported by experimental observations.

Because the red fibers are the main fibers affected by spaceflight, and the red fibers are mainly postural fibers, the main groups of muscles which are subject to disuse atrophy are hypothesized to be postural muscles. Postural muscles in the human are found mainly in the neck, trunk, and calves [43,44]; but the only postural muscles studied directly in Skylab were those in the calves. More recent studies in Space Shuttle astronauts do indeed demonstrate atrophy of muscles of the anti-gravity muscles in the lower extremities, back and neck [31]. Individual losses in some muscle groups for some Shuttle astronauts (and in space-flown rats) exceeded 50%. The atrophy in the calves decreased as exercise, directed toward the legs, became more intense and more posturally oriented. The altered electromyographic responses and the decreases in the cross-sectional area of the calves support the hypothesis of atrophy of the postural muscles; of course, these altered responses do not exclude atrophy of other muscles that were not examined.

8.2.3 Conclusions: Muscle Atrophy

The Skylab data showed definite losses in whole-body protein and suggested that the protein losses were a result of muscle atrophy, which appears to mainly affect the postural muscles. In zero-g, such muscles are no longer required to support the body weight, and the one-g locomotive function is reduced or eliminated because the legs are not required to support or even to provide locomotion for the body. Exercise may have reversed or inhibited muscle atrophy in the legs, and although the atrophy was not completely eliminated, adherence to an appropriate exercise regimen might possibly result in complete reversal.

8.3 Integrated Musculoskeletal System

The term "musculoskeletal system" is used very loosely by NASA biomedical research managers as if it represents a single integrated discipline. However, it is extremely rare to find researchers who have deviated from their own specialty as "muscle" researchers or "bone" researchers. Nevertheless, there are reasons to maintain the goal of integrating these two components. First, the musculoskeletal system, can be treated as a functional unit, providing the means for humans to easily adapt to moving about and working in a one-g environment. Secondly, eliminating gravity causes both muscle and bone

tissue to degrade for similar reasons – reduced loading and disuse. In both cases, the losses are most significant in the lower extremities, in anti-gravity muscles and weight bearing bones. Third, similar experimental techniques can be used for gathering information about muscle atrophy and bone demineralization including collecting blood and urine samples, metabolic balances, performance measures, and imaging techniques. Finally, exercise may prove to be a common countermeasure for ameliorating or reversing the long-term effects of weightlessness. In fact, it may be preferable to maintain musculoskeletal tissue as a system rather than to provide individual countermeasures effective for only muscle or only bone.

Functionally, muscle and bone are highly interrelated. A contracting muscle is capable of providing high internal loading on the bones to which it attached, although the nature of this loading is not well understood. Because of the interaction between the two tissues, the contribution of the atrophy of muscle toward the skeletal losses must be considered. Unfortunately, data with which this contribution could be assessed is severely limited. One of the few demonstrations of a direct relationship between muscle atrophy and skeletal loss was shown in immobilized rhesus monkeys [45]. In that study enhanced bone resorption was found to occur at the site of muscle insertion and on the periosteal surfaces, resulting in a loss of 30% of the force required to pull the tendon from the bone. A similar and even more striking finding in humans was made in 1981 after a long-term flight on a Russian space station [21]. Using computer tomography, the researchers were able to show that bony projections of the spine to which (non-exercised) anti-gravity muscles were attached, lost about 8% of its mass which correlated well with a 4% decrease in the mass of muscles attached to the bone. The vertebrae itself, which was exercised by simulated gravitational loading, did not lose bone. One type of proof of the relationship between muscle atrophy and bone losses would require demonstrating that the prevention of muscle atrophy will also lead to the prevention or retardation of bone losses. This has not yet been demonstrated.

Attempts to identify an exercise regimen that would reduce or prevent bone loss during bedrest have shown mixed results. An early bedrest study (6-month) indicated that an hour per day of exercise designed to duplicate muscular, one-g, compressional, and tensile forces, failed to change mineral balances, bone density losses, or hormonal plasma concentrations [46]. However, if the subjects stood stationary for three hours a day, bone demineralization was prevented. Potentially, the important differences between the exercise program and quiet standing are the amount of force applied to the calcaneus, the muscle groups involved, and the duration of the stress. The exercises provided particular muscles with much movement and very little force; the standing provided more force, little movement and probably affected a different set of muscles (postural muscles). Therefore, the important preventative factor appears to be the amount of force applied to the bones, and may include the types of muscles used, as well as the duration of the stress.

Prevention of bone demineralization in space crews might require a system that can provide mechanical loads to each area of the body representative of the loads seen in one-g. If this is true, then a needed area of research is to characterize actual bone strains and loading patterns at clinically relevant sites in humans during specific types of movement and exercise in one-g. This will help determine the mechanical loading thresholds for bone mass maintenance and engineer the types of devices to provide the appropriate loads. More fundamental research along these lines would determine the specific manner in which external loads are translated into the molecular and cellular signals that activates or suppresses osteocytic activity. What will likely evolve is a protocol involving a multifaceted exercise prescription perhaps together with drugs, (i.e., diphosphonates), growth hormones, and dietary supplements (i.e., calcium, vitamin D) to maintain the functional integrity of the musculoskeletal system in a weightless environment.

A recent review of musculoskeletal countermeasure programs has concluded that current exercise paradigms and other countermeasure strategies typically used during spaceflight are inadequate to prevent or reduce deficiencies in the musculoskeletal system [47]. While loss of muscle mass in space is diminished but not prevented by exercise, exercise alone has not had the same partial success on bone loss. It may be preferable to maintain musculoskeletal tissue as a system rather than to provide individual countermeasures effective for only muscle or only bone However, aerobic modes of exercise (high frequency, low force), the type most commonly used by astronauts, are far more suited to maintaining cardiovascular condition rather than musculoskeletal health. In contrast, resistive exercise (high force, low frequency) is the most promising countermeasure at present to maintain bone and muscle tissue. Three possible countermeasure approaches were suggested: a) intermittent artificial gravity, b) resistive exercise, c) pharmacoloigc and/or dietary supplement. Combinations of these may also be useful. In summary, the development of successful countermeasures for muscle atrophy and bone demineralization remains an unresolved issue.

References

1. Rambaut, P. C., Leach, C. S., and Johnson, P.C., Calcium and Phosphorus Changes of the Apollo 17 crewmembers, *Nutr. Metab*. 18: 62, 1975.
2. Lutwak, L.,Whedon, G. D., LaChance, P. A., Reid, J. M., and Lipscomb, H., Mineral Electrolyte and Nitrogen Balance Studies of the Gemini VII Fourteen-Day Orbital Spaceflight, *J. Clin. Endo. Metab*. 29: 1140, 1969.
3. Rambaut, P. C., Smith, M. C., Mack, P. B., and Vogel, J.M., Skeletal Response, in *Biomedical Results of Apollo,* R. S. Johnston, L. F. Dietlein and C. A. Berry (Eds), NASA, Washington, D.C., 1975, pp. 303–322.
4. Donaldson, C. L., Hulley, S. B., Vogel, J. M., Hattner, R. S., Bayers, J. H., and McMillan, D.G., Effect of prolonged bedrest on bone mineral, *Metabolism,* 19: 1071–1084, 1970.

5. Rambaut, P. C., and Johnston R. S., Prolonged Weightlessness and Calcium Loss in Man, *Acta Astronautica,* 6: 1113–1122, 1979.

6. Oganov, V. S., and Schneider, V. S., Skeletal System, Chapter 11, *Space Biology and Medicine,* Joint U.S./Russian Publication, Vol. III, Book 1, *Humans in Spaceflight,* C. S. Huntoon, V. V. Antipov and A. I. Grigoriev (Eds.), AIAA, Reston, VA, 1996, pp. 247–266.

7. DeLuca, H. F., and Schnoes, H. K., Metabolism and Mechanism of Action of Vitamin D, *Ann. Review Biochem.* 45: 631–666, 1976.

8. Rambaut, P. C., Leach, C. S., and Whedon, G. D., A Study of Metabolic Balance in Crewmembers of Skylab IV, *Acta Astronautica,* 6: 1313–1322, 1979.

9. Vogel, J., Whittle, M. W., Smith, M. C., Jr. and Rambaut, P. C., Bone Mineral Measurement-Experiment M-78, *Biomedical Results from Skylab*, NASA SP-377, Chapter 20, R. S. Johnston and L. F. Dietlein (Eds.), NASA, Washington, D.C., 1977, pp. 183–190.

10. Schneider, V.S., Leblanc, A.D., and Taggart, L.C., Bone and Mineral Metabolism, Chapter 17, in *Space Physiology and Medicine*, 3rd ed., A. E. Nicogossian, C. L. Huntoon, and S. L. Pool, (Eds.), Lea & Febiger, Philadelphia, 1994, pp. 327–333.

11. Leach, C. S., Rambaut, P. C., and DiFerrante, N., Amino Aciduria in Weightlessness, *Acta Astronautica,* 6: 1323–1333, 1979.

12. Leach, C. S., and Rambaut, P. C., Biochemical Responses of the Skylab Crewmen: An Overview, in *Biomedical Results of Skylab,* NASA SP-377, R. S. Johnston and L. F. Dietein, (Eds.), NASA, Washington, D.C., Chapter 23, 1977.

13. Huntoon, C. L., Cintron, N. M., and Whitson, P. A., Endocrine and biochemical function, Chapter 18, , *Space Physiology and Medicine*, 3rd ed., A. E. Nicogossian, C. L. Huntoon, S. L. Pool, (Eds.), Lea & Febiger, Philadelphia, 1994, pp. 341–342.

14. Schneider, V. S., personal communication, United States Public Health Service, Johnson Space Center, NASA, Houston, TX, 1980.

15. Brand, S. N., *Report of the Bedrest Data Analysis,* TIR 2114-MED-2021, General Electric, Management and Technical Services Co., Houston, TX, 1982.

16. Jaros, G. G., Coleman, T. G., and Guyton, A. C., Model of Short-term Regulation of Calcium-ion Concentration, *Simulation,* 32: 193–204, 1979.

17. Jaros, G. G., Guyton, A. C., and Coleman, T. G., The Role of Bone in Short-term Calcium Homeostasis: An Analog-Digital Computer Simulation, *Ann. Biomed. Eng.,* 8: 103–141, 1980.

18. Brand, S. N., *User's Guide of the Structure and Operation of STCAL and LTCAL.,* TIR 2114-MED-2018, Management and Technical Services Co, Houston, TX, 1982.

19. Brand, S. N., *Vitamin D Subsystem Model,* TIR 2114-MED-2002, Management and Technical Services Co., Houston, TX, 1982.

20. Brand, S. N., *Parathyroid Hormone Subsystem Model,* TIR 741-LSP-9024, General Electric Co, Houston, TX, 1979.

21. Cann, C. E., Response of the Skeletal System to Spaceflight, Chapter 6, *Fundamentals of Space Life Sciences*, Vol. 1, S. E. Churchill (Ed.), Krieger Publishing Co., Malabar, FL, 1997, pp 83–103.

22. Heany, R. P., and Skillman, T. G., Secretion and Excretion of Calcium by the Human Gastrointestinal Tract, *J. Lab. Clin. Med.*, 64: 29–41, 1964.

23. Wronski, T. J. and Morey, E. R., The Effect of Spaceflight on Periosteal Bone Formation in Rats, *Amer. J. Physiol.* 244: 304–309, 1983.

24. Morey, E.R. and Baylink, D.J., Inhibition of Bone Formation during Spaceflight, *Science*, 201:1138–1141, 1978.

25. Leonard, J. I., Leach, C. S. and Rambaut, P. C., Quantitation of Tissue Loss During Prolonged Spaceflight, *Amer. J. Clin. Nutr.,* 38: 667–683, 1983.

26. Thornton, W. E., and Rummel, J. A., Muscular Deconditioning and its Prevention in Spaceflight, in *Biomedical Results from Skylab*, NASA SP-377, NASA, Washington, D.C., 1977, pp. 191–197.

27. Thornton, W. E., Anthropometric Changes in Weightlessness, *Anthropometric Source Book*, vol. I, *Anthropometry for Designers*, NASA RP-1024, NASA, Washington, D.C., 1978.

28. Baker, S. T., Nicogossian, A. E., Hoffler, G. W., Johnson, R. L., and Hordinsky, J., Changes in the achilles tendon reflexes following Skylab missions, *Biomedical Results of Skylab*, NASA-SP-377, NASA, Washington, D.C., 1977, pp. 131–135.

29. LaFevers, E. V., Nicogossian, A. E., Hoffler, G. W., Hursta, W. and Baker, J., *Spectral Analysis of Skeletal Muscle Changes Resulting from 59 Days of Weightlessness in Skylab 2*, NASA TMX-58171 , NASA, Washington, D.C., 1975.

30. Oganov, V. S., and Potapov, A.N., On the Mechanisms of Changes in Skeletal Muscles in the Weightless Environment, *Life Sciences and Space Research*, Vol. XIV, Akademic-Verlag (Berlin), 1976, pp. 137–143.

31. Jaweed, M. M., Muscle Structure and Function, Chapter 16, *Space Physiology and Medicine*, 3rd ed., A.E. Nicogossian, C.L. Huntoon, S.L. Pool, Lea & Febiger, Philadelphia, 1994, pp. 317–326.

32. Kozlovskaya, I. B., and Shenkman, B.S., Muscle Structure and Metabolism, Chapter 10, in *Space Biology and Medicine,* Joint U.S./Russian Publication, Vol III, Book 1, *Humans in Spaceflight,* C.S. Huntoon, V.V. Antipov and A.I. Grigoriev (Eds.), AIAA, Reston, VA, 1996, pp. 231–246.

33. Kazarian, V. A., Rapoport, E. A., Goncharova, L. A., and Bulycheva, S. Y., Effect of Prolonged Weightlessness on Metabolism of Proteins in Red and White Skeletal Muscles of Rats, *Kosm Biol. Aviak. Medit.*, 6: 19–23, 1977.

34. Ahlers, I., Misurova, E., Praslicka, M. and Tigranyan, R. A., Biochemical Changes in Rats Flown onboard the Cosmos 690 Biosatellite, *Life Sciences and Space Research,* Vol. XIV, Akademie-Verlag (Berlin), 1976.

35. Il'ina-Kakuyeva, Ye. I., Portugalov, V. V., and Krivenkova, N. P., Effects of Spaceflight Factors on Skeletal Muscles of rats, *Kosm. Biol. Aviak. Medit.*, 1: 20–25, 1977.

36. Goldspink, G. Postembryonic Growth and Differentiation of Striated Muscle, *The Structure and Function of Muscle*, 2nd ed., Vol. I: Structure, Part I, G. H. Bourne (Ed.), Academic Press, 1972, pp. 181–228.

37. Booth, F. W., Time Course of Muscular Atrophy During Immobilization of Hindlimbs in Rats, *J. Appl. Physiol.: Respir. Environ. Exercise Physiol.*, 43: 656–661, 1977.

38. Fedorov, I. A., Chernyy, A. V., and Federov, A. I., The Rate of Synthesis and Decomposition of Tissue Proteins in Hypokinesia and Increased Muscular Activity, NASA Translation, NASA TM 75203 from *Fiziologickeskiy Zhurnal*, SSSR im. I. M. Sechenova, 63: 1128–1133, 1977.

39. Parin, V. V., Gazenke, D.G., Vuganov, Ve. M., Vasil'yev, P. V., and Kas'yan, I. I. (Eds.), Weightlessness, *Medical and Biological Research,*. Meditsina Press (Moscow), 1974, NASA Technical Translation F-16, 1975, p.105.

40. Thornton, J. E., Hoffler, G. W., and Rummel, J. A., Anthropometric Changes and Fluid Shifts, in *Biomedical Results from Skylab*, NASA SP-377, NASA, Washington, D.C., 1977, pp. 330–339.

41. Rambaut, P. C., Leach, C. S., and Leonard, J. I., Observations in Energy Balance in Man During Spaceflight, *Amer. J. Physiol.*, 233: R208–R212, 1977.

42. Rummel, J. A., Sawin, C. F., Michel, E.L., Buderer, M. C. and Thornton, W. T., Exercise and Long-Duration Spaceflight Through 84 days, *J. Amer. Med. Women's Assoc.*, 30: 173–187, 1975.

43. Hamsin, E., Anatomical and Functional Changes in Joints and Muscles During Prolonged Bedrest, Translated from *Nordisk Medicine*, 85: 293–298, 1971.

44. Lockhart, R. D., Anatomy of Muscles and their Relation to Movement and Posture, *The Structure and Function of Muscle*, Vol. I: Structure, Part I, 2nd ed., Academic Press, 1972, pp. 1–21.

45. Kazarian, L. E., and VonGierke, H. E., Bone Loss as a Result of Immobilization and Chelation, *Clin. Orthop.*, 45: 67–75, 1969.

46. Hulley, S. B., Bayers, J. H., Donaldson,C. L., Hattner, R. S., and McMillan, D. E., *The Effect of Prolonged Simulated Non-Gravitational Environment on Mineral Balance in the Adult Male*, Vol. 1., Final Report NASA CR-1083l4, NASA, Washington, D.C., 1970.

47. Baldwin, K. M., White, T. P., Arnaud, S. B., Edgerton, V. R, Kraemer, W. J., Dkram, R., Raab-Cullen, D., and Snow, C. M., Musculoskeletal Adaptations to Weightlessness and Development of Effective Countermeasures, *Med. Sci. Sports Exerc.*, 10: 1247–1253, 1996.

Update Endnotes

Update #1

Hormonal Control (TBD). Recent research on calcitrophic hormones in bedrest and spaceflight.

Update #2

Bone Activity (TBD). Recent research on direct measurements of bone activity (osteoblastic and osteoclastic) during hypogravic maneuver.

Chapter 9
Integrated Systems Analysis: Simulations of Hypogravity

9.1 Introduction

In previous chapters the systems analysis emphasized the development and testing of hypotheses to explain the observed physiological changes during spaceflight in a variety of body systems. These hypotheses and their effects were demonstrated using relatively simple simulations involving a single regulatory system. This section will examine the application of multiple hypotheses applied simultaneously to multiple systems to study the hypogravic environment. In addition, simulations of spaceflight will be augmented by simulations of ground-based analogs of microgravity. In one instance, our large integrated subsystem model, the Whole-Body Algorithm, will be used to perform the simulations. Thus, this chapter will bring together, or integrate, data from multiple subsystems, multiple subsystem models, multiple hypotheses and multiple types of microgravity stresses.

In order to create realistic simulations of the biomedical changes in spaceflight, it is critical to have available accurate data from spaceflight with which to compare the model responses. Unfortunately, this requirement is problematic because of the operational limitations of collecting data early in flight or in making invasive measurements even on a major mission such as Skylab. The simulation studies described in Chapter 5, for example, indicate that some of the most rapid changes in a host of fluid-related mechanisms occur within the first few hours of spaceflight. This was not fully appreciated during the design of the Skylab experiments; even if it were, it would have been operational unfeasible to gather data so early and so frequently as would be needed to measure these changes.

It became obvious that if realistic simulations of microgravity were to be accomplished, it would be necessary to supplement the spaceflight data with the more extensive data sets from experimental ground-based analogs of microgravity. Specifically, the ground-based hypogravic maneuvers that were considered the most useful included postural changes, water immersion, supine bedrest, short-term head-down tilt and long-term head-down bedrest. All of these approaches have in common a redistribution of blood volume involving a partial emptying of the peripheral vessels in the legs and an engorgement of the headward regions of the circulation. Because the analogs are ground-based and were performed in well-equipped research laboratories, they are capable of providing more subjects, more detailed examination of difficult to measure quantities and examination of the effect of environmental or other external factors.

The simulation model used in the first study described in this chapter is the Whole-Body Algorithm. In the remaining studies the Guyton model of circulatory, fluid and electrolyte control, which is the keystone subsystem of the Whole-Body Algorithm, was used. This approach was taken because the Guyton model was quite suitable for the fluid-related changes that were of interest. In addition, it was less unwieldy to use one model, however complex, rather than an integrated set of models. The simulation models offer a means not only of examining the experimental results and evaluating hypotheses, but also of potentially determining the differences between the various one-g analogs and spaceflight events. After all, all of the analogs are characterized by alterations in fluid (blood) shifts toward the head, but they are not functionally identical. In one aspect, they may be distinguished from each other by the time course and magnitude of fluid movement. Table 9-1 indicates some of the differences of these ground-based analogs and spaceflight, while Fig. 9-1 shows the approximate durations of currently available experimental studies. If we make the tentative assumption that it is possible to simulate reduced gravity by any maneuver that creates headward fluid shifts, Fig. 9-1 suggests that, taken in the aggregate, these analog experiments provide a wide time span with which to provide reduced-gravity validation data for the models.

Our primary interest in these model simulations was to achieve an accurate assessment of fluid disturbances in the hypogravic environment. Such an assessment is characterized by the following quantities: the redistribution of fluid between various compartments and locations such as intracellular/extracellular, plasma/interstitial and lower body/upper body; the changes in electrolyte concentrations associated with these compartments; the changes that occurred in intake and sweat losses of water and electrolytes; and the regulatory mechanisms (renal, hormonal, cardiovascular) which control acute fluid-electrolyte disturbances and long-term adaptive influences. Secondarily, there was an emphasis in examining the circulatory and hemodynamic changes including responses to tilt, exercise and fluid-loading. These areas are readily accounted for by the Guyton model; in addition it was possible to indirectly study some of the other important effects of microgravity such as muscle atrophy and bone demineralization.

Our basic thesis governing the analysis of the spaceflight results is that the physiological changes that occur during weightlessness can best be appreciated by understanding the mechanisms that are necessary to protect the body from the effects of gravity. Therefore, an ideal model with which to analyze the zero-g data would be one that contains all of the gravitational protective mechanisms that are present in normal, ambulatory man. The advantage of such a model is that the simulation of hypogravity could be initiated by simply altering or removing the gravity vector. The hypothesis that would be tested, then, would be that the hypogravic state, if chronically maintained, would lead to the gradual readaptation of those mechanisms that

Table 9-1. Characteristics of Various Hypogravic and Fluid-Shift States

Normogravic or Hypogravic State	External Forces	Time Phase*	Influence on Body Fluids
Postural Change	Full effect of gravity gradient during erect posture	Short term	Fluids pooled in legs
Water Immersion	External pressure gradient equal to blood hydrostatic gradient	Short term	Fluids forced cephalad by external forces
Supine Bedrest	Partial removal of erect gravity gradient	Long term	Elastic forces of tissues redistribute fluids
Head-down tilt & Head-down bedrest	Removal and partial reversal of gravity gradient	Short term Long term	Elastic forces of tissues redistribute fluids and leg tissues dehydrate
Spaceflight	Complete removal of gravity gradient in all body positions	Long term	Redistribution of fluids and dehydration of leg tissues

* Short-term is considered < 24 hrs.
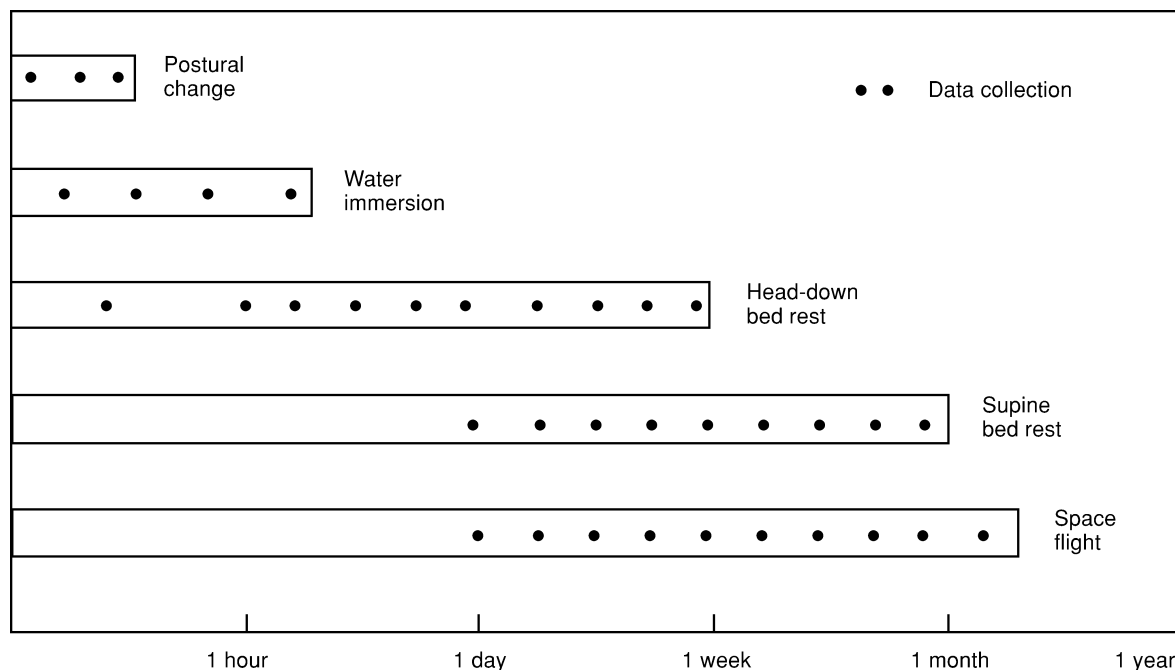
Figure 9-1. Duration of typical hypogravic fluid shift studies in the Skylab era. The length of typical studies are indicated by the bars. The times during which data is typically collected is shown by the solid circles. Data collection is generally sparse during the first day of supine bedrest and spaceflight studies when many dramatic changes occur. Results from other analog studies are therefore necessary to estimate early physiological changes.

have been developed to protect man from his normal ambulatory, relatively unstable, upright position. Unfortunately, a model that can be initialized in the ambulatory state and maintain stability has not yet been designed. An attempt to accomplish this is described later in this section but it was only partially successful.

Consequently, investigation of the thesis through modeling must be approached in a different manner. The simulations of supine bedrest were initiated in the supine model by forcing a redistribution of fluids in a manner that was hypothesized to occur as a result of gravity unloading. In the case of head-down tilt, the introduction of the gravity vector allowed a more realistic simulation of fluid redistributions by simply changing the angle of tilt. In this case, the overall hypothesis being tested was whether the dynamic changes in fluid volumes that occur because of gravity unloading were responsible for many of the observed renal, cardiovascular and hormonal responses. Other hypotheses, reflective of gravity unloading, were also included in the initiation of the simulation. For example,

variations between the physiological stresses shown in Table 9-1 may be explained, in part, by differences in the metabolic activity, the diet and the degree of musculoskeletal degradation of the subjects. Therefore, the investigation of the spaceflight responses, through modeling, has been done as a series of trials based on discrete physiological alterations that are hypothesized to occur upon exposure to hypogravic stresses.

In this chapter the testing of the zero-g hypotheses using a mathematical model and various ground-based analogs is discussed. A summary of the specific hypotheses examined is given in Table 9-2. To test the hypotheses, the long-term circulatory model (Guyton) was modified by incorporating ever-increasing complex processes related to gravity. Hypogravity was first simulated in the unmodified Guyton model without a leg compartment (Chapter 9.2). These simulations demonstrated a need for a leg compartment in the model. Supine bed-rest studies provided data to validate and improve the simulations (Chapter 9.3). Since the model was originally designed as a supine model, it was only possible to simulate supine bedrest by artificially forcing fluids from the leg toward the head and then allowing the model's normal regulatory processes to take over. This approach was extended to simulate the long-term Skylab spaceflight missions (Chapter 9.4). Water immersion was simulated in the same model by providing an external compressive force on the leg fluid compartments that provided a cephaled fluid shift (Chapter 9.5). Water immersion studies were especially useful in providing information on early events of hypogravity. Further modification of the model was undertaken to include gravity, particular the action of the gravity vector on hydrostatic blood columns. This permitted a range of postural tilt studies to be simulated (orthostasis in Chapter 9.6, head-down tilt and head-down bedrest in Chapter 9.7) using a more natural forcing function. In each case, the knowledge gained from one set of studies was applied to the subsequent studies. Data of increasing complexity was examined, interpreted and organized in a way to assist in model validations and hypothesis testing. In the iterative process of performing these functions, the hypotheses addressing spaceflight physiology can be continually examined and reevaluated.

9.2 Supine Bedrest Simulation with a Legless Circulatory Model (Whole-Body Algorithm)

The first simulations of hypogravity were performed with the Whole-Body Algorithm, with the long-term circulatory portion (Guyton model), playing the central role. It was noted that the primary event accompanying a reduced hydrostatic effect is a shift of blood from the legs to the central regions of the vasculature. The resulting increase in blood pressures in this region coupled with the fact that this area contains the major pressure sensors of the body was generally believed to be the causal factor for many of the physiological changes to follow. However, in an attempt to simulate supine bedrest with a legless model initialized in the supine position, some important questions had to be addressed at the outset. First, in a model that does not directly account for gravity, what physiologically acceptable stimulus or forcing function would cause the model to simulate the reduction in hydrostatic effect that accompanies bedrest? Secondly, how could hydrostatic effects be accounted for in a model without legs? At this point in these studies it was not feasible to devote the time necessary to add a leg compartments and explicit gravity components (this would be done at a later time); therefore, some artificial but plausible forcing function was needed.

The approach eventually used was to approximate the headward fluid shift by shifting a portion of blood from the unstressed blood volume to the stressed blood volume. The broad outline of this approach is shown in Fig. 9-2 in which the entire circulatory volume is approximated by a single compartment divided into stressed and unstressed volumes.* The reader should note that only changes in the stressed blood volume (which is a small fraction of the total blood volume) is responsible for changes in vascular pressure. At the start of the simulation, fluid would be suddenly shifted from the unstressed to the stressed volume, keeping the total blood volume constant. The amount of fluid shifted would be approximately the same as that observed to be displaced from the legs when changing from the erect to the supine posture (about 300 ml). The increase in stressed blood volume would initiate the model simulation by increasing the pressure on the pressure receptors, which would in turn, initiate pressure-receptor effects. The fact that the unstressed volume has been reduced is of no consequence since, mathematically, it contributes nothing toward changes in blood pressure. Only the stressed volume is the critical factor affecting pressures, pressure receptors and most all aspects of fluid-electrolyte regulation. In this method total blood volume remains constant while the step change in stressed volume takes place.

In summary, the fluid alterations of bedrest were assumed to be simulated by forcing an amount of fluid equal to that mobilized from the legs during an acute erect-to-supine position from the unstressed to the stressed volume of the circulation. This is similar to an infusion of blood into the central circulation with the exception that it is accomplished at constant blood volume. Once this forcing function was complete (over a period of less than 1-minute) the model would then run on its own and respond to this "blood infusion" into the stressed volume by activation of the model's controller mechanisms. These studies with the legless model only simulated the acute movement of blood from the legs; there was no attempt to simulate the slower migration of fluid from the leg tissues

---

* Consider the circulation to be represented by an empty deflated balloon. The amount of fluid volume that must be introduced into the balloon to *just* inflate the balloon without increasing the internal pressure is called the unstressed volume. Introduction of any further fluid (stressed volume) will cause the balloon to expand with increasing internal pressure. A graphical representation of this concept is shown later in Fig. 9-32.

Table 9-2. Hypotheses Tested during Integrated Systems Analyses

Classification	Question	Hypotheses
Body fluid shifts and distribution	What conditions are necessary or sufficient to simulate a realistic dynamic behavior of: a) total body water b) blood volume c) intracellular/extracellular d) intravascular distribution e) fluid loss from legs?	• Loss of plasma volume and total body water initiated by rapid headward shift of blood and extravascular fluid from legs • Headward shift of blood results in an immediate diuresis which may be modified by state of hydration • Losses of body fluid can primarily be attributed to changes that occur in legs. Short-term losses are due to acute fluid shifts, while long-term losses are due to long-term tissue losses, metabolic factors and circulatory adjutments.
Loss of electrolytes from body	What conditions are necessary or sufficient to simulate realistic behavior of major electrolyte loss from body of a) sodium b) potassium?	• Primary loss of sodium occurs early in flight due to extracellular fluid loss • Loss of potassium due to muscle disuse atrophy, occurring gradually.
Loss of red cell mass	What conditions are necessary or sufficient to simulate the increase in hematocrit?	• Increase in hematocrit due to early plasma volume loss is responsible for increased oxygen supply and decrease in erythropoietic activity.
Change in renal function	What factors controls renal function as defined by: a) urine volume b) sodium excretion c) potassium excretion d) glomerular filtration rate e) renal blood flow?	• Headward shift of body fluids triggers renal mechanisms (neural, hormonal, and hemodynamic) which produce acute losses of electrolytes and fluids. • Continued gradual loss of intracellular and extracellular fluid coupled with changes in sweat losses and dietary intake of fluid and electrolytes can explain longer-term renal response.
Hormonal regulation	What factors controls the major renal and cardiovascular hormonal regulators: a) ADH b) renin-angiotensin c) aldosterone?	• Initial headward fluid shift results in increased stimulation of cardiopulmonary presso-receptor pathways resulting in depression of ADH, angiotensin, and aldosterone at the beginning of flight • Longer term changes in hormone can be partly attributed to changes in plasma electrolyte levels
Changes in cardiovascular system at rest	What conditions are necessary or sufficient to simulate cardio-vascular behavior as defined by: a) cardiac output b) heart rate c) stroke volume d) peripheral resistance e) blood flows to legs, viscera, kidneys f) blood pressures in arteries, veins, atria, pulmonary circulation?	• Acute cardiovascular changes can be attributed to rapid expansion of central blood volume resulting in alterations of flows, pressures, autonomic stimulation, and vasoconstrictor agents (angiotensin, catecholemines) • Longer term changes may be attributed to circulatory system adjusting to: a) continued decrease of gravity load on mechanoreceptors, and b) downward adjustment of blood capacitance affecting retoning of blood vessels and blood volume.
Changes in provocative metabolic and orthostatic stress tests (includes LBNP and bicycle ergometry exercise)	Can the changes in performance of these tests be explained by a) fluid shifts b) reduced blood volume c) exercise conditioning d) vascular retoning?	• Inflight reduction in blood volume can explain most of deviation of LBNP responses at the beginning of flight, and the decrements in exercise performance at recovery • History of exercise conditioning inflight determines in part the immediate postflight exercise response and rate of recovery toward normal • Longer term changes in LBNP during flight is partly attributable to retoning of vascular elements. Other factors not well known.

Overall Hypotheses
1. The dynamic changes in fluid volumes and electrolytes that occur as a result of gravity unloading are responsible for many of the observed renal, cardiovascular, and hormonal responses as well as the decrements in performance of provocative metabolic and orthostatic stresses.
2. Similar types of fluid shifts occur in all stresses considered here (i.e., spaceflight and its analogs), but differ in magnitude and dynamic behavior. Differences in metabolic activity, diet, and degrees of musculoskeletal degradation also exist in these situations. These differences can explain, in part, the variations in overall physiological responses between these stresses, particularly between long-term bedrest and spaceflight.

(A)   Control Position: "Erect"
Total blood volume = Vs + Vo
where   Vs = stressed blood volume
              Vo = unstressed blood volume

5 compartments of the model are represented here
by a single compartment. Leg blood volume is
considered to be included in Vs + Vo

(B)   Acute Shift to Supine
(i) $\Delta V \sim 300$ ml shifted from unstressed to stressed volume

(ii) ΔV represents easily moblized fluid from legs being
     infused into central compartment at constant blood volume

(C)   Physiological Response
(i)   Increased pressures lead to reflex diuresis, i.e., approx.. ΔV is excreted.

(ii) Stressed blood volume reduced to approx. normal

(iii) Total blood volume eventually reduced by $\sim \Delta V$

Figure 9-2. Idealized approach for simulating blood volume distribution during bedrest using the Guyton model. The model is initially in the control position (a); bedrest is initiated by forcing function (b); model response shown in (c).

and further "drying" of the leg vasculature. These processes, which were addressed in more advanced simulations, could remove another 200–300 ml from the legs (see Chapter 9.3). Also later in this chapter, simulations will be described using models with upper and lower body segments that are capable of shifting fluids between these compartments in a more realistic manner.

One other modification that was suggested for simulating bedrest was a cardiovascular effect. The effect was an increase in heart rate by 0.4 beats per minute for each day of simulated bedrest. The cardiovascular effect had been suggested from abundant data of different bedrest studies [1]. Although the modification was added to the model, it did not appear to be critical to the simulations. Simulations were run with and without the cardiovascular effect and the only difference was an increase in heart rate and a corresponding decrease in stroke volume. No other differences in behavior of any other variable, including cardiac output, were observed.

Simulations of the events that occur during supine bedrest were performed with the whole-body algorithm using the legless Guyton model. Before and after simulated bedrest, an additional series of stresses were automatically performed utilizing the short-term subsystem models of the Whole-Body Algorithm. These additional studies consisted of 70° tilt, lower body negative pressure (LBNP) and 50-watt supine exercise. In experimental studies, these tests help to reveal physiological changes that occurred during bedrest that were not always apparent in the resting supine state. These simulations of bedrest and special stress studies will be described next.

9.2.1 Comparison of Simulation with Bedrest Data

The responses of the model to a 28-day bedrest simulation are shown in Figs. 9-3(a) to 9-3(d) using the forcing function described above. Twenty-four variables are depicted. The simulation revealed that many new quasi steady-state conditions were reached at the end of 4 weeks. However, most of the significant changes in the variables had occurred by the end of the first day. Consequently, the model's behavior is shown in more detail for the first 24-hours. While many of these variables have not been measured simultaneously during any single bedrest study, many of the results shown in Fig. 9-3 have been confirmed in different hypogravic maneuevers either during bedrest, water immersion, or spaceflight. The experimental bedrest results, for many of the same variables, are shown in Figs. 9-4 to 9-7. Unfortunately, bedrest investigators fail to measure physiological variables during the first day when many interesting physiological parameters are changing. It was, therefore, only possible to compare the longer term results of the simulation with experimental data.

Based on the simulation data, the physiological adjustments to gravitational stress appear to be quite rapid. Central blood volume is not shown but its value will be parallel to that of the pressures within the circulation. Within the first few simulated minutes, the blood pressures in both the atrial and the arterial segments rose, causing an increase in stroke volume and cardiac output (Fig. 9-3(a)). Heart rate reflexively decreased because of baroreceptor influence and a rapid rise in blood pressure yielded a transient decline in aldosterone and renin (Fig. 9-3(b)). Because of the changes in aldosterone, the urine rate and
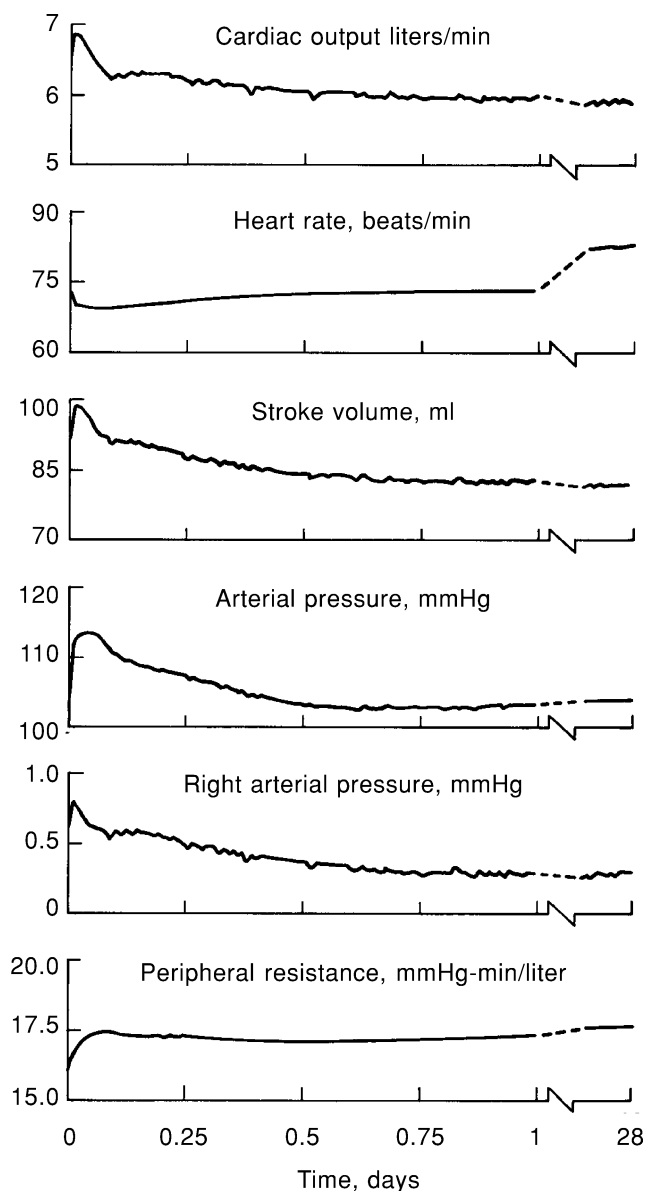
Figure 9-3(a). Simulated responses to 28-days of bedrest, using Guyton model without legs: Cardiovascular function.
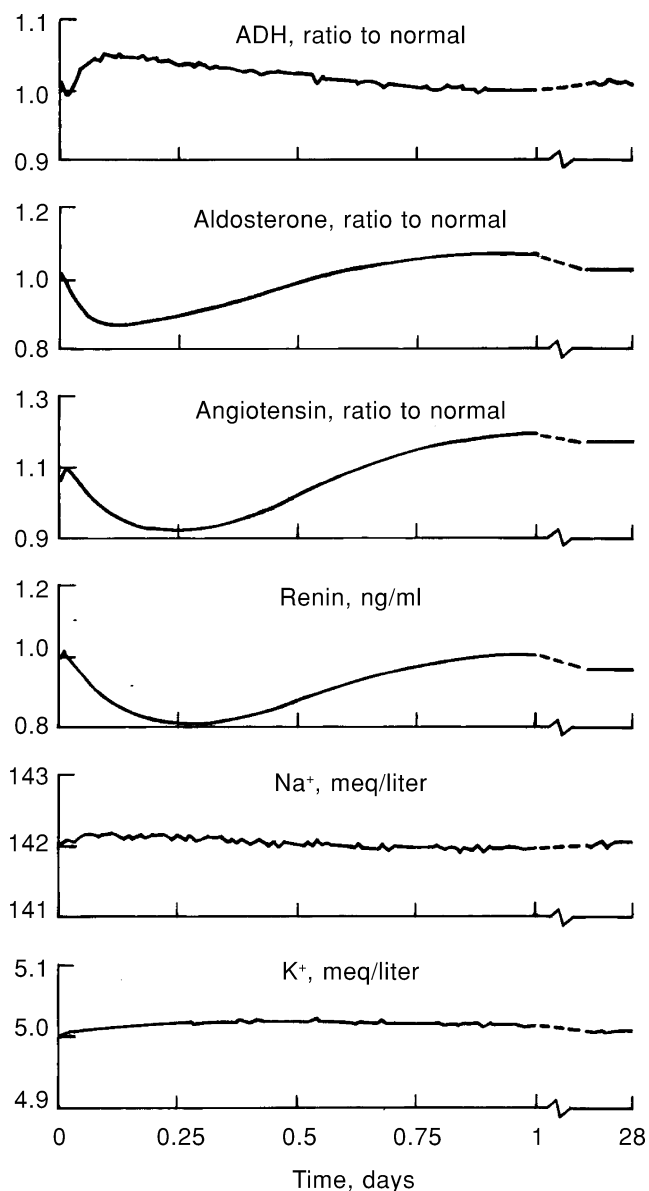
Figure 9-3(b). Simulated responses to 28-days of bedrest, using Guyton model without legs: Plasma concentration of hormones and electrolytes.

urine sodium increased (Fig. 9-3(c)). The increase in urinary fluid loss led to decreases in blood volume, extracellular fluid volume, total body water and vascular hemoconcentration (Fig. 9-3(d)). Because of the changes in central blood volume and pressure, changes in the plasma concentrations of anti-diuretic hormone (ADH), aldosterone, angiotensin and renin occurred. Anti-diuretic hormone is shown to decrease for the first half-hour of the simulation, after which it transiently rises and then declines in a biphasic response. Transient decreases in aldosterone, angiotensin and renin were predicted whereas sodium and potassium plasma concentrations remained essentially unchanged. Many of these variables were not pre-

dicted to return to their pre-bed-rest values at the end of 28-days, the most notable of these being blood volume, extracellular fluid volume, total body water, hematocrit, cardiac output, heart rate, stroke volume, blood pressure, peripheral resistance, renal flow, angiotensin and aldosterone.

An unexpected result was the decrease below control of the right atrial pressure (which is similar to central venous pressure) that occurred within a few hours. The only analogous data at this time was from water immersion studies that showed clearly that central venous pressure increases dramatically immediately upon immersion and is maintained at high levels for several hours [9]. This observation, in fact, is the basis for Gauer's theory of cen-
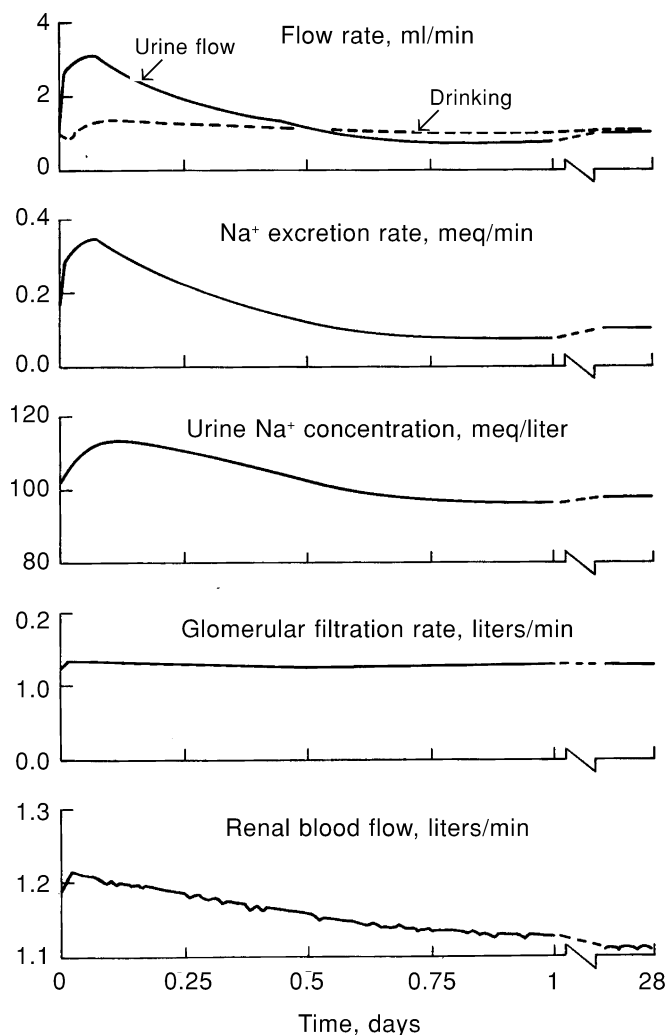
Figure 9-3(c). Simulated responses to 28-days of bedrest, using Guyton model without legs: Renal function.

Figure 9-3(d). Simulated responses to 28-days of bedrest, using Guyton model without legs: Body fluid volumes.

tral blood volume regulation via ADH and renal pathways [10]. The reasons for the model's behavior will be reported later (see Chapter 9.7.5), but at this time it should be noted that it was not until some years later that head-down tilt studies showed that venous pressure falls back toward normal much faster than with water immersion and it was even later that spaceflight studies confirmed that central venous pressure can fall below control almost immediately upon entering microgravity (without even showing an earlier increase) UPDATE#1.

The long-term effects of bedrest were simulated reasonably well with this model. Further examination of the autoregulatory segments of the model were made by removal of all of the autoregulatory components, except for those that were long-term (i.e., time constants greater than one week). Simulations with these changes resulted in almost identical values for all variables at the end of 28-days indicating that very short-term autoregulatory

mechanisms are not significant in longer-term studies – an expected result.

The model's long-term hemodynamic changes were compared with the results from several bedrest studies of 2 to 7 weeks duration (Fig. 9-4). Although hemodynamic agreement between model and data was generally good, variation of experimental data among all the studies was very wide. The cause of the experimental variation was unknown, but it was not necessarily related to the length of the bedrest.

Seemingly conflicting data that showed both increases and decreases in certain hormones, as a result of reduced-gravity effects were reconciled by the model. Figure 9-5

Figure 9-4 legend table:
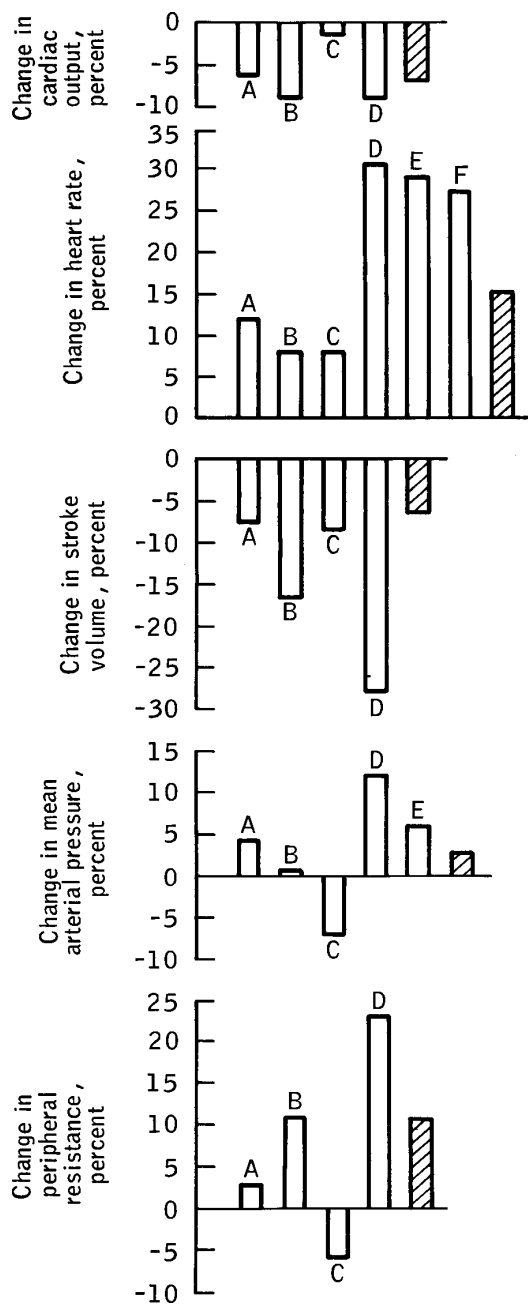
	Reference	Days bedrest	No. subjects
A	2	14	15
B	3	21	5
C	4	28	6
D	1	42	3
E	5	14	6
F	6	21	6
	Guyton model	28	----

Figure 9-4. Hemodynamic response due to prolonged bedrest. Percent change from control. Model vs. data [2,3,4,5,6].

represents the only bedrest data available (at the time of this analysis) showing the prolonged effects of bedrest on plasma renin and urinary aldosterone. No data on angiotensin activity were located. However, since renin is a precursor to angiotensin, the renin data were compared with results of the angiotensin simulation. The pattern predicted by the model, of an initial decrease followed by an increase in plasma concentrations of aldosterone and angiotensin, is supported by the published accounts shown in Fig. 9-5 and in short-term immersion studies (not shown) [11].

The decrease in ADH during the first day of simulation appears to be contrary to the belief of many reviewers of bedrest studies [12,13]; however, no experimental data could be located that would conclusively demonstrate that ADH is below control levels after 1-hour of bedrest. In a recent review on ADH control, it is concluded that although ADH may decrease temporarily during postural change (upright to supine), because of changes in atrial pressure, this effect does not appear to be long lasting [14]. The longer term simulated effects show an increase in ADH, which will almost return to normal after 1-day. An explanation for the simulated ADH bedrest responses may be found in the concept that ADH is under the dual control of osmo- and volume-regulators. Accordingly, the increase in central blood volume may initially decrease the plasma ADH concentration, but the long-term control is probably regulated by the osmolarity of the extracellular fluid and thereby the plasma ADH concentration is raised. The model embodies the dual control mechanism which is described in detail in Chapter 9.8.4.

Data on the body fluid volume changes during 28-days of experimental bedrest are presented in Fig. 9-6. There was generally good agreement between the simulation and experimental results of these variables. Although the model yielded higher hemoconcentration than the experimental data (i.e., compare Figs. 9-3(d) and 9-6)), the difference may be explained by two factors. First, this particular study used frequent blood draws, which diminished red cell volume and the draws were not accounted for in the simulation; and, second, these data and other experimental studies strongly suggest a diminution of red cell mass due to inhibition or cessation of red cell production. The simulation did not predict significant changes in red cell mass; however, the simulation did not use the improved red cell production subsystem that was produced during the course of the systems analysis project (see Chapters 3,6 and Appendix B). This subsystem probably would have predicted the changes observed in red-cell mass more accurately. More advanced simulations, discussed later in this chapter, will demonstrate this effect.

Some experimentally determined changes in renal function during bedrest are shown in Fig. 9-7. Comparison of changes in urine and sodium excretion with the simulation results (Fig. 9-3(c)) indicates reasonably good agreement.

9.2.2 Comparison of Simulations with Post-Bedrest Tilt and Exercise Data

Researchers interested in bedrest as an analog to space-flight have developed several procedures for testing the
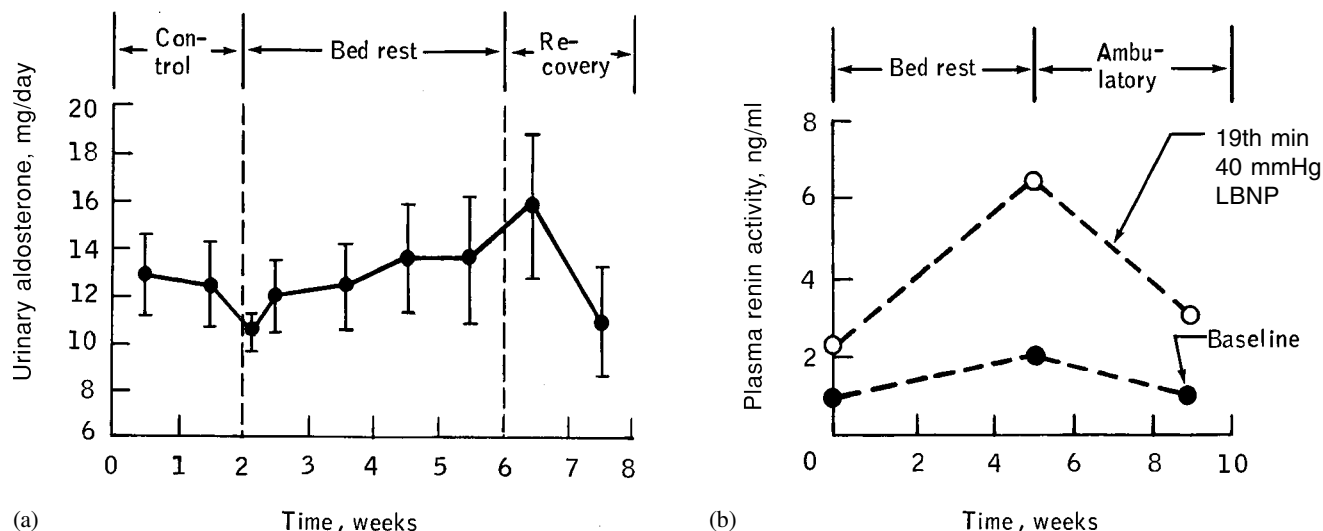
Figure 9-5. Experimental data on the effect of bedrest on (a) aldosterone [2] and (b) renin [7] responses.

effects of bedrest on cardiovascular behavior. These tests include exercise and tilt-table studies. The former is a metabolic stress and the latter is an orthostatic stress; both tests will reveal physiological changes that are not observable at rest. On occasion LBNP will be used instead of the tilt-table to test orthostasis. The ability of the short-term cardiovascular model (Croston's model) to simulate exercise, tilt and LBNP was presented in Chapter 3 (see Chapter 3.2.1.4). Here we will examine the simulated responses to the same stresses, but in the context of the Whole-Body Algorithm. In this case the four week bedrest discussed in the current section was simulated using the long-term circulatory model and then control was passed to the short-term models where tilt and exercise were simulated. Results will be compared with experimental data.

The results of the short-term simulations of 70° head-up tilt and supine exercise, before and after a bed-rest simulation, are shown in Figs. 9-8 and 9-9, respectively. Simulation results are compared to corresponding experimental data from 4-week bedrest studies [3,15]. All results labeled "tilt" or "exercise" are shown as changes from the resting supine position immediately preceding tilt or exercise. These simulated results were produced by the short-term group of models of the Whole-Body Algorithm before and after the long-term model provided a simulation of bedrest. Results labeled "supine" or "rest" in these figures represent the changes in supine resting values because of bedrest alone (long-term model vs. data).

The differences in the initial conditions of the short-term models, between the pre- and post-bedrest states, were based on changes obtained from the long-term model's bedrest simulation. Only total blood volume changes, vascular resistances and local cardiovascular changes were transferred from long-term to short-term models. This is an admittedly simplistic set of hypothesis to allow differentiation between the pre- and post-bedrest physiological states. Other changes observed at the end of the long-term

bedrest simulation included hormonal changes, unstressed volume changes, pulmonary resistance and blood viscosity effects. These changes were not used in the short-term subsystem to simulate tilt and exercise.

Model and experiment agreement in the case of supine exercise was better than in the case of tilt. This result was not unexpected, since the head-up tilt simulations should have been highly affected by physiological changes in the legs during bedrest that would influence fluid pooling upon standing and the model lacked a leg compartment. Some of the changes that might be expected in the lower extremities include leg tissue dehydration, reverse stress relaxation (retoning) and compliance changes during bedrest as well as extravasation of plasma into an altered interstitium during standing. These potential effects indicated that a leg compartment would be important in simulating head-up tilt particularly if excess pooling occurs. This may be one reason why experimental data during tilt is so time-dependent. An example of this can be seen in Fig. 9-8 where experimental values for heart rate are shown at the end of 1-minute and at 5-minutes. The short-term models that simulated tilt do not contain an interstitial compartment that can promote time-dependent pooling. These leg factors would not be expected to influence the simulated exercise results as much, since in supine exercise, pooling of blood in the legs does not occur. If it had, cardiac performance during exercise would be greatly affected.

9.2.3 Summary: Supine Bedrest with a Legless Model

In summary, this preliminary attempt to simulate the effects produced by upper and lower body fluid shifts has demonstrated the capability of the Whole-Body Algorithm to perform a sequential series of short- and long-term stresses automatically and somewhat accurately. No major structural changes in any of the subsystem models were
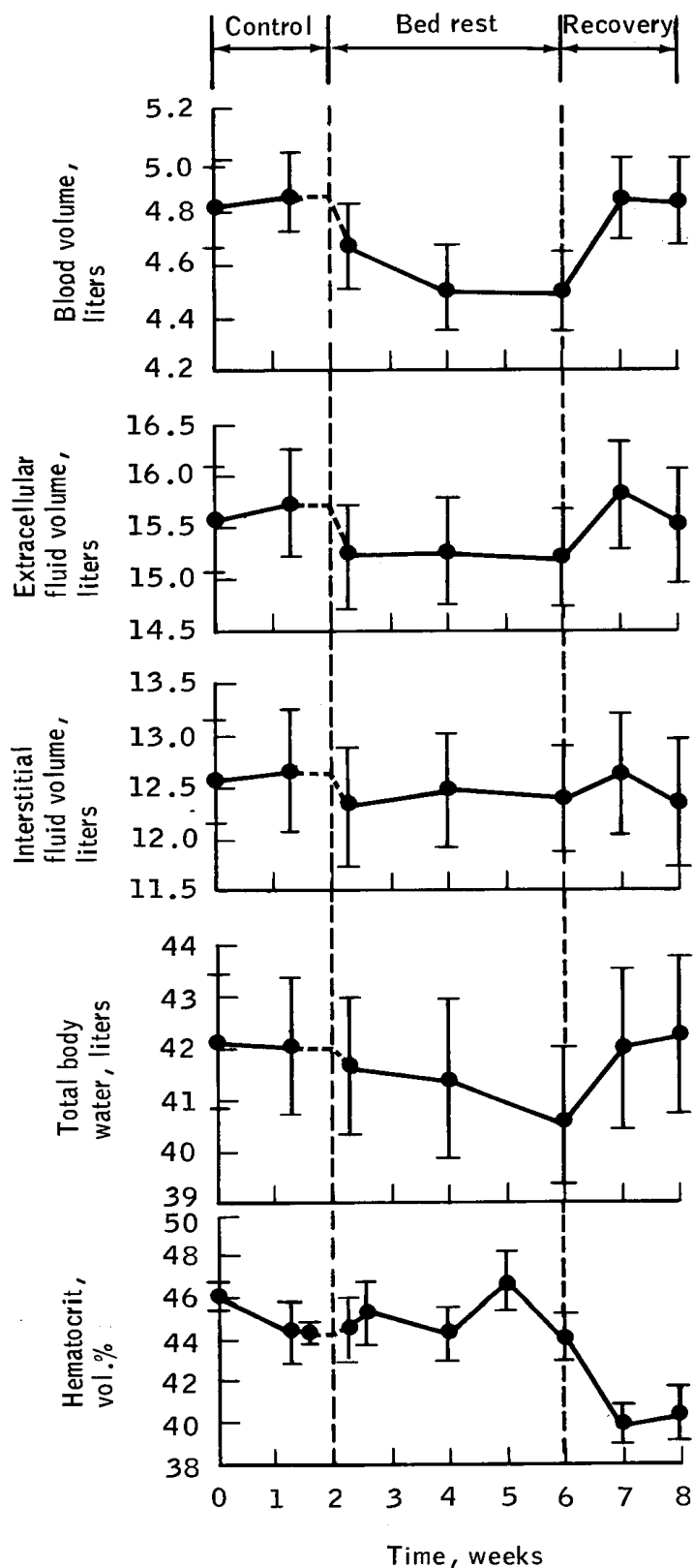
Figure 9-6. Experimental data of body fluid volume changes during a four-week period of bedrest [2].

necessary to perform these simulations. This study should be considered a validation of the structure and function of the Whole-Body Algorithm. Also encouraging was the notion that the response to a simple increase in stressed blood volume could explain many of the fluid and circulatory findings from bedrest studies.

However, some aspects of the model's behavior have suggested that certain modifications would be useful. Some of these include a superior erythropoiesis regulatory system that would predict decreases in red cell mass in long-term hypogravity, inclusion of a leg compartment in the long-term model and inclusion of an extravascular compartment in the short-term models. In addition, further analysis and understanding is needed in the areas of autoregulation of blood flow, stress relaxation and ADH regulation.

Furthermore, the simulations had to be artificially induced by forcing fluids into or out of the stressed fluid compartment. As such, the simulations did not represent physiological changes induced directly by the postural change but those induced indirectly by changes in the stressed fluid volume. In an attempt to make the long-term model capable of initiating its own fluid shifts, a leg compartment and the addition of a gravity vector was considered to be essential additions to the model. The modeling studies with such a modification are presented in the following section.

9.3 Supine Bedrest Simulation Using a Circulatory Model with Legs

9.3.1 Introduction

The addition of leg compartments to the Guyton model was motivated by the need to simulate hypogravic maneuvers more realistically. A number of critical processes occur in the legs in spaceflight including acute fluid shifts, gradual dehydration of the leg tissues and musculoskeletal degradation. The long-range goal to simulate spaceflight by initializing the model in the erect position and then remove the gravity effect was planned to be accomplished in several stages: a) addition of leg compartments, b) addition of gravity effects, c) testing the leg compartment modifications with supine bedrest simulation, d) testing of the gravity effects with postural simulations, e) creation of a model referenced in the erect position and f) simulation of spaceflight by removing the gravity effect from the reference model. The first four of these steps was completed in the course of this project and they are documented in the remainder of this chapter. The project ended, unfortunately, before it was possible to develop an erect reference model. This section will report on the use of a model with legs to simulate long-term supine bedrest. Testing the model for gravity related stresses such as postural changes and head-down tilt will be the subject of subsequent sections.

9.3.2 Model Modifications and Simulation Strategy

The path towards a realistic simulation of postural change and gravity dependency necessitates that the circulatory compartments should be divided into upper and
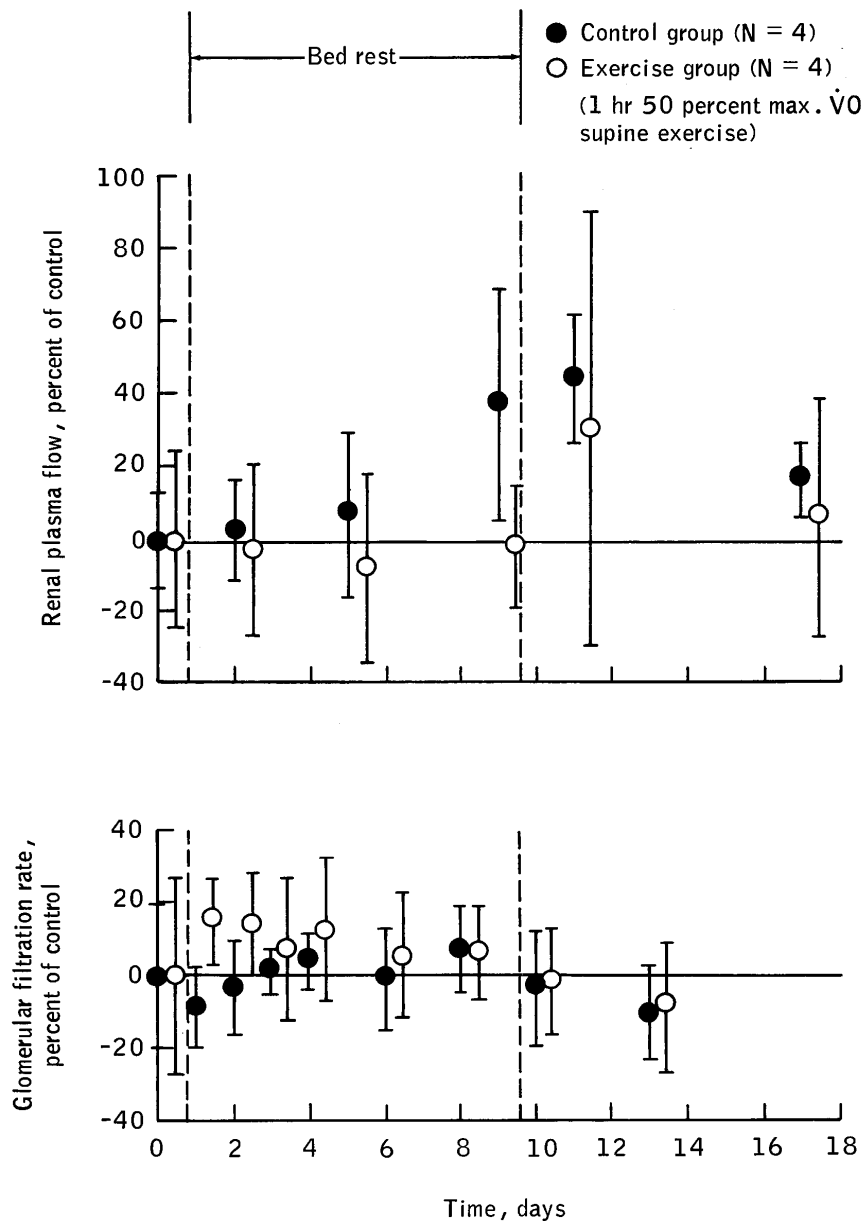
Figure 9-7. Experimental data of renal function during bedrest [8].

lower body segments. The Croston model of cardiovascular regulation was designed from the outset with leg compartments and gravity elements but it is considered a model for short-term events. The more comprehensive Guyton model contains elements that lend themselves to the more desirable behavior of long-term adaptation. Redesigning Guyton's circulatory model so that elements of the leg (lower body) compartments could be specified required the modification of several components of the model associated with fluid volumes and flows. These modifications involved separating or redistributing:

1) the pressures, flows and volumes of the upper and lower circulatory compartments;

2) the flow paths between upper and lower circulatory compartments perfusing muscle and non-muscle, non-renal tissues;

3) the levels of pressure and volume of the upper and lower body interstitial (and intracellular) compartments;

4) the basal capillary filtration and lymph flow between the upper and lower body compartments;

5) the pressure-volume function curves (compliance relationships) of the upper and lower circulatory compartments for arterial and venous segments; and

6) the pressure-volume function curves (compliance relationships) for the interstitial component of the upper and lower body compartments.
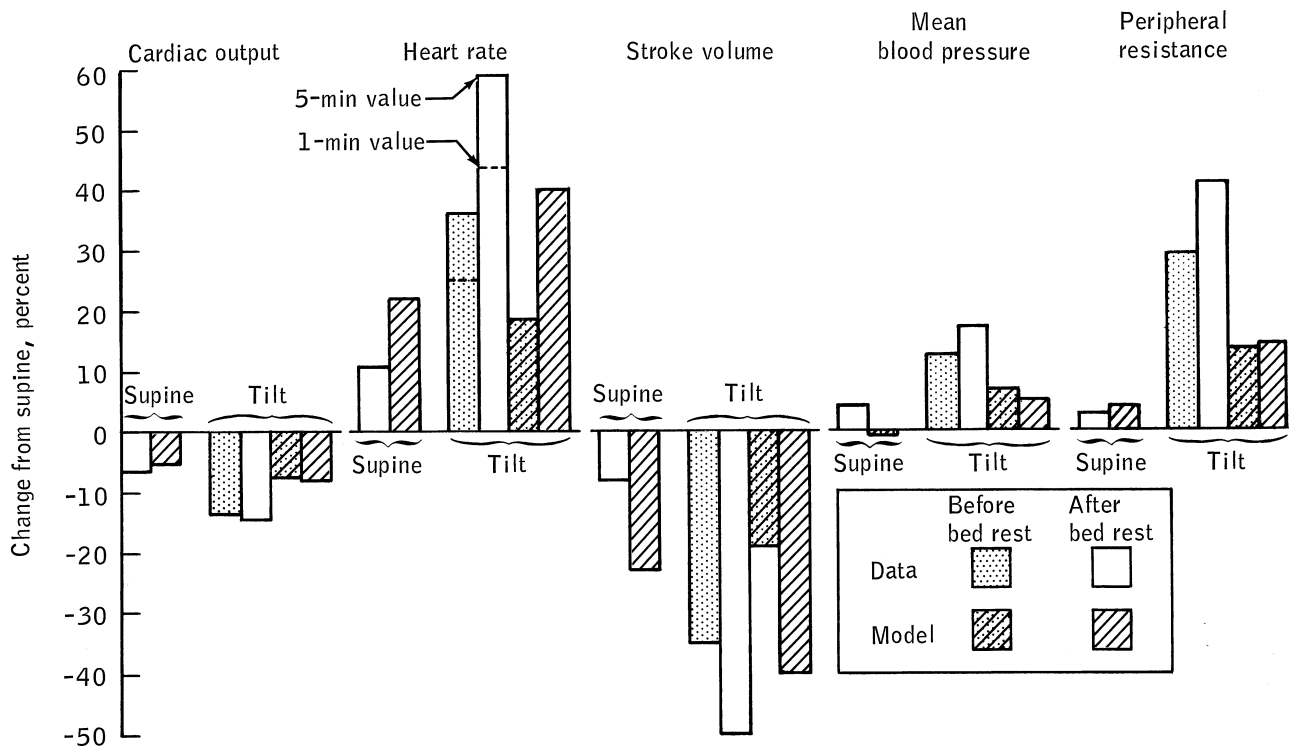
Figure 9-8. Response to 70° tilt from supine: Before and after bedrest comparison of model and data [15].
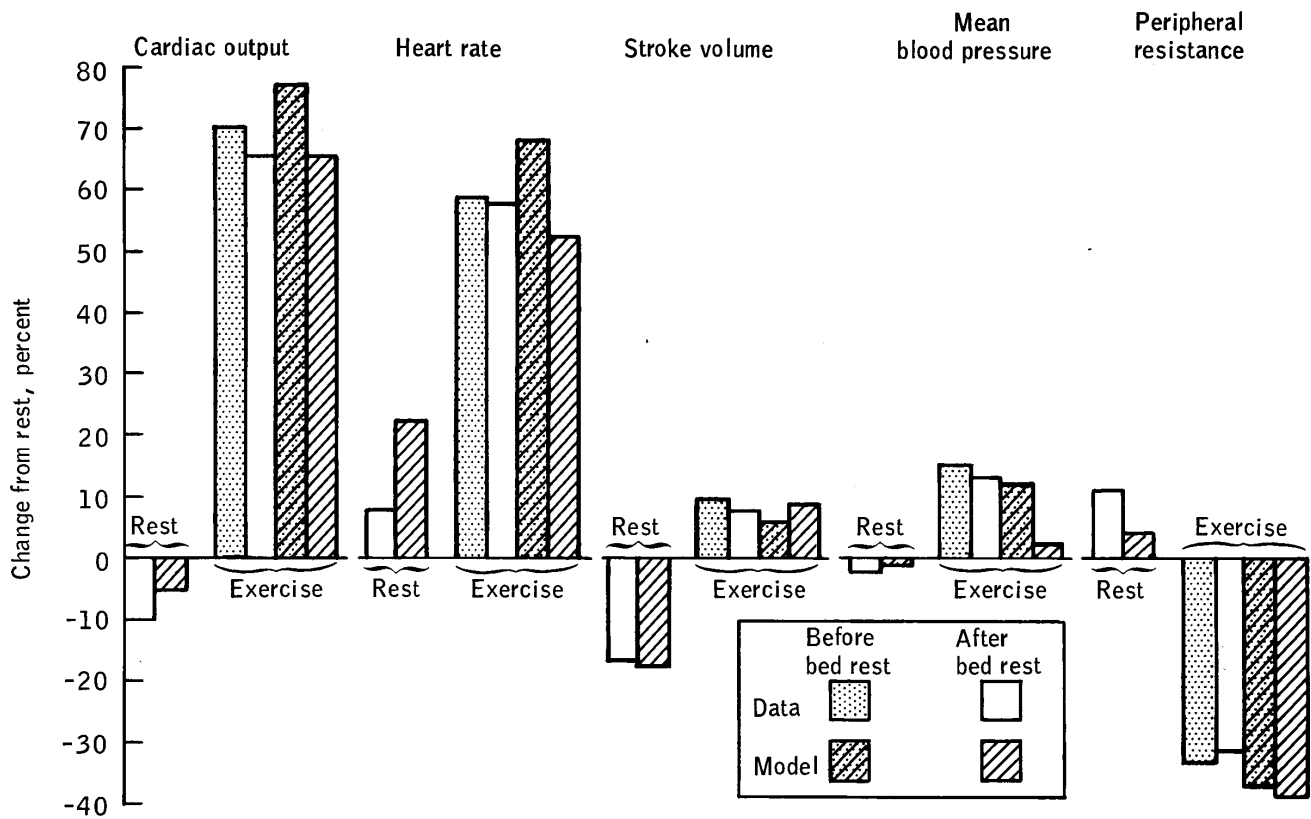
Figure 9-9. Response to 50 Watt supine exercise: Before and after bedrest comparison of model and data [3].

Another critical modification was to add gravity effects to the new circulatory compartments so that removal or adjustment of the gravity vector is explicitly represented in the model. See Chapter 3.2.5, Appendix C.1 and Leonard & Grounds [16] for details of the recompartmentation and gravity related modifications to the model. Chapter 9.6 also reviews special issues associated with these modifications. Figures 3-35 and 3-36 show a schematic of the Guyton model before and after recompartmentation. Taken as whole, this redesign would allow changes to occur in the leg compartments themselves and fluid shifts to occur between the lower and the upper body compartments subsequent to simulated postural changes. After the modifications were made, it was verified that the recompartmented model could reproduce the stability and responses to simple stresses almost identical to the original model.

If the Guyton model, modified with leg compartments, could be initialized in the erect position, a simulation of supine bedrest could be initiated by simply changing the gravity vector from vertical to horizontal position (allowing pooled fluids in the legs to move to the upper body propelled by natural tissue compressive forces) and turning off any position-defined orthostatic defense mechanisms, e.g., proprioceptor. Because such an erect initial state was not available, the problem became that of determining how to simulate a supine bedrest state starting from a supine initial state. Inasmuch as both states are supine, it would not be possible for fluids to move headward in a natural manner. Therefore, it was decided to move fluids artificially without actually changing postural position. This "forced-fluid stimulus" is similar to that presented earlier in Fig. 9-2 using the "legless" Guyton model. Although this is an unnatural forcing function, the studies that emerged, especially regarding mechanisms of leg dehydration, are considered to have value in understanding an important aspect of the hypogravic response.

In this study, our main interest was in the fluid volume responses during supine bedrest, specifically in leg volume. About 400–600 ml of blood are easily mobilized and rapidly transferred between legs and upper body during postural maneuvers. Another 300–500 ml of plasma was normally pooled extravascularly in the leg tissue upon standing. Thus, it appears that up to a liter of fluid is normally pooled in the legs when standing and some or all of it is available to shift cephaled when gravity vectors are removed. The working hypothesis is that fluid shifts from the legs during supine bedrest are the major driving force for many of the observed changes regarding fluid volumes (blood and interstitial), urine excretion and regulators (autonomic and hormonal) of renal and blood pressure control. It appears that the amount of blood originally pooled in the legs is very close to the eventual reduction in blood volume in hypogravity. For that reason special attention is paid, in this section, of the factors that cause leg dehydration in hypogravity.

9.3.3 Experimental Data
**9.3.3.1 Bedrest Data.** There are relatively few published studies which deal with all aspects of bedrest on the human physiological system, or which attempt to integrate the many major studies which have been conducted in the years prior to the current modeling studies, i.e., [6,17,18,19]. One possible explanation for this fact is that differences in scope and methodology, especially as regards the degree and duration of immobilization, make quantitative comparisons between studies difficult or impossible. So rather than attempt to determine a "typical" bedrest response, a specific bedrest study was chosen for simulation.

The study which was used as a baseline for the current set of horizontal bedrest simulations is the Baylor College of Medicine (BCM) 28-day bedrest study [20]. That study was designed as a bedrest control for the first 28-days of the Skylab missions; one can use this data to draw comparisons between microgravity and bedrest. This data was augmented with two other bedrest studies, a 14-day BCM study [17] and a 28-day study of Hyatt [2]. Results of certain fluid volume measurements (total body water, intracellular fluid, interstitial fluid) which were the emphasis of the simulation study, were quite variable as will be shown. However, plasma volume and leg volume changes are more consistent and these data will allow us to examine the processes that control them.

9.3.3.2 Leg Volume Changes in Bedrest and Spaceflight. One of the important objectives of this effort was to create the ability to simulate the prolonged dehydration effects in the legs that are observed during bedrest and weightlessness. Figure 9-10 shows the change in total leg volume during the first month of bedrest and spaceflight. The most dramatic aspect of this data is the four-fold difference in the magnitude of the leg volume changes between spaceflight and supine bedrest. One feature that is common, however, is the rapid decrease within the first few days followed by a more gradual decline that does not stabilize during the time period observed. The leg volume data from spaceflight does not level out even up to 84-days. Recovery is also very rapid, but bedrest yields the most rapid recovery. A critical analysis of the time-course of leg dehydration in spaceflight has been presented in Chapter 5.4.2. (The head-down bedrest and spaceflight data will be scrutinized more closely in later sections of this chapter; here we will concentrate on the supine bedrest data).

If one examines the data more carefully, it can be presumed that the changes that occur the most rapidly are probably due to the easily mobilized fluid in the legs, that of blood and the interstitial fluid that is pooled in the legs upon standing. By measuring the leg volume changes during the first few minutes of the supine position (from erect), approximately 400 ml of blood are inferred to pool in the legs. Judging from volume change on the 28th-day of bedrest (Fig. 9-10) there is probably another 300 ml volume that can be attributed to extravascular sources. This undoubtedly consists of easily mobilized interstitial fluid and of muscle tissues that atrophy from disuse during bedrest. If we acknowledge that recovery of the atrophied tissue takes longer than that of fluid recovery, it is possible to infer from the recovery data that much more tissue is lost during spaceflight than is lost during bedrest.
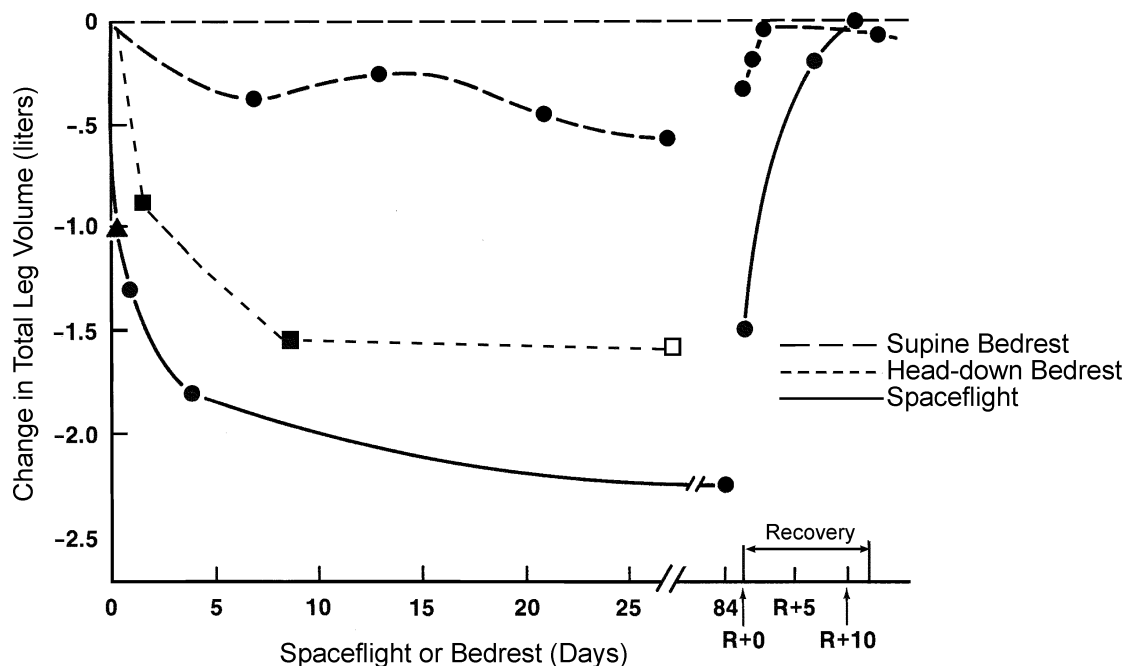
Figure 9-10. Effect of spaceflight and bedrest on total leg volume. Ref.: Supine bedrest [20]; Head-down tilt/bedrest ■ [21], □ [22]; Spaceflight ▲ Apollo Soyez Test Project [23], Skylab, SL4 mean ● [24].

9.3.4 Model Parameters Affecting Leg Dehydration

As was made clear previously in this book, a maneuver from the erect to supine position will result in a rapid headward movement of easily mobilized fluid in the legs. This leg fluid is derived from fluids in the leg vessels and leg interstitium, previously pooled during standing. (See Fig. 5-24 for details of this concept and Fig. 9-11 (bold lines) for a summary). Following this rapid fluid shift there appears to be a more gradual and less significant decrease in leg volume. The continual losses of leg volume, after the first day in the supine position, suggest that mechanisms beyond simple fluid shifts from the leg vasculature are important to understand long-term changes observed during bedrest. The components of the Guyton model were examined for various factors which could help explain the exponential-like decrease in leg volume. Once identified, these factors could be used to test hypotheses regarding fluid shifts and fluid volume changes during bedrest. Table 9-3 addresses the model factors that could influence the long-term dehydration of the legs.

9.3.5 Simulation Hypotheses

Based on the factors in Table 9-3 several promising hypotheses were identified and tested in the model as part of a bedrest simulation. The onset of bedrest simulation would be performed in a manner that will cause the blood pooled in the legs to rapidly shift headward. The hypotheses discussed below are designed to produce a more *gradual* loss of fluids from the legs over the 4 weeks of bedrest. Most of the factors in Table 9-3 were tested in the model but eventually only the first four were deemed important to achieve the desired result.

9.3.5.1 Hypothesis #1 – Decreased O_2 Demand and Autoregulation of Flow. The first hypothesis is based on the fact that bedrest subjects are relatively inactive, compared to ambulatory subjects. Thus, oxygen demand would be reduced. In addition, muscle tissue atrophy which accompanies bedrest or spaceflight will lead to a smaller and more gradual reduction in whole-body oxygen demand, but especially in the legs where the postural muscles primarily reside. In the Guyton model oxygen demand is linked to local blood flow autoregulation, so that a decrease in demand would reduce blood flow through the local tissues as well as reduce local capillary pressure. As shown in the hypothesis diagram of Fig. 9-11 this would lead to an increase in fluid reabsorption as predicted by the Starling forces and ultimately a decrease in interstitial fluid volume.

This "disuse" hypothesis was tested in the model by decreasing the value of oxygen consumption by 7% below the control level. This value is the same as that measured in subjects immobilized with plaster hip casts [25]. There are no comparable values measured directly during a bedrest study. A simulation to demonstrate the hypothesis was performed with the oxygen demand being lowered both by a step decrease of the whole value and by a linear decrease of the value over 28-days; both scenarios seemed plausible. For example, there is probably a rapid decrease in oxygen consumption at the very start of bedrest but also slower changes as metabolism processes change and as tissue wasting occurs.

The response of the model to the step decrease, shown in Fig. 9-12, was an autoregulatory-induced increase in peripheral resistance (not shown) with an associated de-

Bedrest

↓ *Muscle tissue activity* ↓ *Gravity loading of muscles* ↓ *Hydrostatic gradients*

↓ Muscle O₂ demand

↑ Muscle atrophy

↑ Tissue filtration   ↓ Leg blood volume

↑ Arteriolar resistance "autoregulation"

↑ Devascularization   ↓ Loss of cell water and electrolytes

↑ Central blood volume

Leg veins partially empty

↓ Leg tissue capillary pressure

↓ Vascular volume   ↓ Intracellular volume

↑ Diuresis

↓ Pressure in leg veins

↑ Fluid reabsorption

Hypothesis #3

↓ Plasma volume

Reverse stress relaxation forces more fluid from legs

↓ Interstitial fluid volume

↑ Hematocrit

Leg vascular volume ↓ until pressure stabilizes

Hypothesis #1

↓ Red cell production

Hypothesis #2

↓ Red cell mass

↓ Total blood volume

Figure 9-11. Hypotheses for explaining fluid volume changes during supine bedrest. Proposed mechanisms for short-term fluid shifts are shown with bold lines. The other branches of the diagram are for longer-term fluid shifts based on inactivity (Hypothesis #1), reverse stress relaxation of leg veins (Hypothesis #2). and muscle atrophy (Hypothesis #3).

Table 9-3. Model Factors Which Influence Leg Dehydration

Name of Process	Model Component	Description of Process
a) Decrease in oxygen demand	Effect of O₂ metabolic rate on autoregulation	Bedrest inactivity diminishes oxygen demand. Local autoregulation responds by increasing resistance to flow and lowering capillary pressure which favors increased fluid reabsorption from the interstitial fluid.
b) Reverse stress relaxation	Unstressed (filling) volume of leg vein (V_o)	Leg veins empty due to headward fluid shifts. Leads to reverse stress relaxation (decreased V_o) of veins until pressure is restored, thereby further emptying the veins.
c) Muscle atrophy	Decreased intracellular fluid and loss of vascularization	Inactivity leads to muscle atrophy. Model's cellular compartment can be diminished by leaking potassium causing water to follow. Blood vessels associated with muscles are diminished by reducing V_o.
d) Drying of interstitial gel	Amount of hyaluronic acid in the interstitium.	Decrease in hyaluronic acid will decrease gel that contains the largest portion of interstitial fluid. Can also be simulated by decreasing set point of interstitial volume.
e) Compliance of leg blood vessels	Venous compliance	Relationship of pressure and volume of stressed volume in the leg veins. A decrease in compliance will increase leg blood pressure and decrease stressed volume.
g) Tilting to supine position	Angle of tilt	Negative values will simulate head-down tilt and pool blood from legs into upper body.
d) External pressure on leg	External pressure bias on leg blood vessels and leg tissue compartment	Represents natural compressive forces of tissue that force fluids headward upon reclining. Also used for muscle pump on standing or external pressure in water immersion. Effect is to drive fluid from legs.
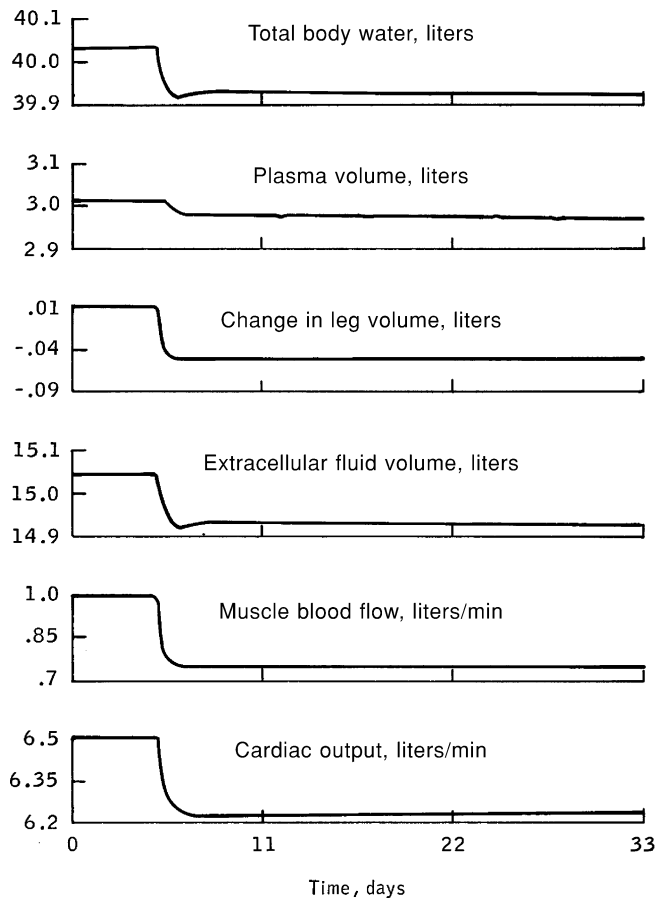
Figure 9-12. Simulation of the effect of a step reduction in oxygen demand in muscles.

crease in cardiac output and muscle blood flow. Leg volume decreased by a small amount, 65 ml, with most of the fluid coming from the interstitium. Modest decreases in plasma volume reflected the increased arterial pressure (not shown). The decreases in plasma volume and interstitial fluid accounted for the losses in total body water.

9.3.5.2 Hypothesis #2 – Reverse Stress Relaxation of the Leg Vasculature. The second hypothesis is based on the knowledge that veins act as viscoelastic materials. When a vein is subjected to a mechanical strain, part of the strain is immediately reversible (the elastic part) and part of the strain is not (plastic deformation, creep, or stress relaxation). The amount of elastic stretch is measured by the compliance, which describes the relationship between pressure changes and volume changes. The filling volume of the venous compartment (V_o) is the volume that can be filled (starting from an empty "flabby" vessel) before pressure changes occur. This is also called the unstressed volume and is capable of non-elastic deformation [26b](see Fig. 9-32 for a graphical illustration of these concepts). During ambulatory periods, the leg veins are often distended and, as a result, a certain amount of stress relax-

ation occurs (i.e., a gradual increase in V_o at constant pressure). During bedrest, however, the leg veins are not distended, but are rather empty and the reverse process, reverse stress relaxation occurs. The filling volume of the leg veins decreases and the transmural pressures increase until transmural pressure across the vein reaches a steady-state condition. As the transmural pressures are gradually increased during reverse stress relaxation, additional blood will leave the leg vascular compartment and shift headward. The effects of bedrest on fluid volume changes, based on reverse stress relaxation in the legs, are shown in Fig. 9-11 (Hypothesis #2).

Reverse stress relaxation in the Guyton model is an automatic mechanism of the large central veins in the body. However, the leg veins of the modified Guyton model were not designed with an inherent function for reverse stress relaxation. Therefore, the unstressed volume of the leg veins was changed manually. The total magnitude used for the stress relaxation effect was 280 ml, the value estimated for the change in leg blood volume because of bedrest. The unstressed volume change was accomplished at an exponential rate (1st order time constant) over 28-days. The major effect of this process was a small gradual rise in arterial pressure that eventually led to a renal-induced reduction in plasma volume of the same magnitude.

9.3.5.3 Hypothesis #3 – Loss of Muscle Tissue and Tissue Vasculature. The third hypothesis is that muscle atrophy due to gravity unloading was responsible for a portion of the long-term changes in leg volume. Muscle atrophy implies losses of skeletal muscle cellular contents and the associated capillary vasculature of the muscle tissue. Figure 9-11 indicates that muscle tissue losses, largely due to inactivity, would decrease interstitial fluid volumes (Hypothesis #1), as well as intracellular volume and the volume of blood normally associated with the lost tissue (Hypothesis #3). To the extent that these losses occur in the legs, leg volume will also gradually decrease.

Is it possible to estimate the amount of leg volume loss due to muscle atrophy? One approach is to note from Fig. 9-10, that the total reduction in leg volume measured at the end of 28-days of supine bedrest was 600 ml. Subtracting the 280 ml of easily mobilized leg fluid measured during postural change from 600 ml yields 320 ml as our estimate for extravascular tissue (interstitial plus intracellular) losses in the legs. Another gross estimate of leg tissue loss would be to use the information that 46% of the decrease in maximum calf circumference was recovered by the end of the first post-bedrest day and then remained constant. If the remaining 54% represents muscle tissue loss and further if this proportion is constant for the total leg loss, than about 320 ml (54% of 600ml) of loss were from extravascular sources, in excellent agreement with the first approach. Using a demonstrated correlation between lean body mass and blood volume [27] and noting the observed blood volume to lean body mass ratio of 89 ml/kg during bedrest [20], a blood volume of 29 ml is calculated representing the blood lost from the body with 320 ml (~0.320 kg) of muscle tissue. (This amount is in

addition to the rapid loss of vascular fluid from the legs at the onset of bedrest).

Which parameters of the model should be altered to simulate the leg volume losses from muscle atrophy just calculated? In the model, the legs do not include a separate cellular compartment but they do contain an interstitial fluid compartment. Therefore, in order to simulate muscle tissue loss, the leg interstitial fluid volume is reduced by 320 ml, the amount previously calculated. Another 30 ml of blood will be "squeezed" from the legs due to devascularization (i.e., the volume associated with the atrophied tissue) by reducing the filling volume (i.e., unstressed volume, V_o) of the leg veins. This is equivalent to invoking reverse stress relaxation. In addition, a small portion of the intracellular volume will be slowly depleted by allowing 10% of intracellular potassium to leak across the cell membrane. This represents the gradual wasting of muscle tissue. Since the intracellular compartment is not a part of the leg structure in the model, this loss is not reflected in leg volume changes, but rather in total body water.

9.3.6 Supine Bedrest Simulation: Overview and Approach

The Guyton model, modified with leg compartments, was used to simulate supine bedrest using the scheme shown in Fig. 9-13. In order to overcome the disadvantage of simulating supine bedrest with a model initialized in the supine position (as discussed in the introduction to this study, Chapter 9.3.1), fluids were forced from the leg compartments and allowed to shift headward. Prior to starting the simulation, the leg veins and leg interstitial compartments were "preloaded" with an amount of fluid believed to be pooled in the legs when erect (see Fig. 9-13(a). It was as if the model were allowed to stand upright for about 30-minutes; about 400 ml excess blood pools in the lower limbs and 300 ml pools in the leg interstitium (see Chapter 9.7.3.2.1). If then, the model was suddenly brought supine, the leg fluid compartments would be "preloaded" at the moment the simulation begins. The leg vein compartment was preloaded by increasing the unstressed volume (V_o) by 400 ml and the leg interstitial compartment was preloaded by increasing the interstitial volume set point (V_I) by 300 ml.

"Release" of these volume excesses provided the initial stimulus for shifting fluid headward and was accomplished by simply reversing the "loading" parameters, V_o and V_I by the same magnitude as the *preload* amount. The duration of the V_o shift was about 30-minutes since it represents the highly mobilized fraction of blood available for shifting between upper and lower body segments during postural change. The duration of the V_I shift was set as a first order exponential change, decreasing 63% of the full value within the first 3.7-days and the remaining 37% over the remaining 24.3-days of the bedrest study (see Fig. 9-13(b and c). The tissue fraction of fluid is reabsorbed across the leg capillary beds into the leg vasculature and then is automatically shifted headward by compliance forces. Two other hypotheses were tested in

this simulation as described in Chapter 9.3.5 (but not explicitly shown in Fig. 9-13): the decrease in oxygen demand due to inactivity (Hypothesis #1) and a small amount (30 ml) of devascularization (i.e., further decrease in V_o) due to muscle atrophy (Hypothesis #3).

The fourth cartoon in Fig. 9-13(d) represents the *response* of the model's control system to the headward fluid load. As described fully in Chapter 5 (and summarized in Fig. 9-11), a relative hypervolemia occurs in the upper body and is relieved by a reduction in plasma volume, i.e., Gauer–Henry mechanism. That is, the physiological volume control mechanisms will maintain the central blood volume at a normal level by renal excretion of excess fluid. This is the belief of a number of researchers and is confirmed by the Guyton model. Prolonged bedrest results in further leg dehydration as suggested by the time profile of leg volume changes. It is suggested that this is due to the hypotheses discussed in Chapter 9.3.4 (see Fig. 9-13(e)).

9.3.7 Supine Bedrest Simulations: Simulation Results

9.3.7.1 Plasma Volume.
The model simulation shows a decreasing plasma volume that compares favorably with all three bed-rest studies (Fig. 9-14). The recovery of the model is slower than that indicated by the data. There is a distinct overshoot of the control level in two of the studies, but not in the simulation.

9.3.7.2 Leg Volume.
The model output of leg volume compared to data from the 28-day Johnson and Mitchell study is shown in Fig. 9-15. Several factors prevent precise comparison between model and experimental response. The experimental data represent changes in total leg volume including those due to decrements in fluid volume (intravascular and extravascular) and solid tissue. The model response, on the other hand, includes only those changes due to leg intravascular and interstitial fluid shifts. The rapid initial decline of plasma volume in the simulation was due to: a) the pooled blood in the leg veins being "released" and propelled toward the central venous compartment by the compressive forces of the leg veins and b) an intravasation of 300 ml of leg tissue fluid into the leg veins which then shift the fluid headward by the same compressive forces as in (a). The continuing slower decrease in leg volume was a result of the tail-end of the 1st order decreases of (a) and (b), (c) a decreased oxygen demand and d) the devascularization mechanism.

Changes in tissue volume as a result of muscle atrophy could not be measured during the bedrest study and were not considered in the simulation. However, this factor could alter the time course of the response. Recovery results indicated that the model recovers leg volume less quickly than the human subjects. All forcing functions used to create the changes were made symmetrically for either decreases or increases in fluid volumes. It has been suggested that this may not be the case in the real system [26a].

9.3.7.3 Extracellular Fluid Volume.
In Fig. 9-16 the differences in the extracellular fluid volume of the simu-
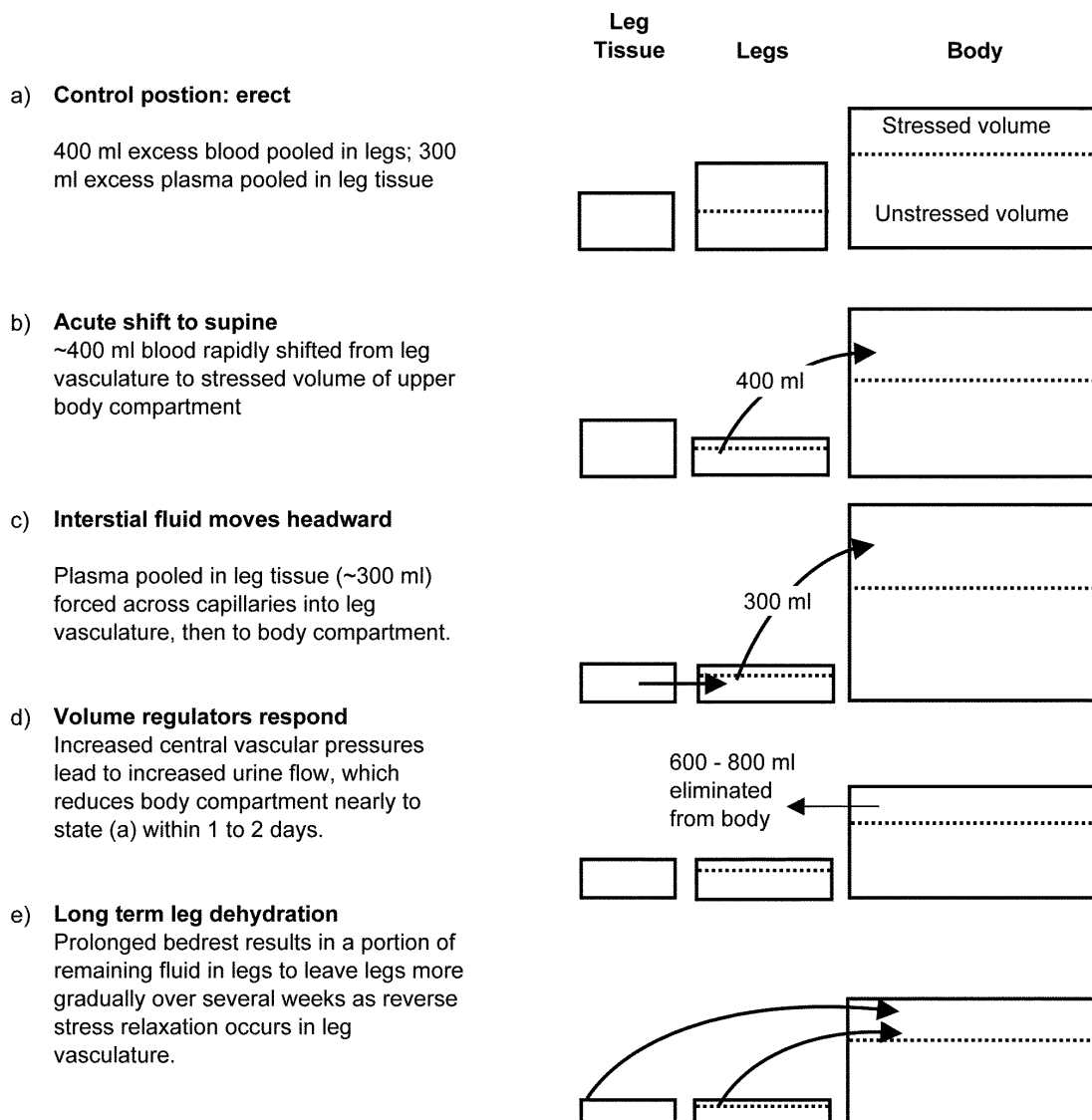
Figure 9-13. Idealized concept for fluid shifts from legs during supine bedrest. This diagram shows the initial preloaded state (a); the forcing stimulus for initiating supine bedrest simulation (b) and (c); the acute response of the model is (d); and the long-term dehydration of the leg (e) as tested by the three hypotheses.

lation and the experimental data from the 28-day BCM study, the 14-day BCM study and the 28-day study of Hyat, are compared. The model's response of extracellular fluid coupled with the leg volume response shown previously suggest that the decrease of the extravascular volume of the legs is excessively rapid and that a volume decrease of less than the 300 ml used for this simulation might be more appropriate. The recovery of human subjects shows an overshoot response which is not duplicated by the simulation. The notation of extrapolated and 30-minute values on the 28-day BCM study indicate two techniques which were used to interpret the isotopic tracer data.

9.3.7.4 Total Body Water. In Fig. 9-17 the total body water response of the simulation is compared to the data from the three experimental studies. The total body water changes include the net changes in both the extracellular and the intracellular fluid compartments. Intracellular fluid was depleted in accord with Hypothesis #3 (see Chapter 9.3.5.3). The simulation predicts both a rapid and then a gradual decline in total body water throughout the duration of the bedrest. The longer term simulation response is in agreement with the data.

9.3.7.5 Other Results. The results of the simulation also show good agreement in other areas of experimental ob-
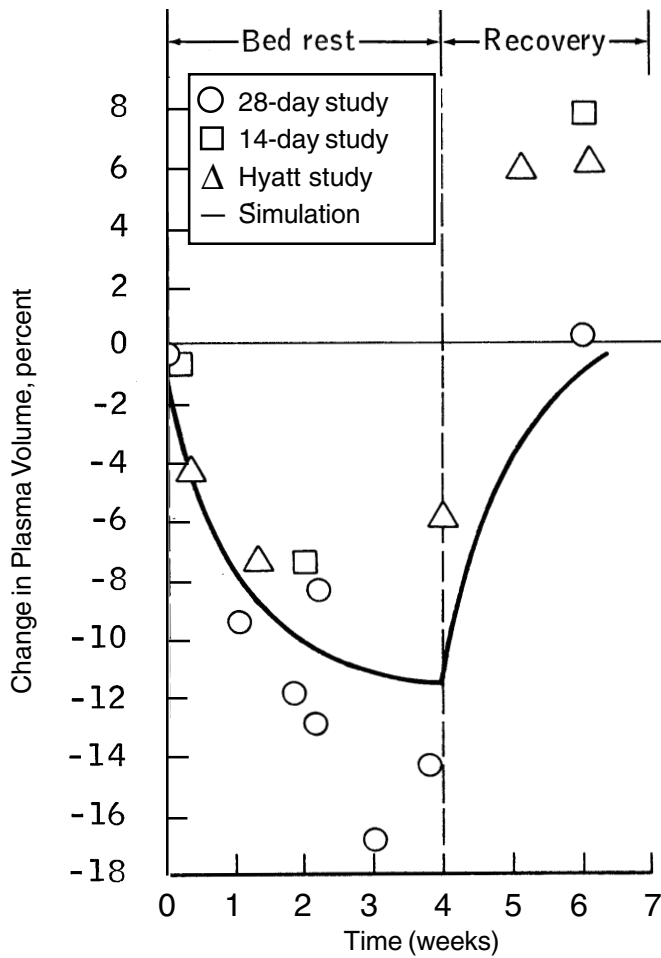
Figure 9-14. Comparison of changes in plasma volume during bedrest: Model vs. data.
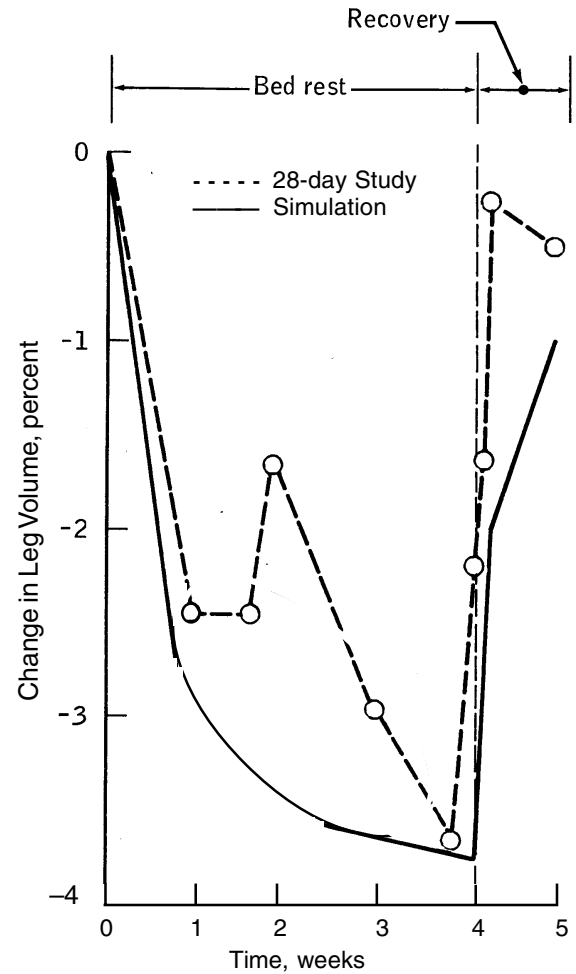
Figure 9-15. Comparison of leg volume changes during bedrest: Model vs. data. Left leg volume data is from 28-day BCM bedrest study. The spike in the data at the end of two weeks of bedrest coincides with the LBNP + saline ingestion crossover study, a factor not accounted for in these simulations.
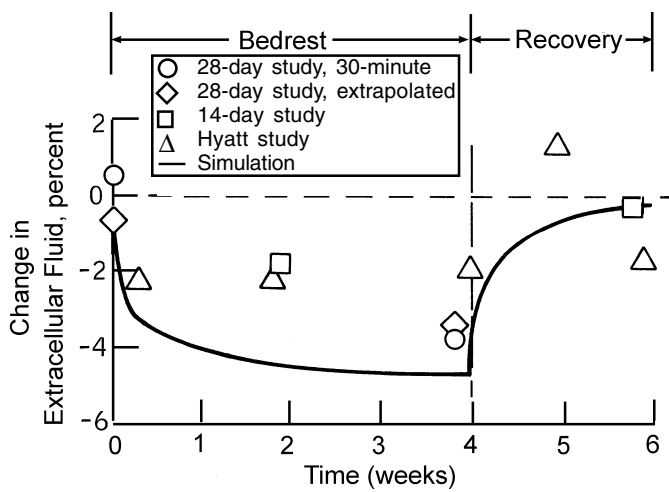
Figure 9-16. Comparison of extracellular fluid volume changes during bedrest: Model vs. data. The notation of extrapolated and 30-minute values for the 28-day bedrest study indicate two techniques which were used to interpret the isotopic tracer data [20]. ◯ - 28-day study; ☐ -14-day study; △ - Hyatt.
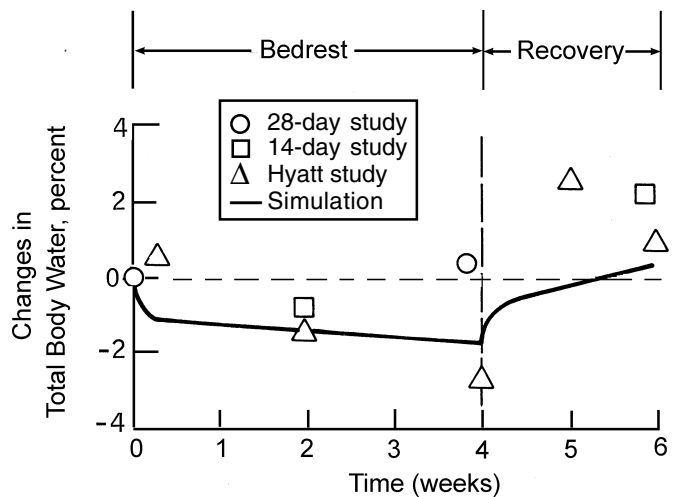
Figure 9-17. Comparison of change in total body water during bedrest and recovery: Model vs. data. ◯ - 28-day study; ☐ -14-day study; △ - Hyatt.

servations including red cell mass, cardiac output, arterial pressure and total peripheral resistance. A 6.7% decrease in red cell mass compared well to the observed value of 6% decrease at the end of bedrest as measured by Kimzey, *et al.* [28]. This favorable comparison indicated the soundness of the improved erythropoiesis algorithm which had been inserted in the model [16,29]; (see Appendix C). Some of the model's hemodynamic parameters which showed a change at the end of 4 weeks simulated bedrest are a 4.2% decrease in cardiac output, a 2.5% increase in arterial pressure and a 7.1% increase in total peripheral resistance. These values show reasonably good correspondence to studies by others [1,3,4,5,6]. The only parameter that was not simulated well was resting heart rate. An increased resting heart rate has been a consistent finding in almost every bedrest study to date. Yet, without additional changes to the autonomic elements, the Guyton model predicts practically no change in resting heart rate for 28-days of bedrest. An empirical algorithm has been applied to the heart rate function to provide realistic heart rate and stroke volume responses for bedrest simulations. The mechanisms that may be responsible for this effect are not presently known.

9.3.8 Summary: Supine Bedrest

Despite the crude approximations that were made, reasonable results have been obtained in simulating the fluid shifts of bedrest. Although it was necessary to use an unnatural forcing function to allow leg fluids to shift headward, the resulting changes in plasma volume, extracellular volume and leg volume were similar to those seen in bedrest. The addition of leg fluid compartments to the model have permitted testing of hypotheses to account for the time course of leg dehydration. The magnitude of 400 ml of shifted blood and a time constant of slightly less than 4-days give good correspondence to experimentally observed losses in plasma volume. The extravascular fluid from the legs, originally estimated to be around 300 ml, leaves the tissue too quickly and may represent an excessively large volume. A decrease in resting oxygen demand of muscle seems warranted and this decrease has positive effects on leg volume changes and hemodynamic parameters. Overall, these simulations provided some insights into the interpretation of the observed fluid volume changes whereby an initial large and rapid decline in the volumes of plasma, interstitium and legs gives way to a smaller and more gradual decrement in these compartments. Most of these changes appear to be explained by fluid and tissue changes in the legs, i.e., leg dehydration and muscle atrophy.

As indicated in Fig. 9-10, the fluid shifts accompanying spaceflight are much larger than those associated with postural changes or supine bedrest. It is possible that the interstitial tissues in the legs contain a larger amount of readily mobilized fluid than has been heretofore recognized under normal terrestrial surroundings. The most promising ground-based, experimental stresses for examining the larger zero-g fluid shifts are water immersion and antiorthostatic bedrest (head-down tilt). These will be examined in the following sections after a simulation study

of spaceflight is presented. All of the remaining studies in this chapter were performed using the Guyton model modified with leg compartments.

9.4 Spaceflight Simulation

9.4.1 Hypothesis Development

An overall goal of the modeling project was to achieve an accurate computer model simulation of the physiological changes observed during spaceflight. Several major obstacles had to be surmounted to accomplish this goal: a) identify the physiological areas of concern, b) develop or acquire the models for studying this area, c) using the model as a guide, identify the experimental variables of interest, d) formulate hypotheses to account for the observed zero-g changes and d) determine how these variables are altered in spaceflight by testing the hypotheses in the model. This approach was used throughout Chapter 5 to analyze the fluid, electrolyte and circulatory responses to spaceflight.

As part of the analysis of Chapter 5 a set of six hypotheses were developed (see Chapter 5.4). Each hypothesis was designed to explain a specific known or suspected physiological change(s) in the Skylab astronauts. Table 9-4 lists these hypotheses and summarizes their major short-term and long-term physiological effects on the simulation. Each item listed is a quantity which has either been measured or postulated to occur in spaceflight. The list taken as a whole represents a comprehensive fluid-electrolyte response pattern to weightlessness. In Chapter 5.4 these hypotheses are analyzed individually and the reader is referred there for a complete discussion of each of them. In this section, we shall report the predicted responses for the case where all of these hypotheses have been combined during a single simulation.

9.4.2 Simulation Approach and Model Modifications

The most important hypothesis considered was the acute shift of fluids toward the head (Hypotheses #1 and #2 in Table 9-4). This was a common characteristic of various hypogravic situations including postural changes, bedrest, water immersion and head-down tilt. Consideration was given to various techniques that would provide the appropriate stimulus for simulating this initial response. Since weightlessness appears, in many respects, to be merely the absence of orthostasis in one-g, it seemed desirable to initialize the model in a steady-state upright position and proceed to remove the gravity vector. This approach was not feasible since the physiological mechanisms that protect man from long-term orthostatic collapse are not known well enough to include in a quantitative model, especially as a reference state [16]. The successful use of six-degree head-down tilt as an experimental ground-based analog to weightlessness suggested another direction. For reasons that were then unknown, the model exhibited instabilities and mathematical discontinuities during a simulated head-down tilt. Neither of these approaches were sufficiently developed at the time to be used in the present study, however, they subsequently re-

Table 9-4. Hypotheses and Their Effects on the Simulation of Circulatory, Fluid and Electrolyte Responses to Spaceflight (Skylab)

Hypothesis	Short Term Effects	Long Term Effects
#1 Blood shift from legs	• Transient decrease in interstitial fluid	• Increased hematocrit • Decreased red cell mass
#2 Filtrate shift from leg tissues	#1 and #2 • Circulatory hyperdynamia • Diuresis • Natriuresis • Decreased sympathetic activity • Decreased angiotensin, aldosterone, and ADH	#1 and #2 • Decreased leg volume • Decreased plasma volume • Decreased body water • Decreased body sodium
	• Transient increase in interstitial fluid	• Decreased interstitial fluid
#3 Potassium release from cells		• Increased K^+ excretion • Decreased body K^+ • Decreased intracellular fluid • Increased plasma $[K^+]$ • Increased Aldosterone
#4 Natriuretic factor	• Increased urine Na^+ excretion • Decreased extracellular $[Na^+]$ • Decreased intracellular osmolarity • Decreased loss of intracellular fluid	• Decreased extracellular $[Na^+]$ • Increased aldosterone • Increased angiotensin • Decreased ADH
#5 Chronic decrease in sweat losses		• Increased renal excretion of water, sodium, and potassium • Increased urine osmolarity
#6 Anorexia and increased sweating early inflight	• Decreased body water • Decreased body potassium • Decreased body sodium • Partial suppression of diuresis & natriuresis	

ceived additional attention and were somewhat successful (see Chapter 9.6 and 9.7).

A third technique was briefly attempted with little success. This involved using the values for fluid intake, evaporative water loss and renal volume excretion that were observed in the Skylab crew (see Chapter 4.4) as forcing functions for the Guyton model. This was done in an attempt to drive the internal physiological mechanisms. Controlling both intake and output proved unsuccessful as a zero-g simulation, but it did demonstrate that the negative water balance which appears appropriate for maintaining normal function in zero-g is a severe stress in one-g and a knowledge of electrolyte balance is as important as water balance for simulating an individual's response to any long-term stress.

The stimulus for weightlessness that was ultimately used in this study took advantage of the fact that the fluid-electrolyte model is extremely stable in a "supine" position. The hypogravic simulation was initialized from this reference state, just as it was in the supine bedrest simulations described in Chapter 9.2 (without "legs") and

9.3 (with "legs"). The following programming was introduced into the Guyton model (modified with legs) in order to perform this Skylab simulation and test the hypotheses:

1. An acute headward shift of leg fluid was accomplished by forcing fluids from the leg blood (Hypotheses #1) and tissue (Hypotheses #2) compartments. See Fig. 9-13 (items a, b and c) for the concept of fluid shifting headward in the model. In this case, however, a greater amount of fluid was shifted than for supine bedrest (i.e., 500 ml of blood and 500 ml of filtrate were forced acutely from the leg compartments) in accordance with observation (Fig. 9-10). For convenience, the longer-term dehydration of the legs was not considered. The leg dehydration phenomena will be revisited in the head-down bedrest study later in this chapter.

2. Potassium was gradually released from the cell compartment in an effort to mimic some of the effects of muscle atrophy (Hypotheses #3). The manner in which this was accomplished is described in Chapter 5.4.2.2.

3. The model was structurally modified to include the natriuretic factor (Hypotheses #4). See Figs. 5-16 and
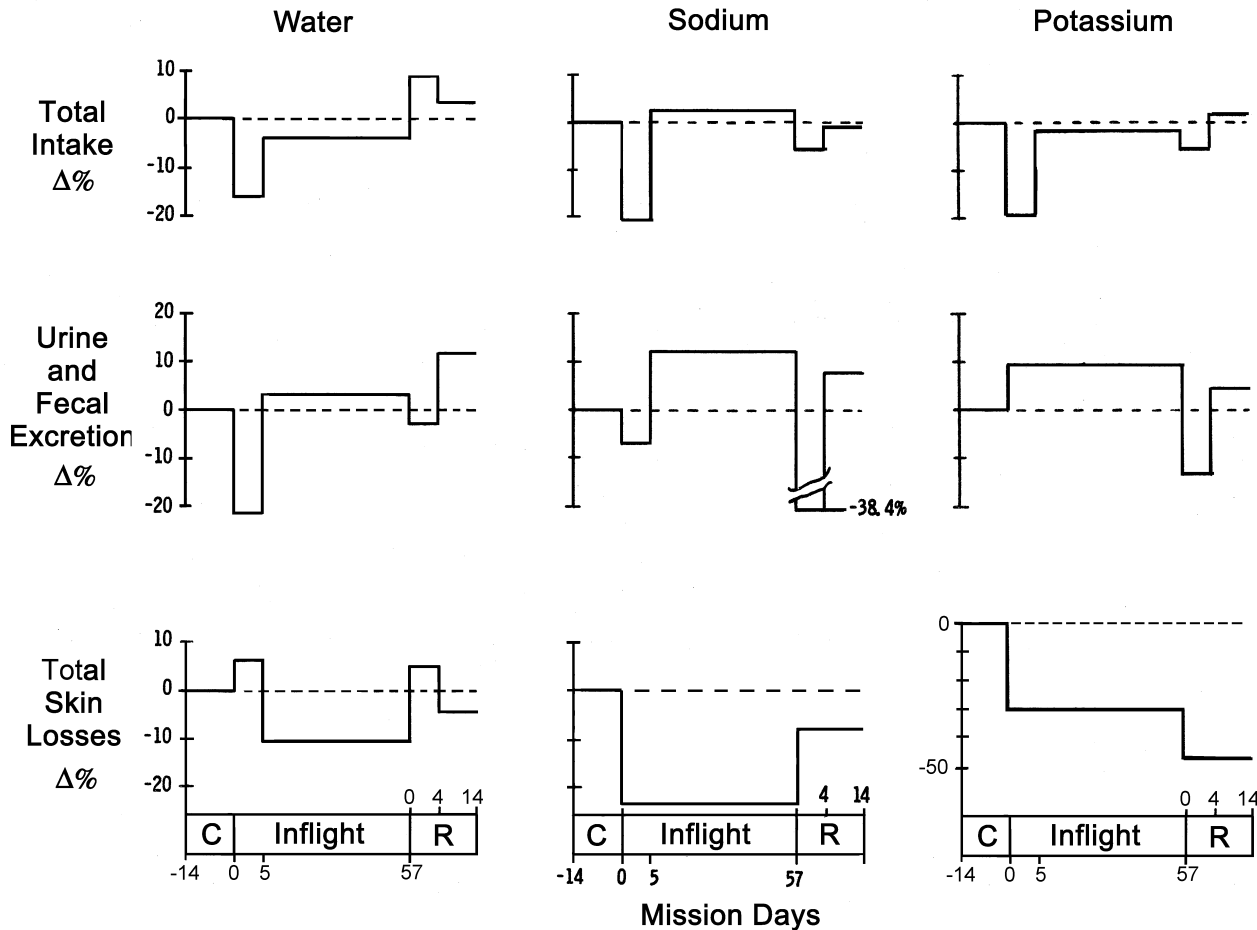
Figure 9-18. Total intake, total excreta and total skin losses for water, sodium, and potassium in the average Skylab crew and for the average mission length. Changes have been partitioned into acute and long-term segments for ease in model use. Total Intake includes dietary intake and metabolic water; Total Excreta combines urine and fecal quantities; Total Skin Losses includes insensible evaporative and sweat losses. For the Skylab simulations in this section, the modified Guyton model was programmed with Total Intake and Total Skin Losses which are fixed parameters. The excreta data was used to compare with model output. Data in this figure was derived from metabolic balances (see Chapter 4) and from a special modeling technique (see Appendix F.3.3). C= preflight control period, R = postflight recovery period.

5-29 and the associated discussions.

4. Dietary intake and sweat rates for water, sodium and potassium were entered into the model according to a previous analysis of a composite Skylab crewman as illustrated in Fig. 9-18 (see also Chapter 4.4 and Table 5-9). This programming was sufficient to test Hypotheses #5 and Hypotheses #6 that deal with short and long term influences of intake and sweat rates.

With regard to the last item, the Guyton model contained no sweat loss mechanism, so a simple formulation was inserted into the model as described in Chapter 5 (Chapter 5.4.2.2). The Guyton model, of course, contains a kidney with renal excretion of water, sodium and potassium as computed variables. Therefore, the urine excretion data shown in Fig. 9-18 was not used as data for programming the model, but rather as data for comparison with the model output. Because the Guyton model contained no representation of fecal output, urine and fecal quantities have been combined. However, fecal excretion is only a small fraction of urine excretion.

9.4.3 Spaceflight Simulation Results

The simulated flight period was 57-days (the length of the average Skylab flight). It was preceded by a 4-day control period and followed by a 14-day recovery period. Recovery periods have not received a great deal of attention during these simulations and hypotheses which might improve their response have not been evaluated. Therefore, the recovery period is not included in all figures. Some of the most important responses in this simulation are presented in Figs. 9-19(a) to 9-19(d).

Figure 9-19(a): The headward shift of a liter of fluid from the legs (blood plus filtrate) results in a rapid loss of plasma. There is a more gradual decline in red cell mass. The model predicts this response as being secondary to hemoconcentration-hyperoxia effects. Hematocrit declines from its initial elevated levels as red cells are lost from the circulation. However, blood volume remains relatively stable at a reduced level due to a compensatory increase in plasma volume. The model also predicts that interstitial fluid volumes (in the upper body) return to normal within several days. Recovery is characterized by a return to control levels for leg volume and blood volume, while hematocrit falls below normal. Discontinuities appear at the end of the fifth inflight day in some cases because this point separated the two-stages (acute and chronic) of dietary/sweat module inputs.

Figure 9-19(b). This figure shows the behavior of some important fluid-electrolyte variables. Total body water and extracellular sodium decrease rapidly because of the fall in extracellular fluid (not shown) and then more slowly as intracellular fluid decreases. The rate at which fluid leaves the intracellular compartment is controlled completely by transcellular osmotic forces. However, this is a complex function of extracellular sodium concentration that is regulated by renal excretion and the release rate of potassium from the cell. The influence of the natriuretic factor caused the plasma sodium concentration to fall, although not as far as observed in spaceflight. Plasma potassium concentration increases primarily because the loss of cell potassium; the concentration would have been higher if not for good renal regulation. The loss (after launch) and eventual recovery (during postflight) of body water, body sodium and body potassium proceed at different rates. These rates were similar to those found for the Skylab crew (see Fig. 5-2).

With the exception of plasma electrolyte concentrations, hematocrit and leg volume, none of the variables shown in Figs. 9-19(a) and 9-19(b) was measured directly *during* the weightless portion of flight. Using traditional and novel modeling techniques it has been possible to develop independent estimates of many of these quantities. The results shown here are in good agreement with those predictions.

Figure 9-19(c): The renal responses of fluids and electrolytes during simulated spaceflight are shown in this figure. Excretions of water and sodium have similar time-courses. After a short period of rapid excretion, the first 5-days of flight are characterized by a loss rate much less than that shown during control. The model is appearing to conserve fluids in the face of decreased drinking and increased sweating. This is followed by a much more constant output slightly higher than control. Steady-state values for water and sodium excretion are elevated by +4% and +12%, respectively. These changes are in excellent agreement with Skylab values. Potassium excretion remains elevated, however, throughout the inflight period by about 4%. This value is lower than that observed during spaceflight because of a potassium loss rate from the cells which was set too low in the model. The predicted steady-state

urine concentration of sodium is about 10% above control, also similar to experimental findings. This occurs at a time when aldosterone is elevated; thus the model exhibits a "sodium escape from aldosteronism" phenomenon similar to other studies of chronic hyperaldosteronism.

The dietary and sweat changes programmed into the model (Fig. 9-18) had a significant influence on the outcome of the simulation, particularly the renal responses of Fig. 9-19(c). It is worthwhile summarizing the important aspects of these metabolic events. The early decrease in intake was ascribed to space motion sickness induced anorexia while the early increases in sweat losses were due to unusual heat and work loads. Both of these early changes had marked effects in causing a fall in the simulated renal excretion of water and sodium; thereby modulating the expected diuresis. During the prolonged phase of flight, mean intake of fluid and electrolytes was not identical with preflight values, but was within ± 5% of control conditions. This small change together with the larger decreases in evaporative loss was also reflected in the both the volume and electrolyte concentration of urine excretion.

Excretion of water and electrolytes is partly under the influence of the hormones shown in Fig. 9-19(c) (ADH, aldosterone and angiotensin). Some dramatic transient effects are predicted early inflight as well as significant departures from preflight levels during the long-term steady-state. Circulatory pressures and plasma electrolyte concentrations are the predominate influences on those hormones. Mean arterial pressure (Fig. 9-19(d)) is elevated by about 2%. Similarly, small changes exist for sodium and potassium concentrations. Yet, the changes in plasma concentrations of ADH, aldosterone and angiotensin (-40%, +16% and +24%, respectively) are significantly larger. If spaceflight is associated with the chronic elevation of central or renal circulatory pressures, then the angiotensin response is paradoxical unless other competing stimuli can be found which oppose that factor. The predicted responses of ADH and angiotensin follow intuitively consistent trends.

Figure 19(d): Although the emphasis of this chapter is on fluid-electrolyte regulation, the Guyton model is capable of simulating hemodynamic events. Figure 19(d) illustrates a variety of common cardiovascular parameters. The first few hours of the simulation do not portray a true picture because of the compressed time scale. The reader is referred to Fig. 9-3 where a similar type of simulation was performed for the first 24-hours of supine bedrest. There you can see that during the first hour or so, the cardiac output, arterial pressure, central venous pressure and renal blood flow actually *increase* before declining below control. Over the next few weeks these cardiovascular parameters gradually return to normal. There are no comparable measurements from the Skylab missions (in resting subjects) to validate these predictions with the exception of mean arterial blood pressure which indicates only a very slight decline from preflight on average over the mission. Because of the lack of inflight measurements, there was no attempt to develop hypotheses to optimize the simulation response as was done for the fluid,
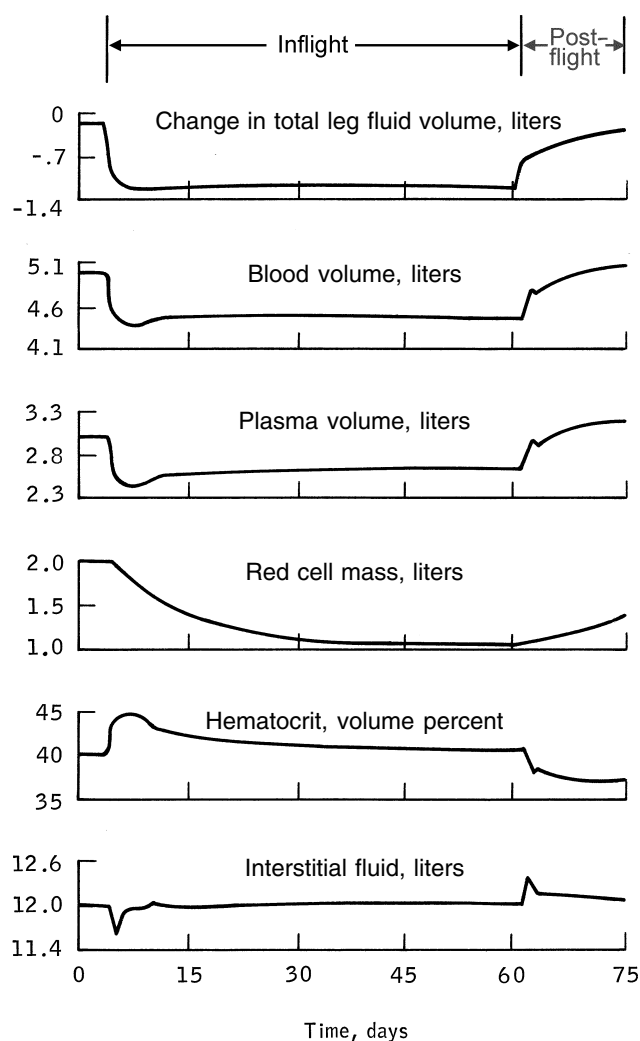
Figure 9-19(a). Simulation of average Skylab mission: Blood and tissue volume. The preflight duration is 4-days; inflight duration is 57-days; and postflight is 14-days. The simulation included all of the proposed hypotheses listed in Table 9-4.

Figure 9-19(b). Simulation of average Skylab mission: Fluid and electrolytes [see caption Fig. 9-19(a)].

electrolye, renal and hormone responses, i.e., Table 9.4. However, hemodynamics will be revisited in the section on head-down tilt bedrest (Chapter 9.7) where experimental data is available.

9.4.4 Summary: Spaceflight Simulation

The responses shown here represent the most accurate simulations performed to date with regard to circulatory, fluid and electrolyte changes. Predictions for the acute, long-term and recovery phases of spaceflight have been compared to the measured spaceflight data for a diverse number of parameters. Table 9-5 lists the parameters that were simulated in this specific study and references the tables and figures in this book that show confirmatory Skylab findings. Other simulations in this book emphasized a number of other physiological functions, including those involved with circulatory, orthostatic, exercise, hematological and metabolic responses. These are cov-

ered in other chapters and other sections of this chapter. In almost all cases reasonable results have been obtained. This was achieved by considering a number of hypotheses as well as a variety of experimental data. Most important, however, these simulations could not have been possible without an accurate model representation of the highly complex physiological system. Taken as a whole, the hypotheses tested have produced a reasonably accurate fluid electrolyte response pattern to weightlessness and these results do account for findings that have been heretofore difficult to explain.

9.5 Water Immersion Simulation

9.5.1 Introduction

Water immersion has proven to be a useful tool for studying fluid volume homeostasis and renal physiology in man [30]. Physiologically, it is characterized by a cephalic redistribution of blood volume from the legs, which is also a seminal event in spaceflight. As such, it has been
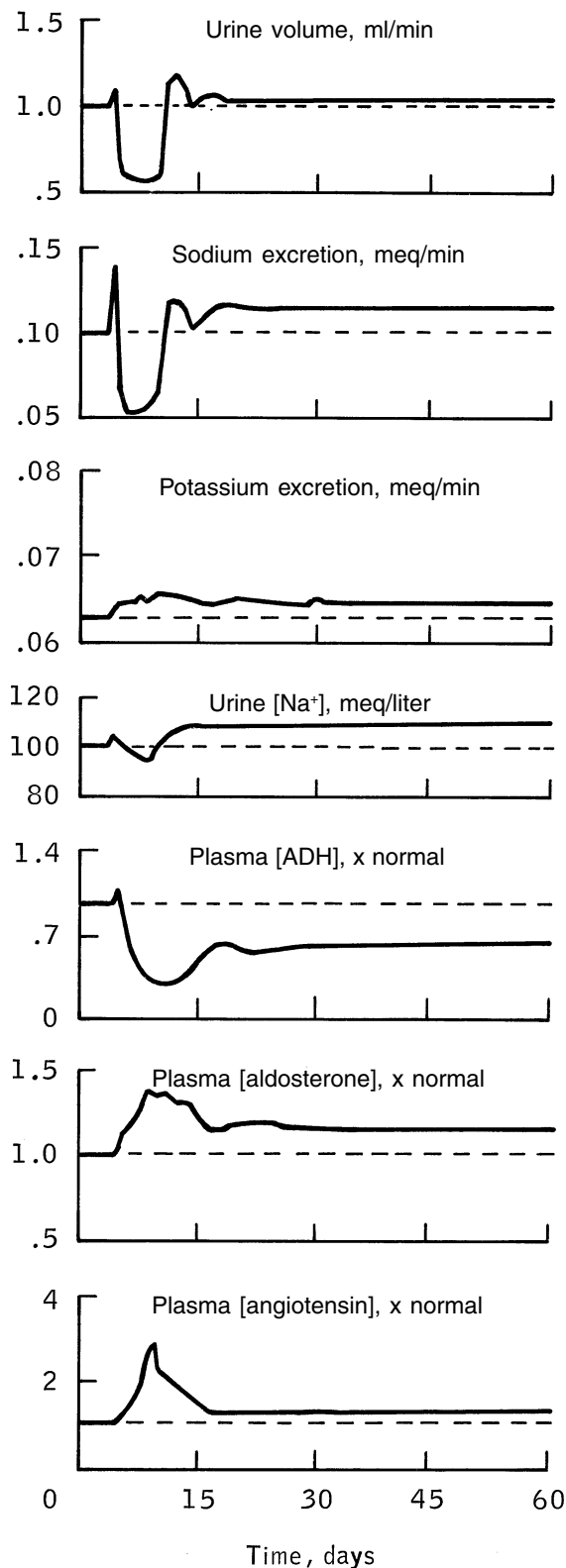
Figure 9-19(d). Simulation of average Skylab mission: Renal and endocrines [see caption Fig. 9-19(a)].
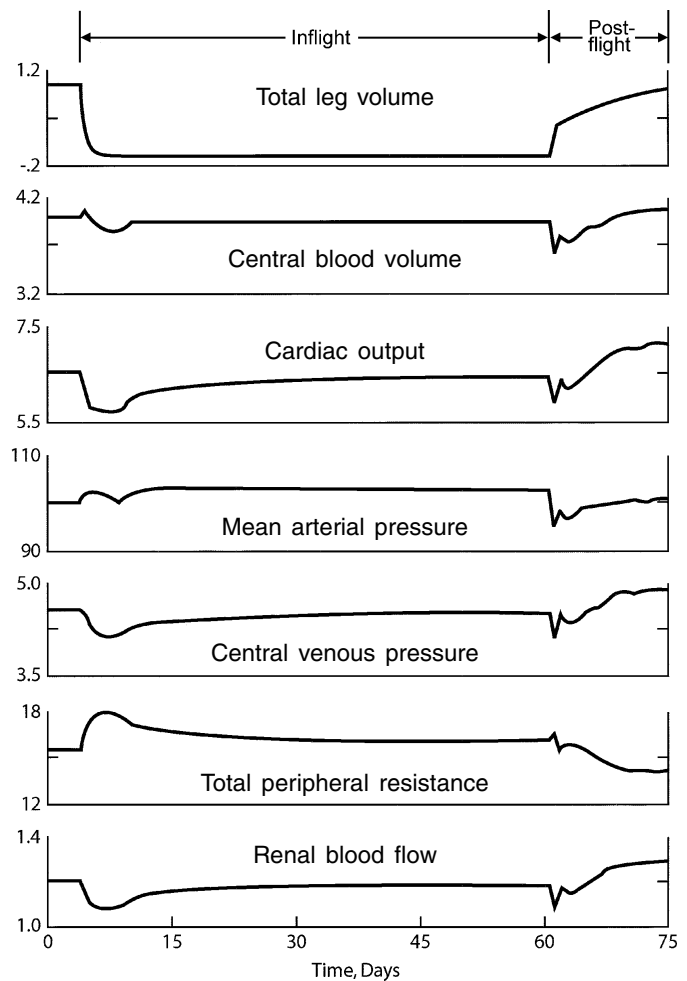
Figure 9-19(d). Simulation of average Skylab mission: Hemodynamics [see caption Fig. 9-19(a)].

used as an excellent means of simulating and examining the details of the circulatory, renal and fluid-electrolyte responses to weightlessness. Because water immersion studies are technically difficult to conduct for periods of longer than 3 to 6-hours, it has been used to help understand the events occurring at the onset of weightlessness. In fact, it is primarily from water immersion investigations that most of the theories (during the 1970's and 80's) regarding the very early effects of zero-g on fluid balance and blood volume control have been obtained [10].

Fluid is shifted from the legs in water immersion due to external water pressures, in contrast to the natural elastic tissue forces which are the primary drivers in weightlessness. The redistribution of blood during water immersion is mediated primarily by an external hydrostatic pressure gradient acting on the body surface (and by innuendo, on vascular columns of the body) which increases by 22.4 mmHg/foot of water depth. This increase in transmural pressure forces blood from the vessels of the lower extremities toward the cephaled region and central

Table 9-5. Variables of the Skylab Simulation and their Experimental Confirmation*

Simulated Variable	Confirmation Table Number	Confirmation Figure Number
Fluid Compartments:		
Total body water	5-2	5-2
Intracellular volume	5-2	
Interstitial fluid	5-2	
Blood volume	5-2	6-2
Plasma volume	5-2	6-2
Red cell mass	5-2	6-2
Total leg volume	5-2	9-10
Body Electrolytes:		
Total body sodium	5-2	5-2
Total body potassium	4-15, 5-2	5-2
Plasma Concentrations:		
Plasma [Na$^+$]	5-5	5-20
Plasma [K$^+$]	5-5	
Hematocrit		6-4, 6-5
Plasma ADH		5-5
Plasma aldosterone		5-5(b)
Plasma angiotensin		5-5(d)
Renal Function:		
Urine excretion	4-14	9-22
Sodium excretion	4-14	5-4(a),9-22
Potassium excretion	4-14	5-4(b)
Urine [Na$^+$]	4-14	

* Skylab simulation refers to Fig. 9-19

venous pool. Although this type of external force does not exist during spaceflight or bedrest, the nature of the fluid redistribution itself is probably similar for all three stresses. Quantitatively, the degree of fluid shift during water immersiont appears to be in between that seen in bedrest and in spaceflight [31].

There are certain facets of the water immersion process that make this maneuver inherently different from the acute response to weightless spaceflight. Several major considerations that may limit the usefulness of water immersion as a zero-g analog are:

1. Water immersion studies are usually limited to periods of less than 6 hours.
2. Immersing a subject to the neck or chin results in negative pressure breathing because the force exerted by the water on the surface of the body has no counterbalance in the airways. Negative pressure breathing, or the positive pressure breathing equipment used to counteract this effect, may interfere with the circulatory, renal and hormonal responses that are under examination [30].
3. During immersion, there is a marked decrease in evaporative water loss. While this simplifies the interpretation of water balance and renal alterations (for example, the predominant route for fluid losses is by way of kid-

ney excretion), it does not permit exact extrapolation of renal responses to the weightless condition where skin water loss is a significant fraction of overall water balance (see Chapter 4). The total quantity of urine voided during immersion might, therefore, be expected to be somewhat higher than that achieved during weightlessness.

4. The pressure on the walls of the thorax, due to the hydrostatic forces of water external to the body, is an effect that is not present in weightlessness and can lead to higher intrathoracic pressure than would be observed in spaceflight. This transthoracic pressure gradient and compression of submerged tissues is probably responsible for the sustained hyperkinetic circulatory state reported during immersion studies [32,33]. As a result, immersion may lead to higher venous pressures, a larger reduction in blood volume than would be expected in zero-g and to a masking of any reflex relaxation effects of peripheral capacitance vessels [34].

In terms of fluid volume regulation, the two most significant responses to the blood redistribution resulting from water immersion are an acute diuresis and a reduction in the plasma volume. At the time of this analysis (early 1980's) there has been no attempt to measure plasma volume *during* spaceflight, but plasma volume loss has been a consistent finding *immediately after* spaceflight Also, the expected diuresis has not yet been measured during any flights, although 24-hour pooled samples were taken on 9 subjects in the Skylab program. One of the questions addressed during the present analysis was to examine the factors which may have led the apparent discrepancy between the observed and expected urinary volume responses, particularly the effect of dehydration.

The physiological events thought to occur during water immersion have been summarized in Chapter 5.3.1. In the following description of simulation and experimental results, reference will be made to that section. A set of baseline simulations of a normally hydrated subject will be presented first. This is followed by studies of the effects of dehydration on the water immersion response.

9.5.2 Simulation of Normally Hydrated Subjects

Simulations of water immersion were performed using the Guyton model with leg compartments, as modified for the bedrest simulations. The simulation was initiated by forcing 500 ml of intravascular and 500 ml of interstitial fluid from the leg compartments. At the time of this study, no data was available to define the magnitude or time course of leg volume shifts during immersion, but the shifts that were imposed in simulation are supported by data from bedrest and orthostatic maneuvers [13,35,36]. Also, it has been shown that central blood volume increases by 700 ml immediately following immersion [37]. The simulations were run for 10-minutes with all short-term autoregulatory components removed and for 6-hours with all autoregulatory components intact. The simulation results are shown in Figs. 9-20 and 9-21. The experimentally determined effects of water immersion are presented in Table 9-6, Figs. 9-22 to 9-25.
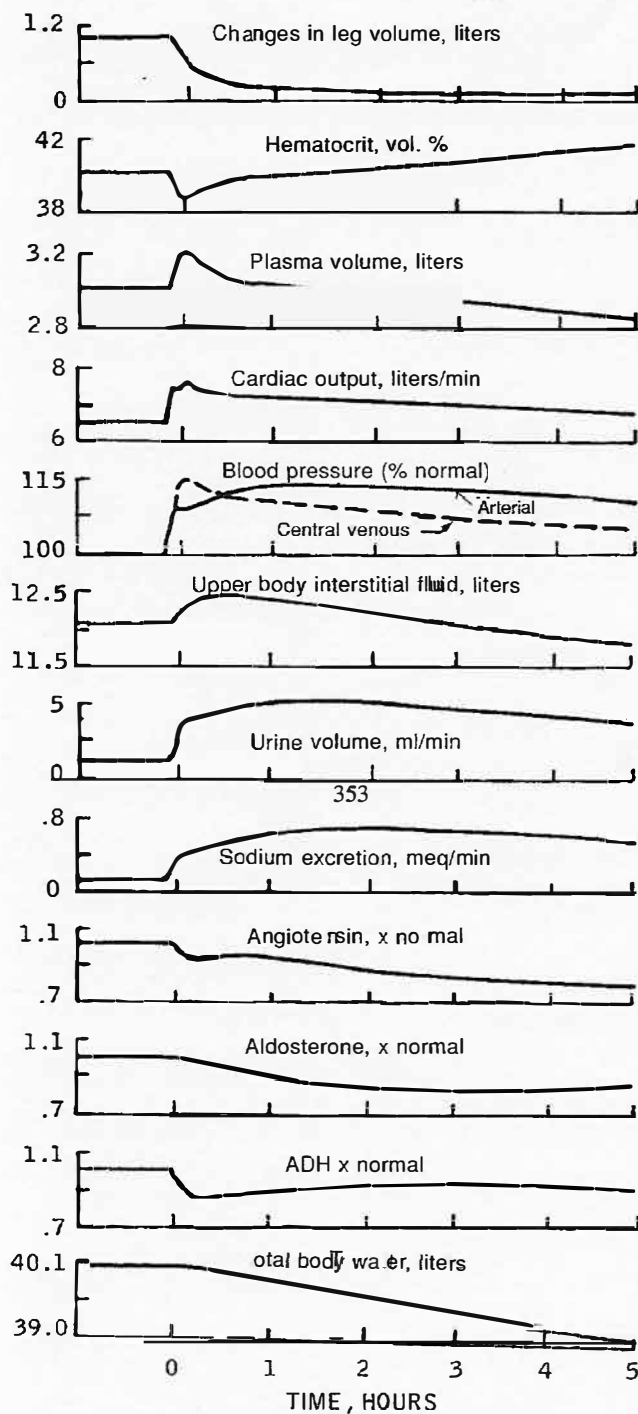
Figure 9-20. Computer simulation of water immersion using the modified Guyton Model.

Figure 9-2 1. Hemodynamic response to 10-minutes of water immersion: Experimental data [37] vs. simulation.
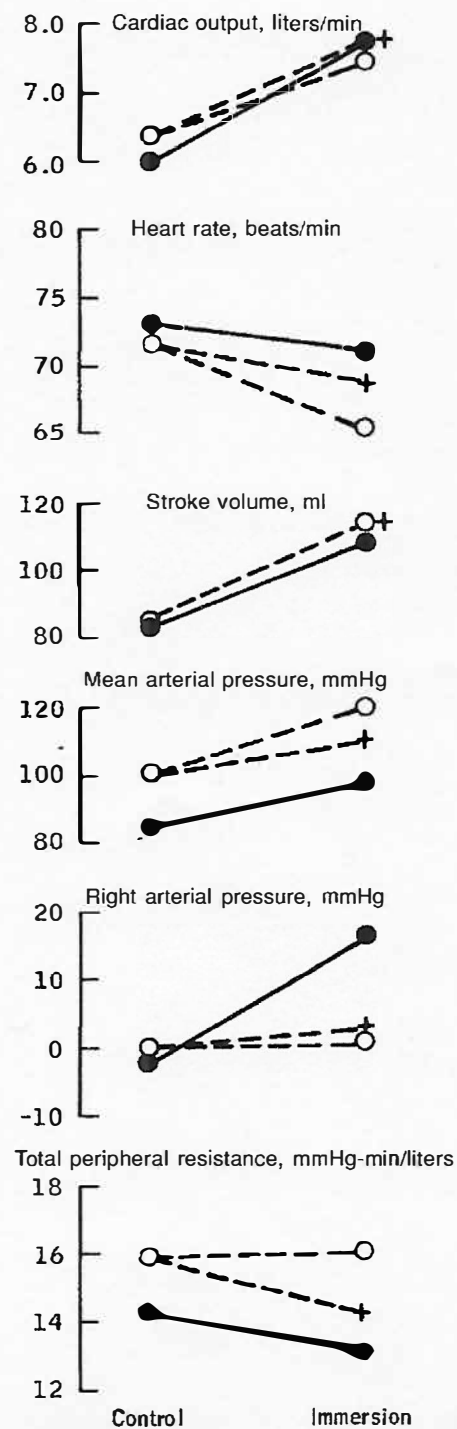
- • Data (Arborelius et al., 1972)
- + Simulation: autoregulation intact
- o Simulation: short-term autoregulation removed

Table 9-6. Experimentally Determined Short-Term (10 min – 6-hour) Immersion Response

Primary Effects:	Reference	Change from Control
Central Blood Volume	(A)	+700 ml
Heart Volume	(G)	+180 ml
Central Venous Pressure	(G,A)	+12 to +18 mmHg
Intrathoracic Pressure	(G,A)	+4 to +5 mmHg
Transmural Pressure	(G,A)	+8 to +13 mmHg
Plasma Volume	(Gr)	+10%

Secondary Effects:		
Circulation		
Stroke Volume	(A)	+35%
Cardiac Output	(A)	+32%
Total Peripheral Resistance	(A)	–30%
Peripheral Venous Tone	(G)	–30%
Arterial Pressure	(A)	+10 mmHg
Endocrines		
Anti-diuretic Hormone	(E,G)	–50% to –88%
Renin	(E)	–75%
Aldosterone	(E)	–70%
Renal		
Urine Volume Rate	(G)	+200%, peak flow +500%
Sodium Excretion Rate	(G)	+50 to 125%
Potassium Excretion Rate	(G)	+30%
Volume		
Plasma Volume	(G)	–10 to –15%
Total Body Water	(G)	–1.5 liters/8 hrs

A = Arborelius and co-workers [37]
G = Gauer and co-workers [10,38]
E = Epstein and co-workers [11,30,39,40]
Gr = Greenleaf, *et al.* [41]

9.5.2.1 Fluid Shifts. The primary effect of water immersion can be characterized by an acute translocation of fluid from the leg to the upper body, primarily the intrathoracic compartment. This primary effect was the basis of the model initialization. In addition to the translocaton of blood, there appears to be a significant increment in plasma volume, demonstrated by a transient decrease in hematocrit. This augmented plasma volume resulted from the external water pressure forcing leg interstitial fluids into the capillaries. Within 1 to 2-hours, however, a significant portion of plasma from the engorged central blood volume finds its way out of the vasculature via renal excretion and via filtration into the interstitium of the upper body (see hypothesis diagram, Fig. 5-17). The result is an interesting biphasic response of the plasma volume, first increasing and then showing a greater net depletion. Experimental findings that depict these changes are shown in Table 9-6, Figs. 9-22 (plasma volume) and 9-23 (hemoglobin); they are also faithfully reproduced in the simulation (Fig. 9-20).

9.5.2.2 Hemodynamic Responses. With the initial acute shift of fluids, an increase in central blood volume, heart volume and blood pressures in the central veins and

Figure 9-22. Percent changes of plasma volume during water immersion. A composite of ten studies, derived from Greenleaf *et al.* [41].

Figure 9-23. Experimentally determined hemodynamic changes during water immersion. Data obtained from (top to bottom) Begin, *et al.* [32], Echt, *et al.* [9], and McCalley *et al.* [42].

21 that yielded a change that was not reproduced in the simulation was the increase in right atrial pressure. Aside from this shortcoming, the simulation of this very short-term response must be considered reasonable, especially since the circulatory, fluid and electrolyte model was designed primarily to describe long-term events.

As noted above, there are serious discrepancies in central venous pressure between model simulation and experiment, with regard to magnitude and time course of response. The same increase in central blood volume that was measured experimentally (about 700 ml) was seen during the simulation. Yet, the venous pressure rose only a fraction in the Guyton model compared to the experimentally reported results. In this case, it is our belief that the experimental blood pressure data is misleading for the following reason. The normal cardiac function curve, in which cardiac output is plotted against right atrial pressure (RAP, similar to central venous pressure), indicates that an increase in RAP by only 2 to 3 mmHg can double the cardiac output [26b]. Increasing RAP by 10 mmHg, as reported by Echt, *et al.* [9] and shown in Fig. 9-23, will cause cardiac output to reach maximum values – about 200% above control. But it has been shown that cardiac output only increases by about 20% in water immersion [32] (see Fig. 9-23). There appears to be a discrepancy between the measured value of venous pressure and the much lower value derived from the accepted cardiac function curve. It is unlikely that venous pressures as large and long lasting as that shown in Fig. 9-23 could occur.

A reasonable explanation for this conflict was alluded to in the introductory discussion where a unique aspect of water immersion was stated to be an increase in intrathoracic pressure due to the external hydrostatic pressure at the level of the heart. During immersion to the neck, the transthoracic pressure gradient in the region of the heart has been estimated to be 20 cm H_2O [32], the same value that was "coincidentally" measured in the central veins. Thus, the rise in central pressure may be an artifact of the measurement; there is an increase in transthoracic pressure (pressure outside the large veins minus pressure inside the veins), but not such a large increase in central venous pressure itself. This condition could be simulated, by introducing into the model, a transthoracic pressure gradient in the region of the heart.

9.5.2.3 Renal and Endocrine Responses. Within the first hour of experimental immersion, there is a significant rise in the urinary excretion of fluid and salts (the latter consisting primarily of sodium), which was reproduced by the simulation (i.e., compare urine and sodium excretion in Figs. 9-20 and 9-24). The urine formed was considerably dilute, demonstrating free-water rather than an osmotic diuresis. In most studies, the peak urine flow occurred within the first hour whereas the natriuresis reached a maximum somewhat later (see Fig. 9-24). This finding suggests independent mechanisms mediating renal sodium and water handling.

pulmonary vessels occur (Table 9-6, Figs. 9-20, 9-21, 9-23). Total peripheral resistance and venous tone decreased, a probable result of autonomic reflexes. These responses have been observed to reach their full magnitude within the first 10-15-minutes of immersion. The simulation results shown in Figs. 9-20 and 9-21 and the experimental data in Figs. 9-21 and 9-23 support the immediate increase in cardiac output and mean arterial pressure. Cardiac output diminishes somewhat but remains elevated over the remaining hours of the simulated and actual immersion test. Central venous pressure, on the other hand, slowly diminishes toward control levels during the simulation (Fig. 9-20) but remains at very high levels during the human study. Furthermore, the increase in magnitude of venous pressure due to water immersion is several hundred-fold (from 4 mmHg to 15 mmHg) in the human (Fig. 9-23) but rises only 15% in the simulation (Fig. 9-20).

The short-term (10-minute) hemodynamic responses to the fluid shifts were further investigated. As shown in Fig. 9-21 a superior simulation was obtained by removing the short-term autoregulatory function of the model. (This function is intended to permit arteriolar resistance elements to respond to short-term fluctuations in local (rather than central) blood pressures). The only variable in Fig. 9-

Numerous mechanisms are available that can potentially contribute to the diuresis and natriuresis of water
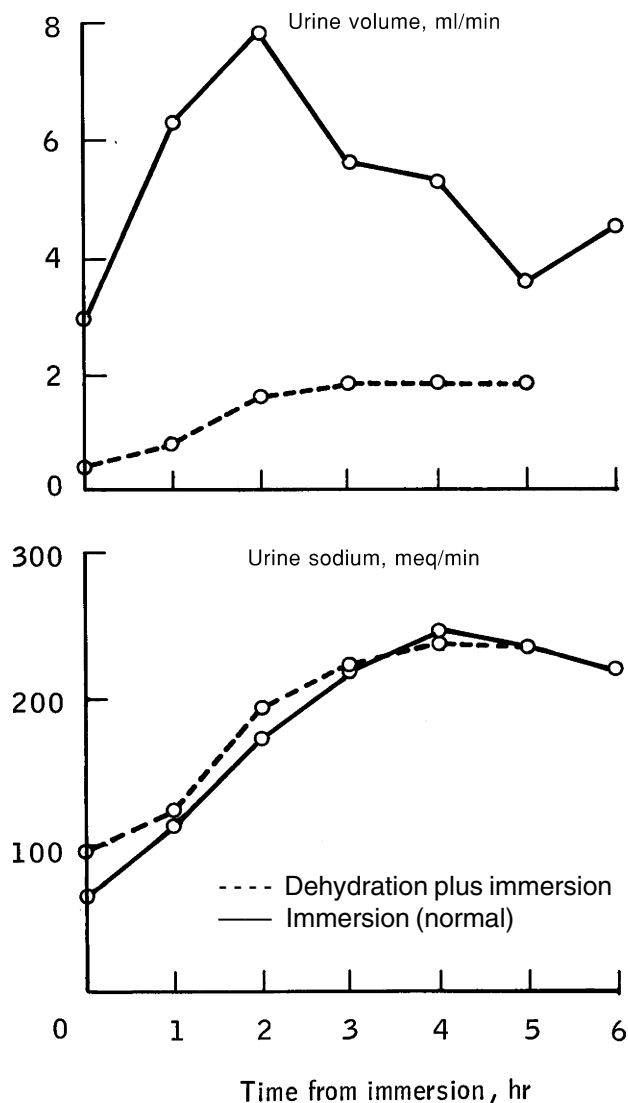
Figure 9-24. Experimentally determined diuresis and natriuresis of water immersion in normal and dehydrated subjects [46].

Figure 9-25. Experimentally determined endocrine changes during water immersion (expressed as percent change from control) Data obtained from Epstein and co-workers [11,39].

immersion. These have been discussed previously in Chapter 5 (see Figs. 5-15 to 5-17). In a review of the renal effects of immersion, Epstein [30] suggested that the factors that were primarily responsible for the diuresis were suppressed ADH, increased prostaglandins (which inhibit the action of ADH) and decreased sympathetic activity. The natriuresis was attributed to suppressed renin-angiotensin-aldosterone, increased prostaglandins, reduced sympathetic activity and release of a natriuretic factor. There is also a lesser role played by hemodynamic effects within the kidney that are observed during expansion of the blood volume [43]. The mechanisms and role of each of these factors are clearly described in Chapter 5. The Guyton model accounts for all these factors except for prostaglandins and intrarenal hemodynamics.

A comparison of endocrine changes during immersion, between a 6-hour simulation and experimental study of similar duration, is shown in Figs. 9-20 and 9-25. In all cases, there is a suppression of renin/angiotensin (one is a precursor of the other), aldosterone and ADH. This is completely in accord with the expected mechanisms based on the analyses of Chapter 5.3.1. While the first two hormones remain suppressed in both simulation and experiment, ADH responded somewhat differently in the human subjects compared to the simulation. Although ADH decreased in both cases, it remained suppressed in experimental studies but returned toward normal in the simulation. This latter behavior in the model was attributed to a decreasing central venous pressure, which effects ADH in an inverse manner. In addition, ADH is also under the influence of plasma osmolality; it is the interplay of these dual controllers, venous pressure and plasma osmolality, that determines the resulting ADH response. This analysis, described by Leonard [44,45], suggests the difficulty in

Table 9-7. Contribution of Plasma and Interstitial Volumes to Body Water Loss During 4-hours Water Immersion*

Compartment	Experiment	Model
Plasma Volume	–75 ml (15%)	–123 ml (16%)
Interstital Volume		
Upper Body	Not measured	–194 ml (25%)
Lower Limbs	Not measured	–473 ml (59%)
Total	–425 ml (85%)	–667 ml (84%)
Total Body Water	–500 ml (100%)	–790 ml (100%)

*Experimental data from Greenleaf, *et al.*, [47].

predicting the time-course of ADH in weightlessness. It also suggests the importance of making careful measurements of blood pressure, serum osmolarity, ADH and volume shifts during water immersion or spaceflight in order to distinguish between the possible alternate scenarios.

9.5.2.4 Plasma and Interstitial Fluid. The net effect of the diuresis and natriuresis on body fluid volume was a reduction in total body water (Table 9-6, Fig. 9-20). Approximately 20 to 25% of the total fluid loss from the body was derived from plasma. This proportion was expected inasmuch as the normal ratio of plasma/interstitial fluid is about 1:4. The increase in plasma volume at the onset of immersion, mentioned earlier, was therefore followed by a gradual decline below control as volume regulator mechanisms reversed the engorgement of the intrathoracic compartment. These observations from experimental studies were faithfully reproduced by the model simulations.

Plasma volume reduction following water immersion may be a result of two independent effects: a diuresis of primarily extracellular fluid and a movement of fluid from the intravascular compartment into the interstitium of the upper body due to normal transcapillary filtration (see Fig. 5-17). The latter of these effects has been difficult to quantify because it is not possible to experimentally distinguish between decreased interstitial volume loss in the lower limbs and any increased interstitial volume in the upper body. However, it is possible to accomplish this feat using computer simulation. This topic has been covered in a detailed manner in Chapter 5 (see Chapter 5.4.2.2, Figs. 5-17, 5-22 to 5-24). Additional analyses of these phenomena were performed in connection with the water immersion study and are presented below.

If one considers the first 4-hours of immersion, a period during which plasma volume may not be significantly changing [47], it is possible to compute the decline in body water and the contribution to this loss from the plasma and interstitial compartments. The results from the computer model and from one immersion experiment are shown in Table 9-7.

Although the absolute values of fluid losses derived experimentally are not identical to those predicted by the model, the percentage contributions of plasma and total

interstitial volumes to total body water losses are quite similar to the observed values. In addition, the experimental data and the simulation responses indicate that substantial amounts of water are removed from the interstitial fluid before plasma volume is largely affected. Furthermore, while the model predicts that most of the interstitial fluid loss originates from the lower limbs as expected, a significant fraction of fluid (25% of the total body water loss) is derived from the upper body interstitial fluid. This appears paradoxical in the sense that it is normally believed that plasma is filtered into these tissues and there is a net gain of tissue fluid (in the upper body) at the expense of plasma volume. However, while the model indicates that outward filtration into tissues does occur (see "upper body interstitial fluid" Fig. 9-20), it is limited in time (about 3-hours) and in magnitude (about 300 ml). The process quickly reverses because of increased plasma colloidal concentration as plasma is filtered through the renal tubules and the upper body capillaries. The model further predicts that if immersion were to continue beyond 4-hours, the upper body interstitial fluid compartment would exhibit a net depletion of nearly the same volume lost from the leg tissues (about 500 ml), but would return to normal within 48-hours. Lymph flow return plays a part in this normalization as well. (See simulation in Fig. 5-23, bottom curve, which represents the upper body interstitial fluid.) For this reason, the role of transcapillary filtration in plasma volume regulation is effective in the short-term but not for long-term control.

This self-limiting feature of transcapillary filtration effectiveness may be blunted if proteins are not perfectly filtered by the capillary membrane and can leak to some extent as a result of pressure distention effects on the membrane pores. This effective increase in protein permeability would permit greater quantities of plasma filtrate to enter the tissue spaces.

This possibility was examined by computer simulation with the results illustrated in Fig. 9-26. Two cases were examined: a) a normal water immersion simulation identical to that shown in Fig. 9-20 and b) an immersion simulation in which protein permeability of the capillary membrane was increased by a factor of ten. Qualitatively, the two primary effects of increasing protein permeability are a reduced plasma colloidal concentration and a normalized (rather than a decreased) upper body interstitial fluid volume throughout the period of study. This study also demonstrated that plasma volume reduction was nearly double for the case of increased protein permeability.

Taken as a whole, the assumption of increased protein permeability resulted in a more realistic simulation of the immersion experiments of Greenleaf and co-workers [41,47]. In particular, a reduction in plasma protein concentration, predicted by the analysis, was reported by Greenleaf *et al.*, [47] in their water immersion study. Of even more relevance, a recent spaceflight study has also suggested that there was an increase in the rate of transcapillary protein transport [UPDATE#2]. A similar analysis was conducted during head-down tilt simulation (see Fig. 9-40). Further details can be found in Ref. [44].
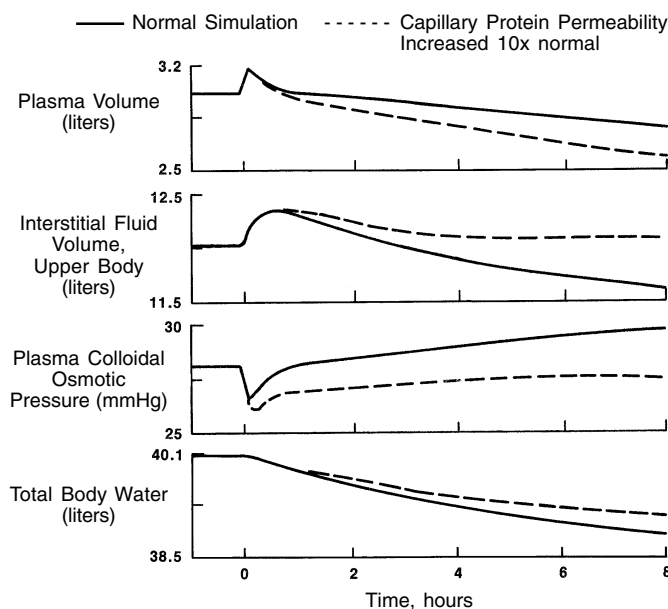
Figure 9-26. Simulation of water immersion: Effect of increasing capillary permeability on transcapillary fluid exchange. Normal simulation (—); Capillary protein permability increased 10 times normal (- - -).

9.5.3 Effect of Dehydration

The preceding characterization of the immersion response was based on well-hydrated and otherwise normal subjects. However, the state of dehydration of the subject, during immersion, is an important determinant of the renal response, of fluid distribution and of the ultimate loss of body water [10]. The effect of dehydration during water immersion was studied experimentally and by computer simulation. The purpose of these studies was to ascertain if the lack of an observed acute diuresis on the Skylab mission could be ascribed to the generally agreed on notion that the crewmembers were dehydrated before the mission and dramatically so, in some cases, during the first week of spaceflight. Some of the results of these analyses are shown in Fig. 9-27 and Table 9-8.

For the simulation analyses, intake of fluid was assumed to be either normal or zero during the 24-hours preceding immersion and the 24-hours during immersion. During the first 6-hours of simulated immersion, the urine volume response for the cases of normal and reduced intake was predicted to be similar. However, increasingly significant differences between these two cases were observed for each succeeding 6-hour period. As a result, the cumulative losses of body water (taken as the balance between renal excretion and drinking) were nearly twice as great for the dehydrated case as for the normally hydrated case at the end of 24-hours (Fig. 9-27).

These simulation studies generally confirmed the experimental results established by Gauer and co-workers [10,33] with regard to renal excretion and plasma regulation when challenged by immersion and dehydration (see
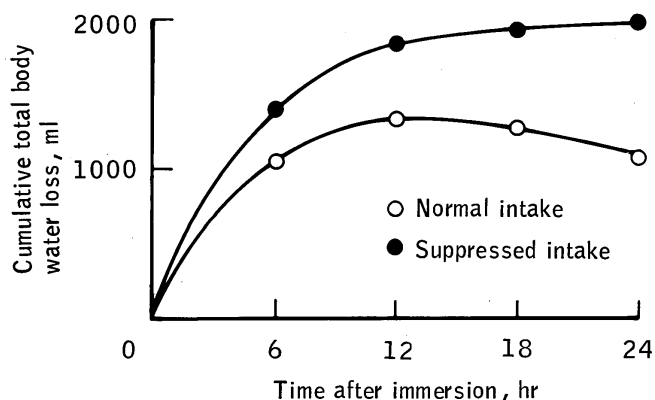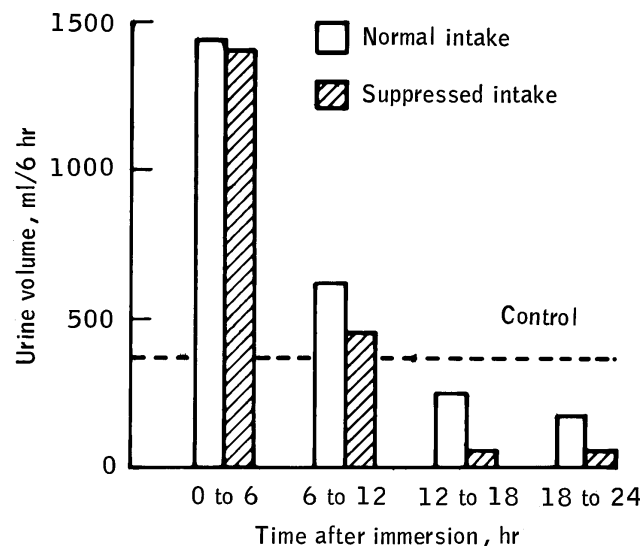
Figure 9-27. Effect of dehydration (via suppressed intake) on simulated immersion response.

Table 9-8 and Fig. 9-24). Specific differences in immersion responses to a normal and a dehydrated state were: a) the absolute increase in water and sodium excretion was smaller (compared to normal immersion controls) whereas the percent urine increase was larger (compared to preimmersion controls); b) immersion was characterized by a larger decrease in free water clearance in the dehydrated subjects than in the hydrated subjects; c) the decrease in plasma volume was more severe in dehydrated subjects; and d) the contribution of plasma volume reduction to excess urine volume excreted during immersion was greater for the dehydrated subjects than for the hydrated subjects.

The effect of salt intake was also studied. It was found that urine flow decreases with reduced sodium intake both prior to immersion and during immersion. This was true for any given level of water intake, both above and below normal. In all cases studied, the urine flow during immer-

Table 9-8. Effect of Dehydration on Pre-Immersion and Immersion Response

	Experiment*		Simulation**	
	Pre-	Immersion	Pre-	Immersion
Urine Volume, V	↓	↓	↓	↓
Δ % V from pre-immersion		↑		↑
Urine Sodium, $U_{Na}V$	↓	↓	↓	○
Δ % $U_{Na}V$ from pre-immersion		↑		↑
Osmolar Clearance, C_{osm}	↓	○	↓	↓
Free Water Clearance, C_{H2O}	↓	↓↓	↓	↓↓
Δ Plasma Volume, $\Delta PV_{immersion}$		↓↓		↓
$(\Delta PV/V)_{immersion}$		↑↑		↑

KEY:
↑ Increase compared to hydrated controls * Behn, Gauer, Kirsh and Eckert [33]
↑↑ Large increase compared to hydrated controls
↓ Decrease compared to hydrated controls ** Guyton's model of Circulatory, Fluid, and Electrolyte Regulation
↓↓ Large decrease compared to hydrated controls
○ No change

sion increased in relation to its pre-immersion diet control; i.e., there was a relative diuresis.

Despite the general agreement between simulations and experiments, it was not possible to replicate the magnitude of the fall in urine excretion during dehydration that was seen in the human subject (see Fig. 9-24). In that case, it can be seen that dehydration caused the absolute quantity of urine flow to be blunted, the peak diuresis to be delayed and the peak of the naturesis to be reached after the peak diuresis, although the natriuresis response itself is unaffected. These simulations did not consider the effects of evaporative water loss, which are reduced to a minimum during immersion, or the difference in the degree of headward fluid shift between the hydrated and dehydrated cases. It can be argued that the magnitude of the fluid shift from the legs in response to immersion would be less in previously dehydrated subjects compared to well-hydrated subjects. We would expect the divergence in the theoretical response between hydrated and dehydrated cases to be even more marked if these factors were considered in the simulation, placing the results in closer agreement with experimental data.

9.5.4 Summary: Water Immersion

Agreement between observed and simulated responses was quite reasonable. The basic characteristics of water immersion were replicated in the model's response, i.e., the translocation of fluid from the legs into the central blood volume and the resulting diuresis and reduction in plasma volume. The realistic behavior of the responses attested to the basic validity of the model and the manner in which the controlling mechanisms were represented. However, the simulation studies of the effects of dehydration on immersion revealed several limitations in model behavior that must await future modifications: a) the experimental results suggest a much greater decrement in immersion diuresis volume as a result of dehydration than is indicated by the model and b) experimental results show a greater dissociation between the immersion diuresis and natriuresis response than could be simulated. The analysis also demonstrated several areas of discrepancy that deserve more research, including: a) the question of whether the 6-hour ADH immersion response is solely under the influence of volume receptor control [47,48], or, as the model indicates, the osmoreceptors as well; b) the role of transcapillary filtration during immersion was shown to be effective in acute studies but not for the longer-term, contrary to the conclusions of some investigators [33]; c) whether transcapillary protein leaks play an important role in reducing plasma volume following immersion as shown by the model simulation; and d) whether central venous pressure measurements during water immersion are as high and sustained as reported in seeming opposition to the traditional operating range for cardiac function.

As a result of the analysis, one can predict that a diuresis should be observable during the first several hours of spaceflight and the probability of demonstrating this response decreases as subjects become dehydrated, as their fluid intake diminishes and/or if urine voids are pooled during the first 24-hours [UPDATE#3]. The nature of the water immersion technique may tend to overestimate the predicted zero-g diuresis because of reduced evaporative water

loss and increased transthoracic pressure gradient. These factors are present in immersion but do not occur in true weightlessness.

9.6 Postural Simulations

The capability of the Guyton model to account for gravity's influence on the fluid columns of the body is described in Chapter 9.3 and Appendix C.2. Much more is known about standing, or orthostasis, than about hypogravity, even though they may be considered inverse physiological stresses. So it is natural to validate a model capable of postural changes by first performing simulations of standing or head-up tilt than for hypogravic situations. A study of head-down tilt, which is a natural adjunct to examining head-up tilt, is reported in the following section.

Earlier in this book the capability of the short-term cardiovascular model (Croston) to perform tilt was demonstrated. Why do we need this capability in the long-term circulatory model (Guyton)? The Croston model is certainly adequate for our purposes of simulating a short-term (10-minute) postural tilt. But it does not contain many of the elements outside of the circulation that ultimately control blood volume, pressure and flows over the longer term as does the Guyton model. We believe that the upright position, like bedrest, does not achieve steady-state within 10–30-minutes; the stationary, erect body continues to adjust probably for hours or days, even though these types of measurements are not made for ethical reasons. The Guyton model's comprehensive inherent capabilities might allow us to determine the factors necessary to simulate long-term orthostasis. The advantage of creating a valid orthostatic model was alluded to earlier, i.e., such a model could more realistically simulate hypogravity by simply changing the angle of tilt from erect to supine (or slightly head-down). This would provide a much more natural simulation. The following postural studies with the Guyton model are preliminary attempts in this direction.

9.6.1 Physiology of Orthostasis

Upon shifting from a supine to an erect position, experimental data reveal physiological changes in the circulatory pressures, flows and blood volume distribution. About 10% of the blood volume is shifted from the upper part of the body (mainly from the thoracic cavity) to the legs, where it is pooled, primarily in the distensible venous segments [27]. Due to hydrostatic pressure on the blood column, the arterial, capillary and venous pressures become markedly elevated in the lower extremities, causing a net capillary filtration into the tissues. This filtration can result in a loss of 5 to 10% of the supine blood volume [13]. In response to the decrease in central blood volume, compensatory pressure regulating mechanisms come into play, preventing a fall in the effective central venous pressure below that of the heart, insufficient cardiac pumping and orthostatic hypotension.

The defenses of the body against orthostatic hypotension consist of both passive and active elements [13,49,50]. Ultrafiltration into the tissues is minimized by increasing tissue fluid pressure and increasing lymphatic flow, reducing the hydrostatic columns in veins by "pumping" blood past leg venous valves and transiently venoconstricting the extremity venules. Systemic arterial pressure is maintained and even elevated, because of activation of intrathoracic and carotid baroreceptors. The reduction in effective blood volume, caused by a shift of blood from the upper to the lower part of the body, is associated with a sustained increase in sympathetic activity to the resistance vessels in muscles and visceral organs and to the heart. Thus, cardiac output and arterial blood pressure are maintained, despite reduced cardiac filling pressure.

The increase in leg vascular resistance also helps minimize venous pooling. Central venous pressure must be maintained to promote adequate right ventricular filling. Although the exact mechanisms controlling this adjustment have not yet been agreed upon, certain factors are important in preventing a debilitating fall in central venous blood volume and pressure. These factors include contraction of large venous channels and venous reservoirs, such as those that exist in the visceral organs; external compression of veins by skeletal muscles in the legs; and an external pressure on the large abdominal veins exerted by both the increased hydrostatic column of abdominal organs and an increase in abdominal muscular contraction, i.e., abdominal reflex [49,52,53,54,55]. Despite the influence of the orthostatic defense mechanisms, the net result of the effects induced by standing is a reduction in central blood volume by leg fluid pooling, a decrease in cardiac output due to reduced stroke volume despite an increase in heart rate and an increase in peripheral resistance which acts to elevate the mean systemic blood pressure [56]. In many individuals the peripheral resistance does not increase sufficiently and blood pressure is not maintained; the ultimate consequence is syncope or fainting. The modeling of syncope was not an objective of the current study.

In order to validate the new features of the modified Guyton model, simulations were performed of both passive tilt experiments and LBNP experiments. These validations offered a relatively simple means of determining that the new gravity-dependent components functioned appropriately and that the controllers in the model were sufficient to face an orthostatic challenge.

9.6.2 Simulation of Tilt and Recovery

Having modified the Guyton model as described above, the main question to be addressed was "are the simple changes made to the model sufficient to simulate a head-up tilt-from-supine response"? The orthostatic maneuver causes a widespread body response that includes: a) baroreceptors; b) autonomic function; c) pressures, flows and volumes of the upper and lower circulatory compartments; d) pre- and post-capillary resistances in muscle and non-muscle tissues in the upper and lower circulatory compartments; e) venous tone in both upper and lower body segments; f) renal blood flow and renal function; g) capillary filtration and lymph flow in both upper and lower compartments; h) secretion of blood pressure and renal regulating hormones; and i) metabolic rate.

These are the responses we wish to replicate. Inasmuch as the major changes of the modified model were associated with the controlled system (i.e., adding new circulatory compartments), it was important to assure that the controllers in the model (autonomic, local and hormonal) were sufficient to regulate orthostasis. The goal was to produce a response that was more qualitatively than quantitatively correct by identifying gross mechanisms that are required not only for short-term and long-term tilt, but for bedrest and weightlessness, these latter situations being the ultimate objective.

The simulation of tilt was initiated by changing the angle of tilt of the gravity vector. The response of the modified Guyton model to a 90° head-upward tilt is shown in Fig. 9-28. The hydrostatic forces produced by the tilt resulted in fluid pooling almost instantaneously in the leg blood vessels and more gradually in the leg tissues. The leg fluid pooling reduced the central blood volume and thereby lowered cardiac output and arterial blood pressure. Blood flows through the legs, upper body and renal pathways were also reduced.

Although the model's responses were generally in the appropriate direction, neither the magnitude nor the dynamic behavior of the responses was consistent with observations of the real system. Pressures and flows would have been reduced even further if compensatory feedback mechanisms, decreasing venous capacitance and increasing peripheral resistance had not been present in the model. However, these feedback mechanisms were not as effective in the model as in the real system. The reduction in arterial pressure and cardiac output, as seen in the simulation, was greater than typically observed in man.

Another shortcoming of the model was related to the blood volume response. Although blood pooling in the legs and fluid shifting into the leg interstitium were appropriate with regard to direction and dynamic behavior, the blood volume only decreased transiently, by about 50 ml, instead of showing a net sustained loss of several hundred ml. On further examination, it was found that fluid was being absorbed from the capillaries in the upper body nearly as rapidly as it was filtering from the leg capillaries. Obviously, further modifications of the model's structure were required.

9.6.2.1 Additional Modifications.
It became apparent that any single mechanism added to the model to allow blood volume to fall would make the blood pressure and cardiac output responses worse. Therefore, a combination of mechanisms was necessary that would inhibit inward fluid absorption in the upper body capillaries and increase venous return and, therefore, the blood flow and arterial pressures. The following modifications were added to the model with the objective of improving the tilt simulation.

a) *Enhanced Venoconstriction.* The sensitivity (gain) of the venous resistance element to efferent baroreceptor signals was increased. This change increased the postcapillary resistance in the upper body capillaries (the major blood flow pathway) in the face of a de-
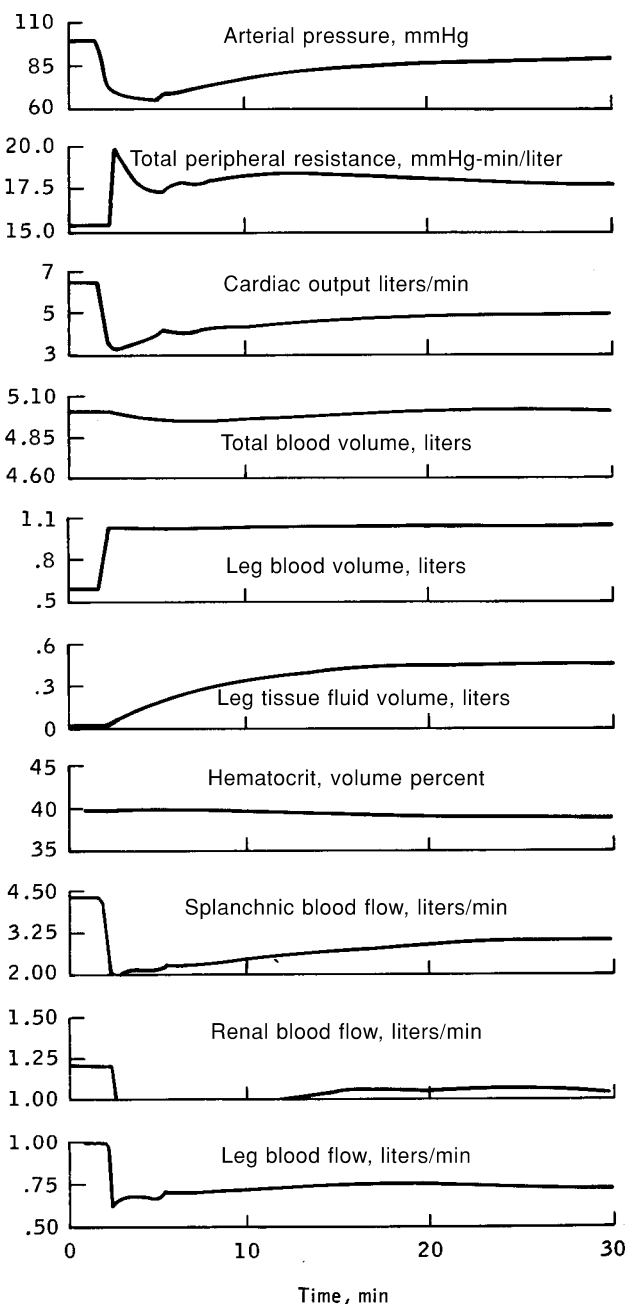
Figure 9-28. Simulation of a 90° head-up tilt from supine using the basic gravity-dependent model without further modification.

creased baroreceptor pressure and thereby permitted an increase in capillary filtration pressure and limited the inward filtration that would have otherwise occurred.

b) *Enhanced Reverse Stress Relaxation.* The original Guyton model contained a stress relaxation element that causes gradual reduction of venous capacitance in the face of a reduced blood volume. A term was added to produce an instantaneous effect that reduces upper body venous capacitance to approximately half the re-

duction in central blood volume. This effect, which had been recommended by Guyton in a recent unpublished version of his model, was simulated by reducing the unstressed venous volume at the moment of tilt. Its effect is to increase venous return, cardiac output and systemic blood pressures.

c) *Reduced Area Available for Capillary Filtration.* The filtration coefficient for the upper body capillaries was reduced in value at the time of tilt. The direct effect was to limit the rate at which interstitial fluid enters the circulation and thereby produce a reduced blood volume.

d) *Muscle Contraction Effect in Legs.* A parameter was added which would provide a pressure, external to the leg blood vessels, simulating the muscle contraction effect that occurs during tilting and, to a much greater extent, during standing. The effect is to reduce leg venous pressure, reduce the amount of fluid pooled in the legs and increase venous return.

These modifications appear reasonable and are supported by tilt-table experiments to be discussed later. The first three modifications are in accord with the generalized splanchnic venoconstriction that has been observed following reduction in central blood volume as a result of either hemorrhage or tilting [53,54]. The first two modifications could also be a result of abdominal compression, autonomic control, or local metabolic effect. The evidence for a decrease in capillary coefficient (item 3) has been inferred from studies of hemorrhage, infusions and standing [57,58]. The last modification (4) could represent a proprioceptive tilt reflex which was simulated as a small increase in external pressure (~10 mmHg).

9.6.2.2 Model Responses After Modification. The four modifications mentioned above were applied individually and in combination to the simulation of tilt. The results are shown in Figs. 9-29(a) to 9-29(e) (dashed curves). The first two mechanisms listed above resulted in the greatest improvements and Fig. 9-30 shows the tilt response as well as recovery from tilt during a simulation in which these effects have been added. The solid curves in Fig. 9-29 represents the simulated response to tilt of the gravity-dependent model without the modifications (as shown in Fig. 9-28). The symbols at the right margin of Fig. 9-29 ("+" or "−") indicate responses that have been improved or made worse, respectively, due to the additional mechanisms. (A plus sign signifies that the modified simulated response is closer to the expected response). The transient "spike" effect at the start of each tilt simulation is an artifact that would not be present if the tilt had not been performed instantaneously. Each of the four modifications resulted in an overall improvement of the model's response to tilt that was reflected in almost all of the variables monitored during this series of simulations.

The Guyton model's responses have provided a comprehensive view of orthostasis. The response of a wide range of model variables obtained during a simulation incorporating all four modifications is illustrated in Figs.

9-31(a) to 9-31(d). Qualitatively, the model variables agree with experimental data. The following is a discussion of the relevant physiology, explaining the responses shown in these figures and including the results of experiments. Although it is desirable to validate the model for much longer periods of time than the 30-minutes of this simulation, there have been no reported data with which to compare an extended time period.

9.6.2.2.1 *Fluid Volume Shifts.* The vertical orientation creates a long hydrostatic column of blood that greatly increases the arterial and venous pressures in the legs (Fig. 9-31(a)). Both of these pressures are increased to the same extent; therefore there is no change in the driving force to flow. However, these high pressures do cause distention of the leg vessels; about 400 to 600 ml of blood rapidly pool in the leg vessels, primarily in the veins [27,51]. A slight muscle contraction effect will reduce by 15% the amount of fluid that otherwise would pool in the leg [49]. The accompanying increase in leg capillary pressures creates a driving force for filtration. At the end of 30-minutes, approximately 500 ml of plasma will have left the circulation and entered the leg interstitial compartment [36]. Concomitantly about 100 to 200 ml of fluid will have entered the circulation through absorption from the upper body capillaries. (This quantity has never been measured experimentally). This results in a net reduction in total blood
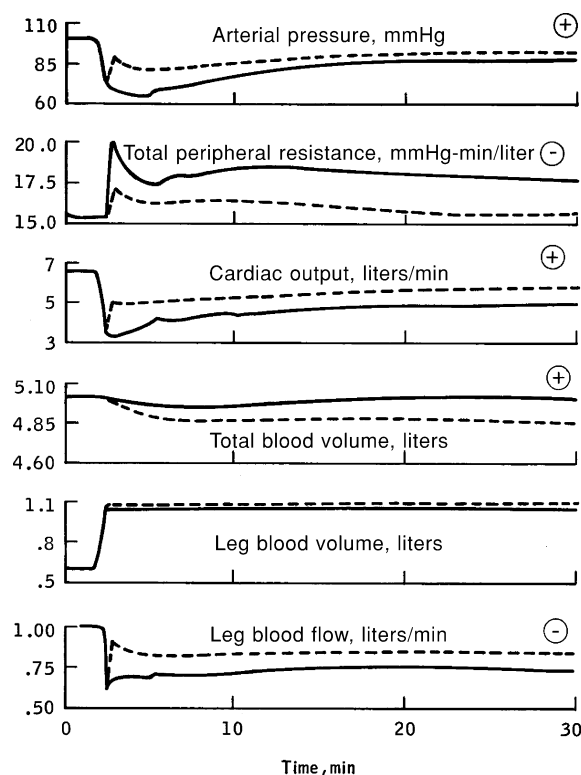
Figure 9-29(a). Simulated 90° tilt response: Effect of instantaneous reverse stress relaxation. Solid lines represents basic model simulaton (Fig. 9-28); dashed lines represents model with modification (see text for meaning of "+" or "−").
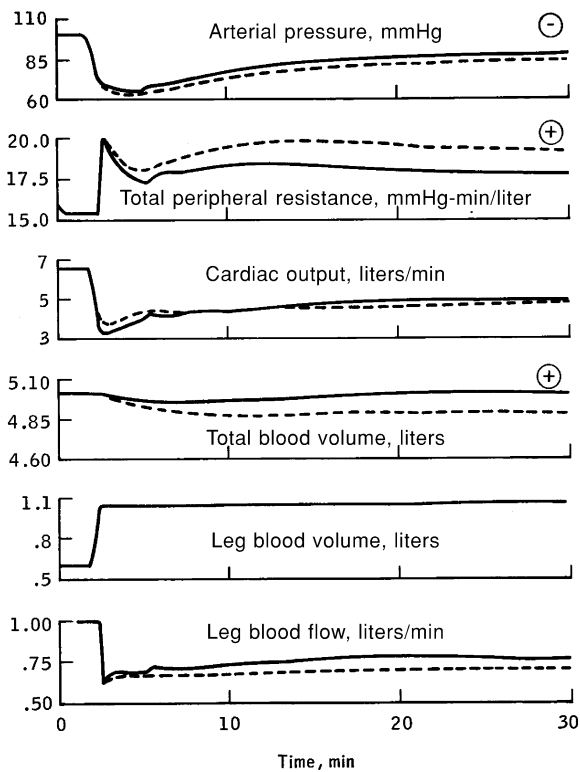
Figure 9-29(b). Simulated 90° tilt response: Effect of enhanced splanchnic venoconstriction. See caption for Fig. 9-29(a).
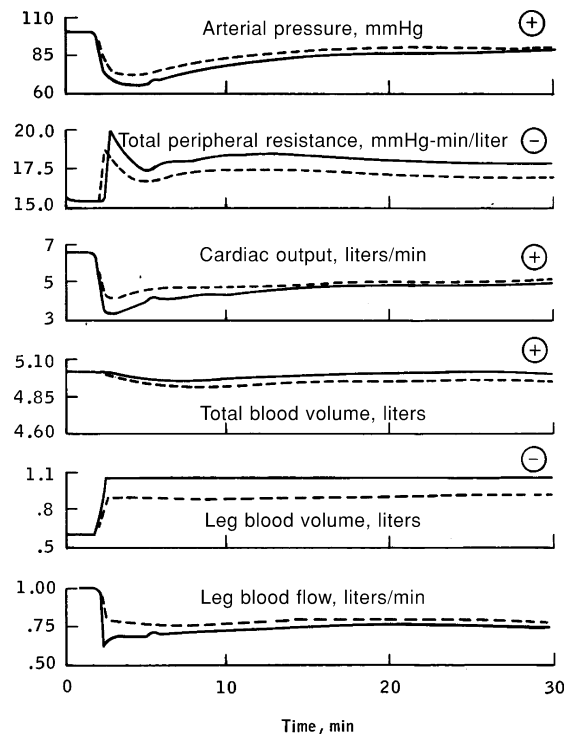
Figure 9-29(c). Simulated 90° tilt response: Effect of muscle pump. See caption for Fig. 9-29(a).
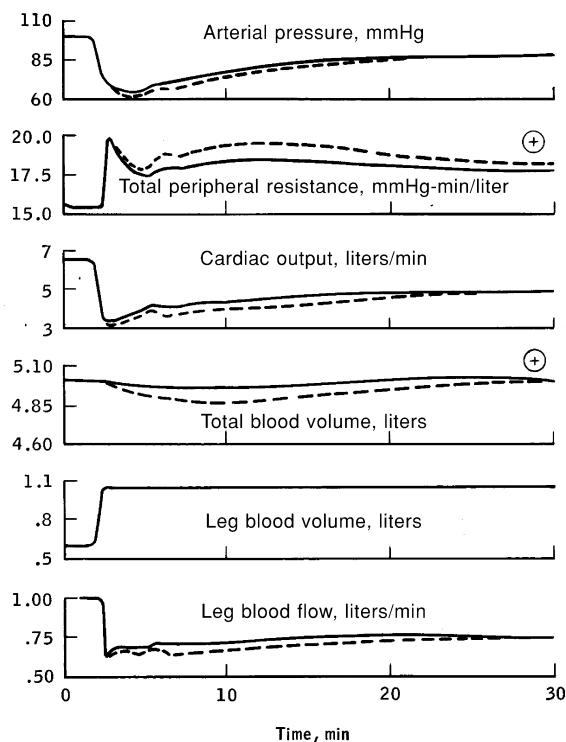
Figure 9-29(d). Simulated 90° tilt response: Effect of reduced capillary filtration coefficient. See caption for Fig. 9-29(a).
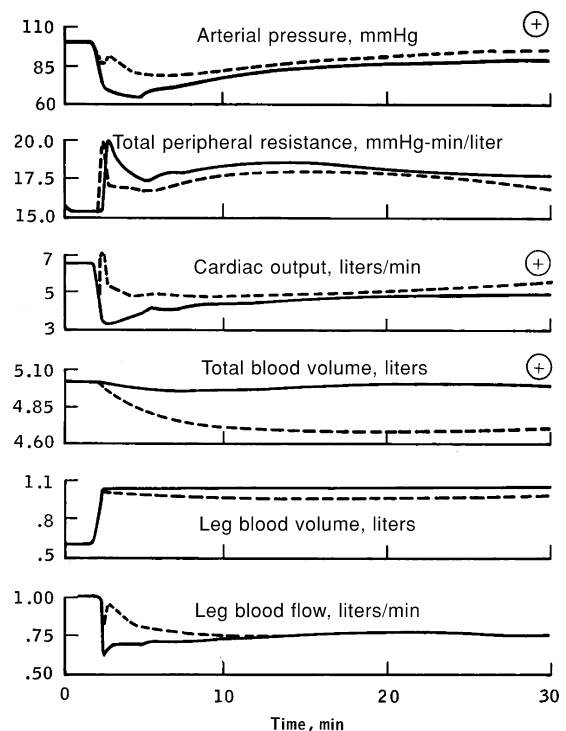
Figure 9-29(e). Simulated 90° tilt response: Effect of combination of four orthostatic mechanisms. See caption for Fig. 9-29(a).
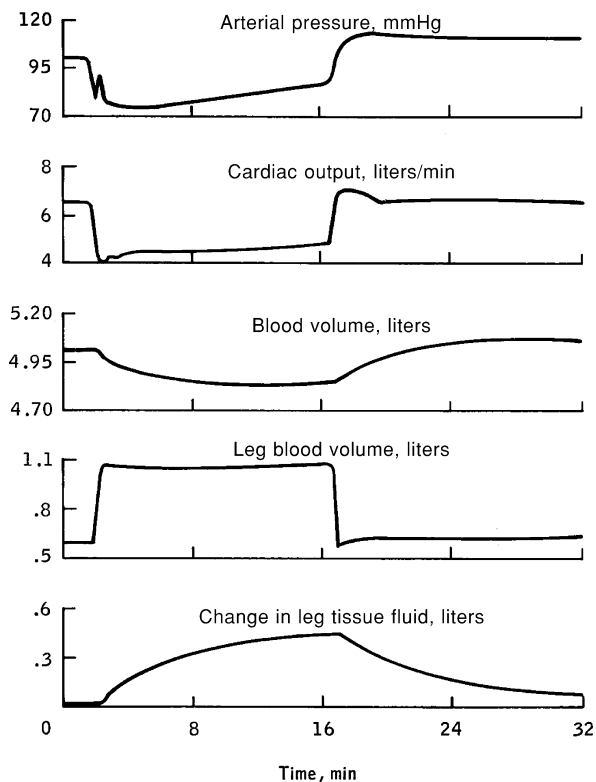
Figure 9-30. Simulated 90° tilt response and recovery with enhanced reverse stress relaxation and splanchnic venoconstriction.

Figure 9-31(a). Simulated 90° tilt response with added orthostatic mechanisms: Fluid shifts and leg blood pressures. Values on right side of graph are changes in value from control at end of 30-minutes.

volume of about 300 ml [52,59]. Since this represents a change in plasma only, the hematocrit increases accordingly [60]. The net deficit of fluid in the upper body (effective central blood volume) is approximately 700 ml: 400 ml due to limb pooling and 300 ml due to net extravascular filtration [36,61].

9.6.2.2.2 *Major Circulatory and Cardiac Changes.*

At the end of the 30-minutes of simulated tilting, the mean arterial pressures have returned to near normal, whereas central venous pressure has remained relatively depressed (Fig. 9-31(b)). The magnitudes of these changes, including the initial reduction in pressures, are appropriate. The time course, however, is in error, because these events are known to occur more rapidly. Cardiac output is decreased by approximately 15%, primarily because of a reduction in stroke volume and despite an increase in heart rate [50,62]. The reduction in stroke volume is a result of a decreased venous return created by the large reduction in central blood volume. The heart rate changes reflect increased autonomic stimulation. Total peripheral resistance increases sharply at first [63] as a result of intense autonomic-baroreceptor activity [64] that later is augmented by angiotensin release and attenuated by autoregulatory effects (see Fig. 9-31(d)). Blood flow to each of the three major tissue segments in the model (renal flow, leg muscle flow and non-muscle, non-renal flow) decreases because

of the general decrease in cardiac output as well as vasoconstriction [50,65,66]. The renal and leg blood flows appear to stabilize at lower levels, but the splanchnic flow tends to return toward normal.

9.6.2.2.3 *Capillary Filtration.*

The filtration of nearly 500 ml of plasma into the leg interstitium, is basically complete within 20 to 30-minutes [63] (see Fig. 9-31(a)). The driving force for this event is an increase in leg capillary pressure of nearly 60 mmHg, equivalent to the hydrostatic column from the heart to the midpoint of the legs. This vascular pressure is opposed by the leg tissue pressure which increases gradually as fluid enters the interstitial spaces [58].

While leg filtration is occurring, the capillaries in the upper body are undergoing a more complex process (Fig. 9-31(c)). At the beginning of the tilt response, the fall in capillary pressure and the rise in colloidal oncotic pressure favor the absorption of fluid from the extravascular
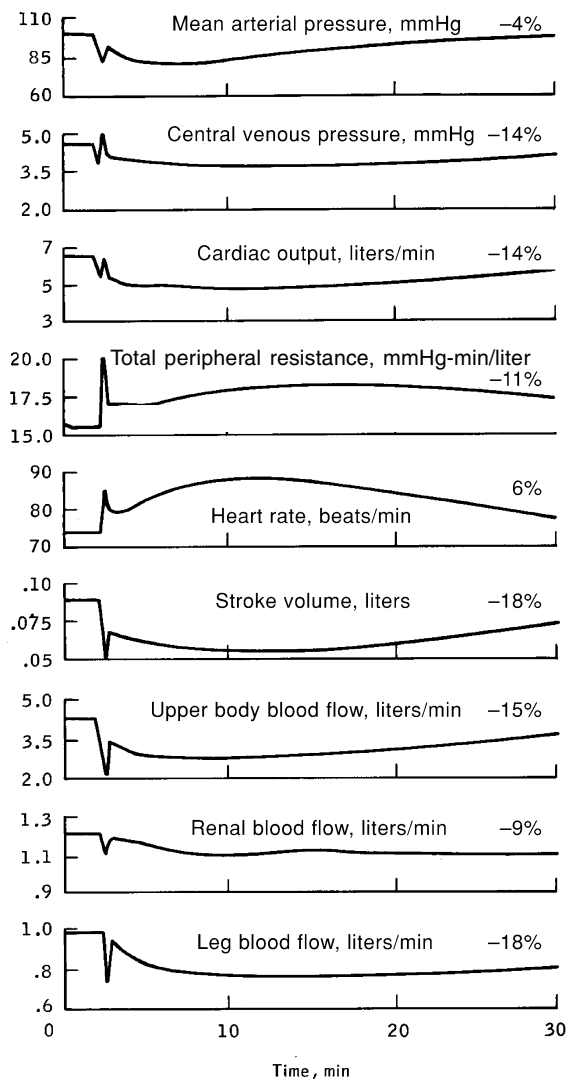
Figure 9-31(b). Simulated 90° tilt response with added orthostatic mechanisms: Major circulatory parameters. Values on right side of graph are changes in value from control at end of 30-minutes.

Figure 9-31(c). Simulated 90° tilt response with added orthostatic mechanisms: Upper body capillary filtration parameters.
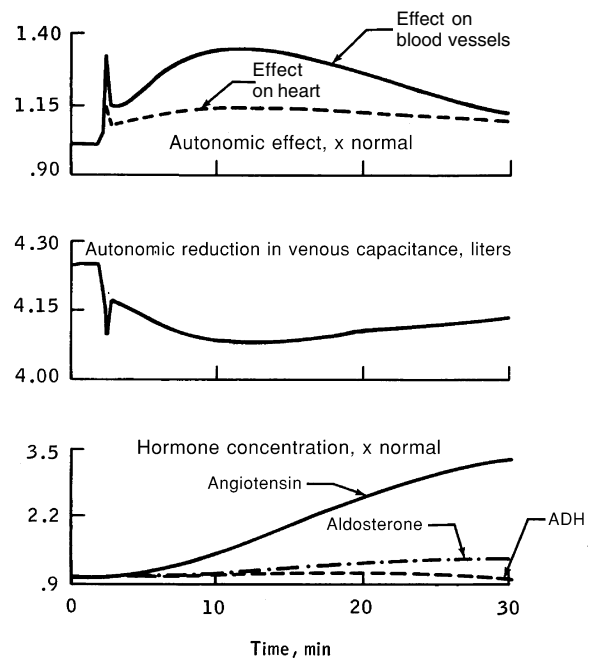
Figure 9-31(d). Simulated 90° tilt response with added orthostatic mechanisms: Autonomic and hormonal responses. Values on right side of graph are changes in value from control at end of 30-minutes.

space into the bloodstream. While colloidal pressures continue to rise, the pre/post capillary resistance ratio decreases because of a rise in venule resistance [61] thus favoring a rise in capillary pressure as well. Capillary pressure rises until the transcapillary forces slows absorption and even reverses it at about 15-minutes following tilt. It is quite remarkable that there may be net transcapillary filtration at a time when arterial and venous pressures are below normal. However, this same behavior, a result of adjustments in the pre/post capillary resistance ratio, has been reported in studies of moderate hemorrhage, another hypovolemic stress [58]. This effect has also been suggested during LBNP studies [67] and not unexpectedly, opposite changes have been suggested during plasma infusions [68]. However, no documentation exists to confirm whether the same phenomena seen in these simulations

occurs during human tilt. Thus, the fall in blood volume due to extravasation of fluid from the legs is partly compensated, hypothetically, by a self-limiting intravasation of fluid from the tissues of the upper body.

9.6.2.2.4 *Neural and Humoral Orthostatic Protective Mechanisms.* Several of the major neural and humoral reflex pathways that are activated during the tilt simulation are shown in Fig. 9-31(d). The autonomic influences include those that produce vasoconstriction, cardioacceleration and contractility and reduction in venous capacitance [49]. The dual effects of venoconstriction and reduced venous capacitance was noted to be among the most potent defense mechanisms for orthostasis. The humoral mechanisms are seen to be slower acting and include angiotensin release, which produces vasoconstriction [69], aldosterone release, which inhibits sodium and water excretion [70] and ADH release, which decreases urinary output and preserves body fluid volumes [14]. All of these mechanisms are mediated in the model by reflex pathways originating at pressoreceptors in the cardiopulmonary, arterial, or renal areas. The realistic time course of these reflexes should be noted; autonomic reflexes are fully operative within a few minutes whereas hormonal responses are slower acting.

9.6.3 Summary: Head-Up Tilt

Validation was accomplished for simulations of 30-minutes head-up tilt. The general agreement between the experimental observations and the model simulations of the many physiological parameters in response to passive tilt attests to the basic soundness of the original Guyton formulation and the new modifications.

An additional set of simulations was undertaken for lower body negative pressure (LBNP) using the modified Guyton model [16]. LBNP was shown, in Chapters 3 and 7, to be an orthostatic-like stress capable of being simulated by a model with a representation of the circulation more detailed than the Guyton model. However, the results with the Guyton model, while not reported here, demonstrated a new capability to simulate fluid shifts along the long body axis [16].

Although other computer models have been capable of simulating a tilt response with greater fidelity with regard to circulatory flows and pressures (especially during the first 10-minutes following tilt), they did not include the wide range of physiological subsystems found in the Guyton model [71,72,73] Thus, the responses shown here are representative of the circulatory, fluid, renal, autonomic and endocrine responses to tilt that have been described by many investigators, each observing only a portion of these physiological reactions.

Longer-term standing using the Guyton model could not be validated at this time because of the absence of experimental data. The model was able to simulate short-term 90° head-up tilt (standing), but it did not achieve a steady-state in this position. The Guyton model was designed from data gathered in the supine, resting position and it would be difficult to redesign the model based on ambulatory initial conditions. Even defining ambulatory initial conditions would not be easy, because these conditions would depend on the history of average activity (standing, walking, or sitting) of the subjects from which the data were gathered. Sufficient data of this type is not available. Furthermore, standing is a complex stress and all the mechanisms that participate in creating orthostatic tolerance are not yet quantitatively understood [49,50].

9.7 Head-Down Tilt and Head-Down Bedrest Simulations

9.7.1 Introduction

Exposure of human subjects to a moderate degree of head-down tilt (anti-orthostasis or negative tilt) for several hours to more than a week, has been used as a ground-based analog of weightless spaceflight [74,75,76].[‡] Head-down tilt has been shown to mimic the major fluid, renal and cardiovascular characteristics of the weightlessness response in a more reliable and reproducible fashion than supine bedrest [77]. An anti-orthostatic animal model has also been used with some success to study cardiovascular deconditioning and musculoskeletal atrophy similar to that which occurs in spaceflight [78,79,80]. The objective of the present analysis is to: a) demonstrate the capabilities of the Guyton model to simulate postural changes and particularly, the short-term and long-term responses of head-down tilt,[§] and b) help interpret the still poorly understood experimental head-down tilt findings. These studies are described more fully in the original reports [81,82].

Although it may appear logical to believe that head-down tilt leads merely to opposite responses to that of a head-up tilt, this is not necessarily so. In the upright position the physiological defense mechanisms must counter the tendency for loss of brain blood flow, while in the head-down position the physiological problem is that of reducing fluid pooling in the fragile thoracic regions which could lead to pulmonary congestion. The body appears better adapted for immediate protection against gravity in the orthostatic position compared to the anti-orthostatic position, the latter case seeming to require longer-term adjustments. It also needs to be noted that in the context of our discussion, orthostasis implies a completely erect upright individual (+90°) while anti-orthostasis represents a much smaller angle to the horizontal (–4 to –6°); the hydrostatic forces are, therefore, not as great in the head-down position as in the upright position.

[‡] Head-down tilt was a relatively new technique at the time this analysis was completed in 1982 and these citations were the extent of the available experimental reports. The more numerous studies conducted since then will not be included in this book, except as a brief update.

[§] The angle of tilt (with the horizontal) for human anti-orthostatic studies has varied from -4 to -12°. Eventually, the science community seems to have settled on a 6° angle of tilt as a standard to simulate microgravity. The present analysis was conducted prior to the establishment of this standard and so considers other angles of tilt as well.

9.7.2 Changes in Leg Fluid and Tissue

We have found that one of the keys to achieving a realistic simulation of supine bedrest or head-down tilt, is a better understanding of events which occur in the legs during alterations of hydrostatic gradients. As was shown in Chapter 9.3 the initial response to a hypogravic stress is an acute movement of blood out of the legs and this is followed by a more chronic condition of gradual leg dehydration. These changes were described graphically in Fig. 9-10. It was shown there that the reduction in leg volume accompanying supine bedrest is much less than that of spaceflight; therefore, most of the fluid regulatory parameters (that respond to headward fluid shifts) change to a lesser degree during supine bedrest than spaceflight. It also was shown in Fig. 9-10 that anti-orthostatic bedrest is associated with leg volume decrements between those of spaceflight and supine bedrest.

It is worth considering that the body fluid losses during spaceflight are primarily derived from leg fluid and tissue losses. This notion is supported by data from Skylab. Those studies reveal a loss of approximately 1.8 liters in leg volume at the end of several days inflight and this was associated with a total body water loss of nearly 1.5 liters (see Chapter 5.4.2.1). The more gradual loss in leg volume during periods beyond a week or so can be ascribed to further leg dehydration as a results of: a) elastic forces, influenced by devascularization and tissue and vessel retoning, which squeeze additional fluid headward and b) loss of solid tissue, mostly muscle, due to disuse atrophy.

Altering a human's posture from supine to -4° head-down tilt allows fluids to shift from the feet to the head. It is easy to understand how blood can flow "downhill" from the leg veins to the veins of the upper body – similar to a horizontal cylinder partially filled with fluid being tipped a few degrees. It is not so easy to visualize how leg blood flow would be affected. As the leg veins lose fluid and pressure, the pressure outside the veins is now unopposed and the vessels collapse or partially collapse; when this happens the resistance to flow should increase. It is also not obvious how leg interstitial fluid drains out of the legs. There is a good deal more leg tissue fluid than there is blood stored in the leg vasculature, as we can infer from comparing leg volume changes measured during short-term lower body negative pressure tests (which affect primarily the blood compartment) with that after long-term head-down bedrest and spaceflight (which affect total leg fluid). Aside from a small contribution of lymph flow, the major portion of leg tissue fluid leaves the legs by crossing the capillary membrane of the leg vasculature and then draining into the upper body. What alterations occur during head-down tilt in the Starling forces that control transcapillary fluid movement? How would these forces be different between the leg capillary beds and those in the upper body during postural maneuvers? To further complicate the picture, long term changes are likely to occur in both the leg veins and leg tissue compartment such as reverse stress relaxation and retoning as well as loss of tissue due to muscle atrophy; these should effect dehydration in the legs as was discussed in Chapter 9.3.3. The Guyton model was not designed with

legs and certainly did not account for postural maneuvers, either short-term or long-term . Therefore, the challenge in this analysis was to account for these processes that are seldom addressed and not well understood, by the use of the mathematical model of the circulation.

9.7.3 Modifications to the Circulatory Model

The direct effect of gravity forces was introduced in three locations in the model: at the inflow to the leg arterial compartment, at the outflow of the leg venous compartments and at the carotid baroreceptors. Hydrostatic forces were computed for any angle of tilt as a function of the vertical distance to the midpoint of the legs or to the neck baroreceptors as measured from the heart (see Appendix C.1). These hydrostatic pressures are algebraically added to the usual dynamic fluid pressures of the circulation.

With the model so modified it was possible to examine by simulation techniques the two postural maneuvers described above which have been most useful for studying fluid responses to gravitational disturbances: head-up tilt (orthostasis) and head-down tilt (anti-orthostasis). By simply specifying any angle of tilt, either head-up, supine, or head-down, it is possible to create a large range of hydrostatic forces in the model, from maximal (at the feet) in the erect position, to zero in the supine position, to negative in the head-down position. Simulations of head-up tilt were examined in Chapter 9.6; in this section we will focus on head-down tilt.

The initial simulations that were performed of head-down tilt (by simply changing the angle of the gravity vector) resulted in leg blood flows and in leg tissue drainage that were not plausible and produced instabilities in the simulated responses, especially at extreme degrees of negative tilt. It was discovered that a more realistic simulation of head-down tilt would be achieved by modeling collapsible leg veins and accounting for dehydration of extravascular leg tissue. This effort is an extension of the analysis of factors affecting long term leg dehydration that were described in relationship to supine bedrest (Chapter 9.3).

9.7.3.1 Modeling Collapsible Veins. The most convenient representation of the elastic properties of arteries and veins is the pressure-volume relationship as illustrated in Fig. 9-32. The volume to the right and left of V_o is "stressed" and "unstressed" volume, respectively. The unstressed volume, or zone of distensibility, is the region in which the vein is in a state of collapse. Notice the nonlinear characteristic shape of the pressure-volume curve. It is convenient in mathematical models to "linearize" this relationship in the "stressed" region as indicated by the dashed line A. This "constant compliance" representation is used in the Guyton model. However, in the original formulation of the Guyton model, the collapsible range was represented by a horizontal line at zero transmural pressure. This simplification is sufficient for many applications of the model. However, this is not an adequate description of collapsible segments and does not permit the model to achieve a full range of unstressed volumes necessary for simulating head-down tilt.
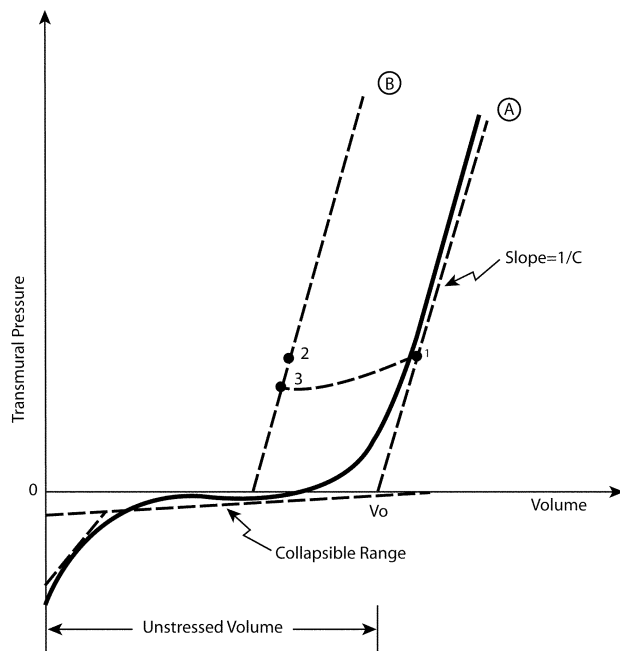
Figure 9-32. Pressure-volume relationships of the veins.. The solid line shows an idealized non-linear "compliance" curve. The dashed lines are linear representations as used in the Guyton model. The unstressed volume, V_o, is the X-intercept of the pressure-volume curve. The region to the right of V_o is the elastic range; vessel compliance is the inverse of the slope. The region to the left of V_o is the area of vessel collapse. The collapsible region can be modeled by using one or more straight lines. The line denoted by "A" shows the normal linear compliance. The normal operating point is shown as "1". If the vessel empties, retoning can take place whereby the compliance line shifts to the left (i.e., "B") and pressure is partially restored; operating point moves to "3". For complete restoration of pressure, the operating point moves to "2".

A superior representation is depicted by the dashed line below the volume axis, either as a single straight line or else broken into linear segments as shown. Modeling in this manner permits the pressure inside the vessel to decrease gradually as the veins empty and collapse. (Otherwise the value of unstressed volume could oscillate between 0 and V_o and the model could be unstable). The decreasing pressure drop for flow as the vein collapses, will cause a decrease in flow [83]. It is also possible to increase resistance to flow using a formulation for collapsible tubes [73] although the data to implement this latter approach was not available.

The normal operating point of a vein is shown in Fig. 9-32 as Point 1. Normally as the volume of the vein gradually is increased or decreased, the *elastic* property of the veins allows the operation point to move up or down on the solid line. However, if the vein is partially drained of fluid, (as in leg veins during head-down tilt) the vessel can also retone, given enough time (Point 2 or 3). The compliance curve has thus shifted from A to B in Fig. 9-32. This passive mechanism is called reverse stress relax-

ation (or "retoning"). Stress relaxation (or "delayed compliance") is movement of the compliance curve to the right and is activated to accommodate over-inflated veins. These processes, derived from the *plasticity* properties of blood vessels, have been incorporated into Guyton's model as one means of controlling venous blood pressure [26b]. This is a different mechanism than active control of venous tone mediated through the sympathetic nervous system.

The modifications of venous collapse were made in only the leg veins of the model, inasmuch as the larger upper body veins do not collapse during head-down tilt, but rather they are engorged. In hypogravic situations, the central veins could act as a large depot for leg fluid. Any additional volume beyond the zone of free distensibility contributes toward increasing venous pressures; this would presumably initiate renal mechanism, which acts to reduce the excess stressed volume. In addition, adaptive mechanisms exist that can accommodate excess fluids. These influences include stress relaxation, vascularization (i.e., increases in number of open capillaries) and altered volume receptor sensitivity.

9.7.3.2 Modeling the Leg Interstitial Compartment.
9.7.3.2.1 *Transcapillary Fluid Movement.* In Chapter 5.4.2.2 the importance and processes of capillary fluid exchange during the acute stage of weightlessness were discussed. The new configuration of the leg filtration mechanisms in the modified computer model is shown in Appendix C (Fig. C-2). Tissue fluid pressure is determined by the elastic characteristics of the tissue (see below) and its state of hydration and acts to oppose capillary pressure. During standing capillary pressures in the feet will increase by 60–75 mmHg. As much as 500 ml plasma may filter into the tissues within 30-minutes; after that this effect is limited by the opposing tissue pressure, a reflex reduction in capillary surface area and by concentration of plasma colloids which are not easily filterable. Little is known about the Starling forces and their dynamics for the reverse situation of head-down tilt[UPDATE#4]. Capillary pressure certainly will be expected to decrease (as a result of diminihsed hydrostatic pressures in the leg) and favor movement from the leg tissues into the leg vasculature. But what is the intensity and time-course of this process and what factors influence it? One of the keys for answering this is a better understanding of the factors that influence leg tissue pressure. This is addressed next.

9.7.3.2.2 *Pressure-Volume Relationship of the Tissues.* Guyton has proposed a composite diagram showing the relationship of interstitial fluid pressure to total interstitial fluid volume (Fig. 9-33; solid curve). Also shown is the relationship between free fluid and non-mobile fluid in the interstitium (dashed line). According to experimental observation, normal interstital fluid is in the negative interstitial fluid pressure range. As can be seen by Fig. 9-33, normal tissues have essentially zero free fluid. However, as the interstitial fluid pressure rises into the positive range, the compliance (slope of the solid curve) increases dramatically and large quantities of free fluid

Figure 9-33. Estimated tissue pressure-volume relationship of entire human body. Redrawn from Guyton, *et al.* [26a].

Like the veins, the interstitial matrix is not entirely elastic in structure because it exhibits the phenomenon of stress relaxation and reverse stress relaxation. One may expect that during acute head-down tilt, free fluids leave the leg tissues quite readily due to the elasticity of the interstitium and the falling capillary pressure. However, loss of tissue fluid is self-limiting as tissue pressure falls. Eventually, reverse stress relaxation partially restores the tissue pressure and this in turn permits further dehydration of the leg tissues. Thus, a greater degree of fluid from leg tissues may be lost during head-down bedrest from subjects who have been previously ambulatory or standing for long periods of time and who are well hydrated.

9.7.4 Verification Studies

Preliminary simulations were performed to test the candidate approaches for modeling the leg elements. Two types of verification studies were performed: a) a postural study demonstrating the model's fluid shift capability between erect, supine and head-down maneuvers and b) a sensitivity analysis demonstrating the ability of the model to simulate various angles of head-down tilt.

9.7.4.1 Simulation of Postural Maneuvers. The capability of the modified model to predict fluid volume changes for a variety of postural changes and gravity vectors are shown in Fig. 9-34. In these simulations, consecutive short-term postural changes were performed, from the supine (initialization) to the erect, back to the supine and followed by an anti-orthostatic position (–4°). The head-down tilt was then allowed to continue for a longer period (48-hour). The forcing function in all of these cases and for the remainder of the simulations in this chapter was the angle of tilt; there were no artificial forcing functions used to move fluid as was done in previous sections of this chapter for supine bedrest and water immersion. However, as mentioned above, the compliance of the leg tissue compartment was set to a value that would ensure inward filtration when the hydrostatic forces of standing were removed.

Two important kinds of fluid shifts are examined in Fig. 9-34: a) movement of blood between upper and lower body and b) plasma exchange between intravascular and extravascular compartments. The model realistically demonstrates the rapid blood volume shift of about 400–600 ml that occurs during normal short-term postural changes and the somewhat slower shift of an additional 500 ml plasma that is normally pooled in the leg extravascular tissues upon standing. This implies that in the erect posture about a liter of fluid is pooled in the leg compartments (veins and interstitium) partially at the expense of a large reduction in central blood volume and total blood volume. Tilting to the supine position returns fluid to the upper body and essentially reverses the previous changes. Tilting head-down -4° for a short period merely accentuates the magnitude of the fluid shifts that were already observed in changing posture from erect to supine. However, longer exposure to head-down tilt (right half of Fig. 9-34) dramatically reverses many of the short-term head-

begin to appear. This non-linear compliance of the tissues is potentially significant to the quantitative understanding and simulation of head-down tilt and weightlessness.

During postural change from supine to erect, a large quantity of free tissue fluid is mobilized and the operating point shifts to the high compliance range where tissue pressures are positive. Conversely, during head-down tilt or prolonged weightlessness, when leg tissues become dehydrated, little free fluid is present and tissue compliances are much lower. Although the interstitial compartment of the *upper body* includes a non-linear compliance relationship, this feature was introduced in the model's *leg compartments* as a manual change in tissue compliance to achieve the desired degree of leg dehydration. In the simulation studies, it was found, in fact, that in order to achieve the proper degree of leg tissue dehydration during head-down tilt, it was necessary to decrease leg tissue compliance several fold compared to the simulation of standing. The change in tissue compliance was one of the more significant modifications considered for the simulation of head-down tilt; it initiated the driving forces of the model, rather than the forced volume shift initiations required for the supine bedrest simulations (Chapter 9.3).

Figure 9-34. Simulation of fluid shifts during acute postural changes followed by bedrest. The angle of tilt with respect to the horizontal is shown at the top.

down shifts, except for the drainage of fluid from the legs, which becomes more severe. Therefore, although the model predicts that almost a liter of leg fluid has shifted cephaled by 2-days of anti-orthostasis (as measured from the initial supine reference), central blood volume has returned to nearly normal, due to the reduction in total blood volume. In the model, the loss of blood volume (and total body water) during prolonged head-down tilt is due primarily to feedback renal excretion pathways, while blood volume loss in the short-term erect position arises from filtration into the leg interstitium. In both cases, the loss of plasma is reflected by a hemoconcentration that is more severe in the anti-orthostatic position.

The simulations of Fig. 9-34 also demonstrate that measurements of leg volume changes during bedrest (or spaceflight) studies can be quite misleading unless the

reference posture is clearly defined. For example at the end of 48-hours of head-down tilt, the simulation results indicate a decrement of total leg volume (leg blood volume plus leg tissue volume) of about one liter if measured from the supine position and about two liters if measured from the erect position. It should be also clear that the time at which subjects remain either in the erect or supine position before the reference (or control) measurements are made is also crucial.

9.7.4.2 Sensitivity Analysis. The results of a series of simulations at –4°, –8° and –12° tilt are shown in Fig. 9-35. The objective of this study was to show that increasing the angle of tilt increases the severity of leg fluid shifts and to examine related physiological aspects. In so doing, the simulation will serve as a verification of the model's ability to account for negative tilt. The manner in which the legs are modeled will influence the amount of total fluid shifted from the legs. Therefore, the predictions shown in Fig. 9-35 will presumably be modified as more realistic leg elements are developed and as data becomes available.

As the angle of tilt increases, the effect on shifting fluids from the interstitium is proportionately greater than the shift of leg blood. This result may be expected in that most of the fluid from the leg vasculature drains out for only small negative angles, similar to the effect seen during LBNP when the greatest amount of leg pooling occurs during the lowest pressure differentials. In previous simulations of supine bedrest, the blood volume changes were nearly equivalent to the losses of blood from the legs. These anti-orthostatic simulations, by contrast, indicate that blood volume losses are always greater than that shifted from the legs. This condition arises because of an excess hydrostatic pressure at the volume receptors, which is maintained throughout negative tilt. This is a situation not previously encountered in the supine position. It may be expected that a similar phenomena is present in human subjects.

Our analysis suggests that at –4°, leg capillary pressures decrease only about 5 mmHg as measured from supine, compared to a 60–75 mmHg increase in the erect position. This suggests a much slower dynamic response during a slight head-down tilt than during a more severe head-up tilt. In addition to the decrease in capillary pressure, the model simulation reveals alterations in plasma colloidal pressure, tissue pressure and pre- and postcapillary resistances (not shown), all of which favor inward filtration through the capillaries. Absorption of tissue fluid would be expected to continue until the tissue pressures declined and a balance of Starling transcapillary forces was again achieved. The model presently predicts the resulting leg tissue fluid losses over 24-hours, in the 4° head-down position, to be nearly equivalent to that gained by the tissues in 30-minutes of standing.

9.7.5 Simulation of Head-Down Tilt

At the time these model analyses were performed (1978 to 1982), there were only a few published experimental studies on head-down tilt using human subjects. Two of
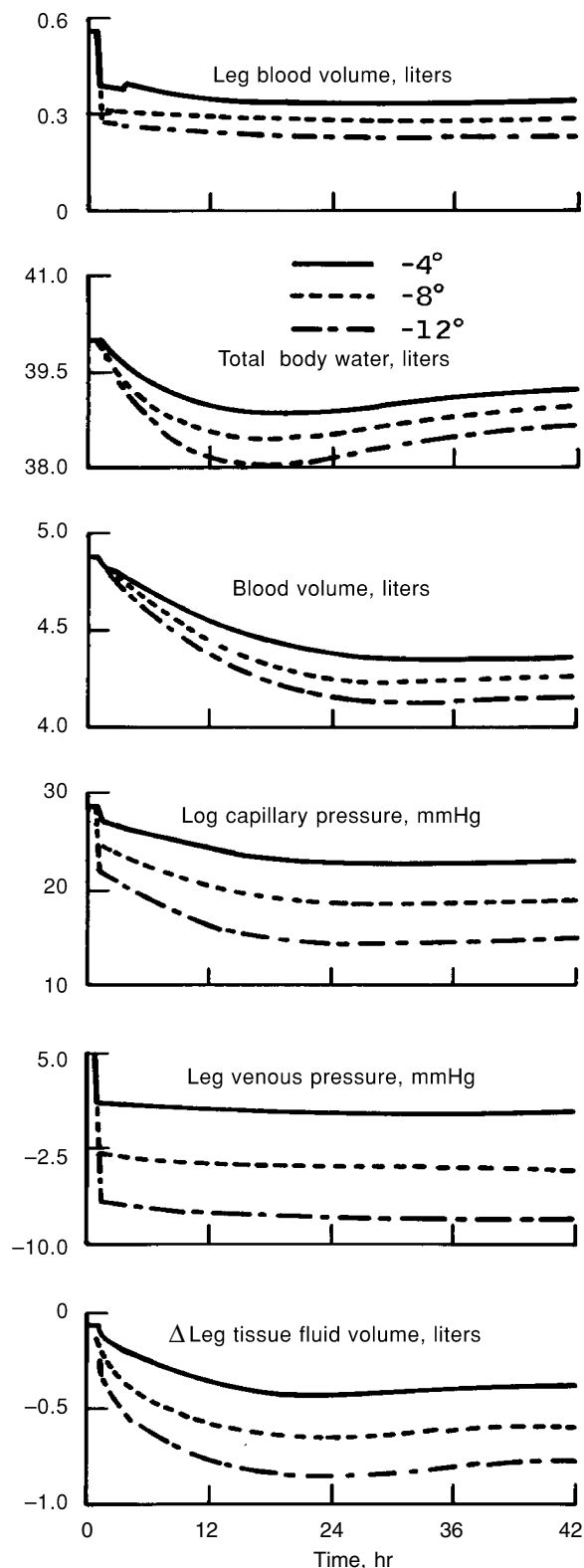
Figure 9-35. Sensitivity analysis of anti-orthostatic simulation: Influence of angle of tilt.

these investigations were useful for validating the technique for simulating head-down tilt. The first of these [34,74] concerned a 24-hour tilt (–5°) and the second study [84] was a head-down bedrest (–6°) for 7-days. Thus, it was possible to study both a short-term and long-term anti-orthostatic bedrest response by comparing model behavior with experimental data. All of the results shown here were performed with the modified version of the Guyton model.

As was true in the studies of supine bedrest and water immersion, head-down tilt is characterized by an acute shift of blood from the legs into the central circulation. The physiological response that accompanies this maneuver, the fluid-shift hypothesis, has been discussed in detail in Chapter 5 (in particular see Figs. 5-15 to 5-17). While most of the acute changes predicted by theory are reflected in the model simulations, they had been difficult to verify experimentally until the studies of Nixon and Blomqvist [34,74].

9.7.5.1 24-Hour Head-Down Tilt Study

9.7.5.1.1 *Simulation.* Computer simulations of the first 24-hours of 5° head-down tilt are shown in Fig. 9-36. These results demonstrate an expected behavior for a variety of fluid volume, hemodynamic and renal-endocrine parameters based on the fluid-shift hypothesis. The initial response (the "acute stress phase") is in accord with the predictions in Fig. 5-15. The loss of fluids from the legs during head-down tilt is closer to that seen in spaceflight than was the case for supine bedrest (see Fig. 9-10). Accompanying the headward shift of leg fluid, there are increases in central blood volume which leads to increases in circulatory pressures, stroke volume and cardiac output, a decrease in heart rate (demonstrating the altered sympathetic outflow) and alterations of the renal-regulating hormones (including ADH, aldosterone, angiotensin and natriuretic factors). The increase in renal water and salt excretion is ultimately expressed as a decline in extracellular fluid, blood volume and total body water.

An interesting aspect of this simulation is the so-called "rebound" effect, after the first hour or two, in which most of the circulatory variables reverse direction. Except for fluid volume changes, which remain depressed, all other variables examined in Fig. 9-36 exhibit a transient biphasic behavior, with a return to baseline. It is particularly noteworthy that in several instances these quantities are predicted to eventually overshoot (or undershoot) baseline conditions. For example, venous pressure, stroke volume, cardiac output, ADH, angiotension and aldosterone appear to reverse direction at the end of the 24-hour period compared to their values during the acute stress phase. Therefore, during the first few hours of head-down tilt, the model predicts a situation similar to that predicted by the fluid-shift hypothesis (Fig. 5-15). But after about 12-hours, while one might find a reduced blood volume as predicted, most of the other elements of that hypothesis might show measured values in *opposite* directions to that predicted on theoretical grounds (see Figs. 5-15 and 5-17).

The simulation analysis, therefore, demonstrates the importance of considering the dynamic properties of regu-
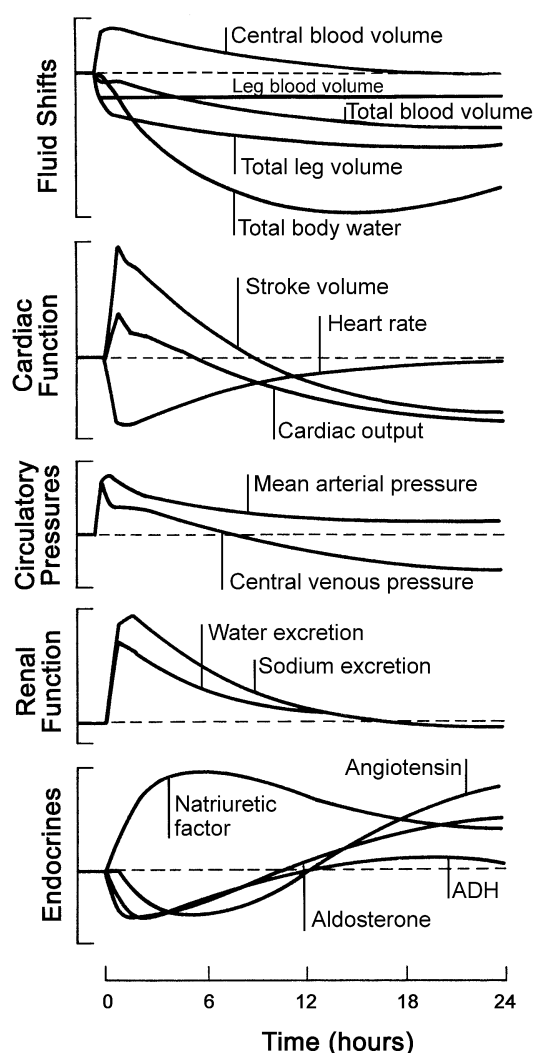
Figure 9-36. Simulation of head-down tilt (-5°) using the modified circulatory model. Values have been omitted from the ordinate for clarity and in order to emphasize the general behavior of the dynamic response for a variety of variables. Comparison should be made with experimental results of Figs. 9-37(a) and 9-37(b). Quantitative values are provided in Table 9-9.

latory systems in order to explain otherwise unexpected or counterintuitive results. For example, if measurements during head-down tilt were performed only after 12-hours, the model predicts that an investigator would find angiotensin levels elevated, renal excretion stable, or venous pressures below normal. These results might appear paradoxical in the face of presumed central hypervolemia and at odds with the concepts outlined earlier. Such "paradoxical" findings, have in fact characterized many previous bedrest and spaceflight studies [85,86]. The simulation analysis suggests that rather than invalidating the theoretical expectations, these types of results merely indicate that earlier and more frequent measurements should have been performed in order to capture the acute biphasic phenomena. In other words, the hypothesis diagrams of Figs.

5-15 to 5-17 (typical of those found in the literature) are really a static picture representing only the acute primary responses to headward fluid shifts; a more realistic dynamic analysis would allow for secondary changes that may cause a reversal of direction in various parameters.

9.7.5.1.2 *Comparison of Model and Data.* Validity of the computer simulations was assessed by comparing the model responses with the experimental studies of Blomqvist and co-workers [34]. A graphical schematic summary of that study has been reproduced from a published report [74] in Fig. 9-37(a) (fluid-shifts and renal-endocrine responses) and Fig. 9-37(b) (hemodynamic responses). Comparing Figs. 9-36 and 9-37, it can be observed that the general behavior of the model's responses is remarkably similar to the experimental findings.

The experimental response to head-down tilt confirms the simulation results for the major hemodynamic, renal and endocrine parameters, in that most of the changes return to control levels within a 24-hour period. It appears that cardiovascular and blood volume regulation was achieved in the human subjects in a manner suggested by a more detailed analysis of the model; that is, by a combination of renal diuresis, transcapillary filtration, accom-
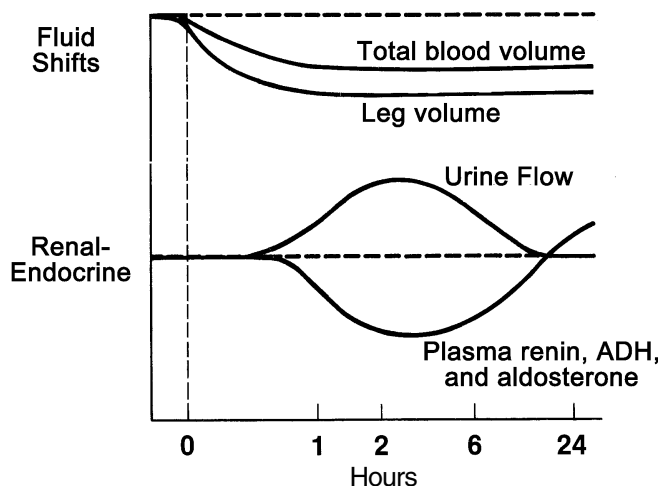
Figure 9-37(a). Experimental fluid-shift and renal-endocrine responses of human subjects to 5° head-down tilt. Idealized responses reproduced from Blomqvist and co-workers [74]. The abscissa has a logarithmic-like scale.
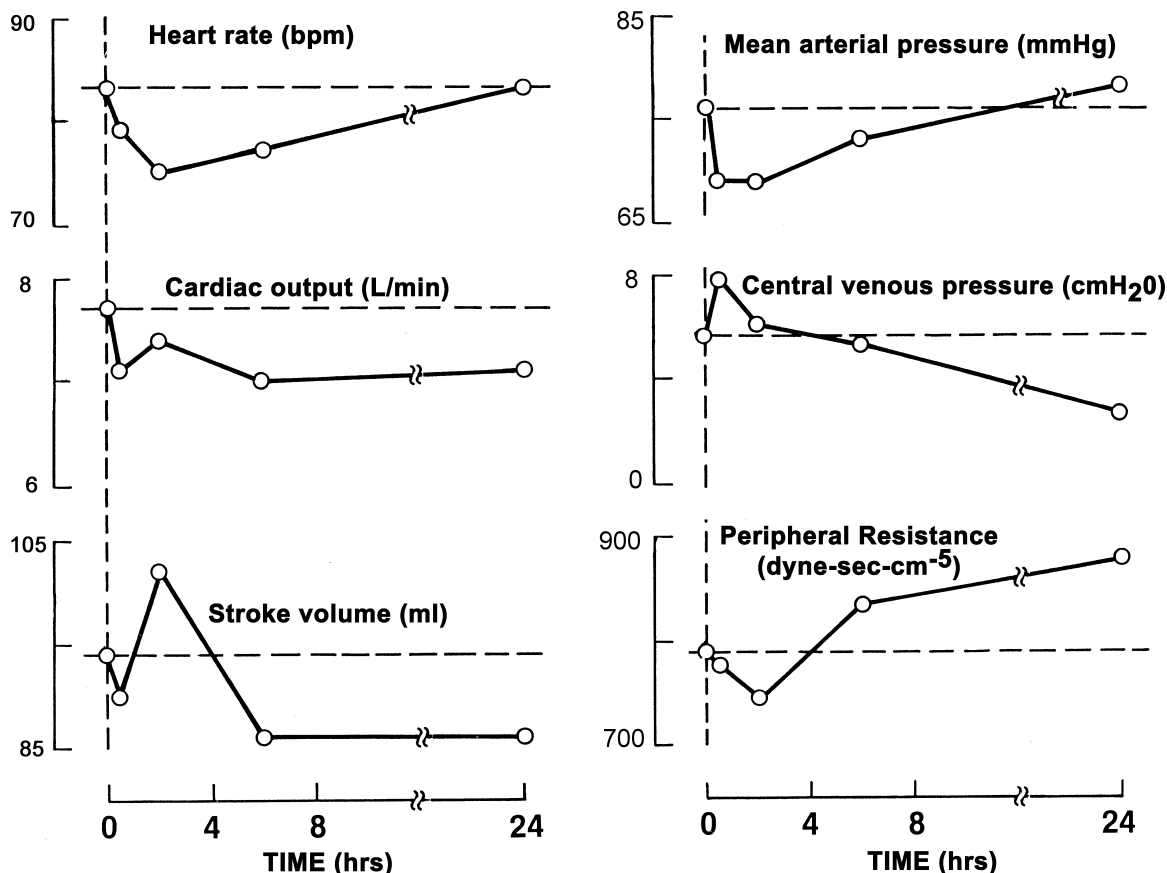
Figure 9-37(b). Experimental hemodynamic responses of human subjects to 5° head-down tilt. Data from Ref. [74]. Compare with model response in Figs. 9-36 and 9-38 (for peripheral resistance).

Table 9-9. Comparison of Simulation and Experimental Response for 24-hour Head-Down Tilt (-5°) Study.

Quanity	Value @ 24-hours Compared to Control	
	Head-down tilt*	Model
Fluid shifts:		
Total body water	−1300 ml	−1130 ml
Leg volume	− 900 ml	− 710 ml
Leg blood volume	nd	− 256 ml
Leg interstitial volume	nd	− 454 ml
Total blood volume	−425 ml	− 563 ml
Hematocrit	+ 7.5%	+12.5%
Urine rate, 1st 8hr/24 hr	127%	190%
Hemodynamics:		
Cardiac output	−7.8%	−11.1%
Stroke volume	−8.5%	−9.8%
Heart rate	0%	+1.4%
Arterial pressure	+3.7 mmHg (+ 4%)	+2.6 mmHg (+3%)
Central venous pressure	−2.4 cm H_2O (−49%)	−0.5 cm H_2O (−9%)
Left atrial pressure	nd	−0.7 cm H_2O (−49%)
Peripheral resistance	+11.3%	+16%
Hormones:		
Angiotensin	+25%	+27%
Aldosterone	+35%	+17%
ADH	+57%	+ 3%
Natriuretic factor	nd	+14%

nd = not determined
* Data from [Refs. 34,74]

modation by vascular capacitance elements and a reduction in blood volume, associated with a transient suppression of volume-regulating hormones. At the end of the experimental period, many of the observed quantities exhibited a deviation from control values and these changes were similar to those predicted by the simulation, at least in direction if not in magnitude (see Table 9-9).

The early rise in urinary excretion noted in the experimental study was also observed in the simulation (i.e., compare Figs. 9-36 and 9-37(a)). Also, the model succeeded in differentiating between the eventual fall below control in venous pressure at a time when arterial pressure was elevated (at 24-hours). Finally, the interesting biphasic behavior of the ADH, aldosterone and angiotensin hormones was seen in both experimental and simulation studies (see Chapter 9.8 for a detailed analysis). The enhanced activity of a natriuretic factor, predicted by the simulation, was not measured experimentally.

Blomqvist's studies were the first reported observation, during a hypogravic type of maneuver, that the renal-regulating hormones return to and overshoot, their control values during a 24-hour period. It was gratifying to us to note that this phenomenon of suppression, recovery and overshoot was predicted by computer-model simulations a number of years prior to these validation experiments [87]; (see Chapter 9.2.1). It is our belief that understanding such a transitory response to central hyper-volemia is essential to reconcile data from short-term and long-term hypogravic studies [88]. Specifically, short-term studies such as water immersion indicated hormone suppression, while results from Skylab and certain longer-term bedrest studies demonstrate that angiotensin and aldosterone become elevated over days or weeks. Rather than viewing this as conficting results, the model behavior suggests they are simply highly dynamic points on a time-continuum.

In preliminary simulations of head-down tilt, the model predicted that ADH suppression was short-lived (i.e., less than 30-minutes) before increasing above control in response to a rising plasma sodium concentration(see Fig. 9-3(b). An elevation in either ADH or sodium concentration is unrealistic during acute hypogravic stress in light of more recent studies [11,34,41,48] which indicate that both quantities diminish, for at least a number of hours. Two model modifications were introduced that produced a more realistic response. First, a renal-natriuretic factor was introduced which permitted plasma sodium concentration to be maintained near or below normal levels (see Fig. 5-30). Secondly, the sensitivity of ADH to venous pressure was increased by a factor of 15 relative to that of plasma sodium concentration, as suggested by recent studies [26a, 89] (see Chapter 9.8). As a result of these modifications, in response to head-down tilt, ADH diminished for several hours until central venous pressure returns

to normal (Fig. 9-36) in agreement with the experimental data (Fig. 9-37(b)).

The longer-term changes in all of the measured hemodynamic variables were identical in direction and close to the magnitude predicted by the model (compare Fig. 9-36 with 9-37(b)). In most cases, the short-term changes were predicted by the model as well. The simulated peripheral resistance is not shown in Fig. 9-36 but rather in Fig. 9-38(bottom); there is close agreement with the experimental findings shown in Fig. 9-37(b). However, a transient dip in arterial pressure and the failure of cardiac output to rise, during the first several hours in the human subjects, could not be explained by the researchers and was not predicted during the simulation. Several of the hemodynamic responses are particularly intriguing. At 24-hours after head-down tilt, both the model and experimental results demonstrate an elevated arterial pressure and peripheral resistance and a diminished cardiac output and venous pressure (Table 9-9, Figs. 9-36, 9-37(b) and 9-38). A detailed model analysis was conducted to determine the cause of these changes (especially the fall in venous pressure) that were not immediately apparent or expected [82]. The following conclusions were drawn from that analysis:

a) The main cause of the net reduction in venous pressure back to the baseline is the loss of blood volume
b) The main cause of the venous pressure declining below the baseline is a rise in peripheral resistance
c) Stress relaxation of the large veins modulated the rise in venous pressure but was not a major contributing factor to the fall in venous pressure.

These conclusions led to a more detailed examination of the factors that caused peripheral resistance to increase. Total peripheral resistance in the Guyton model is proportional to four factors: a) an autoregulatory factor which attempts to regulate blood flow according to the oxygen needs of the tissue, b) a viscosity factor which increases frictional resistance to flow, c) an angiotensin factor which is proportional to angiotensin levels (angiotensin is a potent vasoconstrictor) and d) an autonomic factor which is a signal from the baroreceptors. The dynamic influence of these various factors on resistance during a head-down tilt simulation is shown in Fig. 9-38. Note that different factors appear to dominate the control of resistance at different time periods. The autoregulatory factor and the autonomic factor respond in opposite directions to the increased flow to the tissues and increased arterial pressure immediately following head-down tilt; they essentially cancel out each other's influence. The hemoconcentration, which develops during head-down tilt secondary to rapid plasma volume losses, alters the oxygen supply-demand balance at the tissue level to favor tissue hyperoxia. This in turn causes an autoregulatory increase in resistance, thereby reducing blood flow and returning the tissue oxygen supply toward normal. An additional influence of hemoconcentration on resistance is due to the viscosity effect that increases frictional resistance. Angiotensin increases above normal following 12-
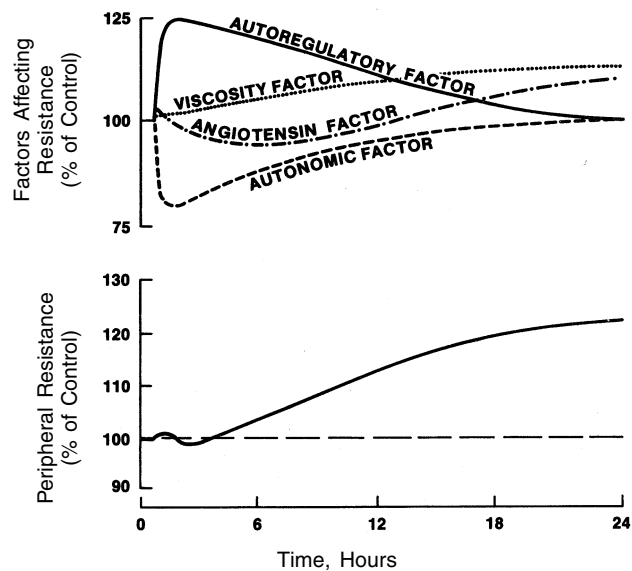
Figure 9-38. Simulation of 5° head-down tilt showing the total peripheral resistance response. Peripheral resistance in the Guyton model is computed as being proportional to the four factors shown in the top graph.

hours of simulated head-down tilt and this has a vasoconstrictor effect as noted above.

Whether or not the responses in Fig. 9-38 are quantitatively accurate is not of major concern at this juncture. It is certainly relevant that increases in hematocrit, angiotensin and total peripheral resistance have been noted in supine bedrest and head-down tilt [34,84]. Peripheral resistance has been measured to increase 15–20% in these cases in excellent agreement with the model predictions. Although no definitive explanation for the resistance changes had been offered (at the time) it is well known that exercise conditioning decreases resting total peripheral resistance, so one might infer the opposite effect during hypokinesia or deconditioning.

9.7.5.2 One Week Head-Down Bedrest
9.7.5.2.1 *Simulation.* As indicated above, both the simulation and experimental results of head-down tilt indicate that many of the physiological disturbances and regulatory influences have not stabilized at the end of 24-hours. In order to determine the behavior of these parameters over longer periods, simulations of a 7-day head-down tilt were performed and were then compared to the experimental findings [84]. Simulations of the 7-day head-down bedrest study were performed in a similar manner to the 24-hour study. That is, the angle of tilt with respect to the horizontal was set to –6° (rather than –5°) and the responses were observed over a period of 7 simulated days. In addition, a decrease in dietary intake similar to the *ad libum* human diet was imposed in the simulation. The average reduction in dietary intake was close to 28%. (The actual reduc-

tion for water, sodium and potassium in the diet, by weight, was 24%, 29% and 30% respectively). Model parameters controlling dietary water, sodium and potassium were reduced by these amounts.

9.7.5.2.2 *Overall Response*. Table 9-10 lists a number of important physiological parameters (similar to those presented in Table 9-9 for the 24-hour study) and their simulated changes from control measured at the end of 7-days. Also shown, for comparison, are the corresponding experimentally measured changes. The simulated responses are in reasonable qualitative agreement with observations in the human subject. Other than using the initial parameters mentioned above, there was no attempt to optimize the simulated response.

9.7.5.2.3 *Fluid Volumes and Hemodynamics*. The acute shift of blood and tissue fluid from the legs to the central circulatory region leads to regulatory changes and produces the long-term fluid and hemodynamic responses shown in Fig. 9-39. The model predicts that most of these disturbances stabilize after the second day. At this time, the legs have lost about 650 ml from both intravascular and interstitial sources while the plasma volume decreases by about 550 ml. Associated with these fluid losses is an almost complete correction of central blood volume. Cardiac output and venous pressure (reflected by end-diastolic volume) eventually reach a level that is below control levels while arterial pressure essentially shows no change. These responses are a continuation of the trend observed at the end of the 24-hour head-down tilt study (compare Figs. 9-36 and 9-39).

During head-down tilt, the model predicts that a significant fraction of the fluid in the interstitial compartment of the leg is drained into the circulation (see Fig. 9-35, bottom curve). However, an unexpected prediction was the loss in upper body interstitial fluid (Fig. 9-40, second from top, solid line). Conventional wisdom suggests that headward fluid shifts should promote transcapillary filtration and thereby an increase in central interstitial fluid. (This is based in part on the reports of puffy faces and head congestion during spaceflight). However, computer analysis of this event suggests that as plasma volume diminishes, plasma protein concentration becomes elevated which favors transcapillary fluid *absorption* from the interstitium. This phenomena is only partially offset by the tendency of the heightened blood pressure to filter fluids in the opposite direction. The resultant of these two opposing transcapillary forces is not easy to predict intuitively and one should use this model prediction of a temporary net inward filtration to encourage experimental verification. However, it is not possible to experimentally measure interstitial fluid of the upper body separately from that of the legs in the human subject. Therefore, the model was used to examine these quantities in greater detail. Model analysis of this phenomenon was first conducted in the simulation of water immersion where it was followed for only 8-hours (see Fig. 9-26) while in Fig. 9-40 the simulation duration is 7-days. By extend-

Table 9-10. Comparison of Simulation and Experimental Responses for 7-Day Head-Down (-6°) Bedrest Study

Quantity	Value @ 7-days Compared to Control	
	Head-down Bedrest*	Model
Fluid Shifts		
Total Body Water	–600 ml	–805 ml
Blood Volume	–400 ml	–650 ml
Plasma Volume	–240 ml	–550 ml
Red Cell Mass	–180 ml	–100 ml
Leg Volume	–460 ml	–650 ml
Hemodynamics		
Cardiac Output	–9.5%	–10.7%
Arterial Pressure	+9.5%	0%
Venous Pressure	–2.0% (EDV)	– 8.6%
Peripheral Resistance	+14.0%	+11.0%
Renal Function		
Water Excretion	–39%	–31%
Sodium Excretion	–39%	–33%
Potassium Excretion	–13%	–16%
Electrolytes:		
Plasma [Na^+]	–3.0 meq/l	–6.7 meq/l
Plasma [K^+]	–0.5 meq/l	–0.5 meq/l
Total Body Potassium	ND	–4%
Plasma Endocrines:		
Angiotensin	+116%	+55%
Aldosterone	–28%	–24%
ADH	–65%	–37%

*Data from Ref. [84]
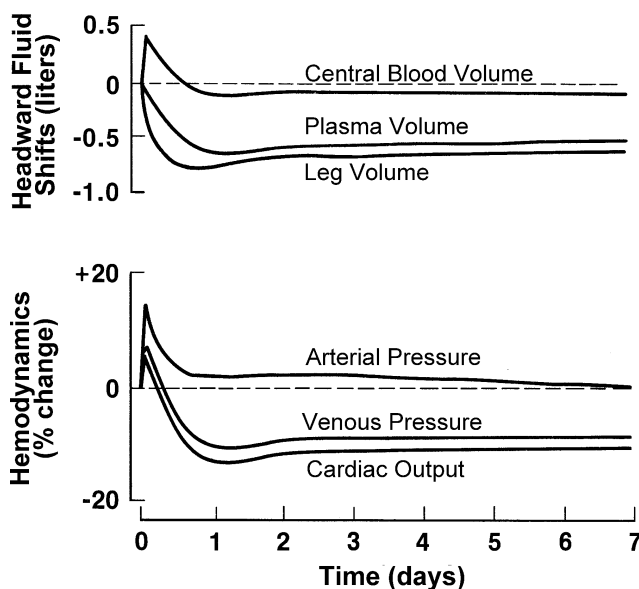
Figure 9-39. Simulation responses of fluid shifts and hemodyamics during head-down bedrest.
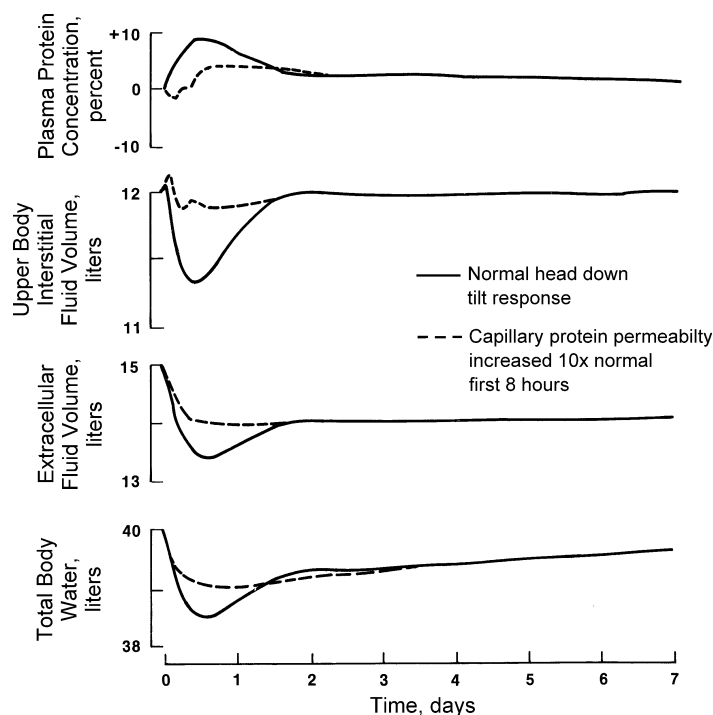
Figure 9-40. Effect of acute increase in capillary permeability on head-down bedrest response.

ing the time period a 700 ml decline followed by a dramatic rebound of upper body interstitial fluid is revealed which restores that compartment's fluid volume before settling at a normal stable level. The rebound occurs as a result of a reduction in lymph flow, normalization of plasma colloids and readjustments of the pre/post capillary resistances to favor filtration.

There is no evidence to confirm the veracity of this simulation, but such swings in fluid volumes have never been reported. Also, it has been shown that water immersion results in dilution of plasma colloids [47] and not their concentration. (No such measurement was available for head-down bedrest). Therefore, a hypothesis was formulated that suggested that plasma colloids would not concentrate and upper body interstitial fluid would not deplete so readily, if transcapillary protein permeability were increased. The rational for this hypothesis is provided in a previous section (Chapter 9.5.2.4). The hypothesis was evaluated by permitting the protein permeability in the capillaries to increase 10-fold from its resting value during the first 8-hours of head-down bedrest (when pores in the capillary wall would most likely be stretched open); thereafter it was returned to normal. The most obvious difference due to this hypothesis is to significantly minimize the large swings in interstitial fluid volume and plasma colloids, thereby reducing the magnitude of total body water depletion. These changes affected the response during the first two days. After that time the effects of the early permeability changes had disappeared. In addition to producing a more plausible simulation of water immer-

sion and head-down bedrest, a transient increase in protein permeability of the capillaries was claimed to be responsible for the reduction in plasma volume during spaceflight.[UPDATE#2]

9.7.5.2.4 *Endocrines and Electrolytes*. Alterations of renal-endocrine function and electrolyte metabolism have been the subject of various spaceflight investigations because they provide important clues about fluid volume control during weightlessness. A number of these quantities measured during the 7-day head-down bedrest are indicated on the left side of Fig. 9-41. They have been placed in the categories: plasma electrolytes, plasma endocrines and renal excretion. The plasma electrolytes are important determinants of the secretion rates of renal-regulating hormones (ADH, angiotensin and aldosterone) which in turn are capable of exerting a powerful influence on renal excretion of fluids and electrolytes. For example, ADH is influenced by and provides renal control of, plasma sodium concentration. These cause and effect relationships are discussed in Chapter 5 and are indicated in Figs. 5-8 and 5-11.

The data shown in Fig. 9-41 indicate several changes, which at first glance, appear paradoxical. For example, there is a decrease in aldosterone, which is associated with a diminished plasma sodium concentration and with a significantly elevated angiotensin level. In addition, urine flow is diminished in spite of a reduced level of ADH. There is also a reduction in sodium excretion, which is associated with a decrease in aldosterone. In each case, the normal relationships between hormone, electrolyte and renal excretion appear to be violated (see Fig. 5-11). Nevertheless, these effects, observed in the human (Fig. 9-41, left side), have all been reproduced in the simulation of head-down bedrest (Fig. 9-41, right side).

When a model is able to predict an unexpected event that turns out to be observable, examination of the model is warranted to help identify the true causal factors. Such an analysis has suggested that in the face of competing factors the following mechanisms prevail [82]:

a) Of the two factors that can normally reduce ADH (an increase in atrial pressure and a decrease in plasma sodium), the most plausible candidate during long-term head-down bedrest is the measured decline in plasma sodium.

b) Plasma potassium was the only one of three aldosterone-controlling factors in the model to change in the appropriate direction to explain the measured decline in aldosterone.

c) The decline in plasma sodium can also explain, in theory, the increases of angiotensin observed in the study.

Thus, this analysis is able to suggest how changes in plasma electrolytes can account for, both qualitatively and quantitatively, the long-term changes in renal-regulating hormones observed during one week of head-down bedrest.

9.7.5.2.5 *Renal Excretion.* The fluid and sodium renal output responses of the model, as shown in Fig. 9-41, can
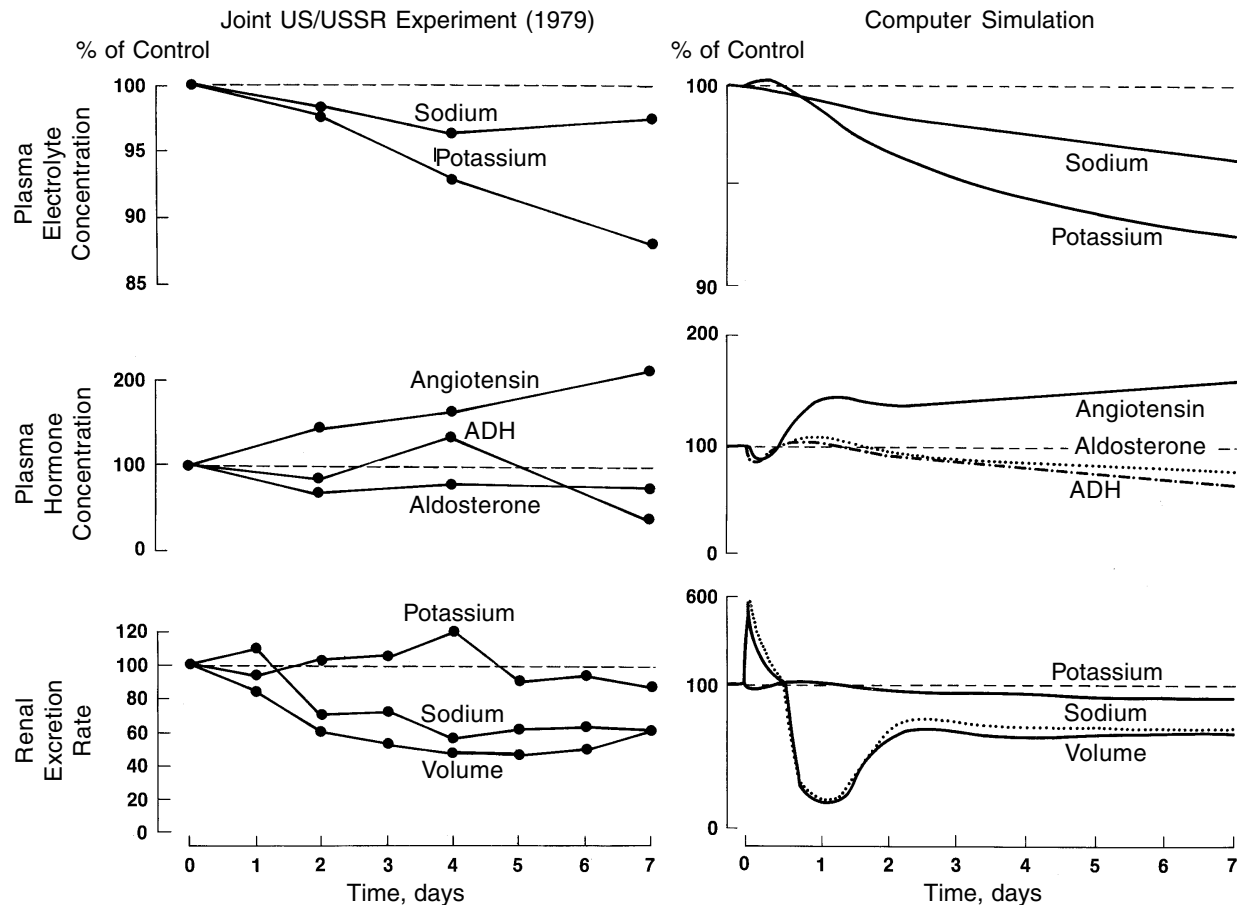
Figure 9-41. Electrolytes, hormones, and renal excretion during head-down bedrest. Left side shows experimental data. Right side shows simulation. In the simulation, like in the human subjects, the water, sodiumk, and potassium dietary intake was reduced 24%, 29%, and 30% respectively. In addition, a potassium "leak" from the cells (20% of the pre-bedrest dietary potassium), was imposed, representing muscle atrophy.

be conveniently separated into an acute response and a longer-term response. Urine measurements were pooled over 24-hours; thus, the models acute response cannot be confirmed directly but can only be inferred from the 24-hour pooled samples. Accordingly, the distinct diuresis does not appear to be confirmed in the human subjects, but a natriuresis was measured. After 2-days of bedrest, the longer-term phase indicates that a near steady-state plateau is reached during the simulation at a reduced level for the three renal substances shown, in complete agreement with the data. These results collectively indicate that the model's prediction of the acute response was not as valid as its prediction of the longer-term response.

Renal excretion, it appears, cannot be explained on the basis of hormonal mechanisms. The measured (and simulated) decreases in both ADH and aldosterone would normally be expected to enhance the excretion of water and sodium and not the reverse as shown in Fig. 9-41. In order to correctly simulate the experimental plasma electrolytes, hormone levels and renal excretion data, it was necessary to impose the dietary restrictions for fluid, sodium and po-

tassium that were measured for the human subjects (see Chapter 9.7.5.2.1). The steady-state renal excretion of the model exactly balances dietary intake. Thus, in chronic situations when dietary factors have been altered, renal regulation of water, sodium and potassium in the mathematical model is controlled by non-hormonal mechanisms, such as plasma electrolytes and renal hemodynamics.

9.7.5.2.6 *Effect of Diet.* The model results have, therefore, suggested the importance of dietary intake in causing the observed long-term changes in renal-endocrine behavior and fluid-electrolyte metabolism during the bedrest study. Figure 9-42 demonstrates this effect more clearly. The effect of dietary changes alone can account for the changes seen at the end of 7-days of head-down tilt with dietary restriction. On the other hand, the acute effects of the first 2-days predicted by the model are peculiar to head-down tilt and are not affected by alterations in diet. It is common to find significant reductions in dietary allotment during bedrest studies, so this conclusion may have applicability that is more general.
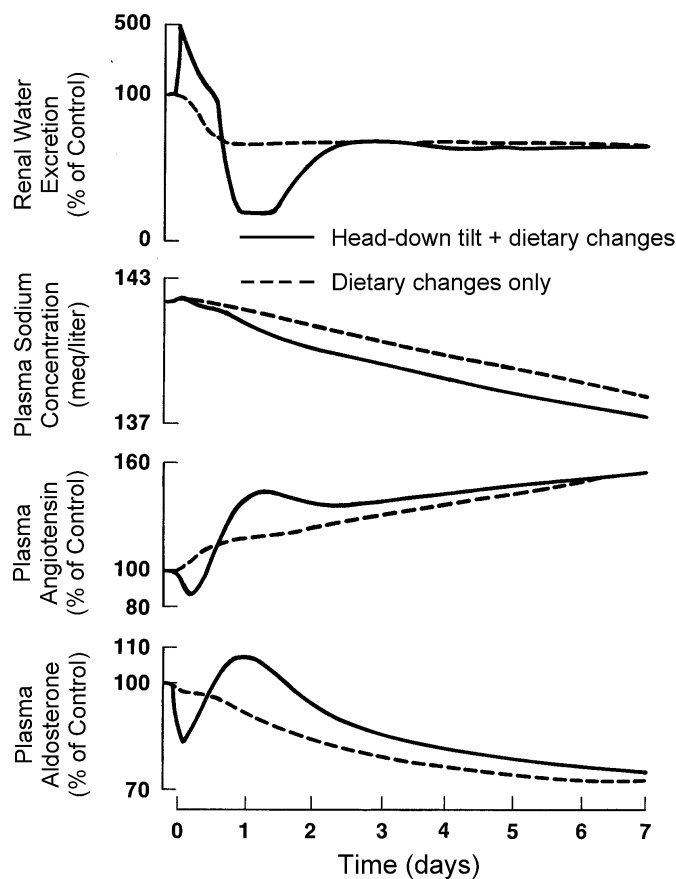
Figure 9-42. Effect of dietary change on head-down bedrest. Solid lines indicates head-down simulation including dietary changes. Dashed lines indicate simulation of dietary changes alone. Dietary changes consisted of: fluid intake (-30%), sodium intake (-30%) and potassium intake (-15%).

9.7.5.2.7 *Potassium Metabolism*. A interesting feature of the renal excretion data shown in Fig. 9-41 (left side) is that renal potassium losses in the human are relatively unaltered in comparison to water and sodium excretion. This occurs in spite of the fact that the dietary intake of all three substances was reduced *in the human subjects* by approximately the same amount, i.e., 25 to 30%. (Normally, if a substance that is normally excreted in the urine has its intake reduced, the urine excretion at steady-state is reduced by a similar amount). It is also interesting that, when the true change of −30% dietary potassium was first imposed *on the model*, it led to reductions in potassium excretion that were unacceptably low (not shown) compared to the data. What can be responsible for this behavior? One likely possibility is that, in the human studies, intracellular stores of potassium have been mobilized because of muscle atrophy induced by bedrest inactivity. Cell potassium could thereby, "leak" into the extracellular fluids and eventually be excreted via the kidneys. Thus, there are two effective routes of potassium input into the

extracellular fluids: from the diet and the cell. The effective sum of these two sources would influence the renal excretion of potassium.

This hypothesis was examined in the model. It was important to first estimate the magnitude of the contribution of cell potassium to renal excretion in the human subjects. This was done by solving a mass balance equation for potassium entering and leaving the extracellular fluid compartment. At steady-state, the net potassium balance must be zero, thus:

$$K^+ \text{ Balance (extracellular)} = 0$$
$$= K_{diet} + K_{cell} - K_{renal-} - K_{fecal+sweat}$$

where K_{diet} is the daily amount of dietary potassium, K_{renal} is the daily potassium renal excretion amount, $K_{fecal+sweat}$ is the daily amount of potassium leaving the body from fecal and sweat routes and K_{cell} is the daily amount of potassium leaking from the cellular compartment due to muscle atrophy. In the pre-bedrest control period, K_{diet} and K_{renal} are known while K_{cell} is assumed to have a zero value; this allows a calculation for $K_{fecal+sweat}$. The equation is again solved for the steady-state bedrest period in which diet and renal potassium values are measured quantities and $K_{fecal+sweat}$ is assumed to have the same value as pre-bedrest; thus, a value for K_{cell} may be computed. This value of K_{cell} was calculated to be 20% of the pre-bedrest dietary intake of potassium per day. By multiplying this value by 7-days a total cell potassium loss was derived. This value was then used in the model to simulate the consequences of muscle atrophy.

A "potassium leak" was applied in the model, which allowed the total cell potassium loss calculated, as described above, to be removed from the cell compartment over the 7-day bedrest period in an exponential manner. In Chapter 5.4.2.2, the simulated release of cell potassium was examined in detail, revealing sequential changes in plasma potassium concentrations, hormones, excretion and fluid volumes (see Figs. 5-25 and 5-26). The net long-term effect of this sequela, in the model, is a permanent loss of body potassium and a reduction of intracellular water. Body potassium was not measured during the head-down tilt study, but a loss of about 400 ml intracellular fluid could be inferred from the human data.

In terms of the model simulation, the total amounts from the two routes for changing extracellular potassium (dietary and cellular) can be lumped together into the dietary input. Thus, if dietary potassium were normally 100 meq/day, the value during bedrest would fall by 30% or 30meq (as measured in the humans). If cellular potassium achieved the value of 20 meq/day (as calculated above), a dietary change of −10 meq/day (i.e., −30 + 20 = −10) would "effectively" represent both potassium pathways. For convenience, this is the approach used in the simulations shown in Figs. 9-41 and 9-42. The alternative approach of having a true cellular potassium leak was later examined and appeared to be even more realistic. Primarily, it permits the potassium dietary intake of the model to be reduced to more realistic levels without significantly
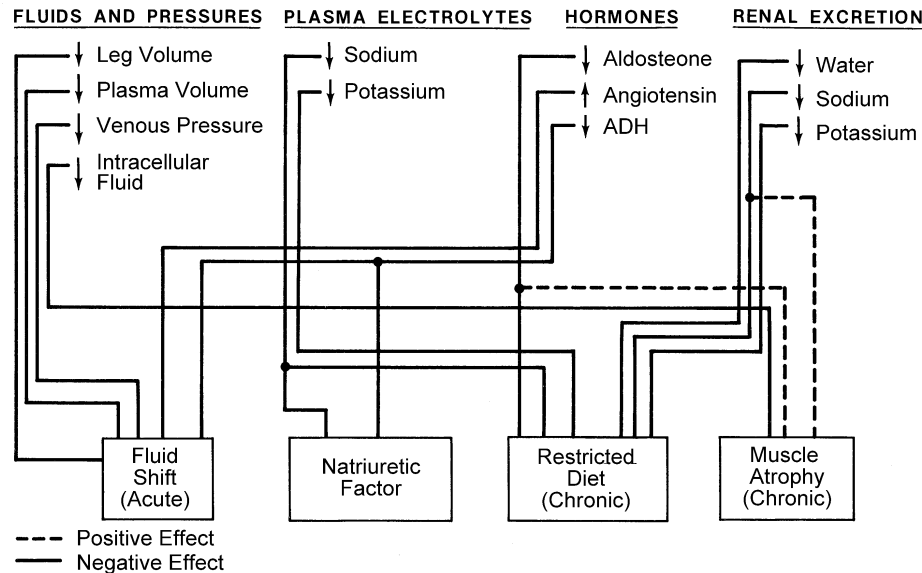
Figure 9-43. Hypothesis for head-down bedrest observations. Experimental findings of interest are shown at top. Acute phase can be explained by fluid shifts (left box), while long-term phase involves accounting for factors shown in the three boxes to the right.

changing the plasma potassium levels or potassium excretion rates which were already in good agreement with the data in the original simulations. Also, intracellular fluid volume becomes more stable in its dynamic behavior.

In summary, the invocation of a muscle atrophy-induced potasium loss from the intracellular compartment resulted in a more accurate simulation of long-term head-down bedrest (see Ref. [82] for further details of this analysis).

9.7.5.3 Summary: Head-Down Tilt.
Once the modifications were made to the model regarding the venous and leg tissue compartments, short-term head-down tilt was adequately simulated by simply adjusting the angle of tilt. Longer-term head-down bedrest was more complicated and required the addition of several other factors that were hypothesized to have an important influence. Figure 9-43 illustrates the model hypotheses that were invoked in the head-down bedrest study (bottom of figure) in order to reproduce the set of experimental findings (top of figure). These hypotheses included accounting for a natriuretic factor, a restricted dietary intake and muscle atrophy in addition to the simple fluid shifts of the acute phase.

The study of short-term and long-term head-down tilt provided the most useful picture of the dynamic nature of the hypogravic adaptation processes that we have found to-date. According to the model and experimental responses, during the first hour or so of head-down tilt, there are significant disturbances in the fluid-regulating systems which are exemplified by internal fluid shifts and elevated pressures and flows in the thoracic circulation. This is followed by a short period in which feedback mechanism (both active and passive) act to correct these disturbances. Thus, with the exception of the fluid com-

partments which remain suppressed (i.e., leg volume and total blood volume), all other variables examined exhibit a transient biphasic behavior during the first 24-hours, with a return toward baseline. However, it has also become clear that the body appears to be seeking a new baseline, that is, the head-down position seems to alter the "normal" physiological state. This is demonstrated by the fact that the longer-term head-down bedrest does not result in a state identical to the original pre-tilt state. Offsets from normal were noted for blood pressures, flow resistances, plasma electrolytes, hormone levels, renal excretion and so on. The underlying causes of a number of these long-term biphasic changes were not always obvious and were in fact counterintuitive. They have become more understandable by examining the intricate model relationships and by testing hypotheses that often required altering these relationships.

In particular, much of the data can be explained by a shift from short-term volume control to long-term metabolic control. Volume control refers, in general to regulation of extracellular fluid volume by thirst and renal mechanisms and in particular, to the vascular control systems that respond to acute headward fluid shifts. Metabolic control, in this case, is taken to mean those events that directly influence the metabolism of dietary substances and are affected by physical activity. In these model simulations, the definition of metabolic control becomes more specific and refers to the consequences of alterations in dietary intake, sweat rates, oxygen uptake and intracellular loss of electrolytes resulting from muscle atrophy. A secondary effect includes the elevated hematocrit and resulting enhancement of oxygen supply. These phenomena are offered as explanations to account for some of the

reported differences between acute and chronic zero-g analog studies as suggested by Fig. 9-43. This thesis is explored in greater detail in Chapter 9.8.

A number of recommendations for improving the simulations of head-down tilt can be found in Appendix G. Because the modified Guyton model has been validated for hypogravic stress, it can be used for more advanced studies, including development of countermeasures, as described below.

9.7.6 Fluid-Loading Countermeasure Simulation
9.7.6.1 Introduction. One of the most clinically significant concerns about spaceflight is the orthostatic intolerance that develops during flight and becomes manifest during the return to Earth and subsequent early postflight period. Orthostatic intolerance resulting from bedrest and spaceflight has been addressed in various part of this book (see Chapters 3.2.6.6(a), 7.4, 7.5, 9.2.2 and 9.6). The capabilities of the two cardiovascular models (Croston and Guyton) for simulating orthostasis, providing insight into the mechanisms of orthostatic intolerance and in helping to design a lower-body pressure garment countermeasure have been demonstrated. Also, the impact of orthostatic intolerance on human health and mission success, during reentry from space, has been described in Chapter 7. In this section, the analysis of another countermeasure for ameliorating orthostatic intolerance will be presented – this one based on oral fluid-loading of the circulatory system. Fluid loads will be imposed on the model following a simulation of head-down tilt, mimicking a spaceflight mission.

The replacement of fluids and electrolytes lost during the course of spaceflight using oral fluid-loading is now a common practice for astronauts about to return from space. An improvement in orthostatic tolerance is brought about by a partial reversal of some of the adaptive changes that occurred in weightlessness, especially changes in cardiovascular parameters such as blood volume and blood pressure. The effects are transitory and therefore, fluid loading is generally administered just a few hours prior to re-entry to achieve peak beneficial effects during the re-entry phase. Data from bedrest [91,92], acceleration studies [93] and Shuttle flights [94] provide some evidence of its effectiveness as a countermeasure to cardiovascular deconditioning.

It was demonstrated in Chapter 7 that the loss of blood volume is often a key factor involved in the reduction of orthostatic tolerance observed following exposure to weightlessness or similar one-g conditions such as bedrest. Other factors contributing to this condition include a degraded baroreceptor responsiveness, increased venous compliance and impairment of autonomic signals and catecholemines release, but the extent of their contributions is only recently becoming understood [90]. Orthostatic intolerance can occur, clinically, without loss of blood volume, but blood volume loss always exacerbates the problem.

The simulation model can be effective in examining this countermeasure, especially since the physiology of fluid loading is not completely understood. Although data is available to show the intercompartment distribution of

fluid loads under normal conditions (see Chapter 3.2.5.3), it is not known how circulatory status is specifically affected by the volume and salt concentration of the fluid load in the presence of re-entry g-forces. As emphasized in Chapter 7.5, it is during the high-g phase of Shuttle reentry where the debilitating effects of orthostatic intolerance are most likely to occur. During administration of fluid loads preceding reentry, it is not known how much of the ingested fluid remains in the circulation and for how long under these conditions. It is also desirable to know the optimum time to administer the fluid load prior to reentry, as well as the effective combination of fluid volume and salt concentration that will maximize blood volume and presumably minimize orthostatic intolerance. The computer simulation studies presented below were undertaken to obtain theoretical answers to questions that were difficult to address experimentally in an operationally-oriented environment.

9.7.6.2 Simulations of Fluid-Loading. Simulations of fluid-loading were performed with the modified Guyton model [95]. This model is superior to the Croston pulsatile model for this purpose because of two reasons: a) it has the capability of realistically adjusting circulatory fluid loads by fluid exchange between the vascular and extravascular compartments and by renal excretion and b) it has been validated to simulate the cardiovascular effects of prolonged hypogravity, a necessary prerequisite for studying fluid loads during postmission return to Earth.

Weightless conditions were simulated by placing the Guyton model in a head-down tilt position of –6°s, identical to the simulations shown previously in Chapter 9.7.5.2. The physiological parameters were allowed to attain new steady levels relative to preflight values by running the model for a period of 3-days. (Although most Shuttle missions last about a week, it was shown that the hemodynamic response does not change significantly after 3-days– see Fig. 9-39). The STS-1 re-entry g-profile with a peak g-force of approximately 1.5 G was used to simulate re-entry g-stress (see Fig. 7-21). The time course of parameter variations was tracked from the beginning of re-entry to touchdown (TD) and 25-minutes thereafter under one-g conditions. The results presented here are limited to the cardiovascular response (although fluid-electrolyte and hormonal systems responses are also generated) since it is the primary determinant of orthostatic intolerance.

The time of ingestion prior to re-entry and the salt concentration of the fluid-load were varied and their influence upon the parameter changes was examined. The volume of fluid-load in all circumstances was one liter, ingested at a constant rate over a period of 10-minutes. This is the maximal amount of fluid-load used by the Shuttle crewmembers. It was not necessary to vary the volume to understand the response patterns as a function of time produced by fluid-loading, since varying the volume has the effect of only amplifying or attenuating the elicited changes in physiological parameters. Thus, the percentage of fluid ingested that remains in the circulation during reentry is a critical quantity that the simulation

provides and it is independent of the total fluid volume ingested.

9.7.6.3 Simulation Results. Simulations were performed with and without fluid-loading. Ingested fluids with three different tonicities were simulated: isotonic, hypotonic and hypertonic, referring respectively to, fluid-load with normal plasma concentration of sodium, fluid-load with no sodium and fluid-load with twice the normal plasma sodium concentration. Figure 9-44 shows the effect of increasing the salt concentration of the fluid ingested 2-hours prior to re-entry. The effectiveness of the countermeasure is judged from this simulation by the amount by which blood volume is restored towards normal. Note that blood volume prior to the simulated mission is 5.0 liters and that after 3-days of simulated hypogravity the blood volume falls to 4.5 liters. During reentry, the blood volume falls approximately another 0.5 liters as a result of capillary filtration in the interstitial compartment of the lower limbs. It is this loss of nearly one liter blood volume from its normal value that leads to orthostatic intolerance during and following reentry. Ingestion of pure water does little to reverse this effect but the effect with hypertonic fluid is much greater.

It is also possible to visualize the effect of the countermeasure on other indices of cardiovascular status such as heart rate, cardiac output and blood pressure. The effectiveness of the countermeasure improved with increasing salt content in terms of restoring the cardiovascular parameters toward preflight levels. Also note that the time course of changes for different salt concentrations was similar for most responses. Since the loss of fluids is not the only causative factor behind spaceflight-induced cardiovascular deconditioning, compensation for fluid loss alone cannot be expected to reverse completely the adaptive manifestation of weightless exposure.

An analysis was conducted to understand the effect of varying the time of ingestion prior to reentry [96]. Moving the fluid intake closer to reentry (less than 2-hours) had the effect of improving the effectiveness of the countermeasure (especially for hypertonic fluids) by moving the responses closer to preflight levels, but the differences were only slight. Ingestion times longer than 12-hours prior to reentry have little impact on the reentry response.

An additional analysis was performed to simulate the addition of a powerful anti-diuretic agent simultaneous with the fluid load [97]. This agent has the effect of blunting the increased renal glomerular filtration rate that follows the fluid load and retain the ingested fluid in the body rather than allowing it to be excreted. This was indeed found to be the case (Fig. 9-45). For example, if blood volume is reduced by 500 ml due to several days of hypogravity, the ingestion of a liter of isotonic saline increases total blood volume by about 150 ml (at the end of 2-hours) and the addition of an anti-diuretic agent can increase this amount by an additional 150 ml. The increase in plasma volume is not greater even if renal excretion is inhibited, because of transcapillary filtration (see Fig. 3-38). While the restoration of plasma volume is not
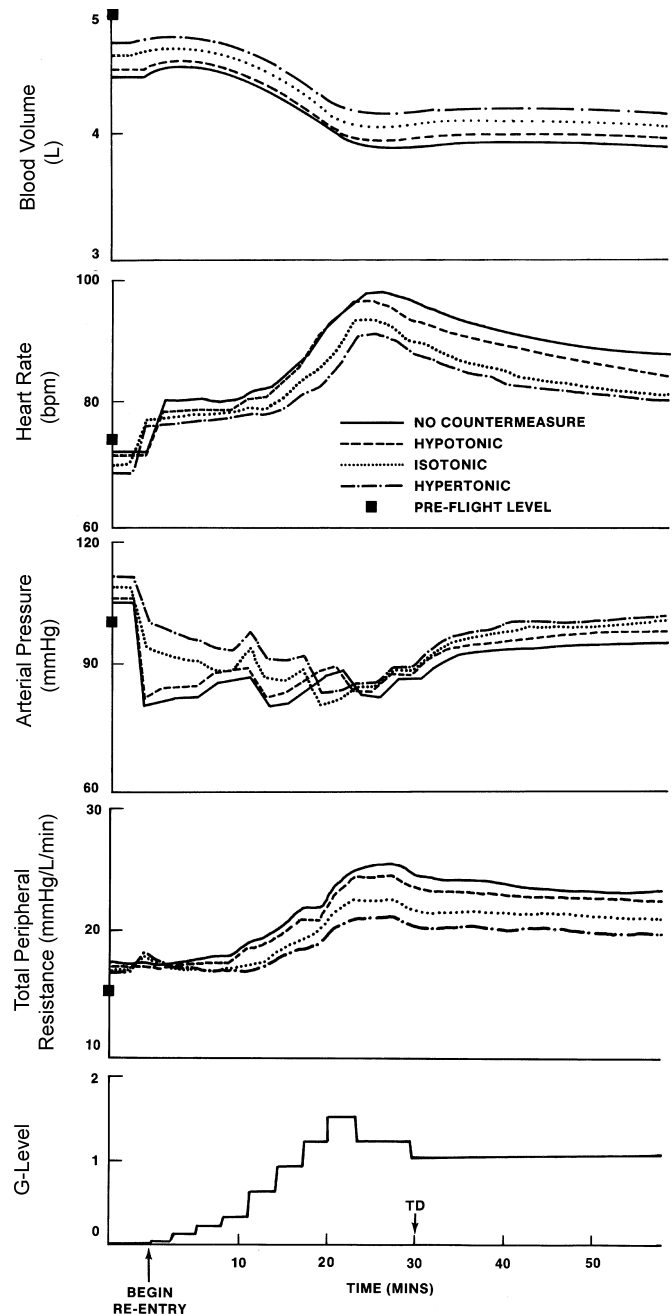
Figure 9-44 Effect of varying the salt concentration of the fluid-load on cardiovascular response during re-entry. Ingestion time is 2-hours prior to re-entry (not shown on these charts). The preflight control level is indicated by the solid square on the ordinate. The level without any countermeasure is shown by the solid line.

large, even 200 ml increase in blood volume has been shown to dramatically restore circulatory parameters towards baseline levels [92]. Thus, as much as 60% of the blood-volume loss can be restored by using fluid-loading in combination with an anti-diuretic.
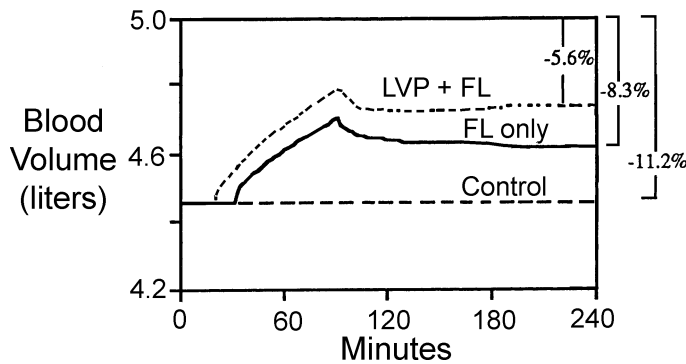
Figure 9-45. Time course of changes in blood volume due to lysine vasopressin (LVP), an anti-diuretic and fluid loading (FL). The baseline blood volume before head-down tilt is 5 liters, which was decreased, after 3-days of head-down bedrest, by 11.2% with no countermeasure (control – dashed line). Of this loss, 2.9% (11.2% less 8.3%) was restored by one liter isotonic saline fluid load (FL – solid line) and an additional 2.7% (8.3% less 5.6%) by LVP (LVP + FL — dotted line). Reproduced from Ref. [96].

9.7.6.4 Summary: Fluid-Loading Countermeasure.
Inasmuch as fluid-loading affords some measure of protection against orthostatic intolerance during re-entry it has been made an operational requirement for Shuttle astronauts. The recommended fluid-load is one liter of isotonic saline, administered 2-hours prior to re-entry. The simulations study presented here favors increasing the salt concentration of the fluid-load administered perhaps with an anti-diuretic. This conclusion is supported by the results of bedrest studies [93]. These authors used a hypertonic electrolyte drink with approximately twice the normal osmolarity to restore 2/3 of the loss in +G tolerance noted in normal subjects following a 2-week bedrest with no countermeasures. It has been shown that the effect of fluid-loading on ameliorating orthostatic intolerance at the end of Shuttle flights decreases with the duration of spaceflight [94]. Evidently, fluid-loading does little to reverse such adaptive manifestations of weighlessness as changes in baroreceptors gain setting or autonomic signal that are believed to occur in spaceflights lasting longer than a few days. The present study also demonstrated the usefulness of modeling and computer simulation in addressing questions of operational interest.

9.8 Integrated Analysis of Hormonal Regulation

9.8.1 Introduction
A group of renal-regulating hormones, consisting of anti-diuretic hormone (ADH), aldosterone and renin-angiotensin, has been the focus of many spaceflight related studies [19,30,47,74,98]. These hormones regulate the ionic composition of body fluids, particularly the plasma concentrations of sodium and potassium (see Fig. 5-8). A knowledge of inflight hormone disturbances should, therefore, provide insight into the status of the fluid-electrolyte systems and in revealing the mechanisms that control renal excretion during weightlessness.

However, the findings from spaceflight have been difficult to interpret or to reconcile with endocrine data obtained from one-g analogs of weightlessness such as water immersion, head-down tilt and bedrest. The results often appear inconsistent, conflicting and paradoxical in relationship to known concepts of endocrine control.

For example, the Skylab studies have revealed the following: wide differences between individual crewmen's ADH responses, reductions in ADH accompanied by normal or decreased urine flow, increases in sodium-retaining aldosterone in the face of a developing natriuresis and elevated levels of angiotensin (known to be stimulated by hypovolemia) at a time when there is an accumulation of fluid in the upper body. Also, the expectation that water immersion studies would predict the direction of endocrine changes in spaceflight was never realized. Supporting evidence, that might help explain this seemingly anomalous behavior, such as measurements made during the onset of weightlessness, are entirely lacking. At least, this was the situation during the early 1980's when the current analysis was conducted. The purpose of the following study was to subject the data that had accumulated during the early years of human spaceflight to the rigorous analysis provided by mathematical and computer simulation. The desired result was to unravel the ambiguities and arrive at a common testable hypothesis. A more complete report on this analysis is available [99,100].

9.8.2 Endocrine Response Data
The analysis began with an examination of the endocrine data from a variety of hypogravic experimental studies whose common characteristic was a reduction in hydrostatic gradients of the blood column resulting in an acute headward shift of fluid. A guiding hypothesis in this study was that all stresses that induce headward fluid shifts may be presumed, in the absence of other influences, to lead to similar responses. It is well known that these maneuvers lead to reductions in body water, plasma volume and electrolytes. Accordingly, it appears reasonable to compare results from such diverse stresses as water immersion, head-down tilt, supine bedrest, head-down bedrest and spaceflight. This argument, in fact, is one basis for utilizing the ground-based studies just mentioned, as analogs of spaceflight and making inferences from them regarding the physiological responses to weightlessness.

Figure 9-46 organizes the endocrine data for the three major renal-regulating hormones, taken from a number of hypogravic studies, whether performed in one-g or zero-g, whether short-term or long-term, into a qualitative, composite description. In the process of integrating this data one must be aware of the fact that each of the hypogravic maneuvers presented here has been studied over a different time-frame (see Fig. 9-1). Thus, at the time this study was conducted, the acute responses to the initial zero-g headward fluid shifts can be inferred only from data collected during water immersion and short-term head-down tilt maneuvers. Other experiments such as bedrest contrib-
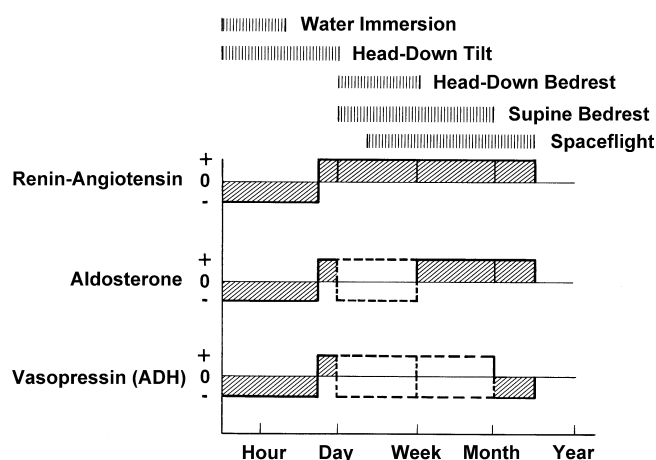
Figure 9-46. Hormonal changes found in plasma or urine during hypogravic studies: a composite. Chart was based on studies from Ref [19,30,47,74,98]. Blank horizontal columns indicate that different studies reported either both an increase or decrease in the same variable. Bars on top of graph indicate typical time periods associated with the hypogravic maneuver.

ute data primarily for long-term changes. Based on the above argument we assume that the data in Fig. 9-46 is truly part of a time continuum for a general hypogravic condition and not dependent on the particular stress.

Based on water immersion and head-down tilt studies, all three hormones exhibited suppression during the acute period where spaceflight data are lacking [39,41,74]. Following this acute phase, renin-angiotensin is the only hormone system that demonstrates a consistent behavior, i.e., a significant elevation in plasma concentration. During spaceflights lasting more than one-month aldosterone was found to be elevated and ADH suppressed [86], al-

though during intermediate periods, data from various bedrest studies and spaceflight are not always in agreement (blank areas in Fig. 9-46). It is the general behavior shown in Fig. 9-46 that needs to be understood. In particular, it is desired to reconcile the differences between the acute and chronic responses as well as the differences among the separate experimental studies.

9.8.3 Analysis of Hormone Controllers

Guyton and co-workers [26a] have incorporated into their model a schema for understanding endocrine regulation and fluid-electrolyte control. This has been presented earlier in this book (Chapters 3.2.5 and 5.0; see Figs. 5-8 and 5-11) and will be summarized below.

A schematic description of the factors which influence the three hormones (as they are represented in the mathematical model of Guyton) reveal that each hormone is responsive to two general types of controlling stimuli: volume disturbances and electrolyte disturbances (Fig. 9-47). The volume stimuli (as reflected by atrial, renal, or arterial pressures) may provide control only during acute disturbances, because of the existence of several types of adaptive mechanisms indicated in Fig. 9-47 and because the volume disturbances are often corrected by other non-endocrine related volume-regulating mechanisms. Three different types of pressure-related adaptive mechanisms are indicated, including receptor adaptation (i.e., adaptation of pressure receptors by increasing receptor tissue compliance or decreasing tissue tension), renal autoregulation (i.e., automatic adjustment of renal artery resistance to maintain blood flow reasonably constant) and baroreceptor resetting (i.e., adjustment of the set point to accommodate chronic changes in pressure). However, the influence of the electrolyte disturbances (as reflected by plasma sodium and potassium concentrations) is not known to adapt over time. Therefore, these electrolyte-sensing systems may
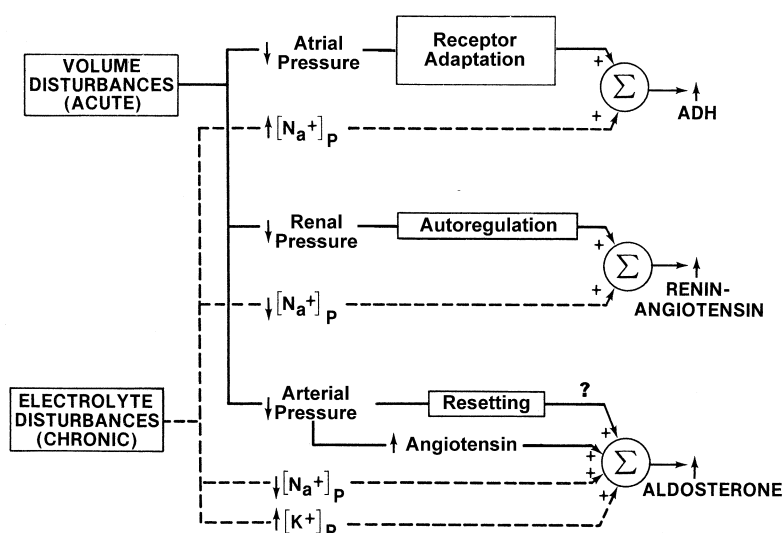
Figure 9-47. Influence of volume (——) and electrolyte (----) controllers on hormonal secretion. The stimuli are shown in the direction that causes each of the hormones to increase in value.

be the primary basis for the long-term control of these hormones in comparison to the volume sensors.

All of the hormone stimulating factors shown in Fig. 9-47 are known to change at one time or another during hypogravic maneuvers. For example, during the onset of hypogravity, headward fluid shifts cause blood pressures to become elevated leading to an initial suppression of hormone levels which aids the renal-correction of the volume disturbance (see Chapters 5.2 and 5.3). However, the long-term response is variable and appears to depend upon metabolic factors (such as diet, sweat loss, physical activity and muscle atrophy) that can alter the plasma electrolytes. Thus, the hyponatremia and hyperkalemia observed in the Skylab crew help explain the elevations of angiotensin and aldosterone and suppression of ADH which were also observed (Chapter 5.3). Discrepancies in hormone levels reported between different hypogravic studies can perhaps be explained by the fact that hormones normally exhibit a highly dynamic behavior which can be obscured by failing to monitor their levels at appropriate times and which can be altered by changes in diet, exercise levels, muscle atrophy and other test conditions. These various changes, occurring simultaneously, complicate any attempt to perform an integrated analysis of hormone behavior.

9.8.4 Analysis of ADH Control

An example of how computer modeling may be useful in accounting for the dynamics of endocrine control during spaceflight is presented below for the case of ADH changes. Two different approaches to understanding ADH control have been proposed, one based on the control of blood volume and the other controlling plasma osmolarity. In the first case, ADH would respond to minor disturbances in central blood volume as reflected by pressure changes in the cardiac atria [101]. In the second case, changes in plasma osmolarity would influence the secretion of ADH [14]. In both cases, the action of ADH on renal water and salt excretion are proposed to bring the stimulating variable under control.

Control of ADH according to these two different pathways is shown in Fig. 9-48, based directly on experimental evidence in the rodent. Specifically, it has been shown that ADH has a sensitive, linear dependency on plasma osmolarity while the corresponding sensitivity on blood volume is highly non-linear, showing little influence at small volume changes and a larger influence (larger than
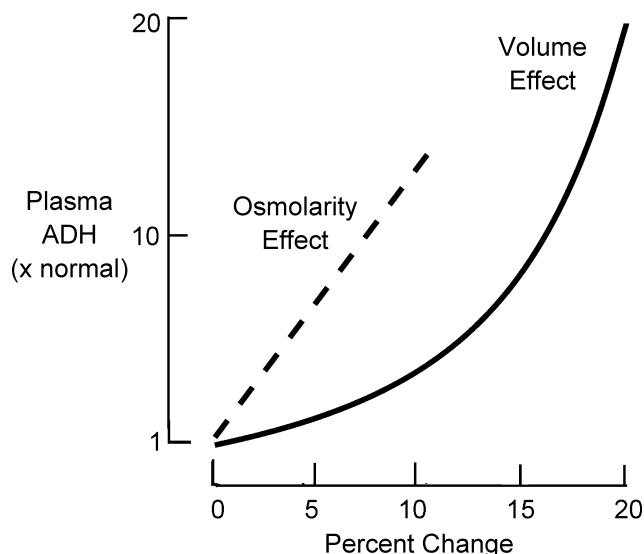
Figure 9-48. Effect on ADH caused by changes in plasma osmolarity or blood volume. Solid line: Effect on ADH due to blood volume depletion. Dashed line: Effect on ADH due to increase in plasma osmolarity. Redrawn from Ref. [89].

the sensitivity to osmolarity) at volume changes greater than 15 to 20% of total blood volume. Therefore, it appears that under certain stressful conditions, large, acute changes in blood volume can become the dominant factor controlling ADH secretion, while under most normal physiological conditions ADH responds to and regulates, changes in plasma osmolarity.

Guyton and co-workers [26a] have attempted to integrate both these points of view by proposing an integrative mechanism for fluid-electrolyte balance. See Fig. 5-19 for a detailed description and Fig. 9-49 for a simplified schematic. The elements in this scheme include a volume receptor-ADH pathway that responds to acute, rather than prolonged volume (and, therefore, atrial pressure) disturbances. The lack of long-term effectiveness of this pathway is credited to receptor adaptation. This is consistent with the concept that volume receptor tissues are elastic and adapt to changing pressures within reasonable periods of time. Thus, pressure changes, if maintained, exert a smaller and smaller influence on ADH. Guyton's concept also includes a sensitive osmotic receptor-ADH pathway
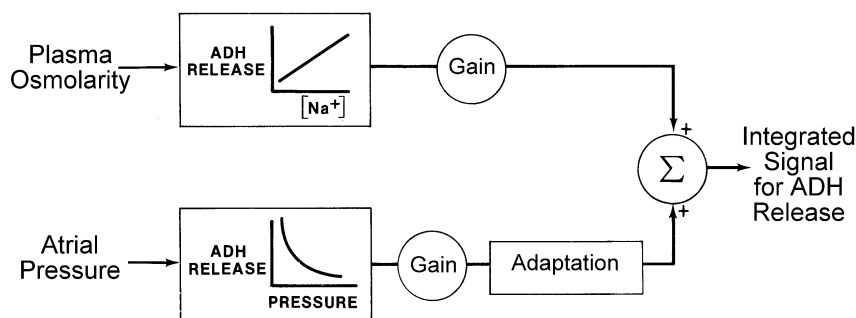
Figure 9-49. Dual control concept for ADH release: osmo vs. volume control. This is the basic concept embodied in the Guyton model.

that can override inputs from the volume receptors and an ADH-thirst drive which receives inputs from both volume and osmoreceptors. In this view, ADH has a short-term role in contributing to the correction of large changes in blood volume, but it has an even more important responsibility (together with thirst-drive) for long-term control of plasma osmolarity. The ability of volume receptors to adapt to sustained volume disturbances, the decreased effectiveness of ADH on urine output over long periods of time and the fact that there are other more powerful mechanisms available for long-term control of blood volume (see Fig. 5-10) support the argument for a minor role of ADH in the long-term control of body fluid volume. Interpretation of disturbances in ADH levels must, therefore, take into consideration the dual volume osmoreceptors pathways affecting ADH, the relative sensitivities of these volume receptors and their ability to adapt.

Modeling and computer simulation studies have suggested that ADH secretion could respond to weightlessness according to the schematic of Fig. 9-50. ADH is assumed to be under dual control of venous pressure and plasma sodium concentration, as outlined above. The following assumptions are made regarding these stimuli under hypogravic conditions: (a) the central venous pressure response is similar to that found during head-down tilt (see Chapter 9.7.5), (b) hyponatremia develops within several days (see below) and (c) ADH is primarily pressure/volume sensitive during the acute phase which may last until pressures begin to decline toward control levels, after which time the sensitivity gradually shifts to favor osmo-control due to some form of volume-receptor adaptation or pressure normalization.

Although based on several untested assumptions, this hypothesis appears to explain the average ADH response as measured in the Skylab crew and illustrated in Fig. 5.5(a). The complex triphasic response of Fig. 9-50 includes the early decrease in ADH (data during the first day was not collected but is inferred from water immersion, head-down tilt and the inverse of the first postflight day), a diminished ADH during the last two-months of spaceflight and the equivocal responses between these two points in time (see Fig. 9-46) due to competition between pressure and osmo-control.

The ADH waveform shown in Fig. 9-50 is not the only possible response as indicated in the complete report [99]. For example, the peak formed between the early and later phases of the response may not occur if adaptation occurs quickly and/or if osmotic stimuli exert a consistent, predominant influence. Also, under certain dietary regimes (or other metabolic influences) plasma sodium may increase, rather than decrease as considered in the above analysis. Consistent with this would be a long-term elevation (rather than suppression) of ADH.

9.8.5 Simulation of Endocrine Responses to Hypogravity

The control of the three renal-regulating hormones shown in Fig. 9-47 are part of a much larger feedback system that can apparently regulate circulatory and extracel-
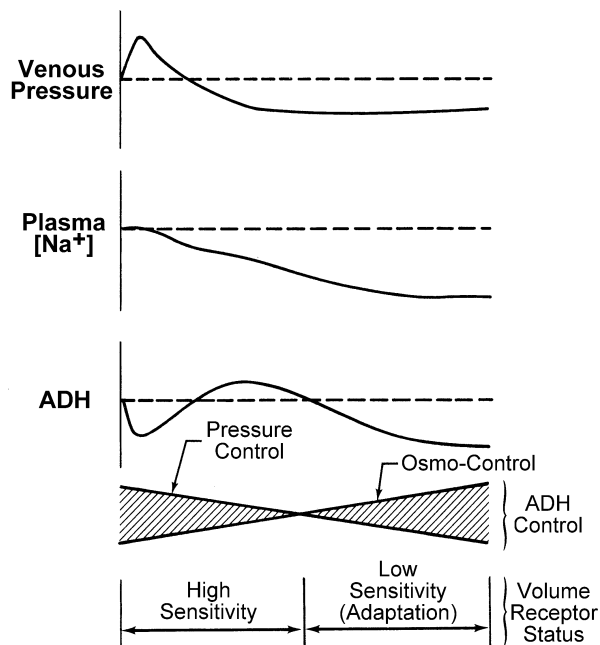
Figure 9-50. Hypothesis for ADH control during spaceflight. Idealized changes in venous pressure and plasma sodium concentration are based on space-based and ground-based data. The stimulus-response behavior shown here was obtained from computer simulation of head-down tilt using the Guyton model.

lular disturbances of various kinds. Figure 5-8 illustrates three distinct types of control mechanisms, including hormones, autonomics and hemodynamics which act to maintain extracellular volume and composition, as well as blood pressure and renal excretion. Thus, the resultant behavior of the hormones of interest for a hypogravic stress is likely beyond intuition and computer model analysis would be useful to understand the totality of the response.

Figure 9-51 illustrates the hormonal responses of ADH, aldosterone and angiotensin obtained in the mathematical simulation of a 7-day head-down (–6 deg) bedrest study (see Chapter 9.7.5.2). A similar set of simulated results were presented in Fig. 9-41 but in that case, the simulation included dietary changes in water and salt based on the intake of human subjects. In Fig. 9-51 there are no changes in dietary intake from control levels, although, as in Fig. 9-41, there is a release of a small amount of potassium from the cellular compartment that represents an effect of muscle atrophy (see Chapter 9.7.5.2.7)). The most notably characteristic observed in Fig. 9-51 is the triphasic nature of each response. The behavior of aldosterone and angiotensin appears to be similar to the ADH response that was presented in Fig. 9-50. In the light of this analysis it is proposed that the short-term suppression of the renal-regulating hormones are a result of volume control following headward fluid shifts in hypogravity while the long-term behavior can be explained as chronic adaptation to metabolic factors. The long-term trend was clearly not due to pressure effects because at 7-days venous pres-
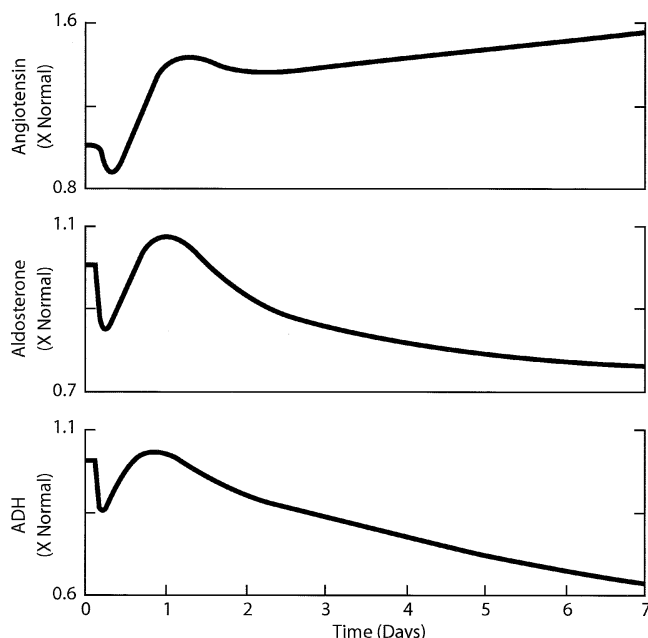
Figure 9-51. Hormone responses during simulation of (-6 deg) head-down bedrest

sure was depressed and arterial pressure was nearly normal (see Table 9-10 and Fig. 9-39). The specific changes in plasma electrolytes that could be responsible for the long-term hormone behavior were reviewed in Chapter 9.7.5.2.4. In most cases the model could account for the observed changes. However, the magnitude of the increase in angiotensin levels in either spaceflight or bedrest seems to be much greater than can be explained by the measured decrements in sodium. The possible involvement of renal pressure and renal hemodynamics should be explored to further elucidate other explanations of angiotensin release.

9.8.6 Summary: Hormone Regulation

This analysis suggests that the renal-regulating hormones represents a tightly coupled system that responds acutely to volume disturbances and chronically to electrolyte disturbances. During hypogravic maneuvers this leads to an initial suppression of hormone levels and a long-term effect which varies depending on metabolic factors. This shift from volume-control to osmo-control may be postulated to derive from an inherent sensitivity of hormones for electrolyte stimuli and/or from a gradual adaptation of pressure disturbances. In addition, the simulations reveal that if pressure effects rapidly normalize, a transition phase may exist which leads to a dynamic multiphasic endocrine response waveform. This hypothesis can qualitatively account for the observed changes in these hormones during Skylab and ground-based analog studies. Where discrepancies between different studies are found, this may be a result of competing and time-varying stimuli which differ between subjects and test conditions.

Confirmation of the above hypothesis will require careful measurements, throughout the time range of interest, of competing factors such as blood pressure, serum electrolytes and fluid volume shifts which must be obtained simultaneously with endocrine levels. These measurements need to be made not only in space but in ground-based analogs such as water immersion and head-down bedrest. Particular attention should be given to obtaining measurements at the onset of hypogravity. Because various metabolic factors such as sweating, muscle atrophy and diet can have a strong modifying effect on hormone behavior, they should be carefully controlled and monitored.

9.9 Conclusions

The studies described in this chapter represent an examination of integrated hypotheses proposed to explain many of the physiological changes observed during exposure to hypogravity. A key approach of these studies was the use of mathematical models and their ability to simulate a number of ground-based analogues of zero-g as well as spaceflight. Data from these hypogravic maneuvers were used to modify the simulation models and to validate simulation results. The simulations presented here build directly upon the subsystem hypothesis development and data analysis of the previous chapters. The studies of this chapter differed from those of the previous chapters in that hypotheses were tested as an integrated set rather than individually, in models that are complex representation of human physiology. The Guyton model, used throughout these studies, became the common framework upon which to integrate and compare diverse stresses and hypotheses. This powerful contribution of the modeling approach is not one that can be easily replicated by human thought and intuition.

9.9.1 Summary of Physiological Findings

A listing of the important physiological responses to weightlessness that have been simulated in this chapter are given in Table 9-11. The broad conclusions drawn from these studies concerning the physiology of hypogravity are shown in Table 9-12 and Fig. 9-52. It is not easy to encapsulate in one diagram the numerous insights derived from examining the experimental findings and performing model simulations. Nevertheless, Fig. 9-52 suggests that there are three broad consequences of gravity unloading: altered hydrostatic gradients leading to headward fluid shifts, unloading of musculoskeletal tissues leading to disuse atrophy and altered metabolism derived from an altered diet and exercise regime. All of these combine to create disturbances in many interrelated body systems, with some universally observed consequences that include loss of body mass and tissues and upon return to one-g a decrease in orthostatic tolerance and work performance. With the exception of a few physiological areas that were not covered in this project (notably vestibular processes) the concepts implied by the simple diagram of Fig. 9-52 can arguably be said to be the basis of space physiology research since the 1970's.

Table 9-11. Important Physiological Responses to Weightlessness Which Have Been Simulated

- Acute fluid shifts from legs
- Longer term leg dehydration
- Redistribution of blood towards head
- Changes in blood flow and pressures
- Changes in cardiac output, heart rate and stroke volume at rest
- Altered secretion of hormones: ADH, angiotensin, aldosterone
- Acute increase in urine water, sodium, and potassium
- Influence of suppressed fluid intake on acute response
- Redistribution of intracellular/extracellular fluid
- Redistribution of intravascular/interstitial fluid
- Effect of protein permeability on capillary filtration
- Altered sympathetic discharge to heart, vessels, and kidneys
- Decreased plasma volume and increased hematocrit
- Suppressed erythrocytosis and decreased red cell mass
- Influence of natriuretic factor on renal function
- Change in osmotic concentration of body fluids
- Influence of diet and sweat losses on long-term hypogravic response
- Fluids, electrolytes and hormonal consequences of muscle atrophy
- Decreased body water, sodium, and potassium
- Cardiovascular adaptation to long-term spaceflight
- Cardiovascular and fluid volume responses to postural maneuvers
- Decreased orthostatic tolerance upon recovery
- Decreased exercise performance upon recovery

Table 9-12. Conclusions About Spaceflight Physiological Adaptation Derived from Modeling Studies

These studies have:

- Shown that weightlessness can be better understood by partitioning the response into short-term (about 5-days) and longer term segments

- Resulted in a generalized hypothesis of the fluid-electrolyte weightlessness response; confirmed by simulation and experimental findings.

- Demonstrated that headward shifts of fluid from the legs are primarily responsible for acute body losses of extracellular fluid and electrolytes. Also muscle atrophy, primarily in legs, is responsible for long-term loss of intracellular tissue, nitrogen and potassium.

- Suggested that of the three routes for depletion of plasma volume (renal, deficit drinking, transcapillary filtration), the last two are not likely to have long-lasting effects. Renal excretion is a high gain mechanism for correcting central blood volume excesses.

- Shown that early fluid losses occur by deficit intake, but suggested that losses would have occurred anyway by renal regulation if intake were normal

- Predicted diuresis during first several hours of spaceflight which may be obscured by reduced fluid-electrolyte intake secondary to space sickness early in flight

- Predicted hemoconcentration during flight contributes to suppression of red cell production

- Suggested a reduction in evaporative water and sweat electrolyte losses rather than an expected increase can help explain patterns of renal excretion; evaporative water loss changes confirmed by analysis

- Suggested that observed reduction in plasma osmolarity can partially explain measured losses of electrolytes and changes in hormonal levels

- Suggested hypotheses to explain "paradoxical" changes in hormonal levels: During long-term spaceflight ADH may be influenced primarily by sodium levels (rather than central blood volume), and aldosterone may be influenced more by plasma potassium levels (rather than sodium).

- Suggested presence of natriuretic factor opposing the sodium retaining influence of aldosterone

- Demonstrated loss of potassium from cellular compartment can account for many long-term effects including enhanced aldosterone, increased K^+ excretion, elevated plasma K^+, decreased intracellular fluid, and decreased body K^+

- Predicted that acute blood volume losses which are maintained cause long-term adaptive adjustments in circulatory flows, pressures, and capacitances including: flow autoregulation, baroreceptor adaptation, and stress relaxation of blood vessels

- Suggested that the failure of blood volume to return to normal in hypogravity, even after long periods, is indirect evidence of the presence of volume receptors in the upper body and perhaps their resetting to new thresholds
- Suggested a concept for the behavior of renal-regulating hormones in hypogravity based on acute control of blood volume and longer term control of plasma electrolyte concentrations

The simulation studies also highlighted the following differences and limitations of the one-g analogs:

a) Each stress provides a picture of hypogravity over a different slice of time. Thus, water immersion results are obtained normally over a 4 to 6-hour period, short-term head-down tilt for 24-hours, long-term head-down bedrest for up to 7-days and Skylab data represents a mean response during a 3-month interval. It is normally the case that the longer the time frame of any particular study, the less energy the researchers invest in measuring acute changes. While a simulation model can examine both acute and chronic segments equally, the data for comparison must come from different types of studies. The lack of a common time frame of study and inconsistent methodological procedures in each case makes true comparison difficult.

b) There are unique aspects of each analog. In water immersion, hydrostatic forces compress the tissue fluids from outside the body and in supine bedrest or head-down tilt there is little or no physical activity. Dietary intake, especially of fluids, electrolytes and calories can also be considerably different. It was shown in these studies that it is possible to account for a number of physiological observations on the basis of dietary change alone.

c) With bedrest in particular, it is difficult to separate the effects of gravity unloading with that of a reduction in metabolic activity. Exercise conditioning alters many of these same systems, often in opposing ways as

hypogravic stress. In addition, it is difficult to experimentally dissociate the effects of hydrostatic forces on the one hand and deformation forces on the other. The use of model simulations, where cause and effect can eventually be teased out, allows the researcher to more easily separate out these different factors.

d) It was observed that all of the hypogravic stresses, when simulated with the Guyton model, were more *qualitatively* similar than different in the short term. This was ascribed to the observation that the volume of leg fluids that are shifted headward are different in each case: they are minimal with supine bedrest, maximal in spaceflight and somewhere in-between for head-down tilt. *Quantitative* differences in the acute circulatory responses appeared to be dependent in large part because of the magnitude and time course of the headward fluid shift. These acute fluid shifts are strong enough to mask out other concurrent effects. However, the longer term responses could be considerably different from each other, depending on factors such as the degree of activity, diet and fluid intake. In an analysis of body composition (Chapter 4.6), an observed negative energy balance is thought to have had a great effect on the metabolic systems of the body during spaceflight.

e) Finally, there are differences concerning some critical measurements. Central venous pressure was predicted to trend below control in the simulations following a short upward spike; this finding was observed experi-
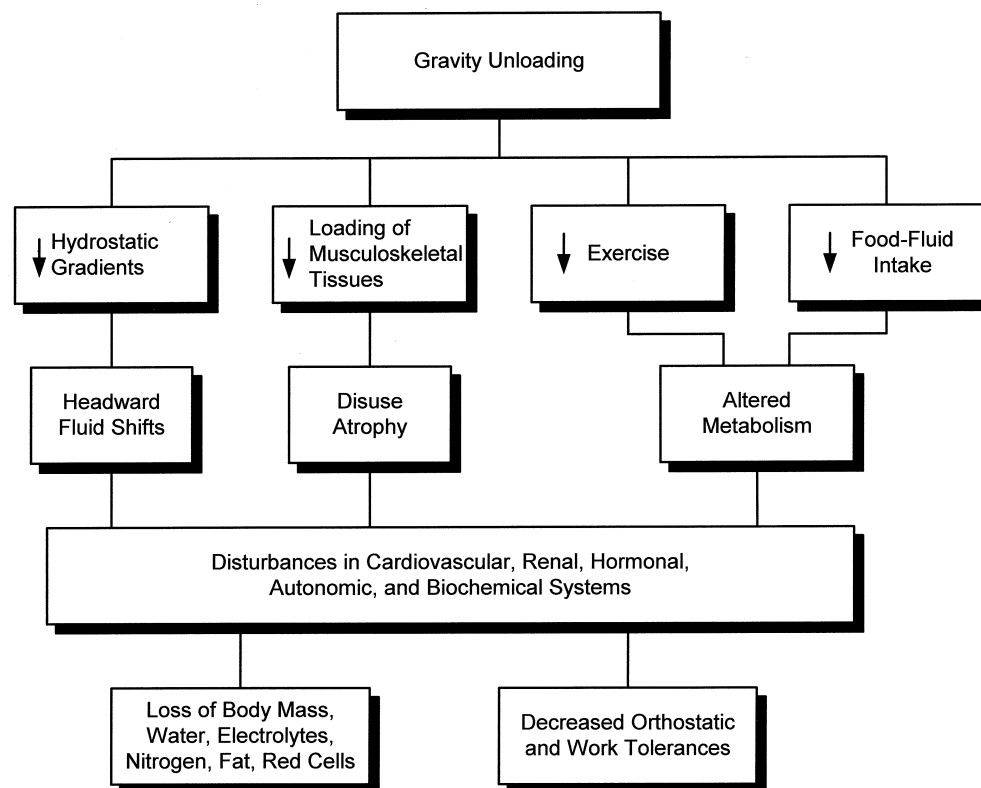
Figure 9-52. Physiological effects of hypogravity. Major effects of gravity unloading as discerned from the analyses of Skylab and zero-g analog findings.

mentally in head-down tilt (but not supine bedrest) and the decrease in venous pressure was later confirmed in spaceflight. In water immersion, the CVP rose so high as to become suspicious – perhaps an artifact of the external water pressure. A diuresis was observed in supine bedrest, head-down tilt and water immersion but, oddly, never during spaceflight. The simulations predict that a diuresis might be attenuated due to body dehydration (lack of drinking, space motion sickness) and by transcapillary filtration, but it would not be eliminated.

While these differences might be clear to the careful observer, they became more apparent when viewed through the prism of a comprehensive modeling analysis.

9.9.2 Summary of Simulation Techniques

The first study in this chapter was a simulation of supine bedrest and associated tilt and exercise tests using the Whole-Body Algorithm. These tests essentially validated this highly integrated model for hypogravic environments. A wide spectrum of physiological responses were achieved with the Whole-Body Algorithm, including the resting bedrest responses and the post-bedrest orthostatic and exercise responses. However, for the remaining studies in this chapter, the model of choice was the Guyton model, modified for examining gravitational maneuvers by the addition of leg compartments and gravity induced hydrostatic pressures, as well as other changes described more fully in Chapter 3 and Appendix C. The stand-alone Guyton model was much more convenient to work with than the much larger Whole-Body Algorithm, primarily because of computer limitations. Although the Guyton model was limited to a narrower range of physiology than the Whole-Body Algorithm, it was an excellent vehicle to study one of our major areas of interest, that is, circulatory, fluid and electrolyte regulation. It is a testament to the wisdom of the creator of the Guyton model that it proved to be adaptable for gravitationally related stresses including weightlessness, situations for which it was never intended.

A useful result of this study is the demonstration that various types of maneuvers, which have been used as experimental analogs of weightlessness, can all be simulated by a common mathematical model. The analogs that have been discussed in this chapter include supine bedrest, head-down tilt (short-term), head-down bedrest (long-term) and water immersion. Head-up tilt or standing was also emphasized because of its obvious relationship to gravitational influences and because there is a larger body of knowledge about this maneuver than the others. In all cases the same quantitative model was used which embodies elaborate but essential relationships describing circulatory, fluid and electrolyte regulation. Thus, a conclusion of this series of studies is that adaptation to weightlessness is a normal response of the feedback control circuits of the body to gravitational disturbances. Furthermore, the modeling process has confirmed the belief of other researchers that one-g analogs truly seem to affect many of the same physiological mechanisms that are activated during space-

flight. The mathematical model can be thought of as functioning as an analog to zero-g physiology in the same way as water immersion does, or the manner in which animals are used as surrogates for human studies.

The original Guyton model did not contain the capability of recognizing changes in gravity or responses to postural maneuvers (Chapters 9.2). Therefore, one of the first important modifications included the addition of leg vascular and extravascular compartments, so that the fluid redistribution characteristic of weightlessness could be reproduced and studied (see Chapter 9.3.2 and Appendix C). During the simulations of supine bedrest (Chapter 9.3), spaceflight (Chapter 9.4) and water immersion (Chapter 9.5) early in this project, the effects of gravity were not included and it was only possible to initiate headward fluid shifts by some artificial means (Figs. 9-2 and 9-13). In order to more realistically portray the shifts of fluid between the leg compartments and the head, it was necessary to model both external forces (the gravity vector) and internal forces (tissue elasticity) that contribute to this fluid shift. Therefore, the next logical stage of model development included a representation of the gravity vector as it affects the fluid columns of the body. Further modifications of the model were necessary during simulation of the erect posture to account for orthostatic defense mechanism that were not originally present in the model (Chapter 9.6 and Appendix C). Finally, the most realistic simulation of weightlessness was achieved by performing head-down tilt and head-down bedrest (Chapter 9.7).

The successful simulation of each stress that was studied was not achieved with the basic model alone; rather some additional functionality was required to be included in the model or it was necessary to test some new hypothesis. Thus, supine bedrest presented an opportunity to examine the gradual dehydration of the legs as a result of tissue and vessel retoning and unloading and atrophy of muscle tissue. Head-down tilt simulations required additional modifications to the leg vasculature in order to prevent venous collapse in the face of negative body angles and to allow fluid drainage from the leg tissues. Problems in these areas were not apparent during previous simulations of simple supine bedrest. Realistic simulations of head-up tilt (orthostasis) required additional assumptions reflecting leg muscle pumps, abdominal compression and reduced venous capacitance by stress relaxation. In order to provide more realistic simulations of water immersion and head-down tilt, transient changes in the capillary membrane's permeability to protein were invoked. The acute response of hypogravity was simulated in water immersion and head-down tilt by simple fluid volume shifts. But longer-term, chronic changes exemplified by the spaceflight and head-down bedrest simulations required metabolic changes including those associated with diet, sweating, exercise and muscle tissue loss. An example was provided that demonstrated how the model could be used to evaluate and design countermeasures to reverse some of the untoward effects of microgravity. Validation of the model for each new situation, therefore, required structural and programming changes in the model that eventu-

ally would enhance the range of model capabilities and lead to improved simulations of weightlessness. In all cases the modification was plausible and realistic, often being based on quantitative experimental evidence. The fact that modifications were required should not necessarily be construed as evidence of model inadequacy because this is the normal approach in modeling research. The end result is hopefully an improved model and an enhanced understanding of the underlying basis of zero-g adaptation.

References

1. Birkhead, N. C., *et al.*, Cardiodynamic and Metabolic Effects of Prolonged Bed Rest, *AMRL-TDR-63-37*, 1963.
2. Hyatt, K. H., Smith, W. M., Vogel, J. M., Sullivan, R. W., Vetter, W. R., Calder, B. E., Bohnn, B. J. and Haughton, V. M., *A Study of the Role of Extravascular Dehydration in the Production of Cardiovascular Deconditioning by Simulated Weightlessness (Bed Rest)*, NASA CR-114808, 1970.
3. Saltin, B., Blomqvist, G., Mitchell J.H., Johnson Jr., R.L., Wildenthal, K. and Chapman, C., Response to Exercise After Bed Rest and After Training: A Longitudinal Study of Adaptive Changes in Oxygen Transport and Body Composition, *Circulation*, 38, suppl. VII, pp. VII-1 -VII-78,1968.
4. Stevens, P. M., Miller, P. B., Cilbert, C. A., Lynch, T. N., Johnson, R. L. and Lamb, L. E., Influence on Long-Term Lower Body Negative Pressure on the Circulatory Function of Man During Prolonged Bed Rest, *Aerospace Med.*, 37, pp. 357-367, 1966.
5. Vallbona, C., *et al.*, *The Effect of Bed Rest on Various Parameters of Physiological Function*, Part VIII, The Effect on the Cardiovascular Tolerance to Passive Tilt. NASA CR-178, 1965.
6. Taylor, H. L., Henschel, A.. Brozek, J. and Keys, A., Effects of Bed Rest on Cardiovascular Function and Work Performance, *J. Appl. Physiol.*, 2: 223-239, 1949.
7. Fasola, A. F. and Triebwasser, J. H., The Renin Response to Lower Body Negative Pressure Stress Testing and the Effect of Exercise During Prolonged Bed Rest, *Preprints of the 1970 Annual Scientific Meeting of the Aerospace Medical Association*, 1970, pp. 63-64.
8. Fuller, J. H., Bernauer, E. M. and Adams, W. C., Renal Function, Water and Electrolyte Exchange During Bed Rest with Daily Exercise, *Aerspace Med.*, 41: 60-72, 1970.
9. Echt, M., Lange, L. and Gauer, O. H., Changes of Peripheral Venous Tone and Central Transmural Venous Pressure During Immersion in a Thermo-Neutral Bath, *Pflugers Arch.*, 352: 211-217, 1974.
10. Gauer, O. H., Recent Advances in the Physiology of Whole Body Immersion, *Acta Astronautica*, 2: 31-39, 1975.
11. Epstein, M. and Saruta, T., Effect of Water Immersion on Renin-Aldosterone and Renal-Sodium Handling in Normal Man, *J. Appl. Physiol.*, 31: 368-374, 1971.
12. McCally, M. and Graveline, D. E., Physiologic Aspects of Prolonged Weightlessness: Body Fluid Distribution and the Cardiovascular System, *N. Engl. J. Med.*, 269: 508-516, 1963.
13. Piemme, T. E., Body Fluid Volume and Renal Relationships to Gravity. Hypodynamics and Hypogravics, The Physiology of Inactivity and Weightlessness, M. McCalley, (Ed.), Academic Press, 1968, pp. 133-161.
14. Goetz, K. L., Bond, G. C. and Bloxham, D.D., Atrial Receptors and Renal Function, *Physiol. Review*, 55: 157-205, 1975.
15. Hyatt, K. H., Kamenetsky, L. G., Smith, W. M. and Vogel, J. M., *A Study of Post-Recumbency Orthostatism and Prophylactic Measures for Prevention of this Phenomenon*, NASA CR-92178, Part I and 2, 1968.
16. Leonard, J. I. and Grounds, D. J., *Study Report: Modification of the Long-Term Circulatory Model for the Simulation of Bed Rest,* (General Electric Co., Houston, TX.; TIR 782-LSP-7011), NASA CR-160186, NASA, Washington, D.C., 1977.
17. Johnson, P. C. and Mitchell, C., *Report of-14-day Bed Rest Simulation of Skylab*, NASA-CR-147758, The Methodist Hospital, Houston, TX, 1975.
18. Vogt, F. B. and Johnson, P. C., Plasma Volume and Extracellular Fluid Volume Changes Associated with 10 Days Bed Recumbency, *Aerospace Med.,* 38: 21–25, 1967.
19. Greenleaf, J. E.,, Van Derveer, D. and Dorchak, K. J., *Adaptation to Prolonged Bedrest in Man: A Compendium of Research,* NASA TM X-3307, NASA, Washington, D.C., 1976.
20. Johnson, P. C. and Mitchell, C., *Report of 28-Day Bed Rest Simulation of Skylab*, Part 1 and 2, NASA CR-151353, The Methodist Hospital, Houston, TX, 1977.
21. Baish, F., Beck, L., Karemaker, J. M., Arbeille, P., Gaffney, F. A. and Blomqvist, C. G., Head-down Tilt Bedrest HDT'88 – An International Collaborative Effort in Integrated Systems Physiology, *Acta Physiol. Scand.*, 144, S604: 1–12, 1992.
22. Convertino, V. A., Doerr, D. F. and Stein, S. L., Changes in Size and Compliance of the Calf After 30 Days of Simulated Microgravity, *J. Appl. Physiol.,* 66: 1509–1512, 1989.
23. Hoffler, G. W., Bergman, S. A. and Nicogossian, A. E., Inflight Lower Limb Volume Measurement, in *The Apollo–Soyuz Test Project: Medical Report* (NASA SP-411), A. E. Nicogossian (Ed.), NASA, Washington, D.C., 1977.
24. Thornton, W. E., Hoffler, G. W. and Rummel, J. A., Anthropometric Changes and Fluid Shifts, in *Biomedical Results from Skylab* (NASA SP-377), R. S. Johnston and L. F. Dietlein (Eds.), Washington, D.C., U.S. Government Printing Office, 1977.
25. Deitrick, J. E., Whedon, G. D. and Shorr, E., Effects of Immobilization Upon Various Metabolic and Physiologic Functions of Normal Men, *Amer. J. Med.*, 4: 30-36, 1948.
26a. Guyton, A. C., Taylor, A. E. and Granger, H. J., *Circulatory Physiology II: Dynamics and Control of the Body Fluids*, W. B. Saunders Co., Phila., 1975.
26b. Guyton, A. C., *Circulatory Physiology III: Arteial Pressure and Hypertension*, W. B. Saunders Co., Phila., 1980., pp. 61–64.
27. Sjostrand, T., Volume and Distribution of Blood and Their Significance in Regulating the Circulation, *Physiol. Review*, 33: 202-228, 1953.
28. Kimzey, S.L., Leonard, J.I., Buderer, M.C. and Johnson, P.C. A Computer Simulation of the Regulation of Erythropoiesis During Space Flight, *Annual Scientific Meeting of the Aerospace Medical Assoc.*, 1976.
29. Leonard, J. I., Kimzey, S. L. and Dunn, C. D. R., Dynamic Regulation of Erythropoiesis: A Computer Model of General Applicability. *Exper. Hematology*, 9: 355–378, 1981.
30. Epstein, M., Renal Effects of Head-Out Water Immersion in

Man: Implications for an Understanding of Volume Homeostasis, *Physiol. Reviews*, 58: 529-581, 1978,

31. Thornton, W.E., Hedgter, V., Coleman, E., Uri, J.J. and Moore, T.P., Changes in Leg Volume During Microgravity Simulation, *Aviat. Space Environ. Med.,* 63: 789–94,, 1992.

32. Begin, R., Epstein, M., Sackner, M.A., Levinson, R., Dougherty, R. and Duncan, D., Effects of Water Immersion to the Neck on Pulmonary Circulation and Tissue Volume in Man, *J. Appl. Physiol.*, 40: 293-299, 1976.

33. Behn, C., Gauer, O. H., Kirsch, K. and Eckert, P., Effects of Sustained Intrathoracic Vascular Distension on Body Fluid Distribution and Renal Excretion in Man, *Pflugers Arch.*, 313, p. 123, 1969.

34. Nixon, J. V., Murray, R. G., Bryant, C., Johnson, R. L., Jr., Mitchell, J. H., Holland, O. B., Gomez-Sanchez, C., Vergne-Marini, P. and Blomqvist, C. G., Early Cardiovascular Adaptation to Simulated Zero Gravity, *J. Appl. Physiol.-Respir. Environ., Exercise Physiol.*, 4, pp. 541-548, 1979.

35. McCally, M., Kazarian, L. E. and Von Gierke, H. E., Cardiovascular and Metabolic Effects of Bed Rest and Immobilization—Simulated Weightlessness, *Proceedings of the 21st International Astronautical Congress*, 1971, pp. 264-282.

36. Henry, J. P., *Orthostasis and the Kidney*, Wright Air Development Center Technical Report 55-478, 1955, pp. 4-14.

37. Arborelius, M., Jr., Balldin, U. I., Lilja, G. and Lundgren, C. E. G., Hemodynamic Changes in Man During Immersion with the Head Above Water, *Aerospace Med.*, 43, pp. 592-598, 1972.

38. Gauer, O. H. and Henry, J. P., Circulatory Basis of Fluid Volume Control, *Physiol. Rev.* 43: 423–81, 1963.

39. Epstein, M., Pins, D. S. and Miller, M., Suppression of ADH During Water Immersion in Normal Man, *J. Appl. Physiol.*, 38, pp. 1038-1044, 1975.

40. Epstein, M., Cardiovascular and renal effects of head-out water immersion in man: Application of the model in the assessment of volume homeostasis, *Circulation Res.* 39: 619–28, 1976.

41. Greenleaf, J. E., Shvartz, E., Kravik, S. and Keil, L. C., Fluid Shifts and Endocrine Responses During Chair-Rest and Water Immersion in Man, *J. Appl. Physiol.: Respir. Environ. Exer. Physiol.,* 48, pp. 79-88, 1980.

42. McCally, M., Plasma Volume Response to Water Immersion: Implications for Space Flight, *Aerospace Med.*, 35, pp. 130-132, 1964.

43. Vander, A. J., *Renal Physiology*, 2nd ed., McGraw Hill Book Co., New York, N.Y., 1980.

44. Leonard, J. I., *Water Immersion and its Computer Simulation as Analogs of Weightlessness*, NASA CR-17146 (General Electric TIR 2114-MED-2005, Houston, TX), NASA, Washington, D.C., 1982.

45. Leonard, J. I., Understanding Metabolic Alterations in Spaceflight Using Quantitative Models: Fluid and Energy Balance, *Acta Astronautica*, 13: 441–57, 1986.

46. Epstein, M., Duncan, D. and Fishman, L. M., Characterization of the Natriuresis Caused in Normal Man by Immersion in Water, *Clin. Sci.*, 43, pp. 275-287, 1972.

47. Greenleaf, J. E., Schvartz, E. and Keil, L. C., Hemodilution, Vasopressin Suppression and Diuresis During Water Immersion in Man, *Aviat. Space Environ. Med.* 52: 329–36, 1981.

48. Khosla, S. S. and DuBois, A. B., Fluid Shifts During Initial Phase of Immersion Diuresis in Man, *J. Appl. Physiol.*:

Respirat. Environ. Exercise Physiol., 46: 703–708, 1979.

49. Guyton, A. C., Jones, C. E. and Coleman, T. G., *Circulatory Physiology: Cardiac Output and Its Regulation*, 2nd ed., W. B. Saunders Co., Phila., 1973.

50. Rushmer, R. F., *Effects of Posture*, Cardiovascular Dynamics, 3rd ed., W. B. Saunders Co., Phila., 1970, pp. 210-219.

51. Shepherds, J. T. and Vanhoutte, P. M., *Veins and Their Control,* W. B. Saunders Co., Phila., 1975.

52. Hellenbrandt, F. A. and Franseen, E. B., Physiological Study of the Vertical Stance of Man, *Physiol. Review*, 23, pp. 220-255, 1943.

53. Rowell, L. B., *The Cutaneous Circulation, Physiology and Biophysics*: Circulation, Respiration and Fluid Balance, T. C. Ruch, H. D. Patton and A. M. Scher, (Eds.), W. B. Saunders Co., Phila., 1974, pp. 185-199.

54. Folkow, B. and Neil, E., *Circulation*, Oxford University Press, 1971.

55. Zoller, R. P., Mark, A. L., Abboud, F. M., Schmid, P. G., Heistad, D. D., The Role of Low Pressure Baroreceptors in Reflex Vasoconstrictor Responses in Man, *J. Clin. Invest.*, 51: 2967–72, 1972

56. Lamb, L. E., Circulatory Problems in Prolonged Space Flight, *Hypodynamics and Hypogravics: The Physiology of Inactivity and Weightlessness*, M. McCalley, Ed., Academic Press, 1968, pp. 163-179.

57. Mellander, S. and Oberg, B., Transcappilary Fluid Absorption and Other Vascular Reactions in the Human Forearm During Reduction of the Circulating Blood Volume, *Acta Physiol. Scand.*, 71, pp. 37-46, 1967.

58. Mellander, S., Interaction of Local and Nervous Factors in Vascular Control. Symposia Angiologica Santoriana, 3rd Int. Symp., Fribourg, 1970, Part I, *Angiologica* 8, pp. 187-201, 1971.

59. Fawcett, J. K. and Wynn, V., Effects of Posture on Plasma Volume and Some Blood Constituents, *J. Clin. Path.*, 13, p. 304, 1960.

60. Tan, M. H., *et al.* Effect of Posture on Serum Lipids. N. Engl, *J. Med.*, 289, p. 116, 1973.

61. Wood, E. J. and Eckstein, J. W., A Tandem Forearm Plethysmograph for Study of Acute Responses of the Peripheral Veins of Man: The Effect of Environmental and Local Temperature Change and the Effect of Pooling Blood in the Extremities, *J. Clin. Invest.*, 37, pp. 41-50, 1958.

62. Tuckman, J. and Shillingfor, J., Effect of Different Degrees of Tilt on Cardiac Output, Heart Rate and Blood Pressure in Normal Man, *British Heart Journal*, 28, pp. 32-39, 1966.

63. Tarazi, R. C., Melsher, H. J., Dustan, H. P. and Frohlich, E. D., Plasma Volume Changes with Upright Tilt: Studies in Hypertension and in Syncope, *J. Appl. Physiol.*, 28, pp. 121-126, 1970.

64. Brigden, W. M., Howarth, S. and Sharpey-Schafer, E. P., Postural Changes in the Peripheral Blood Flow of Normal Subjects with Observations on Vasovagal Fainting Reactions as a Result of Tilting, Lordotic Posture, Pregnancy and Spinal Anesthesia, *Clin. Sci.*, 9, p. 79, 1950.

65. Culbertson, J. W., *et al.*, The Effect of the Upright Posture Upon Hepatic Blood Flow in Normotensive and Hypertensive Subjects, *J. Clin. Invest.*, 30, pp. 305-311, 1951.

66. King, S. E. and Baldwin, D. S., Renal Hemodynamics During Erect Lordosis in Normal Man and Subjects with Orthostatic

Proteinuria, *Proc. Soc. Exptl. Biol. Med.*, 86, p. 634, 1954.

67. Foux, A., Seliktar, R. and Valero, A., Effects of Lower Body Negative Pressure (LBNP) on the Distribution of Body Fluids, *J. Appl. Physiol.*, 41: 719-726, 1976.

68. Leonard, J. I. and Abbrecht, P. H., Dynamics of Plasma-Interstitial Fluid Distribution Following Intravenous Infusions in Dogs: An Experimental and Computer Simulation Study, *Circulation Res.*, 33, pp. 735-748, 1973.

69. Oparil, S., Vassaux, C., Sanders, C.A. and Haber, E., Role of Renin in Acute Postural Homeostasis, *Circulation*, 41, pp. 89-95, 1970.

70. Gowenlbck, A. H., Mills, J. N. and Thomas, S., Acute Postural Changes in Aldosterone and Electrolyte Excretion in Man, *J. Physiol.*, 146, pp. 133-141, 1959.

71. Croston, R. C. and Fitzjerrell, D. G., Cardiovascular Model for the Simulation of Exercise, Lower Body Negative Pressure and Tilt Experiments, *Modeling and Simulation*, 5, Proceedings of the Fifth Annual Pittsburgh Conference, W. G. Vogt and M. H. Hickle, (Eds.), Instrument. Society of America, 1974.

72. Boyers, D. G., Cuthbertson, J. G. and Luetscher, J. A., Simulation of the Human Cardiovascular System: a Model with Normal Responses to Change of Posture, Blood Loss, Transfusion and Autonomic Blockade, *Simulation*, 18, pp. 197-206, 1972.

73. Snyder, M. F. and Rideout, V. C., Computer Simulation Studies of the Venous Circulation, *IEEE Transactions on Biomedical Engineering*, BME-16, 1969, pp. 325-334.

74. Blomqvist, C.G., Nixon, J.V., Johnson Jr., R.L., Mitchell, J.H., Early Cardiovascular Adaptation to Zero Gravity, Simulated by Head-down Tilt, *Acta Astronautica,* 7: 543–553, 1980.

75. Volicer, L., Jean-Charles, R., Chobanian, A. V., Effect of Head-down Tilt on Fluid and Electrolyte Balance, *Aviat. Space Environ. Med.,* 47: 1065–1068, 1976.

76. Kakurin, L. I., Lobachik, V. I., Mikhailov, V. M. and Senkevich, Yu. A., Anti-Orthostatic Hypokinesia as a Method of Weightlessness Simulation, *Aviat. Space Environ. Med.* 47: 1083–1086, 1976.

77. Nicogossian, A. E., Huntoon, C. L. and Pool, S. L., *Space Physiology and Medicine*, 3rd ed., Lea & Febiger, Baltimore, 1994, p.364

78. Popovic, V., Antiorthostatic Hypokinesia and Circulatory Changes in the Rat, *Proc. Aerospace Med. Assoc.,* pp. 152–153*,* 1981.

79. Morey, E. R., Space Flight and Bone Turnover: Correlation with a New Rat Model of Weightlessness, *Bioscience*, 29: 1968–1972, 1979.

80. Muscacchia, X. J., Deavers, D. R., Meininger, G. A. and Davis, T. P., A Model for Hypokinesia: Effects on Muscle Atrophy in the Rat, *J. Appl. Physiol.: Respirat. Environ. Exercise Physiol.* 48: 479–486, 1980.

81. Leonard, J. I., Grounds, D. J. and Fitzjerrell, D. G., *Development of an Hypothesis for Simulating Anti-Orthostatic Bed Rest*, NASA CR-160200, (General Electric TIR 741-LSP-8023, Houston, TX), NASA, Washington, D.C., 1978.

82. Leonard, J. I., *Analysis of Head-Down Tilt as an Analog of Weightlessness Using a Mathematical Simulation Model*, NASA CR-171870, (General Electric Co. TIR 2114-MED-4003, Houston, TX), NASA, Washington, D.C., 1984.

83. Altman, Philip L. and Dittmer, Dorothy S., *Biology Data Book*, Federation of American Societies for Experimental Biology, 2nd ed., Vols. 1, 2 and 3, 1972.

84. Joint Soviet-American Experiment on Hypokinesia, Experimental Results, NASA TM-76013, 1979 (Also private communications from H. Sandler and C. S. Leach).

85. Hyatt, K. H., Hemodynamic and Body Fluid Alterations Induced by Bed Rest, in *Hypogravic and Hypodynamic Environments,* R. H. Murray and M. McCally (Eds.), NASA SP-269, NASA, Washington, D.C., pp. 187–209, 1971.

86. Leach, C. S. and Rambaut, P. C., Biochemical Responses of the Skylab Crewmen, in *Biomedical Results from Skylab,* R. S. Johnston and L. F. Dietlein (Eds.), NASA SP-377, NASA, Washington, D.C., pp. 204–216, 1977.

87. Fitzjerrel, D. G, Grounds, D. J. and Leonard, J. I., *Interfacing Major Physiological Subsystem Models: An Approach for Developing a Whole-Body Algorithm*, (General Electric TIR 741-MED-5009, Houston, TX), NASA CR-160232, NASA, Washington, D.C., 1975.

88. Leonard, J. I., Leach, C. S. and Rummel, J. A., Computer Simulations of Postural Change, Water Immersion and Bed Rest: An Integrative Approach for Understanding the Spaceflight Response, *The Physiologist,* 22: S31–S32, 1979.

89. Dunn, F. L., Brennan, T. J., Nelson, A. E. and Robertson, G. E., The Role of Blood Osmolarity and Volume in Regulating Vasopressin Secretion in the Rat, *J. Clin. Invest.,* 52: 3212–3219, 1973.

90. Convertino, VA. Mechanisms of Microgravity Induced Orthostatic Intolerance: Implications for Effective Countermeasures. Overview and Future Directions. J. Grav. Physiol. 9: 1–12, 2002.

91. Greenleaf, J.E., Van Beaumont, W., Bernauer, E.M., Haines, R.F., Sandler, H., Staley, R.W., Young, H.L. and Yusken, J.W., Effects of Rehydration on +G_z Tolerance After 14-days Bedrest. *Aerospace Med.,* 44: 715–22, 1973.

92. Hyatt, K.H. and West, D.A., Reversal Bedrest-Induced Orthostatic Intolerance by Lower Body Negative Pressure and Saline. *Aviat. Space Environ. Med.,* 48: 120–24, 1977.

93. Greenleaf, J.E., Brock, P.J., Haines, R.F., Rositano, S.A., Montgomery, LD. and Keil, L.C., Effect of Hypovolemia, Infusion and Oral Rehydration on Plasma Electrolytes, ADH, Renin Activity and +G_z Tolerance. *Aviat. Space Environ. Med,* 48: 693–700, 1977.

94. Charles, J.B. and Lathers, C.M., Cardiovascular Adaptation to Spaceflight, *J. Clin. Pharm.* 31: 1010–1023, 1991.

95. Srinivasan, R.S., Simanonok, K.E. and Charles, J.B., Computer Simulation Analysis of the Effects of Countermeasures for Orthostatic Intolerance, *Physiologist,* 35: S165–S168, 1992.

96. Srinivasan RS, Leonard JI, White RJ. Mathematical Modeling of Physiological States. in *Space Physiology and Medicine*, (Eds.) A.E. Nicogossian, S.R. Mohler, O.G. Gazenco, A.I. Grigoriev, VA Reston. Reston, VA: American Institute of Aeronautics and Astronautics and Moscow, Russia: Nauka Press, 1996, vol III, Chap. 26, p. 559– 594.

97. Srinivasan, R.S., Simanonok, K.E., Fortney, S.M. and Charles, J.B., Simulation of the Fluid Retention Effects of a Vasopressin Analog Using the Guyton Model of Circulation, *Physiologist,* 36: S114–S115, 1993.

98. Murray, R.H. and McCally, M.(Eds.), *Hypogravic and Hypodynamic Environments.* NASA SP-269, NASA, Washington, D.C., 1971.

99. Leonard, J.I., *The Behavior of Renal-Regulating Hormones During Hypogravic Stress*, General Electric Co., Houston, TX, TIR 2114-MED-5002, 1985.

100. Leonard, J.I., Computer Simulation Analysis of the Behavior of Renal-Regulating Hormones During Hypogravic Stress. *The Physiologist,* 25, S65–S66, 1982.

101. Gauer, O.H., Henry, J.P. and Behn, C., The Regulation of Extracellular Fluid Volume, *Ann. Rev. Physiol.*, 32: 547–595, 1970.

102. Leach, C.S., Alfrey, C.P., Suki, W.N., Leonard, J.I., Rambaut, P.C., Inners, L.D., Smith, S.M., Lane, H.W. and Krauhs, J.M., Regulation of Body Fluid Compartments During Short-Term Spaceflight. *J.Appl.Physiol.* 81: 105–116, 1996.

103. Buckey, J.C. Jr, Gaffney, F.A., Lane, L.D., Levine, B.D., Watenpaugh, D.E., Wright, S.J, *et al.*, Central Venous Pressure in Space, *J. Appl. Physiol.* 81: 19–25, 1996.

104. White, R..J. and Blomqvist, C.G., Central Venous Pressure and Cardiac Function During Spaceflight. *J. Appl. Physiol.* 85: 738–746, 1998.

105. Buckey, J.C. Jr. Central Venous Pressure, in, *Gravity and the Lung: Lessons from Microgravity*, Prisk, G.K., Paiva, M. and West, J.B. (Eds), Marcel Dekker, Inc., N.Y. 2001, pp. 225–253.

106. Hargens, A.R., Tipton, C.M., Gollnick, P.D., Mubarak, S.J., Tucker, B.J. and Akeson, W.H., Fluid Shifts and Muscle Function in Humans during Acute Simulated Weightlessness, *J. Appl. Physiol.*, 54: 1003–09, 1983.

107. Parazynski, S.E., Hargens, A.R., Tucker, B.J., Aratow, M., Styf, J. and Crenshaw, A., Transcapillary Fluid Shifts in Tissues of the Head and Neck During and After Simulated Microgravity, *J. Appl. Physiol.*, 71: 2469–75, 1991.

Update Endnotes

UPDATE #1. Central Venous Pressure

The analysis in the water immersion section revealed a suspected problem with the high and sustained measurements of central venous pressure during water immersion reported by researchers. The magnitude of the reported values are well outside the range of right atrial pressures which are generally accepted in the control of cardiac function and are in disagreement with the model of Guyton as well. In this case, rather than indicting the model, it is suggested that the measurements are skewed by an artifact of the immersion technique. That is, the external hydrostatic pressure at the level of the heart during immersion is transmitted to the circulation and the pressure transducers. If this is true, the value of water immersion in understanding the spaceflight response becomes questionable. In spaceflight, recent findings (years after the above simulation analysis was performed) indicate that central venous pressure falls rather than increases [103]. While this appears to agree with head-down tilt studies and the Guyton model computer simulation, spaceflight measurements found no increase in venous pressure, even at the onset of microgravity. The reasons for the changes in space seem to be different than those found in one-g or computer studies. Current hypotheses have been subjected to computer modeling [104] and critically reviewed [105].

UPDATE #2. Transcapillary Fluid Movement

(Related to Chapters 9.5.2 and 9.7.5.2) In the water immersion and head-down tilt studies, an analysis was performed in which the model predicted an increase in transcapillary protein permeability in the upper body possibly as a result of headward fluid shifts. Relevant to this model prediction made many years ago, is a recent spaceflight study of body fluid regulation, that has shown a decrease in plasma protein concentration (including albumin) [102]. Those investigators suggested that an increased rate of transcapillary protein transport into the interstitium might account not only for the decreased plasma proteins but was a cause of the reduction in plasma volume.

UPDATE #3. Early Diuresis

In the spaceflight experiment of Leach, *et al.* [102] the diuresis at the onset of microgravity was not observed even though it was an important objective of the research and inspite of an expectation that it should occur. The astronaut subjects were requested to maintain their hydration at normal levels but this could not be guaranteed because there is a desire on their parts to minimize their intake of fluid prior to launch. In addition, astronauts waiting on the launch pad (often for several hours) are in a sitting position, on their back, with their feet and knees above their head. Inasmuch as this position should produce many of the fluid distribution and renal effects as head-down tilt, there is a likelihood that the diuresis expected upon insertion into weightlessness could be considerably blunted.

In the same study, the plasma volume was shown to decline within 2-days. It was hypothesized by the researchers that plasma volume decreased, not because of the expected diuresis, but because of fluid transport into the interstitium presumably due to an increase in upper body transcapillary protein permeability.

UPDATE #4. Transcapillary Starling Forces During Head-Down Tilt.

(Related to 9.7.3.2.1) The earliest studies of transcapillary fluid shifts during head-down tilt indicated that dehydration of lower leg tissues resulted from inward filtration due to a decreased capillary blood pressure. Interstitial fluid pressure in leg muscles decreased, fluid colloidal concentrations did not change and capillary pressure was not measured; therefore, the results were not conclusive [106]. But these researchers believed that there is a drop in capillary blood pressure in tisssues below the heart that is responsible for tissue dehydration. More recent studies of the head and neck areas suggested that facial edema during head-down tilt is caused primarily transcapillary filtration mediated by elevated capillary pressures and decreased plasma colloid osmotic pressure and attenuated somewha by elevated interstitial fluid. Support was provided in this study for the Guyton model's behavior whereby there is a transition from inward capillary filtration in the legs and outward filtration above the heart duriing head-down tilt [107].

Chapter 10
Discussion and Conclusions

10.1 Introduction

The goals of this project were to apply new analytical methods to analyze the major medical experiments of Skylab, to develop and test individual physiological subsystem hypotheses using computer models, and to integrate these hypotheses into a unified and internally consistent understanding of the physiological adaptation to weightlessness. The systems analysis effort has yielded two major kinds of results or end-products. First, is an array of systems analysis methods, tools, and techniques that have proven valuable for the processing and interpretation of experimental data in general, and spaceflight data in particular. Second, is an improved understanding of the physiological events that occur during human adaptation to weightlessness, and the concomitant identification of areas suitable for future study. Both of these perspectives will be summarized in this chapter.

The systems analysis methodology, particularly the use of mathematical models, holds much promise as an analytical tool and continues to be of great interest to a portion of the space research community. In contrast, many of the conclusions, interpretations, and recommendations developed in the project regarding spaceflight physiology are likely, because of the passage of time, to have been superceded by research that is more recent. However, because of the limited pool of researchers and flight opportunities, the field of space medicine has moved slowly relative to its earth-based cousin. Thus, while there are likely to be some physiological insights that are still worthwhile to present day researchers, the conclusions presented here, while not necessarily outdated, are not meant to represent current thinking in the field. Rather, this book represents, as was stated at the outset, an historic record of a unique project in NASA's life science program.

A major contribution of the systems analysis approach was the organization and integration of various functions that were not previously available to the space life sciences program on a systematic basis. Integration was applied to such categories as multiple physiological disciplines, multiple models and subsystems, multiple control systems within those models, multiple environmental and metabolic stresses on the body, multiple hypotheses, and multiple sources of ground-based and spaceflight data (Fig. 10-1). The most important of these integrating functions and activities include the following:

a. integration of multiple data sets from different investigative areas (i.e., cardiovascular, musculoskeletal) into a common database and analysis system to provide an interdisciplinary cross correlation capability;

b. integration of multiple physiological and environmental stresses (i.e., bedrest, water immersion, spaceflight) to construct an acceptable description of the weightlessness response;

c. integration of experimental data with concepts of physiological control (i.e., biosystem models) in order to compare real-world and theoretical behavior and generate verifiable predictions;

d. integration of physiological mechanisms relating to homeostatic control of an organ system within the framework of a mathematical model, i.e., regulation of blood pressure by integrating baroreceptors, chemoreceptors, hormonal control and renal control;

e. integration of physiological subsystem models into a larger, more complex "whole-body model" to study theoretical interactive effects, i.e., integrate cardiovascular, respiratory, thermal, and fluid volume regulation; and

f. integration of subsystem hypotheses related to zero-g adaptation into a unified theory showing overlapping and interactive effects between subsystems, i.e., gravity unloading, fluid shifts, metabolism, short and long term effects.
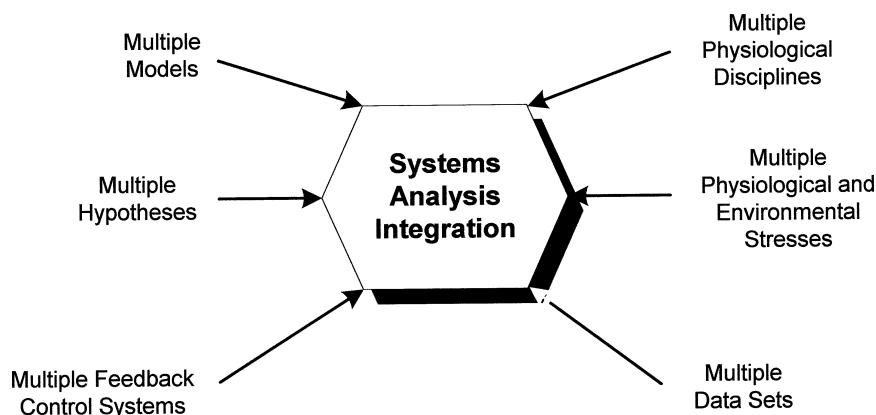
Figure 10-1. Systems analysis is ideally suited for integrating a variety of categories in complex research projects.

Why is "integration" of such great value? Integration permits one to systematically examine all the elements associated with a particular function or activity. Integration provides a "big picture" perspective from which it is easier to discern the commonalities and differences of the subelements and to look for synergies, especially in complex research projects. Systems analysis provided the tools for integration and resulted in a comprehensive approach to these complex problems. In NASA life sciences, there was no other group specifically engaged in an interdisciplinary or integrative analysis of a large portion of the Skylab database.

Of the two categories of end-products mentioned above, major accomplishments in the first of these, *development of systems analysis technology,* include (see Chapter 3 and Table 10-1):

a) The Skylab Integrated Medical Data Analysis System (SIMDAS) for interdisciplinary analysis using databases, statistical analysis and modeling systems,
b) The suite of individual subsystem models describing cardiovascular, fluid-electrolyte, erythropoietic, respiratory, thermal, and calcium regulation,
c) Development and validation of a first generation Whole-Body Algorithm for simulating spaceflight adaptation, and
d) An Integrated Metabolic Balance Analysis System for reexamining the unique Skylab metabolic balance and body composition data.

The most notable accomplishments in the second category, an *improved understanding of the physiological processes in microgravity,* include:

a) A new interpretation of the extensive metabolic and whole-body measurements from Skylab (Chapter 4);
b) An analysis and interpretation of all data related to disturbances in body fluid volumes (Chapter 5),
c) Development of hypotheses to explain the loss of red cells in spaceflight (Chapter 6);
d) Development of hypotheses of the mechanisms leading to orthostatic intolerance and decreased aerobic capacity following spaceflight (Chapter 7); and
e) Differentiation between fluid-shift effects of zero-g, water immersion, supine bedrest and head-down tilt/bedrest (Chapter 9), and
f) Limited progress was achieved with the more recent development of a calcium model and analysis of musculoskeletal data (Chapter 8).

As in most large scale studies composed of many component parts, there was a flexible approach to each area of analysis, the path chosen being dependent on the questions being asked, the models and data available, and the resolution required for the results. Nevertheless, there were certain common elements in the approach that can be summarized (below), now that all phases of the project have been addressed.

Table 10-1. Systems Analysis Technology Developed to Analyze Spaceflight Data

System	Function	Significance
Skylab Integrated Medical Data Analysis System	▪ Contains data from spaceflight and ground-based studies ▪ Analysis system includes statistical programs, special purpose programs and simulation models	▪ A database/analysis system that permits automated interdisciplinary analysis
Subsystem Simulation Models	• Validated mathematical models for: –Cardiovascular regulation –Fluid-electrolyte regulation –Respiratory regulation –Thermoregulation –Erythropoiesis regulation –Calcium regulation	• Permits a large array of quantitative models to be applied to solving problems in space physiology
Whole-Body Algorithm	• Integrates cardiovascular, fluid-electrolyte, respiratory, thermal, and erythropoietic regulatory models into one large model representing the major organ functions of the body	• Permits multi-organ simulation of prolonged flight adaptation interspersed with environmental (temperature, gas composition) and clinical (LBNP, exercise) tests, similar to the Sklylab protocol • Permits study of interactive effects between subsystems
Integrated Metabolic Balance Analysis System	• Computes metabolic balances for fluids, electrolytes, nutrients, and energy • Uses Skylab metabolic balance and whole-body data	• Provides description of time-varying changes in body composition during zero-g adaptation. • Estimates dietary and exercise requirements for zero-g

10.2 Important Factors of the Systems Analysis Approach

10.2.1 Critical Questions

Certain features of the systems analysis approach were particularly useful in guiding the evaluation of spaceflight data. Most importantly, the context of the analysis was established by the desire to answer several critical questions that were stated in the Introduction (Chapter 2), which can be briefly summarized as follows: a) Can the spaceflight findings be explained in terms of disturbances and responses of well-known homeostatic systems?; b)What are the common elements in the spaceflight response?; c) Is there a typical "zero-g response" as revealed by data from space and ground-based analogs of zero-g?; d) How can the differences between the responses of the crewmen from the three Skylab missions be explained?; and f) Can a unified theory of physiological adaptation to weightlessness be formulated?

10.2.2 Critical Subsystem Issues

As a starting point in the analysis of each physiological subsystem, an in-depth review was performed to reveal those "critical issues" in the observed responses that might become fruitful for more detailed analysis. This review not only consisted of examining the spaceflight data and complementary ground-based information but also the physiological processes and feedback control mechanisms involved in each physiological area. The mathematical models were useful in this latter task to help understand system behavior. A selection of these areas of unusual or unexplained events that were singled out for special attention in this project are listed in Table 10-2. Many of the most significant issues that were raised by researchers prior to and following Skylab are included in this list.

10.2.3 Hypothesis Formulation

These issues were systematically addressed by formulating and evaluating physiological hypotheses. Formulation of hypotheses was facilitated by examining each physiological system in terms of its regulating features and model behavior. Critical disturbance points of the feedback system could be tentatively singled out for detailed quantitative analysis by simulation. Spaceflight and ground-based data were reexamined for evidence to support the candidate hypothesis. All hypotheses that were eventually considered were not usually identified at the start of each analysis, but as part of the iterative cycle of model simulation and comparison with data as suggested by the process flow diagrams of Fig. 2-6 and 3-1. With each reiteration, the model pointed the way to new areas that lacked clarity. The hypotheses considered and evaluated in each investigative area are summarized in Table 10-3. The detailed analysis of these hypotheses and effects constituted a major portion of the total effort and led to the conclusions discussed subsequently in this section.

10.2.4 Integration of Hypotheses

An important objective of these studies was to search for basic phenomena common to the major physiological events in space and to determine areas of overlap ripe for interdisciplinary analysis. In many cases, a hypothesis or an effect of exposure to weightlessness that was important in one subsystem was later found to be useful to explain events in other subsystems. An example of one such overlapping area was the reduction in blood volume that was found to be of central importance in the behavior of the cardiovascular system, the fluid volume control system, the erythropoietic system and the metabolic systems. The most important of these overlapping areas are shown in Table 10-4. Where a particular effect is not associated with a specific physiological subsystem in this table, there is no implication that an association does not exist, only that it was not examined in this study. Also, certain effects such as insufficient exercise, inadequate diet, or thermal disturbances, all of which were present to varying degrees in the Skylab missions, may not be present on future flights, so this table is not of general value. Nevertheless, this tabulation does indicate the degree of hypothesis integration that was accomplished.

10.2.5 Hypotheses Testing

Evaluation of the hypotheses was accomplished by several means, including model simulation analysis, statistical analysis, and, in only a few cases, experimentation. The use of models was, by far, the most prevalent technique and the most unique in this project. Hypothesis testing is normally accomplished, in the case of simulation analysis, by comparison of the computer predicted responses with those observed experimentally. Models could predict the consequences of a particular hypothesis whose plausibility might be questioned if these consequences did not agree with known measurements. Models could also qualitatively distinguish between alternative hypotheses. Examples of this type of test include the hypothesis whether red cells that disappeared during spaceflight were regenerated or not while in space or whether or not exercise training could counteract the degraded exercise performance otherwise seen in microgravity?

Some hypotheses could be tested by simply altering a parameter value. In other cases new feedback pathways, such as a naturetic factor, were tested and found to enhance the simulation response. Still another approach was to clamp the value of a normally time-varying quantity to test its importance in producing certain effects. A number of useful modeling techniques were used for studying system behavior as altered by an hypothesis including sensitivity analysis, dynamic and steady-state responses, and examination of feedback mechanisms. Once a simulation was produced with the desired outcome it was easy to assess the relative contribution of individual mechanisms, thus providing a basis for generating new hypothesis.

The ability of a model to reproduce, in a *qualitative* manner, the behavior of a dozen or so measured variables, added to the robustness of the simulation and the probability that the hypothesis could be correct. This was much more useful to this project than *quantitatively* estimating the value of a particular parameter, i.e., parameter estimation or curve-fitting. Good agreement between model and data was not always essential. That is, it is not always

Table 10-2. Selected Observations from Skylab Experiments Addressed by Systems Analysis

---

Fluid-Electrolyte System

- Rapid loss of water early in flight
- Much larger decrease in leg fluid volume compared to bedrest
- Absence of measurable diuresis following headward fluid shifts contrary to expectations
- Unusual combination of hormonal changes compared to bedrest and water immersion
- Presence of hyponatremic plasma maintained throughout flight
- Increased water and sodium excretion throughout mission without continuous body losses
- Differences in ADH response between missions
- Decreased evaporative water loss in presence of hypobaric atmosphere
- Disproportionate losses of potassium and cell water

Cardiovascular System

- Absence of acute cardiovascular disturbances expected from headward fluid shifts
- Decreased orthostatic tolerance as measured by LPNP tests during flight and recovery
- Maintained aerobic capacity *during* flight despite decreased blood volume and decreased orthostatic tolerance
- Decreased aerobic capacity *immediately following* flight
- Differences in aerobic capacity among the three Skylab missions

---

Erythropoietic System

- Blood volume loss, as measured by plasma volume and red cell mass losses, not related to mission duration
- Inflight loss of red cell mass despite normoxic environment
- Delay in postflight recovery of red cell mass on shortest mission
- Significant differences in rates of red cell loss among the three Skylab crews

---

Musculoskeletal System

- Progressive loss of calcium from body
- Urinary calcium stabilizes at elevated level while fecal calcium increases progressively with flight duration
- Changes in PTH during spaceflight dissimilar to changes in bedrest
- Apparent decreases in rates of nitrogen losses as a function of flight duration and increasing levels of exercise

---

Body Composition

- Apparent disproportion in rates of water, muscle, and fat losses in relation to their normal ratio in body tissues
- Decreases in body mass losses with flight duration
- Water losses in astronauts apparently independent of flight duration
- Large differences in body composition changes between the crews of the three Skylab missions
- Body composition changes related to differences in diet and exercise on each mission
- Apparent similar energy requirements in zero-g and one-g contrary to prior belief

---

Table 10-3. Hypotheses Tested by Simulation, Metabolic, or Statistical Models

Cardiovascular System

1. Acute cardiovascular disturbances expected from headward fluid shifts

2. Long-term adaptation of blood volume, pressures, and flows expected from:
   a) stress relaxation
   b) baroreceptor and volume receptor resetting
   c) autoregulation of blood flow
   d) changes in metabolic activity

3. Decreased orthostatic tolerance and maintained aerobic performance *during* flight due to:
   a) reduced blood volume
   b) collapse of leg veins
   c) increased compliance of leg veins early in flight
   d) retoning of leg veins and reduction of unstressed volume late in flight
   e) altered sensitivity of baroreceptors
   f) continued activity from cardiopulmonary volume receptors
   g) hemoconcentration opposing blood loss to maintain oxygen delivery

4. Effects of *inflight* exercise training:
   a) enlarged heart
   b) increased contractility of the heart
   c) reduced sympathetic activity
   d) decreased arteriolar vasodilation during exercise
   e) increased leg capillary density
   f) increased vagal activity at rest

5. *Postflight* decreased aerobic performance and orthostatic tolerance:
   a) reduced blood volume
   b) increased sympathetic activity affecting heart and peripheral vessels
   c) incomplete compensation of venous capacitance for reduced blood volume

Fluid-Electrolyte System

1. Changes in renal excretion, hormone secretion, body fluid volumes, and fluid composition observed in flight due to:
   a) headward fluid shifts
   b) loss of extracellular fluid and sodium
   c) loss of cellular electrolytes
   d) presence of a natriuretic factor
   e) decreased evaporative water and electrolyte sweat losses
   f) anorexia early in flight
   g) altered ratio of fluid/electrolytes in diet
   h) preflight dehydration
   i) hyponatremia of extracellular fluid

Erythropoietic System

1. Inflight loss of red cell mass resulting from:
   a) hemoconcentration
   b) increased arterial oxygen tension
   c) shifts in oxy-hemoglobin affinity
   d) increased renal blood flow
   e) inadequate diet
   f) inadequate exercise
   g) altered bone-marrow responsiveness
   h) hemolysis early in flight
   i) loss of lean body mass
   j) regeneration theory vs. continuous loss theory

2. Postflight recovery kinetics affected by:
   a) hemodilution
   b) delay in plasma volume recovery
   c) hemolysis
   d) bone marrow transit time delay
   e) increased oxy-hemoglobin affinity
   f) ineffective erythropoiesis

Musculoskeletal System

1. Atrophy of muscles and bone induced by:
   a) gravitational unloading
   b) postural disuse
   c) exercise disuse
   d) inadequate diet
   e) high levels of cortisol
   f) muscle-bone interaction
2. Loss of calcium caused by:
   a) decreased intestinal absorption
   b) inhibited vitamin D production
3. Increased fecal calcium results from decreased intestinal absorption mediated by inhibited vitamin D production.
4. Feedback influence of parathyroid hormone may limit calcium loss.
5. Calcium loss does not stabilize and may become progressive.
6. Muscle loss stabilizes with increasing flight duration.

Body Composition and Energy Metabolism

1. Are rates of water, muscle, and fat losses proportionate to ratio in body tissues?
2. Can body fat losses be predicted from energy balance considerations?
3. Is water loss independent of flight duration?
4. Are the various methods for estimating lean body mass losses (total body water, total body potassium, biostereophotometry, nitrogen balance, potassium balance) in agreement?
5. Is muscle loss dependent on the level of inflight exercise?
6. Does the anorexia of motion sickness significantly influence body composition changes?
7. Are energy requirements in zero-g and one-g similar?

Table 10-4. Examples of Integrated Quantitative Hypotheses Testing

Skylab Hypothesis or Effect	Cardiovascular	Body Fluid Volume & Renal Regulation	Erythropoietic	Musculoskeletal	Thermoregulatory	Body Metabolism
1. Effect of Gravity Vector Per Se	X	X		X	X	
2. Effect of Headward Fluid Shifts	X	X	X			
3. Effect of Blood Volume Loss	X	X	X			
4. Effect of Atrophy and Cell Demineralization	X		X		X	
5. Effect of Exercise Conditioning	X		X	X		X
6. Effect of Metabolic Rate	X	X	X		X	X
7. Effect of Diet		X	X	X		X
8. Effect of Thermal Disturbance	X	X				X

necessary that the model be an exact description of reality. The most valuable results occurred when simulations did not match expectations and when there were surprises. The heuristic characteristics of modeling added value by suggesting improvements to the models, new hypotheses, and new experiments even if agreement was poor.

In most laboratories, hypotheses are tested by designing new experiments on the back of the results of the last experiment. This was not a feature of the current project because it was planned as being a more theoretical study and experiments in space were many years apart. However, collaborations with several investigators who performed human and animal studies led to the ability for systems analysis to contribute to new experiments, in one case this consisted of erythropoiesis studies in the mouse (see Chapter 6.5.4) and in another case, to a head-down bedrest study in humans (see Chapter 9.7). Results of those studies, in turn, led to refinements in hypotheses and modeling studies. Modeling was also useful in designing protocols for advanced flight experiments on the Shuttle Spacelab. In the only case highlighted in this book, the erythropoiesis model helped formulate the blood draw protocol for a hematology experiment so that blood sampling would not skew the results (see Chapter 6.5.6). Recommendations for the next generation of flight experiments were generated in most areas studied (the reader is referred to Appendix G for more detail). In addition to hypothesis testing and recommendations for future experiments, there are a couple of examples in which the models were utilized to evaluate the plausibility and efficacy of countermeasures against orthostatic intolerance (see Chapters 7.5.4 and 9.7.6). Taken together, these capabilities for hypothesis testing resulted in a greater utilization of valuable information acquired from spaceflight.

10.2.6 How Models Shaped Data Analysis

Models were very useful in indicating which data was most crucial. The hypothesis testing approach often re-

quired dietary, metabolic rate, or environmental data to drive the simulation, and still other types of data with which to compare the model responses. This often led to reexamining data that was not readily obtainable or that had already been analyzed by more traditional, e.g., statistical, methods. Satisfying these data requirements led, in one instance, to the integrated metabolic balance analysis for describing body composition changes during spaceflight. In another situation, the study that led to an analysis of evaporative water loss in the Skylab crew was suggested originally by the need to validate the sweating mechanism in the thermoregulatory model for weightlessness. Both of these unanticipated analyses provided results that proved useful in their own right as well as contributing to improved simulations.

10.2.7 Simulation of Analog Studies

An important part of the analysis was the simulation of a number of different ground-based studies, each related to the spaceflight stresses in some important manner. These one-g studies often provided more abundant data than were available from spaceflight investigations. In addition, they were helpful in understanding the basic responses, both in the human and in the model, to simple or well-known environmental and metabolic disturbances without the confounding influence of spaceflight. Thus, in the case of studying acute fluid shifts in spaceflight and upon recovery, some important experimental situations examined included the responses to fluid loading, hemorrhage, and postural changes. Similarly, in the analysis of erythropoietic regulation during weightlessness, it was found useful to review the results from red blood cell infusions, dehydration, and descent-from-altitude studies. Some ground-based studies were specifically designed to simulate weightlessness. These hypogravic stresses included supine and head-down bedrest and water immersion. These stresses have some common characteristics of spaceflight, namely, a reduction in hydrostatic gradients

Table 10-5. Stresses Related to Spaceflight that were Studied Using Simulation Models

• **HYPOGRAVIC STRESS**	• **FLUID SHIFTS (NON-GRAVIC)**
- Supine Bedrest	- Hemorrhage
- Head-down Tilt/Bedrest	- Fluid Infusions
- Water Immersion	- Water and Salt Loading
- Spaceflight	- Dehydration
• **ENVIRONMENTAL DISTURBANCES**	• **METABOLIC STRESS**
- Hypoxia	- Exercise (Trained & Untrained)
- Hypercapnia	· Diet Restriction
- Temperature	
- Ambient Pressure	• **ERYTHROPOIETIC STRESS**
	- Altitude Hypoxia and Descent
• **ORTHOSTATIC STRESS**	- Red Cell Infusion
- LBNP	- Erythropoietic Injection
- Tilt Table	- Anemia
- Postural Change	- Polycythemia
- Centrifugation	- Hemoglobin disorders
- Shuttle Reentry	

and a rapid headward shift of fluid. Some of these studies emphasized the short-term phase of hypogravity while others described the longer-term processes. Taken together these analog studies provided a better understanding of the complete temporal spectrum of hypogravic responses. Confidence in the computer simulations were achieved by validating the models for such a wide variety of experimental and clinical conditions. A partial list of these simulations is presented in Table 10-5**.** The simulation models helped to reveal the regulatory processes operative in these situations and provided a quantitative basis for testing whether the same mechanisms were operative in spaceflight.

10.2.8 Testing Differences Between Missions

The goal of much of the analyses was to isolate and identify the effects of microgravity, but this was not always possible because of the confounding effects of variations in diet, exercise and flight duration among the Skylab crewmembers. In cases where these factors seemed important (such as in studying body composition, erythropoiesis regulation, or cardiovascular responses to exercise) each mission was examined separately. A considerable effort was made to account for diet and exercise in as quantitative a manner as possible. For example, a systematic study was undertaken to document a composite or average level of crew diet on a daily basis, including the caloric (i.e., fat, carbohydrate, and protein) and non-caloric (water, electrolytes) components. These data were then utilized as model forcing functions to obtain more realistic simulations of the fluid-electrolyte regulatory response. In the case of erythropoiesis regulation, the interpretation of the differences between red cell mass loss on the three missions was accomplished, in part, on the basis of exercise and dietary considerations using both statistical and mathematical modeling techniques. Similarly, the cardiovascular stress test results suggested an involvement of exercise conditioning effects that was examined by developing "physically trained" and "physically untrained"

cardiovascular models. These analyses all pointed toward specific hypotheses implicating dietary and exercise factors and recommendations for controlling these factors in future flight experiments.

In addition to the effects of duration, exercise and diet, there were other differences between spaceflight and ground-controls. The Skylab environment also included reduced ambient pressures, increased oxygen and carbon dioxide ambient gas tensions, isolated instances of elevated temperatures, and transient but large variations in gravitational stress forces at launch and re-entry. In some cases it was possible to reassess the Skylab data by accounting for these known changes, especially for the erythropoiesis analysis. Just like diet and exercise, the models, especially the Whole-Body Algorithm, included parameters that could adjust for these changes. While several of the individual models were useful in this regard, the analysis, unfortunately, did not progress to the point where the Whole-Body Algorithm was utilized for a more comprehensive analysis.

10.2.9 Time-Dependent Analysis

It proved advantageous in a number of cases to segment the analysis into short-term (or acute) and long-term (or chronic) response periods. This concept was based on the suggestion from modeling studies, that showed that the mechanisms that participate in the short-term response (the time during which the most prominent fluid and circulatory disturbances occur) are different from those that lead to adaptation during prolonged spaceflight. Also, the most dramatic disturbances in the body seem to occur during the first several days following launch and reentry. This suggested a logical division of the spaceflight period into acute and chronic segments as a convenient method of examining the spaceflight data and performing computer simulations. (Also, in general, physiological processes appear to be much better understood for acute changes, than for long-term adaptation). The models ca-

pable of simulating both short and long-term responses are the circulatory, fluid, and electrolyte model, the erythropoiesis model and the calcium regulation model; the remaining models, the pulsatile cardiovascular model, the respiratory model and the thermoregulatory model are capable of simulating only short-term responses.

10.3 Major Conclusions from Physiological Systems Analysis

This study addressed most of the physiological systems that have been extensively examined during previous spaceflights, particularly during the Skylab program. For purposes of summation, the investigative areas will be grouped into the same five categories used throughout this volume: fluid-electrolyte regulation, erythropoiesis regulation, cardiopulmonary function, musculoskeletal function, and body metabolism and composition (see Table 2-1). Table 10-2 indicates the broad spectrum of physiological issues and adaptive processes that were considered in each area, although these did not always coincide with the original objectives of the corresponding Skylab experiments.

As shown in Table 10-6, the study of the *fluid-electrolyte system* emphasized the regulation by renal and endocrine controllers, of fluid volume compartments and electrolyte composition as well as differentiating between acute and chronic responses. The *cardiopulmonary systems* analysis was directed at the study of circulatory regulation during rest in zero-g and as a result of orthostatic challenges and exercise stress testing. The analysis of the *erythropoiesis regulatory system* covered one major issue, that is, the loss of red cell mass during exposure to zero-g. In order to address this issue, however, the entire schema of erythropoietic, blood volume, and oxygen transport regulation had to be considered as well as energy balance effects. Of concern in the *musculoskeletal area* was the precise description of hard and soft tissue loss. In the case of bone demineralization, formulation of a quantitative model of calcium regulation was in its initial stages of validation. "Why do astronauts lose weight in space?" was the central question addressed by the extensive analysis of *metabolic balance and body composition*. A more detailed list of topics and accomplishments in each area can be found in Appendix G. The major conclusions and the interpretation of the spaceflight findings emanating from this study are summarized in the sections that follow, first in terms of the individual physiological subsystems and then as an integrated hypothesis.

Conclusions drawn from the interpretation of the spaceflight data should be accepted with caution, as they are limited, in large part, by a number of constraints imposed on the collection of data. For example, with regard to the Skylab missions:

a) There were a relatively small number of subjects on each flight, making statistical treatment of the data difficult, especially for findings beyond the first 28 days.

b) The restriction on invasive measurements, as well as on measurements collected early in the mission lim-

Table 10-6. Investigative Areas and Issues Considered in Study

Fluid-Electrolyte System
Body FIuid VoIume Regulation
Body Fluid Electrolyte Regulation
Renal and Endocrine Control
Acute vs Chronic Responses

Cardiopulmonary System
Circulatory Status at Rest in Zero-g
Response to Orthostatic Tolerance Test (LBNP)
Response to Shuttle Reentry
Response to Metabolic Stress (Exercise)
Exercise Training Effect

Erythropoiesis Regulation
Blood Volume Loss
Erythropoiesis Regulation
Renal vs Bone Marrow Effects

Musculoskeletal System
Soft Tissue Losses (Lean Body Mass)
Bone Demineralization and Calcium Regulation

Body Composition
Energy Balance (diet and exercise)
Water and Electrolyte Balance
Dynamics of Body Composition Changes
Components of body mass loss

ited the amount of useful data that could be collected. That is why simulation models and supplementary data from zero-g analogs became so critical.

c) Conclusions drawn from the data need to be limited to the relatively homogeneous population of the astronaut subjects – i.e., physically fit men in their late thirties. Generalization to broader populations in terms of age, sex and physical training involves some additional uncertainty.

d) There were differences between the three Skylab missions (such as ambient temperature excursions, space motion sickness, daily caloric intake, and levels of personal exercise) that undoubtedly increased the variance of the data for the combined crewmembers.

e) A number of factors were present in spaceflight in addition to weightlessness (see last section) but experimental controls to account for these were not completely successful. Thus, it is not possible to offer definitive conclusions regarding a spaceflight effect as arising solely because of gravitational changes.

In addition, there are limitations and errors associated with the methods of analysis used in this project. These will be discussed later in this chapter. The physiological processes described below are gleaned from three sources:
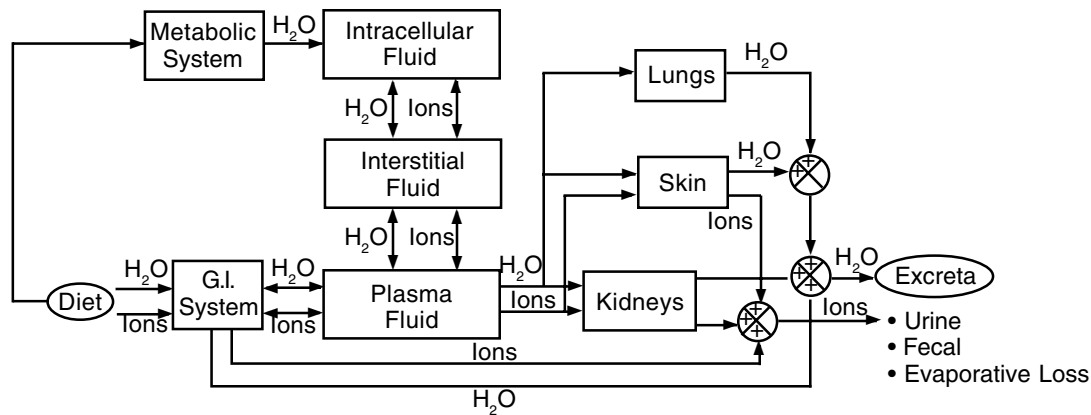
Figure 10-2. Fluid-electrolyte characteristics of the human body. Assessing the values of all the volumes and flow rates indicated here and how they changed during the course of a long spaceflight became an important goal of this project.

spaceflight data, primarily from Skylab; ground-based data, largely from studies of water immersion, head-down tilt and bedrest; and simulation studies, principally using the appropriate subsystem (stand-alone) mathematical model. The analyses on which these descriptions are based are described in detail in the previous chapters (Chapters 4 to 9). These summaries serve as the conclusions of those chapters. While today, many of the tentative conclusions discussed in the next sections may appear either well-accepted or outdated, they were considered to be novel when the original research was completed 20 years ago.

10.3.1 Fluid-Electrolyte Response to Weightlessness

A major emphasis of this project was an understanding of the control of whole-body fluid-electrolyte metabolism during the acute and adaptive phases of spaceflight. Figure 10-2 is a schematic of the body's fluid compartments and all the routes of fluids and electrolytes entering and leaving these compartments and the body itself. A knowledge of the alteration of the body's fluid volumes is central to an understanding of weightlessness by virtue of its influence on the circulation. Therefore, identifying the status of the body's fluid systems in spaceflight, and how it changes over time, became an important goal in this project. As indicated in Fig. 10-2, this would include knowledge of the volume and electrolyte composition of several fluid compartments (plasma, interstitial, intracellular) and the major flow paths for water and electrolytes (dietary inputs, metabolic water, fecal loss, urine excretion, and evaporative water) into and out these compartments.

Although this approach was not part of the original experimental design on Skylab, it was thought that innovative data analysis techniques combined with judicious use of the simulation models could identify most of these compartments and pathways and thus, an approximation of the fluid volume status during spaceflight. In addition, the mathematical models, containing the physiological control systems (hemodynamic, neural, hormonal) that

regulate the quantities shown in Fig. 10-2, could provide critical insight about the regulatory behavior of the entire system. A fundamental analysis of fluid control in space can be found in Chapter 5 while the application of these principles to simulation studies of different types of hypogravity are presented in Chapter 9.

Analysis of this disciplinary area, including circulatory adjustements, benefited from separating the regulatory behavior into an acute phase and a chronic, adaptive phase. The Guyton model was well suited for this two-pronged approach, because, it, more than any other model in our repertoire, included a number of long-term adaptive mechanisms that appeared to have as significant a role in spaceflight as they do on earth.

10.3.1.1 Acute Response. There is unequivocal evidence that hypogravic stresses such as bedrest, water immersion, and spaceflight result in significant fluid redistribution within the body. The removal or reduction of the hydrostatic pressure in the blood column, coupled with the normal tissue elastic forces and muscle tone of the lower body, results in shifts of blood and tissue fluid from the lower body to the intrathoracic circulation. The consequences of this event are widespread and long lasting, as suggested by Fig. 10-3, which is based on water immersion and head-down tilt studies as well as model simulations. As a result of acute central volume expansion, the following complex sequela of neuro-humoral reactions occur with rapid secondary changes in the cardiovascular and renal systems:

a) Decreased sympathetic outflow to the kidneys, peripheral vessels, and heart leading to peripheral vasodilation

b) Increased venous return leads to enhanced cardiac output,

c) Reduced secretions of renin, angiotensin, aldosterone and ADH promoting vasodilation and elimination of water and salt,

d) enhanced renal excretion of fluid and electrolytes as

a result of the alterations in sympathetic activity, hormone secretion, and blood pressures and flows;

e) increased transcapillary filtration of plasma into the interstitium favored by increased hydrostatic pressures, and

f) a decrease in thirst following reduction in angiotensin levels and augmented by space motion sickness anorexia.

Thus, the volume controllers near the heart interpret the headward shifted fluids as excess volume and activate three potential pathways to reduce the blood volume including capillary filtration, renal excretion and a thirst mechanism. Of these, the renal mechanisms are the most complex and powerful and can be further separated into three groups, mediated by neural, hormonal, and hemodynamic factors. The net result of these processes is the loss of extracellular fluid and electrolytes, which has been observed frequently following weightless spaceflight. According to model simulations these fluid adjustments tend to reduce central blood volume to normal levels, thus opposing the notion that central hypervolemia may lead to cardiopulmonary fluid congestion.

Measurements were not possible on Skylab during the first few hours, but based on 24-hour pooled urine voids, urine flow in the Skylab crew was not increased during the first several days. Does this invalidate the fluid-shift theory described above? Although experimental evidence for this theory is sparse during spaceflight, it is possible to make generalizations concerning the contribution of the three major pathways shown in Fig. 10-3.

a) **Transcapillary Filtration.** Simulations predict that the role of transcapillary filtration is minor and self-limiting as a means of relieving central hypervolemia unless transcapillary protein permeability increases dramatically. Modeling studies showed that hemoconcentration results from the shift of blood from the legs but not from the shift of previously pooled leg tissue fluid, although both fluid pools are mobilized. If plasma colloids are also concentrated by the same mechanisms, the model predicts a dramatic attenuation of filtration into the tissues of the upper body early in flight. Alternatively, the model allows for the possibility of an increase in capillary protein permeability that actually enhances filtration and further depletion of plasma volume. In either case, the simulations predict that, in the absence of edema, the total amount of fluid that can be accepted into the interstitium is limited.[*]

b) **Thirst Mechanism and Drinking.** It can be easily computed from the measurements of water balance, that the entire loss of body fluids observed in the Skylab crew could be accounted for by deficit fluid intake (possibly as a result of space motion sickness, a volunteer curb on fluid intake, or some mechanism peculiar to hypogravity) rather than renal excretion.

c) **Renal Mechanism.** Model and ground-based studies suggest that if thirst is not a factor, a renal diuresis is likely to be the preferred pathway of fluid regulation in the well-hydrated subject. Computer simulation analysis of the early flight period agrees with the findings from daily-pooled inflight urine samples that there is a suppression of renal excretion of water and sodium during the first several days. However the model also predicts a distinct diuresis during the first six hours that follow acute heardward fluid shifts, and that this diuresis is reduced but not abolished with a decrease in fluid intake, i.e., dehydration. It is postulated that a diuresis was not observed because void-by-void urine samples could not be obtained and because an early diuresis would be masked in a 24-hour pooled sample in the presence of diminished fluid intake. The short-term renal response to spaceflight in well-hydrated subjects has only recently been studied.[*]

Based on model analysis and postflight measurements, plasma volume is depressed about 0.5 liters throughout the flight (see Figs. 10-5 and 10-15). The failure of plasma volume to return to normal during prolonged flight (even with ad libum fluid intake) is presumptive evidence of the fluid-shift hypothesis of Fig. 10-3 involving blood volume controllers and perhaps a change in volume set-point. Failure to demonstrate any of the particular mechanisms such as reduced ADH or a diuresis during the acute stress phase does not necessarily invalidate the overall theory, because alternative pathways can be activated to achieve the predicted plasma volume loss. Thus, although an expected diuresis has not yet been observed early in flight, volume receptors and renal excretion pathways may be continually responding to the tendency for fluids to pool headward and thereby act to maintain a reduced blood volume. The renal pathway for controlling blood pressure (and thereby controlling blood volume) has been shown by Guyton to be the only mechanism in the body to have infinite gain, meaning it is capable of 100% correction of any deviation from control values (see Chapter 5).

Whatever the mechanism, most of these early fluid losses from the blood and from the body, appear to be ultimately derived from observed decrements in leg volume involving a contraction of the plasma, interstitial, and possibly intracellular fluid spaces of the lower limbs. Almost the entire decrement of body water and sodium that occurs during the flight, representing extracellular losses occurs within the first two days after the onset of weightlessness. At the end of this period, the legs and the body will have lost nearly 1.5 liters of fluid. Symptoms of distention of neck and head veins, facial puffiness, and a feeling of congestion in the head indicate the tendency of fluids to continue to pool in the upper body. In addition, during the early stages of flight, it can be deduced that significant quantities of potassium are escaping from intracellular compartments, bringing with it cell fluid. These early losses

---

[*] Recent flight experiments on the Shuttle Spacelab could not confirm either a microgravity-entry diuresis nor an increase in central blood pressures. See Chapter 9 endnotes and Chapter 7 for more recent findings on the acute phase of fluid and circulatory changes during spaceflight.
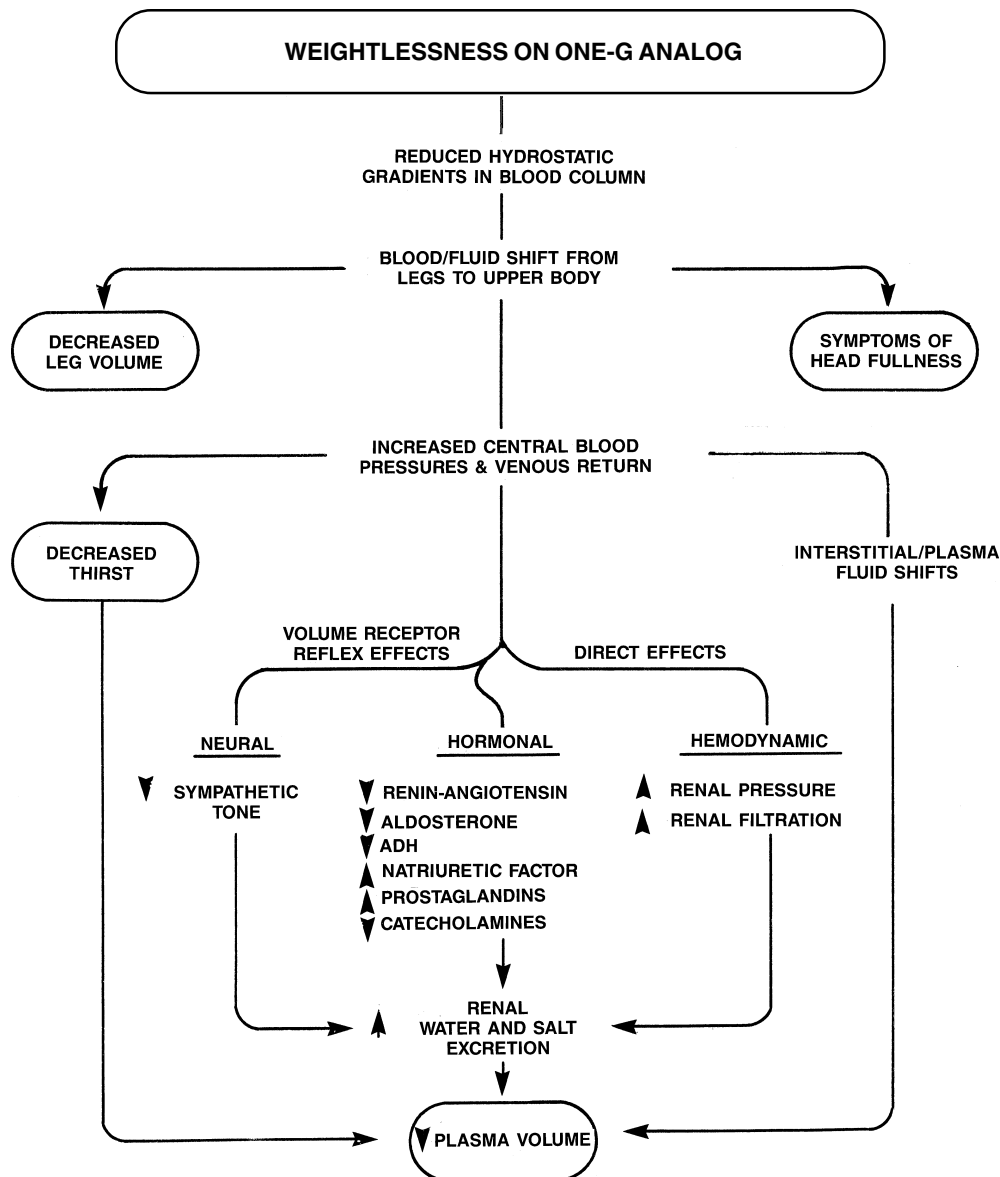
Figure 10-3. Hypothesis diagram to illustrate how headward fluid shifts induced by weightlessness lead to a decrease in plasma volume. The three major pathways that lead to decreased plasma volume, thirst mechanism, renal mechanisms and transcapillary filtration are discussed in the text. While most of the neural-endocrine-hemodynamic mechanisms shown here are short-lasting, certain quantities, such as decreased leg volume, head-fullness, and decreased plasma volume are observed over long periods. Enclosed quantities were measured during flight or postflight on Skylab crew.

of intracellular fluids may also be derived, in large part, from the legs, i.e., muscle atrophy of lower limb postural muscles. The leg compartments, therefore, would seem to play a critical and broad role in the acute fluid response.

10.3.1.2 Longer-Term Response. The long-term adaptive phase can be considered to begin after the initial loss in body fluids. This phase is characterized by maintenance of extracellular volume and electrolyte composition at new homeostatic levels, a return to body water balance although the components of that balance (i.e., intake, sweat, excretion) are reset to new levels, and a continued loss of intracellular material in response to reduced zero-g mechanical loading effects. Nitrogen and potassium balances demonstrate that the greatest cellular losses occur during the first month in space, undoubtedly a result from disuse atrophy of the musculoskeletal organs. Hormonal agents, especially those affecting circulatory and renal function, are disturbed from their preflight levels and undoubtedly participate importantly in the adaptive processes. For example, an-

giotensin and aldosterone have reversed direction from the acute stress phase and are now elevated, although ADH remains suppressed.

A number of important observations during this period (from Skylab) are indicated in Fig. 10-4 (top). At the bottom of the illustration are five hypotheses that were formulated and evaluated in the modified Guyton model (see Chapter 5.4.2) in order to reproduce the observations. The connecting lines show the hypotheses that are associated with a particular physiological change. In a few cases, indicated by lines that join each other, there are multiple factors underlying a particular observation. Figure 10-5 shows a number of computer simulations of spaceflight, illustrating most of the quantities shown in Fig. 10-4. The dynamic changes in both short and long-term phases of flight are reasonable representations of the observed findings that may have occurred in the Skylab crew (compare with data in Chapter 5.1.2). The most significant conclusions that were obtained from these simulations, especially those related to the long-term fluid-electrolyte response in hypogravity are discussed below:

a) As noted above, plasma volume does not appear to return to normal but rather is reduced by about 500 ml throughout prolonged spaceflight; the resulting hemoconcentration profoundly effects the oxygen supply-demand balance leading to erythrosuppression.

b) Metabolic balance studies indicate that sodium losses stabilize within several days of flight (see Fig. 10-10). This implies that extracellular fluid volumes also reach a new equilibrium level.

c) Longer-term intracellular fluid losses may be expected to occur because of cellular degradation (i.e., from muscle disuse atrophy) augmented by high circulating levels of cortisol and from osmotic loss of water following a primary release of osmolar substances, e.g., potassium, from cells.

d) A release of potassium from the intracellular compartment (and from the body – see Fig.10-10) continues throughout the flight and can help account for many long-term effects observed in the Skylab crew. These effects include increased renal excretion of potassium, decreased body potassium, decreased intracellular fluid, increased plasma potassium, and enhanced aldosterone secretion.

e) The proportion of potassium loss to intracellular water loss measured in the Skylab crew was successfully simulated only when body fluids were allowed to become mildly hypo-osmotic. Plasma hypo-osmolarity and hyponatremia were consistently observed in the Skylab crew and also in some bedrest studies. It was necessary to postulate a natriuretic factor not previously included in the model, in order to reduce plasma sodium concentrations in accord with Skylab measurements.

f) Without the presence of a naturetic factor is it not clear why hyponatremia persists during prolonged hypogravity inasmuch as ADH and aldosterone are normally capable of correcting this condition. Dilu-

tion of body fluids may be considered a sacrifice of osmo-control for fluid volume control. Excreting a dilute urine, the normal response to reflexly correct hyponatremia, may not be possible in spaceflight because of the additional loads on the kidney resulting from dietary and sweat alterations and musculoskeletal degradation. However, chronically maintained hyponatremia was shown in model simulations to exert a long-term suppressant effect on ADH and cause hypersection of renin-angiotensin and aldosterone, as well as a depressed thirst drive, all of which are in accord with the Skylab findings.

g) Aldosterone secretion is increased not only due to hyponatremia, but also to hyperkalemia, the latter resulting in large part from release of cellular potassium. Also, aldosterone appears to be exerting its main effect on potassium rather than sodium excretion. In addition, the model also predicts that the observed increase in angiotensin levels exerts a long-term hyper-secretory effect on aldosterone.

h) Several lines of indirect evidence strongly suggest that inflight evaporative water losses and electrolyte sweat losses were reduced from preflight levels. This is significant, since it was previously expected that evaporative water losses would be greater in the hypobaric environment of Skylab. Although respiratory and skin diffusion losses may have been increased during sedentary activity, it was postulated that the magnitude of sweat loss reduction was even greater, leading to a net daily reduction in evaporative water loss. An analysis of factors directly associated with weightlessness (i.e., lack of sweat drippage, absence of natural convection, and biochemical effects) suggest a sweat suppression effect secondary to a high degree of skin wetness.

i) Renal losses of water and sodium were somewhat increased during the adaptive phase of flight. However, this did not indicate continued loss of these substances from the body inasmuch as sweat losses may have been correspondingly reduced, as suggested from metabolic balance studies. The simulation model demonstrated that renal excretion of water and salts could be accurately predicted from a knowledge of dietary intake and estimated sweat losses.

j) Interstitial fluid volume (not including the leg tissues) tends to return to normal within several days after a major volume disturbance such as that which occurs during the onset of weightlessness. The factors involved in this adjustment include: lymph flow, elevated plasma colloidal osmotic pressures, and physio-chemical forces between gel and free fluid in the interstitium. The simulation model (Guyton) does not include a separate head compartment and therefore did not assess the degree of tissue swelling in this region as was noted in the Skylab crew.

k) The systems analysis suggests that the major renal-regulating hormones (aldosterone, angiotensin, and ADH) represent a tightly coupled system that responds acutely to volume (i.e., pressure disturbances) and
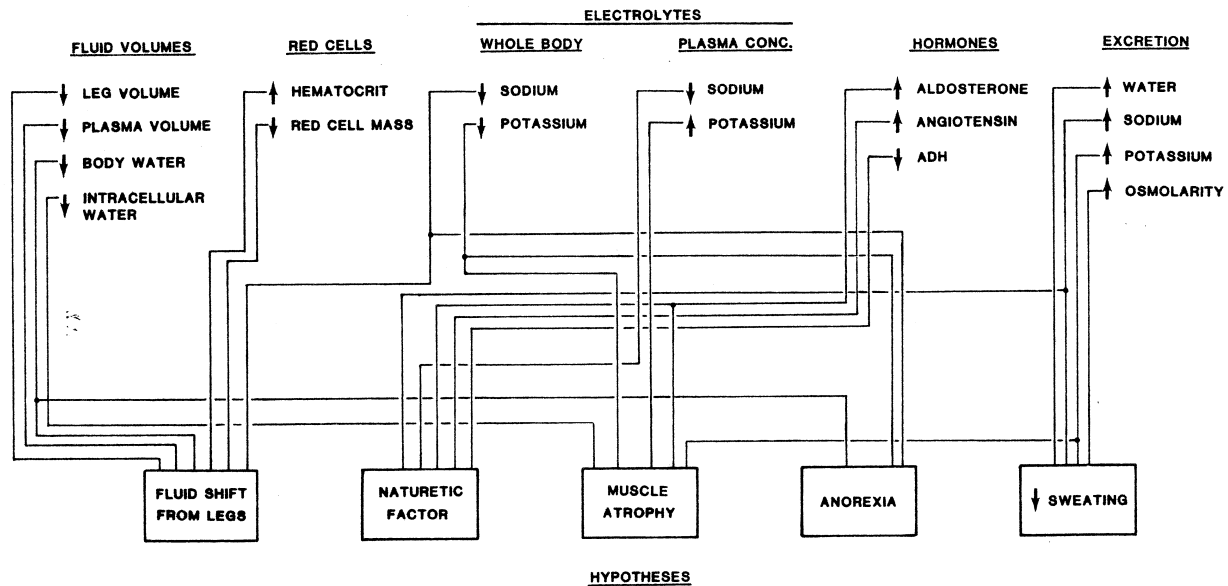
Figure 10-4. Schematic illustration of the special hypotheses (bottom) that were introduced into the Guyton model in order to simulate the set of observations (top) obtained during the Skylab experiments. All of the observations and hypotheses considered here are associated with the chronic phase of spaceflight, with the exception of anorexia that refers to the reduced dietary intake resulting during the first few days of flight. In the first Skylab mission, however, reduced dietary intake persisted throughout the mission. Refer to Chapter 9.4 for details. Suppressed red cell mass is discussed in Chapter 10.3.2.

chronically to electrolyte disturbances. During hypogravic maneuvers, this leads to an initial suppression of hormone levels (resulting from headward fluid shifts and central blood volume expansion) and a long-term effect that varies depending on metabolic factors, e.g., diet, sweat loss, physical activity, and muscle atrophy, that can alter the plasma electrolytes and thus influence hormone behavior. This shift from *volume/pressure control to osmo-control* creates complex and often competing stimulating factors that can result in a multi-phasic pattern of hormone response (see Fig. 10-5, bottom graph). The computer simulation of the Skylab missions revealed that the combination of hyperkalemia and hyponatremia can account for the levels of these hormones during the chronic phase of flight.

The reader is also referred to Table 5-10 for a comprehensive summary of observed changes in various indices of fluid-electrolyte status observed in the Skylab crew together with interpretations from the present analysis.

10.3.2 Hematology

The most important hematological finding during Skylab was a reduction in the circulating blood volume and red cell mass (RCM) during the inflight period. Before Skylab, the working hypothesis was that the pure oxygen gaseous atmospheres in the Gemini and Apollo space capsules represented a toxic stimulus and resulted in early destruction of significant numbers (as great as 20% loss)
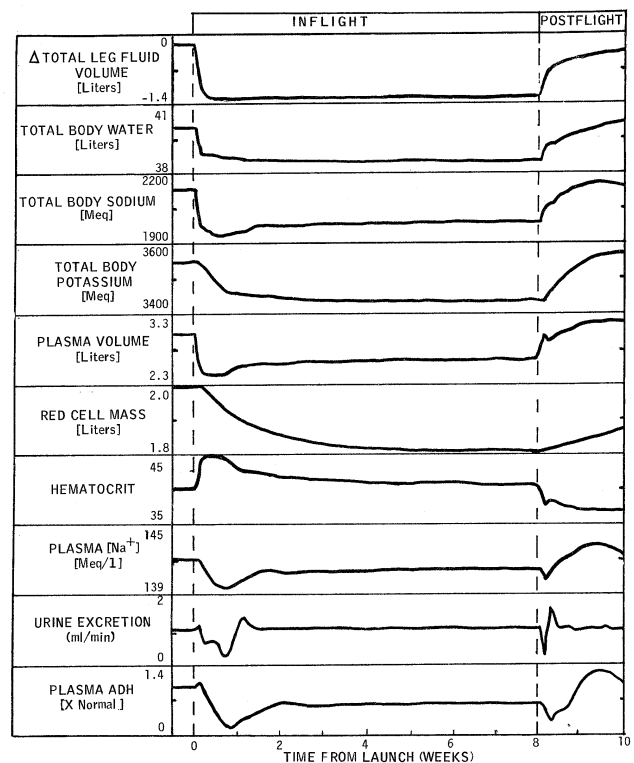
Figure 10-5. Simulations of the Skylab mission using the Guyton model. The model incorporated the hypotheses indicated in Fig. 10-4. This is a composite of the simulations shown and discussed in Chapter 9.4, using fluid and electrolyte balance data from the nine Skylab astronauts. All of the quantities shown, except for blood volume, were measured directly or indirectly during spaceflight and they agree with observations (see Table 9-5).

of red cells. For the Skylab crewmen who lived in a normoxic environment, this hypothesis was no longer tenable to explain their (11%) loss of red cell mass. In the absence of a consistent finding of increased red cell destruction, it was assumed that this loss was likely a result of suppressed erythropoietic activity. However, no conclusive proof of this theory is available and no one mechanism has been identified which is consistent with all the data. Therefore, examination of this issue was included in the systems analysis project (see Chapter 6).

10.3.2.1 Approach. In the absence of inflight measurements (only pre- and postflight measurements were made), the time course of blood volume, plasma volume and red cell mass changes during the Skylab missions were predicted by the modified Guyton model (see previous section and Chapter 5) and the model of erythropoiesis regulation (see Chapter 6). Several approaches were utilized using the theoretical model of erythropoiesis regulation to help understand the mechanisms that were likely to have produced these changes. These approaches included: (a) parameter sensitivity analyses, which helped identify the factors most likely to have a sensitive influence on erythropoiesis; (b) dynamic simulation of experimental studies such as altitude hypoxia, descent from altitude, and red cell infusions which validated the model and helped reveal behavior of the real system; and, (c) collaboration with investigators, performing human bedrest and food-deprived rodent studies, to test in the biological system those hypotheses suggested by the computer model. Examination of this relatively simple model revealed that diminished erythropoiesis activity (the prevailing hypothesis for spaceflight RCM loss) can be caused indirectly by hyperoxia of a renal oxygen sensor via erythropoietin, acting on the bone marrow, or by direct alteration of stem cell kinetics at the marrow controller. Both of these pathways were examined.

10.3.2.2 Renal Hyperoxia. A central finding from these theoretical and experimental studies was that moderate increases in hematocrit (11.5% on Skylab) resulting from an acute loss of plasma volume, if unopposed by other factors involving oxygen delivery to tissues, can proportionately increase oxygen tension at a renal sensing site (i.e., tissue hyperoxia) and exert a sensitive suppressant effect on erythropoietin and red cell production (Fig. 10-6). The erythropoietic regulatory system may be viewed, when operating in this fashion, as a hemoglobinometer; i.e., red cell production and hemoglobin concentration decreases to eventually relieve the hyperoxic condition. According to this notion, the suppressive effect on erythropoiesis lessens with flight duration as the hematocrit approaches preflight levels; this is accompanied by a diminished red cell mass. The accuracy of the prediction of the degree and time course of red cell loss was improved by insuring model agreement with the spaceflight obtained hemoglobin measurements. Nevertheless, the lack of corroborating inflight plasma volume measurements makes the prediction problematic. In any event, modeling and

bedrest studies suggest that RCM during spaceflight will decline in a linear fashion and stabilize as hematocrit normalizes. Therefore, the Skylab finding of red cell loss can be tentatively explained in terms of normal feedback regulation of the erythropoietic system in the face of sustained decreases in plasma volume.

The ability of hemoconcentrated blood to suppress erythropoietic activity was qualitatively similar in a number of quite different situations, including red cell infusion, descent from altitude, water deprived dehydration, bedrest, or spaceflight. However, as revealed by computer simulation, the quantitative effect was not always the same. Some of the differences between the spaceflight and bedrest responses could be attributed to differences in the timecourse and magnitude of plasma volume loss. More importantly, however, it was found that, equal degrees of hemoconcentration did not result in the same degree of erythro-suppression for bedrest and spaceflight, nor for the 59-day and 84-day Skylab missions. This suggested that other factors may have been present which either augmented or opposed the hemoconcentration effect.

10.3.2.3 Bone Marrow Effects. Two additional factors were therefore examined: diet and exercise. Findings from animal studies suggesting that dietary restriction can reduce, and exercise can enhance, erythropoiesis appear to account for the above noted discrepancies in a number of cases. An inadequate diet (negative energy balance), has been shown to lead to suppressed erythropoiesis by mechanisms that may bypass the hormone regulator and act directly on the bone marrow controller (see Fig. 10-6). This could explain the occasional findings that erythropoietic activity decreases in the presence of normal levels of erythropoietin. However, both dietary and exercise effects on erythropoietic activity have not been well defined in the human subject and the lack of appropriate controls during spaceflight studies does not permit a definitive conclusion. Nevertheless, these effects appear capable of explaining some of the unusual findings on Skylab as noted below.

Two theories were examined to explain the findings that as the Skylab missions increased their duration, the returning crews were found to have smaller average losses of red cell mass. The time course of red cell loss in spaceflight is not known because of difficulties of performing this measurement inflight. However, according to the "regeneration theory" postulated by the Skylab research team, and based on a composite of postflight measurement of all crewmembers, it was thought that red cells disappear by some yet unknown mechanism during the first month and then begin to replenish (or regenerate) during the second and third months. This notion would predict that after durations in space longer than 3 months, the RCM might return to normal. However, it was not possible to reproduce these events in the model using any plausible hypothesis, as a generalized theory of erythropoietic regulation in weightlessness.

An alternate theory was proposed based on the observation that decreasing losses of RCM in Skylab were associated not only with longer flight duration but also with
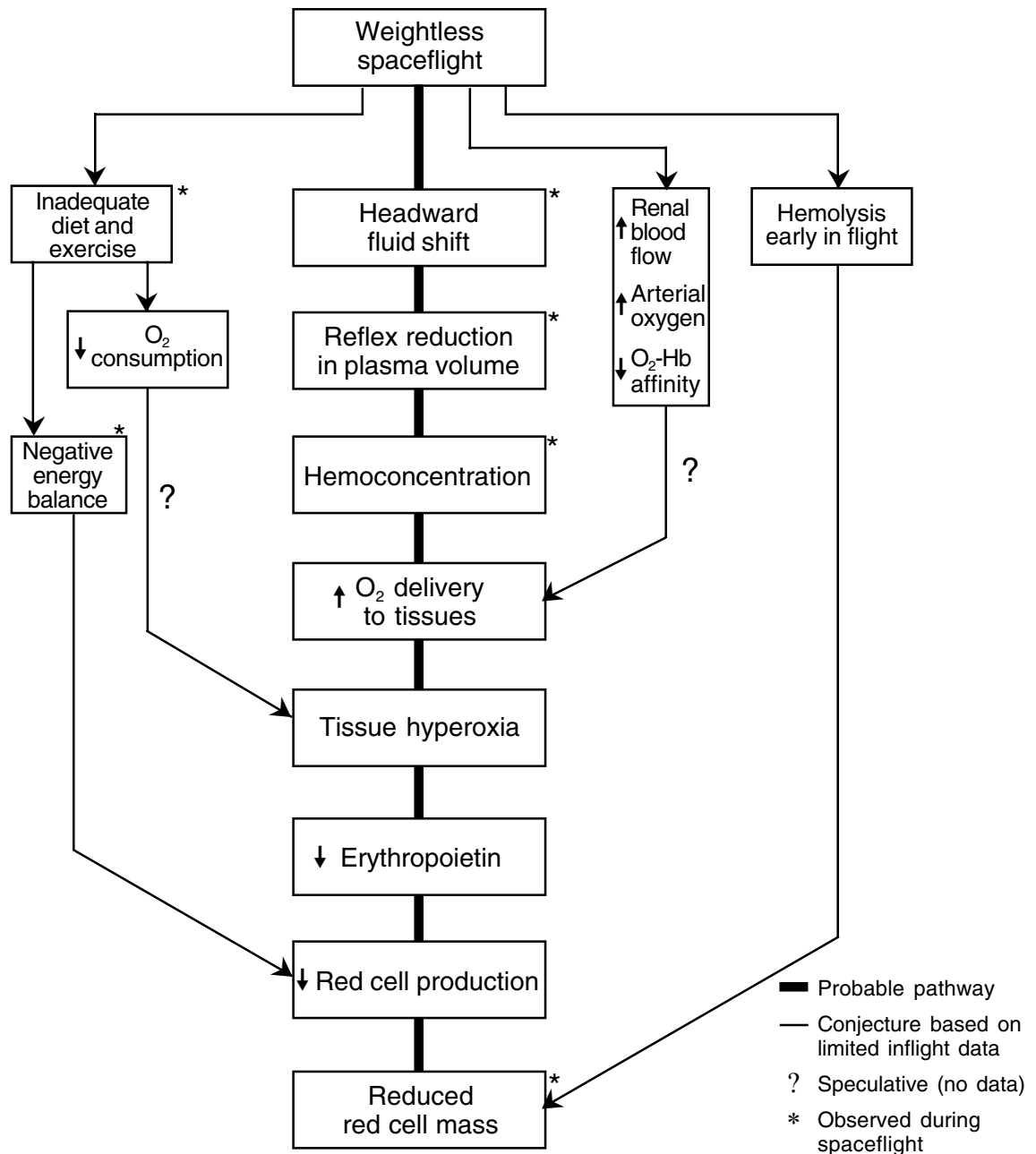
Figure 10-6. Hypotheses for spaceflight induced loss of red cell mass. The most likely pathway is dominated by fluid regulation and reduced erythropoietin. Metabolic mechanisms induced by negative energy balance that act directly on bone marrow stem cells can be a contributing factor. Hemolysis has not been a consistent finding although selected destruction of young cells (apoptosis) has recently been proposed. Other possible pathways are speculative.

increasing levels of diet and exercise. These metabolic factors had demonstrable effects on changes of body tissue and cardiovascular condition during flight, and, as noted above, their further involvement in maintaining the oxygen transport-erythropoietic system was postulated. A more plausible "continuous loss" theory was proposed which suggested that there are two components to the suppression of red cell production: one related to energy balance (diet and exercise) and one related to water balance (hemoconcentration). Differences among the crewmen's RCM losses were thereby considered a result of different levels of dietary intake and exercise, superimposed on a common loss due to hemoconcentration. According to this concept, the kinetics of RCM disappearance would not include regenerative behavior as postulated by NASA investigators, but would be more similar to the continuous, linear losses observed in bedrest. Statistical correlations between diet levels and red cell losses on Skylab, as well as model analysis, also tend to support this theory. Thus, it is not necessary to invoke the occurrence of red cell regeneration to explain the Skylab data. If this theory is correct it could also explain the unusually large RCM losses observed during the relatively short Gemini and Apollo flights. It those cases, the combined influence of hemoconcentration, negative energy balance and decreased physical exercise may have been additive to the destructive effects of 100% oxygen which has already been implicated as the primary cause of red cell loss.

10.3.2.4 Other Factors. Other factors that may have enhanced oxygen delivery and produced similar effects as hemoconcentration cannot be ruled out (i.e., shifts in blood flow, P_{50}, and arterial pO_2) but direct data are only available to support the hemoconcentration effect. Nevertheless, the model system predicts that even small changes in a variety of parameters (perhaps smaller than can be measured experimentally), if sustained for long enough periods of time, could lead to a progressive and significant degeneration of red cell mass.

The simulation analysis failed to rule out some small degree of acute red cell destruction as contributing to either the reduced RCM during hypogravity or the delayed recovery of red cells following some spaceflights and bedrest. Unusual removal of cells from the circulation could possibly arise from the mechanical stresses of launch, splenic sequestration, exercise hemolysis during flight, or postflight hemolysis of cells made more fragile by weightlessness or bedrest.[†] However, a major role of inflight cell destruction is unlikely on Skylab, because this would contradict the observations that hemoglobin concentration is significantly elevated and that overt signs of hemolysis were found only on the shortest flight.

10.3.2.5 Recovery. Computer simulation predicted that in most cases the observed repletion of red cells during the

period of recovery from hypogravity could be attributed to hemodilution-induced hypoxia, i.e., an effective anemia resulting from inflight RCM depletion and followed by postflight plasma refilling. The delayed recovery of RCM during the 28-day Skylab mission and the 28-day bedrest simulation of that mission was attributed in part to a normal 3-4 day bone marrow transit time and a time-lag in plasma volume recovery. The presence of an acute reticulocytosis following bedrest and its absence after a Skylab mission of the same length suggests somewhat different mechanisms were operative in each case. The involvement of shifts in oxy-hemoglobin affinity, mild hemolysis, or ineffective erythropoiesis were suggested as areas of future study. Also, it is possible that the history of exercise during spaceflight compared to the history of inactivity during bedrest may account for some of the observed differences.

10.3.3 Cardiovascular Regulation

Of all the physiological systems of interest, the cardiovascular system has been studied for the longest period of time in the spaceflight program. However, because of the complexity of this system, and because of operational constraints limiting the collection of crucial data, a good description of cardiovascular adaptation to zero-g was still lacking even following the Skylab missions. Most of the earlier spaceflight experiments and measurements were appropriately designed to reveal possible pathophysiological aberrations that would limit the capacity of man to work in zero-g and prevent normal function upon return to earth. These tests provided a gross clinical description of the system under orthostatic and exercise stresses and demonstrated that spaceflight does not impair crew health or performance. However, some fundamental measurements of the systemic circulation, including blood flows, venous pressures, vascular resistances and tone as well as possible alterations in the neural and hormonal controllers, would not be made for a decade or longer after the Skylab experiments. Acute changes of the cardiovascular system upon entering space could only be inferred from ground-based hypogravic maneuvers. Also, longer-term adaptive changes undoubtedly occur but were obscured by limited knowledge of these aspects of cardiovascular physiology even in one-g environments. For example, the effects of exercise conditioning on circulatory parameters is a subject still under intensive study. Therefore, the analysis of these short and long-term events has resulted in a description of cardiovascular alterations that is somewhat incomplete and somewhat speculative.

Three broad areas of cardiovascular regulation in weightlessness have been considered: the resting (unstressed) cardiovascular system, orthostatic testing, and exercise testing. These three areas are discussed next and are illustrated in Fig. 10-7. See also Chapter 7 for a detailed presentation.

10.3.3.1 The Resting Cardiovascular Response to Weightlessness. The most dramatic changes in the resting cardiovascular system probably occurred early in flight, long before the first Skylab measurements could be

---

[†] Recent flight experiments on the Shuttle Spacelab support the notion that younger erythrocytes are selectively marked for early destruction at the bone marrow level in the presence of hemoconcentration. See endnotes of Chapter 6 for a discussion of recent findings.
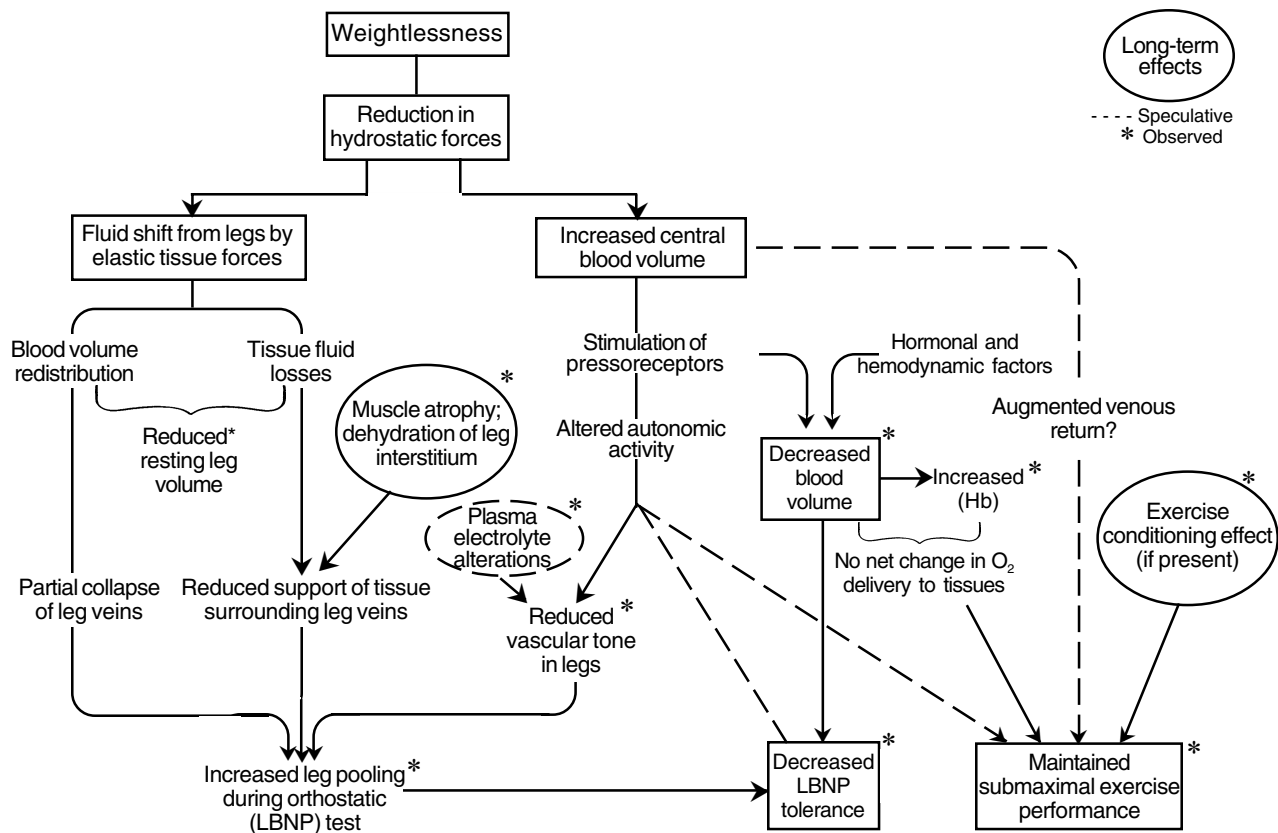
Figure 10-7. Hypotheses of the major events and mechanisms in the cardiovascular system during spaceflight. These postulated effects can explain the findings at rest and from provocative LBNP and exercise testing relatively early in the flight period. During prolonged flight (not shown), adaptive effects that lead to retoning of the leg vessels and resetting of the baroreceptors, permits orthostatic tolerance to return towards normal. Immediately, postflight, orthostatic tolerance is degraded (compared to preflight) largely because the reduced blood volume tends to pool in the legs. Exercise performance is also degraded during the first postflight day as body water increases causing a relative anemia and poorer oxygen delivery to the tissues.

performed. As simulated by the modified Guyton model and demonstrated by one-g experimental analogs of weightlessness, the following scenario is postulated. At the onset of microgravity, the primary event of the headward fluid shift leads to central blood volume expansion, increased venous and arterial pressures, increased stroke volume, and elevated cardiac output. Secondary reflexive reactions following stimulation of central mechanoreceptors include a decrease in heart rate and decreased peripheral resistance. These reflexes, together with enhanced transcapillary filtration and excess renal excretion, tend to correct both the central blood volume and associated pressures. The Guyton model predicts a complete normalization of central blood volume within several hours, and as this occurs the circulatory and cardiac variables also return to normal and some eventually over- or undershoot. Thus, while arterial pressure may return to normal, peripheral resistance and heart rate increases, and cardiac output and venous pressure decreases compared to control; as indicated in the previous sections, total blood volume is ultimately reduced at the expense of fluid leaving the lower limbs (see Chapter 9.7.5.1).

Whether this entire scenario occurs is still a matter of controversy inasmuch as it has not been possible to perform a complete cardiovascular assessment very early inflight. Those measurements that are possible are complicated by emotional stresses resulting from launch activity. Also, some of the headward fluid shift may have occurred while the crew is preparing for launch in the feet-up position. Inflight measurements taken some hours after launch, some of more recent vintage, confirm a decrease in leg volume, plasma volume, and central venous pressure; a modest increase in heart rate, and no change in mean arterial pressure. Measurements of resting cardiac output and peripheral resistance have yielded inconsistent results. Only the CVP measurements were obtained just after entering zero-g; the others some hours later. Engorgement of neck veins and facial tissues and feelings of head fullness that continue throughout the flight are symptomatic of the continued tendency of fluids to pool in the upper body in zero-g.

Final adjustment of circulatory parameters (flows, pressures, resistances), in order to accommodate the redistri-

bution of fluids, appears to occur much more slowly than the initial fluid volume adjustments. Although arterial pressures return close to normal, there may exist a residual central blood volume expansion. Therefore, one of the long-term effects of spaceflight may be a decreasing influence of high-pressure baroreceptors and an increasing influence of low-pressure volume receptors. Whether volume receptor adaptation occurs is unknown. A residual excess volume in the vicinity of the low pressure cardiopulmonary receptors may account for the longer term increase in resting heart rates noted in the majority of the Skylab crew (and in bed-rest subjects) as well as a possible increase in stroke volume, e.g., Bainbridge reflex and Starling effect. Both of these factors argue in favor of a long-term increase in cardiac output by influences acting directly on the heart.

However, there are also general systemic influences that must be considered in an assessment of long-term blood flow alterations. As indicated in Figs. 10-6 and 10-7, the hemoconcentration (secondary to reflex reduction of plasma volume) together with a possible reduction in metabolism of certain organ systems (such as postural muscles) could lead to a relative increase of oxygen delivery at the tissue level. As a result, local autoregulatory (resistive) elements may reduce blood flow so that oxygen delivery coincides with oxygen demand.

Other long-term mechanisms are capable of assisting the circulation adapt to reduced total blood volume, an emptying of leg veins and blood pooling in the upper body. Over time, the circulatory system attempts to adjust the capacity of the blood vessels to the actual blood volume, thereby maintaining mean circulatory pressures. Blood volume adjustments, if maintained chronically and if they effect the pressure within the vessels, can lead to changes in vascular compliance via poorly understood local (delayed compliance) and central (autonomic influence on venous compliance) pathways. Thus, it may be expected that in zero-g, a retoning or devascularization of leg vessels occurs to accommodate the reduced blood volume in that segment of the circulation while stress relaxation of veins in the upper body may occur to accommodate fluid expansion in central regions. The actual role of these long-term mechanoreceptor, autoregulatory, and stress relaxation mechanisms have not been well studied. Also, their *net* effect is unknown because accurate measurements of flow, volume, and pressure have not been simultaneously performed in the space environment. Some of these adaptive trends may be interpreted as the removal or reversal of orthostatic defense mechanisms no longer needed in spaceflight.

Cardiovascular function was evaluated during the Skylab missions by an orthostatic stress test (lower body negative pressure, LBNP), and by an exercise stress test (bicycle ergometry). The most prominent findings from these tests were a decrease in orthostatic tolerance during and following flight and a post-flight decrease in aerobic capacity. Hypotheses to explain these findings were formulated and tested in the pulsatile cardiovascular model. It was convenient and useful that the same model for the cardiovascular system be used to analyze both LBNP and exercise,

each of which present different challenges to the cardiovascular system with significantly different responses.

10.3.3.2 Analysis of Orthostatic Testing. The observed decrease in orthostatic tolerance is not unexpected in the light of significant loss of blood volume (500–600 ml). Upon application of lower body negative pressure (one-g or zero-g) or standing (one-g), the increase in leg pooling coupled with a reduced blood volume significantly lowers central blood volume and venous return to the heart. The model simulations quite accurately predicted the increased heart rates and decreased pulse pressures characteristic of the Skylab crews' intolerance to orthostasis. The inflight heart rate response to maximal LBNP (50 mmHg) was shown to be nearly equivalent to a 15% hemorrhage. However, blood volume loss alone was not sufficient to explain all of the observed findings. For example, an increase in leg volume pooling during LBNP (compared to the degree of pre-flight LBNP pooling) was noted during spaceflight. The most promising explanation of this phenomenon, as suggested by simulation analysis, was the partial collapse of leg veins in association with a reduced leg blood volume during the pre-LBNP control period. Small increments of LBNP would be expected to draw significant quantities of blood into the empty leg veins, more so in zero-g than in one-g.

The response to orthostasis was observed to stabilize and even improve in some subjects during the latter part of the mission. One of the more promising hypotheses to explain these findings was a long-term downward adjustment of vascular capacity in the legs (in response to the reduced leg fluid volume) that could be manifested physiologically by retoning, devascularization, or reverse stress relaxation. Changes in plasma electrolyte concentrations (increased potassium and calcium, decreased sodium) may also be involved in altering vascular tone. Little is known concerning autonomic influences on venous tone during long-term adaptation to hypogravity.

One of the keys to understanding the circulatory changes in zero-g may be better description of the vascular and extravascular compartments in the legs. Simulations of headward movement of fluid upon entering zero-g and the subsequent repooling of fluid in the legs upon application of LBNP or one-g recovery can be made more realistic by including more accurate descriptions of collapsible leg veins, non-linear leg tissue pressure-volume relationships, tone of extravascular muscle, peripheral transcapillary filtration, and the active and passive control mechanisms which influence these elements. Differentiating the upper and lower body capillary beds with respect to regulation of the pre- and post-capillary resistances and the elastic character of the interstitial tissues surrounding these beds is not yet possible from available data. The loss of tone of supporting muscles surrounding deep leg veins during prolonged weightlessness is an additional complicating factor in modeling both intravascular and extravascular leg elements. A number of these effects have been included in the modifications to the Guyton model, but many of the details are poorly understood. The pulsatile cardiovascular model is limited to

short-term events because it is a closed system and does not contain capillary leaks. The lack of data in these areas of circulatory regulation, while discouraging, still permits the models to be used for hypothesis testing and suggesting new experimental approaches.

10.3.3.3 Analysis of Shuttle Reentry. During the early testing phase of the Space Shuttle program, there was concern of circulatory dysfunction during the Shuttle atmospheric reentry phase. In contrast to all previous manned spaceflights (where crewmembers descended by parachute in a semi-reclining position with hands-off control), the crew of the Shuttle orbiter was to be exposed to acceleration forces in the head-to-foot direction (sitting position) after having also suffered a weightlessness induced-blood volume loss. Acceleration forces were known to reach a maximum of twice the normal sea-level g-forces and blood volume losses in spaceflight have been measured at about 500 ml. The pooling of fluid in the legs at such high g-forces combined with a loss of blood volume had the potential to render the crew orthostatically intolerant at a time their performance level needed to remain high for a hands-on landing. Simulations were performed with the short-term cardiovascular model (LBNP version) to study the combined behavior of the two stresses – high g-forces and blood volume loss – on the circulatory system. The operational question of immediate concern was "what is the maximum tolerable $+G_z$ at any given level of blood volume loss?"

The model was first validated for its ability to respond to high g-forces and blood volume losses by simulations of centrifuge and hemorrhage experiments respectively. The validated model was then used to study the dual effects of blood volume loss and levels of g-force on carotid blood pressure. Previously obtained data have related carotid pressure to vision impairment as reflection of orthostatic intolerance. It was thus determined that even with modest blood volume losses of 10–15%, the tolerance to increased gravitational loading is reduced significantly. Evidence from Shuttle flight crews, both during reentry and in tilt studies immediately following reentry, confirmed a tendency for syncope; the model was able to replicate these results and show that they could be ascribed to blood volume loss and reentry g-forces. Finally, more advanced simulation studies were used to design two countermeasures for "reentry intolerance". In one of these, the lower limb external pressure required for an anti-g compression suit was determined (Chapter 7), and in the other the volume and timing of a fluid-loading protocol was established (Chapter 9). This entire study, including simulations of basic changes on the circulatory system, simulations of operational conditions, and model-aided development of countermeasures, indicates the versatility of these mathematical models.

10.3.3.4 Analysis of Exercise Response. Tolerance to exercise was essentially maintained during the flight period. It was only after return to earth that aerobic capacity was found to diminish. This is similar to results reported for bedrest. Analyses performed with the whole-body algorithm permitted the circulatory adaptations of long-term bedrest to initialize the short-term LBNP and exercise model so that pre- and post-bedrest stress tests could be simulated. Results from these studies suggested that decrements in blood volume in association with some reduction in unstressed volume in the legs could quantitively account for most of the observed changes in post-bedrest exercise (and LBNP) and postflight exercise in the crews of the two shortest Skylab missions. These changes, reflecting what has been termed circulatory deconditioning of zero-g, included increased heart rate, decreased stroke volume, and decreased cardiac output during postflight sitting exercise compared to preflight testing.

However, there was a notable qualitative difference between the degraded post-flight exercise responses of the different crews. For example, heart rate was lower, stroke volume was smaller and blood pressure was higher during exercise testing of the 84-day crew compared to the 28-day and 59-day crews. This was tentatively ascribed to an inflight exercise training effect since the level of personal daily exercise increased on each longer flight. A systems analysis task was therefore devoted to developing the most feasible explanation of the interaction of zero-g adaptive changes (deconditioning) and exercise training (conditioning).

In this regard, the cardiovascular exercise model was modified and validated to represent the simulation of a highly trained subject's response to bicycle exercise in one-g. These "training" modifications included a larger heart, increased contractility of the heart, reduced sympathetic activity, decreased arteriolar vasodilation (neurogenic) during exercise, increased leg capillary density, and increased vagal activity at rest. This model was used in the "trained" and "untrained" mode to simulate the postflight bicycle ergometry experiments. The results led to the conclusion that a training effect was quantitatively consistent with the exercise responses for the crew that trained the hardest.

The most acceptable hypothesis tested to explain this crew's response was a combination of effects that included increased sympathetic activity on heart rate, increased peripheral resistance, increased contractility, a reduction in blood volume, and a reduction in unstressed volume in the legs. Each of these influences acting alone was not sufficient to explain the totality of situations examined which consisted of resting in the supine and sitting positions and exercise in both positions. (The supine exercise position tends to minimize the effect of blood volume loss on exercise performance). The combined set of hypotheses is not a unique set of cardiovascular changes but at this time represents a feasible combination of conditioning and deconditioning effects.

The absence of any notable decrease for inflight exercise capacity for all crewmembers indicates that the contracted blood volume is an appropriate adaptation to zero-gravity. Nevertheless, the nature of the adaptation is not clear. The current analysis suggested that normal oxygen delivery was maintained in the face of diminished

blood volume by the hemoconcentration of weightlessness, and by the tendency of fluid to pool in the upper circulation, thereby augmenting venous return to the heart. Conversely, the hemodilution upon recovery would be expected to contribute to the postflight degradation in exercise performance.

10.3.4 Musculoskeletal Responses to Weightlessness

The Skylab findings support the concept of a generalized atrophic response of the total musculoskeletal system during extended exposure to hypogravity. Losses in bone and muscle mass were among the more significant physiological changes observed in the astronaut subjects (see Fig. 10-8).

10.3.4.1 Muscle Atrophy. The losses in muscular tissue were particularly well documented in the Skylab crew (see Chapter 4). One of the systems analysis projects demonstrated that lean body mass was reduced by approximately 1.5 kg ($N = 9$) over the inflight period. This was revealed by several independent methods that showed losses in body water, potassium, nitrogen, and body volume. More direct evidence of muscle and collogen breakdown was provided by the measured increase in renal excretion of urinary 3-methylhistidine, hydroxylycine, and hydroxyproline. Also, excesses of intracellular electrolytes and amino acids appeared in the plasma and urine. Further analysis of spaceflight data indicated a significant degree of local muscle loss in the legs and perhaps in the skeletal muscle groups that normally control anti-gravity or posture. The data supporting these contentions come from spaceflight studies showing a gradual loss of leg volume, decreased leg strength, a reduction in duration of the Achilles reflex, and, in animals, diminished mass and response of red fiber groups.

It is well known that atrophy of skeletal muscle occurs in response to disuse, inadequate functional load, and insufficient food intake. Spaceflight may be associated with more than one of these conditions. The absence of gravity results in diminished use of the lower limbs for postural support and locomotion, reduced body weight loading on weight-bearing tissues, and perhaps interference with proprioceptor reflexes which can influence muscle metabolism and function. A reduced caloric intake appears to be capable of increasing the loss of body protein, but increased caloric intake may not prevent this loss. The muscle disuse atrophy hypothesis receives support from the finding that the more intensive exercise performed by the crew of the longest flight (mainly exercise of the leg muscles) was associated with the smallest decreases in leg volume and strength. Little is known, however, about the changes occurring in other muscle groups, particularly those used for postural support in the upper body. If postural muscles are the primary targets of loss induced by zero-g, appropriate locally applied exercise might reverse this trend. Because each Skylab crewmember exercised, it is not possible to quantitatively predict the zero-g effect of complete lack of exercise. There is no rea-

son to question, however, that exercise does maintain strength, muscle tone, and probably mass in the legs and improves circulatory condition similar to one-g training.

10.3.4.2 Bone Demineralization. Evidence for inflight loss of bone mass comes primarily from observations of calcium metabolic balance and bone density. Inflight calcium balances were consistently negative on all flights, a result of excess urine excretion throughout the missions and a progressive increase in fecal calcium loss as a function of mission duration. Bone densitometric data indicated losses in the calcaneus (of the heel), but not in the radius and ulna (of the arm), suggesting that losses are concentrated in load-bearing bones. A significant correlation between changes in calcaneus bone density and calcium balance for the nine crewmen was demonstrated. Additional evidence of demineralization is suggested by increases in urinary hydroxyproline and hydroxylycine which may indicate breakdowns of the collagen matrix in the bone. As expected, plasma and urine biochemistry showed significant increases in calcium and phosphate, but the calcium regulatory hormones did not reveal a consistent trend. Analysis of all these data suggest that bone losses became progressively more severe on each longer mission, in contrast to the trend toward stabilized losses noted for muscle.

The initiation of bone loss is assumed to come from a reduction of mechanical forces induced by gravitational unloading, and/or reduced musculoskeletal interactions. These forces (piezoelectrical, compressional, tensile, and shearing forces) are known to be important in the normal maintenance and repair of bone. It appears logical that external forces, appropriately applied, might reverse the decalcification process. However, the search for suitable countermeasures has not met with notable success. The effect of exercise on bone demineralization remains unresolved.

Current understanding of the physiology of calcium metabolism, including the systems analysis, provides a partial explanation of the biomedical findings. Upon release from the bone into the extracellular pool, calcium and its concentration in plasma is under the control of a feedback system which is mediated by a hormonal system which influences renal excretion and gastrointestinal absorption as well as new bone formation. The observed elevation of urinary calcium may have been a result of increased plasma calcium concentration decreased parathyroid hormone, and increased renal tubular sodium (see Fig. 10-8). Progressive losses of fecal calcium have been tentatively attributed to a net decrease in dietary absorption of calcium from the gastrointestinal tract. The active metabolite of vitamin D (1, 25 dihydroxycholecalciferol) is an important regulator of GI tract absorption, and a decrease in circulating levels of this substance could explain the fecal data. As suggested in Fig. 10-8, a depression of parathyroid hormone and Vitamin D could have a negative feedback effect on demineralization and limit the losses of calcium from the bone. These preliminary hypotheses have been incorporated into proposals for future flight experiments that will examine several features of
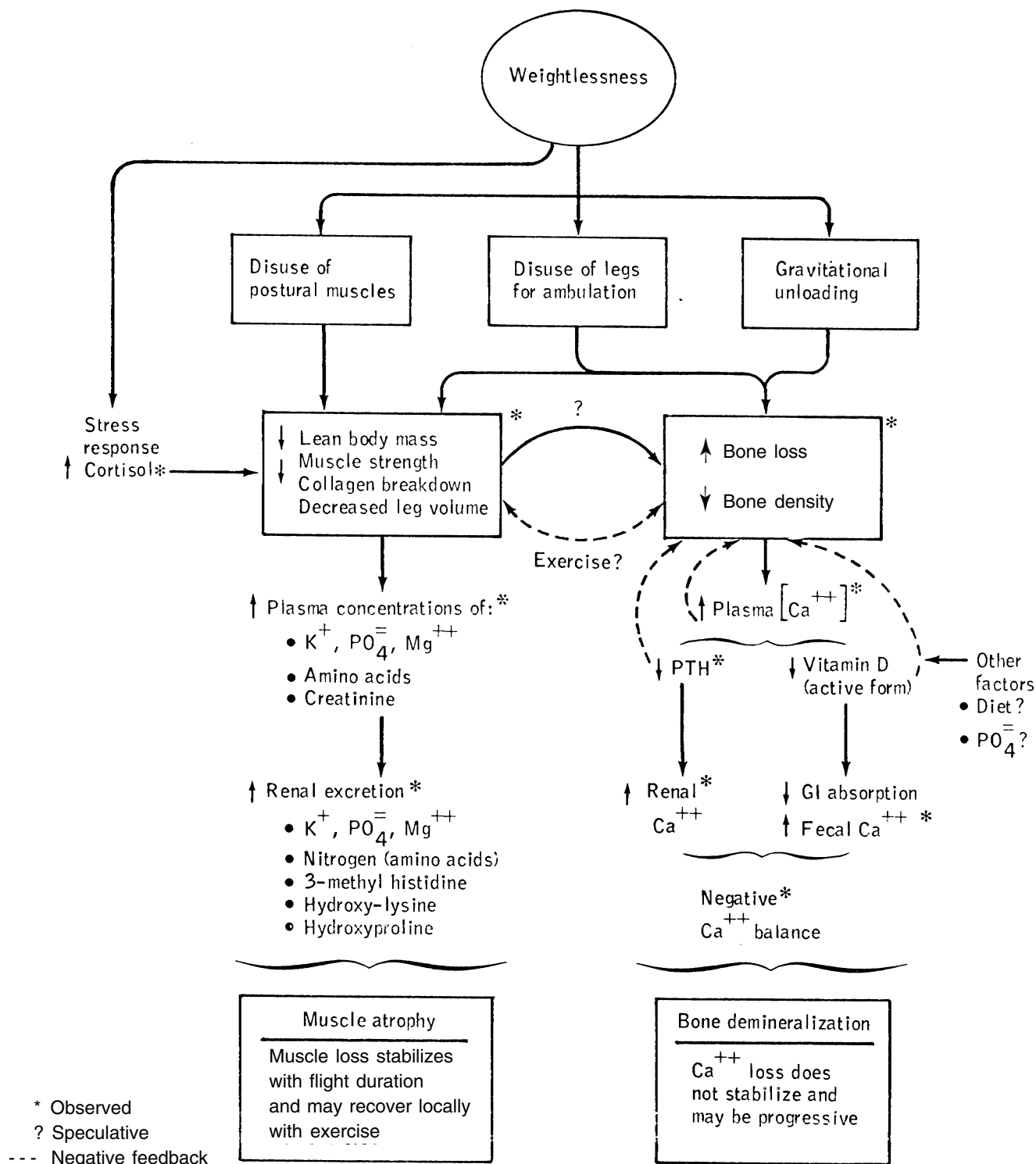
Figure 10-8. Highly simplified schematic indicating the postulated effects of spaceflight on the musculoskeletal system. For a more detailed hypothesis of bone demineralization, see Fig. 8-9.

calcium regulation, including fluxes into and out of the bone and GI tract, hormonal regulation, and the effect of exercise as a countermeasure.

The systems analysis approach for understanding bone demineralization in space centered on understanding the complex feedback systems of calcium regulation including the development of a mathematical model. Various interpretations of spaceflight and bedrest findings were addressed which helped formulate the hypothesis of calcium metabolism adaptation to long-term spaceflight that is summarized above. Although the model is not yet complete, formulation of the model was instrumental in unifying spaceflight and bedrest data and in identifying critical areas in the regulatory system that might become altered in zero-g. When fully developed the model should be able to provide guidance in understanding these mechanisms. Can the acute renal calcium excretion be explained as an initiating event or as a feedback response? Can some primary disturbance in the calcitropic hormones cause renal excretion and bone loss or is there a primary event at the bone level due to alterations in mechanical forces? What biological activity is occurring in the bone tissue during these events?

10.3.5 Body Composition Changes

The analysis of body composition changes during spaceflight, performed during this project (see Chapter 4), offered a more complete answer to the question of "why do astronauts lose weight during spaceflight?" than was heretofore available. Figure 10-9 shows the relationship of the compartments associated with body composition. Accordingly, the body mass can change in accord with alterations in three major substances: muscle (dry), fat (normally low water content), and body water. The changes in body water, in turn, can be said to be caused by changes in one or more components of the water balance, or alternatively, by changes in the major fluid compartments of the body. From an energy balance perspective, the loss of body tissue (muscle and fat) implies an imbalance between caloric intake (diet) and caloric output (work + heat). All of these quantities were examined by an integrative analysis of the energy balance, mass balance, water balance, and body fluid volume of the Skylab astronauts to formulate estimates of body composition changes.

While the original Skylab experiments were designed to measure body composition changes only at the beginning and end of flights, a method was developed to combine pre- and postflight data with daily inflight metabolic data so that cumulative changes of body composition during flight could be estimated. The changes in several of these body composition compartments, as computed in this project, are shown in Fig. 10-10 for the first month in space. Some of the changes reflect the same complex relationships between diet, exercise, physical condition, and energy balance that are normally observed in terrestrial conditions. In addition, certain changes in the fluid and musculoskeletal compartments can be directly attributable to the weightless environment. Interpretation of the Skylab data, with the view of identifying and isolating
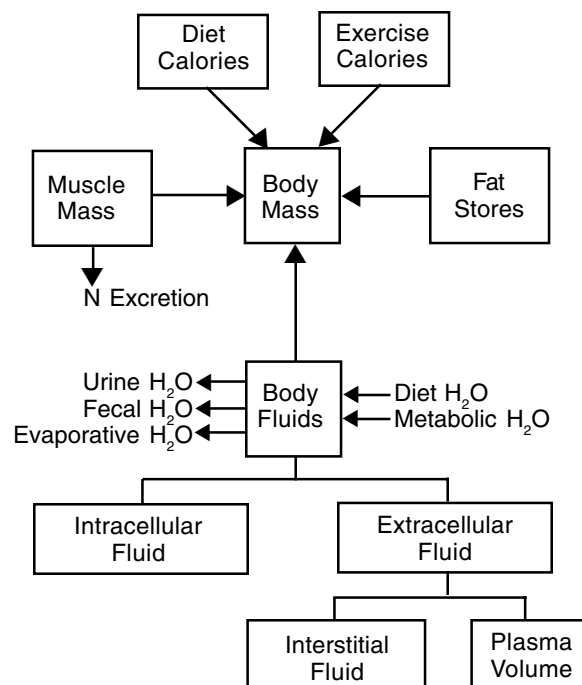
Figure 10-9. The compartments which make up the metabolic systems of the body. Assessing the values of these quantities was required in order to understand why astronauts lose weight during the course of a long spaceflight.

the zero-g factors, is made more difficult because each successive crew remained in flight a month longer, exercised longer and harder, and received a larger caloric intake per kilogram of body weight. Nevertheless, the data obtained from indirect metabolic balance techniques does lend itself to a reasonable interpretation that must eventually be verified by measurements that are more direct. For purposes of summation, it is convenient to consider each major body constituent separately:

10.3.5.1 Body Water. There appears to be an obligatory loss of at least one liter of body water that occurs during the first two days of spaceflight (Fig. 10-10(a)). Each of the crewmembers lost varying amounts of water early inflight, some less and some more than a liter, but at the end of one-month inflight, the body water response appeared to converge toward a one-liter loss. The initial body water deficit was primarily a result of reduced fluid intake since urine and evaporative water losses, on the average, were below control during this period. Those crewmembers exhibiting severe space motion sickness symptoms reduced their intake by the greatest amount and lost the greatest amount of body water. When normal intake was resumed following severe bouts of motion sickness, some body water repletion was evident. The reduction in body water is maintained throughout the flight in spite of ad libitum drinking. Shifts of up to two liters of fluid from the legs,

Total Body Water (liters)

Total Body Sodium (meq)

Total Body Potassium (meq)

(a)

Days from launch

Days from recovery

Change in body weight, kg

Change in body tissue, kg

Change in body protein, kg

Change in body fat, kg

Days from launch

Days from recovery

(b)
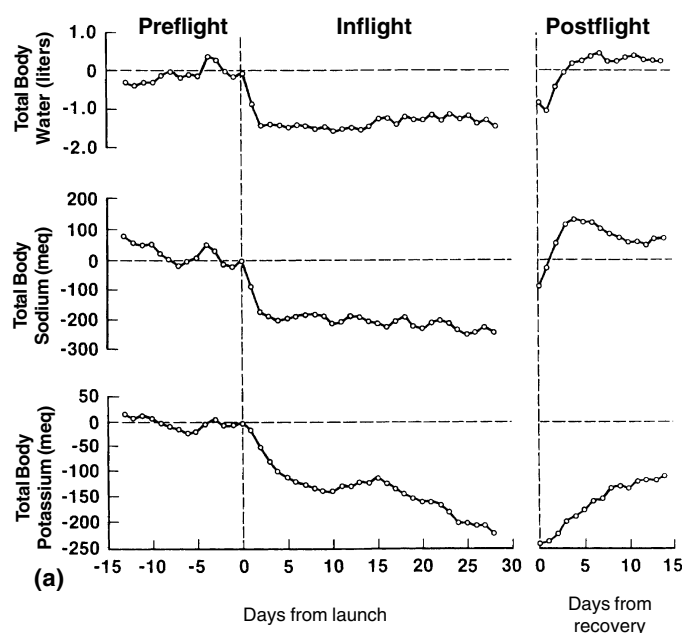
Figure 10-10. Body composition changes for all mission phases (including first month inflight) for all Skylab crewman (N=9; mean ± SE). Values are shown as change from morning of launch. Body mass was measured directly; all other quantities were derived using daily metabolic balance measurements. a) Body Water and electrolytes: Because sodium and potassium are the major cations of the extracellular and intracellular compartments respectively they reflect fluid changes in those compartments. b) Body weight and tissues: Tissue weight (dry) consists of fat and protein. Changes in lean body mass are approximately five times those shown for protein.

observed on Skylab, can easily account for these body water losses.

10.3.1.2 Body Electrolytes. Upon entering weightlessness, metabolic balances shifted in the negative direction for all of the electrolytes studied including sodium, potassium, calcium, phosphate, magnesium, and nitrogen. The rates of loss were most severe for the first month of flight. Cumulative estimates of loss computed for sodium, potassium and nitrogen indicated that the sodium losses were rapid and then stabilized after several days similar to the behavior of body water, while potassium and nitrogen losses were more gradual and did not stabilize until the second month (Fig.10-10(a)). Electrolyte losses from both intracellular and extracellular compartments were significant compared to their total body amounts, but contributed negligibly to changes in body mass. Nevertheless,
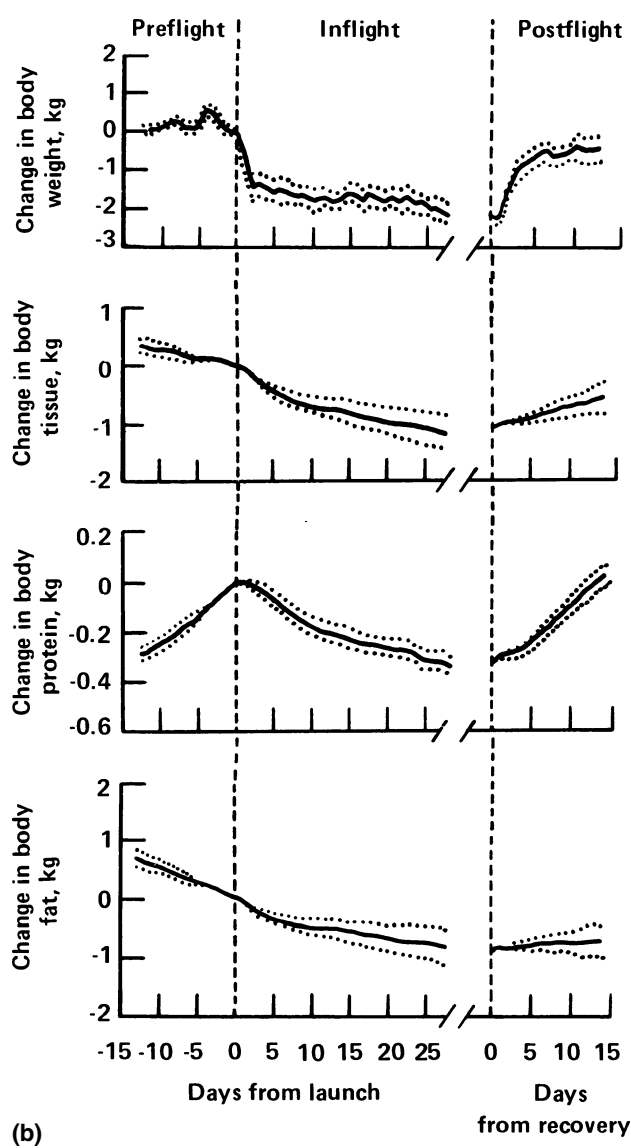
they reveal other more significant changes. For example, sodium losses reflect reductions in extracellular water, while potassium losses are indicative of intracellular fluid losses (primarily muscle). Taken as a whole, these data indicate that spaceflight induces a rapid loss of extracellular fluids and salts, while disappearance of intracellular constituents takes considerably longer.

10.3.1.3 Body Weight (Mass). Body mass was the only whole body component measured directly during flight (Fig 10-10(b)). A weight loss of 3.8% (2.7 kg) was observed in the nine Skylab crewmembers during their inflight period. This was attributed to a 2.5% loss (1.5 kg) in lean body mass and a 10.4% loss (1.2 kg) in body fat. Water, fat and protein contributed approximately 48%, 39% and 13% respectively, toward the total body mass loss by the end of the mission. Body mass, measured daily during

spaceflight, decreased most rapidly at launch and recovery, reflecting changes in body water. After the initial rapid inflight decline, body mass either continued to decline, stabilized, or recovered somewhat depending on the effects of diet, exercise, and weightlessness on major tissue compartments such as fat, muscle, and water. There were significant differences between the three Skylab missions (see Chapter 4), which could be attributed to differences in diet and exercise.

10.3.1.4 Body Tissue. The loss of body tissue (dry weight of fat and muscle), particularly fat, appeared to be directly related to the difference between net energy utilization and net caloric intake (Fig. 10-10(b)). The results support the premise that body fat is the substance preferentially used to compensate for energy deficits that result from inadequate energy intake. A negative energy balance was observed on the first two Skylab missions. An adequate diet, in relation to the workload, was present only on the third and longest mission. Three generalizations can be made regarding the effects of exercise and diet on tissue storage. First, an inadequate diet will result in fat and muscle losses. Second, when diet is adequate to maintain body mass, but exercise is insufficient, the muscles will atrophy and fat will be deposited. This seems to have occurred in the crew of the 84-day mission. Third, with an adequate diet during periods of exercise training a loss of fat and increases in lean body mass will occur. This situation was observed on all missions during the preflight control period.

10.3.1.5 Body Fat. Of all the components examined, the changes in fat stores appeared to vary the most between crews. This undoubtedly reflected the wide range of caloric intakes in the controlled diets and the varying degrees of exercise performed. Fat losses have been observed consistently in association with inadequate food intake in crews of Gemini and Apollo missions. On the other hand, the crew of the longest Skylab flight exhibited a mean gain in body fat, implying a more than sufficient diet despite their higher workloads during exercise. On average for the nine Skylab crew, there was a small loss of body fat (Fig. 10-10(b)).

Caloric intake was less than adequate for the two shortest Skylab flights, for two reasons. First, the caloric content of a strictly controlled diet was based on the erroneous assumption that inflight energy requirements were less than those of a one-g environment. Second, almost all of the crewmen experienced space motion sickness during the first week of flight, and this resulted in anorexia of some significance. Because of the second of these effects, fat losses were particularly rapid during the week following launch. In general, the changes in body fat appear to be explained by the balance between caloric intake and energy expenditure and do not appear to have been influenced by weightlessness.

10.3.1.6 Body Protein. According to an analysis of metabolic balance studies of nitrogen and potassium, it was determined that protein losses are initiated almost immediately after entering weightlessness and then decrease exponentially with time during the first month (Fig. 10-10(b)). It is only after the first month of flight that protein losses appear to stabilize. These losses occurred in spite of a high protein diet and in the presence of exercise training. The lack of suitable controls makes it difficult to assess whether the stabilization of protein loss results from increasing exercise, increasing diet, or from some long-term adaptive influence. All of these findings are consistent with the hypothesis that the postural muscles are virtually unused in weightlessness and that they therefore atrophy from disuse.

10.3.1.7 Caloric Requirements for Spaceflight. The food intake for the nine crewmen ranged from 39.6 to 48.5 kcal/d-kg Bwgt while the caloric value of the tissue lost varied from -4% (a gain in tissue mass) to 26% of caloric intake. On the basis of a regression analysis of the body mass loss in relation to the caloric intake, it was estimated that a caloric intake of 46-50 kcal/d-kg Bwgt would have prevented significant tissue loss (primarily fat) for the Skylab astronauts.

10.4 Integration of Subsystem Hypotheses

10.4.1 Overall Hypothesis

Although the separation into individual physiological subsystems has been convenient and has yielded a number of new insights as shwon above in Chapter 10.3, the central approach of systems analysis is to eventually integrate this information and view the behavior of the body as a whole. Figure 10-11 is offered as an integrated hypothesis for the human physiological response to weightlessness. Most of the major systems of the body are represented except for those that were not part of the current analysis, such as the vestibular and immunological systems. This scenerio was generated primarily from the systems approach that has been presented in this book and outlined in the beginning of this chapter. Considerable detail has been omitted for the sake of clarity so that generalization can be made about the interactions between subsystems and the behavior of the combined systems. The following broad picture has emerged.

Disturbances in the cardiovascular, fluid-electrolyte, erythropoietic, musculoskeletal, and metabolic systems that are found during and after flights of varying duration appear to be attributed to two, and possibly three, major effects of weightlessness. These are, first, the absence of hydrostatic forces, resulting in acute fluid shifts within the body, and second, the absence of deformation forces, resulting in disuse and degradation of normally load-bearing tissues. The first of these effects leads to a rapid series of events, including redistribution of circulating blood, emptying of the leg vessels, and eventually a reduction in extracellular body fluids, the most important of which is blood volume. The consequences of the second effect are a more chronic reduction in bone and muscle mass. Thus, most of the intracellular and extracellular losses of fluid, salts and musculoskeletal tissues can be explained by these two mechanisms. Many of these changes can be ob-
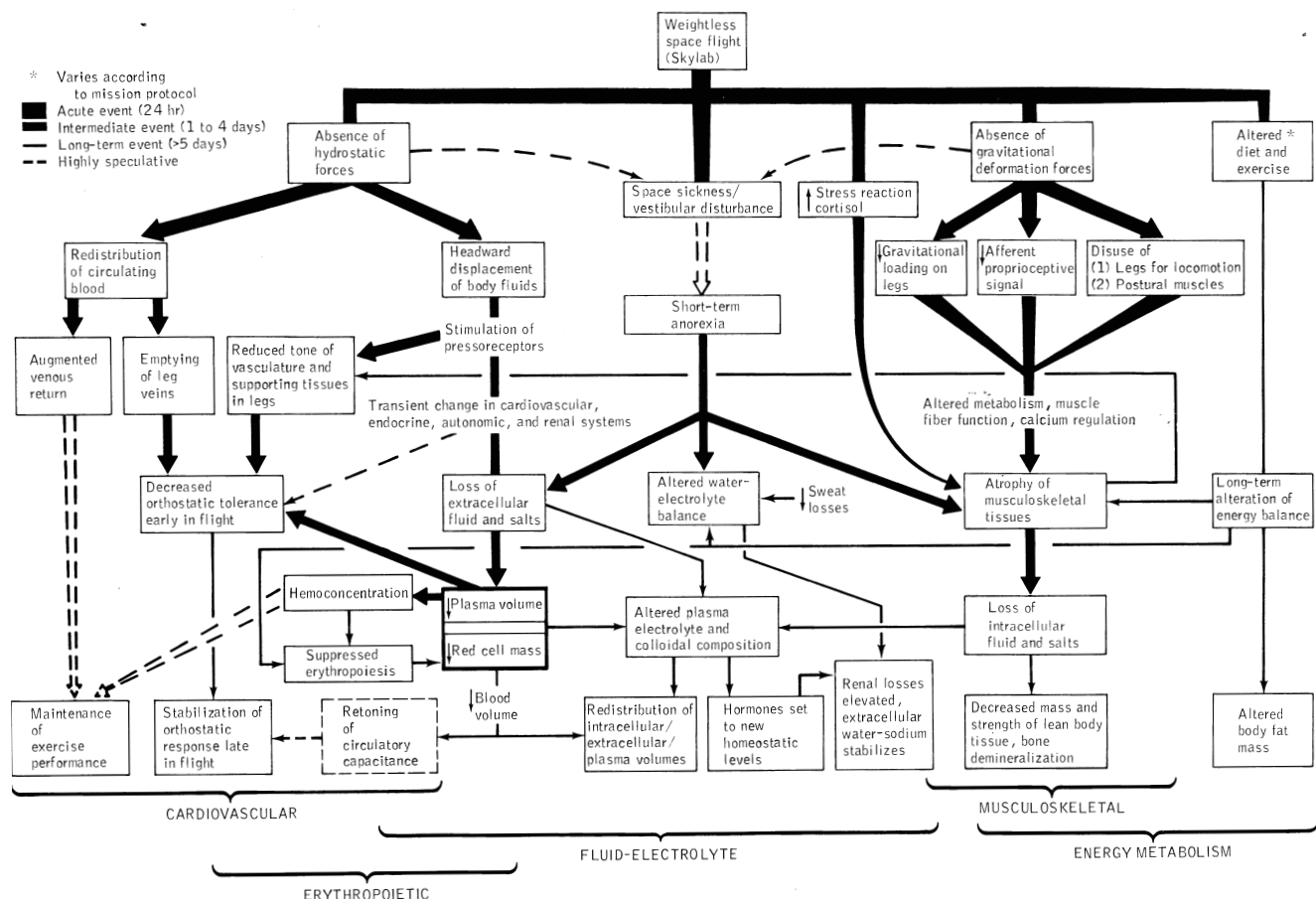
Figure 10-11. Integrated hypothesis of physiological adaptation to prolonged spaceflight.

served during spaceflight itself, while others manifest themselves more clearly after return to Earth. As suggested by the diagram, these two effects are not completely separate, and probably converge to some common pathway by mechanisms much more complicated than indicated here.

In addition, a third factor, alteration of metabolic state, reflected by changes in dietary intake and exercise, was found to play an important role in the physiological adjustments of the Skylab crew. An inadequate intake of fluid and food, resulting in negative energy balance, whether brought on early in flight as the result of space motion sickness, or more chronically because of a controlled but deficient diet as occurred in the first 2 Skylab crews, contributed substantially to the loss of body water and electrolytes during the first week and to the gradual loss of body fat, body protein and perhaps to the suppression of erythropoiesis in the ensuing weeks. Similar processes may have occurred in astronauts of Gemini and Apollo missions because of the inadequate caloric content of their diet. Also, the lack of an expected diuresis could have been influenced by the deficit intake of water just prior to launch. Finally, the seemingly obligatory degradation of musculoskeletal tissue creates a pool of circulating me-

tabolites that adds to the load of waste products that must be processed by the kidneys, thereby altering plasma biochemistry, hormonal secretion and renal function. To the extent that these metabolic factors are under voluntary control (i.e., diet and exercise), they may not be part of a generalized zero-g response but rather specific to Skylab. The circulatory and renal systems are central to many of these processes, both acute and long-term, because of the need to maintain a hypovolemic state in weightlessness and to eliminate the waste-products of tissue atrophy.

These three primary effects of spaceflight have both acute and long-term effects which lead to the notable and consistent findings of a loss in weight, a change in body composition, redistribution of fluid volumes, new homeostatic levels of renal, cardiovascular, and endocrine parameters, a decreased tolerance for orthostasis, and additionally, upon return to a one-g environment, a decreased aerobic capacity. Figure 10-11 also indicates a direct effect on the neurovestibular system, particularly the unweighting of the otolith organs that (together with other orientation cues) is believed to contribute to space motion sickness. It is this latter effect that contributes to the negative energy balance of susceptible crewmembers.
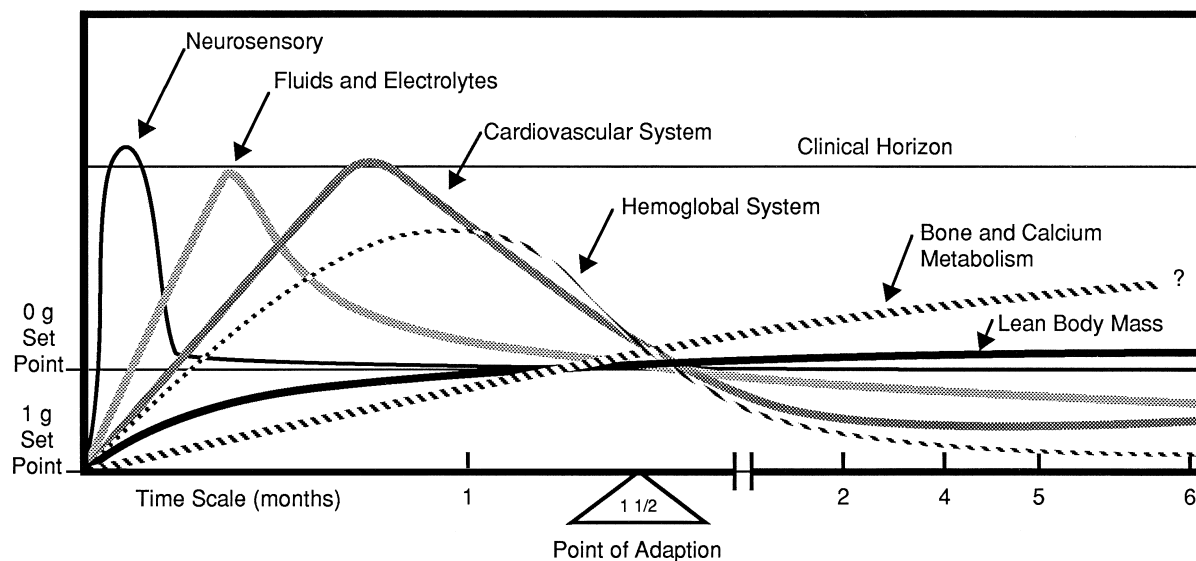
Figure 10-12. A highly idealized view showing the approach toward homeostasis of physiological systems during spaceflight. Each physiological subsystem has a different time course of adaptation and appears to be driving towards a new homeostatic level. Note that the time scale is exponential.

Adaptation to weightlessness is said to occur when the body adjusts to these changes and reaches a new homeostatic level. Figures 10-12 and 10-13 are an attempt to show the relative time course of adaptation for each major physiological system or for loss of body tissue, respectively. The return to new baseline values in Fig. 10-12 reflects the establishment of a new homeostatic level appropriate to weightlessness. The most rapid effects are observed in the vestibular system and the systems that respond to fluid volume regulation, i.e., headward fluid shifts. The significant decrements in body water, plasma volume, and sodium that have been observed in crewmen returning from space can be attributed to losses that occurred during the first several days of flight (Fig. 10-13). At the other extreme are the body structures that respond to slower acting processes and which manifest their zero-g response by gross losses in red cell mass and bone calcium. However, even a slowly responding system such as that which controls bone demineralization is under the influence of rapidly acting hormonal regulators. Muscle tissue appears to degrade at an intermediate rate, as exemplified by nitrogen and potassium losses. Depending on the degree to which caloric intake matches energy requirements, fat stores can be included in this intermediate group as well (see Fig, 10-13). The time course of adaptation, or the rates of disappearance from the body, depends on the nature of the disturbance and on the time constant of the correcting homeostatic system.

10.4.2 Homeostatic Control

At the time of the Skylab program, it was not known whether the changes observed in spaceflight were dysfunctional responses (pathological) or based on commonly accepted feedback mechanisms (adaptive). The studies
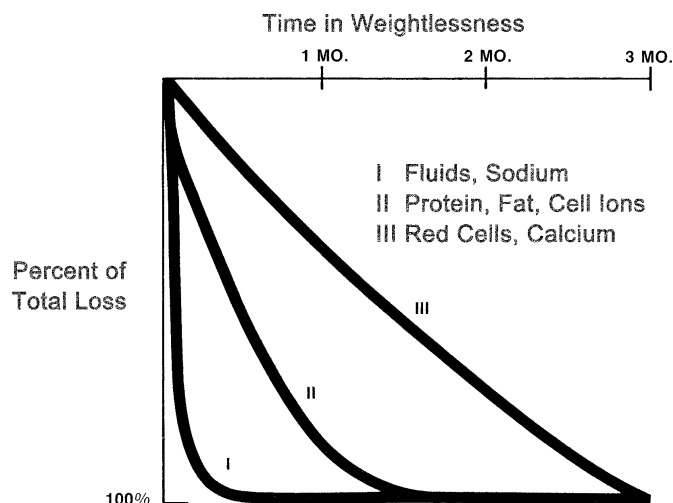
Figure 10-13. Various substances disappear from the body during weightlessness adaptation leading to a change in body composition. This figure, like the previous one, illustrates the different time courses of these substances.

discussed in this volume have supported the concept that, within the time span which man has so far been studied in space, most of these responses to weightlessness can be explained in terms of normal feedback regulatory processes.[*] But it was not always possible to explain the long-term adaptation phase of spaceflight in terms of regulatory

---

[*] The few instances of possible pathology might include a minor degree of erythrocyte hemolysis and development of motion sickness.

feedback mechanisms more suited to corrective action of acute disturbances. This suggested a logical division of the spaceflight response into acute and chronic segments for purposes of systems analysis. A classical example of the temporal range of feedback processes concerns the blood volume and pressure controllers that reduce plasma volume when challenged by the acute cephaled shifts of peripheral fluid. These controllers include fast acting baroreceptors-sympathetic pathways, slower acting renal mechanisms, and long-term adaptive effects that retone the blood vessels to accommodate more or less blood volume. Another of many examples concerns the behavior of the renal regulating hormones, such as ADH or aldosterone, whose acute response to hypogravity could be explained by volume/pressure controllers but whose long-term response could only be accounted for by controllers responding to electrolyte concentration. In order to determine the extent of feedback involvement in each case, it was necessary to develop the appropriate model of the system under investigation, to identify plausible disturbance points in the regulatory pathways that would produce the response of interest, and then to perform simulations of the system to verify that the predicted responses are quantitatively in agreement with observed responses.

10.4.3 Central Importance of Blood Volume Regulation

A concept that clearly emerges from the model simulation studies is the primacy of the circulatory system. From a systems point of view, it was known that the general behavior of many organs, including the renal, respiratory, thermoregulatory, hormonal, erythropoietic, and fluid control systems, depends largely, on normal function of the circulation. Because of the initial headward fluid shifts and subsequent downward blood volume regulation, the control of blood volume and pressure has turned out to be central to the understanding of the responses to weightlessness and the return to Earth. The ability to assess the causes and consequences of blood volume loss during spaceflight was facilitated by the fact that the circulatory system was represented, at varying levels of detail, in our entire repertoire of models, and in three particularly useful models, those of fluid-electrolyte, erythropoiesis, and cardiovascular regulation.

The cartoon in Fig. 10-14 illustrates the shift of blood and leg tissue fluids that are normally pooled in the legs in one-g into the central circulatory compartments in zero-g. The consequences of this fluid shift phenomenon are widespread, as suggested throughout this book and summarized in Fig. 10-14. Not only do they activate the numerous blood volume and renal-endocrine controllers as indicated in Fig. 10-3, but they affect the hematological, pulmonary, cardiovascular, and perhaps the vestibular system as well as the physical characteristics of the astronauts. The usefulness of ground-based analogs to simulate spaceflight is often judged by the number of such effects that can be reproduced. The homeostatic reduction in plasma volume that is thought to occur (see Fig. 10-5) returns central blood volume towards normal, reduces the total plasma volume and produces a mild hemoconcentration. This event has the following consequences:

a) Hemoconcentration results in enhanced oxygen delivery to the tissues, causing a reduction in red cell production and red cell mass, due in part from suppression of erythropoietin (see Fig. 10-6). Thus, plasma volume and red cell mass are regulated by independent mechanisms. Red cell mass is ultimately under the control of an *oxygen regulator* which balances oxygen supply and demand while plasma volume is under control of a *volume regulator* sensing central fluid pressures. Although not measured directly during flight, the blood volume reduction can, arguably, be attributed to an acute plasma volume loss, followed by a more gradual loss of red cell mass, a scenario simulated by the modified Guyton model (Fig. 10-15). A potentially significant insight from this model simulation is the prediction that as red cells are depleted, volume regulators replenish the plasma component just enough to maintain total blood volume at a new and reduced level. This inverse relationship between plasma volume and red cell mass was, in fact, observed in the Skylab crew (see Fig. 6-2. This supports the notion of a tightly controlled blood volume level with an altered zero-g setpoint.

b) An increase in peripheral flow resistance also results from the increased viscosity of the hemoconcentrated blood, as well as from autoregulatory controllers responding to tissue hyperoxia. The circulatory effects of increased resistance, as predicted by our models are to suppress venous pressures and cardiac output below control levels.

c) Other circulatory adaptive effects, such as blood vessel retoning, are likely to occur in prolonged flight as the body attempts to reduce the capacitance of the circulation to accommodate a reduced blood volume. The Guyton model is one of the few models in existence that accounts for this and other similar mechanisms in the long-term adaptation of the circulation.

d) The effect of blood volume loss (and postflight hemodilution) are believed to be largely (but not wholly) responsible for the impaired circulatory responses during exercise and orthostatic tests noted in astronauts returning from space. During flight the increase in hemoglobin concentration likely helps maintain exercise performance in the face of a depleted blood volume.

10.4.4 Summary of Integrated Hypothesis

The integrated hypothesis has emphasized several critical ideas:

a) there are only a few direct effects of weightlessness on the body from which a cascade of physiological responses ensue,

b) there are both acute and longer-term (adaptive) components to the weightlessness response,

c) a number of physiological systems participate in this response,
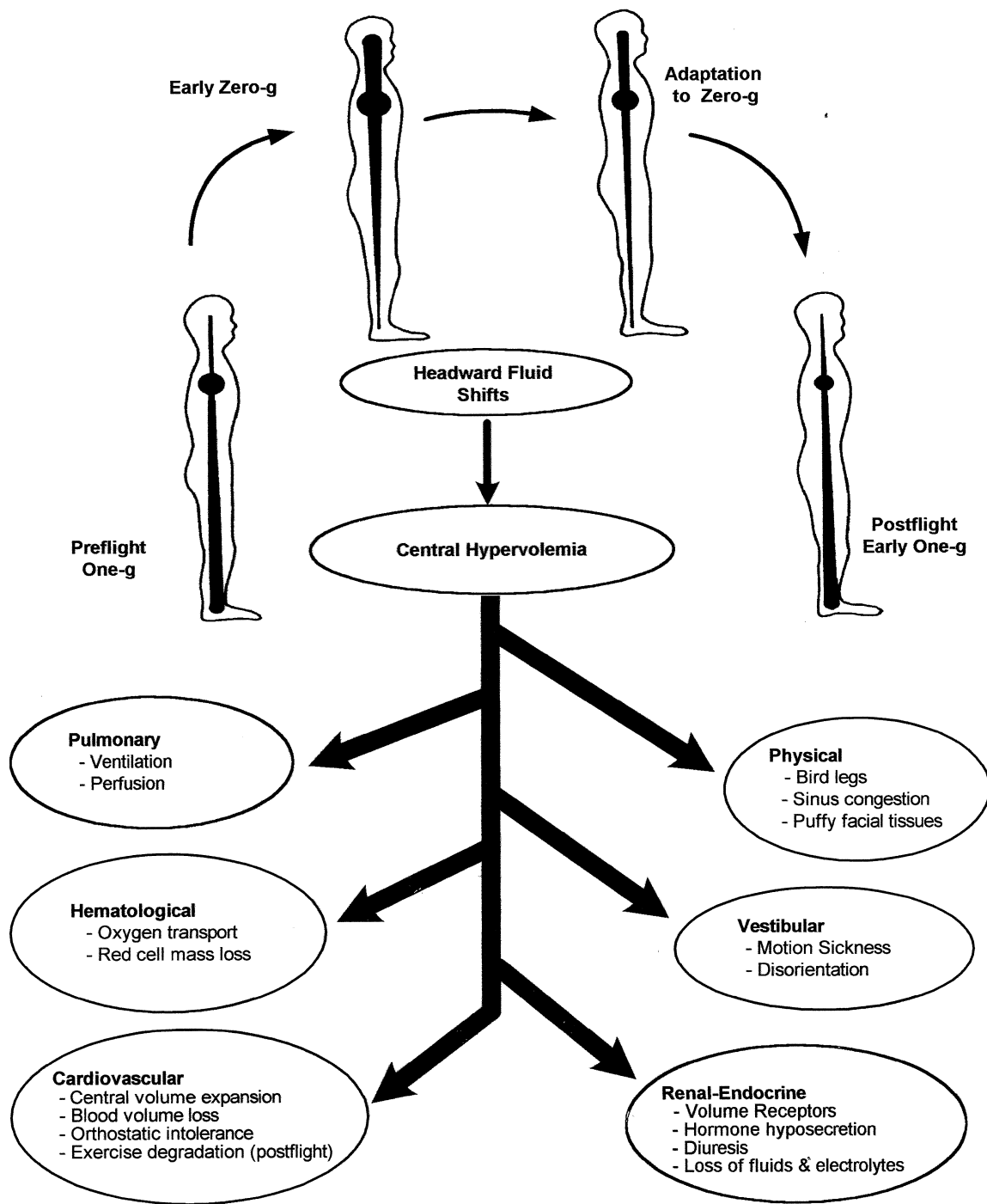
Figure 10-14. The wide-spread effects of headward fluid shifts. The cartoon on top indicates that blood and fluid normally pooled in the legs in one-g are shifted headward in zero-g. During spaceflight adaptation, volume controllers normalize central fluid volumes. Upon return to earth, the reduced blood volume is believed to play an important role in causing orthostatic intolerance and reduced exercise performance. There are widespread and measurable consequences at every stage of this scenario, including the recovery period, as indicated by the lower portion of the figure. The vestibular effects are uncertain but have been proposed by various researchers.
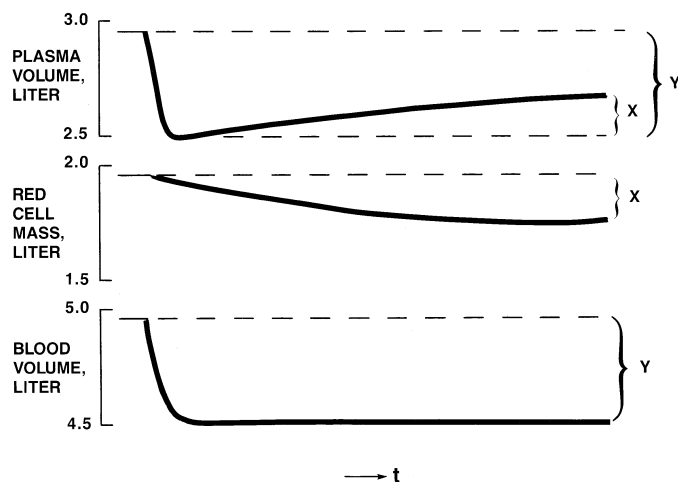
Figure 10-15. Plasma volume, red blood cell mass and blood volume changes during a head-down tilt simulation by the Guyton model modified by the inclusion of a more accurate erythropoiesis subsystem (Appendix X). Plasma volume rapidly declines by the amount Y, and then gradually rebounds by an amount, X, to compensate for the loss of red cells. This results in a constant blood volume at a reduced level, Y.

d) the response is highly dynamic and interactive between all of the major systems, suggesting the importance of an interdisciplinary approach,

e) the responses to weightlessness do not appear to be pathological but can be explained in terms of normal feedback regulatory processes that are also operative on earth,

f) the time course to achieve a new homeostatic state for zero-g is different for each major physiological system, and

g) the most significant and consistent consequences of these fundamental changes include a change of body composition, blood volume loss, alteration of blood biochemistry (hormones, electrolytes), cardiovascular deconditioning, atrophy of musculoskeletal tissue and short-term vestibular disturbances.

This broad view of adaptation to spaceflight, together with the more detailed subsystem hypotheses, is the culmination of the systems analysis effort, and represents a response to the critical questions posed earlier in this chapter. The approach taken here was designed to mine the lucrative Skylab database during a time when spaceflight was inaccessible. Whether or not the effort was worthwhile should be evaluated in an historical context; i.e., prior to Skylab a generally agreed upon overall hypothesis for adaptation to weightlessness was lacking. Like any theoretical analysis, these ideas need to be treated with appropriate caution. Any ideas that conflict with irrefutable data that were somehow not considered should be discarded, of course. More likely, there will be conflicting viewpoints based on other hypotheses or weak data. In these circum-

stances, the obvious course is to provide the crucial experiments that will provide a factual basis for a more correct view. In many cases, we have proposed such an experimental program.

10.5 Effectiveness and Limitations of the Modeling Approach

10.5.1 General Modeling Process

In general, it was the consensus of those working on this project that mathematical models are useful and effective tools for testing physiological system hypotheses in an interdisciplinary context especially where experimental opportunities are limited as in human space research. Nevertheless, there were limitations to the modeling process and lessons to be learned for future studies. Some general conclusions, lessons learned and recommendations are discussed below, first regarding the general modeling process, and then, because of its special nature, the Whole-Body Algorithm.

a) **Models Should Complement Research Environment**. The state of the art in mathematical modeling in the early 1970's (when this project was underway) was the representation of entire organ systems or multi-organ systems. At the same time, biomedical spaceflight research was in its embryonic form and consisted almost entirely of identifying gross changes of different organ systems. Thus, there was good alignment between the type of data being collected by NASA and the level of detail in currently available physiological models. Had the nature of the research been concerned more with changes at the biochemical and cellular level, as it is today, these same models would have been much less effective.

A large scale modeling program becomes cost effective when it is difficult or expensive to collect worthwhile data. The current project took place during the 10 year hiatus in spaceflight operations between the end of the Skylab biomedical program (Feb. 1974) and the start of the Shuttle Spacelab research program (Nov. 1983). If Space Station science operations truly became routine, there may be less incentive for science program managers to invest in an extensive modeling program. However, development of an advanced whole-body model would be extremely useful in preparing for NASA's long-term goal of the exploration of Mars.

b) **Models Limit the Analysis**. It was obvious from the outset that the models currently available or those that could be developed would be restricted to the analysis of only a subset of the experimental measurements in the extensive Skylab database. Models, by their very nature, do not include all the details of the real system. The approach taken for data collection in the Skylab missions was to measure a large number of variables, not merely those that had previously been shown to be disturbed during spaceflight, nor necessarily fundamental factors in each physiological sys-

tem. Thus, there were large quantities of data that could not fit within the framework of the predictive simulation models. In some cases, as in the study of body composition, it was still possible to create simple metabolic models that yielded extremely useful results of a descriptive rather than a predictive nature. In other cases, the models, however complex, simply did not include many potentially important effects. Thus, in the area of fluid-electrolyte and hormonal regulation, data concerning such substances as growth hormone, thyroxine, insulin, and catecholamines were not considered in a quantitative manner. Similarly, the evaluation of the electromechanical properties of the heart and the immunological responses of the crewmen, although studied in space, did not lend themselves to a rigorous simulation analysis. Models were also not available at the time to study such potentially important factors as acid-base balance, cell metabolism, or vestibular function. In the time since this study began, however, many promising developments in modeling these systems have taken place and these ought to be considered if further work is planned in spaceflight systems analysis.

c) **Data Limits the Analysis**. Notwithstanding the above comments concerning the abundance of data relative to model complexity, another limitation in the approach resulted from a scarcity of data in those areas where the models *were* well suited for analysis. Measurements were limited, in the Skylab study, to non-invasive collection procedures, but most of the model parameters and variables reflect invasively obtained quantities. Data collection was also severely restricted during the first 24 hours of each flight, during the time that dramatic physiological change took place. Unfortunately, the predictive accuracy of the majority of models used in this study is much greater for short-term or acute stress conditions compared to longer-term events. Therefore, it was not possible to verify the model predictions in a variety of circumstances. Table 10-7 lists examples of the more common quantities measured during spaceflight that could be simulated with the current suite of models (left column); also shown are an equal number of very useful quantities that were not measured in Skylab but that were within the capabilities of model prediction. Because of the unavailability of this data, the modeling approach, with its predictive capabilities, was able to make a more significant contribution.

d) **Importance of Experimental Program.** The importance of using models for data interpretation within the framework of an active experimental program has been emphasized throughout this book. This demands, first, an active involvement of experienced researchers and, secondly, the ability to influence new experimental studies. Indeed, we found that the strongest outcome was generally achieved when the system modelers and the subject-matter expert scientists operated as a team. This was not always the case and it was necessary at those times for the modelers to de-

velop a firm foundation of the physiology. Researchers who do not make the effort to appreciate the usefulness of modeling usually are too skeptical of this tool, e.g., it is incomplete, it is too quantitative, to trust the potential insights and benefits. Also, there was limited opportunity in this project to become involved with new experimental studies, the exceptions being a U.S.–Russian bedrest study (Chapter 9.7) and the hematological studies in dehydrated mice (Chapter 6.5.4). However, the modeling project did provide the basis for a number of ideas that were incorporated into proposals for future flight experiments (see Appendix G).

e) **Not All Models Useful.** Not all of the models used in the project were equally useful. For example, the thermoregulatory and respiratory models, although important elements in the whole-body algorithm, received relatively little attention in the task of spaceflight data evaluation. These models were originally included (prior to the first Skylab flight) because of the belief that disturbances in environmental temperatures and ambient gas compositions, if they occurred, would be important factors in interpreting the crew's responses. However, there were only isolated instances of environmental disturbances and for the most part there were no unusual thermoregulatory and respiratory problems. The models that proved most useful for hypothesis testing were the modified Guyton model, the pulsatile cardiovascular model (in both LBNP and exercise modes), and the erythropoiesis model. The former of these was the most complex and the latter the least complex of all the models used in the project, emphasizing the notion that even simple models can be extremely useful. Nevertheless, the lesser used stand-alone models were critical components of the Whole-Body Algorithm.

f) **A New Reference State Needed.** One of the conclusions of this study is that it is not an easy task to mathematically simulate the true nature of zero-g. The two major characteristics of weightlessness are the elimination of hydrostatic gradients on blood columns and the elimination of loading on weight-bearing tissues. The human body, altered by these two characteristics in zero-g, is usually contrasted with that found in the upright ambulatory position in one-g, for the latter is the position in which the effects of gravity are most prominent. It may, therefore, be argued that a true simulation of weightlessness should begin with a model referenced in the upright position and should contain hydrostatic and tissue elements which respond to gravity. In such a model, removal of the gravity vector might then automatically promote the headward redistribution of circulating fluids (in response to the absence of hydrostatic gradients) and the degradation of atrophy of musculoskeletal tissues (in response to the absence of load). This rationale is conceptually identical to that which underlies experimental simulation of weightlessness by bedrest. However, the existing mathematical models are initialized in the

Table 10-7. Selected Quantities Predicted by Simulation Models

PARAMETERS FOR WHICH INFLIGHT DATA EXISTS	PARAMETERS FOR WHICH INFLIGHT DATA DOES NOT EXIST*
Total body water	Extracellular water
Leg volume	Intracellular water
Body potassium	Interstitial water
Extracellular sodium	Plasma volume
Plasma sodium	Red cell mass
Plasma potassium	Red cell production rate
Plasma proteins	Plasma erythropoietin
Plasma hemoglobin	Tissue oxygenation
Plasma angiotensin	Autonomic activity
Plasma aldosterone	Volume receptor stimulation
Plasma ADH	Natriuretic factor
	Capillary filtration
Urine volume	Cardiac output
Urine sodium	Peripheral resistance
Urine potassium	Venous pressure
Evaporative water loss	Local blood flows
Blood pressure	Body temperature
Leg blood flow	Circulatory, renal, fluid, and hormonal changes on first inflight day
LBNP heart rate	LBNP cardiac output
LBNP blood pressure	LBNP venous pressures
LBNP leg volume	LBNP blood volume and flow distribution
Exercise heart rate	Exercise cardiac output
Exercise oxygen uptake	Exercise stroke volume
Exercise minute ventilation	Exercise blood gases

*Skylab era

supine, not the upright, position, and do not contain all of the mechanisms that are representative of ambulatory man. The fallacy of the supine reference position is made clearer by realizing that the supine condition, if extended, is not much different from the weightlessness adapted state. (This is the basis for using supine bedrest as a spaceflight analog). It is our belief that if one begins with a model referenced in the erect position, long-term spaceflight could be approximated by simulating the chronic supine position.

Most of the crucial mechanisms that allow man to remain in the upright position are those that protect against orthostatic collapse and those that maintain integrity of musculoskeletal tissue in the face of down-ward weight loading. Unfortunately, many of these mechanisms are not yet known or quantified, so that mathematical simulations using this approach are not yet feasible. Nevertheless, it was still possible to approximate some of these gravitational effects in the current modeling effort in a somewhat artificial manner. For example, headward fluid shifts were accomplished either by mathematically forcing fluids from the legs, applying external pressures on the extremities, or by tilting the model in a head-downward position. Similarly, the effects of muscle atrophy were simulated, in part, by allowing the release of cellular electrolytes into the extracellular compartments. This approach avoided the problem of modeling the pri-

mary physio-chemical-mechanical forces that occur with the loss of gravity, and it was successful in reproducing many short-and long-term effects observed in hypogravity environments. The task of identifying more basic model forcing functions was begun with the studies of orthostatic mechanisms, cardiovascular deconditioning, and gravity loading effects on bone demineralization. Simulations of weightlessness with greater realism will most likely be achieved by more fully appreciating and quantifying the mechanisms that permit man to function in his normal upright position. Such an approach would necessitate a deeper understanding of gravitational and spaceflight physiology.

10.5.2 Whole-Body Algorithm

10.5.2.1 Accomplishments. A great deal has been learned in the design and development of the Whole-Body Algorithm (Chapter 3). The WBA was conceived as a means to study multiple system physiological processes and interactions, multiple and sequential stresses, and overall system hypotheses including zero-g effects. A number of diverse stresses (over a range of stress levels) have been simulated including environmental disturbances (ambient temperature changes, hypoxic and hypercapnic gas mixtures), metabolic changes (supine and sitting exercise), and special experimental situations (tilt-table studies, LBNP, and bedrest). Simulation of short-term stresses resulted in simultaneous and integrated responses from the cardiovascular, respiratory, and thermoregulatory subsystems and the accuracy of a large number of responding variables were verified. The capability of each subsystem model was extended by adding functionality not in the original model (Appendix D). In all cases, whenever a particular subsystem model had been previously tested on a stand-alone basis, its performance as part of the WBA proved to be at least as good and in some cases better, with respect to agreement with available data and stability of response.

The versatility of the WBA was illustrated by its ability to combine these stresses and automatically sequence between the long and short-term model subsystems. This capability was demonstrated by a 4-week bedrest study preceded and followed by tilt and exercise stress tests (Chapter 9). In this case the long-term subsystem model was found to reproduce many experimentally observed changes in circulatory dynamics, body fluid-electrolyte regulation and renal function as the body adapts to hypogravity. The shorter-term components of the WBA successfully reproduced differences in tilt and exercise tests before and after bedrest. Both steady-state and transient responses were found to be reasonably accurate. A myriad of operational and computer-related problems were solved during its development. Taken together these are significant accomplishments.

10.5.2.2 Lessons Learned and Recommendations. Although a measurable degree of success has been achieved, the WBA is by no means complete and it really represents a stage of development. Many aspects and ca-

pabilities of the model have yet to be tested. The validation process has uncovered inadequacies in the response to many of the stresses and suggestions for correcting these have been discussed in earlier chapters (also see Appendix G). Some of the most useful insights gained from the experience with developing and using the Whole-Body Algorithm include the following:

a) **Greater Stability.** In the course of running simulations with the WBA it was observed that the model was extremely stable from an operational perspective. In some models, especially in the initial simulation trials, there is a tendency for the output variable (signal) to oscillate and eventually become unstable. Guyton (private communication) made a similar observation concerning the development of his model and attributed this phenomenon to the extreme stability of the real system because of redundant feedback pathways. This suggests that interacting subsystem models, if properly formulated, inherits some the innate stability and compensatory characteristics of the real system.

b) **WBA Too Cumbersome.** Complexity may have limited the usefulness of the whole-body algorithm, which contains well over a thousand parameters and variables and a large number of physiological subsystems. A model of this size is somewhat cumbersome and unwieldy, and simulations take a relatively long time to perform. This was due, in large part, to the limitations of the computer systems that were in use 25 years ago. In addition, the WBA turned out to be not as well suited for studying a single subsystem response, as were the individual subsystem models on a stand-alone basis. For example, often only a small portion of the Whole-Body Algorithm was needed to test the erythropoiesis response to a hypoxic stress. It was much more convenient, in those cases, to use the stand-alone model for erythropoiesis regulation. Perhaps for these reasons, most of the systems analyses performed in this project and the most useful results were achieved with the individual stand-alone models rather than with the Whole-Body Algorithm.

c) **WBA Not Fully Utilized.** The WBA, as developed in this project, is very versatile, capable of simulating many different conditions. Limited resources permitted the examination of only a few specific conditions, all related to spaceflight. It was not possible to address numerous other applications. Thus, even before developing a more *advanced* model, it may be useful to put the *current* model to more complete use. For example, simulation of exercise (with or without simultaneous environmental stresses) is one of the areas in which this model may be superior to all others. Although exercise was an experimental procedure during Skylab, measurements were confined to the cardiovascular responses to this stress. Therefore, the model's capability to integrate thermal, respiratory, and cardiovascular responses to exercise could not be used to advantage. In general, there is a scarcity of data describing multi-subsystem responses to almost

any stress and when this fact is combined with a difficulty in performing rapid experimental iterations, the utility of such a complex model as the WBA becomes questionable.

d) WBA Should Integrate Spaceflight Hypotheses. The full potential of the whole-body algorithm has not yet been realized, not only due to insufficient data, but also because the present effort has largely emphasized the subsystem analysis in the stand-alone models. The analysis of subsystem hypotheses is now largely complete in several important investigative areas. The next phase of application will be to incorporate descriptions of these subsystem hypotheses into the whole-body algorithm. When this is accomplished, then that model will serve its main function as a central repository of a detailed integrated, multi-system hypothesis of zero-g adaptation. In this way it will be possible to discover how the hypotheses developed for one system could have important consequences on another system. Thus, the WBA can then be used to study interactive effects between subsystems, responses to multiple stresses, and the dynamic behavior of short-term and long-term regulators, capabilities which the present model contains but which have not been fully explored.

e) Top-down or Bottoms-up? A major question at the outset of developing a large-scale multi-subsystem model is whether the design should be "bottoms-up" or "top-down". The first approach consists of combining previously existing subsystem models so that they function together, while the second approach is to design each subsystem to function as a part of a single model from the outset. In spite of some obvious limitations, the Whole-Body Algorithm was designed with a "bottoms-up" approach and the reasons for doing so were discussed in Chapter 3 (Chapter 3.2.6.2). Briefly, the bottom-up approach can lead to a working model more swiftly but there are operational, structural, and conceptual problems. On the other hand, the top-down approach is a more logical and natural one, but requires a large investment in talent, time and money. In the end, there was general agreement that a top-down approach would result in a superior model (see section below and Chapter 11).

10.5.2.3 Future Directions of the WBA. Work on the WBA essentially stopped once the concept was demonstrated. This was a result of limited resources and changes in priorities rather than in belief that the basic approach was incorrect and should be abandoned. Thus it was apparent at the time that many voids existed in the integrated model that was created. Much work is needed in the areas of modeling metabolic and biochemical processes, renal function, vestibular function and a host of others. An advanced model that integrates these systems may prove to be very useful for evaluating countermeasures and predicting crew health during spaceflight. Developing models that mimic a particular individual's unique physiology is an even more far-reaching goal. There has been little

modeling of disease processes on a subsystem or system level. These voids should be among the objectives addressed by an advanced total body system model.

However, in designing an advanced total body system model, one must consider an even more basic problem than simply filling the voids of these models. It almost seems like a contradiction in terms, but the model must be simplified before a more complex model can be developed; this may require a totally different approach than building a total body model by connecting subsystem models together. At the heart of the systems analysis approach is the identification of the essential details of a system and to discard or reduce in size, the non-essential elements. Several of the essential elements identified for an improved Whole-Body Algorithm include: a) a top-down design approach, b) the need for a single central nervous system and a circulatory system, c) an associated research program for developing a model validation database and a interdisciplinary spaceflight database, and d) developing a central repository and communication system that will allow modelers from many laboratories to participate in building a large-scale physiological model. These and other recommendations are discussed further in Chapter 11 and listed in Appendix G.

10.6 Concluding Remarks

The project, on which this book is based, set out to develop and utilize a general systems approach for conducting and analyzing research on the human adaptation to weightlessness. The approach discussed herein has been valuable in evaluating hypotheses and important mechanisms, identifying elements requiring further experimental description, providing a basis for analysis of selected data, and assisting in the development of a general hypothesis for gravity unloading. Specifically, all of the objectives originally established at the outset of this project (see Introduction, Chapter 2.1.2) have been addressed and realized to a large extent, as described below:

1. The objective of "*developing new and improved mathematical approaches for solution of problems in spaceflight life sciences*" was achieved with the development of an integrated database and analysis system including statistical capabilities, special purpose programs and simulation models including the development of a preliminary large-scale model of the human (see Chapter 3 and Table 10-1).

2. The objective of "*organizing, integrating and analyzing spaceflight and supportive ground-based research data across interdisciplinary lines*" has been realized in each of the areas addressed including fluid-electrolyte regulation, body composition, erythropoietic regulation, cardiovascular regulation and musculoskeletal function. This effort has resulted in an advanced, but more narrowly focused, analysis of spaceflight data than was previously available from the original Skylab reports. A major data analysis activity was the interpretation of the vast quantity of

Skylab metabolic data (see Chapter 4). Data that had previously been published was reevaluated and reinterpreted with the systems analysis tools in the light of recent findings from ground-based studies and Soviet missions.

3. The objective of "*attempting to explain the experimental findings*" by "*testing individual physiological subsystem hypotheses using quantitative approaches*" was perhaps the unique contribution of this project and was described at length in Chapters 5 through 9 and summarized in the current chapter. Hypotheses were contributed by spaceflight investigators and were naturally generated by the systems analysis process. Because the models embodied current theories of homeostatic control in the requisite organ systems, it was possible to use computer simulation as the basis of a hypothesis testing approach. Comparing model results with the spaceflight findings led to insights about the behavior of the system under weightlessness conditions and to the veracity of the hypothesis.

4. A fourth, and highly ambitious, objective was to "*integrate these hypotheses into a unified and internally consistent understanding of physiological adaptation to weightlessness*". The process of identifying what appear to be fundamental influences of gravity on each physiological system and then examining interactions between systems has led to the recognition of several common pathways (see Fig. 10-11). These pathways have suggested clues for a tentative integrated physiological hypothesis for spaceflight adaptation that is consistent with the Skylab data. Feedback pathways that regulate acute changes in flight eventually give way to less understood adaptive (or chronic) processes. In order to solidify these tentative conclusions more data must be collected under various conditions, including spaceflight and ground-based studies and using human and animal subjects.

5. The final objective listed at the outset was to apply the experience gleaned from this project "*to improve experimental design and data analysis*". Because of the capability of the models used in this project to test hypotheses and predict quantities or processes that were not examined directly in space, the potential exists for proposing confirmatory experiments. During the latter phases of the project, the systems analysis team formed collaborations with researchers who were engaged in animal research, human bedrest studies, operational medicine, and proposal preparation for experiments on the new Space Shuttle. The systems analysis approach helped to solidify the hypotheses, to provide the research rationale, and to simulate the proposed experimental protocols. Many of these proposed experiments have already been realized. As was emphasized more than once, full potential of the systems analysis method will best be realized by maintaining an iterative cycle between model development and experimental research.

In spite of the limitations in the modeling process and the difficulty in achieving a rapid iterative experimental process, these studies have resulted in an improved understanding of the physiological events that occur during human adaptation to weightlessness. When this understanding is enhanced, it should be possible to use advanced models to define appropriate indices of health (normal adaptation) during spaceflight, to predict individual responses to weightlessness, and to develop countermeasures to the deleterious effects of spaceflight and subsequent recovery.

Chapter 11
Advanced Applications and Future Directions

11.1 Introduction

We have demonstrated, in some detail in this book, the advantages of mathematical modeling. These include the identification of system structure, simulation of intact system behavior, estimation of quantities which are normally not measurable, and hypothesis testing to understand specific mechanisms and help interpret experimental findings. The next step in the NASA Life Sciences program is to put these newly developed tools to work in support of the current and future spaceflight programs. A balanced program is envisioned for applying the current simulation and analysis systems to new areas and filling the gaps in the current capability by developing new systems. This should be complemented by an appropriate experimental research program. As we have seen from experience, a synergy of melding experimental and theoretical activities is crucial for a successful outcome.

Based on the results of the current program we would expect model applications in several specific areas. Among these is the use of the models with the zero-g hypothesis mechanisms incorporated in them for more advanced studies of integrated physiology. Such a model system would also be suitable for assisting with the design and interpretation of flight experiments and for continuing the integration of ground-based and spaceflights studies. The preliminary effort in developing an erythropoietin mouse model should be extended in developing multi-species models for all appropriate physiological systems where animal experiments play a critical role.

The innovative project of combining subsystem models that was begun in the current project (i.e., whole-body algorithm) should be continued. An advanced large system model that utilizes a top-down design approach should have considerable promise in helping to understand interactions between major body systems and long-duration adaptive phenomena. Also customizing this model so that it can differentiate between individual subjects or classes of subjects is a more realistic strategy of accounting for the nuances in physiological responses than a one-size-fits-all approach.

A major role of models is also is seen in the development of computer-assisted health care systems. Simulation models can be developed for understanding the pathophysiology of a disease state and evaluating alternative therapies and countermeasures. Pharmacokinetic models are becoming more common for helping to understand drug distribution and behavior in the body with the purpose of optimizing drug dosing schedules. Models can be oriented toward such clinical problems as minimizing the amount of blood drawn from a patient or optimizing expensive imaging tests. Other types of computational

methods and biomedical databases can be added to develop a system which serves as an adjunct to space medical operations, including real-time physiological monitoring of the spaceflight crews, diagnosing medical conditions, and selecting treatment regimes. Beyond these space applications, a number of recent innovations in medicine and physiology have shown much promise including expert systems and teaching models.

The general systems analysis approach that provided the foundation and structure to the current project is also being applied to managing portions of the space life sciences research program. This is especially true for activities where decisions by mission planners must be made to allocate limited resources for science experiments and ensure safety of space crews. A systematic approach to resource allocation has been used in managing science during the Shuttle Spacelab era and in planning for exploration-class missions.

These ideas for advanced applications and future directions of systems analysis and modeling will be explored below.

11.2 Systems Analysis as an Aid for Designing Spaceflight Medical Experiment

An important use of simulation models has been to predict experimental results or stress responses that cannot be determined directly because of excessive risk, cost, or delay. The more highly developed the model, the greater the predictive capabilities. However, a powerful use of simulation models is, as a research tool, to aid in designing and interpreting experiments rather than to take the place of experimentation. An example of this approach is provided in Chapter 6.5.7 where the use of the model for erythropoiesis regulation in developing a flight experiment is described. When used for these purposes, it is not always necessary that the model be an exact description of reality; a gross approximation will often be sufficient. Certain special techniques, such as sensitivity analysis, error analysis, and parameter estimation, have been developed that greatly enhance the use of simulation models in this regard. The following outline briefly discusses many of the uses that simulation models afford the scientist/planner in designing experiments (details have been omitted in the interest of brevity only; the techniques discussed have been developed sufficiently to begin applying them immediately to any physiological system which is not well understood and for which a gross descriptive model has been formulated):

a) Models can be used to rapidly simulate long-term experiments in relatively brief periods. The simulation

would help establish the exact conditions that are desired for the upcoming experiment.

b) Models that predict unsteady state responses can be used to indicate the times when variables are changing more rapidly and thus suggest the time protocol for making data measurements.

c) Traditional methods of stressing systems, such as inducing single step changes in a system parameter, often do not produce as much insight into a system as more unusual types of stresses such as multiple, sequential or time varying stresses. Models can usually predict, better than human intuition, the effects and advantages of using these types of experimental stresses.

d) Sensitivity analysis is a systematic and quantitative method of identifying the most important parameters of a system; i.e., those that have the greatest influence on given response variables. This method would provide a rational basis for deciding priority of experimental measurements and cost allocations.

e) Error analysis, when combined with sensitivity analysis, can lead to an even more powerful ordering of priorities. This technique provides an estimate of the relative contribution of errors of the major system parameters to the final system response. This information can be used to define the limits of allowable experimental error and hence suggest acceptable measurement techniques.

f) Simulation may be used to design decisive experiments by determining those conditions under which competing theories or hypotheses predict the most divergent experimental results.

g) Physiological function of particular systems is often evaluated clinically by measuring only a few system variables (such as heart rate and blood pressure for cardiovascular evaluation). As more knowledge is gained, these "performance criteria" are reevaluated and improved (e.g., the use of exercise stress and non-invasive measurements to evaluate cardiorespiratory function). Simulation can be used to aid in this process of developing performance criteria that are sensitive to deteriorating physiological function. This can be done by testing complex combinations of parameters and correlating them with simulated stress and pathological states. This in turn would suggest experiments to test any favorable simulated results.

h) The interpretation of experimental results can also be aided and extended by modeling. Parameter estimation procedures involve adjusting parameter values in a model until certain simulated responses compare favorably with experimental measurements. This results in estimating values for parameters and responses of the system that would otherwise be difficult or impossible to measure directly.

An analogy can be made for relating computer simulation using math models to help understand experimental research in the same way as animal models are used to help understand the human response to experimental intervention. However, the analogy becomes more complex because we have shown that the computer model can be used to simulate the spaceflight response of both the animal and the human. A major portion of NASA's life science research is devoted to animal studies which often serve as a surrogate for the human in both ground-based and space-based research. Figure 11-1 attempts to show these relationships between math models, animal models and human studies as used for gravitational studies. Also shown are the various functions, described above, that models contribute to this interaction. The models provide a framework for coordinating and interpreting a diversity of biological studies whose ultimate objective is the understanding of human responses to weightlessness.

Figure 11-1 also shows a concept that has been stressed throughout this book, that modeling is an integral part of the research cycle. Full potential of the systems analysis method is realized when there exists an iterative cycle between model development and experimental observation.

11.3 Advanced Total Body System Models

The research reported in this book has revealed that the adaptive response to spaceflight is manifested in all of the body systems that have been studied. It has also become apparent that many unresolved biomedical problems still exist and that our understanding of physiological adaptive mechanisms is incomplete under either earth-bound or space conditions. Therefore, a useful strategy to study spaceflight adaptation would be to examine the human body as a total system. This was the underlying motivation for creating the *whole-body algorithm*. We can no longer treat the human body as if it were divided into academically defined organ systems (i.e., cardiovascular system, neural system) acting independently. It is not enough to only address the problems caused by the loss of bone or exposure to space radiation. Rather, a more optimal approach is to develop a fully integrated view of the body, with all parts connected and fully interacting in a realistic manner.

As was discussed in the last chapter, the *whole-body algorithm* was a preliminary effort, almost a computer exercise; it was meant to be followed by more advanced models. The first version of the *whole-body algorithm* is already unwieldy and difficult to work with as well as being time consuming to operate. It is already apparent that much work is needed in the areas of modeling metabolic and biochemical processes, renal function, vestibular function, calcium regulation, and pharmacokinetics among others. There has been little done in the area of modeling to understand disease processes on a subsystem or system level. Some of the more important recommendations for improvements to the current *whole body algorithm* is provided in Appendix G. There is also a compelling rationale to begin this type of effort from a clean slate, as discussed below.

After nearly 3 decades of inactivity in the area of large-scale physiological models, NASA is beginning to commit resources to the development of a "digital human" – a
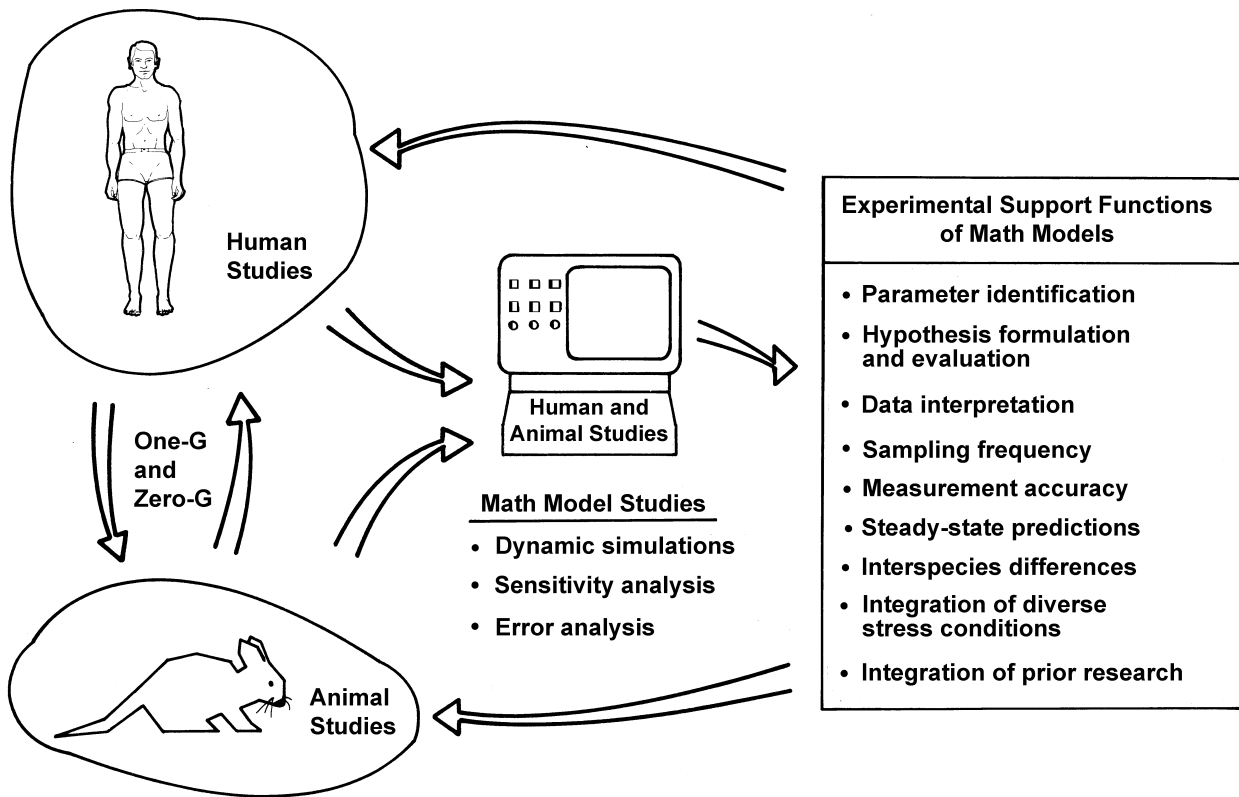
Figure 11-1. Interaction of biological and computer models in support of human experimentation in the space program.

quantitative description of a healthy human being that contains state-of-the-art information on each component of the body and how these components relate to each other [1]. The *digital human* will contain virtually everything known about human physiology, from biochemical to cellular to organ to system information (vertical integration) and then to interactions among the body's system (horizontal integration). A concept for integrating components in this manner was presented in Chapter 2 (Fig. 2-1). Such a representation of the human body through digital information will be the backbone of a new approach to integrative physiology and medicine. This approach capitalizes on the investment that has been and continues to be made in the molecular approach to biology, and at the same time on the new and emerging capabilities in computing, information storage, modeling, and fast, parallel processing that characterize today's technology (Fig. 11-2). It is envisioned that the payoff from the *digital human* will be great. This model will allow us to understand the function of the healthy body as we never have before, and to identify the knowledge gaps that are hidden from our view today when we look at the many parallel and interacting proceses at work within the body. It will enable us to probe into the causes and mechanisms responsible for the many changes that occur when the environment changes, as it does during spaceflight, or when some pathway or component within the body becomes dysfunctional, as it does

during injury or disease.

The following cross-cutting themes will be central to the approach to be taken because they represent fundamental physical, chemical, and biological processes that govern system behavior across vertical and horizontal levels of integration:
· biochemical and electrical signaling;
· biomechanics and movement;
· energetics and metabolism;
· fluid, electrolyte and acid-base balances;
· mass and energy transport and conservation;
· hierarchical organization of function from molecule to cell to organ;
· homeostatic regulation, multi-level control in hierarchical systems, and their dependence on the functional state of the person; and
· adaptation and limits to achieve steady states in continuous environmental stresses.

Integration across systems (similar to the current *whole-body algorithm*) is key to the success of the modeling approach because the loss of stability and homeostasis under stress likely involves the interaction of varied human responses, biological functions, and mechanisms at all levels. Because of genetic and experiential differences among individuals, this integration needs simultaneously to address generic human responses and individual
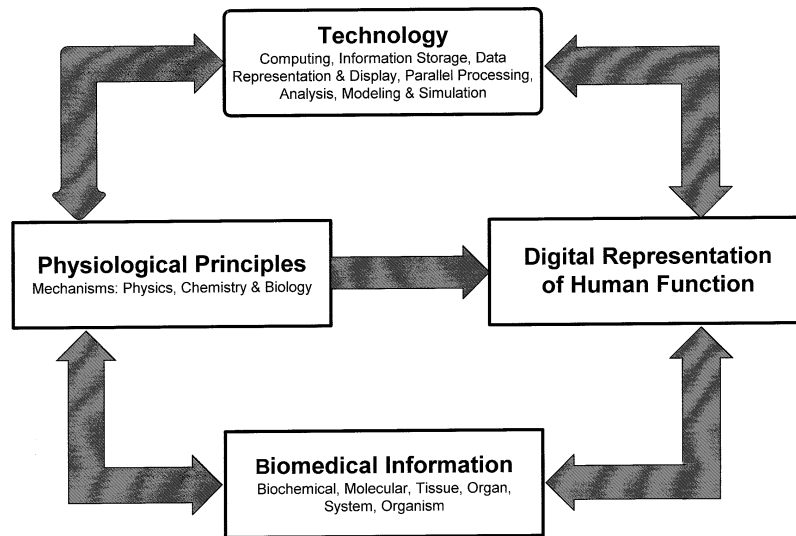
Figure 11-2. Major elements that are needed to create a digital human.

functional characteristics. The research necessary to develop the *digital human* encompasses "classical" medical disciplines (i.e., cardiovascular, renal, endocrinology) as well as "cross-cutting" disciplines such as immunology, neurobiology, nutrition, aerospace engineering, bioengineering, bioinformatics, molecular biology, and biotechnology.

The proposed model is envisioned to embody a wide range of human function. Some of those under consideration include movement, repair and healing, homeostatic regulation and control, environmental adaptation, and sensory perception. This will necessitate the integration of a variety of specific models and simulations of anatomical and physiological attributes including, among others, models of membranes, cells, neurons, sensory processes, circulation, respiration, hemodynamics, metabolism, endocrine function, organs, reproduction, skeleton, muscles, digestion, and movement control.

Developing such an ambitious model will require time, resources, and proper planning. We must first develop appropriate strategies and themes for defining, organizing and integrating human function; then we must identify the critical research necessary to gather the data and information that is lacking. We should begin by consolidating existing knowledge of physiological function, but we must determine whether incorporating this information into model simulations leads to instabilities and a breakdown in homeostasis.

The creation of this complex model will necessitate a modular approach for combining mechanism–based computational models. Synthesis and integration of these components, each created by teams of researchers in geographically diverse laboratories, and with different computer languages, will be not only a technological challenge, but scientifically we must understand how these individual units work together, as they do in the real func-

tioning human. Such software modules should be extensible, reusable, interoperable, and retargetable, and they need to be based on cellular, tissue, and organ-level mechanisms. Not all of the specific models may be required for a particular simulation; only those modules needed would be integrated. The resulting integrated simulation would probably be executed over a distributed network. It should be possible to exploit WEB-supported models and databases such as the High Level Architecture (HLA) for simulations of the Department of Defense, the Common Object Request Broker Architecture (CORBA), the designs incorporated in the Physiome Project and the National Library of Medicine's Visible Human, and the Department of Energy's nascent program on the Virtual Human.

The goal of this modeling research is to provide a tool for planning an exploration-class manned space mission. A typical Mars-type mission might involve trips of six months to one year each way, with a stay on Mars of one to two years. The *digital human,* personalized for each crewmember, could provide the ability to simulate this mission, understand the physiological adaptation, support the development of appropriate countermeasures, and address the critical questions for increased safety, better health and improved performance on such a prolonged and gravitationally-varied journey. This would not be an exercise in descriptive mathematics and programming, but a more comprehensive effort to organize factual and conceptual information to make it ultimately useful during long-term space travel within the solar system.

11.4 Computer Assisted Health Care Systems

The concept of a whole-body representation of human physiology and function can lead to applications in disease states and health care issues. For example, large-scale
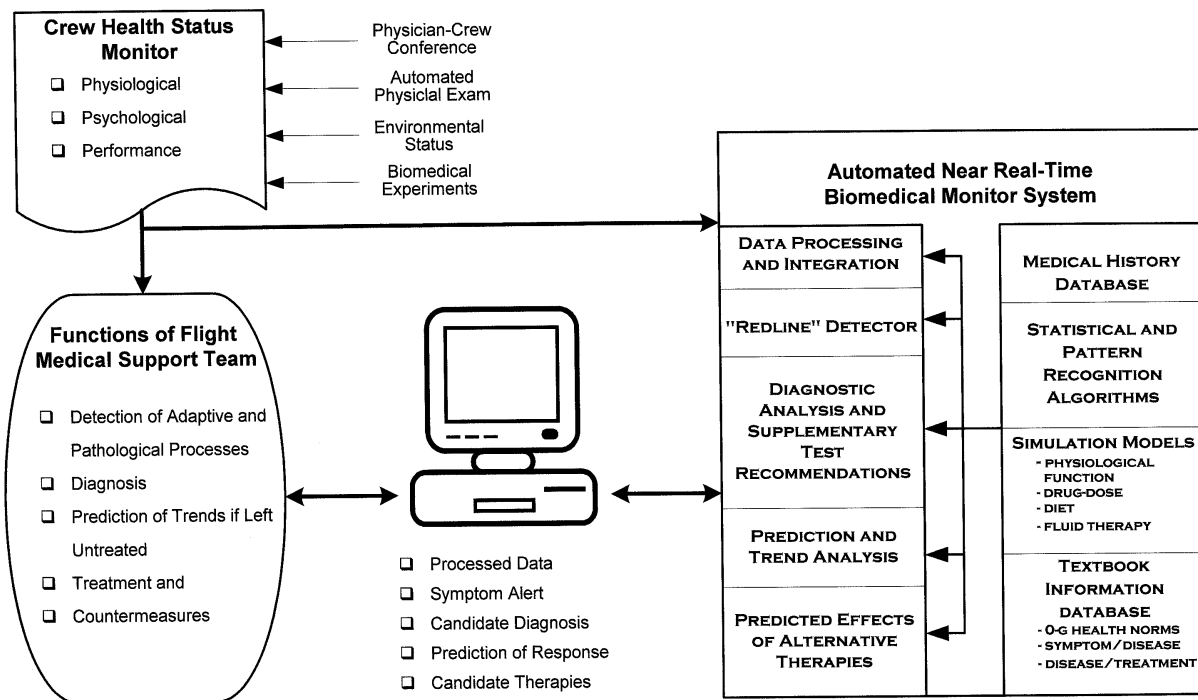
Figure 11-3. Concept for a computer-assisted remote health care system originally proposed for use in the Space Shuttle.

models could be used for real-time monitoring of patients, providing extrapolations of trends in important health parameters, identifying the critical parameters to monitor for patient care, aiding in diagnosis, and indicating patient response to simulated therapy. This has obvious implications for space-based medicine, that is, in situations where resources are limited and patients are treated from remote locations.

Models also lend themselves to establishing normal health status of crewmembers and predicting deviations from the reference state. The "classic" symptoms from which diseases are normally diagnosed on earth may be significantly altered by the zero-g environment. In the same way, earthbound treatment procedures may be inadequate or inaccurate when applied to the space bound patient. An appropriately validated model could become a powerful tool for translating these "classic" terrestrial symptoms and treatments into spaceflight environment symptoms and treatments. The use of models in a predictive mode assumes that the models have been verified for the response of interest in the environment of interest and "tuned" for the individual being observed. Once this has been accomplished, it would be possible to define a "redline" safety boundary and determine when these limits have been exceeded. Also, models can help identify the manner in which diseases develop by simply altering one or more of the normal pathways of the physiological system. Once a mathematical model of a pathology is validated, the human system's response to the disease can be simulated and therapies can be identified and evaluated.

In this regard, the utility of models to help design countermeasures for orthostatic intolerance has been demonstrated in Chapters 7 and 9.

A concept for a computerized real-time biomedical monitoring and health care system is shown in Figure 11-3. The system envisioned would have the capability to: a) automatically integrate spaceflight health monitoring data, including measurements of physiological, psychological, performance and environmental status, b) detect acute or chronic off-nominal conditions, c) predict future health status assuming no remedial action is taken, and d) search for appropriate treatments. This capability would be provided by a computer software system consisting of an extensive biomedical database and programs for data processing, pattern recognition, Monte Carlo searches, and statistical and trend analysis. In addition, the utilization of mathematical models of major physiological systems should provide significant advantage in this biomedical monitoring process. Models envisioned for this system would have such uses as: a) establishing indices most sensitive to particular changes in body function, b) establishing acceptable tolerance limits for monitoring instruments, and c) helping to distinguish between normal adaptive changes as a result of weightlessness and pathological conditions that might be modified by the space environment. Furthermore, the simulation models have a capability to be used in a real-time mode for such purposes as: a) predicting difficult to measure parameters from non-invasive measurements, b) predicting trends for pathological conditions, and c) prediction of effects of alternative thera-

pies for pathological states as well as countermeasures for normal adaptive states. Special modeling techniques such as sensitivity analysis, error analysis, and parameter estimation, are well developed for identifying critical parameters and indices of system performance when applied to integrated subsystem model simulations of environmental and metabolic stresses. Extensive medical textbook information would also be included in this proposed system that could be rapidly searched for symptoms, diseases and alternative therapies with prediction of possible consequences and probabilities of success attached to each treatment or countermeasure. A total system approach such as this could be designed as an adjunct to the needs of a flight surgeon or physician, whether remote or on-site.

The above concepts for a computer assisted health care system were proposed in the mid-1970's for use on the then-future Space Shuttle [2]. In the ensuing years, the capabilities of mathematical models have improved but they have not fully developed their potential in space-based health care as originally envisioned. On the other hand, we have witnessed great strides in the related fields of remote medical sensing, telemedicine and bioinformatics for earth-based purposes. While modeling is still not a vital part of these new paradigms of medical administration, there is great promise. Pilot projects have shown that medical care can be administered in a distributed manner by using the Internet to feed patient data to specialists from different medical centers. These teams could then use appropriate mathematical models to aid in monitoring and diagnosing, providing therapeutic modalities and actual drug dosing recommendations. The patients data can be entered into a nationwide database and statistical models could be used to formulate the most current relationships between sign/symptom, disease/treatment, and treatment/side effect. Standing in the way of creating truly deterministic predictive models capable of simulating both normal and pathological events is the lack of understanding of long-term adaptive processes and disease states. A systematic approach is needed to organize and integrate such information from space and earth-based laboratories.

11.5 Bioinformatics

Bioinformatics is a relatively new term that refers to the cataloging of biological information and the computational methods for manipulating this information. Mathematical models and their use obviously falls under this characterization. It should have become evident to the reader of this volume that the process of modeling feeds on data. Data is used to determine the values of model parameters, special data sets are used to validate a model, and when models are used in a predictive mode, data is used to both drive the model and more importantly as a basis for judging the accuracy of model response. NASA has been on the forefront of insuring the availability of biological data and the development of advanced computational technology as demonstrated by the four facilities or organizations discussed below. The first two of them

are related to archiving research data and the last two are organizational units for developing innovative modeling applications.

11.5.1 NASA's Life Sciences Data Archive

The idea of providing a depository of life sciences data collected in spaceflight to be used by the scientific community and mission planners is an old one, but it was not until the early 1990's that the concept became a reality. NASA's Life Sciences Data Archive (LSDA) contains information and data from spaceflight experiments conducted from 1961 to the present, and includes human, animal and plant studies. The goal of LSDA is to archive and distribute life sciences data from the last 40 years via a web site [3], and to also archive life sciences data from future Shuttle missions and the International Space Station. A major purpose of the LSDA is to help researchers in preparing for future flight experiments. The authors of this book all played major roles in planning and managing this potentially important program.

In its ideal form, each flight experiment (and limited number of ground-based experiments) will contain an overview of the experimental objectives, approach and results; names and backgrounds of all investigators; descriptions of all parameters measured, experimental protocols and hardware; experiment data; and bibliographic information for NASA project documents and scientific publications. There is a complete search capability for locating information by keywords and cross-searching techniques. This capability allows users to compare data across missions, experiments, and disciplines and perform queries for locating, retrieving, or requesting data. At the time of its inception, this was one of the first life sciences database on the World Wide Web Internet. Some issues and recommendations concerning the LSDA's policy on limiting data access due to privacy concerns can be found in Appendix G

11.5.2 SPACELINE Bibliographic Data Base

SPACELINE is a NASA sponsored library-style archive containing documents and publications describing the scientific results of all projects funded by NASA's Life Sciences Division. This includes ground-based and flight research and human, animal and plant studies. It includes not only peer reviewed publications but all other research documents published by NASA, its contractors and grantees. Most of SPACELINE's holdings can be retrieved via the National Library of Medicine's PubMed (Internet) feature [4,5]. Dissemination of this information is designed for the scientific and educational communities and the public.

11.5.3 NASA Center for Bioinformatics

The NASA Center for Bioinformatics at Ames Research Center (Moffett Field, CA) and Stanford University School of Medicine recently established a National Biocomputation Center on the university's campus in Palo Alto, CA [6]. The new center is a national resource to further the use of virtual reality in medicine.

The purpose of the Center is to apply advanced com-

puter technology to the study of biological systems. The Center is dedicated to the development and application of advanced visualization, 3D imaging, and computation and simulation technologies to support the NASA mission for the human exploration and development of space.

Researchers at the Centre are working on a variety of virtual reality computer tools to aid in complex reconstructive surgery and other procedures. Surgeons can use the big-screen workbench, special gloves, as well as computer tracking wands and other devices to manipulate 3-D computer images of patients. This technology will enable surgeons to plan complex surgical procedures and to visualize the potential results of reconstructive surgery in a three-dimensional virtual environment simulator.

In the future, virtual reality will allow surgeons to rehearse a great many complex procedures before operations. The team expects that, eventually, virtual reality will be a powerful teaching tool for medical students. A digital library of computerized "virtual patients" will be created that physicians can use to share information about uncommon procedures. Some biocomputation researchers envision a virtual hospital could be established which may eventually link the best medical minds worldwide as well as treat patients.

11.5.4 Integrated Human Function

The National Space Biomedical Research Institute (NSBRI) [7] in collaboration with NASA is leading an effort to develop an overall understanding of the human body's response to spaceflight by integrating across research areas in specific body systems. Working from the principal that the body needs to be studied in an integrated fashion, they hope to create analytical and predictive models that answer questions involving multiple human subsystems. Such models will integrate human function across multiple scales of organiztion and widely varying time scales, using both vertical (hierarchical) and horizontal integration involving such diverse organizational scales as molecule, cell, tissue, organ, and organism.

If this description sounds similar to the description provided earlier to describe the *digital human* it is because the Integrated Human Function program of NSBRI has been created to begin creating this advanced integrated system model. One of the first applications will be a human exercise model, involving cardiovascular, respiratory and thermoregulatory subsystems. This integrated approach will eventually allow researchers to predict potential problems, simulate health conditions and plan adequate responses to situations that might occur on a long-duration mission. Understanding how the body's systems interact from the molecular and cellular level to the whole human will enable medical planning and therapy that can benefit space and ground research and patient care.

11.6 Systems Analysis and Science Management

The great expense of spaceflights and the limitations on payloads and personnel make it incumbent for space mission planners to choose carefully those experiments that offer the greatest return. With the probability of exploration-class space missions on the horizon, there are also great biomedical risks for the safety of space crews. There is a necessity for a process for optimizing risk management decisions based on immediate and long term scientific goals as well as political and economic realities. Scientists and planners should be provided with as much information as possible for this task as well as analysis techniques that will help assimilate and integrate this information. The broad area of systems analysis has proven to be a valuable approach for systematically organizing information and in deducing from this network the consequences of alternative plans.

11.6.1 Science Planning During the Space Shuttle Era

The systems analysis team that produced the research results discussed in this book also developed the process of selecting and managing the life sciences research payloads (i.e., experiments) for the Shuttle Spacelab. The Spacelab missions are, in one sense, simply a collection of separate experiments that would be performed in space. In reality, they are highly complex, integrated research projects, that use the same astronauts as subjects and investigators and a common pool of resources, to be precisely implemented in a one to two week period. Selection of scientific experiments are conducted, first by a scientific peer review, and then by NASA project and mission management teams who recommend an integrated experiment payload package. Figure 11-4 summarizes the process for achieving a recommended payload. The approach is a systems analysis one, whereby the problem is broken down into component parts and the decisions of one component feed into other parts in such a manner that an optimum payload can be formulated based on well defined criteria. Some of the more important steps in this process include:

a) Identification of critical hypotheses in each major discipline as determined by principal investigators, NASA advisory panels, National Academy of Sciences, and systems analysis.
b) Identification of critical measurements and hardware for obtaining data;
c) Analysis of probability of scientific success based on achieving optimal data collection (i.e., minimum subject population, access to critical time periods);
d) Identification of experimental commonalities and redundancies with other experiments; analysis of synergies gained by combining similar experiments;
e) Determining resource needs for each experiment, including crewtime, power, money, and hardware;
f) Estimation of mission resource allocation; and
g) Evaluation of feasibility of experimental protocols with respect to resources.

In this scenario, computer models of physiological systems are used to identify critical hypotheses and measurement protocols. These models are also instructive in demonstrating the synergy of similar experiment proposals.
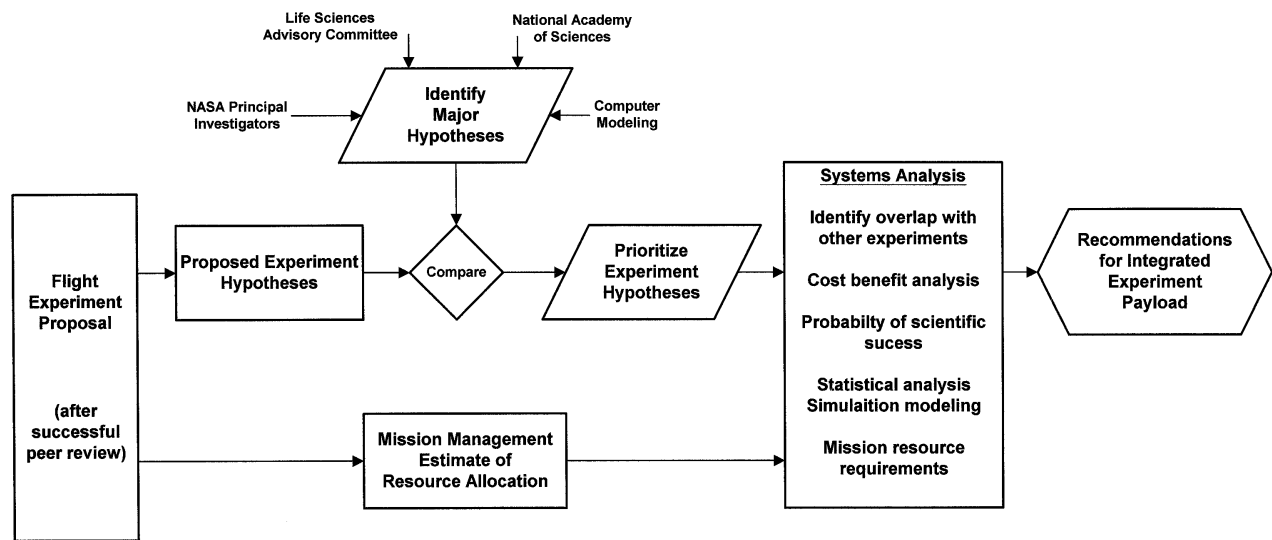
Figure 11-4. Systems approach to develop Shuttle experimental payloads.

Other types of management models are then called into play to identify various experiment options and support the development of enhanced payloads with the end-goal of optimizing science return. A similar approach is also used by NASA to guide ground-based research programs.

11.6.2 Science Planning for Exploration-Class Space Missions

The systems analysis process has also been called upon by life science planners to develop an approach to identify and mitigate risks to crew health, safety, and performance during more advanced exploration-class missions such as a Mars journey. The main objectives of this approach are to provide information for defining acceptable levels of risks, assess progress toward effective risk mitigation, and to provide a guide for prioritization of research and technology. The major processes and functions of this approach, known as the *critical path roadmap* [8] is shown in Figure 11-5, and includes the following:

- Identify the mission requirements to set the context for the risks to be addressed;
- Identify the most mission-critical risks to human safety, health, and performance;
- Identify the risk factors associated with each risk, i.e., conditions which increase the risk;
- Prioritize the risks by assessing their significance and severity with and without countermeasures employed;
- Identify the critical questions that must be addressed to understand and mitigate the risk. These critical questions provide the basis for underlying research projects, and address issues involving risk assessment and acceptability, physiological mechanisms and processes, countermeasure development and validation, and medical diagnosis and treatment;

- Define the deliverables, i.e., specific end-items that include scientific knowledge about underlying mechanisms, risk characterization and assessment, countermeasure protocols, strategies, or procedures for risk reduction, or technology development. Tasks for achieving the deliverable can then be established;
- Determine the level of readiness of each countermeasure or technology item and the criteria for their evaluation (i.e., risk mitigation requirements); and
- Analyze the costs and benefits associated with the risk and its possible mitigation; is the cost acceptable?, is the risk acceptable?

An example of the risks, risk factors and their consequences are shown in Figure 11-6 for the area of Cardiovascular Alterations. The risk mitigation approaches (i.e., countermeasures) are shown at the bottom of this figure with a connecting dashed lines indicating that they are capable of blocking risk factors, risks/outcomes or final consequences. Charts like these were prepared for all discipline areas to help managers and researchers understand these relationships and the purpose of the highly directed research program. There is an obvious role for simulation modeling in this schema. Potential risks can be assessed by studying the simulated response of individual crewmembers to the spaceflight environment and determining if it passes a clinically significant threshold of safety. Models can also be used to evaluate countermeasures and other risk mitigation procedures. An example of such an assessment of risk and risk mitigation was shown in Chapter 7, where orthostatic intolerance thresholds were simulated in the face of Shuttle reentry g-stresses, and it was shown how pressure-suit garments could alleviate the tendency to faint.
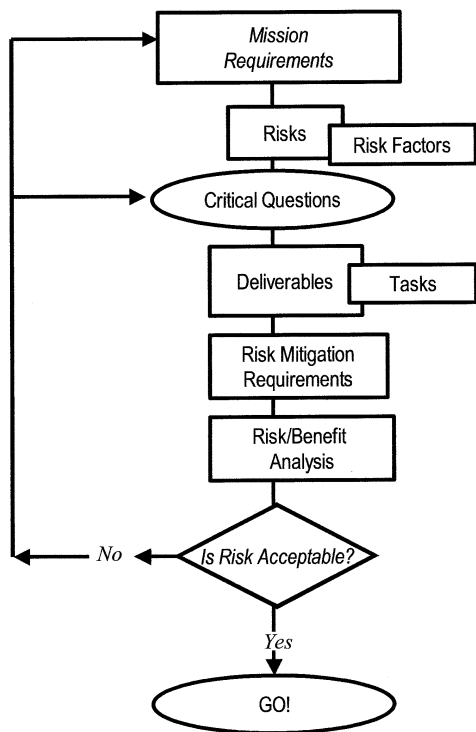
Figure 11-5. Key elements of the Critical Path Roadmap for identifying risk mitigation requirements.

References

1. White, R.J., Bassingthwaighte, J.B., Charles, J.B., Kushmerick, M.J., and Newman, D.J., Issues of Exploration: Human Health and Well-Being During a Mission to Mars, COSPAR,19??

2. Leonard, J.I., Furukawa, S., Van Nordstrand, P., Systems Identification and Application Systems Development for Monitoring the Physiological and Health Status of Crewmen in Space. (TIR-MED-5012, General Electric Co., Houston, TX), NASA CR-160235, Washington, DC, 1975.

3. See Life Sciences Data Archive website: http://lsda.jsc.nasa.gov

4. See SPACELINE website: http://spaceline.usuhs.mil/

5. See National Library of Medicine/PubMed website: http://www.ncbi.nlm.nih.gov/

6. See National Biocomputation Center website: http://biocomp.stanford.edu

7. See National Space Biomedical Research Institute (NSBRI) website: http://www.nsbri.org/

8. See Critical Path Roadmap website: http://criticalpath.jsc.nasa.gov
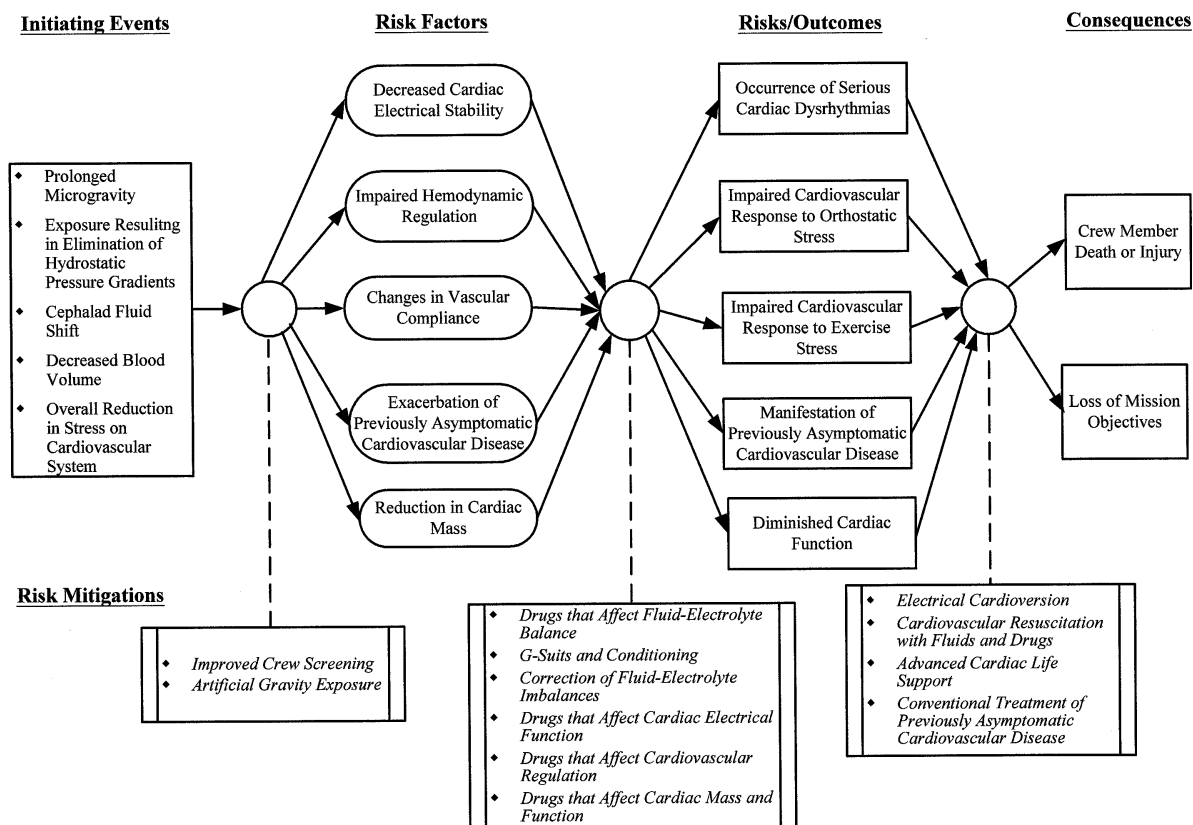
Figure 11-6. An example of the risks, risk factors, and risk mitigation approaches for the Cardiovascular discipline area.

Appendix A
The Modeling and Simulation of Feedback Control Systems

The purpose of this Appendix is to explain the basic vocabulary and principles of model development so that the reader may better grasp the description of the simulation models. Examples that describe the steps leading to the development of a computer algorithm of a model subsystem are provided, and the simulation techniques used to assess model behavior and accuracy will be discussed.

A.1 Definitions of Terms and Concepts

A.1.1 Parameters and Variables

Two general types of quantities are used in mathematical models: *parameters* and *variables*. The value of a *parameter* is generally constant with respect to time, whereas the value of a variable changes with time (i.e., is *time-varying*). Biological parameters often vary slowly with time but may be assumed to be constant in the mathematical model.

Parameters may be considered *independent* of system actions. Variables may also be considered independent if they influence the system from the outside, i.e., ambient temperature. Parameters and *independent variables* are also called *input functions*, or *forcing functions*. More often, variables are *dependent* (also called output functions), since they vary according to the relationships within the system. An objective of a systems analysis is to specify the state of the system; that is, to specify the values of all dependent variables at every instant of time.

A.1.2 Classification of Mathematical Model Systems

Mathematical models are classified according to the types of equations they employ [1].

A.1.2.1 Distributed and Lumped Parameter Systems.
In *distributed parameter systems*, the values of variables depend on time as well as space coordinates, and the system must be analyzed by solving *partial differential equations*. In a *lumped parameter system*, each element is treated as if it were concentrated ("lumped") at one particular point, which is called a *node* or a *compartment*. The use of lumped parameters greatly simplifies the analysis because *ordinary differential equations* are used to describe the changes with time. To account for spatial changes that occur in such a system (e.g., the value of blood pressure is different in arteries, capillaries, and veins), compartments are added for each major space location until one reaches the level of compartmentalization (lumping) commensurate with the basic purpose of the model being designed.

Generally, as subdivisions are included in a model, the fidelity and accuracy of the model's response increases. For example, in this project, two circulatory models were employed, one composed of 7 compartments and the other

of 28 compartments. The 7 compartment model can only simulate mean blood pressures in arteries and veins, whereas the 28 compartment model can simulate pulsatile flow and provide systolic and diastolic pressure for all anatomical portions of the vasculature (i.e., aorta, arteries, arterioles, capillaries, venules, veins, and vena cava).

All models described in this publication are lumped parameter systems. Whether the lumping of components and the simplifying of input–output relationships are appropriate depends entirely on the intended purpose of the model. Lumped, compartmental modeling is in keeping with a basic facet of the systems approach: to simplify the problem and define the essentials of its solution.

A.1.2.2 Linear and Nonlinear Systems.
In modeling, systems generally consist of components with a known (or assumed) relationship. In a broad sense, a component of a system may be thought of as having the property to transform certain inputs into certain outputs. Such relationships are often (loosely) termed *transfer functions* (although transfer function has a rigorous meaning only in terms of Laplace transforms).

Mathematically, the components of a system may be represented by several operators, which transform one function into another. If all the operators for the system are linear, in the loose sense that their operation on two independent functions produces two independent results, then the system itself is said to be *linear*. Otherwise, the system is said to be *nonlinear*. Mathematically, much more is known about the behavior of linear systems.

Unfortunately, most biological systems—with their threshold and saturation behavior, sigmoidal dose-response relationship, and dead time—are nonlinear; analysis of such systems revolves around *numerical methods* and the use of *computers*. Obtaining rapid, accurate, numerical solutions of nonlinear system equations is absolutely essential in biological modeling and often represents a separate challenge. Solutions of nonlinear models are more likely to yield counter intuitive results than those of linear models. Most of the models used in this project can be classified as nonlinear.

A.1.2.3 Other Classifications and Nomenclature.
Models can be developed for either *predictive* or *descriptive* purposes. A predictive model must only produce accurate predictions of the output variables in the system. For example, a single equation may be used to predict the fractional saturation of hemoglobin with oxygen at different levels of oxygen partial pressure. In this case, the modeler is not concerned with a relative replication in the model of the interactions between the variables in the system. The relationships employed in the predictive model to

generate the predicted output need not conform to the mechanisms in the real system that lead to the same outputs. In contrast, descriptive models not only must generate predictions in agreement with real system output but *also* must employ intermediate relationships that are realistic representations of the true processes that generate the observed outputs.

The vast majority of biological systems are *continuous* systems, in which values are always changing with time, and they are best described by *differential equations*. These equations are typically solved with numerical procedures on digital computers by transforming them into *finite-difference equations*. In this process, the variables actually appear to be constant for the duration of the *integration step size* and, therefore, more properly belong to a *discrete* system. This approximation of continuous biological systems by discrete numerical systems can produce inaccuracies and instabilities in the solution, unless appropriate care is taken and the system is carefully verified.

The models described in this project can also be said to be *deterministic*, since the input–output relationships for each component are based on simple physical laws (i.e., flow-pressure, diffusion, mass action) and are therefore fixed, predictable, and reproducible. In reality, most biological systems are *stochastic*, in the sense they are subject to random noise, and their responses can be described by statistical laws and in terms of probabilities and expected values.

Riggs [1] makes the observation that "all naturally-occurring systems are, in the final analysis, time-varying distributed-parameter, quantized, stochastic, nonlinear systems. That we can sometimes obtain useful information by treating these wayward creatures as if they were fixed lumped-parameter, continuous, deterministic, linear systems is little short of miraculous."

A.1.3 Biological Control Systems

It is difficult to conceive of any biological quantity that is not controlled or influenced by one or more factors. For example, blood pressure influences and controls the rate of baroreceptor neural firing. In this situation, baroreceptor neural firing is *controlled*, or *regulated*, within narrow limits at the expense of the other system quantities, the limits of which may vary widely. The relationship between blood pressure and baroreceptor neural firing would be construed as an *open-loop* system for controlling baroreceptor neural firing. Further examination of the process shows that the baroreceptor afferent signal is processed by the central nervous system (CNS) and results in an efferent neural signal that controls peripheral resistance. This relationship between baroreceptor firing and peripheral resistance is an open-loop system for controlling peripheral resistance. However, it is known that peripheral resistance directly regulates blood pressure. Once this control is added to the system, the complete loop of physical changes (blood pressure, peripheral resistance) and information transmission (afferent and efferent signals) forms a *closed-loop* control system. The difference between the closed-loop and open-loop systems is obviously the pres-
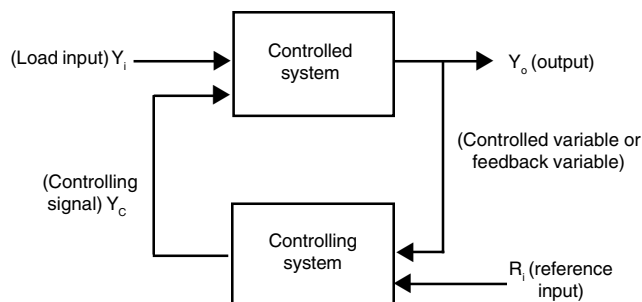
Figure A-1. A generalized feedback control system. Most biological homeostatic systems can be reduced to these basic components.

ence of the relationship of peripheral resistance to blood pressure. Blood pressure in the closed-loop system is called the *feedback variable*.

A feedback control system, as described previously, is composed of two major elements, or components: the *controlled* system and the *controlling system* or *controller*. Figure A-1 is a diagram illustrating the relationships of these elements. The purpose of the controlled system is to transform inputs from the outside (*load inputs, disturbances*, or *stress stimuli*) and inputs from the controller (*controlling signals*) into *responses* (*outputs*). The reference input of Fig. A-1 is also referred to as a *set-point*, and it represents a normal or desired value of a feedback variable. Differences between the set-point and the actual feedback variable result in corrective action by the controller; this correction permits the output to revert toward normal values in the face of the disturbance. Consequently, the presence of *feedback control* in biological systems allows important quantities to fluctuate within limits necessary for maintaining life in the face of many metabolic and environmental disturbances encountered by the organism.

In man-made technological control systems, the set-point is a physical quantity that can be varied at will (e.g., a thermostat setting for a home heating system). Biological systems, however, often have neither a reference input not an error detector. The establishment of a set-point, or an *operating point*, in mathematical models of biological systems is often included for convenience, only because the real system behaves as if it were controlled by such a reference value [1,2].

In terms of the example described previously, blood pressure is the controlled feedback variable (Y_o) and peripheral resistance can be considered the controlling variable (Y_c). The controlled system consists of components that transform changes in blood pressure into changes in peripheral resistance (i.e., baroreceptor afferent signals, CNS processing, efferent signals, effect of autonomics on vasculature resistance). A typical blood pressure load disturbance (Y_i) might be an infusion of blood into the circulatory system (which implies that a description of the volume-pressure relationships of the circulation must be included in the controlled system) or the introduction of an upright tilt disturbance (which implies that a description of gravity effects on blood volume distribution must

be included in the controlled system). The set point (R_1) is the "normal" value for blood pressure.

A.2 Formulation of a Computer Model

It would be instructive to review the steps that lead from conceptualization of a model to digital computer implementation. Model systems can be graphically represented by some combination of boxes that represent the elements of the system. Such a representation is called a *block diagram*, which includes logic diagrams, schematics, flow diagrams, and system diagrams. An important step in constructing a model of any system is to draw a block diagram representing the blocks and their interconnections. This type of diagram, or series of block diagrams, becomes a "roadmap" or a "key" for taking a system apart and putting it back together. Some of the most common basic symbols used in a special form of block diagram, called an analog diagram, are shown in Fig. A-2. The analog diagram is an adaptation of the diagrammatic method so useful with linear systems. The mathematical operations are self-explanatory. As an example of the loosely termed "transfer function," the graphical transfer function in the figure might represent the relationship between cardiac output x and right arterial pressure y. This transfer function can then represent a measured cardiac function curve.

As a specific example of the programming process, the subsystem of the circulatory, fluid, and electrolyte model that deals with angiotensin formation has been chosen. Figure A-3(a) can be construed as a hypothesis diagram for the open-loop control of renin-angiotensin. This diagram indicates the major factors that control angiotensin formation and the many effects of angiotensin on other subsystems. It is generally agreed that two of the major influences on renin release (a precursor to angiotensin formation) from the juxtaglomerular cells of the kidneys are renal perfusion pressure and the load of sodium filtered through the tubules (i.e., glomerular filtration times plasma sodium concentration). Renin enters the circulation and forms angiotensin, which has a slight negative feedback effect on renin formation (see dashed line in Fig. A-3(a)). The final effect of angiotensin is considered to be widespread, affecting vascular resistance, renal resistance, aldosterone secretion rate, thirst and drinking, and the rate of tubular fluid reabsorption.

To progress to a computer model of this system, each of the pathways connecting any two variables must be described in as much detail as necessary, commensurate with the objectives of the model design. Therefore, the next level of detail is shown in the block diagram of Fig. A-3(b), in which the relationships between variables are qualitatively organized. Functional relationships are identified wherever data describing hormonal secretion rates or hormonal effects are available. This diagram was developed from some very general algebraic relationships, and the mathematical operations of summation, division, multiplication, and integration are indicated.

Figure A-3(c) is the same diagram as Fig. A-3(d), reorganized to reflect the computer program names for each

Addition/Substraction: $x, y, z \rightarrow x + y - z$

Transfer function (graphical)

Multiplication: $x, y, z \rightarrow = xyz$

Transfer function (algebraic): $y = 1 + 3x + 2x^2$

Multiplication by constant fact K: $x \rightarrow K \rightarrow Kx$

Transfer function (multiple variables): $y = (2x + v + 3w)u$; inputs v, x, w, u

Summation: $+x$, $+y$, $-z \rightarrow \Sigma \rightarrow x + y - z$

Division (or multiplication): $y \rightarrow \div \rightarrow \dfrac{x}{y}$
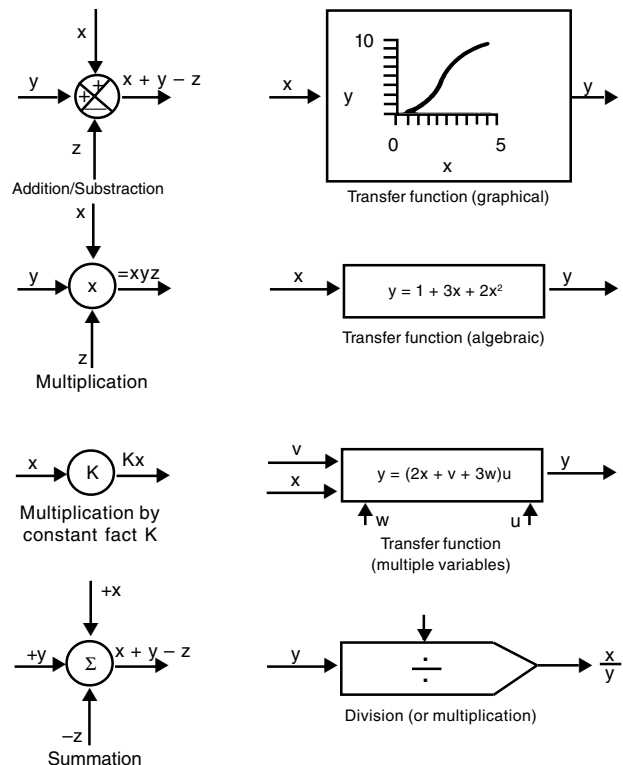
Figure A-2. Symbols used in block diagrams representing mathematical operations.

variable and the quantitative transfer functions for each element. It was common at one time to simulate models on analog computers, and Fig. A-3(c) is known as an analog diagram because it represents a circuit diagram for programming this segment of the model on an analog computer. However, a digital computer requires a different programming language, and Fig. A-3(d) is the Fortran version of the renin-angiotensin subsystem. The reader should be able to identify the meaning of the Fortran expressions from the previous diagrams. Note that the first statement represents a function relating renal pressure and renin secretion. In the analog computer, this function would be represented by a function generator; in the digital computer, it is represented by a table of x–y values (not shown) from which the desired operating points are interpolated. The exponential functions (e.g., EXP(–I/RNK)) in Fig. A-3(d) are numerical approximations for integration, in which "I" is the integration step size.

It can be appreciated that the discipline of translating an ordinary physiological hypothesis diagram into a quantitative computer representation can lead to a better understanding of the biological system. Available data from diverse sources are integrated into a common framework; other data are excluded as being nonessential for the given level of detail (i.e., importance of data can be ranked), and missing information, which suggests the need for new experiments, is quickly identified.

Renal arterial pressure ↓

↓ Glomerular filtration

↓ [Na⁺] Plasma

↑ Renin

(−)

↑ Angiotensin II concentration

↑ Vascular resistance

↑ Renal resistance

↑ Aldosterone secretion rate

↑ Thirst and drinking

↑ Tabular fluid reabsorption rate

(a)

Renal arterial pressure

Renin

PAR

Pressure effect on renin secretion

Na⁺ tubular flow sup- pressive effect on renin secretion

Plasma [Na⁺]

Renin

GFR x Na+

Glomerular filtration rate

Renin secretion rate

Renin destruction rate

Initial plasma renin

∫

Total plasma renin

Plasma volume

÷

Renin plasma conc

Angio release

Renin conc

Angiotensin secretion rate

Angiotensin destruction rate

Initial plasma angiotensin

∫

Total plasma angiotensin

Plasma volume

÷

Angiotensin plasma conc

Angio effect

Angio conc

Effects of angiotensin on:

Vascular resistance

Renal resistance

Aldosterone secretion

Thirst and drinking

Tubular fluid reabsorption

Negative feedback effect of angiotensin concentration

Time delay

Angio conc

Angiotensin plasma conc

(b)

Figure A-3. Formulation of a control system algorithm (a) Hypothesis diagram showing factors which influence renin-angiotensin production and the quantities which they influence. These represent the assumptions for one of the hormonal subsystems in the Guyton model. (b) A more detailed block diagram of the hypothesis diagram of Fig. A-3(a) showing the mathematical operators relating each quantity. (c) An analog computer diagram of the renin-angiotensin system. This diagram contains sufficient information to wire a patch panel for programming an analog computer. (d) A Fortan algorithm for the renin-angiotensin control system as it appears in the Guyton model. The symbols can be interpreted from the preceding diagrams.

A.3 Simulation Techniques

Once a model is implemented on a computer and verification procedures ensure that it is operating appropriately, the model is ready to be tested for accuracy. A model that is deemed credible can be used to describe the behavior of the system in terms familiar to control engineers and can be used to predict system responses in terms that can be tested by biological experimentation. Some of the more important techniques used to produce model credibility and to predict system behavior are discussed below.

A.3.1 Dynamic Simulation

In the context of this study, obtaining the solution to a model means introducing some type of load disturbance (i.e., a parameter perturbation) and solving the model's differential equations iteratively, using numerical techniques. This process, known as dynamic simulation, is accomplished using high-speed digital computers and results in time-varying values of the dependent variables. These responses are examined in qualitative terms for their reasonableness by analysts who are familiar with the physiological system or, more often, they are compared quantitatively with experimental data. In this project, simulation responses were available from digital computers in tabular and graphical form and could be compared with previously stored data.

A.3.2 Sensitivity Analysis

Sensitivity analysis is a method for studying system responses due to variation in parameter value [3]. The conceptual basis of sensitivity analysis is simple; small variations are made in the values of the system parameters of a model, and the effects of these changes are observed individually in the solution (see Appendix E). Sensitivity functions that describe the observed effects may be computed, and these are interpreted to extract information about the dynamic system that could not be obtained from simply finding solutions with a particular set of input conditions. Sensitivity analysis provides the following.

1. A quantitative means of comparing the relative importance of individual parameters on any system variable;
2. A means of determining interactive effects of two or more parameters on model behavior;
3. A tool to help assess the validity of a particular model without the need to collect and use extensive measurements from the real system;
4. Information in a form that can be easily interpreted by those familiar with the subject matter of the model but not necessarily knowledgeable of simulation techniques;
5. A means of assigning relative importance to all parameters, a process that can be valuable both to the simulator in performing parameter estimation or stability analysis and to the experimenter in allocating resources for data collection;
6. A practical method of analyzing and comparing two different models designed to represent the same physical system.

A sensitivity analysis is very useful when performed early in model development, before model validation. This analysis is particularly important to the experimenter, who can help evaluate the model based on the relative sensitivities of the parameters without really knowing much about the model. The technique also is useful for involving the experimenter early in the modeling process, another important factor for eventual model acceptance [6]. The results of the sensitivity analysis must be evaluated in the light of other known information about the real system. For example, the fact that a parameter has a very significant effect on a particular variable of the model is of little importance if it is known that the parameter in the real system is relatively constant or that changes in other parameters are capable of canceling the original effects.

Although sensitivity analysis can be considered to a be a special case of dynamic simulation, there are several important differences between these two procedures.

1. Sensitivity analyses are characterized by comparatively small perturbations.
2. Sensitivity analyses often are performed by varying one parameter at a time.
3. Sensitivity analyses often are performed to obtain sensitivity functions rather than solutions of the dependent variable.
4. Sensitivity analyses usually entail comparisons between two or more simulation runs rather than between model results and experimental data.

Examples of sensitivity analysis are provided in the descriptions of the erythropoietic model (Chapter 3.2.4.2) and of the thermoregulatory model (see Appendix E).

A.3.3 Variation of Parameters

Once a parameter has been identified as being particularly influential, either by sensitivity analysis or from direct knowledge of the real system, it is often desirable to determine the effect of different parameter values on specific variables. For example, the volume of blood is known to be important in the blood flow/pressure response to upright tilt from the supine position. It is reasonable to ask, "How does the response change as more and more blood is removed?" Another way to pose this question is, "What is the effect of hemorrhage on standing?" Documenting this effect with a simulation model of circulatory control is relatively straightforward; the parameter representing blood volume is assigned a series of values (i.e., a percentage of the control or normal value) and, at each level, a dynamic simulation is performed. The resulting time-varying responses (of, for example, heart rate, cardiac output, or blood pressure) can be plotted as overlays on the same graph. If steady-state responses are desired, the graph often is constructed with blood volume on the abscissa and the response variable on the ordinate (see Fig. 7-8).

A.3.4 Error Analysis

Parameters values are never known with 100% accuracy. If the standard deviation (SD) around the mean value can be estimated for each parameter, it is possible to place

statistical confidence limits on a model's behavior. For the example discussed previously, assume an experiment is performed in which blood volume reduction is measured as –10% ± 1.5% (SD). Dynamic simulations can be performed for three values of blood volume: –8.5%, –10%, and –11.5%, corresponding to the mean minus SD, the mean, and the mean plus SD, respectively. The response, for example, for heart rate could also be expressed in terms of a mean and a deviation. This expression would represent a prediction of the minimum error interval in the response variable, because of the inherent design of the system and the uncertainty in measuring blood volume, but would not include any experimental errors that could occur in measuring the response variables. Conversely, if a decrease in the confidence interval of a response variable to a given width was desired, it would be possible, using these techniques, to determine the minimum experimental accuracy required in measuring the independent parameter.

Error analysis becomes especially desirable in large-scale systems containing many parameters that promulgate errors through the model, and in certain nonlinear systems in which the interactive effects of different parameters lead to amplification of individual errors. Unfortunately, even though the techniques to accomplish this analysis are rather straightforward, there are few examples in the literature of physiological systems.

A related problem that has application to error and sensitivity analysis is the effect of noise on the behavior of the system. Noise can be described as a statistical disturbance of a particular variable, and it is characterized by statistical properties such as mean value, probability distribution, or spectral density. Model output variation which results from noise can be found by including a distribution function for each parameter or variable that exhibits noisy behavior. This problem becomes extremely relevant in parameter estimation analysis when model output is compared to data having a significant noise level [4].

A.3.5 Stability Analysis

At this point it is appropriate to mention stability analysis of dynamic systems because of the inverse relationship between sensitivity and stability in negative feedback systems. In general, sensitivity to disturbing factors can be reduced by an increase in feedback gain (in technological systems at least). However, instability occurs as a consequence of this gain increase. Thus, systems with high gain may have low sensitivity to external perturbations but may also be operating on the borderline of instability. Most biological systems are normally stable, and they do exhibit low sensitivity. Whether they are working somewhere near the stability limit by way of high gain factors is not known but should be studied on a case-by-case basis [5]. An analysis of stability can become an important measure of the competence of a model, in that if both model and actual system can be thrown into instability due to the same parametric changes, there is reason for having greater confidence in the mathematical representation.

Little practical work has been done on stability analysis of complex physiological systems. Formal techniques

for investigating stability in linear systems and in simple nonlinear systems have been reported [4,6]; but, for the most part, studying large-scale nonlinear models is a trial-and-error experience. Systems that exhibit oscillatory or periodic behavior in normal operation (e.g., eye movement, respiration) can often be made unstable more easily than systems that behave monotonically. Inherent instability is dependent on the properties of the system and is normally not a function of the specific disturbance. If the system is inherently stable, all transients will ultimately disappear regardless of the disturbance causing them. Conversely, any disturbance to an unstable system will initiate oscillations that increase in amplitude with time.

Stability can arise from either inherent features of the real system or from structural features of the mathematical model (such as a long integration interval). The techniques of sensitivity analysis can reveal both types, although it is not always possible to distinguish between the two. Like sensitivity, stability is a function of the operating point; therefore, all possible operating points must be tested for stability. A careful, systematic sensitivity analysis may often reveal not only points of instability but their causes as well.

A.3.6 Parameter Estimation

The object of parameter estimation (or identification) analysis is to determine the value of one or more parameters in a model. The parameters selected for estimation are usually impossible or difficult to measure directly in the real system. In practice, the technique involves repetitive adjustment of the parameter values until some objective judgment of acceptable correlation between model output and corresponding measurements in the system prototype has been satisfied (see Fig. A-4). The automatic optimization of parameters has been the object of considerable attention [7], consequently, there is a large body of literature on parameter estimation in physiological systems and algorithms.

The error criterion used in parameter estimation is usually a difference function of the form

$$e(t) = y(t) - y^*(t)$$

where y^* is a dependent variable that has been measured in the real system, y is the corresponding model variable, and t is time. The error criterion E is a function of e, usually $|e|$ or e^2, integrated over a specified time interval; e.g.,

$$E = \int_0^T |e| \, dt$$

Since y is dependent on the system parameters q_i, e can be expressed as $e(t) = e(t, q_1, q_2, \ldots, q_m)$. The criterion for the best fit between data and model is achieved when E reaches a minimum value.

Not every parameter can be estimated with the same degree of accuracy. Parameter estimation is used most effectively on parameters exerting a strong influence on a particular model variable that can be easily measured in
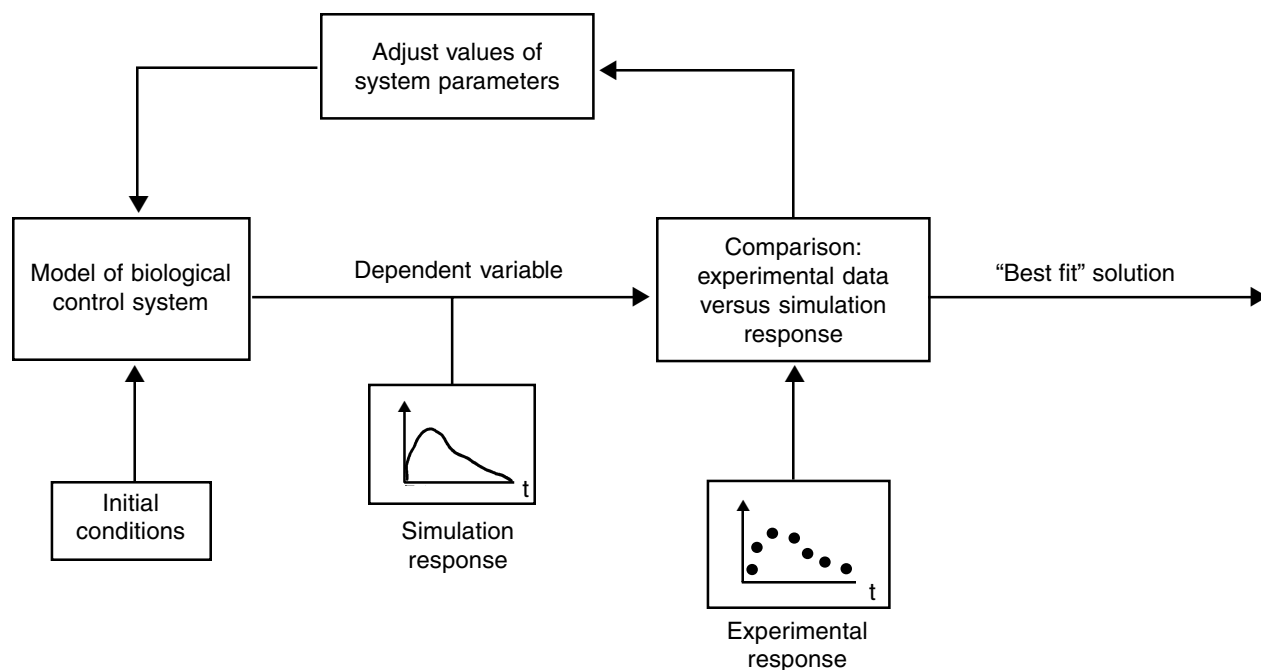
Figure A-4. Simulation procedure for parameter estimation. This method of fitting model output to experimental results can produce values for system parameters that are difficult to measure directly.

the real system. A useful technique for determining which parameters can be estimated with greatest precision is sensitivity analysis, discussed earlier in this Appendix. If sensitivity analysis is used before parameter estimation, it is possible to select those parameters with the highest sensitivity coefficients as the best candidates for parameter estimation analysis. When the parameter sensitivity is low, then that parameter value cannot be estimated with as much certainty. The low-sensitivity parameter should be set at a reasonable constant value determined from other sources.

If the problem of sensitivity analysis is expressed as determining the behavior of a model given all the parameter variations, then the inverse problem would be to determine (or identify) the parameter variations capable of producing a given behavior of the real system. Unlike sensitivity analysis, variation of parameters, error analysis, and stability analysis, parameter estimation requires data measurements from the real system. This inverse problem may not have a unique solution. Nevertheless, it would be valuable to know the various solutions possible, since this knowledge would be a great aid in hypothesis testing. If several different parameter perturbations could produce similar model results, it might be possible to accept the most reasonable, based on physiological plausibility; alternatively, this information could provide the basis for further experimental testing.

A.4 Model Validation

The validation process is primarily concerned with demonstrating the accuracy and the capability of simulation models. Two general criteria must be met before model credibility can be established. First, a quantitative variable or parameter validity criterion must be met, and, second, a qualitative "plausibility" criterion must be met. The first condition refers to tests in which model output is compared directly to experimental data, whereas the second condition includes all other tests in which only the general behavior of the model is examined on a more subjective basis. In the first case, a high degree of fidelity in model response is expected, whereas in the second, the model responses need only be "reasonable." No validation procedure is appropriate for all models. Rather, validation depends on the nature of the model and the goals and objectives of the modeling study.

A.4.1 Quantitative Tests

An important aspect of validation involves comparing the behavior of the model's dependent variables with that of their experimental counterparts for the same stress. Differences between model behavior and experimental data can often be corrected or minimized either by introducing new, previously omitted elements into the model's structure or by modifying the existing structure (i.e., adjusting the value parameters that are not well known).

The extent to which the validation process can be carried is often limited by data availability. Thus, if only steady-state data are available, validation in the dynamic, or transient, mode cannot be performed, even though the model has that capability. Similarly, if only a relatively small number of experimental variables have been measured during a particular stress, then it is possible to validate the model for the responses of only those measured variables; simulated values of all other variables can be

obtained but should be considered as predictions requiring experimental verification. The response of the body to a given stress is almost always related to the level or intensity of that stress, and more often than not, the relationship is nonlinear. Therefore, to validate the model properly, it is desirable to obtain data not merely for a given stress but for a range of intensities of that stress. If it is important to simulate more than one type of stress, the validation process will result in a more accurate model if the experimental response of the same variable is known for each of the desired stresses. Thus, an idealized set of experimental data suitable for complete validation of a complex model should include the following.

1. Steady-state data
2. Transient data
3. Data for a wide range of stress intensities
4. Data for all major dependent variables of interest or importance
5. Data for a variety of stresses

In addition, since experimental protocol, measurement techniques, and number and type of subjects may vary widely from one investigation to another, even when studying the same stress, it is desirable to obtain many of these data from the same experimental study.

The data used to validate the model should meet several conditions:

1. The data used for model validation should be different than that used in model development. The model must be capable of predicting beyond the data from which the model was generated.
2. The data must be of sufficient precision to make the test meaningful. The data should cover the range of interest and should have a minimum level of noise. The latter condition is best assured by including data representing a large subject population.
3. The data should be gathered under conditions similar to those represented in the model. Not all data are appropriate for use in validation. The assumptions about the biological system being studied are often reflected in the experimental protocol used to gather the data, and these are often not the same assumptions used in the model.

Obtaining good agreement between a simulation response and data is especially important when trying to simulate a diverse number of variables having constantly changing values. Agreement between simulation response and data is often improved by adjusting parameter values. This procedure is the same as that described under parameter estimation techniques. More than one combination of parameter values may lead to a good "fit." In these cases, it is important that all changes be reasonable and consistent with known physiological processes.

A.4.2 Qualitative Tests

The purpose of modeling and simulation, in the context of the current study, is not necessarily to produce an optimal fit between experimental data and model output, although this result would not be undesirable. Rather, the objectives are to help understand the behavior and interactions of the system and its components and to assist in new experimental approaches. Model credibility, in this case, can also be established by performing fewer quantitative tests.

Often, the model analyst is content to verify initially that the "shape" of the data and model output agree. This situation would occur if the modeler were primarily interested in the validation of model dynamics as contrasted to the exact fit of model output and data. In this case, it is not considered critical that the absolute magnitude of the response be without error; this type of discrepancy can often be remedied by the adjustment of a system parameter.

An important criterion for indicating whether a model is good enough to be used for forming conclusions about the real system is that a one-to-one correspondence and similarity of form must exist between model and real system. So-called "black box models" (i.e., models which represent overall behavior of systems without representing their underlying mechanisms) are not good models for making predictions regarding general system behavior; at best, they may be used as descriptions of data. Thus, there is always some model that can fit a particular set of experimental data (usually by adjusting one or more parameters), but only the biological plausibility of a particular model justifies preferring it to all others. Therefore, the inclusion of a greater number of adjustable parameters in a model, although perhaps providing a better agreement with the data, does not necessarily add insight into the physiological mechanisms.

The techniques described earlier in this Appendix—sensitivity analysis, error analysis, stability analysis, and variation of parameters—do not require extensive data sets. They can be very useful in establishing the plausibility of a model without necessitating excessive analysis of the mathematics of the model and all the explicit and implicit assumptions. Sensitivity analysis, in particular, can be important in this regard by quickly and systematically analyzing these component relationships without the need of actual subject data. This capability is particularly useful in comparing two different models.

For a model to contribute to a particular investigative field, it must ultimately be judged by scientists familiar with that area. When these scientists are not the people who developed and validated the model, it is important that lines of communication between them be established as early in the modeling process as possible. Model validation, ideally, should be an interdisciplinary process. During this project, the experience has been that general simulations, sensitivity analyses, or parameter variation studies performed without comparison to good experimental data appear to make less of an impact on experimenters not familiar with systems analysis than the same work supplemented with at least a single simulation showing reasonably good agreement with experimental data.

References

1. Riggs, D.S., *Control Theory and Physiological Feedback Mechanisms*, Williams and Wilkins Co., Baltimore, MD, 1970.
2. Milhorn, Jr.,H.T., *The Application of Control Theory to Physiological Systems*, W. B. Saunders Co., Philadelphia, PA, 1966.
3. Cruz, Jr., J.B., *System Sensitivity Analysis, Benchmark Papers in Electrical Engineering and Computer Science*, Dowden, Hutchinson, and Ross, Stroudsburg, PA, 1973.
4. Rosen, R., *Dynamical System Theory in Biology*, Vol. I: *Stability Theory and Its Applications*, Biomed Engineering Series, Wiley-Interscience, New York, NY, 1970.
5. Jones, R.W., *Principles of Biological Regulation: An Introduction to Feedback Systems*, Academic Press, New York, NY, 1973.
6. Tomovic, R. (D. Thornquist, transl), *Sensitivity Analysis of Dynamic Systems*, McGraw-Hill, New York, NY, 1963.
7. Johnson, L.E., Computers, Models, and Optimization in Physiological Kinetics, *CRC Crit. Rev. Bioeng.*, vol. 2, Feb. 1974, pp. 1-37.

Appendix B
Detailed Description of the Model for Regulation of Erythropoiesis

This Appendix contains the complete mathematical description of the erythropoiesis regulatory model. As this is the simplest of all models considered in this project, it provides a convenient example of how a physiological model is constructed. Reference should also be made to the overall description of the model provided in Chapter 3.2.4 and a diagrammatic view of the model in Fig. 6-10, as well as simulations of the model throughout Chapter 6.

The model developed for the spaceflight hematological program was designed to examine the relative influence of the controlling factors of erythropoiesis on total red blood cell (RBC) mass. The formulation was based on the generally accepted concept that the overall balance between oxygen supply and demand regulates the release of a hormone, erythropoietin, from renal tissues sensitive to oxygen tension levels and that this substance in turn controls bone marrow red cell production [1,2,3].

The amount of oxygen delivered to the tissue is accounted for in the model by the combined influence of several factors: hemoglobin concentration, lung oxygenation of hemoglobin, blood flow, and oxygen-hemoglobin affinity [4]. From this amount of oxygen, a certain fraction is extracted by the tissue depending on the oxygen demand parameter. Oxygen enters the cellular spaces by diffusion along an oxygen tension gradient between the venous capillaries and the cell [5]. Decreasing the oxygen supply in relation to the demand reduces tissue oxygen tension that is, in effect, monitored by a local oxygen detector [6] and results in increased rates of erythropoietin release [7]. Erythropoietin is released into the general circulation, and its final plasma concentration is determined by its rate of release, its volume of distribution, and the rate at which it is metabolized [8], the latter being represented in the model by the hormone plasma half-life. The target organ for erythropoietin is the bone marrow. The production rate and release of red cells in the model are determined by the plasma erythropoietin concentration [9]. A time delay exists between marrow stimulation and red cell release [10]. Destruction of cells is represented in the model by a lifespan parameter. Hemoglobin concentration in blood is based on the addition of new cells to existing cells and plasma.

It is known that red cell production is modulated by factors other than those considered in the model. These include iron levels [11], hormones other than erythropoietin [12], neural stimulation [13], as well as inhibitors and activators of erythropoietin [14]. Although it may be desirable to include these effects in future model applications, quantitative information regarding them is presently lacking or the need for their inclusion is not yet warranted.

Overall oxygen transport is under the control of homeostatic mechanisms in addition to the erythropoiesis system. Thus, some of the fixed parameters of the model such as blood flow, capillary diffusivity, arterial oxygen tension, plasma volume, and oxygen-hemoglobin affinity can be considered variable elements of circulatory, ventilatory, biochemical, and fluid regulatory feedback mechanisms that are beyond the scope of the current model's design objectives. Larger models that incorporate many of these features are available and these have been shown to be compatible with an erythropoiesis subsystem model [15]. Although these mechanisms are not included explicitly in the present erythropoiesis model, their influence can be tested, in most cases, by manual alteration of existing model parameters.

B.1 Mathematical Description of Model

B.1.1 Oxygenation of Blood

The oxygen concentration of arterial blood (neglecting oxygen dissolved in plasma) after passage through the lungs can be expressed as the product of the carrying capacity of a gram of hemoglobin ($CHbO$; i.e., 4 moles O_2 per mole Hb), times the hemoglobin concentration (Hb), times the fractional degree of oxygen-hemoglobin saturation (S_aO). It is convenient to use hematocrit rather than hemoglobin concentration as an index of red cell concentration in blood. These quantities are related by the mean corpuscular hemoglobin concentration, such that $MCHC = Hb/Hct$. Therefore, for arterial blood [1]

$$\begin{aligned} C_aO &= S_aO \times Hb \times CHbO \\ &= S_aO \times Hct \times MCHC \times CHbO \end{aligned} \tag{B1}$$

At full hemoglobin saturation, $S_aO = 1.0$, and Eq. (B1) then represents the maximum oxygen-carrying capacity of blood at a given hematocrit. In most instances, the parameters $MCHC$ and $CHbO$ will be invariant, so that the arterial oxygen concentration is influenced only by the hematocrit and hemoglobin saturation. In practice, the arterial oxygen tension (P_aO) is assigned a value,[*] and a corresponding value of S_aO is determined from the oxygen-hemoglobin equilibrium curve (OEC), an operation that can be expressed in functional form as

$$S_aO = OEC(P_aO) \tag{B2}$$

---

[*] See Table B-1 for symbol definitions, units, and normal values.
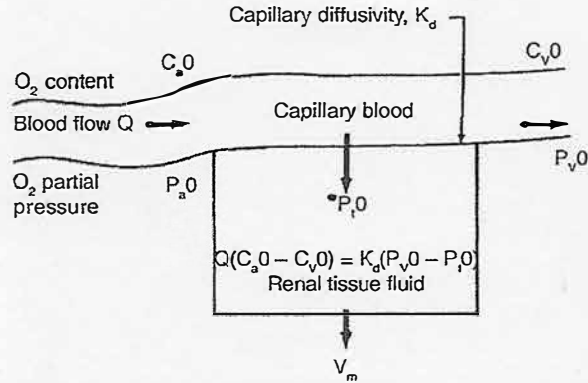
Figure B-1. Two-compartment steady-state model of renal tissue oxygenation.

Figure B-2. Renal controller function for erythropoietin production rate showing effect of gain G_1.

B.1.2 Oxygen Delivery at Tissues

Oxygen transport at the tissue level is schematically represented in Fig. B-1. In the present model, the tissue of concern is taken to be the erythropoietin-producing cells known to be located primarily within the kidneys. It is assumed that the oxygen sensor as well as sites of erythropoietin production, is responsive to the mean oxygen tension of the kidneys. This assumption permits tissue oxygen tension to be derived from an oxygen balance using blood flows, arteriovenous oxygen concentrations, oxygen consumption, and transcapillary diffusion resistances common to the kidneys, which are considered to be a homogenous tissue.

The elements of tissue oxygenation were determined using a two-phase model consisting of capillary blood and tissue fluid [16]. It is assumed that the blood compartment is well mixed with an oxygen partial pressure (P_vO) equal to that in the venous outflow. Oxygen diffuses from blood to tissue along a gradient of oxygen partial pressure ($P_vO - P_tO$), where P_tO is the oxygen tension of the homogenous tissue. The amount of oxygen unloaded from the blood is given by the difference in oxygen concentration between arterial and venous blood ($C_aO - C_vO$). At equilibrium, the rate of oxygen transfer to the tissues is identical to the tissue oxygen consumption (V_m) and to the unloading of blood oxygen as determined by the arteriovenous oxygen concentration. In other words,

$$\underbrace{Q \times (C_aO - C_vO)}_{\text{Rate of oxygen unloading}} = \underbrace{K_d \times (P_vO - P_tO)}_{\text{Rate of oxygen diffusion}}$$
$$= V_m \tag{B3}$$

where Q is the rate of regional blood flow and K_d is the diffusive transfer coefficient between blood and tissue.

The venous partial pressure may be obtained by solving Eq. (B3) for C_vO

$$C_vO = C_aO - (V_m/Q) \tag{B4}$$

then computing venous hemoglobin saturation from a formulation analogous to Eq. (B1)

$$S_vO = C_vO/(Hct \times MCHC \times CHbO) \tag{B5}$$

and determining P_vO from the OEC, expressed in functional form as

$$P_vO = OEC(S_vO) \tag{B6}$$

Tissue oxygen tension can now be derived from Eq. (B3) as

$$P_tO = P_vO - V_m/K_d \tag{B7}$$

The assumption of steady state in this formulation implies rapid equilibration of oxygen in the fluid phase and is not meant to suggest a constant tissue oxygen tension during the simulation of an erythropoietic disturbance. Since the erythropoietic process itself has been modeled dynamically, the hematocrit will be time-varying until red cell production achieves its own steady state. In this model, the hematocrit is a major influence on alterations in tissue oxygen tension. In addition, other quantities in this algorithm (P_aO, V_m, K_d, P_{50}, Q) are non-regulatory parameters and can also influence tissue oxygen tension if they are manually altered.

B.1.3 Erythropoietin Production and Distribution

Erythropoietin release is assumed to be governed by the tissue oxygen tension. A limited number of studies [5,17,18,19] suggest a relationship of the form[†]

$$\overline{E_p} = E_o \exp\left(- G_1 \overline{P_t O}\right) \qquad (B8)$$

where $\overline{E_p}$ is the rate of erythropoietin production, $\overline{P_t O}$ is the tissue oxygen partial pressure, G_1 is the gain or slope of the function plotted linearly as the natural log of $\overline{E_p}$ vs. $\overline{P_t O}$, and E_o is the $\overline{E_p}$ intercept at $\overline{P_t O} = 0$. Setting $E_o = \exp(G_1)$ ensures that Eq. (B8) will always pass through the normal operating point ($\overline{E_p} = 1.0$, $\overline{P_t O} = 1.0$) irrespective of values of G_1. In certain cases, it may be desirable to postulate a shift in the normal operating point as well as gain, and in those cases, E_o and G_1 may be adjusted separately. Figure B-2 illustrates the semi-logarithmic relationship between tissue oxygen tension and erythropoietin production and shows the influence of G_1.

The concentration of erythropoietin in the plasma (E) is a function of the rate of production (E_p), the rate of clearance or destruction (E_d), and the volume of distribution (V_e). If it is assumed that the rate of disappearance is proportional to the plasma concentration (i.e., $E_d = K_e \times V_e \times E$, where $K_e =$ clearance constant $= \log_e 2$/plasma halflife), then the following first-order differential equation can be written for the rate of change of erythropoietin concentration [8,17]:

$$\frac{dE}{dt} = \frac{E_p}{V_e} - K_e E \qquad (B9)$$

The steady-state concentration of E (at $dE/dt = 0$) is, therefore

$$E(o) = E_p(o)\big/ K_e V_e \qquad (B10)$$

Eq. (B9) can be normalized by letting $\overline{E} = E/E(o)$ and $\overline{E_p} = E_p/E(o)$ and substituting Eq. (B1) into Eq. (B9):

$$\frac{d\overline{E}}{dt} = K_e\left(\overline{E_p} - \overline{E}\right)$$
$$= \frac{\log_e 2}{TE_{1/2}}\left(\overline{E_p} - \overline{E}\right) \qquad (B11)$$

a form that has the advantage of being independent of distribution volume and, further, independent of erythropoietin half-life ($TE_{1/2}$) at steady state, since $\overline{E}(o) = \overline{E_p}(o)$. The value of $TE_{1/2} = 12$ hours was chosen for humans, but this does not appear to be well established for normal subjects [20].

B.1.4 Red Blood Cell Production

An equation expressing the semilogarithmic dose-response relationship between red cell production (RCP) and erythropoietin concentration (E) can be given as

$$\overline{RCP} = G_2 \log_e \overline{E} + P_1 \qquad (B12)$$

As has been the convention, RCP and E have been normalized with respect to their steady-state control values, G_2 is the gain or slope of the response curve, and P_1 is the value of $\overline{RCP}$ when $\overline{E} = 1.0$ and is normally taken as unity.

The accuracy of Eq. (B12) may diminish considerably at very low and very high values of erythropoietin levels. For example, at decreasing values of $\overline{E}$ approaching zero, the production rate tends toward minus infinity rather than zero, whereas at high $\overline{E}$ values, the relationship does not exhibit a maximal production rate that is known to exist. Therefore, two additional equations were formulated and piecewise fitted to Eq. (B12) to account for suppressed and maximal erythropoiesis (see Fig. B-3). Their precise description is somewhat speculative, although this bone marrow function curve closely corresponds to the sigmoid shape of most biological dose-response relationships [21] and to those observed by others for the bone marrow [22,23,24].

In the present study, it was assumed that there is no basal production of red cells unless erythropoietin is present (i.e., $P_o = 0$). Maximal red cell production is assumed to be six times normal [17] ($P_m = 6$) and the upper limit of accuracy of Eq. (B12) was arbitrarily chosen at $\overline{RCP} = 5$.

Iron uptake studies of red cells indicate a bone marrow transit time for red cell production of 3.5 to 4.5 days [10]. This effect was included in the model using a simple first-order time delay[‡] with a time constant T_{BM}. The inclusion of this transit delay clearly improved the realism of the dynamic response of the model, especially following sudden changes in tissue oxygen tension.

B.1.5 Red Cell Destruction and Red Cell Mass

The lifespan of the red cell dictates the destruction rate of cells. A model of red cell destruction was assumed in which cells are destroyed randomly and no cells survive past a given lifespan [25]. In that case, the rate of destruction (RCD) is simply proportional to the amount of cells present at any time. If that amount is given as RCM, then the rate of red blood cell destruction will be

$$RCD = K_r \bullet RCM$$
$$= \log_e 2 \bullet RCM \big/ TRC_{1/2} \qquad (B13)$$

where $TRC_{1/2} =$ red cell half-life and $K_r =$ red cell clearance constant $= \log_e 2/TRC_{1/2}$. At normal values used in the

---

[†] The bar over the symbols represents normalized values. Thus, $\overline{X} = X/X(o)$ where $X(o)$ is the control or pretreatment condition and X is a value during the post-control or treatment phase. The use of normalized values simplified comparison of model response with data from various laboratories.

[‡] If Y is the steady-state value predicted from a dose-response relationship, then the response delayed with a time constant T is obtained by the solution of the differential equation $T \, dy/dt + y = Y$. In finite difference form, suitable for iterative computer solution, this becomes $y_2 = y_1 + (Y - y_1) (H/T)$ where $H =$ integration step size, $y_1 =$ value of y at the ith iteration, and $y_2 =$ value of y at the $i + 1$th iteration.
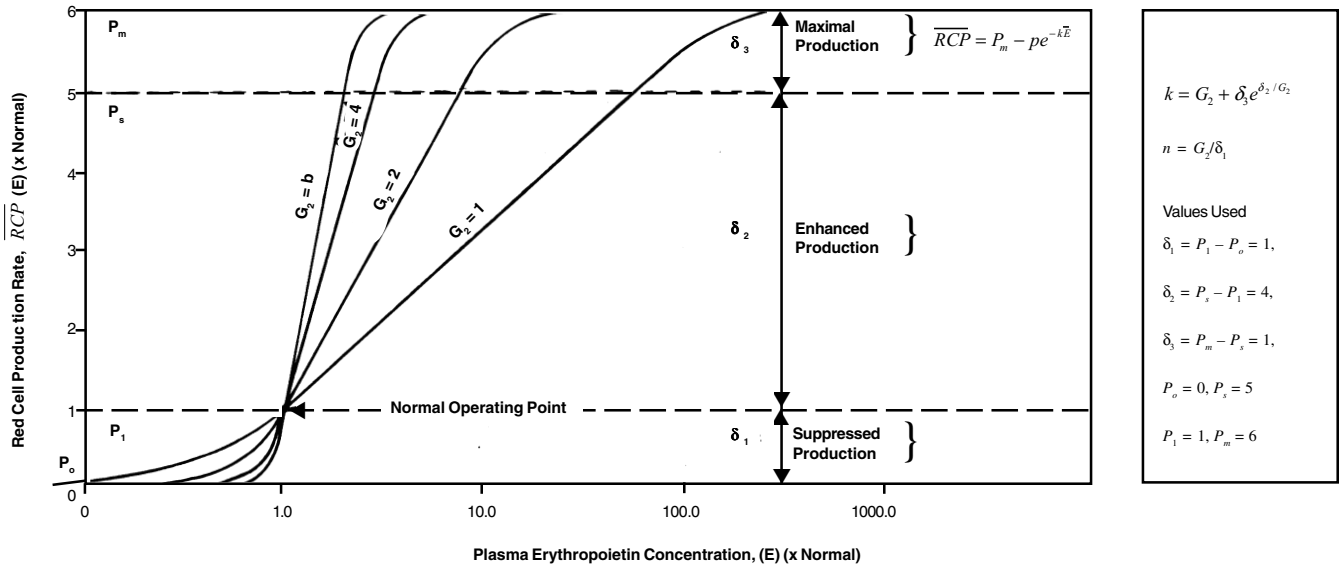
Figure B-3. Bone marrow controller function for red cell production rate showing equations used to piecewise fit the dose-response curve and demonstrating effect of gain G_2 (semi-log plot).

model, the rate of red cell destruction is 1.1% of the total amount present or 22 ml of packed cells/day.

The instantaneous change in total circulating red cell mass is the net difference between red cell production and red cell destruction rates:

$$\frac{d(RCM)}{dt} = RCP - RCD \qquad (B14)$$

The quantity RCP is obtained from Eq. (B12) using the transformation $RCP = \overline{RCP} \times RCP(o)$, where $RCP(o) = RCD(o) = K_r \cdot RCM(o)$.

Finally, the current value of RCM, obtained by integration of Eq. (B14), is combined with the plasma volume to obtain the whole-body-hematocrit of the circulation:

$$Hct = \frac{RCM}{PV + RCM} \qquad (B15)$$

and the feedback loop begun in Eq. (B1) is closed.

B.1.6 The Renal/Bone-Marrow Axis as a Proportional Controller

A more visual understanding of the relationships for renal and bone marrow function can be obtained by determining the overall dose-response curve of the combined kidney/bone marrow axis; that is, the relationship between tissue oxygen tension and red cell production. The results are shown here only for the midrange of erythropoietin production and were obtained by mathematically combining the renal function (Eq. (B9)) with the steady-state plasma distribution function of erythropoietin (Eq. (B11); $\overline{E} = \overline{Ep}$) and the bone marrow function (Eq. (B12)). In this way, erythropoietin is eliminated as an explicit variable; i.e.,

$$\overline{RCP} = G\left(1 - \overline{P_tO}\right) \qquad \left(\text{for } \overline{P_tO} < 1\right) \qquad (B16)$$

where $G = G_1 \times G_2$. This is a simple inverse linear relationship that has previously been used in the models of Guyton and co-workers [15] and Hodgson [5]. In this form, the gain of the renal/bonemarrow (open loop) system is seen to be the product of the two gain factors, G_1 and G_2. Similar (although nonlinear) gain-product relationships were obtained for the extreme of hyperoxia and maximal hypoxia. The results of this analysis have been plotted in Fig. B-4 for a range of values of G. This function represents the entire controller circuit of the erythropoiesis model. In general, hypoxic tissue is predicted to have a greater effect on red cell production than hyperoxic tissue, as indicated by the relative slopes. However, at higher gain factors, the suppression of erythropoiesis can be considerable for relatively small increases in tissue oxygenation.

Equation (B16) is a typical controller function for a linear proportional control system in which the actuating error signal is the deviation of $\overline{P_tO}$ from its control value (unity) and G is the constant of proportionality or controller gain. The control value of $\overline{P_tO}$ is taken as an arbitrary reference standard and is not meant to imply that there is an internal set-point. It becomes clear from this control function that the primary controlled variable is tissue oxygen tension rather than red cell production, red cell mass, or hematocrit, which can be considered controller variables. The control system always adjusts the controller variables in a direction that returns the controlled variable toward normal after an initial load disturbance (see Fig. A-1 in Appendix A).

The controller gain is a major determinant of the final feedback compensation following a disturbance and, within limits, the speed at which a disturbance is corrected.
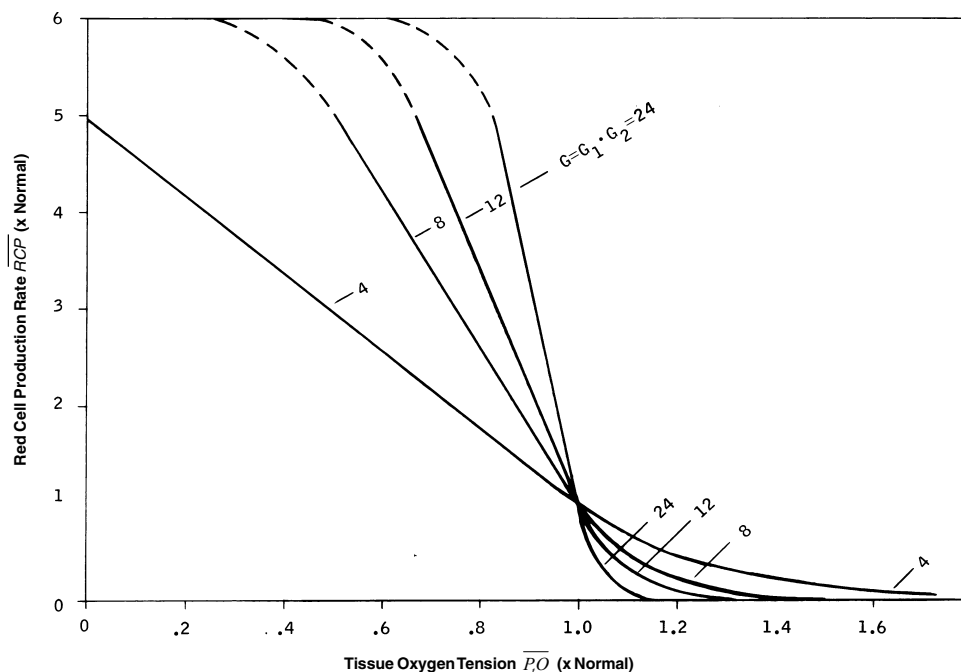
Figure B-4. Combined renal/bone-marrow controller function showing effect of tissue oxygen tension on erythropoiesis for various values of overall gain *G*.

Although increasing the gain increases the feedback effect, it may be at the sacrifice of an oscillatory approach to the steady state. Systems of higher order than this one will tend to become unstable as controller gain increases. Oscillations in the erythropoiesis system are known to occur in special cases, and analysis of these systems in terms of control system theory has proved to be rewarding [26,27].

B.1.7 Model Operation

The system of Eqs. (Bl), (B2), (B4) through (B8), and (B11) through (B15) are solved by computer simulation using an iterative procedure. Equations (B11) and (B14) are integrated numerically using a simple Euler algorithm [28] and initial conditions $E(o)$ and $RCM(o)$, respectively. The program is currently implemented on a Univac 1110 and a PDP 11/40 using Fortran language. Remote terminals including graphic display of the simulation responses (and experimental data simultaneously, when desired) have greatly facilitated user interaction and have enhanced the convenience of model validation.

Perturbing the model away from its normal steady state (initial conditions) is accomplished by altering one of the model parameters.§ These quantities are normally constant in value but can be altered during a run to simulate either independent stress stimuli or long-term regulatory adjustments. Thus, hypoxia may be simulated by decreasing arterial oxygen partial pressure (P_aO), and hemolysis may be simulated by decreasing the red cell lifespan. In some cases, alteration of more than one parameter may be desired as in the simulation of altitude hypoxia that involves a primary change in arterial pO_2 and a compensatory shift in oxygen-hemoglobin affinity (P_{50}). Parameter values may be time-invariant with values fixed before a simulation run or they may be entered as a function that varies with time as the run progresses. Experimental data may be used to drive the model in this fashion. Thus, it is possible to simulate a wide variety of stresses and to test a large number of hypotheses regarding regulating mechanisms.

B.1.8 Parameter Estimation

Table B-1 lists the values of the system parameters, chosen as representative of the human system. Also shown are the steady-state control values (i.e., initial conditions) of the major dependent (output) variables. The precise values of most of the quantities shown in Table B-1 are not critical, however, to the general behavior of the model's response when expressed in percent deviation from control. An exception to this occurs for the highly nonlinear functions such as the oxygen equilibrium curves and the renal and bone marrow function curves. The location of the operating point on these curves can change the nature of the output response. Also, the shapes of these curves, as defined by the gains and threshold parameters, are critical to the magnitude of the response. These will be discussed next.

---

§   The term "parameter" is used to denote time-invariant quantities that are not altered by the dynamic properties of the model as opposed to "dependent variables" that are time-varying and form the connecting links of the feedback circuit, i.e., P_tO, E, RCP, Hct, etc. (see Appendix A).

Table B-1. Parameters and Initial Conditions

Symbol	Definition	Value	Units
Parameters			
$CHbO$	Carrying capacity of hemoglobin	1.34	ml O_2/g Hb
E_o	Intercept of erythropoietin function	20.09	x normal
G_1	Gain of erythropoietin function	3	Nondimensional
G_2	Gain of red cell production function	2	Nondimensional
K_d	Capillary diffusivity	0.567	ml O_2 min^{-1} mmHg^{-1}
		4.25	mI O_2 min^{-1} kPa^{-1}
$MCHC$	Mean corpuscular hemoglobin concentration	0.375	g Hb/ml RBC
P_aO	Oxygen tension in arterial blood	95.0	mmHg
PV	Plasma volume	3.0	Liters
P_m	Maximum production rate of red cells	6	x normal
P_o	Minimum production rate of red cells	0	x normal
P_1	Normal production rate of red cells	1	x normal
$P50$	Oxygen tension of hemoglobin at 50% saturation	26.7	MmHg
Q	Renal blood flow	1.2	Liters/min
TBM	Bone marrow transit time	4	Days
$TE_{1/2}$	Plasma half-life of erythropoietin	12	Hours
$TRC_{1/2}$	Red cell half-life	63	Days
V_m	Oxygen uptake of kidneys	20	ml O_2/min
Initial Conditions			
C_aO	Oxygen content of arterial blood	19.6	mI O_2/100 ml blood
C_vO	Oxygen content of venous blood	17.9	ml O_2/100 ml blood
$\underline{E}$	Erythropoietin concentration in plasma	1.0	x normal
	Erythropoietin production rate	1.0	x normal
Hct	Hematocrit	40	ml packed RBC/100 ml blood
P_tO	Oxygen tension in renal tissue fluid	20	mmHg
P_vO	Oxygen tension in venous blood	55.3	mmHg
RCM	Red cell mass	2.0	Liters
RCP	Production rate of new red blood cells	22	ml of packed cells/day
S_aO	Saturation of arterial hemoglobin with oxygen	97.6	Percent
S_vO	Saturation of venous hemoglobin with oxygen	89.3	Percent

An equation for the oxygen equilibrium curve was obtained from Aberman and co-workers [29]. Their study included a computer algorithm that converts oxygen tension to saturation and, with iteration, oxygen saturation to tension. The agreement between measured and computed values is claimed to be better than 0.2%. In addition, the algorithm includes the capability of altering $P50$ values (see Fig. B-5).

Analysis of Adamson's data [18] from which the erythropoietin release function was obtained, leads to an estimated value of $G_1 = 2.8$. In simulation studies of bedrest and hypoxia [30,31] values of G_2 were determined by parameter estimation to range from 2 to 5. No data exist to confirm these estimates directly. It is permissible to use the gain factors as adjustable parameters, within reasonable limits, in order to test hypotheses and possibly provide improved agreement between model and experiment data. In addition to the gains or sensitivities, the other parameters of these functions (E_o, P_o, P_1) that can be thought of as threshold indices are also not well known and are available for parameter estimation during a simulation. Changing these latter quantities implies a shift of the normal rating points (($E_p = 1$, $\overline{P_tO} = 1$) for Fig. B-2; ($\overline{RCP} = 1$, $\overline{E} = 1$) for Fig. B-3). The value of K_d was obtained from Eq. (B7) by dividing the oxygen uptake by $P_vO - P_tO$. The value of P_tO was arbitrarily assumed to be 20 mmHg, and P_vO was computed from Eqs. (B1), (B2), and (B4) through (B6).

B.1.9 Steady-State Errors

It is an inherent property of most biological homeostatic mechanisms in general and proportional control systems in particular that there will be at least some residual steady-state deviation from the normal operating point
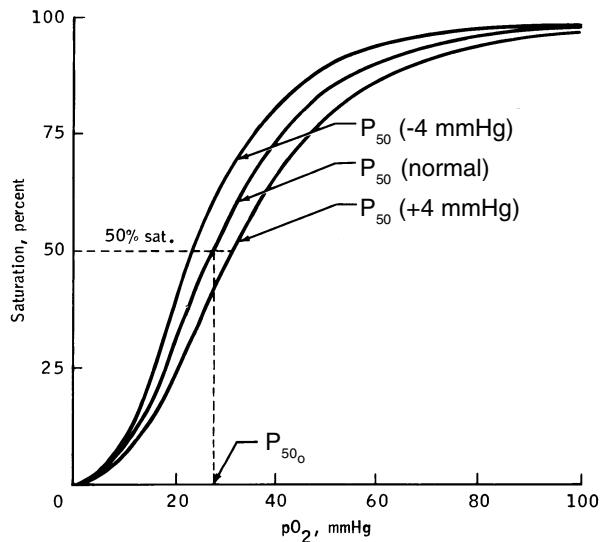
Figure B-5. Oxygen-hemoglobin equilibrium curves drawn directly from computer model output showing effect of changing the $P50$ parameter. The $P50$ value is the oxygen tension at which 50% of the hemoglobin is saturated and is, therefore, an index of oxyhemoglobin affinity. The position of the OEC may vary in accordance with known effects of hydrogen ion, CO_2, temperature, or 2,3DPG (diphosphoglycerate). The effects of DPG are of interest because of its possible contribution to erythrokinetic changes during bedrest or weightlessness.

Figure B-6. Steady-state analysis of long-term determinants of tissue oxygen tension. (a) Segment of feedback circuit that results in the term *dRCM/dt* becoming zero at steady state when destruction and production rates are equal. (b) Reversal of diagram in Fig. B-6(a) starting from the zero point and showing mathematically equivalent influences on tissue oxygen tension.

when the system is disturbed by a constant load. This "steady-state error" will vary in size depending on the gain of the system and the magnitude of the load disturbance. The sensitivity coefficients of Table 3-6, for example, indicate the steady-state errors of red cell production resulting from small changes in parameter disturbances.

A basis for understanding steady-state errors in the current model is as follows. At any equilibrium state, the term *dRCM/dt* in Eq. (B14) must be identically zero. Therefore Eqs. (B13) and (B14) imply that, at steady state, daily red cell production and destruction rates are equal. Furthermore, if red cell lifespan is constant, a steady-state alteration in red cell mass implies a proportionate change in red cell production. Most load disturbances are accompanied by changes in circulating red cell mass (Fig. 6-13). This implies that red cell production and one or more of the factors that affect red cell production (including tissue oxygen tension, erythropoietin, hematocrit, controller gain, and set-point) must have incurred a steady-state error, however small. It can be appreciated from Fig. 6-13, that steady-state errors in tissue oxygen tension are reduced at the expense of larger errors in red cell mass and hematocrit.

Steady-state analysis may also provide insight into the independent determinants of the controlled variable [32]. Figure B-6(a) shows the effect of tissue oxygen tension on red cell production (the controller function of Fig. B-4) and the balance between red cell production and destruction. Feedback control ensures that the various elements of the model are adjusted until the rate of red cell mass change, *dRCM/dt*, becomes zero and that steady state

is defined by this condition. It is mathematically permissible to set *dRCM/dt* to equal zero and work backward from this point to visualize those factors that determine tissue oxygen tension (Fig. B-6(b)). There are only two such factors in our model: red cell destruction (which determines production rate) and the relationship between tissue oxygen tension and red cell production. Only these factors and those quantities that affect these factors will ultimately determine tissue oxygen tension. Experimental evidence is severely lacking on the determinants of the shape of the controller function curve, although it appears that it may be under the influence of neural and biochemical factors (see Chapter B.2.2). The factors that are responsible for normal red cell destruction are also not apparent [10]. Except for overt pathology, rates of destruction are generally considered to be a constant fraction of total circulating red cell mass.

Aside from these experimental shortcomings, it is important to note that the factors usually agreed to play a role in acute changes of tissue oxygenation (i.e., blood flow, capillary diffusivity, oxygen uptake, P_{50}, hematocrit) are not represented between the zero point and the tissue oxygen point in Fig. B-6. Although they may be considered dependent variables in the system, none of them, from a mathematical point of view, are independent determinants of the *final* level at which the tissue oxygen tension will stabilize in the steady state. Although *dRCM/dt* will always return to its initial zero value, the tissue oxygen tension may exhibit a steady-state error due to the inherent properties of the control system in the face of a constant disturbance. However, based on the preceding analysis, the authors believe that even tissue oxygen tension will return to its initial value (zero steady-state error) when both of the following conditions are satisfied: (1) a constant daily rate of red cell destruction and (2) a constant controller relationship between tissue oxygen tension and red cell production.
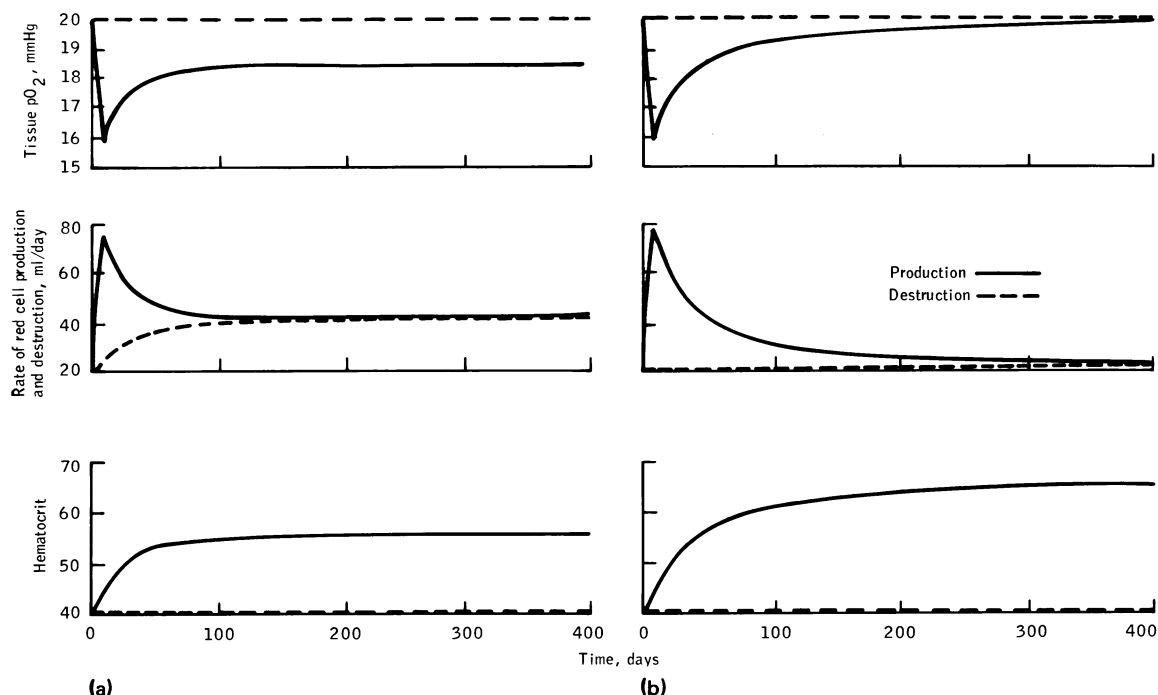
Figure B-7. Effect of destruction rate on long-term control of tissue oxygen tension. (a) Normal simulation response to hypoxic stress. (b) Hypoxic simulation with destruction rate clamped at control value and showing regulation of tissue pO_2 back to normal despite reduced P_aO.

As an example of the last point, a simulation of hypoxia was performed (Fig. B-7b) in which arterial oxygen tension (P_aO) was set at some low value for the entire run and red cell destruction was clamped at its control value of 22 ml of packed cells/day. Tissue oxygen tension decreased and then began to return toward normal as red cell production and hematocrit rose, similar to the simulations with the intact system shown in Fig. B-7(a). However, since the destruction rate was not permitted to increase, a greater net rate of red cells entered the circulation than would have occurred had destruction rate rose in accord with the mass action law of Eq. (B13). As a result, tissue oxygen tension continued to rise and red cell production rates declined. When the system reached its new steady state, red cell production and tissue oxygen tension returned exactly to the prehypoxic control conditions in accord with the concepts discussed in the previous paragraph. This was despite an arterial oxygen tension that was still significantly depressed and at the expense of hematocrit and circulating red cell mass that were considerably above normal.

It is perhaps easy to visualize that a primary change in destruction rate, as in hemolytic anemia, leads to secondary changes in tissue oxygen tension. It is more difficult to conceive of destruction rate being a determining factor of tissue oxygenation in a stress like hypoxia in which it appears, at first, that the decreased oxygen loading of arterial hemoglobin is the primary stimulus for hypoxia. However, it is important to distinguish between the initial stimulus of the acute phase, where blood pO_2 is controlling, and the ultimate stimulus of the steady-state condi-

tion, where destruction rate (and controller function) is controlling. These conclusions from a theoretical model may warrant further experimental examination. The simulation of hemolytic anemia presented in Chapter 6 (see Fig. 6-18) illustrates the capability of the control system to minimize steady-state errors.

B.2 Discussion

B.2.1 Renal pO_2 Sensor

A major assumption in the controlled system is the description of the renal oxygen detector. The evidence strongly indicates that the balance between oxygen supply and demand at intrarenal sites is the primary stimulus for erythropoietin release [33]. Furthermore, these detector sites must monitor venous or tissue pO_2 rather than arterial pO_2 since anemia or increased oxygen-hemoglobin affinity lead to increased erythropoietin production without significantly altering arterial blood oxygen tension [5,34,35]. The receptors sensitive to tissue pO_2 may be those cells that excrete erythropoietin or its precursor [13]. The present model is in accord with these concepts.

It has been suggested that the kidney has unique characteristics that enable it to function as a sensitive oxygen chemoreceptor and, in particular, be responsive to changing hemoglobin levels. The peculiar renal microcirculation and the uniquely low arteriovenous oxygen difference provide a gradient of tissue oxygen tension that amplifies changes in blood oxygen delivery [14,35]. In addition, the auto-regulatory features of the kidney ensure that

blood flow and oxygen uptake are effectively stable over a wide range of oxygen tensions and blood pressures [36,37] Moreover, if blood flows should be altered, the kidney, in contrast to other organs, will exhibit proportionate changes in oxygen uptake [38]. This means that the ratio V_m/Q (the only term in which blood flow appears in the model (Eq. (B4)) may be relatively constant, and renal blood flow would not be expected to markedly influence tissue oxygenation.

The preceding discussion suggests that the powerful influence which oxygen uptake, per se, was found to have in the model (Fig. B-1 and Fig. 6-13) may be mitigated in the real system by concurrent changes in blood flow. Similarly, it is possible that an elevation of V_m, by whatever cause, promotes tissue hypoxia and results in local regulatory increases of K_d, the effective capillary diffusivity. This is now known to be true for skeletal muscle [39] but has not been confirmed for the kidney. Such regulation would, however, further dampen the effect of oxygen uptake because K_d appears only in the ratio V_m/K_d in Eq. (B7). It may be desirable to add these local regulatory effects— between oxygen uptake, blood flow, and capillary diffusivity—to the model. A current alternate approach is to assume they are constant and to examine their influence, if the data so suggest, in improving the accuracy of simulation. Under these circumstances, and in accord with Eqs. (B1) to (B7), tissue pO_2 would be a function of the hemoglobin concentration of the blood, the arterial oxygen saturation of hemoglobin, and the shape and position of the OEC [6].

It should be emphasized that the site of the intrarenal detector has not yet been confirmed and that the quantitative aspects of its oxygen supply-demand balance (including direct measurement of P_tO) remain unknown. Justification of this segment of the model is based on indirect evidence, gross characteristics of the kidney as a whole, and determinants of tissue oxygenation derived from other tissues.

The use of a steady-state formulation for tissue oxygenation (Eqs. (B1) to (B7)) in a dynamic model is justified because, in the well-perfused kidney, equilibrium of oxygen tension due to pure convection and diffusion may be achieved in the order of seconds to minutes following a load disturbance. This can be compared to the much slower changes of the erythropoietin distribution or bone marrow red cell production process. Estimates of true equilibration times were obtained from the non-steady-state version of this algorithm [16,40] that was originally employed in the NASA studies. The steady-state description permitted the use of a larger integration step size in the numerical algorithms and increased the solution speed significantly without decreasing the accuracy of the response for the long periods of time in which the investigators were interested.

B.2.2 Bone Marrow Controller System

An accurate description of the relationship governing erythropoietin release is not yet available, presumably because of the difficulty in measuring intrarenal oxygen levels and the uncertainty surrounding the specific location of the receptor cells. The formulation used to relate tissue oxygen tension to erythropoietin release is in accord with the study of Adamson [18], who found a semilogarithmic inverse relationship between daily urinary erythropoietin excretion and hematocrit in humans. A parallel between urinary and plasma erythropoietin [7] as well as between hematocrit and tissue [41] pO_2 was assumed in deriving Eq. (B8). A similar relationship has been used by Hodgson [5], whereas Parer [42] has derived a linear relationship, and Mylrea and Abbrecht [17] have used arterial oxygen-hemoglobin concentration (i.e., $Hb \times S_aO$) rather than tissue oxygen tension as the independent variable. At the present time, sufficient data do not exist to reveal the precise shape of this function.

Measurement of plasma erythropoietin has, until recently, been restricted to levels above basal [1]. Therefore, no data are available to confirm the relationship to reduced release rates of erythropoietin. This region is of particular interest because of its application of simulation to bedrest, spaceflight, and related disturbances in which chronic elevation of hematocrit follows plasma volume shifts.

There is an abundance of information demonstrating that in experimental animals, a linear relationship exists between red cell production and the log of erythropoietin concentration (Eq. (B12)). This has been observed, for example, in bioassay animals in which doses of erythropoietin are injected either singularly with iron uptake used as the index of erythropoietic activity [2,24] or administered at frequent intervals for up to several weeks with production rate expressed in terms of increased red cell mass [9,23]. It is reasonable to assume that a similar dose response relationship exists for the human, although confirmatory evidence is lacking. In vivo estimates of the human function curve, especially for the suppressed erythropoiesis range, will be possible as erythropoietin becomes available in large quantities and as more sensitive assay methods for this hormone are developed.

The shape and position of the renal and bone marrow function curves have been found to be crucial elements in the control of erythropoiesis in general and in the long-term control of tissue oxygenation in particular. Model parameters have been incorporated to allow for shifts in sensitivities and thresholds away from the normal operating points. Values of controller sensitivities have not been well established in the human by direct methods and only to a limited extent in experimental animals [5] Several studies suggest that alterations in these parameters occur during certain physiological stresses such as dehydration and hypoxia [43,44] and during pathological disturbances such as abnormal hemoglobin [34], erythrocytosis [18] and hemolytic anemia [45]. It appears that the rate of red cell production is determined not only by the concentration of erythropoietin but also by the size of the stem cell pool [46]. If the pool size increases, the bone marrow response to a given dose of erythropoietin should be greater than normal (i.e., an effective increase in G_1). The availability of iron to the erythron may also influence this function [11]. Certain hormones, such as androgens, as well as neural stimuli are assumed to exert their effect on erythro-

poiesis by their modification of erythropoietin release [12,13] (i.e., an effective change in G_1). It is possible, using the current model, to predict these parameters within narrow limits provided both the dynamic behavior of erythropoietin and red cell production rates are measured simultaneously during hematologic stress. Unfortunately, such data are seldom available, especially for humans.

B.2.3 General Comments

Feedback regulation of tissue oxygen tension is accomplished solely by adjustments of hemoglobin levels resulting from the output of a renal/bone-marrow controller. Other parameters that are known to effect acute changes in tissue oxygenation are incorporated explicitly in the model but are non-regulatory in nature and can be altered manually to test various hypotheses. Similarly, the characteristics of the controller can also be adjusted to test their effect on long-term control of tissue pO_2 and red cell mass. Such parameter adjustment (other than for the primary disturbance) has not been found to be essential, in most cases, to simulate the basic behavior of the dynamic and steady-state response. However, fine-tuning of param-

eters is required to scale the model output and achieve closer agreement with experimental values. In some cases, these studies indicate the need to propose additional regulatory elements to provide, for example, a more realistic simulation of the erythropoietin response to hypoxia. Other features of a general nature have also been identified that will increase the utility of the model even further, including (1) the effect of blood volume and viscosity on oxygen transport and (2) a description of stem cell kinetics and reticulocytosis [47,57].

B.3 Formulation of Mouse Model

B.3.1 System Parameters

The computer model for erythropoietic control was adapted to the mouse system by altering the system parameters originally given for the human, to those that more realistically represent the mouse [48]. Parameter values were obtained from a variety of literature sources as indicated in Table B-2. The immediate application of the mouse model was the study of the mouse as a potential experimental model for spaceflight. Data for the simula-

Table B-2. System Parameters for Erythropoiesis Control Model

Parameter	Model symbol	Parameter value Human	Parameter value Mouse	Reference	Units
Red cell mass*	RCM	2000	0.63	B-49	ml
Plasma volume*	PV	3000	0.77	B-49	ml
Blood volume	BV	5000	1.40	B-49	ml
Whole-body hematocrit	Hct	40.0	45.0	B-49	ml of packed RBC/100 ml blood
Mean corpuscular hemoglobin concentration*	MCHC	0.375	0.300	B-50	g Hb/ml RBC
Hemoglobin concentration	Hb	15.0	13.5	B-50, B-51	g Hb/100 ml blood
O_2 capacity of blood*	CaO	20.1	19.0	B-51	mI O_2/100 ml blood
O_2 capacity of hemoglobin	CHbO	1.34	1.41	B-50, B-51	mI O_2/g Hb
pO_2 tension at one-half *Hb* saturation*	P50	27	39	B-52	MmHg
Arterial pO_2*	P_aO	95	78	B-53	mmHg
Arterial *Hb* saturation	S_aO	0.97	0.99	B-52	Percent
Renal metabolic rate*	V_m	20	0.04	B-54	ml O_2/min
Renal blood flow*	Q	1200	1.83	B-55	ml/min
Normal tissue pO_2*	P_tO	20	20		MmHg
Erythropoietin half-life*	$TE_{1/2}$	12	3.25	B-56	Hours
Red cell lifespan*	TRC	126	20	B-17	Days
Erythrocyte maturation time*	$TBM\ TE_{1/2}$	4	3.5		Days
Normal RBC production rate*	RCP	22	0.0437	B-49	ml RBC/day
RBC turnover rate	RKC	1.1	6.93	B-49	Percent/day

* Fundamental value from which other parameter values may be derived. Relationships used in deriving these other parameters are as follows:
 Blood volume: $BV = RCM + PV = 0.63 + 0.77 = 1.4$ ml
 Whole-body hematocrit: $Hct = RCM/BV = 0.63/1.4 = 0.45$ ml packed RBC/ml blood
 Hemoglobin concentration: $Hb = Hct \times MCHC = 45 \times 0.3 = 13.5$ g Hb/100 ml blood
 Capacity of hemoglobin: $CHbO = C_aO/Hb = 19.0/13.5 = 1.41$ ml O^2/g Hb
 Arterial Hb saturation: $S_aO =$ function (P_aO) (See oxygen-hemoglobin dissociation curve (Fig. B-8).)
 RBC turnover: $RKC =$ turnover rate/100 $= 0.693/$RBC half-life $0.693/20/2 = 0.0693$ per day $= 6.93\%$ per day
 Steady-state destruction rate $= RCM \times RKC = 0.63 \times 0.0693\ 0.0437$ ml/day
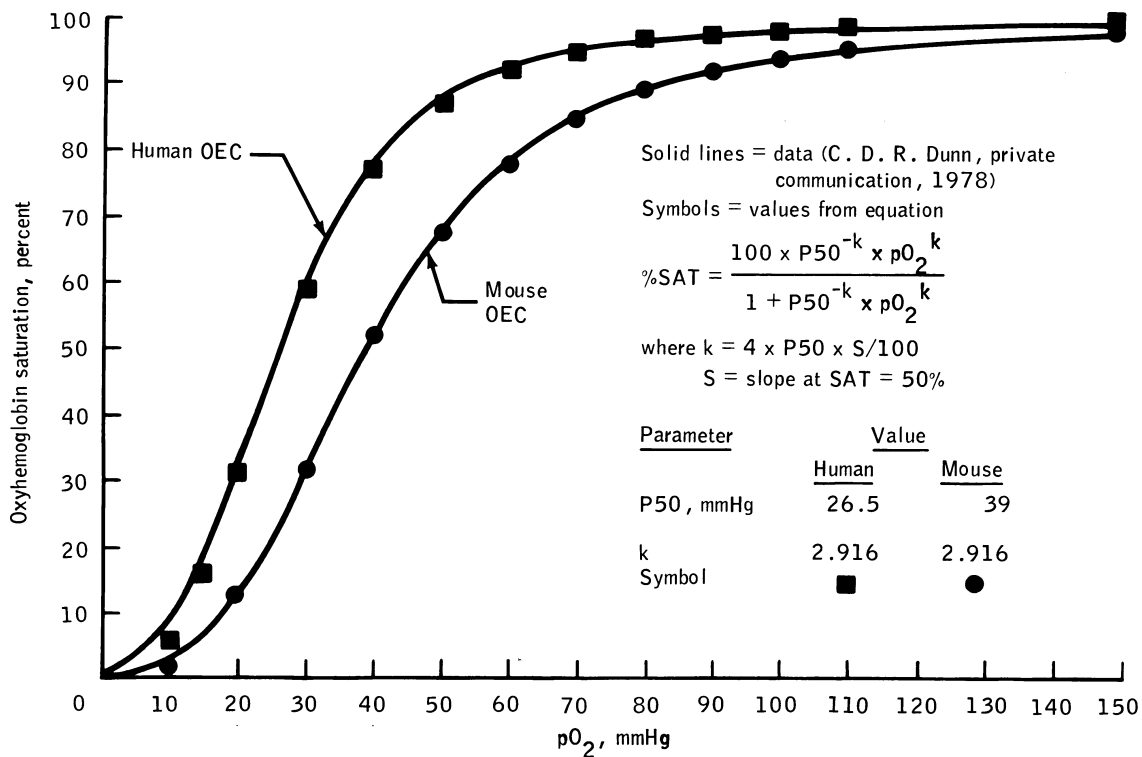
Figure B-8. Oxygen-hemoglobin equilibrium curves for human and mouse: experimental versus theoretical values.

The figure shows oxyhemoglobin saturation (percent) versus pO_2 (mmHg) for Human OEC and Mouse OEC.

Solid lines = data (C. D. R. Dunn, private communication, 1978)

Symbols = values from equation

$$\%SAT = \frac{100 \times P50^{-k} \times pO_2^{\ k}}{1 + P50^{-k} \times pO_2^{\ k}}$$

where $k = 4 \times P50 \times S/100$

S = slope at SAT = 50%

Parameter	Human	Mouse
P50, mmHg	26.5	39
k	2.916	2.916
Symbol	■	●

Table B-3. Absolute Versus Specific Parameter Values

Parameter	Absolute units			Specific units*		
	Human	Mouse	Units	Human	Mouse	Units
Red cell mass	2000	0.63	ml	28.6	25.2	ml/kg body wt.
Plasma volume	3000	0.77	ml	42.9	30.8	ml/kg body wt.
Blood volume	5000	1.40	ml	71.4	56.0	ml/kg body wt.
Renal blood flow	1200	1.83	ml/min	4.28	6.10	ml/min^{-1} g^{-1} tissue
Renal O_2 consumption	20	0.04	ml/min	0.73	0.133	ml/min^{-1} g^{-1} tissue
Body O_2 consumption	250	0.51	ml/min	0.00357	0.0255	ml/min^{-1} g^{-1} tissue

*Based on

Body weight = 70 kg man and 25 g mouse

Renal mass = 280 g (0.4% body wt.) in man and 0.3 g (1.2% body wt.) in mouse

Table B-4. Oxygen Balance at Kidney

O₂ supply equals

BF x O₂ concentration ⟵ | Kidney | ⟶ O₂ venous

O₂ demand

Parameter	Human	Mouse	Units
Oxygen demand	20.0	0.04	ml O_2/min
	0.073	0.153	ml O_2 min^{-1} g^{-1}
Oxygen supply			
P_aO, arterial	95.0	78	mmHG
S_aO, arterial	97.4	98.6	Percent saturation
O_2 concentration	196.0	188	ml O_2/liter blood
BF, blood flow	1200	.0 1.83 ml		
blood/min			
O_2 supply	235.0	0.343	ml O_2/min
	0.839	1.143	ml O_2/min^{-1} g^{-1}
Oxygen venous			
P_vO, venous	56.0	57	mmHG
S_vO, venous	89.0	86	Percent saturation
pO_2, tissue	20.0	20	mmHg
Percent oxygen	8.7	13.4	Percent
extraction =			
(O_2 demand)/(O_2 supply)			

tions were obtained from C. D. R. Dunn (University of Tennessee Memorial Research Center) and included studies of dehydration and hypoxia. The strain of mice used in these studies was C3H with an approximate weight of 25 grams. Parameter values were chosen for this strain where possible. In certain cases, the literature values were superseded by values obtained directly from Dunn's studies. In a few cases, mouse data were not available and data for the rat were substituted. A comparison of system parameters for the mouse and human models is shown in Table B-2. Aside from the obvious differences expected in fluid volumes, blood flows, and metabolic rates, large differences were observed in the following: erythrocyte lifespan (126 days vs. 20 days)[**] erythropoietin half-life (12 hours vs. 3.25 hours), and normal arterial pO_2 (95 mmHg vs. 78 mmHg). The shorter lifespan of the mouse red blood cells implies a turnover of erythrocytes that is six-fold faster. That is, the daily rates of red cell production and destruction (as well as reticulocyte index) are approximately six times higher in the C3H mouse than the human.[††] Other parameters that were found to be more similar between the two species were as follows: hematocrit (40 vs. 45), mean corpuscular hemoglobin concentration (0.375 vs. 0.30), and maximum oxygen-carrying capacity of hemoglobin (1.34 vs. 1.41).

[**] First and second numbers in parentheses refer to human and mouse, respectively.
[††] Typical values for mice red cell lifespan found in the literature indicate only a threefold increase. Values used here were found by Dunn to be much different in the C3H strain.

Although the arterial pO_2 in the mouse is much lower than in the human, the oxygen saturation of hemoglobin of both species is nearly identical (97% vs. 99%). This is a result of the distinctly different oxygen-hemoglobin dissociation curves shown in Fig. B-8 and reflected in the different P_{50} values (26.5 mmHg vs. 39.0 mmHg). The P_{50} differences imply that, at the same level of tissue oxygen tension, oxygen is more easily unloaded in the mouse than in the human. It should be noted that the normal pO_2 of arterial blood assumed here (78 mmHg)) was obtained from rat data [51,56] and has been used in a previous model validated for the mouse with reasonably good results [17]. No corresponding mouse data could be located. Values for renal blood flow of the mouse were not available, and data from rats were used (6 ml min^{-1} g^{-1} tissue).

B.3.2 Scaled Parameters

Some parameters of the mouse model differ considerably from the human model because of scaling factors alone. The values used in the model are given on an absolute basis for the whole animal rather than as a specific property in terms of "per gram of tissue." In terms of specific units, the differences between the mouse and human system are much smaller, as shown in Table B-3.

B.3.3 Oxygen Balance

The balance of oxygen supply versus oxygen demand is crucial to the feedback regulation of erythropoiesis. A parameter reflecting this complex balance is the tissue oxygen tension that is believed to govern the release of erythropoietin. The oxygen balances for the human and mouse systems as used in the model are given in Table B-4.

Oxygen consumption per gram of renal tissue in the mouse is approximately twice that for the human. (Overall total oxygen consumption per gram body weight is nearly seven times greater in the mouse.) This higher oxygen demand of the mouse is satisfied in two ways in the model. First, there is a 50% greater efficiency in oxygen extraction as indicated in Table B-4. (Note that, in both species, the amount of oxygen delivered at rest is more than sufficient; i.e., roughly 10 times that required by the tissues.) Second, there is a 30% higher blood oxygen supply per gram of tissue because of greater tissue blood flow in the mouse.

The normal tissue oxygen tension is arbitrarily assumed to be identical in both model systems; i.e., 20 mmHg. The equation describing oxygen diffusivity to the tissues from venous capillaries is given in the steady state as

Net oxygen delivery = tissue oxygen consumption
$$= (pO_2 \text{ vein} - pO_2 \text{ tisue}) \text{ x } K \quad \text{(B17)}$$

where K = conductivity coefficient = O_2 diffusivity times the capillary surface area. The ratio K_{man}/K_{mouse} would be expected to reflect the surface area ratio between species if diffusivity is assumed similar in mouse and man. Therefore, if S is capillary surface area, then

$$\frac{S_{\text{man}}}{S_{\text{mouse}}} = \frac{K_{\text{man}}}{K_{\text{mouse}}}$$

$$= \frac{(O_2 \text{ consumption})_{\text{man}}}{(O_2 \text{ consumption})_{\text{mouse}}} \times \frac{(pO_2, \text{vein} - pO_2, \text{tissue})_{\text{mouse}}}{(pO_2, \text{vein} - pO_2, \text{tissue})_{\text{man}}}$$

$$= \frac{20\,\text{ml/min}}{0.04\,\text{ml/min}} \times \frac{(57.5 - 20)\,\text{mmHg}}{(56.4 - 20)\,\text{mmHg}} = 515$$

This is in good agreement with the surface area ratio of 650 of the glomerulus derived from data in Ref. 54 (p. 174), lending support to the general representation of the kidney in the computer model.

B.3.4 Functional Relationships

Three functional relationships are included in the computer model: (1) oxygen-hemoglobin equilibrium curve (OEC), (2) erythropoietin release as a function of tissue pO_2, and (3) erythrocyte production rate as a function of erythropoietin concentration. The first of these is shown in Fig. B-8 and will subsequently be described in detail. The form of the function curves for erythropoietin and red cell release will be assumed identical in the mouse and human models. There is no reason at the present time to take issue with this assumption, particularly since the bone marrow function was originally obtained from the mouse. These curves (as shown in Figs. B-2 and B-3 and as used in the models) are represented in normalized form (i.e., percent of control) so that any species may be represented. The gain factors G_1 and G_2, representing the slope of the relationships, may be different between species. This is of little concern in the basic design of the model because these parameters will be adjusted during the simulation process and their actual values will be estimated by "fitting" the model output to the experimental data.

The equation describing the sigmoidal OEC is a form of the Hill equation and is shown in the insert of Fig. B-8. The two solid lines represent human and mouse blood, respectively, and were recently obtained from blood samples of the C3H mouse [49]. The value of P_{50} is explicitly stated in the equation so that shifts in oxygenhemoglobin affinity may be easily described. The value of the exponent k, found from the best fit of the mouse curve, also provides a good fit of the human curve as shown in Fig. B-8. Thus, the only difference between the equation describing the human and mouse OEC is the value of P_{50}.

References

1. Adamson, J.W. and Finch, C.A., Hemoglobin Function, Oxygen Affinity, and Erythropoietin, *Ann. Rev. Physiol.*, 37: 351-369, 1975

2. Fisher, J.W., Busuttil, R., et al., The Kidney and Erythropoietin Production: A Review, Erythropoiesis *Proceedings of the Fourth International Conference on Erythropoiesis*, K. Nakao, J. W. Fisher, and F. Takaku, Eds., University Park Press, 1975, pp. 315-336.

3. Jacobson, L.O., Goldwasser, E., Fried, W. and Plzak, L., Role of the Kidney in Erythropoiesis, *Nature*, 179: 633-634, 1957.

4. Finch, C.A. and Lenfant, C., Oxygen Transport in Man, *New England J. Med.*, 286(8):407-415, 1972.

5. Hodgson, G. Application of Control Theory to the Study of Erythropoiesis, *Regulation of Hematopoiesis*, Vol. 1, Chap. 15, A. S. Gordon, Ed., Appleton-Century-Crofts (New York), 1970.

6. Beutler, E. "A Shift to the Left" or "A Shift to the Right" in the Regulation of Erythropoiesis, *Blood*, 33:496-500, 1969.

7. Krantz, S.B. and Jacobson, L.O., *Erythropoietin and the Regulation of Erythropoiesis*, University of Chicago Press, 1970.

8. Reissman, K.R., Diederich, D.A., Ito, K. and Schmaus, J.W., Influence of Disappearance Rate and Distribution Space on Plasma Concentration of Erythropoietin in Normal Rats, *J. Lab. & Clin. Med.*, 65:967-975, 1965.

9. Van Dyke, D.C. and M. Pollycove, *The Relation of Erythropoietin to Anemia and Polycythemia, Erythropoiesis*, L. O. Jacobson and M. Doyle, Eds., Grune and Stratton (New York), 1962, pp. 340-350.

10. Harris, J.W. and Kellermeyer, R.W., *The Red Cell: Production, Metabolism, Destruction, Normal & Abnormal*, Harvard University Press (Cambridge), 1970.

11. Finch, C.A. and Denbelbeiss, K., et al., *Ferrokinetics in Man, Medicine*, 49:17-53, 1970.

12. Peschle, C., Marone, G., Sacchetti, L. and Condorelli, M., The Hormonal Influences on Red Cell Production: Physiological Significance and Mechanism of Action, *Erythropoiesis-Proceedings of the Fourth International Conference on Erythropoiesis*, K. Nakao, J. W. Fisher, and F. Takaku, Eds., University Park Press, 1975, pp. 99-117.

13. Baciu, I., The Humoral and Neural Regulation of Erythropoiesis. Translation of "Die humorale und nervose Regelung der Erythropoese", *Klinische Wochenschrift*, 48(3):133-143, 1970; (NASA Translation: TT F-13, 157).

14. Gordon, A.S. and Zanjani, E.D., Some Aspects of Erythropoietin Physiology, *Regulation of Hematopoiesis*, vol. 1, ch. 19, A. S. Gordon, Ed., Appleton-Century-Crofts (New York), 1970.

15. Guyton, A.C. , Coleman, T.G. and Granger, H.J., Circulation: Overall Regulation, *Ann. Rev. Physiol.*, 34:13-46, 1972.

16. Middleman, S., *Transport Phenomena in the Cardiovascular System*, Wiley-Interscience (New York), 1972, pp. 1-115.

17. Mylrea, K.C. and Abbrecht, P.H., Mathematical Analysis and Digital Simulation of the Control of Erythropoiesis, *J. Theor. Biol.*, 33(2):279-297, **1**971.

18. Adamson, J.W., The Erythropoietin Hematocrit Relationship in Normal and Polycythemic Man: Implications of Marrow Regulation, *Blood,* 32(4): 597-609, 1968.

19. Erslev, A.J., Erythropoietin in Clinical Medicine, *Erythropoiesis-Proceedings of the Fourth International Conference on Erythropoiesis*, K. Nakao, J. W. Fisher, and F. Takaku, Eds., University Park Press, 1975, pp. 425-433.

20. Waldman, T, Discussion on the Metabolic Fate of Erythropoietin, *Erythropoiesis*, L. O. Jacobson and M. Doyle, Eds., Grune and Stratton (New York), 1962, pp. 136-137.

21. Riggs, D.S., *Control Theory and Physiological Feedback Mechanisms*, Williams and Wilkins Co. (Baltimore), 1970.

22. Camiscoli, J.F. and Gordon, A.S., Bioassay and Standardization of Erythropoietin, *Regulation of Hematopoiesis*, Vol. I, A. S. Gordon, Ed., Appleton-Century-Crofts (New York), 1970, pp. 369-394.

23. Gurney, C.W., Degowin, R., Hofstra, D. and Byron, J., Application of Erythropoietin to Biological Investigation, *Erythropoiesis*, L. O. Jacobson and M. Doyle, Eds., Grune and Stratton (New York), 1962, pp. 151-161.

24. Dunn, C.D.R., Jones, J.B., Jolly, J.D. and R. D. Lange, Progeni-

tor Cells in Canine Cyclic Hematopoiesis, *Blood*, 50:1111-1120, 1977.

25. Berlin, N.I., Life Span of the Red Blood Cell, *The Red Blood Cell*, ch. 12, C. Bishop and D. M. Surgenor, Eds., Academic Press (New York), 1964.

26. Mackey, M.C., Unified Hypothesis for the Origin of Aplastic Anemia and Periodic Hematopoiesis, *Blood*, 51:941-956, 1978.

27. King-Smith, E.A. and Morley, A., Computer Simulation of Granulopoiesis: Normal and Impaired Granulopoiesis, *Blood*, 362:54-262.1970.

28. Arden, B.W. and Astill, K.N., Numerical Algorithms: Origins and Applications, Addison-Wesley Publishing Co. (Reading, Mass.), 1970.

29. Aberman, A., Cavanilles, J.M., et al., An Equation for the Oxygen Hemoglobin Dissociation Curve, *J. Appl. Physiol.*, 35(4): 570-571,1973.

30. Leonard, J.I., Kimzey, S.L. and Dunn, C.D.R., Dynamic Regulation of Erythropoiesis: A Computer Model of General Applicability, *Exper. Hematology*, 9:355-378, 1981.

31. Kimzey, S.L., Leonard, J.I. and Johnson, P.C., A Mathematical and Experimental Simulation of the Hematological Response to Weightlessness, *Acta Astronaut.*, 6:1289-1303, 1979.

32. Guyton, A.C., Coleman, T.G., et al., Relationship of Fluid and Electrolytes to Arterial Pressure Control and Hypertension: Quantitative Analysis of an Infinite-Gain Feedback System, *Hypertension: Mechanisms and Management*, G. Onesti, K. E. Kim, and J. H. Moyer, Eds., Grune and Stratton (New York), 1973.

33. Grant, W.C. and Root, W.S., Fundamental Stimulus for Erythropoiesis, *Physiol. Rev*., 32:449-498, 1952.

34. Adamson, J.W., Parer, J.T. and Stamatoyannopoulous, G., Erythrocytosis Associated With Hemoglobin Rainier: Oxygen Equilibria and Marrow Regulation, *J. Clin. Invest.*, 48(3):1376-1386, 1969.

35. Metcalfe, J. and Dhindsa, D.S., The Physiological Effects of Displacements of the Oxygen Dissociation Curve, *Oxygen Affinity of Hemoglobin and Red Cell Acid Base Status*, P. Astrup and M. Rorth, Eds., Academic Press (New York), 1972, pp. 613-628.

36. Aperia, A.C., Liebow, A.A. and Roberts, L.E., Renal Adaptation to Anemia, *Circulation Res.*, 22:489-500, 1968.

37. Selkurt, E.E., *The Renal Circulation. Handbook of Physiology*, Sec. 2: Circulation, vol. 2, W. F. Hamilton and Philip Dow, Eds., Chap. 43, American Physiological Society (Washington, D.C.), 1963.

38. Pitts, R.F., *Physiology of the Kidney and Body Fluids*, 2nd ed., Yearbook Medical Publishers (Chicago), 1968.

39. Granger, H.J, Goodman, A.H. and Cook, B.H., Metabolic Models of Microcirculatory Regulation, *Fed. Proc.*, 34(11):2025-2030, 1975

40. Duvelleroy, M.A., Mehmel, H. and Laver, M.B., Hemoglobin-Oxygen Equilibrium and Coronary Blood Flow: An Analog Model, *J. Appl. Physiol.*, 35(4):480-484, 1973.

41. Thorling, E.B. and Erslev, A.J., The "Tissue" Tension of Oxygen and Its Relation to Hematocrit and Erythropoiesis, *Blood*, 31:332-343, 1968.

42. Parer, J.T., Oxygen Transport in Human Subjects With Hemoglobin Variants Having Altered Oxygen Affinity, *Respir. Physiol.*, 9:43-49, 1970.

43. Dunn, C.D.R. and Lange, R.D., Erythropoietic Effects of Space Flight, *Acta Astronaut.*, 6:725-732, 1979.

44. Kretchmar, A.L., Erythropoietin: Hypothesis of Action Tested by Analog Computer, *Science*, 152:367-370, 1966.

45. Erslev, A.J. and Silver, R.K., Compensated Hemolytic Anemia, *Blood Cell*, 1:509-525. 1975.

46. Lajtha, L.G., Oliver, R. and Gurney, C.W., Kinetic Model of a Bone-Marrow Stem-Cell Population, *British J. Hematol.*, 8:442-460, 1962.

47. Leonard, J.I., Study Report-Improvements and Validation of the Erythropoiesis Control Model for the Simulation of Bed Rest, (General Electric Co., Houston, Tex.; TIR 741-LSP-7012.) NASA CR-160187, NASA, Washington, D.C., 1977.

48. Leonard, J.I., System Parameters for Erythropoiesis Control Model: Comparison of Normal Values in Human and Mouse Model, (General Electric Co., Houston, Tex.; TIR 741-LSP-8024.) NASA CR-160401, NASA, Washington, D.C., 1978.

49. Dunn, C.D.R., Effect of Dehydration on Erythropoiesis in Mice: Relevance to the "Anemia" of Space Flight, *Aviat. Space & Environ. Med.*,49:990-993, 1978.

50. Green, E.L. (Ed.), *Biology of the Laboratory Mouse*, McGraw-Hill (New York), 1967, pp. 351-372.

51. Altman, P.L. and Dittmer, D.S., *Biology Data Handbook*, Vols. 1, 2, and 3, Federation of American Societies for Experimental Biology (Bethesda, Md.), 1972.

52. Ulrich, S., Hilpert, P. and Bartels, H., Uber die Atmungrfunktion des Blutes von Spitzmausen wuBen Mausen und syrischen Goldhamstern, *Pfluegers Arch.*, 277:150-165,1963.

53. Abbrecht, P.H. and Littell, J.K., Erythrocyte Life Span in Mice Acclimatized to Different Degrees of Hypoxia, *J. Appl. Physiol.*, 32(4):443-445, 1972.

54. Spector, W.S., *Handbook of Biological Data*, W. B. Saunders Co. (Philadelphia), 1961, p. 174.

55. Arendshorst, W.F., Autoregulation of Blood Flow in the Rat Kidney, *American J. Physiol.*, 228(1):127-133, 1975.

56. Abbrecht, P.H. and Littell, J.K., Plasma Erythropoietin in Men and Mice During Acclimatization to Different Altitudes, *J. Appl. Physiol.*, 32(1):54-58, 1972.

57. Wichmann, H.E. and Loeffler, M. (Eds.), Mathematical Modeling of Cell Proliferation: Stem Cell Regulation in Hemopoiesis, CRC Press, Boca Raton, FL, 1985.

Appendix C
Guyton Model for Circulatory, Fluid, and Electrolyte Control: Modifications and Recommendations

The original version of the model developed by Arthur Guyton and used extensively as a basis for much of this work was built as a general-purpose model of overall circulatory regulation and was used by the authors to simulate a wide variety of real situations, including congestive heart failure, various types of hypertension, fistula, and hypoproteinemia [1,2]. Despite these successes, the model, as originally constructed, did not have the level of detail required to respond to the challenge of the microgravity environment. Modifications were made to the model to rectify this limitation and expand its capabilities. These modifications are available in report form [3,4], but they are presented and summarized here for the convenience of the interested reader.

The original version of the Guyton model is presented in Fig. C-1. A legend of symbols, definitions, and units is included. In addition, Fortran language versions of both the original and the modified model are obtainable [5,6].

There are two parts to this appendix. The first part summarizes the modifications that were concerned primarily with recompartmenting the circulatory subsystem to include leg volume and controller elements; adding gravity-dependent functions to the controlled and controller systems; and revising and updating the baroreceptor block, red blood cell block, and the angiotensin block. These modifications have extended the capability of the original model so that the effects of gravity and its removal on fluid distribution may be simulated more realistically. The second part is a set of recommendations for improving the capability of the model to simulate orthostatic (tilt and standing) maneuvers.

C.1 Modifications to the Guyton Model

C.1.1. Leg Circulatory Compartment

Two additional compartments have been added to the model of the circulatory system, one to represent the arteries in both legs and the other to represent the veins (see Fig. 3-36). Each compartment is characterized by a total blood volume, blood pressure, and compliance (see Table C-1). The values for volumes and compliances of the leg compartments were derived from the model of the 28-compartment pulsatile cardiovascular sub-system of the Whole-Body Algorithm. The blood volumes and compliances of the upper circulatory compartments were adjusted to keep the total volume and compliance of the arterial and venous vessels nearly identical to those in the original Guyton model.

C.1.2 Blood Flow Pathways and Metabolic Rates

The original Guyton model contained three blood flow pathways: renal, muscle, and the remainder of the circula-

tion. In the modified version, these three pathways remain intact; however, the muscle flow pathway represents the entire leg flow, and the non-muscle, non-renal pathway together with the renal flow represents total upper body flow. In this modified model, leg blood flow and total body muscle blood flow are identical. Muscle and non-muscle, non-renal flows were readjusted by changing their basic resistances so that cardiac output was similar to that of the unmodified version of the Guyton model and leg flow was similar to that of the leg blood flow of the short-term pulsatile cardiovascular model of the Whole-Body Algorithm. Metabolic demand in terms of oxygen consumption was also readjusted in proportion to the new blood flow rates.

C.1.3 Resistances of the Leg Blood Vessels

The single resistance in the muscle blood flow pathway of the original version was replaced by two variables in series to allow capillary filtration to occur in the muscles. These represent a precapillary arteriolar resistance and a postcapillary venular resistance, the values of each being dependent on autonomic and angiotensin effects. In addition, the venular resistance responds to passive distention due to hydrostatic pressure, whereas the arteriolar resistance includes autoregulatory and viscosity effects. These formulations for the leg muscle tissue are similar to that of the non-muscle, non-renal precapillary and postcapillary resistances in the original Guyton model with the following exceptions.

First, the passive distention effect resulting from hydrostatic pressure was not included as a determinant of the leg arteriolar resistance. This exclusion was based on the belief that, upon standing, a strong myogenic local reflex acts to constrict arteriolar vessels (as well as capillary sphincters) in response to the high hydrostatic load. The myogenic reflex opposes the passive distention effect. It was felt that the passive distention effect should be removed until the myogenic effect is included in the model. Otherwise, the effect of standing would create arteriolar distention great enough to overcome autonomic vasoconstriction, a condition that does not normally exist in the real physiological system.

Second, the veins are not known to participate in the myogenic response but, rather, should be highly responsive to passive distention under the high hydrostatic pressures of standing. Consequently, a passive distention effect was added to the leg venule resistance. This formulation permitted a 1 mmHg change in pressure to cause a 1% change in resistance in accordance with data reviewed by McDonald [7]. The net effect of excluding the passive distention effect in the leg arterioles and adding this effect to the leg venules is to favor a higher precapillary/postcapillary resistance ra-
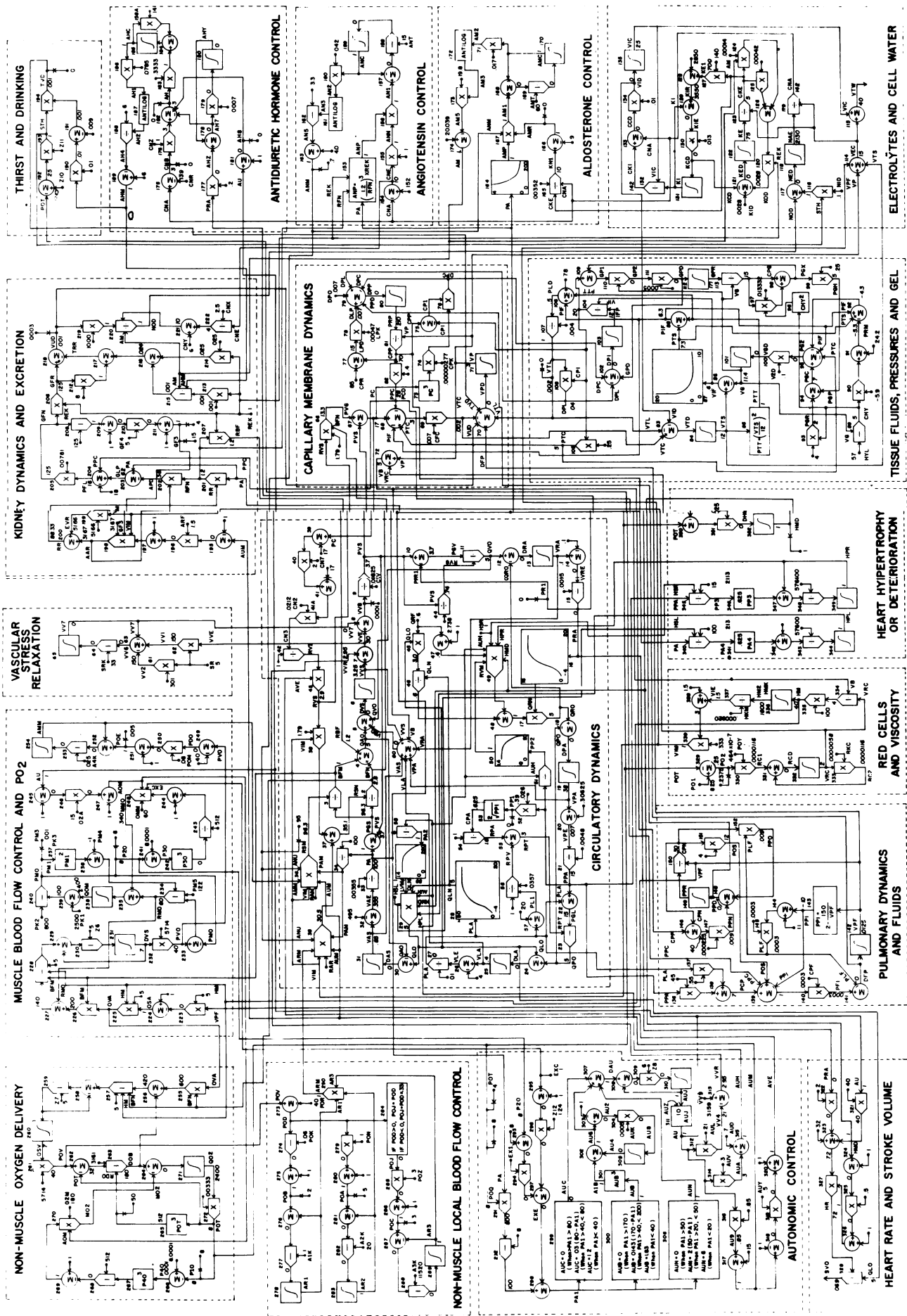
Figure C-1. Systems analysis diagram for regulation of the circulation according to Guyton and co-workers. Reprinted from Ref. [1] with permission of the publisher. Units are the following: volume in liters; mass in grams; time in minutes; chemical units in meq; pressure in millimeters of mercury; and control factors in arbitrary units but in most instances expressed as the ratio to normal—for instance, a value of 1 represents normal. Normal values are given on the lines that represent the respective variables. The important dependent and independent variables in the analysis are listed in the key. Additional variables are present for purposes of calculation but generally have no physiological significance.

Figure C-1 Key

AAR   afferent arteriolar resistance
AHM   antidiuretic hormone multiplier, ratio of normal effect
AM   aldosterone multiplier, ratio of normal effect
AMC   aldosterone concentration
AMM   muscle vascular constriction caused by local tissue control, ratio to resting state
AMP   effect of arterial pressure on rate of aldosterone secretion
AMR   effect of sodium to potassium ratio on aldosterone secretion rate
AMT   time constant of aldosterone accumulation and destruction
ANC   angiotensin concentration
ANM   angiotensin multiplier effect on vascular resistance, ratio to normal
ANN   effect of sodium concentration on rate of angiotensin formation
ANP   effect of renal blood flow on angiotensin formation
ANT   time constant of angiotensin accumulation and destruction
ANU   nonrenal effect of angiotensin
AOM   autonomic effect on tissue oxygen utilization
APD   afferent arteriolar pressure drop
ARF   intensity of sympathetic effects on renal function
ARM   vasoconstrictor effect of all types of autoregulation
ARI   vasoconstrictor effect of rapid autoregulation
AR2   vasoconstrictor effects of intermediate autoregulation
AR3   vasoconstrictor effect of long-term autoregulation
AU   overall activity of autonomic system, ratio to normal
AUB   effect of baroreceptors on autoregulation
AUC   effect of chemoreceptors on autonomic stimulation
AUH   autonomic stimulation of heart, ratio to normal
AUK   time constant of baroreceptor adaptation
AUL   sensitivity of sympathetic control of vascular capacitance
AUM   sympathetic vasoconstrictor effect on arteries
AUN   effect of CNS ischemic reflex on autoregulation
AUV   sensitivity control of autonomics on heart function
AUY   sensitivity of sympathetic control of veins
AUZ   overall sensitivity of autonomic control
AVE   sympathetic vasoconstrictor effect on veins
A1K   time constant of rapid autoregulation
A2K   time constant of intermediate autoregulation
A3K   time constant of long-term autoregulation
A4K   time constant for muscle local vascular response to metabolic activity
BFM   muscle blood flow
BFN   blood flow in nonmuscle, nonrenal tissues
CA   capacitance of systemic arteries
CCD   concentration gradient across cell membrane
CHY   concentration of hyaluronic acid in tissue fluids
CKE   extracellular potassium concentration
CKI   intracellular potassium concentration
CAN   extracellular sodium concentration
CNE   sodium concentration abnormality causing third factor effect
CPG   concentration of protein in tissue gel
CPI   concentration of protein in free interstitial fluid
CPN   concentration of protein in pulmonary fluids
CPP   plasma protein concentration
CV   venous capacitance
DAS   rate of volume increase of systemic arteries
DFP   rate of increase in pulmonary free fluid
DHM   rate of cardiac deterioration caused by hypoxia
DLA   rate of volume increase in pulmonary veins and left atrium
DLP   rate of formation of plasma protein by liver
DOB   rate of oxygen delivery to nonmuscle cells
DPA   rate of increase in pulmonary volume
DPC   rate of loss of plasma proteins through systemic capillaries
DPI   rate of change of protein in free interstitial fluid
DPL   rate of systemic lymphatic return of protein
DPO   rate of loss of plasma protein
DRA   rate of increase in right atrial volume
DVS   rate of increase in venous vascular volume
EVR   postglomerular resistance
EXC   exercise activity, ratio to activity at rest
EXE   exercise effect on autonomic stimulation
GFN   glomerular filtration rate of undamaged kidney
GFR   glomerular filtration rate
GLP   glomerular pressure
GPD   rate of increase of protein in gel
GPR   total protein in gel
HM   hematocrit
HMD   cardiac depressant effect of hypoxia
HPL   hypertrophy effect on left ventricle
HPR   hypertrophy effect on heart, ratio to normal
HR   heart rate
HSL   basic left ventricular strength
HSR   basic strength of right ventricle
HYL   quantity of hyaluronic acid in tissues
IFP   interstitial fluid protein
KCD   rate of change of potassium concentration
KE   total extracellular fluid potassium
KED   rate of change of extracellular fluid concentration
KI   total intracellular potassium concentration
KID   rate of potassium intake
KOD   rate of renal loss of potassium
LVM   effect of aortic pressure on left ventricular output
MMO   rate of oxygen utilization by muscle cells
MO2   rate of oxygen utilization by nonmuscle cells
NAE   total extracellular sodium
NED   rate of change of sodium in intracellular fluids
NID   rate of sodium intake
NOD   rate of renal excretion of sodium
OMM   muscle oxygen utilization at rest
OSA   aortic oxygen saturation
OSV   nonmuscle venous oxygen saturation
OVA   oxygen volume in aortic blood
OVS   muscle venous oxygen saturation
O2M   basic oxygen utilization in nonmuscle body tissues
PA   aortic pressure
PAM   effect of arterial pressure in distending arteries, ratio to normal
PC   capillary pressure

PCD   net pressure gradient across capillary membrane
PCP   pulmonary capillary pressure
PDO   difference between muscle venous oxygen pO$_2$ and normal venous oxygen pO$_2$
PFI   rate of transfer of fluid across pulmonary capillaries
PFL   renal filtration pressure
PGC   colloid osmotic pressure of tissue gel
PGH   absorbency effect of gel caused by recoil of gel reticulum
PGL   pressure gradient in lungs
PGP   colloid osmotic pressure of tissue gel caused by entrapped protein
PGR   colloid osmotic pressure of interstitial gel caused by Donnan equilibrium
PGV   pressure from veins to right atrium
PIF   interstitial fluid pressure
PLA   left atrial pressure
PLD   pressure gradient to cause lymphatic flow
PLF   pulmonary lymphatic flow
PMO   muscle cell pO$_2$
POD   nonmuscle venous pO$_2$ minus normal value
POK   sensitivity of rapid system of autoregulation
PON   sensitivity of intermediate autoregulation
POS   pulmonary interstitial fluid colloid osmotic pressure
POT   nonmuscle cell pO$_2$
POV   nonmuscle venous pO$_2$
POY   sensitivity of red cell production
POZ   sensitivity of long-term autoregulation
pO$_2$ oxygen deficit factor causing red cell production
PPA   pulmonary arterial pressure
PPC   plasma colloid osmotic pressure
PPD   rate of change of protein in pulmonary fluids
PPI   pulmonary interstitial fluid pressure
PPN   rate of pulmonary capillary protein loss
PPO   pulmonary lymph protein flow
PPR   total protein in pulmonary fluids
PRA   right atrial pressure
PRM   pressure caused by compression of interstitial fluid gel reticulum
PRP   total plasma protein
PTC   interstitial fluid colloid osmotic pressure
PTS   solid tissue pressure
PTT   total tissue pressure
PVG   venous pressure gradient
PVO   muscle venous pO$_2$
PVS   average venous pressure
QAO   blood flow in the systemic arterial system
QLN   basic left ventricular output
QLO   output of left ventricle
QOM   total volume of oxygen in muscle cells
QO2   nonmuscle total cellular oxygen
QPO   rate of blood flow into pulmonary veins and left atrium
QRF   feedback effect of left ventricular function on right ventricular function
QRN   basic right ventricular output
QRO   actual right ventricular output
QVO   rate of blood flow from veins into right atrium
RAM   basic vascular resistance of muscles
RAR   basic resistance of nonmuscular and nonrenal arteries
RBF   renal blood flow
RC1   red cell production rate
RC2   red cell destruction rate
RCD   rate of change of red cell mass
REK   percent of normal renal function
RFN   renal blood flow if kidney is not damaged
RKC   rate factor for red cell destruction
RMO   rate of oxygen transport to muscle cells
RPA   pulmonary arterial resistance
RPT   pulmonary vascular resistance
RPV   pulmonary venous resistance
RR   renal resistance
RSM   vascular resistance in muscles
RSN   vascular resistance in nonmuscle, nonrenal tissues
RVG   resistance from veins to right atrium
RVM   depressing effect on right ventricle of pulmonary arterial pressure
RVS   venous resistance
SR   intensity factor for stress relaxation
SRK   time constant for stress relaxation
STH   effect of tissue hypoxia on salt and water intake
SVO   stroke volume output
TRR   tubular reabsorption rate
TVD   rate of drinking
VAS   volume in systemic arteries
VB   blood volume
VEC   extracellular fluid volume
VG   volume of interstitial fluid gel
VGD   rate of change of tissue gel volumes
VIB   blood viscosity, ratio to that of water
VIC   cell volume
VID   rate of fluid transfer between interstitial fluid and cells
VIE   portion of blood viscosity caused by red blood cells
VIF   volume of free interstitial fluid
VIM   blood viscosity, ratio to normal blood
VLA   volume in left atrium
VP   plasma volume
VPA   volume in pulmonary arteries
VPD   rate of change of plasma volume
VPF   pulmonary free fluid volume
VRA   right atrial volume
VRC   volume of red blood cells
VTC   rate of fluid transfer across systemic capillary membranes
VTD   rate of volume change in total interstitial fluid
VTL   rate of systemic lymph flow
VTS   total interstitial fluid volume
VTW   total body water
VUD   rate of urinary output
VV7   increased vascular volume caused by stress relaxation
VVR   diminished vascular volume caused by sympathetic stimulation
VVS   venous vascular volume
Z8   time constant of autonomic response

Table C-1. Steady-State Values of Major Physiological Parameters in Modified Guyton Model

Parameter	Value	Parameter	Value
Blood volume, liters		Flow Resistances, mmHg/liter/min	
Right heart	0.109	Total peripheral	15.60
Pulmonary	0.413	Renal	83.39
Left heart	0.431	Leg (muscle)	96.31
Total cardiopulmonary	0.953	Non-renal, non-muscle	22.20
Upper artery	0.714	Large veins	0.60
Leg artery	0.146	Leg arteries (fixed)	0.95
Total artery	0.860	Leg veins (fixed)	0.35
Upper veins	2.750	Pulmonary	2.76
Leg veins	0.440		
Total veins	3.190	Body fluid volume, liters	
Total stressed volume	0.877	Blood	5.003
Total unstressed volume	4.126	Plasma	3.007
Total upper body volume	4.417	Red cell	1.999
Total leg volume	0.586	Interstitial	12.013
Total blood volume	5.003	Free fluid	0.545
		Gel	11.467
Blood pressure, mmHg		Total body water	40.038
Upper arterial	100.1	Extracellular	15.042
Leg arterial	99.3	Intracellular	24.996
Upper venous	4.55		
Leg venous	4.89	Metabolic rate, ml O_2/min	
Right heart	0.63	Nonmuscle, nonrenal	252.0
Pulmonary	18.87	Leg (muscle)	58.0
Left heart	0.97	Total	310.0
Compliances, liter/mmHg		Concentration, meq/liter	
Upper arteries	0.00265	Plasma sodium	142.0
Leg arteries	0.00112	Plasma potassium	5.00
Upper viens	0.07905	Plasma protein	70.1
Leg veins	0.00772		
		Hematocrit, vol.%	39.95
Blood flow, liters/min			
Cardiac output	6.47	Stroke volume, liters	0.088
Renal	1.20		
Leg (muscle)	0.98	Heart rate, beats/min	73.3
Nonrenal, nonmuscle	4.30		

tio upon standing which tends to reduce leg capillary pressure towards leg venous pressure. According to Mellander [8], this is an appropriate response to limit outward filtration of plasma in the erect posture.

C.2 Effect of Gravity on Pressure Gradients

The average hydrostatic pressure gradient in the legs (PG_L) due to gravity has been expressed as

$$PG_L = H_L \times F \times \sin\phi \qquad (C1)$$

where H_L is taken as the distance (in centimeters) from the heart to the knees. (The knee was used as a convenient reference point to find the average hydrostatic effect in a lumped leg compartment.) The term F converts pressure from centimeters water to millimeters mercury, whereas ϕ is the angle (in radians) of body tilt measured from the horizontal. The pressure gradient PG_L is introduced into the formulation for leg flow at the input to the leg arterial compartment, where it aids flow, and at the output of the leg venous compartment, where it opposes flow.

The gravity effect on the carotid baroreceptors must also be included since the tilt angle changes the hydrostatic pressure at these important sensors. The hydrostatic gradient at the baroreceptors is given by an equation similar to Eq. (C1) except that the term H_L is taken to be the distance between the heart and the carotid receptor. The
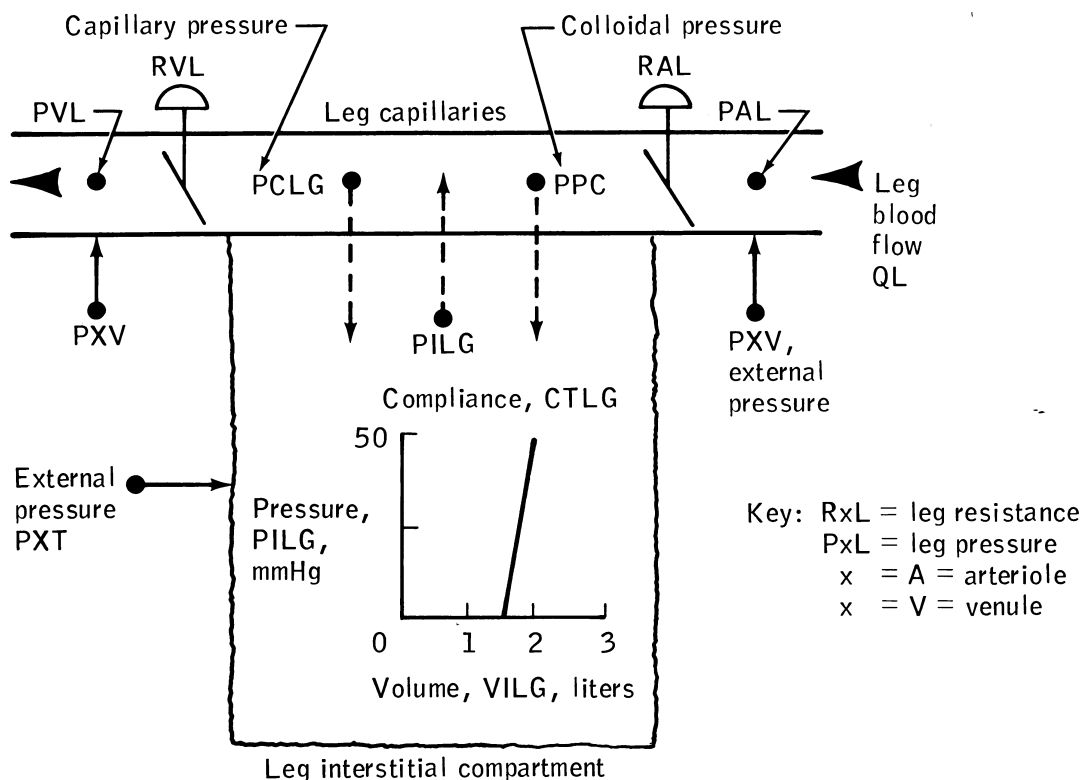
Figure C-2. Schematic diagram of leg filtration mechanisms.

pressure gradient so calculated is subtracted from the effective blood pressure sensed at the carotid body during a tilt simulation. Any angle of tilt may be simulated by adjusting ϕ, and other postures such as sitting may be studied by reducing the height H_L.

C.3 Venous Valves

The effect of venous valves has been added by permitting blood flow from the venous leg compartment to assume only positive values. Because this leg compartment can only be filled by arterial blood (rather than reverse venous flow from upper body veins), transient conditions can exist in which outflow to the veins is extremely low. This occurs, for example, during the onset of lower body negative pressure simulation. This situation was not possible in the original Guyton formulation.

C.4 Leg Plasma/Interstitial Filtration

A mechanism was added to permit plasma to filter into a new interstitial leg compartment. This mechanism is illustrated in Fig. C-2 in schematic form. Blood flow in the leg tissues is driven under an arterial-venous pressure gradient (PAL – PVL) across an arterial resistance RAL and a venous resistance RVL. The capillary pressure (PCLG) is computed as a function of upstream and downstream pressures and the precapillary/ postcapillary resistance ratio,

in accordance with the Landis–Pappenheimer formulation:

$$PCLG = RCLG * PAL + (1 - RCLG)*PVL$$

where $RCLG = RVL/(RVL + RAL)$. Filtration rate into the leg interstitium ($QLEG$) is based on the transcapillary hydrostatic pressure and oncotic pressure gradients multiplied by a leg capillary filtration coefficient ($CFLG$).

$$QLEG = (PCLG - PILG - PPC) * CFLG$$

where $PILG$ is the leg interstitial pressure and PPC is the plasma colloid osmotic pressure. It is assumed that interstitial colloid osmotic pressure is negligible. The value of $PILG$ is determined from the leg interstitial volume ($VILG$) and the tissue compliance ($CTLG$).

Because of the lack of detailed information regarding the leg tissues and tissue pressure changes during standing, this represents a highly simplified model of leg filtration having the following major assumptions.
1. Leg tissue fluid volume is equal to 1.5 liters in supine steady state.
2. Linear compliance permits tissue pressures to rise by about 40 mmHg during standing when the fluid volume is increased by approximately 500 ml because of plasma filtration. This large pressure increase is necessary to oppose excessive filtration because of the equally high change in capillary pressure.
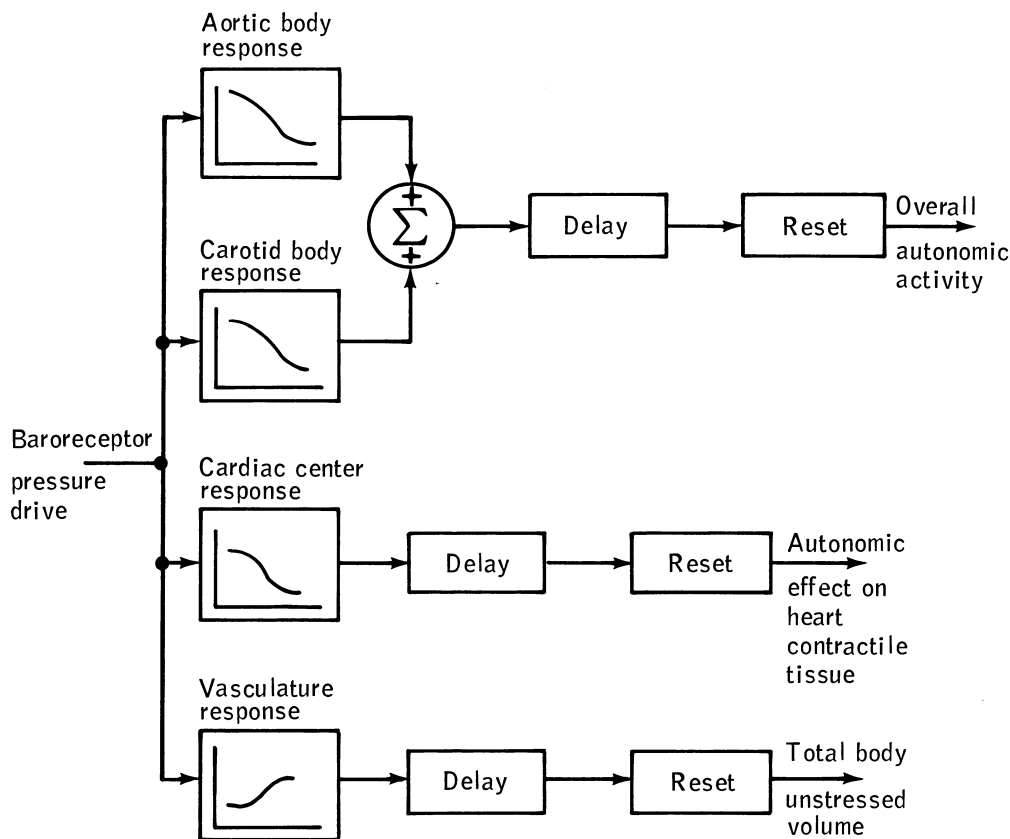
Figure C-3. Block diagram of baroreceptor system.

3. The effects of lymph flow, tissue colloidal concentration, and tissue gel have not been included.

The total resistance to blood flow through the leg muscle is given by the sum of the two variable resistances

$$RL = RAL + RVL$$

and the blood flow rate of the leg is taken to be the difference of pressure between the leg arteries (*PAL*) and veins (*PVL*) divided by the resistance

$$QL = (PAL - PVL)/RL.$$

C.5 External Leg Vascular Pressure

An external pressure term (*PXV*), shown in Fig. C-2, was included in the formulation for leg arterial and venous pressure, as was an external tissue pressure term (*PXT*). These terms are normally zero. By setting *PXV* and/or *PXT* to values less than zero, the effects of lower body negative pressure can be simulated. Values higher than zero will simulate various events such as positive pressure leg garments, water immersion, dehydration of the legs, and a muscle pump mechanism, all of which have the effect of

reducing venous leg blood volume and aiding in venous return during standing.

C.6 Vascular Stress Relaxation Effect

A term representing instantaneous stress relaxation was added to the stress relaxation block of the original model. This term appears as a constant factor (normally zero), which was found to be necessary to aid venous return during tilt simulation. In that case, reverse stress relaxation was used. Its physiological counterpart may be a combination of stress relaxation and the abdominal compression postural reflex, as well as a central venoconstrictor effect [9].

Stress relaxation of the vascular system was extended by the inclusion of new components with different time constants for action. These new components are associated with 6-hour and 14-day relaxation phenonmena.

C.7 Baroreceptor System

The baroreceptor system in the original Guyton model was changed by direct inclusion of separate aortic and carotid effects and by separate inclusion of the autonomic influence on both contractility of the heart and whole-

body unstressed volume. Appropriate delays and resetting mechanisms were used. A flow chart for the modified system is given in Fig. C-3.

C.8 Modified Red Blood Cell Production Algorithm

A new algorithm for red cell regulation was also implemented in the recompartmentalized Guyton model. This new block was based on the erythropoiesis regulatory simulation model previously described in Chapter 3 and 6. This model has greater capability than the blood cell subroutine in the original Guyton model, especially with respect to the simulation of hemopoietic responses to hypoxia, red cell infusion, and bedrest. A detailed description of this algorithm, as it appears in the modified Guyton model, is presented in Ref. [3].

The new red blood cell algorithm was based on a kidney sensor of oxygen partial pressure located in tissue of constant metabolic rate and perfused with venous capillary blood, flowing at a constant rate. These restrictions permit erythropoiesis to be responsive primarily to changes in hematocrit and arterial oxygen partial pressure, shifts of oxyhemoglobin dissociation, and disturbances in oxygen-carrying capacity of hemoglobin.

C.9 Renin-Angiotensin System

The original version of the Guyton model did not possess a detailed representation of the renin-angiotensin system. In particular, renin secretion as such was not present, and the model did not respond correctly to low-level angiotensin II infusion. This original model contained what was essentially a black box, with angiotensin level dependent on tubular sodium flow. To extend the range of applicability of the model, the black box was replaced with a more physiologically oriented section. A flow chart of the added system is contained in Appendix A (Fig. A-3). The new system improved the mechanism for releasing angiotensin into the circulation and permitted thirst and salt intake as well as renal afferent and efferent arteriolar resistances to depend on angiotensin levels.

C.10 Recommendations for an Improved Orthostatic Model

The addition of gravity dependent elements to the Guyton model, discussed in Chapters 3.2.5 and 9.6, provided new capability to simulate changes in postural positions. The cardiovascular model of Croston is capable of even greater realism for short-term orthostatic tests. However, the Guyton model, with a circulatory system open to fluid transfer with adjoining compartments as well as with the external environment, and long-term controllers is theoretically capable of longer-term simulations. In the current project, the Guyton model failed to achieve the robust blood pressure control during standing that is seen in the human subject. It also did not achieve a longer term steady state during standing. Additional modifications are there-

fore required in the Guyton model for longer-term orthostatic capability. The object of these modifications would be to produce a model capable of maintaining normal, healthy ambulatory function. It is our hypothesis that understanding the hypogravic state is predicated on a better understanding of the orthostatic state. The recommendations below may serve as a start in this direction.

Table C-2 and the associated Fig. C-4 illustrate a number of mechanisms that are believed to aid in orthostatic protection. Orthostatic protection insures that blood pressure levels are preserved at close to a normal level during standing. Some of these mechanisms have already been included in the Guyton model and are discussed in Chapter 9 and the first part of this Appendix. These include:

a) a leg tissue compartment that can normally receive about a half liter of plasma during standing;
b) a muscle contracting effect that decreases transmural pressure and decreases leg fluid pooling;
c) valves in the leg veins that allows blood flow to move only toward the central regions;
d) a passive distention effect at the leg veins affecting postcapillary resistance and decreasing leg filtration;
e) autonomic and angiotensin effects on leg arteriolar resistance which limits flow to the legs, raises arterial pressure, and decreases capillary filtration.

In addition, there are other suggested areas for model improvements as follows:

C.10.1 Factors Affecting Venous Capacitance

It is clear that a more faithful simulation of tilt requires a greater degree of compensatory venous return than was seen in the studies reported in Chapter 9. Venous return can be effectively enhanced in the model or in man by reducing capacitance of the central veins and perhaps leg veins. The mechanisms that are involved in these changes arise from centrally mediated high pressure and low-pressure baroreceptors in the upper body, from vasoconstriction hormones, and from local effects such as reverse stress relaxation and passive elastic recoil. Contraction of the leg and abdominal musculature, considered also to be important compensatory reflexes to orthostatic pooling, are probably mediated via central and local mechanoreceptors [10,11].

Observations on the behavior of the capacitance vessels in the human have been restricted to the limbs, but even here inconsistent results have been found during tilt studies [12]. It is not possible at present to determine whether changes in splanchnic blood volume are induced actively or passively, although this generally is considered to be an important fluid source during acute hypovolemia [13,14]. Boyers, *et al.* [15], using a model for tilt simulation, found it necessary to employ a low pressure autonomic input sensitive to central blood volume or pressure which acts, in part, on the veins to enhance venous return. Evidence for this effect is not yet strong [16]. The current version of the Guyton model does not include low pressure autonomic effects other than those used to influence ADH release. Perhaps a new autonomic reflex path-
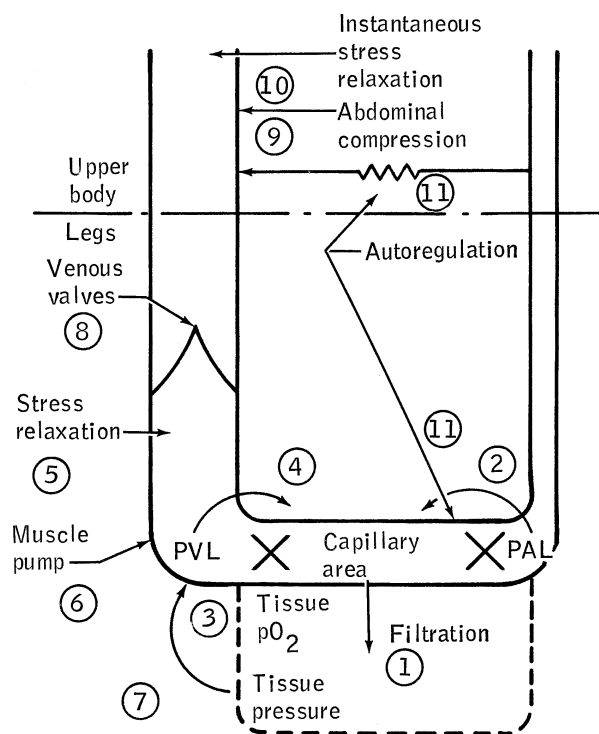
Figure C-4. Modifications for an improved tilt simulation. The numbers correspond to the elements in Table C-2. (PVL = Venous pressure in legs and PAL = arterial pressure in legs).

way, mediated by low-pressure receptors which influence venous resistance and capacitance, can be postulated and incorporated for future evaluation.

C.10.2 Stress Relaxation of Veins

In the erect position, reverse stress relaxation takes place in the large veins of the model following decrements of central blood volume. This may occur more rapidly and intensively than heretofore suspected according to recent evidence from Guyton's laboratory and others [17,18]. Such an effect greatly enhanced the present tilt responses reported in Chapter 9.6. Quantitative studies on the compensatory effects of stress relaxation and stress relaxation recovery following blood volume changes are meager [19]. It is important to ascertain where in the circulation it occurs. If stress relaxation has an influence on the smaller leg veins it would act in a direction to gradually increase blood pooling, as is known to occur during standing.

C.10.3 Pre- and Post-Capillary Resistance

Previous simulations with the Guyton model have led us to suggest that autoregulation effects (a mechanism which adjusts precapillary resistance to meet local oxygen demands) may be too strong and rapid in dampening peripheral resistance changes following intravascular fluid shifts either headward or feetward as occurs during postural changes. More recent studies on our part indicate that a more powerful influence on postcapillary resistance may be required rather than an attenuation of autoregula-

tion. Evidence for this hypothesis is only suggestive. Nevertheless, it is important to note that venous capacitance and venous resistance changes are theoretically independent in the model, but not necessarily in the human vasculature. Thus, any changes in the model that effect autonomic influence on capacitance, such as discussed above, should also be considered for their influence on postcapillary resistance. In addition, it is important to consider that under various conditions there may be a dissociation in the reflex changes of the (arterial) resistance and (venous) capacitance vessels due to competing control elements or perhaps redistribution of efferent autonomic signals [20,21]. The role of pre-/post capillary resistance takes on new importance in the Guyton model now that there are two distinct capillary beds. These elements have been implicated in the regulation of regional blood flow, number of patent capillaries, nutritional exchanges, plasma volume, and venous return.

C.10.4 Improved Leg Circulatory Elements

While the degree of fluid pooling in the legs appears to have been adequately simulated by the current model it should be realized that this is a preliminary study and that many factors which control fluid pooling, filtration and blood flow in the legs have not been included [22]. Fluid pooling in legs during standing is known to be reduced by the leg muscle pump, venous valves, autonomic vasoconstriction and humoral (angiotensin) mechanisms as well as by a buildup of fluid pressure in the interstitium [19]. All these effects have been included to some extent in the model. However, their mathematical representation was only estimated; quantitative data were mostly lacking. In addition, there is evidence for the presence of other major effects not presently included such as: a) catecholamine influence [23], b) postural sway [11], and c) myogenic vasoconstriction [21]. This latter effect acts in the face of high transmural pressures to increase precapillary resistance, induce sphincter closure and reduce filtration area. Several other effects are detrimental to orthostatic tolerance such as stress relaxation and passive distention of arteries and veins. These effects may be required for longer-term simulations. For example, it has been suggested that postural sway and the venous (muscle) pump are responsible for maintaining orthostatic tolerance during prolonged standing or minimal upright activity. An improvement in the leg muscle elements would do more than enhance the tilt response. Because of the large mass of the skeletal muscles, passive and active fluid mobilization, especially when reinforced by the mechanical effect of muscle contraction, provides the potential for large changes in capacity within the entire circulation during a wide variety of stress conditions.

C.10.5 Leg Interstitial Compartment

The leg interstitial compartment was modeled quite simply as a water reservoir with a linear compliance. For the present effort this appears to be adequate. However, absent from this formulation is a lymphatic system, a tissue gel, colloids and a nonlinear compliance, all of which

Table C-2. Mechanisms for Improving Fidelity of Tilt Simulations

Element Modification	Justification
1) Filtration of plasma between leg vasculature and interstitial fluid	Transfers about 300 – 500 ml plasma. The interstitial fluid volume increases during standing and decreases during supine.
2) Autoregulatory effect on leg capillary surface area	A local myogenic reflex that has been postulated to occur in response to increased leg hydrostatic pressures by decreasing effective capillary surface area. The effect is to limit the filtration of plasma.
3) Autoregulatory effect on leg venous resistance	Decreases venous resistance when standing and lowers capillary pressure. Although evidence is not strong for this effect, it appears to be necessary to prevent severe edema. The autoregulatory effect in the model with legs currently only affects arteriolar resistances.
4) Passive distention effect on leg veins	Decreases venous resistance proportional to the increase in hydrostatic pressure.
5) Stress relaxation of leg veins	Postulated mechanism similar to upper vein stress relaxation. It will not improve the short-term maintenance of blood pressure and venous return, but it will permit a more realistic gradual slow pooling of blood in legs and thereby improve bedrest and long-term standing simulations.
6) Muscle pump effect	Increases venous return from the legs and decreases leg pooling.
7) Effect of increasing leg tissue fluid pressure on transmural pressure of leg veins	Similar effect as the muscle pump, but is an automatic regulatory effect rather than a fixed parameter.
8) Venous valves	Slightly delays the rapid pooling of blood in legs by permitting leg blood flow in only headward direction.
9) Abdominal compression effect	Standing reflex that compresses splanchnic veins and releases a small quantity of stored blood. Effect is to restore venous pressure and enhance venous return.
10) Instantaneous stress relaxation (and reverse stress relaxation) in large veins	Allows rapid reverse stress relaxation in large veins during standing to enhance venous return. This effect was found to be necessary to simulate appropriate response to tilt, infusion and hemorrhage.
11) Short-term autoregulatory flow effect	Preliminary observations have shown that short-term autoregulation is too strong and too rapid. It does not allow flow resistances to decrease appropriately since it counteracts the central reflex vasoconstriction, so the effect was decreased.
12) O_2 consumption	During standing O_2 consumption increases by 10 to 20%. This increases autoregulatory flow and autonomic stimulation.
13) Renin-angiotensin response	Preliminary results showed that the renin response to the off transient to tilt was too slow. Angiotensin affects vessel constriction, urine flow, and aldosterone production. See text for recommendations.
14) ADH response	Preliminary results showed that the ADH response was not sustained as it is in the real system during tilt or zero-g
15) Cardiopulmonary autonomic response	Decreasing cardiopulmonary volumes are known to elicit autonomic responses during tilt, suggesting a low pressure receptor. The model currently has only high pressure receptors for volume and pressure control.

are important elements of the upper body tissue fluid compartment [24]. Data are not available to model a completely realistic distributed parameter interstitial compartment system.

C.10.6 Improvements in Endocrine Systems

This recommendation concerns improving the endocrine system of the Guyton model. The response to tilt of ADH, angiotensin, and aldosterone were in good agreement with available data. However, there are areas which can be immediately addressed that might improve responses to tilt and other stresses. First, it was noted that during the off transient to tilt, angiotensin did not fall as rapidly as it does in the tilt recovery of man [25]. This was believed to be due, in part, to the arterial pressure response which was unrealistically low for a short period and, in part perhaps, to an inadequate description of the renal pressoreceptor releasing site of renin. Several model descriptions have recently become available that would assist in improving this response [26,27]. Secondly, the aldosterone algorithm of the Guyton model has been recently revised [28], and it is suggested that if feasible, it be incorporated into the NASA/GE gravity dependent model. Finally, data has recently appeared which may allow a revision of the ADH algorithm. This concerns the ADH response to immersion and a quantitative description of the relative influence of blood volume and osmolarity on ADH concentration [29,30]. Unfortunately, there is still much conflict in the literature regarding the regulation and physiological role of ADH during postural changes both during short-term and prolonged studies [31].

C.11 Conclusion

A few other factors should be considered in an orthostatic model. Increasing the effects on cardiac contractility or heart rate on improving venous return have not been considered thus far in our studies. Also, in most individuals, orthostasis leads to syncope sooner or later during quiet standing. Some individuals are more prone to this, perhaps because of an inadequate sympathetic response. In the current project no attempt was made to model syncope, but it should be a future goal, especially in attempting to differentiate between individuals who are or who are not prone to syncope. Finally, it should be noted that many of the recommendations discussed above await more physiological studies (rather than mathematical definition) prior to developing algorithms for incorporating them into a model.

References

1. Guyton, A.C., Coleman, T.G. and Granger, H.J., Circulation: Overall Regulation, *Ann. Rev. Physiol.,* 34: 13–46,1972.
2. Guyton, A.C., Jones, C. and Coleman, T.G., *Circulatory Physiology: Cardiac Output and Its Regulation,* 2nd ed, W. B. Saunders Co., Phil. PA, 1973.
3. Leonard, J.I. and Grounds, D.J., S*tudy Report: Modification of the Long Term Circulatory Model for the Simulation of Bed Rest,* (TIR 742-LSP-7011, General Electric Co., Houston, TX) NASA CR-160186, NASA, Washington, D.C., 1977.
4. White, R.J. *A Long Term Model of Circulation: Final Report*, (General Electric Co., Houston, TX; TIR 741-MED-4021) NASA CR147674, NASA, Washington, D.C., 1974.
5. White, R.J., *Summary Report on a Basic Model of Circulatory, Fluid, and Electrolyte Regulation in the Human System Based Upon the Model of Guyton,* (TIR 741-MED-3042, General Electric Co., Houston, TX) NASA CR-160212, NASA, Washington, D.C., 1973.
6. Archer, G.T., *User's Instructions for the Guyton Circulatory Dynamics Model Using the Univac 1110 Batch and Demand Processing (With Graphics Capabilities)*, TIR 741-MED-4004, General Electric Co., Houston, TX, 1974.
7. McDonald, D.A., *Blood Flow in Arteries*, Williams and Wilkins Co., Baltimore, MD, 1960.
8. Mellander, S., Interaction of Local and Nervous Factors in Vascular Control, *Angiologica*, 8: 187–201, 1971.
9. Guyton, A.C., private communication.
10. Guyton, A.C., *Textbook of Medical Physiology*. 5th ed., W. B. Saunders Co., Philadelphia, PA, 1976
11. F. A. Hellenbrandt and E. B. Franseen, "Physiological Study of the Vertical Stance of Man, *Physiol. Review*, vol. 23, p. 220–255, 1943.
12. Shepherd, J.T. and Vanhoutte, P.M., Veins and Their Control, W. B. Saunders, Philadelphia, 1975.
13. Rowell, L.B., The Splanchnic Circulation, in *Physiology and Biophysics*, T. C. Ruch, H.D. Patton and A. M. Scher, Eds., W. B. Saunders, Philadelphia, 1974, Chapter 12, pp. 215–233.
14. Guyton, A.C., *Circulatory Physiology II: Arterial Pressure and Hypertension*, W.B.Saunders, Philadelphia, 1980, pp. 284–286,
15. Boyers, D.G., Cuthbertson, J.G. and Luetscher, J.A., Simulation of the Human Cardiovascular System: a Model with Normal Responses to Change of Posture, Blood Loss, Transfusion, and Autonomic Blockage, *Simulation*, 28: 197–206, 1972.
16. Zoller, R.P., Mark A.L., Abboud F.M., Schmid P.G., Heistad, D.D., The Role of Low Pressure Baroreceptors in Reflex Vasoconstrictor Responses in Man, *J. Clin. Invest.*, 51: 2967–2972, 1972.
17. Shoukas, A.A. and Sagawa, K., Control of Total Systemic Vascular Capacity by the Carotid Sinus Baroreceptor Reflex, C*irc. Research*, 33: 22, 1973.
18. Drees, J.A. and Rothe, C.F., Reflex Venoconstriction and Capacity Vessel Pressure-Volume Relationships in Dogs. *Circ. Res*., 34: 360, 1974.
19. Guyton, A.C., Jones, C.E. and Coleman, *T.G., Circulatory Physiology: Cardiac Output and its Regulation*, 2nd ed., W.B. Saunders Co., Philadelphia, 1973.
20. Epstein, S.E., Stampfer, M. and Beiser, G.D., Role of the Capacitance and Resistance Vessels in Vasovagal Syncope, *Circulation*, 37: 524–533, 1968.
21. Mellander, S. Interaction of Local and Nervous Factors in Vascular Control, *Symposia Angiologica Santoriana,* 3rd Int. Symp., Fribourg, 1970, Part I, Angiologica, 8: 59–73, 1971.
22. Rushmer, R.F., Effects of Posture, in *Cardiovascular Dy-

namics, 3rd ed., Saunders, Philadelphia, pp. 210–219, 1970.

23. Sundin, T., The Influence of Body Posture on the Urinary Excretion of Adrenaline and Noradrenaline, *Acta Physiol. Scand.*, 313: 1–57, 1956.

24. Guyton, A.C., Granger, H.J. and Taylor, A.E., Interstitial Fluid Pressure, *Physiol. Rev.*, 51: 527, 1971.

25. Oparil, S., Vassaux, C., Sanders, C. A., and Haber, E., Role of Renin in Acute Postural Homeostasis, *Circulation*, 41: 89–95, 1970.

26. Luetscher, J. A., Boyers, D. G., Cuthbertson, J. G., and McMahon, D.F., A Model of the Human Circulation: Regulation by Autonomic Nervous System and Renin-Angiotensin System, and Influence of Blood Volume on Cardiac Output and Blood Pressure, *Circ. Res.,* 32–33 (Suppl. I: Hypertension):184–198, 1973.

27. Blaine E.H., Davis J.O. and Harris P.D., A steady-state control analysis of the renin-angiotension-aldosterone system, *Circ. Res.,* 30: 713–730, 1972.

28. White, R.J., private communication.

29. Epstein, M., Pins, D.S. and Miller, M., Suppression of ADH During Water Immersion in Normal Man, *J. Appl. Physiol.*, 38: 1038–1044, 1975.

30. Dunn, F.L., Brennan, T.J., Nelson, A.F., and Robertson, G.L., The Role of Blood Osmolarity and Volume in Regulating Vasopressin Secretion in the Rat. *J. Clin. Invest*, 52: 3212–3219, 1973.

31. Kimura T., Minai K., Matsui K., Mouri T. and Sato T., Effect of Various States of Hydration on Plasma ADH and Renin in Man, *J. Clin. Endocrinol. Metab.,* 42: 79–87, 1976.

Appendix D
Design, Development, and Validation of the Whole-Body Algorithm

This Appendix contains a detailed description of the design, development, and validation of a model that, for reasons revealed in the discussion, has been termed a Whole-Body Algorithm (WBA). This discussion is meant to supplement that of Chapter 3.

D.1 Summary of Subsystems

The individual subsystem models used in this project were carefully selected and modified to simulate the response of a human subject to the stresses under investigation in the Skylab medical experiments. These models are summarized in the following paragraphs.

D.1.1 Long-Term Fluid and Electrolyte Subsystem Model

The long-term model of circulatory, fluid, and electrolyte control, originally developed by Dr. A. C. Guyton, has been substantially modified to include the most current formulations for many of the regulatory functions and implemented in an interactive time-sharing mode. The systems analysis of overall circulatory regulation, as developed by Guyton, includes a large number of the physiological subsystems that affect the circulatory system. This model consists of 354 blocks. Each block represents at least one mathematical function that describes an important physiological facet of circulatory regulation, including autonomic, metabolic, renal, hormonal, and fluid transport function.

The circuit of blood flow in the Guyton model is divided into five volume segments: system arteries, system veins, right atrium, pulmonary arteries, and pulmonary veins-left atrium. Exchange of water, proteins, and electrolytes (sodium and potassium) is permitted between the plasma, interstitial, and intracellular fluid compartments by way of diffusion, active transport, transcapillary exchange, and lymph flow. Heart function is represented in a high degree of detail, which includes ventricular muscle strength, heart hypertrophy and deterioration, and autonomic and sympathetic stimulation. These characteristics of the model can be viewed as the controlled system, whereas the controlling system consists of three major components: local control, hormonal control, and autonomic control. The inclusion of such elements as hormonal control, autoregulation, baroreceptor adaptation, erythropoiesis control, protein formation and destruction, venous stress relaxation, and cardiac-conditioning factors clearly indicates that the Guyton model was originally developed to serve as a long-term model, i.e., simulate long-term adaptive events.

Many and varied experiments have been simulated with the Guyton model, including some involving infusions of water, electrolyte, plasma, and angiotensin. Various pathologic conditions have also been simulated, including congestive heart failure, loss of kidney function, and nephritic proteinuria. The long-term simulation chosen as a test for the Whole-Body Algorithm was bedrest, because it appears to be a reasonable analog to zero-g. The addition of gravity-dependent stress factors and the inclusion of leg compartments in this subsystem greatly improved the subsystem's response to bedrest and weightlessness. Additional improvements were made by modifying the original algorithm for red blood cell control [1] (see Appendix C).

D.1.2 Cardiovascular Subsystem Model

A model of the human cardiovascular system capable of simulating bicycle-ergometry exercise was developed under this project by Dr. R. Croston. Subsequent modifications to this model were made to enable simulation of lower body negative pressure (LBNP) and tilt. The original model of the cardiovascular circulatory system was divided into 28 compartments, which described pulsatile blood flow, pressure, and volume. The model was modified to include gravity effects, muscle pumping, venous tone, venous valves, respiratory rate, and intrathoracic pressure. Heart-period control, peripheral resistance, venous tone, and other variables included in the new model were based on classical cardiovascular mechanisms. In addition, metabolic control mechanisms for oxygen uptake, for oxygen deficit, and for metabolite accumulation were included to enable simulation of metabolic changes. The feedback signals for the control algorithms in the model came from the chemoreceptors and from neurogenic response to muscular activity and to anticipatory stimuli. Exercise workload, work rate, gravity, resting oxygen consumption, and blood volume were required inputs. Typical outputs were oxygen uptake, oxygen deficit, total metabolites, heart rate, various blood flows, systolic pressure, mean arterial pressure, diastolic pressure, stroke volume, and venous pressure.

D.1.3 Respiratory Subsystem Model

The third major subsystem selected for inclusion in the Whole-Body Algorithm was the respiratory system. The model previously developed by Dr. F. Grodins was chosen as the best available (in 1975) representation. In this model, the controlled system is divided into three compartments (lung, brain, and tissue). The blood passes through the lungs, and, after a transport delay dependent on vascular volume and blood flow rate, the arterial blood arrives at the brain or the tissue compartment. In this model, carbon dioxide (CO_2) and oxygen (O_2) exchange rates are governed by metabolism. Venous blood leaving the brain combines, after a time delay, with venous blood from the

tissue to form mixed venous blood. After another delay, this mixed venous blood enters the lungs to complete the cycle of gas transport and exchange. The real system is composed of receptor elements that monitor chemical concentrations and of afferent nerves that transmit this information to the central nervous system, the neural centers, to motor nerves, and to the respiratory muscles that drive the thorax lung pump. In the model, conversely, this process is represented by chemical concentrations at receptor sites (which are inputs to the system) and by ventilation rate (which is the major controlled variable). Typical short-term stresses for which this model is suited include hypoxia, hypercapnia, and acid base disturbances. Modification of the original model provided the capability to simulate exercise.

D.1.4 Thermoregulatory Subsystem Model

A dynamic model of physiological regulation of body temperature, originally developed by Dr. J. Stolwijk and later modified slightly, basically accounts for the body's reaction to external temperature (environment) and for the effects of metabolic heat production (exercise). The controlled system consists of a representation of the thermal characteristics of the various body compartments. These compartments (or nodes) were designed to represent head, trunk, arms, hands, legs, and feet. These compartments were further divided into concentric layers designated as blood core, muscle, fat, and skin. Each node appropriately produces metabolic heat and also exchanges convective heat with adjacent compartments. The skin exchanges heat with the environment by way of radiation, convection, and evaporation. The thermoregulatory model receives temperature signals from all tissue compartments, and, after integration and processing, the control system sends commands to all appropriate compartments to change metabolic heat production, blood flow, or the rate of sweat secretion.

D.2 Design and Development

The Whole-Body Algorithm was designed to provide the capability of simulating long-term and short-term stresses with a single "master" model. The long-term simulation is accomplished by a circulatory, fluid, and electrolyte subsystem model, which may be used to provide initial operating conditions for a set of three short-term models representing the cardiovascular, respiratory, and thermoregulatory systems. These three short-term models, which are designed to simulate the response to acute changes both in the environment and in short-term experiment stresses, operate in parallel and interchange information as often as every 0.05 second of simulation time. Using this approach, a Whole-Body Algorithm evolved that could simulate with equal facility those adaptive changes occurring over a period of days, weeks, or even months and those experimental stresses in which significant changes might occur in a matter of seconds.

D.2.1 Approach to Whole-Body Algorithm

Since all subsystem models were designed as feedback control systems with identifiable controller elements,

they have a certain formal compatibility. The technical plan for integrating these subsystem models included verifying the subsystem modeling approach, verifying the compatibility of each subsystem model, providing for system expansion, and unifying the system software programs and languages and the subsystem computational approach. The plan also included identifying interfaces between subsystem models, providing uniform experimental checkout of each subsystem and of the assembled algorithm, examining all interfacing closed loops for stability, developing the executive program to control execution of the subsystems, and validating the Whole-Body Algorithm.

This plan led to development of a Whole-Body Algorithm that is limited only by the detail of the individual subsystem models, the lack of physiological experiment data to further refine the models, and the lack of knowledge regarding certain physiological phenomena. This model provides a basis for studying physiological phenomena and a basic model that can be refined as new parameters are recognized.

D.2.2 Subsystem Interfaces

The individual models have been described above in the form in which they were used in the Whole-Body Algorithm. In this section, the interfaces developed to represent the appropriate interaction between these subsystems are described. A diagram illustrating these interfaces is presented in Fig. D-1, where the interface variables are defined as shown.

The general philosophy of interfacing the subsystems was to combine the various models in a manner causing the least number of modifications to the basic model formulations, even at the cost of an occasional loss of computing efficiency. Since the units used in each model were substantially different, it was frequently necessary to convert the units of variables passed between models. The rule for the Whole-Body Algorithm was that conversion factors, where necessary, would be applied on the receiving end of the transfer. It is recommended that all future models be converted to a single set of consistent units.

D.2.2.1 Long-Term/Short-Term Interface.
Although technically the least difficult to accomplish, the long-term/short-term interface (Fig. D-1) was one of the most important in the Whole-Body Algorithm. This interface provided the capability to simulate the spaceflight event sequence (see Fig. 2-2). From the modeling viewpoint, the basic plan was to use the long-term model to initialize the short-term models for simulating any short-term experiments or transient environmental conditions. After steayd-state conditions were reached, the long-term model could be initialized for simulation of the subsequent long-term phase. Since the long-term/short-term interchange under this plan is sequential rather than simultaneous, the modeling problem consisted primarily of providing for the transfer of the interface variables through a common block and of modeling the mechanisms necessary to use these variables on either side of the interface in a physiologically representative manner.

CBF = trunk core blood flow
HBF = head blood flow
MBF = muscle blood flow
SBF = skin blood flow
RBF = renal blood flow
C0 = cardiac output
VO2 = oxygen uptake
RF = respiratory frequency
TC = trunk core temperature

PaO_2 = arterial oxygen partial pressure
$PaCO_2$ = arterial CO_2 partial pressure
RO2R = resting oxygen requirement
BV = total blood volume
UBV = total unstressed blood volume
IWL = insensible water loss
OHC = oxyhemoglobin concentration
HM = hematocrit
NBF = nonmuscle blood flow

Figure D-1. Subsystem interfaces of Whole-Body Algorithm.

A major problem encountered was the transfer of state variables between models lacking identical initial conditions. This particular problem manifested itself as a drift from control steady-state conditions in the models at the time of transfer. A procedure to solve this interface problem involved choosing a supine resting (but not basal) state as the initial condition. This state was assumed to exist before any short-term stress was initiated and is closely related to the passive zero-g state. To properly represent this state, all subsystem models had to be initialized to this state at the time of transfer by matching metabolic rates (equivalent to the resting supine oxygen uptake), initial blood volumes, and major blood flows.

An additional problem was caused by the creation of new environmental conditions by the short-term models. The long-term/short-term interface had to include the capability to reinitialize the long-term model with the steady-state values of variables computed by the short-term loop (insensible water loss, oxyhemoglobin concentration, and skin blood flow) after simulation of the environmental stress. Including this capability provides the structure for simulating the entire spaceflight sequence with environmental stresses performed throughout the interval. The next problem was to select, when simulating non-environmental stresses, the variables to exchange other than those required to represent transient environmental changes in the supine resting state. These variables should be direct functions of the long-term stresses being simulated and of the resultant hypotheses related to the level of physiological detail present in the models. By assumption, the short-term experimental stresses (other than environmental) would always include complete recovery to the state that existed before the stress. Hence, these stresses would not be allowed to perturb the long-term model.

The requirements for simulating bedrest made it necessary to identify important interfacing variables to more accurately simulate that condition. Bedrest is associated with the headward redistribution of blood and the resultant changes in blood volume, vasomotor conditions, hematocrit (due to plasma filtration), and blood flow through the major flow paths. Changes in total blood volume and total unstressed blood volume provide the necessary in-

formation to the short-term models for initializing blood volume and vasomotor changes (except tone changes, which were not considered in the initial bedrest hypothesis). Hematocrit was passed through the interface to provide the respiratory subsystem effect due to changes in red blood cell concentration. The blood flow changes in the renal, muscle, and non-muscle paths of the long-term model were passed through the interface to provide flow changes in the major flow paths of the short-term cardiovascular models. These flow changes are converted to a corresponding resistance changes and applied to the respective flow paths represented in the cardiovascular model. The renal blood flow changes was represented by a resistance change in the renal arterioles; the muscle blood flow changes was represented by a resistance change in the leg arterioles; and the non-muscle blood flow change was represented by a change in the resistance of the superior mesenteric artery. These hemodynamic changes were then reflected in the respiratory and thermoregulatory subsystems by way of the flow parameters in their respective interfaces with the cardiovascular subsystem during the simultaneous operation of these short-term models.

Model changes, other than those required to accommodate the variables passed through the interface as discussed previously, are associated with the specific hypotheses concerning the physiological changes that occur during bedrest. These modifications, as well as the requirements for additional variables to be passed through the interface to represent these specific hypotheses, will change as different hypotheses are considered. One value of the design approach selected for the Whole-Body Algorithm is the relative ease with which new interface pathways and hypotheses can be added and tested without total disruption of the system. These hypotheses and the required model changes are discussed in detail in Chapter 9. The hypotheses dealing with the occurrence of long-term rate changes and reverse stress relaxation during bedrest has been left in the Whole-Body Algorithm formulation. These points should be considered when repeating the simulation of bedrest with additional or different hypotheses.

It should be noted that all interfaces between the subsystems were designed for the simulation of the one-g response to the stresses of interest with the hypothesized physiological changes and responses as documented here. The assumption of different conditions, other stresses, other hypotheses, or other combinations of stresses and hypotheses would require the passing of additional or different variables through the interfaces. In most cases, additions to or improvements in the subsystem models would be required to accommodate the changes desired. The Whole-Body Algorithm was designed as a research tool to facilitate these structural changes.

D.2.2.2 Cardiovascular/Respiratory Interface. The interface between the cardiovascular and respiratory subsystems presented the most difficulty and, therefore, received the most attention. The difficulty was related to the physiological interaction and interdependence of these two short-term subsystems and to the fact that a larger

number of short-term stresses of interest to this project have responses manifested in these subsystems.

The initialized (resting) metabolic rate was different in each model, and this difference was the first problem encountered in the interacting of these two models. This problem was, in fact, encountered in all the model interfaces. The initial metabolic rate in the cardiovascular model was represented as a resting (non-exercising) oxygen uptake for an alert and ready subject. In the other models, the metabolic rate was initialized much closer to a basal rate. This problem was solved by using the resting oxygen requirement from the cardiovascular model to drive all subsystem models to a state of mutual equilibrium. Then the new state achieved was used as the initial conditions for subsystem models for all subsequent simulations.

The other interface elements of these two models were chosen to represent elements that changed significantly during the stresses of interest and that would significantly affect the subsystem model on the other side of the interface. The model having the better physiological representation of the variable of interest determined the direction in which these variables were passed. In most cases, this selection was made easily, since the counterpart variable of the interfaced subsystem model was generally represented non-physiologically or empirically in the other subsystem model. For example, respiration in the cardiovascular model was poorly represented by external pressure on the thoracic blood compartments. In some case, however, modifications in the receiving model were necessary to ensure proper model response to the passed variable, specifically when the receiving model had not been designed to respond to stresses generated in the sending model (e.g., the cardiovascular response to environmental stresses). For example, it was necessary to model changes in inspired gas concentrations where the model simulated the action of chemoreceptors, which are sensitive to changes in arterial partial pressures of oxygen and carbon dioxide. The chemoreceptor reflex was added to the cardiovascular subsystem model to ensure sensitivity to increases in carbon dioxide and decreases in oxygen in a manner similar to the baroreceptor response to changes in blood pressure. The premise for chemoreceptor control was derived from Scher [2] and is shown in Fig. D-2. The basic expression derived to produce the chemoreceptor autonomic reflex is

$$AUNC = 1.0 + (0.03448 \ \Delta pCO_2 - 0.016 \ \Delta pO_2)$$

where AUNC is the chemoreceptor autonomic effect and ΔpCO_2 and ΔpO_2 are changes in arterial carbon dioxide and oxygen partial pressures, respectively. Based on information from Duffin [3], it was necessary to limit the effect of the changes in arterial pCO_2 and arterial pO_2. Results of this study showed that the response of the carotid chemoreceptor was very low or zero for arterial pO_2 greater than 80 mmHg and for arterial pCO_2 less than 30 mmHg. The resulting autonomic factor was then applied to the calculations of peripheral resistance, heart rate, and strength of heart contractions in the manner depicted in
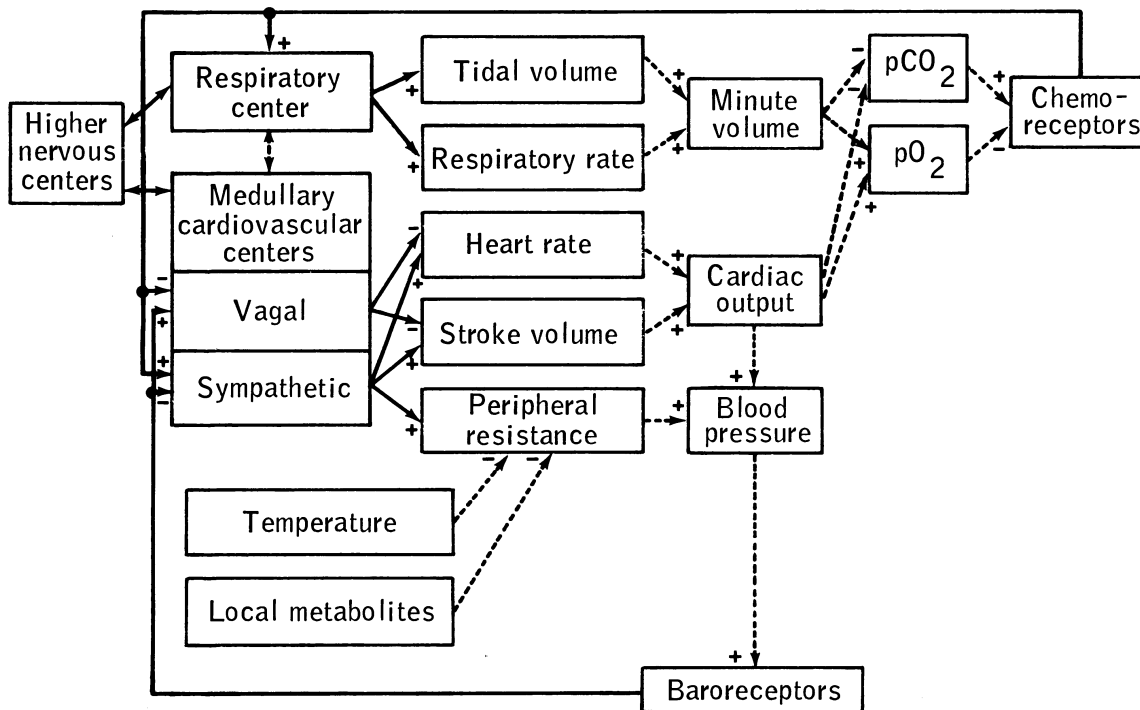
Figure D-2. Block diagram of autonomic control system. The major components of the cardiovascular and respiratory control systems are shown. A plus sign indicates that an increase in the input to a component increases its output; a minus sign indicates a decrease in output. When pressure rises at the baroreceptors, the sensory nerves will increase firing and there will be decreased firing in sympathetic fibers and increased firing in vagal fibers to produce vasodilation, decreased heart rate, decreased stroke volume, and decreased peripheral resistance. Decreases in heart rate and stroke volume will decrease cardiac output, which, combined with decreased peripheral resistance, will decrease blood pressure and, in turn, decrease pressure at the baroreceptors. An increase in arterial carbon dioxide partial pressure (pCO_2) or a decrease in arterial oxygen partial pressure (pO_2) at the chemoreceptors will increase the sensory discharge to cause decreased vagal and increased sympathetic activity, which will result in increased heart rate, increased stoke volume, and increased peripheral resistance. The heart rate and stroke volume increases produce an increase in cardiac output, which, combined with the increased peripheral resistance, increases the blood pressure. The combination of increased blood pressure and increased respiratory minute volume resulting from respiratory effects should produce increased transport of oxygen to the tissues.

Fig. D-2. These values in turn change blood pressure (which acts on the baroreceptors and closes a second feedback loop), as well as stroke volume and cardiac output. Cardiac output is passed to the respiratory subsystem model and thus completes the feedback loop across the interface.

The cardiovascular and respiratory subsystems, when initially exposed to exercise, responded in an unrealistic manner. It was noted, after all interface links were established, that a very good response from both subsystems was elicited for high exercise levels (150 to 200 watts) but that a poor response (worse than that for the stand-alone models) was elicited for the lower levels (100 watts and below). This problem was traced to a poor representation of the time-varying rate of oxygen uptake in the respiratory subsystem model. Since oxygen uptake is numerically integrated in the cardiovascular subsystem model (that is, the area to the left of the curve of oxygen uptake compared to time) to calculate oxygen deficit, a significantly different circulatory response resulted. An altered response would

be expected, in this case, because oxygen deficit affects many control functions in the cardiovascular model.

The studies of Whipp and Wasserman [4] indicate that variation of oxygen uptake with time for exercise levels greater than 100 watts cannot be represented accurately by the single exponential function used in the respiratory model (see Fig. D-3). Using this information, a new multiple exponential function for the higher exercise levels and an improved single exponential function for lower exercise levels were derived as shown in Fig. D-4 for 100 and 200 watts. Note that the curve for 200 watts, which is represented by multiple exponential function, breaks after approximately 2 minutes of exercise, as was indicated by the experimental data. This break corresponds to the anaerobic threshold, which is also indicated by the experimental data (Fig. D-3). When the exponential function (rate of change of oxygen uptake, or VO_2) is plotted on a semi-logarithmic scale, it becomes a straight line the slope of which is related to the time constant. Each exer-
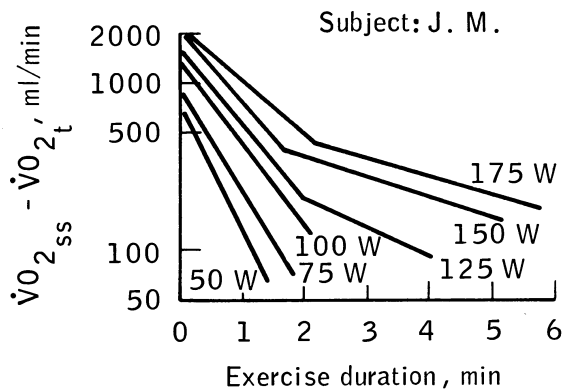
Figure D-3. Rate of change in oxygen uptake VO₂ as a function of exercise duration for selected workloads. The subscript ss indicates steady state; t indicates transient (from Ref. 4).

Figure D-4. New oxygen-uptake functions modeled in the respiratory subsystem.

cise level requires not only a different time constant but a minimum of two exponential functions to represent oxygen-uptake rates for exercise levels greater than 100 watts. The curves for this subject also show the anaerobic threshold to be very near the 2-minute mark of the exercise period for all levels above 100 watts. After these new oxygen-uptake functions were included in the respiratory subsystem model, the oxygen-deficit function in the cardiovascular model was tuned for these data and a good response from both subsystems was elicited for all levels of exercise (see Chapter 3).

D.2.2.3 Cardiovascular/Thermoregulatory Interface.
The principal functions of the thermoregulatory subsystem model are to simulate changes caused by variations in environmental parameters (for example, temperature, relative humidity, barometric pressure, cabin ventilation, clothing) and to simulate increases in metabolic production of heat (exercise). The function of the cardiovascular system, in the context of thermoregulation, is to provide a fluid medium for convective heat transfer away from tissues warmer than the blood and into tissues cooler than the blood.

The blood supply to the skin is of great significance to both cardiovascular and thermoregulatory subsystems. The skin exchanges heat with the environment through the pathways of radiation and convection. The amount of heat exchanged through these pathways is a function of the skin temperature and the various environmental factors mentioned previously. The temperature of the skin is determined through a heat balance of these environmental heat exchanges, through conduction to the adjacent fat compartment, and through convective heat exchange with the blood supply. The skin temperature acts in a feedback loop within the thermoregulatory subsystem, using the mechanisms of vasoconstriction and vasodilation to control the production of sweat and the skin blood flow. Therefore, since the skin blood flow is largely a function of the state of thermoregulation, the value for this parameter is computed and passed from the thermoregulatory subsystem to the cardiovascular subsystem. The other parameter passed from the thermoregulatory to the cardiovascular subsystem is the direct influence of temperature on heart rate. The temperature of pacemaker cells is known to influence heart rate. Since the thermoregulatory subsystem computes temperatures in the trunk core, this parameter is passed to the cardiovascular subsystem and is used to compute an additive term for the heart rate which is directly proportional to the change in temperature. Selkurt [5] indicates that the magnitude of this effect is approximately 13 to 20 beats/min °C.
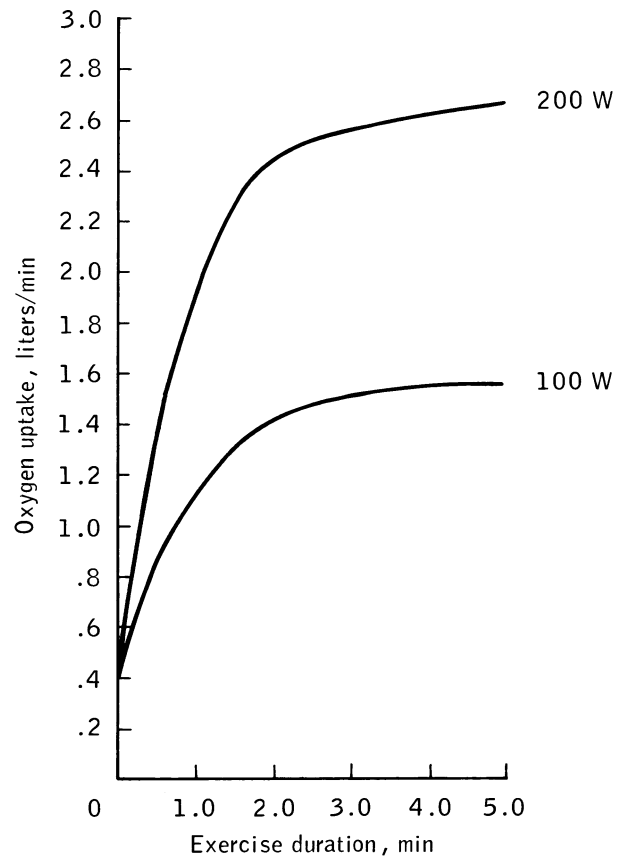
The remaining parameters of the cardiovascular/thermoregulatory interface are passed from the cardiovascular subsystem to the thermoregulatory subsystem (see Fig. D-1). The representation of the circulatory blood flow in the original thermoregulatory model was very crude and, therefore, caused significant inaccuracies in its response. These inaccuracies were expected to be relieved by interfacing the model with a fully developed cardiovascular model. This task was difficult, since the 28 blood-volume compartments of the cardiovascular subsystem had relatively little resemblance to the 40 geometrical body tissue compartments of the thermoregulatory subsystem. Correspon-

dence was found, however, between the two systems on a broader level. The blood flows that could be used directly from the cardiovascular model were the venous return from the brain and the sum of venous return flows from the heart, the kidney, and the liver. These two flow paths were used to replace the head core and trunk core blood flows, respectively, in the thermoregulatory model. The total muscle blood flow was passed from the cardiovascular to the thermoregulatory model as well. The muscle blood flow was distributed to various muscle tissues throughout the body, using the original distribution fractions in the thermoregulatory model as reported by Stolwijk [6] for rest and for bicycle-ergometry exercise. The remainder of the cardiac output was distributed to the remaining core and fat blood flows. This procedure provided a workable interface between the two models. However, in future studies, refinement of these blood flows using experimental data to acquire better representation of temperature distribution for the transient response to exercise is recommended.

A final variable passed from the cardiovascular to the thermoregulatory subsystem was the metabolic rate. This variable replaced an input parameter to the original thermoregulatory subsystem that had remained constant through an experiment. This refinement was required in the thermoregulatory model to improve the transient response to exercise. The arteriovenous oxygen difference computed in the cardiovascular subsystem included consideration of factors such as oxygen debt, oxygen deficit, and oxygen uptake in working muscle. These interface variables much more accurately represented the metabolic expenditures which resulted in the production of heat. The increase in metabolic rate from a basal to a resting state, as required by the design approach, was seen in the thermoregulatory model as mild exercise. Since metabolic heat generated during bicycle ergometry was distributed heavily to the leg muscles, adjustments had to be made to distribute the resting metabolic heat more equitably to other muscle compartments by using a distribution ratio proportional to the muscle mass fraction for each compartment.

An additional modification to the thermoregulatory subsystem was the addition of a countercurrent heat exchange formulation in the model's blood supply to improve performance in a cool environment. The new algorithm, as illustrated in Fig. D-5, represented the blood compartment as being in intimate thermal contact with the core compartments of the trunk, the arms, the legs, and the returning venous blood. These mechanisms are increasingly important in a cooler environment, where the venous return flows from muscle and skin are significantly cooler than the arterial blood supply.

In summary, the cardiovascular/thermoregulatory interface addressed the shortcomings of the cardiovascular model in the area of skin blood flow during exercise, the shortcomings of the thermoregulatory model in the area of blood flow rates, and the factors affecting metabolic use of oxygen. The principal result of an increase of skin blood flow in the cardiovascular subsystem was an increase in cardiac output, which, in turn, affected all other flows in the cardiovascular system. A primary benefit of this sub-

system interaction was that conditions of various levels of skin blood flow during exercise could be studied. With this combined model, the competitive effect of skin and muscle blood flow could be studied at various ambient temperatures for several levels of prolonged exercise and other conditions.

The chemoreceptor effect on the cardiovascular system and the respiratory system as well as the thermal-receptor effect on heart rate were bypassed during the exercise simulation. These effects, known to exist under abnormal conditions at rest, did not appear to be significant during exercise in normal environments. The reason for this apparent inconsistency during exercise and rest is not known. The importance of these receptors should be reevaluated if multiple stresses, such as exercise in hypoxic or hot environments, are to be considered.

D.2.3 Computer Program Architecture

Extensive planning for a software structure for the Whole-Body Algorithm was required before it could be implemented. Design considerations required a model capable of simulating long-term adaptive changes as well as short-term acute experimental stresses. The approach taken was to run the long-term model for the desired amount of adaptation time and to initialize the short-term models with its results. Then, the short-term models were executed simultaneously and, on completion of the short-term experiment, significant effects of the short-term stresses were passed back to the long-term model to provide for further simulation of the adaptive process.

This procedure furnished the structure whereby entire spaceflights could be simulated using the Whole-Body Algorithm. The total amount of computer core required for the Whole-Body Algorithm was 29,200 decimal words. To operate within the limits of a 20,000-word core size (in the time-sharing mode), it was necessary to overlay the program. In the overlay process, which is commonly used in the programming of operating systems, parts of the program are stored on mass storage devices (disks) until a specified portion of the program (a segment) is required during the execution. At that time, the segment is brought into core and used until another segment of the program is required. Using this technique, programs such as the WBA may have a total size that is much larger than the available core size. Communication between programs through common blocks enables the updating of variables that are changed during execution.

The second advantage of this approach was that whenever the Whole-Body Algorithm completed a short-term experiment, control was retuned to another segment brought into core. If the short-term models were called again, the programs were returned to core in their initialized state as updated by the long-term simulation. Therefore, a new short-term simulation could begin without memory of the past simulation. Such an approach assured that all computed variables were reset to their initial values without the need for additional computer programming.

To obtain synchronous operation of the short-term subsystems modes, an executive program was developed.

All variables are known except those on left-hand sides of the equations.
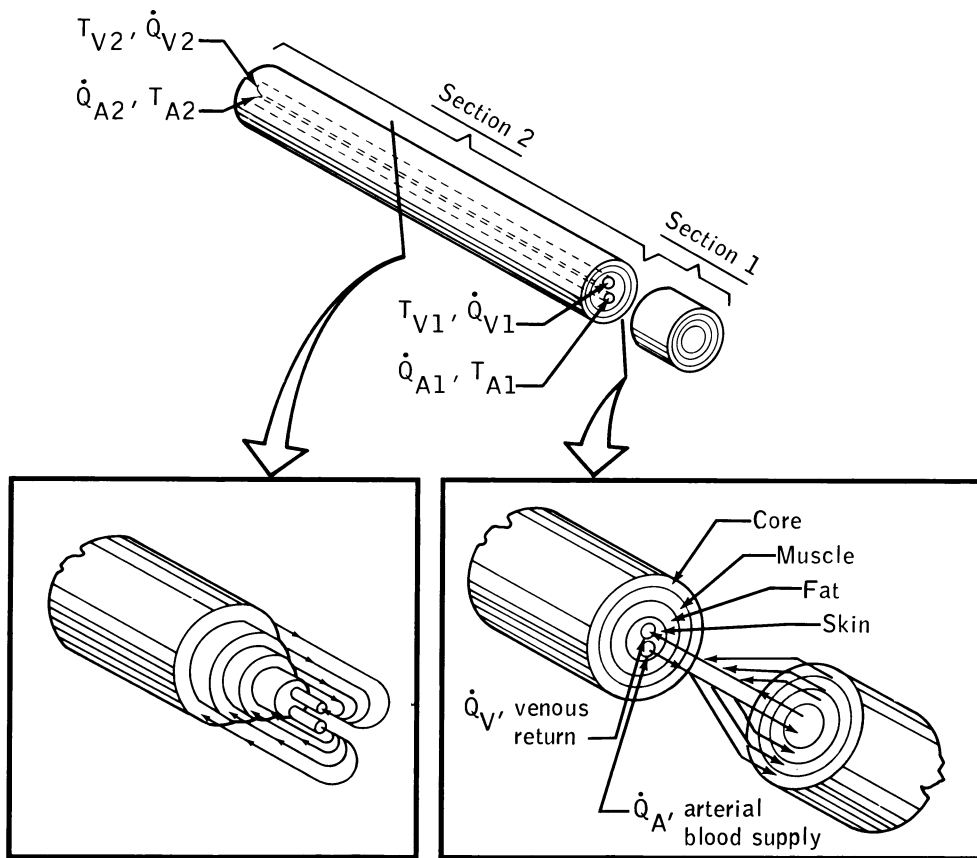
$$\dot{Q}_{V2} = \dot{Q}_{A2}$$

$$\dot{Q}_{V1} = \dot{Q}_{A1}$$

$$T_{V1} = \frac{\sum_{i=1}^{4}\left(BF_{i1}{}^{*}T_{i1}\right)}{\dot{Q}_{A1}}$$

$$T_{V2} = \frac{\sum_{i=1}^{4}\left(BF_{i2}{}^{*}T_{i2}\right)}{\dot{Q}_{A2} - \dot{Q}_{A1}}$$

$$CCH = \left(T_{V1} - T_{C1}\right){}^{*}\dot{Q}_{V1} + \left(T_{V2} - T_{C1}\right){}^{*}\left(\dot{Q}_{A2} - \dot{Q}_{A1}\right) + \left(T_{A2} - T_{C1}\right){}^{*}\dot{Q}_{A2}$$

$\dot{Q}_{V2}$ = blood flow rate (venous return, section 2)

T_{V1} = temperature of blood (venous return, section 1)

T_{C1} = temperature of core compartment, section 1

BF = blood flow

CCH = total countercurrent heat exchange

Figure D-5. Schematic diagram of countercurrent heat exchange.

The function of the executive program was to compare the value of time in the various subsystems and advance the time in the appropriate subsystem accordingly. The maximum difference in integration step sizes between the short-term subsystems occurred between the cardiovascular (0.002 second) and the thermoregulatory (3 second) models. It was possible for one subsystem to advance by several integration steps before another subsystem was advanced by even one step. Additional software details are contained in Ref. 7.

D.3 Validation Studies

From the outset, it was apparent that to obtain the idealized data set required to completely evaluate and validate the Whole-Body Algorithm would not be possible. A literature search revealed that very few transient data were available for any of the stresses, and responses to graded levels of stresses were not available for many of the cases considered; exceptions were a few easily measured variables such as heart rate and ventilation rates. Experimental studies documented in the literature were almost always concerned with only one major physiological system and entirely neglected other important systems. For example, investigators who reported cardiovascular responses to graded levels of environmental temperatures failed to measure body temperatures or ventilation rates. In many cases, it was impossible to obtain confirming data, and validation was based on a single source. The task of validating the Whole-Body Algorithm was more difficult than the validation of many other physiological models because it contains more subsystems, more parameters, and more dependent variables than other physiological models.

All the short-term stresses chosen for simulation were similar to those already used to validate at least one of the short-term subsystem models operated alone. A summary of the short-term models and the corresponding stresses for which they were tested on a stand-alone basis is shown in Table 3-8. If validation had been restricted to testing subsystems of the Whole-Body Algorithm that had been tested previously on a stand-alone basis, data collection and validation would have been simpler, since portions of the necessary data were available and documented. However, all the models were not previously capable of responding to all the stresses. The formulation of the Whole-Body Algorithm has increased the capability of each of these models and provided a basis, through the interfacing links and simultaneous operation of all the models, for simulating additional stresses in an integrative manner. For example, the thermoregulatory model has been previously validated for a thermal stress at rest; however, the respiratory and cardiovascular subsystem models had no capability until now, to simulate thermal stresses. Thus, it was necessary to attempt to locate a validation data set that included responses of these additional subsystems. Unfortunately, as previously discussed, physiological study of whole-body integrated responses to stresses is not usually undertaken and many of the desired data were unavailable. Nevertheless, a wide variety of responses have been tested and the overall capability and potential of the Whole-Body Algorithm is evident from the results presented in Chapter 3.

In a model as versatile and complex as the Whole-Body Algorithm, it is possible to test an endless variety and combination of situations, stresses, and parameter changes. To limit these tests to a reasonable number and still demonstrate the validity of the model, several guidelines were imposed as follows.

1. Only one stress at a time would be imposed on the model; multiple-stress validation simulations, such as exercise in a hot environment, would not be performed.
2. A number of relevant short-term stresses would be used to validate all three subsystem models in the short-term section of the model.
3. The long-term portion of the model would be validated with only a single stress.
4. The emphasis on validation would be in the steady-state domain, although the capability to simulate dynamic changes would be demonstrated.
5. The model would be capable of performing experiments of short duration with the short-term subsystems and of passing changes representing new physiological steady state to the long-term subsystem, yet this capability would not be validated. Rather, an attempt was made to determine long-term fluid-electrolyte changes or other adaptation effects which resulted from thermal stress, hypoxia, etc.
6. The reverse situation—automatically reinitializing the short-term subsystem models with changes resulting from a long-term stress—would be validated with a pre-and post-bedrest, exercise, and tilt stress following several simulated weeks of bedrest. This simulation would demonstrate the capability of the long-term subsystem to dynamically adapt through certain elements such as pressure-receptor resetting, autoregulation of blood flows, and stress relaxation.
7. During validation of the Whole-Body Algorithm no changes to the parameters of the model were permitted in order to create a better fit to the data beyond that already included in the stand-alone models prior to inclusion in the WBA.
8. The data sets used for validating the individual models could be used to verify that the integrated model responds in a reasonable manner similar to the stand-alone model response.

Table 3-9 is a summary of information related to the validation tests performed under these guidelines. The bedrest validation of the Whole-Body Algorithm is presented in Chapter 9.2 and will not be discussed further here. The following discussion is meant to supplement the simulations described in Chapter 3.

D.3.1 Simulation of LBNP and Tilt
D.3.1.1 Physiological Response to Tilt and LBNP.
The physiological changes that occur when an individual assumes the erect position provide a hemodynamic stress on the entire circulatory system. The capability of the vasculature, the heart, and the nervous system to appropriately react to this stress formed the basis of the tilt-table test and the Lower Body Negative Pressure (LBNP) test.

Upon shifting from supine to erect position, changes occur in circulatory pressures and flows as well as in blood volume distribution. The arterial, capillary, and venous pressures become markedly elevated in the dependent ex-

tremities to cause a net capillary filtration into the tissues. This filtration can result in a loss of 5 to 10% of the supine blood volume [8]. An additional 10% of blood volume is shifted from the upper part of the body (mainly from the thoracic cavity) to the legs, where it is pooled primarily in the distensible venous segments [9]. Venous segments below the heart tend to distend, whereas those above the heart tend to collapse. In the absence of compensatory mechanisms, the effective central venous pressure would probably fall below that of the heart and result in insufficient cardiac pumping and orthostatic hypotension.

The defenses of the body against orthostatic hypotension consist of both passive and active elements [8,10,11]. Ultrafiltration into the tissues is minimized by increase of tissue fluid pressure and lymphatic flow, reduction of the pressure level in the veins by enhanced muscle pumping, and transient venocontriction of the extremity venules. Systemic arterial pressure is maintained, and even elevated, by activation of intrathoracic and carotid blood pressure receptors. The reduction in effective central blood volume caused by a shift of blood from the upper to the lower part of the body is associated with a sustained increase in sympathetic activity to the resistance vessels in muscles and visceral organs and to the heart. This response maintains cardiac output and arterial blood pressure despite reduced cardiac filling pressure. The increase in leg vascular resistance also helps minimize venous pooling. Central venous pressure must be maintained to promote adequate right-ventricular filling.

The exact mechanisms controlling this adjustment have not yet been explained, but it is believed that three factors are important in preventing a debilitating fall in central venous blood volume and pressure: (1) contraction of large venous channels and venous reservoirs such as those in the visceral organs, (2) external compression of veins by skeletal muscles in the legs, and (3) an external pressure on the large abdominal veins exerted both by an increased hydrostatic pressure on abdominal organs and as an increase in abdominal muscular contraction. The net effects induced by standing or tilting and by the influence of the orthostatic defense mechanisms are a reduction in central blood volume, a decreased cardiac output due to reduced stroke volume (despite an increased heart rate), and an increase in peripheral resistance, which acts to elevate the mean systemic blood pressure [12]. Orthostatic hypotension develops when one or more of the compensatory mechanisms are not adequate.

Lower body negative pressure tests, in which an increased transmural pressure is created in the blood vessels below the waist, can also cause a considerable degree of venous pooling in the lower extremities, similar to that found in tilt-table experiments [13]. Other hemodynamic changes are also similar to the tilt response, such as decreases in cardiac output and stroke volume and increases in heart rate. However, investigators believe that there are certain fundamental differences between these two stresses [14,15]. The most important difference is that a hydrostatic gradient exists in tilt but not in LBNP. The tilt experiment causes a gravity gradient from the heart to the extremities in every vascular segment, with varying amounts of blood pooling. The quantity of pooled blood depends on the length of the segment and its distance from the heart. The effect of these two different kinds of stresses on the cardiovascular system will be evident in the following results. Lower body negative pressure has been used in experimental studies as a means of creating an effective "hemorrhage" in the central portions of the vasculature [16] as well as of providing a hemodynamic stress for crewmen in weightless spaceflight.

D.3.1.2 Simulation of LBNP/Tilt with the Whole-Body Algorithm. The tilt experiment is simulated in the short-term subsystem model by applying the gravity pressure gradient terms to the vascular compartments. The overall effect is a decrease in blood volume above the heart and an increase in all segments below this region. In simulating LBNP, a negative pressure term applied externally to the leg vessels increases the transmural pressure and results in a calculated increase in blood volume of the leg compartments.

The cardiovascular subsystem model contains representation of many of the elements previously discussed that are involved in the physiological response to tilt and LBNP. The model has elements that simulate the shift in blood from upper to lower segments of the body, the baroreceptor reflex and the resulting sympathetic effects on heart and vasculature, the muscle leg pump, venous valves, collapsible and distensible veins, and stress relaxation. Extravascular compartments are not represented in the short-term model, and hence, transcapillary filtration and lymph flow are not simulated. Such a limitation is not as restrictive as it would first appear for the following reasons. First, filtration into the tissues on standing is not rapid; the process requires as long as 30 minutes to reach a steady state [12]. Second, the baroreceptor reflexes are fully developed within the first minute following postural changes [10]. Third, most measurements of hemodynamic variables during LBNP and tilt ae usually completed within the first 5 minutes following the stress, well before the major effect of ultrafiltration is felt.

Furthermore, although tilting may result in extravasation of plasma, there is not conclusive evidence that the same is true during LBNP. Thus, the only real limitation that exists in simulating tilt is that the model's response should be compared to experimental measurements taken within several minutes after the stress is imposed.

Additional discussion of the physiology and simulation of postural change is presented in Chapter 9.6. Simulations of LBNP during spaceflight is discussed in Chapter 7.4.

D.3.2 Simulation of Respiratory Gas Disturbances: Hypoxia and Hypercapnia
D.3.2.1 Physiological Response to Hypoxia. An adequate supply of oxygen is essential to meet the varied metabolic requirements of every body cell. Oxygen transport from the inspired air to the individual cells involves many processes and organs, each with its own regulatory system. The essential components of the oxygen supply

system are ventilatory gas exchange, cardiovascular system function including cardiac pumping capability and blood flow distribution, hemoglobin affinity for oxygen, and hemoglobin concentration. All of these elements are present in the Whole-Body Algorithm in varying degrees of detail. In the normal subject, this complex system is adjusted to maintain an adequate tissue oxygen tension that meets the tissue requirements for the body as a whole. In the stressed individual in whom either metabolic requirements or oxygen supply are abnormal (as in exercise, hypoxia, or anemia), the system readjusts its oxygen supply capability to maintain adequate oxygen supply to the more critical organs such as the heart, the brain, and, in the case of exercise, the muscles tissue [17].

The most common experimental method to induce hypoxia consists of decreasing the oxygen content of the inspired gas. Since oxygen transport to the body cells is ultimately governed by diffusion, which is dependent on the partial pressure gradient, the critical indicator of oxygen level is its partial pressure (both in the inspired air and in the blood) rather than the absolute concentration (ml) O_2 per ml blood). Breathing air with less than normal oxygen will not cause noticeable effects either in pulmonary ventilation or in overall cardiovascular function until the inspired pO_2 level falls significantly from its normal value of 158 mmHg (corresponding to an inspired oxygen concentration of 21%). Thus, mild acute hypoxia is not considered a strong stimulus for physiological response [18]. Acute inhalation of 8 to 10% oxygen results in moderately severe hypoxia. Some of the more noticeable acute physiological effects are a sharp increase in pulmonary ventilation and a large rise in heart rate as well as in cardiac output [19]. The small changes in blood pressure that accompany this stress suggest that considerable vasodilation has occurred [20]. Little quantitative information is available for man regarding the redistribution of blood that results in overall peripheral vasodilation. In general, blood is believed to be shunted to tissues with high oxygen extraction (heart, muscle, and brain) at the expense of flow to tissue with low oxygen extraction (skin, viscera, and kidney). Severe hypoxia results in a reflex bradycardia and a significant and large vasoconstrictor effect. Because the WBA is not capable of simulating severe hypoxia, these extreme effects are not discussed herein.

The body has developed a complex of regulating systems that are integrated both at the central nervous system (CNS) level and at the local organ level. It is generally accepted that the hypoxia-induced increase in ventilation is a direct result of a decreased arterial pO_2, causing increased peripheral and central chemoreceptor activity [3]. Much less is known about the determinants of the accompanying cardiovascular changes. For many years, it was believed that the chemoreceptors were mainly responsible for stimulating most of the cardiovascular effects of hypoxia (or hypercapnia), but such a view is no longer tenable. The effects of chemoreceptors and other factors on the heart, the resistance vessels, and the capacitance vessels are shown in Fig. D-6 [2,19,21,24]. Figure D-7 is a schematic view of the integration of these factors during

the hypoxic or hypercapnic stress. It is obvious that the chemoreceptors provide only a part of the control necessary to withstand a decrease in oxygen supply. The actual degree and direction of cardiac and vasomotor behavior depend on the degree of hypoxia, the particular vascular bed, the animal species under investigation, and the relative influence of these competing local, autonomic, and hormonal factors. It is experimentally difficult to separate the various autonomic effects, and little quantitative information is available regarding the relative influence of these determinants in man.

A complicating factor that must be considered is that under the influence of low blood pO_2, the respiratory minute-volume output increases and, consequently, carbon dioxide is expired in greater than normal amounts. Thus, hypoxia is usually associated with hypocapnia, which is know to cause variation in central nervous activity, often in a direction that minimizes some of the cardio-respiratory effects of hypoxia [22,25].

D.3.2.2 Physiological Response to Hypercapnia. Carbon dioxide is a substance that is normally inspired in extremely small quantities (approximately 0.3 mmHg partial pressure). However, because large quantities of CO_2 are produced in the body by cell metabolism, the partial pressures in the blood are relatively high (approximately 40 and 46 mmHg) in arterial and venous blood, respectively). Blood carbon dioxide is one of several important chemicals used by the body to indicate local and overall rates of metabolism. These agents appear in various feedback pathways that adjust vascular resistance and blood flow to supply sufficient oxygen to meet the demand and to carry away toxic products of metabolism. During acute hypercapnic stress, the resting individual is confronted with an unfavorable environment for elimination of metabolic carbon dioxide and must therefore increase minute ventilation. The body responds to acute carbon dioxide inhalation in many ways. For example, it responds as if metabolism has suddenly increased, such as it would in exercise or as if an accumulation of metabolites has occurred by local occlusion of blood vessels. Besides the ventilatory response, other changes observed are an increase in blood pressure, heart rate, stroke volume, and cardiac output with a decrease in overall vascular resistance [26]. Except for the marked increase in blood pressure, the overall response to hypercapnia is similar to those previously described for hypoxia. Unlike oxygen, which does not appear to cause significant whole-body responses until its blood partial pressure has been reduced to about 40% of normal levels, the response to carbon dioxide is more linear and dramatic changes can be observed when blood pCO_2 changes only slightly from normal physiological values [3].

Although the *ventilatory* response to hypoxia and hypercapnia have been well studied and essentially understood (primarily a chemoreceptor-activated response), few studies of the *cardiovascular* effects of these disturbances, particularly for carbon dioxide inhalation, have been reported. Except for the brain (which is under local rather
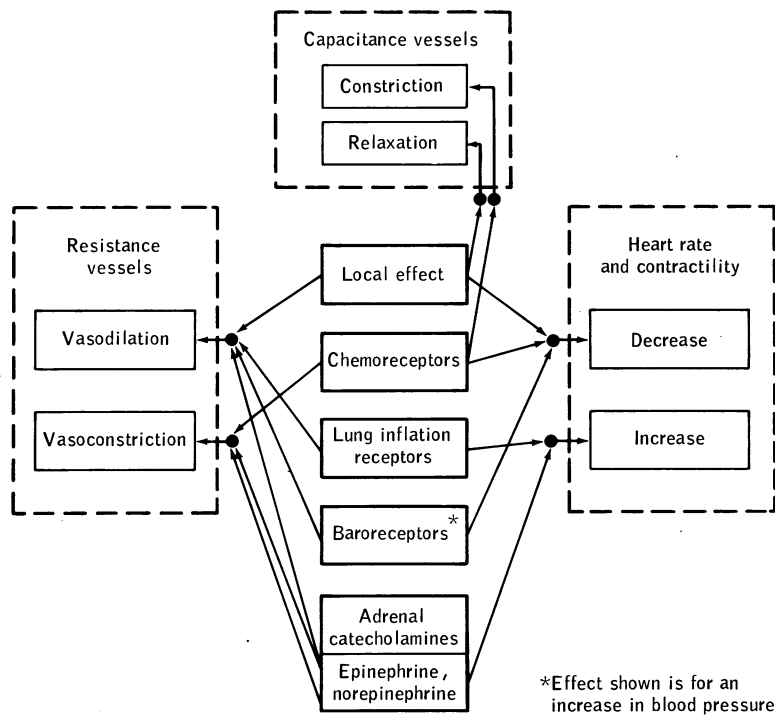
Figure D-6. Determinants of cardiovascular regulation during hypoxia and hypercapnia.
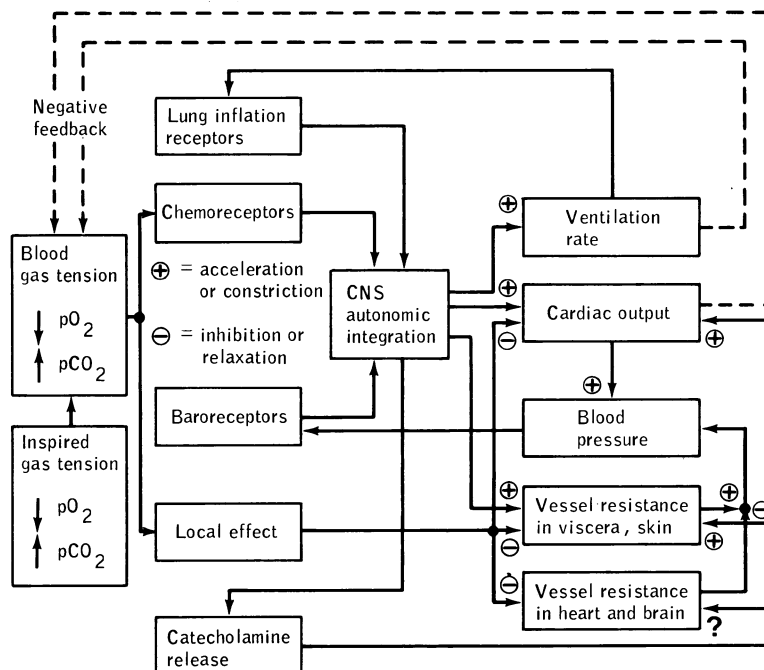
Figure D-7. Integrated cardiorespiratory regulation during hypoxia or hypercapnia.

than autonomic control), little attention has been paid to blood flow redistribution during hypercapnia.

It appears that the same mechanisms activated by breathing oxygen-poor mixtures are also activated by increase in carbon dioxide levels and act in very much the same way, but here, also, little quantitative information is available in man [22]. The scant attention paid to changes in the cardiovascular system during hypercapnia represents a severe challenge to modeling. For example, although peripheral blood flow resistance is known to decrease during hypercapnia, the mechanism is not clear. The few available studies in man have suggested that only the brain and heart are known to vasodilate [26].

D.3.2.3 Simulation of Hypoxia and Hpercapnia with the Whole-Body Algorithm.

The respiratory model was capable of simulating reasonable ventilatory responses to hypoxia and hypercapnia before its incorporation into the Whole-Body Algorithm. The controlling mechanism was a chemoreceptor sensor responding to low levels of oxygen and high levels of carbon dioxide. However, the cardiovascular subsystem model was not capable of responding to change in blood gas tensions, and additional modeling was required to account for this effect. In attempting to cope with the lack of qualitative data regarding mechanisms controlling the cardiovascular system and with few previous modeling guidelines to follow, it was decided that only a gross approximation of the real system was justified.

The first major assumption was that the feedback systems (Figs. D-6 and D-7) responding to low levels of oxygen responded to increasing levels of carbon dioxide in the same qualitative manner. For example, it was assumed that both hypoxia and hypercapnia produce a local vasodilating effect and a depressant effect on the heart. Although all the evidence is not yet available to support this assumption in its entirety, there is little evidence to contradict it. The second major assumption was that, for the purposes of this preliminary study, it would be possible to lump many of these effects into an effective "chemoreceptor" feedback pathway. The sensor of this pathway would have a graded response to increasing arterial levels of carbon dioxide and decreasing levels of oxygen. This response is similar to the response of the ventilatory system chemoreceptors. The appropriate sensitivities of these new chemoreceptors to each of the gases would depend on available data regarding integrated effects in the intact animal. The actual level of oxygen and carbon dioxide tension in the blood at any moment would be obtained from the respiratory model that had previously been shown to provide good agreement with published studies. In terms of the elements shown in Fig. D-6, the cardiovascular "chemoreceptror" was used to represent a combination of local effects, chemoreceptor effects, lung inflation reflex, and adrenal catecholamine effects. The baroreceptor representation in the model was not changed and could function independently of the "chemoreceptor." This configuration in the Whole-Body Algorithm is summarized in Fig. D-2.

To appropriately simulate the data available for hypoxia and hypercapnia in normal resting man, it was necessary to allow the chemoreceptors to affect heart rate, cardiac contractility, muscle flow resistance, renal flow resistance, and the resistance of flow through bone and fat in a manner generally seen in experimental animals. Since the sensitivities of the chemoreceptors to oxygen and to carbon dioxide were not the same, these feedback pathways were not expected to respond identically for both hypoxia and hypercapnia.

Brain blood flow was a variable already controlled by the respiratory subsystem model, and no changes were necessary in that section of the model. A chemoreceptor effect on coronary and skin blood flow was not included, despite data that demonstrated changes in these organs. Since their basal flow was small compared to cardiac output, it was felt that their effect on the overall system would be minimal.

Hypocapnia and hypoxia were simulated simply by changing the values of the parameters representing inspired air concentrations of oxygen, carbon dioxide and nitrogen.

D.3.3 Simulation of Thermal Stress
D.3.3.1 Physiological Responses to Thermal Stress in Resting Man.

If a resting man is exposed to a hot environment for short periods, changes are observed not only in the thermal regulating system but in other major physiological systems as well, notably the circulatory and ventilatory systems. Indeed, in a strict sense, all of these subsystems act as a functional unit to reduce the thermal stress on the body. Sweating, insensible heat loss from the lungs, redistribution of blood flows (notably to the skin tissues), and cardioacceleration all are manifestations of thermoregulation and require a multiple system of regulatory loops [27,28].

The effects of heat exposure are first manifested by an increase in skin temperature. As further heating takes place, the temperatures in all deep tissue masses tend to increase. In response, the body makes several adjustments (Fig. D-8) that act to remove this excess heat load and reduce its effects. These changes are discussed in the following paragraphs.

Blood flow through skin tissue increases as a result of both local and centrally mediated effects. Increased skin blood flow brings greater quantities of warm blood to the body surface, where its thermal energy can be transferred through the skin and, ultimately, by radiation and conduction to the environment. The normal skin blood flow of 150 to 200 ml/min can increase to 3500 ml/min and perhaps higher under maximum vasodilation [29]. The increase in skin blood flow tends to increase skin temperatures. If the environment is warmer than the body surface (that is, if ambient temperature is greater than 32° to 34°C, the body will gain heat by conduction and radiation; if cooler, it loses heat. Radiation is usually the more important route of heat exchange.

Because of the reduced or negative temperature gradient between skin and surroundings, circulatory adjustments alone are not adequate for dissipating heat by radiation at ambient temperatures above 32° to 34°C. At

Core temperature ← Skin temperature → Conduction and radiation

Central autonomic integration

Thermoregulatory, cardiovascular, and respiratory effectors

Sweating and evaporation

Skin blood flow

Skin flow resistance

Splanchnic and renal flow resistance

Peripheral resistance

Heart rate

Cardiac output

Minute volume

Pulmonary evaporative loss

——— Direct or reflex effects
- — - Final feedback effects

Figure D-8. Integrative physiological regulation of thermal stress at rest.

these temperatures, sweating is initiated; evaporation of the sweat removes heat from the body surface. Evaporative heat loss by sweating is a particularly effective cooling mechanism. Maximum sweating levels of nude resting man approach 400 ml/hr at ambient temperatures of 48°C. This maximum sweating level represents 270 watts of cooling power [30]. At these high temperatures, sweating and pulmonary water loss becomes the only avenues of heat loss. A humid environment and clothing decrease evaporation of sweat and increase the heat load, whereas an increase in free-air velocity on the skin decreases the heat load. The major circulatory change appears to be a shift of blood flow from central circulation to peripheral vasculature.

In resting man, renal, hepatic, and splanchnic flows have been observed to decrease (by some as yet unknown mechanism) when he is exposed to severe heat stresses, whereas skin blood flow increases [31]. This readjustment of arteriolar resistance elements results in a decreased peripheral resistance.

Heart rate has been observed to increase gradually with increasing body temperatures; this increase probably results from autonomic stimulation from the thermoregulating centers. This effect on the heart, together with the decrease in peripheral resistance, results in an increase in cardiac output by as much as 80% [28,32]. No striking changes in stroke volume (or blood pressure) have been seen, despite a tendency for increased myocardial contractility [33].

The major response of the respiratory system to thermal stress is an increase in minute volume. Whether this effect is directly related to temperature is not know, but the effect is gradual and mild until deep body temperatures are increased from the normal value by more than 1° to 1.5°C, where marked increases in minute volume have been demonstrated [34]. The great effectiveness of the overall thermoregulatory system is such that, during rest, the core temperature is unlikely to rise more than 1°C even when ambient temperatures are increased by 30°C [35].

D.3.3.2 Simulation of Thermal Stress with the Whole-Body Algorithm. The thermoregulatory subsystem model contained the major thermoregulatory elements, and it was capable of accurate and detailed simulation of thermal

stress in resting man even before it was integrated into the Whole-Body Algorithm. For example, it contained elements for conduction, radiation, sweating, skin blood flow regulation, shivering, and insensible pulmonary water loss. However, except for skin blood flow, the cardiovascular segments of the stand-alone model were only crudely developed and had no capability of simulating important cardiovascular parameters such as blood pressure, peripheral resistance, heart rate, and stroke volume. It was felt that the pulsatile cardiovascular model, when joined with the thermoregulatory model, would contribute this information as well as improve the cardiovascular portion of the thermoregulatory subsystem. Conversely, the thermoregulatory model's description of skin blood flow regulation during heat stress was markedly superior to the same formulation in the pulsatile cardiovascular model. As discussed previously, there are thermal effects on the cardiovascular system besides skin blood flow regulation. These effects concern resistance changes in visceral organs and thermal effects on heart rate. Compared to the available data relating heart rate to deep body temperature [30,32,34,36], little information was available concerning blood flow redistribution in response to changes in ambient temperatures. Consequently, only the former effect has been introduced in this version of the Whole-Body Algorithm. These and other changes have been described in detail earlier in this appendix. The effect of temperature on ventilation has been omitted from the model because this factor is not important for the ambient temperatures of interest in the preset studies [34].

The simulation of an environmental thermal stress was accomplished by changing values of the ambient dry-bulb input parameter. Wall temperatures, affecting the radiant elements of heat transfer, were also adjusted to be equal to the dry-bulb temperature, and wet-bulb temperature was set to correspond to a relative humidity of 35%.

References

1. Leonard, J.I., Kimzey, S.L. and Dunn, C.D.R., Dynamic Regulation of Erythropoiesis: A Computer Model of General Applicability, *Exper. Hematology*, 9:355-378, 1981.

2. Scher, A.M., Control of Arterial Blood Pressure, *Physiology and Biophysics*, Ruch, T.C., Patton, H.D. and Scher, A.M. (Eds.), Ch. 10, W. B. Saunders Co. (Philadelphia, PA), 1974, pp. 146-169.

3. Duffin, J.,The Chemical Regulation of Ventilation, *Anaesthesia,* 26:142-154, 1971.

4. Whipp, B.J. and Wasserman, K., Oxygen Uptake Kinetics for Various Intensities of Constant-Load Work, *J. Appl. Physiol.*, 33(3):351-356, 1972.

5. Selkurt, E.E., *The Renal Circulation, Handbook of Physiology*, Sec. 2: Circulation, vol. 2, W. F. Hamilton and Philip Dow, Eds., Ch. 43, American Physiological Society (Washington, D.C.), 1963.

6. Stolwjik, J.A.J., *A Mathematical Model of Physiological Temperature Regulation in Man*, Final Report, Contract NAS 9-9531, NASA CR-1855, 1971.

7. Marks, V., *User's Instructions for the Whole Body Algo-rithm*, (General Electric Co., Houston, TX; TIR 741-MED-5009), NASA CR-1855, NASA, Washington, D.C., 1971.

8. Piemme, T.E., Body Fluid Volume and Renal Relationships to Gravity*, Hypodynamics and Hypogravics—The Physiology of Inactivity and Weightlessness*, Michael McCally, Ed., Ch. 5, Academic Press (New York, NY), 1968, pp. 133-161.

9. Sjostrand, T., Volume and Distribution of Blood and Their Significance in Regulating the Circulation, *Physiol. Rev.*, 33(2):202-228, 1953.

10. Guyton, A.C., Jones, C.E. and Coleman, T.G., *Circulatory Physiology*: *Cardiac Output and Its Regulation*, 2nd ed., W. B. Saunders Co. (Philadelphia, PA), 1973.

11. Rushmer, R.F., Effects of Posture, *Cardiovascular Dynamics*, Ch. 7, 2nd ed., W. B. Saunders Co. (Philadelphia, PA), 1961, pp. 171-192.

12. Lamb, L.E., Circulatory Problems in Prolonged Space Flight, *Hypodynamics and Hypogravics—The Physiology of Inactivity and Weightlessness*, Michael McCally, Ed., Ch. 6, Academic Press (New York, NY), 1968, pp. 163-179.

13. Wolthuis, R.A., LeBlanc, A., Carpentier, W.A. and S. A. Bergman, Jr., Response of Local Vascular Volumes to Lower Body Negative Pressure Stress, *Aviat. Space & Environ. Med.*, 46(5):697-702, 1975.

14. Wolthuis, R.A., Bergman, S.A. and Nicogossian, A.E., Physiological Effects of Locally Applied Reduced Pressure in Man, *Physiol. Rev.*, 54(3):566-595, 1974.

15. Blockley, W.V., Identification of a Fundamental Inadequacy in LBNP as a Circulatory Challenge in Deconditioning Assessment, *Preprints of the 1970 Annual Scientific Meeting of the Aerospace Medical Association*, 1970, pp. 67-68.

16. Murray, R.H., Thompson, L.J., Bowers, J.A. and Albright, C.D., Hemodynamic Effects of Graded Hypovolemia and Vasodepressor Syncope Induced by Lower Body Negative Pressure, *American Heart J*., 76(6):799-811, 1968.

17. C. A. Finch, C.A. and Lenfant, C., Oxygen Transport in Man, *New England J. Med*., 286(8):407-415, 1972.

18. Dripps, R.D. and Comroe, J.H.,Jr., The Effect of the Inhalation of High and Low Oxygen Concentrations on Respiration, Pulse Rate, Ballistocardiogram and Arterial Oxygen Saturation (Oximeter) of Normal Individuals, *Amer. J. Physiol*, 149(2):277-291, 1947.

19. Abramson, D.I., *Circulation in the Extremities*, Academic Press (New York, NY), 1967.

20. Kontos, H.A., Levasseur, J.E., et al., Comparative Circulatory Response to Systemic Hypoxia in Man and in Unanesthetized Dog*, J. Appl. Physiol.*, 23(3): 381-386, 1967.

21. Shepherd, J.T., *Physiology of the Circulation in Human Limbs in Health and Disease*, W. B. Saunders Co., (Philadelphia, PA), 1963.

22. Sagawa, K., Overall Circulatory Regulation, *Ann. Rev. Physiol.*, 31:295-330, 1969.

23. Hatcher, J.D. and Jennings, D.B. (Eds.), *Proceedings of the International Symposium on the Cardiovascular and Respiratory Effects of Hypoxia*, Hafner Publishing Co. (New York, NY), 1966.

24. Korner, P.I., Integrative Neural Cardiovascular Control, *Physiol. Rev.*, 51(2):312-367, 1971.

25. Reynolds, W.J. and Milhorn, H.T., Jr., Transient Ventilatory Response to Hypoxia With and Without Controlled Alveolar

PC O$_2$, *J. Appl. Physiol.*, 35(2):187-196, 1973.

26. Richardson, D.W., Wasserman, A.J. and J. L. Patterson, Jr., General and Regional Circulatory Responses to Change in Blood pH and Carbon Dioxide Tension, *J. Clin. Invest.*, 40:31-43, 1961.

27. Benzinger, T.H., Heat Regulation: Homeostasis of Central Temperature in Man, *Physiol. Rev.*, 49(4):671-759, 1969.

28. Thauer, R., Circulatory Adjustments to Climate Requirements, *Handbook of Physiology*, Sec. 2, Circulation, Vol. III, W. F. Hamilton and Philip Dow, Eds., Ch. 55, American Physiological Society (Washington, D.C.) 1963, pp. 1921-1966.

29. Rowell, L.B., *The Splanchnic Circulation, Physiology and Biophysics*, Ruch, T.C., Patton, H.D., and Scher, A.M. (Eds.), Chap. 12, W. B. Saunders Co. (Philadelphia, PA), 1974, pp. 215-233.

30. Selkurt, E.E. (Ed.), *Physiology*, 3rd ed., Little, Brown and Co., (Boston, MA), 1971.

31. Rowell, L.B., Brengelmann, G.L., Blackmon, J.R. and Murray, J.A., Redistribution of Blood Flow During Sustained High Skin Temperature in Resting Man, *J. Appl. Physiol.*, 28(4):415-420, 1970.

32. Wyss, C.R., Brengelmann, G.L., et al., Temperature, *J. Appl. Physiol.*, 36(6):726-733, 1974.

33. Rowell, L.B., Brengelmann, G.L. and Murray, J.A., Cardiovascular Responses to Sustained High Skin Temperature in Resting Man, *J. Appl. Physiol.*, 27(5):673-680, 1969.

34. Saxton, C., Respiration During Heat Stress, *Aviat. Space & Environ. Med.*, 46:41-46, 1975.

35. Stolwjik, J.A.J. and Hardy, J.D., Temperature Regulation in Man: A Theoretical Study, *Pfluegers Arch.*, 291(2):129-162, 1966.

36. Damato, A.N., Lau, S.H., et al., Cardiovascular Response to Acute Thermal Stress (Hot Dry Environment) in Unacclimatized Normal Subjects, *Amer. Heart J.*, 76(6):769-774, 1968.

Appendix E
Sensitivity Analysis: A Simulation Technique with Application to the Human Thermoregulatory System Model

Analysis of the effects of parameter variation on the output (dependent) functions of a mathematical model can be important in predicting errors that may occur when designing technological control systems and in understanding the importance of specific parameters in biological systems. One of the simplest ways of understanding the response of a model system to parameter variation is called sensitivity analysis.

The conceptual basis of sensitivity analysis is straightforward. Small variations are made in the values of the system parameters of a model, and the effects of these changes are observed in the dependent variables during a simulation procedure. Following this step, sensitivity functions (described later) that describe the observed effects are computed. Such functions contain a considerable amount of information about the dynamic system under investigation. The most important use of sensitivity analysis is to determine the relative influence of different parameters on the system's response. This information is useful in assessing the validity of a model without the need for extensive model-to-data comparison studies and in guiding experimenters toward the investigation of the most important parameters in a real system.

The literature of physiological systems contains few examples that illustrate the formal application of sensitivity analysis, especially with regard to large-scale models [1,2]. The studies of ecological systems by Miller [3,4] provided the framework for the present study. Several texts are devoted exclusively to sensitivity analysis [5,6], but their sensitivity analysis is applied to nonbiological systems.

This appendix consists of a discussion of methods to compute sensitivity functions and contains examples of the manner in which these functions can be used to obtain meaningful information about a complex mathematical model of human thermoregulation. A more detailed study is available [7].

E.1 Theoretical Background

E.1.1 Definition of Sensitivity

Consider a model with an output (dependent) function y, which depends also on a (normally fixed) parameter q. Let y^o be the reference (or normal) value of y obtained when $q = q^o$, and let Δy represent the change in y that results from a change in q to $q^o + \Delta q$. The incremental sensitivity coefficient is defined as

$$\Delta S = \frac{\Delta y}{\Delta q} \tag{E1}$$

and the differential sensitivity coefficient is defined as

$$S(t,q) = \frac{\partial y(t,q)}{\partial q}$$
$$= \lim_{\Delta q \to 0} \Delta S \tag{E2}$$

when this limit exists.

The term sensitivity function is often used instead of sensitivity coefficient to emphasize that S is not always constant but is dependent both on time t and on the value of q. In this appendix, S will be considered the mathematically rigorous definition of sensitivity, whereas ΔS will be an approximation. Values for S (or ΔS) may be obtained by several methods, both analytically and numerically, but the primary interest here will be on a numerical approach.

E.1.2 Supplementary Behavior

The simulation of any model usually involves determining the supplementary motion that results from a parametric disturbance. Sensitivity analysis can provide a convenient method for determining supplementary behavior. Supplementary behavior is defined as the difference between the varied behavior of the system $y = y(t, q + \Delta q)$ and the fundamental behavior (or reference solution) of the system $y^o = y(t, q)$. Thus,

$$\Delta y = y(t, q + \Delta q) - y^o \tag{E3}$$

Eq. (E3) can be expanded by a Taylor series. By neglecting higher order terms, it can be reduced to

$$\Delta y = S(t,q)\Delta q \tag{E4}$$

In the general case for a system with m parameters, the analogous form is

$$\Delta y(\Delta q_i,...,\Delta q_m) = \sum_{i=1}^{m} S_i \Delta q_i \tag{E5}$$

This important relationship allows one to predict the behavior of a system following a parametric variation using simple algebra and without the necessity of performing a simulation. However, knowledge of the sensitivity function, or sensitivity functions, is required. In many cases, this method of analyzing supplementary behavior is often more convenient than a direct simulation of the varied system.

E.1.3 Methods of Determining Sensitivity Functions

Assuming that the equations describing the dynamic system are known and are easily differentiable, sensitivity equations can be derived on the basis of the definition given by Eq. (E2). In practice, the system equations and the sensitivity equation are solved simultaneously on an analog or a digital computer. The solution to the sensitivity equations consists of the sensitivity coefficients. The sensitivity equations are generally linear even if the original system is nonlinear. For a system with n variables and m parameters, there are $n \times m$ sensitivity coefficients that may be obtained from a solution of the sensitivity equations. For large-scale systems, the derivation and the solution of the sensitivity equations become somewhat impractical; more straightforward numerical methods can be used to obtain the sensitivity functions.

In those cases where neither the analytic solution nor the explicit formulation of the sensitivity equations is readily obtainable, an empirical method is available. This technique involves varying a single parameter by a small increment about its normal value and performing a single computer simulation. The sensitivity coefficient is obtained by comparing the value of the output variable from this run with its value during a run in which none of the parameters are perturbed from their reference positions. For the general case having m parameters q_i (where $i = 1, \ldots, j, \ldots, m$) and q_j as the particular parameter of interest, the incremental sensitivity function that describes the change in y due to the variation Δq_j is given by

$$\Delta S_j\left(t, \Delta q_j\right) = \frac{y\left(t, q_j + \Delta q_j\right) - y\left(t, q_j\right)}{\Delta q_j} \quad \text{(E6)}$$

If a parameter is perturbed by a small amount (for example, 1%) and the sensitivity function is sufficiently smooth, the value of ΔS_j determined from Eq. (E6) will be approximately equal to the true sensitivity coefficient defined by Eq. (E2). This method requires that each sensitivity function S_i ($i = 1, \ldots, m$) be determined by a separate simulation during which only a single parameter is perturbed.

E.1.4 Logarithmic Sensitivity Coefficients

An alternative approach to sensitivity analysis is one that uses the function

$$\bar{S}_j = \frac{\partial \ln y}{\partial \ln q_j}$$

$$= \frac{q^\circ_i}{y^\circ} S_j \quad \text{(E7)}$$

where $\bar{S}_j$ is called the logarithmic sensitivity coefficient (function). Note that $\bar{S}_j$ may be approximated by the ratio of $\Delta y / y^\circ$ to $\Delta q_j / q^\circ_j$ in the same way that S_j is approximated by the ratio of Δy to Δq_j. If $\bar{S}_j$ is known, then the percent change in the output variable y is given by $\bar{S}_j$ multiplied by the percent change in parameter q_j.

Once the sensitivity functions are determined for each parameter, it is possible to estimate the variation in y for any combination of parametric changes. Let U_i be defined as the fractional change of a parameter from its normal value

$$U_i = \frac{\Delta q_i}{q^\circ_i}$$

$$= \frac{q_i - q^\circ_i}{q^\circ_i} \quad \text{(E8)}$$

Equation (E5) can be rewritten using the definitions given in Eqs. (E7) and (E8) as follows.

$$\Delta y / y^\circ = \sum_{i=1}^{m} \bar{S}_i\left(\Delta q_i / q^\circ_i\right)$$

$$= \sum_{i=1}^{m} \bar{S}_i U_i \quad \text{(E9)}$$

Solving this expression for y yields fewer parameter disturbances.

$$y\left(t, \Delta q_i, \ldots, \Delta q_m\right) = y^\circ\left(1 + \sum_{i=1}^{m} \bar{S}_i U_i\right) \quad \text{(E10)}$$

This result allows the value of y to be computed easily for any number of single- and multiple-parameter changes, so long as these changes are small, in some sense. The agreement between the values of a response variable y as predicted by Eq. (E10) and those predicted by a complete model system has been found to be surprisingly good even when parameter values are changed by 100%, when highly complex models are used, or when highly nonlinear models are used [7]. The deviation becomes more pronounced as the operating point moves farther from the normal value because Eq. (E5) does not include the higher order terms of the Taylor expansion. These terms can become increasingly significant for larger perturbations.

The sensitivity coefficient defined by Eq. (E1) or (E6) depends on the total deviation of the parameter (Δq) from some normal value and the time or time period for which the sensitivity coefficient is computed. If the system is in a steady state, the sensitivity coefficient no longer depends on time. When the system under study is highly nonlinear or when the value of a parameter may vary within broad limits, sensitivity analysis can be difficult. When the dynamic system has many parameters ($q_1, q_2, \ldots, q_m$) with values not known to a high degree of accuracy, the difficulty will be compounded, since sensitivity functions may depend on the particular values of all parameters. In the general case, the sensitivity coefficient $S(t, q_1, q_2, \ldots, q_m)$ is a quantity associated with every point of parametric

space (i.e., every operating point) and changes with the position of the point. Thus, it is essential to carefully define and specify the times and parameter limits that are of primary interest.

E.2 The Performance Criterion

In many cases, when dealing with a model having many dependent variables, it is desirable to define a single measure of overall system performance. Such a measure, which can be called a *performance criterion*, could be extremely useful in performing sensitivity analysis and parameter estimation. Then, the effects of multiple-parameter variations can be related to changes in this single variable rather than in a large number of dependent variables. However, the definition of a performance criterion is not straightforward, since it depends on the purpose for which the simulation is performed and on subjective judgments.

If Y is the performance criterion selected, then the measure of deviance, as defined by Miller [3], is of the form

$$D = f(Y - Y^\circ)$$

where Y° is the normal value of Y. Note that Y itself may depend on one or all of the system parameters. The measure of deviance D can be subjected to sensitivity analysis in the same way as other system variables. The sensitivity coefficients are obtained by forming the partial derivatives $S_i = \partial D/\partial q_i$, where q_i ($i = 1, \ldots, m$) are the m parameters of the system. Approximate values of S_i can be found by the method of parameter variation previously described following Eq. (E6). Thus,

$$\Delta S_i = \frac{D(q_i + \Delta q_i) - D(q_i)}{\Delta q_i}$$
$$= \frac{D(q_i + \Delta q_i)}{\Delta q_i} \tag{E11}$$

Note that the value of $D(q_i)$ is zero by definition. The number of sensitivity coefficients of a large-scale system of n dependent variables and m parameters is reduced from $m \times n$ to m when a single performance criterion is used as a measure of overall system behavior since S_i is computed only for the variable D.

Although the choice of an overall performance criterion of a model is somewhat arbitrary, experience has provided certain guidelines in its formulation. These are discussed in the following paragraphs.
1. An overall performance criterion is a function of one or more of the systems dependent variables. This function is usually (but not necessarily) one of the following forms or a combination of them.

$$D = \sum_{j=1}^{n} |e_j| \tag{E12a}$$

$$D = \sum_{j=1}^{n} e_j^2 \tag{E12b}$$

$$D = \sum_{j=1}^{n} \left| \frac{e_j}{Y_j^\circ} \right| \tag{E12c}$$

$$D = \sum_{j=1}^{n} \left(\frac{e_j}{Y_j^\circ} \right)^2 \tag{E12d}$$

where Y_j° is the value of the performance criterion in the unperturbed case at some time t_j, Y_j is the corresponding value of the performance criterion in the simulation of interest, and $e_j = Y_j - Y_j^\circ$. The functions of Eqs. (E12a) through (E12d) are similar to the error criteria, or goodness of fit criteria, used in parameter estimation. In parameter estimation analysis, the parameter values of a simulation model are adjusted until model response agrees with the experimental data according to a specified criterion function. In these cases, the term $Y - Y^\circ$ is the difference between the model response and the experimental response. Because of these similarities, the techniques of sensitivity analysis can be used advantageously in parameter estimation [7].
2. The choice of variables used in forming the performance criterion should be related to the most important variables of the system or to a combination of variables that are representative of some index of overall behavior. This choice could, of course, change as the objectives of the simulation study change. For example, the Guyton model of circulatory regulation has been extremely valuable in elucidating the mechanisms that control long-term fluid volumes and blood pressure changes. Although the Guyton model contains more than 300 dependent variables, it is conceivable that a meaningful performance criterion can be formulated from only two variables, arterial blood pressure and extracellular fluid volume, since all the other variables are known to exert some influence on these two. It would be possible and is sometimes desirable to construct a performance criterion that gives more weight to one variable than another and also gives different weights to the transient and steady-state responses. Miller [3] has shown that a number of reasonable, but different, choices for the performance criterion all produce very similar results in a particular example. He states, "generally a balanced measure of all the output variables is more successful, and it is unwise to use one single output variable as a 'general indication of model behavior.'"
3. The value of D should be zero when there is no perturbation of parameters and should be positive otherwise.
4. The performance criterion chosen should correlate well with other possible performance measures and with intuitive estimates of model change.
5. The variables chosen to formulate D should be capable of easy and accurate measurement in the labora-

tory, even though these experimental measurements are not used in sensitivity analysis. The first reason for this requirement is that the results can be more easily interpreted and their validity judged if the behavior of these variables in the real system is known for certain situations. The second reason is that sensitivity analysis can be a very powerful tool for selecting those parameters for parameter estimation and this latter technique does depend very heavily on experimental measurements. The measure of deviance can be used in the same form in sensitivity analysis as the error criterion in parameter estimation analysis.

Although the discussion of performance criteria has been with regard to a mathematical model's behavior, these functions are useful from a clinical medicine viewpoint as well. For example, maximum oxygen uptake has long been used as a measure of a cardiopulmonary function under stress. It would be possible to use simulation models of various subsystems to examine other variables or combinations of variables as overall indices of subsystem behavior. The methods described in this appendix would provide preliminary criteria. The most promising of these could then be subjected to clinical trials.

In the next section, the usefulness of the performance criterion in sensitivity analysis will be developed by applying these techniques to a complex human thermoregulatory model.

E.3 An Example of Sensitivity Analysis

In this section, some of the techniques of sensitivity analysis will be applied to a complex model of the thermoregulatory system that has been described in Chapter 3 of this document. For simplicity, the steady-state version of the model will be used exclusively. This means that static sensitivity coefficients will be determined and parametric sensitivity during transient states will not be considered. The following presentation is not meant to be a complete sensitivity analysis but, rather, is suggestive of the type of analysis that might be performed.

E.3.1 Computing Sensitivity Coefficients

A traditional analysis of parametric variation is illustrated in Fig. E-1, in which the effects of metabolic rate RM (exercise) on certain important variables have been plotted. Table E-1 contains definitions of the symbols used in this model. Similar figures using other parameters for the abscissa such as TCAB, TW, PCAB, and VCAB could be prepared.

The sensitivity coefficients $S_i = \partial y_i/\partial RM$ (where y represents any variable) could be generated by computing the slope of the curves shown. Since the slopes are somewhat steeper at the lowest values of RM, the sensitivity coefficients are different at either end of the abscissa. For this reason, sensitivity coefficients are usually related to a perturbation from a specific operating point. Two operating points will be considered in this example, characterized by the input parameters shown in Table E-2. The first
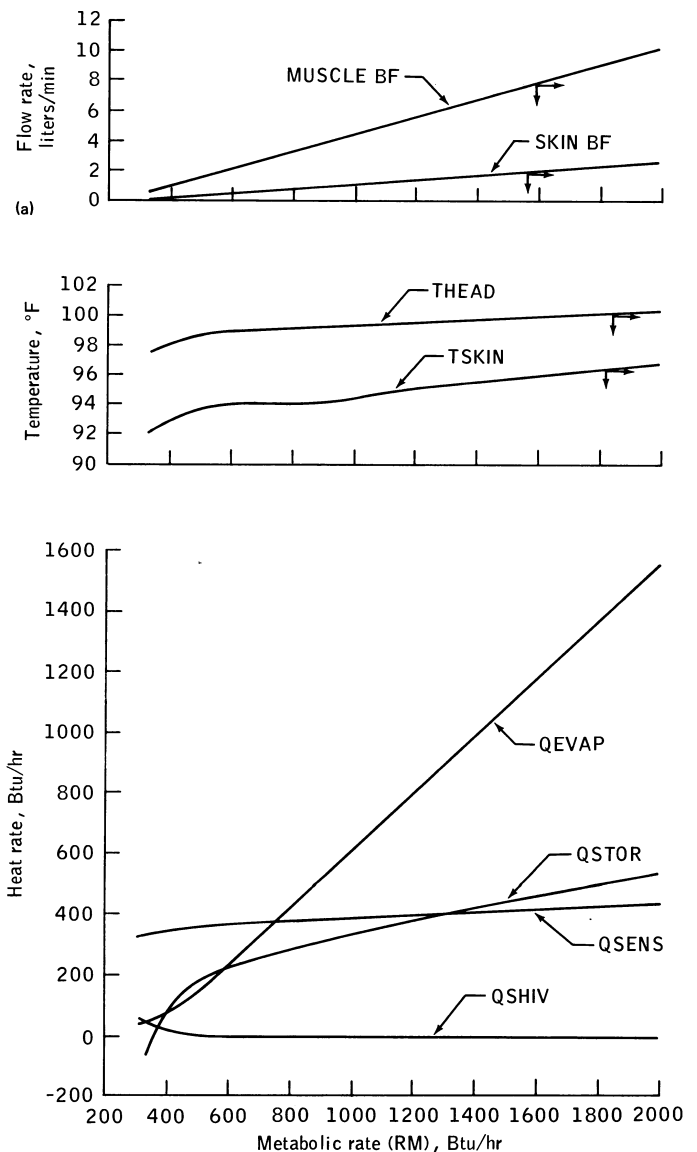
Figure E-1. Effect of changing metabolic rate on selected thermoregulatory variables. (a) MUSCLE BF and SKIN BF; (b) THEAD and TSKIN; and (c) QEVAP, QSTOR, QSENS, and QSHIV.

case represents a moderately relaxed, supine subject and the other an exercising, standing subject, both in comfortable environments.

The sensitivity coefficients have been computed for a selected variety of parameters and variables for each of the two operating points. As shown in Table E-3, each value has been computed by varying a single parameter, listed on the left, by +10% away from the operating point and determining the change in the particular variable shown across the top of the table using computer simulation of the model. The logarithmic sensitivity coefficients were determined from Eq. (E7).

There is a large variation of values among the coefficients shown in Table E-3; the higher the value, the greater

Table E-1. Thermoregulatory Model Glossary Terms

Symbol	Definition
Mathematical notation	
C	Heat capacity
D	Measure of deviance
$D_{COMPUTE}$	Computed deviance
$D_{PREDICT}$	Predicted deviance
e	Measure of error: difference between unperturbed and perturbed model output or between model output and corresponding experimental results
f	Function
i,j	Subscripts denoting iteration
m	Number of parameters
N	Number of variables
q	System parameter
S	Differential sensitivity coefficient
$\overline{S}$	Logarithmic sensitivity coefficient
T	Temperature
t	Time
U	Fractional perturbation of a parameter
Y	Performance criterion
y	Dependent variable
Δ	Change
ΔS	Incremental sensitivity coefficient
$\circ$	Superscript denoting the unperturbed state of the model
Program notation	
CLOV	Clothing resistance
PCAB	Barometric pressure
MUSCLE BF	Muscle blood flow
QBASAL	Basal metabolic rate
QEVAP	Heat loss due to sweat evaporation
QSENS	Sensible heat loss
QSHIV	Heat generated due to shivering
QSTOR	Heat stored in body relative to a reference state
RM	Metabolic rate due to exercise
SKIN BF	Skin blood flow
TCAB	Ambient temperature
TDEWC	Ambient dewpoint temperature
THEAD	Head core temperature
TSET	Set-point temperature
TSKIN	Mean skin temperature
TW	Ambient wall temperature
UEFF	Efficiency of exercise
VCAB	Free-air velocity

the effect of a given parameter on the designated variable. The skin and head temperatures are relatively insensitive to any environmental parameter, which is expected, since negative feedback temperature regulation is an important feature of the model. Similarly, exercising muscle blood flow (case 2) is insensitive to all the parameters studied except for metabolic rate, whereas, perhaps surprisingly, the model predicts a generally higher sensitivity of the rest-

Table E-2. Input Parameters for Two Operating Points

Input parameter	Value	
	Case 1*	Case 2**
RM, W (BTU/hr)	330	1165
QBASAL, W (BTU/hr)	283	283
UEFF, percent	0	13.5
TCAB, (°F)	68	75
TW, (°F)	68	75
TDEWC, (°F)	50	55
PCAB, (lb/in2)	14.7	14.7
CLOV, (clo)	0.35	0.5

* Moderately relaxed

** Medium exercise

ing muscle flow (case 1) to all the input parameters. Other differences in sensitivity between the two cases shown can be easily noted from this table (especially the effects on QSHIV, QEVAP, and QSTOR). This analysis enables one to easily determine the sections of the model that are most and least sensitive to a particular parameter. For example, both free-air velocity (VCAB) and clothing resistance (CLOV) are seen to have their greatest influence on shivering in the relaxed state and on sensible heat loss in the exercising state. Also, it appears that many of the variables studied are more sensitive to wall temperature than to air temperature. In general, it appears that RM, TCAB, and TW exert a more profound influence on the model than do TDEWC, VCAB, and CLOV. A determination of whether these sensitivities are physiologically appropriate is beyond the scope of this study. However, the ranking of parameter importance as shown here provides a rapid method, for someone familiar with the thermoregulatory system, to evaluate certain characteristics of the model.

E.3.2 Use of the Performance Criterion

As mentioned previously in this appendix, it is desirable to formulate a single performance criterion which represents overall model behavior. In the case of the thermoregulatory model, the variable QSTOR, representing the amount of heat stored in the body relative to the reference state, appears to satisfy the requirements previously mentioned for a performance criterion. In the 41-node model, QSTOR is defined as

$$QSTOR = \sum_{i=1}^{41} C_i \left(T_i - TSET_i \right) \qquad \text{(E13)}$$

where T_i is the temperature of the ith body node, $TSET_i$ is the reference set-point (corresponding to the temperature in a neutral thermal environment), and C_i is the heat capacity (BTU per degree Fahrenheit) of the ith node. When the subject is in a neutral environment, $T_i = TSET_i$ and QSTOR = 0. Inasmuch as the individual body segment temperatures are the net result of all the thermal forces

Table E-3. Sensitivity Coefficients From 10% Change in Parameter Values

Parameter	Sensitivity coefficient for—							
	QSTOR	QEVAP	QSENS	QSHIV	SKIN BF	MUSCLE BF	THEAD	TSKIN
Case 1*								
RM	5.18	0.56	0.08	–6.77	0.10	0.37	0.00	0.02
TCAB	2.57	0.26	–1.16	–9.03	0.26	–3.15	0.00	0.05
TW	2.94	0.25	–1.23	–9.64	0.10	–3.36	0.00	0.05
TDEWC	–0.03	–0.81	–0.00	–0.70	0.09	–0.29	0.00	0.00
VCAB	0.49	0.04	0.15	0.66	0.06	0.18	0.00	–0.01
CLOV	0.69	–0.07	–0.18	–1.56	0.10	–0.59	0.00	0.01
Case 2**								
RM	0.62	1.51	0.11	0.00	1.35	1.28	0.01	0.01
TCAB	0.42	1.04	–1.62	0.00	1.04	0.01	0.01	0.04
TW	0.53	1.13	–1.77	0.00	1.11	0.01	0.01	0.04
TDEWC	–0.06	0.00	–0.01	0.00	0.18	0.01	0.01	0.00
VCAB	–0.03	–0.09	0.14	0.00	–0.03	0.01	0.00	0.00
CLOV	0.11	0.14	–0.21	0.00	0.21	0.01	0.02	0.01

* Rest
** Exercise

acting on the body, QSTOR is a good indicator of overall model performance. (A similar and related criterion might be mean body temperature.) The variable QSTOR has already been used successfully to define the limits of thermal comfort for manned spaceflight. The outside tolerance limits have been set at QSTOR = ±300 BTU. (These limits would be exceeded by slightly more than a 1°F) change in mean body temperature, an indication that QSTOR is very sensitive to changes in heat balance.)

The sensitivity coefficients for QSTOR relative to several input parameters have already been presented in Table E-3. As can be noted, QSTOR is many times more sensitive to the parameters studied near the resting operating point than in the exercising state. As a consequence, it can be argued that the absolute values of the input parameters should be known to a higher degree of accuracy during the resting state as opposed to the exercising state to enable achievement of the same degree of model accuracy.

The degree of linearity of QSTOR about the exercise operating point has been tested, and the results are summarized in Table E-4. The values in this table have been obtained in exactly the same manner as those already described in Table E-3, except that QSTOR is the only variable studied and each parameter has been varied over a ±60% range from the operating point. The results suggest that the sensitivities are extremely constant over a wide range.

The parameters studied thus far have been input (environmental) parameters to the model; the values of input parameters are usually known to a fairly high degree of accuracy. However, the model contains many other param-

eters, called system parameters, that are properties of the controlled or controlling systems and do not vary from run to run, as do the input parameters. These parameters represent various controller gains in the hypothalamic thermoregulatory centers of the model that control sweating, shivering, vasodilation, and vasoconstriction. The values of system parameters are not known with great certainty. Examples of these parameters are skin/air-interface heat-transfer coefficients, tissue thermal conductivities, basal blood flow rates, and thermoregulatory control mechanisms.

The sensitivity coefficients of the seven thermoregulatory control parameters have been investigated with respect to overall model performance as measured by QSTOR to illustrate several points. (See Table E-5.)

E.3.3 Prediction of QSTOR From a Sensitivity Model

It can be shown that the value of a particular variable in a complex model can be predicted from simple algebraic equations that are functions of the sensitivity coefficients without the need to perform simulations of the entire model on high-speed computers. Here, the attempt is to predict values of QSTOR for a wide range of simultaneous parameter variations.

Let D be a measure of deviance from some operating point,

$$D = \frac{QSTOR - QSTOR°}{QSTOR°} \qquad (E14)$$

Table E-4. Values of the Overall Performance Sensitivity Coefficient* for Single-Parameter Changes About the Nominal Operating Point for Exercise**

	QSTOR° = 97.2 W (332 BTU/hr)					
Parameter	**Sensitivity coefficient for percent change, of —**					
	0.5	1	10	20	40	60
	Increase					
RM	0.626	0.627	0.619	0.738	0.696	0.668][***]
TCAB	0.345	0.346	0.416	0.420]	0.276	0.169
TW	0.530	0.532	0.527	0.464]	0.291	0.242
TDEWC	–0.055	–0.054	–0.058	0.063]	0.059	0.019
VCAB	–0.028	–0.028	–0.026	–0.025	–0.024	–0.023]
CLOV	0.109	0.109	0.106	0.102	0.095	0.093]
UEFF	–0.065	–0.065	–0.064	–0.064	–0.064	–0.064]
	Decrease					
RM	0.630	0.630	0.640	0.663	0.721	1.61]
TCAB	0.348	0.348	0.368	0.388]	0.450	0.653
TW	0.534	0.535	0.559	0.579]	0.632	0.744
TDEWC	–0.051	–0.051	–0.047	–0.043	–0.036]	–0.030
VCAB	–0.026	–0.027	–0.028	–0.029	–0.032	–0.028]
CLOV	0.113	0.111	0.115	0.120	0.131	0.045]
UEFF	–0.061	–0.063	–0.063	–0.063	–0.063	–0.063]

*   Equation (E15)
** See Table E-2 for absolute values of parameters at operating point.
***See text for explanation of brackets

Table E-5. Sensitivity Coefficients for Thermoregulatory Control Parameters with Respect to Overall Performance

Each Parameter Varied Separately by 10%

System Parameter	Normal value	Sensitivity coefficient	
		Rest	Exercise
CSW, W/ (BTU/hr–°F)	705	0.040	0.407
SSW, W/ (BTU/hr–°F)	63.9	0.091	0.068
CDIL, * (lbm/hr–°F)	143	0.115	0.174
SDIL, * (lbm/hr–°F)	9.2	0.025	0.019
CCON, (°F^{-1})	2.78	0.001	0.000
SCON, (°F^{-1})	2.78	0.000	0.000
PCHIL, (BTU/hr–°F)	25.7	2.1	0.000

* Mass of blood

Table E-6. Values of Parameters and Sensitivity Coefficients Used for Predicting Changes in QSTOR

Parameter	Value			$\bar{S}_i$
	Nominal	Min.	Max.	
RM, W (BTU/hr)	1165	330	2000	0.627
UEFF, percent	13.5	5	22	–0.0647
TCAB, (°F)	75	55	75	0.346
TW, (°F)	75	55	75	0.532
TDEWC, (°F)	55	45	65	–0.0536
VCAB, (ft/min)	30	10	50	–0.028
CLOV, (clo)	0.5	0.1	0.9	0.109

The relative sensitivity coefficients S_i in Table E-4 have been determined by varying one parameter at a time

$$\bar{S}_i = \frac{\partial D}{\left(\dfrac{\partial q_i{}^\circ}{q_i{}^\circ}\right)}$$

$$\doteq \frac{\left[\dfrac{(QSTOR - QSTOR^\circ)}{QSTOR^\circ}\right]}{\left[\dfrac{(q_i - q_i{}^\circ)}{q_i{}^\circ}\right]} \qquad (E15)$$

where q_i is the value of any parameter, q_i refers to the corresponding value at the operating point, and the symbol $\doteq$ means "is approximately equal." Rewriting Eq. (E9) for n parameters and substituting QSTOR for y results in a formula for predicting D

$$D_{\text{PREDICT}} = \sum_{i=1}^{n} \bar{S}_i U_i \qquad (E16)$$

where U_j is defined by Eq. (E8). In this example, the concern is with varying only those parameters listed in Table E-4 and having those values for $\bar{S}_i$ listed in the ±1% columns. Furthermore, the parameter values about the operating point for case 2 (Table E-2) will be restricted to a range that has been shown to have reasonably constant sensitivity coefficients (see brackets in Table E-4). These ranges are shown in absolute values in Table E-6.

A series of 24 runs was simulated with the thermoregulatory model. Each run consisted of changing all seven parameters simultaneously. The actual parameter values for a given run were obtained by choosing values randomly within the limits given previously and assuming that all values have the same probability of being chosen. For each run, a value of D was computed (D_{COMPUTE}) from Eq. (E14) using the simulated values of QSTOR and compared to the value of D_{PREDICT} determined from Eq. (E16). The values of $\bar{S}_i$ used in Eq. (E16) are shown in Table E-6, whereas values for U_i were determined from the random perturbations for each parameter. It should be emphasized that the sensitivity coefficients in Eq. (E16) were obtained from simu-

lations performed by varying one parameter at a time by 1% to predict values for D, whereas computed values for D result from simulations in which all parameters are varied over a much wider range simultaneously.

The results of this study are shown in Fig. E-2. The dashed line represents perfect agreement between D_{PREDICT} and D_{COMPUTE}. The origin represents the operating point. Although the agreement becomes very poor for negative deviations from the operating point, it is encouraging to see a reasonable correlation of all runs that can be described by two straight lines intersecting the origin despite the very wide range of random parameter variations. Thus, D_{PREDICT} allows a good estimate of D (and therefore QSTOR) between the range of $-0.2 < D_{\text{PREDICT}} < +0.7$. For example, assume that it is desired to estimate the value of QSTOR for the following conditions: RM = 1300 BTU/hr; TCAB = TW = 80° F; and all other input parameters are identical to those given in Table E-2, case 2. Then, Eq. (E16) can be represented by only three terms which describe the perturbations of RM, TCAB, and TW from the operating point, so that

$$D_{PREDICT} = 0.627\ \frac{1300 - 1165}{1165} + 0.346\ \frac{80 - 75}{75}$$

$$+ 0.532\ \frac{80 - 75}{75}$$

$$= 0.131 \qquad (E17)$$

This value can be used to estimate, from Fig. E-2, $D_{\text{COMPUTE}} = 0.125$, which corresponds to QSTOR = 374 BTU. The value actually obtained during simulation of this particular condition is QSTOR = 379 BTU. Values of D outside the range mentioned previously can also be predicted once the correlation between D_{PREDICT} and D_{COMPUTE} has been established although the errors will be larger (Fig. E-2). The deviation from the theoretical line in Fig. E-2 probably results from two errors: first, the assumption that sensitivity is constant (especially for RM) over a range for which it is not really constant (Table E-4) and, second, the fact that higher order sensitivity coefficients were neglected.
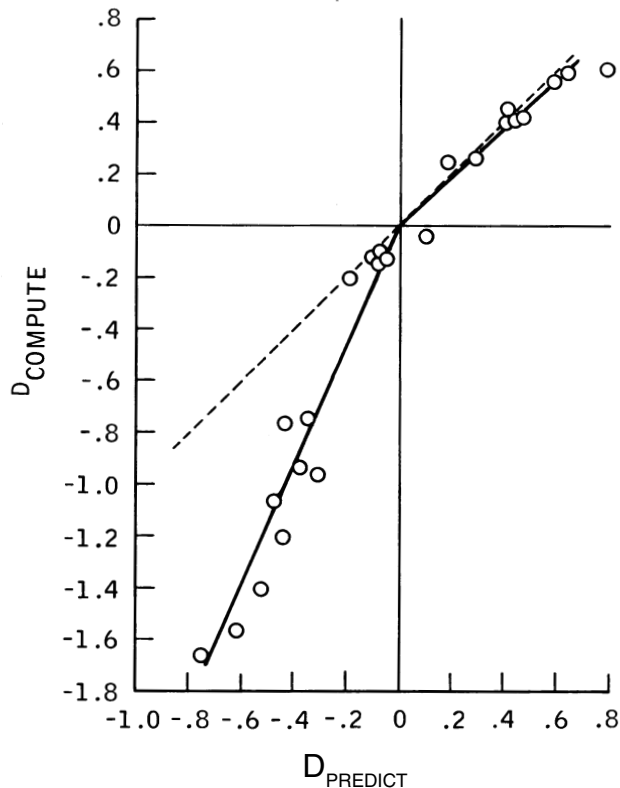
Figure E-2. Overall measure of deviance of thermoregulatory model due to variation of all input parameters simultaneously: comparison of computed and predicted results.

It would be possible to prepare a family of curves similar to those shown in Fig. E-2 for a series of important operating points. Once this has been done, QSTOR could be reasonably well predicted over a wide range in the manner just illustrated. Other variables besides QSTOR could be handled in the same way. Then, the relative values of each term in Eq. (E16) would also provide a quantitative measure of the importance of each parameter.

The usefulness of predicting model behavior with simple algebraic equations rather than by direct simulation of the original analog system (which involves solutions of differential equations or computer based numerical analysis) is, of course, obvious. Fundamentally, this procedure is not new, since it is based on linearization of a system using a Taylor series expansion. However, the coefficients of the Taylor series in this case are the sensitivity functions, which have intrinsic meaning by themselves. In addition, the results are expressed in terms of linear algebraic equations rather than linear differential equations. The technique illustrated in this example appears to be applicable to most nonlinear, multivariable, multi-parameter models. However, the following disadvantages have also become apparent: (1) all the sensitivity coefficients must be computed in the desired time period, (2) the degree of accuracy of the method around the operating point

should be established by some independent check, (3) in highly nonlinear systems, higher order sensitivity functions may have to be computed, or, alternatively, (4) a series of first-order sensitivity functions may have to be computed at closely spaced operating points. In addition, the equations for this procedure no longer describe a deterministic system, even though the coefficients were generated from one. There is a danger that persons not familiar with the use of this method may extend it beyond its limitations. Notwithstanding these restrictions, the method appears to be powerful enough to be suitable for certain types of application even with complex models, especially where high-speed, large-core computers are not available.

Another important application of sensitivity analysis is to investigate the interdependence of parameters. In Fig. E-3, the metabolic rate and ambient temperature have been varied simultaneously over a wide range and QSTOR contour lines were drawn. The convergence of contour lines toward the lower left shows that QSTOR becomes more sensitive to simultaneous changes of TCAB and RM as these parameters decrease in value. Also, there appears to be a region of very high sensitivity near 550 BTU/hr and 80°F, a commonly encountered environment. Further sensitivity analysis using these and other parameters would be suitable for obtaining human tolerance limits and may reveal minimum or maximum points of sensitivity. An analysis of second-order sensitivity coefficients of the type $\partial^2 y/\partial(q_1 \bullet q_2)$ would also help to reveal mutual interaction effects between parameters.

These results have been illustrated for the steady-state case. For models that are capable of predicting time-dependent behavior, the quantitative relationships of sensitivity coefficients are more complex than for the simpler steady-state relationships. For example, in the computation of sensitivity coefficients for studying transient behavior, it is important to define the time limits of interest, since sensitivity coefficients may be time-dependent.

E.4 Conclusions

Sensitivity analysis can be extremely useful early in the model development process. Identification of the relative importance of parameters can be made even in models that are somewhat inaccurate [4]. A person familiar with the subject matter of the model (but not necessarily familiar with simulation techniques) can make a judgment concerning the validity of the model, based on the reasonableness of the sensitivity relations. The possibility of identifying the most important parameters of a system and determining the accuracy needed in their measurement (using error analysis techniques) means that one could predict the effort required to produce a valid model before massive resources were committed. It can also suggest the relative priority in data collection because certain measurements will be more critical than others for understanding system behavior. One of the most important advantages of sensitivity analysis during these early stages of development is that it does not require extensive data collection to determine qualitative model validation.
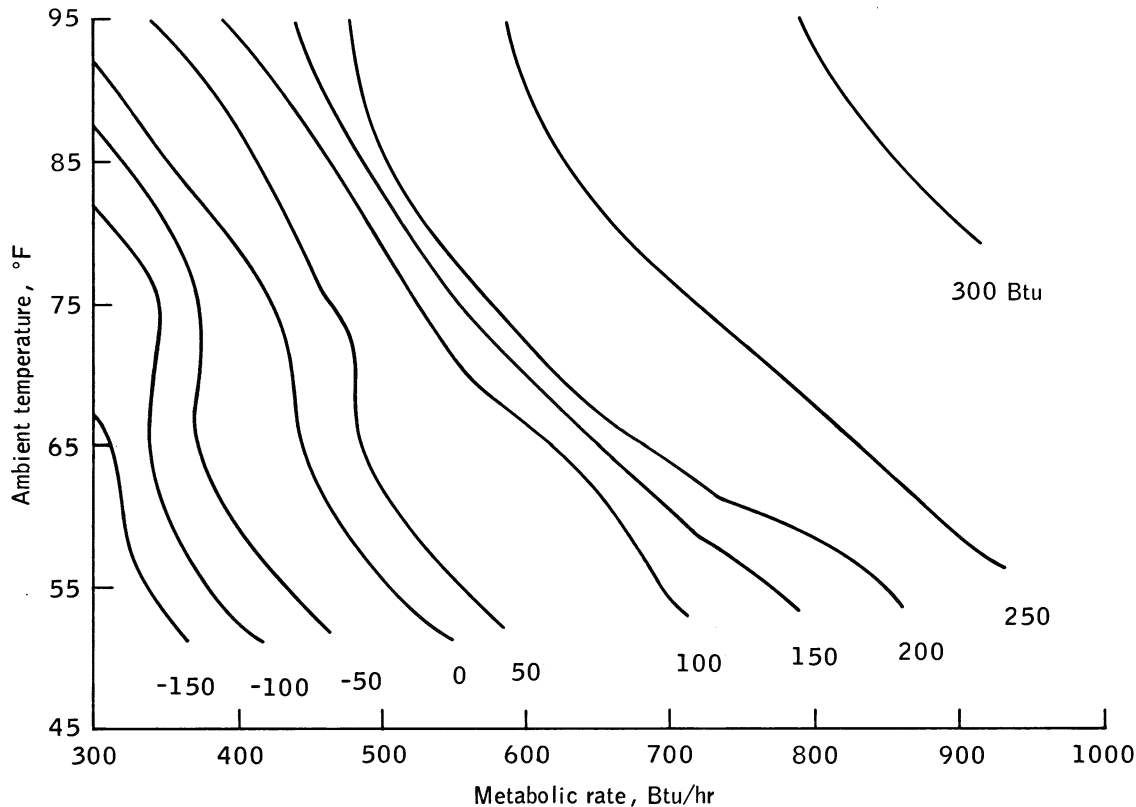
Figure E-3. QSTOR contour lines for simultaneous changes in ambient temperature and metabolic rate.

Once the model has been validated and its credibility ascertained, the techniques of sensitivity analysis can be used to perform advanced simulation studies such as noise analysis, parameter estimation, stability analysis, and inverse sensitivity, all of which are derived from sensitivity considerations. The examples discussed in this appendix demonstrate the capability of using sensitivity coefficients to form simple linear models of complex systems. The use of these algebraic models for making rapid, first-order calculations of system behavior should be explored further. In addition, certain aspects of the system may have to be modified more carefully by introducing new elements or by using improved parameter values. A sensitivity analysis performed on a validated model could provide the motivation, direction, and support for this effort. Finally, when a model is used for making inferences regarding untested situations, sensitivity analysis is useful for predicting uncertainty in model behavior, based on measurement errors in input data.

References

1. White, R. J. and Navar, L. G., Formal Sensitivity Analysis Applied to Physiological Systems, *Proceedings of the 28th Annual Conference on Engineering in Medicine and Biology*, Alliance for Engineering in Medicine and Biology (Arlington, Va.), 1975, p. 431.

2. White, R.J., Croston, R.C., and Fitzjerrell, D.G., "Cardiovascular Modeling: Simulating Human Response to Exercise, Lower-Body Negative Pressure, Zero Gravity and Clinical Conditiions, *Adv. Cardiovasc. Phys.*, Ghista, D.N. (Ed), vol 5 (Part I), S. Karger, Basel, Switzerland, 1983, pp. 195-229.

3. Miller, D. R.. Model Validation Through Sensitivity Analysis. *Proceedings of the 1974 Summer Computer Simulation Conference*, 11:911-914, AFIPS Press, Montvale, N. J., 1974.

4. Miller, D. R., An Experiment in Sensitivity Analysis on an Uncertain Model. *Simulation*, 23(3):101-104, 1974.

5. Cruz, Jose B., Jr., System Sensitivity Analysis, *Benchmark Papers in Electrical Engineering and Computer Science*, Dowden, Hutchinson, and Ross (Stroudsburg, Pa.), 1973.

6. Tomovic, R. and Vukobratovic, M., *General Sensitivity Theory*, American Elsevier (New York), 1972.

7. Leonard, J.I., *The Application of Sensitivity Analysis to Models of Large Scale Physiological Systems*, (TIR 741-MED-4028, General Electric Co., Houston, Texas; Contract NAS 9-12932), NASA CR-160228, NASA, Washington, D.C., 1974.

Appendix F
Integrated Metabolic Balances: Details

This Appendix provides a more detailed discussion of the methods of computation and assumptions used to derive the results, tables, and figures in Chapter 4, the Integrated Metabolic Balance Analysis. Also included are descriptions of error analyses and supplementary data as they pertain to the specific studies. The Appendix is divided into subsections that generally correspond to the sections of Chapter 4.

F.1 Skylab Water Balance Analysis

The discussion of the Skylab Water Balance Analysis in Chapter 4.2 only presents and interprets the results of that analysis. This part of Appendix F contains details of the approach used in the analysis. Further details are also available [1,2].

F.1.1 Assumptions and Methods of Calculation

The daily change in total body water (i.e., daily water balance), ΔTBW, is given by the algebraic sum of all liquid quantities entering or excreted from the body according to the following relationship [3]:

ΔTBW
= water intake (food + drink) + metabolic H_2O
- water excreted (urine + feces)
- evaporative water loss (skin + respiratory)   (1)

Water intake and water excreted were measured on a daily basis during the Skylab missions and it was possible to estimate metabolic water from the known units of fat, protein, and carbohydrate consumed. However, it was not possible to compute a daily water balance using only this information since daily evaporative water loss, a significantly large quantity, was not measured. An alternative water balance equation can be derived which is independent of both evaporative water loss and any liquid quantity consumed or excreted by developing a complete gravimetric (mass) balance. The daily change in body mass, ΔBWGT, can be found by summing up the total masses (liquids and solids) of all input (+) and (-) output quantities,

ΔBWGT
= dry weight of food + water intake (food + drink)
- dry weight of excreta (urine + feces)
- water excreted (urine + feces)
- evaporative water loss (skin + respiratory)
- weight of metabolic CO_2 + weight of
  metabolic O_2 - dry skin loss   (2)

Thus, combining Eq. (1) and (2),

ΔTBW = ΔBWGT - dry weight of food
+ dry weight of excreta (urine + feces)
+ metabolic H_2O + metabolic CO_2
- metabolic O_2 + dry skin loss   (3)

The "dry skin loss" in these equations refer to sweat solids, sebaceous residues, desquamated epithelium, as well as nail and hair clippings. The metabolic H_2O, CO_2, and O_2 refers to those insensible quantities produced or consumed by metabolism of food stuffs as well as the catabolism of body tissue (primarily body fat and protein).

All of the quantities on the right side of Eq. (3) were measured directly except for the metabolic H_2O, CO_2, and O_2 and the dry skin loss. The metabolic quantities can be estimated from the foodstuffs, while the dry skin loss can be estimated from the infrequent total body water measurements. The procedure used to compute these indirectly measured quantities is given below.

The term net insensible metabolic losses (IML) is defined as

IML
= metabolic H_2O + metabolic CO_2 - metabolic O_2
= IML (foodstuff) + IML (body tissue)   (4)

The insensible metabolic losses associated with foodstuffs were determined indirectly from the daily amounts of carbohydrate (CHO), fat (FAT), and protein (PRO) in the ingested diet according to accepted stoichiometric relationships [3,4,5] for reduction of food to carbon dioxide, water, and urinary nitrogen:

H_2O(met) = EFF(0.555 CHO + 1.071 FAT + 0.413 PRO)   (5)

CO_2 (met) = EFF(0.829 CHO + 1.427 FAT + 0.775 PRO)ρ(CO_2)   (6)

O_2 (met) = EFF(0.829 CHO + 2.019 FAT+ 0.967 PRO)ρ(O_2)   (7)

The densities carbon dioxide and oxygen, ρ(CO_2) and ρ(O_2), were taken as 1.977 and 1.429 g/1, respectively. EFF is an efficiency factor to allow for incomplete digestion across the gastrointestinal tract. A value of EFF was obtained for *each* Skylab crewman based on a solids (mass) balance of food and feces according to the relationship:

$$EFF = \frac{\text{Total mission dry food - total mission dry feces}}{\text{Total mission dry food}}   (8)$$

An average value of EFF ($\pm$SD) of 0.962 $\pm$ .005 was obtained; the individual crew values used in this study are given in Table F-1.

Table F-1. Digestive Efficiency Factor of Skylab Crews, EFF*

Mission	Man	Pre-flight	In flight	Post flight	Weighted Avg.**
28-day	1	0.967	0.966	0.968	0.967
	2	0.954	0.966	0.947	0.957
	3	0.961	0.965	0.972	0.965
59-day	1	0.967	0.965	0.982	0.968
	2	0.958	0.960	0.953	0.958
	3	0.959	0.959	0.967	0.960
84-day	1	0.950	0.955	0.948	0.953
	2	0.960	0.969	0.973	0.968
	3	0.963	0.961	0.959	0.961
Mean		**0.960**	**0.963**	**0.963**	**0.962**
SD		**±.006**	**±.004**	**±.012**	**±.005**

*   EFF = 1 - $\dfrac{\text{Fecal Solids}}{\text{Food Solids}}$

**   The average values shown were weighted by the number of observations in each phase of the flight for each mission.

Substituting Eqs. (5) to (7) into Eq. (4) leads to the following relationship

IML(foodstuff) =
EFF (1.009 CHO + 1.007 FAT + 0.563 PRO).   (9)

Body protein (ΔProtein Loss) and body fat (ΔFat Loss) catabolism occurred during the course of the Skylab mission. It would be expected that these quantities would contribute to the net insensible metabolic losses in a similar manner as equivalent amounts of foodstuffs; i.e.,

IML (body tissue) =
1.007 (ΔFat Loss) + 0.563 (ΔProtein Loss)   (10)

It was not possible to estimate the metabolic losses associated with body tissue metabolism on a daily basis. However, this term was included numerically in the estimate for dry skin loss, which was averaged over the entire mission.

One of the purposes of this study was to obtain not only estimates of daily water balance, but also to sum these daily balances to compute the total body water changes over large time intervals (up to several months). Errors in the estimates of daily water balance would, therefore, be cumulative over time. It has been estimated previously that dry skin loss amount to at least 12-20 gm/day [6,7]. Exclusion of the difficult to measure insensible metabolic losses that are a result of body tissue catabolism potentially adds another 20 - 40 gm/day error in the water balance [8]. Summing these up, it can be seen from Eq. (3) that failure to take skin and body tissue losses into account could underestimate daily water balance by at least 30 - 60 gm/day and produce errors at the end of a one-month period of 1 - 2 liters in total body water calculations. Thus, it was important to accurately estimate these quantities. This was achieved by rewriting Eq. (3) using Eq. (4).

ΔTBW = ΔBWGT
    – dry weight of food
    + dry weight of excreta
    + IML(foodstuff) + IML(body tissue)
    + dry skin loss   (11)

Define ΔTBW(balance) as the right side of Eq. (11) excluding the last two terms, i.e.,

ΔTBW = ΔTBW(balance) +
        IML(body tissue) + dry skin loss   (12)

In other words ΔTBW(balance) is the water balance typically obtained from directly measured quantities excluding corrections for skin and body tissue losses. The left side of Eq. (12) represents the true change in total body water as measured, in the case of the Skylab crew, by tritium dilution techniques before and after a period of several weeks or months. Let this direct measurement of total body water change be designated by TBW (direct), and let the non-measured quantities be termed a correction factor, CF. Then

CF = IML(body tissue) + dry skin loss   (13)

Use of Eq. (12) yields

CF = $\overline{\Delta\text{TBW}}$(direct) – $\overline{\Delta\text{TBW}}$(balance)   (14)

where

$\overline{\Delta\text{TBW}}$(balance)
= $\overline{\Delta\text{BWGT}}$ – $\overline{\text{dry weight of food}}$
+ $\overline{\text{dry weight of excreta}}$ + $\overline{\text{IML}}$(foodstuff).   (15)

The bar above the terms in Eqs. (14) and (15) represent average daily quantities during the particular period between TBW measurements. During the Skylab experiments, total body water measurements were obtained at the beginning and end of each flight phase: preflight, inflight, and postflight. (In the case of the 59-day mission, the measurement at the start of inflight was not obtained). The value ΔTBW(direct) was taken as the difference between any two consecutive tritium dilution measurements, and the value ΔTBW(balance) was computed from the uncorrected balance, Eq. (15), using the total quantities consumed, excreted, or changed during this same time interval.

Thus, in the majority of cases, it was possible to compute a separate correction factor for each flight phase for each crewman. (Values for the terms in Eqs. (14) and (15) can be found in Tables 4-6 and F-4). These values, expressed in gm/day, are shown in Table F-2. It can be observed that the average CF value for preflight and inflight phases were similar, indicating that the sum of skin and tissue losses were similar during these phases. The low

Table F-2. Water Balance Correction Factor, CF [gm/day]

Mission	Man	Preflight	Inflight	Postflight
28-day	1	41.7	56.3	69.6
	2	100.0	126.5	32.1
	3	89.2	65.9	-11.2
59-day	1	66.6	66.6	-116.1
	2	97.7	97.7	-49.0
	3	63.6	63.6	14.7
84-day	1	24.9	26.0	74.1
	2	54.4	42.9	-7.8
	3	95.6	12.9	-27.9
Mean		**70.2**	**61.8**	**3.6**

Table F-3. Urinary Specific Gravity (s.g.)*

Mission	Man	Preflight	Inflight	Postflight
28-day	1	1.019	1.020	1.017
	2	1.028	1.027	1.020
	3	1.009	1.013	1.009
59-day	1	1.016	1.021	1.016
	2	1.021	1.021	1.019
	3	1.023	1.025	1.022
84-day	1	1.016	1.021	1.014
	2	1.020	1.021	1.017
	3	1.028	1.031	1.015
Mean		**1.020**	**1.022**	**1.017**
SD		**±0.006**	**±0.005**	**±0.004**

∗ Value shown are the everages of daily urine samples obtained during the designated period.

(and even negative) values for the postflight phase was possibly a result of a normal dry skin loss that was masked by a greater body tissue *gain* during the recovery period.

The final form of the water balance equation used in this study can be written by combining Eqs. (9), (11), and (13):

ΔTBW =
ΔBWGT - dry weight of food + dry weight of feces
+ urine volume x(s.g. - 1.0) + EFF(1.009 CHO
+ 1. 007 FAT + 0. 563 PRO) + CF   (16)

where "s.g." is the specific gravity of urine obtained for each sample and is given in Table F-3, and "urine volume x (s.g. - 1.0)" represents the dry urine weight. (See also Fig. 4-5 and 4-6 for a pictorial representation of Eqs. (16) and (18).

With the exception of s.g. and CF, each term in Eq. (16) was measured daily and continuously over the entire preflight, inflight, and postflight periods. The average values of these terms for each crewman are shown in Table F-4.

The change in total body water during a period of N consecutive days, $\Delta TBW(N)$ can be determined by algebraically summing (i.e., integrating) the daily water balance of each successive day, ΔTBW_i, over the interval. Thus,

$$\Delta TBW(N) = \sum_{i=1}^{N} \Delta TBW_i$$
$$(17)$$

In the water balance study $\Delta TBW(N)$ was computed for each day of the mission starting from either the day of launch or the day of recovery and summing backward and forward in time from these reference points. Thus, $\Delta TBW(N)$ had a value identically zero at the morning of launch or the morning of recovery. Mean values of $\Delta TBW(N)$ were used in this report by averaging the values for the three crewmembers on each flight ($n = 3$) or by pooling two ($n = 6$) or three ($n = 9$) flights. The method of obtaining variances of $\Delta TBW(N)$ is presented at the end of this Chapter. The effect that the correction factor has on estimating $\Delta TBW(N)$ is illustrated in Fig. F-1.

Evaporative water loss is a critical quantity in the whole-body water balance. Evaporative water losses (EWL) were estimated on a daily basis by rearranging the water balance Eq. (1),

EWL =
= water intake(food + drink)
+ metabolic H_2O
- water excreted(urine + fecal) - ΔTBW   (18)

where ΔTBW is the quantity obtained from Eq. (16). (Another formulation for EWL is provided in Appendix F.2).

Average evaporative water loss for the entire Skylab crew is illustrated in Fig. F-2 for a 2 week period before and after launch and recovery. The changes in EWL during the mission are too small to easily discern in Fig. F-2 but can be noted in Table F-5.

Water balance graphs were prepared (see Chapter 4, Figs. 4-9 and 4-10) using the following definitions for intake and output:

Total water intake =
 = water(drink) + water(food) + metabolic H_2O,   (19)

Total water output =
= urine volume + fecal water +
+ evaporative water loss   (20)

Equations (19) and (20) form the basis of a partitional water balance that is provided in Table F-5. This table presents data for each of the 3 Skylab missions and serves as backup for Table 4-26 which is accompanied by a brief interpretation. The changes in body water cannot only be

Table F-4. Mean Values of Terms in Water Balance Equation for Skylab Crew [gm/day]*

	Crewman:	1	2	3	4	5	6	7	8	9	Skylab Means**
No. of days Observed	Pre	30	30	30	20	20	20	26	26	26	
	Inf.	28	28	28	59	59	59	84	84	84	
ΔBody Weight	Pre	-30.0 ± 68.8	-46.7 ± 65.5	-56.7 ± 60.4	+5.0 ± 83.2	-35.0 ± 118.8	+80.0 ± 122.6	30.8 ± 67.2	-30.8 ± 79.8	0.0 ± 57.4	-9.16 ± 14.1
	Inf.	-39.3 ± 68.0	-96.4 ± 91.4	-114.3 ± 77.8	-66.1 ± 45.1	-61.0 ± 45.2	-71.2 ± 69.0	0.0 ± 34.4	-16.7 ± 45.9	-16.7 ± 37.7	-53.5 ± 12.8
Food Solids	Pre	556 ± 8	619 ± 7	610 ± 13	545 ± 6	561 ± 8	819 ± 10	617 ± 9	600 ± 11	616 ± 6	616 ± 27
	Inf.	578 ± 9	610 ± 9	585 ± 12	596 ± 8	572 ± 12	822 ± 19	639 ± 5	621 ± 5	646 ± 6	630 ± 26
Insensible Metabolic Loss (food)	Pre	470 ± 7	525 ± 18	520 ± 13	471 ± 5.4	472 ± 8	690 ± 10	518 ± 8	515 ± 10	519 ± 6	522 ± 22
	Inf.	498 ± 9	522 ± 10	506 ± 11	527 ± 7.1	487 ± 10	701 ± 16	541 ± 4	536 ± 5	548 ± 6	541 ± 21
Urine Solids	Pre	25.5 ± 1.4	23.8 ± 1.7	24.6 ± 1.1	22.3 ± 1.3	23.3 ± 1.6	34.5 ± 1.5	27.8 ± 1.5	27.0 ± 1.8	53.0 ± 3.2	29.1 ± 3.2
	Inf.	28.6 ± 1.3	30.6 ± 1.7	33.0 ± 1.9	24.5 ± 0.8	29.4 ± 0.8	37.4 ± 0.8	33.7 ± 0.9	32.7 ± 1.3	57.5 ± 1.6	34.2 ± 3.2
Fecal Solids	Pre	18.4 ± 3.7	28.4 ± 5.3	23.7 ± 5.9	18.1 ± 5.1	23.8 ± 3	33.6 ± 3.9	31.2 ± 2.1	24.1 ± 3.7	22.8 ± 5.1	24.9 ± 1.8
	Inf.	19.7 ± 4.3	20.5 ± 5.6	20.2 ± 3.0	20.7 ± 3.4	23.2 ± 3	33.6 ± 2.8	28.7 ± 2.4	19.2 ± 2.7	25.1 ± 3.2	34.2 ± 1.6
Correction Factor	Pre	41.7	100.0	89.2	66.6	95.7	63.6	24.9	54.4	95.6	70.2 ± 6.9
	Inf.	54.3	126.5	65.9	66.6	95.7	63.6	26.0	42.9	12.9	61.8 ± 11.5
ΔTBW**	Pre	-30.1 ± 67.5	11.0 ± 83.9	-8.6 ± 58.4	38.3 ± 81.5	18.8 ± 116.4	82.2 ± 122.6	15.1 ± 67.8	-10.0 ± 77.8	74.2 ± 55.7	21.1 ± 12.6
	Inf.	-14.5 ± 86.4	-8.4 ± 9.4	-74.7 ± 78.0	-23.1 ± 42.6	2.1 ± 47.2	-56.7 ± 67.8	-9.2 ± 34.4	7.35 ± 45.7	-19.0 ± 36.4	-23.2 ± 25.6

* Values are mean ± SE, *N* = 9
** ΔTBW obtained from Eq. (16)

Table F-5. Partitional Water Balance for Each Skylab Mission (N = 3) [ml/day; mean ± SE]

Daily Water Balance Quantities	SL-2			SL-3			SL-4		
	Preflight	Inflight	Postflight	Preflight	Inflight	Postflight	Preflight	Inflight	Postflight
Input:									
Water Ingested (food & water)	2941±536	2932±533	3140±577	2678±295	2597±302	2794±371	3293±225	2937±227	3359±354
Metabolic Water	340±10	328±5	359±16	368±47	362±67	387±44	351±3	359±5	371±13
Output:									
Urine volume	1640±536	1702±428	1835±477	1333±116	1356±98	1374±73	1660±161	1672±93	1986±387
Fecal Water	79±8	67±5	18±5	90±25	77±18	64±22	77±26	61±8	70±20
Evaporative Water	1573±82	1522±133	1619±125	1576±272	1552±435	1653±534	1881±274	1574±160	1652±288
Net Water Balance:									
Mean	-9	-32	28	46	-26	90	26	-11	52
SE	±12	±22	±9	±19	±17	±53	±25	±4	±8
No. of Days Observed	30	28	14	20	59	17	26	84	18

Table F-6. Changes in Body Fluid Compartments for Each Skylab Mission (N = 3) [Liters ± (SE)]

Body Fluid Compartment	28-Day Mission	59-Day Mission	84-Day Mission	Skylab Mean
Total Body Water	-1.22±0.47	-0.60±0.64	-0.63±0.11	-0.82±0.25
Extracellular Fluid	-0.13±0.17	-0.87±0.41	0.00±0.52	-0.33±0.24
a) Plasma volume	-0.28±0.14	-0.43±0.10	-0.53±0.08	-0.41±0.06
b) Interstitial fluid *	+0.15±0.50	-0.44±0.46	+0.53±0.48	+0.08±0.76
Intracellular Fluid**	-1.08±0.64	+0.27±1.04	-0.63±0.63	-0.49±0.44

* Derived from extracellular fluid and plasma volume
** Derived from total body water and extracellular fluids
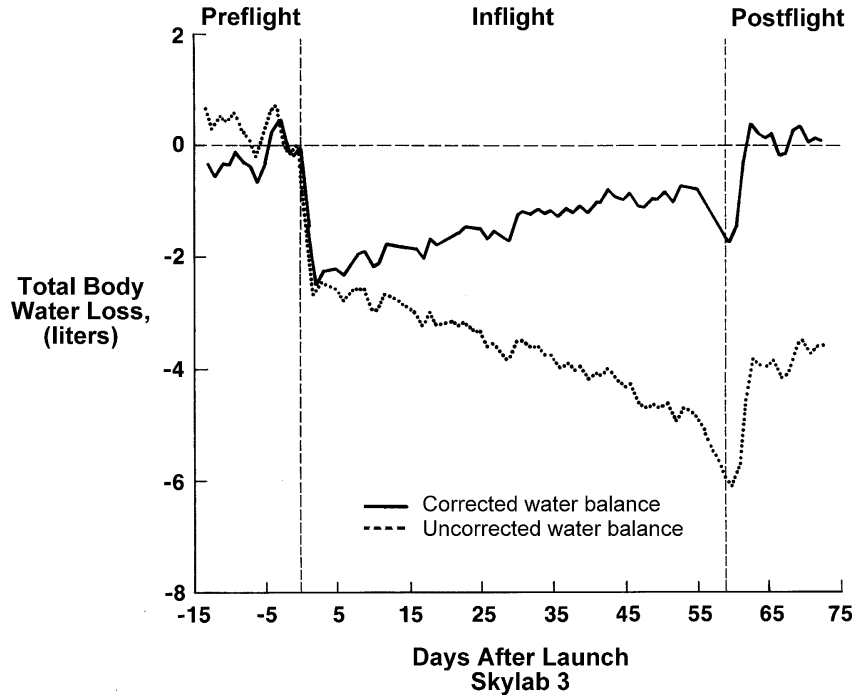
Figure F-1. Comparison of total body water for the Skylab crew on 59-day mission ($N = 3$) computed with and without correction factors (CF) in the daily water balance. (Values are shown as changes from morning of launch; (———) with correction factor and (- - -) without correction factor.

partitioned into rates of input and output but into fluid compartments of the body. Table F-6 presents the changes in the intracellular, extracellular and plasma compartments over the duration of each Skylab mission. The combination of data in Tables F-5 and F-6 provides the first complete gross assessment of fluid status in weightlessness.

The metabolic balance analysis accounts for changes in total dry body tissue (ΔTIS), protein (ΔPRO) and fat (ΔFAT) computed from the following assumed relationships:

$$\Delta BWGT = \Delta TBW + \Delta TIS$$
$$= \Delta TBW + \Delta PRO + \Delta FAT \quad (21)$$

Thus, changes in total tissue weight can be found by subtracting ΔTBW from ΔBWGT. Daily changes in total body protein were determined from the nitrogen balance:

$$\Delta PRO = 6.25 \, (N \, (\text{diet}) - N \, (\text{urine}) - N \, (\text{feces}) \,) \quad (22)$$

Daily changes in body fat were computed from Eq. (21) as:

$$\Delta FAT = \Delta BWGT - \Delta TBW - \Delta PRO = \Delta TIS - \Delta PRO \quad (23)$$

Total body changes in these quantities over any interval of N days can be found by summing up (integrating) the daily balances analogously to Eq. (17) for total body water changes:

$$\text{Change in Total Body Tissue} = \Delta TIS(N) = \sum_{i}^{N} \Delta TIS_i \quad (24)$$

$$\text{Change in Total Body Protein} = \Delta PRO(N) = \sum_{i}^{N} \Delta PRO_i \quad (25)$$

$$\text{Change in Total Body Fat} = \Delta FAT \, (N) = \sum_{i}^{N} \Delta FAT_i \quad (26)$$

where N is the number of days of interest, usually a complete mission phase.

F.1.2 Water Balance Error Analysis

The use of an average constant value for CF in the daily water balance rests on the assumption that day-to-day skin and body tissue losses are similar (see Eq. (13)), and implies a linear rate of tissue change. Information indicating the variability of skin losses either on Earth or in space is unavailable. The assumption of a linear rate of fat loss was confirmed in the water balance study and body fat loss was believed to make the largest contribution to the correction factor in that study. Rates of protein losses or gains were also found to be nearly linear during the preflight and postflight periods. Protein loss inflight appeared to occur linearly over the first month before approaching a steady state. Thus, the assumption of linearity of the CF is reasonably correct for the entire preflight, inflight, and postflight periods except for the later portions of the inflight phase. Thus, this assumption should not introduce significant error into daily water and cumulative balances.

The use of the correction factor insures that changes in total body water over each flight phase, as obtained from the corrected water balance, will be in absolute agreement with directly measured total body water. Estimates of the CF, therefore, were highly dependent on the accuracy of the direct tritium dilution method. These estimates have been shown to be realistic when compared to independent data of skin losses and body tissue losses. The use of direct total body measurements in conjunction with the balance method has been previously recommended as a technique to correct metabolic whole-body balances for otherwise unaccountable losses and to minimize accumulative error [9].

Random experimental error for this method includes sampling and instrumental errors associated with measuring the terms in Eq. (16); that is, body weight, dry food, urine volume and s.g., dry fecal mass and carbohydrate, fat and protein. Random errors associated with instrumentation were previously estimated to be less than ±65 g/day [2].

Since the quantities defined in Eqs. (17), (24), (25), and (26) are sums of other random variables and if these random variables can be assumed to be independent, then errors (variances) associated with the summed quantities can be expressed as:

$$\sigma^2_{MN}(X) = \sum_i^N \sigma^2_M(\Delta X)_i \tag{27}$$

where
$$\sigma^2_{MN}(X)$$

represents the variance of the change in *X* (i.e., *X* = total body water, tissue, protein or fat) for the average of M subjects at the end of N days;

$$\sigma^2_M(\Delta X)_i$$

is the variance on the *i*th day of the average balance of *X* for *M* subjects. In this fashion, the errors are observed to be accumulative, starting from the reference day (*i* = 1, launch or recovery day). The cumulative error represented by Eq. (27) is probably an over-estimation of true error, since most of the variance in the balance on any particular day was due to random error. If the correction factor, CF, were deleted, it might be appropriate to use the above accumulative error in the calculation, since the daily water balance would always be underestimated by this quantity. For these reasons, both accumulative and non-accumulative errors were computed in this study. Accumulative errors were used in the 14-day analysis while non-accumulative errors have been plotted for the extended period (30-day and entire mission) analysis. The non-accumulative variances for *M* subjects on the *N*th day were computed in the following fashion:

$$\sigma^2_{MN}(X) = \sum_i^N \frac{\left[\Delta X_i - \Delta \overline{X}\right]^2}{M-1} \tag{28}$$

where ΔX_i is the water, tissue, fat, or protein balance for the *i*th crewmember on the *N*th day and $\Delta \overline{X}$ is the average

balance of *M* crewmen on the *N*th day. Further details of the error analysis can be found in the literature [2].

Equation (28) is derived from the traditional formulation for standard deviation and standard error that is used throughout this book, specifically,

$$\text{Standard deviation (SD)} = \sqrt{\sum_i^n \frac{\left[X_i - \overline{X}\right]^2}{n-1}}$$

$$\text{Standard error (SE)} = \frac{SD}{\sqrt{n}}$$

where *n* is the number of samples, i is the iteration, X_i is the value of interest, and $\overline{X}$ is the mean value.

F.2 Skylab Evaporative Water Loss Analysis

The next part of this Appendix presents details of the Skylab Evaporative Water Loss Analysis not found in Chapter 4. Further details are available in the literature [10,11].

F.2.1 Assumptions, and Methods of Calculation

Two standard balance equations were combined to estimate evaporative water loss, EWL, from the input and output of fluids and solids for each crewman [3,12,13]. The first was the water balance equation, Eq. (1), and the second was the mass balance equation, Eq. (2). Solving Eq. (2) for EWL:

(a) ± 14 days around launch

(b) ± 14 days around recovery

Figure F-2. Average evaporative water loss for the Skylab crew (*N*=9) at launch (a) and recovery (b).

Table F-7. Measured and Derived Metabolic Data for Preflight and Inflight Phases; Average Daily Values for Each Mission

		28-Day Mission	59-Day Mission	84-Day Mission	Skylab Mean ± SE
No. of days observed	Pre	30	20	26	
	Inf.	23	54	79	
Total water Ingested	Pre	2941	2678	3293	2971 ± 208
	Inf.	2911	2670	2953	2845 ± 212
Food (Dry)	Pre	594.9	641.5	611.0	615.8 ± 27.2
	Inf.	598.5	686.4	638.2	641.0 ± 28.1
Urine	Pre	1610	1333	1660	1535 ± 172
	Inf.	1824	1386	1681	1630 ± 158
Fecal Water	Pre	78.4	90.0	77.2	81.8 ± 10.9
	Inf.	69.5	78.7	60.9	69.7 ± 6.9
Fecal Solids	Pre	23.5	25.2	26.0	24.9 ± 1.8
	Inf.	21.0	26.6	24.3	24.0 ± 1.7
Change in Body Weight	Pre	-44.5	16.7	0.0	-9.3 ± 14.5
	Inf.	-55.1	-25.9	3.8	-25.7 ± 12.5
Diet Protein	Pre	107.4	123.4	120.0	116.9 ± 6.5
	Inf.	102.3	117.9	120.0	113.4 ± 6.6
Diet Fat	Pre	105.0	113.3	110.5	109.6 ± 3.3
	Inf.	79.1	75.3	101.1	85.2 ± 4.5
Diet Carbohydrate	Pre	355.1	378.8	356.4	363.4 ± 17.5
	Inf.	394.4	468.3	393.5	418.7 ± 22.1
Metabolic Water	Pre	352	381	363	365 ± 15
		346	391	375	371 ± 15
Insensible Gas Loss	Pre	164.4	176.7	166.6	169.2 ± 8.3
($CO_2 - O_2$)	Inf.	182.2	217.0	183.3	194.1 ± 10.4

*All liquid quantities are expressed in ml/day, all other quantities are in gm/day

**Data from the first 5 mission days were not included in determining these values

EWL = dry weight of food
+ total water ingested from food and liquids
– (urine volume x urine s.g.) – wet weight of feces
– weight of CO_2 expired
+ weight of O_2 used - gain in body weight   (29)

Note that the term "dry skin loss", used in the previous section, Appendix F.1, were neglected in this balance equation (primarily losses of sweat solids) and that this omission can be a source of systematic error. Because the differences in evaporative loss between flight phases were rather small, it was important to estimate the magnitude of these errors and locate their origins if possible. EWL estimated by these balance methods included *insensible* water losses from the respiratory tract and dermis, as well as *sensible* sweat losses. Metabolic water, CO_2, and O_2 were determined indirectly from the daily measured amounts of protein, fat, and carbohydrate in the ingested diet according to the relationships shown in Eqs. (5) to (7). Individual urinary specific gravity values were used in the computa-

tions (see Table F-3). Average measured and derived values for the terms in these balances are presented for each mission in Table F-7.

The evaporative water loss results presented in this study were obtained using the mass balance equation, Eq. (29). All terms in that relationship were measured either directly or indirectly on a continuous daily basis. Since total body water (TBW) was measured only several times for each subject, EWL as computed from the water balance equation (Eq. (1) or (18)), represented an average value for the period between the TBW measurements. A comparison between these two formulations (water balance and mass balance) served as a check on the accuracy of the experimental procedures (see Table 4-6). Other factors such as blood draws and sweat solids were estimated to be only 12-20 gm/day, a relatively insignificant amount relative to daily EWL [6,7]. Therefore, these factors were not considered in the analysis.

For the first few days of each flight, the crews experienced motion sickness, anorexia, temperature stresses, and

Table F-8. Propagation of Error Analysis of Mass Balance Equation in Determining Evaporative Water Loss*

I	Quantity	Inflight Mean $\overline{X_i}$	Total Error		Instrument Error	
			Standard Error $S_{\overline{X_i}}$	Total Error Contribution $S^2_{\overline{X_i}} / S^2_{\overline{X}} \times 100$	Instrument Error E_i	Instrument Error Contribution E_i^2 / E^2
1	Food (wet)	1063	$\pm\,50$	4.2%	$\pm\,3$	0.2%
2	Water (drink)	2389	$\pm\,190$	60.6%	$\pm\,10$	2.3%
3	Urine x s.g.	1612	$\pm\,140$	34.7%	$\pm\,10$	2.3%
4	Feces (wet)	92	$\pm\,8$	0.1%	$\pm\,3$	0.2%
5	$(CO_2 - O_2)$	192	$\pm\,9$	0.1%	$\pm\,10$	2.3%
6	ΔDaily Body Wgt	-53	$\pm\,13$	0.3%	$\pm\,64$	92.7%
		EWL = 1609	$S_{\overline{x}} = \pm\,244$	100.0%	$E = \pm 66$	100.0%

$$\overline{X}(EWL) = \overline{X}_1 + \overline{X}_2 - \overline{X}_3 - \overline{X}_4 - \overline{X}_5 - \overline{X}_6 \qquad \text{(Mass Balance Equation)} \qquad \text{(a)}$$

$$S^2_{\overline{X}}(EWL) = \sum_{i=1}^{6} S^2_{\overline{X_i}} \qquad \text{(Propagation of Sampling Errors)} \qquad \text{(b)}$$

$$E^2(EWL) = \sum_{i=1}^{6} E_i^2 \qquad \text{(Propagation of Instrument Errors)} \qquad \text{(c)}$$

*Means and standard errors shown are pooled values for all inflight observations on all nine subjects; unless otherwise noted units are in grams

activities not typical of the remainder of the mission. Major readjustments in fluid and electrolytes also occurred during this period, and atypical, but appropriate changes in EWL were demonstrated. The atypical first five days of the inflight phase were omitted in the analysis. The experimental design provided that each subject serves as his own control; his inflight data were compared to data from his preflight control phase. Statistical analysis of the data included the paired t-test, correlation analysis, and analysis of variance with consideration for the unbalanced number of daily observations in each flight phase [14,15].

F.2.2 Error Analysis

Evaporative water loss is an indirect measurement and is subject to the random errors or variation in the directly measured components of the material balance equation. These random errors were mainly the result of two sources of variation: a) variation between daily observations and between subjects due primarily to biological variability

and environmental disturbances; and b) variation due to limited instrument resolution.

Table F-8 lists the sampling errors (S_{Xi} = instrument error + biological variability) and the instrument errors (E_i) for each term in the mass balance equation. Sampling errors were taken as the standard errors of the mean of each quantity for nine men during the inflight phase. Instrument errors were obtained by estimating the precision of each instrument from preflight and inflight studies [9,16]. The percent contribution of the errors associated with each term toward the total variance of sampling errors and instrument errors are also shown in Table F-8. (The data for the quantity $\overline{X_i}$ in Table F-8 are the mean values for only six of the crewmen corresponding to the subjects presented in Chapter 4, Table 4-6).

Since evaporative loss is given by a linear sum of terms (see Table F-8, Equation (a)) an estimate of the standard error in evaporative loss can be found by summing the square of the errors for each term as shown in Table F-8,

Equations (b) and (c). This is only true, if the errors in each term are statistically independent of one another (i.e., if the correlation coefficients are zero).

While the assumption of error independence is reasonable in computing total instrument error, this is not the case for total sampling error. For example, it is possible that the variation of water intake is highly correlated with the variation in urine output. For the case where high correlations exist, a more accurate estimate of $S_x(EWL)$ can be determined by taking into account the covariances, S_{ij}. The difference between the value of $S_x(EWL)$ in Table F-8 and the corresponding value in Chapter 4, Table 4-6 (244 vs. 89) may arise from the fact that in the former case the covariances were neglected. A more complete estimate of the propagation of errors in which the covariance terms were computed can be found in Ref. [10]. Nevertheless, the simplified analysis of errors presented in Table F-8 is very informative by demonstrating that the errors in computing evaporative water loss are almost entirely due to the total variation associated with measuring water intake and urine. One would expect a large correlation and covariance between water intake and urine since water intake physiologically drives urine excretion.

Random sampling errors can usually be reduced by increasing the number of samples. The large effect of water and urine variability and the high correlation between these quantities allow the precision of the evaporative loss estimates to be improved by measuring water intake with greater accuracy or, even better, by controlling water intake within smaller limits.

Total instrument error is due primarily to the body mass measuring device as shown in Table F-8. Also, it appears from this table that most of the error in the measurement of body weight is due to instrument error. Therefore, the instrument and overall sampling error of the body mass measurement can be reduced by improving the precision of this instrument rather than by increasing the sample size. However, this would not reduce the total error of the estimate of evaporative water loss, since the total instrument error was only a small component of the total sampling error and the average total error of the weight change measurements constituted only a small fraction of the final value of evaporative loss and its total error. The instrument error analysis also illustrates that the limiting resolution of the mass balance technique in measuring evaporative water loss on Skylab (in the absence of significant biological fluctuations) is about ±70 gms, which represents approximately a 4% error.

Systematic errors in the present technique are associated with the neglect of less significant terms in the material balance equation. In particular, failure to account for sweat solids, sebaceous residues, and desquamated epithelium would systematically cause the calculated evaporative loss to be overestimated by about 12-22 gm./day [6,7]. This was a negligible fraction of the total evaporative loss, but could account for about 50% of the discrepancy found between the mass balance and water balance techniques (see Table 4-6). The water balance method does not require accounting for these solid residues. However,

uncertainties in other measured quantities may also account for this disagreement. Thus, it is not likely that serious systematic errors were present in the estimation of evaporative loss in the present study.

F.2.3 Supplementary Metabolic Balance Data

Tables F-9 and F-10 present the measured and derived data respectfully for each Skylab crew member that were used in the balance equations to obtain the presented calculations for evaporative water loss shown in Table 4-5. This is also the detailed backup data used to compute the mean mission values listed in Table F-7.

F.3 Skylab Sodium and Potassium Balance

The following section provides a more extensive discussion of the Skylab sodium and potassium balance analysis than that presented in Chapter 4. Further details of this analysis are available [17].

F.3.1 Assumptions and Methods of Calculations

Metabolic balances were performed for sodium and potassium using the following basic equations:

$$\text{Daily electrolyte balance} = \text{Dietary intake} \\ - \text{Urine exretion} - \text{Fecal excretion} - CF \quad (30)$$

Cumulative electrolyte balance over N days
= Change in total body electrolyte

$$= \sum_{i=a}^{N} \text{Daily electrolyte balance} \quad (31)$$

where CF is a correction factor for sweat losses, unaccounted losses, and error terms; "a" is the day the balance begins (the first day of the mission phase); and "N" the day the balance ends (last day of the mission phase). These equations were added to the computer program that was used to compute the Skylab water balances. The output of the program allowed the visual display of the daily balance, the integrated or total balance, and the contribution of each term in the balance toward producing short-term and long-term changes in the balance. In the balance equations shown, the sweat losses, unaccounted losses, and error terms were combined since sweat losses were not measured during the Skylab program.

In order to obtain reasonable estimates of the time course and magnitudes of the daily balance and the changes in total body potassium and sodium, the balances were computed using correction factors based on matching the *measured* changes in the total body pools of sodium and potassium with the *cumulative balances* as computed from Eq. (31). For sodium, this correction factor was based on the product (plasma sodium concentration) x (extracellular fluid volumes). For potassium, whole-body values were measured directly.

The balance programs were run for a number of cases for both sodium and potassium. For each case, balances

Table F-9. Components of Metabolic Balance for Each Skylab Crewmember: Measured Variables Used in Balance Equations*

Mission	Crewman	Total Water Ingested, ml/d		Food Dry gm/d		Diet Protein gm/d		Diet Fat gm/d		Diet Carbohydrate gm/d		Urine gm/d		Fecal Water gm/d		Fecal Solids gm/d	
		Pre	In	Pre	In	Pre	In	Pre	In	Pre	In	Pre	In	Pre	In	Pre	In
28-Day	1	2500	2405	555.6	583.8	104.6	101.9	104.9	81.3	318.5	377.8	1340	1509	81.0	66.6	18.4	19.4
	2	2316	2239	619.3	619.1	107.9	105.9	101.2	82.2	382.3	408.9	849	1207	90.6	64.6	28.4	23.0
	3	4008	4089	609.8	592.6	109.8	99.0	109.0	73.9	364.4	369.5	2642	2757	63.5	77.2	23.7	20.5
	Mean ± SE	2941 ± 536	2911 ± 591	549.9 ± 19.8	598.5 ± 10.6	107.4 ± 1.5	102.3 ± 2.0	105.0 ± 2.3	79.1 ± 2.6	355.1 ± 19.0	394.4 ± 9.0	1610 ±535	1824 ± 474	78.4 ± 7.9	69.5 ± 3.9	23.5 ± 2.9	21.0 ± 1.1
59-Day	1	2214	2175	544.6	608.8	95.1	87.3	98.1	67.7	331.2	434.7	1392	1169	45.1	45.3	18.1	20.1
	2	2594	2554	560.7	593.1	112.4	111.6	110.1	78.7	315.4	381.0	1110	1453	91.5	74.8	23.8	24.6
	3	3227	3282	819.2	857.3	162.6	154.9	131.8	79.6	489.8	589.3	1498	1535	133.3	115.9	33.6	35.2
	Mean ± SE	2678 ± 295	2670 ± 325	641.5 ± 89.0	686.4 ± 85.6	123.4 ± 20.2	117.9 ± 19.8	113.3 ± 9.9	75.3 ± 3.8	378.8 ± 55.7	468.3 ± 62.4	1333 ± 116	1386 ±111	90.0 ± 25.5	78.7 ± 20.5	25.2 ± 4.5	26.6 ± 4.5
84-Day	1	2888	2630	617.3	641.5	120.7	118.5	108.2	100.6	363.1	398.6	1739	1635	128.6	75.8	31.2	28.4
	2	3325	2797	600.1	622.5	112.5	111.4	107.5	92.0	357.6	395.7	1350	1513	55.7	53.2	24.1	20.1
	3	3667	3433	615.6	650.7	126.9	130.0	115.8	110.6	348.4	386.1	1892	1896	47.2	53.6	22.8	24.3
	Mean ± SE	3293 ± 225	2953 ± 245	611.0 ± 5.5	638.2 ± 8.3	120.0 ± 4.2	120.0 ± 5.4	110.5 ± 2.7	101.1 ± 5.4	356.4 ± 4.3	393.5 ± 3.8	1660 ± 161	1681 ± 113	77.2 ± 25.8	60.9 ± 7.5	26.0 ± 2.6	24.3 ± 2.4
Skylab Mean ± SE		2971 ± 208	2845 ± 212	615.8 ± 27.2	641.0 ± 28.1	116.9 ± 6.5	113.4 ± 6.6	109.6 ± 3.3	85.2 ± 4.5	363.4 ± 17.5	418.7 ± 22.1	1535 ± 172	1630 ± 158	81.8 ± 10.9	69.7 ± 6.9	24.9 ± 1.8	24.0 ± 1.7

* No. of days included in preflight is 30, 20, 26 and inflight is 23, 54, and 79 for the 28-day, 59-day and 84-day missions, respectively. The first 5 inflight days were excluded in Tables F-9 and F-10.

Table F-10. Components of Metabolic Balance for Each Skylab Crewmember: Derived Data Used in Balance Equations

Mission	Crewman	Days Pre	Days In	Metabolic Water ml/d Pre	Metabolic Water ml/d In	Insensible Gas Loss $(CO_2 - O_2)$, gm/d Pre	Insensible Gas Loss $(CO_2 - O_2)$, gm/d In	Change in Body Weight, gm/d Pre	Change in Body Weight, gm/d In
28-Day	1	30	23	330	339	148.1	174.8	-30.0	-17.4
	2	30	23	364	359	176.5	188.9	-46.7	-30.4
	3	30	23	363	341	168.6	182.9	-56.7	-117.4
	Mean ± SE			*352 ±11*	*346 ±6*	*164.4 ±8.5*	*182.2 ±4.1*	*-44.5 ±7.8*	*-55.1 ±31.4*
59-Day	1	20	54	327	352	152.6	198.0	+5.0	-24.1
	2	20	54	337	342	147.7	177.9	-35.0	-24.1
	3	20	54	478	479	229.8	275.0	+80.0	-29.6
	Mean ± SE			*381 ±49*	*391 ±44*	*176.7 ±26.6*	*217.0 ±29.6*	*16.7 ±3.4*	*-25.9 ±1.8*
84-Day	1	26	79	365	377	169.8	185.3	+30.8	+10.1
	2	26	79	358	364	166.1	183.4	-30.8	-7.6
	3	26	79	367	385	163.9	181.1	0.000	+8.9
	Mean ± SE			*363 ±3*	*375 ±6*	*166.6 ±1.7*	*183.0 ±1.2*	*0.0 ±17.8*	*3.8 ±5.7*
	Skylab Mean ± SE			**365 ± 15**	**371 ± 15**	**169.2 ± 8.3**	**194.1 ± 10.4**	**-9.3 ± 14.5**	**-25.7 ± 12.5**

were obtained for the nine Skylab crewmen separately and in several combinations. Individual balances were run for a complete mission, while the average balances for groups of crewmen were run for a maximum of 28 consecutive days. The integrated balances were computed using the launch day as the day of reference. This allows a complete picture for preflight through the first 28 days for any individual crewman, mission, or combination of missions to be obtained. In addition, balances were performed for the 14-day recovery phase for each astronaut.

Average balances were computed for five mission combinations: each of the three missions separately, for all three missions combined, and for the 59-day and 84-day missions combined. Balances were computed for four intervals for each of these five mission combinations. The four intervals included:

a) from 13 days before launch to mission day 14
b) from the day of launch to mission day 28
c) from 13 days before recovery to recovery day 14
d) from 28 days before recovery to the day of recovery.

These balances, when presented graphically, provide a complete picture of the sodium and potassium balances

from 13 days before launch through 28 mission days followed by 14 days of recovery. This interval corresponds to all Skylab days for which data exists for all nine crewmen.

The correction factor, CF, in Eq. (30) was calculated as follows:

$$CF_i = \overline{Bal}_i - \frac{(\Delta TBX_i)}{N_i} \qquad (32)$$

where $\overline{Bal}_i$ is the uncorrected average balance (i.e., diet - urine - fecal) for mission phase i (i = preflight, inflight, or postflight); ΔTBX_i represents the directly measured total body loss of electrolyte X (sodium or potassium) in phase i; and N_i represents the number of days in phase i. While ΔTBX was measured directly for potassium, ΔTBX was not measured for sodium. Therefore, in order to calculate ΔTBX for sodium, the following assumptions were made:

a) Subjects were in steady-state preflight,
b) All changes in total body sodium and potassium come from the exchangeable pools,
c) The exchangeable sodium pools can be represented as the extracellular fluid volume (ECF) multiplied by the plasma concentration of sodium [Na^+] plasma,

Table F-11. Skylab Change in TBW, ECF, and Body Weight During Preflight*

Mission	Days of Measurement	Subject	ΔTBW(liters)	ΔECF(liters)	ΔBWGT(kg)
28-Day Mission	F-21**, F-1	CDR	-0.5		-0.1
		SPT	0.8		0.6
		PLT	-0.3		1.2
59-Day Mission	F-20, F-1	CDR			0.2
		SPT			-1.3
		PLT			1.5
84-Day Mission	F-15, F-1	CDR	0.1	-0.2	0.8
		SPT	0.2	-0.1	-0.4
		PLT	0.7	-0.5	-0.6

* Data from Leach and Rambaut [18]

**F-21 refers to 21-days prior to launch

d) Errors in ECF volume measurement, plasma, and sodium concentration are small.

Using these assumptions, the correction factor for sodium was calculated as follows:

$$CF_i = \overline{Na^+ Bal}_i - [\Delta ECNa^+_j / N_i] \qquad (33)$$

where

CF_i = correction factor for phase i,

i = pre-, in-, or post-flight,

$\overline{Na^+ Bal}_i$ = average uncorrected sodium balance for phase i

N_i = number of days in phase i

$\Delta ECNa_j^+$ = change in extracellular sodium for period j

= $\Delta(ECF \times [Na^+]_{plasma})_j$

j = interval of time where change was measured as indicated below,

j assumes the following values:

for i = preflight; assume no change in TBNa, i.e., $\Delta ECNa^+ = 0$,

for i = inflight, j = (R+0) – (Preflight Mean)

for i = postflight, j = (R+14) – (R+0)

where R= day of recovery from orbit

The available data supports the hypothesis that the crewmen were in a preflight steady-state with respect to total body sodium and potassium. The measured preflight changes in total body water, body weight, and ECF volume were relatively small as shown in Table F-11. If one considers a nine man average, the changes in TBW, ECF, and BWGT were 0.1667 ± 0.21 liters (mean $\pm$ SE), -0.27 ± 0.15 liters, and -0.056 ± 0.31 kg respectively and statistically are not significantly different from zero (t-test).

In addition to the assumptions described above, it was assumed that all changes in total body sodium occurred in the exchangeable pool, which is approximately 70% of the total body sodium [19]. Bone calcium is known to change during spaceflight [20], and some sodium loss might be expected to accompany the loss of bone calcium. If sodium leaves the body in proportion to the sodium and calcium ratio in bone, based on the calcium losses from the body, approximately 1 meq of bone sodium would be lost during the first month inflight. Estimates of exchangeable potassium on the other hand show that it represents from 85 to 96% of total body potassium [19]. Therefore the measurements are generally taken to accurately represent changes in total body potassium.

A further assumption made for sodium was that exchangeable sodium can be approximated by the ECF volume times the plasma sodium concentration, $[Na^+]_{plasma}$. The plasma compartment is in free communication with the interstitium and lymph and these compartments combined account for 57% of the total exchangeable sodium. Nichols [21] demonstrated that these compartments contribute 70% of the sodium loss during acute sodium loss in dogs.

A potential problem with this analysis concerns the errors associated with the measurements themselves. The inflight change in total body sodium was calculated using the following equation:

$$\Delta TBNa(inflight) = ECF_2 \times [Na^+]_2 - ECF_1 \times [Na^+]_1 \qquad (34)$$

Table F-12. Preflight Total Body Potassium, TBK (meq)

Subject	F-20 & F-21	F-14 & F-16	F-7 & F-8	F-1 & F-2
1	3252	3309	3280	3301 3202
2	3876	3969	3937	3849 3952
3	3822	3839	3949	3920 3803
4	3333	3367	3314	3340
5	3094	3080	3034	3039
6	4536	4602	4687	4760
7	3228	3258		3197
8	3758	3698		3562
9	3612	3678		3551
Mean	**3612**	**3644**		**3607**
±SE	**±448**	**± 463**		**± 521**

* F-20 represents the 20th day prior to launch

where   1 = measured just prior to launch
          2 = measured at recovery

The error in computing ΔTBNa is about two times that of the error in the calculation of either preflight or postflight extracellular sodium alone, since each term above contributes to the change. If the error associated with the sodium concentration is nominally +1 meq and the error of the ECF volume measurement is 0.5 liter (3-4%), the error in ΔTBNa(*inflight)* has a possible value of about 172 meq.

Inasmuch as the calculated value of ΔTBNa inflight was approximately 100 meq, the error is greater than the quantity being calculated. The daily balance is still within acceptable accuracy since the error divided by the average mission length (e.g.,172/57) equals only 3.0 meq/day. Neither does it much affect the difference between flight phases. The error in the plasma Na$^+$ concentration may be less than 1 meq decreasing the potential error in ΔTBNa in proportion to the error of [Na$^+$]$_{plasma}$.

Total body potassium (TBK) was measured *directly* in Skylab using whole-body isotope counts and was not dependent on ECF volume measurements, which were a large potential source of error for computing body sodium. Therefore, the correction factor for potassium was calculated directly according to Eq. (32).

Table F-12 lists the individual preflight TBK measurements from which the mean values of ΔTBK (preflight) were computed and shown in Table F-13. Table F-14 shows the average values of potassium balance (KBal (uncor-

rected)). Table F-15 summarizes the calculations for preflight and inflight potassium skin losses.

Using the inflight values of $\overline{CF_K}$ in Table F-15, it is possible to obtain a corrected daily average for potassium balance:

$$\overline{KBal}(corrected) = \overline{KBal}(uncorrected) - \overline{CF_K} \text{. (35)}$$

These results are presented in Table F-16. From these values, the monthly total cumulative losses of potassium at the end of each month of the mission can be obtained as follows:

Total cumulative loss at the end of the inflight period i (i = I, II, or III)

$$= \overline{KBal}(corrected)_i \text{ x } N_i \qquad (36)$$

where N the number of days in the inflight period i. These values are presented in Table F-17.

Absolute values of TBK were determined by subtracting the monthly losses from the directly measured TBK (preflight mean). The methods of calculating these absolute TBK values are presented below, along with a set of sample calculations.

F.3.2 Sample Calculation (Subject #5):
F.3.2.1 Preflight Skin Loss. From Table F-12, the changes in TBK during the preflight period are calculated as follows,

Table F-13. Changes in TBK from Preflight Average*

Subject	N	Preflight Mean±SD	Postflight	ΔTBK
1	5	3269 ± 43	2998	-271
2	5	3917 ± 52	3678	-239
3	5	3867 ± 64	3528	-339
4	4	3339 ± 22	3151	-188
5	4	3062 ± 30	3029	-33
6	4	4647 ± 98	4485	-162
7	3	3228 ± 31	3108	-120
8	3	3673 ± 100	3348	-325
9	3	3614 ± 64	3169	-445
Mean		**3624**	**3388**	**-236**
SE±		**± 484**	**± 471**	**± 125**

* Preflight value is mean of *N* measurements; only one postflight measurement was made.

Table F-14. Crew Average for Uncorrected Potassium Balance (meq/day)

Mission	Subject	Periods Preflight	Inflight I*	Inflight II	Inflight III
28-day	1	19.27	6.24		
	2	20.80	3.18		
	3	16.75	4.20		
59-day	4	14.66	0.79	9.35	
	5	16.17	0.92	13.17	
	6	20.20	5.16	21.77	
84-day	7	12.29	1.84	0.83	2.45
	8	14.94	4.95	8.08	9.42
	9	17.48	8.95	2.33	14.10
(Mean ± SE)	**(1-9)**	**16.95 ± 2.80**	**4.03 ± 2.67**	**9.26 ± 7.65**	**8.66 ± 5.86**
	(4-9)	**15.96 ± 2.70**			
	(7-9)	**14.90 ± 2.60**			

* inflight periods I, II, and III refer to the first, second, and third inflight months

Table F-15. Estimation of Preflight and Inflight Potassium Skin Losses*

Subject	Preflight**			Inflight			
	Direct ΔTBK (meq)	Uncorrected KBal (meq/day)	$\overline{CF_K}$ (meq/day)	Direct ΔTBK (meq)	Uncorrected KBal (meq/day)	N days	$\overline{CF_K}$ (meq/day)
1	0	19.27	19.27	-271	6.24	28	15.92
2	+25	20.80	19.55	-239	3.18	28	11.72
3	+40	16.75	14.75	-339	4.20	28	16.31
4	+7	14.66	14.31	-188	5.07	56	8.43
5	-55	16.17	18.92	-33	7.05	56	7.63
6	+224	20.20	9.00	-162	13.47	56	16.36
7	-31	12.29	13.84	-120	1.37	84	3.14
8	-196	14.94	24.74	-325	7.48	84	11.35
9	-61	17.48	20.53	-445	8.46	84	13.76
Mean	**5**	**16.95**	**17.21**	**-236**	**6.28**		**11.62**
±SE	**± 111**	**± 2.80**	**± 4.67**	**± 125**	**± 3.50**		**± 4.55**

ΔTBK (direct, preflight)
= TBK(F-1) – TBK(F-20)
=3039 - 3094 = -55 meq

From Table F-14, the uncorrected preflight potassium balance is,

$\overline{KBal}$(uncorrected, preflight) = 16.17 meq/day

From Table F-15, the preflight potassium correction factor for skin losses is,

$\overline{CF_K}$ = $\overline{KBal}$(uncorrected, preflight)
- ΔTBK (direct, preflight)/N days
= 16.17 - (-55/20 days) = 18.92 meq/day

F.3.2.2 Inflight Skin Losses. From Table F-15, the inflight change in TBK measured directly is,

ΔTBK (direct, inflight) = -33 meq

From Table F-14 the uncorrected inflight potassium balance is

$\overline{KBal}$(uncorrected, inflight) for period I = 0.92 meq/day
for period II = 13.17 meq/day

From Table F-15, the inflight potassium correction factor for skin losses is,

$\overline{CF_K}$ = [($\overline{KBal}$(uncorr)xN)$_I$ + ($\overline{KBal}$(uncorr) x N)$_{II}$
- ΔTBK(direct)]/(N_I + N_{II})
= [0.92 x 28 days + 13.17 x 28 days - (-33)] / 56 days
= 7.63 meq/day

F.3.2.3 Corrected K⁺ Balances. The potassium balances can be corrected simply by subtracting the correction factor, CF_k from the uncorrected potassium balance:

$\overline{KBal}$(corrected) = $\overline{KBal}$(uncorrected) – $\overline{CF_K}$

So that from Tables F-14 and F-15:

$\overline{KBal}$(corrected, preflight) = 16.17-18.92 = -2.75 meq/day

and

$\overline{KBal}$ (corrected, inflight) for period I = 0.92 - 7.63 = -6.71
for period II = 13.17 - 7.63 = 5.54

F.3.2.4 Monthly Inflight Losses (Gains), ΔTBK. The changes in TBK for each monthly inflight period is computed by summing the daily corrected balances over the 28 days in each period (see Table F-16 and F-17).

Table F-16. Crew Average for Potassium Balance (Corrected for Skin Losses), meq/day

Mission	Subject	Periods			
		Preflight	Inflight I*	Inflight II	Inflight III
28-day	1	0.00	-9.68		
	2	1.25	-8.54		
	3	2.0	-12.11		
59-day	4	0.35	-7.64	0.92	
	5	-2.75	-6.71	5.54	
	6	11.2	-11.20	5.41	
84-day	7	-1.55	-1.30	-2.31	-0.69
	8	-9.80	-6.40	-3.27	-1.93
	9	-3.05	-4.81	-11.43	0.34
Mean ± SE	**1-9**	**0.35 ± 5.54**	**-7.60 ± 3.32**	**-0.86 ± 6.37**	**-0.76 ± 1.14**
	4-9	**-0.02 ± 6.9**			
	7-9	**-4.8 ± 4.39**			

* Inflight periods I, II, and III refer to the first, second, and third inflight months

Table F-17. Crew Averages for Monthly TBK Changes* (meq)

Mission	Man	Periods			
		Preflight	Inflight I**	Inflight II	Inflight III
28-day	1	0	-271		
	2	+25	-239		
	3	+40	-339		
59-day	4	+7	-214	+26	
	5	-55	-188	+155	
	6	+224	-314	+152	
84-day	7	-31	-36	-65	-19
	8	-196	-179	-92	-54
	9	-61	-135	-320	+10
Mean ±SE		**-5 ± 111**	**-213 ± 93**	**-24 ± 179**	**-21 ± 32**
Cumulative Shift from Preflight			**-208**	**-227**	**-243**

* TBK changes = KBal (corrected) x N (days)
** Inflight periods I, II, and III refer to the first, second, and third inflight months

Inflight I Loss = -6.71 x 28 = -188 meq
Inflight II Gain = +5.54 x 28 = +155 meq

F3.2.5 Total Body K⁺ During Mission. The value for TBK at the end of the several inflight periods is obtained as follows:

TBK(*preflight mean, direct*) =	3062
Inflight I ΔTBK =	- 188
TBK at end of Period I =	2874 meq
Inflight II ΔTBK =	+155
TBK at end of Period II =	3029 meq

F.3.3 Alternative Method for Computing Electrolyte Sweat Losses

During the evaluation of Hypothesis #5 (Chapter 5), another technique was discovered that could be useful for indirectly estimating sweat losses of sodium and potassium for the Skylab crew. Figure F-3 depicts a simplified fluid-electrolyte model of the body for the purpose of illustrating the exchange of fluid and electrolytes between intracellular and extracellular compartments including intake, sweat, and renal losses. The quantities that have been measured directly or derived are indicated with an asterisk. If only the water and sodium exchange across the extracellular compartment are considered (i.e., exclude potassium and water exchange with the intracellular compartment), the extracellular sodium concentration can be uniquely determined by knowing the initial concentration and any net changes which occur in the balance between intake and output from this compartment. This is similar to the problem of determining the concentration of a substance, *X*, in a holding tank after a certain quantity of water and *X* has been added. Conversely, if the change in concentration of *X* is known, the amount of substance added can be derived. In this manner, it is possible to determine the sodium sweat component by using the experimental extracellular sodium concentration data and the other components of the metabolic balances. Similarly, potassium losses (from sweating and cell loss) can be estimated from the plasma potassium concentration.

All the elements shown were included in the Guyton model and the current version of the model can be used to evaluate this technique; alternatively, it may be desirable to formulate a much simpler model based on Fig. F-4. A suggested mode of operation is shown in that graphic. Known values of intake and renal losses are input into the model, and values for electrolyte losses are assumed. The normal mode of using the Guyton model does not include forcing renal excretion as required by this method; thus, the name "push-pull" has been adopted (i.e., fluids are both pushed and pulled from the model). Predicted sodium and potassium responses are then compared to the experimental response. Extracellular electrolyte concentrations and total body losses of electrolytes in a given time period can both be compared. Iteration to obtain the "best fit" between experimental and predicted results leads to an estimated value of the electrolyte losses.

Preliminary results using this method have been encouraging. They have suggested that potassium and particularly sodium sweat losses were actually higher than control during the first few days of flight, before being reduced below control as originally estimated in Fig. 9-18. This is in keeping with the results of evaporative water losses which show the same trend. This information was utilized in a simulation of combined hypotheses which are shown in Chapter 5 (Figs. 5-32 and 5-33).
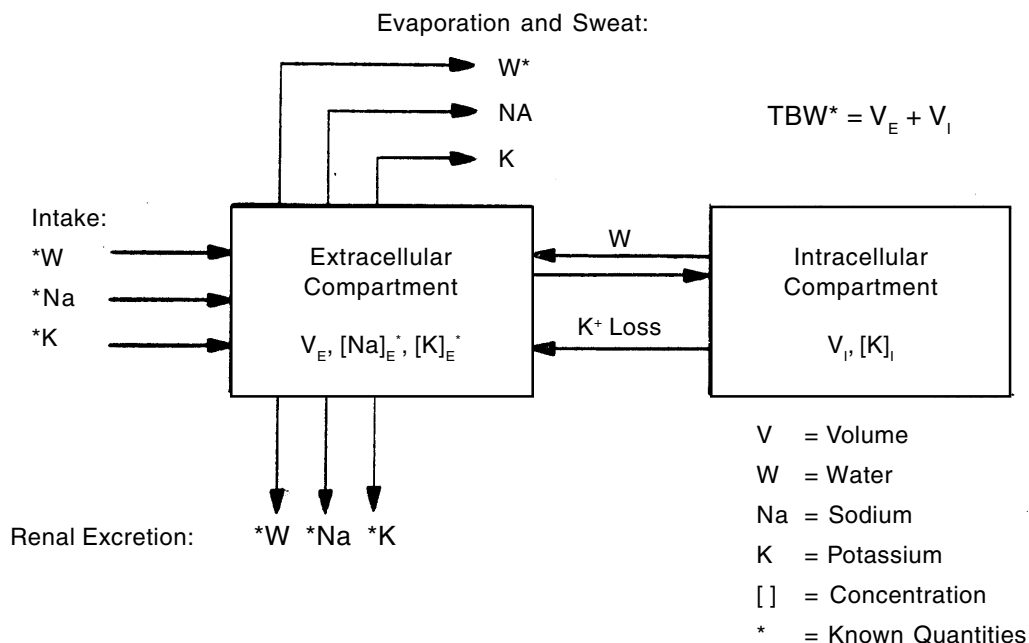
Figure F-3. Simplified fluid-electrolyte model.
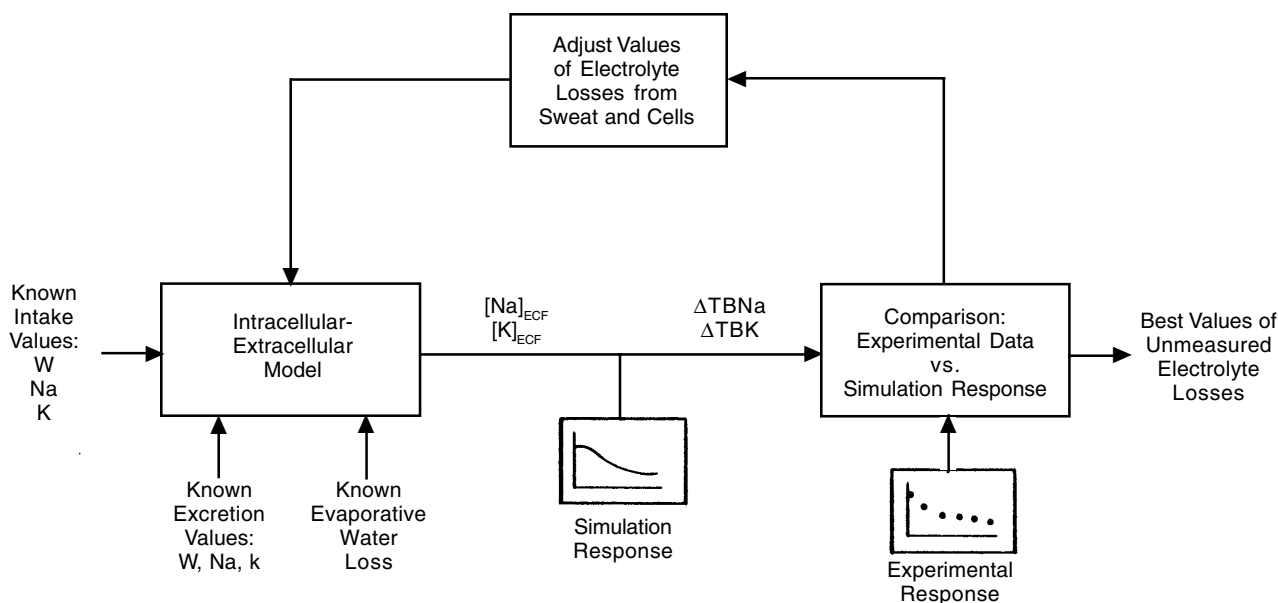
Figure F-4. Push-Pull simulation procedure for estimating unknown electrolyte loss rates.

F.4 Quantification of Tissue Loss Resulting From Prolonged Spaceflight

This section describes details of the Skylab lean body mass analysis that, for convenience, were not presented in Chapter 4.5. The reader is also referred to the original reports for a full discussion [22,23].

F.4.1 Methods of Calculation and Assumptions

Table F-18 summarizes alternative methods that were used in this study to quantify lean body mass (LBM)*. According to the references cited in Table F-18, the LBM [24] has a water content of about 73%, a potassium content of 60-70 meq/kg (in men), and a density of about 1.1 gm/cm³. In contrast, body fat contains less water (14%) and negligible potassium content, and has a lower density of about 0.9 gm/cm³. It is possible to estimate the relative proportions of fat and lean tissue in the body by measuring total body water (TBW), total body potassium (TBK), or body density (D), and assuming a simple two-compartment model (fat and fat-free). Body density is commonly derived from body mass or weight (BWGT) divided by body volume (BVOL). All of these measurements were available from the various Skylab experiments (see Table F-19). Empirical relationships have been suggested for predicting lean body mass from combinations of either TBW and TBK or TBW, TBK, BVOL and BWGT. Losses in lean body mass were obtained by using the relationships shown in

Table F-18 and by comparing the preflight period with the first postflight day of recovery. An inflight metabolic nitrogen balance provided an additional measure of lean tissue loss. The cumulative algebraic sum of nitrogen balances, obtained each day of the mission, indicates the net loss (or gain) of body nitrogen. Since protein contains an average of 16% nitrogen by weight, and lean body mass is composed of 19.4% protein, it is possible to quantify protein and lean body mass from the cumulative nitrogen balance [24,25].

Table F-20 presents individual subject results for inflight LBM changes derived from each method. This table is presented in summarized form in Chapter 4.5, Tables 4-16 and 4-20. The values in this table were used to perform correlation analyses between the various methods and these are discussed in Chapter 4.5. Further detailed calculation of each method can be found in the original report [22].

F.4.2 Experimental Approach
F.4.2.1 Measurements. Total body water (TBW) and total body potassium (TBK) were obtained by the isotopic dilution of isotopic hydrogen and potassium, respectively [18]. Body volume (BVOL) was computed from a stereophotogrammetric method involving four cameras to make two stereoscopic pairs of photographs from the front and back and using computer analysis to determine the volume of different body regions and of the body as whole [34]. Body mass (BWGT) was measured by conventional scales in terrestrial environment and by the principles of oscillating masses during spaceflight [16].

The nitrogen balance consisted of daily monitoring of dietary intake and daily collections and analysis of urine and fecal excreta [35]. Only preflight and postflight measurements were possible for TBW, TBK, and BVOL. Body mass and metabolic balances of nitrogen and potassium

---

* In this study, it was assumed that the difference between the lean body mass (body mass less storage fat) and fat-free mass (body mass less all other extractable fat); i.e., the essential body fat (about 2% of body weight), is negligible.

were determined daily throughout the preflight, inflight, and postflight period.

F.4.2.2 Pooling of Subjects. The periods of weightlessness associated with each of the three Skylab missions were 28 days, 59 days, and 84 days. Data presented in this and other reports [8] show that the largest losses in weight occurred during the first month and suggest that minimal changes were associated with the last two months, especially for body weight, body water, and lean body mass. For this reason, as well as the limited number of subjects available (three crewmembers on each flight), it was decided to pool the results of all nine subjects in summarizing changes in body composition. However, the data were also examined and discussed with respect to duration of flight. Paired t-tests were used to assess statistical significance of inflight changes.

F.4.3 Errors in the TBK Method

In Chapter 4.5, it was discussed that the method based on TBK did not at first provide reasonable results (labeled "uncorrected" in Table 4-16). A correction factor was successfully applied based on the assumption that a significant amount of potassium leaves the cellular compartment independently of other cell constituents due to osmotic considerations. The inflight changes of lean body mass calculated from the simple, *uncorrected* formula (LBM = TBK/65) was –3.63 ± 1.93 Kg while that calculated by applying a *correction* for an inflight osmotic effect was –1.55 ±1.96 Kg. This latter value is in better agreement with the other methods studied. The following section discusses the possible errors in the TBK method and demonstrates precisely how the correction was applied.

F.4.3.1 Sources of Error. The unreasonably high values for LBM losses derived from the uncorrected TBK method were examined by considering the following factors:

a) The factor of 65 meq K+/kg LBM used in the calculations (see Table F-18) may be inappropriate for the astronaut population. Values from the literature reveal that the potassium content of lean body mass is normally within the range of 60 - 70 meq K+/kg [28,36,37]. If the mean inflight LBM loss of 1.5 kg obtained by the average of the other methods is accepted, then the measured inflight loss of 235 meq K+ would require a concentration of 235/1.5 = 157 meq K+/kg LBM, and this value is so far out of the normal range that other explanations must be sought, such as those described in (b) and (c) below,

b) The possibility must be considered that the measured values of TBK were erroneous and that the potassium losses were overestimated due to systematic errors in the technique. The total accuracy of the isotope dilution method for ^{40}K may be several percent [38]. A systematic error of this magnitude could explain most of the discrepancy in the calculation of LBM loss. It had been noted that in certain pathological situations, this technique was subject to large errors in predicting LBM [39]. However,

preflight values were reasonable, and it was not clear how the inflight conditions or postflight measurements could challenge the suitability of this method.

c) A significant fraction of the measured TBK loss may have been unaccompanied by other cellular components such as nitrogen and water (which together constitute about 90% of LBM). As discussed in Chapter 4.5 the ratios water:potassium:nitrogen in lost body mass are often greater than the normal cellular ratios of these components. Although it is not clear why this should happen, and the metabolic balance data for nitrogen and potassium do not support this conclusion, this phenomenon is still a possibility on Skylab.

In addition to the high values of lean body mass loss predicted by the uncorrected TBK method, the expected intracellular water loss also appears rather high. Using a value of 160 meq/liter for the intracellular potassium concentration [40], it would be expected that 1.5 liters of cell water would be lost with the observed decrement of 236 meq potassium assuming iso-osmotic loss and that potassium was the most significant osmotically active substance undergoing change. This was large compared to the total weight loss of 2.39 kg, the measured total body water change of 0.8 liters, or the derived intracellular water loss of 0.5 liters [18].

One explanation for these discrepancies could have been a mild, but persistent dilution of sodium concentration and osmolarity in extracellular fluid as measured from plasma samples obtained at regular intervals throughout the flight [18]. This was also noted in several bedrest studies [41,42], and while it has not yet been explained, osmotic balance requires that intracellular fluid be similarly dilute [19]. Also, it can be calculated that a lesser amount of water will be expected to accompany potassium osmotically from the cell if body fluids become hypotonic (see Fig. 5-28; [22]). Therefore, two components of potassium loss have been postulated: an *osmotic loss* which satisfies osmotic balance in the face of extracellular dilution and a *muscle atrophy loss* which was accompanied by nitrogen and other cellular constituents. This assumption has been translated into quantitative terms using the changes in plasma sodium concentration as correction factors. A sample calculation appears below.

F.4.3.2 Correction of the TBK Method. A mean change in plasma sodium concentration of –4.53 mEq/l was measured during the inflight phase over a three-month period (see Table F-21). Assume that a portion of the potassium leaving the cellular compartment unaccompanied by protein and water is equivalent to the amount necessary to dilute intracellular potassium to the same extent as sodium is diluted in the extracellular compartment (i.e., a mean decrease in sodium concentration of 4.53 meq/l measured throughout the inflight phase). Also assume that this is a generalized potassium loss throughout the intracellular compartment; i.e., 29.6 liters (measured preflight).

Therefore, this component of the potassium loss, to satisfy osmotic equilibrium, can be estimated to be

Table F-18. Mathematical Description of Methods Used in Determining Body Composition Changes*

Method	Concept	Equation
Total Body Water	Lean body mass is 73.2% water [26]	$LBM = TBW/0.732$
Total Body Potassium	Lean body mass contains 65 meq K+/kg [27,28]. This value is age dependent and has been adjusted to mean age of astronauts (40.7 years)	$LBM = TBK/65$
Total Body Water + Total Body Potassium	Lean body mass is estimated from sum of body water + cell solids + bone mineral. Cell solids estimated from TBK and bone mineral assumed to be a constant proportion of cell solids [28]. Assume inflight bone mineral loss does not contribute significantly to body weight change [29].	$LBM = TBW + \dfrac{TBK}{320.6} + \dfrac{0.334\,TBK\,*}{320.6}$ where TBK* = preflight value
Cumulative Nitrogen Balance	Cumulative inflight nitrogen balance assumes negligible loss of sweat component. Protein contains 16% nitrogen [30]; LBM contains 19.4% protein [24].	$N\,Bal = N(diet) - N(urine) - N(feces)$ $\Delta Protein =$ $\quad N\,Bal \times Mission\,Length \times 6.25$ $\Delta LBM = \Delta Protein/0.194$
Body Density (Stereophotometric)	Body segmented into fat and essential body mass compartments, each having characteristic density. Densities determined from average of four different studies [26,31-33]: Fat (0.9168 gm/cm³), LBM (1.0997 gm/cm³).	$LBM = BWgt\left(6.01 - \dfrac{5.51}{D}\right)$
"Combined" Method (Stereophotometric)	Lean body mass is the difference between body weight and fat mass. Body fat is estimated as the difference between measured volume of body and sum of the calculated volumes of body water and cell solids [28]. Method uses combination of all data shown in Table F-19. Results of this method reported here were taken directly from Whittle [29] and cannot be derived precisely from values given in Table F-19 because of the use of certain correction factors in the original calculations.	$LBM = BWGT$ $-\,0.901\left(Body\,Vol - \dfrac{TBW}{0.994} - \dfrac{TBK}{448.6} - \dfrac{0.334TBK\,*}{847.8}\right)$ where TBK* = preflight value

Note 1. All quantities expressed as kg (LBM, FAT, BWGT, Protein) or milliequivalents (TBK).
Note 2. Assume essential body fat is negligible; i.e., fat free mass = lean body mass.
Note 3. Symbols: TBW=total body water; TBK=total body potassium; LBM=lean body mass; BWGT=body weight; D=body density; N=nitrogen

osmotic loss = 4.53 meq/1 x 29.6 liters = 134 meq K+

The actual loss of potassium that can be claimed to be a result of muscle atrophy (i.e., accompanied by nitrogen and water) is the difference between the measured inflight loss (Table F-19) and the osmotic loss:

muscle atrophy loss = 235 - 134 = 101 meq K+

The *lean body mass* (LBM) loss attributed to muscle atrophy is obtained from the relationship (Table F-18):

$\Delta LBM = (\Delta TBK/65) = (101/65) = 1.57$ kg

The *protein loss* (PRO) is assumed to be 19.4% of the LBM loss:

$\Delta PRO = 0.194 \times 1.57 = 0.30$ kg

Altenatively, the protein:potassium ratio of the LBM is known to be 3.06 gm/meq [36], so that

$\Delta PRO = 3.06 \times 101 = 0.31$ kg.

The *fat loss* is:

$\Delta FAT = \Delta BWGT - \Delta LBM = 2.69 - 1.57 = 1.12$ kg.

The *intracellular water* loss accompanying 101 meq K+ can be estimated from the concentration of cell K+ [40]:

$\Delta intracellular\,water = \left[\dfrac{101\,meq}{160\,meq/liter}\right] = 0.64\,liters$

These calculations are summarized below for both the uncorrected and corrected cases:

Table F-19. Body Composition Parameters Before and After Skylab Mission

Subject	Body Wgt (Kg)[1] Pre	Post	Δ	Body Volume (liters) Pre	Post	Δ	Total Body Water (liters) Pre	Post	Δ	Total Body Potassium (meq) Pre	Post	Δ
1	62.2	60.2	-2.0	59.00	56.62	-2.38	41.55	40.8	-0.75	3270	3000	-270
2	77.9	74.3	-3.6	75.22	70.65	-4.57	48.80	48.0	-0.80	3915	3680	-240
3	80.2	76.0	-4.2	76.42	71.26	-5.16	52.15	50.0	-2.15	3865	3530	-340
4	68.6	64.6	-4.0	63.55	59.98	-3.57	42.50	41.9	-0.60	3340	3150	-190
5	61.8	58.7	-3.1	56.74	53.58	-3.16	39.10	39.6	+0.50	3060	3030	-35
6	88.0	84.1	-3.9	81.23	77.36	-3.87	53.60	51.9	-1.70	4645	4485	-160
7	67.8	67.8	+0.1	63.87	64.52	+0.65	41.85	41.0	-0.85	3230	3110	-120
8	71.5	68.6	-2.9	68.38	65.04	-3.34	45.40	44.9	-0.50	3675	3350	-325
9	67.6	66.1	-1.5	63.71	61.98	-1.73	45.65	45.1	-0.55	3615	3170	-445
Mean	71.7	68.9	-2.8*	67.57	64.55	-3.02*	45.62	44.8	-0.82*	3625	3390	-235*
SD	± 6.7	± 8.1	± 1.4	± 8.36	± 7.56	± 1.72	± 5.00	± 4.4	± 0.75	± 484	± 471	± 125

*p > 0.995 that postflight is different from preflight
Note 1. Preflight body weight is mean of daily measurements during 2-3 week period to launch. Postflight body weight value is the first shipboard measurement after reentry.Measurements of other parameters were made less frequently preflight and were made on either the 1st or 2nd day postflight.

Table F-20. Inflight Changes in Lean Body Mass for Each Skylab Subject using Various Methods*

Subject	TBW	TBK	TBW + TBK	Cumulative Nitrogen Balance	Body Density	Combined Method
1	-1.02	-2.09	-1.17	-0.87	-2.43	-1.96
2	-1.10	-1.80	-1.16	-2.00	+2.21	-0.86
3	-2.93	-2.91	-2.74	-1.54	-4.20	-3.65
4	-0.82	-0.32	-0.67	-1.88	-7.47	-2.85
5	+0.69	-0.09	+0.48	-1.48	-4.61	-1.12
6	-2.32	+1.34	-1.43	-1.54	-2.07	-3.38
7	-1.16	-0.45	-0.94	-3.35	-4.49	-1.89
8	-0.68	-2.15	-0.94	-1.84	+3.31	-0.39
9	-0.75	-5.45	-1.65	-0.13	+4.06	-0.36
Mean	+1.12	-1.57	-1.14	-1.63	-1.74	-1.83
SD	±1.03	±1.96	±0.85	±0.87	±4.03	±1.25
Normalized to ΔBWGT = -2.72	-1.22	-1.58	-1.15	-1.85	-1.56	-1.64

*in kilogram

Body Composition Changes from TBK Loss

	Uncorrected	Corrected for Dilution	Other Estimates
ΔLean body mass (kg)	-3.63	-1.57	-(1.2 to 1.6)
ΔFat (kg)	+0.94	-1.12	-(1.0 to 1.5)
ΔProtein (kg)	-0.70	-0.31	-(0.2 to 0.4)
ΔIntracellular water (liter)	-1.50	-0.64	-0.5

While this is a speculative exercise, the predicted body composition variables (middle column) were in better agreement with other independent measurements discussed in Chapter 4.5 (last column) after the correction was applied. The computations for each crewman, based on the above method, are shown in Table F-21.

F.4.4 Errors in the Nitrogen Balance

Errors in the nitrogen balance technique have been reviewed by Hegsted [9], and discussed by Grande [24], Calloway [30], Forbes [43], Wallace [44], and Steffee [45]. The two major errors most often mentioned were: (a) the fact that certain losses are not measured in the usual balance study, especially fluid or nutrients lost through the skin, thereby making the balances falsely high, and (b) there is a consistent bias in most balance studies arising from an overestimation of intake (the subject may not eat all of the food offered, but cannot consume more than is offered) and an underestimation of output (it is difficult to collect all excreta and impossible to collect more excreta than was actually produced) thus making the balances falsely high. In the Skylab metabolic experiments, collection of excreta and measurement of food and water intake were carefully performed and corrections were included for food not eaten at each meal. However, it must be recognized that it was more the responsibility of the crewmen than the principal investigators to perform the actual collection and reporting tasks during the inflight phase. Nevertheless, the crewmembers were highly trained and well motivated subjects and it is unlikely that consistent errors were introduced.

With regard to other errors in the nitrogen balance, it has been estimated that dermal losses of nitrogen were found to be less than 0.5 g/day for sedentary men in a comfortable environment. Sweating due to heavy exercise may result in not more than another 0.5 g/liter of evaporative loss [9,30] (it has been estimated that sweat losses of the Skylab crew were less than one liter/day). The Skylab subjects exhibited such high net nitrogen retentions during the preflight phase of the study (3 gm/day) that it cannot be reversed by subtracting even 1 gm/day of unmeasured dermal losses. Further, it is important to note that the preflight Skylab nitrogen balances are in good agreement with the net retention found by other investigators for the particular dietary levels observed.

In attempting to explain the positive nitrogen balances that are normally seen in most normal subjects, Steffee [45] suggests that another route of unmeasured losses may be molecular nitrogen (gas). He says "there is now increasing evidence to indicate that this route, hith-erto regarded as unlikely in mammalian organism, may be an important factor in nitrogen loss during generous intakes of protein in healthy subjects or during some pathological condition. The evidence, based on various approaches, has been reviewed and appears to provide a likely explanation for the positive balance values". It should be noted that a positive nitrogen retention, if real, argues as well for a positive total body potassium retention during the preflight phase. But TBK measurements do not suggest any change in this quantity, a discrepancy we cannot resolve.

The presence of these errors in the nitrogen balance should serve as a warning to interpret the balance results with some degree of caution. They do not, however, negate the fact that the Skylab crewmen's nitrogen balance changed direction upon launch and again upon recovery (see Fig. F-9). The positive nitrogen balances observed during the preflight phase could have been expected because of the following: a) the dietary nitrogen consumed in the calibrated preflight phase was probably higher than in the crew's daily life prior to flight and b) the increased activity of the crew as they exercised according to a rigid schedule may have had an anabolic effect on lean body mass. The dramatic shift in direction during the inflight phase to a negative balance is in keeping with the concept of atrophy of unused postural muscles in a microgravity environment. This concept would also argue for the observed postflight recovery of nitrogen when the subjects return to a world of gravity and must reactivate and rebuild the postural muscles. The leveling off of nitrogen loss after the first month during the last two flights suggests that there was a lower limit of protein loss reached irrespective of the level of exercise or time inflight.

F.5 Energy Balance and Body Composition of Weight Loss During Prolonged Spaceflight

This section of the Appendix presents the details of the approach, assumptions and methods of computation associated with Chapter 4.6. Further details can be found in Leonard [46,47].

F.5.1 Computational Procedures and Assumptions

The analysis for deriving body compositional changes were based on two formulations: a) an equation of body composition and b) an equation for energy balance. In the first of these equations, the change in body weight (ΔBWGT) was assumed to result from changes in total body water (ΔTBW), body protein (ΔPRO), and body fat (ΔFAT). Thus,

$$\Delta BWGT = \Delta TBW + \Delta PRO + \Delta FAT \qquad (37)$$

For the second equation which describes energy balance, net energy utilization (E_{util}), was computed as the sum of energy intake from diet (E_{diet}) minus energy excreted in urine (E_{urine}) and feces (E_{feces}) plus energy available from body tissue catabolism (energy from body fat, E_{fat} and body protein, E_{pro}). Thus,

Table F-21. Inflight ΔLBM from TBK Method (Corrected for Dilution Effect)

Subject	ICF (liters)	[ΔNa] (meq/l)	ΔTBK Estimated Osmotic Loss (meq)	ΔTBK Measured (meq)	ΔTBK Corrected (meq)	ΔLBM (Kg)	ΔProtein (Kg)	ΔFat (Kg)	ΔBWGT (Kg)
1	25.4	-5.3	-135	-271	-136	-2.09	-0.406	+0.08	-2.01
2	33.3	-3.65	-122	-239	-117	-1.80	-0.349	-2.29	-4.09
3	36.6	-4.10	-150	-339	-189	-2.91	-0.565	-1.27	-4.18
4	24.6	+6.8	-167	-188	-21	-0.32	-.62	-3.64	-3.96
5	24.4	-1.11	-27	-33	-6	-0.09	-0.018	-3.03	-3.12
6	34.7	-7.18	-249	-162	+87	+1.34	+0.260	-5.25	-3.91
7	28.0	-3.25	-91	-120	-29	-0.45	-0.087	+0.60	+0.15
8	29.0	-6.37	-185	-325	-140	-2.15	-0.417	+0.44	-1.71
9	30.3	-3.0	-91	-445	-354	-5.45	-1.06	+4.05	-1.40
Mean	**29.6**	**-4.53**	**-135**	**-236**	**-101**	**-1.55**	**-0.30**	**-1.14**	**-2.69**
SD	**4.4**	**2.02**	**64**	**125**	**128**	**1.97**	**0.38**	**2.78**	**1.53**
		(p < 0.001)	(p < 0.01)	(p < 0.01)	(p < 0.05)	(p < 0.05)	(p < 0.05)	NS	(p < 0.01)

Key: ICF – Intracellular fluid (measured preflight)

[ΔNa] = Average change in sodium plasma concentration (inflight - preflight)

ΔTBK (osmotic loss) = ICF x [ΔNa]

ΔTBK (corrected) = ΔTBK (measured) - ΔTBK (osmotic loss)

ΔLBM = ΔTBK/65

ΔProtein = ΔLBM x 0.194

$$E_{util}{}^* = \text{Work (internal + external) + Heat lost}$$
$$= E_{diet} - E_{urine} - E_{feces} + E_{fat} + E_{pro} \quad (38)$$

As suggested by Eq. (38), the net energy available from food and tissue metabolism is assumed to be utilized entirely to perform work and produce heat. $E_{util}{}^*$ is starred (*) to designate that it could not be measured directly or indirectly on a daily basis (i.e., by measuring work and heat lost or oxygen consumption) as were the other terms in Eq. (38). It was assumed that $E_{util}{}^*$, expressed as a daily average quantity for the preflight, inflight, or postflight phases, was constant throughout that phase for each crew member.

For convenience, the remainder of the computational procedures related to these equations are described in three parts: (F.5.1.1) determination of $E_{util}{}^*$, (F.5.1.2) determination of daily estimates of ΔTBW and ΔFAT and the latter's caloric equivalent, E_{fat} and (F.5.1.3) determining cumulative estimates of weight and tissue changes. In addition, (F.5.1.4) the computational procedures are provided for estimates of energy requirements that would prevent loss of body weight during spaceflight.

F.5.1.1 Determination of Mean Energy Utilization, $E_{util}{}^*$.
$E_{util}{}^*$ was determined from Eqs. (37) and (38) by assuming each term in these formulations represented overall mission quantities. For example, ΔBWGT, which normally refers to daily changes in body mass would, in this part of the analysis, refer to change in net mass between the day of launch and day of recovery. When used in this way, the term is designated with a bar, thus $\Delta \overline{BWGT}$. Each term in Eq. (37), so designated, can be estimated except for $\Delta \overline{FAT}$. Body weight changes, $\Delta \overline{BWGT}$, were measured daily and directly, body water changes ($\Delta \overline{TBW}$) by isotope dilution techniques at launch and recovery, and protein losses ($\Delta \overline{PRO}$) estimated from cumulative daily nitrogen balance using a factor 6.25 to determine the protein equivalent of nitrogen [30]. Refer to Table F-22 for a summary of the methods used to compute each term in this analysis.

Overall mission fat losses for each subject were thereby calculated by solving Eq. (37) for $\Delta \overline{FAT}$. Using the caloric equivalent of this loss, $\overline{E_{fat}}$, it was possible to derive the cumulative energy utilized, $\overline{E_{util}{}^*}$, from Eq. (38) in which $\overline{E_{diet}}$ was determined from the caloric equivalent of dietary content of protein, fat and carbohydrate [3,4], $\overline{E_{urine}}$ from urinary nitrogen (N_{urine}) and taken to be 8.32 x N_{urine}. $\overline{E_{feces}}$ was measured directly by bomb calorimetry, and $\overline{E_{pro}}$ was estimated from the caloric equivalent of the nitrogen balance losses (i.e., $\overline{E_{pro}}$ = 5.65 x 6.25 x $\overline{N_{BAL}}$). Each of these terms representing daily quantities was summed over the entire mission phase and used in Eqs. (37) and (38). The value of $\overline{E_{util}{}^*}$ obtained from this calculation was divided by the number of mission days to estimate $E_{util}{}^*$. Values of $E_{util}{}^*$ so computed, are shown in Table F-23.

F.5.1.2 Daily Estimates of Body Water and Body Fat Changes.
Daily changes in body fat were determined by solving Eq. (38) for E_{fat}, using the derived constant value of $E_{util}{}^*$ and daily measured values of the other components E_{diet}, E_{urine}, E_{feces}, E_{fat}, and E_{pro}. Daily body fat changes were converted from energy (E_{fat}) to mass equivalents (ΔFAT) and used to compute ΔTBW from Eq. (37). Daily body mass changes (ΔBWGT) and body protein changes (ΔPRO) used in this computation were estimated as previously described.

F.5.1.3 Cumulative Estimates of Weight, Water, and Tissue Changes.
Cumulative changes in each of the quantities in Eq. (37) were calculated by summing the consecutive daily balances over any desired time interval. The interval of each day's balance period was taken to be from morning to morning. The experimental protocol specified that each day would begin after the last urine and fecal void prior to breakfast. Body mass measurements were made each day after overnight fasting. It was convenient to use the morning of the day of launch as the reference point from which cumulative balances were computed. Thus, the prelaunch period required a backward calculation from the point of reference (i.e., launch).

The calculation schema outlined above is shown in the idealized graph Fig. F-5. The average net dietary intake (i.e., $E_{diet} - E_{urine} - E_{feces}$) is indicated by the lowest solid curve. The dashed horizontal line represents the average daily energy utilization, $E_{util}{}^*$, for the inflight period. The difference between mean energy utilization and net dietary intake is the deficit between net calories derived from the diet and the energy actually required. This energy difference is assumed to be supplied by fat and protein tissue catabolism (carbohydrate stores in the body being assumed insignificant) as suggested by Eq. (38). The area bounded between the horizontal dashed and lower solid lines and any two time intervals is the energy equivalent of the cumulative tissue loss (protein + fat) during that interval. If daily protein changes can be assumed from the nitrogen balance (hatched area in Fig. F-5), it is possible to derive daily fat losses from this area of the graph as shown. The difference between total weight loss and the sum of fat and protein losses is then taken to be the daily change in body water, as indicated by Eq. (37).

The data corresponding to the idealized representation of Fig. F-5 is presented in Fig. 4-23. Figure F-6 show a similar analysis except that each mission is shown separately. Considering only the inflight period, the difference between the net caloric intake and the energy utilization curves is diminished for each longer mission. This was a result of increased caloric intake (per kg of BWGT). These differences, averaged over the inflight period are -448 kcal/day, -360 kcal/day, and +23 kcal/day for the 28-day, 59-day and 84-day missions respectively; (a negative sign indicates a dietary deficiency whereby tissue is catabolized, and a positive sign indicates a dietary excess whereby tissue is stored).

F.5.1.4 Estimates of Inflight Caloric and Exercise Requirements to Prevent Loss of Body Weight.
After completing the above calculations it was possible to undertake regression analyses of the type described by Whittle [48] in attempts to estimate the caloric and exer-
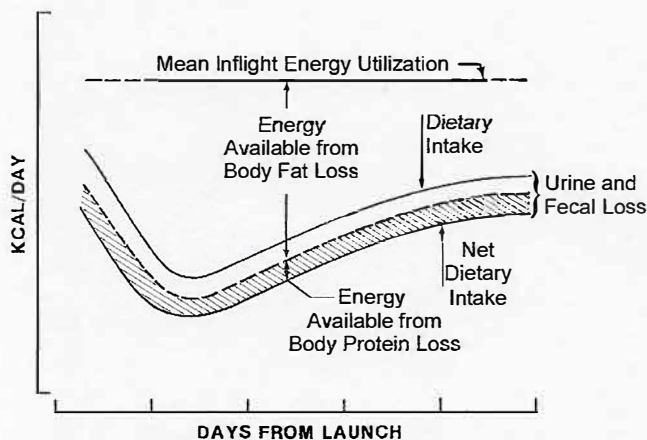
Figure F-5. Estimation of tissue loss from energy balance components. This figure is an idealized version of Fig. 4-23.

cise requirements that would maintain preflight body weight during the inflight phase. For these analyses a regression equation was derived and employed:

$$\Delta M / \Delta T = C \times (E_O - E_R) \qquad *(39)$$

where ΔM = change in body mass, body fat, or body protein (gm/kg BWGT) over an inflight time interval, ΔT

* C is a constant, the slope of the line in Fig. 4-29, and is not needed in the analysis.

(days), E_O = observed energy intake from food (kcal/d/kg BWGT) or observed energy expenditures for exercise (kcal/d/kg BWGT), and E_R = energy required from food at which no change in body mass or body fat occurs (kcal/d/kg BWGT) or energy required for exercise at which no change in body mass or body protein occurs (kcal/d/kg BWGT).

Using Eq. (39) both caloric intake and exercise energy expenditures could be separately correlated with the average rate of body mass loss ($\Delta M/ \Delta T$). In addition, caloric intake could be correlated with body fat assuming that an adequate diet would prevent loss of body fat. Similarly, exercise could be correlated with body protein on the assumption that an adequate exercise level would prevent the loss of body protein. The introduction of the term $\Delta M/ \Delta T$ allows us to account for the effect of different mission lengths. Two sets of regression analysis were performed: a) using data for the entire mission, and b) using data for only the first month of each flight (see Table F-30].

F.5.2 Supplementary Data for Energy Balance Analysis

In Chapter 4.6 the results from the body composition and energy balance analysis are presented as mean values for each of the three Skylab missions. Tables F-24 to F-30 are referred to in Chapter 4.6, and show the corresponding results for each crewman. Figures F-7 to F-10 are an alternate method of viewing the daily estimated changes of body weight, body water, body protein, and body fat that are also illustrated in Fig. 4-28.
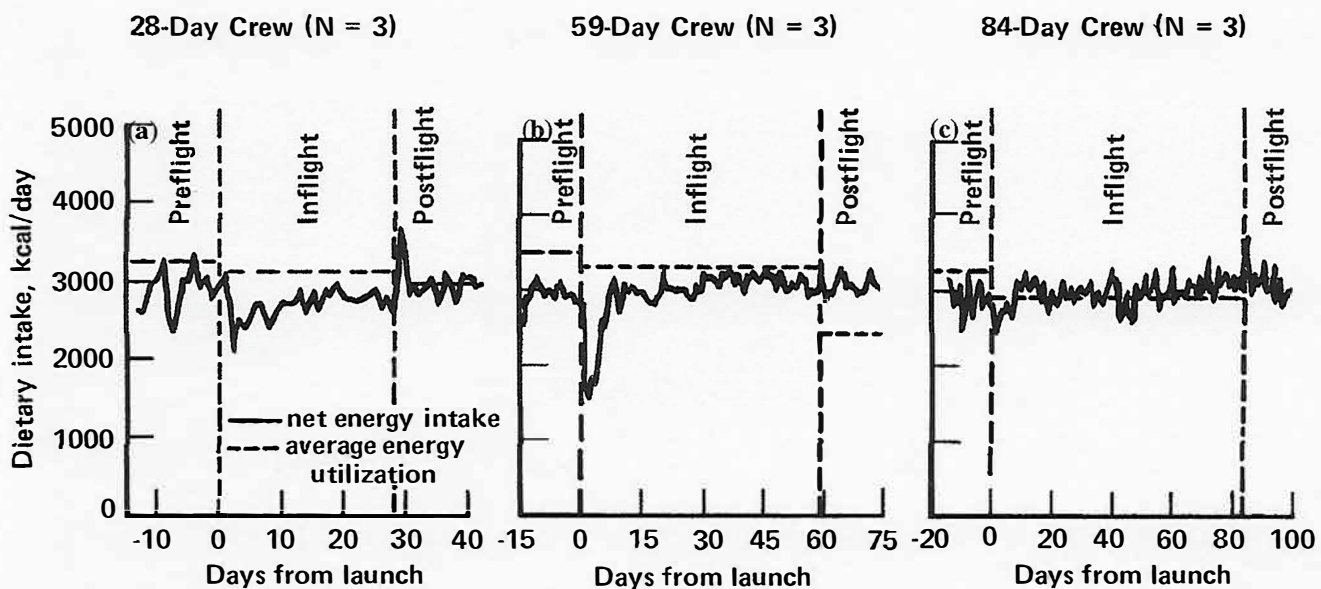
Figure F-6. Net food intake for each of the three Skylab missions (*N*=3). The difference between net energy intake (solid line) and average energy utilization (horizontal dashed line) represents the energy content of lost tissue, $\Delta \overline{TIS}$. Inflight values are: (a) 28-day mission $\Delta \overline{TIS}$ = -448 Kcal/day; (b) 59-day mission, $\Delta = \overline{TIS}$ -360 Kcal/day; (c) 84-day mission, $\Delta \overline{TIS}$ = +23 Kcal/day.

Table F-22. Methods for Computing Terms in Body Composition Equations

Quantity	Symbol	Method of Computation
Change in Body Mass, gm	$\Delta \overline{BWGT}$ and $\Delta BWGT$	Direct body mass/weight measurements
Change in Body Water, gm	$\Delta \overline{TBW}$	Isotope dilution (tritium) method performed before and after flight
	ΔTBW	Solve Equation (37) for ΔTBW
Change in Body Protein, gm	ΔPRO and $\Delta \overline{PRO}$	Nitrogen balance: $\Delta PRO = 6.25 \times N_{BAL} = 6.25 \times (N_{diet} - N_{urine} - N_{feces})$
Change in Body Fat, gm	$\Delta \overline{FAT}$	Solve Equation (37) for $\Delta \overline{FAT}$
	ΔFAT	$\Delta FAT = -E_{fat}/9.461$
Energy in Diet, kcal	E_{diet}	From stoichiometric relationships and known amounts of carbohydrate, fat, and protein in diet: E_{diet} = 4.182 x diet carbohydrate (gm) + 9.461 x diet fat (gm) + 5.65 x diet protein (gm)
Energy in Urine, kcal	E_{urine}	From urine nitrogen: $E_{URINE} = 8.32 \times N_{urine}$ (gm)
Energy in Feces, kcal	E_{feces}	From bomb calorimetry
Energy in Catabolized Protein, kcal	E_{pro}	$E_{pro} = -5.65 \times PRO$
Energy in Catabolized Fat, kcal	$\overline{E}_{fat}$	$E_{fat} = -9.461 \times \Delta \overline{FAT}$
	E_{fat}	Solve Equation (38) for E_{fat} using $E_{util}*$
Net Energy Utilized, kcal	$\overline{E_{util}}*$	From Equation (38)
	$E_{util}*$	$E_{util}* = \overline{E_{util}}*$ /days of mission phase

Note:

(1) Bar over symbol denotes overall mission phase mass losses or cumulative energy quantities summed over mission phase. Symbols without bars referred to daily values of that quantity. Δ = change in quantity, * denotes computed value.

(2) $\overline{E_{diet}}$, $\overline{E_{urine}}$, $\overline{E_{feces}}$, $\overline{E_{pro}}$, and $\Delta \overline{PRO}$ are computed by summing the daily amounts of each quantity (as defined above) over each mission phase; (i.e. = $\overline{E_{diet}} = \sum E_{diet}$)

(3) Units are in gm or gm/day and kcal or kcal/day depending on the period for which they are computed.

Table F-23. Net Utilization (E$_{util}$*) [kcal/day]

Subject	Preflight	Inflight	Postflight
28-day mission			
1	2737	2861	3493
2	3522	3572	2729
3	3448	2969	2706
59-day mission			
4	3037	3049	1485
5	3354	3170	2248
6	3994	3678	3633
84-day mission			
7	2879	2842	3306
8	3130	2973	2833
9	3773	3031	3322
Mean	**3319**	**3127**	**2862**
±SD	**+414**	**+300**	**+682**

Table F-24. Tissue Components of Body Mass That Were Lost During the Inflight Phase [gm]

Mission	Crewmember	ΔBody Weight	ΔTotal Body Water	ΔTissue Solids	ΔProtein	ΔFat
28-day	1	-1100	-405	-695	-170	-52.
	2	-2700	-180	-2520	-390	-2310
	3	-3200	-2090	-1110	-300	-810
	Mean	**-2330**	**-890**	**-1440**	**-290**	**-115.**
	±SD	**±1100**	**±1080**	**±960**	**±110**	**±85.**
59-day	4	-3900	-1395	-2535	-365	-2170
	5	-4200	+125	-3725	-285	-343.
	6	-4200	-3345	-855	-295	-560
	Mean	**-3900**	**-1530**	**-2370**	**-320**	**-205.**
	±SD	**±300**	**±1740**	**±1440**	**±40**	**±1440**
84-day	7	0	-770	+770	-650	+1420
	8	-1400	-615	-785	-355	-42.
	9	-1400	-1600	+200	-30	+230
	Mean	**-930**	**-995**	**+62**	**-350**	**+410**
	±SD	**±810**	**±530**	**±790**	**±310**	**±93.**
	Skylab Mean	**-2390**	**-1140**	**-1250**	**-315**	**-93.**
	±SD	**±1460**	**±1090**	**±1425**	**±170**	**±1440**

*Time period considered is from morning of launch (one-g) to morning of recovery (zero-g)

Figure 7. Change in body weight during each Skylab mission ($n = 3$). Values are shown as changes from morning of launch.

Figure 8. Change in body water during each Skylab mission ($n = 3$). Values are shown as changes from morning of launch.
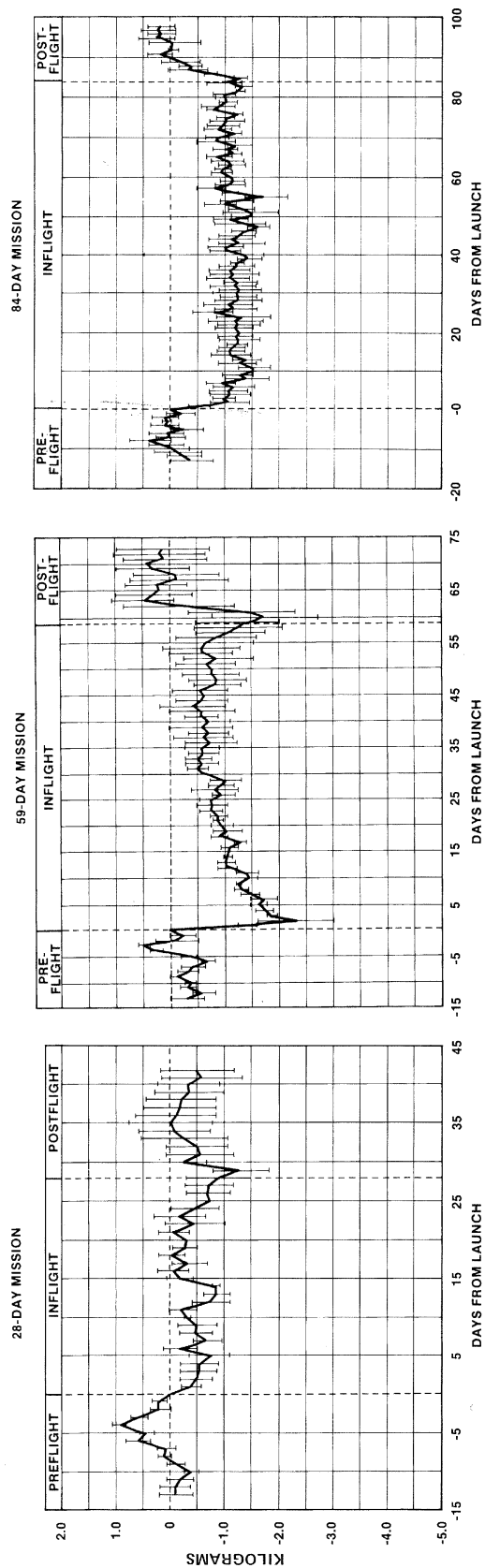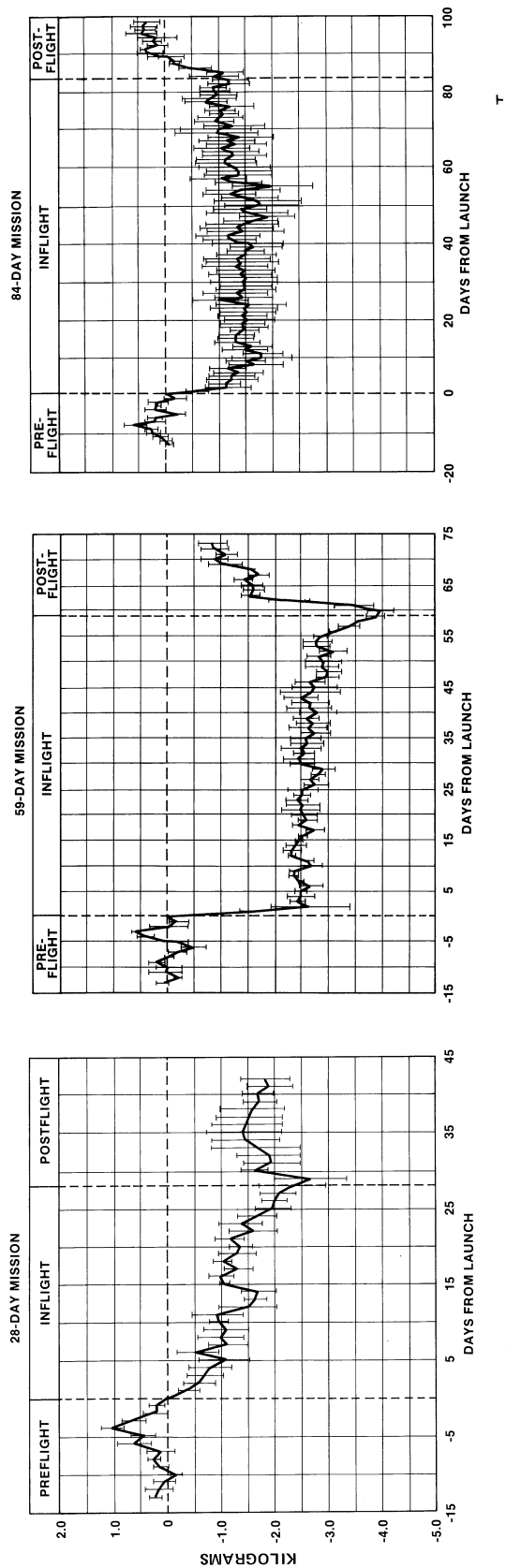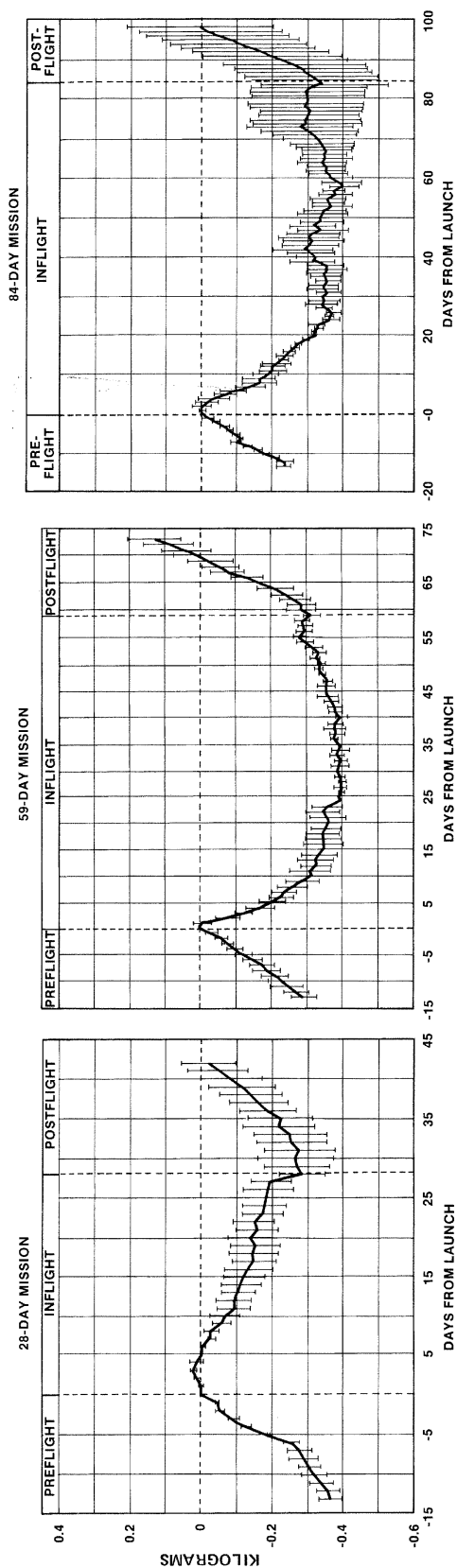
Figure 9. Change in body protein during each Skylab mission ($n = 3$). Values are shown as changes from morning of launch.
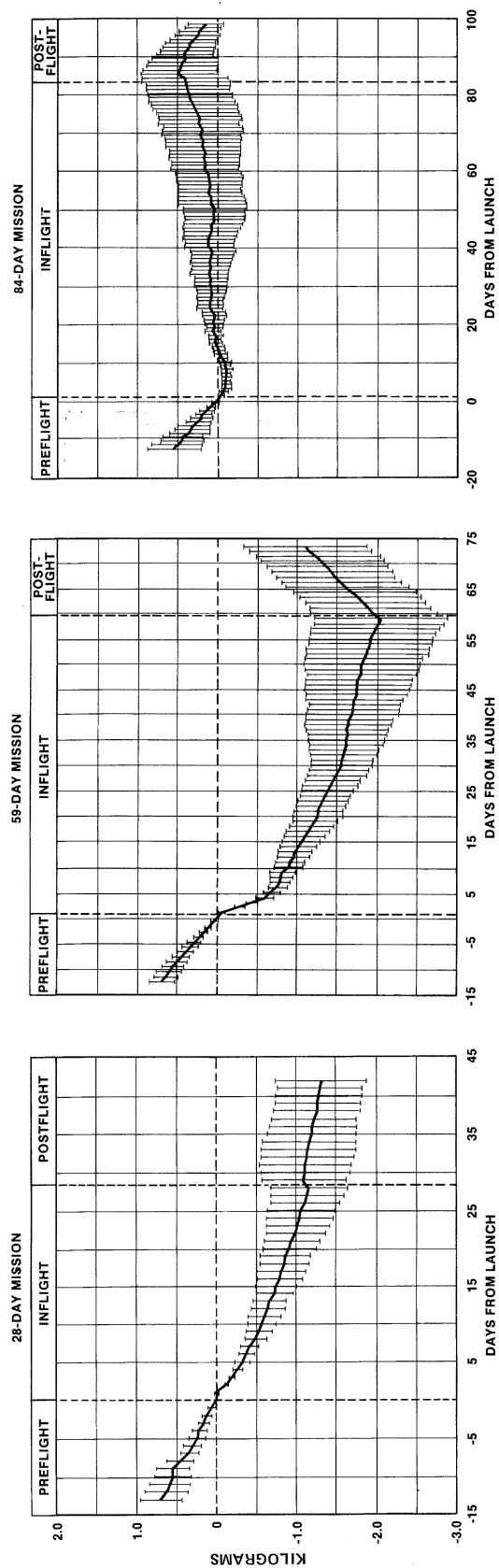
Figure 10. Change in body fat during each Skylab mission ($n = 3$). Values are shown as changes from morning of launch.

Table F-25. Changes of Body Weight/Mass and Body Water Before and After Skylab Missions [Kg]

Crewman	Body Weight			Total Body Water		
	Preflight Mean	Δ_1 [a]	Δ_2 [b]	Preflight Mean	Δ_1	Δ_2
1	62.21	-2.0	-1.1	41.55	-0.75	-0.41
2	77.89	-3.6	-2.7	48.80	-0.80	-0.18
3	80.18	-4.2	-3.2	52.15	-2.15	-2.09
4	68.56	-4.0	-3.9	42.50	-0.60	-1.37
5	61.82	-3.1	-3.6	39.10	+0.50	+0.12
6	88.01	-3.9	-4.2	53.60	-1.70	-3.34
7	67.75	+0.1	0	41.85	-0.85	-0.77
8	71.51	-2.9	-1.4	45.40	-0.50	-0.62
9	67.60	-1.5	-1.4	45.65	-0.55	-1.60
Mean	**71.73**	**-2.8**	**-2.4**	**45.62**	**-0.82**	**-1.14**
±SD	**±8.72**	**±1.4**	**±1.5**	**±5.00**	**±0.75**	**±1.09**

(a) Δ_1 = Change from preflight mean to first shipboard measurement at recovery. Body mass waas measured within several hours of recovery. Body water was measured on first or second day of recovery.

(b) Δ_2 = Change from preflight mean to morning of day of recovery (a zero-g state). Total body water changes estimted by correcting for wtaer intake and excretion between recovery a.m. and first shipboard measurement.

Table F-26. Components of Energy Balance During Skylab Preflight Phase [kcal/d]

Energy Balance Component	Crewman								
	1	2	3	4	5	6	7	8	9
Total Diet[a]	2916	3166	3175	2851	2996	4214	3224	3149	3269
Excreta: Urine[b]	106	105	110	93	108	166	116	121	135
Feces	142	158	143	110	125	171	160	146	129
Total Excreta	248	263	253	203	233	337	276	267	264
Body Tissue Loss: Protein[c,e]	-104	-110	-106	-108	-121	-143	-117	-78	-98
Fat[d]	173	730	632	497	712	260	47	326	866
Total Tissue[e]	69	620	526	389	591	117	-70	248	768
Net Energy Utilization[f]	2737	3523	3448	3037	3354	3994	2878	3130	3773

a) Diet (kcal/day) = 4.182 diet carbohydrates (gm/d) + 9.461 x diet fat (gm/d) + 5.65 x protein (gm/d)
b) Urine energy = 8.32 x urine nitrogen (gm/d)
c) Energy from protein tissue loss = 5.65 kcal/gm
d) Energy from fat tissue lost = 9.461 kcal/gm
e) Minus sign denotes a gain of body tissue
f) Net energy utilization = Diet Excreta + Energy from body tissue lost

Table F-27. Components of Energy Balance During Skylab Inflight Phase [kcal/d]

Energy Balance Component	Crewman								
	1	2	3	4	5	6	7	8	9
Total Diet[a]	2888	3031	2873	2888	2860	3927	3271	3149	3361
Excreta: Urine[b]	132	150	135	111	138	186	152	146	160
Feces	106	107	104	111	131	181	161	102	146
Total Excreta	238	257	239	222	269	367	313	247	306
Body Tissue Loss: Protein[c]	34	79	60	35	28	28	44	24	2
Fat[d,e]	178	720	274	348	551	90	-160	48	-26
Total Tissue[e]	212	798	334	383	579	118	-116	72	-24
Net Energy Utilization[f]	2861	3572	2968	3049	3170	3678	2842	2974	3031

(See footnotes for Table F-26)

Table F-28. Energy Balance Terms Related to Diet[a,d]

Crewman	Days Observed Pre	Days Observed Inf	CHO (gm) Pre	CHO (gm) Inf	FAT (gm) Pre	FAT (gm) Inf	PRO (gm) Pre	PRO (gm) Inf	E_{diet}(kcal)[b] (calculated) Pre	E_{diet}(kcal)[b] (calculated) Inf	E_{diet} (kcal)[c] (bomb) Pre	E_{diet} (kcal)[c] (bomb) Inf
1	30	28	319	376	105	79	105	101	2916	2888	2632	2498
2	30	28	382	402	101	80	108	105	3166	3031	2901	2580
3	30	28	364	394	109	72	110	97	3175	2873	2881	2497
4	20	59	331	426	98	66	95	95	2851	2888	2561	2586
5	20	59	315	368	110	76	112	107	2996	2860	2688	2511
6	20	59	490	565	132	77	163	148	4214	3927	3716	3488
7	26	84	363	398	108	100	121	118	3224	3271	3152	3202
8	26	84	358	395	108	92	113	111	3149	3149	3088	3085
9	26	84	348	385	116	109	127	128	3269	3361	3194	3285
Skylab Mean			**363**	**412**	**110**	**83**	**117**	**111**	**3218**	**3139**	**2979**	**2859**
±SD			**52**	**60**	**10**	**14**	**19**	**18**	**400**	**349**	**358**	**400**

a) CHO = dietary carbohydrates; FAT = dietary fat; PRO = dietary protein

b) E_{DIET} (Calculated) = total energy derived from diet = (4.182)CHO + (9.461) FAT + (5.65) PRO

c) E_{DIET} (Bomb) = total of diet measured by bomb calorimetry. (The number of samples used to obtain E_{DIET} (Bomb) was somewhat less than that used to compute E_{DIET} (Calculated).

d) Regression coefficients for E_{DIET} (Calc) vs. E_{DIET} (Bomb): r = 0.93 (Preflight), r = 0.91 (Inflight); ratio Inflight/Preflight for E_{DIET} (Calc) = 0.975, for E_{DIET} (Bomb) = 0.96.

Table F-29. Energy Available versus Energy Utilized [kcal/day-kg BWGT]

Mission	Subject	Ediet Pre	Ediet Inf	Ediet net Pre	Ediet net Inf	Eutil Pre	Eutil Inf
28-day	1	46.9	46.4	42.9	42.6	44.0	46.0
	2	40.7	38.9	37.3	35.6	45.2	45.9
	3	39.6	35.8	36.4	32.9	43.0	37.0
	Mean	**44.7**	**40.4**	**38.9**	**37.0**	**44.1**	**43.0**
	±SD	**±4.5**	**±5.5**	**±3.5**	**±5.0**	**±1.1**	**±5.2**
59-day	4	41.6	42.1	38.6	38.9	44.3	44.5
	5	48.5	46.3	44.7	41.9	54.3	51.3
	6	47.9	44.6	44.1	40.5	45.4	41.8
	Mean	**46.0**	**44.3**	**42.5**	**40.4**	**47.6**	**45.9**
	±SD	**3.8**	**±2.1**	**±3.4**	**±1.5**	**±5.4**	**±4.9**
84-day	7	47.6	48.3	43.5	43.7	42.5	42.0
	8	44.0	44.0	40.3	40.6	43.8	41.6
	9	48.4	49.7	44.5	45.2	55.8	44.8
	Mean	**46.7**	**47.3**	**44.7**	**43.2**	**47.3**	**42.8**
	±SD	**±2.3**	**±3.0**	**±2.9**	**±2.3**	**±7.3**	**±1.7**
	Skylab Mean	**45.0**	**44.0**	**41.4**	**40.2**	**46.4**	**43.9**
	±SD	**±3.6**	**±4.5**	**±3.3**	**±3.9**	**±4.9**	**±4.0**

a) E_{diet} = total energy available from dietary carbohydrates, fats, proteins (calculated)

b) $E_{diet\ net} = E_{diet}$ – energy in urine and feces

c) E_{util} = energy utilized = $E_{diet\ net}$ + energy obtained from protein and fat catabolism.

Table F-30. Diet, Exercise and Tissue Weight Change Data Used for Regression Analysis*

Subject	Caloric Intake (kcal/d-kg)	Average Daily Exercise Work (kcal/d-kg)**	ΔBWGT	ΔFAT (gm/d-kg)	ΔPRO
1	46.4	2.35	-0.632	-0.302	-0.0966
2	38.9	1.35	-1.238	-0.977	-0.179
3	35.8	1.62	-1.426	-0.361	-0.133
4	42.1	3.68	-0.964	-0.537	-0.090
5	46.3	3.83	-0.987	-0.941	-0.0788
6	44.6	4.84	-0.809	-0.108	-0.0572
7	48.2	4.00	0	+0.249	-0.114
8	44.0	5.09	-0.233	-0.071	-0.0594
9	49.7	4.76	-0.247	+0.041	-0.0855

* These data used in regression analysis of Table 4-25

** Derived from Michel and co-workers [49] by dividing useful bicycle work by 22% efficiency. To compute total exercise performed over the mission in watt-minute (W-min), multiply value in table for average daily exercise work (kcal/d-dg) by BWGT x 70 W-min/kcal x 0.22 x N, where N is the number of inflight days in the Skylab Mission.

References

1. Leonard , J.I., *Skylab Water Balance Analysis,* (General Electric Co. TIR 782-LSP-7003), NASA CR-167461, NASA, Washington, DC, 1977.

2. Leonard, J.I., *Skylab Water Balance Error Analysis*, (General Electric Co. TIR 782-LSP-7006), NASA CR-160402, NASA, Washington, DC, 1977.

3. Consolazio, C. F., Johnson, R. E., and Becora, L. J., *Physiological Measurements of Metabolic Functions in Man*, Mc.Graw-Hill (New York), 1963.

4. MacHattie, L. A., Graphic Visualization of the Relations of Metabolic Fuels, Heat, O2, CO2, H2O, and Urine N, *J. Appl. Physiol.*, 15, 1960, pp. 677-683.

5. Calloway, D. H., Pace, N., (Eds.), Life Support Requirements of Astronauts, Part 1, *Basic Data. Envir. Biol. Med.,* Vol. 1, 1972, pp. 65-202.

6. Roth, E. M., Teichner, W. H., and Mirarchi, P. O., Contaminants Standards in *Compendium of Human Responses to the Aerospace Environment*, E. M. Roth, (Ed.), NASA, Washington, DC, 1968, sect. 10-16, pp. 13-36.

7. Webb, P., (Ed.), *Bioastronautics Data Book*. NASA SP-3006, NASA, Washington, D. C., 1964. Sect. 13, p. 10.

8. Rambaut, P. C., Leach, C.S., and Leonard, J. I., Observations in Energy Balance in Man During Spaceflight, *Am. J. Physiol.*, Vol. 233, *Reg. Integ. And Comp. Physiol.,* vol 2, pp. R208-R2121977

9. Hegsted, D. M., Balance Studies, *J. of Nutrition,* 106:3, 1976, pp. 307-311

10. Leonard, J. I., *Analyses of Evaporative Water Loss in the Skylab Astronauts*, (General Electric Co. TIR 741-LSP-7017), NASA CR-167462, NASA, Washington, DC, 1977.

11. Leach, C.S., Leonard, J.I., Rambaut, P.C., and Johnson, P.C., Evaporative water loss in man in a gravity-free environment, *J. Appl. Physiol: Respirat. Environ.Exercise Physiol.* vol. 45, 1978, pp.430-436.

12. Bernauer, E. M., Mole, P. A., and Johnson, R. E., Calculation of Metabolic Mixture and Water Balance Using Fortran Programs, *Metabolism*, vol. **16**, 1967, pp. 899-909.

13. Gee, G. F., Kronenberg, R. S., and Chapin, R. R., Insensible Weight and Water Loss During Simulated Spaceflight, *Aero. Med.* vol. 39, 1968, pp. 984-988.

14. Roy, J., Laha, R. G., and Chakrawarti, I. M., (Eds.), *Handbook of Methods if Applied Statistics*, Vol. I. Techniques of Computation, Descriptive Methods and Statistical Inference, John Wiley Co., Inc., New York, 1966.

15. Snedecor, G. W., *Statistical Methods*, 5th ed., Iowa State University Press, Ames, Iowa, 1956.

16. Thornton, W. E., and Ord, J., Physiological Mass Measurements in Skylab. in *Biomedical Results from Skylab*, SP-377, Chapter 19, NASA, Washington, D. C., 1977, pp. 175-182.

17. Grounds, D., *Skylab Sodium and Potassium Balances*, Rep.

TIR-741-LSP-7015, General Electric Co., Houston, TX, 1977.

18. Leach, C. S., and Rambaut, P. C., Biochemical Responses of the Skylab Crewmen: An Overview, *Biomedical Results from Skylab*. NASA SP-377, Chap. 23, NASA, Washington, D. C., 1977, pp. 204-216.

19. Bland, J. H., *Clinical Metabolism of Body Water and Electrolytes*, W. B. Saunders and Cox, Philadelphia, PA, 1963.

20. Vogel, J. M., Whittle, M. W., Smith, M. C., Jr., and Rambaut, P. C., Bone Mineral Measurement in *Biomedical Results of Skylab*, NASA SP-377, NASA, Washington, DC, 1977.

21. Nichols, G. Jr., and Nichols N., Changes in Tissue Composition During Acute Sodium Depletion, *Am. J. Physiol.* vol. 186, 1956. p. 383.

22. Leonard, J.I., *Quantitation of Tissue Loss During Prolonged Spaceflight*, (General Electric Co. TIR 741-LSP-9017), NASA CR-167460, NASA, Washington, DC, 1979.

23. Leonard, J.I., Leach, C.S. and Rambaut, P.C., Quantitation of Tissue Loss During Prolonged Spaceflight, *Amer. J. Clin. Nutr.*, vol. 38, pp. 667-683, 1983

24. Grande, F., Energy Balance in Body Composition Changes, *Ann. Intern. Med.* vol. 68, 1968, pp. 467-480.

25. Yang, M., and Van Itallie, T. B., Composition of Weight Lost During Short-Term Weight Reduction: Metabolic Responses of Obese Subjects to Starvation and Low-Calorie Ketogenic and Nonketogenic Diets, *J. of Clin. Invest.*, vol. **58**, 1976, pp. 722-730.

26. Pace, N., and Rathburn, E. N., Studies on Body Composition III: The Body Water and Chemically Combined Nitrogen Content in Relation to Fat Content, *J. of Biol. Chem.*, vol. 158, 1945, pp. 685-691.

27. Edmonds, C. J., Jasani, B. M., and Smith, T., Total Body Potassium and Body Fat Estimation in Relationship to Height, Sex, Age, Malnutrition and Obesity, *Clin. Sci. and Mol. Med.* vol. 48, 1975, pp. 431-440.

28. Allen, T. H., Anderson, E. C., and Langham, W. H., Total Body Potassium and Gross Body Composition in Relation to Age, *Gerontology*, vol. 15, 1960 pp. 348-357.

29. Whittle, M. W., *The Effects of Prolonged Spaceflight on Human Body Composition*, Ph.D. thesis, University of Surrey, England, 1978. (Available at Biostereometrics Laboratory, Texas Institute for Rehabilitation and Research, Houston, TX.)

30. Calloway, D. H., Odell, A.C.F., and Margen, S., Sweat and Miscellaneous Nitrogen Losses in Human Balance Studies, *J. Nutr.* vol. 101, 1971 pp. 775-786.

31. Chien, S., Peng, M. T., Chen, K. P., Huaug, T. E., Chang, C., and Fang, H. S., Longitudinal Studies on Adipose Tissue and its Distribution in Human Subjects, *J. Appl. Physiol.* vol. 39, 1975.

32. Siri, W. E., The Gross Composition of the Body, in *Advances in Biological and Medical Physics*, vol. 4, Academic Press, 1956, pp. 239-280.

33. Brozek, J., Grande, F., Anderson, J. T., and Keys, A., Densitometric Analysis of Body Composition: Revision of Some Quantitative Assumptions, *Ann. N. Y. Acad. Sci.*, vol. 110, 1963, pp. 113-140.

34. Whittle, M. W., Herron, R. E., and Cuzzi, J. R., Biostereometric Analysis of Body Form: The Second Manned Skylab Mission, *Aviat. Space Environ. Med.* vol. 47, 1976, pp. 410-412.

35. Whedon, G. D., Lutwak, L., Rambaut, P. C., Whittle, M. W., Smith, M. C., Reid, J., Leach, C., Stadler, C. R., and Sanford, D. D., Mineral and Nitrogen Metabolic Studies, Experiment MO71, in *Biomedical Results from Skylab,* NASA SP-377, Chapter 18, NASA, Washington, D. C., pp. 164-174, 1977.

36. Snyder, W. S. (Chairman), *Report of the Task Group on Reference Man,* prepared by Task Group 2 of the International Commission on Radiological Protection, Pergamon Press, (Oxford), G. B., 1975.

37. Womersley, J., Durnin, J. V. G. A., Boddy, K., and Mahaffy, M., Influence of Muscular Development, Obesity, and Age on the Fat-Free Mass of Adults, *J. Appl. Physiol.*, vol. 41, 1976, pp. 223-229.

38. Pierson, R. N., Lin, D. H. Y., and Phillips, R. A., Total Body Potassium in Health: Effects of Age, Sex, Height and Fat, *Am. J. of Physiol.*, vol. 226, 1974, pp. 206-212.

39. Muldowney, F. P., and Healy J. J., Lean Body Mass and Total Body Potassium, in *Compartments, Pools and Spaces in Medical Physiology*. Per-Erik E. Bergner, M.D., C. C. Lushbaugh, M.D. and Elizabeth Anderson (Eds.), 1967, pp. 95-110.

40. Pitts, R. F., Physiology of the Kidney and Body Fluids, in *Year Book Medical Publishers*, 2nd ed., Chicago, Ill., 1968.

41. Chobanian, A. V., Lillie, *A.* D., Tercyak, A., and Blevins, P., The Metabolic and Hemodynamic Effects of Prolonged Bedrest in Normal Subjects, *Circ. Res.* vol. 54, 1974, pp. 551-559.

42. Johnson, P. C., and Mitchell, C. (Eds.), *Report of 28-Day Bedrest Simulation of Skylab*, The Methodist Hospital, Houston, TX, NASA, CR-151354, 1977.

43. Forbes, G. B., Another Source of Error in the Metabolic Balance Method, *Nutr. Rev.* vol. 31, 1972, pp. 297-300.

44. Wallace, W. M., Nitrogen Content of the Body and its Relation to Retention and Loss of Nitrogen, *Fed. Proc.* vol. 18, 1959, pp. 1125-1130.

45. Steffee, W. P., Goldsmith, R. S., Pencharz, P. B., Scrimshaw, N. S., and Young, V. R., Dietary Protein Intake and Dynamic Aspects of Whole Body Nitrogen Metabolism in Adult Humans, *Metab.*, vol. 25, 1976, pp. 281-297.

46. Leonard, J.I., Analysis of Metabolic Energy Utilization in the Skylab Astronauts, (TIR 741-LSP-7018, General Electric Co.,Houston, TX), NASA CR-160402, NASA, Washington, DC, 1977.

47. Leonard, J.I., Energy Balance and the Composition of Weight Loss During Prolonged Spaceflight, (TIR 2114-MED-2012, General Electric Co. Houston, TX), NASA CR-17145, NASA, Washington, DC, 1982.

48. Whittle, M.W. Caloric and Exercise Requirements for Spaceflight: Biostereometric Results from Skylab, *Aviat. Space Environ. Med.*, 50: 163-167, 1979.

49. Michel, E. L., Rummel, J. A., et al., Results of Skylab Medical Experiment M171–Metabolic Activity. *Biomedical Results From Skylab*, Richard S. Johnston and Lawrence F. Dietlein, (Eds.), V: Cardiovascular and Metabolic Function, ch. 36. NASA SP-377, NASA, Washington, DC, 1977, pp. 372–387.

Appendix G
Accomplishments and Recommendations

G.1 Accomplishments of the Systems Analysis Project

The investigative areas will be grouped, for purposes of summation, into four categories: (a) fluid, electrolyte, and renal function; (b) cardiovascular function; (c) hematology; and, (d) musculoskeletal function and body composition. The major systems analysis accomplishments for each area are summarized in Table G-1. The results from these studies have led to an interpretation of the spaceflight findings that are summarized in Chapter 10. In addition to the emphasis on interpreting physiological changes during spaceflight, this project has produced a number of accomplishments regarding the technological tools and information systems which have been indispensable to achieving its overall goals. These technology accomplishments are described in Chapter 3 and summarized in Table 10-1.

G.2 Recommendations for Model and Simulation Improvements

Throughout this book recommendations have been implicitly or explicitly made for improving the mathematical models or examining new model applications. For convenience, these recommendations have been assembled below. Although the recommendations, for the most part, are highly summarized, details can be found in the appropriate parts of the book.

G.2.1 Recommendations for Guyton Model
G.2.1.1 Areas Identified for Future Model Improvements

a) Develop a capability for simulating acid-base balance. This would involve modification of the renal sytem, the buffering system, and the respiratory system.
b) Formulation of upper body circulatory elements representing collapsed veins in modified Guyton model.
c) Validate Guyton model for LBNP simulation.
d) Develop an advanced renal subsystem model including peritubular capillary effects, third factor effects, factors influencing intrarenal blood flow, and the effect of calcium on electrolyte excretion.
e) Hormonal regulation should be updated to reflect current knowledge, especially with regard to multiple and competitive influences, and identification of the different mechanisms which dominate short-term vs. long-term control.
f) Experimental measurements of hormone levels are often obtained from urine samples. Existing models have the capability only of predicting plasma concentrations to hormones. It is recommended that a study be conducted to determine feasibility of adding hormone renal excretion capability to existing models.

g) Develop a new upright reference position for the model in addition to its present supine reference.
h) Test a more natural means of simulating weightlessness by starting with an upright reference control position and then removing the gravity effects from the reference model.

G.2.1.2 Recommendations for Additional Simulation Studies

a) Now that a reasonable simulation of spaceflight has been accomplished, it is important to make a detailed analysis of the mechanisms that control specific responses. In most cases, redundant feedback pathways exist. Determine which pathways predominate.
b) Determine the basic differences between simulations of bedrest, immersion, head-down tilt and spaceflight. What is the appropriate model stimulus for each of these conditions?
c) Use models to create and evaluate circulatory indices of performance, both inflight and postflight. These algorithms should provide a simple measure of circulatory status.
d) The new leg compartments of the modified Guyton model require additional validation studies, especially for characterization of resistance elements, capacitance elements and capillary exchange.

G.2.1.3 Recommendations for an Improved Simulation of Postural Studies.
The ability to simulate postural maneuvers, both head-up and head-down, has proved to be a complex endeavor. Chapters 9.3.2, 9.6.3 and Appendix C.1 have described the model modifications that provided basic structural and mechanistic capabilities to respond to the gravitational vector. Appendix C.2 delineated a set of recommendations for an improved orthostatic model. Here we would like to mention several other recommendations for improving the head-down tilt simulation and, by extension, spaceflight simulation.

a) *Addition of a Head Compartment.* The model at present does not contain a separate vascular compartment above the heart level and does not exhibit collapsed veins in the erect posture, nor refilling and fluid storage during hypogravity and anti-orthostasis. Reports from astronauts typically include symptoms of head fullness, head tissue puffiness and neck vein distention during prolonged hypogravity. Thus, the model may have to be altered in some manner to reproduce these effects. The most feasible approach is the addition of collapsible veins in a separate cephaled compartment.
b) *Improved Resistance to Flow in Legs.* The leg resistance elements (both pre- and post-capillary) are

Table G-1. Accomplishments of Systems Analysis Study

Fluid-Electrolyte Regulation

- Modification of the Guyton model (circulatory, fluid and electrolyte regulation) to include gravity-dependent elements, leg compartments, and improvements in the erythropoietic, renal, autonomic and renin-angiotensin subsystems
- Validation of the modified Guyton model for fluid-loading, hemorrhage, and postural-change studies
- Simulation analysis of the fluid-electrolyte response to hypogravic studies including water immersion, head-down tilt, bedrest, and spaceflight
- Analysis of evaporative water loss in the hypobaric, reduced-convective-flow environment of Skylab using metabolic balance analysis and the modified Stolwijk thermoregulatory model
- Metabolic balance analysis of water, sodium, potassium, calcium, nitrogen, and magnesium including Skylab nine-man composite summaries of dietary intake, renal excretion, and sweat losses
- Composite time profiles of the nine-man Skylab mean responses for plasma and urinary electrolytes, hormones, and total body changes in water, sodium, and potassium
- Analysis of fluid-electrolyte regulatory feedback mechanisms involved in acute and long-term responses to weightlessness
- Interpretation of all Skylab data related to disturbances in body fluid volumes and their composition including a description of the fluid-electrolyte status of the Skylab crewman and an integrated hypothesis to explain the behavior of renal-regulating hormones
- Major support of bedrest and Spacelab flight experiment proposals

Cardiovascular Regulation

- Development of a new pulsatile cardiovascular system model
- Validation of cardiovascular model for exercise, tilt, lower body negative pressure (LBNP) in one-g, and centrifugation.
- Modification of the pulsatile model to include elements responsive to hypoxia and hypercapnia
- Modification of the respiratory model of Grodins to include the capability to respond to exercise
- Simulations of the exercise response using the combined thermoregulatory, respiratory, and cardiovascular subsystem models of the whole-body algorithm
- Simulation analysis of spaceflight LBNP and postflight exercise (supine and sitting) using the pulsatile model
- Simulation of disturbances in the circulatory system during short-term water immersion and head-down tilt and long-term bedrest and spaceflight using the modified Guyton model and the whole-body algorithm
- Composite time profiles of the nine-man Skylab mean responses to LBNP
- Sensitivity analyses for effects of blood loss and venous compliance changes on tilt and LBNP responses
- Analysis to examine possible changes in inflight baroreceptor sensitivity
- Analysis of mechanical and metabolic efficiencies and other performance indices during bicycle ergometry flight experiments
- Modification of the pulsatile cardiovascular model to include physical training (conditioning) effects and evaluation of these hypotheses against Skylab exercise data
- Formulation and evaluation of hypotheses to account for decreased orthostatic tolerance and decreased aerobic capacity during inflight and postflight phases
- Analysis of cardiovascular response during the high-g of Shuttle reentry with reduced blood volume including identifying thresholds for visual grayout
- Utilization of models to develop countermeasures for orthostatic intolerance during and after Shuttle reentry including fluid loading and leg pressure garments
- Support of flight experiment proposal for advanced cardiopulmonary studies

Hematology

- Development of new models for control of erythropoiesis in the human and the mouse
- Simulation analysis of hematological responses to altitude hypoxia and descent, red cell infusions, bedrest, water-restricted dehydration, and spaceflight
- Collaboration in a research program that examined suppressed erythropoiesis in dehydrated mice
- Analysis of all spaceflight and ground-based studies related to loss of red cell mass during hypogravity
- Formulation and tentative evaluation of candidate hypotheses to explain the "anemia" of spaceflight with particular emphasis on explaining the differences in red cell loss among crewmen
- Simulations of clinical syndromes (anemias, polycythemias, and Hb abnormalities) and partial development of a teaching model of erythropoiesis regulation
- Support of a Shuttle Spacelab experiment by predicting expected results, critical measurements, frequency of measurements, and effect of blood sampling on the hematological response to microgravity.

Musculoskeletal System and Body Composition

- Metabolic mass, water and energy balance analyses including a new method for estimating cumulative total body changes (water, fat, protein, electrolytes) as a function of flight duration
- Analysis of body composition changes (lean body mass and fat) based on body water, body potassium, nitrogen-potassium balance, and body density data
- Analysis of inflight requirements for exercise and diet
- Interpretation of components of body weight loss based on fluid and energy regulation and gravity unloading
- Design and development of a new model for calcium regulation, including validation studies of bedrest and spaceflight
- Support of a flight experiment proposal for advanced calcium regulation studies

presently modeled in a similar fashion as the upper body. They both account for passive distention and collapse, autonomic influence, angiotensin, vasoconstriction, and viscosity effects. However, there are undoubtedly some fundamental differences between the lower and upper body resistance capacitance and capillary elements. Mechanisms which are currently under consideration for inclusion in the lower extremity elements include those due to: a) locally produced vasoconstriction (myogenic), b) enhanced autonomic effects, and c) chemical effects (i.e., catecholemines).

c) **Improved Model of Collapsible Veins.** Rather than model the veins according to the linearization of the compliance curve shown in Fig. 9-32, an alternative approach is to allow the veins to completely collapse at any point where transmural pressure approaches zero. This produces a "waterfall" effect where flow is independent of pressure drop. When pressure falls to zero, the resulting cessation of flow causes pressure to rise and the vessel reopens. This approach would likely resolve some current problems encountered with the model at the more extreme tilt angles and improve its stability.

d) **Differentiation of Transcapillary Filtration.** Simulations that are more realistic can be achieved by improving the description of the differential behavior of upper and lower body capillary filtration and the factors which influence this process. We believe that capillary beds in the legs are especially suited to withstand elevated hydrostatic loads and the model should reflect this notion.

G.2.2 Erythropoiesis Regulatory Model
G.2.2.1 Improvements in Model Design.
Many factors have been discussed that are known to affect erythropoiesis, but have not been included in the proposed model. This study has resulted in several specific recommendations for improvements in the model and suggestions for related models.

a) The current model does not include a description of the kinetics of stem cell differentiation in the bone marrow. Such a description would represent the red cell proliferation and maturation cycle from multipotential cells to denucleated red cells. The model, thus modified, would be able to predict the reticulocyte index and have an improved characteristics of the bone marrow transit delay, among other benefits.

b) The current model does not include extrarenal erythropoietin production or extramedullary erythropoiesis.

c) The model should have an updated description of the renal sensor site(s), including the determination of oxygen tension and factors effecting erythropoietin productIon.

d) The kinetics of erythropoietin formation should include descriptions of "pro-Ep-plasma factors" and "Ep inhibitors".

e) Account for the effect of certain factors on erythropoietin that are not included in the current model, such as iron levels, hormones other than erythropoi-

etin (i.e., growth hormone), and neural stimulation, as well as inhibitors and activators of erythropoietin.

f) The effects of blood viscosity and blood volume changes on blood flow and tissue oxygenation should be added to the model.

g) Other factors that control oxygen transport are only currently included as fixed parameters. They could be added as variable elements. These factors include blood flow, capillary diffusivity, arterial oxygen tension, plasma volume, and oxygen-hemoglobin affinity.

h) Include an explicit representation of the DPG effect on oxyhemoglobin affinity; consider implementing a self-regulating mechanism perhaps based on levels of tissue oxygenation

G.2.2.2 Simulation Studies with Improved Model
a) Sensitivity analysis with parametric variation study of improved model

b) Characterization of bedrest response as a function of different plasma volume time profiles and red cell destruction rates

c) Reexamination of spaceflight data in light of model improvements and bedrest validation study.

G.2.2.3 Design and Develop Related Models
a) Teaching model for hematological abnormalities

b) Species-specific animal models for predicting results and integrating data for ground-based and Shuttle animal experiments

c) Ferrokinetic models for iron uptake studies

G.2.3 Cardiovascular Model (LBNP and Exercise)
A number of recommendations for improvements in the short-term cardiovascular model were suggested by the simulations of LBNP and exercise discussed in Chapter 7.

a) If the model is to be used for real-time simulations longer than a half hour it needs a more adequate representation of longer-term mechanisms including tissue filtration, hormonal regulation, baroreceptors adaptation and delayed vessel compliance (stress relaxation and reverse stress relaxation).

b) The current model has a neural component that uses a single autonomic signal for controlling flow resistances, compartmental compliances, and cardiac contractions. This signal combines the effects of sympathetic and parasympathetic neural control. A superior model can be achieved by developing a dual autonomic controller containing separate elements for these functions.

c) The current model is limited to the submaximal range of exercise. To enable the capability for maximal oxygen uptake tests, suggestions have been raised to improve cardiac reserve or cardiac filling representations in the model. Other areas should be examined that control arterial pressure and heart rate at intense levels of exercise.

d) The model should be adapted to differentiate between levels of physical conditioning; i.e., to individualize the model.

e) A more specific type of individualization is the notion that male and females responses to orthostatic intolerance are thought to be quite different after spaceflight. The model should be individualized for these simulations based on gender.

f) An explicit representation of chemoreceptor stimulation should be included to enable the model to respond to changes in the content of inspired gases during exercise.

g) Representation of whole leg compliance (as opposed to leg venous compliance) should be included in the model for comparison with gross leg compliance measurements during LBNP. Also, there is a need for introducing non-linear compliances for the leg veins modeled after the upper body veins.

G.2.4 Calcium Regulatory Model

The model of calcium regulation did not reach the same level of maturity in development and application as the other math models in our repertoire. On the other hand in the years since Skylab, the problem of calcium demineralization in space has assumed a much higher research priority. The initial effort should be to reproduce the best model currently published (see Chapter 8) and then to validate the various sections.

a) Update the current NASA model to include all the features of the most recent model by Jaros and co-workers [Jaros GG, Guyton AC, Coleman TG, Ann. Biomed. Eng., 8:103-141, 1980].

b) Modify the renal and intestinal subsystems so that they are able to reproduce the excreta findings from prolonged bedrest and spaceflight.

c) Modify the hormonal regulation subsystems so that the behavior of the calcitropic hormones are in agreement with published data for a variety of stresses including bedrest.

d) Include in the model a description of bone regulatory forces that control mineralization such as piezoelectric and mechanical stresses.

e) The model will eventually need to include a much improved skeletal subsystem that is representative of the osteoblastic and osteoclastic processes.

f) Application of the model should be directed toward the identification, development and design of countermeasures for ameliorating bone demineralization in spaceflight.

G.2.5 Whole-Body Algorithm (WBA)
G.2.5.1 General Recommendations. Some important general recommendations include the following:

a) *Top-Down Design Approach*. As discussed in Chapter 10, there was general agreement that an advanced version of the Whole-Body Algorithm should be designed as a single integrated system, using a top-down. approach. Such an approach would have the following characteristics: a) a unified programming language, b) a standard set of input-output specifications, c) a standard set of acceptable numerical integration methods, d) a unified documentation method, e) a minimum of redundancy, g) the ability to develop the subsystems independently, knowing that the final products will be compatible, and h) a strongly coupled set of unique subsystems. This is a more logical, realistic and natural approach.

A top down approach would eliminate the deficiencies in the current model of having multiple autonomic nervous systems or circulatory systems. Another problem with the current version is the weakly linked artificial boundary between "short-term subsystems" and "long-term subsystems". Thus, it is not realistic at present to simulate exercise for more than 30 minutes because the hormonal changes, stress relaxation changes, and autoregulation functions a re not present in the short-term models.

Figure 2-2 illustrates one approach that incorporates both horizontal integration (different subsystems linked in parallel fashion) and vertical integration (a hierarchy of biochemical, cellular, tissue, and organ function). The organism level is the top link in the hierarchy; organs are connected to each other wherein each organ is assigned 5 layers – organ system, organ, tissue, cellular, biochemical. New versions of modules can be designed and substituted with a minimum of interfacing difficulties.

b) *Need for a Common Control Center*. The real physiological system is composed of many regulating systems with a common control center (the central autonomic nervous system) and with many commonalities in the basic controlled system (similar fluid compartments, blood pathways, etc.). In contrast, the integration of several self-contained models results in different control centers and different descriptions of the controlled system. An advanced top-down approach should lead to a model that is much more like the real system. Unfortunately, the experimental observations upon which an advanced neural and biochemical control system must be designed, are scarce and in many cases, non-existent. Thus, new experiments must be designed and additional information must be collected before there is a solid basis with which to pursue such a unified control center. Examples of the deficiencies in the current WBA include lack of discrimination between sympathetic and parasympathetic control, lack of a lung stretch receptor reflex; lack of connection between autonomics and catecholamine release.

c) *Validation Database Required.* Validating a large-scale system model such as the Whole-Body Algorithm (or its advanced successor) requires a physiological database that is as equally detailed and integrated. However, it was found that much of the needed data was lacking. One of the limitations of developing this type of model was in finding data sets that stretched across disciplinary boundaries so that a number of model subsystems could be validated at the same time, for the same stress, using data obtained from the same laboratory. It is interesting to note that some of the

most valuable data for validating the Whole-Body Algorithm came from laboratories engaged in both physiological research and modeling. Thus, this project has provided additional support for advocating a continuing interdisciplinary research program concerned with measuring whole-body responses to combinations of environmental and metabolic disturbances. Once a large-scale model is validated it should be capable of integrating large quantities of data such as that available for Skylab. There are admittedly few scientific projects in which such grandiose multi-disciplinary data collection occurs, but for those occasions, large-scale models become a significant tool for data analysis and interpretation.

d) ***Central Repository Concept.*** An advanced "digital human" would require the collaboration of researchers in many laboratories over a wide geographic area. A nationwide time-sharing system would allow contributors to afix their subsystem models into the larger model. A central committee of experts would administer the system, select the best models of each type for inclusion in the system, establish standards for programming language and interfaces, prepare documentation, and approve modifications. This approach would function as a central repository and communication system and could evolve into an important national resource contributing to the development and application of physiological modeling.

e) ***Test the Full Capability of the Existing Model.*** The WBA, as developed in this project, is very versatile, capable of simulating many different conditions. Limited resources permitted the examination of only a few specific conditions, all related to spaceflight. Thus, we did not address the many possibilities for other important applications. Thus, even before developing a more advanced model, it may be useful to put the current model to more complete use. For example, the three short-term models of the WBA could operate independently of the long-term model. This short-term group was a significant accomplishment in itself especially for its ability to simulate such common conditions as the exercise response, or exercise combined with an environmental stress as hypoxia. Each of these three short-term subsystem models (thermoregulatory, circulatory, and respiratory) were originally designed to simulate exercise, but the capabilities for responding to combined stresses have never been thoroughly investigated.

f) ***Individualized Models.*** The eventual goal of these systems analysis efforts is to provide a capability to predict normal responses for individual subjects in the spaceflight environment. Thus, the models, including the WBA, could be "tuned" for each individual crewmember.

G.2.5.2 Specific Recommendations for More Advanced Studies with the WBA

a) Improve and integrate the autonomic control system for both the cardiovascular and repiratory subsystems.

This is particularly needed for central and local integrated autonomic control for all stresses with the same formulation or representation. Better discrimination between sympathetic and parasympathetic control, lung stretch receptor reflex, autonomic control affecting catecholamine release from the adrenal medulla, different representation of similar controllers in each subsystem, and resetting or sensitivity changes in receptors and control centers are other areas which need investigation.

b) Improve definition of the long-term/short-term interface and improvements in the cardiovascular subsystem are needed to better simulate the gray area between short-term and long-term changes (particularly around one hour of simulated time). This is particularly needed to simulate the plasma filtration, stress relaxation changes, autoregulation, and many hormonal changes which do occur following many short term stresses (such as head-up tilt in 1-g).

c) Improve representation and/or validation of long-term adaptation/acclimatization (particularly since this is an area of interest in spaceflight) to long-term stress. Examples of long-term stresses that could be examined with complex integrated models include the long-term effects of thermal stess, hypoxia, and exercise. Data from people living in hot and cold climates and at high altitudes may provide a starting place for such study. Very little modeling activity has been conducted for these purposes.

d) Improve respiratory-thermoregulatory subsystem interface (other than through the cardiovascular subsystem) to improve simulation of respiratory heat losses and thermal influences on respiratory control.

e) Improve the flexibility for simulating different population responses to stress such as the effect of training/conditioning, age, and gender.

f) Continue validation, particularly in the areas of transient responses (both on and off) to exercise and thermal stress and multiple stresses for which data are available. Examples of some of the combined short-term stresses to which the WBA could be fruitfully applied includes: a) exercise + hypoxia, b) exercise + hypercapnia, c) exercise + thermal, d) exercise + dehydration, e) tilt + hypoxia, f) tilt + thermal stress, g) hypoxia + hypercapnia, h) exercise + hypoxia + thermal stress. Further testing of bedrest hypotheses is also needed.

g) Changes in evaporative water loss have long-term effects on renal excretion. Validate the thermoregulatory model for spaceflight evaporative water loss and utilize Whole-Body Algorithm to pass this information to long-term model subsystem.

h) The addition of vestibular and musculoskeletal subsystems to an advanced whole-body model should be considered. After a long-term spaceflight, stresses such as orthostatic intolerance is not only a result of circulatory problems, but muscular and vestibular activity as well. This would provide the capability, not present in the current version, of altering otiolith/propriocep-

tor function or tissue loading functions.

i) The degradation of hard tissues is not currently being considered in the WBA. The accompanying loss of calcium is a disturbing problem for long-term space-flight. Excess calcium in the body fluids also produces alterations in hormone levels and renal function. These effects should be accounted for in more advanced models.

It appears from the foregoing that this development of a whole-body algorithm is not complete and probably never will be complete. It is, however, a very good beginning and this study has not only produced a very useful tool, but has pointed the way for future work in this area.

G.3 Recommendations for Experimental Studies

The ultimate value of a model lies in the degree to which understanding of the system under study is enhanced. However, any worthwhile scientific endeavor should not only answer questions, but to suggest new ones. Thus, a number of testable hypotheses were formulated during the modeling process. All these items are legitimate research issues suitable for experimental study. Some have been addressed by others in varying levels of detail. In many cases, the model has provided a scientific rationale for an alternative hypothesis.

G.3.1 Fluid-Electrolyte and Circulatory Regulation

a) Regarding fluids shifted headward during hypogravic stress:
   i.   does excess fluid remain in the upper body throughout prolonged zero-g stress?;
   ii. is this fluid stored primarily in circulatory compartments or do extravascular spaces accept a significant portion?;
   iii. does cephaled fluid shifts merely fill previously collapsed veins in head and neck or does the volume increase beyond the zone of free distensibility?;
   iv. how much storage volume does this represent?;
   v.   does central hypervolemia return to normal during prolonged periods of spaceflight as predicted by the model or does it persist as suggested by water immersion experiments.

b) During one-g postural change, what is the extent of fluid movement between plasma and interstitium? Is there a significant amount of plasma refilling during standing due to reabsorption from the upper body's interstitial reservoir?

c) What is the origin of fluids which disappear from legs during first several days after launch (i. e., blood, interstitial, intracellular). Also, why is the amount of fluid shifted from legs during weightlessness so much greater than that associated with postural changes in one-g?

d) Recent experiments onboard Spacelab failed to reveal a diuresis. There may still be an issue regarding the voluntary withholding of fluids by astronauts the first day of flight as well as confounding influences of reclining for long-wait periods on the launch pad. The model suggests that a zero-g diuresis and natriuresis cannot be entirely suppressed.A definitive test for a diuresis may have to await the availability of a human centrifuge aboard Space Station. This would allow a subject to adjust to 1-g and then suddenly be exposed to microgravity.

e) Test the hypothesis, predicted by the model, that normally hydrated subjects in spaceflight will exhibit a normal diuresis when challenged by a fluid load. This study should be conducted well after the initial onset of weightlessness and with a statistically significant population.

f) One explanation for the fall in plasma volume during the onset of hypogravity, in the absence of a diuresis, is that transcapillary filtration increases and causes an equivalent loss of plasma volume. The model supports this possibility but suggests that the effects are transitory, and that interstitial fluid will eventually return to normal. Lymph flow and plasma colloidal oncotic pressure are factors to consider in this normalization. Verify the details of transcapillary filtration during spaceflight, including the possibility of increased protein permeability, as suggested by the model. Also, one should attempt todifferentiate between the tr anscapilla ry Starling forces in the legs and above the heart during hypogravity maneuvers.

g) What is the etiology of hyponatremia and its effect on fluid-electrolyte regulating hormones. What is the contribution of natriuretic hormone in producing hyponatremia and in opposing aldosterone's effect on sodium excretion.

h) Confirm the analysis which predicts reduced evaporative water and sweat electrolyte losses (hidromieosis) during prolonged spaceflight.

i) Confirm the model predictions of the effect of potassium release from cells as a factor controlling aldosterone.

j) What are the long-term adaptive mechanisms that are involved in circulatory and renal adaptation to prolonged spaceflight? That is, measurements are needed of central venous pressure, cardiac output, leg blood flow, renal flow, glomerular filtration rate, etc.

k) Additional inflight data is necessary during the first several hours following launch. Particular data that is required includes: urine flow; hematocrit; plasma electrolytes; levels of aldosterone, ADH, and angiotensin; fluid and electrolyte intake; sweat components; and circulatory indices.

l) Test the hypothesis, predicted by the model, that the renal-regulation hormones, angiotensin, aldosterone and ADH, are governed early in flight by pressure-volume regulating factors and later in flight by plasma electrolyte regulation.

m) Conduct a meaningful assessment of renal function in microgravity using renal stress tests in humans (fluid loading, salt loading, dehydration) and animals (glomerular and tubular dynamics using micropunc-

ture techniques).

n) Carefully controlled experiments are required to study metabolic rates, energy utilization, and thermoregulation (i.e., evaporative water loss), during prolonged spaceflight.

G.3.2 Cardiovascular

a) There is currently an inadequate description of the circulatory mechanisms that accommodate redistributed blood volume over prolonged periods of weightlessness. These processes include venous stress relaxation and reverse stress relaxation, vascularization and devascularization, baroreceptors and volume receptor adaptation, and autoregulation of blood flow.

b) The contribution of venous sympathetic activity to circulatory disturbances during spaceflight and recovery, at rest and during orthostasis, needs to be elucidated.

c) No hypothesis for the resting tachycardia of spaceflight has been proposed and our studies have failed to provide additional insight into its etiology.

d) The model has predicted a fall in venous pressure upon entering weightlessness is related to an increase in peripheral resistance. Determine the consequences of the known increases of angiotensin during bedrest and spaceflight on peripheral resistance. Is this a factor in the decline of venous pressure, or are there other causes?

e) The effects of physical conditioning on orthostatic intolerance and exercise performance during and following spaceflight needs to be confirmed and documented.

f) There does not appear to be adequate data describing how simple blood volume loss uncomplicated by weightlessness or similar conditions can modify the normal circulatory response to centrifugation. Such data would be highly useful to separate the effects of blood volume loss from other aspects of cardiovascular deconditioning.

g) Several additional hypotheses remain to be tested in an effort to obtain a more complete picture of the LBNP response during spaceflight and recovery.

   i. The influence of the slow adjustment of the circulatory capacity to a reduced blood volume (reverse stress relaxation). This hypothesis could help explain the increased stability of cardiovascular response to orthostatic testing.

   ii. The influence of sympathetic tone which may be decreased early inflight and increased upon recovery.

   iii. Postulated changes in baroreceptor activity which may occur in the immediate postflight period.

   iv. The influence of fluid stored in the upper body (originally derived from leg fluid) during zero-g which may be available during LBNP stress.

G.3.3 Erythropoiesis Regulation

a) Earth-based human studies showing the effects of exercise training on indices of erythropoiesis (i.e., red cell production, erythropoietin, iron uptake, stem cell distribution, reticulocytosis) are needed to help interpret the red cell response on Skylab. Red cell mass appears to exhibit less of a decrement for crew who exercised the most.

b) Earth based human studies showing the effects of negative caloric balance on the mechanisms of erythropoiesis are needed to help explain the effect of space motion sickness-induced anorexia on erythropoietin.

c) Determine the acute decrease in red cell mass during the first few days of spaceflight. Is this decrement explicable from the reduction in red cell production or is their a destructive element involved (i.e., shortened life span)?

d) Determine whether changes in P_{50} during bedrest and spaceflight has an effect on red cell production.

e) Demonstrate whether or not changes in renal blood flow occur during bedrest or spaceflight and if it has an effect on red cell production.

G.3.4 Musculoskeletal Adaptation

a) Demonstrate that the prevention of muscle atrophy will also lead to the prevention or retardation of bone losses.

b) Characterize bone strains and loading patterns at clinically relevant sites in humans during specific types of movement and exercise in one-g. This information can be used to engineer the types of devices needed to provide representative one-g loads during spaceflight.

G.4 Data Utilization: Privacy Considerations

This project would have been nearly impossible to conduct if the data privacy policy that is currently in force was effective in the Skylab era. Federal guidelines, used by NASA's astronauts, prohibit the release of individual data to the general scientific community (even if coded without identifiers) if the data can be associated with a specific research subject. On a mission with only 3 astronauts (as was the case in Skylab) it would be impossible to shield the identity of the subject by merely using subject codes. Most of NASA's missions have few subjects, and thus, unless the individual data can be averaged with those from many missions (risking data degradation because each mission is different from another) the data cannot legally be used except by the principal investigator. NASA will not permit this data to be released. Average data is certainly not as powerful as the use of individual responses, as was demonstrated in the current project. There should be no need to remind the reader how expensive it is in time, resources and in human life, to collect space-based data. Thus, an extremely important recommendation is to modify the data sharing guidelines pertaining to human scientific astronaut-subjects to allow appropriate data analysis by third parties to occur and to permit the use of individual-subject data.